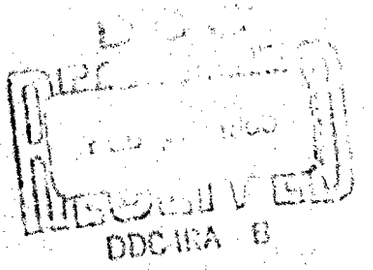
AD610549

PROCEEDINGS OF THE SYMPOSIUM ON SOIL-STRUCTURE INTERACTION

COPY 2 OF 3
HARD COPY $. 9 5c
MICROFICHE $. 3 0c
646D



UNIVERSITY OF ARIZONA
TUCSON, ARIZONA
SEPTEMBER 1964

Best Available Copy

ARCHIVE COPY

PROCEEDINGS OF THE SYMPOSIUM ON SOIL-STRUCTURE INTERACTION

The papers published herein were presented at the Soil-Structure Interaction Symposium conducted by the University of Arizona under sponsorship by the Office of Civil Defense. Publication does not necessarily reflect the views or policies of any agency of the United States Government.

UNIVERSITY OF ARIZONA
ENGINEERING RESEARCH LABORATORY
TUCSON, ARIZONA
SEPTEMBER 1964

PREFACE

The University of Arizona, Engineering Research Laboratory, was host to the Soil-Structure Interaction Symposium on the campus at Tucson, Arizona. Arrangements were sponsored and supported pursuant to a contract between the University of Arizona and the United States Department of Defense, Office of Civil Defense, in cooperation with other agencies of the United States Government.

These proceedings publish the formal as well as the informal material which was presented during the four days, June 8 through June 11, 1964. In general, the individual sessions followed a similar pattern in which previously prepared papers were given by the author after which questions were considered. The formal papers are presented herein under session headings; the less formal discussion is presented later under similar session headings.

The reasoning upon which the symposium was based, and the purposes to be realized, are best exemplified in welcoming addresses given in the opening session by Dr. James R. Shaw, representing the University of Arizona, and Mr. F. J. Tamanini, representing the Office of Civil Defense.

DR. JAMES R. SHAW*

I welcome you to the University of Arizona on behalf of Dr. Harvill** and Dr. Patrick***, who regret very much that they will be unable to join you. I bring you their greetings. The general area of civil defense and survival has been one of major interest at the University of Arizona for a considerable number of years.

The power of atomic bombs and thermonuclear devices staggers the imagination. And the reactions of this tremendous stress situation on the part of people generally have been of great concern to us, particularly in the medical field, as well as in the engineering field. The general attitude was somewhat improved a year ago when the Latham and Martin book, Strategy for Survival (University of Arizona Press, 1963), focused our attention on the problem and gave some hope for the future. We are proud of the young, dedicated, hard-working staff interested in this area; and we are particularly proud of the fact that you honored Arizona by joining here in your discussions. The staff, I might add, joins you in not knowing that this job cannot be done.

From a psychological and psychiatric point of view, people under tremendous stress situations react generally in one of four different ways. At the time of the application of the stress, there is a very large group of individuals who are completely unstable, emotionally. They are a nuisance, they require an expenditure of resources, time, and even control. There is another large group who completely ignore everything. They just fail to recognize any change in anything, push it completely from consciousness, and may even wander around and do nonsensical things. They are not any particular problem or danger because they are in a world by themselves, and isolate themselves by blocking everything from consciousness. There is a third group who are unable to make decisions or evaluate the situation; but who are very anxious to help and will attach themselves very early to true leaders who come out of the rubble or come into the rubble area, assess the situation, and make plans. Then, thank God, there is always the fourth group; who are able to pick themselves up, knock the dust off, look around and see what the situation is, think very clearly, and develop plans to carry out procedures to make the most of it. I feel the group we now have in this room fall into this latter, and very important, category.

This symposium is the first one of its kind in the field of underground survival construction design. The objective of the symposium is a review of the present status of the art and science. You are here to evaluate the potential for further productive research in this general area of interest. I can only join Stuart L. Pittman, Assistant Secretary of Defense for Civil Defense, when he said: "Let us get on with this work, even though when the threat fades there is little appetite for the dismal subject of survival. We owe this to our country. It makes us a tougher nut to crack and it makes war less likely." To this I would like to add that your efforts are in direct support of peace. We wish you great success. We hope that your deliberations here are fruitful.

Mr. F. J. TAMANINI****

It certainly is a pleasure to join the University of Arizona in welcoming this group, the Soil-Structure Interaction Symposium. I would like to take the next few minutes to actually paint a backdrop to the overall program, indicate what is behind it, and how this effort fits into the overall environment. To many of you this may be a slight review or a slight updating.

---

* Associate Director of Research, University of Arizona, Tucson, Arizona.
** President of the University of Arizona, Tucson, Arizona.
*** Director of Research, University of Arizona, Tucson, Arizona.
****Chief Structural Engineer, Architectural and Engineering Development Division, Office of Civil Defense, Department of Defense, Washington, D.C.

In 1961 when the President issued an executive order placing major civil defense responsibilities in the Department of Defense, he established the Office of Civil Defense. At the same time, he made Stuart L. Pittman Assistant Secretary of Defense for Civil Defense. This actually made a workable defense posture available to the country, because now it became possible for the Department of Defense to have a system of weaponry available to it, to have military services, and also to have civil defense in the military establishment. Civil Defense was no longer a separate office under the President or under an agency outside of the Department of Defense. This was a most important shot in the arm, because now the Department of Defense was able to move out in cooperation with the military services in planning what civil defense should be concerned with and what the military services should do to assist Civil Defense. One of the major conclusions established at this time was that the architectural and engineering professions of this country certainly had to be relied upon to do the technical task at hand. The President and Secretary of Defense decided to conduct computer studies and war gaming to decide what challenges confront Civil Defense. This was done. I might state that a major problem confronting the country was that there were not many architects and engineers acquainted with weapons effects, with a shielding methodology, or with protective construction. The Office of Civil Defense decided it must go to the universities and campuses of the country to present programs for the practicing architects and engineers, in order to move ahead in an effort to provide adequate shelter for about 240 million people by 1970. This major program was initiated with several workshops and about eight universities and two service schools. This professional development program has grown to include approximately 115 educational institutions and about 195 qualified instructors who are acquainted with effects of weapons, shielding methodology and protective construction. These numbers are increasing steadily by the splendid cooperation developed with the universities. In the meantime, protective construction manuals, and other publications were also being generated and sponsored by divisions other than the one with which I am associated.

So we have technology coming into operations, and we have professional development programs being integrated by the universities and their staff into the architectural and engineering professions. I might add that to date we have approximately 5800 practicing architects and engineers, including faculty and instructors, who are qualified and certified by the Department of Defense, after taking a very intensive course in radiation shielding methodology. It might be well at this point, to indicate that the national policy for civil defense is concentrated on providing adequate fallout shelter space for everyone in the country. The life-saving potential of fallout shelters can be readily shown. If one thinks in terms of a cigar, a lighted cigar, where ground zero is the burning end which is the high-initial-effects area, and the rest of the cigar is the fallout pattern. The national investment policy is concerned with that area depicted as the fallout pattern area. That is where there is the most life-saving potential per dollar.

However, we offer protective construction programs dealing with structural dynamics. These educational programs were necessary because many of the architects and engineers who had to deal with emergency operating centers, communication centers, control centers and other facilities, needed to know something about overpressure. They had to know something about concomitant effects and the treatment thereof, in addition to the radiation shielding. These courses are limited in number. Only about six or eight hundred have taken this program in protective construction. This is the constructional dynamics or blast program.

We also have two other programs that are part of this readiness program for the country. One is the environmental engineering program, which is orientated toward the mechanical engineer. This again came about because of the requirements to build more environmental control into all our shelters for temperature, ventilation, and so on, which makes more shelter space available at very little cost. We also have a shelter planning program for the principals of architectural engineering firms who are not the slide rule operators or design personnel of the consulting firms but rather the actual individuals who are the first contact with the client.

This program for soil-structure interaction came about because it was called to our attention that there were numerous areas in soil-structure interaction that needed either more information or dissemination of the information that was already currently available, but available only to certain researchers, or certain laboratories or government offices, and not readily available to anyone who would be associated with protective construction or shelters that required additional features other than radiation shielding. So the University of Arizona and our headquarters office discussed the possibility of having this get-together here for reviewing the state of the art and providing a meeting ground for not only researchers but practicing engineers and university faculty in order to see the over-all current picture and perhaps see it better from our vantage position here.

This particular program does not realign civil defense policy. It is no deviation from it. We are not attempting to change the national fallout shelter policy. It is very important that we get this point across to those who are present so that nothing is read into the fact that we are still looking to the future while making progress in the direction of providing the nation with readiness and with shelters. This is the approach of the Department of Defense. I think there is going to be a lot to show, to read, and to study. It is hoped that through the material that comes from this symposium we will realize an improved protective shelter program.

TABLE OF CONTENTS

page

PREFACE i
F. J. Tamanini - Office of Civil Defense
James R. Shaw - University of Arizona

SESSION ONE - MONDAY AM

OPENING ADDRESS

THE BASIS OF CURRENT CRITERIA FOR THE DESIGN OF UNDERGROUND PROTECTIVE CONSTRUCTION, N. M. Newmark - University of Illinois 1

SESSION TWO-MONDAY PM

WAVE PROPAGATION IN SOIL MEDIA

CHARACTERISTICS OF STRESS WAVE PROPAGATION IN SOIL, E. T. Selig - IIT Research Institute 27
DYNAMIC BEHAVIOR OF GRANULAR MEDIA, James V. Zaccor - URS Corporation 62
STATIC AND DYNAMIC CONSTRAINED MODULI OF FRENCHMAN FLAT SOILS, A. J. Hendron and M. T. Davisson - University of Illinois 73
PROPAGATION OF DYNAMIC STRESSES IN SOIL, Lynn Seaman - Stanford Research Institute 98

SESSION THREE-TUESDAY AM

GROUND MOTION AND INSTRUMENTATION

FREE FIELD GROUND MOTION PRODUCED BY EXPLOSIONS, William R. Perret - Sandia Corporation 107
INERTIAL EFFECTS AND SOIL STRENGTH CRITERIA, B. B. Schimming and H. C. Saxe - University of Notre Dame 118
A NEW DEVICE FOR SOIL STRAIN MEASUREMENT, W. B. Truesdale and M. E. Anderson - IIT Research Institute 129
SHOCK-ISOLATING BACKPACKING MATERIALS, A REVIEW OF THE STATE OF THE ART, George C. Hoff - U. S. Army Engineer Waterways Experiment Station 138
EFFECTS OF GAUGE DENSITY AND PLACEMENT ON MEASUREMENT OF ACCELERATION IN SOIL, E. T. Selig and R. W. Rusin - IIT Research Institute 155
A REVIEW OF STRESS AND STRAIN MEASUREMENT IN SOIL, E. T. Selig - IIT Research Institute 172

SESSION FOUR-TUESDAY PM

STATE OF THE ART

THE BEHAVIOR OF SHALLOW-BURIED CYLINDERS, Jay R. Allgood - U. S. Naval Civil Engineering Research Laboratory 189
BURIED TUBES UNDER SURFACE PRESSURE, P. S. Bulson - Military Experimental Establishment, Hampshire, England 211
REVIEW OF SOIL-STRUCTURE INTERACTION, Carl K. Wiehle - URS Corporation 239
STRUCTURAL DESIGN TRENDS IN BURIED FLEXIBLE CONDUITS, Reynold K. Watkins - Utah State University 246
A STUDY OF LOADS ON UNDERGROUND STRUCTURES, D. A. Van Horn - Lehigh University 256

SESSION FIVE–WEDNESDAY AM

SIMILITUDE AND MODEL STUDIES

page

SIMILARITY REQUIREMENTS FOR UNDERGROUND STRUCTURES, Donald F. Young and Glenn Murphy – Iowa State University 285

THE APPLICATION OF SIMILITUDE TO PROTECTIVE CONSTRUCTION RESEARCH, Robert K. Tener – U. S. Army Engineer Waterways Experiment Station 296

A SIMPLIFIED SOIL STRUCTURE INTERACTION MODEL TO INVESTIGATE THE RESPONSE OF BURIED SILOS AND CYLINDERS, C. J. Costantino, P. P. Robinson and M. A. Salmon – IIT Research Institute 305

THE EFFECT OF PORE AIR PRESSURE ON SOIL-STRUCTURE INTERACTION, Delon Hampton – University of New Mexico 315

PHOTOELASTIC STUDY OF WAVE PROPAGATION AROUND EMBEDDED STRUCTURAL ELEMENTS, W. F. Riley – IIT Research Institute 332

SESSION SIX–WEDNESDAY PM

ANALYTICAL AND EXPERIMENTAL STUDIES, PART I

AN INVESTIGATION OF PANEL-ARCHING EFFECTS IN NONCOHESIVE SOIL, W. B. Truesdale and E. Zey – IIT Research Institute 349

ARCHING IN SOIL DUE TO THE DEFLECTION OF A RIGID HORIZONTAL STRIP, Chunduri V. Chelapati – California State College at Los Angeles 356

ATTENUATION OF STRESSES FOR BURIED CYLINDERS, Jerome Q. Burns and Ralph M. Richard – University of Arizona 378

THE BENEFICIAL ACTION OF THE SURROUNDING SOIL ON THE LOAD-CARRYING CAPACITY OF BURIED TUBES, U. Luscher and K. Höeg – Massachusetts Institute of Technology 393

AN EXPERIMENTAL EVALUATION OF SOIL ARCHING, George E. Triandafilidis – Rice University, Delon Hampton – University of New Mexico, and Milan Spanovich – Pittsburgh, Pennsylvania 403

SESSION SEVEN–THURSDAY AM

ANALYTICAL AND EXPERIMENTAL STUDIES, PART II

EXPERIMENTS ON CIRCULAR CYLINDERS WITH FLEXIBLE ROOF PLATES BURIED IN SAND, C. J. Costantino and A. Longinow – IIT Research Institute 423

YIELDING MEMBRANE CONCEPTS, H. P. Harrenstien and R. H. Gunderson – University of Arizona 436

THE RESPONSE OF BURIED CYLINDERS TO QUASI-STATIC OVERPRESSURES, B. A. Donnellan – University of New Mexico 449

RESPONSE OF BURIED STRUCTURAL MODELS TO STATIC AND DYNAMIC OVERPRESSURES, R. L. Marino, Jr. and W. F. Riley – IIT Research Institute 464

INTERACTION BETWEEN A SAND AND CYLINDRICAL SHELLS UNDER STATIC AND DYNAMIC LOADING, John Thomas Hanley – University of Minnesota 487

SESSION EIGHT–THURSDAY PM

DESIGN AND PROTOTYPE STUDIES

PROTECTION OF UNDERGROUND STRUCTURES BY ARCH ACTION ASSOCIATED WITH THE IMPERFECT DITCH METHOD OF CONSTRUCTION, Merlin G. Spangler – Iowa State University 531

MEASUREMENTS OF SOIL-STRUCTURE INTERACTION ON PROTOTYPE PROTECTIVE STRUCTURES, Ralph H. Sievers, Jr. – U. S. Army, Office of Chief of Research and Development 547

THE DESIGN OF BURIED ARCHES TO RESIST BLAST LOADS, William J. Flathau and Richard A. Sager – U. S. Army Engineer Waterways Experiment Station 554

FORCE TRANSMISSION DUE TO COHESIVE SOIL-FOUNDATION INTERACTION UNDER VIBRATORY LOADING, Robert L. Kondner – Northwestern University 574

THE THEORY OF LIMITING EQUILIBRIUM FOR AXISYMMETRIC PROBLEMS: A COMPARISON WITH EXPERIMENT ON SILO SKIN FRICTION, C. J. Costantino and A. Longinow – IIT Research Institute 583

DISCUSSION 593

SESSION ONE—MONDAY AM

OPENING ADDRESS

THE BASIS OF CURRENT CRITERIA FOR THE DESIGN OF UNDERGROUND PROTECTIVE CONSTRUCTION

by
N. M. Newmark*

INTRODUCTION

I intend to talk about some of the aspects of underground protective construction. The title of the talk is given as "The Basis of Current Criteria for the Design of Underground Protective Construction." I am not sure that this talk will be entirely on the subject, but I shall discuss a number of the topics that are important and that have been taken into account in the design of underground protective structures, particularly military structures. It is necessary to discuss structural design criteria because as Mr. Tamanini pointed out, the Civil Defense program has thus far been related only to radiation and fallout shelter design (see Preface). There has been and will always be the possibility of designing fallout shelters to give blast protection as a sort of bonus since it is sometimes possible, without the expenditure of too much additional money, to build into fallout shelters blast protection as well. However, the general interest in the civilian defense program is for lower levels of overpressure than one usually considers important in the military program. I shall limit myself, when it is necessary to provide a limitation on the design criteria, to the region where the overpressure level is of the order of not more than 200 or 300 lb per sq inch. You've probably heard lately that we can consider much higher overpressures for military structures. But the types of behavior one must consider at higher levels are so different that it would confuse the picture to try to present these data.

DESIGN CRITERIA

Figure 1 is intended merely to give some sort of a scale to the discussion. It is apparent from this figure that an overpressure of 200 lb per sq inch will occur at about 2,700 feet from ground zero for a 1-MT weapon. Since this is the sort of upper limit of overpressure that we are interested in, it is interesting to note the rapid decay in peak overpressure occurring beyond this region, i.e., at about 7,000 feet from ground zero the pressure has decayed to 20 lbs per sq inch. These distances scale as the cube-root of the yield, in megatons. Now we are interested in evaluating the phenomena important in the design of protective construction within the region bounded by these ranges. For example, we are concerned with the question whether at this range the direct transmitted stresses through the soil and rock might be of comparable importance to the air-induced stresses. For example, if we take the best data that we have available for, say, a 1-MT surface burst at 2,700 ft distance in a soil or rock medium with excellent coupling, we find that we have a strain of the order of about 0.000083 inches per inch. If the modulus of elasticity of the soil is of the order of 10 million lbs per sq inch, which it is for a good sound rock with a seismic velocity of about 20,000 ft per second, we would get vertically under the source or in a 45 degree cone under the source, a stress of approximately 830 lbs per sq inch. This is more than comparable to the 200 lbs per sq inch air blast pressure. But near the surface at a range of 2,700 ft, we would have values considerably less; on the order of about 300 lbs per sq inch. If, however, the coupling is somewhat less, corresponding to a true-surface burst with no penetration, then, even at 200 lbs per sq inch overpressure, the stresses in the medium directly below at 2,700 feet and horizontally at a range of 2,700 feet would be comparable. And, if we deal with a softer material such as shale or limestone, with a seismic velocity of the order of 6,000 feet per second the stresses in the medium are between 75 and 35 lbs per sq inch, which is considerably less than the pressures transmitted to the ground by the air overpressure. Consequently, for most of the situations in which we are interested, for shallow buried structures subjected to overpressures up to 200 lbs per sq inch, the air blast pressures are predominant in producing the ground velocities, accelerations, and displacements; the direct coupled effects are not important. The air blast pressures vary with time as shown in Figure 2 for a particular overpressure. At lower overpressures, the curve decays slower, but

*Professor and Head, Department of Civil Engineering, University of Illinois, Urbana, Illinois.

even at 100 lbs per sq inch overpressure there is quite a peak to the curve. It has a long base, but most of the impulse is in the early portion. It is only when one drops down to less than about 25 or 30 lbs per sq inch that one gets the so-called "classic" exponential type of curve. This peak pressure has some influence because of the fact that the peak is very quickly washed out with passage through the soft surface materials, and this attenuation affects the response of structures in general. In rock, of course, the peak would be transmitted more effectively, but it is difficult to have a shallow buried structure in rock because to excavate it and then backfill it introduces a material that is different from the natural material.

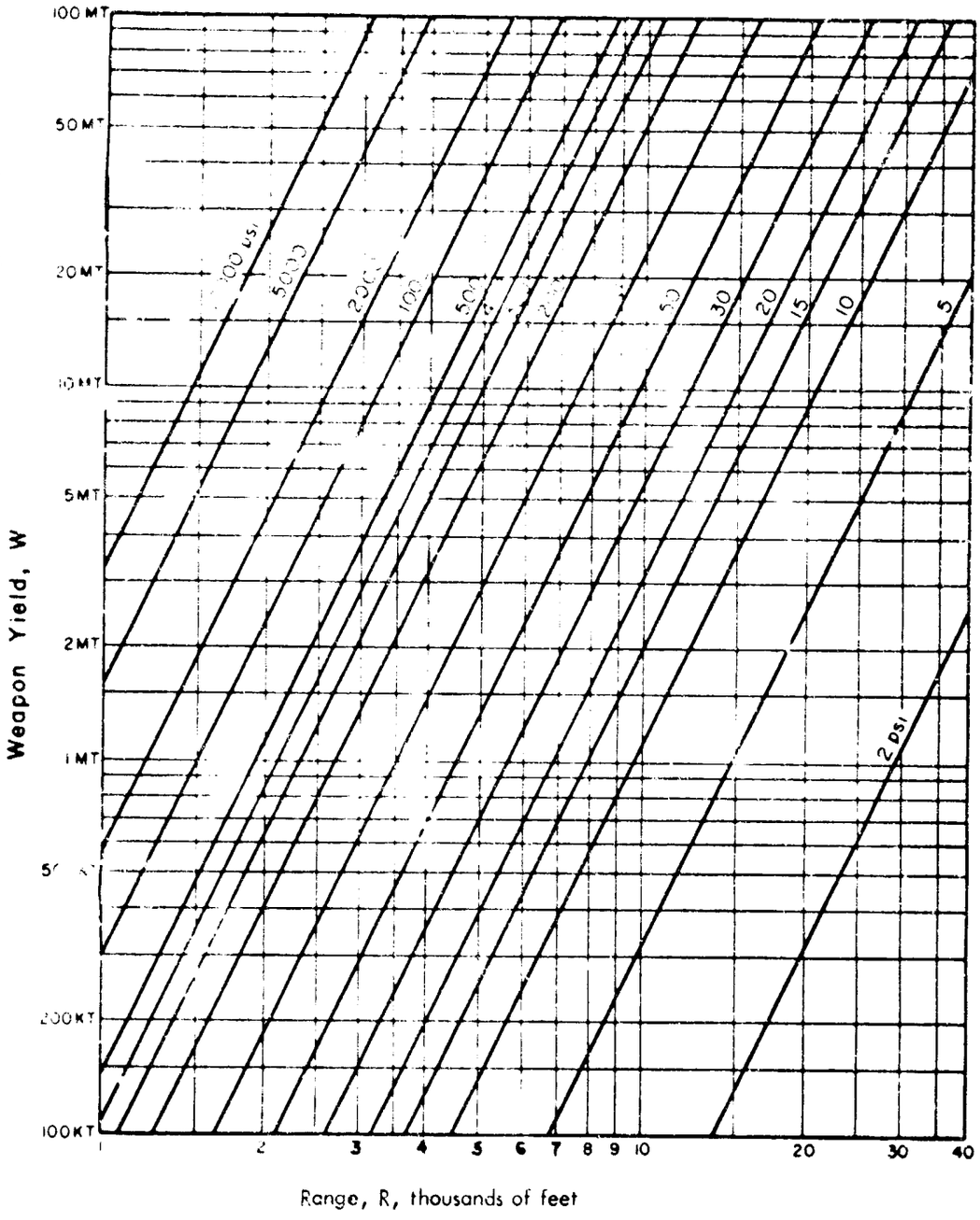


Fig. 1 Peak Overpressure at Ground Surface Versus Range for Various Yields, Surface Burst at Sea Level

Ground Motion

Let us look now at what happens when these air blast pressures are applied to the ground surface and propagate over the surface. Figure 3 shows a pressure wave traveling with a propagation or shock velocity of magnitude U. The velocity of propagation in the soil is C. When C is less than U, the air overpressure travels a distance proportional to U, and the ground shock wave travels a distance proportional to C. When all the positions that the leading edge of the shock can have are drawn, a series of lines are obtained that make an angle α with the horizontal where $\sin\alpha = C/U$. In other words, we get a sloping front of the shock along which vertical pressures occur. It must be emphasized that there are some horizontal pressures resulting from the vertical pressure. However, the pressure is not normal to that line. The sloping shock front is a front of essentially vertical pressures propagating through the ground as long as the air shock velocity (U) is greater than the ground motion velocity (C) or as long as we have superseismic conditions. When C = U, then these velocities are equal. The ground shock front becomes vertical or nearly so; it is vertical at the surface and departs from the vertical at a distance below the surface. Here we have an extreme condition. Moreover, as soon as the air velocity (U) becomes less than the ground shock velocity (C), then the shock in the ground outruns the shock in the air and we have a rather peculiar and unusual situation.

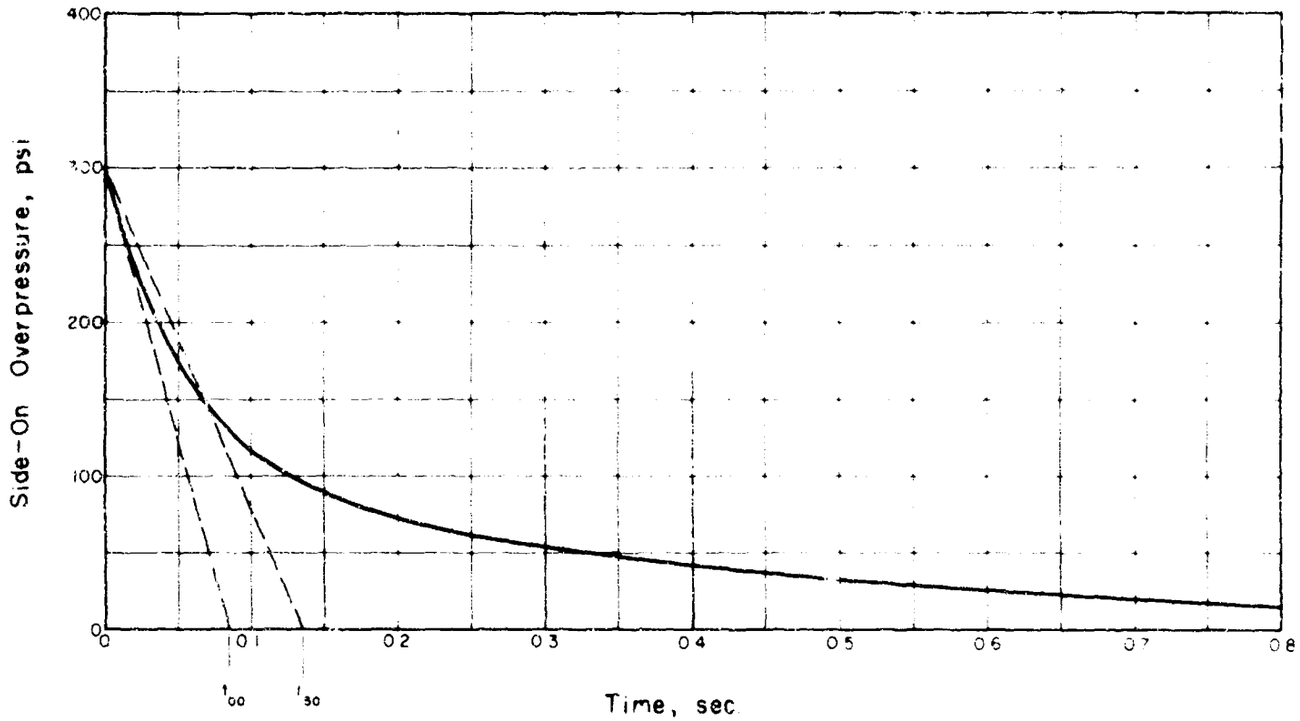


Fig. 2 Overpressure-Time Variation for Examples of Displacement Computation

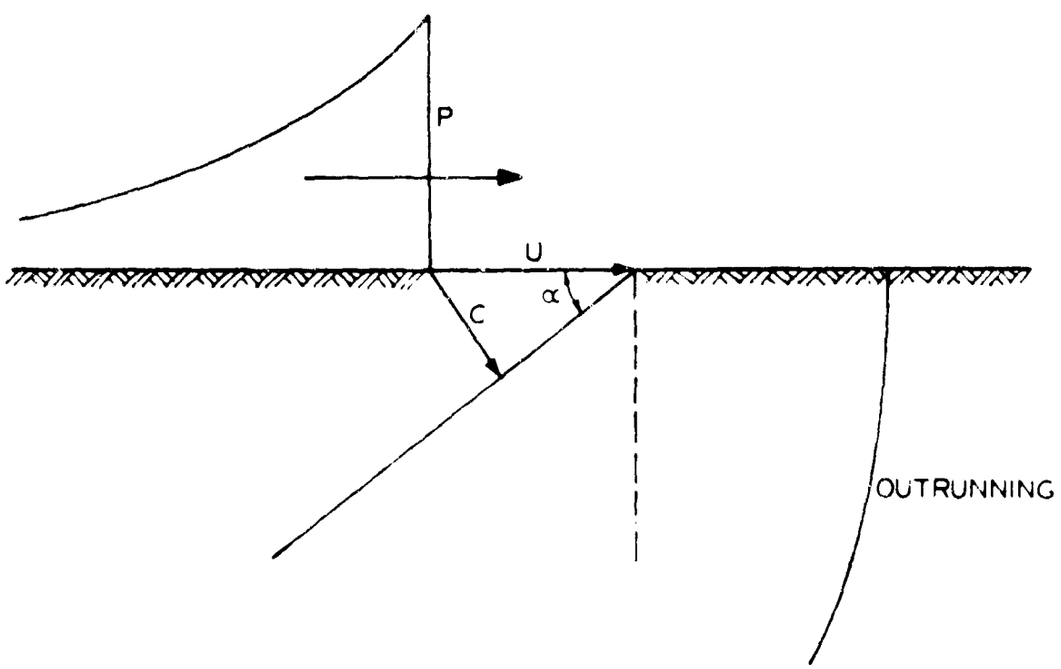


Fig. 3 Wave Propagation

Let us consider the conditions under which this situation will occur. The air shock velocity (U) varies with overpressure. For example, an air overpressure of 200 lbs per sq inch travels at about 4,000 feet per second, an air overpressure of 100 lbs per sq inch travels at a velocity of about 3,000 feet per second, and air overpressure of 50 lbs per sq inch travels at a velocity of about 2,200 feet per second. For a soil with a ground shock velocity (C) of 3,500 feet per second the material seismic velocity will exceed the air blast shock velocity at an overpressure between 100 and 200 lbs per sq inch. This will result in a subseismic or "outrunning" ground shock condition. When this occurs, the shock in the ground precedes the air blast shock wave and reaches the structure first. As a result, we get a wave that is detached in the ground from the pressure in the air. When that happens, a rather peculiar phenomenon of motions and stresses is produced which has been given a great deal of emphasis by investigators, possibly some of it over-emphasized. This can be said because most of the important phenomena involved in the design of structures are essentially the same, whether we have "outrunning" or superseismic conditions. There are some things, however, that must be taken into account especially in consideration of a shallow-buried surface structure. In the "outrunning" case the structure gets a bump from the ground before it gets a bump from the air, and so there is a difference in phasing and in the various effects on the structure which cause problems in connection with shock isolation. If we have layered soil media and if a sublayer of material has a higher seismic velocity, then the shock wave propagates down to this layer, along it, and then up. In this case, an upward motion may result which precedes the downward main motion from the air blast effects. These are things that are of importance in the practical details of design. They have to be considered particularly in shock isolation problems and they are of greater importance at low overpressures than at high overpressures because the lower the overpressures, the slower the shock velocity of the air and the more chance there is of the air velocity being outrun by the velocity in the medium. Typical seismic velocities for different materials are given in Table 1.

TABLE 1
TYPICAL SEISMIC VELOCITIES FOR SOILS AND ROCKS

Material	Seismic Velocity fps
Loose and Dry Soils	600 - 3,300
Clay and Wet Soils	2,500 - 6,300
Coarse and Compact Soils	3,000 - 8,500
Sandstone and Cemented Soils	3,000 - 14,000
Shale and Marl	6,000 - 17,500
Limestone - Chalk	7,000 - 21,000
Metamorphic Rocks	10,000 - 21,700
Volcanic Rocks	10,000 - 22,600
Sound Plutonic Rocks	13,000 - 25,000
Jointed Granite	8,000 - 15,000
Weathered Rocks	2,000 - 10,000

Based on information taken from: "Subsurface Exploration and Sampling of Soils for Civil Engineering Purposes", by Juul Hvorslev, ASCE Research Report, printed by Waterways Experiment Station, Vicksburg, Mississippi, 1948, p. 30, Fig. 4.

Since we're dealing with overpressures that have velocities of the order of 4,000 to 1,200 feet per second, "outrunning" will occur in many of these materials at overpressures which are summarized in Table 2. In alluvium, at pressures less than 40 lbs per sq inch, we get "outrunning"; at higher pressures, we do not. In dry gravel, outrunning possibly occurs somewhere in the same range. In wet gravel, it occurs at higher values. In sandy clay pressures below 100 will give outrunning, but pressures above probably will not. But as one gets into limestone and metamorphic rocks, one finds "outrunning" at overpressures less than 1,000 lbs per sq inch, so we may be in "outrunning" situations in many practical cases.

Figure 4 illustrates what happens when a time dependent pressure applied to the surface is propagated down through the medium. The pressure at the surface, as it varies with time, is shown at the top. There is a very fast rise to the peak, a decay, and a tapering off to zero in some duration. At some time later, after the wave front has reached some depth, the pressure time curve has a longer rise, a lower peak, and a longer decay. These are emphasized in Figure 4 in which the wave front is drawn with a slope so these pressure curves will not overlap, as they indicate a difference in time. As the wave progresses deeper it assumes a very long rise, a very much reduced peak, and a somewhat

lengthened duration. One important quantity that we look at is the total area under these curves--the impulse. In general, at the overpressures we are considering here, for all except very small weapons, this impulse is a constant. Essentially the condition that the total vertical impulse over any horizontal plane is preserved, occurs in any region where the overpressures do not vary greatly over a distance about equal to the depth that we are considering. Therefore, we are talking here of depths that are comparable to the distance over which the overpressure varies a relatively small amount. Moreover, since the area under the curve must be the same and since there is a decay in the peak, there must be a lengthening of a base to keep the impulse constant. It is this change in character or shape of the pressure time curve that is of great importance in design for underground structures. Essentially this phenomenon implies that the deeper you go, the less is the peak pressure that you must resist; the deeper you go, the less is the particle velocity you have; and the deeper you go, the lower is the particle acceleration that is involved in producing effects on equipment in the structure. This rise time to the peak varies, of course, with the type of material. Empirically, it has been more or less established that this rise time is of the order of magnitude of about half the transit time of the shock front to reach the point considered. It can be more or less than this, but this is a good basic value to use in trying to estimate the effects of depth of cover when you have no other information available.

Most of the information we have about the attenuation with depth is empirical in nature. There are some rather crude theoretical studies; the crudest is one for which I am responsible, which I make no apologies for since it gives answers which seem to agree with the experimental data, but I don't think it is of sound enough basis to warrant a good deal of further effort on this same approach. The difficulty, of course, is, when you start making calculations, which we can now do with a computer, the results you get are conditioned upon the assumptions you make in your calculations. The results are critically sensitive to the damping, the viscosity, and so forth, the values of which we can assume, but have great difficulty in measuring. We can assume all kinds of conditions that give about the same general type of attenuation. But the mere fact that any set of assumptions gives agreement with experimental data does not mean that the assumptions are correct. This is one of the things that one learns the hard way in experiment. You can't verify the accuracy of assumptions merely by looking at the results you get when you use these assumptions in calculations. Computers are very useful tools in all of these studies.

TABLE 2
APPROXIMATE OVERPRESSURES AT WHICH OUTRUNNING OF GROUND WAVE OCCURS FOR LARGE YIELD SURFACE BURSTS

Formation	Overpressure* (psi)
Alluvium	less than 40
Gravel (dry)	10 - 100
Gravel (wet)	40 - 500
Sandy Clay	100 - 500
Sandstone	500 - 2000
Shale	650 - 2500
Limestone	1500 up
Metamorphic	1000 up
Granite	3000 up

*Outrunning conditions may be anticipated at overpressures less than those tabulated.

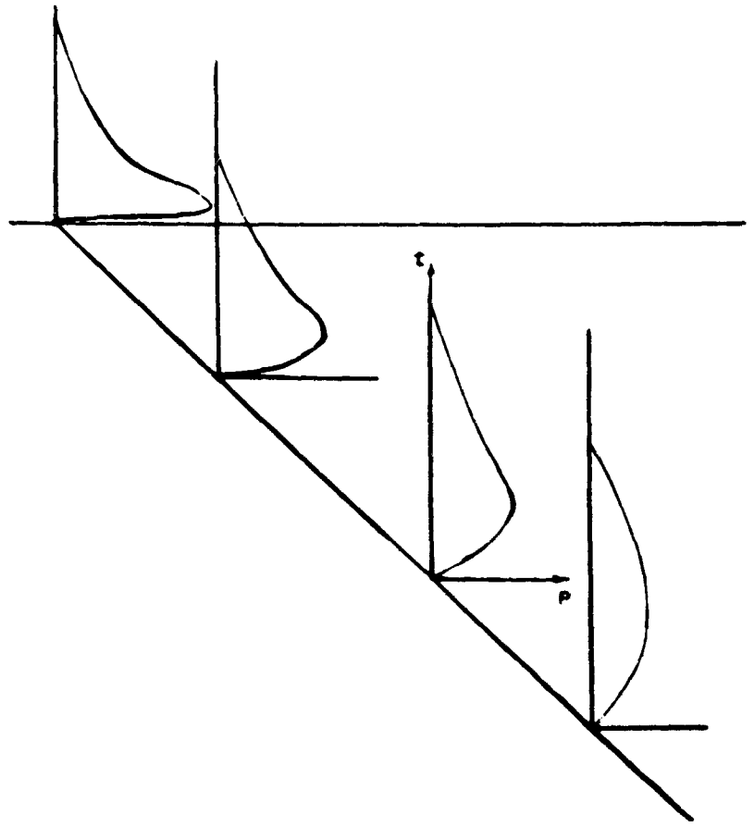


Fig. 4 Attenuation of Soil Pressure Wave with Depth

Some of the data that are available on attenuation with depth presented in a slightly different form are shown in Figure 5. This figure is a summary of the experimental results plotted in a form that was conditioned upon certain assumptions I made several years ago. These were that we had an almost instantaneous or static situation in which we could consider the instantaneous air pressure distributions and could then compute the static soil pressures at various steps by letting the pressure move across the surface and evaluating how the pressure changed with depth. This, of course, is not entirely appropriate because of the fact that shock waves propagate in a somewhat different fashion, and theoretically, for a perfectly elastic material, even if one loads only a small segment of the surface, the pressures would be transmitted through the material without attenuation of the front, even though there was attenuation behind the front. Fortunately, we don't have perfectly elastic materials. In general, the smaller the yield, the faster is the attenuation. For a 40-KT weapon the attenuation at a 40 foot depth is 50% for 200 psi overpressure. For 100 psi overpressure, the attenuated pressure is about 70% of the surface value. Therefore, the higher the overpressure the faster the attenuation, the smaller the yield the faster the attenuation, and so forth.

These various relations are summarized in the following highly empirical equations which are used quite often for design purposes. They have the virtue only that they give consistent results that may be completely wrong, but, if so, they are wrong in a consistent manner.

$$P_z = \alpha P_{so} \tag{1}$$

$$\alpha = \frac{1}{1 + \frac{z}{L_w}} \tag{2}$$

$$L_w = 230 \text{ ft.} \left[\frac{100 \text{ psi}}{P_{so}}\right]^{1/2} \left[\frac{W}{1\text{MT}}\right]^{1/3} \tag{3}$$

Figure 6 is a chart that has been developed to compute the effects of these equations, and gives results that are consistent with the values in Figure 5. For example, for 1-MT and 100 lbs per sq inch and 100 feet we have 70% of the surface pressure, at 25 feet we have 90% and so on. It should be obvious that for shallow-buried structures, buried less than 25-50 feet, and for low overpressures and large yields, we have very little if any attenuation.

Figure 7 shows a more rational presentation of the change of wave form with depth. This is plotted in such a way that we have time plotted always horizontally, pressure always vertically. Figure 7(a) shows the pressure-time curve at the surface. The pressure-time curve at some depth is indicated by Figure 7(b). The rise time at the surface is indicated by the time intercept of the wave peak line and the time to a peak is shown by the abscissa of this line at any depth. Figure 7(c) shows a pressure-depth curve, and this is quite important to look at. It shows instantaneous values of pressure at different depths. We can obtain the pressure-depth curves for various times, and by using the modulus of deformation (the constrained modulus) at a particular depth, we can compute the strain by dividing the constrained modulus into

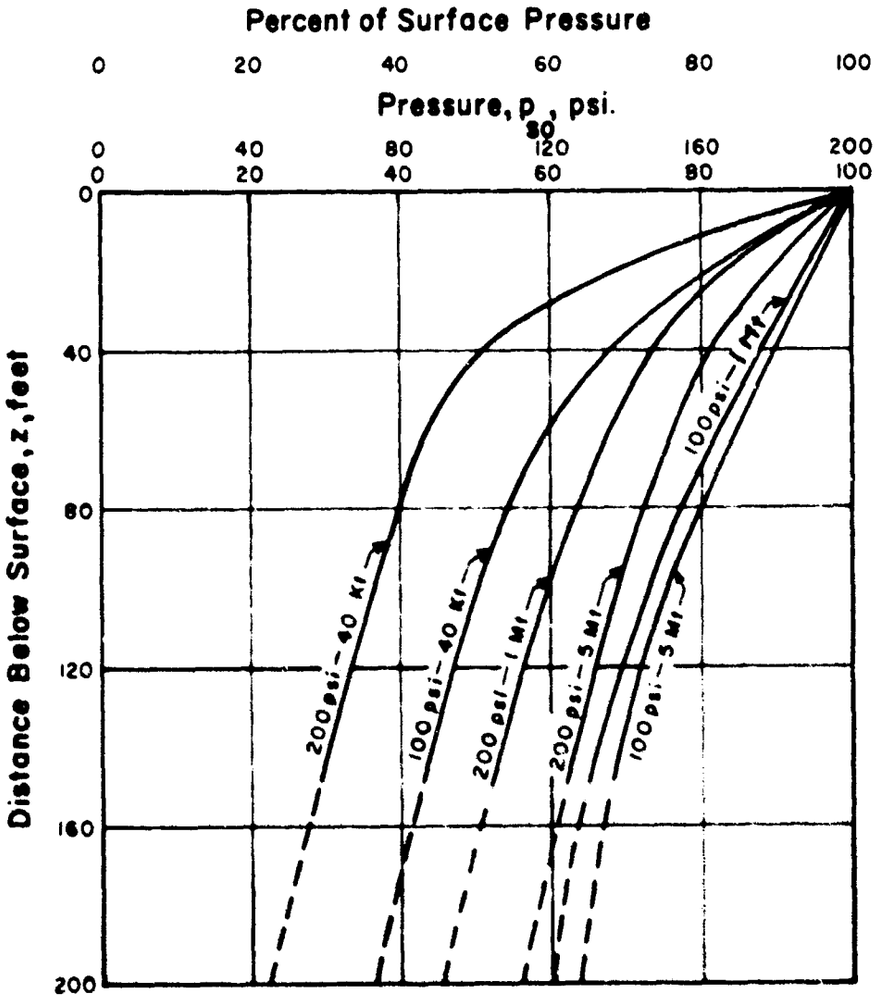


Fig. 5 Change in Maximum Vertical Stress with Depth Due to Spatial Attenuation

the pressure level at that depth. Then we can compute the downward displacement at the surface or at any point below the surface, by integrating the total strain from the wave front up to the point in question. These calculations give instantaneous values of displacement, and if we do the computation for various time intervals we can compute the maximum displacement by looking for the maximum values.

If we have layers we have to take into account reflections and so forth, which we can do, or we can perhaps more crudely approximate this by forgetting about the reflections and assume on the average that they are compensated for; this isn't too bad an assumption if one looks at displacements. It's very bad if one looks at other parameters.

It is possible, therefore, to compute not only the maximum displacement but the displacement time curves at various points, and the differential displacement between two points, and so forth. I would like to call your attention to the fact that the differential displacement between any two points at different depths is always greater than the difference in maximum displacements at those two depths. It has to be greater than that, because the maximum displacements do not occur simultaneously. Therefore, when one is a maximum, the other is at somewhat less than a maximum value. Furthermore, the difference must be less than the maximum strain between those two points integrated over the length since the maximum strain exists only at the one point, not over the entire depth. Therefore, we have some limitations on differential displacement which gives us a clue as to how much, for example, the displacement between top and bottom of the soil around the structure might be. This in turn gives us some measure of the shear that might be transmitted to the structure by the soil and also some measure of the displacement at points where two structures are connected together, or the displacement that must be absorbed by any connection between them.

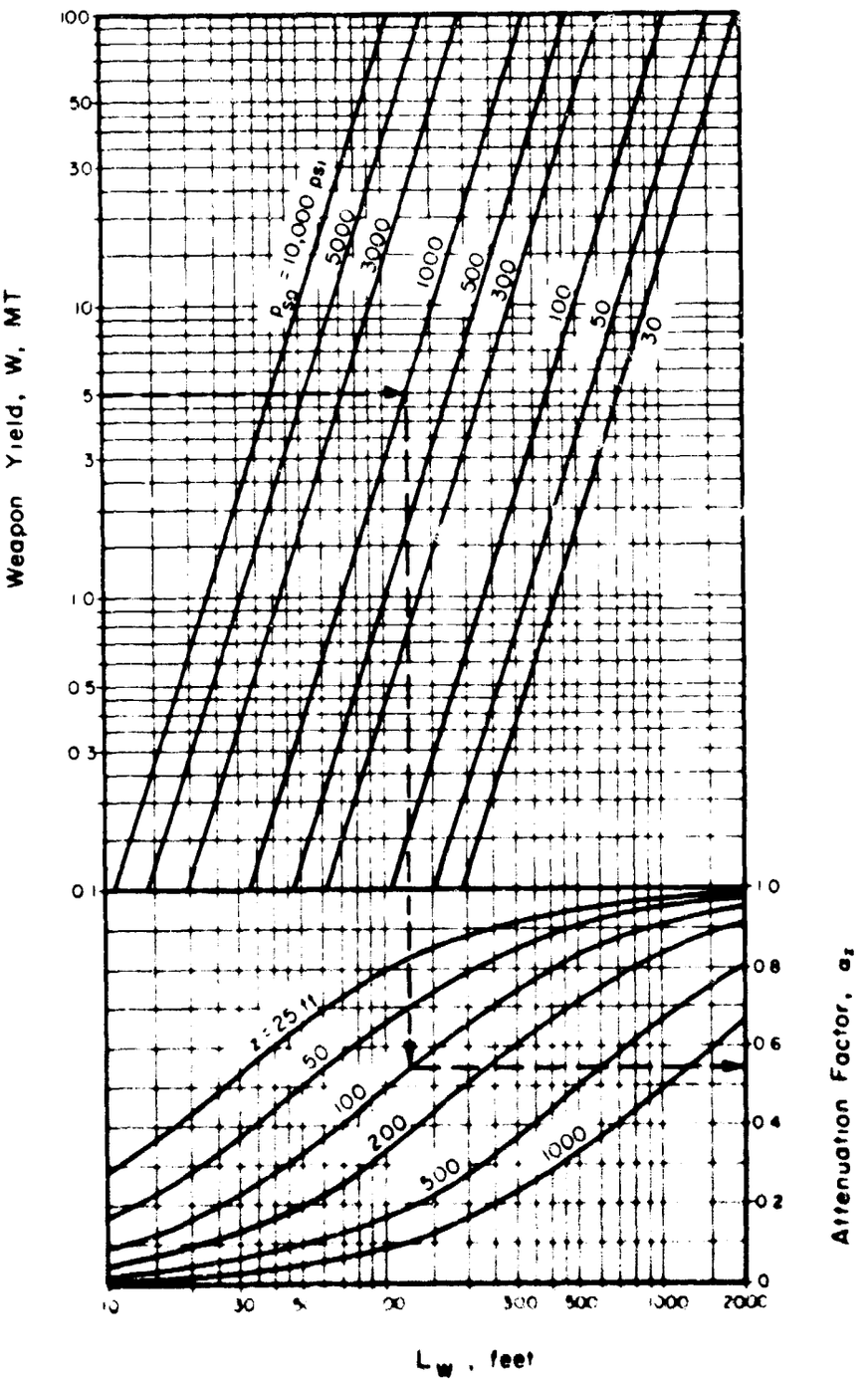


Fig. 6 Depth Attenuation Factor

Figure 8 illustrates the stress-strain curve for soil. The dotted curve is an idealized curve for the purpose of presentation here. For increasing stress we obtain first a softening and then for higher stresses a hardening or locking. As we reduce the load we get a recovery with some permanent set, and the loading and unloading do not follow the same path. It is necessary to define several moduli, initial tangent modulus, m_i, secant modulus, m_p (from which given a stress we can compute the strain), and a recovery modulus (from which we can compute the total elastic recovery, or total recovery, and the permanent set). If we were interested in obtaining displacements we would have to use this form

of stress-strain curve because, after a stratum has been stressed to some point and the stress is released, there is some permanent set in the stressed stratum and some elastic recovery. For purposes of very quick estimates of displacement, it is possible by means of rather crude relationships applicable to one-dimensional wave propagation theory, and by making some necessary assumptions and a few unnecessary ones, to come up with equations of the following sort. The elastic component of displacement in a homogeneous medium can be obtained by the following formula:

$$d_e = 9 \text{ in.} \left[\frac{P_{so}}{100 \text{ psi}} \right]^{1/2} \left[\frac{1000 \text{ fps}}{c} \right] \left[\frac{W}{1MT} \right]^{1/3} \quad (4)$$

For example, in a material having a seismic velocity of 2,000 feet per second, and subjected to an overpressure of 100 psi from a 1-MT weapon, one could expect 4-1/2 inches of elastic displacement at the surface.

The permanent displacement is very difficult to determine unless we have complete stress-strain data for the material. In general where we don't have such information the following entirely empirical equation can be useful:

$$d_r = \frac{P_{so} - 40}{30} \text{ in.} \left[\frac{1000 \text{ fps}}{c} \right]^2 \quad (5)$$

It doesn't differ by more than a factor of 3 or 4 from the correct values in most cases. This gives us a value for which there is no permanent deformation for overpressures less than 40 lbs per sq inch. It is apparent from this relationship that the softer materials have a relatively larger amount of permanent deformation (for overpressures higher than 40 lbs per sq inch).

The relative displacement between any two depths is the summation of the relative strains between those two points. For the first 100 feet, a relationship can be used that depends on the square of the seismic velocity and on the magnitude of the overpressure as shown in the next equation. For example,

$$d_e - d_{ez} < 4.8 \text{ in.} \left[\frac{P_{so}}{100 \text{ psi}} \right] \left[\frac{1000 \text{ fps}}{c} \right]^2 \frac{z}{100 \text{ ft}} \quad (6)$$

For a 100 lbs per sq inch overpressure applied to a soil with a 1000 foot per second seismic velocity, at the 100 foot level the relative displacement compared with the surface value would be less than 4.8 inches.

The one-dimensional wave theory gives us a means of getting the other parameters, velocity and acceleration. The velocity is related to the strain and is equal to the seismic velocity times the strain. This leads to the relation:

$$v_z = 50 \frac{\text{in.}}{\text{sec.}} \left[\frac{P_{so}}{100 \text{ psi}} \right] \left[\frac{1000 \text{ fps}}{c_p} \right] \alpha \quad (7)$$

From this equation, it is apparent that as the pressure decreases or attenuates, the velocity attenuates in the same way.

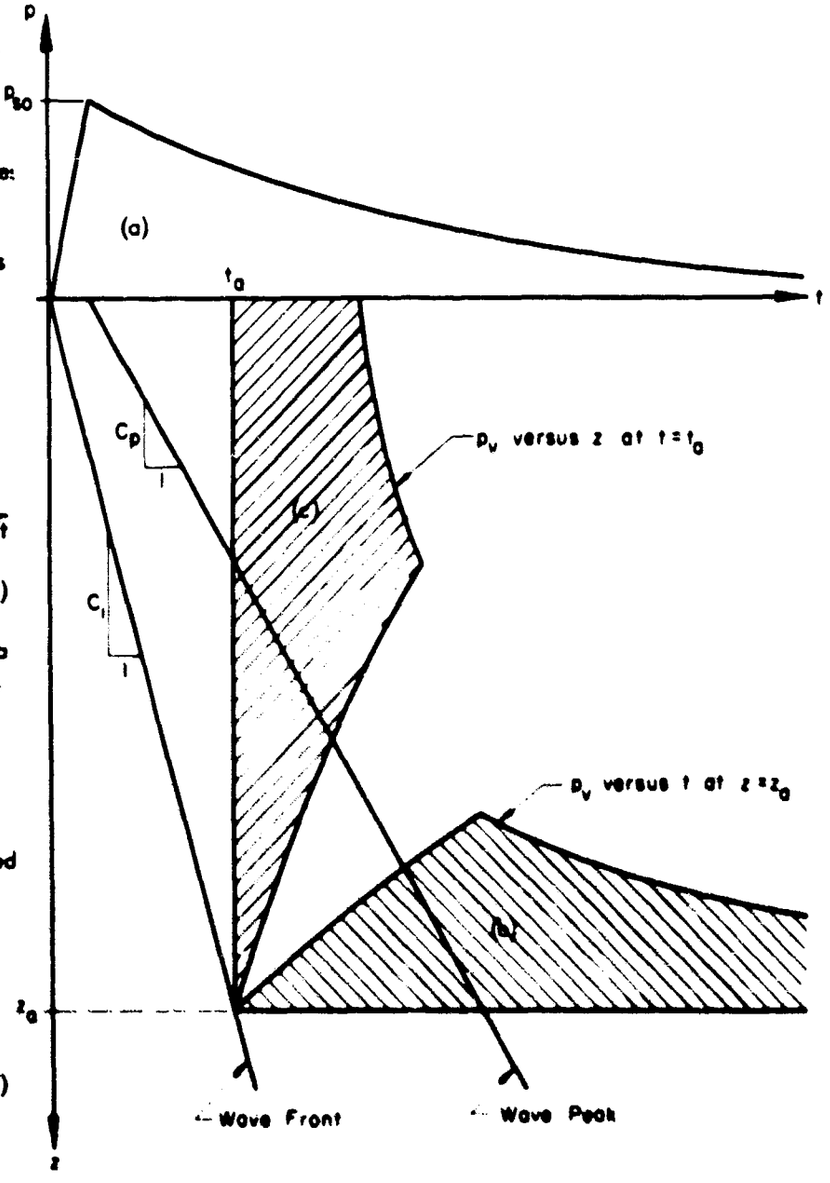


Fig. 7 Change of Wave Form with Depth

The acceleration is a much more difficult quantity to estimate. We can compute it by assuming that the velocity is proportional to the pressure curve, and that the acceleration is the derivative of the pressure curve. The maximum acceleration is, therefore, the maximum velocity divided by some sort of equivalent time that corresponds to the maximum slope of the overpressure time curve. If we assume that the rise time is parabolic, the effective rise time in computing the acceleration would then be one half the true rise time. This can be written as $a_o = 2v_o/t_r$ where t_r is the true rise time to peak velocity. If it is assumed that the rist time is of the order of 0.001 to 0.002 seconds for the points very near the surface, then the equation for peak surface acceleration becomes

$$a_o = 150g \left[\frac{P_{so}}{100 \text{ psi}}\right] \left[\frac{1000 \text{ fps}}{c}\right] \qquad (8)$$

Theoretically, of course, the acceleration can be infinite; it is infinite for a shock. However, it is only infinite for an infinitesimal time. The relationship between overpressure, seismic velocity, and resulting surface velocity is shown in Figure 9.

The computation of acceleration at various depths beneath the surface is made in a manner similar to the surface acceleration as discussed. The only difference is that the rise time is assumed to be one half of the transit time or time necessary for the wave peak to reach that depth. The resulting equation is:

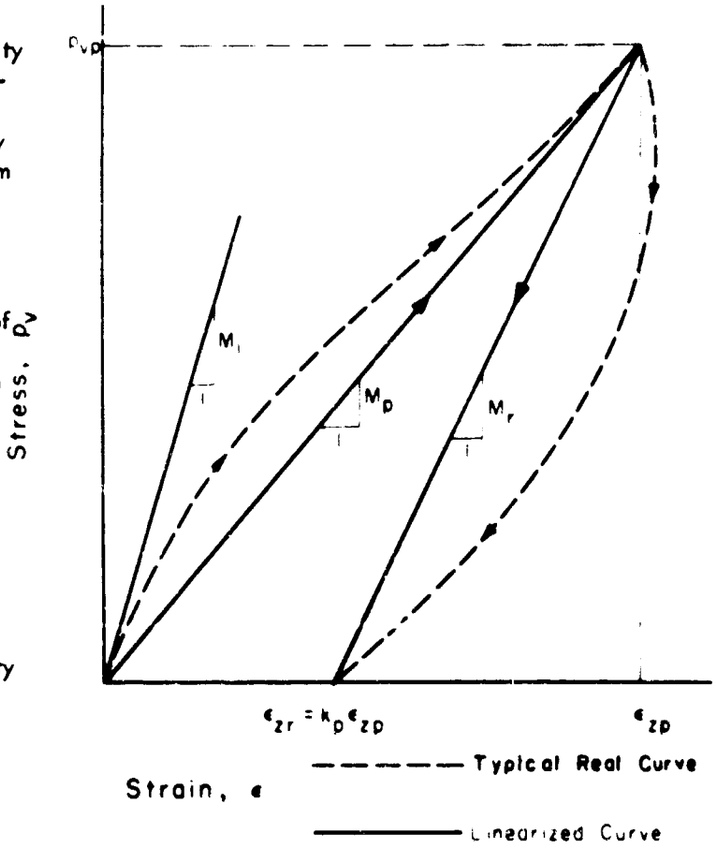


Fig. 8 Real and Linearized Stress-Strain Curves for Soil

$$a_z = 2\frac{v_z}{t_r} = 2g\frac{v_z}{t_r}\frac{1}{386 \text{ in./sec.}^2} \qquad (9)$$

or

$$a_z = 4g\frac{v_z c}{z}\frac{1}{386 \text{ in./sec.}^2} \qquad (10)$$

where $t_r = (1/2)(z/c_p)$. Substituting the equation for the velocity at depth z into this equation yields:

$$a_z = 5g \left[\frac{P_{so}}{100 \text{ psi}}\right] \left[\frac{100 \text{ ft.}}{z}\right] \alpha \qquad (11)$$

However, a_z should not be taken as greater than a_o.

The acceleration at various depths as computed by this equation is independent of the seismic velocity. There are two influences here: the rise time, which varies inversely with seismic velocity, is faster in harder materials; but the particle velocity varies inversely with the seismic velocity. Since accleration is the quotient of these two quantities, the acceleration is nearly independent of seismic velocity. Figure 10 shows the particle acceleration as a function of depth. The curve rounds off near the surface due to its dependence on the surface seismic velocity, which I suggest should never be taken as greater than 2000 feet per second because of the surface effects that are involved.

So much for the vertical pressures which act on the structures that we design, or essentially act on the free-field where we might put the structures. What we want to know are the other forces that act at the same time. These are summarized very briefly and quite empirically in Table 3 which shows the ratio of horizontal to vertical soil pressures, K_o. For dynamic conditions the soil must always be assumed to be undrained. For static, both undrained and drained conditions are permissible. For cohesionless soils the dynamic ratios are of the order of about 1/4; the static ratio is definitely larger. It ranges from about 1/3 for dense soils to 1/2 for loose soils. These K_o values go on up to 1 for saturated soils having a consistency range from very soft to hard. For rock, we can compute K_o from Poisson's ratio μ by use of the expression $K_o = \mu/(1-\mu)$. With this background, we can begin our discussion of soil-structure interaction.

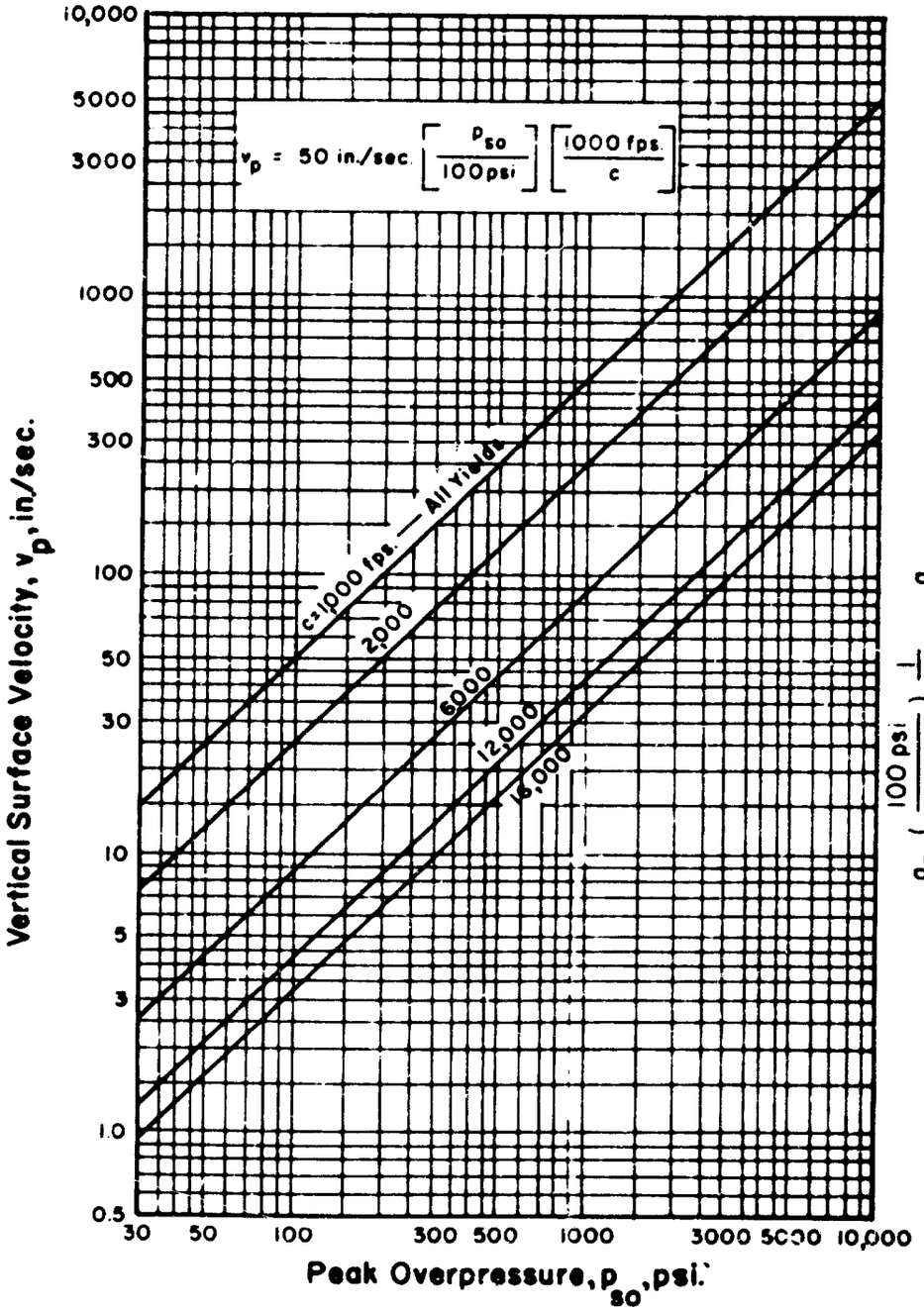


Fig. 9 Air-Induced Surface Vertical Velocity

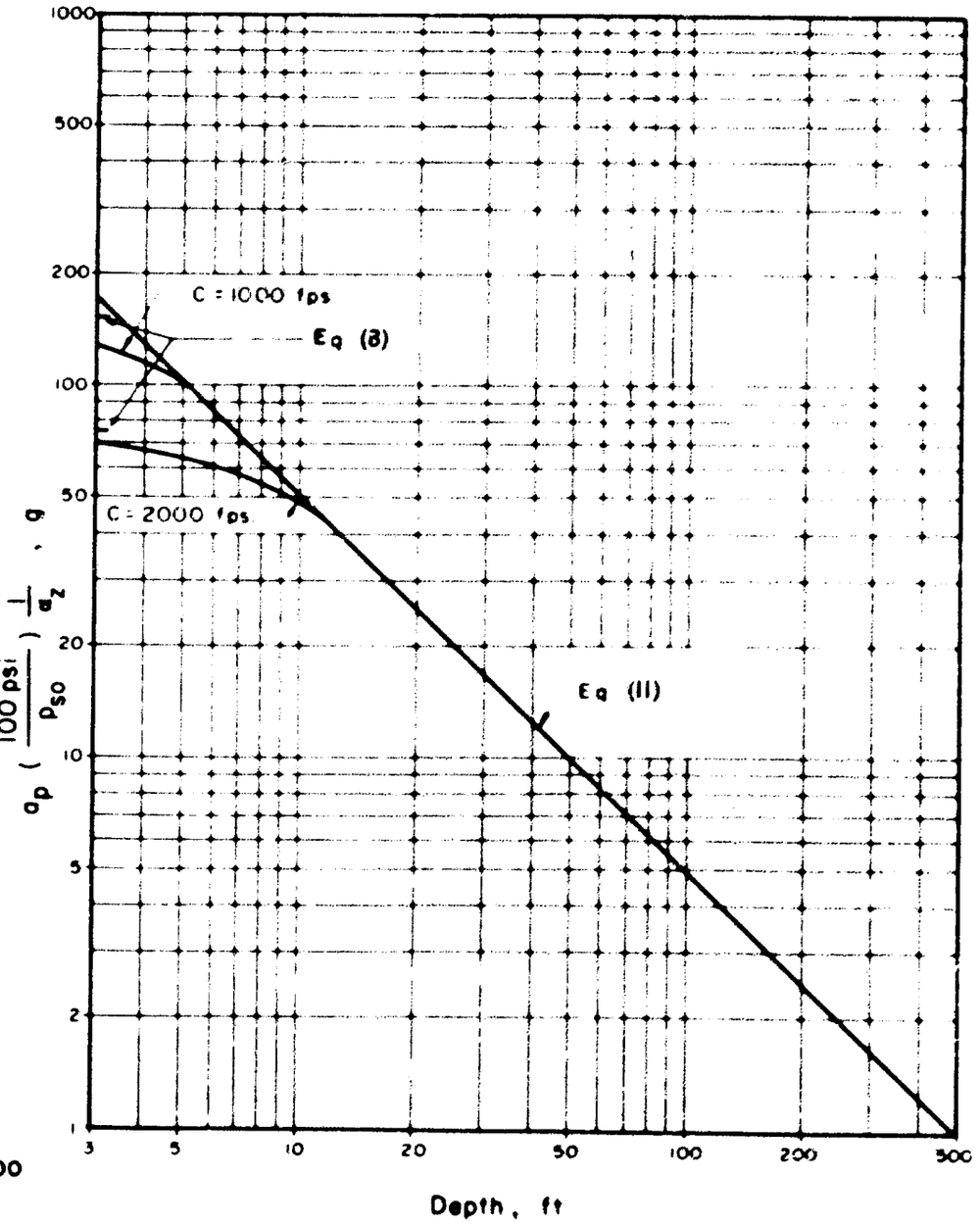


Fig. 10 Variation of Peak Pseudo Acceleration with Depth

TABLE 3
RATIO OF HORIZONTAL TO VERTICAL SOIL PRESSURES

Soil Description	K_o, For Stresses Up to 1,000 psi		
	Dynamic	Static	
	Undrained	Undrained	Drained
Cohesionless Soils, Damp or Dry	1/4	1/3-dense 1/2-loose	1/3-dense 1/2-loose
Unsaturated Cohesive Soils of Very Stiff to Hard Consistency	1/3	1/2	1/2
Unsaturated Cohesive Soils of Medium to Stiff Consistency	1/2	1/2	1/2
Unsaturated Cohesive Soils of Soft Consistency	3/4	1/2 to 3/4	1/2 to 3/4
Saturated Soils of Very Soft to Hard Consistency and Cohesionless Soils	1	1	1/2-stiff 3/4-soft
Saturated Soils of Hard Consistency. q_u = 4 tsf to 20 tsf.	3/4 to 1	1	1/2
Saturated Soils of Very Hard Consistency. q_u 20 tsf.	3/4	1	1/2
Rock	Obtain from tests on rock cores and correlate with seismic data.		

SOIL-STRUCTURE INTERACTION

Figure 11 shows a sketch of an arch near the surface of the ground subjected to a laterally moving surface air overpressure. If the cover is very small or if there is no restraint offered by the embedment in the soil, then the arch will tend to deflect to one side. Because of the fact that it cannot be so pushed without displacing the soil, which has mass and a high inertia, and because of the fact that before it can start to move very fast, the pressure has gone over the top, the arch tends to be pushed back. In other words, this unsymmetrical displacement is almost completely prevented as soon as the cover becomes even moderate. So far as we know, if there is a good sound backfill, even though it is just barely tangent to the surface covered, this kind of motion would be prevented. Another type of deformation, not necessarily associated with the greater depth, is a symmetrical deformation in which the crown goes down and the haunches go out. This results even when the pressure wave travels longitudinally, and even when the depth of cover is enough to prevent the unsymmetrical deformation from taking place. This is true because the cover over the crown, when it is very shallow, cannot prevent the crown from buckling in, except for the fact that, for the crown to buckle elastically, the haunches must buckle out. If, however, the compression in the arch reaches the plastic limit, then we can get deformation of the crown without the haunches moving out, and the arch would have a tendency to collapse. As a result, in general, we would have a collapse condition if the vertical pressure on the crown reaches the value that would correspond to a ring compression equal to the yield point. To reiterate, the restraint offered by the soil tends to keep the arch fixed in position to resist unsymmetrical deflections but yielding and symmetrical deflection are still possible. These conditions are shown respectively in Figure 11, (a) and (b).

Now we get to the very important and critical practical problems. The structures under consideration here are generally constructed in an excavation which is then backfilled. If for any reason the backfill is poorly placed, porous, or bad on one side or the other, deformation can take place more readily and may be more harmful. The greater the depth of cover, the less the effect of backfill, of course, because we get some compaction due just to the weight of the material. Another effect that takes place in the structures is also shown in Figure 11. This effect is the footing motion which, for convenience, is shown only in Figure 11(b). The total load transmitted to the arched element acts on the footing which, having no overburden from the inside of the structure and, therefore, no confinement, may tend to push material up into the structure or may just bite down through the soil. Consequently, there is a possibility of motion here which tends to relieve the effects of the pressures on the structure. This may be bad for the footings; however, it probably is good for the structure. This motion can take place in both the symmetrical and unsymmetrical modes. Actually, it would start at one footing first and then the other but since the pressure travels across the structure so rapidly in comparison to the response time of the structure, the tendency is generally for these motions to take place almost symmetrically.

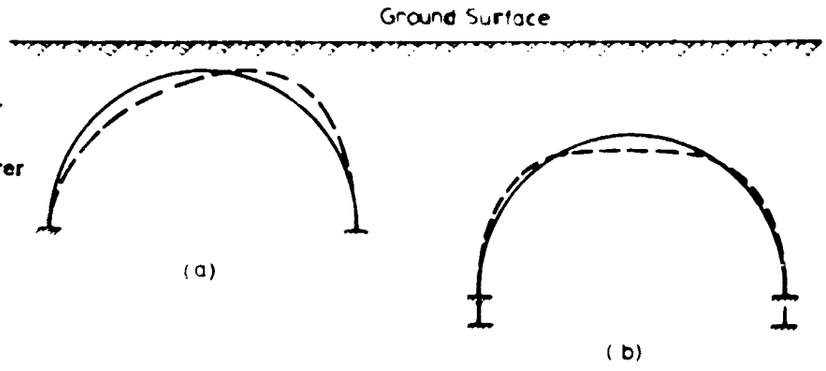


Fig. 11 Response of Buried Arches

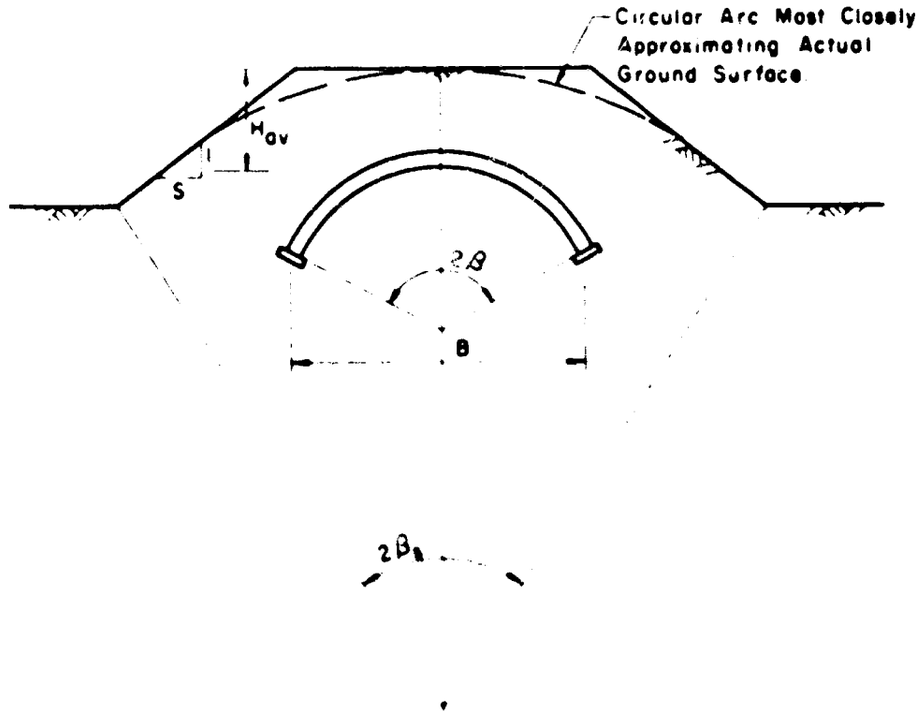


Fig. 12 Typical Partially Buried or Mounded Arch or Dome

In general, the so-called "arching" or relief of pressure due to deformation in a structure of this sort, an arched structure, is less than in a flat roofed structure because of the greater stiffness of an arch in compression as compared to a flat roofed structure in bending. Thus, arching may not take place in arches. There is, of course, an influence of the footing motion on relief of pressure that may be of great significance. Because of the effect of the soil relieving the structure from these unsymmetrical displacements and configuration, there is some necessity for setting requirements on height of cover over the structure and the type of backfill in order to enable the structure to behave properly. Figure 12 illustrates a sort of practical problem of an arch mounded over. Here we have somewhat different loading conditions on the arch because of the force acting on the mound. We actually have a soil arch acting with a structural arch, and this has to be taken into account in the design.

Figure 13 outlines, more or less, the standard criteria for full cover over an arch or dome. These criteria are presented only as points of departure for more rational specifications which may be developed later. In general, one can have steeper slopes, but they should be far enough away from the structure so that the higher intensity reflected pressures acting on the steeper slopes are not transmitted to the structure at some point which would give rise to a non-uniform stress.

For a buried arch, pressures which reach the structure can be divided into two components. Figure 14 shows the first component, a uniform compressive force which increases in intensity as the pressure wave travels across the arch. It reaches a value equal to the surface overpressure after a time of the order of one transit time across the structure. This time would be B divided by U where B is the span and U the air shock velocity. As the uniform component rises from zero to the full value of the side-on overpressure, general overall compression is produced and buckling may occur. Buckling would occur if the arch were not supported by soil, but this buckling is inhibited almost fully by the passive forces of the soil. Calculations have been made to investigate these phenomena assuming various types of spring supports which would simulate the soil pressures. But, in general, buckling does not occur in the usual way under these conditions and ordinarily can safely be neglected.

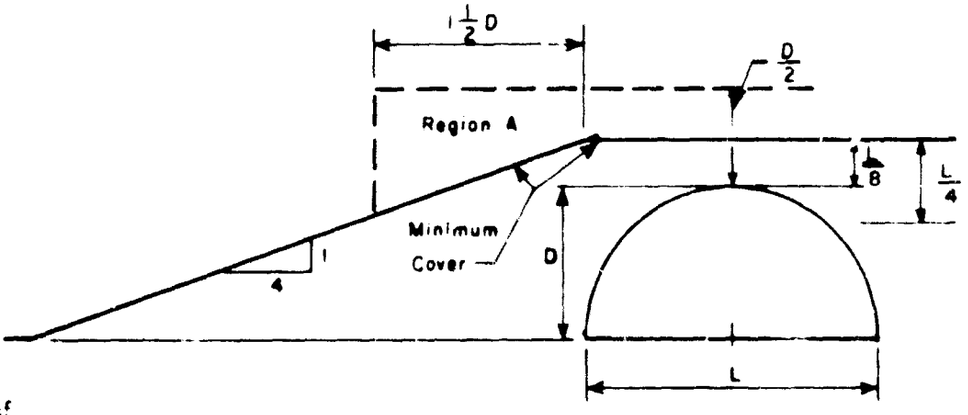


Fig. 13 Definition of Full Cover

The second component is a flexural component inward on one side and outward on the other. This is shown in Figure 15. This rises to a maximum in a time of one half the transit time. Obviously it reaches its maximum value when the pressure acts only over half the arch. It doesn't act at all after the pressures have passed over the arch completely or, in other words, when we have a uniform loading on the surface. Thus, it has a very short time base which, in effect, makes it a more or less impulsive loading. The maximum value for this loading is of the order of one half the surface overpressure. It is easily seen that when the pressures have passed over half the structure and reached the crown we have full pressure on one side and none on the other. We then divide this up into two components. The first component is $1/2\ p_{so}$ uniformly. The second component is $1/2\ p_{so}$ on the half of the structure over which the surface load is acting and $-1/2\ p_{so}$ on the other half. This gives a total of p_{so} on the one half and 0 on the other. We can handle these two components of loading nearly separately; however, we must consider their interaction since the axial ring compression magnifies the effect of the non-uniform component.

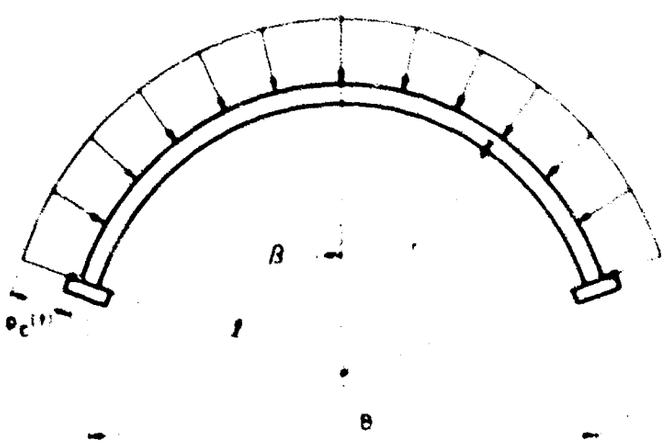


Fig. 14 Uniform Compression Loading

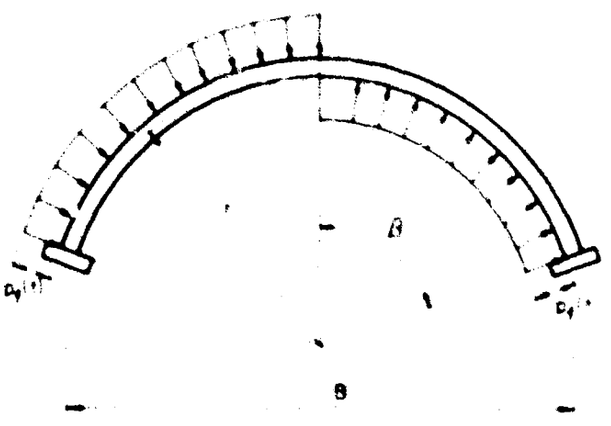


Fig. 15 Flexural Loading

Arching Concepts

Proceeding to the arching concept, we refer to Figure 16 which illustrates a situation in which we have a flat roofed structure acted on by a pressure. Looking at the pressure distribution on an element of the soil above, we notice that the pressure increases as we go toward the surface because of the attenuation of pressure with depth. If the roof deforms, we have lost additional pressure by shear to the surrounding material or to the sides of the structure. This problem has been studied in great detail by a number of people and most of you have papers on this topic. The papers are divided into two groups. One group treats the topic of buried cylinders. This is a nice, simple problem and may lead to results of great practical importance. The other group deals with problems that are related to arching over flat roofed structures and many experiments have been conducted along this line. Unfortunately, we had to arrive at design criteria several years ago, before all of your fine work was available. Thus, the results we arrived at are based on a moderate mixture of judgement and available information from static loading tests. The analysis presented here is the one given in the Air Force Design Manual.

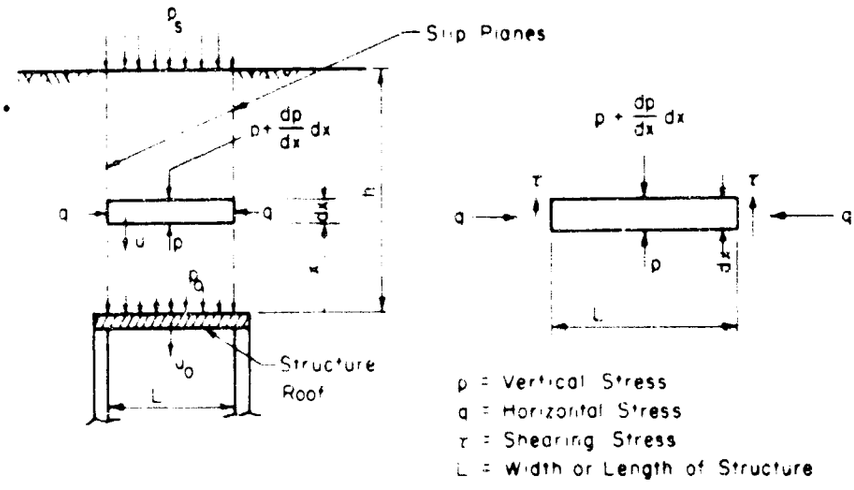


Fig. 16 Force Field Assumed for Underground Structure

What I tried to do in this analysis was to take into account the magnitude of the deformation of the roof because it seemed quite necessary to consider this as one of the parameters. Most of the treatments of arching that had been developed up to that time did not take into account this displacement, or at least assumed it in a range that seemed to be wholly unreasonable. Therefore, I essentially modified what Terzaghi had done (Terzaghi: Theoretical Soil Mechanics) to take account of the magnitude of the displacement. In order to simplify matters, I assumed vertical shear planes and uniform displacements. These assumptions can be corrected for I was not looking for precise expressions, but merely a means of relating the then available data to some set of criteria that could be used to furnish design standards.

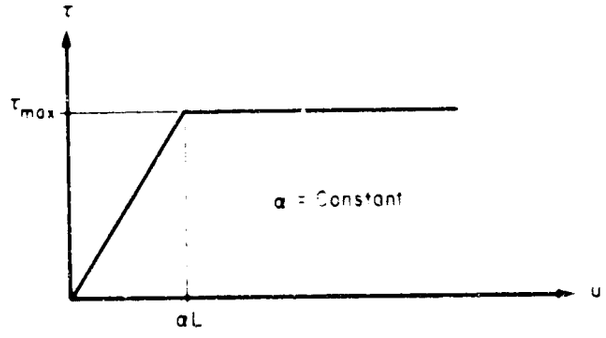


Fig. 17 Assumed Variation of Shearing Stress Versus Displacement

Figure 17 shows the relationship for shearing stress versus displacement on the slip surfaces. I assumed that the shearing stress increased linearly to some maximum at a certain value of displacement and then remained constant. This maximum is not necessarily a constant value, but is equal to the cohesion plus the value of the normal pressure times the tangent of the angle of internal friction.

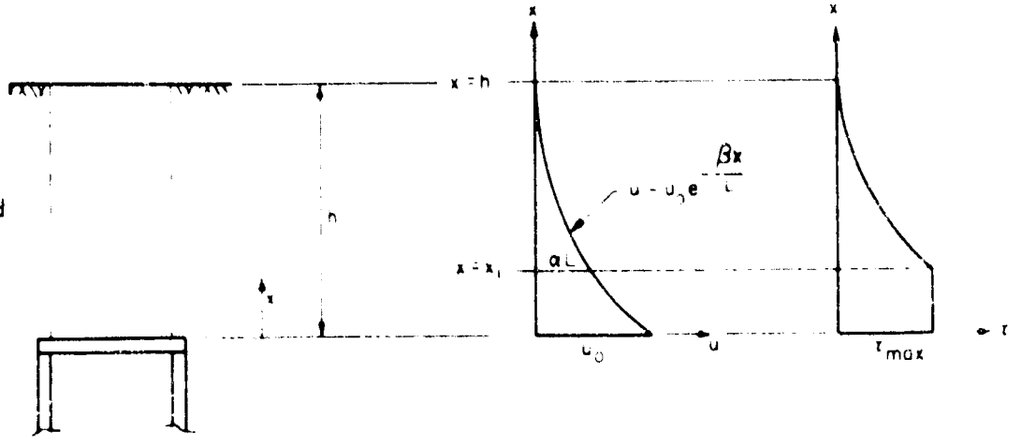


Fig. 18 Assumed Variation of Displacement and Shearing Stress with Depth

Figure 18 indicates some assumptions that were made in the course of the derivation. I assumed that the displacement decayed with distance from the movable surface as an exponential curve. I also assumed the shearing stress to be

proportional to the displacement above X_1 and constant below X_1.

Figure 19 shows schematically a box with a deflected roof. The actual displacement of the roof surface is not uniform, but, when approximated by a uniform value, we get a usable result. I should emphasize the fact that the analysis presented here in a very cursory fashion is primarily for a semi-static condition or a relatively slow dynamic impulse. It is quite obvious, I think, that if one applies a sharp peaked pulse of stress and it travels down, it does not know the structure is there until it reaches the structure; therefore, its influence will be entirely different. If the structure is rigidly supported in some fashion at its base, the initial pulse of loading on the roof of the structure will show no arching. But if there is a rise time in the pressure pulse, then there is time for the pressure to know that the structure is there, and essentially the structure will experience reduced loading. For intermediate conditions, there is an effect that must be taken into account. The large magnitude of arching that we get out of this analysis or related analyses must be considered in light of the fact that these are applicable only for relatively slow rise time pressure curves.

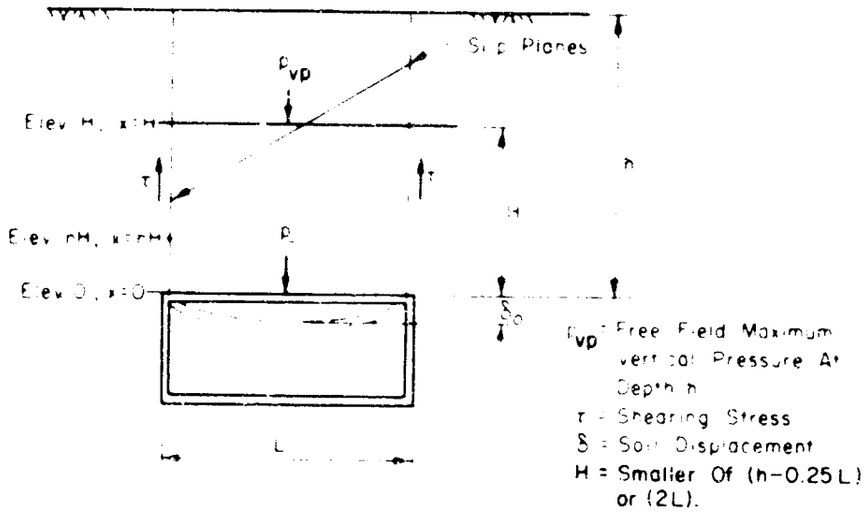


Fig. 19 Cross-Section of Underground Structure

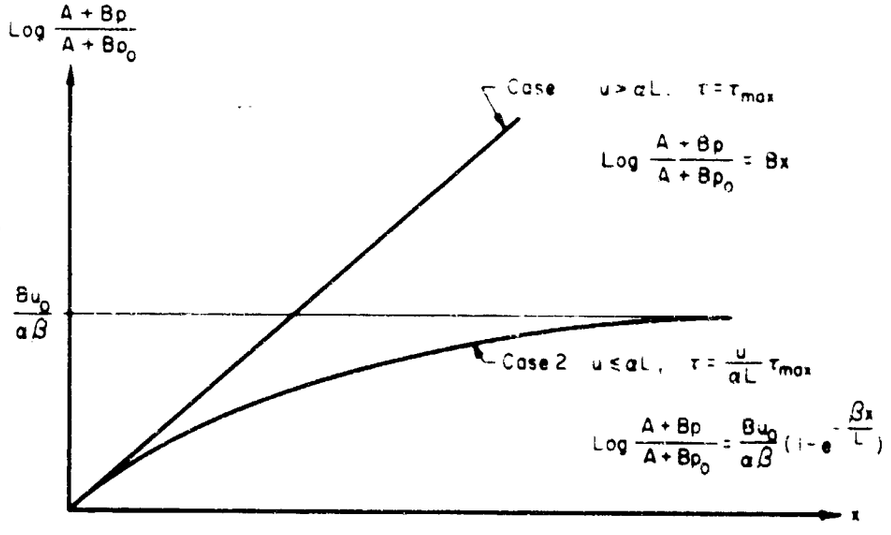


Fig. 20 Variation of Pressure with Depth

Figure 20 is a sort of summary of the results. The expression $\log (A + B_p)/(A + B_{po})$ is plotted as the ordinate versus the distance X as the abscissa. In the argument of the logarithmic expression:

$A = C/R$
$B = K_o \tan \phi/R$
p = the pressure at some distance X above the yielding point
p_o = the pressure on the yielding surface

where

C = cohesion coefficient in shearing stress
R = hydraulic radius of the loaded area = area divided by perimeter
K_o = horizontal coefficient of pressure
$\tan \phi$ = tangent of the angle of internal friction of the soil

Were B equal to 0, we would have only a cohesive resistance. Under these conditions, this analysis says that there is no arching. Were A equal to 0, we would have only a frictional resistance. We then get results that say that the log of p/p_o is either a linear function of displacement or a function which increases to a maximum and remains constant. In other words, p/p_o is an exponential curve of the form e^x for Case 1 and approaches a constant value for Case 2. In the latter Case, we have the shearing stress equal to the maximum value. In the former, it is less than that. In other words, in Case 2 the displacement is less than the value required to produce a yield shear resistance so that we are on the linear

part of the shear curve. Essentially then, for a frictional type of material, p/p_o is some constant given by $p/p_o = e^{(K_o \tan \phi\, u_o/R\alpha\beta)}$. The quantity α is the proportion of the span at which yielding occurs and β is the coefficient in the arbitrarily assumed displacement curve. These numbers are a little difficult to define, but we can arrive at reasonable values from experiments in which we had a number of drums at various orientations to the direction of stress. We could pick constants from these and from other data that were available from field tests at the time this analysis was made. From these I picked values of α of about 2%. In other words, at a displacement of the order of about 2% of the span, we reached the condition where we generated the full shearing stress, otherwise we obtained less than that. We obtained results which say, in general, that the displacement, if it is more than 2%, will give rise to a very large reduction in pressure when the depth of cover is about equal to the diameter. The factor is about 20 or 30 when the depth of cover is twice the diameter and it is fairly large even for smaller depths of cover. When the displacement of the surface is less than 2%, then this factor is considerably less, and the ratio of load on the surface, to load on the yielding roof is of the order of maybe no more than 3 or 2 when the ratio of the depth of cover is of the order of about 1/2 to 1 times the span. These are very crude figures.

There are a number of parameters that enter into the rather complicated expressions, but the results given by this analysis do check quite well with experimental data. Professor Linger has made a number of tests with some modifications of the theory that have indicated quite good agreement with the theory.

To emphasize the main point, the amount of arching is a function of the amount of displacement of the part of the structure on which the pressure acts. If this displacement is small, the arching is negligible. Arching becomes less important as the rise time of the applied pressure pulse becomes shorter.

What governs the amount of displacement in the roof of a structure? In part, this is governed by the design conditions. If we design a reinforced concrete slab for very large pressures and have it quite thick, it cannot deflect very much before it yields and crushes. Consequently, the amount of arching we would get on extremely strong structures would be, in general, less than the amount we would get on extremely weak structures. In other words, if you design something for 10 psi, you might get a very large amount of arching. If you design for 10,000 psi, you would probably get very little.

SHOCK AND VIBRATION

The remainder of the discussion is concerned with shock and vibration. Let us look at a simple spring-mass system, Figure 21, where the base is subjected to some motion; and let us look at the stresses in the spring or the acceleration of the mass when we have a prescribed motion of the base to deal with. In other words, that prescribed motion of the base is either the free-field motion or the free-field motion modified by the structure set into the free-field. The spring and mass may be either an internal part of the structure which is coupled to the external walls, or a piece of equipment supported by some sort of foundation or connection to the structure. The following equations give familiar relationships for the frequency of a spring-mass system:

$$f = \frac{1}{2\pi}\sqrt{\frac{k}{m}} = \frac{1}{T} \qquad (12)$$

$$f = \frac{1}{2\pi}\sqrt{\frac{g}{x_s}} \qquad (13)$$

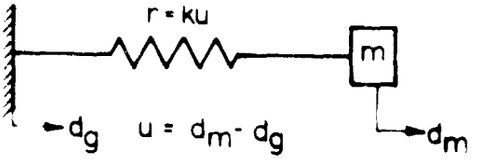


Fig. 21 Simple Mass-Spring System

Figure 22 shows a response spectrum, i.e., the plot of maximum responses of that simple spring-mass system when subjected to a certain type of input. In this figure, the input is in the form of either a double triangle of acceleration, or a single parabolic pulse of velocity, or a displacement that rises to a maximum and remains constant. These are all the same input, of course, just plotted in different ways as shown in the figure. If the base moves in the fashion described by that input, then the response of the system is shown here plotted as a function of the frequency of the system times the duration of this input versus the pseudo-velocity divided by the maximum ground velocity. The pseudo-velocity is equal to the circular frequency of vibration multiplied by the maximum displacement, and the maximum ground velocity is the peak on the parabolic velocity curve. The horizontal lines give constant values of that ratio. The lines sloping upward to the right gives ratios of the maximum displacement in the spring (D) to the maximum ground displacement (Y_o). The lines sloping downward to the right give ratios of maximum acceleration of the mass (A) to the maximum ground acceleration ($\ddot{y}_o$). This is a three-way plot.

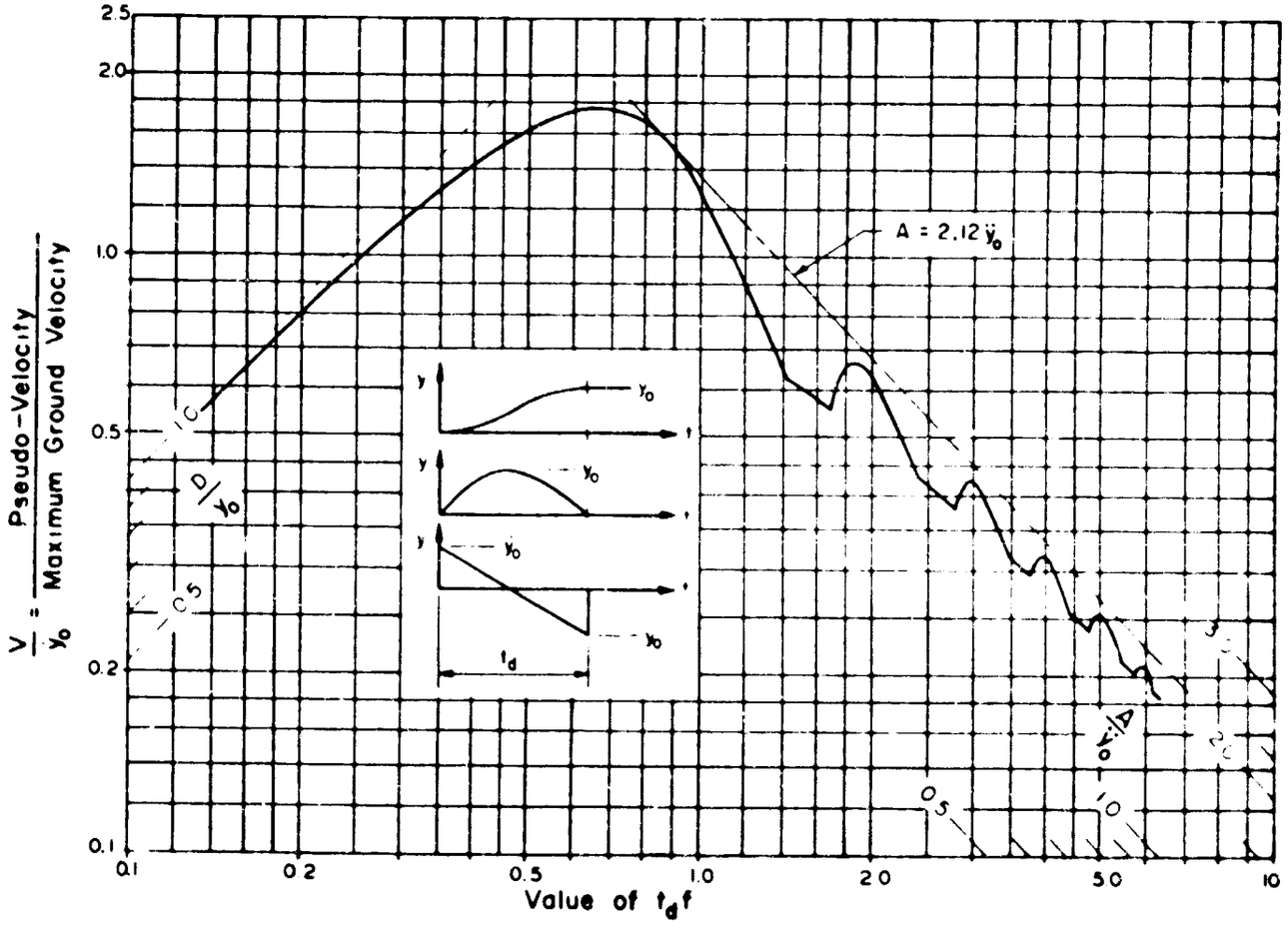


Fig. 22 Deformation Spectrum for Undamped Elastic Systems Subjected to a Parabolic Velocity Pulse

It is interesting to note the general character of the response in the left part of the spectrum. We can characterize the response by saying that the spring relative displacement is equal to the maximum ground displacement. This is obvious because if we have an infinitely large mass supported by an infinitesimally weak spring and we move the base, the mass does not move; but since the base moves, the deformation of the spring is equal to the movement of the ground. It has to be so. The surprising thing is that it is so for such a large range of frequencies. On the right hand side of the spectrum, we have a result that says the maximum acceleration of the mass is just slightly more than twice the maximum ground acceleration. That is because these accelerations are discontinuous. If they were rounded off, we would get a value equal to 1 times the maximum ground acceleration. In other words, if we had a very hard spring and an infinitesimally light mass and we moved the base, then we would move the mass at the same velocity and with the same displacement time relationship. The forces acting on the mass would have to be equal to the mass times the acceleration of the ground to make it move that way, therefore, the force of the spring is a measure of acceleration. This, of course, is the way an accelerometer is designed. The only reason we have the little bumps on the curve is because of the discontinuities.

In between the two extremes, we get a result that gives us something on the order of 1.5 to 1.7 for the ratio of the pseudo-velocity to the maximum ground velocity. There is a little amplification here. The amplification gets progressively higher as we go from left to right or as we move from displacement to velocity to acceleration. The following equations express the relationship between the pseudo-velocity and relative displacement:

$$V = 2\pi f D \tag{14}$$

and between the acceleration and the other quantities:

$$A_g = (2\pi f)^2 D = 2\pi f V \tag{15}$$

where f is the natural frequency and A is a dimensionless acceleration parameter.

Figure 23 shows a set of relationships for a much more complicated shock input. This is the north-south direction ground motion that corresponds to the El Centro earthquake record of May, 1940. The series of curves are for various amounts of viscous damping from no damping ($\beta = 0$) for the upper curve to 40% of critical for the lower. You see that they all have the same general nature. All of the curves, regardless of the amount of damping, come down to $D/y_o = 1$ and approach this for relatively low frequencies. They all approach $A/\ddot{y}_o = 1$ for relatively high frequencies. They approach some amplification factor times the maximum ground velocity for intermediate frequencies, and that amplification factor is 1 for about 20% damping. It is as high as about 4 or slightly more than 4 for no damping. The amplification factor in terms of acceleration along the $\beta = 0$ curve at one points is about 9. This is an indication of the amount of resonance in this long earthquake of about 28-30 seconds duration. However, even that is not a great deal. For simple types of input like those arising from blast or shock, we would not expect such high amplifications.

Figure 24 is one of a series of approximate shock spectra that have been determined in a study by Professor A.S. Veletsos and myself for the Air Force Weapons Laboratory. We can sketch a spectrum in this fashion if we know the acceleration, velocity and displacement curves. It is valid for all types of displacement for which there is no recovery from the maximum, or else a small recovery. On the left, we approach $D = Y_o$, the maximum ground displacement. At the top, we get to about 1.5 times the maximum ground velocity. On the upper right we have about twice the maximum ground acceleration, and finally on the lower right, we get only the maximum ground acceleration. With very good accuracy this represents the results for almost all of the kinds of inputs we get from shock due to nuclear blast. There are more complicated situations considered in a report which will be issued soon by the Air Force Weapons Laboratory.

The system to which the shock spectrum corresponds is shown in Figure 25. It is comprised of a movable base whose motion we know and a spring, a dash-pot, and some supported mass. This represents a piece of equipment or an internal part of the structure.

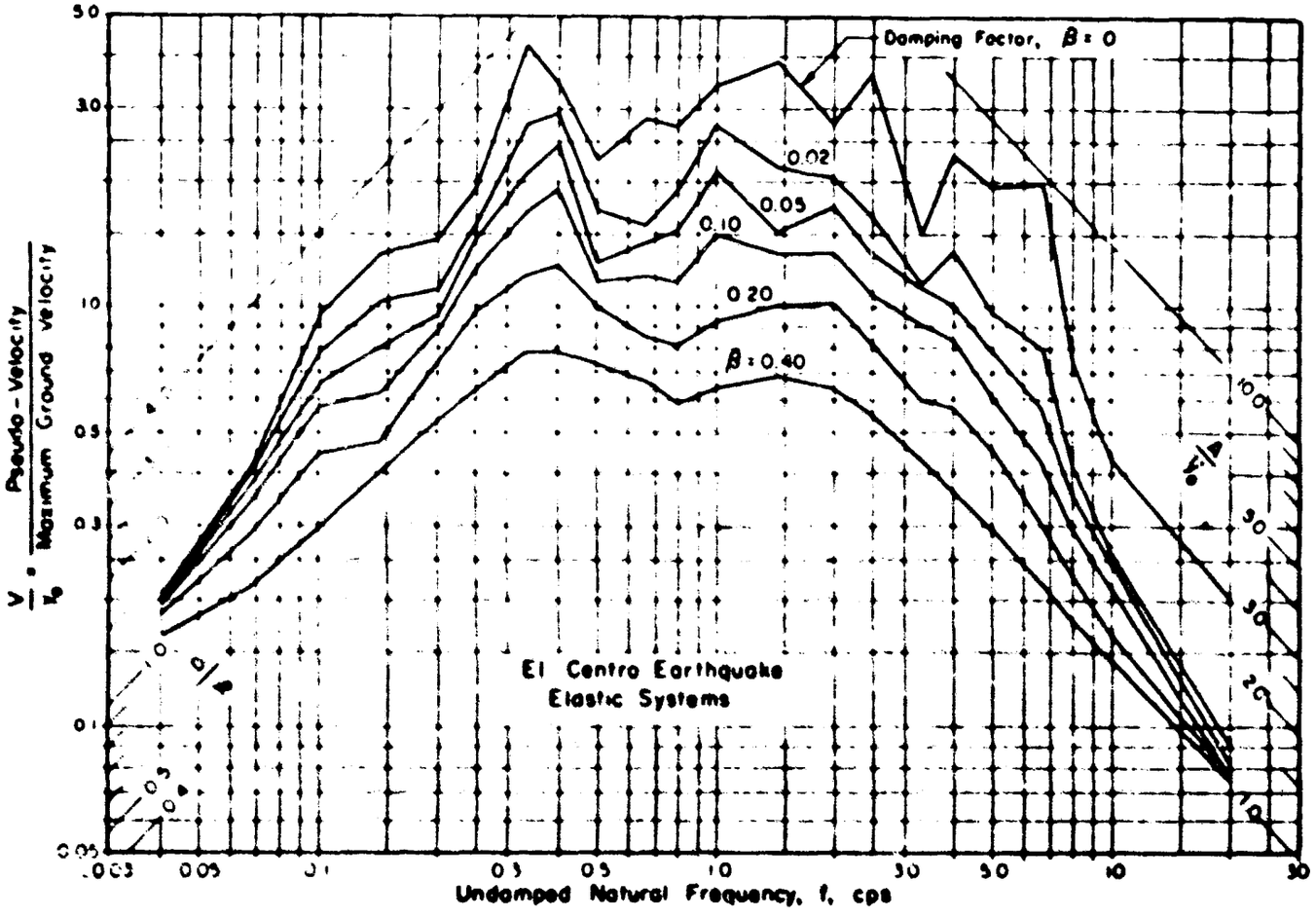


Fig. 23 Deformation Spectra for Elastic Systems Subjected to the El Centro Quake

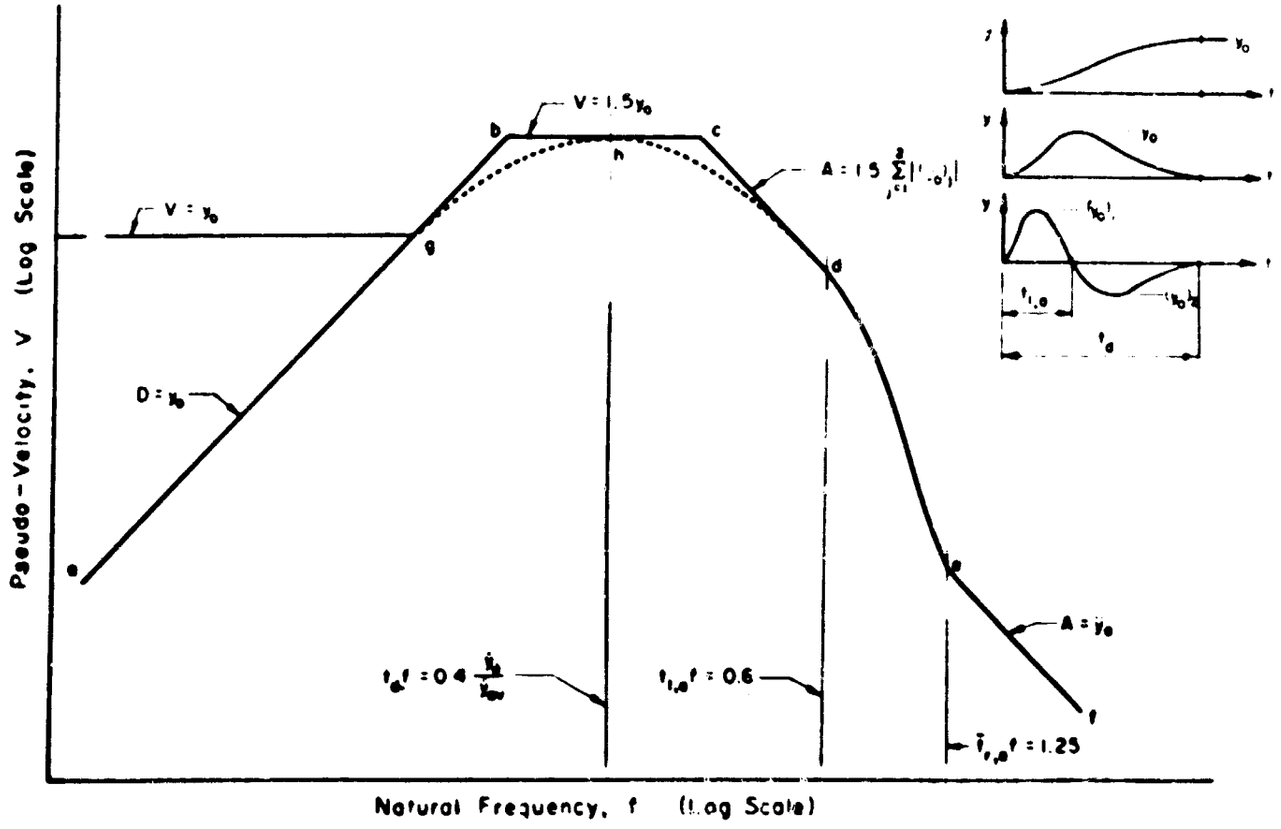


Fig. 24 Design Spectrum for Systems Subjected to a Half-Cycle Velocity Pulse

Figure 26 gives a description of the response spectrum we can use for damping of the order of 5% or 10% and for the kinds of motion we get in nuclear blasts. Errors will not be more than about 30% in general, and will probably not be greater than the uncertainty in the input parameters. On the left hand side of the shock spectrum, we have a line that corresponds to a maximum displacement on this three-way chart equal to the maximum ground displacement. On the top, we have a spectrum velocity 1.5 times the maximum ground velocity. On the right hand side, we have a spectrum acceleration equal to twice the maximum ground acceleration. We omitted the transition and the section where we have only the maximum ground acceleration because it probably is not important. In that range, it is very easy to take account of the accelerations. The normal fastening of the element to a wall gives a good deal of damping so that it really doesn't matter to much.

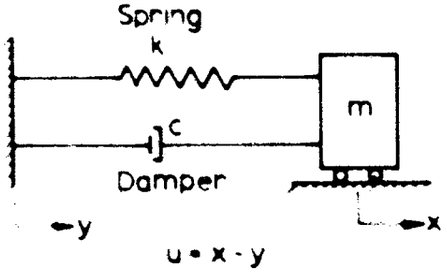


Fig. 25 System Considered

Since the preceding discussion was for elastic situations and since plastic action will often occur, what we are really concerned with is what happens in an inelastic system. Figure 27 is a plot of the curved elastic force-displacement curve for a spring, and a replacement of it by an elastoplastic relationship. The important thing to remember is that there is an arbitrarily defined yield point such that the area under the replacement curve up to this point is the same as that under the actual curve. This u_y, or yield displacement, has a certain magnitude, and the maximum displacement that we are going to permit in our design is the quantity μ times the elastic limit value, where μ is a sort of ductility factor. For $\mu = 1$, we have elastic action; for $\mu = 10$, we have a very highly plastic action approaching an infinite value.

The earthquake spectrum is much more complicated than the nuclear shock spectrum. Because they give about the same general results, the shock spectra shown in Figure 28 for the El Centro earthquake can be used in our discussion. These give directly the elastic components of motion. We would have to multiply each of these curves by μ to get the total motion and displacement of the spring, but we can use these elastic components directly to get accelerations. In Figure 28, the top curve ($\mu = 1$) is the same as the curve for $\beta = .02$ in Figure 23. The other curves in Figure 28 are for

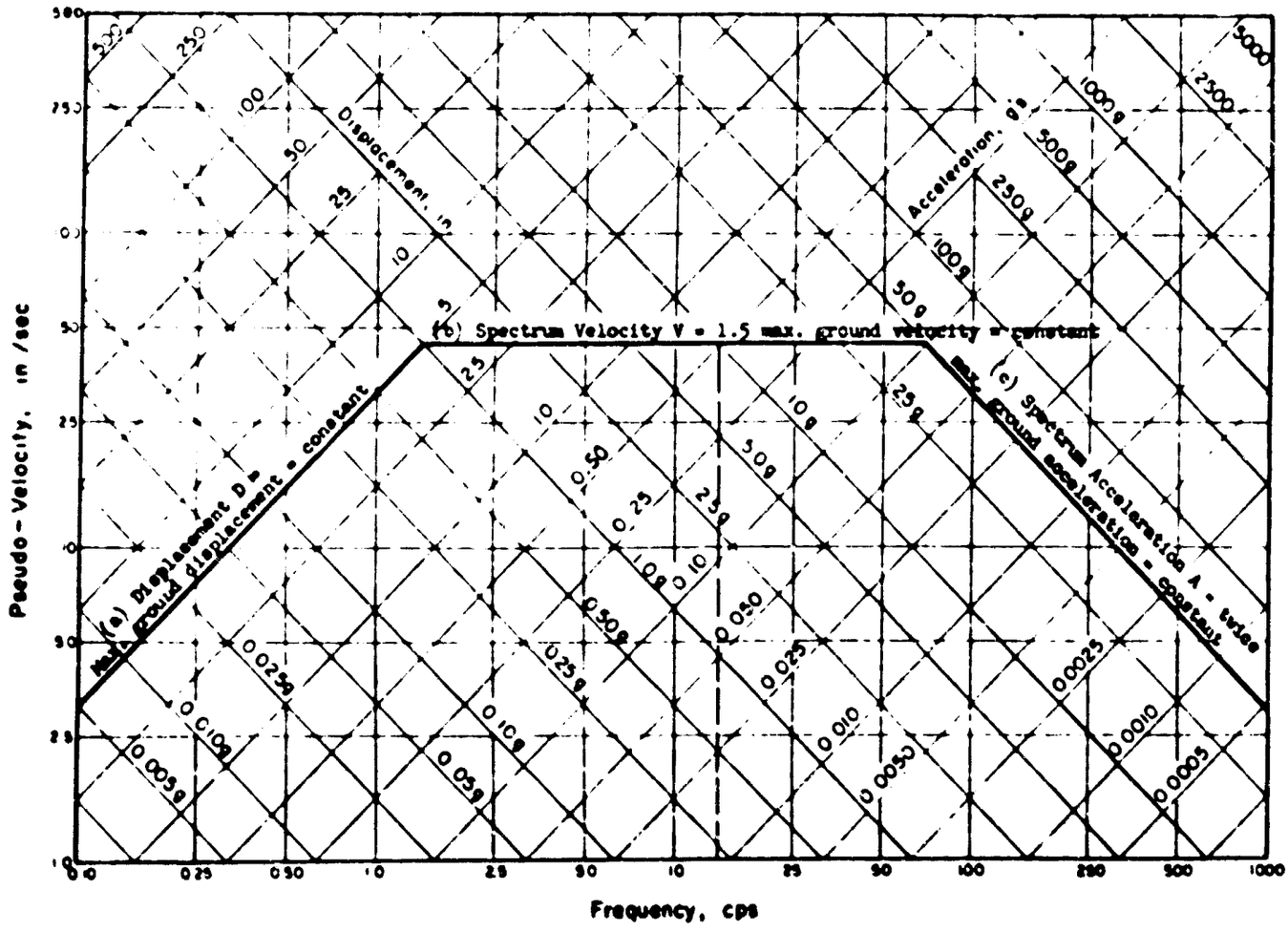


Fig. 26 Combined Shock Spectrum Envelope for Earth Motion

various values of μ from $\mu = 1$ to $\mu = 10$. Figure 29 demonstrates these results better. On the left, the total displacement is preserved. In other words, the displacement of both the elasto-plastic system and the elastic system are about the same. We can, therefore, infer what the elastic component of displacement is, or what the acceleration is, by dividing the elastic response by the ductility factor μ for which we need to design. On the extreme right, the accelerations are the same for both systems and are equal to the maximum ground accelerations. In other words, if the inelastic spring can carry the force which corresponds to the mass times acceleration, it will do so and although it will have an extremely large displacement, the acceleration is not reduced even though the spring is inelastic. In between, we have a

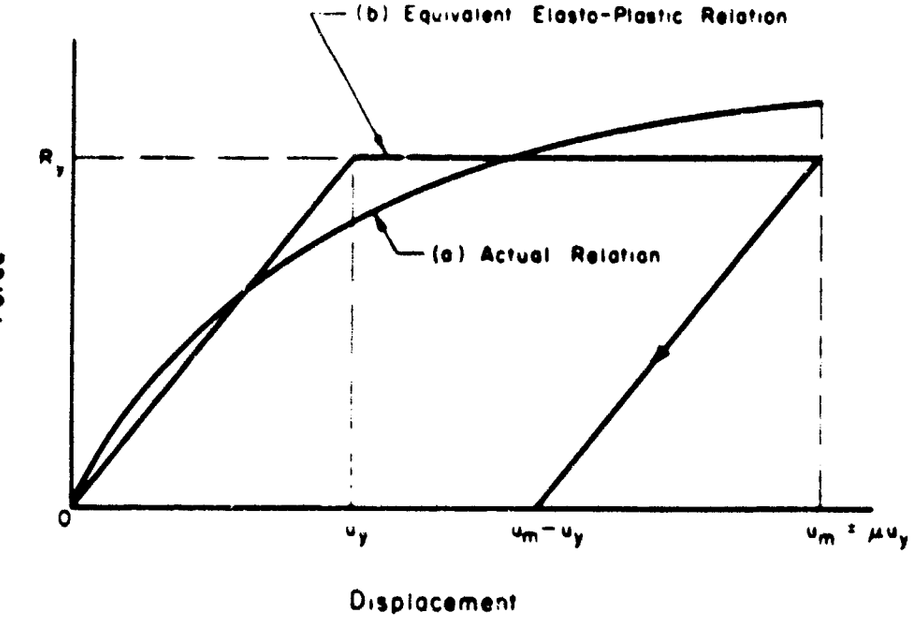


Fig. 27 Replacement of an Inelastic Load-Deflection Relation by an Elasto-Plastic Relation

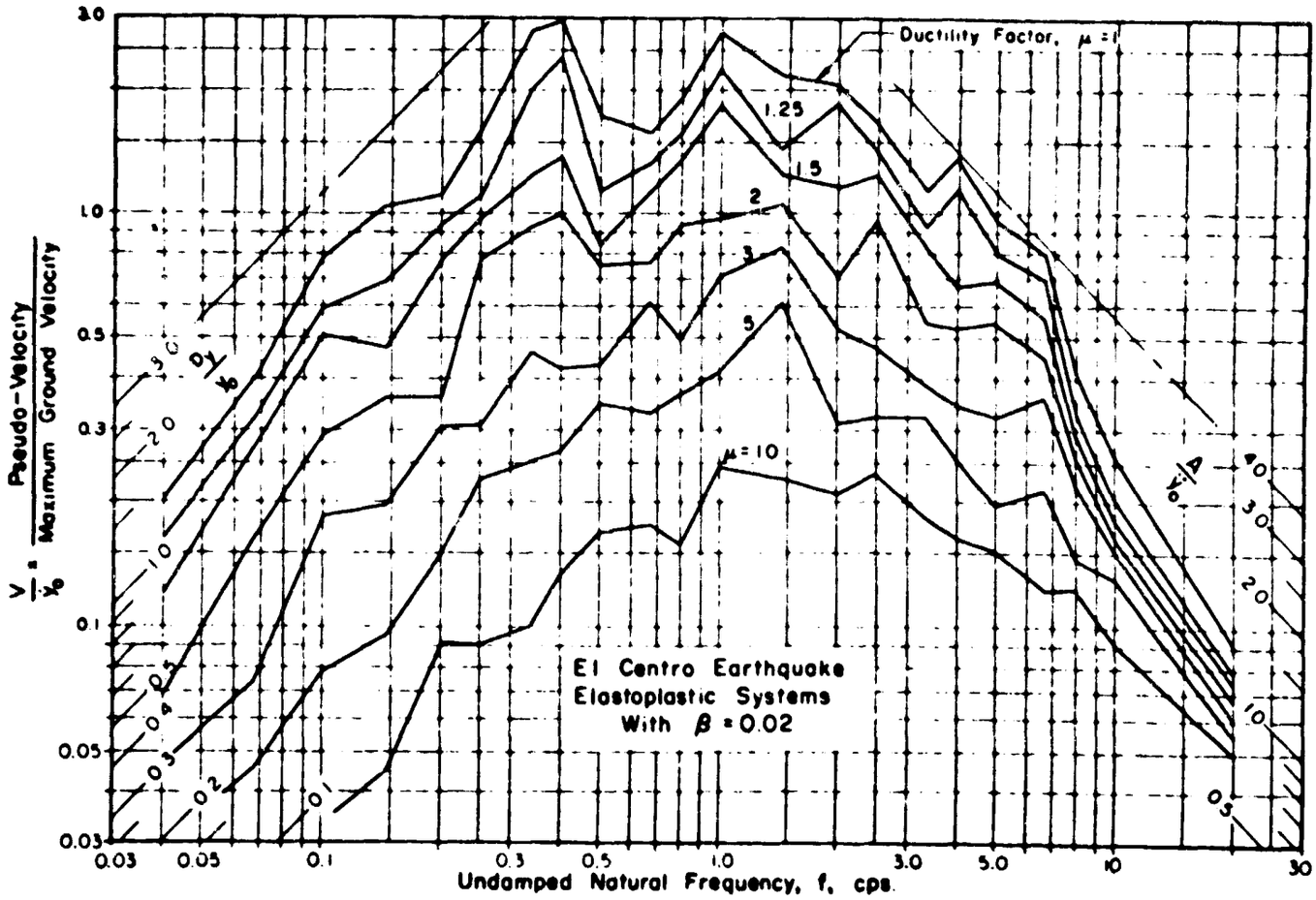


Fig. 28 Deformation Spectra for Elasto-Plastic Systems with 2% Critical Damping Subjected to the El Centro Quake

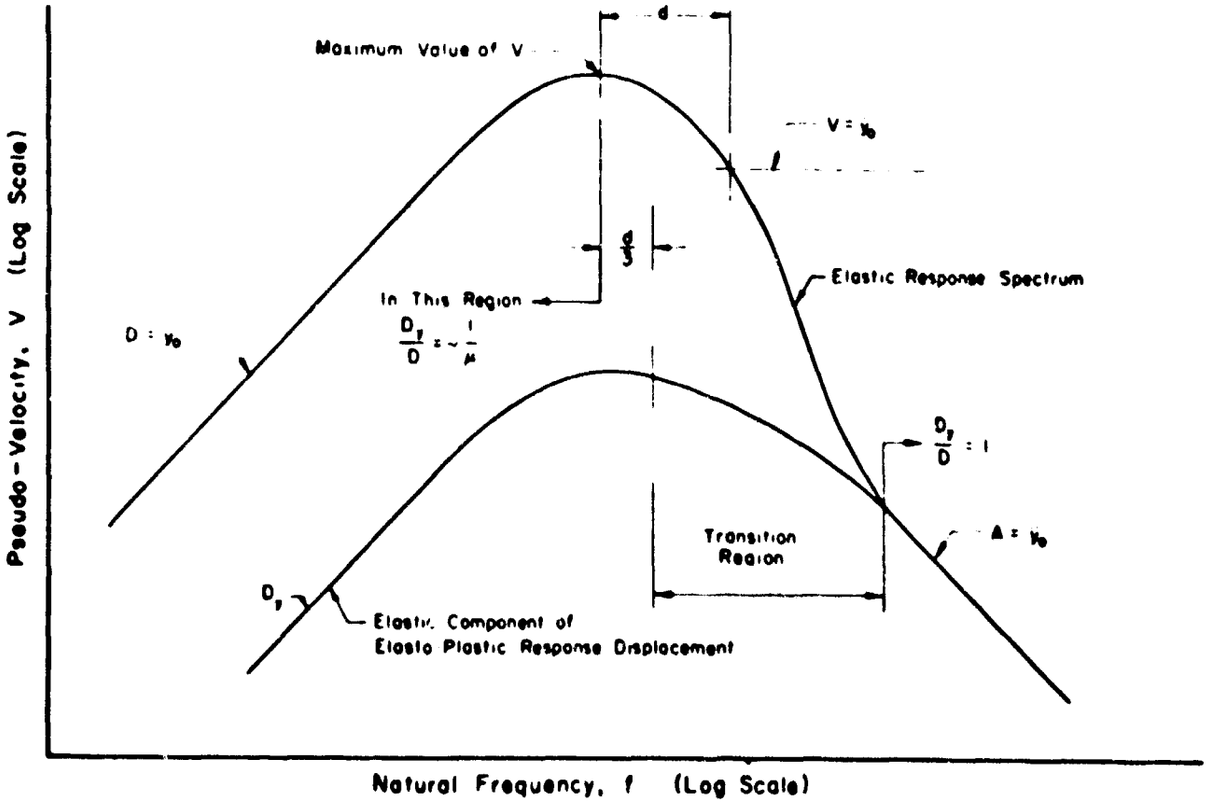


Fig. 29 Approximate Design Rule for Construction of Deformation Spectra for Elasto-Plastic Systems

transition and somewhere here we can deal with the energy being conserved. Actually the conservation of energy is not on the safe side in the low frequency range. It is on the safe side in the high frequency region and it is a good approximation to an interior or intermediate region.

Therefore, we can, in general, divide response spectra up into three parts: on the left, we have low frequencies and we conserve displacement; on the right, we have high frequencies and we conserve force or accelerations; in the middle, we have intermediate frequencies and we conserve energy. We can now deal with any inelastic system subjected to shock without difficulty. This means that we can conserve one or the other of these quantities as shown in Table 4. With being the ductility factor, we note that when displacement is conserved, the total displacement is the same for the elasto-plastic response relative to the elastic response. When energy or velocity is conserved, the total displacement ratio is $\mu/\sqrt{2\mu-1}$ and the acceleration ratio is $1/\sqrt{2\mu-1}$. When force or acceleration is conserved, the total displacement ratio is μ and the acceleration ratio is 1. Thus, we can design an inelastic support, if we wish, by taking these factors into account.

TABLE 4

Quantity Conserved	Elasto-Plastic Relative to Elastic Response	
	Total Displacement	Acceleration
Displacement	1	$1/\mu$
Energy or Velocity	$\mu/\sqrt{2\mu-1}$	$1/\sqrt{2\mu-1}$
Force or Acceleration	μ	1

When we are dealing with the design of an underground structure, even though we may have taken into account the situation as far as motion is concerned, we must take into account the relative motion between two points under transient conditions if we are planning to connect those two points together in any way by wiring, duct work, pipes, or anything else. Figure 30 illustrates two such points, a and b, in a structure where we know the free-field motion and how it is changed in the structure. In other words, it is not appropriate to assume that these will deflect in phase, even though

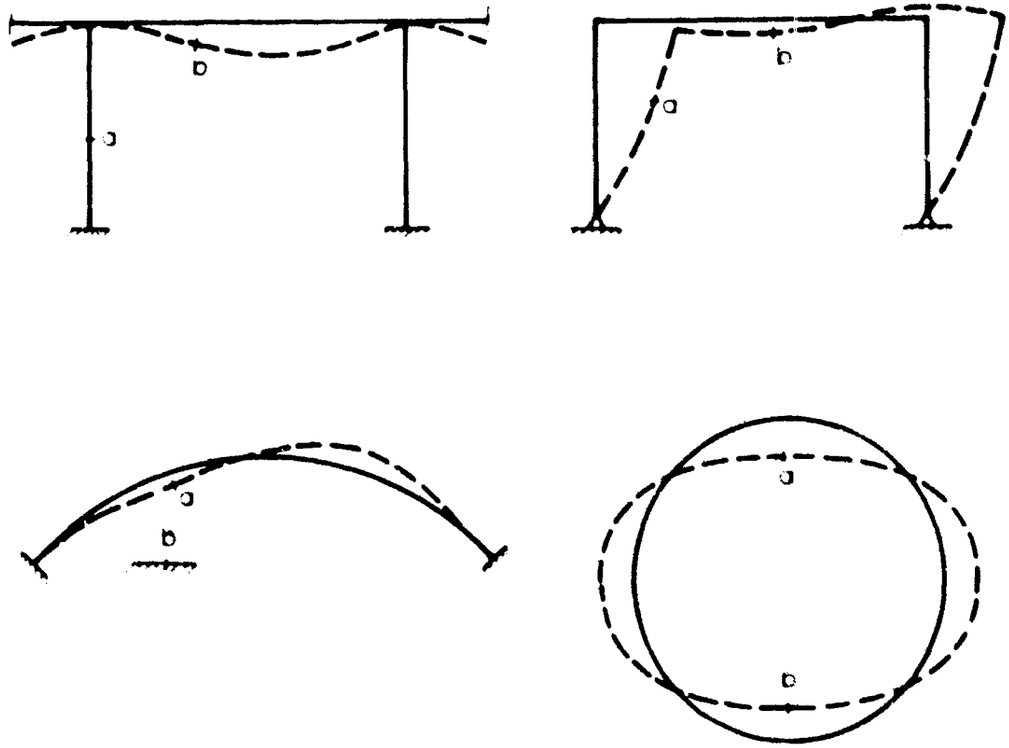


Fig. 30 Relative Displacements within a Structure Associated with Structural Distortion

they may have the same frequency. They can get out of phase. Thus, we must provide for relative displacements between the two points corresponding to the deformation of the structure and the deformation of any piece of equipment mounted on a spring that oscillates when supported at that point. In general, we must provide for the sum of the absolute values of the maximum excursions when we interconnect anything. Otherwise, we will get into trouble with breaking pipes and wires and so forth.

Figure 31 is merely an excuse to talk about certain other things I have neglected up to now. This shows a box resting on a relatively hard stratum surrounded by a softer stratum of material. Under these conditions the deformation of the soft stratum is not transferred completely to the box because it is supported rather well on the hard stratum. But because it is supported in a fashion different from the material along side it, there will be shears transmitted along the sides; negative skin friction if you will. This is akin to the old problem of the force a pile picks up when the earth around it settles relative to the point of the pile. We have to take this into account in the design of the structure.

The displacement of the bottom of this structure is governed primarily by the displacement of the hard stratum. It is determined by the deformation of the structure and also its base. In many cases we can treat this structure as if it were a stratum of soil, particularly when it is sufficiently large. For a given force applied to the roof, we have a certain force at the base which gives us a deformation. We can, therefore, get a sort of equivalent modulus; we can also get an equivalent density from its total weight divided by its total cross-sectional area. We can then compute a seismic velocity for it. We find that in many cases it is comparable to that of a moderately stiff or moderately soft soil. Some calculations that I've made for representative buildings give values of the order of 3,000 to 5,000 feet per second. We can then view this as if it were a stratum of material and deal with reflections from it.

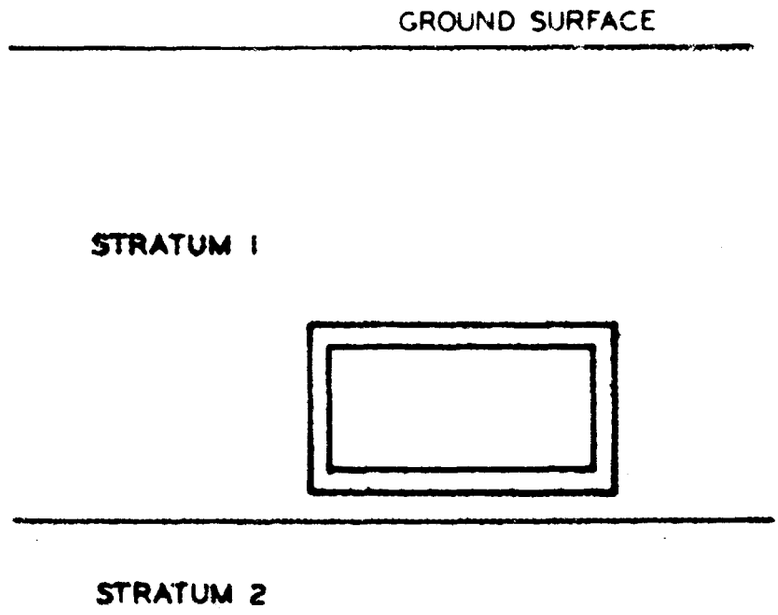


Fig. 31 Effect of Burial in Relatively Soft Soil

When a shock or pressure wave comes down through stratum 1 and reaches stratum 2 there is a reflection. In other words, there is a partial transmittal and a partial reflection at the surface of stratum 2. If this were an infinitally rigid material there would be a reflection factor which would double the stress at this point and also the velocity would become zero.

There is a change in both velocity and stress which must be taken account of when we deal with the phenomena that occur here. If a stress which has been reflected at stratum 2 is coming back to the surface and hits the structure, there will be a negative reflection and the stress goes back and forth. In this case, we find that the magnitude of the strain oscillates about some level, i.e., the same level which it would have if there were no reflection. For many purposes, such as computing displacement, we can forget about the reflection. However, if we want to compute particle velocity and acceleration we must take it into account because instantaneous values do not show these phenomena. When we look at a relatively thin structure, assuming that there is no underlying stratum, the stress hits the top of it and tries to move the whole structure. There may be, over an infinitesimally small period of time, a sort of reflection. If the shock wave were present, there would be reflection. In the absence of a shock wave, this structure moves with the underlying material. Consequently, the net effect is a much smaller reflection factor, approaching almost none at all. This has happened in structures on which we have not been able to measure reflections and this, I think, is completely consistent with the facts that the structure itself has a sort of equivalent seismic velocity and mass which must be taken into account.

A final point is desirable to make. The base of the structure in Figure 31 was a slab. If it had been a series of footings we would have some design problems to provide for the proper motions and displacement of the footings. If it is

a complete slab then the design problem, although it is complicated, resolves itself into one of judgement. We can see that we need not have the footing any stronger than the roof, so that even though it looks like we might get large displacements, the whole area is loaded and the displacement will be no greater than in the soil around it.

This brief introduction to the Symposium was intended to give a survey of the problems involved in soil-structure interaction. The papers that follow will give detailed results of research studies and design applications.



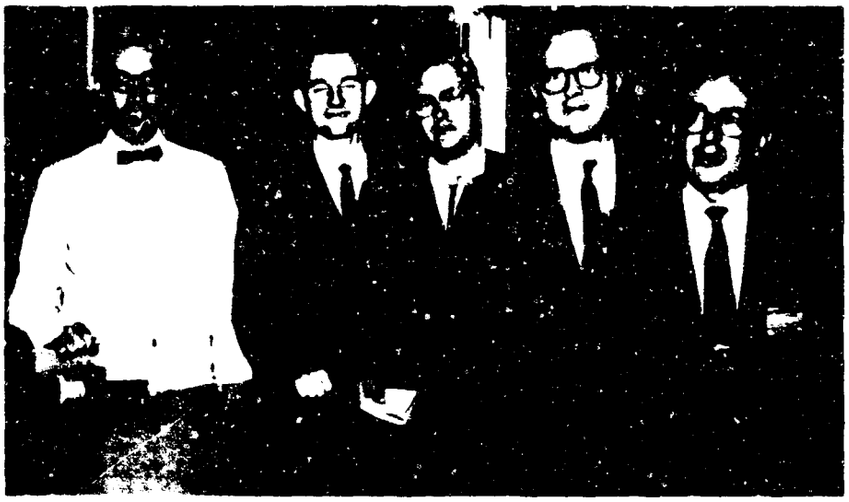
Nathan M. Newmark, Professor of Civil Engineering and Head of the Department at the University of Illinois, has been a member of the staff at Illinois since 1930. He has been engaged in research and instruction in structural engineering for his entire career, and has been in charge of the Structural Research Laboratory since 1946. In 1955, Rutgers University conferred the honorary degree of Doctor of Science on Professor Newmark, who received his Bachelor of Science degree there in 1930. In May 1962, Dr. Newmark was elected a Fellow of the American Academy of Arts and Sciences, and in April 1964 he was named to a Committee of Twenty-Five, appointed by the National Academy of Sciences, to select the charter members of a National Academy of Engineering. He is the author of over 145 papers in the fields of structural analysis and design, applied mechanics, numerical methods of stress analysis, and effects of impact, shock, vibration, wave action, blast and earthquakes on structures. He has served as a consultant to a great many industrial organizations and a number of government agencies in these fields. He has been a member of consulting boards and panels for many of these groups and has been associated with nearly all the nuclear field test programs dealing with effects on structures.

SESSION TWO-MONDAY PM
WAVE PROPAGATION IN SOIL MEDIA

SESSION CHAIRMAN: ROBERT V. WHITMAN

TABLE OF CONTENTS

	page
CHARACTERISTICS OF STRESS WAVE PROPAGATION IN SOIL, E. T. Selig	27
DYNAMIC BEHAVIOR OF GRANULAR MEDIA, James V. Zacco:	62
STATIC AND DYNAMIC CONSTRAINED MODULI OF FRENCHMAN FLAT SOILS, A. J. Hendron, Jr. and M. T. Davisson	73
PROPAGATION OF DYNAMIC STRESSES IN SOIL, Lynn Seaman	98



Participants in Session Two were, left to right, Robert V. Whitman (Session Chairman); Lynn Seaman; M. T. Davisson; E. T. Selig; and J. V. Zaccor.

CHARACTERISTICS OF STRESS WAVE PROPAGATION IN SOIL

by
E. T. Selig*

ABSTRACT

A review is made of the basic characteristics of shock induced stress wave propagation theories and previous research. Attention is primarily devoted to the situations where the slope of the stress-strain curves of the soil decreases with increasing stress or strain, i.e., negative curvature. The effect of elastic, viscoelastic, plastic, locking and general nonlinear, inelastic behavior is discussed. The phenomena are further illustrated by wave propagation experiments in long, horizontal bars of dry sand confined under constant lateral pressure with one end subjected to dynamic loading from an air shock tube. The observed results are compared with theoretical predictions. It is shown that the major features of the observed stress waves can be explained on the basis of the characteristic nonlinear, inelastic stress-strain behavior of the sand without the inclusion of time dependent effects.

INTRODUCTION

The purpose of this paper is to present some of the basic characteristics of stress wave propagation in soils. Considerable attention is given to previous work on the subject and the various basic theoretical approaches are summarized. The phenomena are illustrated by experiments of shock induced wave propagation in bars of sand. The particular lateral boundary condition of constant confining pressure was used, hence the experiments were not strictly one-dimensional. However, the results are useful in evaluating both constrained and confined wave propagation in soils.

A nonlinear, inelastic theory of wave propagation is compared to some of the experimental results to establish the validity of the theory and the significance of the important phenomena. On the basis of this agreement, the theory is extended to show the influence of the soil stress-strain characteristics, specimen boundary conditions and applied loading.

The general definition of stress waves includes the special case where a stress discontinuity or shock exists. It will be shown that even though shock loading is applied to the soil the induced stress waves will not necessarily be shock waves. The nature of the wave depends upon the stress-strain characteristics of the soil--in general, for the condition of constant confining pressure, shock waves will not be transmitted through the soil.

WAVE PROPAGATION THEORIES

A detailed discussion of stress waves in solids has been presented by Kolsky (1). In a medium that cannot sustain finite shear stresses only one type of wave, a pressure wave, can be propagated. It travels with a velocity $\sqrt{k/\rho}$ where k is the bulk modulus and ρ is the density. In isotropic solids of unlimited extent two types of elastic waves may be propagated. These are dilatational waves which travel with the velocity $[(k + 4\mu/3)/\rho]^{1/2}$, where μ is the modulus of rigidity (or $[(\lambda + 2\mu)/\rho]^{1/2}$ where λ is Lame's constant $= k - 2/3\ \mu$), and distortional waves which travel with the velocity $(\mu/\rho)^{1/2}$. In addition, elastic waves may also be propagated along the surface of a solid. These are called Rayleigh waves, and the disturbances associated with them decay exponentially with depth. Because they are two-dimensional they attenuate less rapidly with distance than the other types of elastic waves.

The particle motion of the dilatational waves is along the direction of propagation. The particle motion of distortional waves is perpendicular to the direction of propagation. The particle motion in Rayleigh surface waves is in the plane perpendicular to the surface along which the waves are traveling and parallel to the direction of propagation.

Real solids are never perfectly elastic; instead, there may be hysteresis in the load-unload cycle or viscosity resulting in a dissipation in energy. Many materials also show mechanical relaxation whereby the strains, produced by application of a sudden fixed stress, increase asymptotically with time and the stresses due to application of a sudden fixed strain relax asymptotically with time. Stress waves with periods close to the relaxation time of such a medium are significantly attenuated in the medium.

In materials having nonlinear stress-strain relationships, shock waves and plastic waves may be formed. Shock waves may occur where the stiffness increases with stress so that the higher intensity portion of a pulse travels faster than the initial portion. In a material which is elastic up to a certain stress and then plastic, an elastic wave is propagated through the medium followed by a plastic wave of lower velocity.

* Senior Research Engineer, IIT Research Institute, Chicago, Illinois.

Elastic Waves

The simplest theory of longitudinal wave propagation in a horizontal column or cylindrical bar is that for a perfectly elastic material. This case is governed by the well known wave equation

$$\rho \frac{\partial^2 u}{\partial t^2} = E \frac{\partial^2 u}{\partial x^2} \tag{1}$$

where ρ is the material density, E Young's modulus, u the displacement of a cross section, x the position along the bar and t time. It is assumed that plane cross sections remain plane, that the stress is uniform over the cross section, and that the wave length is much longer than the bar diameter.

Extensions and contractions in the longitudinal direction will be accompanied by contractions and extensions in the transverse direction. Therefore, when the wave length is of the same order as the bar diameter, the stress will become nonuniform on the cross section, and the plane cross sections will become warped.

The solution of Eq. 1 may be written

$$u = f(c_o t - x) + F(c_o t + x) \tag{2}$$

where c_o, the velocity of wave propagation, is equal to $\sqrt{E/\rho}$.

The following observations can be made from these equations:

1. The stress at any point is proportional to the particle velocity.
2. Since the wave velocity is independent of the frequency of the stress, a stress pulse will travel without distortion.
3. The shape of the pulse reflected from a free end is the same as that of the incident pulse, but opposite in sign, i.e., a compression wave will be reflected in tension. The particle velocity and displacement at the free end of the bar are twice those along the bar.
4. A pulse is reflected from a fixed boundary unchanged, i.e., a compression wave reflects as a compression wave. The stresses at the fixed end are double those when the pulse is traveling along the bar.

When the wavelength becomes comparable with the lateral dimensions of the bar, the velocity of longitudinal waves depends upon the wavelength and at very short wavelengths they travel with the velocity of Rayleigh surface waves.

Viscoelastic Waves

One well known departure from an ideal elastic solid is a viscoelastic material. In such a material, energy is dissipated through viscous forces. Maxwell (2) was one of the first to suggest a time-dependent stress-strain relationship as more closely approximating the behavior of a real solid. He proposed a relationship of the form

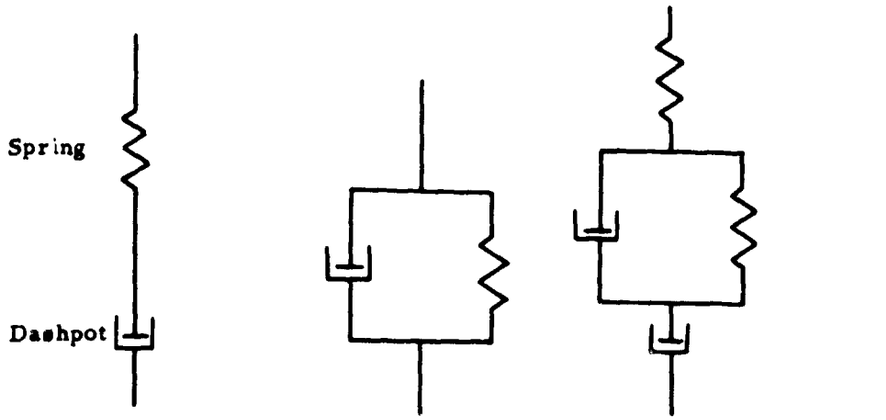
$$\frac{d\sigma}{dt} = E^* \frac{d\epsilon}{dt} - \frac{\sigma}{\tau} \tag{3}$$

where E* is the appropriate elastic constant and τ is the relaxation time. Thus, when a stress is applied for a time which is short compared to τ, the behavior is like that of an elastic solid, while for times long compared to τ the behavior is like that of a viscous liquid.

Three models of viscoelastic solids are shown in Figure 1. The simplest model is the Maxwell solid (Figure 1a) consisting of a spring and dashpot in series. For the Voigt solid (Figure 1b), the stress is equal to the sum of two parts, one proportional to strain and the other proportional to strain rate. The Maxwell model represents stress relaxation while the Voigt model represents creep. The internal friction or damping capacity of the Maxwell solid varies inversely with frequency while that for the Voigt solid is proportional to frequency. Experimental evidence indicates that for most solids, neither is entirely correct and damping capacity is often roughly independent of frequency (1). A more general, but more complicated representation shown in Figure 1c combines the features of the Voigt and Maxwell models in an attempt to more closely represent true behavior.

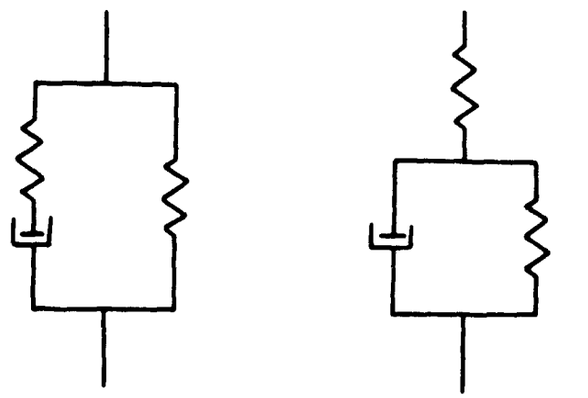
For the Maxwell model, the stress asymptotically approaches zero when a constant strain is applied, hence, the model does not transmit static stresses. In practice, it has been observed that a finite stress usually results. The Voigt model does not represent stress relaxation, since if the strain is fixed the stress is fixed. Another disadvantage of the Voigt model is that it transmits step pulses at infinite speed, i.e., there is no upper bound to the wave propagation velocity. By placing a spring in parallel with the Maxwell model and a spring in series with the Voigt model, these deficiencies are overcome and the two resulting models are mechanically equivalent (Figure 2).

Hillier (2) has derived the equations describing propagation of longitudinal waves in modified Voigt viscoelastic element shown in Figure 2b. The wave velocity and damping of the case where the two springs have equal stiffness are shown in Figure 3 as a function of frequency of applied pulse, p. In Figure 3, τ is the "retardation time," c the wave velocity, c_o velocity based upon the stiffness of one of the two springs alone, and α the attenuation factor.



a) Maxwell Solid b) Voigt Solid c) More General Solid

Fig. 1 Models of Viscoelastic Solids



a) Modified Maxwell b) Modified Voigt

Fig. 2 Modified Viscoelastic Models

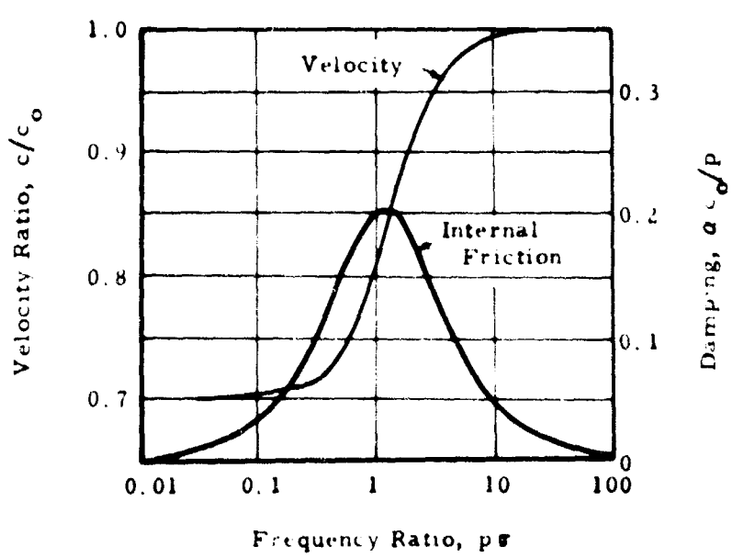


Fig. 3 Characteristics of Modified Voigt Viscoelastic Solid (3)

Damping is a maximum when the period of the vibration is about equal to the retardation time, and falls off rapidly for increases or decreases from this value. The velocity increases significantly with frequency. For very low frequencies, the velocity corresponds to that for the two springs in series without the dashpot, while for very high frequencies it corresponds to that with the spring in parallel with the dashpot inoperative. This velocity change is analogous to the dispersion in a perfectly elastic rod when the wavelength is of the same order as the diameter. However, the effects on velocity are opposite, high-frequency waves traveling faster than low-frequency waves in the viscoelastic solid and slower in the short elastic rod.

Lai and Sauer (4) have computed the transient stress, strain and particle velocity response of a semi-infinite rod represented by the standard, linear, viscoelastic model shown in Figure 2. This is the simplest model which has a finite wave propagation velocity and will support load without infinite creep. The stress-time history applied to the end of the rod is characteristic of an air blast from a nuclear explosion.

For a step pulse applied to the end of the bar the stress variation with time at two points along the bar are compared for the elastic and viscoelastic models in Figure 4. As the distance along the bar increases, the initial jump in stress decreases and the time to reach the steady-state value increases for the viscoelastic material. The wave remains unchanged for the elastic model. The strain and particle velocity vary in the same manner with time.

The stress variation with time for several wave forms and one position in the bar is shown in Figure 5. The stress jump is the same in all cases. For the step function, the stress increases monotonically to the maximum value. For the decaying loading pulse the stress first increases and then decreases as it approaches the loading pulse asymptotically. However, as the decay rate increases the point of maximum stress approaches the wave front so that the jump value becomes the maximum value. The same trends occur for strain and particle velocity.

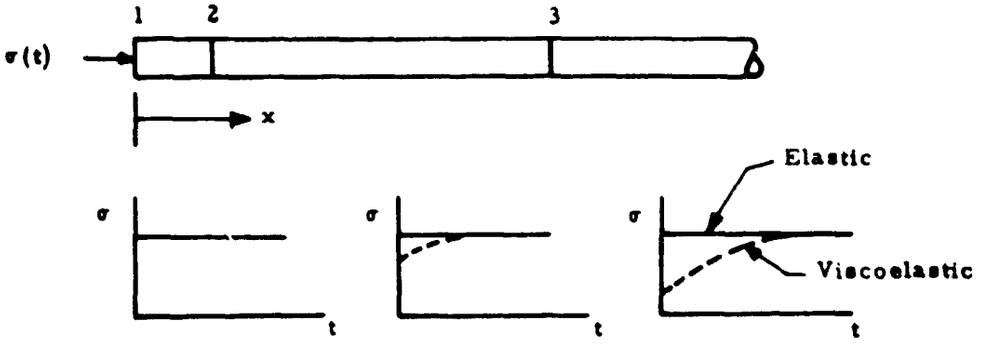


Fig. 4 Attenuation of Stress in Viscoelastic Bar (4)

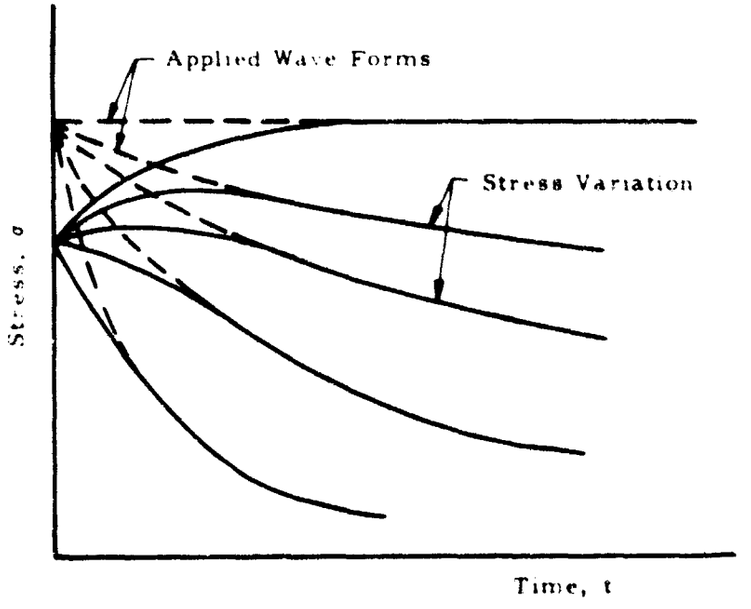


Fig. 5 Effect of Wave Form on Stress Variation (4)

The stress variation for one wave form and several positions along the bar is shown in Figure 6. With increasing distance, the stress jump value decreases, the point of maximum stress occurs at increasingly greater times after the wave front, and the stress values overshoot the loading pulse. The attenuation of the maximum stress with depth is shown in Figure 7 for a given wave form. As the degree of viscoelastic behavior increases for a given position and loading pulse, the maximum strain and particle velocity increase, and the rise time for maximum stress-strain and particle velocity increase.

Typical stress-strain curves are shown in Figure 8 as a function of degree of viscoelastic behavior and wave form. The greatest hysteresis occurs for the slowest decay rate of loading pulse in the model which is least elastic.

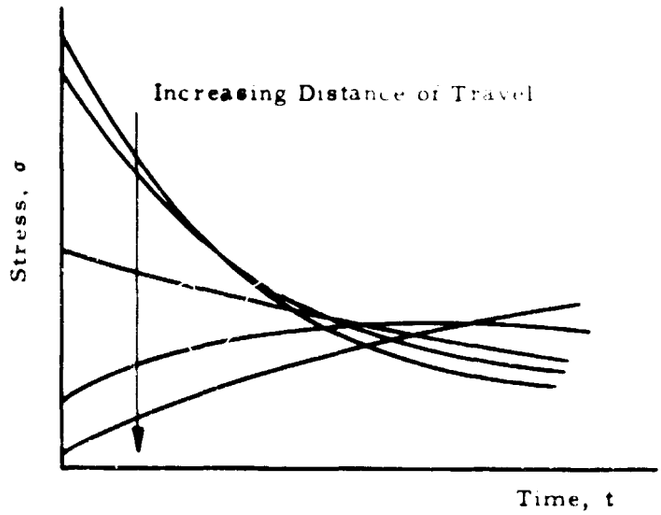


Fig. 6 Attenuation of Wave Form with Distance (4)

Plastic Waves

Waves in materials with nonlinear stress-strain relationships and hysteresis present a much more complex analysis problem (1). The first problems considered involved stress increase, only, applied to infinitely long wires or rods assuming 1) a single-valued stress-strain relationship with a decreasing slope after the elastic limit, 2) non-time-dependent stress-strain response, and 3) a cross section sufficiently small that the effects of lateral inertia could be neglected. Under these conditions, an elastic wave will be propagated at the fastest velocity followed by a transition zone and then a plastic wave at a slower velocity determined by the modulus of the stress-strain curve.

The next step was to consider a finite length of pulse so that unloading occurred. For the stress-strain relationship assumed, an unloading wave will travel down the rod at a faster velocity than the plastic wave. It will eventually catch up with the plastic wave, producing an internal reflection. This causes a plastic wave of lower intensity to propagate forward and an elastic wave of the same sign to propagate backward. For a finite length rod, elastic and plastic waves will also be reflected from the end in a manner depending upon the end conditions.

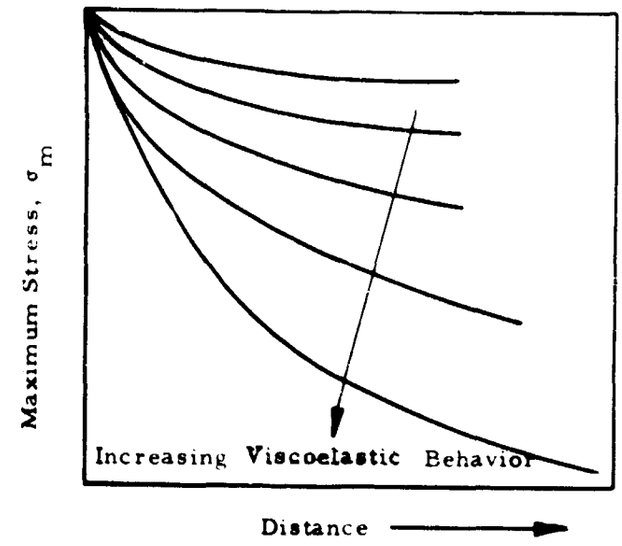


Fig. 7 Attenuation of Maximum Stress with Distance for a Given Decaying Wave Form (4)

A different situation occurs with a material whose modulus increases with stress instead of decreasing. In this case, the larger stresses will travel faster than the smaller ones, eventually overtaking them and creating a steep front or shock. The thickness of the transition zone containing the shock front depends on the properties of the medium and is governed by the extent of energy dissipation. The latter can be quite significant because of the high velocity gradients existing at the shock front.

The general theories for plastic wave propagation in rods have been reviewed by Turnbow (5). Consider a typical stress-strain curve where the slope decreases with increasing stress (Figure 9a). Applying Newton's law to a region of the rod acted on by a net stress $\Delta\sigma$ at a stress level σ, (Figure 9b) one finds that

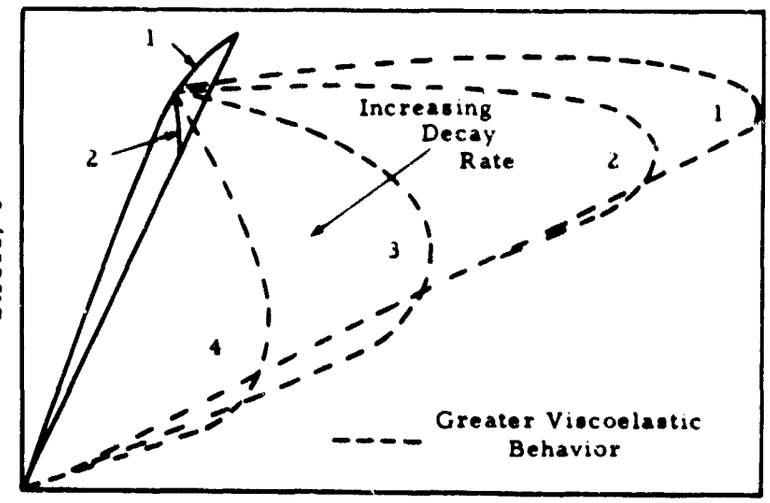
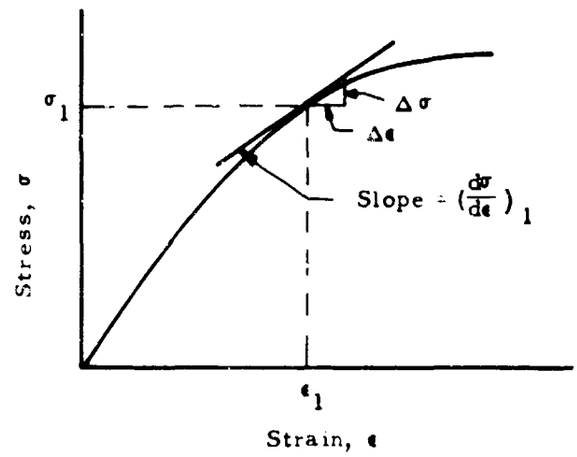
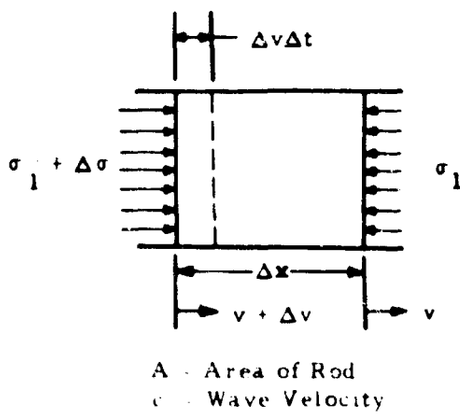


Fig. 8 Viscoelastic Stress-Strain Response (4)



a) Typical Stress-Strain Curve



A = Area of Rod
c = Wave Velocity

$$(\Delta\sigma)\ A = \rho\,\Delta x\, A\,(\frac{\Delta v}{\Delta t})$$

$$\Delta\sigma = \Delta\epsilon\,(\frac{d\sigma}{d\epsilon})_1$$

$$\Delta\epsilon = \frac{\Delta v\,\Delta t}{\Delta x}$$

$$c = \frac{\Delta x}{\Delta t}$$

$$c = \sqrt{(\frac{d\sigma}{d\epsilon})_1 \cdot \frac{1}{\rho}}$$

b) Propagation Velocity of Disturbance

Fig. 9 Derivation of Wave Propagation Velocity (5)

$$c = \sqrt{\left(\frac{d\sigma}{d\epsilon}\right)_1 \frac{1}{\rho}} \tag{4}$$

where c is the velocity of propagation of the disturbance $\Delta\sigma$ and $\left(\frac{d\sigma}{d\epsilon}\right)_1$ the tangent to the stress-strain curve at σ_1.

For the elastic case, Eq. 4 reduces to

$$c = \sqrt{\frac{E}{\rho}} \tag{5}$$

For a material with a stress-strain curve consisting of linear segments, the velocity of portions of the applied stress pulse within these segments would be constant and the pulse would propagate in a series of discontinuities. Several examples are illustrated in Figure 10.

Donnell (6), noting this decrease in velocity with increase in stress due to the nonlinearity of the stress-strain curve, pointed out that at high enough rates of loading energy would be "trapped" in the region of the loaded end of the bar, causing failure near the end when it otherwise might not occur. This mechanism explains observed failure at high rates of loading without resort to strain-rate effects.

When the slope of the stress-strain curve increases with stress, a different situation occurs as indicated previously. The overtaking tendency of the portion of the wave at highest stress levels maintains a sharp fronted wave traveling at a velocity governed by the secant modulus of the stress-strain curve. Several examples are given in Figure 11. The shaded area on the stress-strain diagram represents unrecoverable thermal energy dissipated in the form of heat.

The three basic theories of plastic wave propagation in cylindrical bars are known generally as the von Karman theory, the Malvern theory and the Prandtl theory. They differ only in the assumptions covering the stress-strain relationships (5). This problem is governed by equation of motion

$$\frac{\partial\sigma}{\partial x} - \rho\frac{\partial v}{\partial t} = 0 \tag{6}$$

and the continuity equation

$$\frac{\partial\epsilon}{\partial t} - \frac{\partial v}{\partial x} = 0 \tag{7}$$

where v is the particle velocity.

It is assumed that 1) the stress is uniformly distributed over the cross section, 2) there is no internal damping, and 3) kinetic energy due to lateral motion is small with respect to longitudinal motion.

The von Karman theory (7) assumes a stress-strain relationship independent of rate of loading. This theory has been shown to approximate certain observed behavior, but Dewez and Clark (8) have also shown some results with iron which indicate large strain-rate effects.

Malvern (9) extended the theory to apply to materials in which stress is a function of the instantaneous plastic strain and strain rate. He considered the static stress-strain curve, $\sigma = f(\epsilon)$, as a set of equilibrium states with plastic flow occurring only when $\sigma > f(\epsilon)$. The stress-strain law is then

$$E_o\frac{\partial\epsilon}{\partial t} - \frac{\partial\sigma}{\partial t} = g(\sigma, \epsilon) \tag{8}$$

where E_o is the elastic modulus of deformation. The function $g(\sigma, \epsilon)$ is the strain-rate function and is defined as

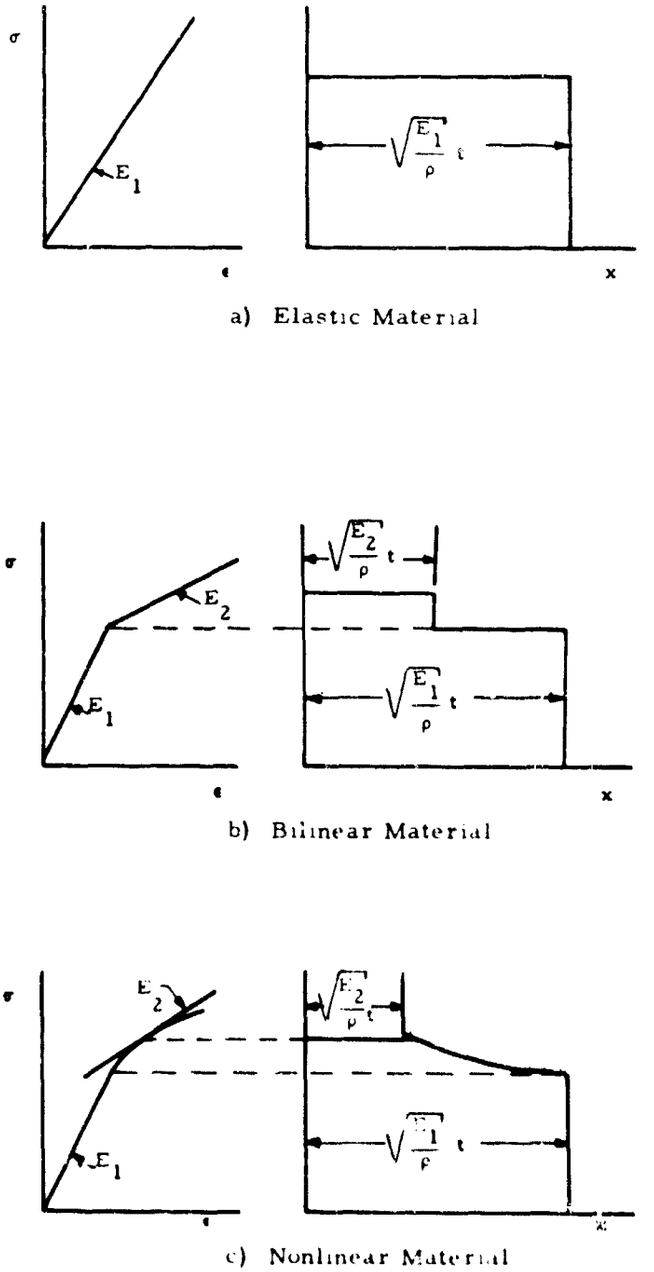


Fig. 10 Propagation of Step Pulse in Rods of Various Stress-Strain Characteristics (5).

$$g(\sigma, \epsilon) = k\left[\sigma - f(\epsilon)\right] \quad \text{for} \quad \sigma \geq f(\epsilon) \qquad (9)$$

$$g(\sigma, \epsilon) = 0 \qquad \text{for} \quad \sigma \leq f(\epsilon)$$

The latter condition reduces Eq. 8 to the elastic case. Although some of the characteristics of observed stress-time relationships were predicted, because of the use of a linear strain law the Malvern theory did not predict other important features of plastic wave propagation. This method does appear to be a plausible means of introducing strain-rate effects, however, because the rate of increase of plastic strain is proportional to the amount by which the instantaneous stress σ exceeds the static stress $f(\epsilon)$ for the same strain.

Prandtl (10) predicted, on the basis of kinetic theory, a dynamic stress-strain law which assumes that the excess stress above the static stress is a logarithmic function of the plastic strain rate, i.e.,

$$g(\sigma, \epsilon) = k_1 \exp\left[\left(\frac{\sigma - f(\epsilon)}{k_2}\right) - 1\right] \qquad (10)$$

Malvern's theory is a linear approximation of Prandtl's theory to simplify numerical computations.

Plass (11) compared the Malvern and Prandtl theories. He showed that moderate changes in the shape of the static stress-strain curve does not appreciably effect the stress, strain, and particle velocity distribution; however, the linear and exponential laws give slightly different shapes to these distributions.

The strain-rate theories, in effect, assume that the material reponds elastically under instantly applied forces and that time is required for plastic flow to occur. The non-strain-rate theories, such as von Karman's, assume that plastic deformation can occur instantly. This point was investigated by Sternglass and Stuart (12), who prestressed a copper strip into the plastic region and then measured the velocity of propagation of superimposed small amplitude waves. They found that the wave front traveled at the elastic velocity and that the velocity of every part of the wave was much greater than the theoretical value given by the tangent modulus at the existing stress level. These results clearly contradict the von Karman theory.

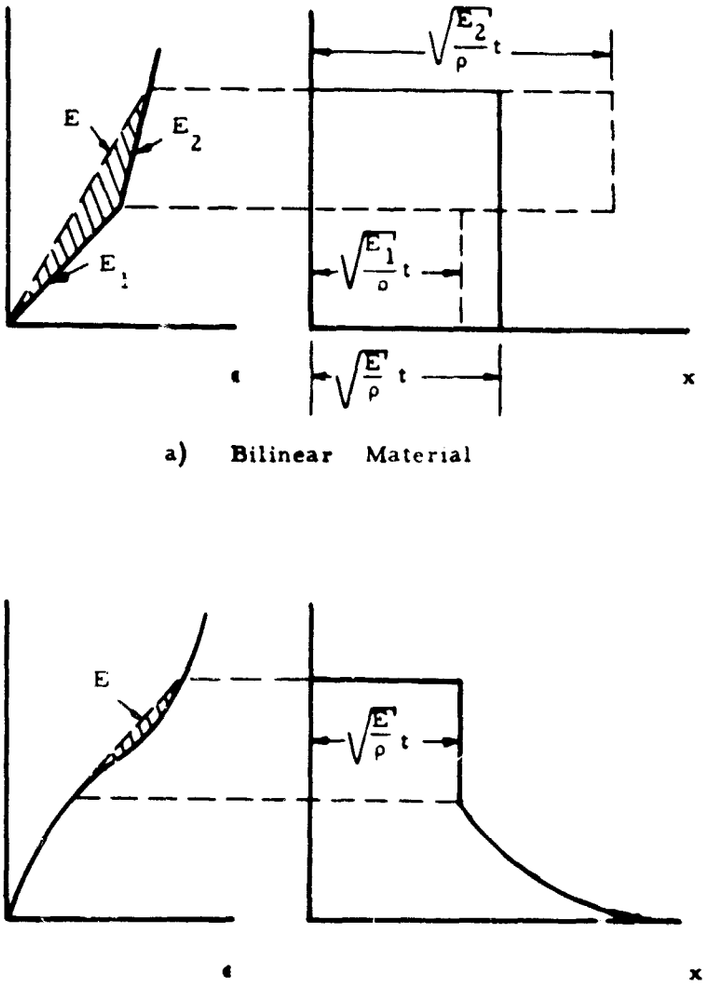


Fig. 11 Propagation of Step Pulse in Rods with Stress-Strain Curves for Increasing Slope (5).

A further comparison of the two theories was made by Karnes (13) in connection with impact studies on short cylinders of copper and lead. He concluded that the von Karman theory predicted the variation of strain with time with reasonable accuracy except in the vicinity of the impact. This theory could also predict the same stress-time variation as the strain-rate theory if a finite rise time is used instead of a step-loading pulse and if the static stress-strain curve is modified to make it "dynamic" by a proportionate increase in stress for a given strain. It was concluded that neither theory satisfactorily explained all of the observed behavior and that radial inertial effects would have to be included in the analysis to properly compare theory and experiment.

The propagation of plastic waves in strain-rate sensitive materials was considered further by Tapley (14). An investigation was made of the effects of lateral inertia on propagation of a plastic disturbance in a short copper bar impacted with a rigid ram. The static stress-strain curve of the material was used and a linear strain-rate law assumed. The results were computed from both the elementary Malvern theory and a theory including the effects of radial motion. Both a step rise and finite rise in velocity at the impact end were assumed.

A comparison of theory and experiment showed that the theory incorporating effects of radial motion and finite velocity rise agrees better with experimental results. The primary effects of including effects of shear and inertia associated with radial motion were found to be:

1. A reduction in the magnitude of the predicted axial stress, strain and particle velocity at a given time.
2. A more oscillatory history for the magnitude of the axial quantities due to the influence of radial effects.
3. The appearance of a dilatational and distortional propagation velocity instead of only the "bar" velocity.

MIT Experiments

An experimental study of stress wave propagation in constrained bars of sand was conducted at MIT (15,16). These wave propagation tests were designed to permit the study of the interrelationship between the stress-strain characteristics and wave transmission phenomena. The testing was limited to dry sands, principally a 20-30 mesh Ottawa sand. Short duration loads were applied by a 50 pound ram striking against one end of a horizontally positioned, long cylindrical sample of sand confined under constant pressure. Impact velocities up to 100 inches per second were possible. The samples were 2 inches in diameter and were as long as 32 inches. Confining pressure was applied to these samples by evacuating air from the interior of the sample. Measurements were made of the impact velocity of the ram wave propagation velocity and the stress-time relationships at the impact and reaction ends of the specimen.

The wave velocities computed from these tests ranged from 1080 to 1420 fps with the majority of the values falling around 1250 fps. A pronounced initial stress peak was developed at the impact end of the specimen. With the higher impact velocities, this peak was several times the strength of the sand under static loading. This phenomenon was attributed to the inertia of sand against lateral expansion and the frictional restraint of the end cap.

In general, especially with lower impact velocities applied to the shorter samples, the impact end stress-time curves dropped to a minimum after the initial peak and then began to increase once more. The second increase in the stress level was thought to be the result of reflection of the pressure waves from the fixed end of the sample. It is suggested that the stress levels which would have been induced in the samples by various impact velocities had there been no lateral inertia or strain rate effect are best represented by the stress level immediately after the peak. These values were seen to increase gradually with an increase in initial impact velocity. Many of the stress-time curves for the reaction end show a well defined knee in the rise portion.

The primary objective of these wave propagation tests was to permit observation of the manner in which a pressure pulse is attenuated by a column of sand. From the theory of wave propagation in a viscoelastic medium and considering the relaxation time associated with lateral inertia effects in Ottawa sand, it was concluded by the authors that the reaction end stresses observed in the tests upon Ottawa sand should not be significantly effected by the lateral inertia effects on the impact end. Based on the comparison of the experimental results with the theoretical equations for plastic and viscoelastic wave phenomena, it was concluded that there was evidence of both plastic and viscoelastic waves in the column of sand.

Smith and Newmark (17) made a computer investigation of one-dimensional stress wave propagation in linear viscoelastic materials. The results were compared with observed behavior in several materials including Ottawa sand.

The approach was to divide the continuous mass of the column of material into a number of lumped masses connected by springs and dashpots. The effects of lateral inertia were neglected. The response of the system to a given dynamic force applied at one end was determined by numerical integration. A major limitation of the viscoelastic model is that it does not account for the effects of nonlinear stress-strain characteristics and the change in yield stress with strain rate. To approximate these effects a yield stress which increases with strain rate was incorporated into the spring elements which were given trilinear characteristics.

The viscoelastic-plastic model of Smith and Newmark was compared with the results of the MIT experiments. The high initial stress peaks at the impact end could not be predicted by the theory if the major features of the remainder of the stress pulse were represented. This discrepancy was attributed to lateral inertia in the sand column on the initiation of impact.

The results of wave propagation in a variety of hypothetical soils were evaluated. The following observations were made:

1. The amount of stress attenuation can be increased by increasing the relaxation time or decreasing the spring stiffness ratio. Both tend to increase the hysteresis loop and spread the wave out.
2. Coulomb damping decreases the stress propagated without changing the general shape of the stress wave.
3. In soils whose stiffness increases with depth the stress may increase with depth, but the accelerations decrease.

Porkin (18) developed a strain-rate sensitive model for one-dimensional wave propagation and compared the predicted behavior with the results of the MIT experiments. He demonstrated that the initial sharp stress peak observed in the experiments can be explained without requiring the presence of lateral inertia as suggested by Smith and Newmark (17). The approach of Porkin is patterned after that of Malvern (9). The boundary conditions in the theoretical model incorporated the stiffness and mass of the gauges at the ends of the specimen used in the experiments.

The results of the analysis showed that it is possible to obtain excellent agreement between the theory and experimental values of peak impact stress in sands over a range of impact velocities from 20 to 100 ips without the use of lateral inertia effects. This does not, of course, disprove the lateral inertia hypothesis, but it does indicate that there are other possible explanations of the observed phenomenon. The author points out that the strain-rate theory is not a

physical theory and no hypothesis concerning the origin of strain-rate sensitivity in dry sands is proposed. Proof of the existence of strain-rate effects in sand would give further support to the Parkin approach. In fact one might question the discard of the lateral inertia phenomena that are known to exist in reality, for a strain-rate mechanism whose significance has not been established.

Whitman, in a discussion of Parkin's paper (18) presents two reasons for the occurrence of the initial stress peak at the impact end of the sand column. The first is due to the frictional restraint of the impacting mass to lateral expansion of the soil column. Until the wave travels several diameters along the specimen, the sand acts as though it were confined by the friction. The second is due to lateral inertia which effectively increases the specimen confining pressure. Thus, at high enough impact velocities the stress should rapidly rise to a value above the static strength and then decrease to the static value after the lateral expansion has had time to take place. This is exactly the behavior observed in the tests. Approximate calculations of the time required for the lateral inertia effects to dissipate gave a range of 0.1 to 0.4 msec. The actual recorded decay times for the stress peak were around 0.4 msec.

Locking Materials

The concept of a "locking material" has been applied to plastic wave propagation in materials. Ideal locking materials were introduced by Prager (19,20) who considered the material to have properties such that beyond a certain strain, stress increase occurred without further increase in strain. Examples of idealized locking materials are shown in Figure 12.

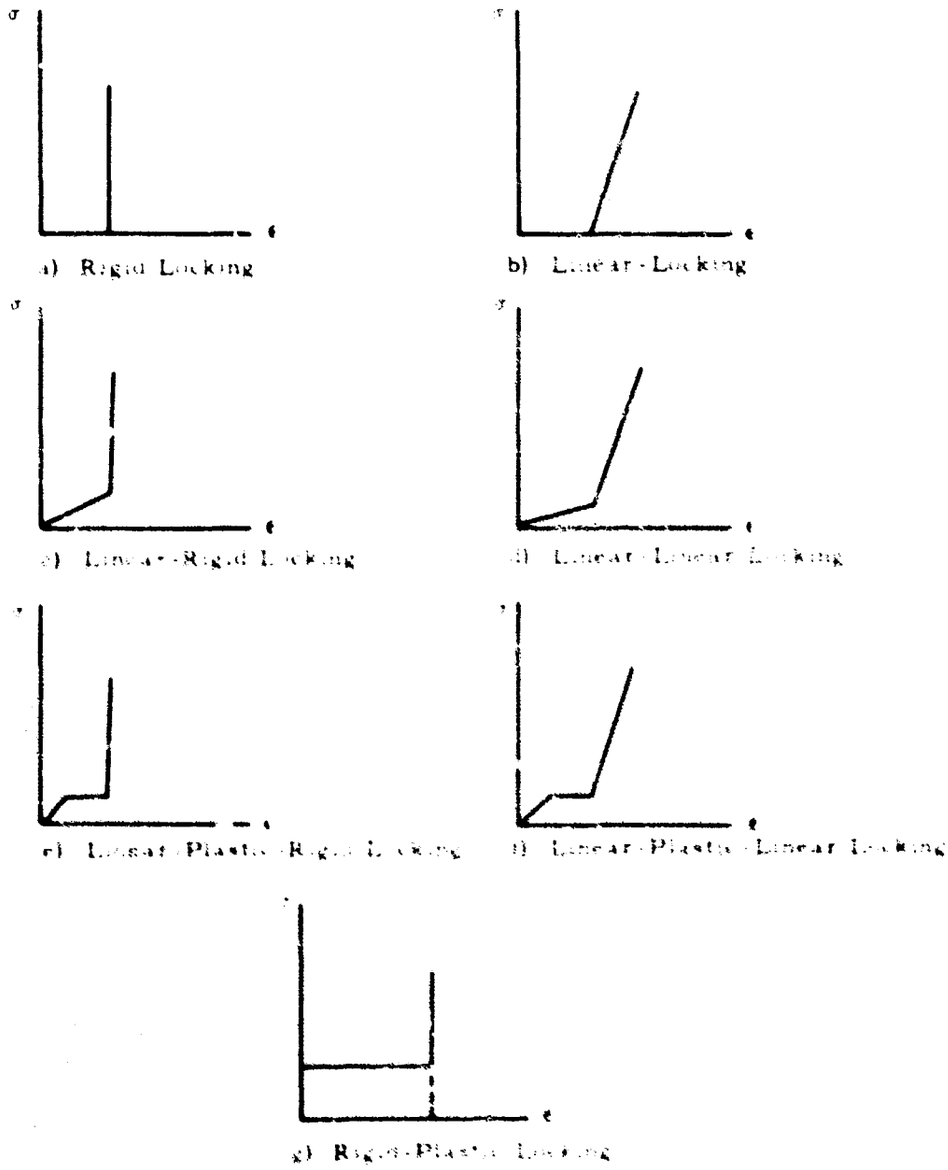


Fig. 12 Idealized Locking Materials

Salvadori, Skalak and W. idlinger (,21,22) have developed equations for the propagation of waves and shocks in locking and dissipative media. The first material considered has the stress-strain characteristics shown in Figure 13. For an applied stress pulse in which the peak stress is greater than p_{cr}, supersonic shock waves will be generated, with the material ahead of the front being in the undisturbed state (density = ρ_i) and the material behind the front compacted into a rigid body of density ρ_c. For peak stress between σ_o and p_{cr}, a subsonic compaction front will develop preceded by an elastic precursor. Elastic waves will be generated for values of stress below σ_o.

A numerical example is given for an applied pressure pulse of the form (Figure 14)

$$P = \frac{p(t)}{p_o} = e^{-\tau} \qquad (11)$$

where P is the non-dimensional pressure, τ is the non-dimensional time and p_o is peak applied pressure. The stress σ at any distance z from the loaded surface will also decay exponentially in the compacted region. In Figure 14, τ_s is the time when σ has decayed to σ_o, and τ_e is the time when σ has decayed to σ_{cr}, at which time compaction ceases.

The position of the various fronts as a function of time is shown in Figure 15. From the results given by the authors, the stress-time history at various distances from the loaded surface has been calculated. These curves are shown in Figure 16 in non-dimensional form. At time τ_s and elastic precursor of constant stress separates out of the wave front leaving a decaying subsonic wave behind. The step in the stress pulse lengthens until time τ_e at which time compaction is complete. After this time the system behaves as a rigid mass (the compacted layer) on a semi-infinite elastic medium. A definite attenuation is caused by non-recoverable compaction. Throughout the propagation, however, the wave front remains a shock front.

The second type of medium considered by Salvadori et al (21) is characterized by the stress-strain diagram in Figure 17. Initial loading occurs along the path OA, unloading occurs along the steeper line AB, and reloading follows the path BAC. The solution is carried out for small strains so that the density may be considered constant.

The loading portion of any wave in such a material will propagate without distortion following the behavior expected in a linear-elastic material with a velocity $c_c = \sqrt{E_o/\rho}$. The unloading portion of the wave will propagate at a velocity $c_1 = \sqrt{E_1/\rho}$. The particle velocity and stress also obey the elastic wave equations because the unloading stress-strain curve is linear. However, displacement and strain are not governed by this equation because the stress-strain curve is offset from the origin.

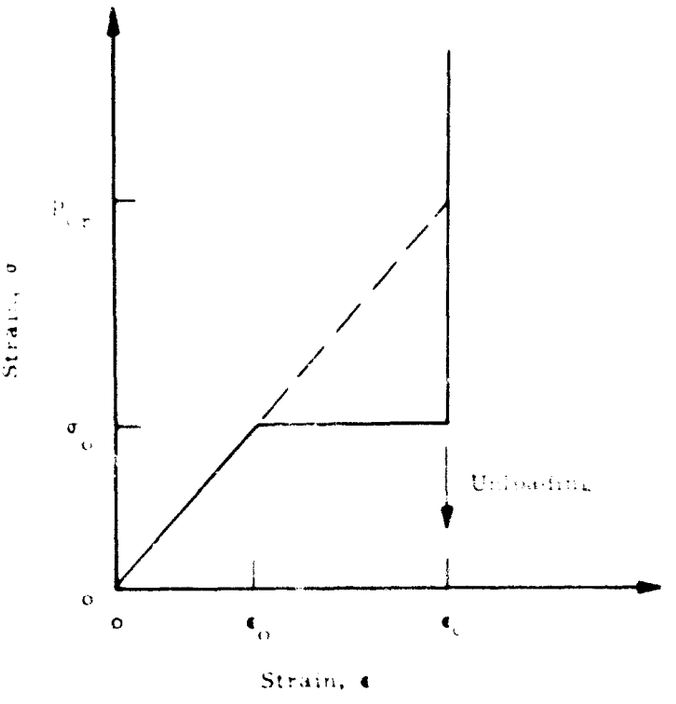


Fig. 13 Linear-Plastic-Rigid Locking Material (21)

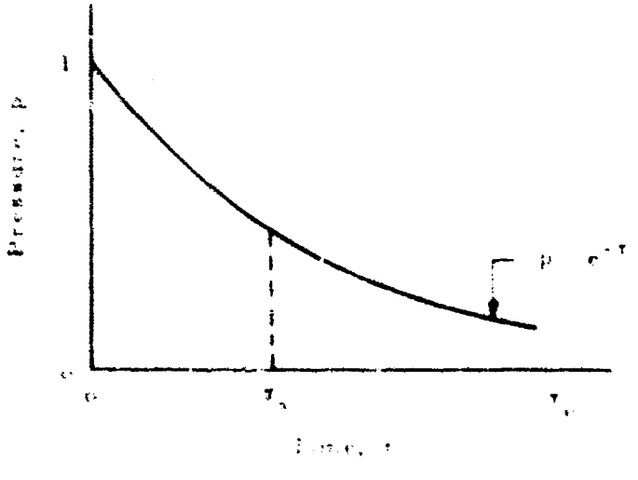


Fig. 14 Applied Pressure Pulse (21)

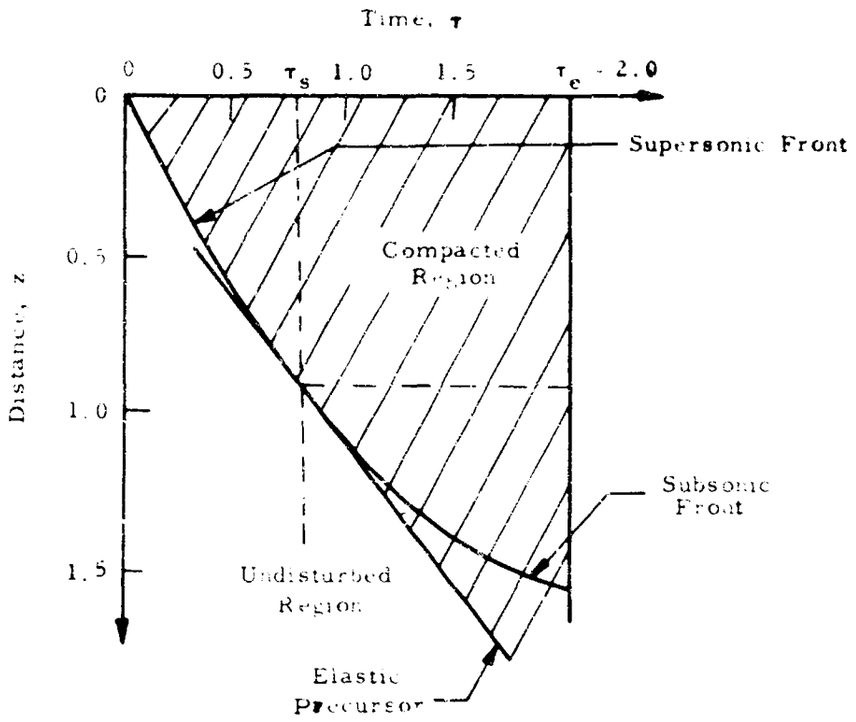


Fig. 15 Position of Waves in Locking Material (21)

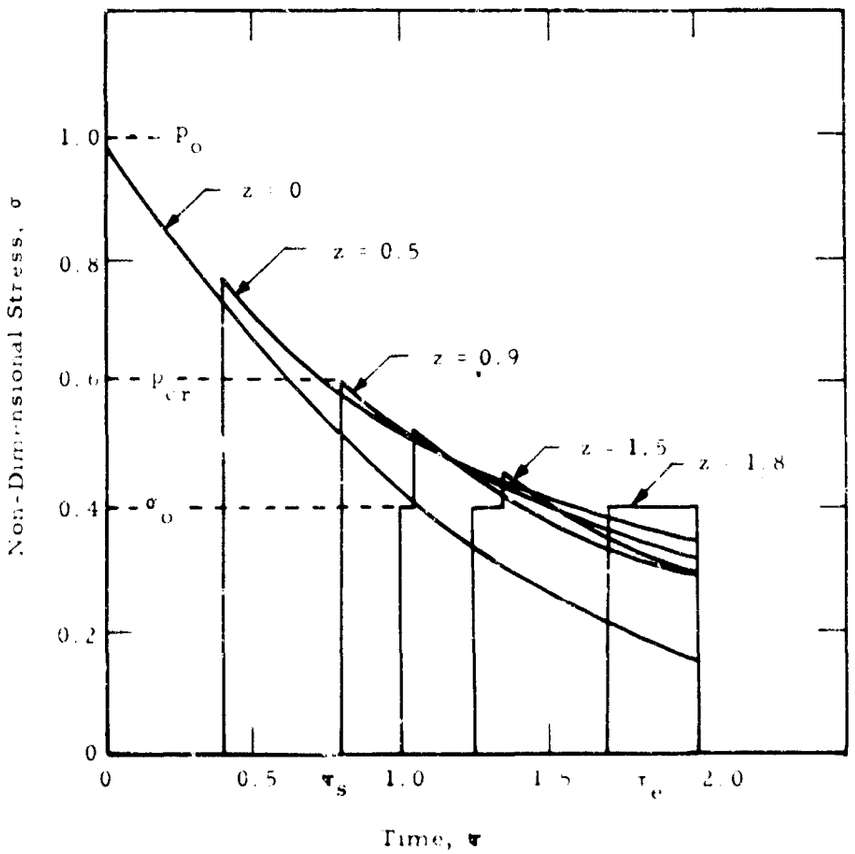


Fig. 16 Waves in Locking Material Under Exponentially Decaying Load (21)

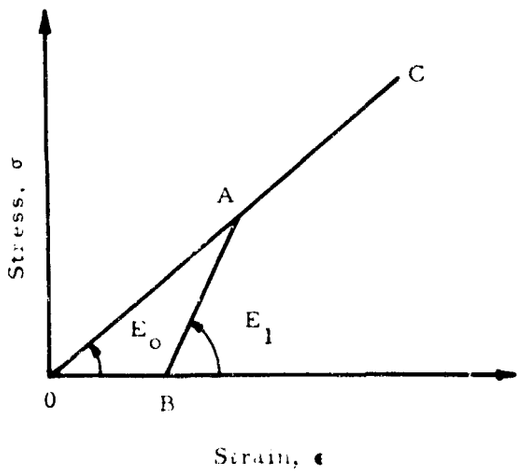


Fig. 17 Stress-Strain Diagram for Dissipative Media (21)

Since velocity c_1 is greater than c_0, the unloading wave will overtake the loading wave. There will thus be a continuous reflection process each time two such waves meet.

A numerical example was calculated for the case of a surface pressure with an instantaneous rise and an exponential decay with time. The variation with time of the peak stress at the traveling wave front is given in Figure 18 for the three cases: 1) unloading modulus equal to loading modulus, i.e., elastic behavior, 2) unloading modulus equal to twice the loading modulus, i.e., partial elastic recovery, and 3) infinite unloading modulus, i.e., no elastic recovery.

The stress wave (in this case a shock wave) propagates with the same general shape in all cases, i.e., instantaneous rise and exponential decay. For the elastic case there is no attenuation for the peak stress. For the inelastic cases appreciable attenuation occurs, increasing with increasing unloading modulus, until eventually the generated stress wave is completely absorbed. The material through which this wave has propagated is thus called a dissipative medium.

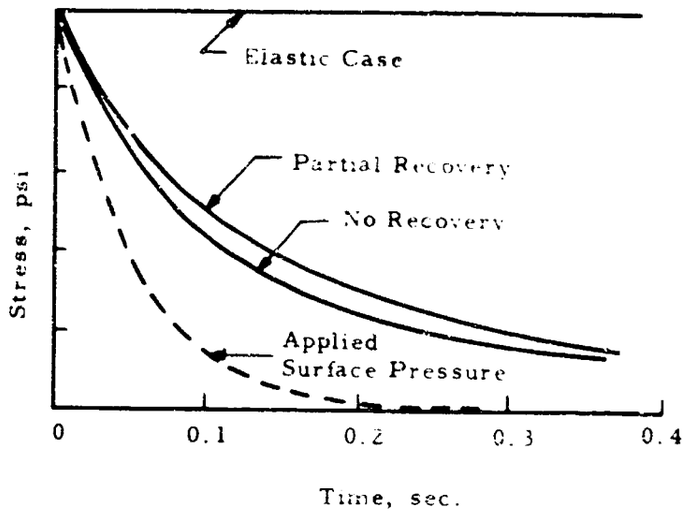


Fig. 18 Attenuation of Peak Stress at Wave Front for Dissipative Materials (21)

Skalak and Weidlinger (22) have extended their previous work on one-dimensional wave propagation to the case of a bilinear material subjected to an exponentially decaying pressure pulse on its free surface. This problem can be solved by the method of characteristics. The stress-strain diagram for this material is shown in Figure 19. Up to stress σ_0 the material compacts, exhibiting an increased modulus, and it unloads along this steeper path. As the modulus of the compaction portion of the stress-strain diagram increases, this material become a locking medium. The results of this analysis are similar to those given for the previous examples. Increasing the modulus of the compaction portion of the stress-strain curve relative to the elastic portion results in a greater attenuation of peak stress and particle velocity.

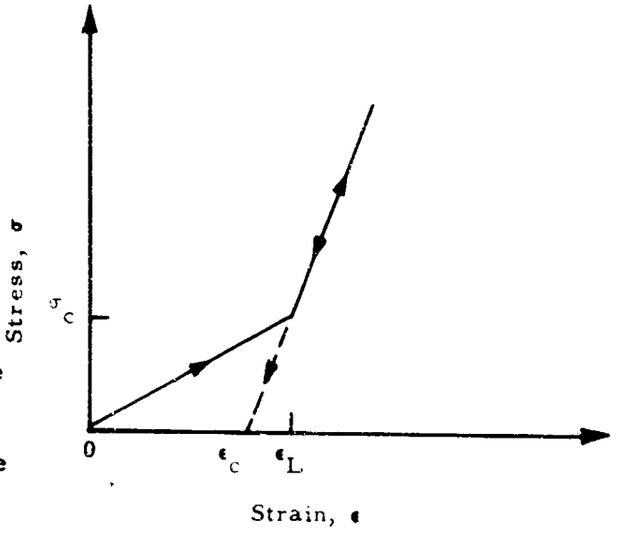


Fig. 19 Bilinear Stress-Strain Diagram (22)

General Nonlinear, Inelastic Materials

The general solution for wave propagation in nonlinear, inelastic materials cannot be solved by the method of characteristics because of the indeterminacy at points where loading and unloading waves meet. Heierli (23,24) has developed an alternative approach for one-dimensional problems which may be used with arbitrary applied pressure pulses, stress-strain characteristics and boundary conditions. This approach, which may be called "method of impulses," involves dividing the applied pressure pulse into a finite number of steps containing a certain amount of impulse.

The method of deriving the equations of conservation of mass and momentum for a region of the material acted on by a step change in pressure is shown in Figure 20. The step change in stress is Δp_{i+1} which moves from position x to $x + \Delta x$ in time Δt. The particle velocities before and after the change are u_i and u_{i+1} respectively. The Eulerian coordinate system is used which means that the position x is attached to the moving particle.

From the condition of conservation of mass the following equation is obtained:

$$\Delta\epsilon_{i+1}\,(\,x_{i+1} + u_i\,\Delta t_{i+1}) = \Delta u_{i+1}\,\Delta t_{i+1} \qquad (12)$$

From conservation of momentum

$$\Delta p_{i+1}\,\Delta t_{i+1} = \rho_i\,\Delta x_{i+1}\,\Delta u_{i+1} \qquad (13)$$

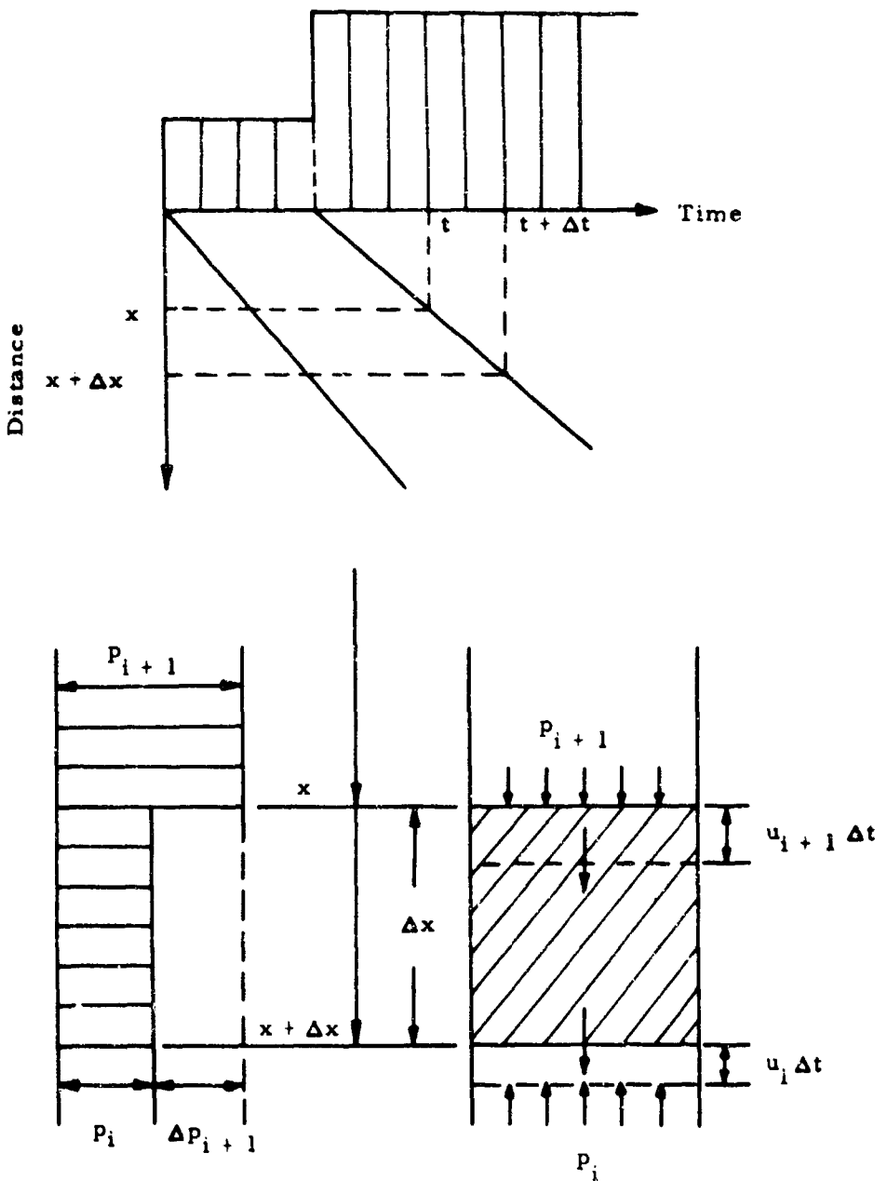


Fig. 20 Propagation of Loading Waves (23)

where ρ_i is the mass density. The stress-strain relationship is given by

$$\Delta p_{i+1} = T_{i+1} \Delta \epsilon_{i+1} \tag{14}$$

where T_{i+1} is the secant modulus or slope of that portion of the stress-strain diagram extending from p_1 to Δp_{i+1}. Combining Eq. 12 and 14 to eliminate $\Delta \epsilon_{i+1}$ gives

$$\Delta p_{i+1}\left(\frac{\Delta x}{\Delta t} + u_i\right) = \Delta u_{i+1}\ T_{i+1} \tag{15}$$

Now the absolute velocity of the step impulse is the quantity in parentheses which will be denoted c'_{i+1}. Combining Eq. 13 and 15 to eliminate Δu_{i+1} and solving for c'_{i+1} gives

$$c'_{i+1} = \frac{u_i}{2} \pm \sqrt{\frac{u^2_i}{4} + \frac{T_{i+1}}{\rho_i}}\ , \text{ where} \tag{16}$$

the $\pm$ signs designate waves traveling in the positive and negative directions respectively. If it can be assumed that u_i is small with respect to T_{i+1}/ρ_i so that u^2_i can be neglected with respect to T_{i+1}/ρ_i the equation reduces to

$$c'_{i+1} = \frac{u_i}{2} \pm \sqrt{\frac{T_{i+1}}{\rho_i}} \approx \pm \sqrt{\frac{T_{i+1}}{\rho_i}} \tag{17}$$

Finally from Eq. 13 an expression for u_{i+1} may be obtained in terms of known quantities:

$$\Delta u_{i+1} = \frac{\Delta p_{i+1}}{\rho_i\left[\frac{-u_i}{2} \pm \sqrt{\frac{u^2_i}{4} + \frac{T_{i+1}}{\rho_i}}\right]} \tag{18}$$

which may be simplified when $u^2_i \ll T_{i+1}/\rho_i$ to

$$\Delta u_{i+1} = \frac{\Delta p_{i+1}}{\rho_i\left[\frac{-u_i}{2} \pm \sqrt{\frac{T_{i+1}}{\rho_i}}\right]} \approx \frac{\Delta p_{i+1}}{\sqrt{T_{i+1}\rho_i}} \tag{19}$$

Using Eq. 16 and 18 or the simplified versions 17 and 19, the loading and unloading waves can be evaluated in nonlinear homogeneous material.

Because the velocity of the unloading waves is greater than the velocity of the loading waves the two will eventually meet causing an impact which will generate a subsequent reflection (Figure 21). The changes which occur in this situation must also be evaluated. After impact the stresses and particle velocities in the region between the reflected waves (shaded area in Figure 21) must be equal. The procedure for calculating the proper stress and particle velocity is as follows:

1. Assume values of Δp_{i+1} above and below the impact point which satisfy the condition that the total stresses are equal.
2. From the stress-strain diagram determine T_{i+1} above and below.
3. Compute Δu_{i+1} above and below and from these values determine the total particle velocity above and below.
4. Continue this process by iteration until the equality of stresses and particle velocities is satisfied with sufficient accuracy.

It should be noted that a nonhomogeneity has been generated at the point of impact because the stress-strain history of the material above and below this point is different. Subsequent waves may be reflected and refracted from this surface. Such occurrences can be handled in the same manner as the impacting of two waves.

Another situation of interest is the reflection of waves from boundaries in the material. If the boundary conditions can be prescribed in terms of either stress or particle velocity then the same method may be used for analyzing this condition as is used for the impacting of loading and unloading waves.

Although the procedure described above may be time-consuming to carry out, especially if small time intervals are required for the impulse steps, the procedure is straight forward and is suited to a wide variety of one-dimensional problems. A number of examples were given by Heierli to demonstrate the application and suitability of the method.

DESCRIPTION OF EXPERIMENTS

Soil

A uniformly graded, dry Ottawa sand was chosen as the soil to be investigated in the wave propagation experiments. The particles were generally well rounded and lie within the range of 20 to 40 mesh. The relationship between the relative density (D_r), void ratio (e), porosity (n) and specimen density is given in Figure 22. The values of maximum static deviator stress obtained from triaxial tests are shown in Figure 23 as a function of specimen density and confining pressure.

For several triaxial specimens a deviator stress equal to approximately 1/2 of the maximum value for the existing confining pressure and density was applied and removed several times in succession and then the specimen loaded to failure. Two moduli of deformation were determined for each cycle: the initial tangent modulus and the secant modulus. The secant modulus has been taken as the slope of the line connecting the end points of each cycle. The values obtained are shown in Figure 24. In general both moduli tend to increase under repeated loading with by far the most significant change occurring between the first and second cycles.

Pendulum

Pendulum impact apparatus was constructed for use in stress gauge calibration as well as for obtaining information on the dynamic stress-strain and strength characteristics of the sand (25). The apparatus (Figure 25) basically consisted of a steel reaction pendulum with soil specimen attached and a second steel pendulum for impacting the specimen. The specimen was either 4 or 8 in. long and 2.8 in. in diameter. The sand was contained in a thin rubber membrane and laterally constrained by a vacuum applied to the pores.

In operation the pendulums were first lined up at the bottom of their swing with the specimen between them. The impact pendulum was then pulled back to a predetermined height and then released to strike the specimen. The acceleration of the two pendulums was recorded throughout the duration of impact. Since the masses of the pendulums were accurately known, the average stress over the ends of the specimen could be computed using the products of the pendulum mass per unit cross sectional area and its acceleration. Since the impacting pendulum was free-swinging prior to impact the impact velocity could be readily calculated from the initial height of the pendulum.

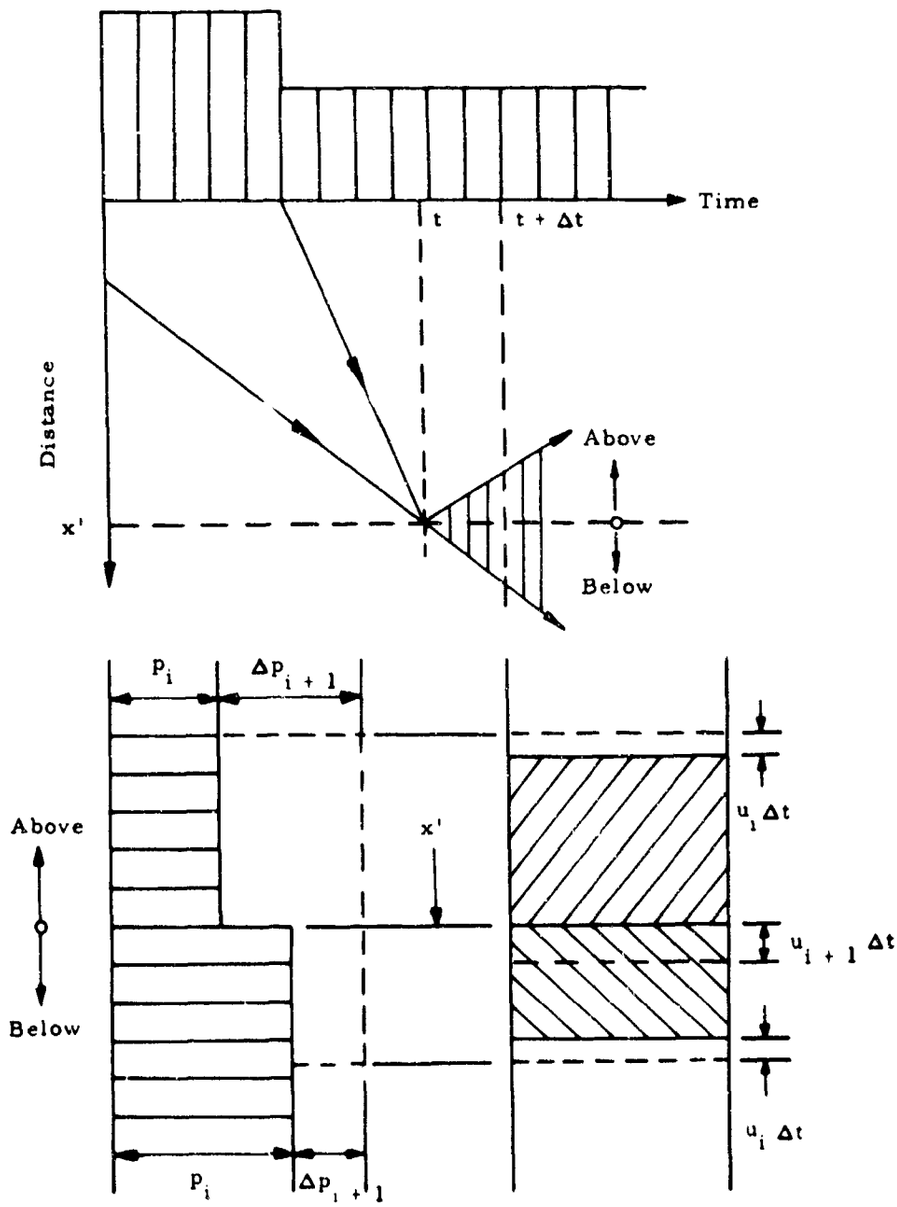


Fig. 21 Propagation of Unloading Waves (23)

Wave Propagation

A schematic diagram of the apparatus for the shock wave experiments is shown in Figure 26. An air shock tube was used to apply a controlled dynamic load to the end of the soil column. The induced shock wave in the soil traveled down the soil column and was recorded at several points by means of embedded stress gauges. There were two important advantages of the shock tube loading: 1) it provided a dynamic loading with essentially zero rise time, and 2) it gave a reproducible load which was independent of specimen response.

The sand specimen was 64 in. long and 2.8 in. in diameter. It was mounted horizontally outside of the shock tube with one end extending into a 2.8 in. diameter hole in the tube. This column was covered on the sides and on the impact end by a thin rubber membrane and constrained by applying a vacuum to the voids. The sand was separated from the air in the shock tube by two 0.008-in.-thick rubber sheets with a thin fabric reinforcement between them. There was enough slack in the material to provide at least a 1/4-in. axial movement of the end of the specimen with no restraint from the membrane.

The specimen was supported along its length by flexible straps (Figure 27). A rigid support block was positioned at the reaction end of the specimen against the end cap and the two were bolted together. The hydrostatic pressure confining the entire sand column was controlled by the vacuum level in the voids of the sand applied through the end cap. A pressure gauge was located at the impact end of the specimen to record the pressure-time history of the reflected shock wave which loaded the specimen.

The stress gauges used in this test series were constructed from 1/16-in.-thick by 1/2-in.-diameter peizoelectric disks surrounded by a steel edge ring (26). In order to provide accurate stress measurements the gauges were calibrated in the shock tube specimens after the specimens were in position for the dynamic tests. The calibration values (psi/mv) obtained in this manner represented the existing embedded sensitivity of the gauge at low stress levels (relative to the strength of the specimen) as influenced by such variables as confining pressure, density and placement conditions. These calibration values were then used to adjust the non-linear calibration curves obtained with the pendulum apparatus which covered the stress levels up to specimen failure.

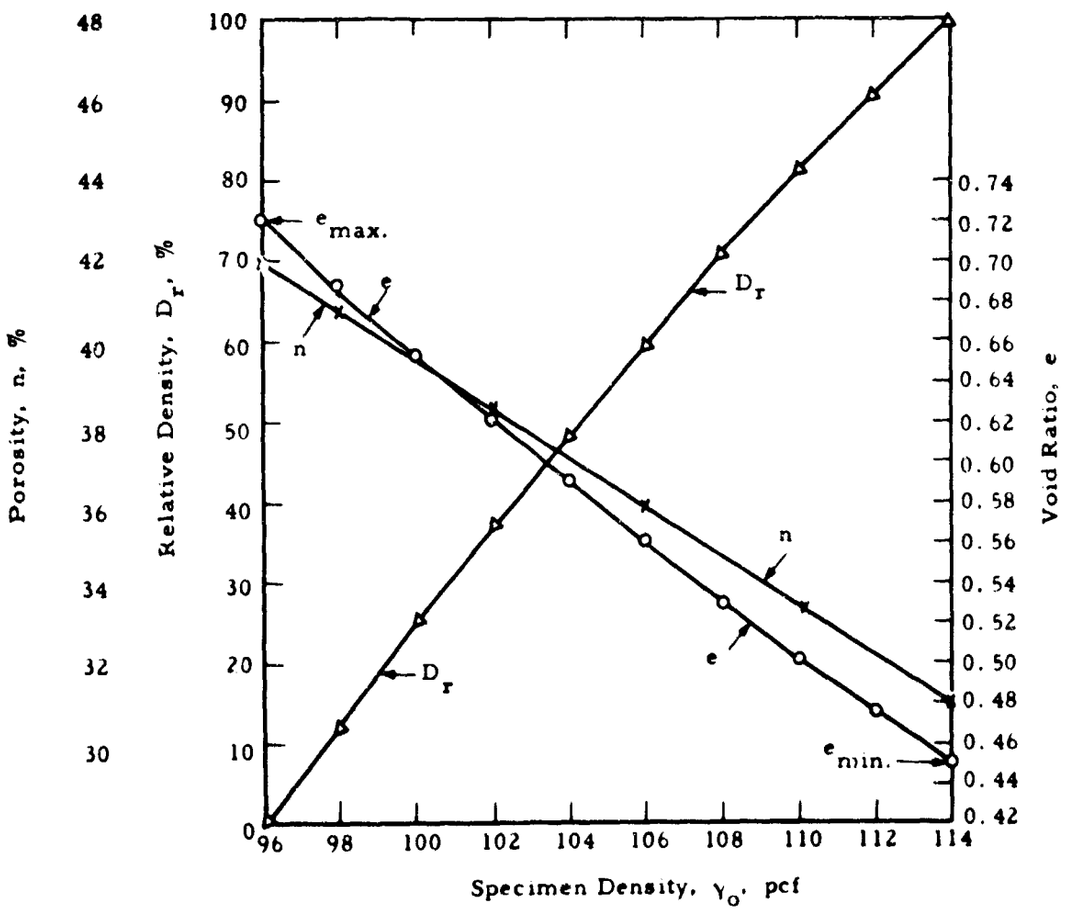


Fig. 22 Relative Density, Void Ratio and Porosity Vs. Specimen Density for Dry Ottawa Sand (20-40 Mesh).

Tests were conducted on specimens representing a range of confining pressures and densities. The applied air shock loading was varied both in magnitude and duration. Each specimen was subjected to multiple impacts with a variation in magnitude of both peak shock pressure and confining pressure. The confining pressure was adjusted to the desired value prior to each impact by regulating the vacuum in the voids of the specimen. It is expected that some change in density and stress-strain characteristics took place with each impact. After the first loading the specimen density was not accurately known because there was no sufficiently accurate method available for measuring this change. All of the test results therefore were correlated with the initial specimen density.

SUMMARY OF EXPERIMENTAL RESULTS

Pendulum Experiments

The initial peak and ultimate stresses obtained in the pendulum tests were compared with the static strength of the same specimens. There was definite evidence that dynamic stresses exceeding the static strength can be developed

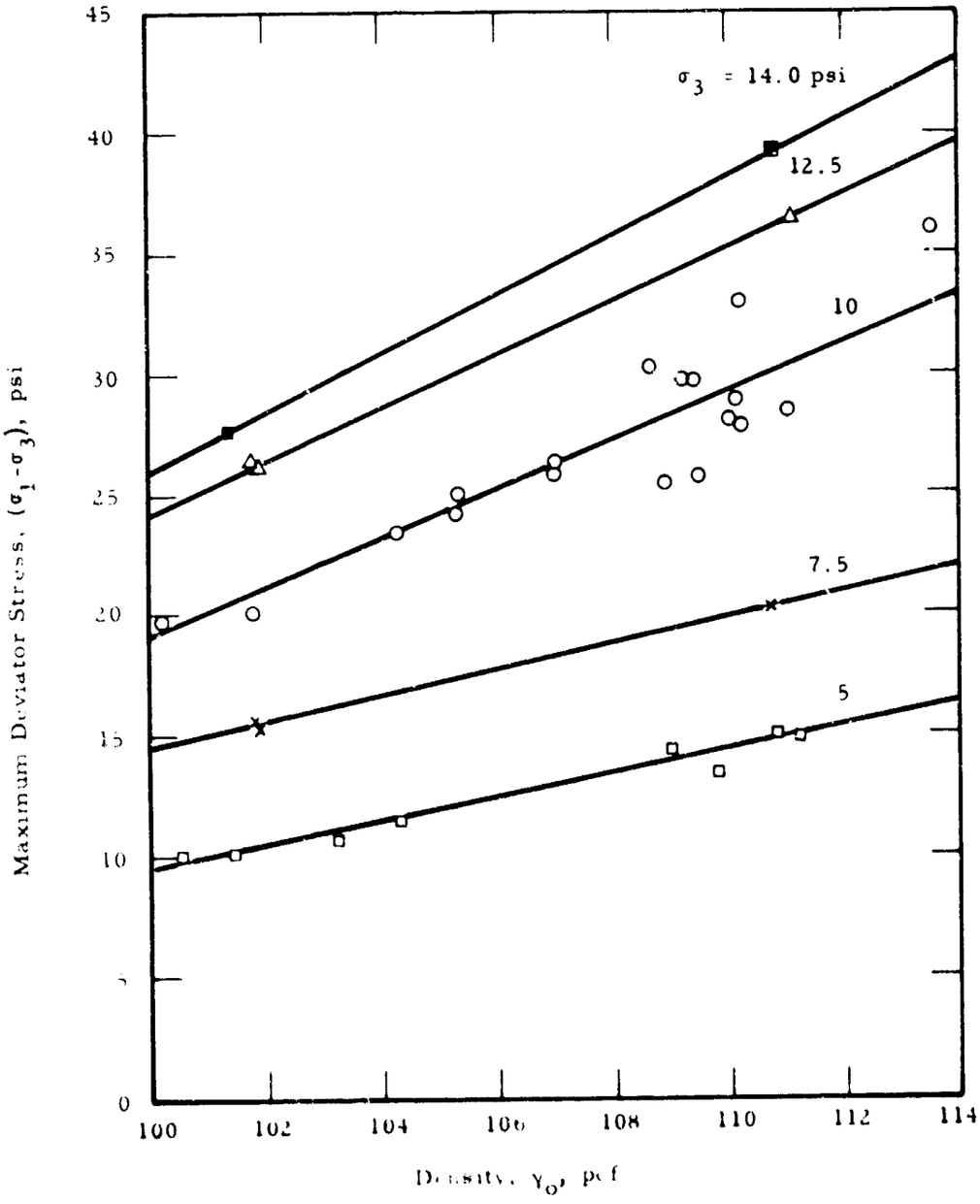


Fig. 23 Variation of Static Strength with Density at Constant Confining Pressure.

in the sand. However, except for the initial peak stresses at the impact end, the increases when they occurred averaged only 12 percent. The initial peak stresses, however, exceeded the static strength by up to 125 percent. This increase is attributed to lateral inertia and frictional restraint on the end of the specimen.

The dynamic stress-strain characteristics obtained from the pendulum tests were essentially the same as those from static triaxial tests, although there was some indication of lateral inertia and viscous effects. The increase in stress for a given strain ranged from zero to 25 percent.

Wave Propagation Experiments

The oscilloscope records from stress gauges positioned at various cross sections along the specimen show the general characteristics of the incident and reflected stress wave. Quantative information obtained from these records consisted of 1) the wave propagation velocity, 2) peak stress attenuation, and 3) change in slope of the shock front.

Specimen density, confining pressure and magnitude and duration of applied shock loading all effect the characteristics of the stress wave induced in the sand. The general nature of this wave and the effect of these factors are illustrated in Figures 28, 29, 30 and 31 by typical oscilloscope records from the test series. These records actually

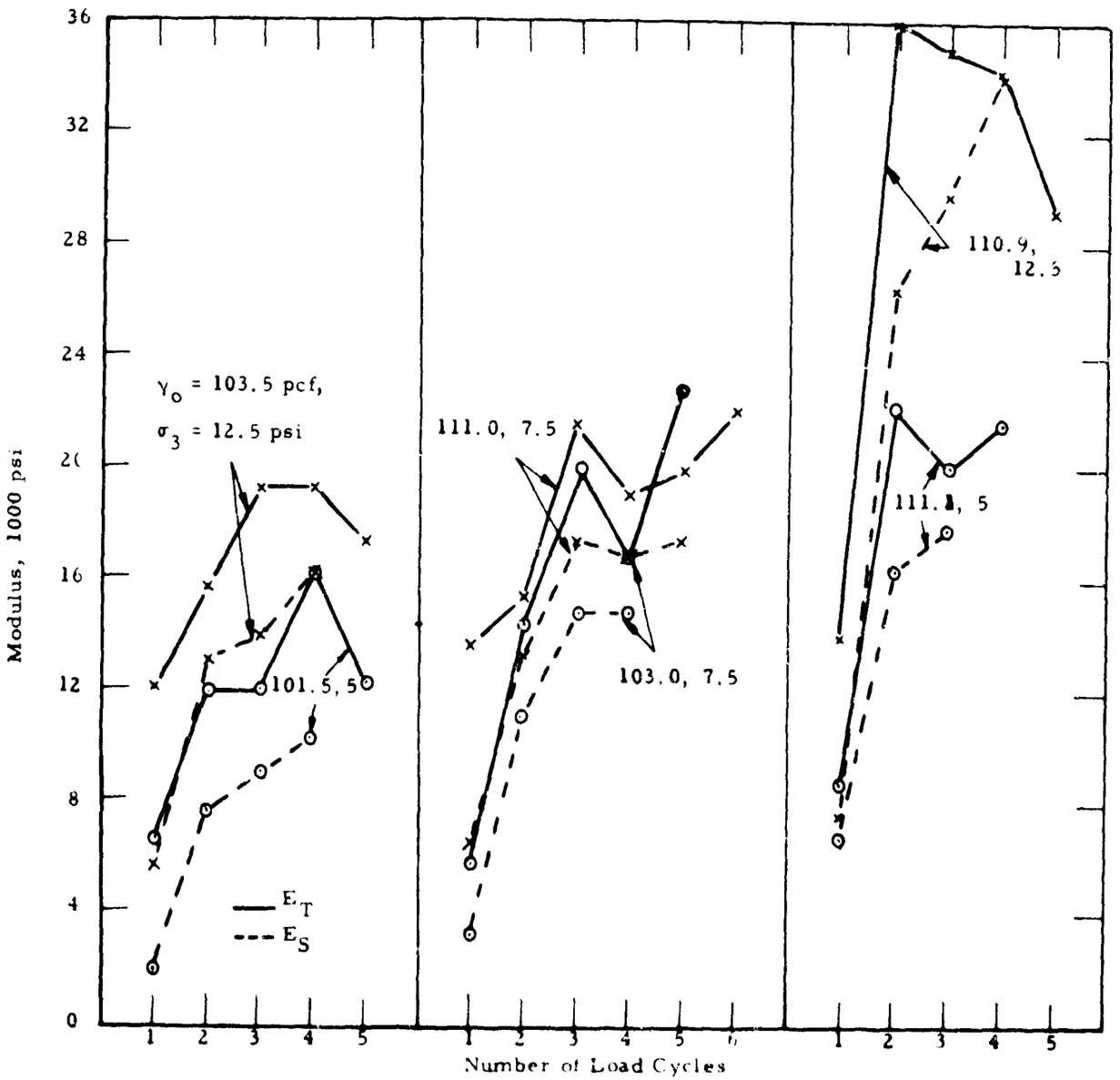


Fig. 24 Variation of Tangent and Secant Moduli with Repeated Load.

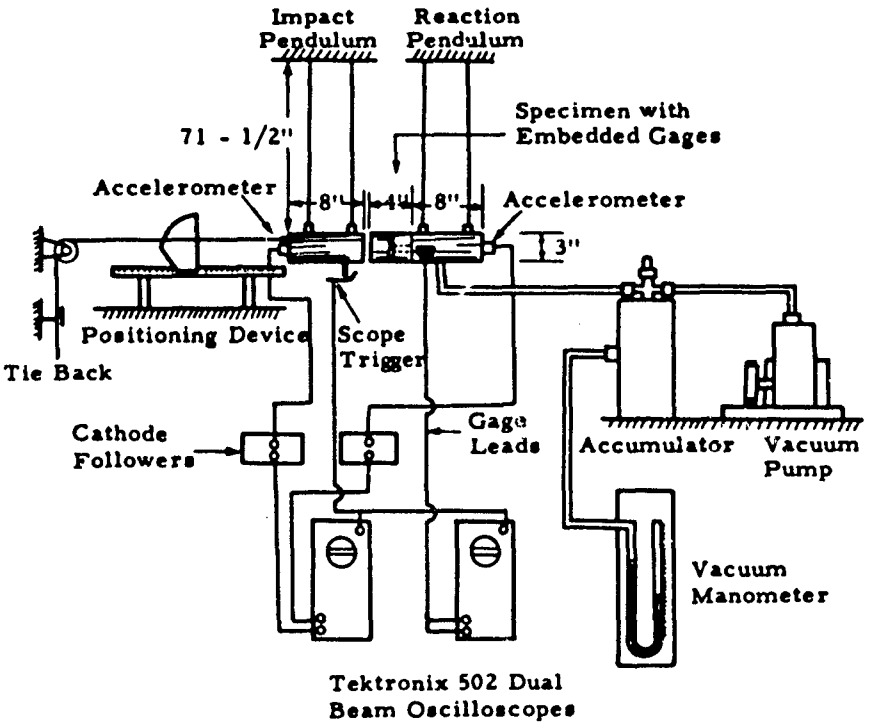


Fig. 25 Schematic of Pendulum Apparatus

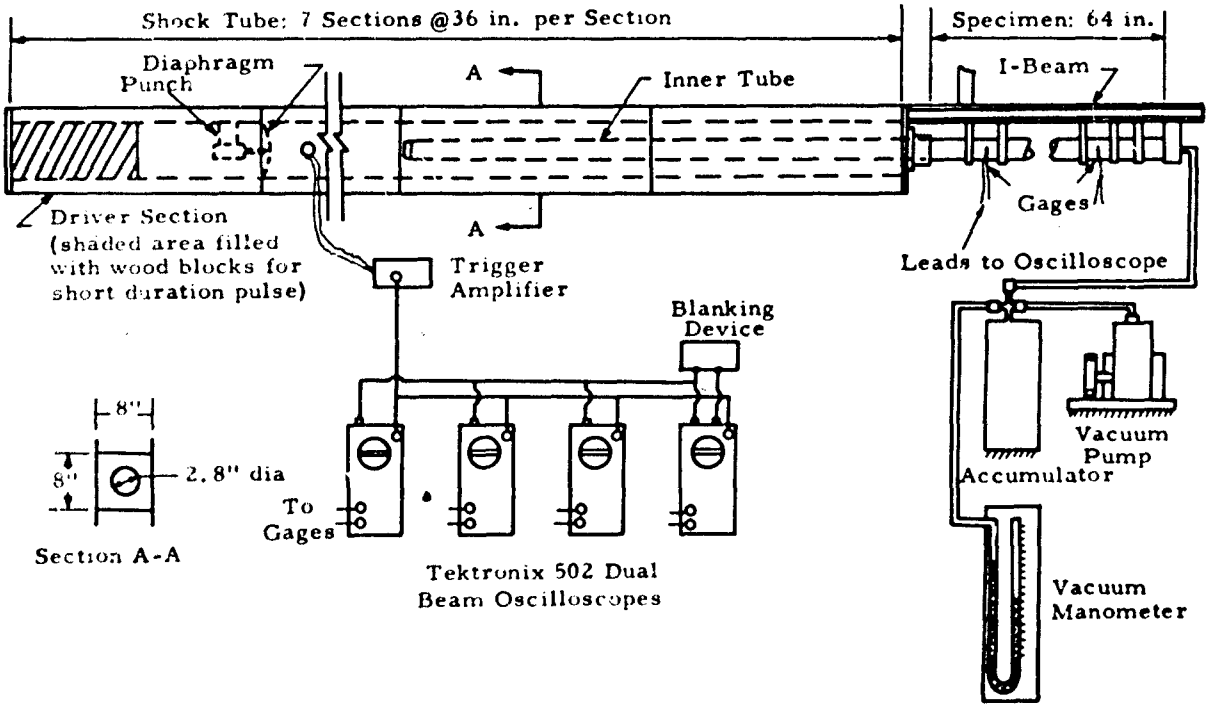


Fig. 26 Schematic of Shock Tube Apparatus

represent millivolt gauge response as a function of time. Because the gauge calibration (mv/psi) is non-linear the true stress pulse has a somewhat different shape than the oscilloscope records. The higher millivolt readings represent less stress per millivolt than the lower readings. Thus the peaks of the records will be flattened out when converted to stress.

The observed propagating waves in the sand are compared in Figure 28 for several different densities and confining pressures where the specimen were loaded with the same shock pulse. (These have been traced directly from the oscilloscope photographic records, thus the vertical scale for each record varies depending upon the gauge calibration.) The spike at the end of the applied air shock pulse is caused by a reflection phenomenon inside the shock tube. Since it does not represent a significant impulse and since it provides a convenient reference point on the wave form the shock tube was not modified to eliminate it.

Two important characteristics of the propagating wave may be observed in these records: 1) change in shape of the wave front and 2) superposition of the incident and reflected waves. A bending over of the incident wave front is clearly evident as the wave traverses the specimen. This distortion increased with a decrease in density and confining pressure for any given position along the soil column. The superposition of the reflected wave on the incident wave may also be seen at gauge positions along the specimen. This reflected wave has an increasingly greater significance with respect to the total wave form as the reflection boundary is approached. In the last record of each sequence the two waves are completely merged and form a single peak.

In Figure 29 the peak applied shock pressure was approximately equal to the static strength of the specimen. This resulted in an appreciable rounding of the wave front, increase in wave length and attenuation of peak stress. Furthermore, the reflected wave was not very pronounced.

In Figure 30 the magnitude of the peak shock pressure was approximately 70 percent of the static strength and the duration was much longer than in the previous test. The peak stress attenuation was at most 16 percent although there was still a significant rounding of the wave front. The incident and reflected waves were not very distinct and the peak point was not as sharp owing to the longer peak duration of the loading pulse.

In Figure 31, the magnitude of the applied peak air shock pressure was only 20 percent of the strength of the specimen. In this case there was no significant attenuation of the peak stress, although there was some decrease in the slope of the wave front. The reflected wave was clearly distinct and may be seen merging with the incident wave as the end of the specimen is approached.

Typical measurements of peak stress variation along the length of the specimen are shown in Figure 32. These curves show that the amount of stress attenuation increased with an increase in peak applied shock pressure for a constant confining pressure. In most cases the peak stress first decreased with distance along the specimen, reaching a minimum near the middle of the specimen and then increased as the reaction end was approached. The increase in stress toward the reaction end was due to the superimposing of the reflected wave upon the peak of the incident wave.

In several tests the peak applied pressure exceeded the static strength of the sand. In all such cases the stress had decayed below the static strength before reaching the first embedded gauge position. This required 50 percent attenuation in one case. Thus, no values of stress greater than the static strength, corresponding to the existing confining pressure and density, were recorded by any of the embedded gauges.

As another indication of the change in shape of the traveling stress wave the average slope of the wave front (psi/msec) was determined for a number of tests. This average rate of stress rise has been determined by dividing the peak stress by the time interval from the beginning of the rise to the peak. In many cases the wave front was appreciably curved; in these cases the initial rate of rise was much greater than the average rate.

Typical results are plotted in Figure 33 as a function of distance along the specimen. The slope attenuated with distance at a decreasing rate--very rapidly in the first few inches since the applied air shock had essentially an infinite slope. At any given distance along the specimen the slope was less the greater the peak applied pressure, all other conditions being approximately the same.

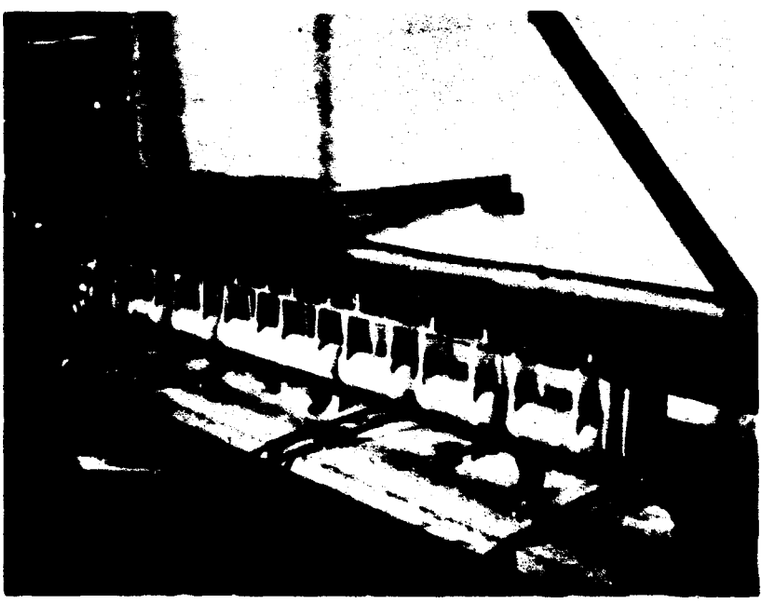
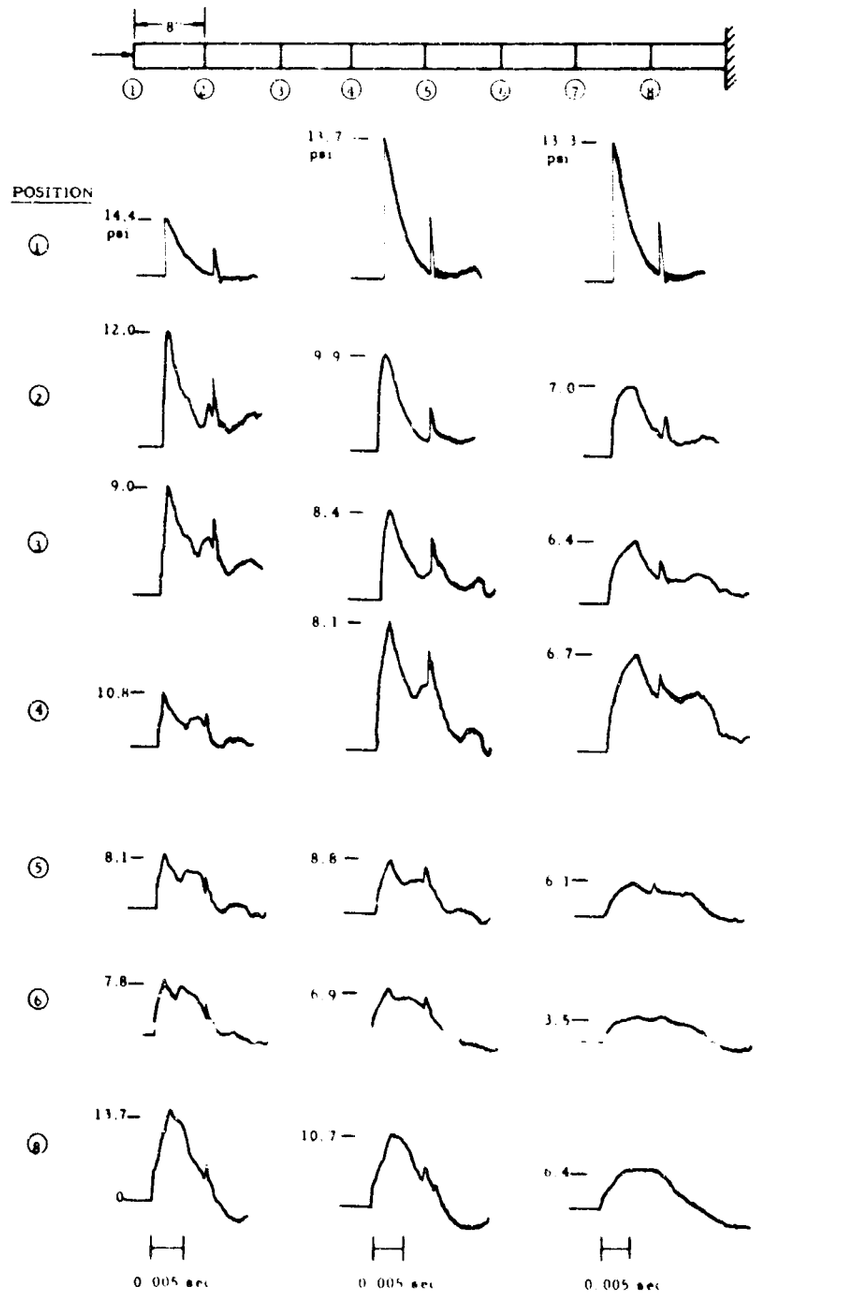
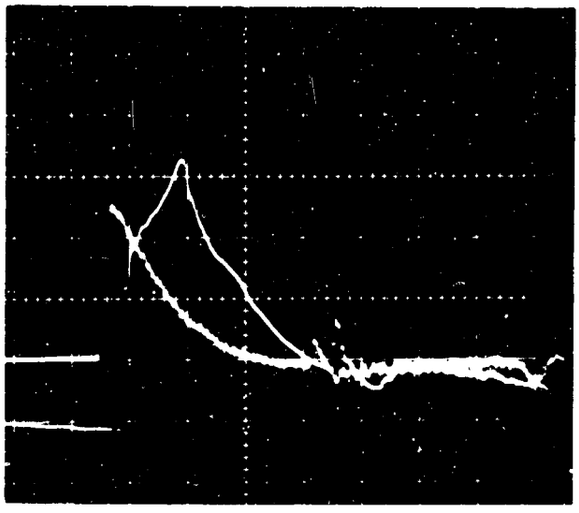


Fig. 27 Specimen in Position for Test



(a) High Density, High Confinement (b) Low Density High Confinement (c) Low Density, Low Confinement

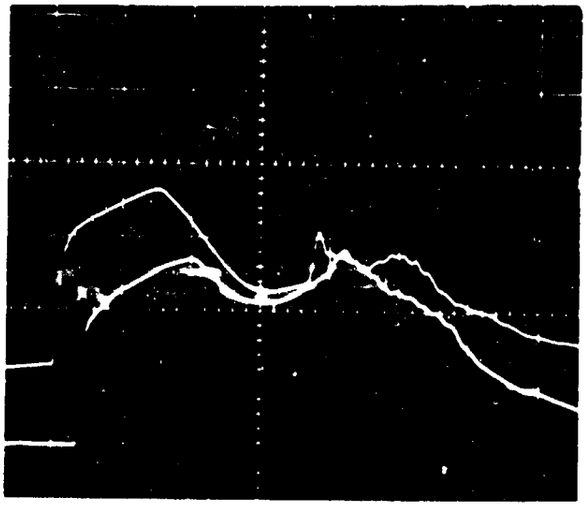
Fig. 28 Typical Shock Wave Records



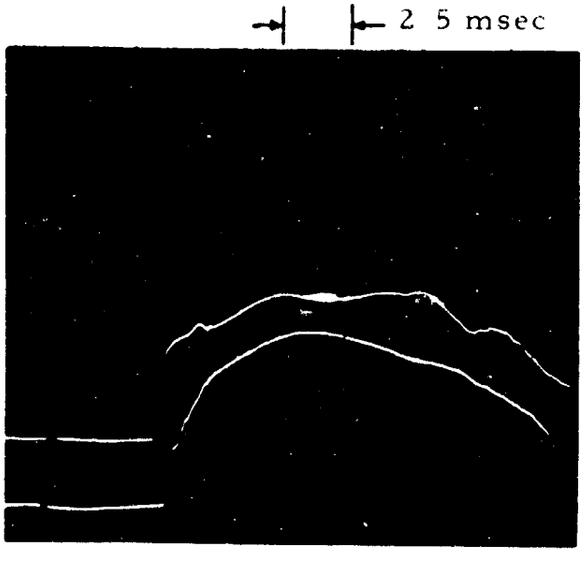
a) $x = 0$ in., $\sigma_{max} = 19.3$ psi
$x = 8$ in., $\sigma_{max} = 15.4$ psi



b) $x = 16$ in., $\sigma_{max} = 14.8$ psi
$x = 24$ in., $\sigma_{max} = 12.4$ psi

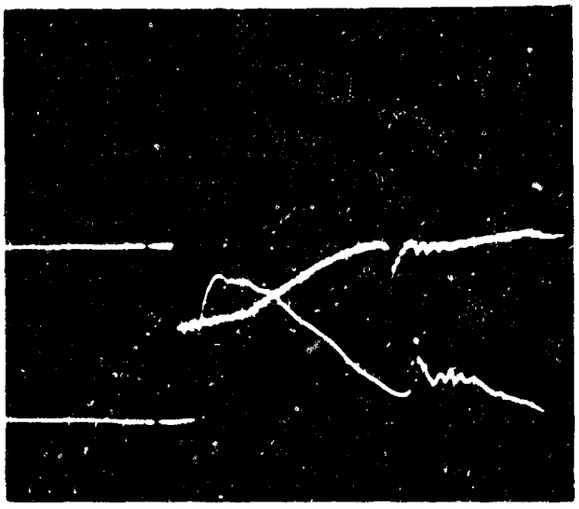


c) $x = 32$ in., $\sigma_{max} = 12.1$ psi
$x = 48$ in., $\sigma_{max} = 11.0$ psi

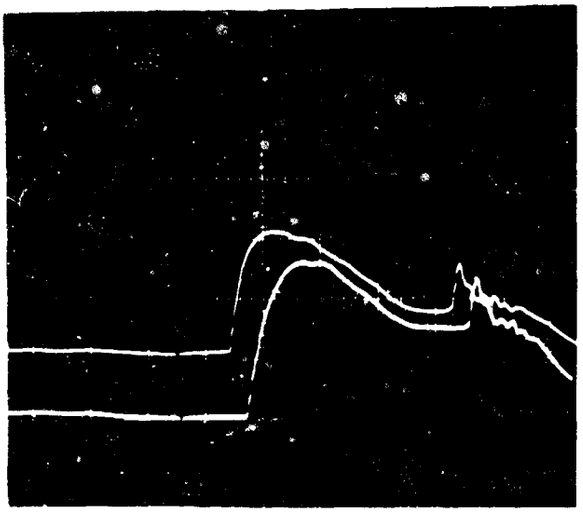


d) $x = 56$ in., $\sigma_{max} = 10.9$ psi
$x = 64$ in., $\sigma_{max} = 16.4$ psi

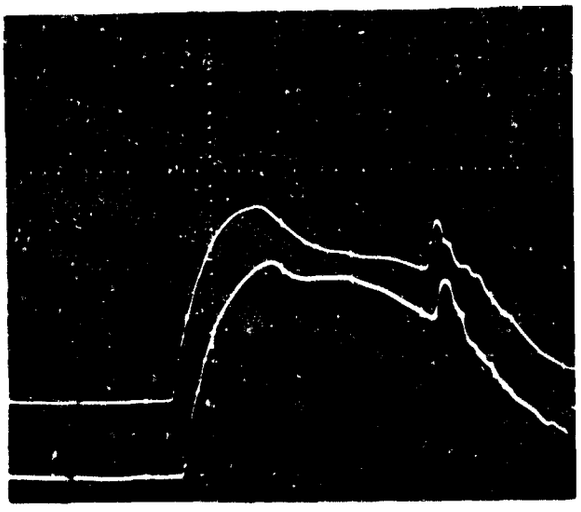
Fig. 29 Observed Stress Waves for Test 11-3
($\gamma_o = 111.0$ pcf, $\sigma_3 = 7.5$ psi)



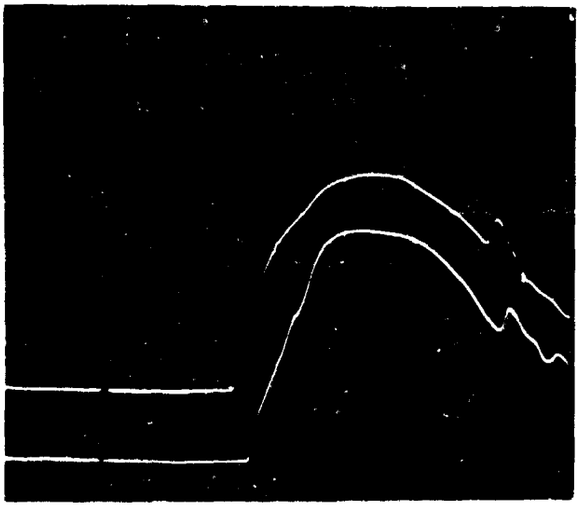
a) x = 0 in., σ_{max} = 12.6 psi
x = 8 in., σ_{max} = 11.6 psi



b) x = 16 in., σ_{max} = 10.6 psi
x = 24 in., σ_{max} = 10.6 psi

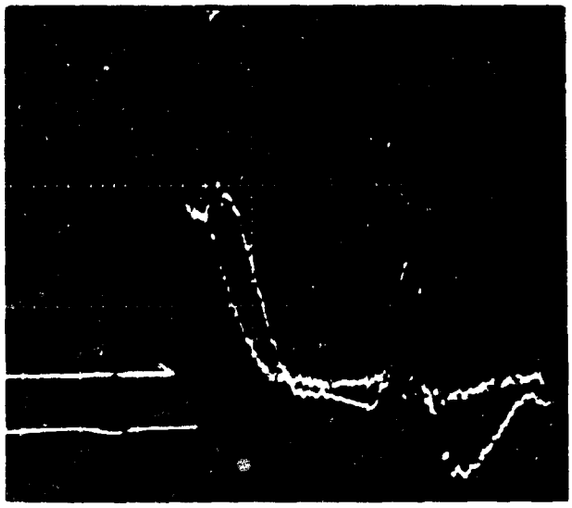


c) x = 32 in., σ_{max} = 11.3 psi
x = 40 in., σ_{max} = 11.4 psi



d) x = 48 in., σ_{max} = 13.0 psi
x = 56 in., σ_{max} = 14.4 psi

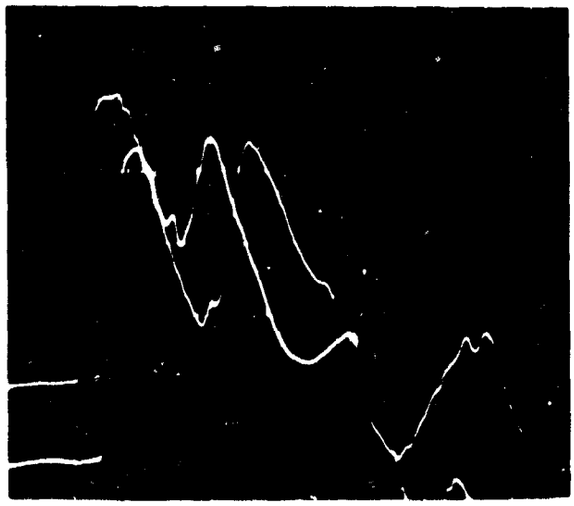
Fig. 30 Observed Stress Waves for Test 7-4
(γ_o = 107.5 pcf, σ_3 = 7.5 psi)



a) x = 0 in., σ_{max} = 4.6 psi
x = 8 in., σ_{max} = 4.7 psi



b) x = 16 in., σ_{max} = 4.7 psi
x = 24 in., σ_{max} = 4.8 psi



c) x = 32 in., σ_{max} = 4.8 psi
x = 48 in., σ_{max} = 4.1 psi



d) x = 56 in., σ_{max} = 4.1 psi
x = 64 in., σ_{max} = 4.4 psi

Fig. 31 Observed Stress Waves for Test 11-5
(γ_o = 111.0 pcf, σ_3 = 7.5 psi)

The velocity of shock wave propagation was determined for each test by plotting the time of wave arrival at each gauge as a function of gauge position. Accurate measurement of arrival time was made from the oscilloscope records using a blanking pulse superimposed upon all channels simultaneously to provide a common reference time. Typical time of arrival plots are shown in Figure 34. These plots are linear, hence the velocity was constant along the length of the specimen. The two variables effecting the velocity are confining pressure and density. A significant increase in velocity with an increase in both of these parameters was observed.

The following conclusions were drawn from the wave propagation experiments:

1. The wave propagation velocity was constant along the length of the specimen and the average velocity varied less than 14 percent for any combination of confining pressure and density, regardless of the stress history.
2. The experimental values of wave velocity based upon time of arrival measurements correlated well with values obtained by other investigators using resonance techniques. The values were much higher than those calculated using the initial tangent modulus from conventional triaxial tests except after many repeated load cycles.
3. The least change in shape of the propagating wave occurred for the highest density, highest confining pressure, smallest applied shock pressure, and longest duration of peak pressure and vice versa.
4. A reflected wave was present in all cases. It was most distinct from the incident wave and had the greatest magnitude for those conditions which created the least wave distortion, i.e., the more elastic cases.
5. The general character of wave distortion was a lengthening of the period and a bending over of the front.

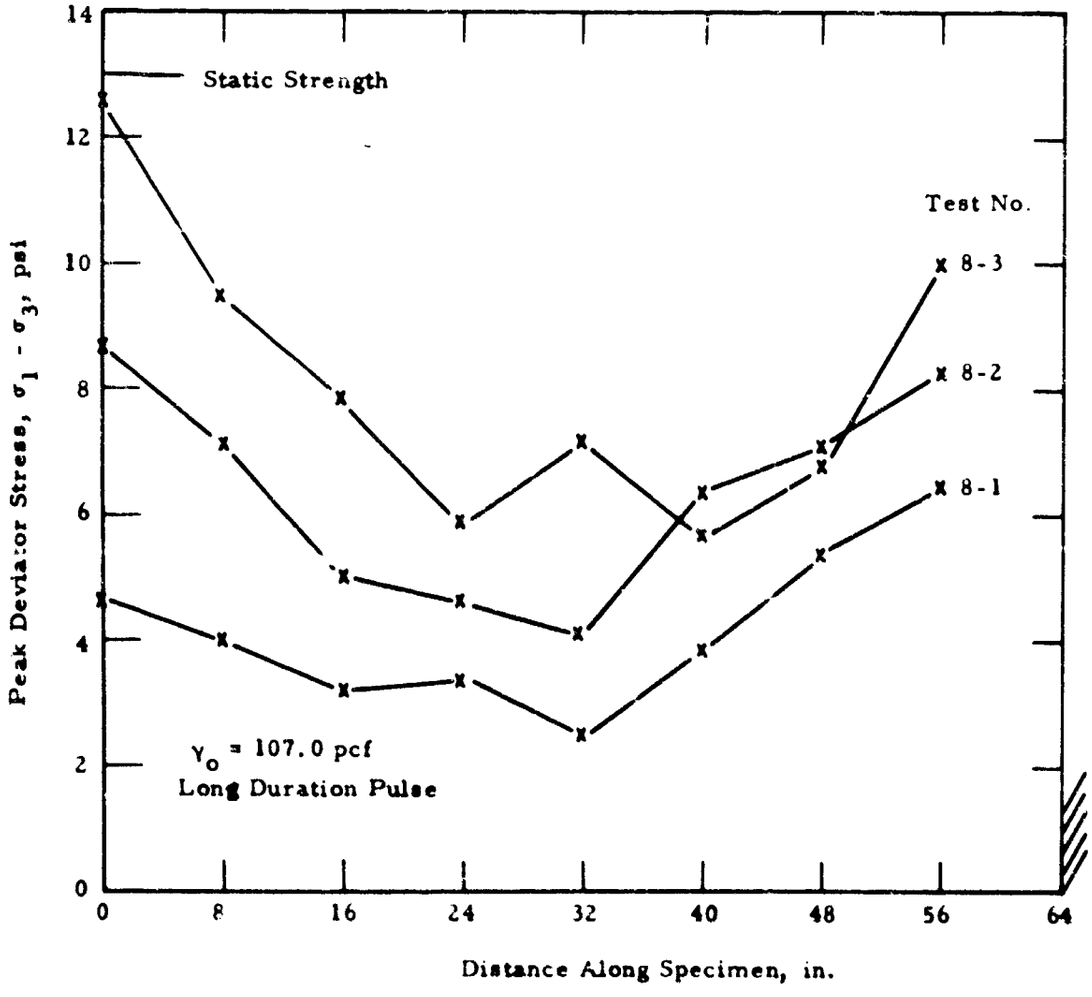


Fig. 32 Variation of Peak Stress Along Medium Density Specimen for 5 Psi Confining Pressure.

6. The peak stress attenuation along the length of the specimen increased as the peak shock pressure was increased with respect to the specimen strength and as the peak stress duration of the applied shock pulse decreased.
7. Values of stress exceeding the static strength of the specimen were not recorded eight inches from the loaded end when the peak shock pressure was greater than the strength.
8. The average rate of stress rise at the wave front decreased rapidly as the wave traveled along the specimen. Most of the reduction occurred in the first several inches.
9. This wave front attenuation increased as the peak shock pressure increased with respect to the specimen strength and as the duration of the peak pressure decreased.

CONCLUSIONS REGARDING WAVE PROPAGATION

The basic theoretical approaches for wave propagation analysis have been discussed. These are the elastic, viscoelastic, plastic, strain-rate and non-linear inelastic theories. It is important to recognize that the essential differences between these various approaches are the assumptions regarding the stress-strain characteristics of the soil. A comparison of theoretical predictions with the experimental results will therefore help to establish the true dynamic stress-strain behavior of the soil as well as help to interpret the observed wave phenomena.

The elastic approach is commonly used as a basis for comparison with other theories; however, it is clearly not adequate for explaining the observed wave propagation behavior. It does not provide an energy dissipation mechanism

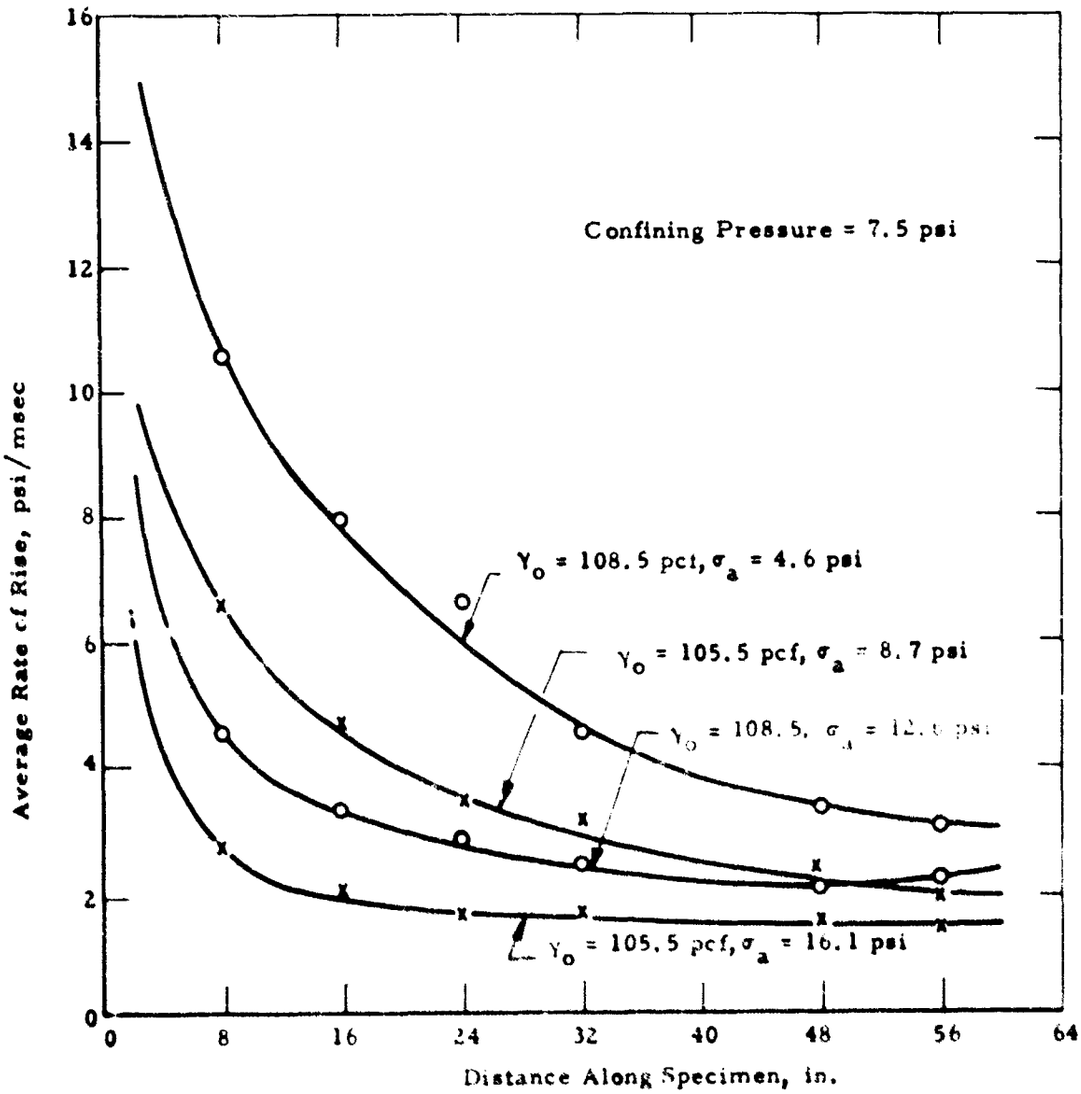


Fig. 33 Attenuation of Shock Front for Short Duration Pulse in Medium Density Specimen.

of a change in shape and attenuation of the stress wave.

The viscoelastic approach does provide energy dissipation and also results in a decay of the peak stress and a change in the wave shape during propagation. But the change in shape, at least with the linear viscoelastic model, is not like that observed in the experiments. Furthermore, the viscoelastic wave velocity increases with rate of loading. The principal reason for the discrepancy must be the difference between the viscoelastic and actual stress-strain response. Both exhibit hysteresis, but the strain is recovered in the viscoelastic case (Figure 8). Hence, although viscous-type effects have been observed in sand, this approach is not adequate by itself for explaining the observed behavior.

The plastic approach to wave propagation assumes a decrease in velocity of stress increments for negative stress-strain curvature (concave downward) as the stress level increases. This results in a spreading out of the wave front as it propagates. If inelastic recovery is included in this plastic model, then energy dissipation and stress attenuation will occur and the general change in wave form observed in the experiments will be predicted. Shocks can only be propagated with positive stress-strain curvature; hence, stress waves rather than shock waves would be predicted for the described experiments.

The actual stress-strain response of the sand specimens used in the experiments was unquestionably nonlinear and exhibited inelastic recovery. Therefore, a theory which does not incorporate these effects cannot be expected to correctly predict the wave propagation behavior. The elastic and plastic theories are in reality special cases of this more general approach. However, strain rate effects were also required in order to consistently explain the observed relationships between the static stress-strain curve, the wave velocity and the wave shape.

It was observed that the wave velocities computed from the static triaxial tests on the first loading of the specimen were much lower than the measured wave velocities. The computed velocities based upon the tangent modulus for specimens subjected to several previous load cycles approached the measured velocities. The actual wave velocities, however, varied less than 14 percent for any given confining pressure and density regardless of the stress history of the specimen. The supposition of a high tangent modulus which exists only at very low stresses cannot satisfactorily explain the discrepancy, because the propagating wave would have to have an elastic precursor or an initial reversed curvature. Neither of these were observed in the experiments. Strain rate effects were therefore assumed to be present.

In the pendulum tests, dynamic stresses at the impact end were observed to exceed the static strength by up to 125 percent. If these are attributed solely to lateral inertia then the effective increase in confining pressure would be about the same percent. Based upon the theories of granular mechanics this would only increase the wave velocity by 12 percent. These excess stresses were observed in the pendulum tests only about as far as one inch from the impact end,

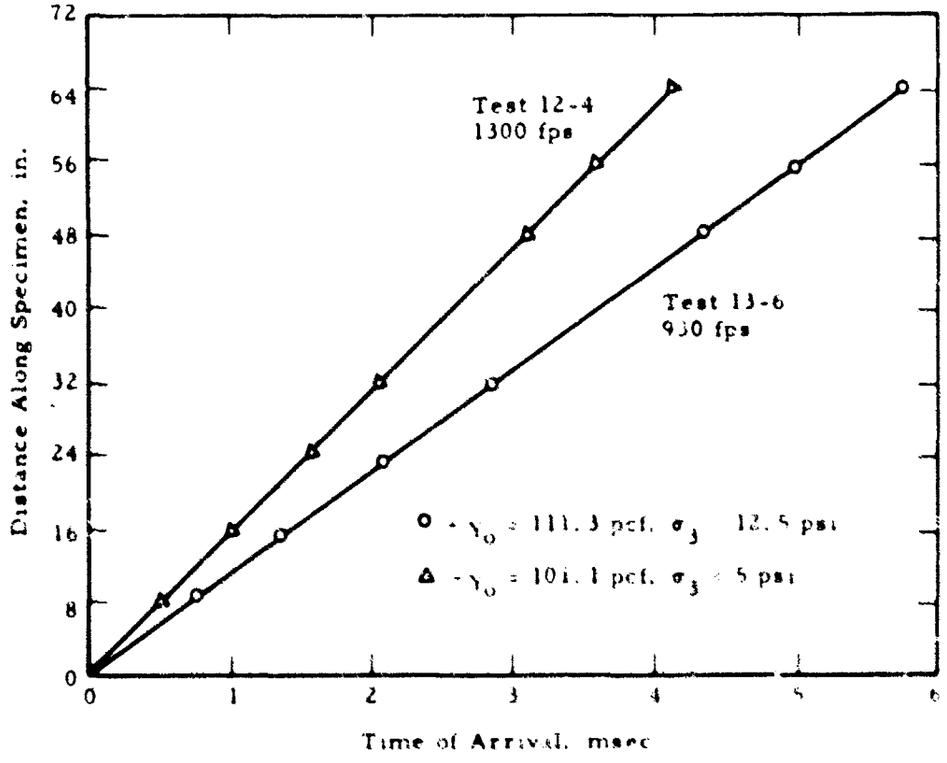


Fig. 34 Typical Shock Wave Time of Arrival Data.

and hence could have been [illegible] exceeded the static strength of the specimen the [illegible] reaching the first gauge station at 2-3 4 diameters [illegible] significantly effect the wave velocity measurements.

In order to illustrate the reasonableness of the nonlinear, inelastic theory, calculations were carried out for one of the experiments using the method of impulses. In this specific case the peak applied shock pressure was approximately 35 percent greater than the static specimen strength. For the calculations a triangular loading pulse was fitted to the actual pulse such as to maintain the same peak pressure and total impulse. The assumed stress-strain curve was obtained from the triaxial test after several repeated load cycles similar to those experienced by the long specimen. To simplify the calculations all unloading and reloading stress-strain moduli were assumed to be constant and equal to the initial tangent modulus.

The results from the theory and experiments are compared in Figures 35 and 36. The peak stress attenuation is predicted quite closely (Figure 35a). The wave front attenuation is in reasonable agreement initially (Figure 35b), although the calculated wave does not deform as rapidly as the actual wave. This is substantiated by the comparison of observed and predicted waves in Figure 36. Although the actual wave spread out more quickly than the calculated wave the general features of the two are the same. It should be emphasized that the static stress-strain curve was used without strain rate corrections to represent the stress-strain behavior of the sand during the passage of the stress wave. Hence the major factor influencing the theory was the nonlinear, inelastic response of the soil.

To illustrate the influence of the major variables a number of other examples were calculated using the method of impulses. The assumed conditions are listed in Table 1. The resulting peak stress attenuations are compared in Figures 37 and 38. The variables considered were 1) the reaction end condition, e.g., fixed or free, 2) the shape of applied air shock loading curve, 3) specimen stress-strain response, and 4) relationship of peak applied pressure to specimen strength.

The following observations were made from these comparisons:

1. There is no attenuation of peak stress for the infinite duration pulse, instead the peak stress increases with time. This increase is shown for 15 and 20 msec after arrival of the wave front at each position. A significant decrease in the rate of stress rise does occur, but it is the least of the five cases considered.
2. For cases I and III, which are identical except for the end condition, the peak stress is maintained for about 8 in. Attenuation begins at this point and is the same for both cases up to 40 in., at which position the reflected wave influences the peak stress. Beyond 40 in. the peak stress increases when the reaction end is fixed and decreases to zero when the reaction end is free. The rate of stress rise attenuates identically for both cases up to 40 in., because up to this position the wave front is not aware of the reaction boundary.
3. Attenuation of the peak stress increases more rapidly when the duration of the applied shock pressure is decreased. Within the accuracy of the computations, however, the rate of stress rise is the same as that for Cases I and III, because the time-to-peak was correspondingly decreased by the faster propagation of the lower stresses.
4. The peak stress and wave front both attenuate more rapidly as the specimen stiffness is decreased.
5. The higher the peak applied pressure relative to the specimen strength, the greater the attenuation.

The results of several experiments in which the parameters were similar to those assumed in the calculations are superimposed on Figure 37. Test 9-1 was performed on a specimen which had not been previously loaded. The results of this test agree best with the calculations using a virgin static stress-strain curve. The agreement would be improved for the initial attenuation if the duration of the assumed peak shock pressure were reduced from 2 to 1 msec, more in line with that existing in the experiment. Tests 7-4 and 8-4 were performed on specimens previously loaded 3 times, specimen 7 to a stress as high as 22.4 psi and specimen 8 to 12.6 psi. A greater stiffness is indicated by the results, more in line with the calculations assuming a stiffer specimen. The actual boundary conditions and the shape of applied shock pressure pulse were closest to those assumed by Case V.

SUMMARY

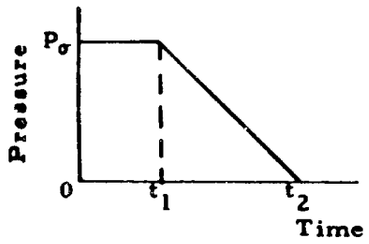
The purpose of this paper has been to review the basic characteristics of stress wave propagation in soil. The dominant influence of the soil stress-strain behavior on the nature of the induced wave has been shown by the various wave propagation theories. Attention has been primarily focused on soils whose stress-strain characteristics have negative curvature. For this class of problems the theories would predict that shock waves will not be created or maintained in the soil; they will only exist for positive stress-strain curvature.

Experiments were performed with horizontal bars of dry sand confined under constant lateral pressure, a situation representing negative stress-strain curvature. It was shown that the significant features of the observed waves could be predicted on the basis of the nonlinear, inelastic stress-strain behavior of the soil without the inclusion of time dependent effects. However, some strain rate effects were required to explain the wave velocity results as well as certain features of the wave shape.

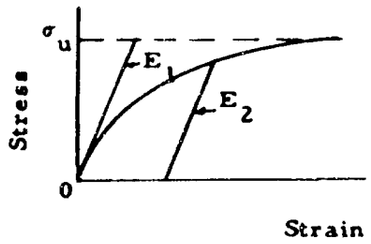
TABLE I

CASES SELECTED FOR COMPUTATION

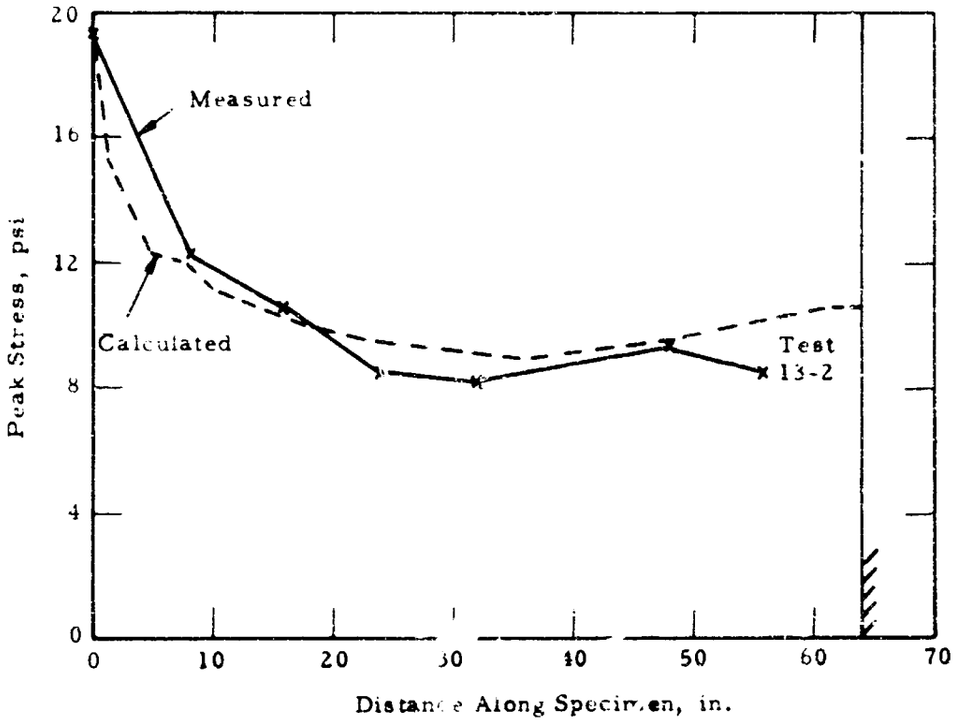
Case	End Condition	p_σ, psi	t_1, msec	t_2, msec	γ_o, pcf	σ_3, psi	σ_u, psi	E_1, psi	E_2, psi
I	Fixed	12	2	10	107	7.5	18	30, 000	30, 000
II	Fixed	12	2	10	107	7.5	18	5, 000	10, 000
III	Free	12	2	10	107	7.5	18	30, 000	30, 000
IV	Fixed	12	∞	∞	107	7.5	18	30, 000	30, 000
V	Fixed	12	0	8	107	7.5	18	30, 000	30, 000
VI	Fixed	14	0	8	107	7.5	18	30, 000	30, 000
VII	Fixed	10	0	8	107	7.5	18	30, 000	30, 000
VIII	Fixed	19.3	0	6	101.1	7.5	15	23, 000	23, 000



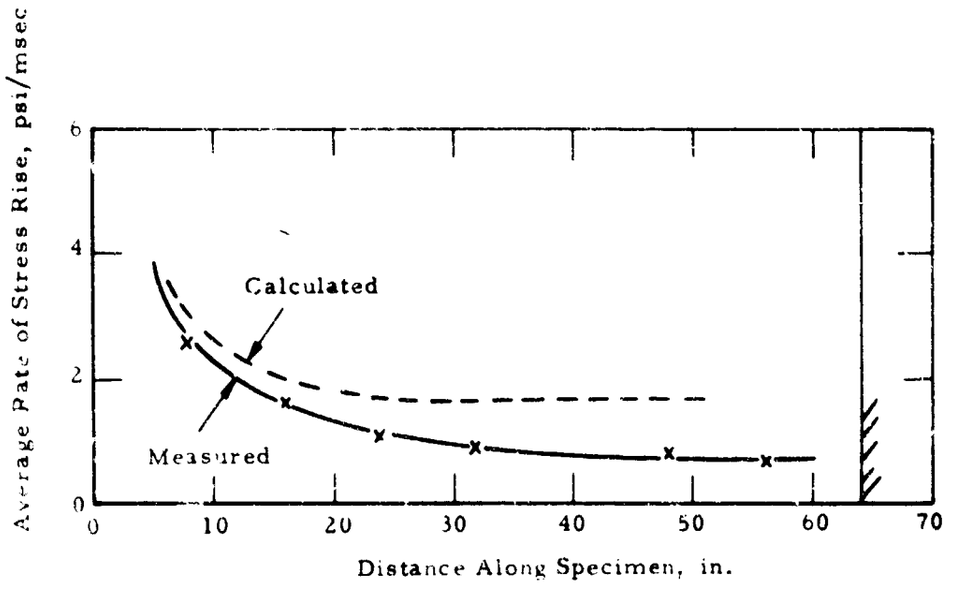
Applied Air Shock Loading



Stress-Strain Curve



a) Peak Stress Attenuation



b) Shock Front Attenuation

Fig. 35 Stress Wave Attenuation for Case VIII Compared with Experiment.

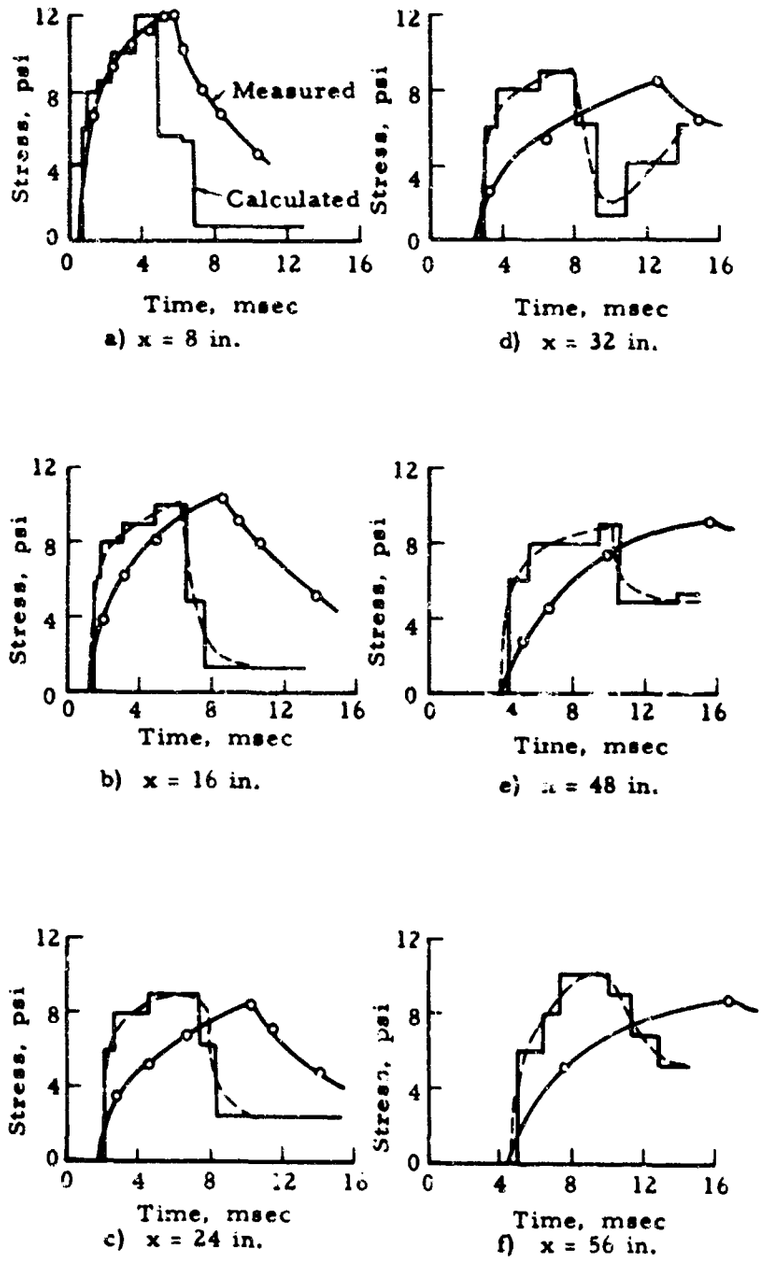


Fig. 36 Calculated Stress Wave for Case VIII.

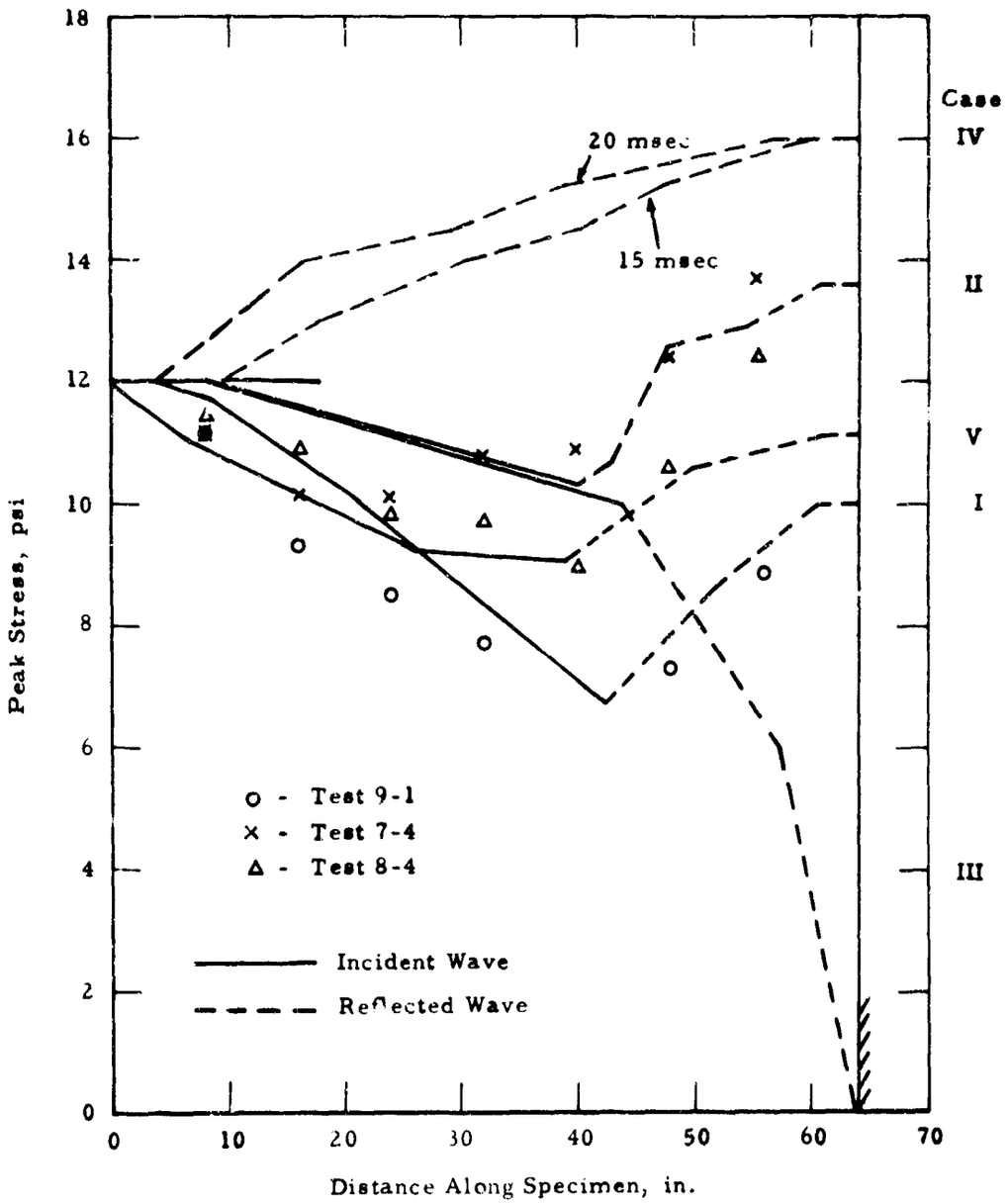


Fig. 37 Calculated Peak Stress Attenuation.

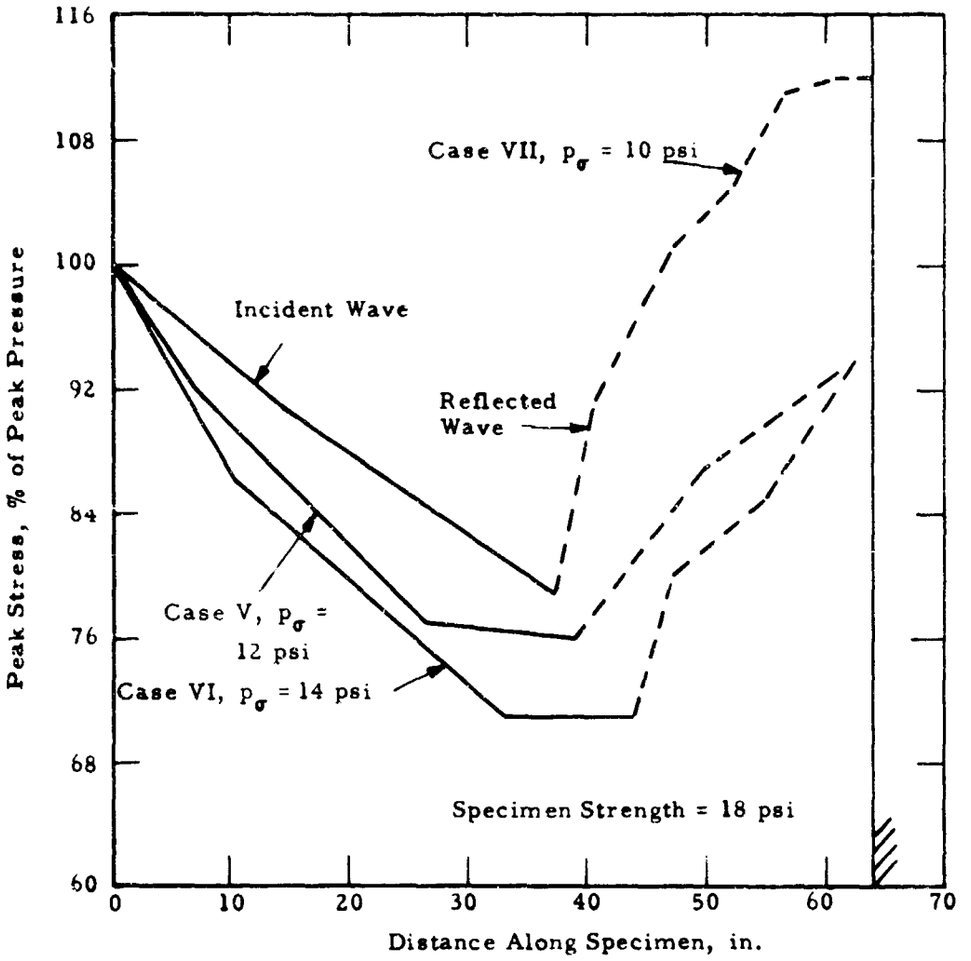


Fig. 38 Effect of Peak Applied Pressure on Stress Attenuation for Constant Specimen Strength

Further studies of wave propagation in soils making use of available analytical tools and experimental techniques are to be encouraged, for they provide an excellent means of extending the knowledge of actual soil stress-strain behavior under dynamic loading as well as information on wave propagation.

ACKNOWLEDGEMENTS

The research reported in this paper was carried out in the Soil Mechanics Laboratory at Illinois Institute of Technology under a grant from the National Science Foundation. The appreciable assistance of Richard Wetzel and Delroy Forbes in the conducting of the experiments is gratefully acknowledged. The suggestions od Dr. E. Vey, Professor of Civil Engineering, during the research, are also appreciated.

REFERENCES

1. Kolsky, H., Stress Waves in Solids, Oxford, Clarendon Press, 1953.
2. Maxwell, C., "Scientific Papers," University Press, Cambridge, Vol. ii, 1890, p. 26.
3. Hillier, K. W., Proceedings, Phys. Soc. B, Vol. 62, 1949, p. 701.
4. Lai, W. amd F. M. Sauer, "Propagation of Stress Pulses in Standard Linear Viscoelastic Materials," Final Report, Part I by SRI for DASA, AD 277770, August 1961.
5. Tumbow, J. W., "Stress-Strain Characteristics of Materials at High Strain Rates, Vol. III, Static Rate Effects and Plastic Wave Propagation," for Sandia Corporation, Contract AT(29-2)-621, by University of Texas, January 1959.
6. Donnell, L. H., "Longitudinal Wave Transmission and Impact," Transactions, Am. Soc. Metals, Vol. 52, No. 1, 1930.

7. vonKarman, T. and P. Dewez, "The Propagation of Plastic Deformation in Solids," Journal of Applied Physics, Vol. 21, No. 10, October 1950, p. 987.
8. Dewez, P. E. and D. S. Clark, "An Experimental Study of the Propagation of Plastic Deformation under Conditions of Longitudinal Impact," Proceedings, ASTM, Vol. 47, 1947, p. 502.
9. Malvern, L. E., "The Propagation of Longitudinal Waves of Plastic Deformation in a Bar Exhibiting a Strain-Rate Effect," Journal of Applied Mechanics, Vol. 18, No. 2, 1951, p. 203.
10. Prandtl, L., "Ein Gedankenmodell zur Kinetischen Theorie der Festen Korper," Zeitch ang. Math. Mech., Vol. 8, 1928, p. 8.
11. Plass, H. J., "A Study of Longitudinal Plastic Waves in Rods of Strain-Rate Material," DRL Report 338, The University of Texas, January 14, 1954.
12. Sternglass, E. J. and D. A. Stuart, "An Experimental Study of the Propagation of Transient Longitudinal Deformations in Elastoplastic Media," Transactions, Am. Soc. Metals, Vol. 75, 1953, p. 427.
13. Karnes, C. H., "Stress-Strain Characteristics of Materials at High Strain Rates, Part IV, Experimental and Theoretical Analysis of Plastic Impacts on Short Cylinders," for Sandia Corporation, Contract AT(29-2)-621, by University of Texas, June 1960.
14. Tapley, B. D., "Stress-Strain Characteristics of Materials at High Strain Rates, Part CI, The Propagation of Plastic Waves in Finite Cylinders of Strain-Rate-Dependent Material," for Sandia Corporation, Contract AT(29-2)-621, by University of Texas, August 1960.
15. Taylor, D. W. and R. V. Whitman, "The Behavior of Soils Under Dynamic Loadings, 2. Interim Report on Wave Propagation and Strain Rate Effect," Contract DA-49-129-eng-227, for Office of Chief of Engineers, AFSWP-117, by MIT, Department of Civil and Sanitary Engineering, July 1953.
16. Taylor, D. W. and R. V. Whitman, "The Behavior of Soils under Dynamic Loadings, 3. Final Report on Laboratory Studies," Massachusetts Institute of Technology, Department of Civil and Sanitary Engineering, Soil Mechanics Laboratory, Contract DA-49-129-eng-227, for Office of the Chief of Engineers, AFSWP-118, August 1954.
17. Smith, R. H. and N. M. Newmark, "Numerical Integration of One-Dimensional Stress Waves," Department of Civil Engineering, University of Illinois, Structural Research Series No. 162, August 1958.
18. Parkin, B. R., et al., "Impact Waves in Sand--A Symposium," Transactions, ASCE, Vol. 127, Part I, 1962, pp. 1269-1335.
19. Prager, W., "On Ideal Locking Materials," Transactions of the Society of Rheology, Vol. 1, 1957, pp. 169-175.
20. Prager, W., "Elastic Solids of Limited Incompressibility," Proceedings, IX International Congress of Applied Mechanics, Brussels, 1957.
21. Salvadori, M. G., R. Skalak, and P. Weidlinger, "Waves and Shocks in Locking and Dissipative Media," Journal, Engineering Mechanics Division, ASCE, Vol. 86, No. EM2, April 1960, pp. 77-105.
22. Skalak, R. and P. Weidlinger, "Attenuation of Stress Waves in Bi-Linear Materials," Journal, Engineering Mechanics Division, ASCE, Vol. 87, No. EM3, June 1961, pp. 1-12.
23. Heierli, W., "Die Dynamik eindimensionaler Bodenkorper im nichtlinearen, nichtelastischen Beriech," Thesis presented to the Eidgenossische Technische Hochschule, Zurich, Switzerland, 1961.
24. Heierli, W., "Inelastic Wave Propagation in Soil Columns," Journal, Soil Mechanics and Foundations Division, ASCE, Vol. 88, No. SM6, December 1962, pp. 33-63.
25. Selig, E. T., "Shock Induced Stress Wave Propagation in Sand," unpublished Ph.D. Thesis, Illinois Institute of Technology, January 1964.
26. Selig, E. T. and E. Vey, "Piezoelectric Gages for Dynamic Soil Stress Measurement," Proceedings, 43rd Annual Meeting, Highway Research Board, January 1964.

DYNAMIC BEHAVIOR OF GRANULAR MEDIA

by
James V. Zaccor*

ABSTRACT

A program of experimental investigation, aimed at discovering the part played by a soil medium in modifying an impulsive load delivered through it, is described briefly. The initial studies and the results reported were limited to granular materials subjected to step shock loadings in which lateral confinement was generated by the applied axial overpressure.

The main purpose of this paper is to demonstrate a quantitative relationship, under these conditions, between measured peak particle displacement and the displacement predicted from the measured velocity of the front of the main stress wave and to indicate the influence of initial stress, or initial effective confining pressures, on the overpressure-strain relationship.

The author also calls attention to precursors propagating ahead of the main stress wave and to the fact that a close relationship is indicated between the precursor wave velocities measured at URS and Hertzian or "seismic" velocities measured in the same material at The Massachusetts Institute of Technology. Further, it was found that these precursor velocities are quite significantly greater than the shock-induced velocities, and that the difference is dependent on both the initial pressure and the applied overpressure. The significance of these observations to design engineering is discussed.

Also of importance is the presentation of information on reflection phenomena occurring at a rigid receiver for shock-induced stress waves, and the information that measured reflection factors exceed two, as should be expected for these materials under these conditions. Discussions of shock and reflection phenomena in soil are presented in the appendixes.

Finally, attention is called to current limited data which appear to correlate measured attenuation of the peak stress, due to interaction of loading and unloading waves for a square-wave input pulse, with hydrodynamic attenuation theory.

INTRODUCTION

The intention of this paper is to present some of the more recent results of an experimental program, currently in progress at URS, aimed at examining behavior of granular material under dynamic loading. The project is sponsored by the Waterways Experiment Station (WES) and is a continuation of a study started under the sponsorship of The Defense Atomic Support Agency which had as its objective development of equipment and techniques for evaluating dynamic behavior of soils. This paper is devoted to a discussion of observations made in connection with traveling waves in which inertial properties play a role.

Objectives

Because interest in wave propagation stems mainly from a desire to know the impulse delivered from a loading source to a receiver, i.e., to a structure, the experimental objective of the program is to measure the distribution of momentum and impulse (pressure-time) as a function of position and time along a column for various media, boundary, and loading conditions. In these studies, energy losses that occur will not be of interest per se, but in regard to their effect on partitioning of energy and redistribution of the total deliverable impulse. Similarly, other behavior processes, such as relaxation or creep, and the degree to which the load-unload cycle produces irreversible strains, will be of interest in considering their effects on redistribution of momentum, i.e., potentially deliverable impulse. It seems reasonable, for example, to expect that irreversible strains could significantly alter the distribution of momentum in a medium that is large compared to the loading pulse length since an effect will be to leave a large mass with a residual velocity that will be converted to impulse, possibly at a nearly imperceptible rate. An effect of this sort has no direct relationship with, say, the more familiar parameter of the area under the stress-strain curve in a load-unload cycle. In addition, it is immediately apparent that if irreversible processes are expected to play such an important role, it is vital not to eliminate them by repeatedly loading the same sample.

*Senior Research Engineer, URS Corporation, Burlingame, California.

Experimental Approach

In attempting to meet the objectives, then, some of the measurements important to this study were indicated, quite simply, by an examination of Newton's second law, which leads to the belief that measurements of stress, particle velocities, and wave velocities of particle velocities, all as functions of time and position along the column, are required. Furthermore, consideration of the impulse-momentum law, which states that the change in force is equal to the rate of change of momentum, i.e.,

$$\Delta F = \Delta(Mv)/t^*, \tag{1}$$

indicates that the simplest experimental arrangement with which to begin a study of propagating waves is to use a very sharp-fronted wave, such as a step shock pulse, so that the momentum is fairly easily defined. For such a case, the momentum equation may be stated in another form, i.e.,

$$\Delta \sigma \ A = \Delta(\rho A x v)/t^{**} \tag{2}$$

or

$$\Delta \sigma = \rho C \Delta v. \tag{3}$$

It is seen that the wave velocity C is the scale factor defining the mass that has undergone a change in particle velocity Δv. Unless the material loaded is an ideal linear elastic medium, or a step shock pulse input is applied, the measurement of many wave velocities C_i*** for corresponding particle velocity changes Δv_i might be required to define the momentum adequately as a function of time, whereas only one wave velocity is required for the step pulse because the material at its front presumably makes a step jump in velocity of Δv directly to the final velocity.

The same wave and particle velocity data are also sufficient to allow determination of the kinetic energy, and, finally, the total work done can be determined at positions along the column from displacement-time and stress-time information. Consequently, it appears that all the data required for studying the momentum and impulse redistribution processes may be obtained by measuring lateral and axial stress-time and displacement-time at enough locations along a column. Particle velocities may be obtained from the slopes of the displacement-time traces, while the wave velocities may be obtained from the travel times between stations. (A description of the experimental apparatus appears in Appendix A.)

EXPERIMENTAL RESULTS

Only the first loadings on dry granular materials have been studied to date, and thus far these tests have been further limited to a 20-30 Ottawa sand and two graded samples. The physical properties of the graded sand samples are indicated in Figure 1. Initial pressures, i.e., seat loads, have been 2 psi or less. In these tests, it has been observed that step stress pulses with slow-rising fronts, e.g., 700 μsec to peak stress, "shock up" after traveling 2 to 4 in. down the column****. The fast-rise portion, if the rounding at the peak is ignored, becomes on the order of 100-400 μsec, as indicated in Figure 2*****. The rounding at the top in these traces is thought to be the effect of short-term relaxation effects.

Further indication that shock waves are propagating may be obtained from examination of the instances in which an unloading wave immediately follows a loading wave, i.e., for a square-wave pulse input. Square-wave loadings have been applied to Ottawa sand placed at a void ratio of 0.51, in which the unloading wave components have been observed to catch and interact with the loading wave. As a result of this interaction, the peak stress decreases with distance traveled along the column. This process of hydrodynamic attenuation has been described in detail in a theoretical treatment by Duvall (1). Analysis of data from one of the experiments in which hydrodynamic attenuation of the peak stress was observed showed excellent agreement with the theory in this reference.

---

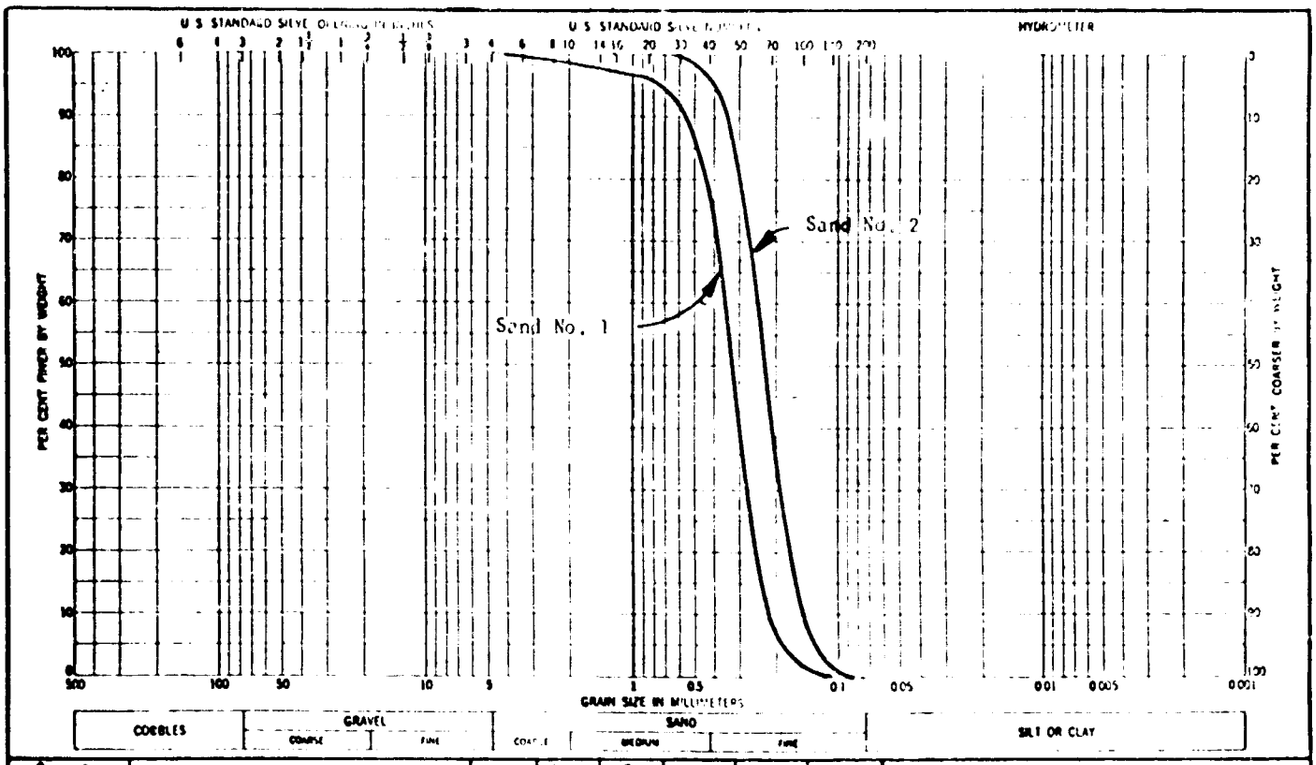
* ΔF is the change in force F, and the rate of change of momentum is given by the product of the mass M and its velocity v divided by the time t for the change to take place.

** The force F in Equation 1 is the product of the stress σ and the cross-sectional area A. The mass M is the product of the density ρ and the volume Ax, where x is the length of column that has undergone the change in velocity Δv. The quantity C is a phase velocity with which the particle velocity change Δv propagates down the column. Consequently (Ct) = (x).

*** For any other condition, the material actually goes through a continuous series of stress changes in arriving at the peak stress, such that each change corresponds to a different wave velocity.

**** The wave is said to have "shocked up" when the fast-rise portion of the traces no longer shows a tendency to steepen further. (A brief discussion of shock phenomena in a soil medium appears in Appendix B.)

***** Even if the rounding is included, the typical measure of rise time (as used in air blast) of 10 to 90 percent of the peak stress is still about 450 μsec for the trace shown (which is among the slowest rise times used).



Sample No.	Local Name	Nat W %	D_{50} (mm)	C_u	$\gamma_{d\,max}$ (pcf)	$\gamma_{d\,min}$ (pcf)	Quan rep.
Sand No. 1	Cooks Bayou Sand	0.1	0.32	1.7	110.8	93.3	75 lb
Sand No. 2	Reid Bedford Model	0.1	0.23	1.6	104.2	87.2	75 lb

Furnished URS by WES

March 1964

Fig. 1 Physical Properties of Sand Samples

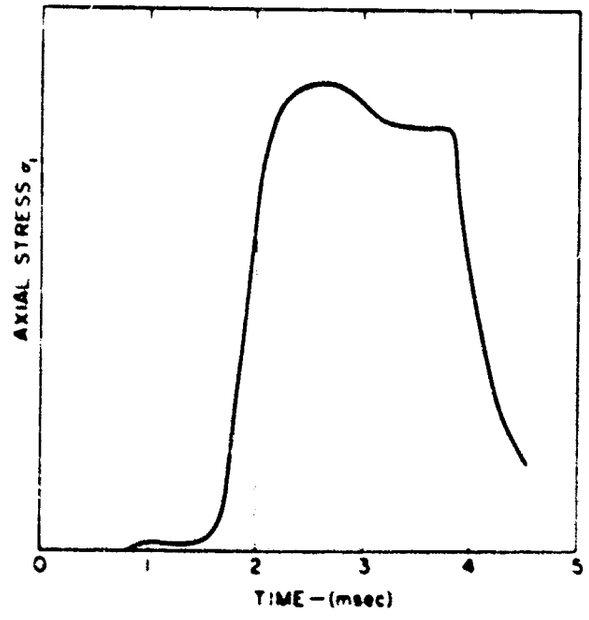


Fig. 2 Stress-Time Trace Measured at the Base of the Sample Column

In studying traveling waves, it is generally considered desirable to make all measurements prior to the occurrence of any reflections from end boundaries. Nevertheless, a great deal may be learned about the conversion of momentum to impulse in a stressed soil element by examining the reflection phenomenon itself. Consequently, as presented in Appendix C, an analysis of data from an actual shock-loading test has been carried beyond the time of reflection of the main wave by the rigid receiver until the particle velocity of the entire column is stopped. It is of interest to note here, however, that for each of the three sands examined, reflected stress at a rigid receiver has always exceeded twice the incident stress.

From data of the type discussed in Appendix C, it is possible to obtain a relationship between stress and total displacement (or strain) at two levels of stress for a uniformly loaded sample. Consider points a and b on the peak reflected-stress trace shown in Figure C-3. It can be calculated from the duration of that stress level and the measured velocity of the reflected wave that the entire sample has been stressed between 80 and 85 psi; in fact, the lateral stress stations also indicated this is true. Therefore, the peak displacement should be associated with the peak reflected stress measured as one condition of strain associated with a uniform loading of the sample. In addition, with a step pulse, the constant level of the incident axial stress allows determination of the total displacement at any point along the sample column, at a time when the entire sample column has been uniformly stressed to the level of the incident stress, simply by reading total displacement at the time of arrival of the incident wave at the rigid reflector. A plot of points for both these displacement conditions appears in Figure 3*.

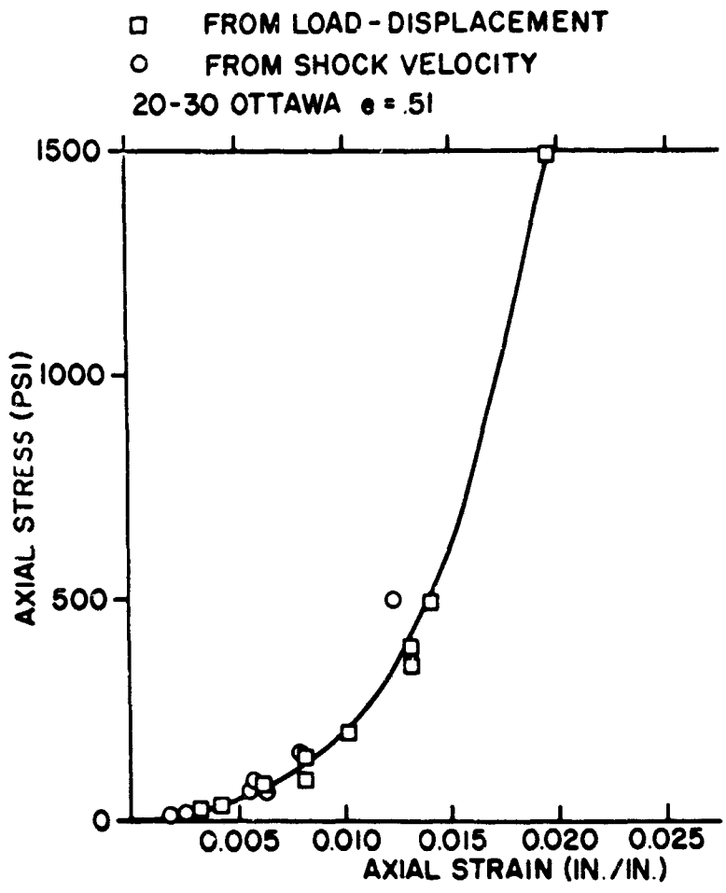


Fig. 3 Envelope of Unique Overpressure-Strain Relationships for Step Shock Inputs

Also plotted in Figure 3 are data points determined from the measured wave velocities (C_{σ_1}) of the peak stress levels (σ_1), calculated simply by using the relationship

$$\epsilon_1 = \frac{\sigma_1}{\rho C^2_{\sigma_1}}. \qquad (4)$$

(In effect, this is a statement that the secant modulus of the stress-strain curve obtained for a shock input is indicative of the wave velocity.) The stress-strain data points for the measured strains and those calculated from the wave velocities appear to match very well.

Shock-Induced Wave Velocities Versus Seismic

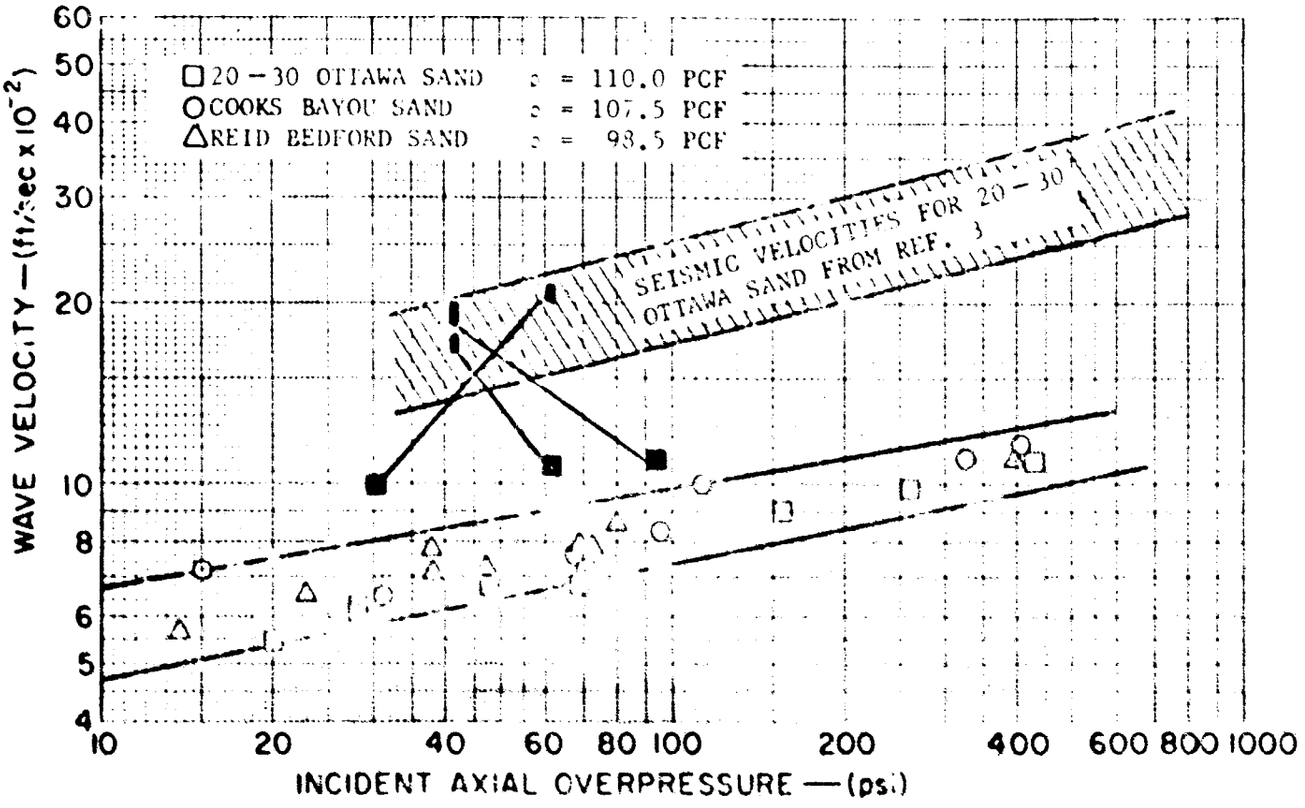
Measured wave velocities for the three sands studied (2) are plotted in Figure 4 as a function of applied axial stress. Also included in Figure 4, for comparison, is a transformed plot of wave velocities measured in Ottawa sand as reported by Whitman (3) at nearly the same void ratio used for the Ottawa sand samples in the test series reported here. The wave velocity data** presented by Whitman show laboratory-measured "seismic" velocities for small stress variations in 20-30 Ottawa sand at a void ratio of 0.53 under various confining pressures. As plotted in Figure 4, however, the curve has been shifted to relate to an axial loading which would develop the corresponding "confining pressure," i.e., lateral pressure, in the URS apparatus. It is seen that these seismic waves propagate considerably faster than the shock-induced waves. Furthermore, the difference between these seismic and shock-induced wave velocities for the 20-30 Ottawa sand is considerably greater than the variation between shock-induced velocities in the three different sands.

* The material does not go through the stress and strain states successively that are indicated by the curve. Rather, the curve is the envelope of a series of unique load-displacement relationships, each obtained for a step pulse loading to a different stress level on a newly prepared sample.

** These waves have been referred to as seismic in Reference 3.

A quantitative measure of the "judgment" that would have been required to correctly predict peak particle displacements (as a result of an applied shock overpressure) from the seismic velocity measurements can be determined by comparing the two wave velocity bands in Figure 4. The "judgment" required to use the seismic velocity predictions should be considered in comparison with the excellent correlation that can be obtained between measured peak particle displacements and the corresponding wave velocities, as has been presented in Figure 3. This correlation requires only that each overpressure applied is properly associated with its own unique propagat n velocity under the appropriate initial conditions. Clearly, it is not reasonable to demand that a single wave velocity, which characterizes a unique set of conditions embracing both initial stress and propagating overpressure (as a seismic velocity might be defined), be representative of all levels of overpressure. Had the seismic velocities been used in Equation 4 for every level of applied overpressure, the predicted peak particle displacements would have been on the order of 600 percent smaller than those measured under shock loadings. In a field application, this discrepancy may be mitigated to some extent if sizable initial conditions of overburden pressure exist.

To summarize, discussion has shown that it is imperative for predicting peak particle velocities and, hence, displacements due to an applied load, to identify the mass involved in the momentum changes. It has also been pointed out that the wave velocity is the scale factor which identifies that mass. It is not sufficient, therefore, to measure simply one wave velocity and apply the momentum equation to predict peak particle velocities. It is also necessary to know the entire spectrum of wave velocities associated with their respective particle velocities and levels of stress propagating. Fortunately, for sharp-fronted waves, the problem becomes simplified to some extent in that all particle velocities, for all intents and purposes, travel with a common wave velocity associated with the peak stress.



Note: Open symbols: < 2 psi seat load, i.e., initial pressure
Fully shaded: 40 to 60 psi initial pressure
Half shaded: precursor velocities versus initial pressure

Fig. 4 Wa e and Precursor Velocities Versus Incident Axial Overpressures

This does not mean that seismic velocities are unimportant. Precursors* will propagate, according to the various laboratory studies, in accordance with an effective confining pressure. In the field, this will be dependent upon the overburden and the degree of cementation. Without doubt, these precursors, being faster than the main wave, will tend to increase the effective mass in the momentum transfer process, hence reducing the maximum particle displacement for a given load; but the magnitude of the effect will be dependent on the level of stress supportable in the precursor relative to the applied overpressure. At present, it is known that the use of precursor velocities for predicting peak particle displacement becomes more legitimate as the supportable level of stress in the precursor increases. Practical application, however, requires quantitative information on the relationships among initial conditions, overpressures, and strains.

A part of that information may well be inherent in data of the type presented in Figures 3 and 4. Consider the hypothesis that initial effective confining conditions (relating, in the field, to effects of cementation and overburden pressures at a given site) might be accounted for, in large degree, by successively shifting the origin of a single stress-strain curve obtained from a confined compression test of the material for zero initial confining pressure. By such a process, one could obtain a family of overstress-strain curves for any initial state of stress. Such a family of curves is shown in Figure 5 for 20–30 Ottawa sand. From these curves, displacements for a given set of initial and overpressure conditions presumably could now be obtained from the appropriate overpressure-strain-initial-stress curve.

So far, three tests to assess this hypothesis have been performed at URS. Though the data are sparse, the few results are encouraging and appear of interest. In these tests, seat loads of 40 and 60 psi were applied axially. Both the velocities of the fronts of the main waves and the displacements of the input end of the column were predictable at a given overpressure from the appropriate curves in Figure 5 and agreed within about 5 percent with the measured values. The three overpressure-strain-initial-stress relationships measured are shown as the shaded points plotted in Figure 5.

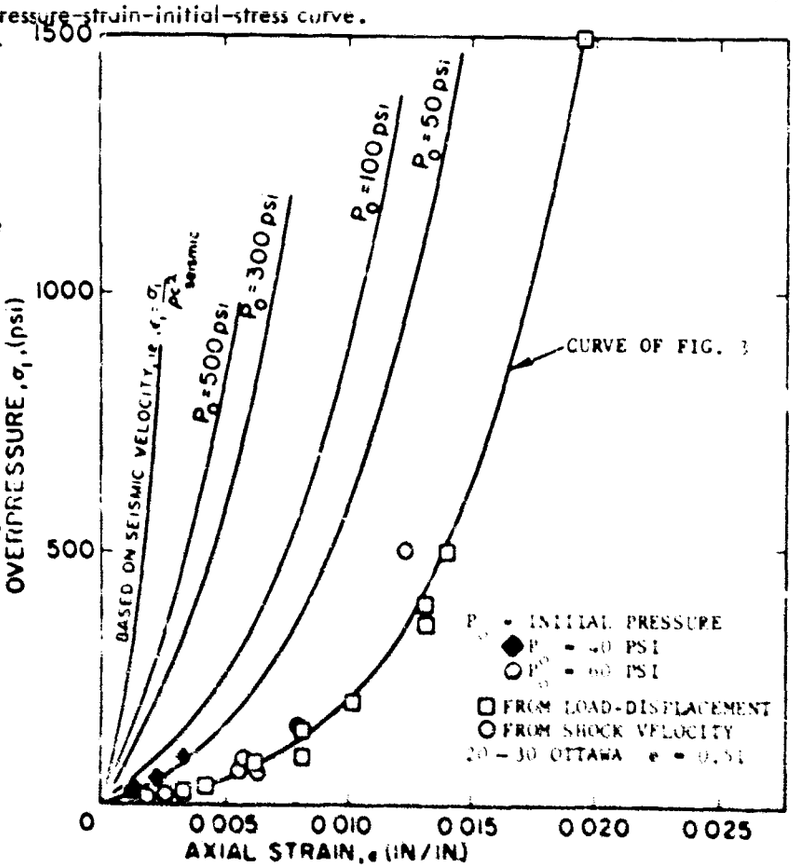


Fig. 5 Axial Overstress-Strain Curves for Various Initial Pressure Conditions in Ottawa Sand

It is of interest that the measured velocities of the observed precursors, when plotted against the set load or initial stress, were within the extremes of the range of the seismic velocities obtained from Reference 3. However, the velocities of the main waves were only between 50 and 60 percent of those of the precursors. The main-wave velocities have been plotted against overpressure and their corresponding precursors have been plotted against the initial stress as the three pairs of points in Figure 4.

In these tests, it was also found that the magnitude of the overstress in the precursor supportable as a result of the seat-load pressure, as determined from the peak reflected stress gauge, was only about 14 percent of the seat-load pressure itself. If it is assumed that, at these low levels of stress, the reflection factor is no more than 2, then the actual incident precursor stress would have been 7 percent of the seat-load pressure. If such a relationship continues to hold, then at an initial pressure of 50[illegible] psi, only a 3[illegible] overpressure could be supported entirely in the precursor. It is of interest that the overstress-strain relationship obtained from the curve in Figure 5 marked "seismic," compares favorable, for stresses up to 35–50 psi, with the overstress-strain relationship from the curve for a 500 psi initial pressure. In addition, it can be seen that if the initial pressure were only one-tenth as great, i.e., 50 psi, but with the same 35 psi overpressure applied, the strain would be 5 times as great as for the case with 500 psi initial pressure or, in effect, for the situation chosen, 5 times as great as would be predicted from the seismic velocities.

*In general, a precursor is a wave that propagates in advance of a main wave, hence, it is relatively small in comparison. In a discrete particulate medium, its magnitude should be relatable to the conditions of interparticulate contact and, consequently, the initial confining pressure. At very low, or zero, initial confining pressures, the level of stress in the precursor may be below the level of easy detection to the extent that it appears to propagate with a lower velocity than is actually correct. In some URS tests with large seat loads, i.e., effectively large initial confining pressures, the velocities of the precursors appeared to be related to the seismic or, perhaps more appropriately in this case, Hertzian velocities obtained from Reference 3.

CONCLUSIONS

The practical significance of the observations described herein is to offer the hope that further studies of the basic behavior of soils under dynamic loads may lead to a method for accounting for overburden and cementation effects in terms of an initial pressure, or some other effective condition of confining pressure. At the least, overpressure-strain-initial-stress studies will allow better quantitative relationships to be drawn, for use in design engineering, between precursor velocities, main stress-wave velocities, and sample strains. Nevertheless, all these effects are related to step pulse loading and have not yet taken unloading into account. Studies of hydrodynamic attenuation processes would allow the additional concepts of wave shape and finite duration to be accounted for.

This paper has also indicated that the nature of the soil behavior, in delivering a pulse to a receiver or structure, is dependent on characteristics of both the input loading and the receiver, as well as of the transmitting medium.

Quantitative evaluation of the loading characteristics (other than the obvious effect of load level) has not been treated here. In regard to the receiver characteristics, it has been indicated that peak reflected stresses may be greater than twice the incident. The practical significance of this, however, could be slight, since the reflection factor will depend on effective boundary conditions, and the size and characteristics of the structure.

REFERENCES

1. Duvall, George E., "Concepts of Shock Wave Propagation," Bulletin of the Seismological Society of America, Vol. 52, No. 4, Oct. 1962, pp. 869-893.
2. Durbin, William L., Correlation of Dynamic Constrained Moduli in Granular Media, (prepared by URS for Waterways Experiment Station) URS 637-15, Burlingame, Calif., July 1964.
3. Whitman, R.V., Nuclear Geoplosics, Part Two, "Mechanical Properties of Earth Materials," Defense Atomic Support Agency, DASA 3203 (II) Draft, Washington, D.C., June 1962.
4. Burmister, Donald M., and Robert D. Stoll, Static and Dynamic Response of Granular Soils, Columbia University, Department of Civil Engineering and Engineering Mechanics, DDC AD No. 415332, New York, N.Y., February 1963.

APPENDIX A - URS DYNAMIC SOIL TEST FACILITY

In the present experimental system used at URS, a sample column about 1 ft. long and 1-1/2 in. in diameter is laterally confined by a 1/4-in. annulus of fluid surrounded by a transparent container. The container is transparent to provide optical entry for tracking lateral and axial displacements of points on the column without making physical contact with the sample*. The objective of the fluid boundary is to provide minimum resistance to axial displacements and maximum resistance to lateral displacements. The fluid is sealed and protected from the applied load so that the lateral stress in the sample and the pressure in the fluid is generated by the axial loading. Kistler pressure transducers are located along the container wall to monitor the fluid pressure, i.e., the lateral stress in the sample. Axial stress is measured at one of the planar ends of the sample at a boundary having a modulus considerably greater than that of the sample so that it is essentially a rigid receiver. At the other planar end boundary, air loadings are applied axially to the column through a piston, which provides a means of measuring displacements of the input end of the sample, prevents penetration of the air loading into the void spaces, and provides a means for unloading the column in a matter of several hundred microseconds simply by bringing the piston to an abrupt stop.

The air loading applied to the piston is the output of a modified shock tube, which has been designed to provide air loadings up to 2,000 psi on the piston, with rise times between 10 and 100 μsec. Stresses in excess of 2,000 psi can be obtained by using compound piston systems, in which the air load is applied to a larger piston than the one that bears on the sample. Loadings with much slower rise times can be achieved by introducing systems of fixed and flexible orifices ahead of the piston. In any event, the piston will slow the rise time of the pulse delivered to the sample column by an amount dependent on both the level of applied stress and the piston mass. With higher applied stresses, the piston is accelerated to the appropriate peak soil-particle velocity at a faster rate. For the pistons used in the tests reported here, rise times at the input end of the sample for low stress levels have been on the order of 700 μsec. At higher stress levels, corresponding rise times as short as 150 μsec have been measured.

APPENDIX B - DISCUSSION OF SHOCK PHENOMENA IN SOIL

The stress-strain curve of a column of laterally confined granular soil characteristically has a positive curvature

$$\frac{d^2\sigma}{d\epsilon^2} > 0,$$

i.e., concave upward about the stress axis.

Interpreting this stress-strain curve as an equation of state allows one to infer that propagation velocities for incremental stress elements increase with increasing axial stress and, as a result, the front of a propagating stress wave will tend to steepen as the wave propagates through the material. This has been confirmed experimentally in granular materials. A further implication is that eventually a stable shock wave would form as the wave proceeded down the column, provided a constant axial stress were maintained at the top. That is, if a step stress wave of infinite duration were put into a laterally confined granular medium not subject to side-wall friction, the shape of the front of the wave should eventually become independent of time.

Further, drawing from more conventional media in which shock waves have been studies, we see that if this stable wave travels at a velocity greater than that of an infinitesimally weak stress signal in the same material, then the wave can be considered a shock. The character of a shock wave in a gas, certainly, is well known and consequently is easily identifiable. The existence of a stable shock wave in a granular medium may prove difficult to demonstrate.

It is relatively easy to provide a sufficiently long expansion chamber in a gas-filled shock tube to allow the complete formation of a stable shock because side-wall friction in a gas is confined to a thin boundary layer next to the wall. However, side-wall friction on a confined granular medium is a dominant mechanism for extracting energy from a wave propagating in the medium, and, unless special arrangements (such as the fluid boundary) are employed, it is not possible to sustain a stable, finite-amplitude, one-dimensional wave. Present-day friction-reducing mechanisms impose limitations on the length of the granular soil column that can be constructed for wave propagation studies.

It is at least possible to say that it is not necessary for a shock in a granular material to be steep-fronted since relaxation effects in an element of soil volume contained in the front may delay attainment of the uniform conditions behind the front.

It is possible to load a column of soil by a pulse sharper than would propagate stably. In this case, the wave in the soil would undergo continuous increase in rise time; that is, the wave front would be apparently flattened or degraded until stable conditions of the shock in the soil were achieved. This occurs since the amplitudes of the highest frequency components of the step wave in air would be degraded exponentially in the soil, with the decay constant for each mode increasing with increasing frequency above the maximum frequency component which the soil will support. On the other

*This is accomplished by means of Optron Corporation Model 680 trackers "locked on" colored sand grains within the sample.

hand, as mentioned earlier, a stress wave entering the laterally constrained soil with a long rise time at the front will gradually steepen until the stable shape of the wave front is obtained. In order to observe both of these conditions, a sizable sample column may be required. To date, only the steepening front has been observed at URS. However, Burmister has reported observing the other condition (4).

Once a stable shock front is physically obtained, then the conservation conditions of mass, momentum, and energy (Hugoniot conditions) can be imposed to relate the uniform states of stress ahead of and behind the shock front. Through the conservation conditions inferences can be made, from measurement of stress and shock wave velocity, regarding state variables, e.g., entropy changes, which would be difficult to measure directly. Once it has been established that a stable front has been achieved, its shape and rise time would give insight into the relaxation effects experienced by the individual granules in passing through the shock front.

APPENDIX C - DISCUSSION OF REFLECTION PHENOMENA

Before looking at reflection phenomena in a column of granular material, a simplified analysis of a similar situation in an ideal linear elastic material should be reviewed.

Linear Case

An important property of the ideal linear elastic material is that all levels of stress are transmitted with the same wave velocity, C. Figure C-1 is a schematic representation of events in a distance-time (X-t) diagram for a sharp-fronted air loading step pulse of magnitude σ_0 applied to the free surface of a stress-free column, the other end of which rests on a rigid receiver. (For the case presented, consider that σ_0 is small compared to the elastic limit.) An X-t diagram is a convenient pictorial way to keep track of the arrival times along the column of characteristics of the wave.

In the case pictured (Figure C-1), a single characteristic, shown by the first diagonal line, is representative of the velocities of all stresses, i.e., the peak stress as well as the front, since the pulse is a step rise in stress. Simultaneous with the arrival of the peak stress, as the stress pulse proceeds along the column, the material undergoes a sudden change in velocity Δv, from zero to v. The material behind the wave, of course, has made a step jump $\Delta\sigma_0$ from zero to the stress level σ_0.

When the wave front arrives at the boundary that has been defined as a rigid receiver, the particle velocity is suddenly stopped, i.e., changed by an amount Δv, as the material velocity returns again to zero from v. Since very little change has occurred in the density ρ, the rate of change of momentum, $\rho C \Delta v/t$, on reflection, is just equal to the rate of momentum change for the incident wave so that the stress behind this reflected front must jump another σ_0, to a total of $2\sigma_0$*. The total stress, resulting from superposition of the incident and reflected stress waves, is generally referred to as the peak reflected stress. The second diagonal line, or the return characteristic in Figure C-1, represents the location of the front of the returning wave of velocity C. This defines the location, as a function of time, of the region where the particle

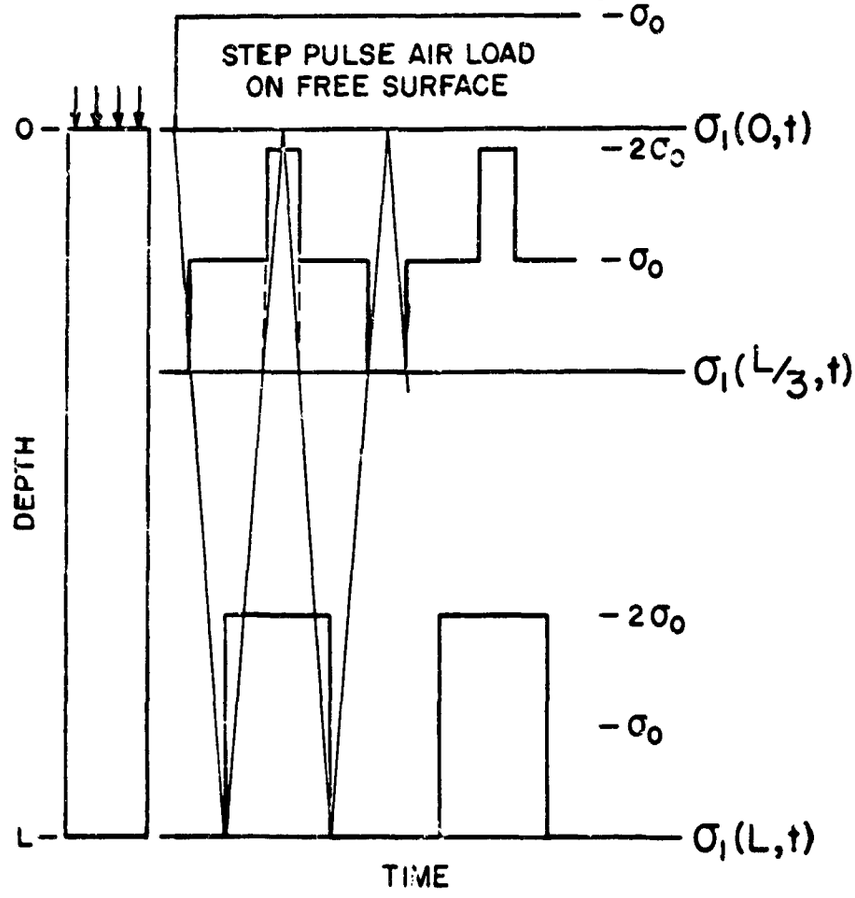


Fig. C-1 X-t Diagram Indicating Stress-Time Histories at Three Locations (X = 0, L/3, and L) Along a Column of Ideal Elastic Material

*If the so-called rigid receiver had either been finite and located in a continuum of the ideal elastic material or if it had been something less than rigid, the stress pulse generated by conversion of the momentum to impulse at the continuum-receiver interface would have been totally different because the rate of change of momentum would have been different.

velocity changes an amount Δv back to zero particle velocity. Space does not permit carrying this analysis further; however, the repeating patterns of stress to be expected for this case are represented at three stations along the column.

Nonlinear Case

Had the material in the column been nonlinear, so that the stress-strain behavior showed ever smaller strains for equal increments of increasing stress, the ratio of the peak reflected stress to the incident stress could be greater than two for reflection at a rigid boundary. In the case of air, for example, it ranges from a factor of two to a factor of eight, depending on the magnitude of the shock strength. This is of considerable importance in determining air-blast loadings on structures. Soil also has a nonlinear response and has been observed in laboratory experiments to shock-up. Consequently, observations of reflection factors greater than two for shock waves in soil are not surprising.

Nonlinear Case: Ottawa Sand

Figure C-2 is an X-t diagram for an actual test in which a step pulse loading of about 32 psi was applied to 20-30 Ottawa sand at a density of 110 lb/ft^2 (or a void ratio of about 0.51). The top and bottom traces are lateral stress-time histories measured at x = 1 and x = 11.8 in., i.e., at measuring stations 1 in. from each end of the column. The middle trace is a history of the axial displacement at x = 5.8 in. Note the precursor and that at the bottom station the rise time of the incident main wave is faster than it is at the top station, where the rise time appears to be about 600 μsec. Careful analysis shows that the incident wave at the bottom station has been interfered with by the reflected pulse; nevertheless, a portion of it can be seen just before reflection. At the top station, it may be seen that the stress remains faithfully constant until the arrival of the reflected wave (except for the bump which corresponds in time to arrival at that station of the reflected precursor). This is what would be expected at a station this close to the input end of the sample for a constant applied axial stress.

Since the lateral stress is, in fact, generated by the axial stress and is directly related to that axial stress, the lateral-stress gauges might also be used to determine the corresponding "free-field" axial stress, provided, of course, the ratio of lateral to axial stress remains constant, which condition has been observed to be true until arrival of an unloading wave. The traces from these stress gauges can be used to determine reflection factors.

For the denser 20-30 Ottawa sand samples studied, reflection factors of 2.5 to 3.2 have been measured in the region of applied stress between 20 and 500 psi. (Actually, the reflection factor may be found in a number of ways.) Looking at the ratio of the peak reflected stress to the incident stress at the two lateral stress measuring stations for the particular loading of Figure C-2, we see that reflection factors of 2.5 and 2.9 are indicated. The upper station reflection factor of 2.5 is not quite correct because an unloading wave (indicated by the dip between 2.9 and 3.0 msec) started to emanate from that location. Another measure of the reflection factor may be obtained from examining the characteristics in the X-t diagram, i.e., by using the wave velocities of the front and the peak particle velocities that are indicated by the diagonal lines intersecting the base lines of the lateral stress traces. The particle velocity changes associated with the reflected and incident waves have been equal, i.e., from 0 to v and from v back to 0, just as in the example of the ideal

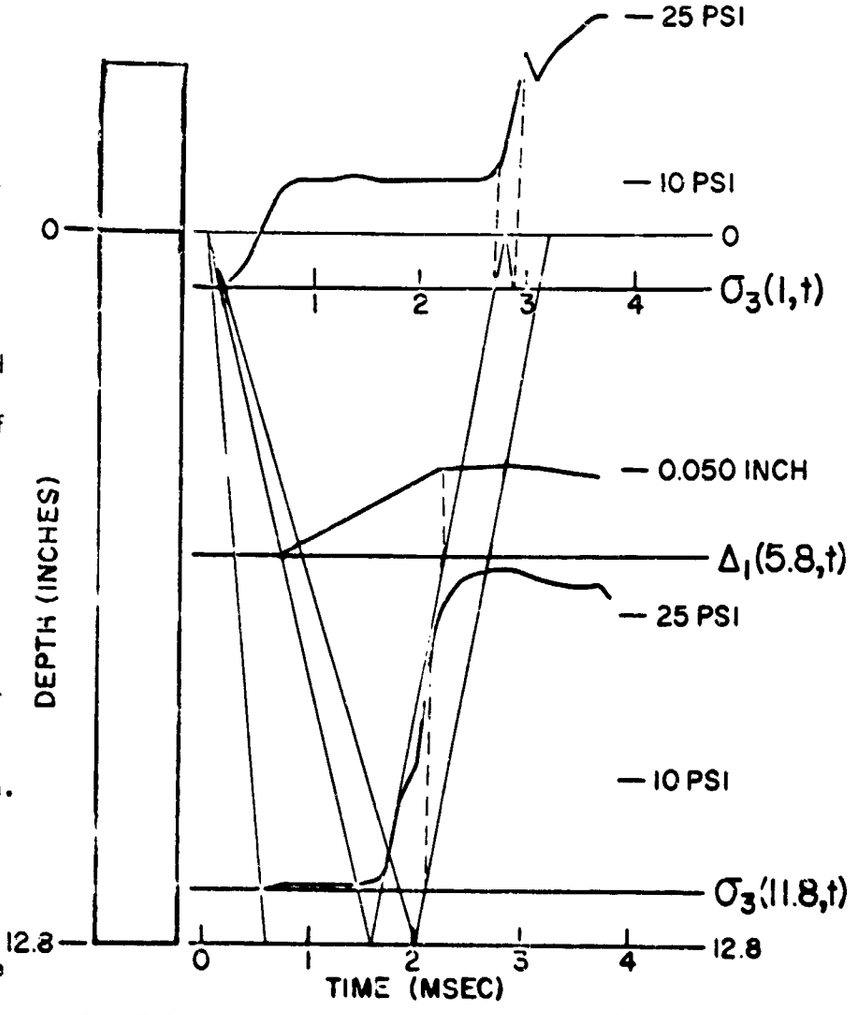


Fig. C-2 X-t Diagram Indicating Lateral Stress-Time and Axial Displacement-Time Histories at the Locations Marked Along a Column of 20-30 Ottawa Sand at 110.0 pcf Density for a Step Pulse Loading to 32 psi

elastic medium. Also, the change in density ρ as a result of the axial strain is still comparatively small, i.e., $\rho_o \sim \rho_i$. Thus, to a first approximation the reflection factor $(\sigma_r + \sigma_i)/\sigma_i$* or $\sigma_r/\sigma_i + 1$ can be obtained from the relationship

$$\frac{\Delta\sigma_r}{\Delta\sigma_i} = \frac{\rho_i C_r \Delta v}{\rho_o C_i \Delta v} \simeq \frac{C_r}{C_i}.$$

For the case under discussion, examination of Figure C-2 shows that 1 plus the ratio of the reflected to the incident wave velocity is approximately 2.7.

The top trace of Figure C-3 is the displacement-time history obtained for the input end of the column and the bottom trace is the time history of the reflected stress for the same test as shown in Figure C-2. Consequently, the same characteristics must be drawn, i.e., the same wave velocities apply and the points of intersection of these characteristics along the column are the same as in the previous Figure. In examining the upper trace, it can be seen that the displacement-time curve indicates that the piston accelerates for a period of time and then achieves constant particle velocity after 600 to 800 μsec, which signifies that there is no differential force across the piston and, hence, that the input end of the soil column is now stressed up to the incident level. Thus, the rise time of the incident wave at the input end of the column is about 700 μsec. (From the upper trace of Figure C-2, it may be recalled that 1 in. further downstream, a rise time of 600 μsec was indicated.) The piston, thenceforth, is seen to move with constant particle velocity until the arrival of the reflected wave front.

The peak displacements in Figures C-2 and C-3 correspond roughly to the arrival of the σ_o level of stress in the returning wave. Many oscillations, that is cycles, of the waves through the sample, occur before equilibrium is reached. They are generally not recorded, but the equilibrium conditions are, as indicated by the broken lines in Figure C-3. Examination of those particular conditions shows the equilibrium stress is 32 psi and the equilibrium displacement of the input end of the column is about 0.080 in. This demonstrates that although a large decrease in stress has taken place (from the peak reflected stress of about 85 psi down to 32 psi), the displacement decrease has been only about 15 percent. It is clear that the ratio of the peak reflected stress to the incident stress (or equilibrium, since the input is a step pulse) is given by 85 ÷ 32, which once again indicates a reflection factor of about 2.7 for the particular case shown.

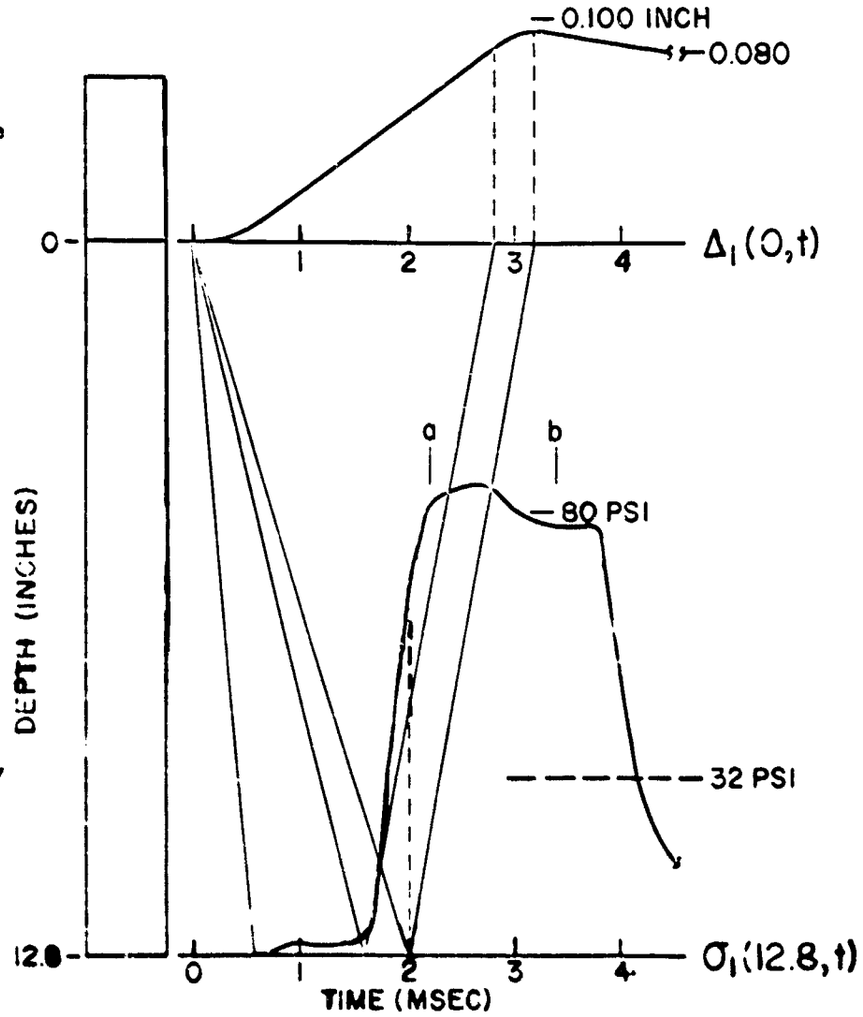


Fig. C-3 X-t Diagram Indicating Axial Stress-Time and Displacement-Time Histories at the Locations Marked Along a Column of 20-30 Ottawa Sand at 110.0 pcf Density for a Step Pulse Loading to 32 psi

SUMMARY

It has been found in a study of shock loadings on granular materials that peak reflected stresses are invariably greater than twice the incident stresses when the reflections occur at a rigid boundary. The method of characteristics has been employed to follow soil response, beyond the time at which reflections occur, with a great deal of success. Reflection phenomena will be of interest in the study of soil-structure interaction where sharp-fronted impulsive loads occur.

*The subscript o refers to conditions ahead of the incident wave, i to conditions behind the incident wave, and r to conditions behind the reflected wave.

STATIC AND DYNAMIC CONSTRAINED MODULI OF FRENCHMAN FLAT SOILS

by
A. J. Hendron, Jr.* and M. T. Davisson**

INTRODUCTION

The advent of megaton sized weapons has necessitated higher degrees of hardness for protective structures. Design requirements for hardened installations require that procedures be developed for predicting ground motions at pressure levels on the order of several thousands of psi. The most versatile procedure used for predicting ground motion (1) is based on observations at the Nevada Test Site at locations where the overpressures were on the order of hundreds of psi. These observations were correlated with dynamic constrained moduli determined in the laboratory under comparable pressures. Because the pressures now of interest are almost an order of magnitude higher, it is desirable that the dynamic constrained moduli of various types of soils be examined at higher pressures in order to investigate the feasibility of using the present ground motion prediction procedures for today's needs. Since most of the field observations have been made at the Nevada Test Site, it is of interest to investigate the static and dynamic behavior of Frenchman Flat soils in one-dimensional compression. The results of both dynamic and static one-dimensional compression tests on undisturbed samples of Frenchman Flat silt are reported in this paper and a comparison is made with the constrained moduli determined on Frenchman Flat soils by other methods.

SITE CONDITIONS

The site from which the undisturbed samples were obtained is located approximately 15 miles north of Mercury, Nevada, in an area known as Frenchman Flat. Three borings designated B-1, B-2, and B-3 were made at the site. B-1 is approximately 4,000 feet from B-2, whereas B-3, is located between B-1 and B-2 at a distance of 1,000 feet from B-1. The surrounding topography is flat, dusty and no vegetation is visible. Frenchman Flat is a playa, or an undrained desert basin. The soil formations are typical of those formed in desert environments involving desert type processes of erosion and deposition.

SOIL PROFILE

Soils Description

The soil may be described generally as a hard friable tan silt with varying structure, cementation and strength. According to the Unified Soil Classification System, the soil is described as a silt of low plasticity, designated ML. In situ, the soil is above the water table and is unsaturated.

Index Properties

Seven hand carved undisturbed samples of Frenchman Flat Playa were obtained from borings B-1 and B-2. The sample depths, Atterberg Limits and moisture-density data in the as received conditions are given in Table 1. The sample from boring B-1 at a depth of 40 feet was non plastic, whereas the liquid limits varied from 30.7 to 37.5 for the other samples; the plastic limits varied from 23.8 to 30.7. Considerable variation was observed in the specific gravity of the soil solids; the values varied from 2.63 to 2.78. The natural moisture contents varied from 8.3 percent to 16.4 percent whereas the dry densities varied from 71.9 pcf to 91.0 pcf. Five of the samples had dry densities in the range from 84 pcf to 87 pcf. The initial degrees of saturation varied from 25 percent to 47 percent.

Results of unconsolidated - undrained triaxial tests on each of the seven samples of Playa silt are given in Figure 1 which indicates a cohesion intercept of 8.5 psi and an angle of internal friction of 34.9°.

Elastic Properties and Seismic Data

The elastic properties of Frenchman Flat silt were determined at the boring locations from the results of in situ vibration tests and seismic compression wave velocity determinations. This work was performed by the Waterways Experiment Station (WES); a detailed description of the procedures and test results are given by Fowler and Fry (2). A summary of the

*1st Lt., U. S. Army Engineer, Waterways Experiment Station, Vicksburg, Mississippi. Also Assistant Professor of Civil Engineering, University of Illinois, Urbana, Illinois, On Military Leave of Absence.
**Associate Professor of Civil Engineering, University of Illinois, Urbana, Illinois.

TABLE I

INDEX PROPERTIES OF UNDISTURBED SAMPLES OF PLAYA SILT

Boring	Depth Ft.	Liquid Limit %	Plastic Limit %	Specific Gravity	Water Content %	Density lb/ft.^{3}	Dry Density lb/ft.^{3}
	0	33.1	25.9	2.78	11.6	96.9	86.8
B-1	20	33.1	25.7	2.63	10.5	94.4	85.4
	40	NP	NP	2.71	8.3	90.8	83.7
	0	30.7	23.8	2.76	9.3	97.1	88.5
	20	37.2	30.2	2.68	13.6	81.6	71.9
B-2	40	30.7	24.8	2.73	12.8	96.5	85.6
	70	37.5	27.3	2.68	16.4	106.0	91.0

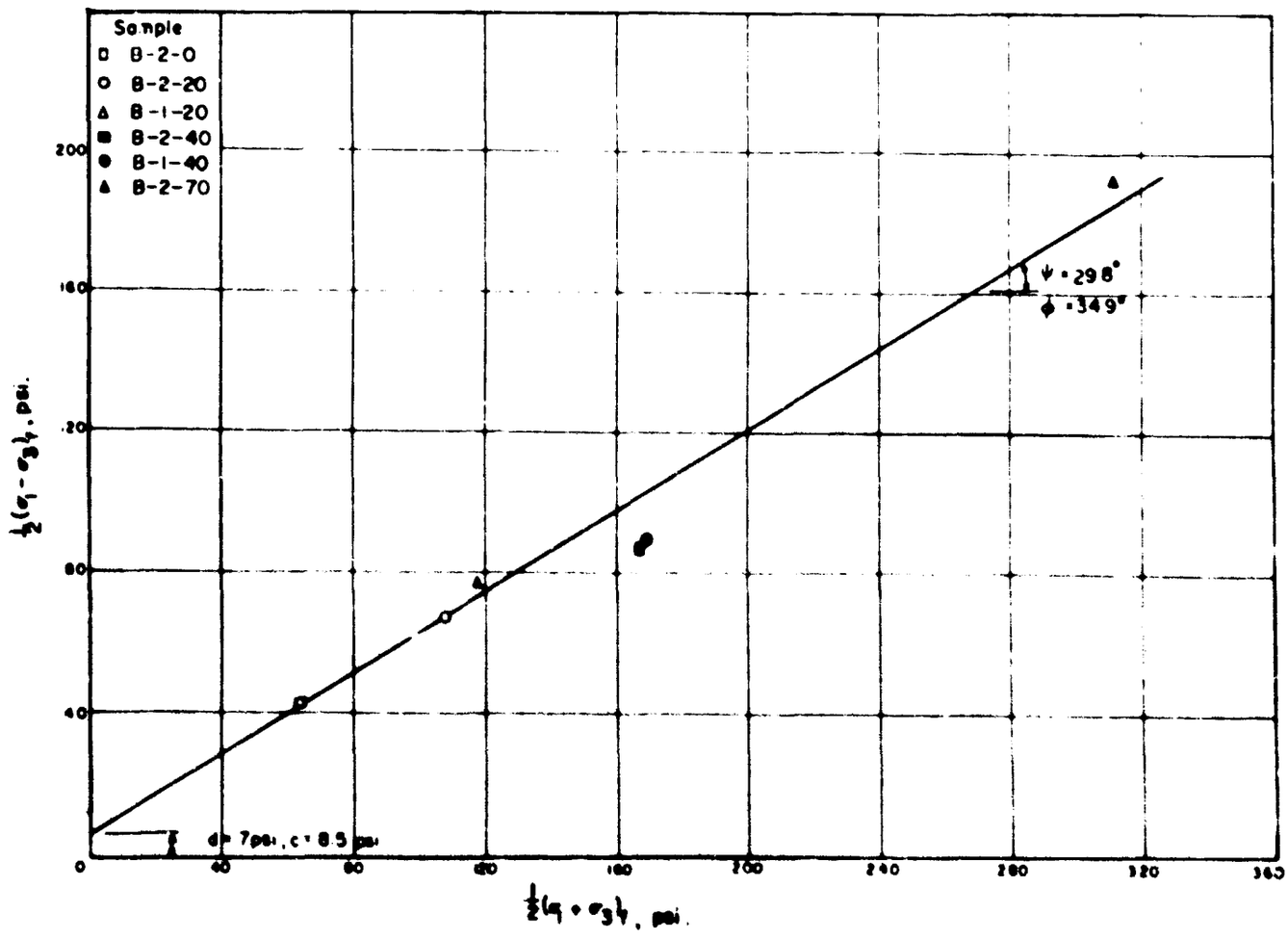


Fig. 1 Modified Mohr-Coulomb Envelope for Playa Silt

elastic soil properties determined by the WES is presented in Table 2. On the basis of the shear velocities determined from field vibration tests, and the compression wave velocities, Young's Modulus E, the shear modulus G, and Poisson's ratio μ, were calculated. Generally, E and G increase with depth with the values of G being approximately 1/3 the corresponding value of E; Poisson's ratio is approximately 0.40. The values of E vary from approximately 6,000 psi at the ground surface to 65,000 psi at a depth of 50 ft.

TABLE 2

SUMMARY OF ELASTIC SOIL PROPERTIES DETERMINED BY WES

Site	Depth Ft	Velocity, ft/sec		E	G	Poisson's ratio
		Seismic Compr.	Vibr. Shear	1000 psi	1000 psi	μ
	0-7	1100	525	7-16	3-6	0.35
B-1	7-21	1750	700	20-43	6-20	0.40
	21-50	2500	1000	40-63	23	0.40
	0-3	890	400	6-10	2-4	0.38
B-2	3-12	1250	550	14-28	5-9	0.44
	12-42	1250	900	28-69	10-25	----
	0-6.5	1100	450	5-21	2-8	0.40
B-3	6.5-24.5	1450	750	20-49	8-16	0.40
	24.5-45	2300	1000	53-63	18-23	0.40

THE BEHAVIOR OF PLAYA SILT LOADED STATICALLY IN ONE-DIMENSIONAL COMPRESSION

Apparatus

One-dimensional compression tests were performed on samples of playa silt to a maximum axial stress of 5480 psi. The test apparatus is illustrated schematically in Figure 2. The apparatus consists essentially of a thin steel ring which

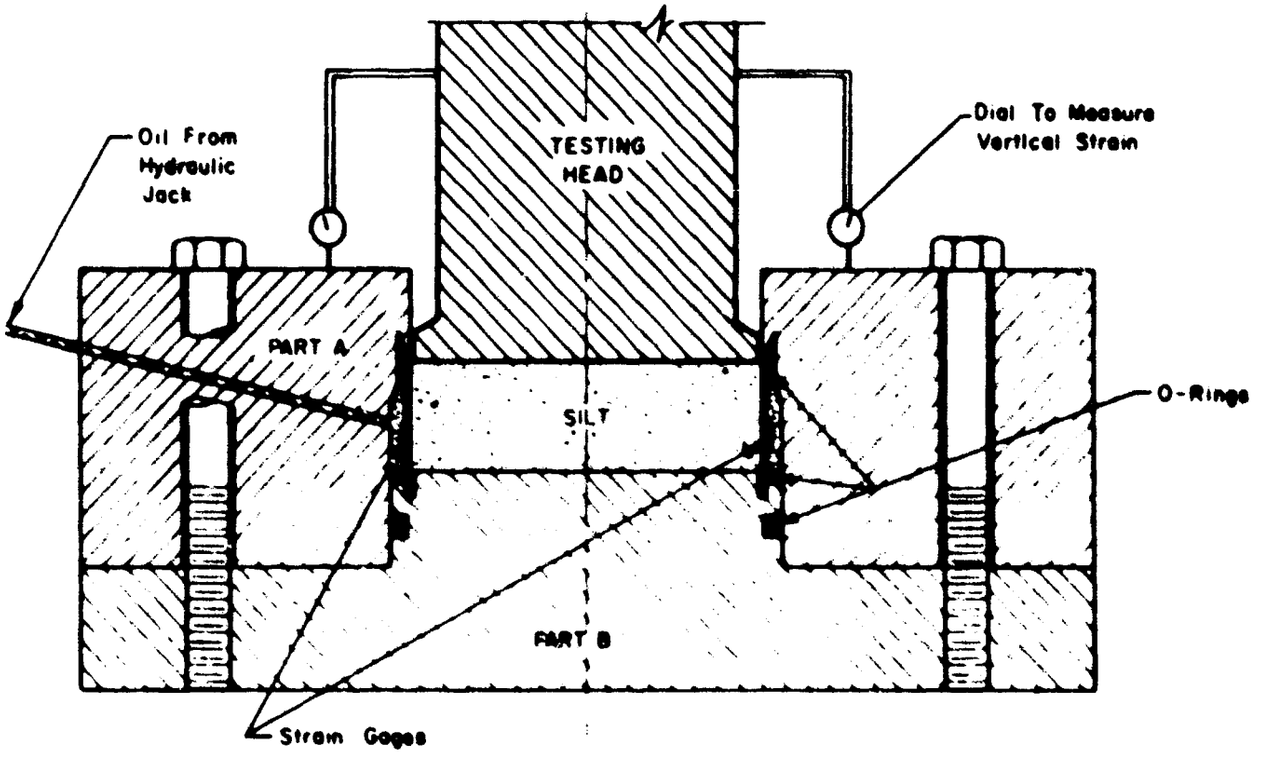


Fig. 2 Schematic Cross-Section of One-Dimensional Compression Apparatus

contains the soil specimen and which in turn is surrounded by an annular space filled with oil. As the soil specimen is stressed axially, radial stresses are induced which tend to increase the diameter of the thin steel ring. Any change in diameter of the ring is immediately detected by the circumferential, metalfilm, strain gauges which are mounted on the flexible ring as shown in Figure 2. In order to maintain a condition of zero radial strain, the oil pressure is modified with changes in axial stress such that the strain indicator remains at a null position during the test. In the null position the radial strains are zero and the oil pressure is equal to the radial pressure acting on the soil specimen. A thorough discussion of the design, calibration, and operation of the device is given by Hendron (3) and the procedure developed for trimming undisturbed soil specimens into the apparatus is given by Hendron and Davisson (4).

Testing Procedure

A seating load of 20 psi was applied to each specimen before zero readings were taken on the dial indicators used to measure the axial strain. A deformation rate of approximately 0.02 inch per minute was applied with a compression testing machine. The lateral stress was continuously adjusted to null the radial strains as the axial stress was varied. The radial stress and the deformation were recorded at predetermined values of the axial stress during loading. During the unloading phase of the test the radial stress and the deformation were recorded simultaneously at arbitrary levels of axial stress.

Stress-Strain Relationships

The axial stress-strain curve for specimen B-1-20, shown in Figure 3, is typical of all seven static stress-strain curves; these curves are given in Figures 4 and 5 for borings B-1 and B-2, respectively. Initially the stress-strain curve is concave downward until a point of inflection is reached, labeled Point A, at which the curve becomes concave upward. Therefore, the specimen initially increases in compressibility as the stress level is increased up to point A; beyond point A the compressibility decreases as the stress level is increased up to the maximum axial stress observed. The unloading portion of the stress-strain curve is very steep (high modulus) in the high pressure ranges, but the modulus decreases markedly below a stress of approximately 200 psi.

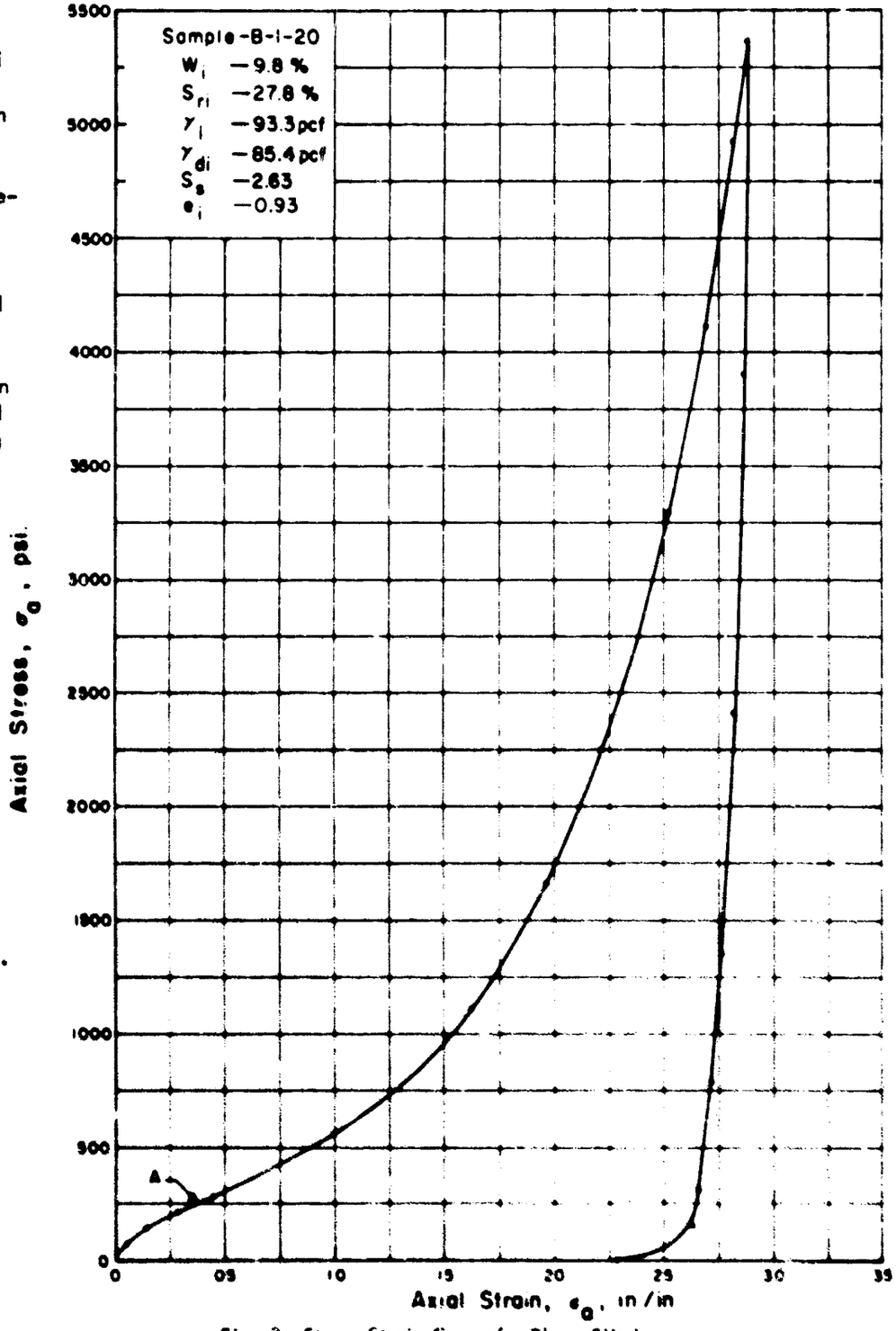


Fig. 3 Stress-Strain Curve for Playa Silt in One-Dimensional Compression

The initial slope of the stress-strain curve is primarily a result of cementation that is typical of the soils at the Nevada test site; it is also caused to some extent by desiccation. The cementation is gradually destroyed as the strain is increased; therefore the stress-strain diagram manifests an initial curvature which is concave downward. Near the point of inflection A, Figure 3, the initial stiffness due to cementation is completely destroyed and the slope of the stress-strain curve begins to increase with the stress level. The phenomenon of the slope of the stress-strain diagram (tangent modulus) increasing with stress level is probably operative from the initiation of loading, but in the Nevada soils it is masked almost entirely by the effects of cementation. The tests performed by Hendron (3) on uncemented, cohesionless soils show a concave upward stress-strain diagram throughout the loading range. It is likely that if some cementation were applied to the four sands tested by Hendron, stress-strain curves similar to those for the Nevada soils would be obtained.

In Table 3 the axial stress and strain values at the inflection points A are tabulated. The average strain value at point A is approximately 4 to 5 percent for all tests on undisturbed samples. The data given in Table 3 for the samples from boring B-2 indicate that the stress levels at which the inflection points occur increase with depth. A similar conclusion could be drawn from boring B-1 except for sample B-1-40 which contained considerable amounts of fine sand and was less cemented than the other samples. Table 3 also lists the maximum axial strains and the ratios of the residual strain to maximum strain for all tests. The maximum strain reached at the peak stress of 5,480 psi ranged from 22.2 percent to 33.8 percent and averaged 27.4 percent for all specimens. The ratio of residual to maximum strain varied from 0.70 to 0.85 and averaged 0.80 for all specimens.

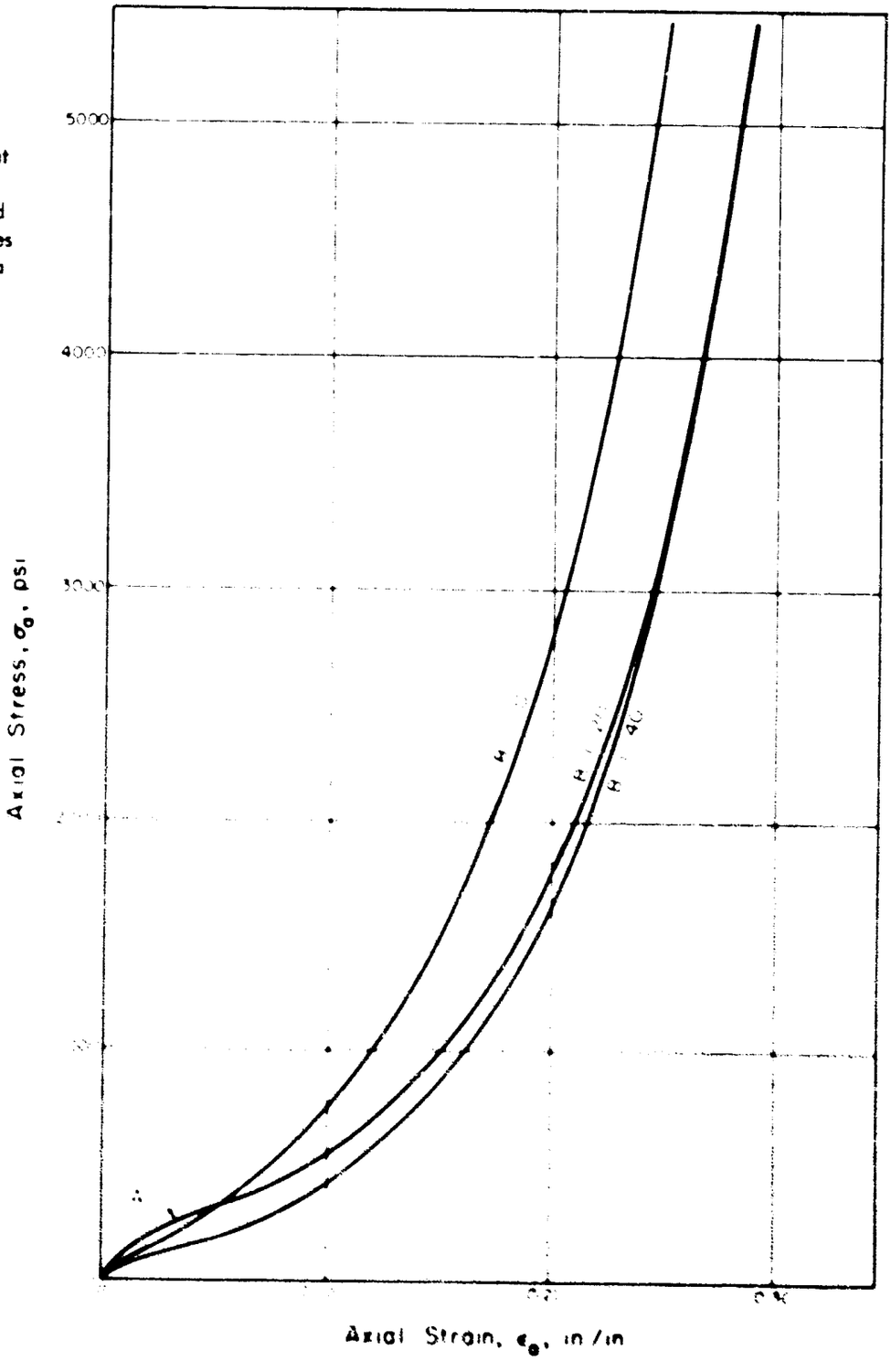


Fig. 4 Stress-Strain Curve for Playa Silt in One-Dimensional Compression

Constrained Moduli-Stress Relationships

Many of the ground motion problems in protective construction may be approximated by assuming that the displacements occur in the direction of stress wave propagation, and that movements perpendicular to this direction are negligible. Under these assumed strain conditions, the constrained modulus becomes the significant soil property because it controls the magnitude of the ground motions. A constrained secant modulus of deformation, M_{cs}, is by definition the ratio of the axial stress to the axial strain under conditions of zero radial strain.

A typical plot of constrained secant modulus versus axial stress is shown in Figure 6 for sample B-1-20. The secant modulus has an initial value at very low stresses which is believed to be primarily the result of cementation and, to a lesser extent, of preload resulting from desiccation. The tests on the specimens from boring B-2 show that the initial values of the secant modulus tend to be essentially the same from depths of 0 ft to 20 ft, but increase with depth from 20 ft to 70 ft; the initial moduli at 20 ft, 40 ft, and 70 ft are 11,800 psi, 23,600 psi, and 30,400 psi, respectively. With increasing axial stress the secant modulus decreases until a minimum value is reached at axial stresses between 200 psi and 1,100 psi. The axial stresses at which the secant modulus reaches a minimum are 50 psi, 500 psi, 700 psi and 1100 psi for specimens B-2-0, B-2-20, B-2-40, and B-2-70, respectively. Therefore the axial stress at which the secant modulus reaches a minimum value increases with depth at boring B-2. The foregoing variation of modulus with depth cannot be detected from the test results on specimens from boring B-1.

Beyond the stress at which the secant modulus passes through a minimum there is nearly a linear relationship between secant modulus and axial stress. Furthermore, at given values of the axial stress the constrained secant modulus of the undisturbed specimens was found to be dependent on the initial void ratio as shown in Figure 7. In general, the constrained secant modulus

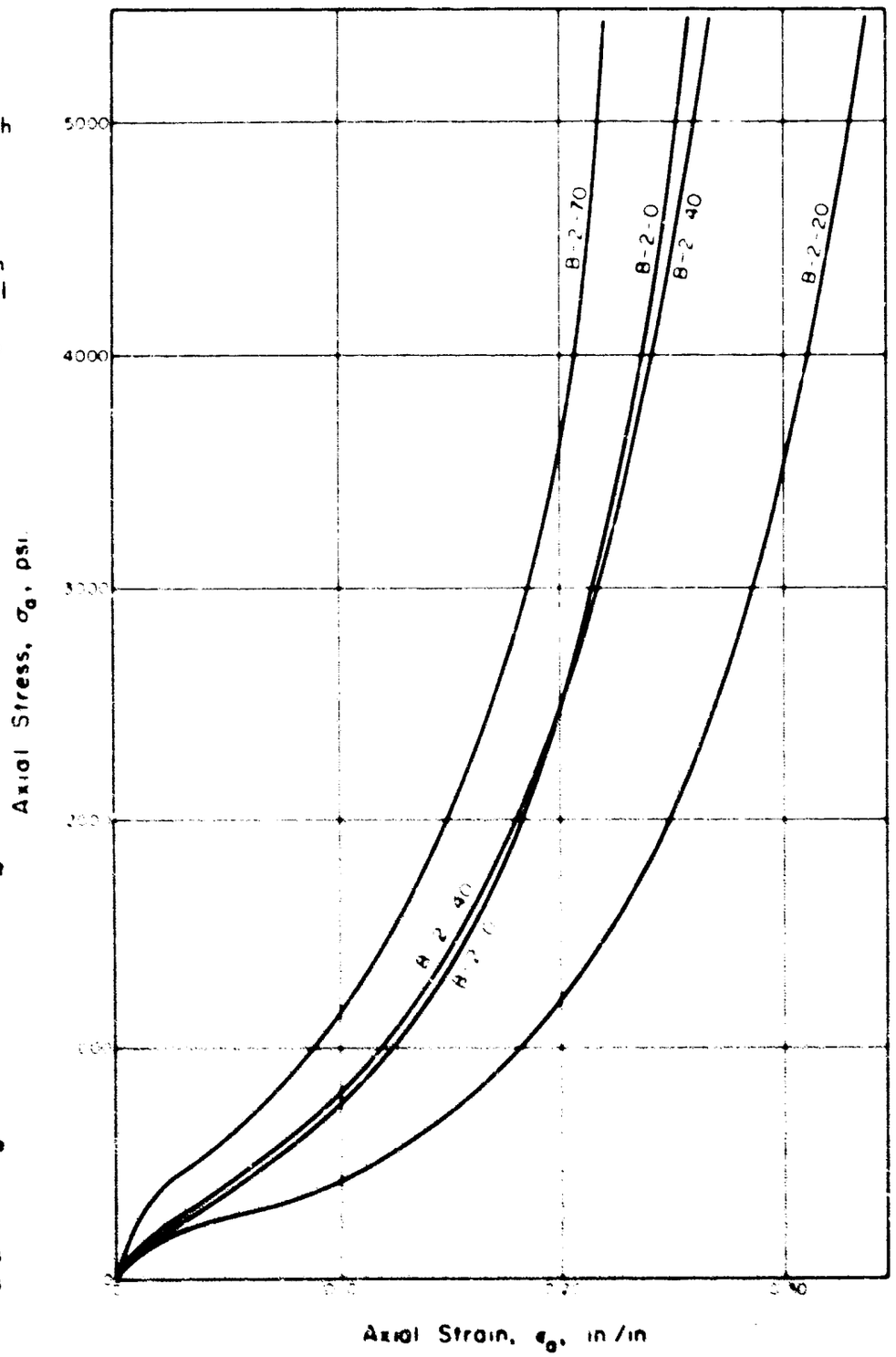


Fig. 5 Stress-Strain Curve for Playa Silt in One-Dimensional Compression

TABLE 3

SUMMARY OF STATIC TEST DATA

Sample Number	Point of Maximum σ_a			Initial S_r, %	Inflection Point		ϵ_a Residual %	K_o Loading	Poisson's ratio $\mu = \frac{K_o}{1 + K_o}$	Ratio of residual strain to maximum strain	Initial Conditions of Sample			
	σ_a, max. psi	ϵ_a, max. %	S_r, max. %		σ_a %	ϵ_a %					w % Water Content	γ_d pcf Dry Density	e_i Void Ratio	G_s g/cm³ Specific Gravity
B-1-0	5480	27.4	65.6	32.3	100	1.7	19.2	0.56	0.36	0.70	11.7	86.8	1.01	2.76
B-1-20	5370	28.9	66.8	27.8	250	4.7	22.8	0.48	0.32	0.79	9.8	84.6	0.95	2.73
B-1-40	5480	29.2	58.5	24.5	55	1.3	24.2	0.47	0.32	0.83	9.3	89.7	1.01	2.71
B-2-0	5480	25.9	61.6	28.4	330	4.3	20.4	0.55	0.36	0.80	9.7	86.5	0.96	2.74
B-2-20	5480	33.8	69.7	28.4	330	7.0	28.7	0.56	0.36	0.85	14.1	71.9	1.33	2.68
B-2-40	5480	26.8	71.5	32.6	415	5.0	21.5	0.51	0.34	0.80	11.5	86.6	0.99	2.75
B-2-70	5480	22.2	96.0	46.6	550	4.1	17.3	0.60	0.38	0.78	14.6	71.0	1.34	2.68
Remolded	5480	27.1	99.6	45.2	100	3.0	22.8	0.51	0.32	0.84	16.3	66.4	1.46	2.71

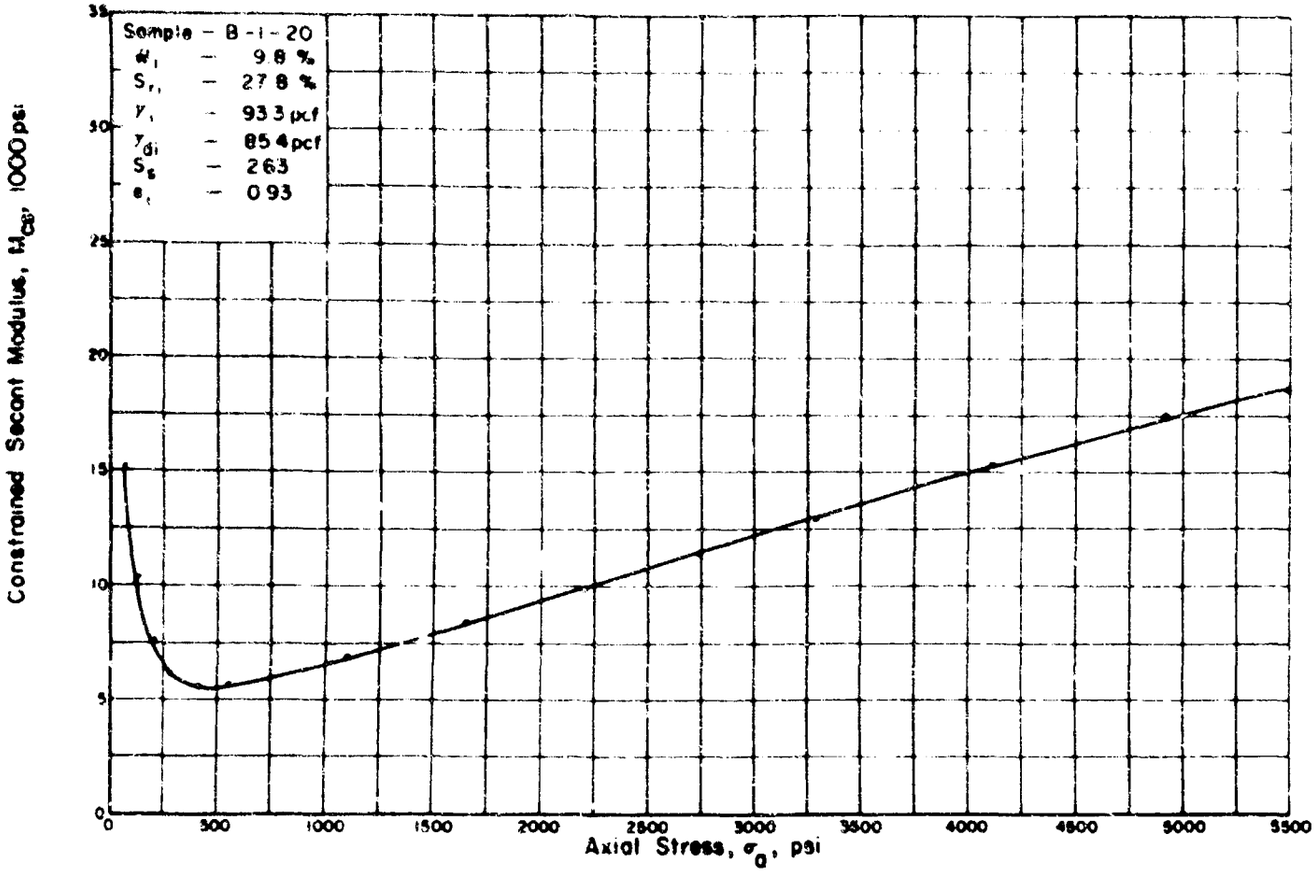


Fig. 6 Relationship Between Constrained Secant Modulus and Axial Stress for Playa Silt in One-Dimensional Compression

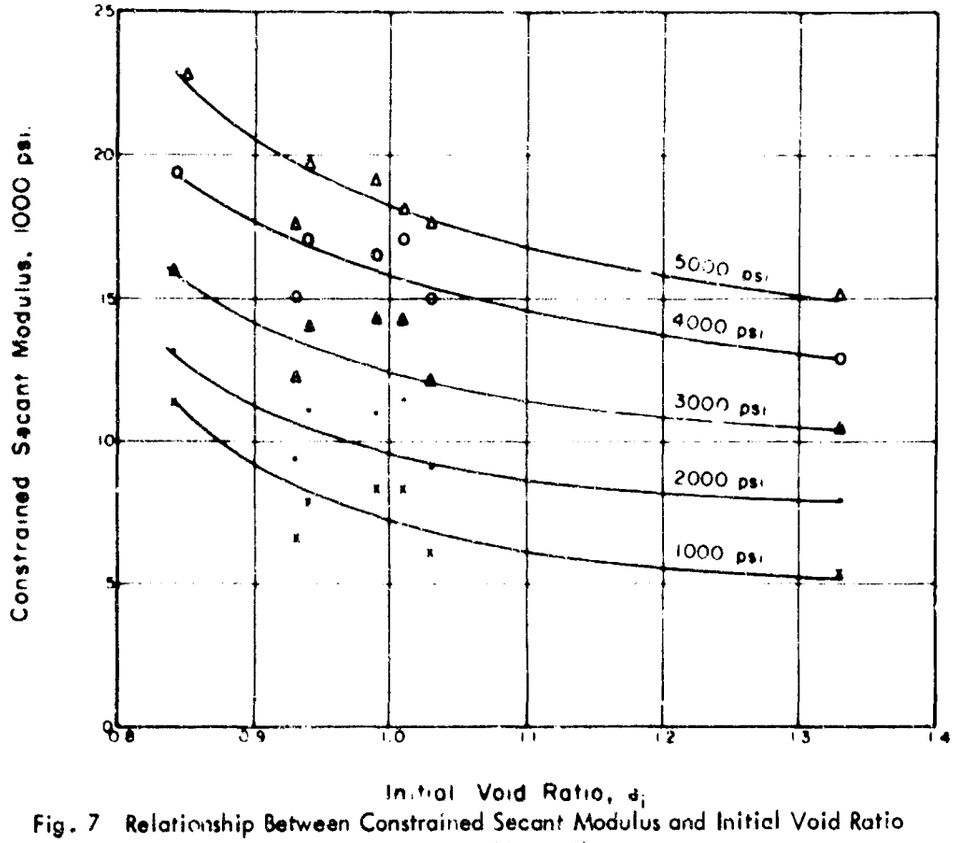


Fig. 7 Relationship Between Constrained Secant Modulus and Initial Void Ratio for Various Axial Stress Levels on Playa Silt

decreases at a decreasing rate as the initial void ratio increases for all levels of axial stress up to 5,000 psi.

Axial Stress-Radial Stress Relationships

Under conditions of one-dimensional compression, radial stresses are induced as a result of an increase in axial stress. The ratio of the effective radial stress to the effective axial stress under conditions of zero radial strain is defined as the coefficient of earth pressure at rest. In this series of static one-dimensional tests full drainage could not occur; therefore, the ratio of the radial stress and axial stress determined during the test is essentially in terms of total stresses. The symbol K_o is used herein to represent the ratio of radial stress to axial stress on a total stress basis although it is normally used as an effective stress relationship.

A typical relationship of the axial and radial stresses for the static tests is shown on Figure 8 for specimen B-1-70. Throughout the entire range of loading the relationship is essentially a straight line; the slope ranges between 0.47 and 0.56. It is believed that for all tests except B-2-70 and the remolded specimen the relationship is probably close to an effective stress relationship because there is no tendency for the slope to increase. The values of K_o for the loading portion of each test are given in Table 3.

As unloading begins the radial stresses are reduced at a slower rate than the axial stress; this results in a concave downward curve that lies above the loading curve as shown on Figure 8. At lower pressures, below approximately 1,000 psi, K_o generally exceeds unity and increases to values in excess of 3 or all specimens at an axial stress of 250 psi. The residual radial stress varied from 150 psi to 350 psi for all samples upon complete removal of the axial stress.

The axial stress-radial stress relationship for test B-2-70 shows a definite tendency for the radial stress to increase rapidly in the latter stages of loading. This is consistent with the high degrees of saturation that are obtained (95 percent) at the maximum stress, as given on Table 3. The effect of the degree of saturation on K_o is shown on Figure 9 for a test conducted on remolded playa silt. At saturations below 80 percent K_o is constant (0.51), but as the degree of saturation approaches 85 percent K_o begins to increase rapidly with the degree of saturation. A more sensitive indicator of the effect of the degree of saturation is the rate of change of the radial stress with respect to the axial stress at a given degree of saturation; this relationship is also shown on Figure 9. At a saturation of 99.6 percent the rate of change of radial stress with respect to axial stress was measured to be 1.01; this is indicative of experimental error because the maximum value cannot exceed unity.

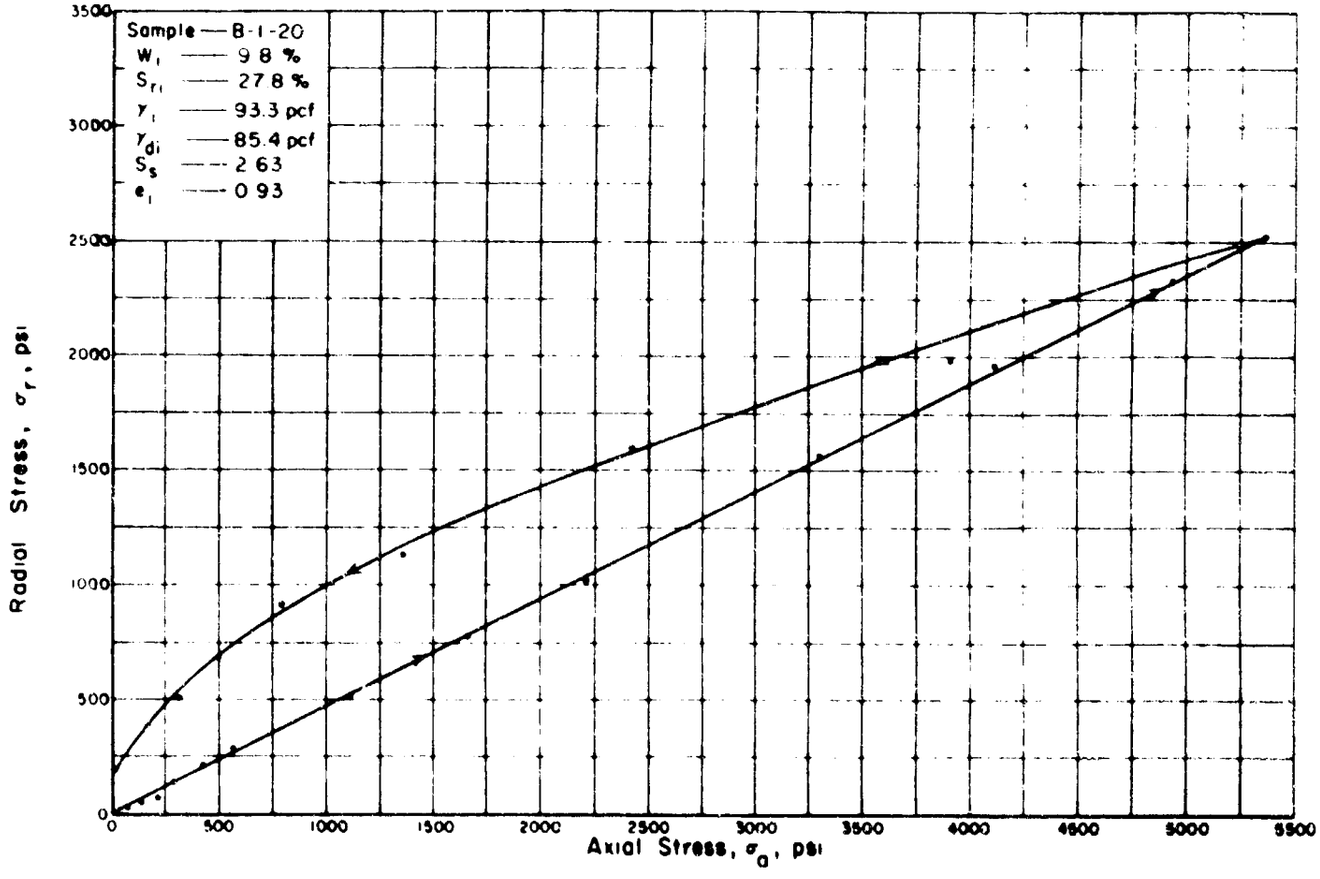


Fig. 8 Relationship Between Axial and Radial Stress for Playa Silt in One-Dimensional Compression

The coefficient of earth pressure at rest K_o is often related to a pseudo-Poisson's ratio for soil by the relationship $K_o = \mu/1 - \mu$, or $\mu = K_o/1 + K_o$. Values of the pseudo-Poisson's ratio for all tests are given in Table 3; they vary from 0.32 to 0.36.

THE BEHAVIOR OF PLAYA SILT LOADED DYNAMICALLY IN ONE-DIMENSIONAL COMPRESSION

General

Dynamic one-dimensional compression tests were performed on specimens from each of the seven undisturbed samples furnished for this study. The test specimen designations are the same as those for the static test series. An additional test was performed on a second specimen carved from sample B-2-70. Therefore, two designations are used for the specimens from boring B-2 at a depth of 70 ft; these are B-2-70a and B-2-70b.

The axial stress-strain behavior and the radial stress concomitant with limited radial strains were measured to axial stress levels varying from 3,900 psi to 20,300 psi. Descriptions of both the apparatus and the experimental procedures are given below. Two different loading machines were used; one is denoted as dynamic whereas the other is denoted as rapid.

Apparatus

A 4-inch diameter steel ring with a height of one inch is used to confine the test specimen. In order to limit the amount of radial strain induced by an applied axial stress, the thickness of the ring in the radial direction adjusted for the range of radial stresses that will be imposed. It is desirable to maintain the radial strains in a null position, as was accomplished in the static tests, but this is not presently practical in a dynamic test; therefore, limited amounts of radial

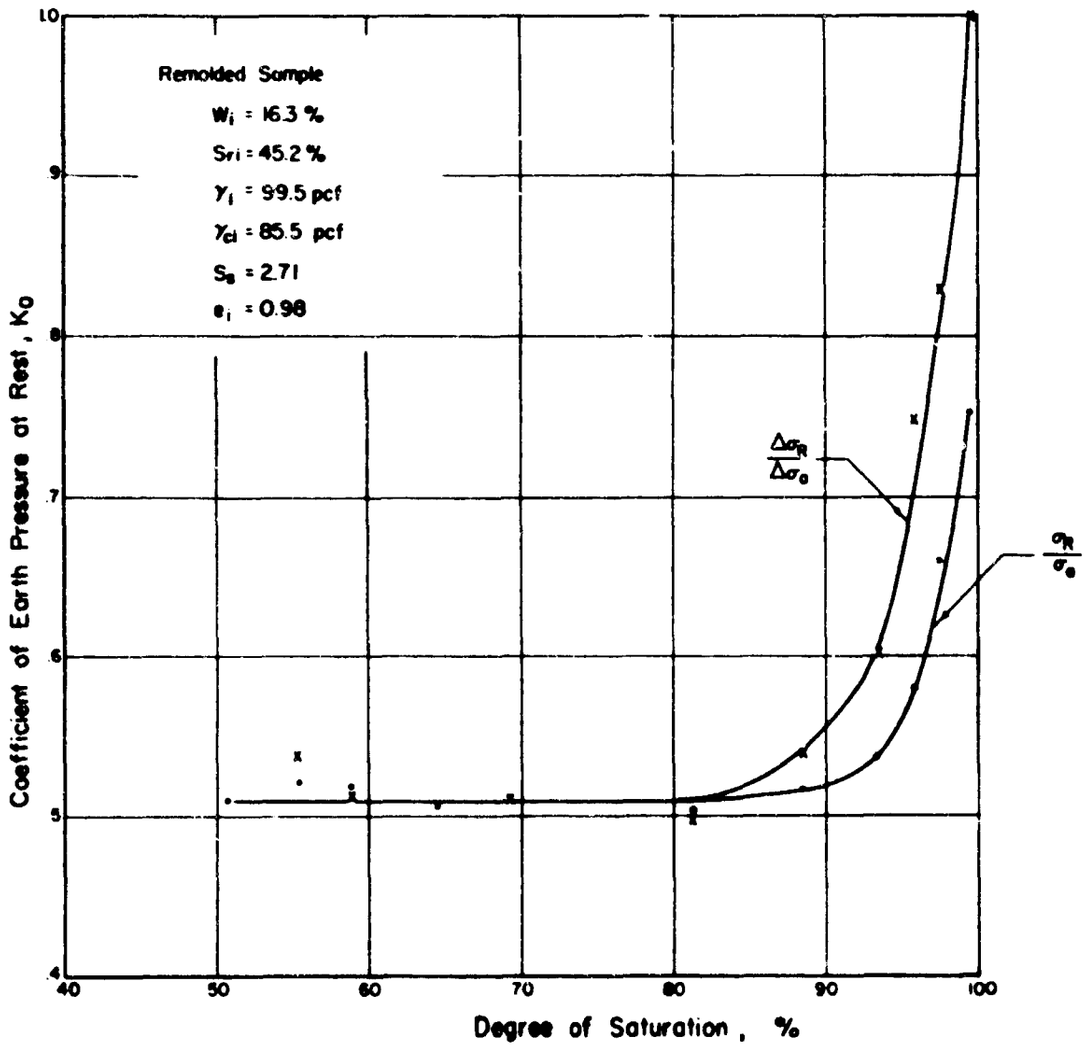


Fig. 9 The Relationship Between the Coefficient of Earth Pressure at Rest and Degree of Saturation for Remolded Playa Silt

strain are allowed to occur. SR-4 gauges were mounted on the outside of the ring to detect the radial strains and furnish a means of determining the radial stress.

The essential feature of the rapid loading machine is that it will apply an axial compressive load of a predetermined magnitude on the specimen in the confining ring in approximately 0.1 second. A schematic of the rapid loading machine is shown in Figure 10. It is essentially a hydraulic ram mounted in a frame; the load is applied rapidly by vigorously operating a lever valve that connects the hydraulic ram to a reservoir of oil subjected to high pressure from a pneumatic source. The load sensing element is a hollow steel cylinder equipped with SR-4 gauges. Axial deformations were measured with a linear variable differential transformer.

The test results obtained for specimen B-2-40 in the rapid test machine are presented on Figure 11. The axial and radial stresses and the axial strain have been plotted against time expressed in milliseconds. The curves are for the initial portion of the test, but they also include a considerable amount of the steady-state or constant-load part of the test. The data were obtained from FM magnetic tape recordings. In addition, oscillograph traces were obtained, but these are not as accurate nor do they have the frequency response of the FM tape system. From the data in Table 4 it is seen that the load increased from zero to its peak value in 128 milliseconds; in addition, it remained on the specimen for 514 milliseconds (dwell time) and was decayed to zero in 86 milliseconds. By summing these time intervals the duration of the test becomes 728 milliseconds.

The essential features of the dynamic loader are the same as those for the rapid loader except for the mechanism that produces the dynamic load. It is possible to apply the full load in approximately 3 milliseconds with the dynamic loader. The axial and radial stress and axial strain instrumentation are the same as used for the rapid loading machine. The loading device itself is entirely pneumatic. As shown in Figure 12, pneumatic pressure is stored in a chamber equipped with a rapid opening valve. At the start of the test the valve is opened and the stored pneumatic pressure escapes and exerts a downward pressure on the piston which loads the dynamometer and the soil specimen. The load is decayed by operating another rapid opening valve that vents the pneumatic pressure to the atmosphere. Further details of the loading equipment are described by Sinnamon and McVinnie (5), and Kane, Davisson, Olson and Sinnamon (6).

The axial and radial stresses and the axial strain have been plotted against time for test specimen B-1-0 on Figure 13. In order to magnify the phenomena which occur at early times, only the first 15 milliseconds of the test data taken from the FM tape recording have been shown.

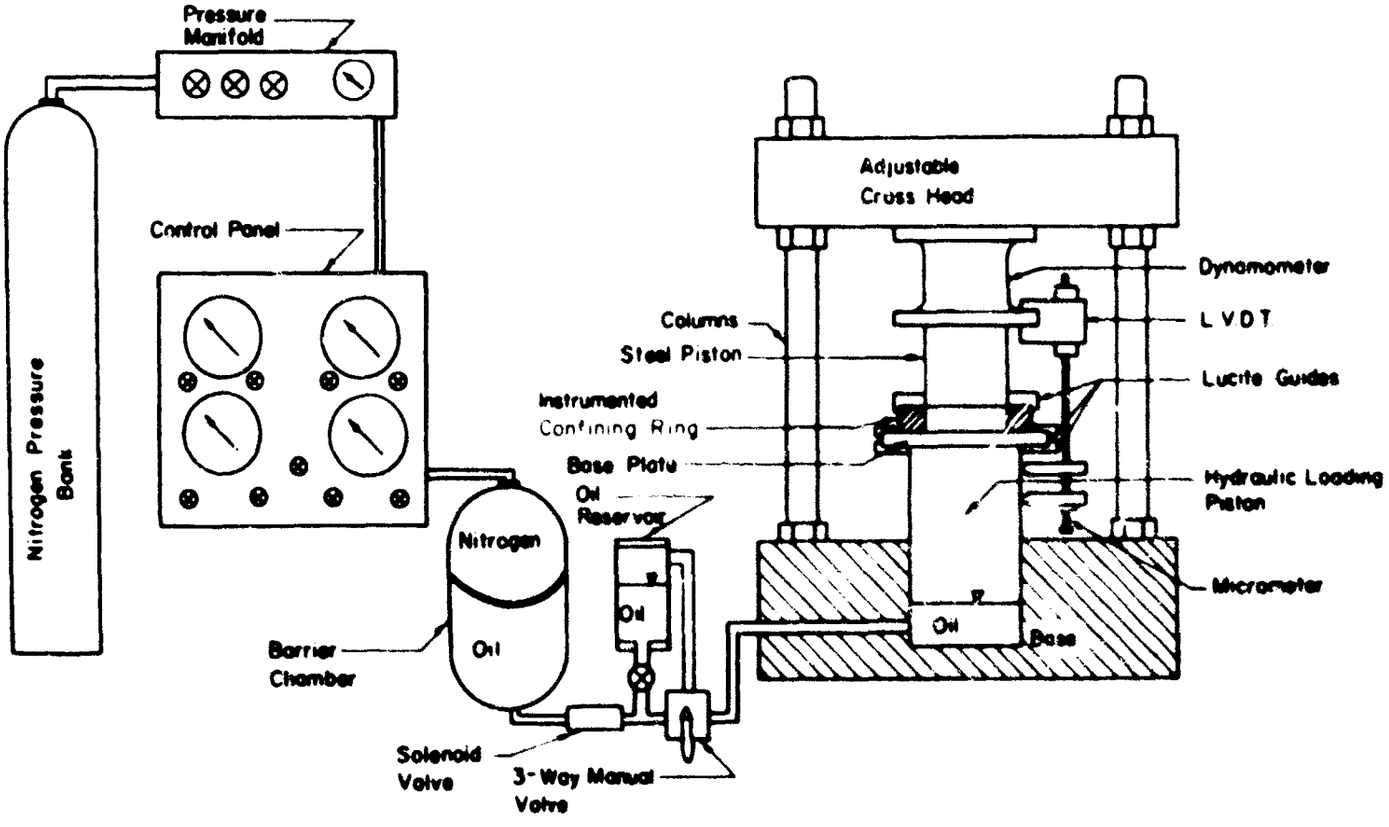


Fig. 10 Schematic of Rapid Loading Machine

Test Procedure

In the rapid loading machine a seating load of approximately 1 to 2 psi was applied to each specimen before recording either the calibrations or the zero readings. The characteristics of the dynamic loading machine, however, required a seating load of approximately 120 psi on the specimen before the zero determinations could be made for axial strain. No attempt has been made to correct the test data for the rather high seating load that was applied.

Stress-Strain Relationships

The stress-strain relationships for the eight dynamic and rapid tests are shown in Figures 14 and 15. Using specimen B-1-0 as an example, it is observed that the stress-strain relationship is concave downward until a stress of approximately 1,000 psi and a strain of approximately 4 percent is reached at the point of inflection A. Beyond point A the stress-strain curve is concave upward in a manner similar to that for the static tests. The rebound or decay portion of the stress strain curve has a steep slope (high modulus) slope down to stresses on the order of 100 psi to 1,000 psi. Below stress levels from 100 psi to 1,000 psi the slope of the curve decreases markedly (low modulus) as the stress decreases. The residual strains vary from 77 percent to 91 percent of the maximum (steady state) strains and average 83 percent; the strain data are listed in Table 4.

A summary of the dynamic and rapid test data including: the rise, dwell and decay times; the axial stresses, strains and degrees of saturation at the peak axial stress; and the steady-state stresses and strains is presented in Table 4. It is noted that for sample B-1-0 a peak stress of 20,300 psi was recorded although the steady-state stress was only 8,200 psi. Therefore, an overshoot equal to approximately 150 percent of the steady-state stress occurs. For the other dynamic tests the overshoot varies between approximately 100 percent and 200 percent. Because the overshoot of the gas loading on the piston surface has been shown by Sinnamon and McVinnie (3) to be on the order of 20 percent to 25 percent of the steady-state stress, it must be concluded that the high observed overshoots are a function of the mass of the piston and the stress-strain properties of the specimen. The weight of the piston assembly is approximately 150 lbs.

On Figure 13 it can be seen that approximately 80 percent of the steady-state strain occurs at the time of the first stress peak (3.1 milliseconds). The remaining 20 percent strain occurs in the next 2 milliseconds and no significant increase

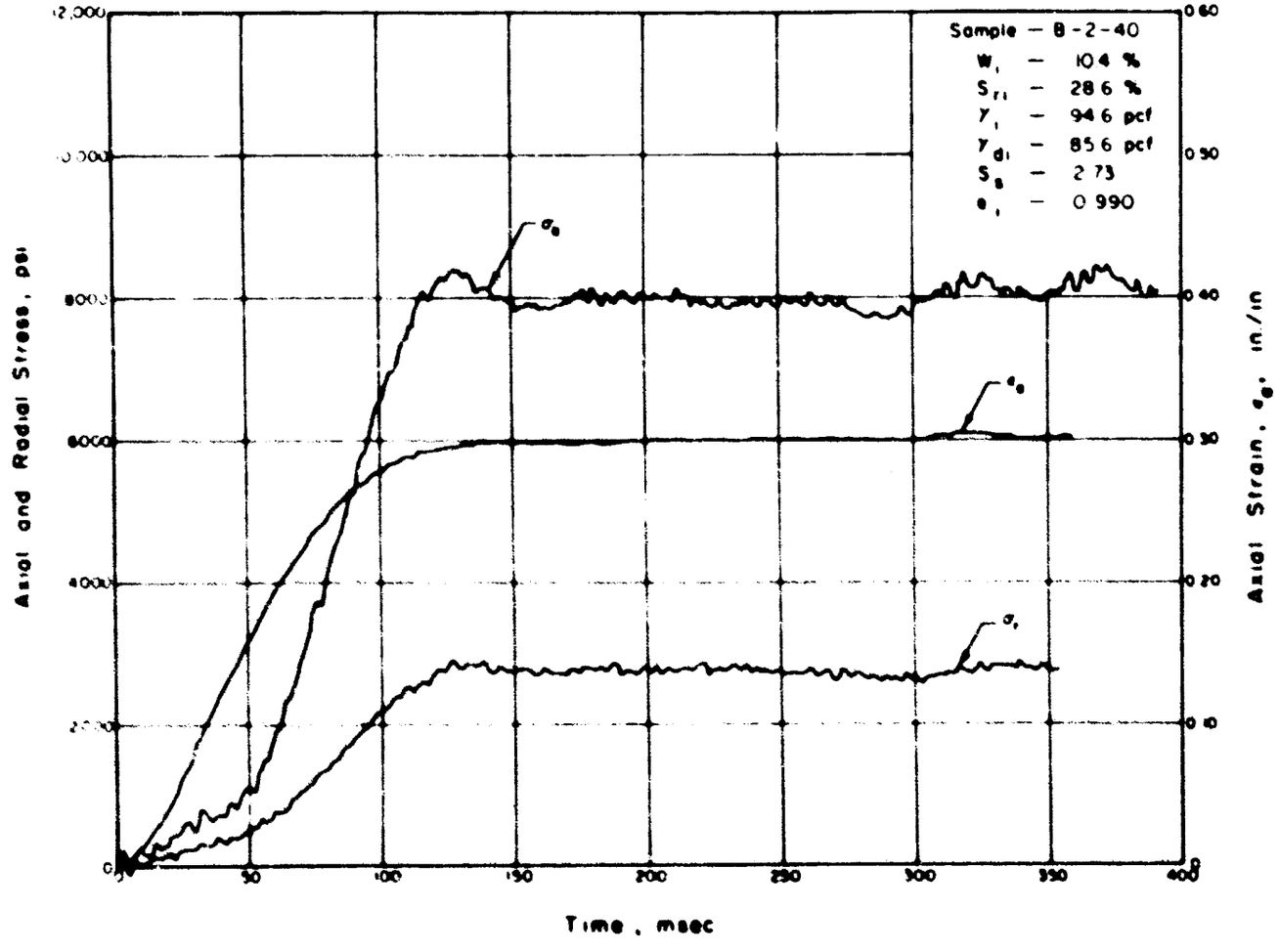


Fig. 11 Rapid Test Data

in strain occurs thereafter. It is probable that if the steady-state stress could have been applied without the overshoot occurring, a lower steady-state strain would have been observed. In this case the strain response would probably have been more like that observed for specimen B-2-40 on Figure 11 where a rise time of approximately 100 to 150 milliseconds was required for the stress and the strain to be in phase. It is believed that the stress overshoot induces strains beyond those that would occur if the steady-state stress were applied without overshoot. Therefore, high overshoots have the effect of forcing the steady-state strain to be nearly in phase with the applied stress, but lagging it somewhat, in this instance by 2 milliseconds.

Constrained Modulus-Stress Relationships

The dynamic and rapid secant moduli M_{cs} have been determined from the stress-strain curves and are presented on Figures 16 and 17. Considering the shape of the stress-strain curves it is clear that the initial secant modulus should be very nearly the modulus determined from seismic and vibration investigations. Because of the concave downward stress-strain relationship, the secant modulus decreases until the point of inflection A is passed. Beyond point A the modulus begins to increase continuously with increases in axial stress. It is noted that a straight line approximates the secant modulus - axial stress relationship between axial stresses of 2,000 psi and 10,000 psi for all 8 tests; if specimens B-1-0 and B-2-70b are excluded, the secant modulus-stress relationship is nearly linear between 1,000 psi and 10,000 psi.

The stress at a given strain in a dynamic test is approximately twice that observed for a static test on the corresponding specimen; therefore, the secant modulus in a dynamic test is also approximately twice that for a static test (or a rapid test). This phenomenon is a function of the permeability of the soil and the initial degree of saturation. In the dynamic tests the air and water in the soil voids do not have time to adjust geometrically to the applied strains as the soil skeleton is stressed. This causes a transient pore pressure which has a variable magnitude from void to void. Part of the observed soil stiffness is, therefore, due to the high bulk modulus of the water in the soil voids. In the rapid tests sufficient time was available for partial air drainage and at least partial redistribution of the pore water in the voids; therefore, the observed moduli were lower than those from the dynamic tests.

TABLE 4
SUMMARY OF DYNAMIC AND RAPID TEST DATA

Sample Number	Time, milliseconds			Initial Peak			K_o	Steady State		Residual	Inflection Point	
	Rise	Dwell	Decay	σ_o, psi	ϵ_o, in/in	Saturation	Loading	σ_o, psi	ϵ_o, in/in	ϵ_o, in/in	σ_o, psi	ϵ_o, in/in
B-1-0	3.1	448	129	20,300	0.230	60.3	0.59	8,200	0.290	0.235	1000*	0.040
B-1-20	3.1	523	111	8,000	0.190	80.0	0.5-0.8	5,500	0.285	0.235	825*	0.043
B-1-40	4.9	535	90	6,400	0.245	43.6	0.46	2,300	0.235	0.200	400*	0.040
B-2-0	145	445	85	3,900	0.245	55.0	0.60	3,800	0.246	0.190	135	0.040
B-2-20	108	609	62	7,600	0.274	62.3	0.54	7,400	0.290	0.240	200	0.045
B-2-40	128	519	86	8,200	0.295	71.5	0.46	6,300	0.310	0.277	400	0.060
B-2-70A	4.2	445	75	6,000	0.200	93.1	0.56	2,300	0.230	0.193	700*	0.030
B-2-70B	3.1	420	112	16,000	0.200	91.2	0.52	8,800	0.270	0.224	950*	0.025

* Does not include 120 psi seating load.

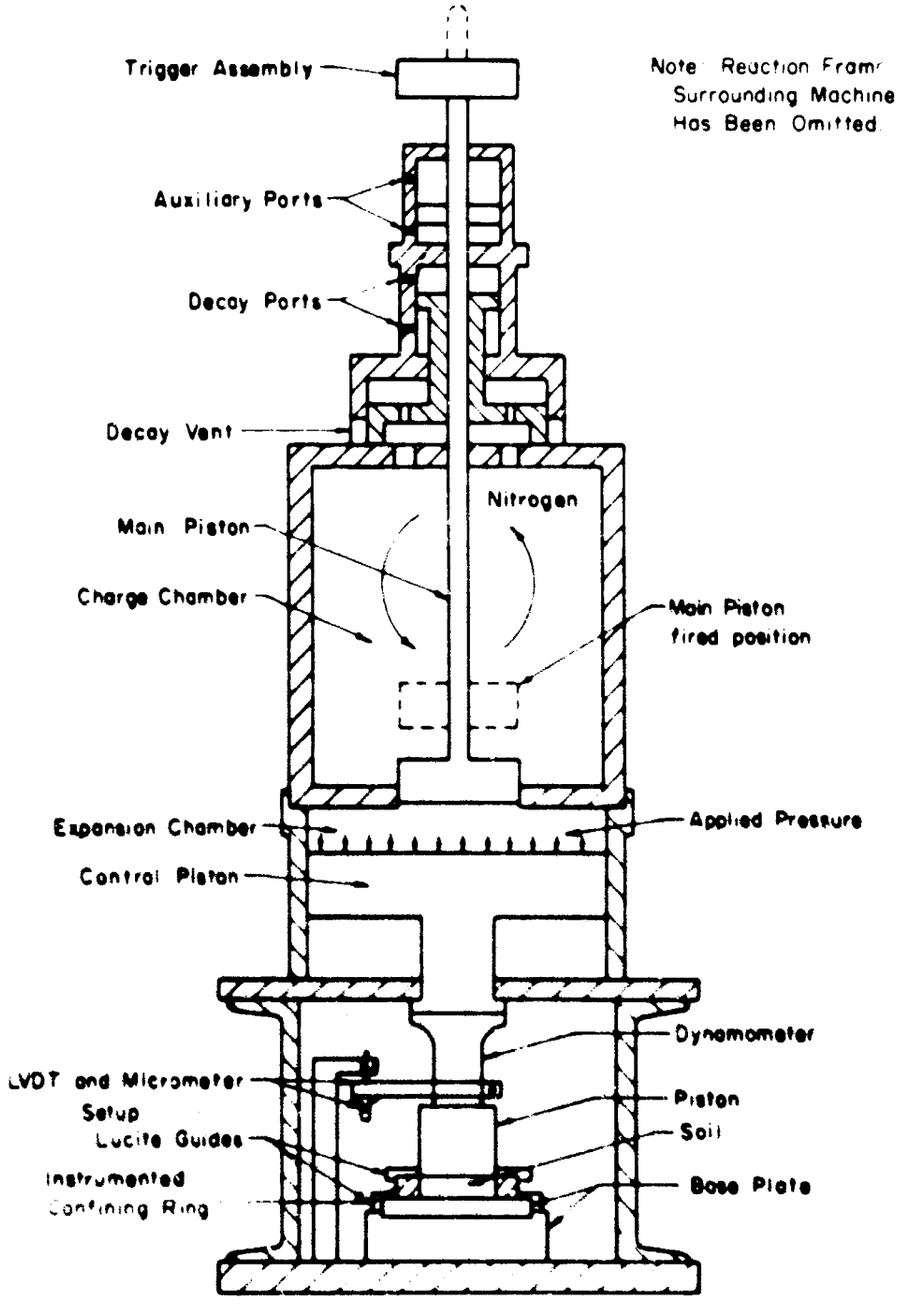


Fig. 12 Schematic of Dynamic Loading Machine

Axial Stress-Radial Relationships

At any given stress level the ratio of the radial stress to the axial stress is called K_o; it should be noted that this ratio as referred to herein is based on total stresses, not effective stresses. The subscript zero usually denotes that no radial strains are involved; however, in the dynamic tests limited radial strains were allowed to occur. A summary of the K_o data upon initial loading is given in Table 4. The values generally range between 0.5 and 0.6 for axial stress levels below 5,000 psi.

Because of the large axial strains, on the order of 20 to 30 percent, a correction was applied to the measured radial strains in order to obtain the radial stresses believed to be more representative. Because a thick ring is used as the radial strain sensing element, it is possible to have several pressure conditions on the inside of the ring that produce the same response in the strain gauges on the perimeter of the ring. For this reason, the confining ring is essentially a load measuring device. An attempt to correct the measured radial stress has been made by dividing the load determined from a hydraulic calibration by the actual area of the specimen. This amounts to dividing the indicated radial stress by the quantity, $1 - \epsilon$.

The K_o data for sample 8-1-0 is given in Figure 18. The loading portion of the curve is nearly linear to the peak stress of 20,300 psi. On this portion of the curve K_o has a value of 0.59. Upon unloading, the value of K_o increases as shown by the solid line. This is in accordance with the behavior of soil specimens loaded statically.

The dashed line indicates that several oscillations occur in this area. The solid line returning to zero axial stress is determined from the unloading portion of the radial stress and axial stress versus time records.

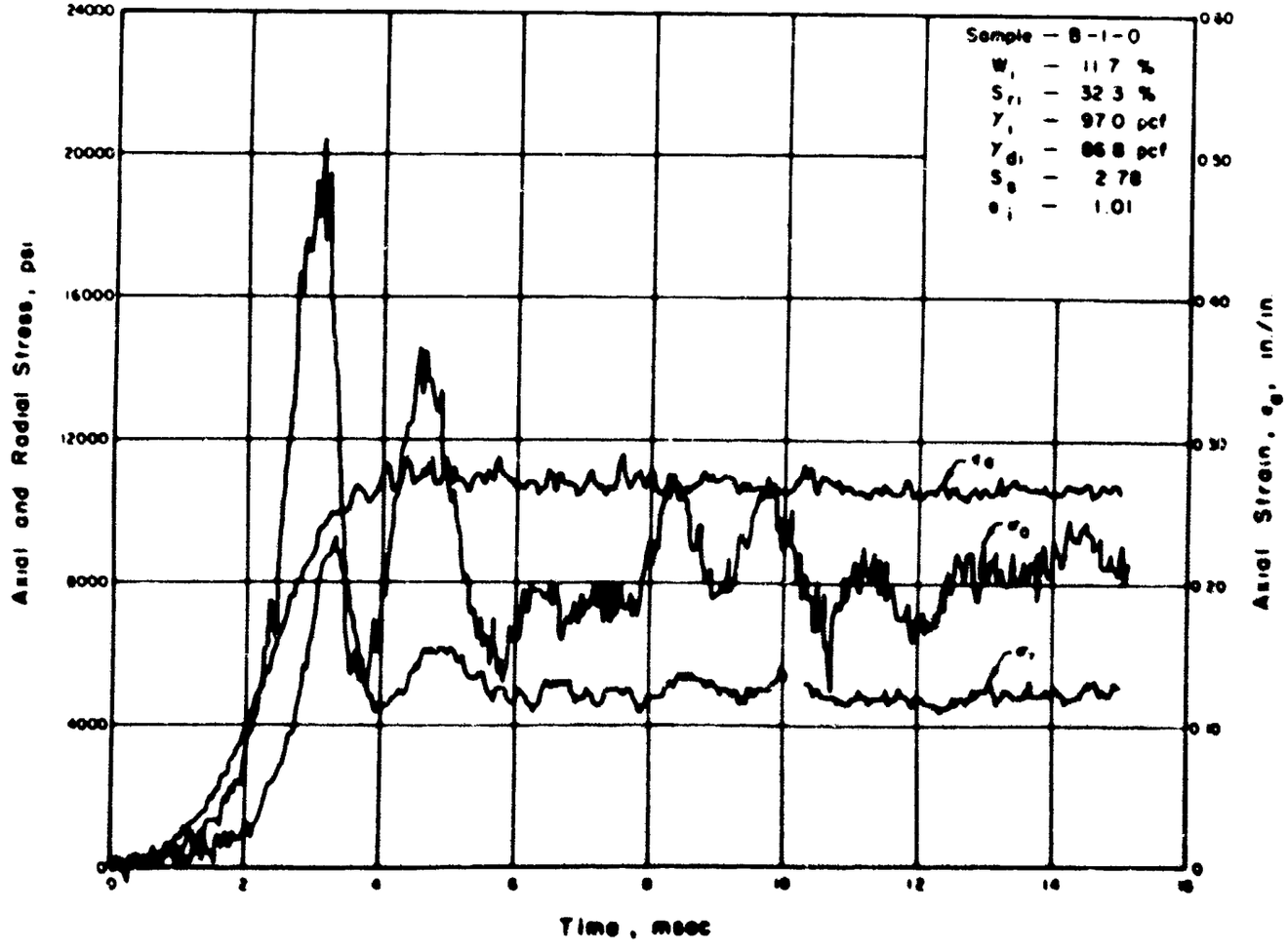


Fig. 13 Dynamic Test Data

INTERPRETATION OF TEST RESULTS

General

In interpreting the data it is recognized that the constrained modulus is the most important quantity under consideration. Also of importance are the values of K_o because lateral pressure predictions are also necessary for the design of underground protective structures. In the lower pressure ranges, the point of inflection A on the stress-strain curves may have considerable significance with respect to stress attenuation. For these purposes the seismic and vibration data, and the static, rapid and dynamic one-dimensional compression tests have been considered together in order to develop a unified picture of the behavior of playa silt.

It must be remembered that the data under consideration are from two different borings approximately 4000 ft apart. Even though the soil deposit is uniform in a given horizon as compared to most soil profiles, there are variations from specimen to specimen that make the interpretation of the test results a matter of considerable individual judgment. Furthermore, at least two or three distinct soil layers have been detected at the Nevada Test Site as evidenced by the data in Table 2. Within each of these distinct soil layers there are variations in the soil gradation within a distance of a few inches vertically. Therefore, it is clear that correlation for this particular soil for which generalizations can be made will be crude because the test specimens are themselves a variable.

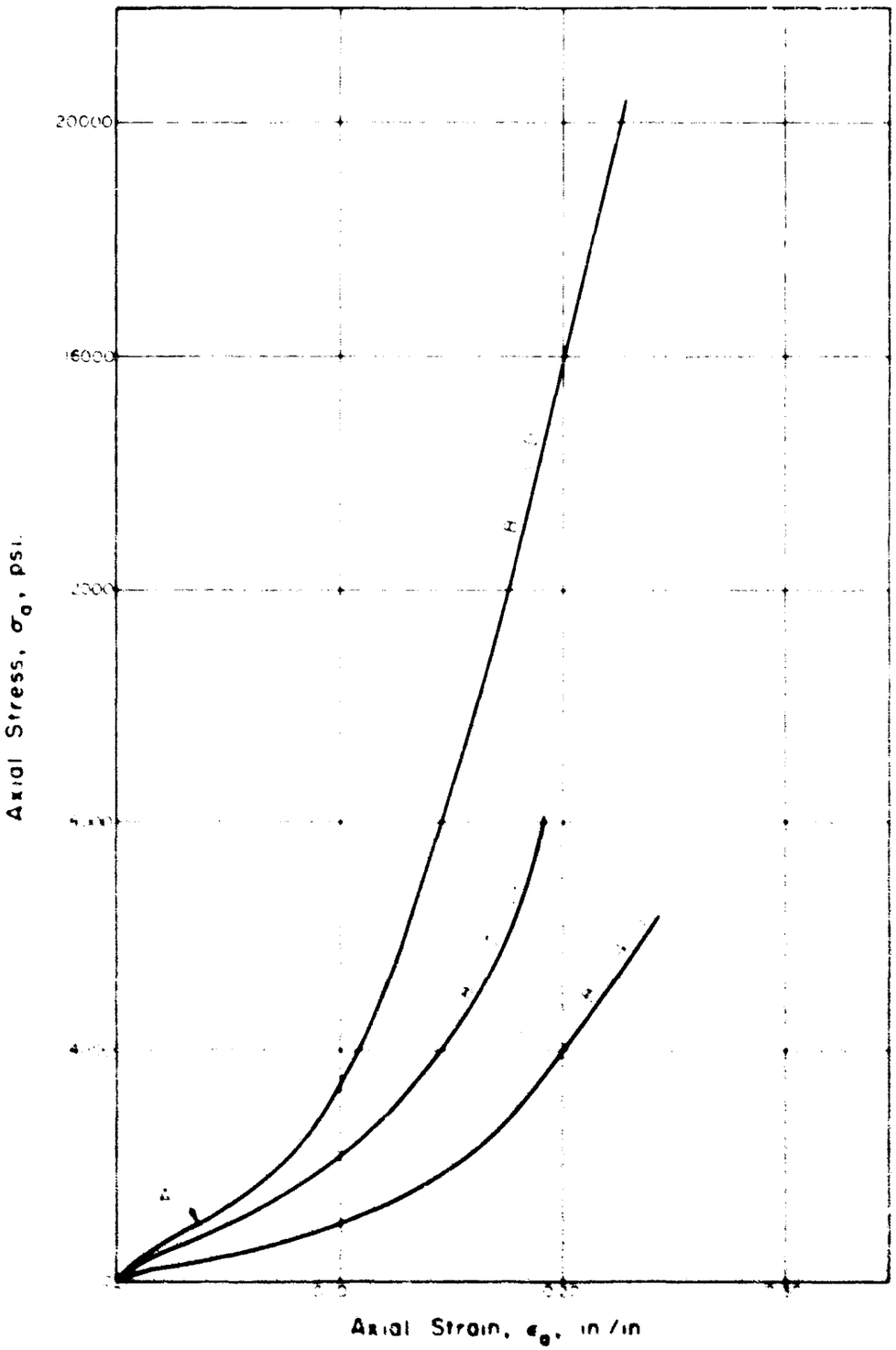


Fig. 14 Stress-Strain Curve for Playa Silt in One-Dimensional Compression

Secant Modulus

A comparison of the secant moduli determined from the rapid and static tests is given on Figure 19 for stress levels up to 5,000 psi. There is nearly a 1 to 1 correspondence between the static and rapid tests. A similar comparison has been made on Figure 20 for the secant moduli from dynamic and static tests. The data suggest that the

dynamic moduli are on the order of 1.85 the static moduli up to an axial stress level of 5,000 psi. The above comparison between static tests and dynamic tests indicates that for rise times on the order of 2 to 3 milliseconds the soil stiffness is approximately doubled. Furthermore, for the three rapid tests with rise times between 100 and 150 milliseconds the results were nearly the same as for the static tests.

Secant moduli-axial stress relationships are shown for all tests in Figure 21. The results from the static and rapid tests fall within a relatively narrow band. The line that has been selected to represent this band is given by $M_{cs} = 4000 + 3\sigma_a$. This equation is not valid for axial stresses below 1000 psi. Although the static tests were not carried to an axial stress beyond 5,500 psi, it is believed that the relationship would be valid to a stress of 10,000 psi; this conclusion is based upon the results of the dynamic and rapid tests which indicate linearity up to 10,000 psi. In a similar manner, the dynamic moduli have been plotted versus the axial stress. Instead of falling within a narrow band, the data tend to diverge as the axial stress is increased. A dashed line with ordinates 1.85 times the ordinates of the line used to represent the static and rapid tests is shown in Figure 21 for comparison with the dynamic data. A slightly different line with the equation $M_{cs} = 13,000 + 4\sigma_a$ has been selected to represent the dynamic test data. This relationship is valid in the axial stress range from 2,000 psi to 10,000 psi. For three of the five dynamic tests, the relationship would be valid down to 1,000 psi. The foregoing information leads directly to a simple procedure for selecting a constrained secant modulus for ground motion studies at the Nevada Test Site for stress levels beyond 1,000 psi. Because the soils of the Nevada Test Site are above the water table, and have a very low degree of saturation, a rapid increase in the secant modulus with increasing axial stress is not detected until stress levels beyond 10,000 psi are reached. This situation is believed to be peculiar to the Nevada Test Site; for more normal soil

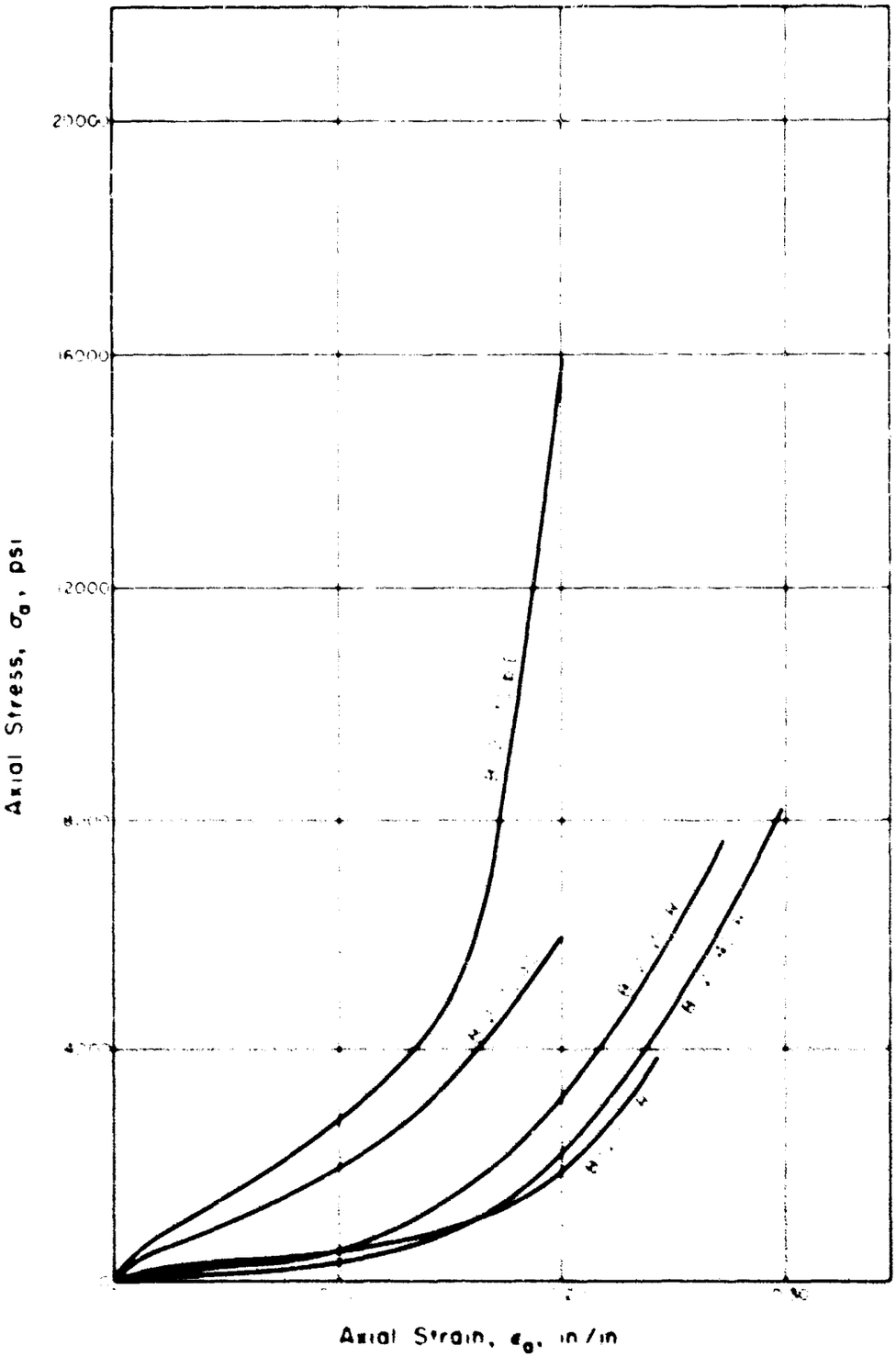


Fig. 15 Stress-Strain Curve for Playa Silt in One-Dimensional Compression

profiles it is probable that the secant modulus would increase rapidly with increases in axial stress at much lower stress levels because the initial degree of saturation is higher.

At stress levels near zero the secant modulus, and also the tangent modulus, would probably be extrapolated to zero stress at a modulus equal to that determined by seismic or vibrational techniques. Considering this interpretation it is clear that a significant decrease in the secant modulus takes place during loading at stress levels below 1,000 psi. If the minimum points on the secant modulus-axial stress relationships are compared to the moduli determined by seismic techniques, it is seen that the secant moduli are on the order of 10 percent to 20 percent of the seismic modulus. At the Nevada Test Site, soil stresses beyond the 10,000 psi to 15,000 psi range would be necessary before the secant modulus would again become as high as that determined from seismic investigations.

Significance of Strain

As mentioned previously the secant moduli determined from dynamic tests are approximately 85 percent higher than the corresponding secant moduli from static tests. However, strains at the point of inflection A for both the static and dynamic stress-strain curves are in the range of 4 percent to 5 percent. At the Nevada Test Site it is believed that the points of inflection may be controlled by cementation more than it is by desiccation or preloading. An interpretation of the observed phenomena is that a strain on the order of 4 percent to 5 percent is required to destroy the effects of cementation and/or preload and desiccation. After the effects of cementation have been

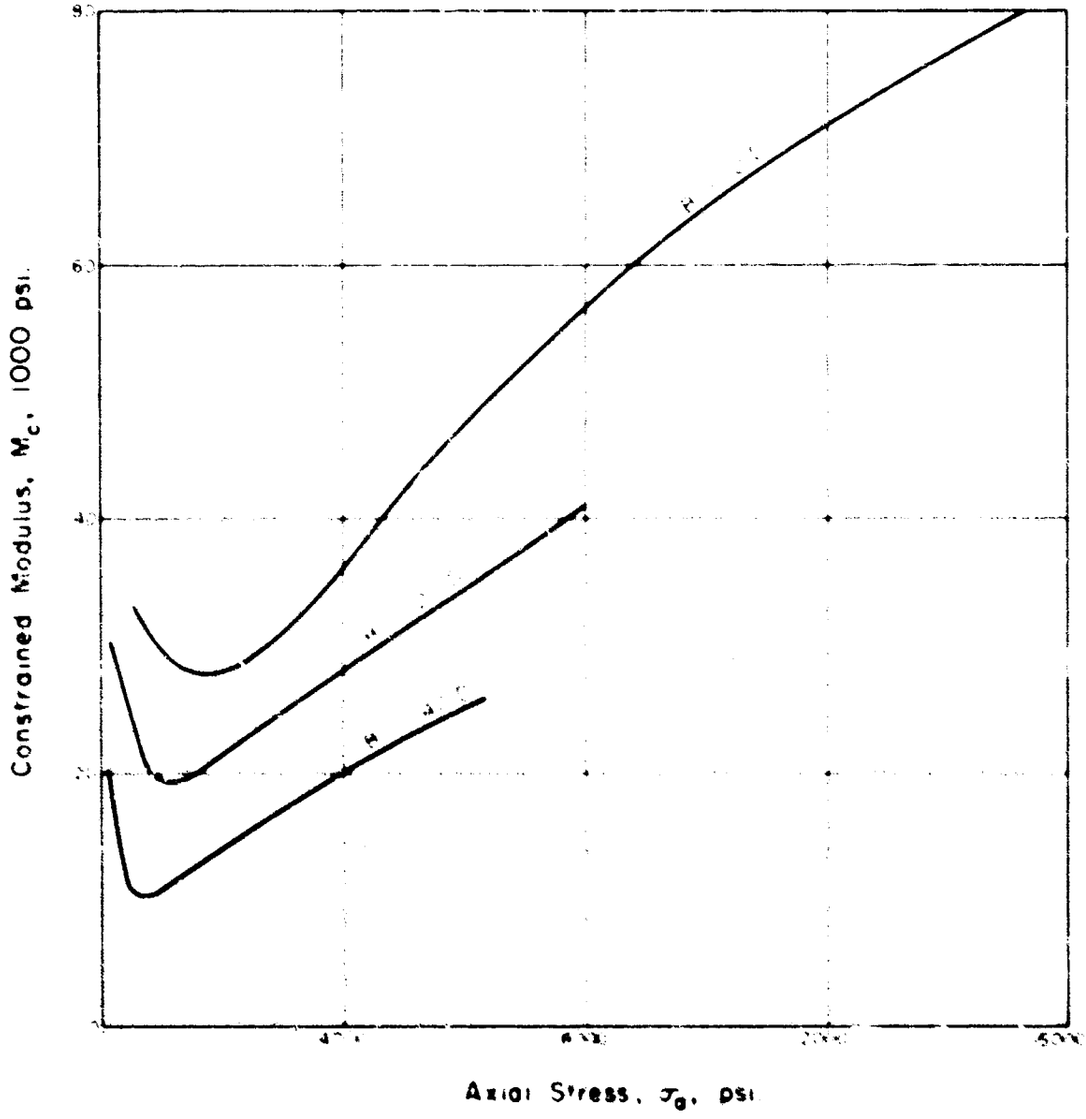


Fig. 16 The Relationship Between Constrained Modulus and Axial Stress for Playa Silt in One-Dimensional Compression

destroyed, the stress-strain curve is concave upward as observed in tests on granular materials without cementation. Therefore, at low axial stress levels, gradual destruction of the cementation and/or preload or desiccation effects cause the tangent modulus to decrease with an increase in the axial stress up to the point of inflection A. Beyond point A the tangent modulus increases which gives a concave upward stress-strain curve. For predicting ground motions at low stress levels, the reversed curvature of the stress-strain curve is significant. However, beyond the point of inflection, at higher stress levels, the reverse curvature at the lower stress levels is not significant except that it causes an increase in the rise time of the pressure time curve with depth.

Another interesting strain phenomenon is observed when the residual strains are compared to the maximum strains. In the static tests the residual strains averaged approximately 80 percent of the maximum strains, whereas in the dynamic tests the residual strains were 83 percent of the steady state strains.

Radial Stresses

On Figure 22 a comparison has been made between the K_o values from the static and dynamic tests in the stress range from zero to 5,000 psi. It is observed that the dynamic values are approximately 10 percent higher than the corresponding static values. For practical purposes there is essentially no difference in the K_o-values; they range between 0.47 and 0.55 for the static tests and 0.46 to 0.60 for the dynamic tests. An average value for K_o between 0.50 and 0.55

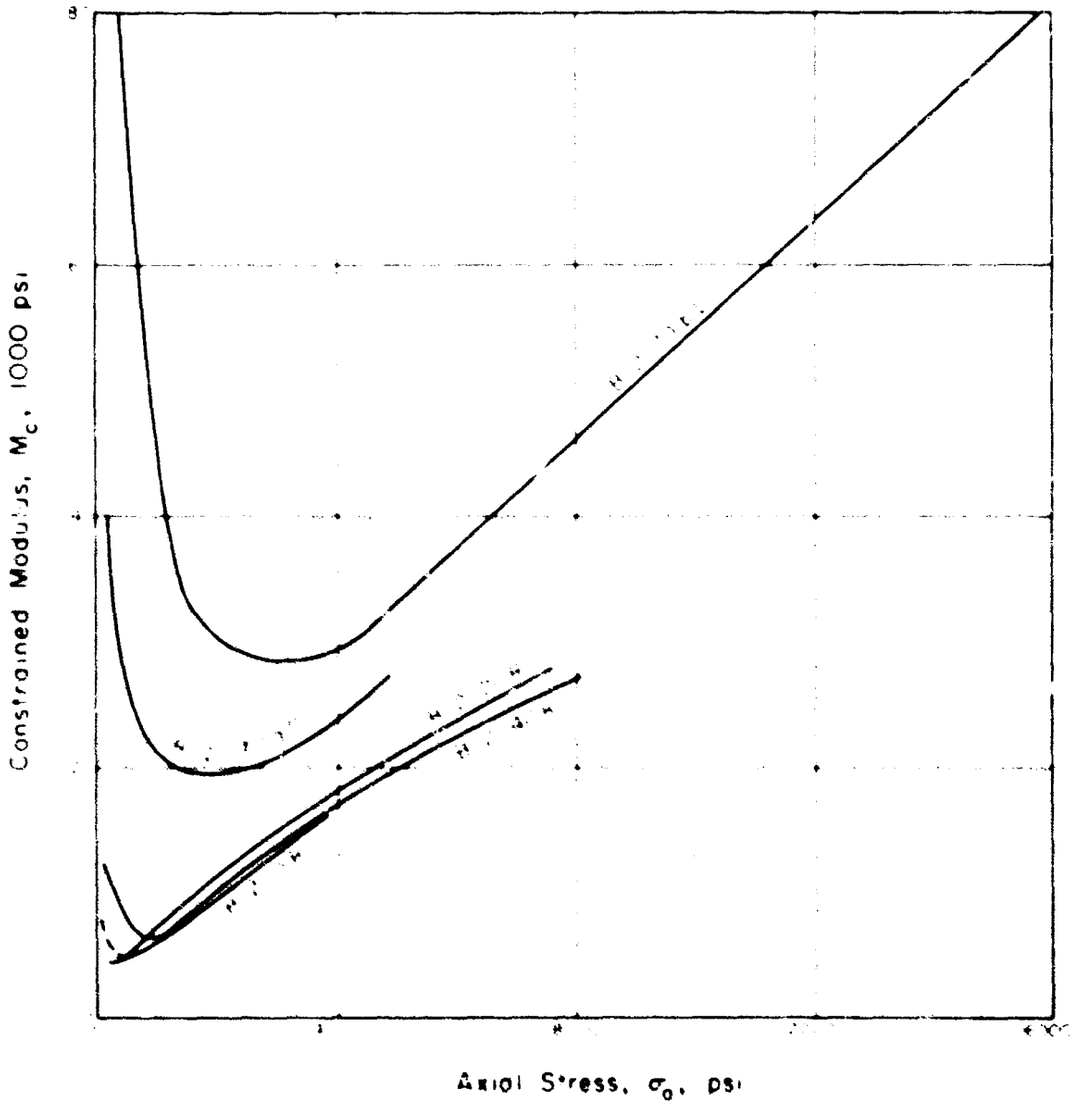


Fig. 17 The Relationship Between Constrained Modulus and Axial Stress for Playa Silt in One-Dimensional Compression

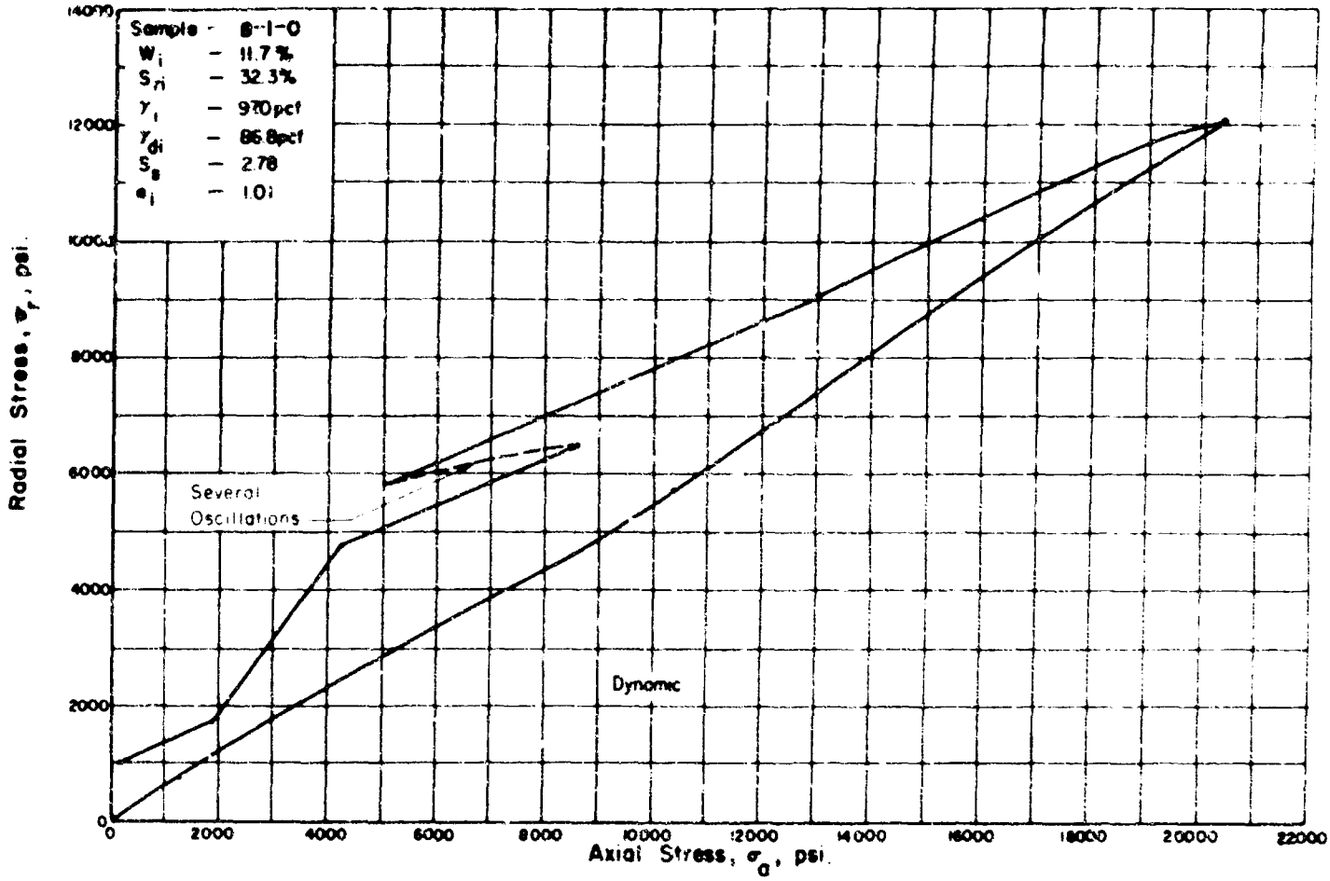


Fig. 18 Relationship Between Axial and Radial Stress for Playa Silt in One-Dimensional Compression

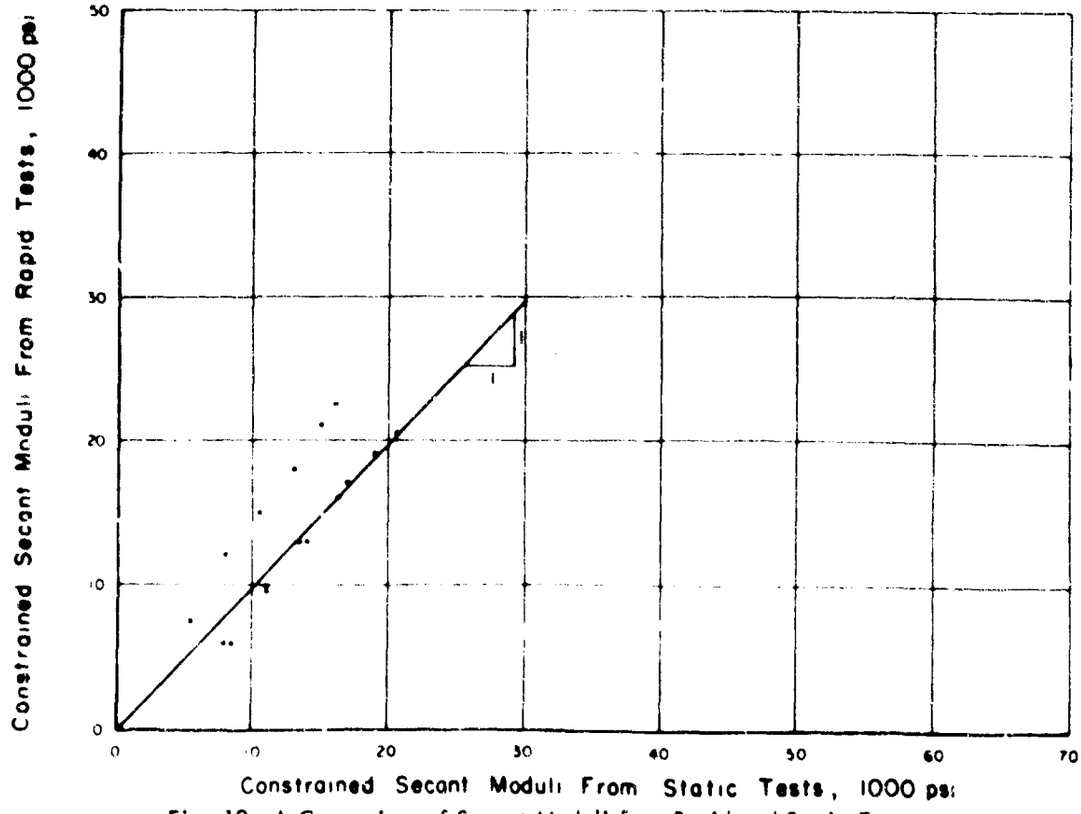


Fig. 19 A Comparison of Secant Moduli from Rapid and Static Tests

would be satisfactory for both the static and dynamic tests in the zero to 5,000 psi axial stress range.

For the remolded specimen tested statically, and for the dynamic tests on specimens B-2-70a and B-2-70b, it was observed that the K_o-values tend to increase when the degree of saturation reaches the range of 80 to 85 percent. This phenomenon occurs because the air permeability of the soil is vastly decreased at high degrees of saturation and the air becomes trapped. Consequently, additional increments of axial stress induce total radial stress increments that tend to approach the increase in axial stress. At sites that have more typical soil conditions than those occurring at the Nevada Test Site (i.e., a degree of saturation in excess of 80 percent), higher K_o-values are likely to be observed below an axial stress level of 5,000 psi than were observed for the tests presented herein.

Constrained Modulus-Depth Relationship at the Nevada Test Site

There are two or three distinct soil layers at the Nevada Test Site with each layer itself having natural variations in its engineering properties. These variations are illustrated on Figure 23 wherein the following have been plotted: the initial constrained moduli for the static, dynamic and rapid one-dimensional tests; the constrained modulus computed from seismic velocities and from the elastic constants determined with the aid of field and laboratory vibration tests. The dashed line indicates that the seismic modulus is on the order of 25,000 psi for the first 20 ft, but that it has a value of approximately 180,000 psi below a depth of 20 ft. The Young's modulus determined with the aid of the field vibration test has a value of 5,000 psi at the ground surface, but is believed generally to increase somewhat with depth; at a depth of 20 ft it has a value of 40,000 psi increasing to approximately 65,000 psi at a depth of 40 ft. The constrained modulus computed from the Young's modulus would be approximately twice the value of Young's modulus; therefore, points have been shown at 10,000 psi at a depth of zero ft and at 80,000 psi and 130,000 psi at depths of 20 ft and 40 ft, respectively. It should be noted that the constrained moduli determined from vibration techniques are less than half those computed from seismic techniques, except at a depth of 40 ft.

The constrained modulus computed from Wilson's laboratory vibration test (1) is higher than the seismic modulus in the upper 20 ft of the soil profile. It is believed that this phenomenon occurs because the confining pressure applied in the laboratory causes a higher modulus to be observed than occurs in the field where the natural material is fissured. Below a depth of 20 ft the vibration tests exhibit a modulus on the order of 1/4 to 1/3 of the seismic modulus.

The initial* constrained secant modulus determined from the static, rapid and dynamic one-dimensional tests, have been plotted on Figure 23 for comparison. The initial secant modulus for the static and rapid tests are on the order of 8 to 15 percent of the seismic modulus, whereas the dynamic moduli are on the order of 15 to 30 percent of the

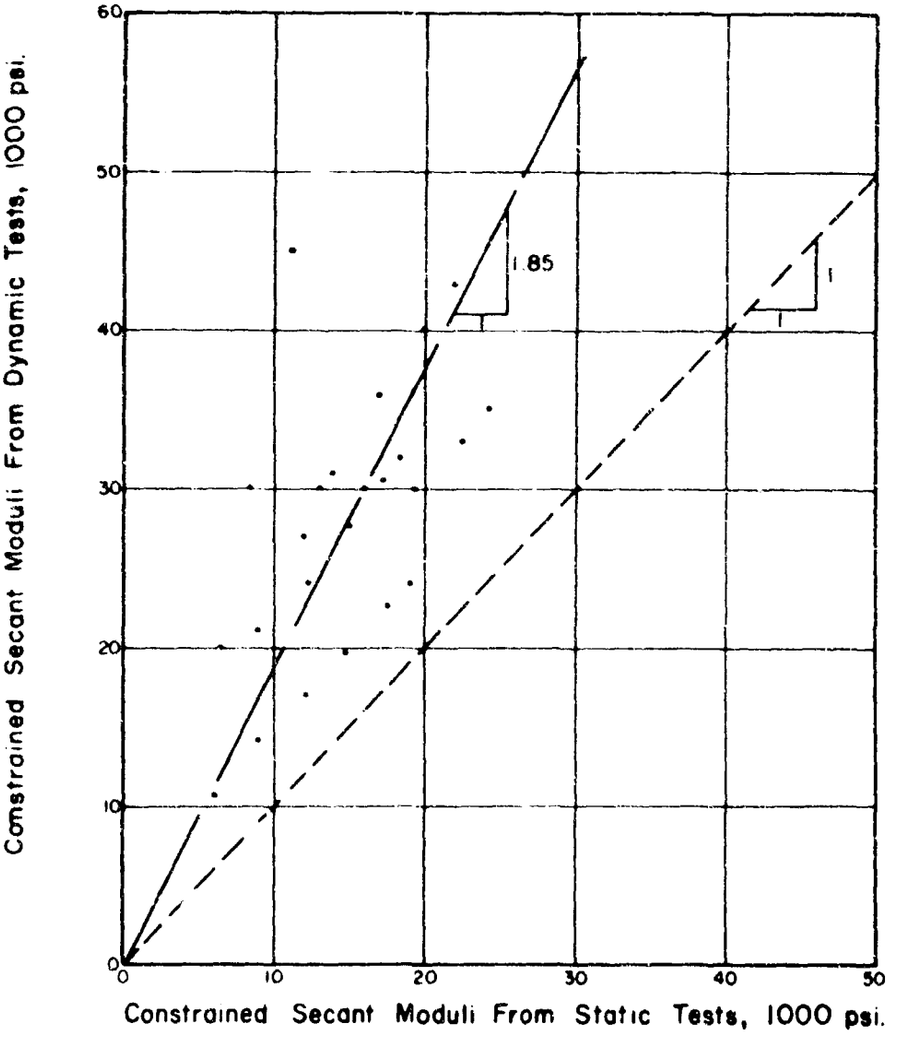


Fig. 20 A Comparison of Secant Moduli from Static and Dynamic Tests

* The initial constrained secant modulus is determined at axial stress levels below 200 psi.

seismic modulus. It is also noted that the constrained modulus at the ground surface determined from Wilson's laboratory vibration test is very close to that determined initially in the dynamic one-dimensional test.

On Figure 24 the secant moduli at an axial stress of 1,000 psi have been plotted for the static, rapid and dynamic one-dimensional tests. The Young's modulus and constrained modulus from the field vibration and seismic tests, and from Wilson's laboratory tests, have also been plotted for comparison. At this stress level the dynamic constrained moduli are on the order of 10 percent to 15 percent of the moduli determined from seismic investigations, whereas the static moduli are on the order of 4 percent to 8 percent of the seismic moduli. The dynamic moduli are also approximately 50 percent of the moduli determined in the Wilson vibration apparatus. At the Nevada Test Site stress levels beyond 10,000 to 15,000 psi will be required before the dynamic secant moduli equal or exceed those determined by the Wilson device, or by seismic means. Clearly, the use of moduli determined from laboratory vibration tests and from seismic investigations requires considerable adjustment to account for the stress level that will occur in the field.

Selection of Modulus for Ground Motion Studies at the Nevada Test Site

At very low stress levels it is apparent that moduli determinations from field or laboratory vibration tests, and from field seismic investigations, are useful. However, as the stress level is increased the percentage of the seismic modulus utilized must be decreased in order to account for the behavior of the soil at stress levels higher than that involved in seismic and vibratory investigations. A better procedure would be to determine directly the variation in the secant modulus with the stress level from dynamic one-dimensional compression tests.

At stress levels beyond the complications of the stress-strain curve caused by cementation, desiccation, or preload, a very simple approximate procedure determined on the basis of the tests presented herein can be used to select the constrained modulus for ground motion studies at the Nevada Test Site. The equation (Figure 21) for the dynamic modulus $M_{cs} = 13{,}000 + 4\ \sigma_a$ may be used for stress levels between 1,000 psi to 2,000 psi and 10,000 psi. Another simple procedure would be to use twice the modulus observed in static one-dimensional tests. Note that these empirical correlations disregard the point of inflection observed at low stress levels; they also disregard any variation in the modulus with respect to depth. If the moduli for higher stress levels are plotted versus depth it will be seen that there is a tendency for the

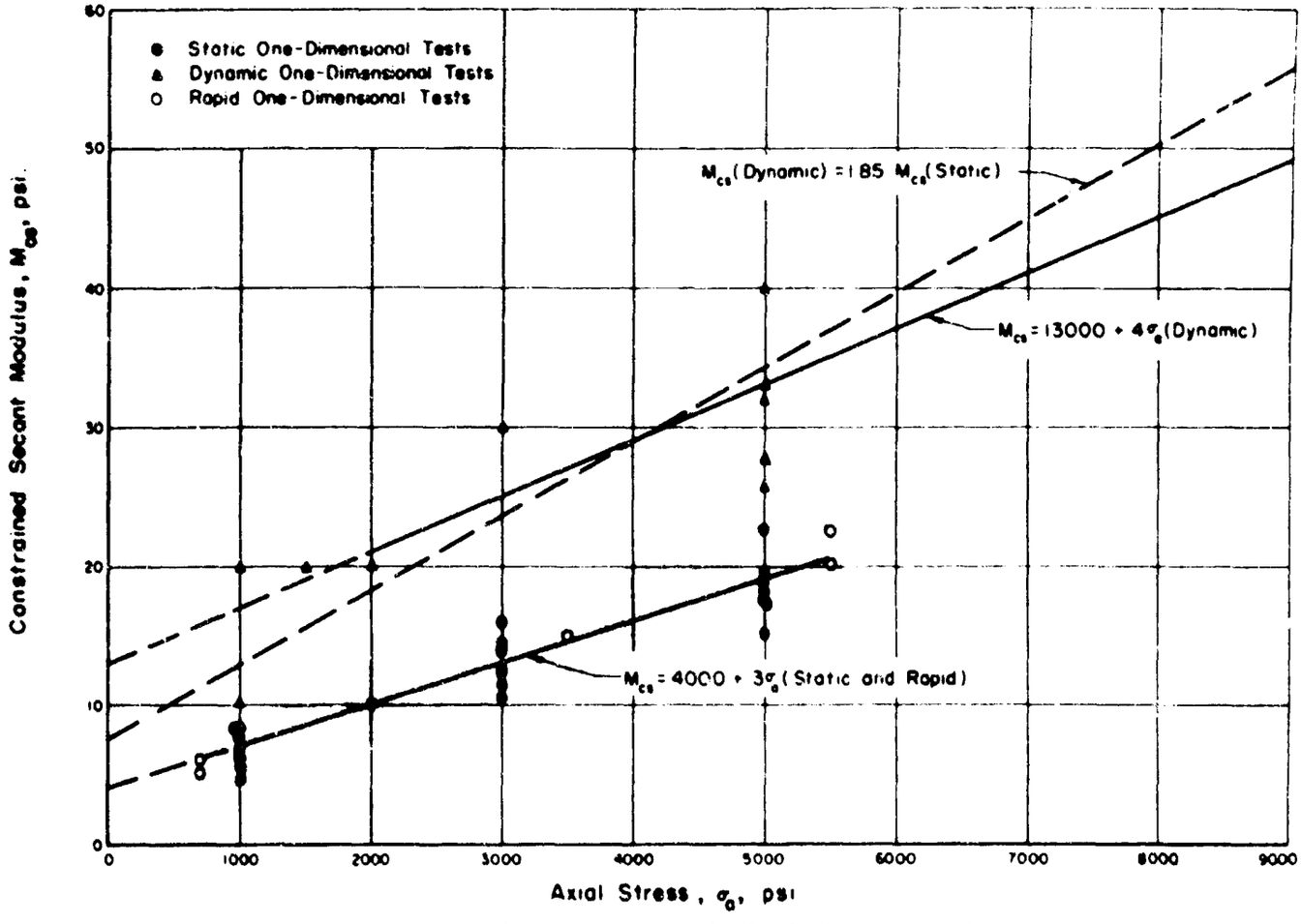


Fig. 21 The Relationship Between Static, Rapid and Dynamic Constrained Secant Moduli with Axial Stress

moduli to become nearly constant with respect to depth. This is reasonable considering that the effects of cementation, desiccation and preload are negligible with respect to the stress level that is applied. However, if the details of stress wave propagation are to be considered in ground motion studies, then the actual shape of the stress-strain curve will have to be considered.

CONCLUSIONS

At a given stress level the dynamic constrained modulus (rise time of 2-3 milliseconds) is approximately twice the static modulus. However, for rise times of 100 milliseconds or longer the modulus is essentially equal to the undrained static modulus.

The constrained modulus is strongly dependent on the stress level. At low stress levels, on the order of several psi, the modulus is essentially equal to that determined by vibration tests, or even seismic techniques. As the stress level is increased the modulus decreases, reaching a minimum at approximately 1,000 to 2,000 psi. Thereafter, the modulus increases nearly linearly with an increase in the stress level.

Under actual field conditions for stress levels below the range of 1,000 to 2,000 psi, the rise time of the peak stress should increase with depth because of the concave downward stress-strain relationship. This conclusion is also substantiated by field observations. Stress levels considerably above these values would be necessary for a shock to form or continue to be propagated.

The prediction of ground motions by using an effective seismic velocity involves considerable judgment. At stress levels of approximately 1,000 to 2,000 psi an effective velocity of 30 percent of the seismic velocity is required. Note that the 75 percent factor commonly recommended would be considerably in error for overpressures in the 1,000 to

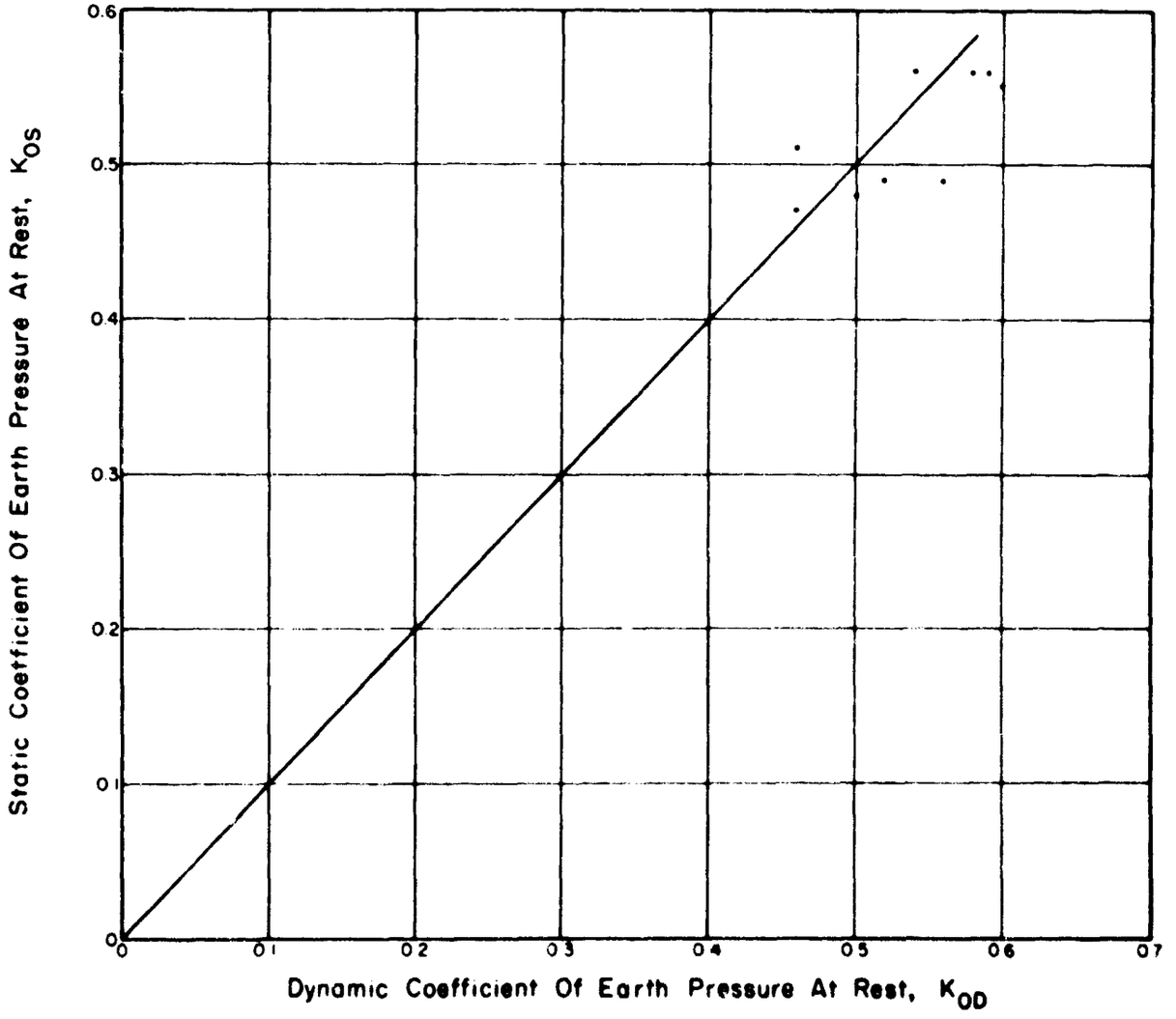


Fig. 22 A Comparison of the Static and Dynamic Coefficients of Earth Pressure at Rest for Playa Silt

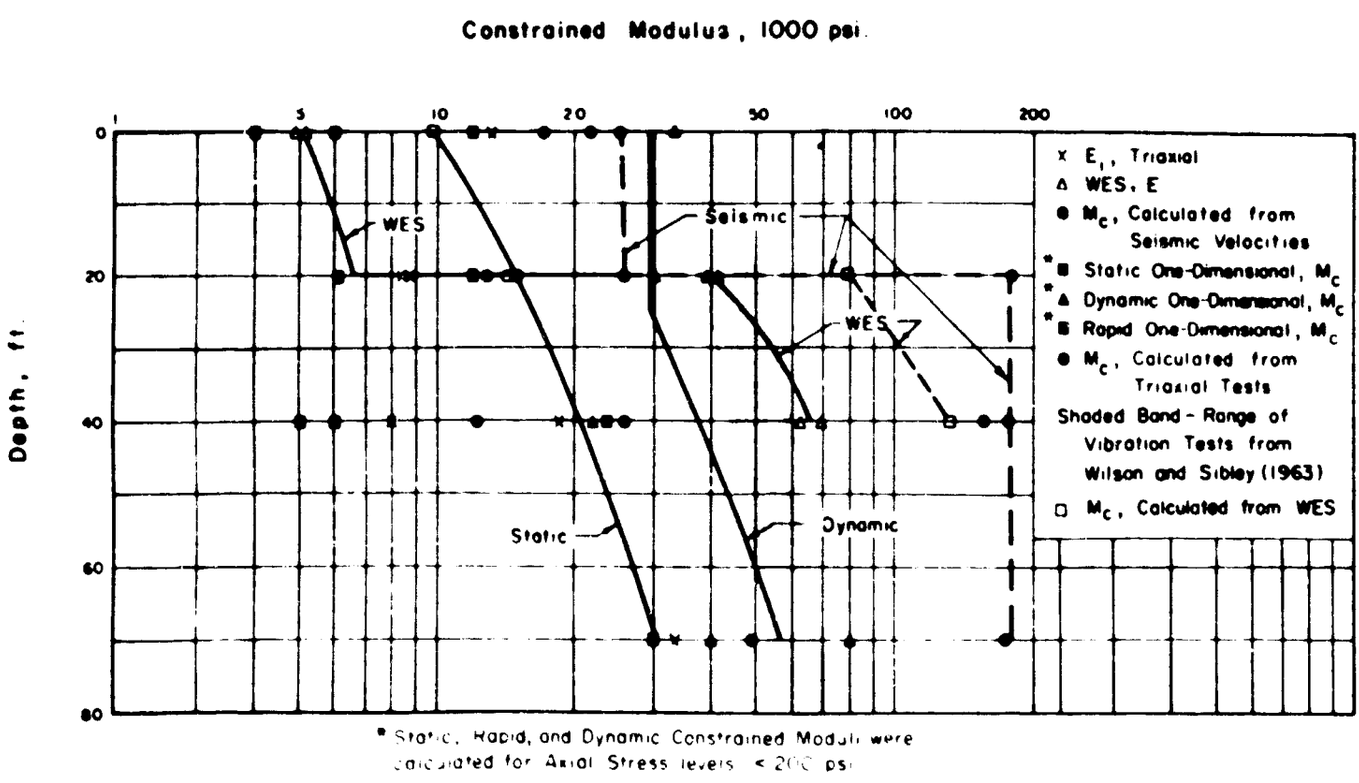


Fig. 23 Summary of Constrained Moduli vs Depth

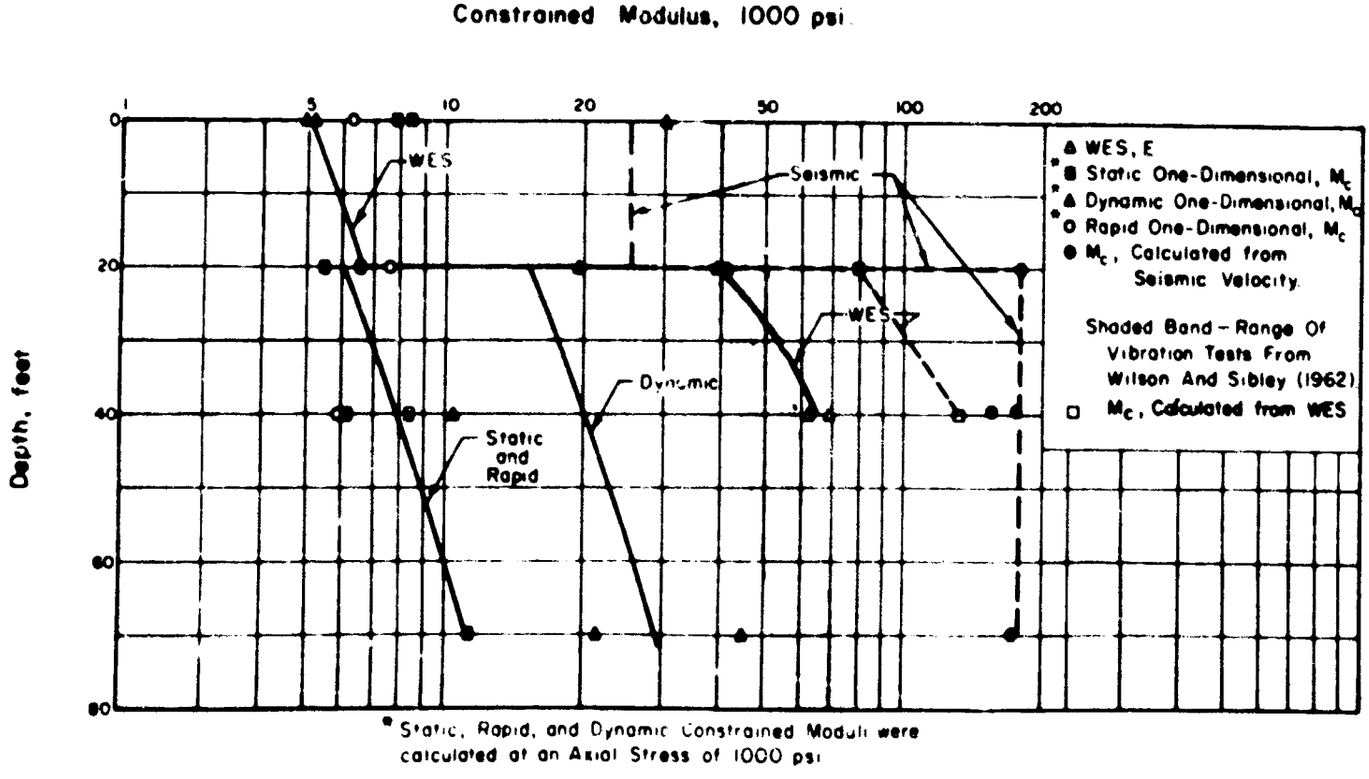


Fig. 24 Summary of Constrained Moduli vs Depth

2,000 psi range.

The playa silt at Frenchman Flat is an unusual soil when compared to those normally encountered in construction. The prediction of ground motions at other sites based on an extrapolation of data obtained at the Nevada Test Site requires a careful comparison of the dynamic constrained moduli of playa silt and the soil in question at the pressure levels of interest.

ACKNOWLEDGEMENTS

This study was conducted with the aid of facilities in the Department of Civil Engineering at the University of Illinois and was sponsored by the Air Force Weapons Laboratory, Kirtland Air Force Base, New Mexico; Captain H. E. Auld was the monitor. Special acknowledgement is made of the personal efforts of Captain Auld in obtaining and preserving the excellent undistrubed samples furnished for this study. The project personnel consisted of Messrs. D. J. Leary and Bijan Mohraz, Research Assistants in Civil Engineering at the University of Illinois. The equipment used for all of the tests was developed during various research efforts in the Department of Civil Engineering at the University of Illinois.

REFERENCES

1. Wilson, S. D. and E. A. Sibley, "Ground Displacements From Air-Blast Loading," Proc. ASCE, No. SM6, pp. 1-31, December 1963.
2. Fowler, J. and Z. B. Fry, "Dynamic Tests, Frenchman Flat, Nevada Test Site, Mercury, Nevada," Misc. Paper No. 4-645, U. S. Army Engineer Waterways Experiment Station, Vicksburg, Mississippi, April 1964.
3. Hendron, A. J., Jr., "The Behavior of Sand in One-Dimensional Compression," Ph.D. Thesis, University of Illinois, Urbana, Illinois, 1963.
4. Hendron, A. J., Jr., and M. T. Davisson, "Static and Dynamic Behavior of a Playa Silt in One-Dimensional Compression," Technical Documentary Report No. RTD TDR-63-3078, AFWL, Kirtland Air Force Base, September 1963.
5. Sinnamon, G. K. and W. W. McVinnie, "Operation Manual and Fabrication Information for Gas Operated 90 kip Dynamic Loading Machine," Report to AFWL on contract AF29 (601)-2876, Kirtland Air Force Base, August 1963.
6. Kane, H., M. T. Davisson, R. E. Olson and G. K. Sinnamon, "A Study of the Dynamic Soil-Structure Interaction Characteristics of Soil," Technical Documentary Report No. RTD TDR-63-3116, AFWL, Kirtland Air Force Base, September 1963.

LIST OF SYMBOLS

e_i - initial void ratio
E - Young's modulus, psi
G - Shear modulus, psi
K_o - Coefficient of earth pressure at rest
M_c - Constrained Modulus, psi
M_{cs} - Constrained Secant Modulus, psi
S_r - Degree of Saturation
S_{ri} - Initial Degree of Saturation
S_s - Specific Gravity of Soil Solids
w% - Water content, %
w_i - initial water content, %

ϵ_r - radial strain, in/in
ϵ_a - axial strain, in/in
σ_r - radial stress, psi
σ_a - axial stress, psi

γ_i - initial density, pcf
γ_{di} - initial dry density, pcf

μ - Poisson's Ratio

PROPAGATION OF DYNAMIC STRESSES IN SOIL

by
Lynn Seaman*

This project, a study of stress wave propagation in soil, has been sponsored by the Defense Atomic Support Agency. The goal of the work has been to predict the phenomena of wave propagation on the basis of data from laboratory compression tests of soil samples. For a start on the problem, the work has been restricted to one-dimensional wave propagation in non-cohesive soils. The results of the study show that for these conditions, wave propagation phenomena caused by blast loading can be predicted from laboratory compression tests through the use of a simple analytical model.

A typical stress wave caused by an explosion is shown in Figure 1. The important parameters are the peak stress and duration of the wave. The time, T, between the arrival of the peak stress and the time at which stress is 0.368 of the peak value is the exponential time constant of the stress wave. The attenuation of peak stress and the change in the time constant, T, are the features of the stress wave which will be predicted.

The soil model which has been analyzed for the predictions is the linear locking or linear hysteretic model. A stress-strain curve for the model is shown in Figure 2. This model has been used by several other researchers (1,2) because it does have some of the character of sand behavior. Loading and unloading occur along different stress-strain characteristics so that a cycle of loading causes some hysteretic energy loss and permanent set. A blast loading provides such a loading and unloading cycle so that energy is lost as a blast wave travels through the soil. The energy loss causes the peak stress to attenuate with depth and causes the stress wave to broaden out with depth. The parameter governing these effects is α, where

$$\alpha = \frac{1 - \sqrt{E_0/E_1}}{1 + \sqrt{E_0/E_1}} = \frac{1 - C_0/C_1}{1 + C_0/C_1}$$

where

E_0 and C_0 are the modulus and wave velocity on the loading curve, and

E_1 and C_1 apply to the unloading curve.

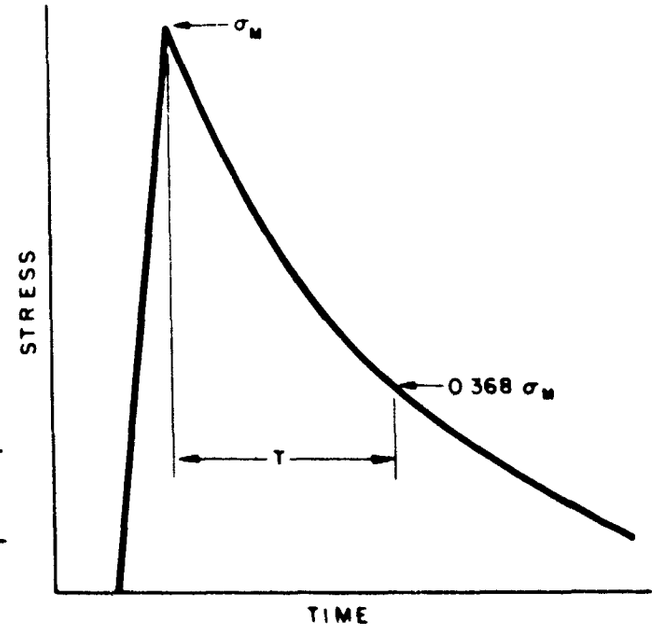


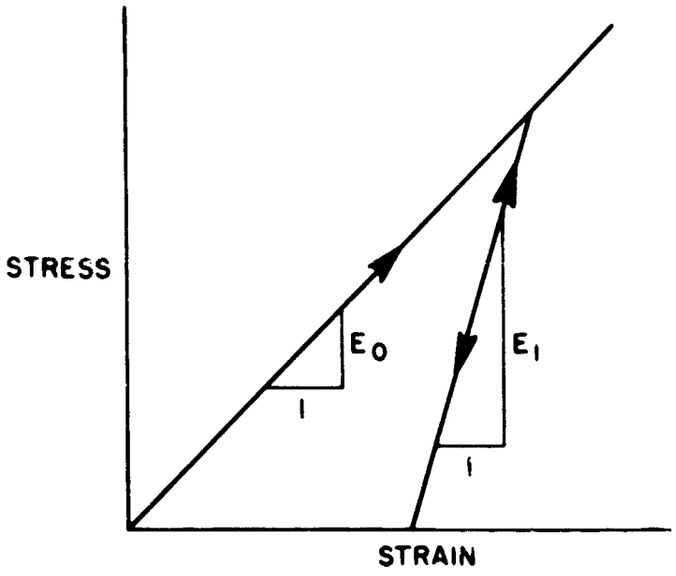
Fig. 1 Typical Stress Wave Form

In Figure 3 is a semilog plot of peak stress versus a non-dimensional depth for a pressure loading with a shock front and an exponential decay. For nondimensionalization the peak stress is divided by the peak surface pressure. The depth is non-dimensionalized by dividing by the wave velocity and the exponential time constant of the applied pressure. However, depth divided by wave velocity is arrival time so the abscissa is also the arrival time. If attenuation were exponential, these lines would be straight. They are initially straight but curve away at greater depths. Values of α for soils are typically around 0.15 to 0.30 and it can be seen that the attenuation rate is not strongly dependent on α in that range.

The broadening out of the stress wave is shown as a function of α in Figure 4. Since the attenuation rate is higher for larger values of α it is to be expected that the stress waves also lengthen out more rapidly for larger α.

The particular values of α which pertain to the sand used on the project were determined in static one-dimensional compression tests on soil samples. The samples were tested at various densities and stress levels. Figure 5 shows a typical stress-strain curve for the project sand. Clearly the sand is hysteretic but not linearly so. The value of α was determined from the slopes of the loading and unloading curves at the peak stress attained. The initial loading cycle on each sample yielded values of α above 0.3. Subsequent loadings gave α values between 0.19 and 0.23. The α values were

*Mechanics Department, Physics Division, Stanford Research Institute, Menlo Park, California.



$$\alpha = \frac{1-\sqrt{\frac{E_0}{E_1}}}{1+\sqrt{\frac{E_0}{E_1}}} = \frac{1-C_0/C_1}{1+C_0/C_1}$$

Fig. 2 Linear Locking Model

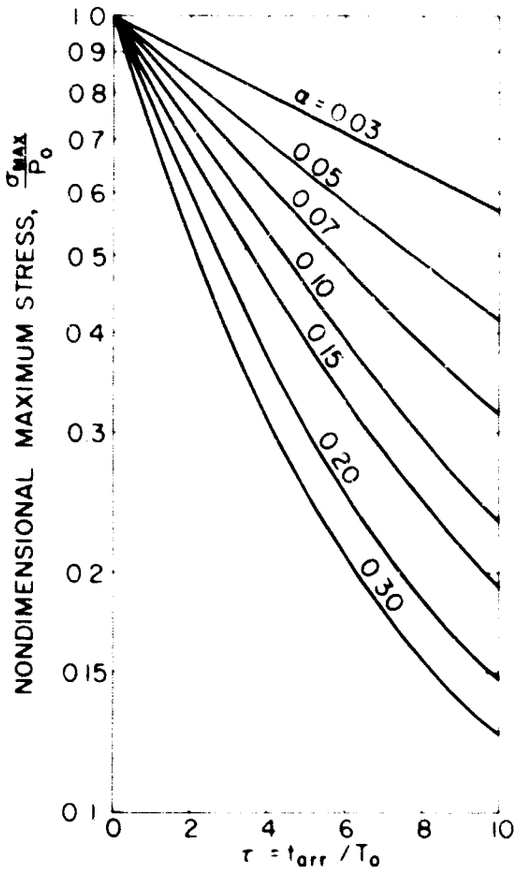


Fig. 3 Attenuation of Peak Stress as a Function of Depth

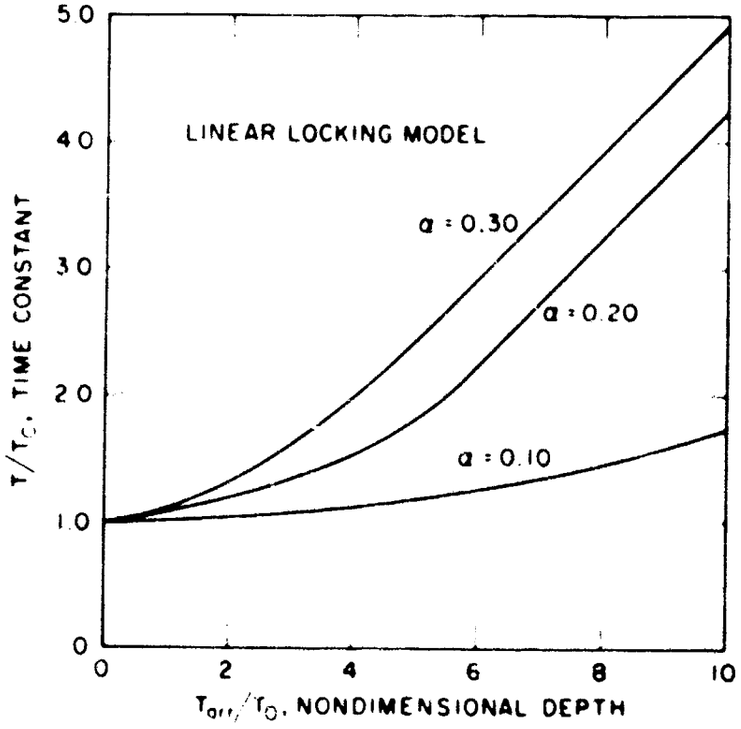


Fig. 4 Time Constant of the Stress Wave as a Function of Depth

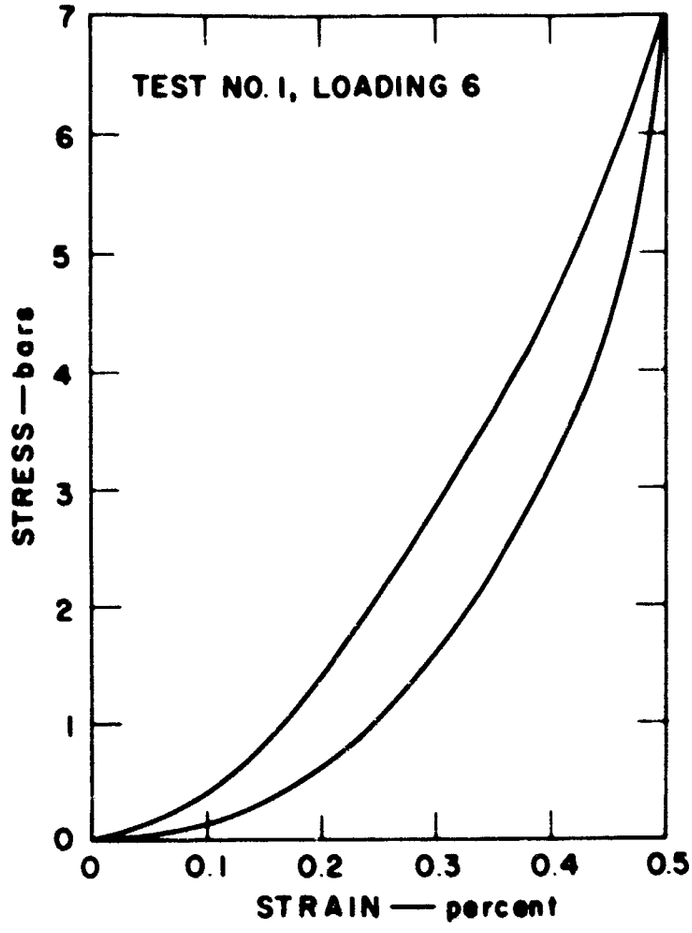


Fig. 5 Stress-Strain Curve for the Project Sand

independent of stress level for the peak stresses used but decreased somewhat with increasing density. The data indicate α = 0.22 for the loosest samples and 0.20 for the densest.

With a known value of the attenuation parameter α, the wave propagation characteristics of the soil can be predicted on the basis of the linear locking model. To substantiate the analysis a series of wave propagation tests were made. The wave propagation experiments were conducted on sand confined in a long tube to produce an essentially one-dimensional condition. A section of the tube is shown in Figure 6. It is made of alternate rings of aluminum and neoprene rubber and is about 1 foot in diameter. The aluminum rings provide the necessary radial confinement while the rubber spacers make the tube very soft in the axial direction. Measurements of axial forces taken by the tube during wave propagation tests show that the tube takes less than 1% of the applied force. The column was built to a height of 15 feet for the tests.

Both stress gauges and accelerometers have been placed at various depths along the column but only the stress gauge results will be discussed here. Two types of gauges were constructed, one with a piezoelectric crystal

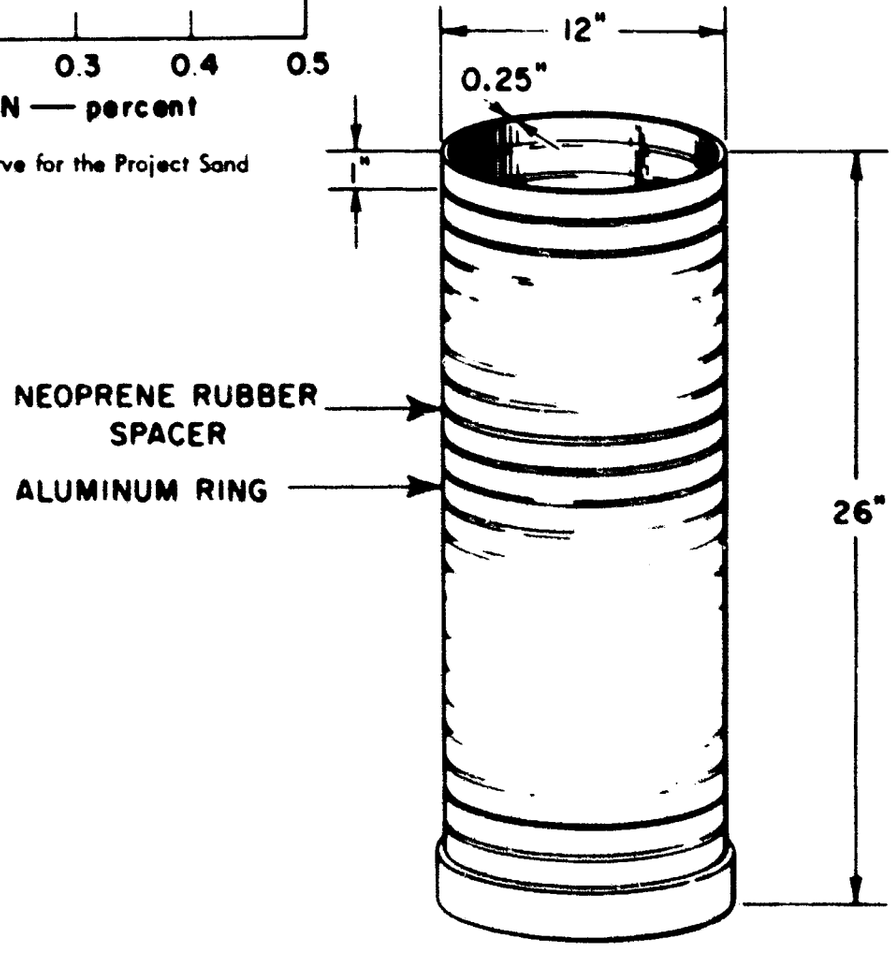


Fig. 6 Soil Tube Section

as the sensing element and one with a diaphragm instrumented with wire strain gauges. Both types are in the shape of flat disks 1-1/2 or 2 inches in diameter. Both are quite stiff with respect to the soil so that their response to loading while embedded in soil is linear. The output of the piezoelectric gauges is about 10 v for 100 psi and that of the diaphragm gauges is 8 mv for 100 psi.

Two means for loading this sand column with a pressure pulse have been used. The first used was a blast loading produced in a Boynton Blast Load Generator. The generator is a dome which is clamped on top of the column. In the second method a large weight is dropped on the column top to produce a stress wave very similar to that from a blast. Comparable stress levels can be obtained in the two types of tests and 100 psi has been used as the nominal peak pressure for all tests. Only the results of the drop weight tests will be described since they show larger stress attenuations and are more conclusive in indicating the correct prediction procedure.

In the drop weight tests a 40 pound weight was dropped about 4 feet onto a steel plate resting on the sand surface in the column. A typical set of stress records produced by such a drop are shown in Figure 7. The record at a depth of

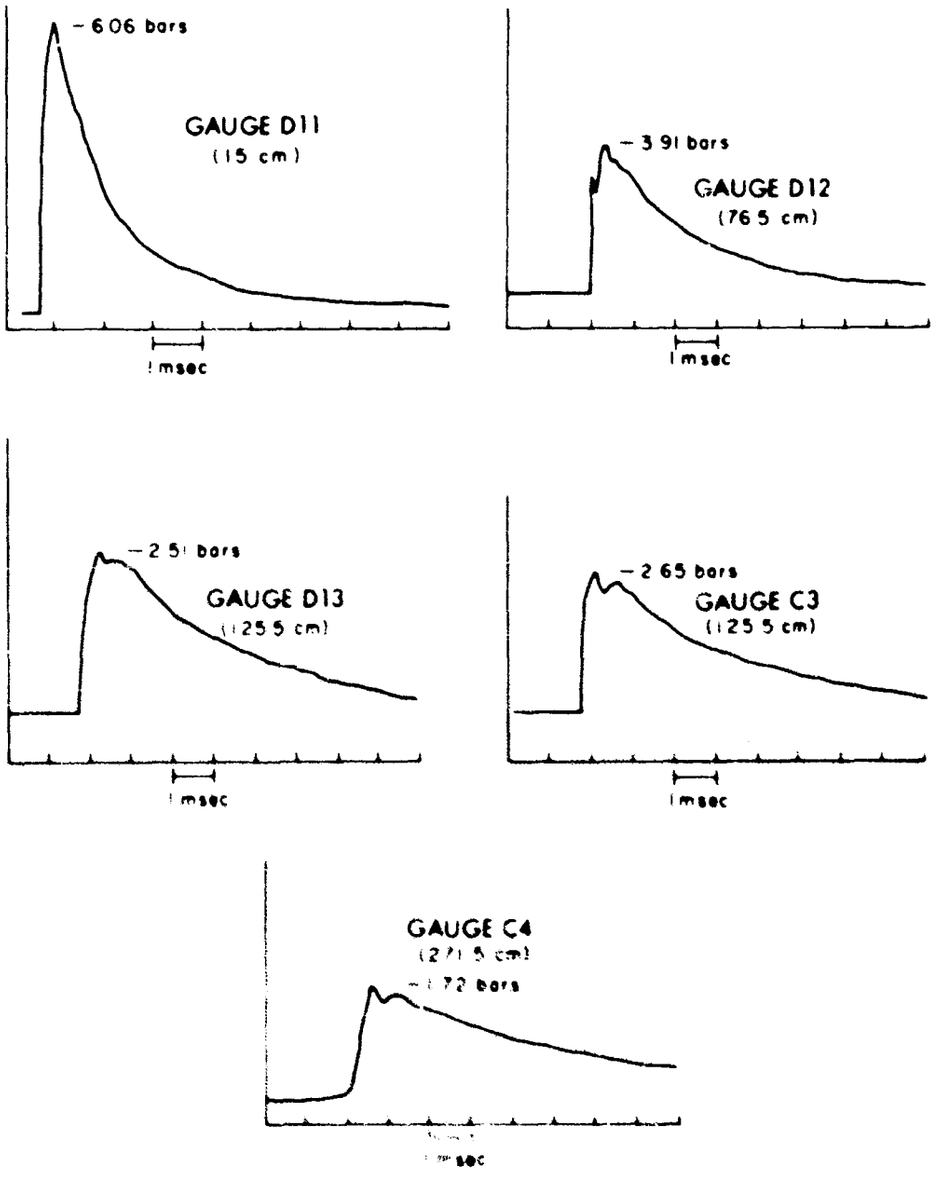
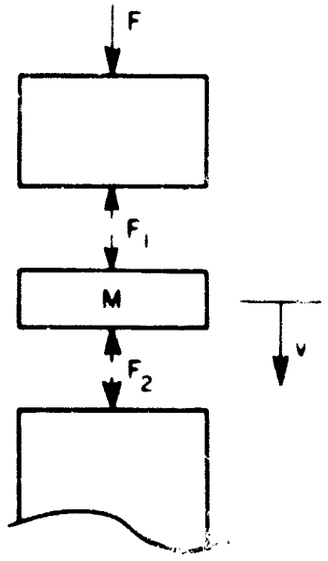


Fig. 7 Typical Stress-Time Records

15 cm shows a rise time of about 0.2 msec and an exponential decay with a time constant of about 1 msec. The lowest record was taken at a depth of 271.5 cm and shows that considerable change has occurred in the stress wave. The rise is not quite as rapid now, the peak is only 30% as nigh as it was near the surface and the stress decay past the peak is considerably more gradual. The intermediate records serve to document the transition which occurs in the stress wave.

Before proceeding to the data obtained, the stress gauge calibration should be outlined. Due to the short duration of the applied stress, a calibration could be made on the basis of the total impulse of the stress wave. Figure 8 shows the geometry to be used. The F's are forces at the top of the column and on a small segment of mass M which has been isolated as a free body. The force balance is written for that segment first and then integrated with respect to time to find the impulse applied to the surfaces of the segment. The equation shows that if the integration is carried from the arrival of the wave to a time when the velocity of the segment has returned to zero, the impulses above and below the segment are equal. If the velocity of the mass above the segment is zero, these impulses equal the applied impulse.



$$F_1 - F_2 = M\frac{dv}{dt}$$

$$\int_{t_1}^{t_2}\sigma_1\,dt - \int_{t_1}^{t_2}\sigma_2\,dt = \int_{t_1}^{t_2}\frac{M}{AREA}\frac{dv}{dt}\,dt = \frac{M}{AREA}(v_2 - v_1)$$

Fig. 8 Impulse Calibration Analysis

The applied impulse is known from the height of drop and the weight. The impulse at the gauge is the area under the stress-time curve. By equating this area to the applied impulse, the gauge calibration for that drop was determined. A new calibration was made for each drop.

Drop weight tests were made with the column at full height and with sand at two different densities. In the first series of tests the sand was at 50% relative density. Data on peak stresses for these tests are shown in Figures 9 and 10. These figures show nondimensional peak stress versus nondimensional depth for ready comparison with the analytical work. In Figure 9 the stress applied at the surface was about 110 psi. In this figure there is also an analytical curve of the predicted attenuation based on the compression data and the linear locking model. Apparently the wave propagation data coincide with the analytical prediction. In Figure 10 the peak stress was 110 psi for the tests with solid black data points and 50 psi for the others. Evidently the attenuation rate is not a function of stress level.

The second series of drop tests were made with the sand at 80% relative density. Since there were 25 drops made in the series only average values are reported here. The attenuation of peak stress is shown in Figure 11 with the same coordinates as the previous two figures. Here three peak stress levels were used ranging from 60 to 125 psi. Again the attenuation rate is independent of peak stress. The data points tend to lie between the curves for $\alpha = 0.15$ and 0.20. Thus there is slightly

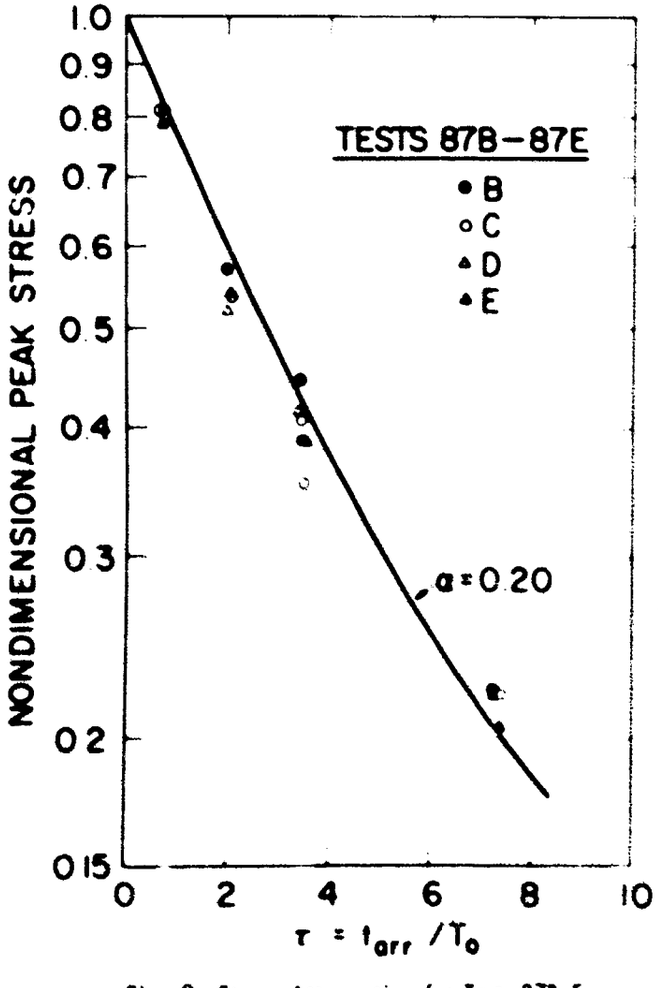


Fig. 9 Stress Attenuation for Tests 87B-E

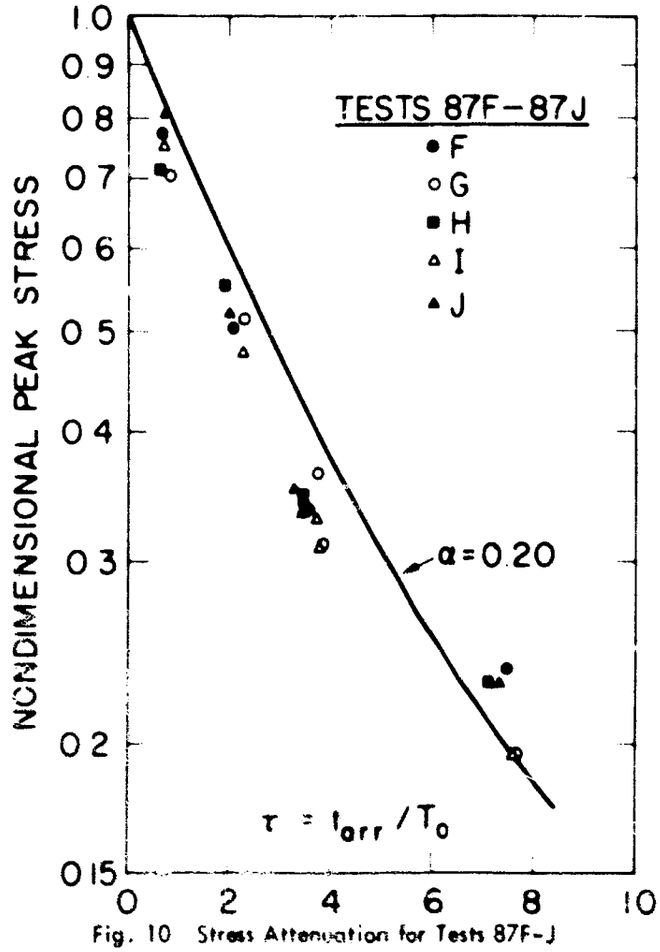


Fig. 10 Stress Attenuation for Tests 87F-J

less attenuation in these tests than there was in the previous series with a looser sand.

The analytical prediction in this case is given by the curve for $\alpha = 0.20$. This slight discrepancy between the data points and the adjusted prediction is probably due to a reduction in the value of α caused by repeated testing.

To be a completely adequate analysis the prediction should also indicate the broadening out of the wave form with depth. In Figure 12 the exponential time constants of the decaying portion of the stress wave are shown as a function of the nondimensional depth parameter. The applied stress evidently had a time constant of 1 msec. The stress waves at greater depths are not strictly exponential so the time at which the stress had decreased to 0.368 of its peak value was taken as the time constant. Such a time constant has no simple mathematical interpretation but it does provide

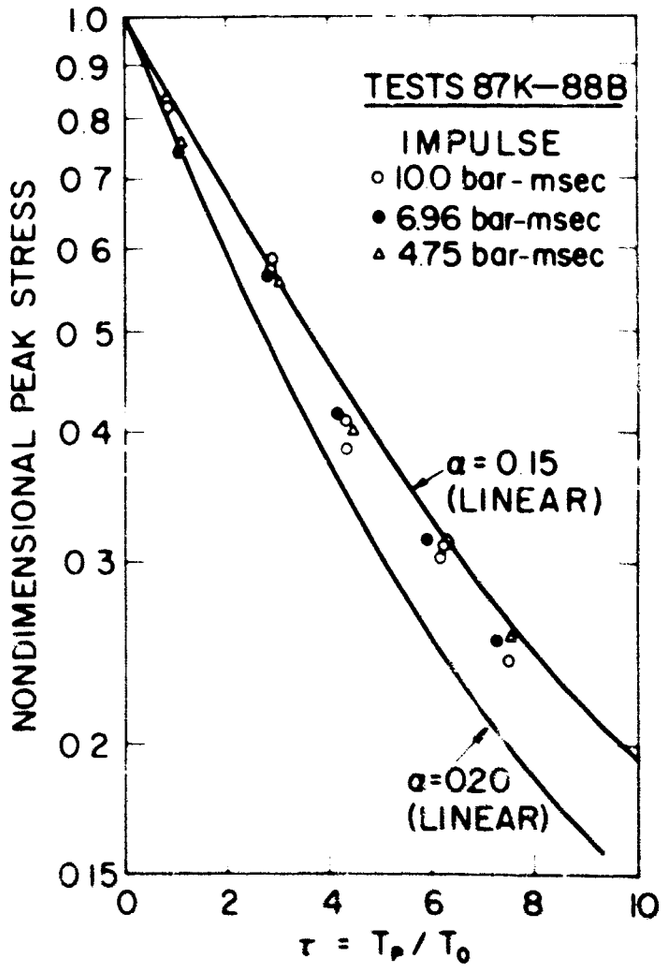


Fig. 11 Stress Attenuation for Tests 87K-88B

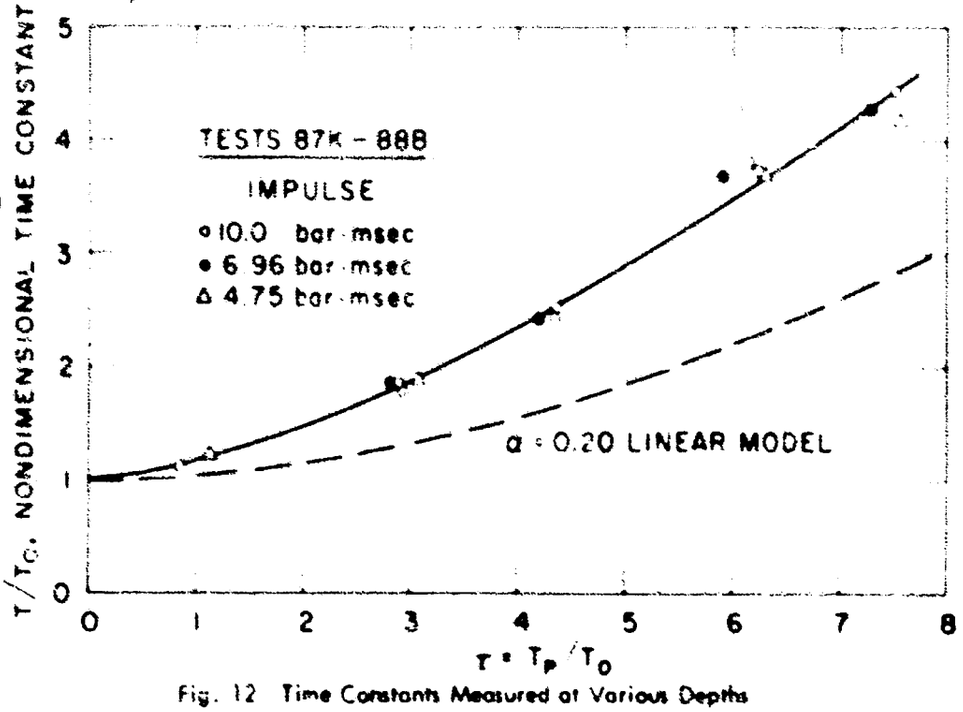


Fig. 12 Time Constants Measured at Various Depths

some description of the change in wave form which occurs as a function of depth. The points lie along a curve, but this is not the analytical curve. For an α value of 0.20, the time constants from the analysis are well below the data points. This rather sizable discrepancy is certainly caused by nonlinearity of the stress-strain curve for the sand. Work which has been begun on a nonlinear hysteretic model similar to the linear model indicates that the nonlinearities of the stress-strain curve have a large effect on the broadening of the stress wave with depth. However, the attenuation rate does not seem to be significantly effected for most values of α .

The next steps in this study of one-dimensional wave propagation are to find the effects of nonlinearity of the stress-strain characteristics, of shocking up or unshocking, and of geostatic stress on the change of wave form with depth. The work will also be extended to include cohesive materials.

The conclusion which has been reached on the basis of this limited number of tests is that wave propagation characteristics in non-cohesive soil can be predicted on the basis of data from laboratory compression tests. The present predictions, which accurately define the attenuation of peak stress, were based on the use of the linear locking model for the soil.

REFERENCES

1. Salvadori, Mario G., Richard Skalak, and Paul Weidlinger, "Waves and Shocks in Locking and Dissipative Media," Trans. American Society of Civil Engineers, 126, Part I, 305, 1961.
2. Heierli, Werner, "Inelastic Wave Propagation in Soil Columns, Proceedings of American Society of Civil Engineers, Paper No. 3347, SM-6, December 1962.

LIST OF SYMBOLS

T_p, T_{arr}, t_{arr} = arrival time for peak stress
σ_m, σ_{max} = peak stress of stress wave
P_o = peak surface pressure
T_o = exponential time constant of the applied pressure wave at the surface
T = exponential time constant of the stress wave

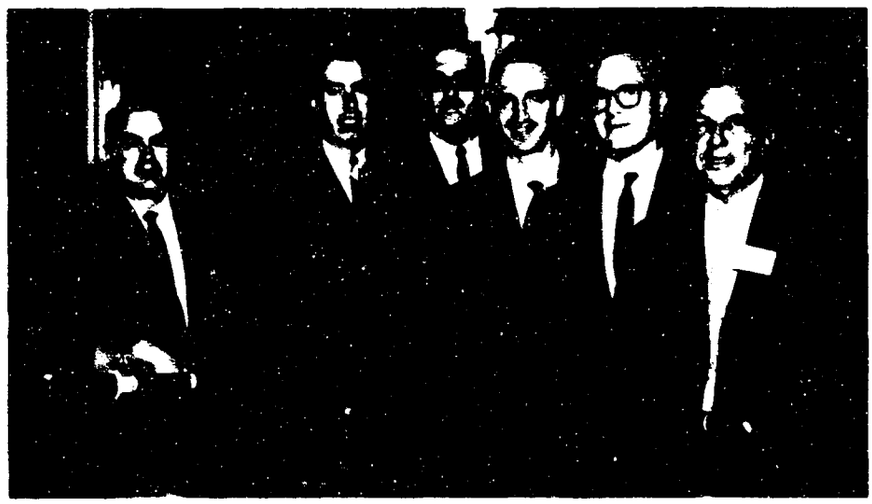
SESSION THREE–TUESDAY AM

GROUND MOTION AND INSTRUMENTATION

SESSION CHAIRMAN: EARL A. SIBLEY

TABLE OF CONTENTS

	page
FREE FIELD GROUND MOTION PRODUCED BY EXPLOSIONS, William R. Perret	108
INERTIAL EFFECTS AND SOIL STRENGTH CRITERIA, B. B. Schimming and H. C. Saxe	118
A NEW DEVICE FOR SOIL STRAIN MEASUREMENT, W. B. Truesdale and M. E. Anderson	129
SHOCK-ISOLATING BACKPACKING MATERIALS, A REVIEW OF THE STATE OF THE ART, George C. Hoff	138
EFFECTS OF GAUGE DENSITY AND PLACEMENT ON MEASUREMENT OF ACCELERATION IN SOIL, E. T. Selig and R. W. Rusin	155
A REVIEW OF STRESS AND STRAIN MEASUREMENT IN SOIL, E. T. Selig	172



Participants in Session Three were, left to right, Earl A. Sibley (Session Chairman); B. B. Schimming; G. C. Hoff; E. T. Selig; and W. R. Perret.

FREE FIELD GROUND MOTION PRODUCED BY EXPLOSIONS

by
William R. Perret*

An explosion is an extremely rapid release of energy within a relatively small volume. The environment of an explosion must react by absorbing and transmitting the released energy. The energy may be released by either chemical or nuclear processes, but reaction of a solid environment such as soil or rock to either type of source will differ only in relation to the energy densities developed.

Energy released by an explosion is manifest in several forms but the most pertinent is development of a large quantity of very hot gas which exerts pressure on its surroundings. When the environment is soil or rock this pressure is very great—megabars for nuclear sources, and hundreds of kilobars for chemical sources. Megabars imply tens of millions of psi; kilobars tens of thousands of psi. Reaction of the environment to pressures of these magnitudes is such that material motions and pressures may be described by hydrodynamic relations. Figure 1 defines schematically the domains characterized by major types of response to the explosion-developed stress-field. Through the hydrodynamic domain pressure decreases generally as the inverse square of radial range by doing work on the environment resulting in melting and vaporization until it reaches a few hundred kilobars. As the pressure decreases below this level the environment retains its solid character and energy is dissipated by crushing, shearing, cracking, and by viscous and frictional processes. In this nonlinear or intermediate zone stresses decrease as an inverse power of the radius between 2.5 and 4 to levels characteristic of the elastic limit of the soil or rock. Finally in the linear or elastic domain stresses, always below the elastic limit, are attenuated at a rate nominally equivalent to the inverse power of radial range, but in practice frequently as an inverse power of the radius between 1.1 and 1.8. The hydrodynamic and part of the nonlinear domain are obviously of no practical interest to structural problems because stress levels are well above those amenable to structural design. However, much of the nonlinear region and part of the linear region are of concern to soil-structure problems since it is pertinent to know in what manner, and at what distances from an explosion, stress fields approach realistic design magnitudes.

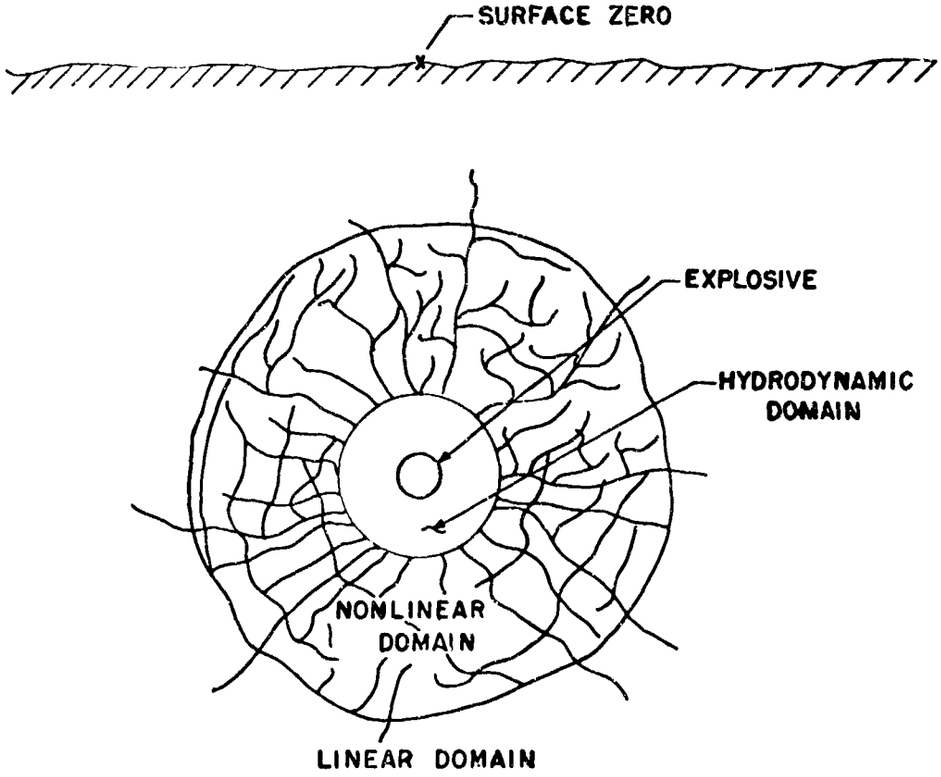


Fig. 1 Schematic Representation of Explosion

It is of interest then to know what means are adaptable to observing the development and attenuation of environmental response to an explosion. The foregoing discussion suggests we should observe stress or stain as a function of time and of distance from the source. However, experience and problems of instrument design and particularly of instrument placement have shown that more reliable and consistent results derive from measurement of particle motion in terms of acceleration or particle velocity. Without going into detail concerning the reasons for greater reliability of particle motion measurements, it is pointed out that perturbations produced by placement of gauges, react considerably more severely on

* Sandia Corporation, Albuquerque, New Mexico.

the response of stress and strain gauges than on the response of accelerometers or velocity gauges. The latter type of guage requires only that the gauge package match in density the surrounding material, that it be bonded securely to its surroundings, and that its dimensions be small relative to the pressure or velocity wavelength.

Full scale experiments to define ground motion produced by large explosions have been undertaken in several earth media over a range of explosion yields from a few pounds of TNT through several kilotons of TNT-equivalent nuclear energy. Correlation of results from various yields is feasible by scaling, assuming similitude. This procedure is valid for similar explosives within similar environments, at least over yield ranges of two or three orders of magnitude.

Let us look at the results of free-field ground motion measurement programs in several types of rock and soil and compare some of these when reduced by scaling to a common yield of one kiloton. These data are peak values derived from records of acceleration or particle velocity as functions of time, or from the time integrals of these records.

Plots of peak acceleration, particle velocity and displacement versus radial range, shown in Figure 2, were derived from a spherical charge of one million pounds of TNT centered 125 feet below the surface of Yucca Flats at the AEC Nevada Test Site. The gauges were at shot depth. These plots imply that none of the gauges were sufficiently remote from the charges to fall in the linear response domain. Data from other explosions in similar desert alluvium indicate that the linear

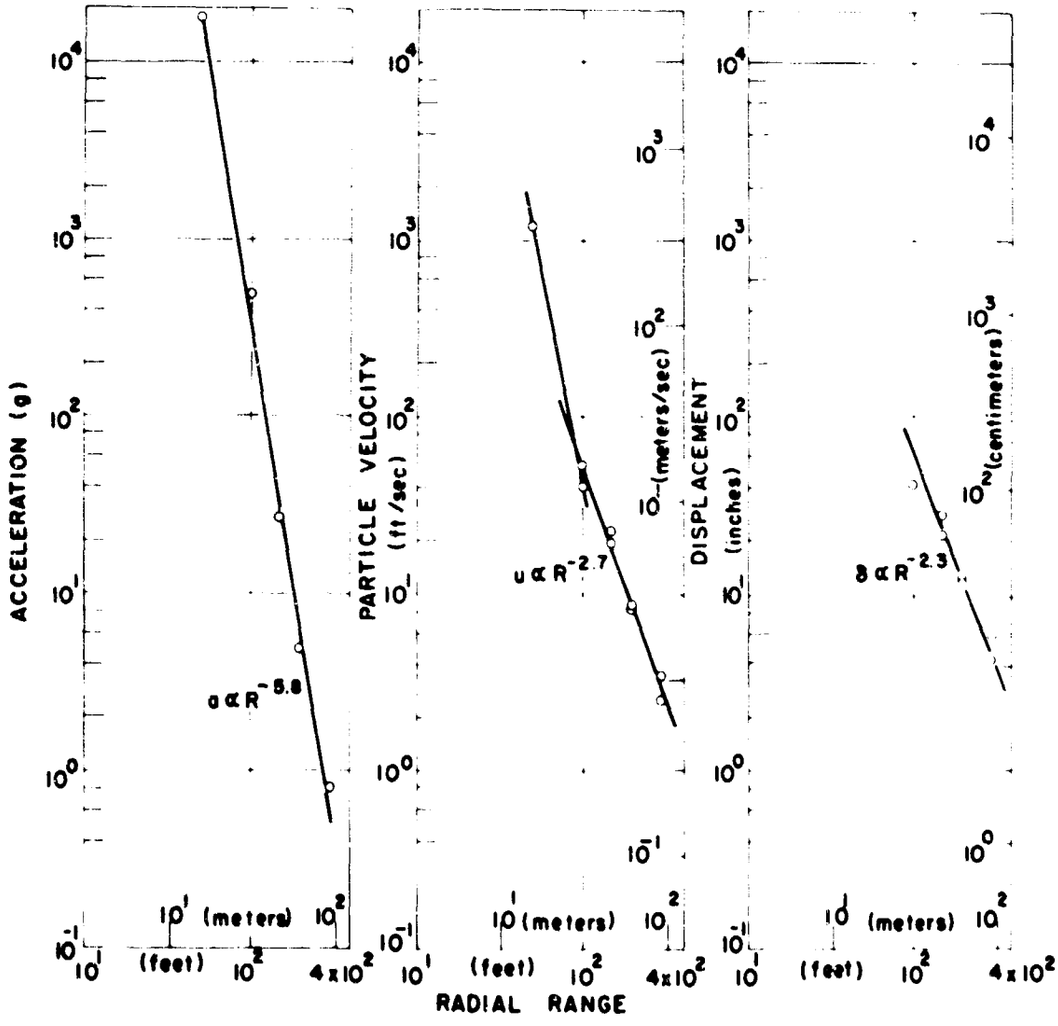


Fig. 2 Peak Accelerations, Velocities, and Displacements for Chemical Explosions

region does indeed exist at a range beyond the most remote gauge.

Similar plots of acceleration and particle velocity data derived from the Gnome, nuclear explosion in salt near Carlsbad are shown in Figure 3. These data do extend through most of the intermediate domain and into the beginning of the linear response region.

In Figure 4 these two sets of data have been reduced by scaling to curves for one kiloton and data from a smaller TNT explosion has been correlated with the Scooter data to indicate the beginning of the linear response region. Here it is apparent that attenuation rates are greater for acceleration than for particle velocity. It is also apprent that there is a much greater difference between peak accelerations in the two media at the same range than between peak particle velocities. The former difference is greater than two orders of magnitude; the latter generally less than a factor of ten.

This difference emphasizes the influence of environmental response on acceleration and the relationship between the various motion parameters and stress or strain. Particle velocity is directly related to compressive stress through the conservation of momentum requirement that stress be equal to the product of the density of the medium, the phase velocity with which the stress is propagated, and particle velocity. Then peak stress and peak particle velocity should vary with range in the same manner; and be directly related, at any particular radial range, to the energy released by the explosion. Acceleration, on the other hand, is the time derivative of particle velocity. Its maximum value will then depend upon the rate of rise of the particle velocity wave. This rate of rise is in turn dependent upon dispersiveness of the material traversed and energy absorption from the higher frequency components of the dispersed wave. The consequence of this is that in the more dispersive and energy absorptive materials such as dry porous soil, the velocity wave spreads out rapidly and the slope of the rising wave front becomes rapidly flatter.

From these curves it is also interesting to speculate on the stress levels represented by the intersection of the two branches of particle velocity curves. If we use the conservation of momentum relationship as at least a good first approximation and use the phase velocity with which peak particle velocities were transmitted it is found that for dry desert alluvium the stress at transition, corresponding to a particle velocity of 0.7 feet per second is about 35 psi; a reasonable value for the elastic limit of this soil at a depth of 125 ft.

The similar calculation for salt, at a particle velocity of 44 feet per second, gives about 18,000 psi which at first glance seems high but agrees reasonably well with the value of 1.2 kilobars found by other types of measurement for the compressional elastic limit for salt. Collateral data from the Gnome experiment has suggested that a second slope transition should have occurred at about 1000 feet from the explosion, corresponding to a particle velocity of 7 feet per second and a stress of about

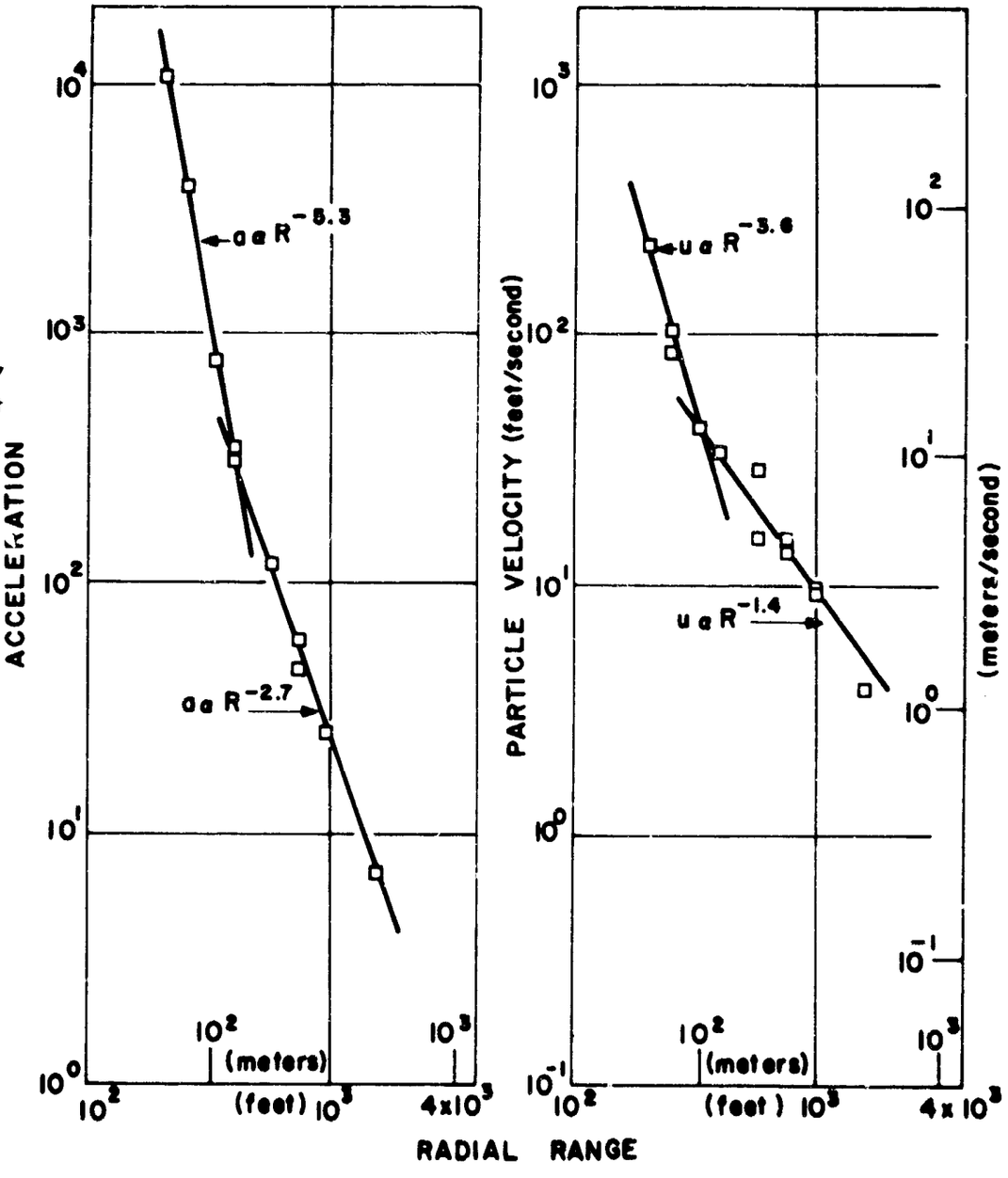


Fig. 3 Peak Accelerations and Velocities for Nuclear Explosions

3100 psi. The dynamic tensile elastic limit of salt under 1200 feet of overburden, the depth of the Gnome shot, is very nearly 3100 psi.

It appears that particle velocity data are the most useful for defining ground shock or motion produced in various rocks or soils by explosions. Figure 5 represents particle velocity data from nuclear explosions in four types of earth materials, all scaled to one kiloton. Attenuation rates in the nonlinear region range between $R^{-3.75}$ in desert alluvium to $R^{-2.41}$ in granite and beyond the transition to quasi-linear response they range from R^{-1} in tuff to $R^{-1.8}$ in weak granite. Transitions in desert alluvium and tuff occur at nearly the same radial range, but the implied elastic limits are about 780 psi for the weak but competent tuff and 60 psi for the granular alluvium. Since the alluvium data was derived from gauges at 1200 feet, roughly ten times the depth of the Scooter gauges, increase from 35 to 60 psi in elastic limit is reasonable.

The two granite curves are from different areas, that represented by steeper sloping curves included several wide shear zones filled with broken granite and very soft clayey gouge along the line of gauge stations. The average elastic limit defined for granite by these curves is about 5800 psi.

The curves presented here are extended only to the approximate maximum radial range at which measurements were made, but they have been extrapolated inward to the approximate limits of the hydrodynamic domain. These are roughly 350 kilobars for granite, 130 kilobars for salt, 15 kilobars for tuff, and 5 kilobars for dry desert alluvium.

The foregoing discussion has been concerned with ground motion produced by underground explosions sufficiently deep to develop only negligible air blast. There is no good reason to believe that that portion of the energy from contact surfact bursts or very shallow explosions which is transmitted directly to the ground should induce response notably different from that described above. The exception to this may be that because of the absence of confinement the decay portion of

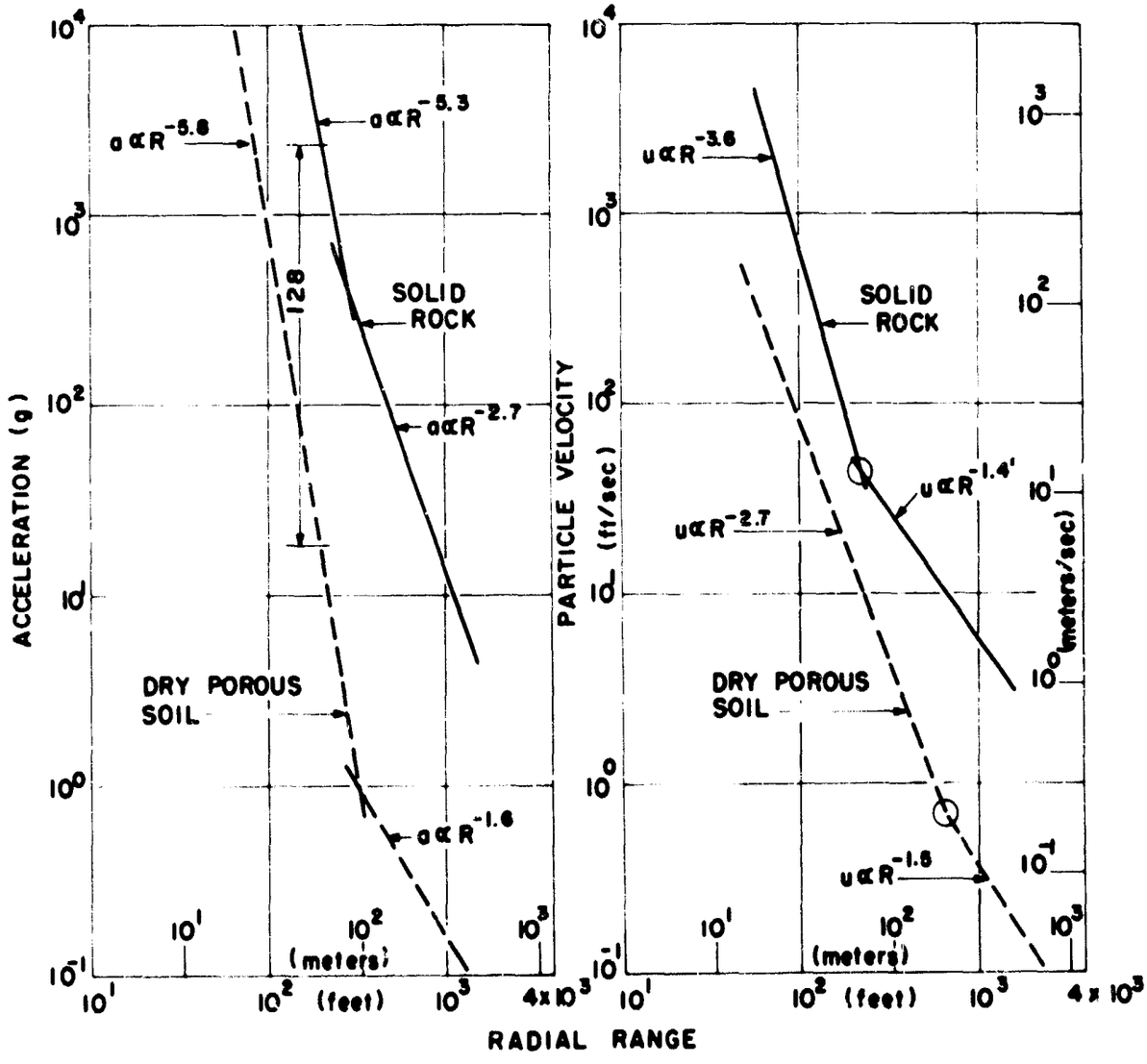


Fig. 4 Summary of Peak Accelerations and Velocities Scaled to One Kiloton Explosions

the wave and thus the impulse might be radically reduced. However, ground motion induced by air blast which often represents a predominant portion of the energy from shallow underground or surface bursts may be expected to differ appreciably from that directly transmitted from an underground explosion. This difference comes about because the air blast remains a shock wave with nearly zero rise time from the region of very strong shock outward to peak pressures well below those of concern to underground structure design.

Energy from an underground explosion ceases to propagate as a true shock wave in the vicinity of the transition from the hydrodynamic regime. Therefore, in the region of stress pertinent to underground structure design the term ground shock is a misnomer since nearly all of the energy which was associated with high frequencies has been dissipated. Conversely, air blast, as it is incident at the ground includes a relatively large high frequency energy component at all pressure levels of interest. Consequently as the energy propagates downward into the earth from air blast incident at the surface it will lose by absorption its high frequency component much more rapidly than other components of its spectrum. .This has two consequences; at any pressure level, except those near the onset of hydrodynamic response, air blast induced earth stress will be degraded much more rapidly than will stresses of equal magnitudes produced by an underground explosion, and airblast induced earth stress derived from large yield explosion will not lose energy so rapidly as will those from small yield explosions because positive phase duration of the air blast which varies as the cube root of energy yield, eliminates low frequency components from the spectrum of low yield sources, thus forcing proportionally more of the energy into the high frequency components.

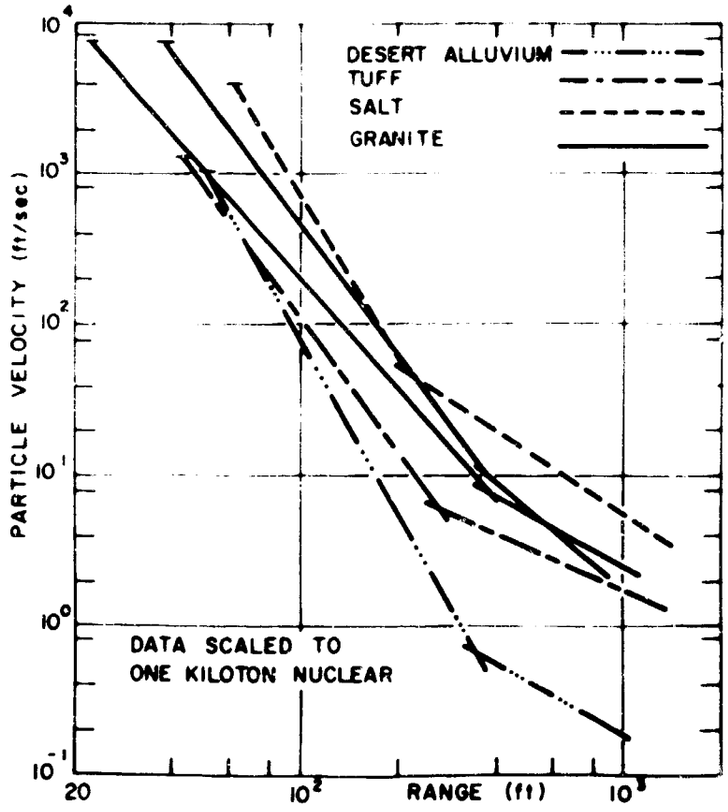


Fig. 5 Summary of Peak Velocities for One Kiloton Nuclear Explosions

An experiment was conducted about seven years ago to investigate the kind of ground motion and particularly the vertical displacement induced by air blast from the 37 kiloton Priscilla explosion 700 feet above Frenchman Flat at the Nevada Test Site. Two types of gauges, accelerometers and relative displacement gauges, were placed at five depths between the ground surface and 200 feet in four locations as shown in Figure 6 .

Airblast incident at the surface at each of these stations, shown in Figure 7, gave peak pressures of 270, 187, 120 and 59 psi. Displacements induced by the pressure and derived from the relative displacement gauges decreased with depth and with peak incident overpressure. Figure 8 presents the time-history of displacement induced by 270 psi overpressure and a maximum impulse of 14.2 psi-seconds at the surface and at depths of 10, 30, 60 and 100 feet. Rebound after initial downward displacement is followed by a residual downward displacement which decreases with depth to zero at 100 feet.

Residual displacements at the surface at all four measurement stations are compared in Figure 9 with the results of preshot and postshot first order surveys. Agreement in these comparisons within 0.2 inch at each station may be taken as an index of the reliability of the displacement gauge performance.

Maximum displacements observed at each gauge position for each station are plotted as a function of depth in Figure 10. Data from each station defines an exponential attenuation represented by the equation

$$\delta = \delta_o e^{-0.014D}$$

where δ and δ_o are displacements in inches at depth D in feet and at the surface, respectively. All data points, with the exception of those at the surface, deviate from the curves by only negligible amounts. The surface data fall significantly above the curve in each case, implying a higher rate of attenuation close to the surface.

Figure 11 is a plot of attenuation with depth of the peak particle velocities derived from integrated acceleration records. This emphasizes the two-phase attenuation suggested by the surface displacements. Here acceleration decreases exponentially as roughly $e^{-0.05D}$ down to the depths of the order of 40 feet or less and then exponentially at rates of about one tenth the shallower ones. This transition suggests two of the points dwelt upon earlier; the absorption of high frequency energy components and the transition to linear or elastic response, since the transitions occur at particle velocities indicative of stresses in the range from 30 to 150 psi.

Finally, contours of maximum displacement plotted on a vertical plane through the line of gauge stations, Figure 12 , indicate a transient broad flat depressed bowl, the half-inch contour extends from the surface at about 1500 to 1600 feet range from ground zero to a depth of about 140 feet at 650 feet range. No transient data are available closer to ground zero, but it may be surmised from the residual displacement survey shown in an earlier figure that there was a downward distortion near the center of the bowl.

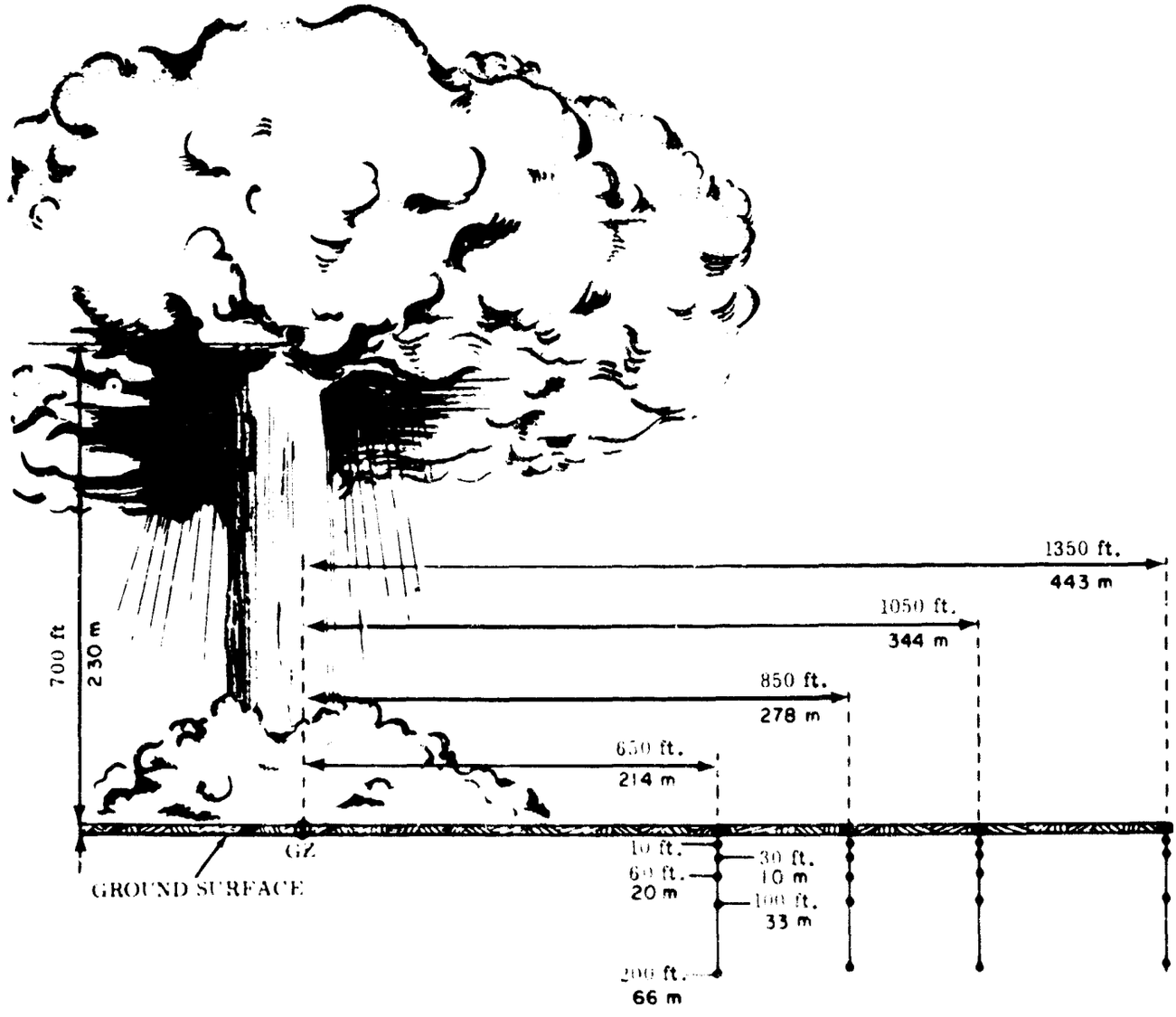


Fig. 6 Placement of Instrumentation for Priscilla Shot

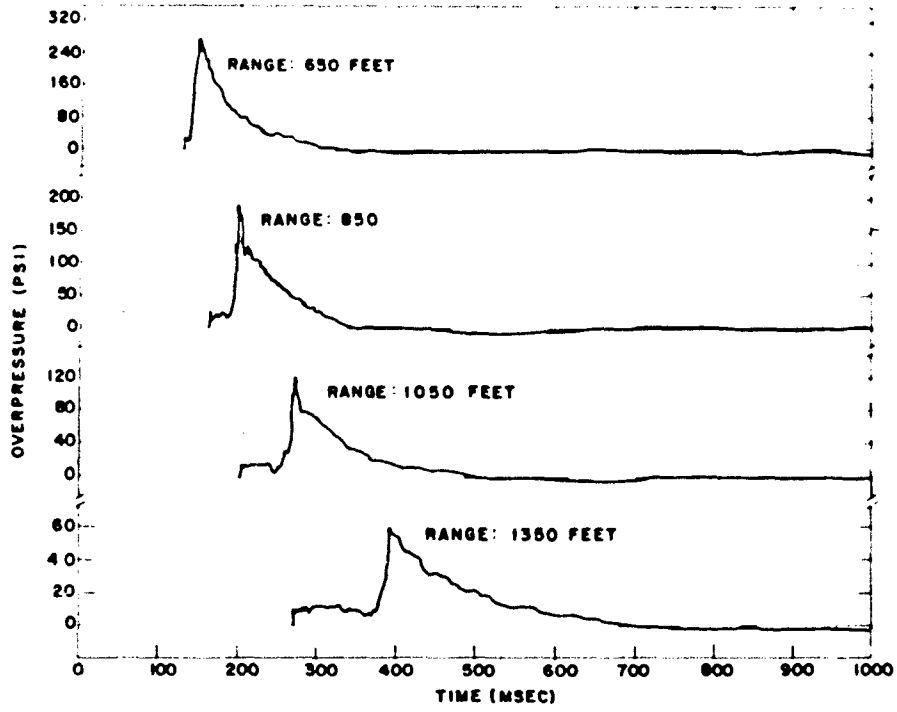


Fig. 7 Overpressures at Various Locations for Priscilla Shot

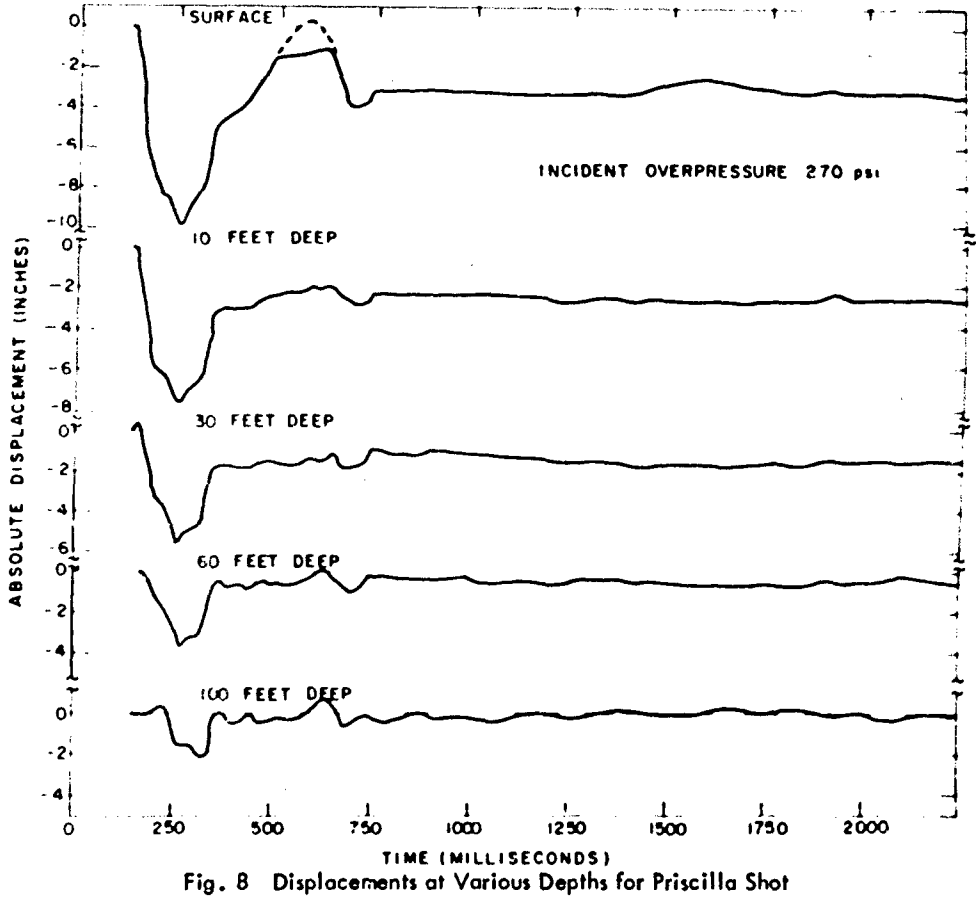


Fig. 8 Displacements at Various Depths for Priscilla Shot

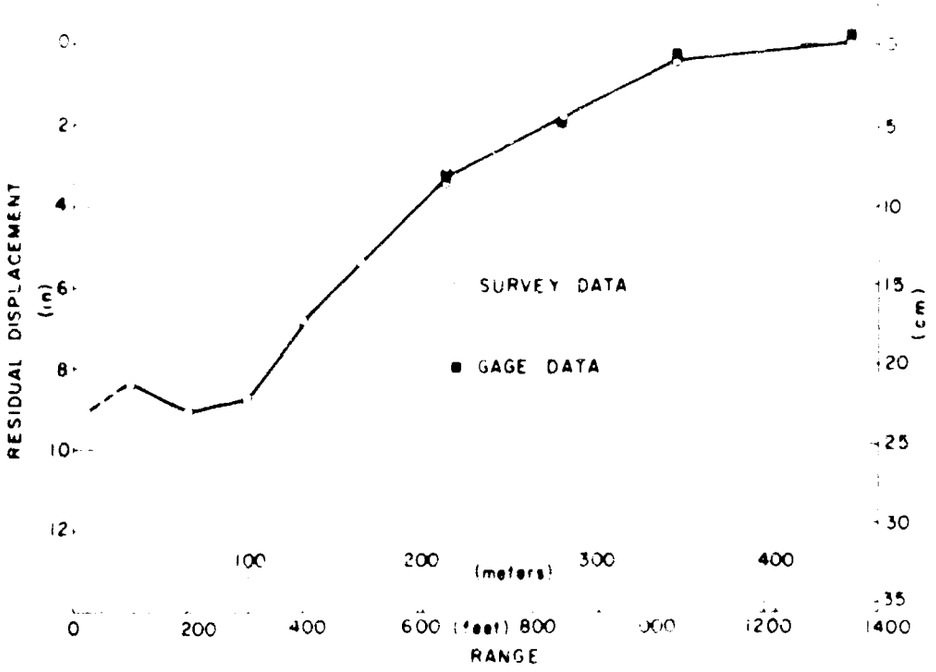


Fig. 9 Residual Displacements for Priscilla Shot

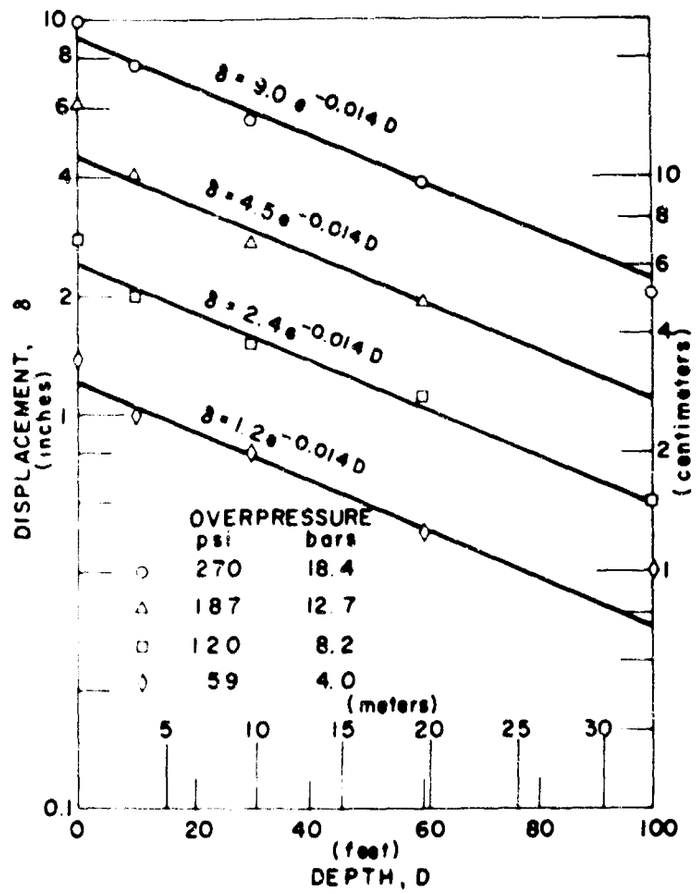


Fig. 10 Attenuation of Peak Displacements with Depth for Priscilla Shot

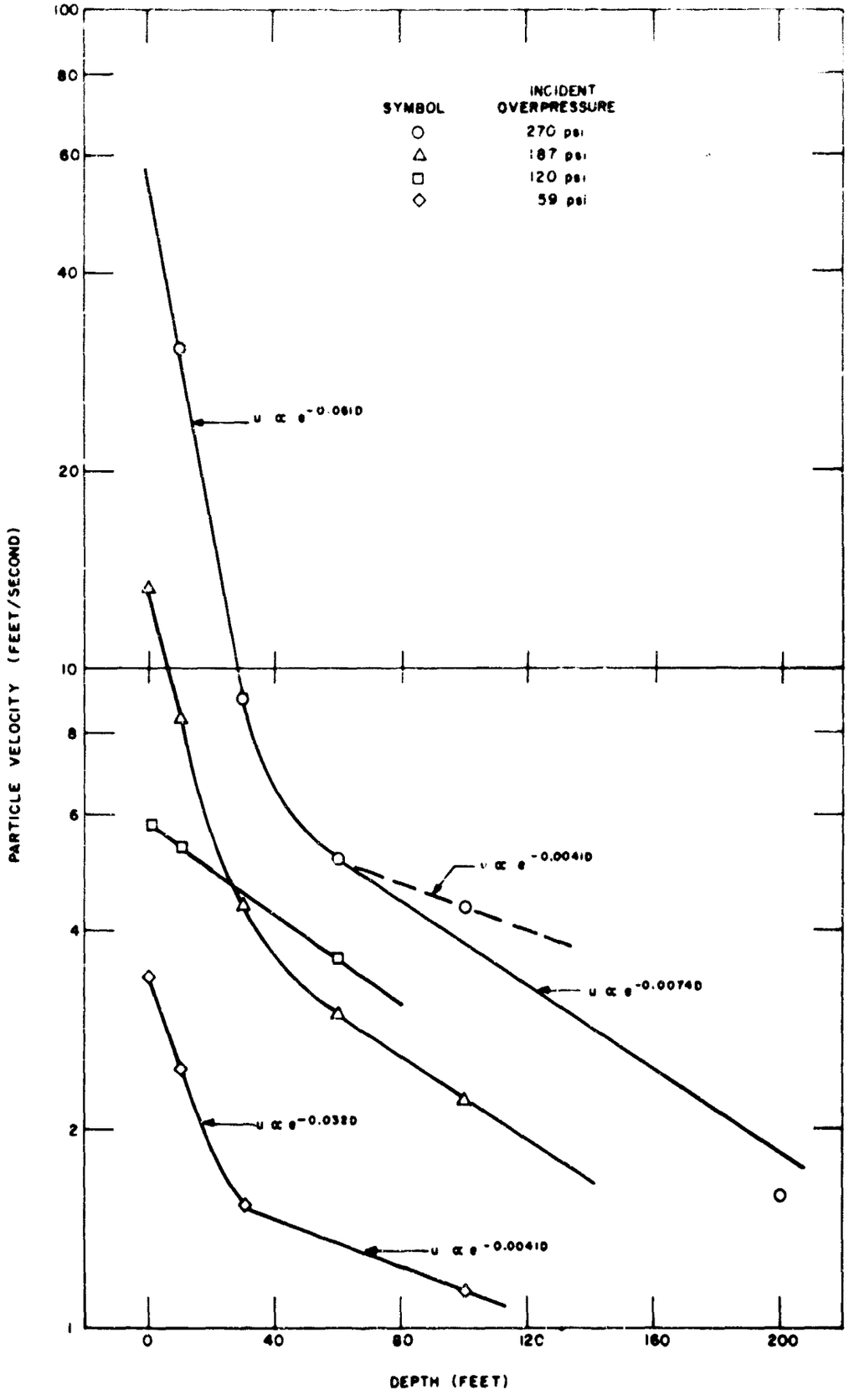


Fig. 11 Attenuation of Peak Velocity with Depth for Priscilla Shot

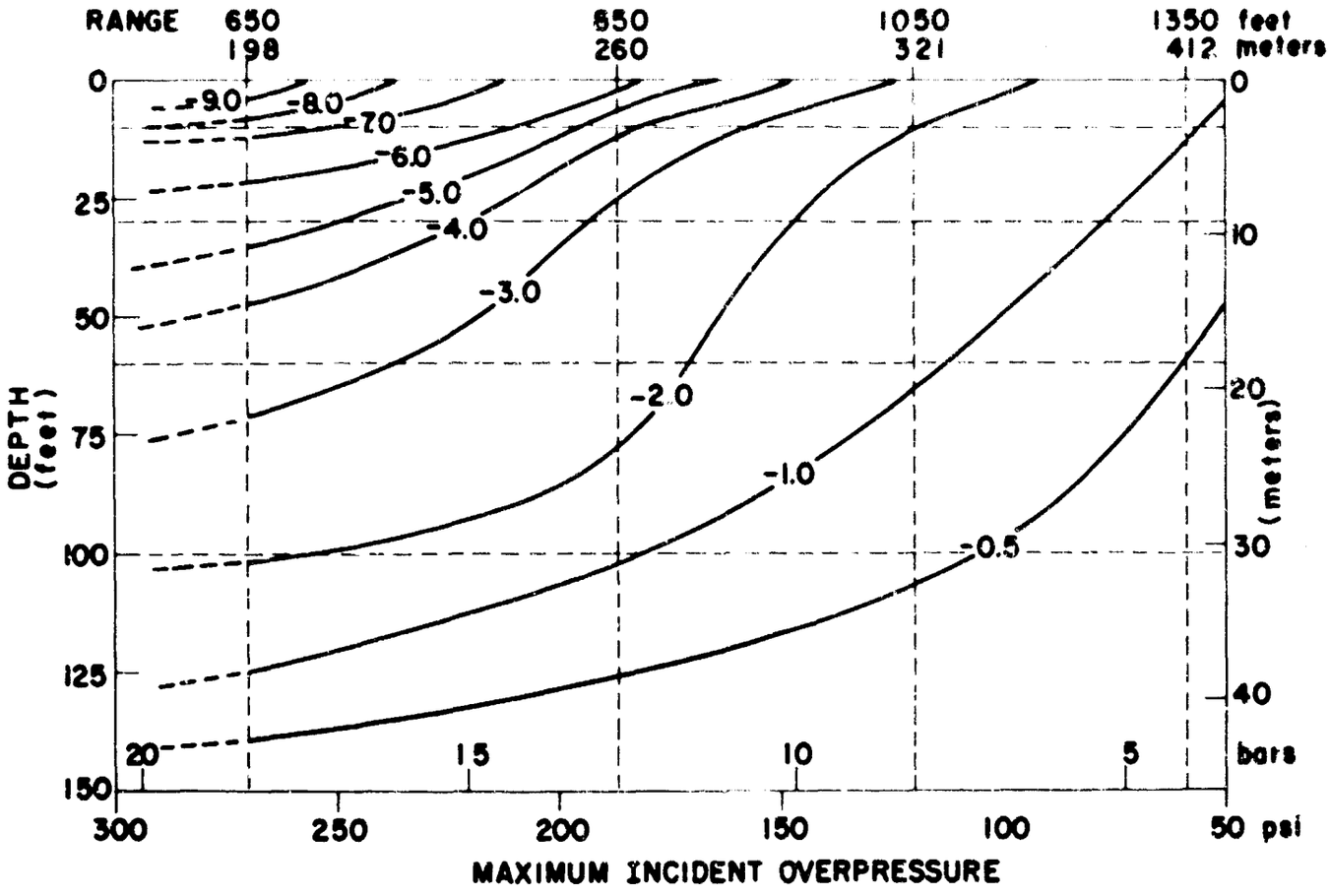


Fig. 12 Contours of Downward Displacement in Inches

REFERENCES

Chemical Explosives

1. Sachs, D. C. and L. M. Swift, "Small Explosion Tests, Project Mole," Final Report, AFSWP-291, Volumes I and II, (Unclassified), Stanford Research Institute, Menlo Park, California, December 1955.
2. Murphey, B. F., "Particle Motions Near Explosions in Halite," SC-4440(RR), Project Cowboy, (Unclassified), Sandia Corporation, Albuquerque, New Mexico, June 1960.
3. Perret, W. R., A. J. Chabai, J. W. Reed, and L. J. Vortman, Final Report, Project Scooter, SC-4602(RR), (Unclassified), Sandia Corporation, October 1963.

Nuclear Explosives

4. Salmon, V. and S. R. Hornig, "Earth Acceleration vs. Time and Distance," WT-517, Operation Tumbler, (Unclassified), Stanford Research Institute, Menlo Park, California, February 1953.
5. Perret, W. R. and V. L. Gentry, "Free-Field Measurements of Earth Stress, Strain and Ground Motion," WT-716, Operation Upshot-Knothole, (Unclassified), Sandia Corporation, Albuquerque, New Mexico, February 1955.
6. Swift, L. M., D. C. Sachs, and F. M. Sauer, "Ground Acceleration, Stress and Strain at High Incident Overpressures," WT-1404, Operation Plumbbob, Priscilla Event, (Unclassified), Stanford Research Institute, Menlo Park, California, May 1960.
7. Perret, W. R., "Ground Motion at High Incident Overpressures," WT-1405, Operation Plumbbob, Priscilla Event, (Unclassified), Sandia Corporation, Albuquerque, New Mexico, June 1960.
8. Swift, L. M. and D. C. Sachs, "Surface Motion from an Underground Detonation," WT-1528, Operation Plumbbob, Rainier Event, (Unclassified), Stanford Research Institute, Menlo Park, California, March 1960.

9. Perret, W. R., "Subsurface Motion from a Confined Underground Detonation," Part I, WT-1529, Operation Plumbbob, Rainier Event, (Unclassified), Sandia Corporation, Albuquerque, New Mexico, August 1961.
10. Adams, W. M., R. L. Flanders, W. R. Perret, R. G. Preston and D. C. Sachs, Summary Report of Strong Motion Measurements, Underground Nuclear Detonations, ITR-1711, Operation Hardtack II, (Unclassified), January 1960, see also Journal of Geophysical Research, Volume 66, Number 3, March 1961.
11. Weart, W. D., "Particle Motion Near a Nuclear Detonation in Halite," PNE-108F, Project Gnome, Plowshare Program, (Unclassified), Sandia Corporation, Albuquerque, New Mexico, December 1961, see also Bulletin of the Seismological Society of America, Volume 52, Number 2, December 1962.
12. Swift, L. M., "Intermediate Range Earth Motion Measurements," PNE-111F, Project Gnome, Plowshare Program, (Unclassified), Stanford Research Institute, Menlo Park, California, December 1961.
13. Perret, W. R., "Free-Field Ground Motion Studies in Granite," POR-1803, HardHat Event, Nougat Series, (Official Use Only), Sandia Corporation, Albuquerque, New Mexico, April 1963.
14. Swift, L. M., "Measurement of Close-In Earth Motion," VUP-2101, HardHat Event, Nougat Series, (Unclassified), Stanford Research Institute, Menlo Park, California, March 1962.

INERTIAL EFFECTS AND SOIL STRENGTH CRITERIA

by
B. B. Schimming* and H. C. Saxe**

INTRODUCTION

The strength of soils under dynamic loading conditions has received a considerable amount of attention in this country in the past quarter century. The primary testing apparatus in the past investigations has been the triaxial device.

As part of the United States Air Force blast protective construction research program, a dynamic direct shear device has been developed in the Civil Engineering Department at the University of Notre Dame. A wide variety of soils have been tested for sensitivity to load rate effects. The purpose of this presentation is to report some of the preliminary results of the testing program.

EXPERIMENTAL FACILITY

The equipment involved in this study has been previously described by Saxe, Graves and Schimming (1) and will be briefly reviewed here. The dynamic direct shear apparatus will subsequently be referred to as DACHSHUND I (Dynamically Applied Controlled Horizontal SHear - University of Notre Dame I).

The method of load application consists of a pneumatic system which is capable of applying a 1000 pound load to the soil specimen in both the vertical and horizontal directions. For a dynamic test, air is passed into the accumulator tanks from the air compressor through a pressure regulator. When the air pressure has reached a predetermined value in the accumulator tanks, air is passed into the rear of the cylinders behind the pistons which are restrained by the trigger assembly. Upon actuation of the solenoid operated triggers, which releases the pistons, the accumulated force on the pistons is suddenly transmitted to the soil specimen. For all of the tests described in this paper, the normal or confining load was applied statically, either pneumatically or with weights placed on the specimen. The horizontal shear load was applied statically and dynamically.

In a static test, the horizontal piston is not restrained by the trigger. As pressure is gradually developed in the horizontal cylinder, it is immediately transmitted to the specimen. The rate of force application is regulated manually at the control panel.

The shear box can accommodate a 4 inch diameter, 3/4 inch thick specimen. The lower half of the box is the moveable portion and is made of aluminum to minimize inertial effects. It is supported by an air bearing supplemented by four small ball bearings recessed into the brass support plate to resist eccentric normal loads.

The measurement of loads transmitted to the soil specimen is accomplished by the use of thin-walled cylindrical transducers. Three load cells are employed: one in the vertical direction and two in the horizontal direction. The lower or "action" load cell moves with the horizontal piston. The upper or "reaction" cell is attached to the upper half of the shear box and a rigid support connected to the base of the machine. The upper half of the shear box is supported on four columns which are flexible in the direction of motion. Hence the reaction load cell also measures the horizontal force on the specimen and in conjunction with the action load cell allows the appraisal of horizontal inertial forces and friction losses at the base of the moveable portion of the shear box.

Displacements in both the horizontal and vertical directions are measured with potentiometric transucers.

All transducer outputs are displayed on oscilloscopes and recorded with Polaroid cameras.

EXPERIMENTAL RESULTS

Figure 1 is a comparison of the static and dynamic strengths of a dry Ottawa sand (# 20-30 sieves) in both a loose and dense state. The solid lines represent the static strength envelopes obtained from a series of tests conducted on DACHSHUND I which compared favorably with results previously reported by Burmister (2) using a conventional direct shear device. The time to failure or test duration was approximately 40 seconds.

The data points represent dynamic tests in which the time to failure was approximately 3 to 4 milliseconds. The normal load was applied statically with air pressure in the vertical cylinder while the shear load was applied dynamically. The resulting comparison demonstrates the insensitivity of dry sand to load rate effects. Similar conclusions have been previously reported by Whitman (3).

* Assistant Professor, Department of Civil Engineering, University of Notre Dame, Notre Dame, Indiana.
**Professor and Head, Department of Civil Engineering, University of Notre Dame, Notre Dame, Indiana.

A second series of tests were conducted on a Jordan Buff Clay sold commercially by the United Clay Mines, Trenton, New Jersey. The characteristics of this clay are as follows:

Liquid Limit	54%
Plastic Limit	26%
Shrinkage Limit	22%
Plasticity Index	28%
Specific Gravity	2.74

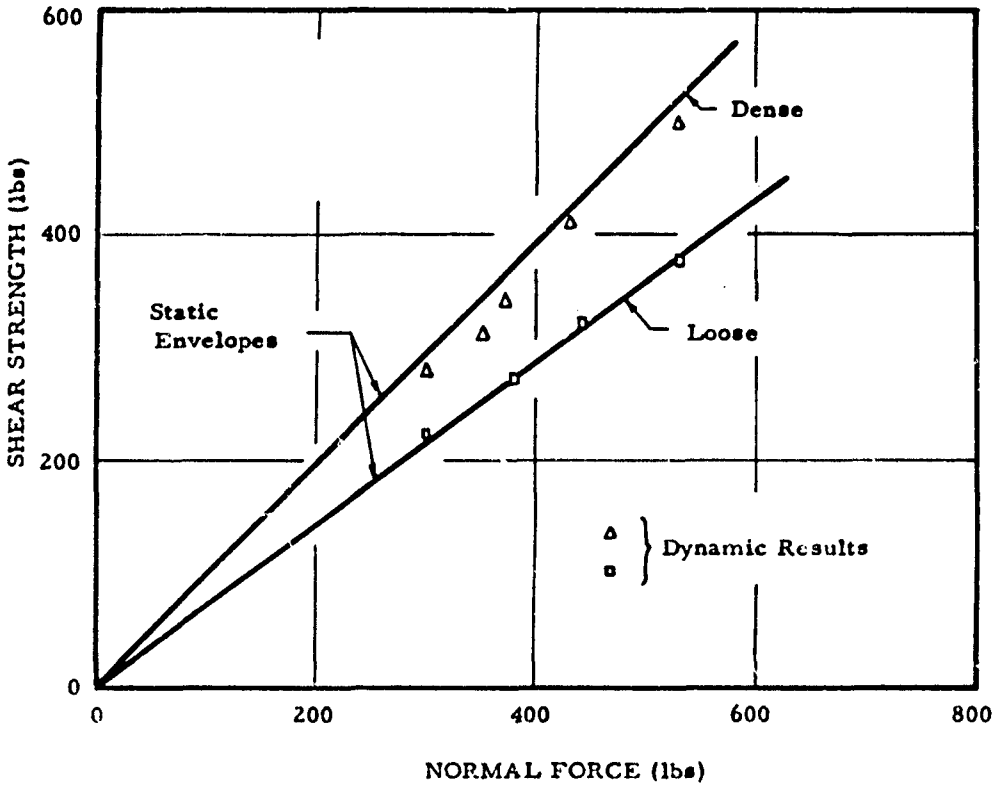


Fig. 1 Comparison of Dynamic and Static Strength Envelopes: Sand

The clay was purchased in powder form, mixed with distilled water to a moisture content of approximately 31% and compacted to a wet density of 114 lbs/cu.ft.

Figure 2 is a typical set of dynamic test results for the compacted clay, comparing the action and reaction load cell response. The initial spike in the action trace was attributed to the inertia of the moving tray and the strength was assumed equal to the value of the trace after this initial peak which is in agreement with the reaction trace.

The static and dynamic strength envelopes for the Jordan Buff Clay are shown in Figure 3. The dynamic envelope is comprised of tests whose time to failure was in the 0-5 millisecond range while the static envelope involved test durations of approximately 40 seconds. An examination of Figure 3 indicates that at any particular value of the normal load, the dynamic shear strength is approximately twice the static value. These results certainly demonstrate the time dependent strength characteristics of the unsaturated clay under consideration.

Consistent with objectives of the study, a number of other soils, including a sandy silt, a lake marl and a silty clay were tested statically and dynamically as previously described.

The primary difference in the static and dynamic failure envelopes for those soils possessing cohesion was an increase in the cohesion parameter under dynamic conditions with little or no change in the friction angle. This is typified by the behavior of the lake marl as shown in Figure 4.

In an attempt to correlate this strength variation with soil type, the ratio of dynamic cohesion to static cohesion was plotted versus the 50% grain size in Figure 5.

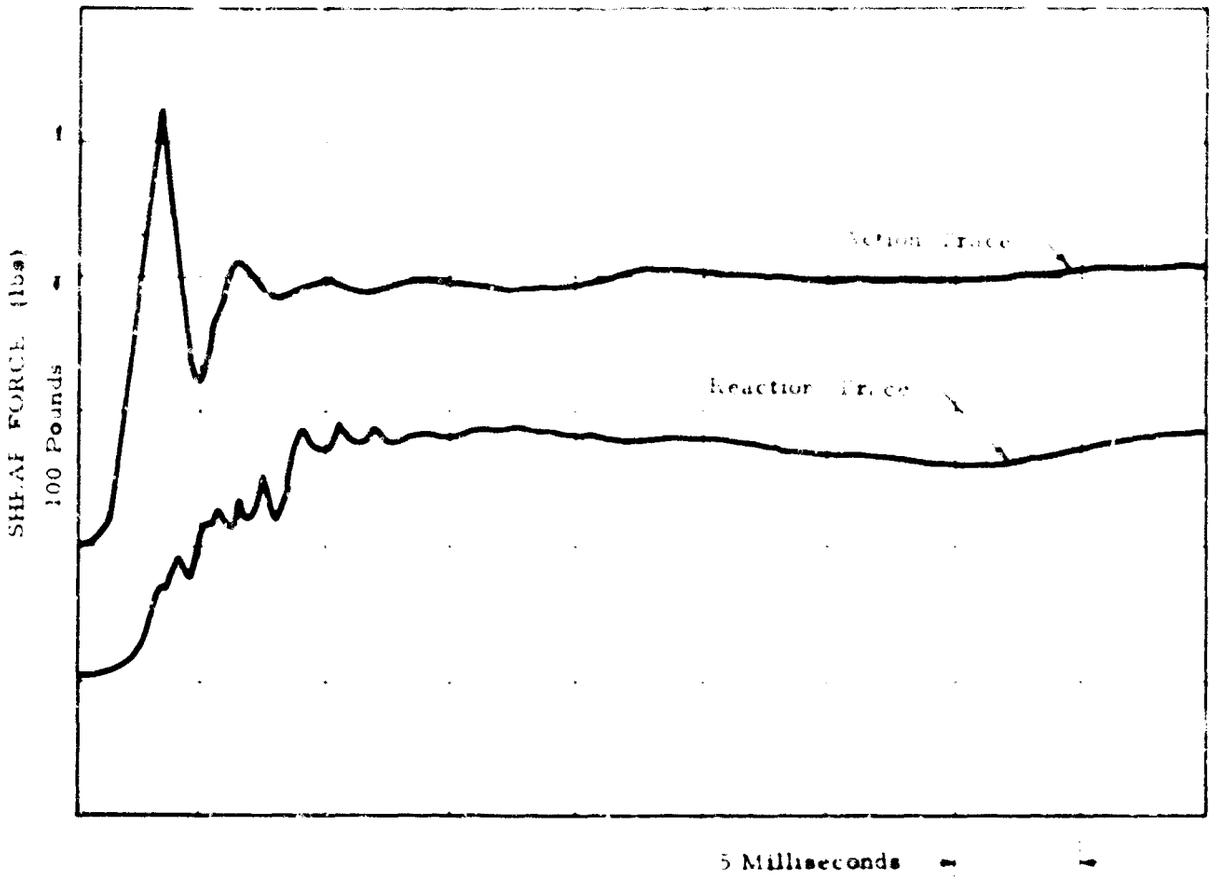


Fig 2 Action and Reaction Load Cell Traces: Clay

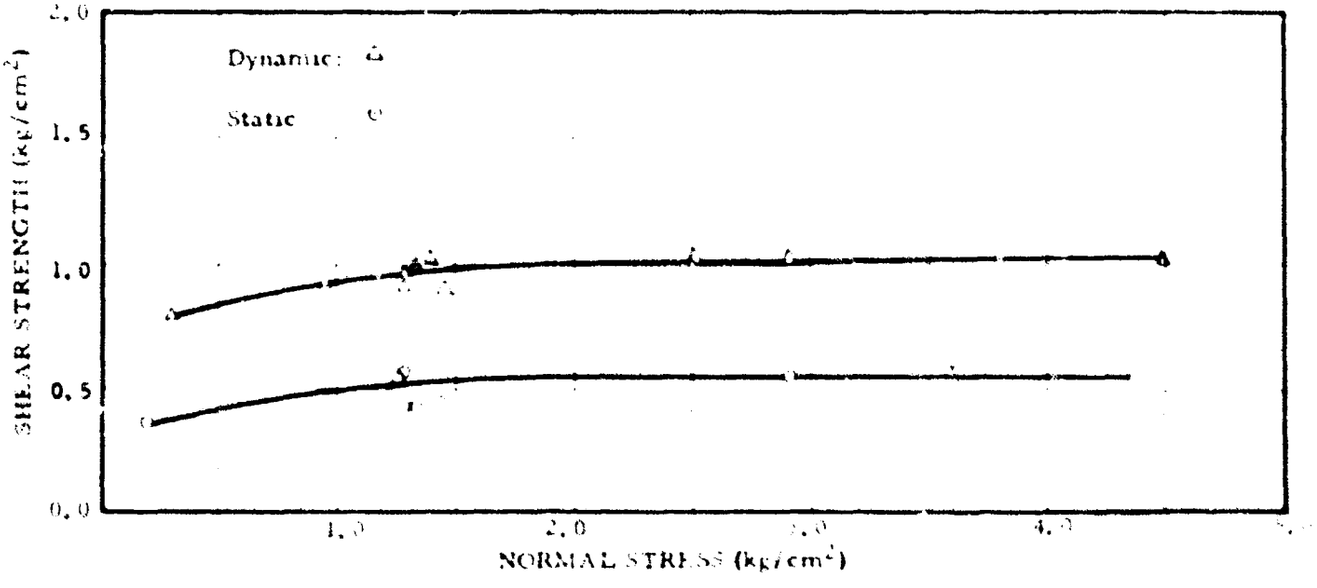


Fig 3 Dynamic and Static Strength Envelopes for Jordan Buff Clay

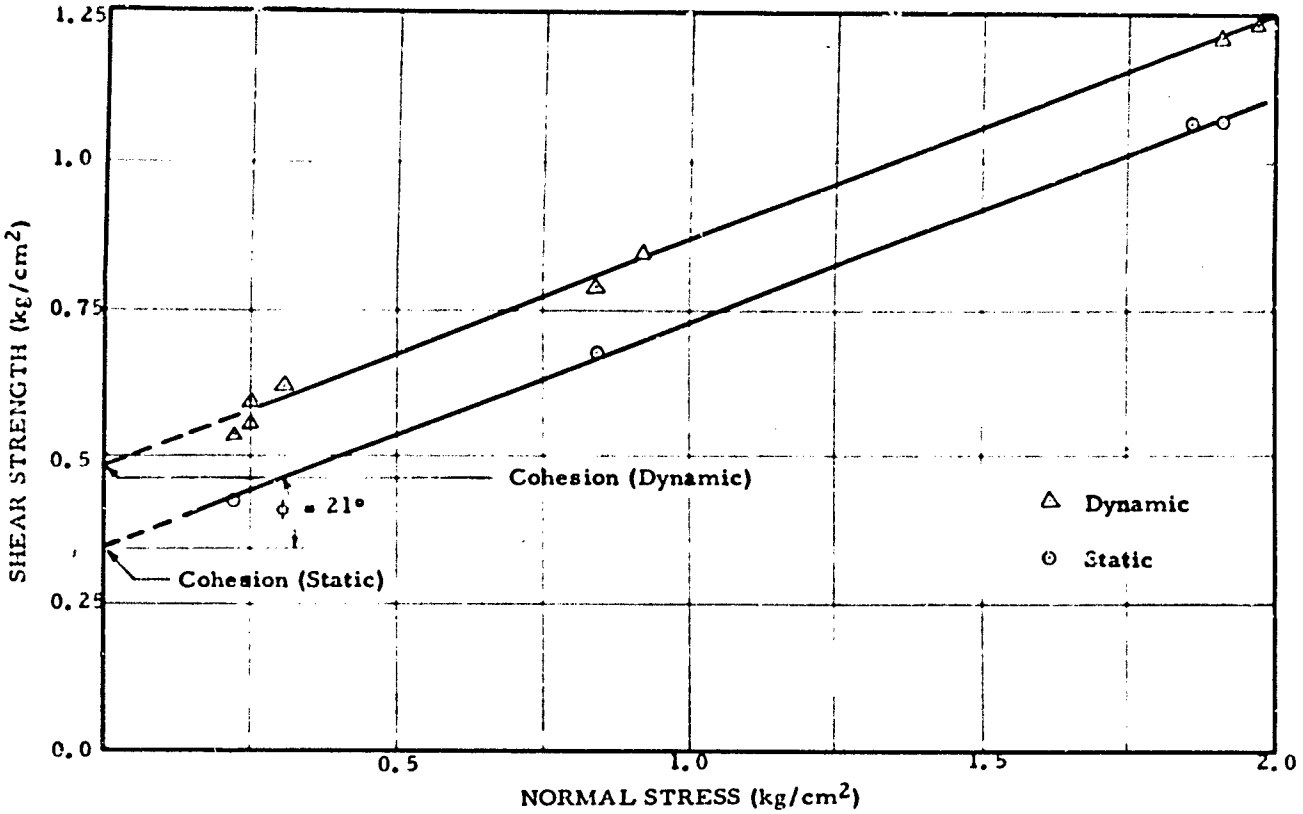


Fig. 4 Dynamic and Static Strength Envelopes for Notre Dame Lake Marl

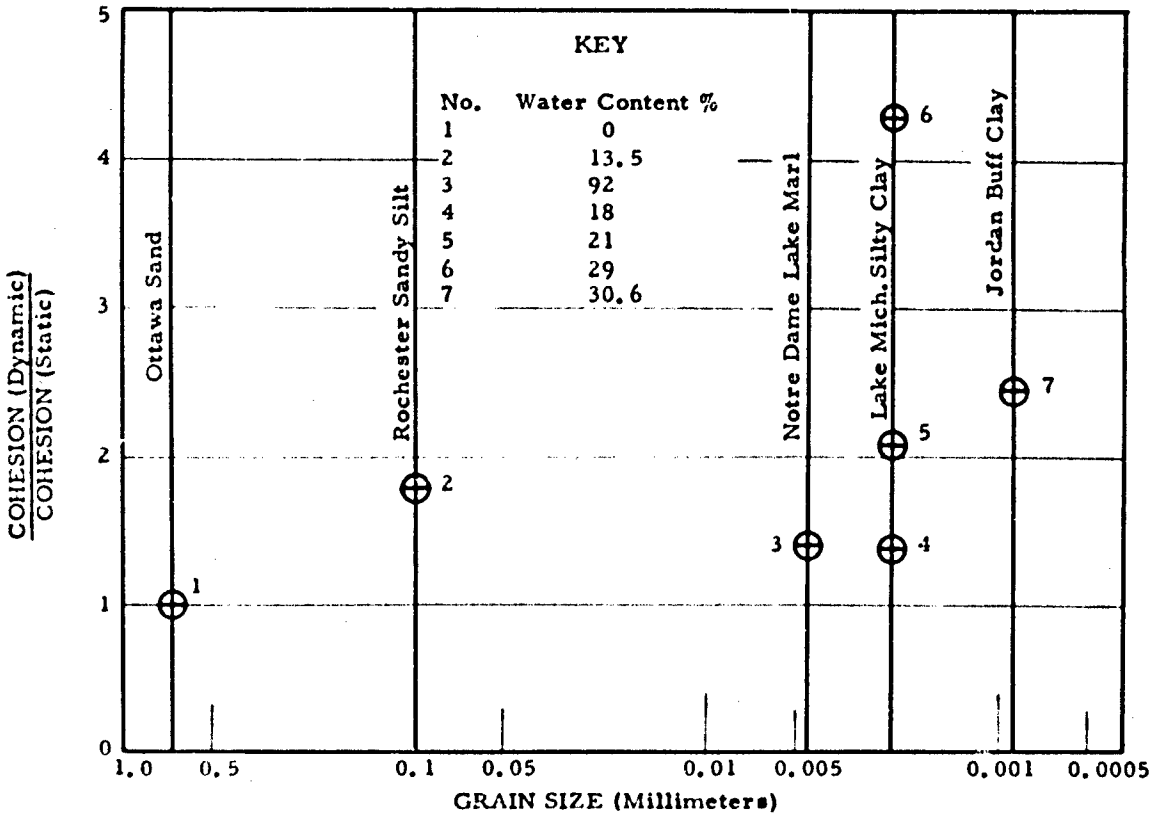


Fig. 5 The Dependence of Displacement Rate Effect on Grain Size

Although this ratio tends to increase with decreasing grain size, there is a wide variation for any one particular cohesive soil, such as the silty clay. However, this variation appears to be consistent with the moisture content of the soil. Thus, the ratio of dynamic to static cohesion was plotted versus the liquidity index defined as the moisture content minus the plastic limit divided by the plasticity index, in Figure 6.

Although there is insufficient data to draw a general conclusion, there appears to be a correlation between the strength ratio and the position of the soil in the plastic range.

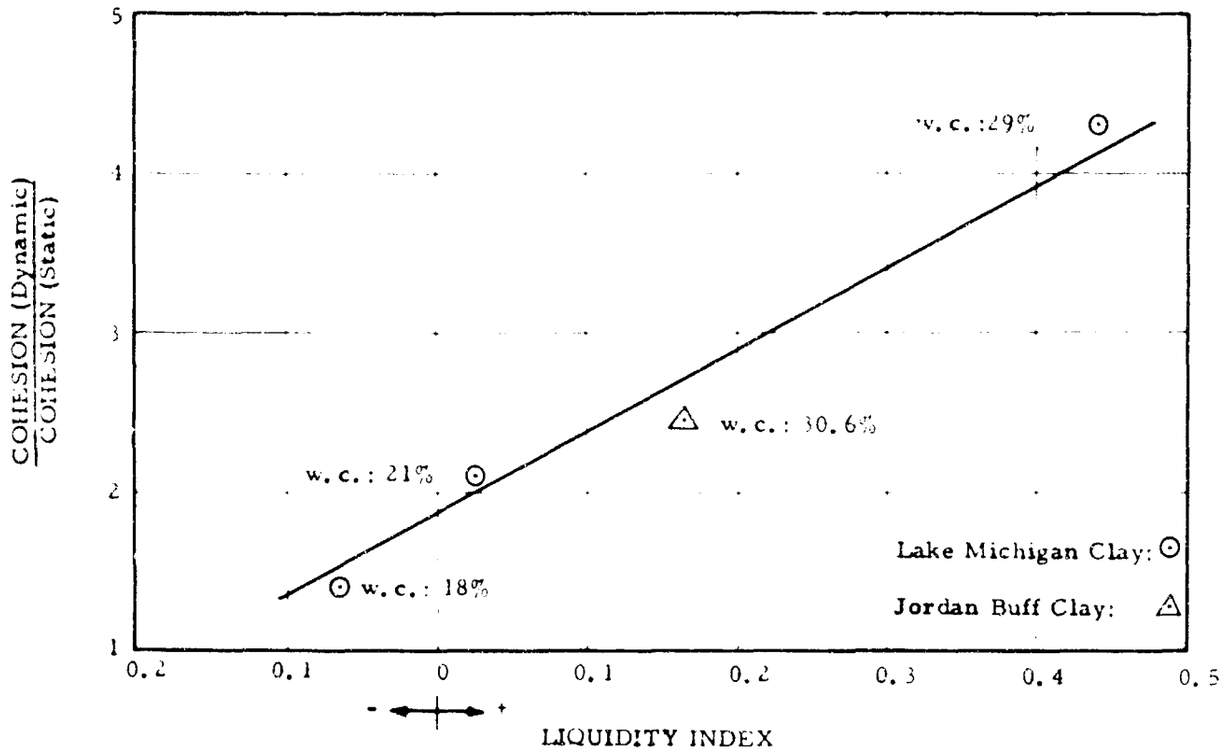


Fig. 6 The Dependence of Displacement Rate Effect on Liquidity Index

INERTIAL CONFINEMENT

The most comprehensive investigation of the behavior of soil under transient loads took place at the Massachusetts Institute of Technology between 1951 and 1954 under sponsorship by the Corps of Engineers, United States Army. Earlier work had been done by Casagrande and Shannon (4) at slower rates of loading.

One rather interesting aspect of the MIT dynamic compression tests is shown in Figure 7. The presence of the sharp initial peak or "spike" in the impact end load cell trace was described by Whitman (3) as a "lateral inertia effect" which he described as follows: "Lateral strains must occur before failure can take place, and in very rapid tests inertia delays the development of lateral strains. Thus, it is possible to develop, during very short periods of time, stresses far in excess of the peak resistance." This lateral inertia effect is shown schematically in Figure 8.

Parkin (5) chose to interpret this peak in a different manner. His analysis was prefaced by the following statement: "Although it cannot be denied, in principle, that effect due to lateral inertia may exist, the purpose of the present study is to test an alternative theory by comparing numerical results derived from it with experiment. In essence we ask if it is possible to exclude all appeals to the effects of lateral inertia and to choose a specific constitutive relationship for the medium which, in conjunction with a sufficiently detailed one-dimensional representation of the experimental arrangement, is able to account for the observed behavior." These contradictory viewpoints stimulated a considerable amount of discussion.

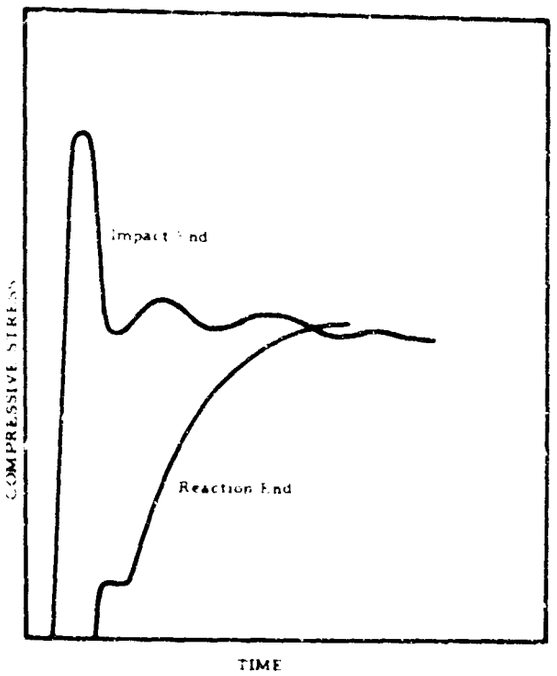


Fig. 7 Stress-Time Relations - Whitman (3)

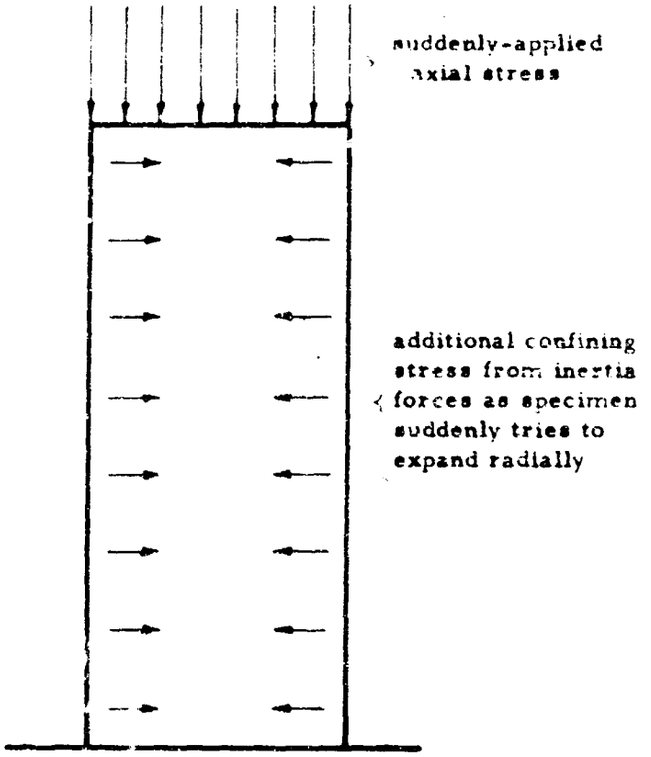


Fig. 8 Lateral Inertia Effect - Whitman and Healy (6)

Fulton and Hendron (7) supported the lateral inertia viewpoint as indicated by the following statements: "The main inconsistency is that there are lateral deformations and, thus, lateral inertia effects in a sample under constant lateral stress that are ignored by the one-dimensional equation of motion." "It does not seem logical to discard the lateral inertia phenomena that are known to exist in reality for a strain rate mechanism whose significance is questionable."

Selig and Vey (8) also joined the discussion, but concluded that "It is obvious that as far as stress propagation is concerned, the peak stress value is of little consequence and only the stress attained after the sudden drop occurs is actually propagated through the soil."

In Whitman's (9) discussion of Parkin's paper, he rather thoroughly defends the "lateral inertia" concept and reiterates that the inertial peak of the impact stress versus time curve was in all likelihood the results of phenomena associated with the boundary conditions peculiar to the test.

In order to possibly contribute to this problem, it becomes apparent that it would be desirable to conduct a dynamic strength test under radically different boundary conditions. Also if the "lateral inertia" effect could be treated as a variable, some insight would be gained. The presence of a dynamic direct shear device at the University of Notre Dame offered the opportunity to investigate these factors.

Figure 9 indicates the various components of normal force that may be operable on the failure plane during a dynamic direct shear test. If the soil tends to dilate (expand) during shear, the indicated inertial forces which are analogous to lateral inertia in the triaxial test may be present.

It appeared that the most reasonable way to explore this situation was to accentuate the effect as indicated in Figure 10. Case (b) represents the conventional pneumatic application of normal load where W_1 is the weight of the vertical piston assembly. For case (a), the vertical pneumatic system is tilted out of the way and the normal load, W_2, is applied with lead weights. W_2 was chosen to be much larger than W_1 to accentuate any effects of inertial confinement.

A typical set of reaction load cell traces for the two different methods of confinement are presented in Figure 11 for a dense 20-30 Ottawa Sand. The upper trace is for a normal load of 150 pounds provided by the lead weights while the lower trace is also for a normal load of 150 pounds, but applied pneumatically.

The shear strength which is taken after the initial peak when there is agreement between the action and reaction load cells is approximately 250 pounds for the top trace and 140 pounds for the lower trace. In addition, the period of sustained shear resistance for the top trace is shorter than for the lower trace. This would tentatively point to the temporary nature of the inertial confinement which ceases when expansion is completed.

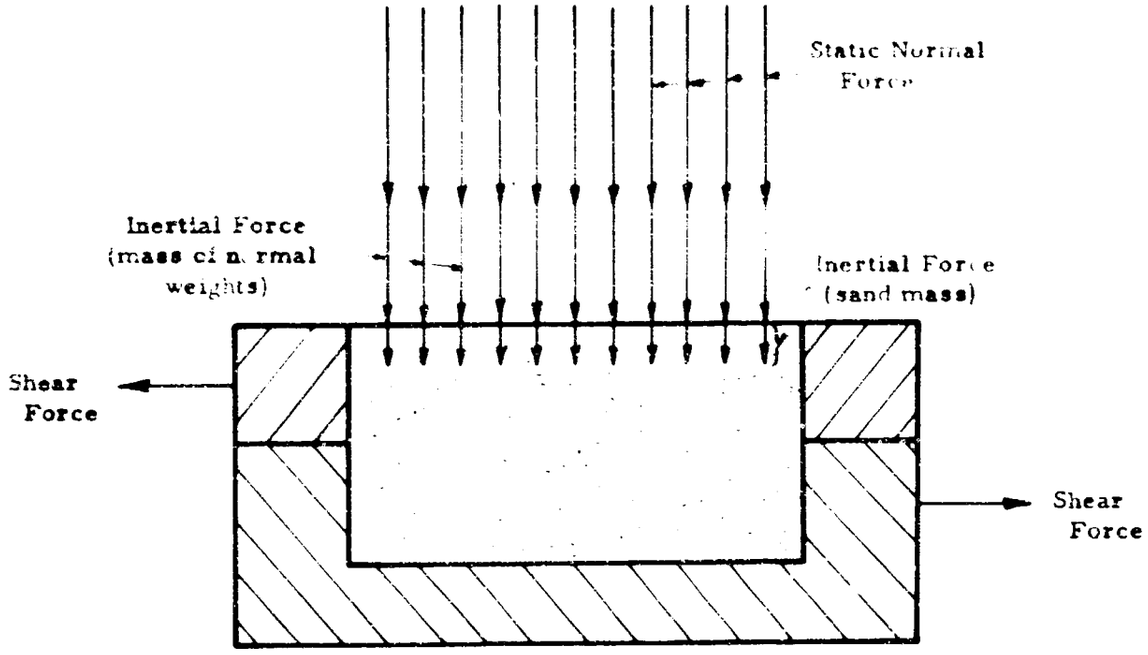


Fig. 9 Forces Involved in Dynamic Direct Shear

$$W_2 >>> W_1$$

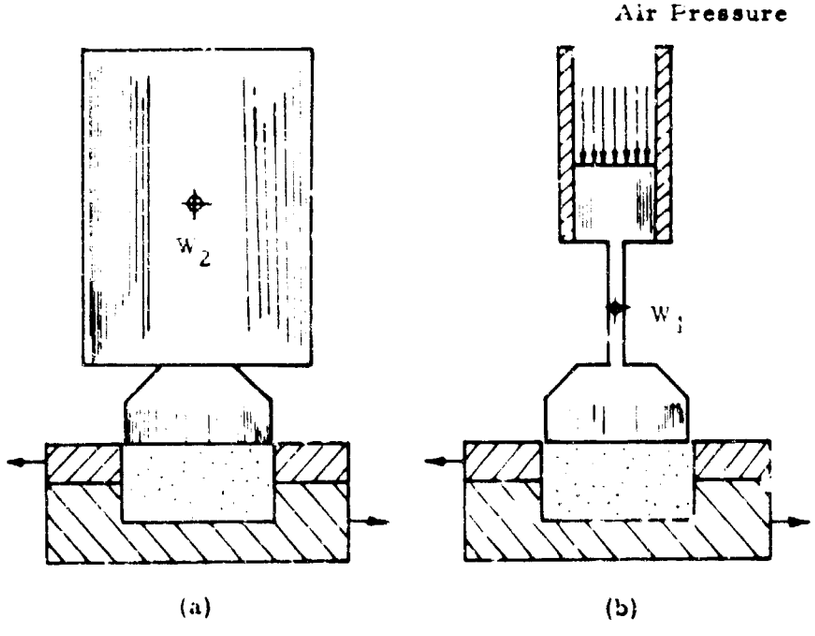


Fig. 10 Methods for Application of Normal Forces

Figure 12 gives the comparison of strength values obtained for the two different methods of normal load application over a range of normal loads. The friction angle for pneumatic application of normal load is approximately 43 degrees which is in agreement with accepted values for the dense Ottawa sand. The friction angle for normal loads applied with the lead weights is 61 degrees which is considerably larger than the static or conventional dynamic value.

DISCUSSION OF INERTIAL CONFINEMENT

With the present configuration of DACHSHUND I, transient forces and displacements can be measured in the normal direction when the pneumatic system is used; however, when lead weights replace the pneumatic system, the dynamic measuring system in the normal direction cannot be utilized. Thus, certain assumptions regarding the displacement behavior in the normal direction are required. Studies at the Massachusetts Institute of Technology have unveiled some factors that are particularly pertinent to this disucssion. Healy (10), using a torsional device, has shown that the magnitude of dilation (expansion) in a dense sand is essentially independent of normal load. Whitman (6) has reported the results of static direct shear tests on dense sand which controlled the magnitude of dilation. These results indicate that if the specimen is not allowed to expand completely, failure cannot be achieved.

These conclusions suggest the conceptual model shown in Figure 13. In order that the middle grain in this model be free to move, which amounts to failure, the upper and lower grains must provide space for the middle grain movement by displacing vertically. If this "passage" is not provided, failure cannot occur and in addition the amount of expansion is not dependent on the normal force between grains.

Based on the assumption that this model is valid in the dynamic range for the two different methods of normal load application previously discussed, some comparisons can be made. In both cases the total expansion will be the same and also the rise-times to failure are measured to be approximately the same. Thus the velocity and accelerations in the normal direction could be anticipated to be comparable.

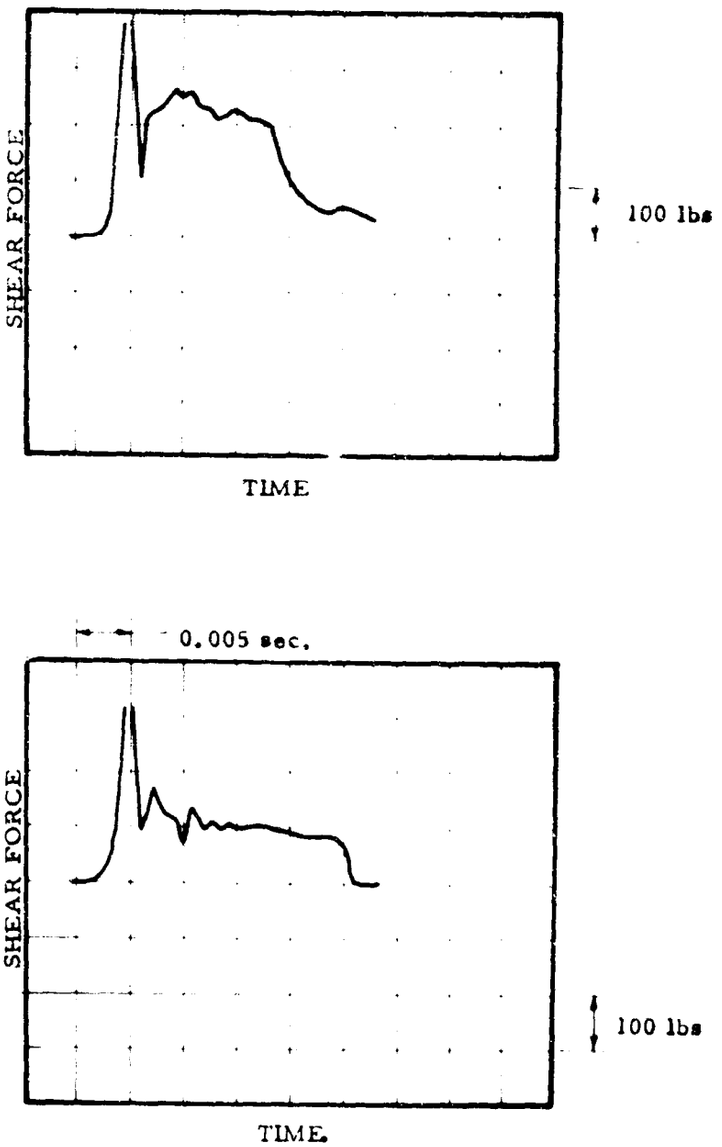


Fig. 11 Reaction Traces for Different Methods of Normal Force Application

On this basis of equal accelerations, any increase in force in the normal direction would be directly proportional to the mass of the moving vertical assembly. For the lead weight configuration this mass is, of course, directly proportional to the normal load. Thus for any particular values of static confinement, as shown in Figure 14, an increase in normal load (Δv) due to the inertial effects will occur which is proportional to the static value of the normal load. Therefore, the "actual" envelope will also be a straight line passing through the origin but with a reduced friction angle. It could be expected that the magnitude of this shift would place the "actual" envelope coincident with the lower envelope in Figure 14, due to the insensitivity of sand to load rate effects independent of inertial effects.

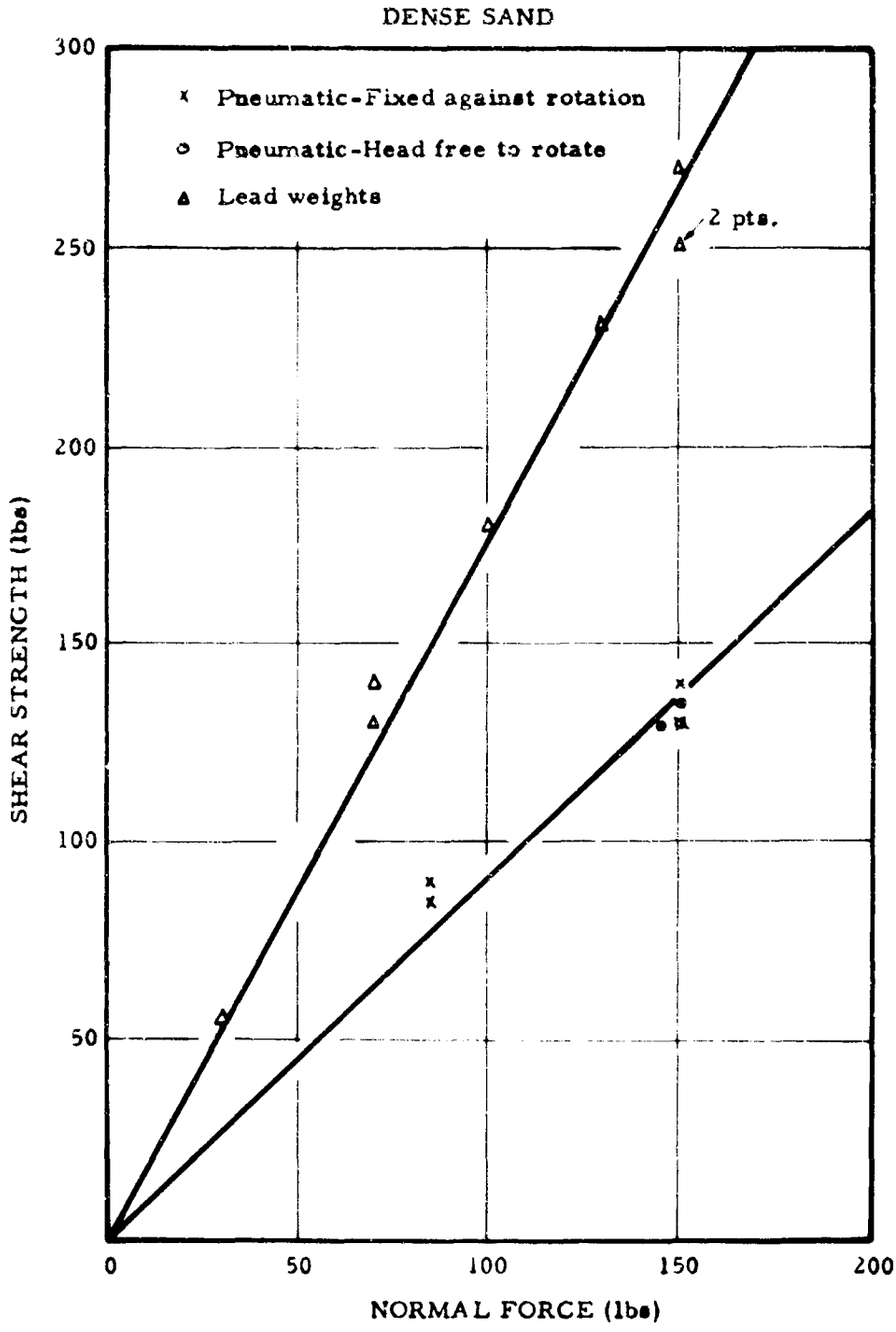


Fig. 12 Strength Envelopes for Different Methods of Normal Force Application

CONCLUSIONS

Based on the results of this investigation, the following conclusions may be drawn:

1. The variation in strength of cohesive soils as a function of rate of load application is best reflected by the cohesion parameter.
2. Apparent "lateral inertial" effects have been observed under boundary conditions quite different than those imposed by the triaxial test thus substantiating their existence independent of the testing device.
3. For soils that dilate when sheared, the inertial forces normal to the failure plane may alter the apparent dynamic strength of the soil.

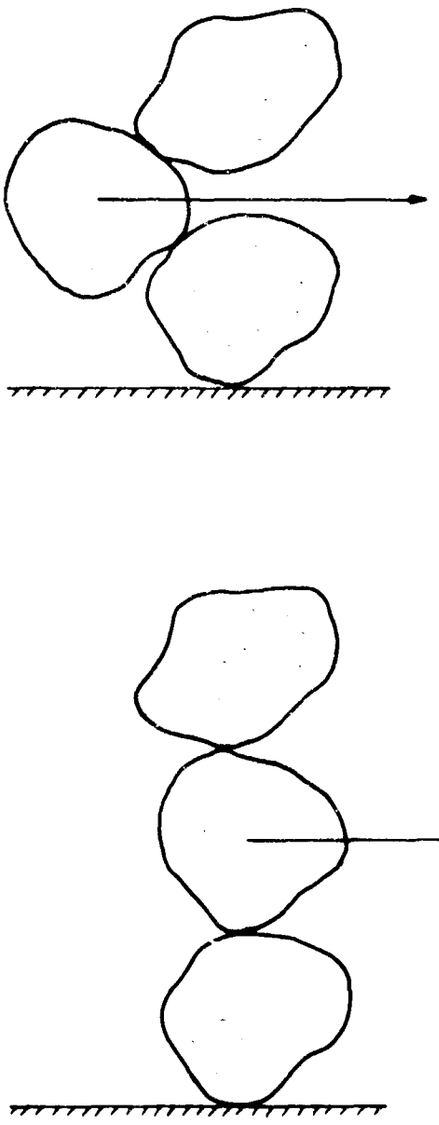


Fig. 13 Conceptual Model of Failure Mechanism

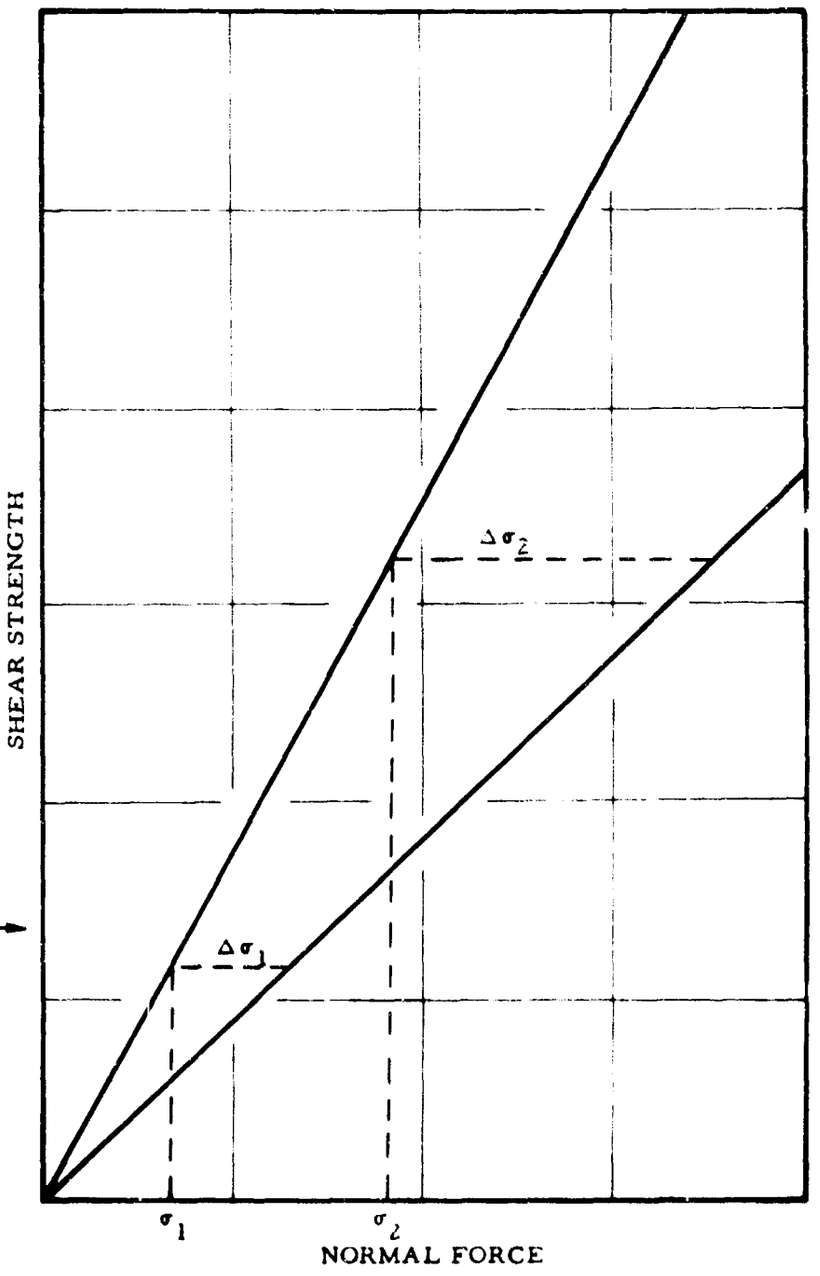


Fig. 14 Interpretation of Strength Envelopes

ACKNOWLEDGEMENTS

The authors wish to thank the United States Air Force, Air Force Systems Command, Research and Technology Division, Air Force Weapons Laboratory, for permission to use part of the data from Contract AF 29(601)-5174 in the preparation of this paper.

In addition, recognition should be given to Theodore Kretschmer, Vincent Dmevich and Helmut Haas for their assistance in the testing program.

REFERENCES

1. Saxe, H.C., L.D. Graves and B.B. Schimming, "Development of an Apparatus for the Dynamic Direct Shear Testing of Soils," Air Force Weapons Laboratory Technical Documentary Report No. RTD TDR-63-3055.
2. Burmister, D.M., "The Place of the Direct Shear Test in Soil Mechanics," Symposium on Direct Shear Testing of Soils, ASTM Special Technical Publication, No. 131, June 1958.
3. Whitman, R.V., "The Behavior of Soils under Transient Loadings," Proceedings, 4th International Conference on Soil Mechanics and Foundation Engineering, Vol. 1, 1957.
4. Casagrande, A. and W.L. Shannon, "Stress-Deformation and Strength Characteristics of Soils under Dynamic Loads," Proceedings, 2nd International Conference on Soil Mechanics and Foundation Engineering, Vol. V, 1948.
5. Parkin, B.R., "Impact Waves in Sand: Theory Compared with Experiment on Sand Columns," Proceedings, ASCE, Soil Mechanics and Foundations Division, Vol. 87, No. SM3, June 1961, Part 1.
6. Whitman, R.V. and K.A. Healy, "Shear Strength of Sands During Rapid Loading," Proceedings, ASCE, Soil Mechanics and Foundations Division, Vol. 88, No. SM2, April 1962.
7. Fulton, R.E. and A.J. Hendron, Discussion of "Impact Waves in Sand: Theory Compared with Experiment on Sand Columns," Proceedings, ASCE, Soil Mechanics and Foundations Division, Vol. 87, No. SM6, December 1961, Part 1.
8. Selig, E.T. and E. Vey, Discussion of "Impact Waves in Sand: Theory Compared with Experiment on Sand Columns," Proceedings, ASCE, Soil Mechanics and Foundations Division, Vol. 87, No. SM6, December 1961, Part 1.
9. Whitman, R.V., Discussion of "Impact Waves on Sand: Theory Compared with Experiment on Sand Columns," Proceedings, ASCE, Soil Mechanics and Foundations Division, Vol. 88, No. SM1, February 1962, Part 1.
10. Healy, K.A., "The Response of Soils to Dynamic Loadings, Report 13. The Dependence of Dilation in Sand on Rate of Shear Strain," U.S. Army Engineers Waterways Experiment Station, Department of the Army, Rand D Subproject 8-S12095-002 under Weapons Effects Board Subtask No. 13.009.

A NEW DEVICE FOR SOIL STRAIN MEASUREMENT

by
W. B. Truesdale* and M. E. Anderson**

DESCRIPTION OF SOIL STRAIN GAUGE

The determination of strain requires the measurement of the change in position of two points spaced a finite distance apart. The IITRI gauge (1,2) developed for measuring static and dynamic strains in soil is shown in Figure 1. The gauge consists of: 1) driver and sensor coils to be placed in the soil, 2) driver and sensor coils on an adjustable precision coil mount, and 3) the electronic auxiliaries. The electronics include an oscillator with a driver amplifier, a signal amplifier, a ring demodulator, filter, and meter. Output terminals are provided for connection to a cathode ray oscilloscope for observing and photographically recording transient strains during dynamic tests.

Figure 2 shows the basic components for application as a soil strain sensor. The embedded coil disks serve as the strain sensing element and must be placed in the soil in a nearly parallel and axially concentric orientation. The externally positioned coils serve as a null reference. As the soil is deformed induced differential coil movements are determined by the resulting electronic signal.

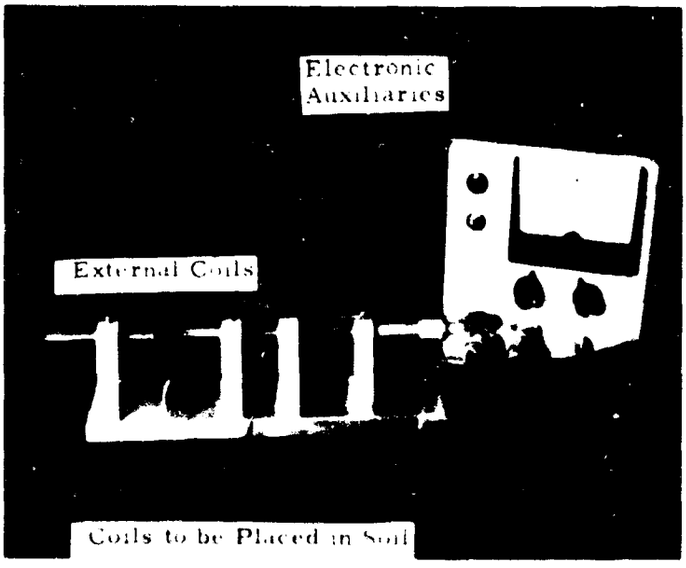


Fig. 1 Soil Strain Gauge.

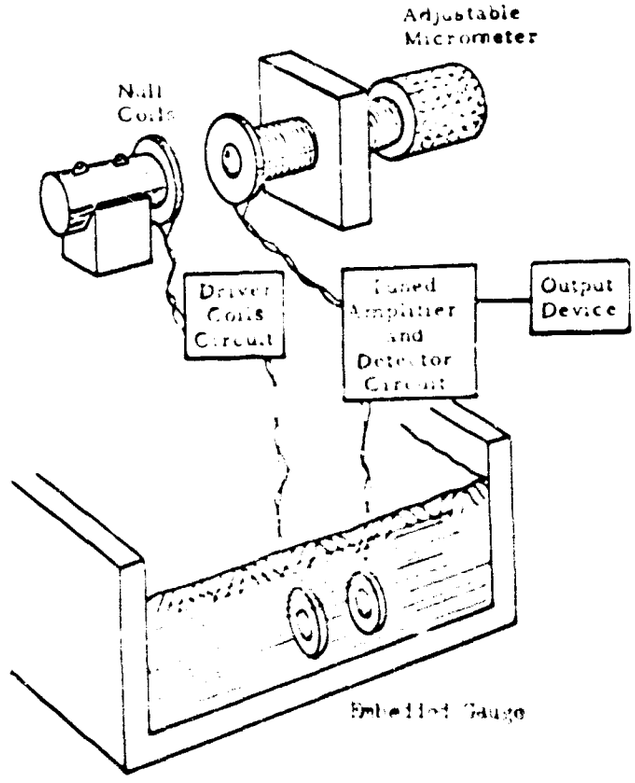


Fig. 2 Pictorial Diagram of Soil Strain Gauge.

* Associate Research Engineer, Soil Mechanics Section, IIT Research Institute, Chicago, Illinois.
** Manager, Instrumentation and Recording Section, IIT Research Institute, Chicago, Illinois.

PRINCIPLES OF OPERATION

The soil strain gauge employs the differential transformer principle; the driver and sensor coil in each set are analogous to primary and secondary transformer windings, respectively. The electronics are designed to measure small changes in mutual inductance caused by a change in flux detected by a sensor coil. The circuitry is more easily described with the aid of the block diagram shown in Figure 3. The instrument electronics consist of the following:

1. A low distortion 50 KC oscillator and temperature compensated power output stage.
2. A high gain four stage amplifier.
3. A synchronous detector whose output is read on a 100-0-100 microamp meter and is also available at output terminals provided for connection to a cathode ray oscilloscope.

A high frequency signal (50 K cps) is applied to the "driver" coils. The magnetic field produced by this high frequency current induces a voltage in the sensor coils, the magnitude of which is a function of the amount of magnetic flux linkage and hence, a function of the coil spacing. The percentage voltage change which occurs across a sensor coil for small changes in spacing is small. However, the two sensor coils are connected in a bridge circuit so that the output signal is the difference of the individual coil output voltages. Since this signal is the change with respect to a null, or zero voltage reference, the measured percentage change in output voltage is greatly increased.

All four coils in the driving and sensing circuit are grounded on one side. This allows a uniformly distributed capacitance to be formed from the ground to the hot side of the coil, facilitating the balancing of the bridge circuit. The bridge comprises the two secondary sensor coils and two matched 7.5K ohm resistors.

The output voltage from the bridge is amplified in a four stage signal amplifier to increase sensitivity so that very small changes in spacing may be detected. Broad-band low-noise silicon transistors are used throughout the amplifier stages to provide stability.

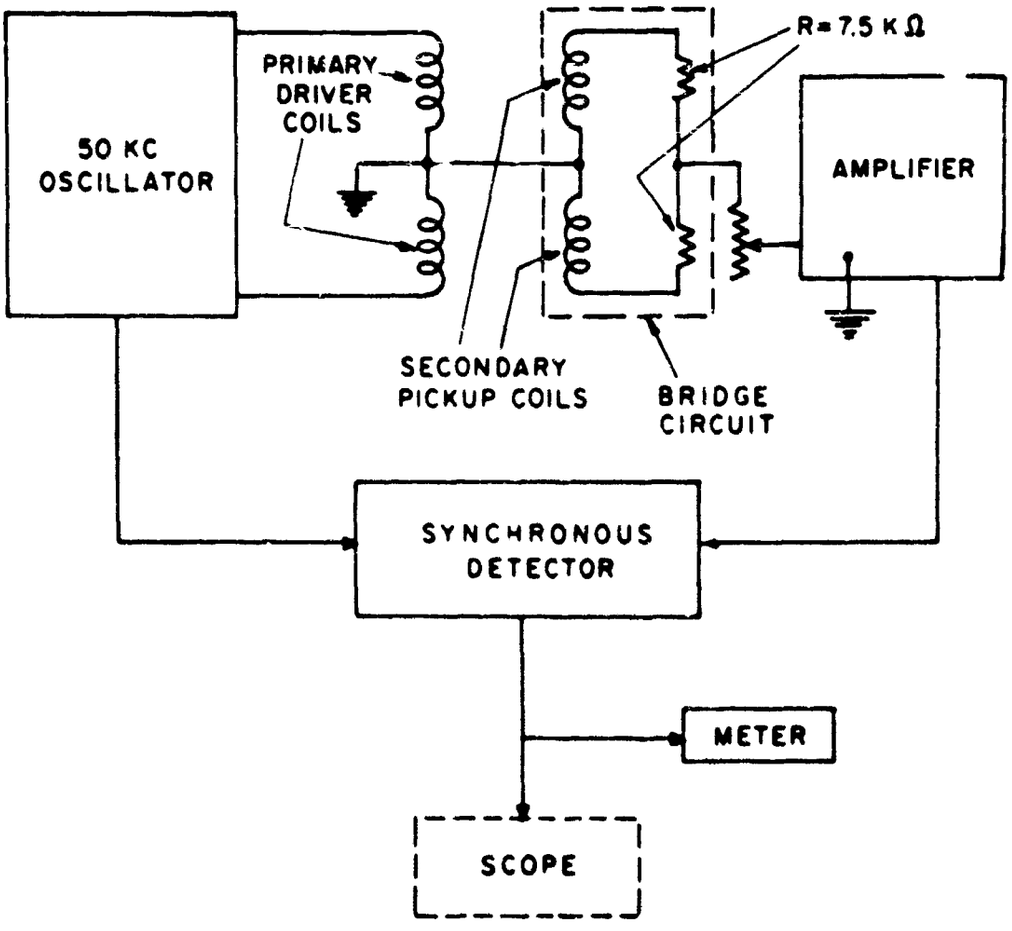


Fig. 3 Block diagram of soil strain gauge.

GROUND MOTION AND INSTRUMENTATION

The voltage signal of interest is the envelope of the high frequency carrier; the amplitude of which is proportional to changes in the coil spacing. To separate the envelope from the high frequency carrier the output from the signal amplifier is applied to two terminals of a conventional ring demodulator. This type of demodulator is sometimes called a synchronous detector and permits operation with a suppressed carrier. The other two terminals of the demodulator are driven by the 50 KC reference voltage. The demodulator output is zero when the carrier input is zero or nulled, and is either positive or negative in polarity when the two sensor coil voltages are not equal. The polarity depends on which coil has the larger voltage, thereby indicating whether the coils have moved closer together or farther apart.

OPERATIONAL PROCEDURE

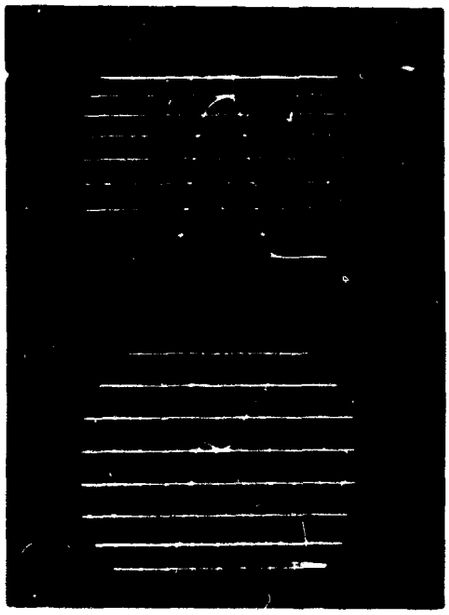
Static Measurements

When the externally positioned coils are at the same spacing as the embedded coils the gauge output is nulled. As deformation occurs in the soil mass the change in spacing of the embedded coils is determined by adjusting the spacing of the reference coils to continually renull the meter. Incremental changes can be read directly off the micrometer head.

Dynamic Measurements

Gauge output must be displayed on an oscillo[illegible], or some other suitable high impedance recording device. The gauge must be calibrated in place, because its sensitivity varies with spacing of the coils and with the degree of misalignment of the embedded coils. The procedure for calibration is, however, accomplished quickly and simply with the reference coils. Since the coil sets, external and embedded, are identical the output of the reference coils for a given displacement from the nulled position is of equal magnitude to the output of the embedded coils for an identical displacement from the nulled position. Figure 4 displays records of transient strains superposed on calibration records.

The horizontal traces represent the calibration record, and are obtained by displacing the reference coils in incremental steps off the null position and photographing the resulting incremental increases in voltage displayed on the oscilloscope. The reference coils are then returned to the null position and the polarity of the signal output to the oscilloscope reversed. (This is necessary because the output of the embedded coils is of opposite polarity to the reference coils.) The instrument is then ready to record a transient strain.



Coil Spacing 0.35 inch

Fig. 4 Calibrated Scope Record

COIL DISPLACEMENT PARAMETERS

The coils laid in the soil as well as those attached to the precision adjustable coil mound must be as closely aligned as possible on the same axis in parallel orientation. This is necessary because the flux density of the magnetic field varies not only with the perpendicular distance from the plane of the coil but also with radial distance from the coil center line.

Figure 5 depicts the coil displacement parameters. To reduce the sensitivity of the gauge to lateral displacement of the coils with respect to each other, either during placement in the soil or during a test, the sensor coil windings are wound to a smaller diameter than the driver coil windings. This permits a slight amount of relative lateral movement while the sensor coil remains in a portion of the magnetic field of constant flux density.

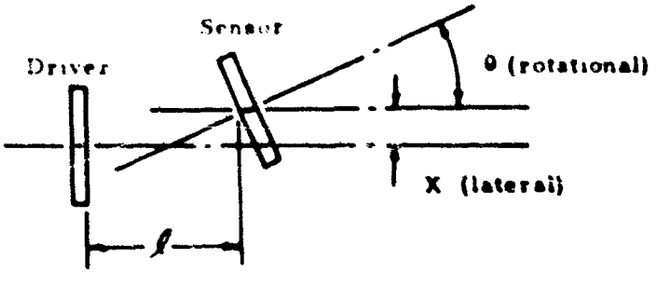


Fig. 5 Coil Position Parameters

Rotational misalignment effects are relatively less severe than lateral misalignment. Theoretically, pure rotation of the sensor coil should have very little effect on gauge output since half of the coil moves closer to the driver coil while half moves away. Thus, while half the coil moves into a portion of the field of increased flux density, half also is in a portion of reduced flux density. However, rotation of either the driver or sensor coil influences the gauge output signal.

Figure 6 compares output signal versus axial, lateral, and rotational displacements at a separation of 0.5 inches. The output for the coils opening and closing was obtained with the coils in each set aligned in an axially concentric and parallel position, i.e., with reference to Figure 5 both λ and θ were zero. The output obtained for an incremental decrease in spacing of either coil set was identical, however, slight differences occurred for incremental increases in spacings. The differences in output are due to the fact that the coil sets are not, in fact, identical. This may be due to variations in the number of turns with which the coils were wound or to inherent variations in the wire itself.

The lateral and rotational output is shown for displacements to both sides of the aligned position. It is seen that the influence of lateral misalignment is symmetrical about the nulled position. Rotational misalignment is not. This is partially due to the difficulty of rotating the coils without changing the axial spacing, but is primarily an effect of the rotating coil lead wires which moved either closer to, or farther away from the other coil as the rotation took place.

Figures 7, 8 and 9 show the influence of misalignment of the coils on the gauge output. The test coils refer to the coils which were misaligned and simulate the possible position of an embedded set of coils. The reference coils were aligned as well as possible, as would be the situation in actual use. Both coils were initially nulled in an aligned position at a spacing of 0.5 in. When the test coils were moved through a lateral and/or rotational displacement, the spacing of the reference coils was adjusted to renull the meter. The change in the spacing from 0.5 in. is the error which would be introduced in determining the separation of the test coils, were they embedded in a soil specimen misaligned as indicated on the figures. It can be seen that the output for axial displacement of the reference coils still serves as an adequate calibration for the test coils.

The absolute magnitude of misalignment which can be tolerated varies with spacing, especially with respect to lateral displacement. In general, it has been found that if the coils can be placed with not greater than 10°-15° relative rotation and/or lateral offset of 10 percent of the coil spacing they will perform quite satisfactorily. Experience has shown that with proper care the gauges can be consistently placed within these tolerances.

PLACEMENT IN SOIL

Satisfactory alignment of the embedded coil disks has been obtained by inserting a rod through the center of both coil disks during placement. The following procedures recommended for placing the gauge are of course arbitrary and may be changed to suit a particular application or the convenience of the user.

Placement in Dry Sand

The soil bed is prepared to the level at which it is desired to place the gauge. The first coil is laid on the sand surface and the alignment rod placed through the center of the coil (Figure 10a) so that it is perpendicular to the soil surface. The rod is of stepped diameter, the larger diameter being 0.10 in. and the smaller of 0.04 in. The smaller diameter passes through a hole in the center of the coil. The step in the diameter of the rod serves to hold the coil flat on the soil surface. Additional sand is then placed to raise the level of the surface to a height above the coil approximately equal to the desired spacing. The second coil has a hole in the center large enough to permit it to be slid down the shaft of the alignment rod to rest on the sand surface. A slight amount of pressure is placed on this coil to hold it flat on the surface (Figure 10b) while it is covered with sand. It is recommended in placing both coils that lead wires be covered immediately as movement of the lead wires during placement can cause rotational or lateral misalignment of the coil disks. After the upper coil has been covered with about 1 inch of soil the rod is removed. At that point coil spacing is determined by adjusting the position of the reference coil on the micrometer mount to null the instrument.

If vibration is to be applied to the test bed to obtain greater sand densities it is recommended that the alignment rod not be withdrawn until after vibration is completed.

Placement in Compacted Soils

Again the soil bed is prepared to the level desired for placement of the gauge, the first coil layed on the soil surface and the rod placed through the center of the soil. Additional soil is then placed and compacted around the rod to obtain the cover necessary to give the desired gauge spacing. The second coil is then slid down the shaft and placed on the soil surface. Additional soil is compacted to a height of 2 to 3 inches above the top coil and the alignment rod removed.

A good deal of care is required in placing the gauges in compacted materials. A Harvard Miniature Tamper was a 20 lb spring and modified 1 in. diameter tamping head is recommended. Obviously this device is not suitable for preparation of large test beds. In these applications it will probably be better to prepare the test bed and excavate for

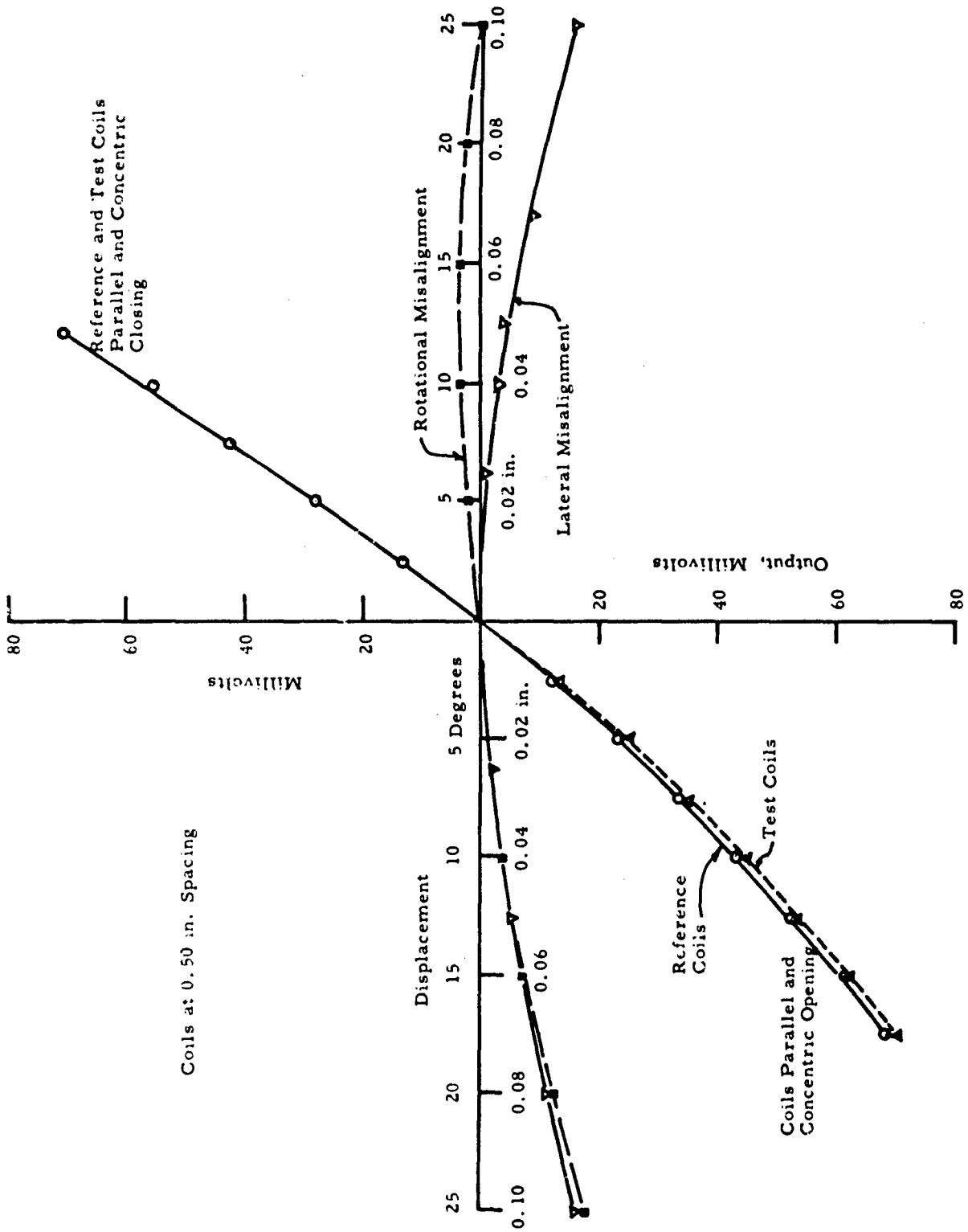


Fig. 6 Relative Coil Displacement Vs. Output Signal

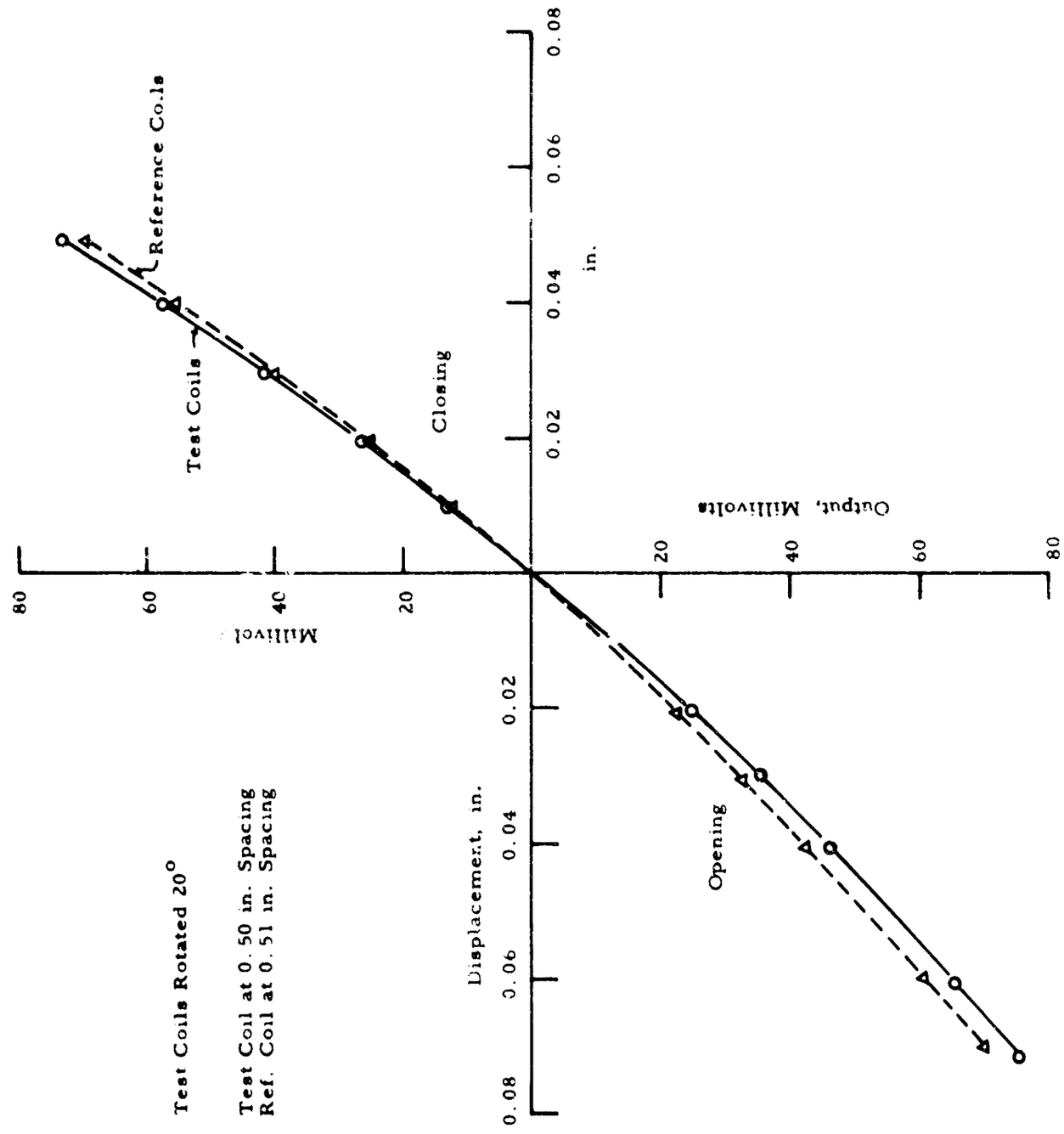


Fig. 7 Relative Output Displacement Vs. Output Signal

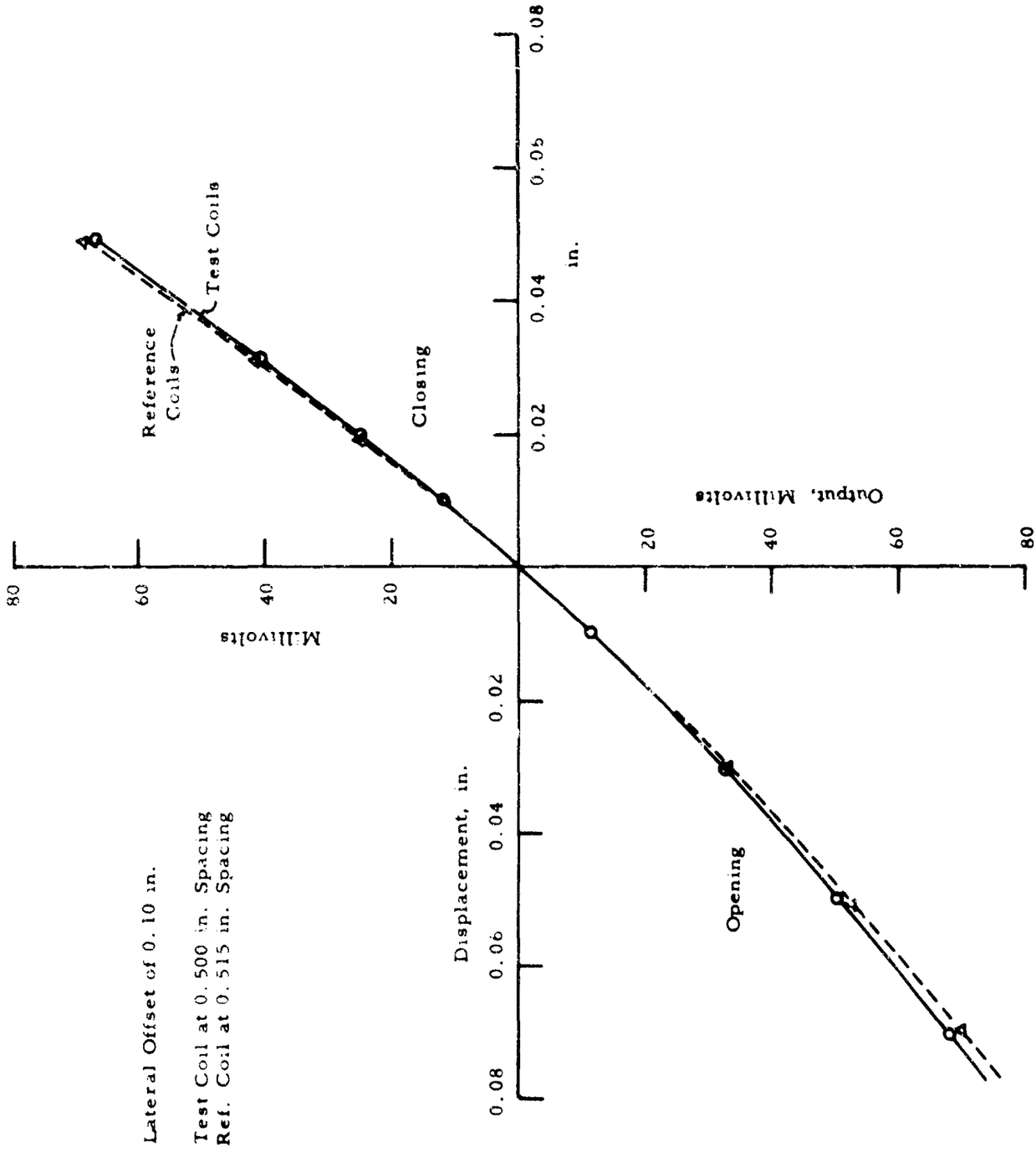


Fig. 8 Relative Coil Displacement Vs. Output Signal

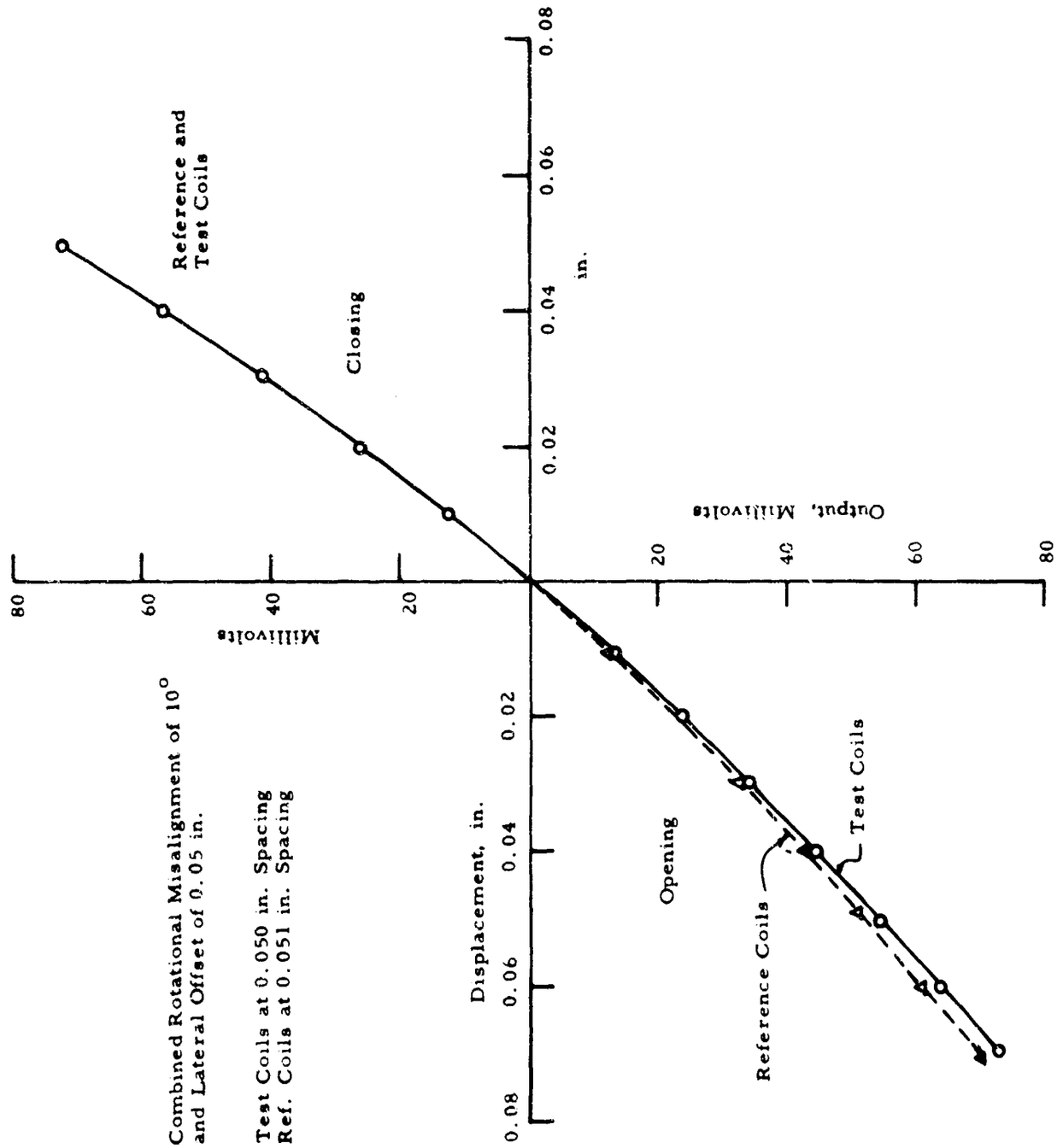


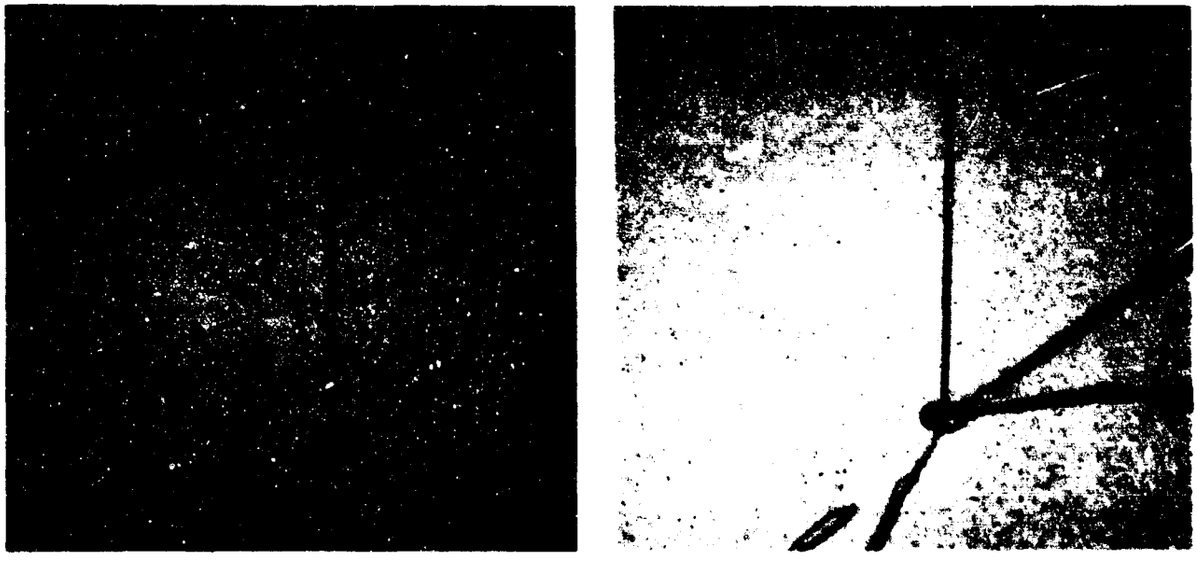
Fig. 9 Relative Coil Displacement Vs. Output Signal

gauge placement. Techniques would then be required to refill the excavation at the same density as the remainder of the test bed. It has been found to be quite difficult to maintain good alignment when applying significant compactive effort in the immediate vicinity of the gauge.

CONCLUSION

The soil strain gauge is adaptable to a wide variety of soil strain measurement applications and has many desirable features. These features include:

1. The gauge components are physically uncoupled to minimize placement problems and gauge influence on the surrounding soil.
2. Precise initial spacing of the two coils inserted in the soil is not required; this can be determined accurately after placement.
3. When the coils are placed within specified alignment tolerances, precise initial and differential measurements are obtained.
4. Wide frequency response accommodates measurement of transient strains with rise times in excess of 100 microseconds as well as strains occurring under static loadings.
5. Calibration for dynamic tests is quick and simple.
6. The coils are expendable because of their low cost.



(a) First Coil (b) Second Coil

Fig. 10 Coil placement techniques

ACKNOWLEDGEMENT

The strain gauge described in this paper was developed by the IIT Research Institute for the Air Force Weapons Laboratory under Contract No. AF29(601)-5343. Mr. F. Peterson monitored the research contract on behalf of the Air Force. Acknowledgement is hereby tended to the Research Directorate, Air Force Weapons Laboratory, who has supported the program and authorized the publication of its findings.

REFERENCES

1. Truesdale, W. B., "Development of a Small Soil Strain Gauge," IITRI for AFWL, TDR-63-3, March 1963.
2. Keller, R. W. and M. E. Anderson, "Development of a Soil Strain Gauge for Laboratory Dynamic Tests," IITRI for AFWL, TDR-64-7.

SHOCK-ISOLATING BACKPACKING MATERIALS, A REVIEW OF THE STATE OF THE ART

by
George C. Hoff*

SYNOPSIS

From a review of the types and effects of nuclear blast loading on buried structures, a basic design criteria for backpacking materials has been established and is reviewed along with the techniques used in determining the energy-absorbing characteristics of the backpacking materials. An example is developed to show how backpacking materials, when placed around buried structures, will absorb a portion of the applied shock energy thereby reducing the forces which reach the structure.

Various programs in the development of such materials as foamed plastics, honeycombs, insulating concretes, granular materials, and other similar materials which could be adequately used as backpacking are reviewed with limited data being presented.

INTRODUCTION

The field of structure-medium interaction has long commanded the attention of individuals concerned with the design and construction of buried structures. With advances in the use of thermonuclear weapons, the difficulty in understanding structure-medium interactions and therefore the designing of buried structures has become further complicated by the introduction of complex ground motions and very high applied loads. The design of buried structures to resist these effects usually results in design loads which are so high that overconservative design would be extremely costly. On the other hand, catastrophic failure of the structure due to under-design cannot be tolerated.

The applied forces for which a blast-resistant structure must be designed are transient in nature and their probability of occurrence is small. The magnitude of these forces depends on a number of factors over which a designer has no control. To eliminate some of the many unknowns imposed on the structural design of buried structure, the designer may employ various structural systems in selected environments which will increase the probability of survival of the structure and its contents. It is the purpose of this paper to review the state of the art of a technique that can be used for controlling the magnitude of the forces being applied to buried structures by blast loading, i.e., the use of backpacking materials for shock isolation of buried structures.

BACKGROUND

Approximately 50 percent of the fission energy of a low-altitude detonation (less than 100,000 feet) is utilized in the production of blast and shock (41). The effective energy of the burst will be dependent upon the actual height of the explosion, as well as upon its energy yield, but the general phenomena are similar in all cases. Nearly all the shock energy appears as air blast which indirectly transmits energy to the ground. Some energy is also transmitted directly into the ground. Regardless of the mode of transmission, tremendous amounts of energy are introduced into the earth, and, although some energy dissipation occurs through internal damping and the process of doing work on the media, considerable shock energy is still present at great distances from the explosion. The character and strength of the shock reaching a buried structure may be influenced by the stress-strain characteristics of the media the shock travels through (26). In order to prevent excessive amounts of this shock energy from reaching the structure, a suitable method for dissipating the energy must be developed. This paper deals with the concept of using backpacking materials and reviews the types of materials currently under investigation for this purpose.

Recent investigations

Interest in the use of backpacking for shock-isolation of entire buried structures has generated many ideas as to the feasibility and composition of various systems and materials that could be satisfactorily used as backpacking. As early as 1953, Engineering Research Associates, et al (9), in a report to the USA Corp of Engineers on Underground Explosion Test Programs suggested that: "The space between the lining and the tunnel surface should be filled with a material of low density that will absorb the energy of the flying rock, distribute the pressure from fallen rock, and provide a mismatch of acoustic impedance so that reflection will take place at the tunnel surface rather than at the surface of the lining."

*Project Engineer, Engineering Mechanics Section, Corp of Engineers, U.S. Army Engineer Waterways Experiment Station, Vicksburg, Mississippi.

In 1957, Vaile (42) reported on the beneficial use of a frangible backfill in isolating and protecting underground structures in operation PLUMBBOB from violent ground motions in their vicinity. During operation PLUMBBOB, vertical concrete pipes covered with concrete slabs were lined one layer thick on the sides and bottom with empty glass quart gin bottles. When compared to the control pipe for the experiment, which had soil backfilled directly against it, it was found that the peak accelerations produced by shear forces exerted on the sides of the isolated pipes were reduced to 26 percent of those experienced by the control pipe. This reduction was attributed in part to the collapse and crushing of the glass which dissipated a portion of the shock energy.

In two related studies performed by Sevin, et al (30,31), at the Armour Research Foundation (now the Illinois Institute of Technology Research Institute), various devices were employed on or about cylinders buried in silica sand in order to alleviate shock-induced motions of the cylinders. These devices consisted of 1) wrapping the cylinders in flexible and rigid polyurethane foams; 2) the use of air voids between the media and cylinder; 3) the use of pre-expanded polystyrene beads as a crushable backfill aggregate and, 4) the use of sand of varying densities as backfill aggregate separated from the overall bed by a stove pipe. The conclusions reached were that polyester urethane foams placed around a cylinder and other materials functioning as a loose backfill aggregate were effective in attenuating the response of the isolated structures.

Da Deppo and Werner (5), in a study on the influence of mechanical shielding on the response of buried cylinders, introduced a crushable layer directly over the buried cylinder. The use of this crushable material greatly reduced the magnitudes of the loads reaching the cylinder.

Fowles and Curran (10), in presenting theoretical descriptions of the propagation of a pressure pulse in a potential backpacking material, suggest that foamed or distended materials are effective in reducing the peak pressures delivered to a structure when an impulse is applied to the opposite surface of the foam.

In discussing the methods of mitigating the effects of shock for lined tunnels in rock, Newmark and Merritt (26) state that the current design concept for protective linings in competent rock includes the provision for a highly deformable material between the face of the rock and the lining. "It would appear that the magnitude of . . . forces (generated by small impacts) reaching the lining could be significantly reduced if a crushable material is introduced between the face of the rock and the lining (26)."

Smith and Thompson (36), suggest that the shock energy reaching a buried structure in rock can be partially dissipated by 1) a reflection of energy, and 2) by energy absorption. They suggest that these requirements be met by interposing a material between the structure and the confining medium that has a low shock impedance with respect to that of the confining medium. The impedance mismatch which occurs will cause some energy to be reflected. If the low-shock impedance material is also very deformable under applied loads, it will absorb the energy present in the form of ground motions, thereby meeting the two requirements.

Design Criteria

A review of the investigations cited above and other similar projects provides an insight as to what is necessary in designing a backpacking system for shock-isolation purposes. In general, a suitable backpacking should be a frangible or crushable material possessing a low breaking or crushing stress level and a high degree of compressibility. If possessing these characteristics, the material should dissipate a portion of the shock energy, thereby reducing the magnitudes of the forces reaching the structure and should accommodate the deformations of the cavity in which the structure has been placed. Due to the large relative costs of construction versus design overpressures (3) the scope of interest of this paper will be restricted to design overpressures less than 1000 psi; that is, the magnitude of stress transmitted to the structure through the backpacking material will be less than 1000 psi. Assuming single burst loading where closure of the cavity is imminent, deformations of the backfill to accommodate this closure should be approximately 30%. In other cases, it may be considerably less.

THEORY

Pressure-volume, Stress-strain Relationships

The majority of the materials investigated both in the past and at present generally fall into two distinct categories: 1) materials having no distinct yield point and some degree of compressibility, and 2) materials possessing a distinct yield point plus some degree of compressibility. Ideally these materials can be represented by pressure-volume curves for a single-rigid locking solid (Figure 1) and an elastic-rigid locking solid (Figure 2) respectively (10).

Consider first the case of a simple-rigid locking solid (Figure 1). The original volume is designated V_o. Under a very small applied pressure, the specific volume decreases to V_1 at no appreciable increase in the pressure. At V_1, the material locks with no further decrease in volume occurring with additional increases in the pressure.

In the case of the elastic-rigid locking solid (Figure 2), the pressure-volume curve is very similar to that of the simple-rigid locking curve but with the addition of an elastic region containing a definite yield point. As in the previous case, the initial specific volume is represented by V_o. Under the application of pressure the material behaves as an isotropic elastic solid until P_e, the elastic yield pressure is reached. Beyond that pressure, the material behaves like a simple-rigid locking solid.

Under blast loading conditions, the loaded area is normally so great that the portion of the medium under consideration and its inclusions can be assumed to be laterally confined with displacements occurring only in the direction of loading. By applying this assumption of lateral restraint to the ideal pressure-volume curves, they can readily be converted to stress-strain curves for simple-rigid and elastic-rigid locking solids subjected to one dimensional compression (Figure 3). To indicate more clearly the behavior of real materials, the locking portion of the curves has been shown as an inclined line representing the elastic behavior of the solids composing the materials under consideration. With the addition of this elastic portion, the simple-rigid and elastic-rigid locking solids will hereafter be referred to as plasto-elastic and elasto-plastic materials respectively. This conversion to a stress-strain relationship provides a convenient tool for evaluating the energy dissipating capability of the materials.

Energy Absorption

The energy absorbed by a material depends on two factors: 1) the deformation of the material, and 2) the forces in the material during the deformation (8). The product of the strain and the unit force results in the amount of energy absorbed by the material:

$$E_n = \bar{\sigma} \times \epsilon = \text{area under the stress-strain curve (Figure 4)} \quad (1)$$

E_n is expressed as the energy per unit volume of material and can be shown for all cases to be,

$$E_n = \int_0^{\epsilon} \sigma \cdot d\epsilon \quad (2)$$

Before proceeding, a distinction should be made between the terms, "energy absorbed" and "energy dissipated". Figure 5 represents a typical stress-strain curve for a material possessing elasto-plastic properties. The entire shaded area represents the energy absorbed per unit volume by the material to a given strain ϵ_2. When the applied forces are removed from the material, some strain ($\epsilon_2 - \epsilon_1$) may be recovered due to the elastic properties of the material. The energy regained during this recovery is known as rebound energy. The actual energy dissipated by the material then is equal to the absorbed energy minus the rebound energy (8), or,

$$\text{Absorbed Energy} = \text{Dissipated Energy} + \text{Rebound Energy} \quad (3)$$

Much work has been done in the past both by industry and government in the development of energy-dissipating theories and mechanisms. It is not my purpose here to make a thorough survey of all the literature on the absorption of energy but rather to discuss the use of backpacking materials for dissipating shock energy reaching buried structures. An annotated bibliography of literature pertaining to the absorption of impact energy has been prepared by Ali and Benson (2), which, although concerned with the problem of absorption of impact energy in the air drop of supplies and equipment, reviews the theory and design of energy-absorbing systems plus the energy-absorbing materials which may be available. This bibliography may be referred to for a more comprehensive review of the energy-absorption concept.

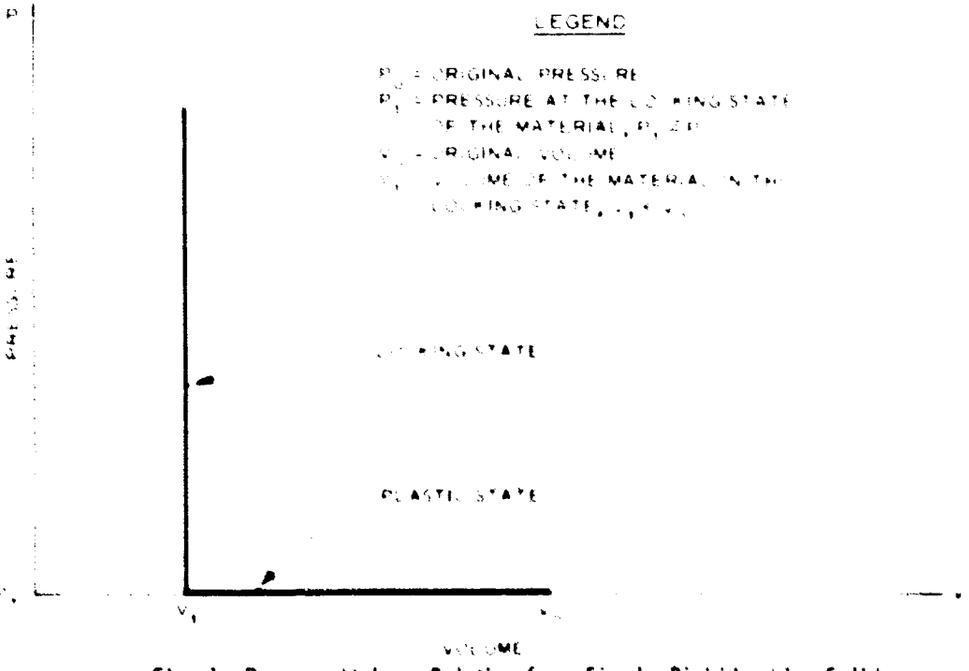


Fig. 1 Pressure-Volume Relation for a Simple-Rigid Locking Solid

From the energy relationships described previously, it becomes obvious from the shape of the stress-strain curve that elasto-plastic materials are more efficient energy absorbers than the plasto-elastic materials. Both materials are under consideration for use as backpacking, however, because the plasto-elastic materials may be more economical and thus more attractive when large volumes are necessary.

Stress Transfer

When the closure of a cavity containing a backpacked liner is uniform, the deformation of the backpacking will also be uniform, and hence, if the backpacking is homogeneous and isotropic, the circumferential stress transferred to the structure will also be uniform. The magnitude of the load reaching the structure will depend on the load-deformation characteristics of the backpacking plus the amount of deformation occurring. If, however, the deformation or stress in the backpacking is non-uniform, the liner will tend to deform into an oval or elliptical shape as shown in Figure 6.

Newmark (25), in discussing the factors to be considered in designing blast and ground shock-resistant structures, approached this problem by permitting the lining to deform by such an amount so as to develop in the backpacking appropriate resisting stresses against the deformation. The lining must, in this case, have requisite strength in compression and in buckling, and must be able to deform sufficiently, without failure or fracture, in order to develop the required resistance.

In developing the stress-transfer theory, Newmark (25) allowed a and b (Figure 6) to represent the displacement of the cavity walls. However, because of the deformations, y, of the liner itself, the net change in thickness of the backpacking at the sides is b - y and a + y. By assuming a general situation of load-deformation for an elasto-plastic material (Figure 7), it can be readily seen that the magnitude of the net differential pressure between points b and a, assuming the lining does not deform, is much greater than the net differential pressure between points b - y and a + y are expressed as $q + p_1$ and $q - p_1$, respectively, it can then be said that the average of these pressures is the uniform component of load, q, and that the difference from the average is p_1, the inward or outward component of load. It is this component of load, p_1, which tends to produce the elliptical or oval deformation of the lining. As can be seen from the ideal curve in Figure 7, the larger the net differential pressure is, the greater p_1 is. When p_1 is large, the deformations of the lining are large. When lining deformations are large, the backpacking is compressed more, thus causing the pressure differential to become smaller, which in turn reduces p_1 and thus the deformations of the lining and so on until an equilibrium is reached at a uniform pressure q. If the deformations of the cavity are such that point b lies on the yield plateau of the load-compression curve for the backpacking, the maximum stress transferred to the structure will be equal to or less than the yield strength of the backpacking.

This same approach to stress transfer can be implemented using a load-deformation relationship for plasto-elastic materials but with a little more difficulty as it is relatively impossible for a lining interacting with the progressively increasing stress-strain relationship of a plasto-elastic material to develop a resistance characterized by a nearly uniform compression on all sides.

Thickness Determinations

In general, the backpacking is most effective when designed to have an energy absorbing capacity equal to that of the core of material removed to form the cavity (25). For a plane wave of stress, assuming average deformations of the cavity, the total strain energy, both elastic and plastic, which would have existed in the core of material that was removed can be evaluated and equated to the relationship shown in Equation 2. By trial and error procedures σ, the average plastic stress in the backpacking and, ϵ, the plastic strain in the backing, can be evaluated (17). The total plastic strain plus volume

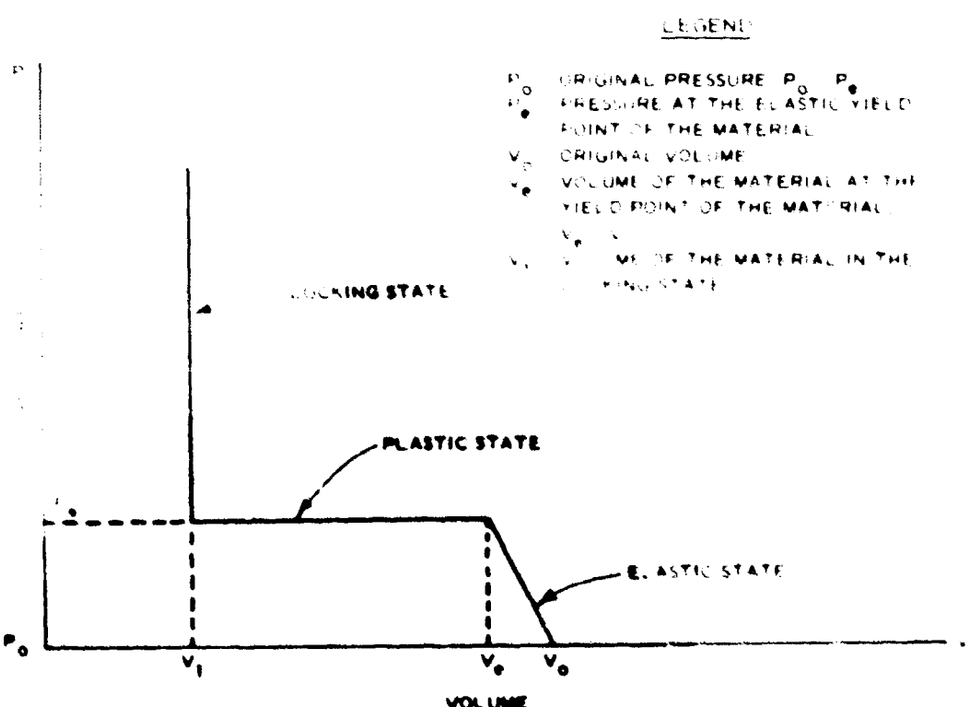
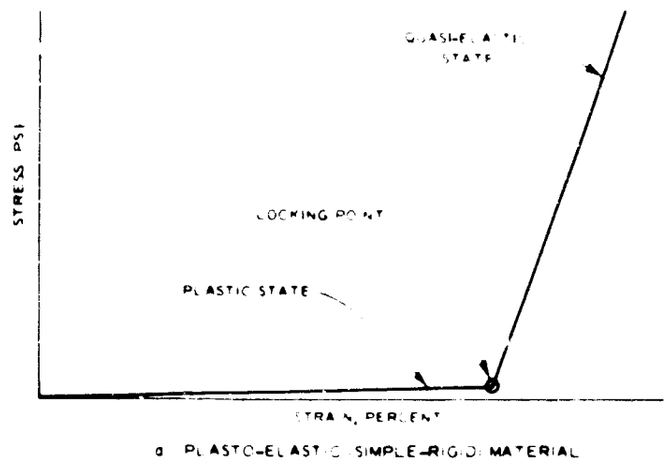
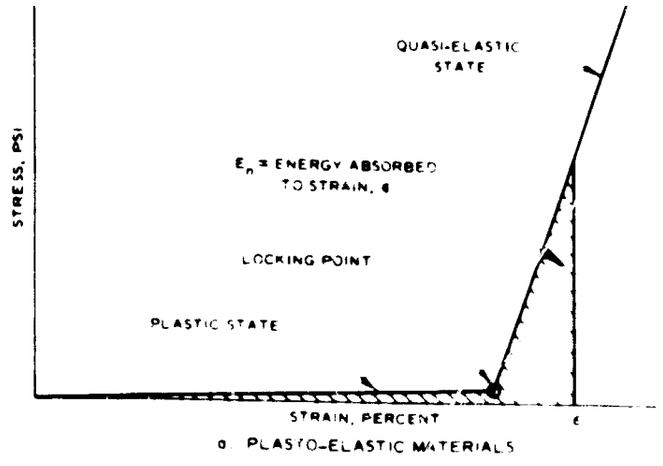


Fig. 2 Pressure-Volume Relation for an Elastic-Rigid Locking Solid

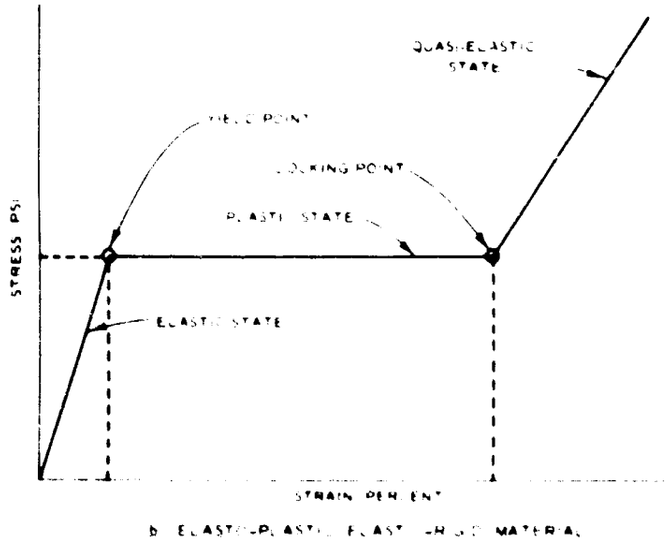


a PLASTO-ELASTIC SIMPLE-RIGID MATERIAL

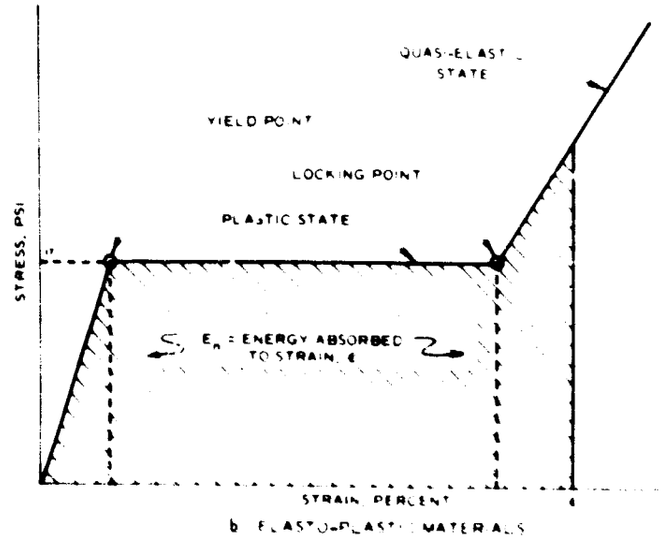


a PLASTO-ELASTIC MATERIALS

Fig. 3 Ideal Stress-Strain Relations



b ELASTO-PLASTIC ELASTIC-RIGID MATERIAL



b ELASTO-PLASTIC MATERIALS

Fig. 4 Ideal Stress-Strain Relations Showing Energy Absorbed to a Given Strain, ϵ

allowances for the solid elastic particles of the backpacking form the basis for determining the thickness, t_f, of the backpacking. When the cavity is in rock, the bulking phenomena* and the kinetic energy of spall projectiles must also be considered in the thickness determination (25).

MATERIALS

The two ideal stress-strain relationships shown in Figure 3 define the properties of a variety of materials. Figure 8 shows the relationship between the ideal and typical stress-strain curves for both types of materials.

The typical curve shown in Figure 8a represents the stress-strain relationship for materials that do not possess a definite yield point (plasto-elastic) but are still very compressible, either elastically or inelastically, or both. Granular materials are a representative material for this type of curve. Some plastics and rubbers also possess these characteristics. However, the plasto-elastic materials discussed in this paper will be primarily the granular materials.

Figure 8b represents the typical stress-strain curve for elasto-plastic materials compared to the ideal curve. Insulating concretes and plastic foams are good representatives of this class of materials, although some granular and other materials also exhibit this type of behavior.

*A reduction in diameter (of the cavity) occurs, arising from the fact that the rock is crushed and displaced around the outside of the cavity. In the process of doing so, it "bulks" and increases in volume thereby decreasing the volume of the cavity (25).

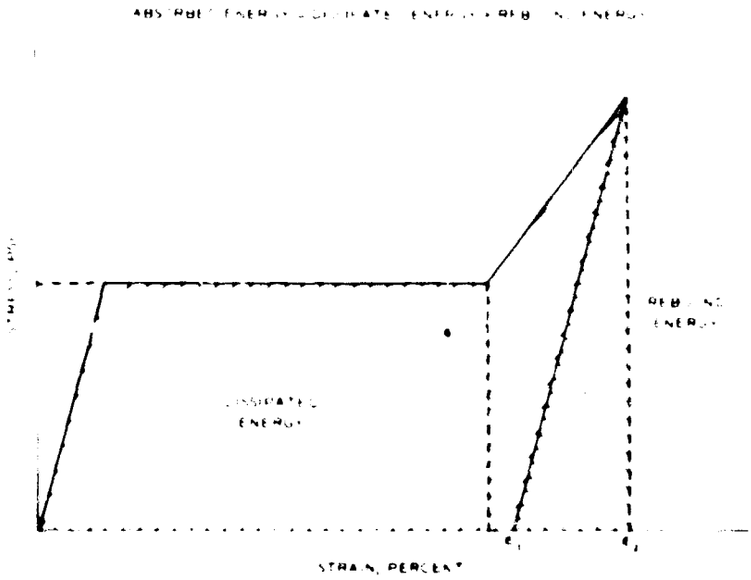


Fig. 5 Ideal Stress-Strain Relation Showing Absorbed Energy, Dissipated Energy, and Rebound Energy (Ellis, et al, 8)

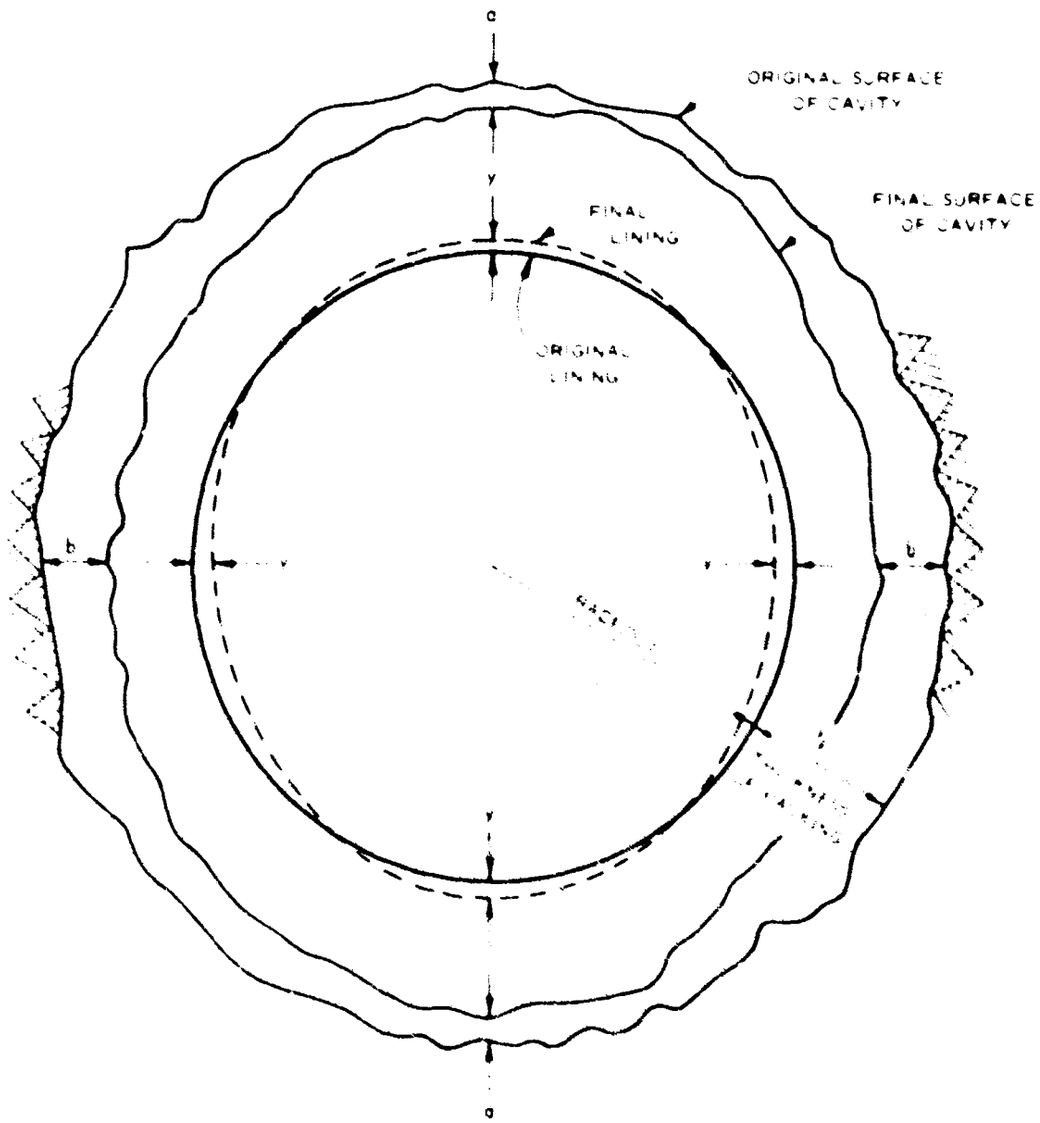


Fig. 6 Deformation of Lining and Packing (Newmark, 25)

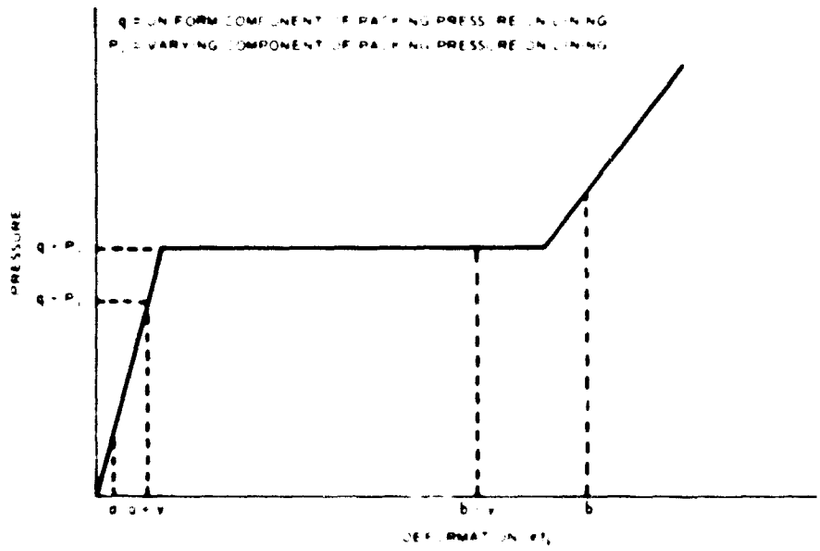


Fig. 7 Ideal Load–Compression Relation for Packing (Newmark, 25)

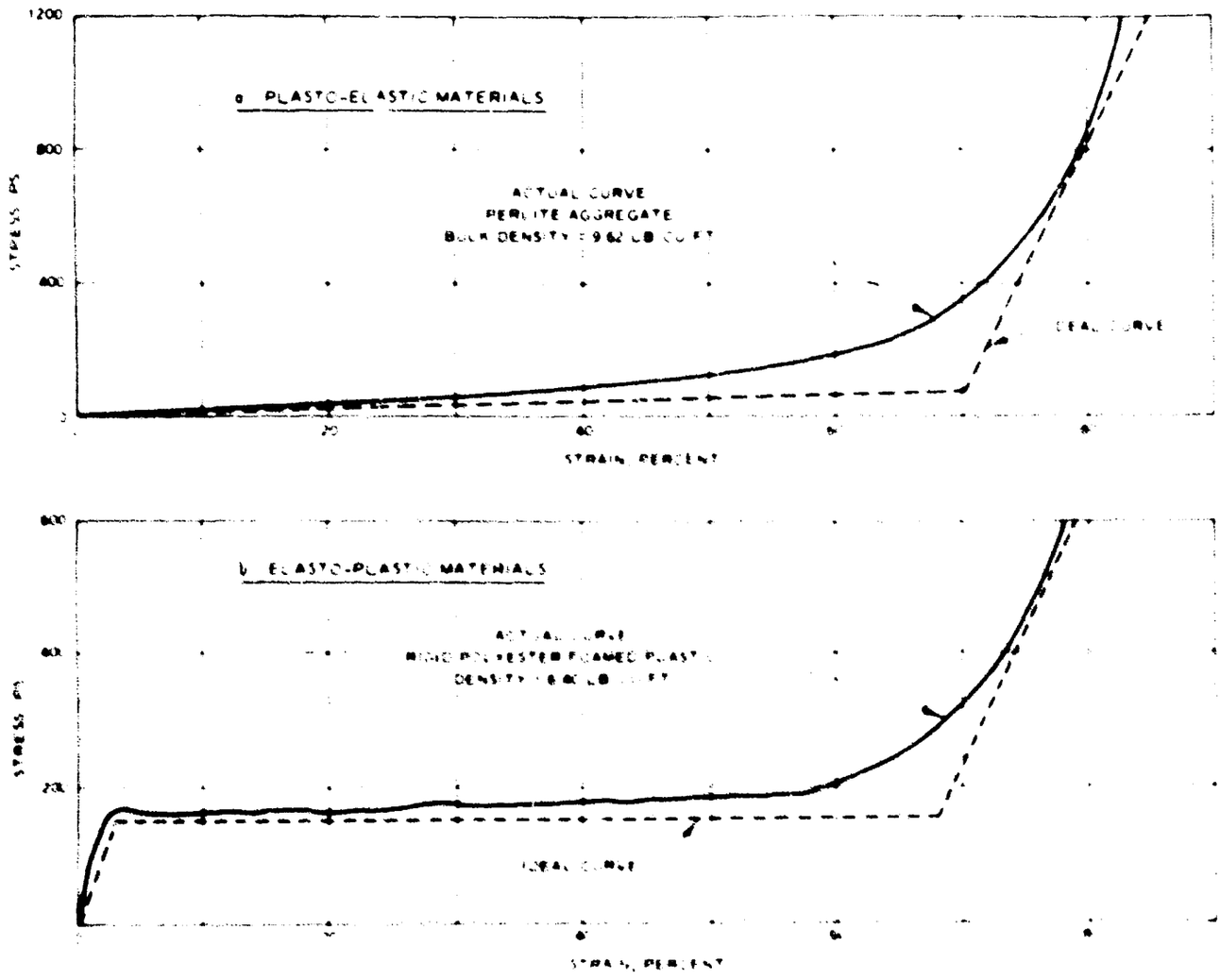


Fig. 8 Ideal and Typical Stress-Strain Relations (Klotz, 20)

Cost

In the following discussion, no attempt will be made to compare any of the materials on the basis of actual cost in place, but for general information purposes, it may be mentioned that granular materials are, with few exceptions, the least expensive materials. The insulating concretes, which cost more in place than the granular materials, are less expensive than the most economical foamed plastics and honeycombs in place by a factor of 10 or more.

Such factors as the actual material used, degree and amount of isolation required, the environment in which the structure is located, construction techniques, and other related factors, while all somewhat interdependent, contribute in varying degrees to the total in-place-cost of the material, thus making any cost comparison except a general one almost impossible. The cost of the backpacking system and, hence, its feasibility, should be evaluated for each proposed structure considering the known environment, assumed loading, and desired response that will be unique to that structure.

Plasto-Elastic Materials

Granular Materials. Numerous studies have been made to define the energy-absorbing mechanisms of granular materials subjected to applied states of stress. The bulk of these studies, however, have been concerned with granular materials of considerable strength that were subjected to stresses well in excess of our present level of interest. Excellent summaries of the state of the art pertaining to the mechanisms and behavior of these granular materials have been compiled by Deresiewicz (7) and Whitman (43).

The general stress-strain relationship in granular materials is very complicated and is to a large extent dependent on the magnitude of the applied pressure. Hendron, et al (12), in reporting on the energy-absorption capacity of granular cohesionless materials on one-dimensional compression provides a description of a typical stress-strain curve and consequently the energy-absorbing mechanisms for granular materials which, although concerned with materials subjected to much higher stress levels, adequately illustrates (Figure 9) the phenomena necessary for backpacking using granular materials.

The behavior in Region 1, the very low stress-range, reflects rearrangement of the particles. When vesiculated granular particles are subjected to the same low stresses, fragmentation by shearing and crushing also occur during the particle rearrangement, thus resulting in a concave upward curve for the same region (20). The absorbed energy in both cases is nonrecoverable.

As the stress increases (Region 2), the particles begin to lock together in a stable matrix of elastic particles. Some rearrangement is still taking place, but the overall behavior is essentially nonlinear elastic in nature, therefore, allowing most of the energy absorbed to be recoverable.

In Region 3, the stress magnitude is such that the particles begin to crush and further rearrange themselves. Most of the energy dissipated here in forming new surface and consolidating the particle is nonrecoverable.

Region 4 behavior is similar to that of Region 2 with some additional crushing taking place.

As can be seen from the upper curve in Figure 9, the average stress required for compaction depends on many things including the initial void ratio of the granular mass, the angularity of the particles, the duration and magnitude of the loading, and the inherent strength of the mineral which composes the grain. Because our interest is in materials whose stress level at approximately 50% strain is less than 1000 psi, we will be concerned mainly with Region 1 and perhaps the lower portions of Region 2.

Normally the strength of the grains of competent naturally occurring material are too great to provide the large deformations required before 1000 psi applied pressure is reached. Some naturally occurring grains, however, do possess this deformation capability, because of the very friable, vesicular nature of this grain. Klotz (20) reported on one such material, volcanic cinders, in an investigation of various materials for use as backpacking for operation NOUGAT, Shot HARDHAT. Other naturally occurring



Fig. 9 Qualitative One-Dimensional Stress-Strain Curve for Granular Material (Hendron, et al, 12)

materials can be altered by various mechanical and thermal methods to produce grains of a composition suitable for shock isolation purposes. Such materials as expanded clay (15), expanded shale, expanded slag, coke, coal cinders (20), vermiculite (15,27,36), and perlite (15,27), have been investigated for their shock-dissipating characteristics by numerous investigators with some of the results of their static tests being shown in Figure 10a.

Artificial grains can also be used for shock-isolation purposes. The waste products of various plastic-foam manufacturing processes often can be adapted for use as granular material. The industrial waste as well as artificial grains manufactured in the form of chips or aggregate, often provides adequate shock-dissipating characteristics. Such artificial materials (Figure 10b) as phenolic micro-balloons (10,15), expanded polystyrene beads (15,30), plastic foam chips (15,20), foamed metallic waste, and foamed rubber waste (15) have been evaluated and found adequate. There are many waste materials which could prove adequate, but because waste is not deliberately manufactured, availability and perhaps cost would probably be limiting features.

Foamed Materials. Many foamed materials do not possess a definite yield point but begin to deform with the application of very small pressures. The resulting stress-strain curve is progressively locking and can be assumed to represent a plasto-elastic material. Examples of this type of foamed material are shown in Figure 11 (1).

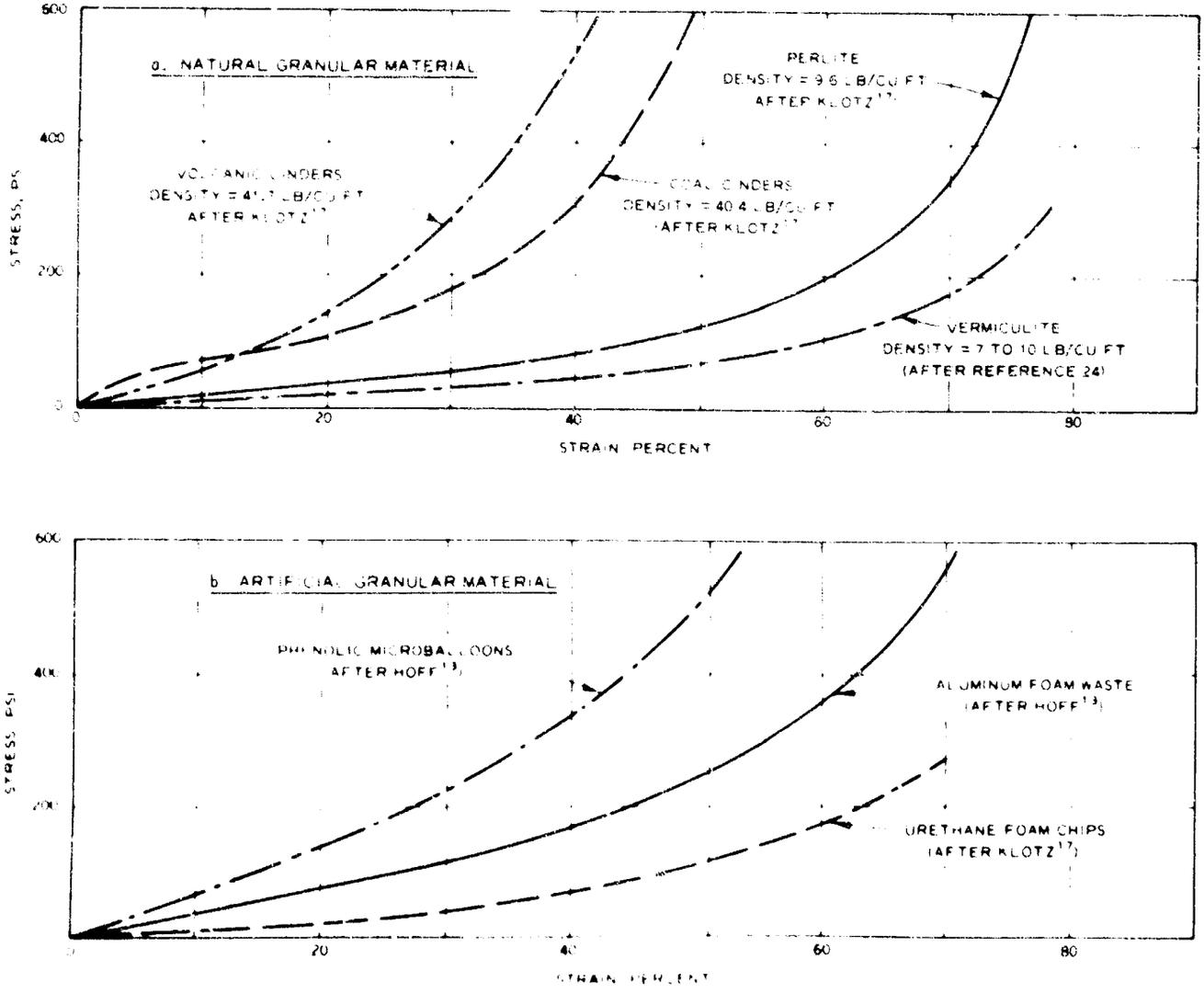


Fig. 10 Typical Stress-Strain Curves for Granular Plasto-Elastic Materials

Elasto-Plastic Materials

Many investigations into the energy dissipating characteristics of various elasto-plastic materials have been conducted over the years in connection with the packaging industry and the Quartermaster Corps' requirements for air-drop cushioning (1,2,28,38). From these investigations emerged a family of foamed plastics and honeycombs whose stress-strain relationship approximate that of the ideal elastic-rigid locking solid. These materials can be fabricated so that the binder will furnish the crushing stress level desired with the fractional volume of voids or pores in the material being controlled so as to obtain the necessary deformations. This is not the final answer, however. A good many of the foamed plastics and honeycombs are very expensive and are relatively difficult to handle and place in sufficient quantities and in adverse environments which may be dictated by the design and location of a buried structure. These problems, in general, fostered the need for a relatively inexpensive construction material which would serve the same purpose. Research at the University of Illinois (20), University of Texas (33,35,36), and the Waterways Experiment Station (15), has shown that insulating concretes, i.e., concretes having oven-dry density of less than 50 pfc, while not as efficient as foamed plastics and honeycombs in some respects, will provide the desired shock-isolation characteristics. The disucssion in the next few paragraphs will be restricted to these three types of materials, i.e., foamed plastics, honeycombs, and insulating concretes, as it is the author's belief that they are most representative of what can at the present time be used most effectively as an elasto-plastic material for shock-isolation.

Plastic Foams. Not all plastic foams possess an elasto-plastic stress-strain relationship. As shown previously, the "flexible" plastic foams often produce a plasto-elastic stress-strain relationship as shown in Figure 11. "Rigid" plastic foams generally produce the elasto-plastic relationship. Both types transfer stress and dissipate energy, but, as shown before, the elasto-plastic material is more efficient in both respects.

A variety of rigid foamed plastics are available and suitable for shock-isolation purposes, but, more often than not, they are extremely expensive. The rigid polyurethane foam is perhaps the most widely investigated (15,20,32,35,40), and used (10,23,30), for this purpose. Figure 12 shows a number of stress-strain curves for a rigid polyurethane foam. Despite its high cost, rigid polyurethane is still attractive as it is available in most areas, is fairly homogeneous and

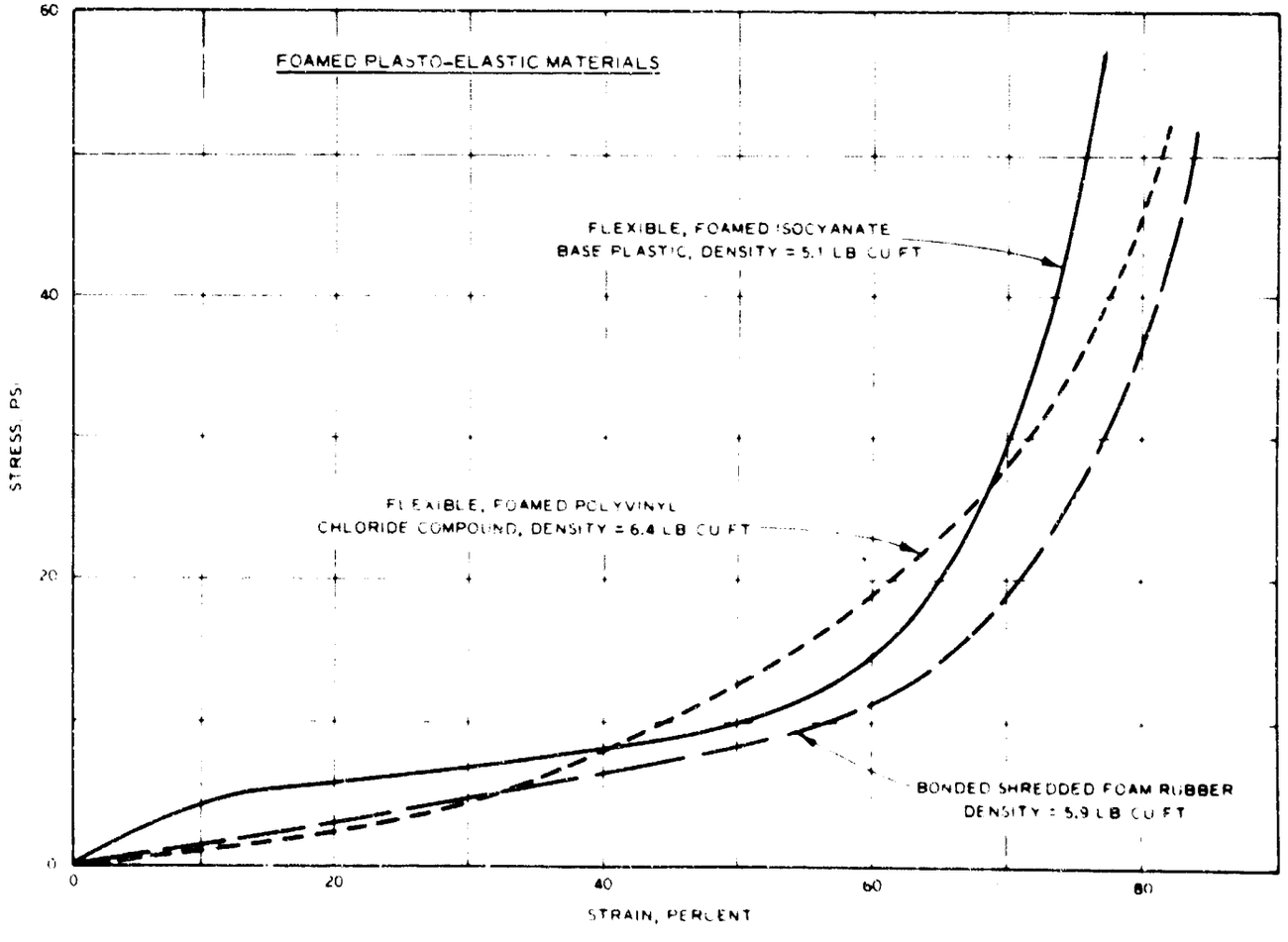


Fig. 11 Typical Stress-Strain Curves for Foamed Plasto-Elastic Materials (Ali, 1)

isotropic when formulated properly; it possesses the desired stress-strain relationship (Figure 12); it possesses the capability of being fabricated in the field and, if closed cell, is somewhat nonsusceptible to ground-water infiltration which would reduce its energy-dissipating potential.

Other types of foam which have been reported as suitable energy dissipators are polystyrene (15,22), and polyvinyl chloride (10,15). These two materials are also very expensive and are normally available only in relatively small pieces as compared to the needs of isolating a structure. The cost of assembling and fitting the small pieces around a structure would be very great.

Research into and development of the capability of casting large volumes of foamed plastics around tunnel liners is currently being undertaken and, if successful, will undoubtedly influence their in-place-cost so as to make them more attractive for shock isolation purposes.

Honeycombs. The use of prefabricated honeycombs has proved an effective means of energy dissipation and stress transfer. Honeycombs have the advantage of being very isotropic if designed properly so that the maximum stress in the packing can always be limited. They can also be largely impervious to ground-water infiltration. The main disadvantage honeycombs have is the large costs that will be incurred in the placing of the material around the structure.

There are two basic types of honeycombs: paper and metallic honeycombs. Paper honeycombs are used primarily at stress levels less than 100 psi (1,8,16,19,39) (Figure 13), while the metallic honeycombs are more effective at stresses in excess of 100 psi (1, 11, 13, 21, 29, 38) (Figure 14). Because of the nature of the composition of the honeycombs, it is doubtful if a good bond between the honeycomb and the structure will be obtained. Manufacturers (11), however, claim that an excellent forming and bond can be obtained with metallic honeycombs.

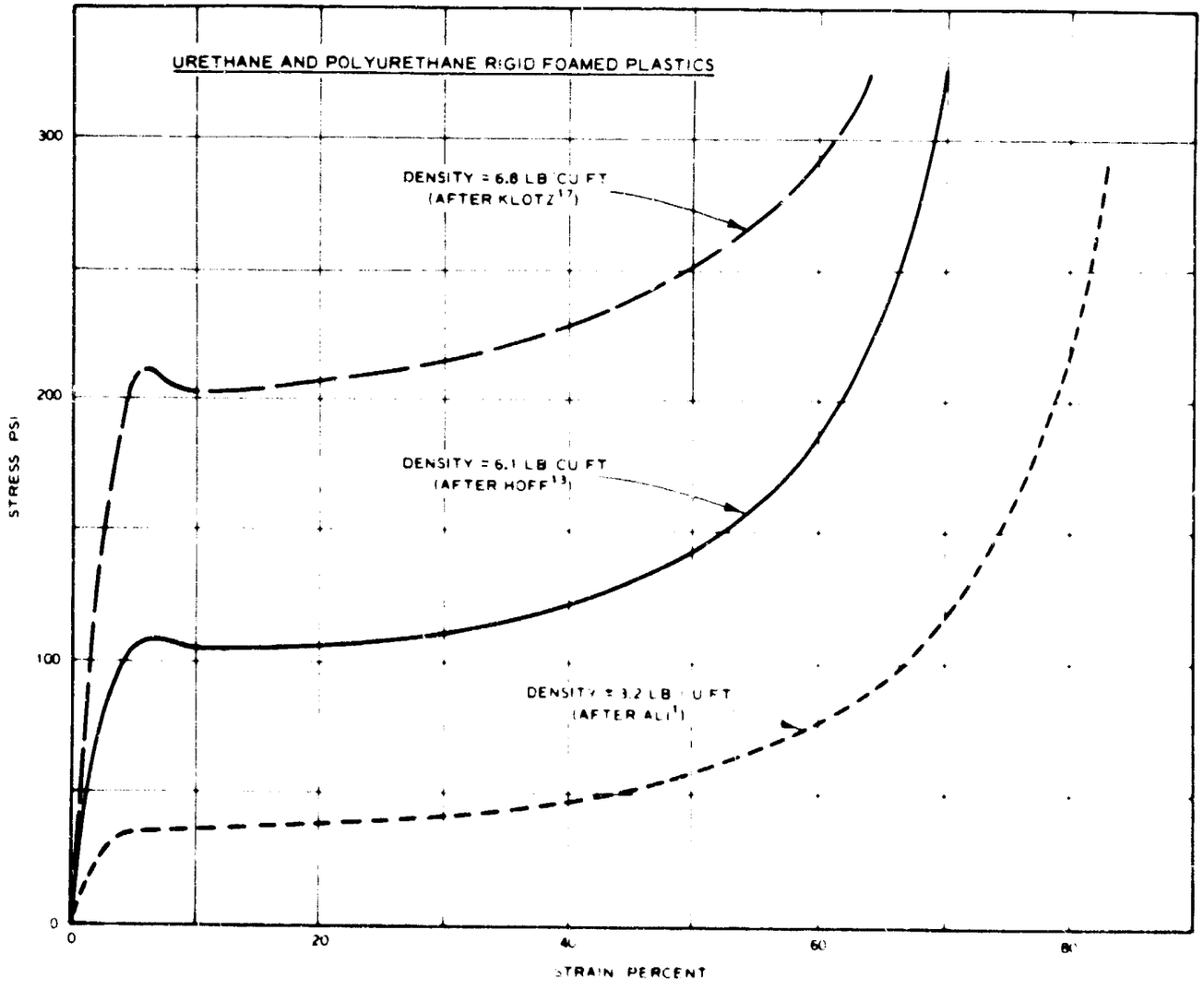


Fig. 12 Typical Stress-Strain Curves for Urethane and Polyurethane Rigid Foamed Plastics

Insulating Concretes. Insulating concretes are best defined as concretes made with portland cement, water, air, and possible aggregate additions to form a hardened material which will have an oven-dry density of 50 pcf or less.

As in the case of the foamed plastics, the hardened matrix provides the crushing stress level while the voids necessary for deformation are provided by the air and in part by the aggregate. The strength of the hardened portland-cement paste can be readily controlled but the deformations present some problems. If an aggregate is used, it must be very weak and friable. Regardless of its strength, however, it still contributes somewhat to the overall strength of the hardened mass. Experience has shown that the addition of too much aggregate in order to obtain more deformation, adversely affects the workability of the concrete, thus making it very difficult to handle and place. The solution is that most insulating concretes, such as vermiculite (4,15,33,35,36), and perlite (20,27) concrete, require as much as 20 to 30 percent entrained air in order to become suitable shock dissipators. Cellular concrete (14,15,20), which may or may not contain a fine sand or filler, can often be found with air contents as high as 75% of the total concrete volume.

These air voids, while desirable from the point of view of deformation, tend to absorb moisture when it is available from the surroundings. The voids, upon becoming filled with fluid, lose their effectiveness for shock dissipation as they then transmit shock loads through the fluid. Tests (15,36), have shown that very large water pressures are necessary to saturate these concretes over a short period of time but the long-time saturation effect of a considerably smaller pressure is not known. It is the author's opinion that this absorption problem is not insurmountable and could be remedied, at least in part, by the use of such methods as chemical "waterproofers," sandwich construction, grout curtains, and well-point systems.

Typical stress-strain curves for three of the most popular insulating concretes are shown in Figure 15, along with a curve for concrete made with a plastic aggregate (expanded polystyrene beads) (15). All of these concretes are relatively inexpensive when compared to the cost of the foamed plastics and honeycombs and can be fabricated and placed in most environments using conventional construction equipment.

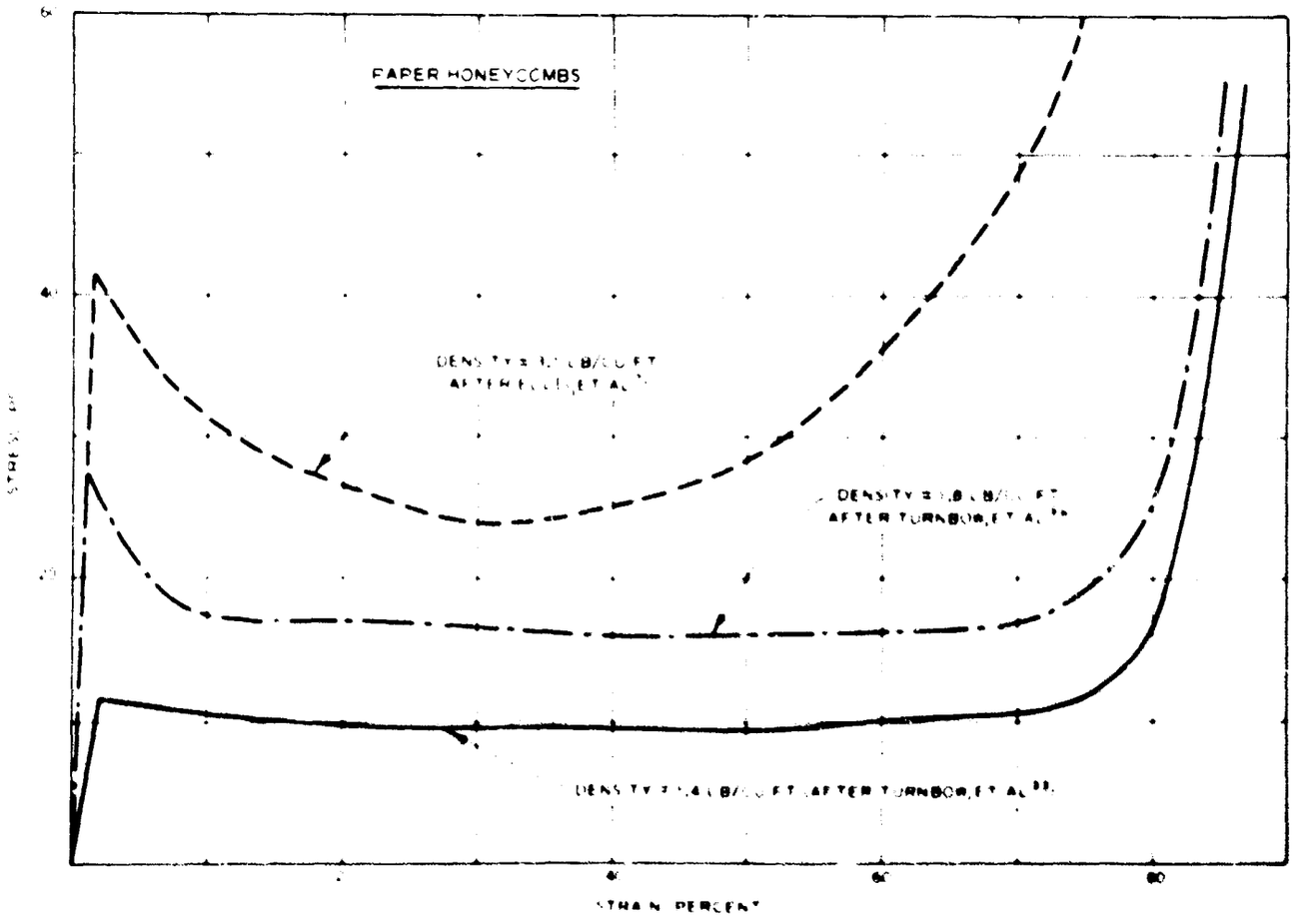


Fig. 13 Typical Stress-Strain Curves for Paper Honeycombs

Other Materials

As evidenced by the introduction of a plastic aggregate into a portland-cement matrix shown in Figure 16, it becomes obvious that many different types of materials systems possessing an elasto-plastic stress-strain relationship can be developed simply by the inclusion of air or a collapsible aggregate into a suitable binder. Various types of ultra-lightweight concretes, plastics with aggregate inclusions, and such foamed binders as epoxy (15), asphalt, gypsum, sulphur (6,21,37), and various chemical compounds all possess possibilities as shock dissipators.

SUMMARY

The behavior of a buried structure subjected to blast loading must be evaluated on the basis of the loads reaching the structure. Research has shown that the use of a properly designed backpacking material placed around the structure dissipates a portion of the shock energy present in the free field, thereby reducing the magnitude of the forces reaching the structure. The response of the backpacking then and that of the structure are completely interdependent and the design of one cannot be considered without the design of the other.

Unfortunately, sufficient data have not been accumulated to date to evaluate quantitatively the combined response. Both laboratory and field programs have been initiated to remedy this deficiency. Analytical models are being developed at the Illinois Institute of Technology in an attempt to describe the response of backfilled structures in soil. Other work is also being conducted to measure the response of backpacked models subjected to blast loading.

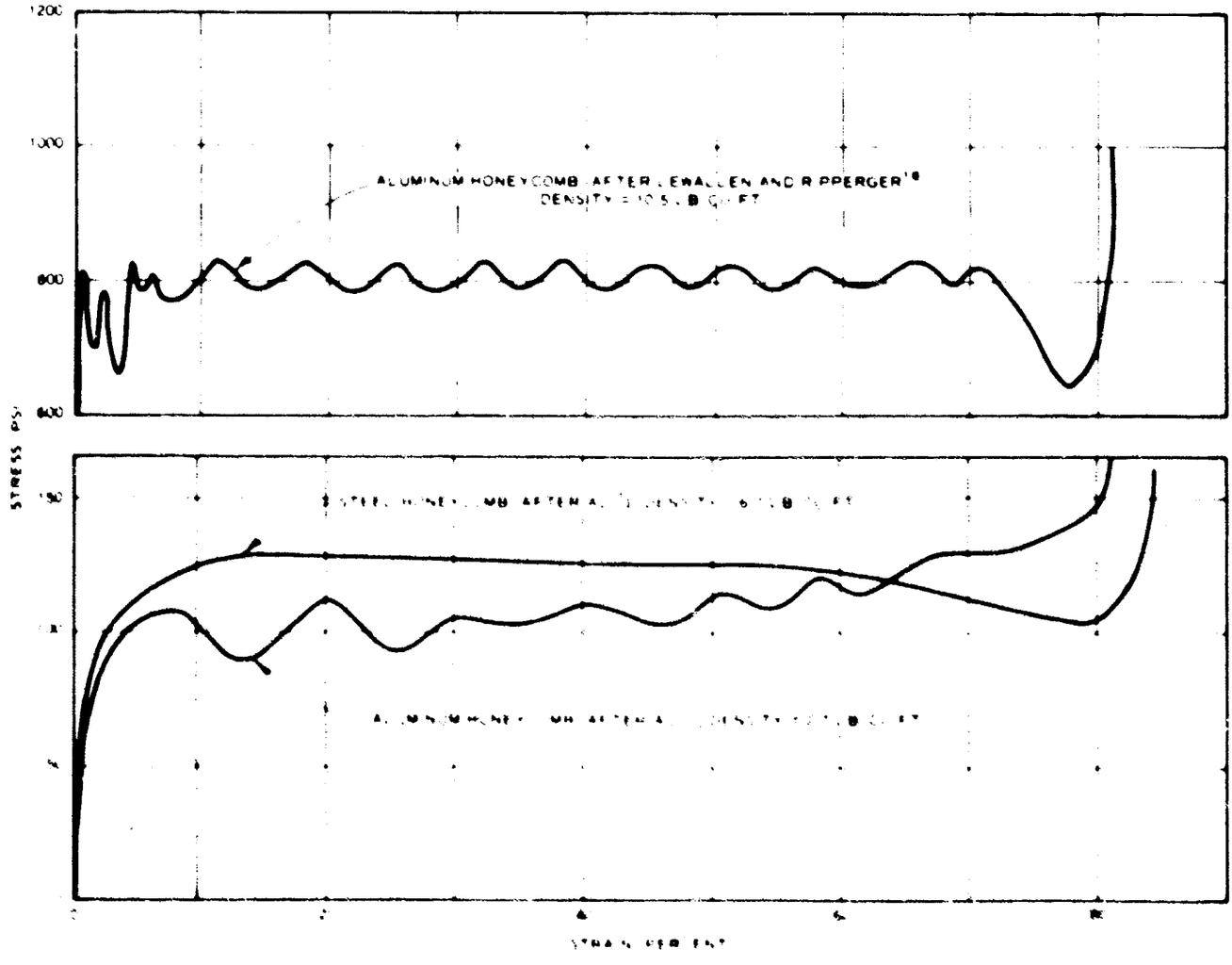


Fig. 14 Typical Stress-Strain Curves for Metallic Honeycombs

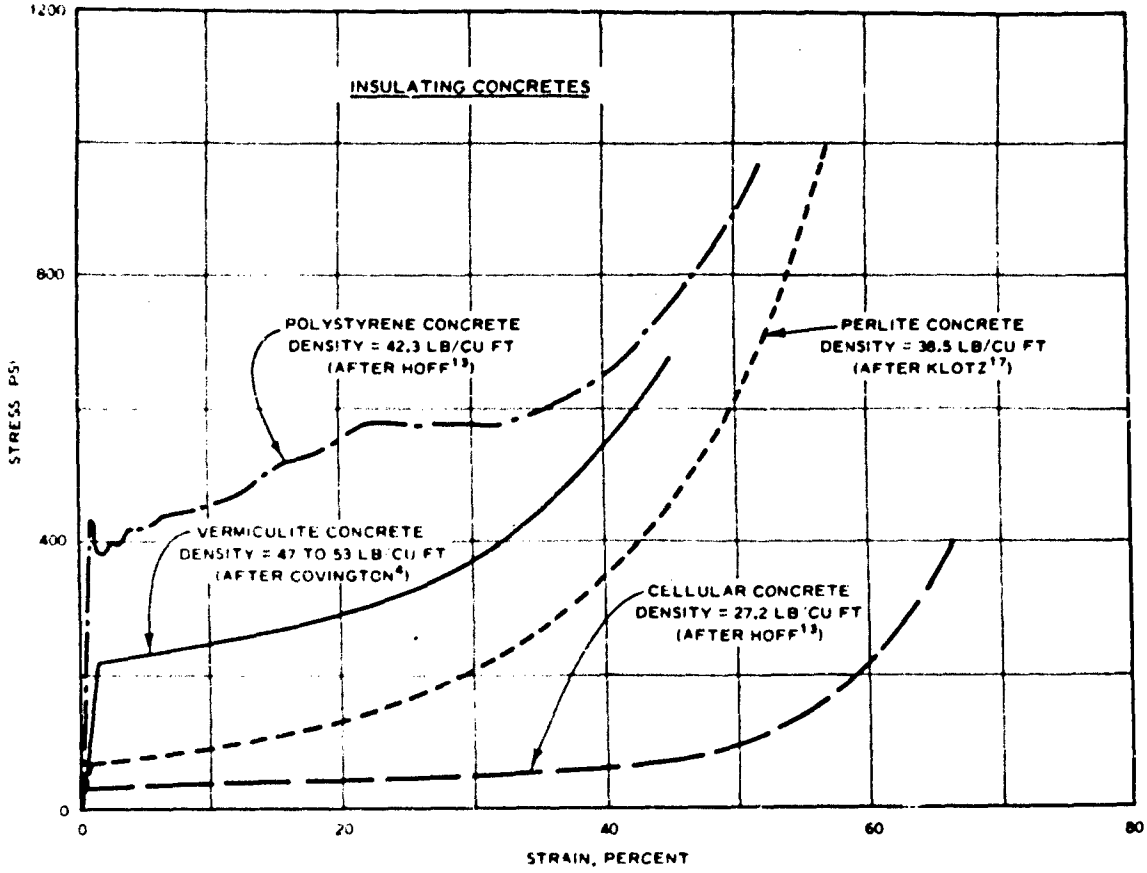


Fig. 15 Typical Stress-Strain Curves for Insulating Concretes

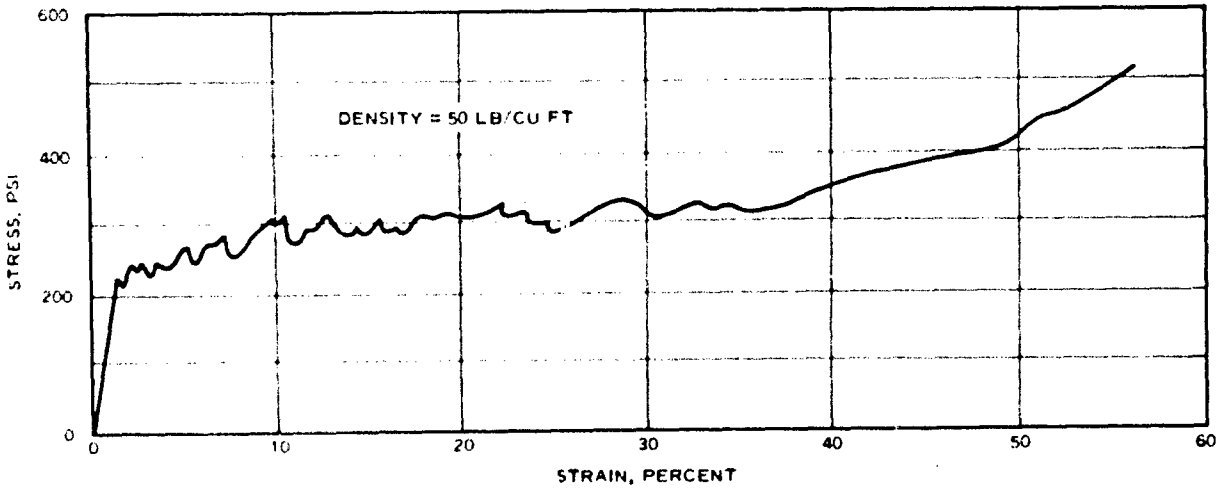


Fig. 16 Typical Stress-Strain Curve for Foamed Sulfur (Nevill, 24)

SOIL-STRUCTURE INTERACTION

Each of the types and systems of materials reviewed undoubtedly has many unique problems associated with its use as backpacking. However, the implementing of adequate research and development of the materials in question would probably solve the majority of these problems. An excellent example of this is the study currently being conducted at the Southwest Research Institute (c,24,37) on the feasibility of foaming bulk sulphur for use as a shock-isolation material around buried structures. A relatively low-cost foamed sulphur possessing an elasto-plastic stress-strain curve, (Figure 16), plus some other desirable features, has been developed and the feasibility of its large scale application is being studied.

This type of laboratory research coordinated with such field programs as operation NOUGAT, Shot HARDHAT (23), operation HARDTACK (34), and other related programs will, together with the development of suitable shock-isolation backpacking materials, probably result in less vulnerable buried structures at reduced costs.

ACKNOWLEDGMENTS

This paper is based on a research project entitled "Shock Absorbing Concrete" (15), currently being conducted at the U. S. Army Engineer Waterways Experiment Station under the sponsorship of the Defense Atomic Support Agency, Washington, D. C. Appreciation is expressed to all personnel of the U. S. Army Engineer Waterways Experiment Station who assisted in preparing this paper. Colonel Alex G. Sutton, Jr., Corp of Engineers, was Director and Mr. J. B. Tiffany the Technical Director of the Waterways Experiment Station during the preparation of this paper.

REFERENCES

1. Ali, Ahmin, "Cushioning for Air Drop, Part 8, Dynamic Stress-Strain Characteristics of Various Materials," Structural Mechanics Research Laboratory, University of Texas, Austin, Texas, June 1957.
2. Ali, A., and L.R. Benson, "Cushioning for Air Drop, Part 9, Bibliography of Literature Pertaining to the Absorption of Impact Energy," Structural Mechanics Research Laboratory, University of Texas, Austin, Texas, June 1957.
3. Christensen, W.J., "Vulnerability of Underground Protective Construction," Navy Civil Engineer, Vol. 1, No. 2, March 1960.
4. Covington, Clarke, "Dynamic Energy Absorbing Characteristics of Lightweight Vermiculite Concrete," Structural Mechanics Research Laboratory, University of Texas, Austin, Texas, June 1961.
5. Da Deppo, D.A., and J.F. Werner, "The Influence of Mechanical Shielding on the Response of a Buried Cylinder," Engineering Research Laboratory, University of Arizona, Tucson, Arizona, February 1962.
6. Dale, J.M., A.C. Ludwig, and G.E. Nevill, Jr., "Feasibility of Foamed Sulphur as a Material for Shock Isolating Large Underground Structures," Southwest Research Institute. Final Report for the Air Force Weapons Laboratory under the USAE Waterways Experiment Station Contract No. DA 22-079-ENG 374, San Antonio, Texas, May 1964.
7. Deresiewicz, H., "Mechanics of Granular Matter," Advances in Applied Mechanics, Vol. 5, Academic Press, Inc., New York, New York, 1958.
8. Ellis, B.C., E.A. Ripperger, and J.N. Thompson, "Design of Cushioning Systems for Air Delivery of Equipment, Structural Mechanics Research Laboratory, University of Texas, Austin, Texas, August 1961.
9. Engineering Research Associates, Bureau of Mines, and the Armour Research Foundation, "Underground Explosion Test Program," Volume II, Rock, Contract No. DA-04-167-ENG-298, for USA Corp. of Engineers, Sacramento District, April, 1953.
10. Fowles, G.R., and D.R. Curran, "Experimental Testing of Shock Attenuating Materials - Final Report," AFSWC-TDR-62-22, Poulter Laboratories, Stanford Research Institute, Menlo Park, California, March 1962.
11. General Grid Corporation, "Energy Absorbing Characteristics of Trussgrid and Spiralgrid," Edgewood Arsenal, Maryland, June 1963.
12. Hendron, A.J., Jr., R.E. Fulton, and B. Mohraz, "The Energy Absorption Capacity of Granular Materials in One-Dimensional Compression," University of Illinois, Final Report, Contract No. AF-29(601)-4302 for Air Force Special Weapons Center, Kirtland Air Force, New Mexico, January 1963.
13. Hind, D., and M.D. Chamberlain, "The Use of Aluminum Honeycomb as a Decelerating Medium," Technical Note No. 670, Sperry Gyroscope Company, Limited, November 1962.
14. Hoff, George C., "Energy Dissipating Characteristics of Lightweight Cellular Concrete," Journal of the Mississippi Academy of Sciences, Abstract, Volume 9, Mississippi State University, State College, Mississippi, 1963.
15. Hoff, G.C., "Shock Absorbing Concrete," Prepared for the Defense Atomic Support Agency, Washington, D.C. by the USAE Waterways Experiment Station, Vicksburg, Mississippi.
16. Hopf, J.P., "Equilibrium Moisture Content of Paper Honeycomb and Its Effect on Energy Absorption," Project No. 7-87-03-0048, Report No. 1, Forest Products Laboratory, Madison, Wisconsin, December 1955.
17. Jones, R.E., and D.L. Hunzicker, "Calculating Cushion Thickness by Analysis of Stress-Strain Curves," Forest Products Laboratory, U.S. Department of Agriculture, Contract No. AF 33(616)-51-4065 for Wright Air Development Center, Wright-Patterson Air Force Base, Ohio, January 1954.

18. Karnes, C.H., J.W. Tumbow, E.A. Ripperger, and J.N. Thompson, "High Velocity Impact Cushioning, Part 4, The Effect of Moisture Content and Impact Velocity on the Energy Absorption Characteristics of Paper Honeycomb," Structural Mechanics Research Laboratory, University of Texas, Austin, Texas, Mc 1959.
19. Karnes, C.H., J.W. Tumbow, E.A. Ripperger, and J.N. Thompson, "High Velocity Impact Cushioning, Part 5, Energy-Absorption Characteristics of Paper Honeycomb," Structural Mechanics Research Laboratory, University of Texas, Austin, Texas, May 1959.
20. Klotz, L.H., "Evaluation of Tunnel Liners in Granite, Shot HARDHAT, Operation NOUGAT, Static Stress-Strain Curves for Various Materials Investigated for Use as Packing," University of Illinois, Final Report, Contract No. AF-29(601)-4993 for Air Force Weapons Laboratory, Kirtland Air Force Base, New Mexico, February 1964.
21. Lewallen, J.M., and E.A. Ripperger, "Energy-Dissipating Characteristics of Trussgrid Aluminum Honeycomb," Research Memorandum No. 5, Structural Mechanics Research Laboratory, University of Texas, Austin, Texas, March 1962.
22. Matlock, H., E.A. Ripperger, J.W. Tumbow, and J.N. Thompson, "High Velocity Impact Cushioning, Part 2, Energy Absorbing Materials and Systems," Structural Mechanics Research Laboratory, University of Texas, Austin, Texas, August 1957.
23. Merritt, J.L., and N.M. Newmark, "Evaluation of Tunnel Liners in Granite, Shot HARDHAT, Operation NOUGAT, Proposed Tests of Lined Tunnels in Granite," University of Illinois, Final Report, Contract No. AF-29(601)-4993 for Air Force Weapons Laboratory, Kirtland Air Force Base, New Mexico, February 1964.
24. Nevill, G.E., Jr., Private Communication, Southwest Research Institute, San Antonio, Texas, March 2, 1964.
25. Newmark, N.M., "Design of Structures for Dynamic Loads Including the Effects of Vibration and Ground Shock," Department of Civil Engineering, University of Illinois, Urbana, Illinois, July 1963.
26. Newmark, N.M., and J.L. Merritt, "Nuclear Geoplosics, Part 5, Effects on Underground Structures and Equipment," University of Illinois, 3203 (V) Draft Prepared for the Defense Atomic Support Agency, Washington, D.C., under Contract Nos. DA-49-146-XZ-027 and DA-49-146-XZ-030, July 1962.
27. Quarterly Report No. 3, Contract DA-49-146-XZ-028, "Isolation of Underground Structures from Dynamic Loads," DASA, Structural Mechanics Research Laboratory, University of Texas, Austin, Texas, February 1961.
28. Rempel, J.R., "Shock-Wave Attenuation in Elastic Rigid Foams," Poulter Laboratories, Stanford Research Ins itute, Contract No. AF-29(601)-4363 for Air Force Weapons Laboratory, Kirtland Air Force Base, New Mexico, October 1963.
29. Ripperger, E.A., and M.D. Reifel, "Size Effects in Trussgrid Aluminum Honeycomb," Research Memorandum No. 6, Structural Mechanics Research Laboratory, University of Texas, Austin, Texas, November 1962.
30. Sevin, E., "Ground Shock Isolation of Buried Structures," Armour Research Foundation, Contract No. AF-29(601)-1134 for Air Force Special Weapons Center, Kirtland Air Force Base, New Mexico, August 1959.
31. Sevin, E., S. Shenkman, and E. Welch, "Ground Shock Isolation of Buried Structures," Armour Research Foundation, Final Report, Contract No. AF-29(601)-2586 for Air Force Special Weapons Center, Kirtland Air Force Base, New Mexico, July 1961.
32. Shield, R., and C. Covington, "High-Velocity Impact Cushioning, Part 6, 108C and 100C Foamed Plastics," Structural Mechanics Research Laboratory, University of Texas, Austin, Texas, March 1957.
33. Shield, R., E.S. Perry, E.A. Ripperger, and J.N. Thompson, "Shock Mitigation with Lightweight Vermiculite Concrete," Structural Mechanics Research Laboratory, University of Texas, Austin, Texas, February 1962.
34. Sieven, R.H., and A.R. Stacy, "Structural Response and Permanent Displacement Measurements - Operation HARDTACK," WT-1708, Defense Atomic Support Agency, Field Command, Alburquerque, New Mexico, October 1960.
35. Smith, E.F., E.S. Perry, N. Burns, and J.N. Thompson, "Effects of Shape of Load Pulse on Shock-Mitigating Characteristics of Vermiculite Concrete and a Polyurethane Plastic," Structural Mechanics Research Laboratory, University of Texas, Austin, Texas, July 1962.
36. Smith, E.H., and J.N. Thompson, "A Study of Vermiculite Concrete as a Shock-Isolating Material, "University of Texas, Contract Report No. 6-83 for USAE Waterways Experiment Station, Vicksburg, Mississippi, October 1963.
37. Southwest Research Institute, "Sulfur Technology at SWRI, Current Areas of Research and Engineering," San Antonio, Texas, May 1964.
38. Swafford, J., "Determination of the Energy Absorption Characteristics of Various Low Density Foam Type Plastics," Report No. A483 McDonnell Aircraft Corp., St. Louis, Missouri, March 1964.
39. Tumbow, J.W., H. Matlock, and J.N. Thompson, "Cushioning for Air Drop, Part 3, Characteristics of Paper Honeycomb Under Dynamic Loading," Structural Mechanics Research Laboratory, University of Texas, Austin, Texas, August 1956.
40. Tumbow, James W., "Cushioning for Air Drop, Part 7, Characteristics of Foamed Plastics Under Dynamic Loading," Structural Mechanics Research Laboratory, University of Texas, Austin, Texas, June 1957.
41. USAEC, "The Effects of Nuclear Weapons," Revised Edition, U.S. Government Printing Office, Washington, D.C., April 1962.

42. Vaile, R.B., Jr., "Isolation of Structures from Ground Shock," Operation PLUMBBOB, WT-1424, Stanford Research Institute, Menlo Park, California, 1957.

43. Whitman, R.V., "Nuclear Geophysics, Part 2 - Mechanical Properties of Earth Materials," 3203 (11) Draft Prepared for the Defense Atomic Support Agency, Washington, D.C., under Contract Nos. DA-22-079-ENG-224 and DA-49-146-XZ-030.

LIST OF SYMBOLS

a, b	=	displacements of cavity walls
E_n	=	energy absorption per unit volume of material
$P1$	=	varying component of packing pressure on liner
P_e	=	pressure at elastic yield-point of the material
P_o	=	original pressure
P_1	=	pressure at the locking state of the material
q	=	uniform component of packing pressure on liner
r	=	radius
t_f	=	thickness of backpacking
V_e	=	volume of material at pressure P_e
V_o	=	original volume
V_1	=	volume of material in the locking state
y	=	deformation of liner
$\epsilon, \epsilon_1, \epsilon_2$	=	strain
σ	=	stress
$\bar{\sigma}$	=	average stress

EFFECTS OF GAUGE DENSITY AND PLACEMENT ON MEASUREMENT OF ACCELERATION IN SOIL

by
E. T. Selig* and K. W. Rusin**

ABSTRACT

A study has been made of the various factors which affect the behavior of accelerometers in soil. Previous field and laboratory experience has been reviewed. This is supplemented by an experimental investigation of embedded accelerometers to determine the importance of gauge density and placement procedures on gauge response.

The most important factors influencing motion measurement appear to be 1) gauge density in relation to the soil, and 2) placement conditions. Reproducibility of peak acceleration measurements was within ± 15 percent on the average. For a variation in accelerometer density of 45 percent, a 12 percent difference in peak accelerations was observed for pendulum tests in sand and a 37 percent difference for shock tube tests in clay. Changing the static compaction pressure for placement of gauges in clay specimens from 12 psi to 42 psi resulted in a decrease of 22 percent in the peak accelerations recorded.

INTRODUCTION

While the physical concept of acceleration measurement in a soil mass is well known, a number of experimental difficulties are encountered in measuring it correctly. The factors influencing gauge performance are generally related to 1) gauge design, 2) gauge placement, and 3) instrumentation. The purpose of this paper is to discuss these various factors and the extent of their importance.

To supplement information available in the literature, a number of laboratory experiments were planned using small piezoelectric accelerometers embedded in specimens of sand and clay. The specimens were subjected to impact and air shock loading. The specific emphasis of these tests was to determine the influence of gauge density and placement effects on the response of embedded soil accelerometers.

PREVIOUS EXPERIENCE

Until recently very few controlled experiments have been conducted to study the response of embedded gauges for measuring soil motion, i.e., acceleration, velocity and displacement. Thus, information about the factors affecting behavior of these gauges is largely qualitative. It is generally believed that matching the density of the gauge and the grout to that of the in situ soil is important if the gauge is to reliably follow the soil motion. It is also considered important to make the seismic impedance (density times wave velocity) match that of the in situ soil unless the dimensions of the grouted region are small compared to the wave length of the pulse. However, placement conditions, including stiffness of the distrubed region, must also be important, e.g., a soft region around the gauge may permit the inertia of the gauge to cause a lag in response.

It is possible to obtain much information on the effects of gauge placement from available reports. In the earlier studies the significance of placement and other factors affecting gauge response was not fully recognized and therefore little attention was given them. In the majority of field test programs there was little opportunity to study the factors influencing placement. The time schedule did not usually permit a thorough gauge evaluation prior to the test and the limitation on the number of channels of instrumentation generally precluded duplicate measurements under different placement conditions. In many instances when it seemed likely that placement significantly influenced the gauge response, sufficient detail describing the gauges and the placement methods was not available to permit more than a qualitative evaluation. During the last few years the placement problem has been recognized, partly as a result of many unsatisfactory data, and a number of laboratory studies have been initiated to obtain more specific information.

Various methods of placement gauges have been attempted. They generally fall into two categories: 1) recompacting soil around the gauge, and 2) grouting. The observed test results do not show either method to be clearly better than the other, although the uncertainty of the results permits only an approximate comparison. The choice between grouting and recompacting is usually made for other reasons. For example, grouting is about the only reasonable

* Senior Research Engineer, IIT Research Institute, Chicago, Illinois.
**Field Engineer, Soil Testing Services, Incorporated, Northbrook, Illinois.

placement method when the gauges are located far beneath the soil surface in a bore hole. In addition, there is usually less uncertainty regarding the method of placement when grouting is used since descriptions of tamping procedures are often misleading and, in fact, there is sometimes doubt that the prescribed procedures are really followed by field crews.

Density discontinuities between the gauge, the disturbed soil or grout immediately surrounding the gauge, and the in situ soil have generally been considered an important factor influencing gauge performance. Therefore, test procedures frequently prescribe that the in situ density be duplicated if possible by the grout or the recompacted soil. Attempts have even been made to match the dynamic modulus of the grout to that of the surrounding soil. Although grouting is usually considered easier to perform than soil compaction, some difficulty results from air entrapment in the grout thereby causing cavities, and also from incomplete drying of the grout.

Grout motion measurements in connection with nuclear field tests began as early as Operation Greenhouse and have been involved in nearly every major test series since then (1). A large percentage of the data has not been useable, however, because of data scatter, or instrumentation difficulties. Initially most of the gauges used were accelerometers because available velocity gauges had poor frequency response or were too complex and expensive. Velocity and displacement information was obtained from the acceleration records by direct integration. Often correlation of the integrated values with directly measured velocity and displacement has been poor. Elaborate base line corrections have sometimes been introduced into the integration to improve results, but, in general, it has been found that integration, at least when done numerically from the printed records, is not satisfactory for obtaining velocity and displacement. This is, in part, because the typical acceleration pulse is composed of a large-amplitude short-duration pulse followed by small amplitude oscillations which are difficult to resolve accurately, but which can have a large effect on peak velocity or displacement.

In recent years the interest in ground motion measurements for field tests has shifted from acceleration to velocity. The reasons for this change in emphasis appear to be the following: 1) velocity is associated with energy level and is useful in correlating with phenomena such as structural damage, 2) velocity scales well, and 3) velocity changes less abruptly than acceleration, hence measurements should be less affected by placement conditions and density mismatch. Some investigators believe that maximum confidence can be placed in peak displacement measurements. The reason given is that displacements change less rapidly than accelerations and hence the peak values are less affected by the time variation of particle motion preceeding the peak displacement. For example, the gauge may lag the soil motion initially, but eventually catch up and perhaps even lead the soil motion. It is likely that in this case the peak displacement will be much less in error than the peak acceleration which occurs when the motion is first induced.

Motion gauges have been constructed principally from variable reluctance (or linear differential transformers), piezoelectric and electromagnetic transducers. The variable reluctance type has been the most frequently used in nuclear field tests because the piezoelectric transducers, while having a much higher limit on frequency response, are more significantly affected by the electromagnetic radiation from the blast and are less suitable with long cables. A number of self-recording gauges have also been used to eliminate the need for instrumentation cables. The results from these gauges have not appeared to be as satisfactory in general as the other types and the self-recording gauges are usually larger and more complex. A description of most of the gauges which have been used for motion measurement has been prepared (1).

The accelerometer most frequently used in the past nuclear tests was the Wiancko variable-reluctance type. The Wiancko accelerometers were mounted in canisters before being embedded in the soil and oriented to the direction in which the acceleration was to be measured. In Operation Castle field test program three of these accelerometers were placed in a canister to measure the three perpendicular components of acceleration; however, only two stations gave dependable data. A higher frequency, higher sensitivity accelerometer was developed by NOL and Schaevitz for use in Buster-Jangle. On Hardtack-II a Northam variable reluctance accelerometer was used for high G measurements but this gauge was difficult to mount and had weak terminals that could be broken easily.

Since the gauges using the variable reluctance principle are capable of measurements only up to frequencies of a few hundred cycles per second, piezoelectric accelerometers were also used in Project Cowboy to extend the range of acceleration measurements. The canisters carrying the gauges were placed with a grout matching the properties of the in situ material.

An ERA self-recording accelerometer was used in Operation Tumbler. During operation, a three-channel magnetic tape was driven past a seismic element with a small permanent magnet attached. One channel recorded timing marks and the other two the orthogonal components of acceleration. Although difficulties involved in external recording required with the Wiancko were eliminated, the ERA accelerometer did not appear to have the accuracy or reliability of the Wiancko. The ERA gauge also needed extensive calibration and adjustment prior to installation.

The first attempt to measure the velocity of soil directly was apparently made on Hardtack-II. A gauge was developed by SRI for this purpose, based on the principle of a mass whose resistance to motion is largely due to viscous damping (sometimes considered an overdamped accelerometer). Due to its construction only vertical velocities could be obtained. A modified version was designed after Hardtack-II to measure horizontal velocities. The basic element of this gauge was a miniature highly damped pendulum. After several trial applications reasonable performance was obtained with the gauges.

GROUND MOTION AND INSTRUMENTATION

Efforts have also been devoted to the development of gauges for measuring transient displacement directly. Sandia, BRL and SRI have been the principal participants. Although little information on the effects of placement is reported, it is generally believed that large displacements are the easiest of the ground motions to measure from a placement point of view.

Other laboratory investigations of embedded accelerometer behavior have been carried out at Stanford Research Institute (2). The purpose of this study was to determine, if possible, the discrepancy between recorded acceleration and true soil acceleration and to find the optimum accelerometer configuration for determining soil motion. Miniature Enedvco piezoelectric accelerometers were encased in a variety of metal and plexiglass caps to provide a range of thickness-diameter ratios and densities. The thickness-diameter ratios were either 0.16 or 0.32 and the gauge density varied from 1.0 to 2.4 times that of the soil. The gauges were embedded in dry sand and subjected to a pressure pulse with about one millisecond rise.

Details of placement were found to have the greatest affect on peak acceleration. Considerable variation in peak acceleration was observed for supposedly identical tests with placement repeated; however, there was much less variation for repeated loading with the same placement. The peak velocities obtained by integrating these acceleration records were much more reproducible than accelerations. Within the reproducibility of the results no trends with respect to gauge density or aspect ratio were observed.

LABORATORY EXPERIMENTS

A number of the factors influencing the performance of embedded gauges have been discussed. It is evident that, on the whole, available information is insufficient for an evaluation of the significance of these factors. A series of laboratory experiments were conducted to obtain more information. Attention was concentrated on two aspects, the effect of 1) variation of gauge density with respect to soil density, and 2) placement conditions, including soil compaction and grouting. The two soil samples used were a uniform dry Ottawa sand (90 percent between 20 and 40 mesh) and a compacted plastic clay (liquid limit = 63, plasticity index = 31, principal clay mineral = kaolinite).

Basically, two types of experimental facilities were involved. The first, pendulum impact apparatus, utilized hydrostatically confined cylinders of sand having properties which could be accurately controlled and reproduced. This apparatus was used to evaluate 1) guage reproducibility, 2) the effects of gauge density, and 3) controlled variation in soil properties. The second facility, a rigid chamber filled with clay and loaded by an air shock tube, permitted an evaluation of 1) gauge response under shock loading, 2) the effects of placement conditions, and 3) gauge density.

Pendulum Apparatus

The pendulum apparatus (Figure 1) is a simple device for applying controlled impact loads to small cylinders of sand confined by means of an internal vacuum. The two pendulums are steel cylinders of approximately equal size and weight. An accelerometer is attached to each pendulum to measure motion during impact. The sand specimen is encased in a rubber membrane and attached to the reaction pendulum by means of the confining vacuum. The second pendulum is used to impact the specimen. The specimen density, confining pressure, and impact velocity may be varied to give a range of test conditions.

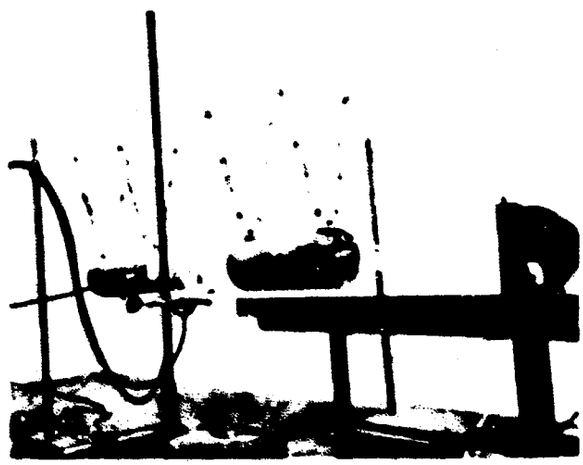


Fig. 1 Pendulum Apparatus

The sand specimen was prepared on the reaction pendulum using a mold split longitudinally and through the cross section at which the embedded accelerometer was to be located. The mold was first filled to this cross section by pouring the sand from a prescribed height. The gauge was set in place on the leveled sand surface and the remainder of the specimen was formed. A diagram of the specimen with the gauge in position is shown in Figure 2. The specimen was 4 in. in length and about 3 in. in diameter. One end of the embedded accelerometer was coincident with the center cross section of the specimen. Since the rubber membrane was also split at this cross section, the electrical conductors from the gauge exited from the specimen at this point.

Specimen densities ranged from 99 pcf to 101.4 pcf (approximately 18 percent and 33 percent relative density, respectively) at confining pressures of 0 and 12.0 psi. The accelerometer densities were 114 and 177 pcf, about 14 and 77 percent higher than the sand.

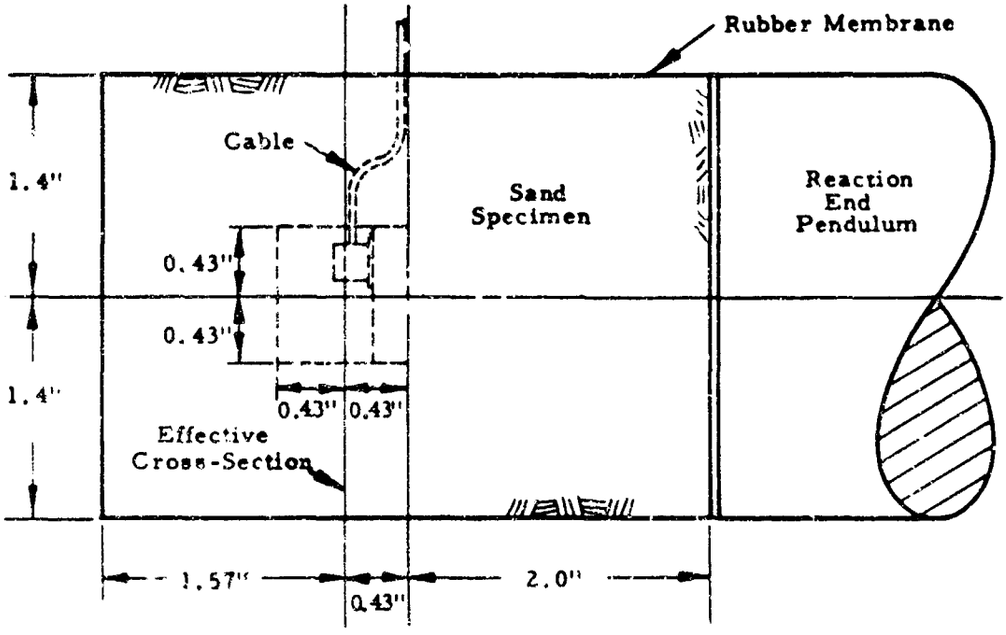


Fig. 2 Location of Accelerometer in Pendulum Specimen

Shock Tube Apparatus

The shock tube apparatus (Figures 3, 5) provided a method of studying air shock induced accelerations under conditions more nearly simulating those in the field. A completely confined specimen of clay was used and the accelerometer compacted or grouted into a hole bored in the soil. The clay was contained in a glass-sided box 24 in. deep, 24 in. long, and 4 in. wide. To facilitate a comparison of results the same specimen was used for all of the tests and subjected to an identical loading for a variety of gauge density and placement conditions.

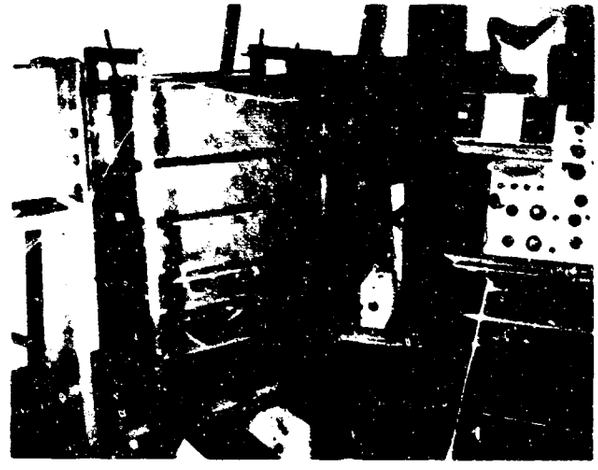


Fig. 3 Apparatus for Shock Tube Experiments

Shock pressures of up to 6.5 psi were provided by using the bursting diaphragm method. Rise time of the air shock was essentially zero, duration of the peak pressure about 5 msec and total pulse duration about 15 msec.

Compaction of the clay was carried out in the vertical plane, i.e., parallel to the 4 in. direction, using five layers and a compactive effort of 5 ft-lb per blow. The number of blows per layer was sufficient to cover the area twice. The initial moisture content of the clay was 32 percent and the average soil density 115 pcf. The accelerometer densities were thus about equal to and 54 percent higher than the soil. This was maintained throughout the tests by covering all exposed soil surfaces with plastic wrap. An unconfined compressive strength of 2-1/4 tons per sq ft was measured with a pocket penetrometer.

With the glass side removed, the hole for the gauge was made in the center of the specimen (parallel to the 4-in. direction) using a 2-in. diameter thin-wall tube. The hole extended from the front surface to the back, i.e., the entire 4 in. The material removed was broken into finer pieces for ease in replacing around the gauge.

Three methods of placement were used:

1. Soil was compacted around gauge with a compaction pressure of 42 psi.
2. Soil was compacted around gauge with a compaction pressure of 12 psi.
3. Gauge was grouted in place with a plaster-of-paris compound ($CaSO_4$).

The bore hole was filled approximately half way with the clay using the desired compaction effort or using grout. The gauge was positioned, and soil carefully compacted around it with the same effort. Then the remainder of the hole was filled and the front glass put into place. The bore hole with gauge and compacting device is shown in Figure 4. The compaction device was a pocket penetrometer with an extension which has a diameter of 0.875 in. When compacting in the narrow space around the gauge, the extension was removed and a correspondingly lower scale deflection was used to

adjust for area differences. With the minimum compactive effort it was necessary to break up the soil into fine particles. This was accomplished by using a number 10 mesh sieve and grating the soil through it. As an independent check on the soil and loading conditions and for standardization purposes, another accelerometer, also shown in Figure 4 was placed in the lower left hand corner of the box (see Figure 5). However, because problems with moisture and pressure sensitivity did not perform satisfactorily and was eliminated after the first series of experiments.



Fig. 4 Preparation for Placement of Gauges in Clay

Accelerometer

The selection of accelerometer for the experimental study was dictated primarily by size, but also by method of cable attachment and frequency response range. To provide for a variation in density and configuration it was decided to enclose a small piezoelectric accelerometer within a machined case with a maximum dimension of 1 in. Because of this size limitation, which is imposed by the pendulum specimen, a "subminiature" commercial model was selected*. Its natural frequency (105 kc) was ample for high frequency response; the low frequency response was provided by using a Kistler Charge Amplifier** in the circuit between the accelerometer and the recording oscilloscope. The electrical cable was attached at the side of the gauge thus permitting it to be placed in the soil in the plane of the motion to minimize cable restraint on accelerometer response. The shape of the accelerometer permitted a case design with a L/D ratio of one or less.

The accelerometer case constructed for the study is shown in Figure 6. Considerable experimenting with the design was required to eliminate the effects of cable forces, case pressures and moisture from the acceleration signal. Each case was made up of a base, thin cylindrical wall and cap held together with three screws. The accelerometer transducer was mounted off center on the base to permit clamping of the cable within the case. Two cases were constructed,

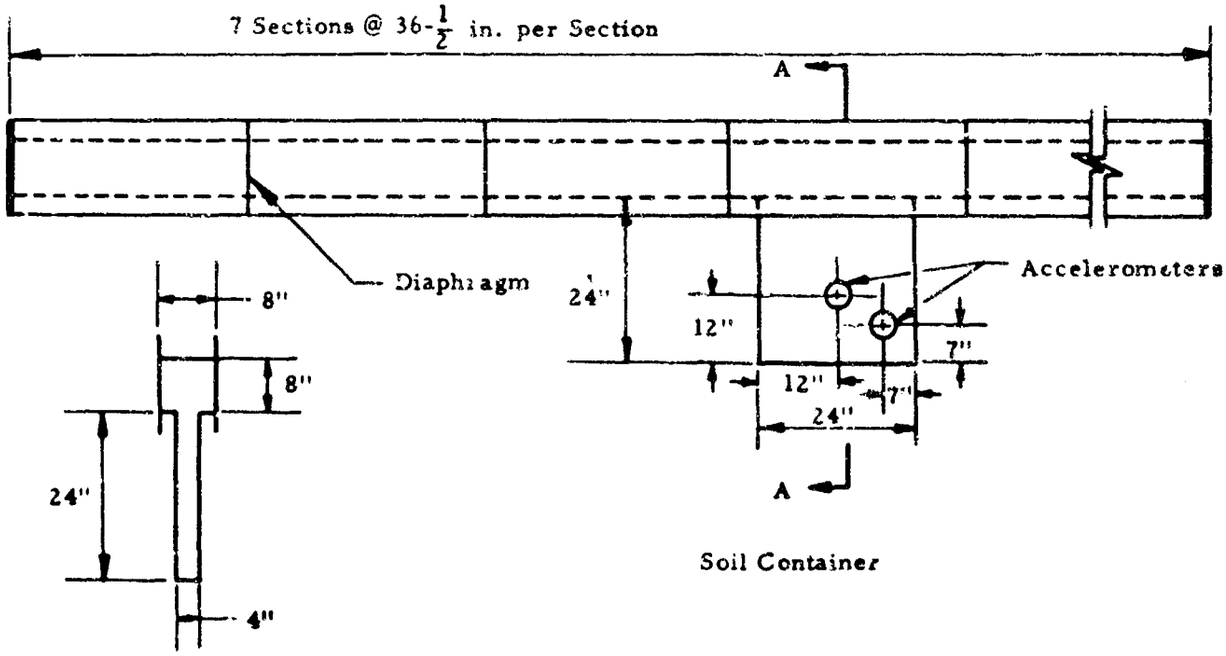


Fig. 5 Schematic of Shock Tube Apparatus

* Columbia Research Laboratories 607-1.
**Kistler Instrument Corporation, N. Tonawanda, New York, Model 566.

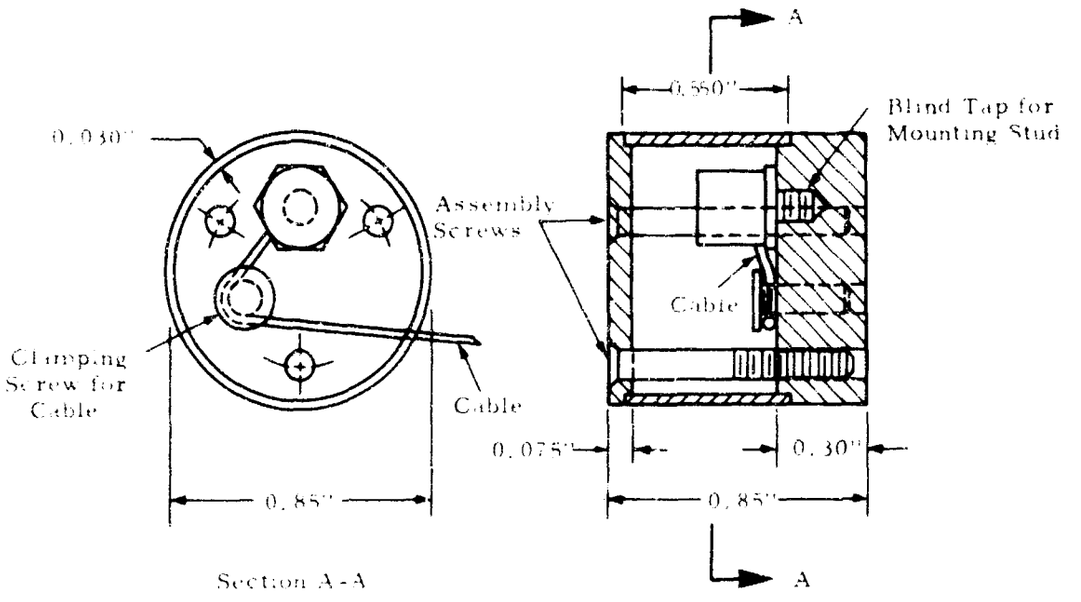


Fig. 6 Accelerometer Design

one all from aluminum and the other with an aluminum base, but a steel wall and cap. The average densities of the assembly were 114 pcf and 177 pcf respectively. When used in clays the case was coated with a liquid latex compound. This eliminated the moisture problem if the gauge was not permitted to stay in the clay for more than about 12 hours.

RESULTS OF PENDULUM EXPERIMENTS

Typical pendulum and embedded accelerometer records are shown in Figures 7 and 8. Basically the embedded gauge record has three characteristic features: a sharply peaked, short duration acceleration, followed by a longer duration deceleration and a final damped oscillation. The latter represents the vibration of the specimen at the completion of impact. At the lower confining pressures the peak impact pendulum deceleration is substantially reduced because of the lower specimen stiffness. This results in reduced intensity of impact so that the positive and negative portions of the embedded accelerometer record are lower in magnitude and longer in duration than at the higher confining pressures.

Three tests (Series A) were performed with the aluminum accelerometer to investigate reproducibility and the specimens were subjected to essentially identical impact sequences. The acceleration results for Series A are shown in Figure 9. The peak positive acceleration is plotted as a ratio of the maximum impact pendulum deceleration. This acceleration ratio was used rather than soil acceleration alone in an attempt to compensate in part for minor variations in density and impact sequence from specimen to specimen. Either the maximum impact pendulum deceleration or maximum reaction pendulum acceleration could have been used since they are both about equal. For each of the four specimens, the data are divided into groups representing the various confining pressures and impact velocities.

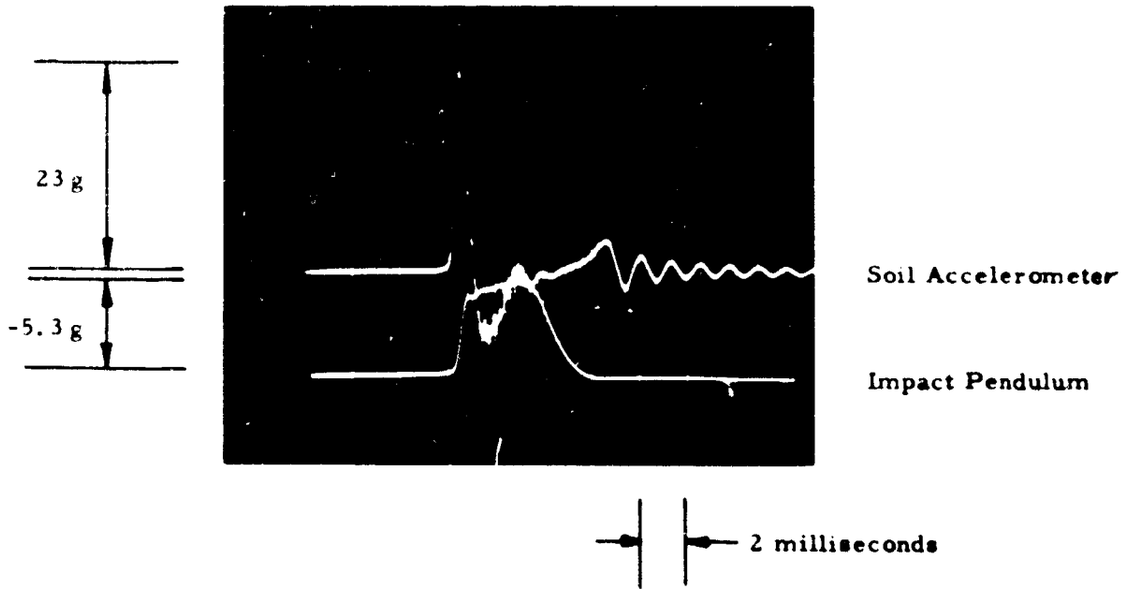
The range of values for each group in Figure 9 may be taken as an approximate indication of reproducibility of the test. The maximum deviation of values from the average for each group ranged from 4 to 58 percent. The largest variation occurred for the 12.5 psi, 0.76 fps group which represents the first few impacts. There was usually a substantial increase in peak soil acceleration between the first and second impacts (the first impact is not shown for all tests). This may be due to alignment of specimen, or placement, but is thought to be primarily due to the fact that the specimen stiffness changed most between the first and second impacts. The maximum deviation was 20 percent without the first group. The average deviation was 15 percent including the first group and 10 percent without this group.

The presentation of data in terms of acceleration ratio obviously does not correct for the effects of impact velocity and confining pressure. As the impact velocity increased, the ratio increased, hence the soil acceleration increased with respect to the impact pendulum deceleration. This might be expected because the higher the impact velocity the faster the soil must accelerate from at rest up to the speed of the impacting pendulum, all other factors equal. The higher ratios at the lower confining pressures for the same impact velocity might be unexpected since the specimen was less stiff. However, both the soil acceleration and impact deceleration decreased at the lower confining pressure, but the latter decreased more thus increasing the ratio. These effects on the ratio are merely a consequence of data presentation and have no effect on conclusions since the various groups are not being compared.

A second series of tests (Series B) was conducted to determine the effect of density mismatch on accelerometer response. Typical acceleration records are shown in Figure 10. The records are of the same general shape as for Series A. There was no discernable difference in the shapes between the steel and aluminum accelerometer records.

The results of Series B are presented in Figure 11 in terms of both positive and negative peak acceleration ratios. The negative ratios, i.e., ratio of first negative peak of soil gauge acceleration to peak impact pendulum deceleration were small and difficult to measure accurately so they were not examined in detail. There is a more or less random variation of these values with overlap from group to group. The positive ratios fall into groups with respect to confining pressure and impact velocity as before.

Test reproducibility was again evaluated by computing the deviation of values within each group for each accelerometer. For the aluminum accelerometer the deviation values ranged from 5 to 50 percent and averaged 17 percent. For the steel accelerometer the values ranged from 1 to 45 percent and averaged 10 percent. The difference between these two sets of results is probably not a function of accelerometer type. As for Series A, the greatest deviation was associated



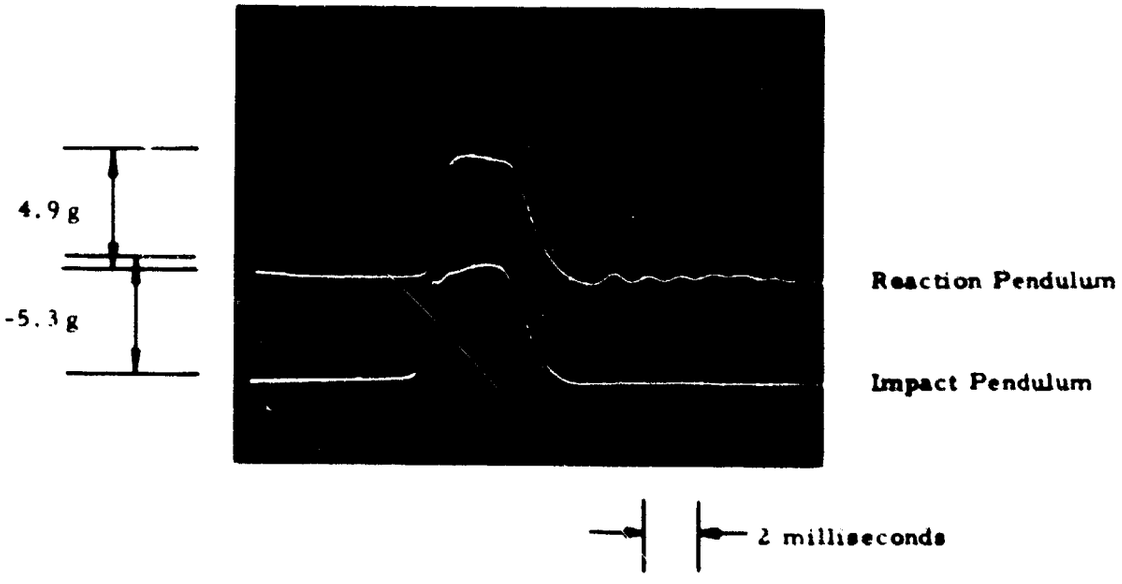
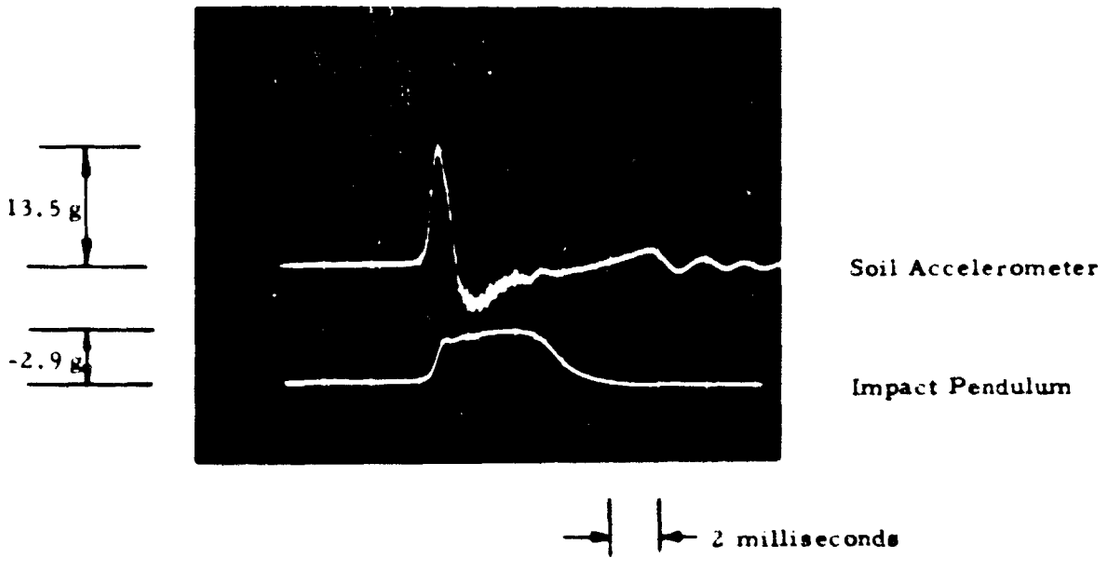


Fig. 7 Typical Pendulum Accelerometer Records (Confining Pressure = 12.5 psi, Impact Velocity = 0.76 ft/sec, Aluminum Accelerometer)

with the first few impacts, i.e., there was always a significant difference between the first and second impacts for any specimen. In all other cases successive impacts within any one group reproduced reasonably well.

As another measure of reproducibility, individual ratios representing essentially identical conditions (confining pressure, impact velocity and impact number) were compared for two specimens with the same type accelerometer. This will improve reproducibility figures because there was always some change in the ratio for successive impacts on one specimen even with all other conditions held constant. On this basis, the deviation for the aluminum accelerometer ranged from 1 to 28 percent, averaging 10 percent; the deviation for the steel accelerometer ranged from 1 to 34 percent and averaged 6 percent.

The variation in the average group ratio between the steel and aluminum accelerometer may be taken as an indication of the effect of density mismatch. Figure 11 shows a consistently larger ratio for the steel accelerometer compared to the aluminum accelerometer. The percent increase in average group values ranged from 5 to 25 percent and



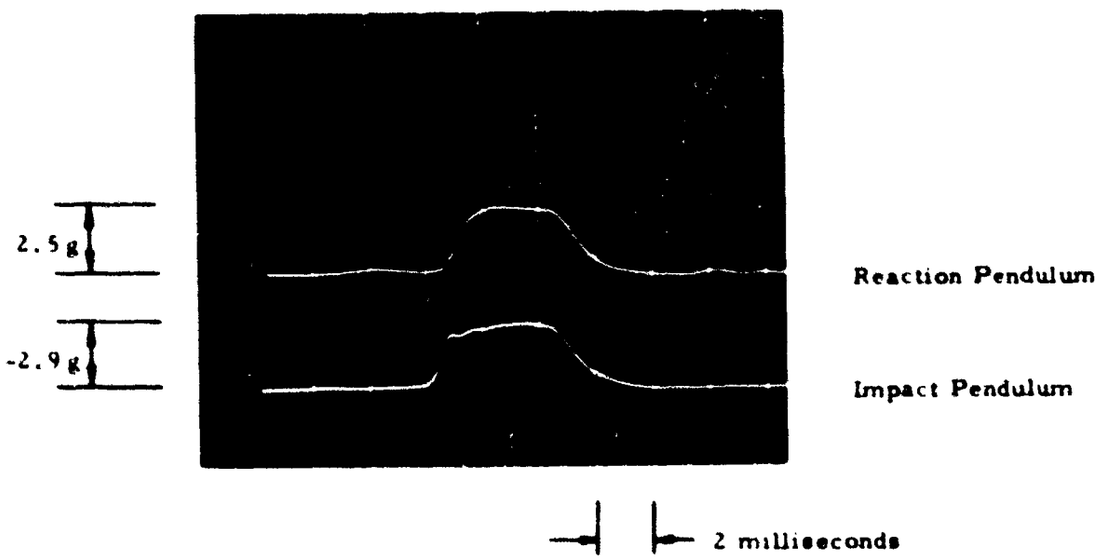


Fig. 8 Typical Pendulum Acceleration Records (Confining Pressure = 5 psi, Impact Velocity = 0.76 ft/sec, Aluminum Accelerometer)

averaged 12 percent. Thus, for an increase in gauge density of 45 percent it appears that there was about a 12 percent increase in gauge response for the same input.

Although it is possible that the change in accelerometers may have changed the specimen response or even the input conditions, the difference may also be explained in terms of gauge density. Consider the embedded accelerometer as a simple single-degree-of-freedom mass-spring system as illustrated in Figure 12. The stiffness, k, and damping, c, occur within the soil specimen and are in part a result of the gauge interaction with the soil. The accelerometer mass is m, the motion of the accelerometer case is z(t), and the equivalent motion of the cross section is y(t). Let the initial acceleration-time history of the cross section be represented by a half-sine-wave pulse. The motion of the accelerometer will follow that of the cross section with an accuracy which depends upon the natural frequency of the system ($\sqrt{k/m}$) and the damping, c.

The theoretical accelerometer response for this idealized system is shown in Figure 13, for several values of frequency and damping(3). If the values of k and c are assumed to be the same for both the aluminum and steel accelerometers then the natural frequency of the aluminum system would be greater than that for the steel system by an amount equal to

$$\sqrt{\frac{\gamma \text{ steel}}{\gamma \text{ aluminum}}}$$

where the γ represents the accelerometer densities. For this study the ratio of natural frequencies is 1.24, i.e., the natural frequency of the aluminum accelerometer is about 25 percent greater than that of the steel. Figure 13 shows that for low damping coefficients the lower natural frequency results in a greater peak recorded acceleration than the higher natural frequency. The observed results in Figure 11 can thus be explained in terms of a low-damped mass-spring system. Of course, this explanation is no proof because at higher damping the reverse is true. However, free vibrations of the specimen at the end of impact (Figure 10) suggest a low degree of damping.

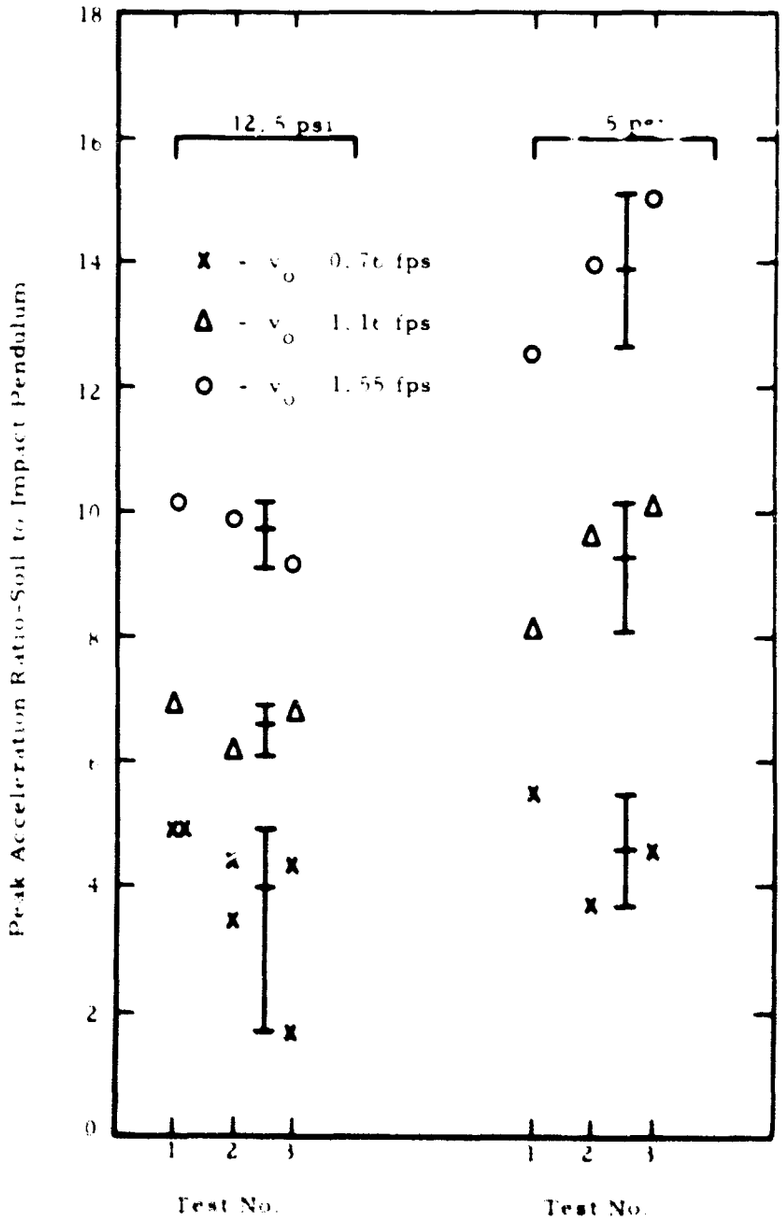


Fig. 9 Acceleration Results for Pendulum Series A

An analysis of the rise time of the embedded gauge records was made in an attempt to further verify the effect of gauge density. No significant differences were noticed with this method. However, this does not pose a contradiction because the accuracies of the rise time measurements were not sufficient to establish any correlation.

Integration of one of the embedded accelerometer records was performed for comparison with the velocity curves obtained by integrating the pendulum accelerations (Figure 14). The final velocity of the reaction pendulum and that of the soil are in agreement. At earlier times the gauge velocity was intermediate to that of the pendulums, i.e., the ends of the specimen.

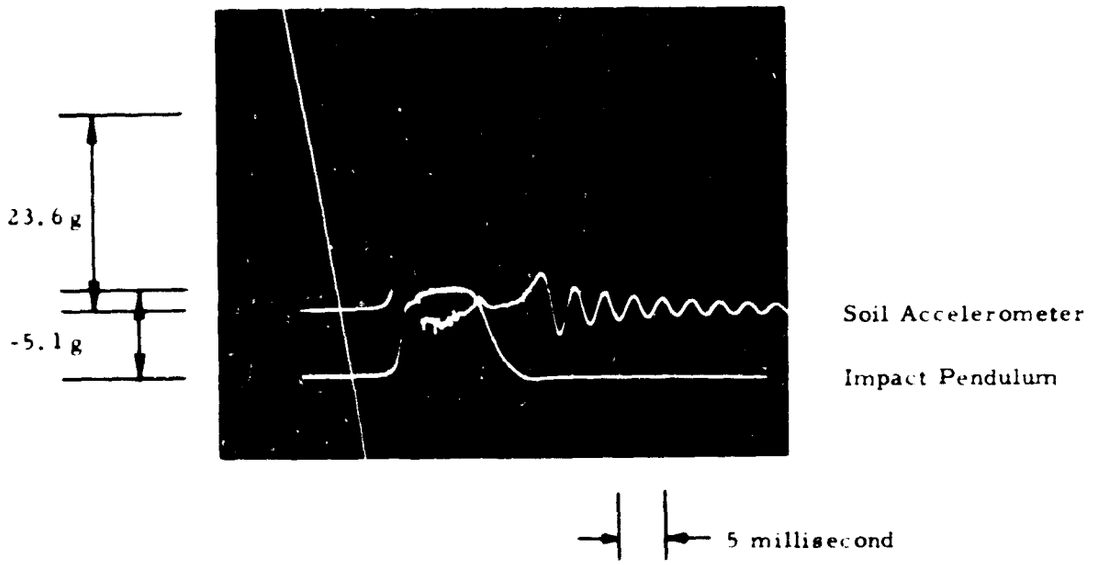


Fig. 10 Accelerometer Response in Series B (Confining Pressure = 12.5 psi, Impact Velocity = 0.76 fps, Aluminum Accelerometer)

RESULTS OF SHOCK TUBE EXPERIMENTS

Typical soil accelerometer records are shown in Figure 15. The distinguishing features are two or three major oscillations of roughly 700 to 900 cycles per second with higher frequency harmonics superimposed. These major oscillations apparently represent the free vibration of the clay specimen since a frequency of 800 cycles per second corresponds to a wave velocity of 3200 fps for the 2-ft deep specimen. The soil acceleration is of course complicated by the presence of many reflections of the shock pulse from the rigid boundaries of the specimen.

The acceleration of the bottom of the soil container was measured for several shock pulses to ascertain whether motion of the container had a significant influence in the soil accelerations. The maximum container accelerations were about 10 percent of the maximum soil accelerations, hence it was concluded that the embedded gauge records could provide a meaningful measure of gauge placement effects.

Two features of the gauge records, the average rate of acceleration rise up to the first peak and the magnitude of several prominent peaks, were used for analysis. The peaks selected were the first positive one, the first negative one and the greatest negative one (usually the second major negative peak). The accuracy of the analysis is limited in part by the superimposed high-frequency oscillations. These oscillations may increase or decrease the peak values of the major oscillations depending upon the phase relationship between the two.

To illustrate the results, the relationship between the three soil acceleration peaks for the aluminum accelerometer embedded with the heavy soil compaction is shown in Figure 16. After one series of measurements, the gauge was removed and embedded in the same manner. This provided an indication of reproducibility of placement. The variation between the results for the two sets of data was no greater than the range of values for each series alone. With one or two exceptions this same degree of consistency was indicated by the other test series. The variation of the positive peaks for any one set of conditions, including reproducibility between two identical series, ranged from about $\pm$ 5 to $\pm$ 29 percent and averaged $\pm$ 15 percent. The greatest variation occurred for the negative peaks reaching about $\pm$ 50 percent. For each test series there was a consistent increase in peak acceleration with increase in peak shock pressure, as would be expected.

Figure 17 indicates the influence of gauge density and placement conditions on positive peak acceleration. The results with the negative peaks were similar. Both positive and negative peaks were consistently greater for the condition of light compaction compared to heavy compaction. This relationship held for both the aluminum and steel accelerometer and for all applied shock pressures. The increase ranged from 0 to 57 percent, averaging 22 percent; the zero difference occurred for the lowest air shock pressures. This increase may be explained on the basis of a damped, mass-spring system as described in the pendulum studies (Figure 12). The stiffness, k, is less for the light compaction resulting in a lower natural frequency and hence the possibility of an overshoot of the peak accelerations.

The effect of the grout appears to be inconsistent. For the aluminum accelerometer, the peak accelerations with the grout were equal to or less than the values for both maximum and minimum soil compaction. For the steel accelerometer the reverse was true. With the volume of grout used it was expected that little, if any, difference between the two accelerometer masses would be observed.

For a particular set of conditions the peak positive accelerations were less for the aluminum accelerometer than for the steel accelerometer, excluding the grout tests. The reverse was true for the peak negative accelerations. The increase in positive peaks averaged 28 percent. The increase followed the same trend indicated in the pendulum tests although the amount was about triple. This difference is most likely because of the higher frequency of motion produced by the shock loading. If the peaks are viewed as oscillations about some mean acceleration then there would be an upward shift of this mean for the steel accelerometer, thus justifying the decrease in negative peaks.

As a further aid in comparing accelerometer performance, the average rate of rise of acceleration up to the first positive peak was measured. Values for 4-psi peak shock pressure are shown in Figure 18. The steel accelerometer consistently showed a faster rate of rise than the aluminum, although the difference was small for the maximum compactive effort. On the basis of the mass-spring analogy, the reverse would be expected, i.e., the aluminum accelerometer should lead the steel in rate of rise.

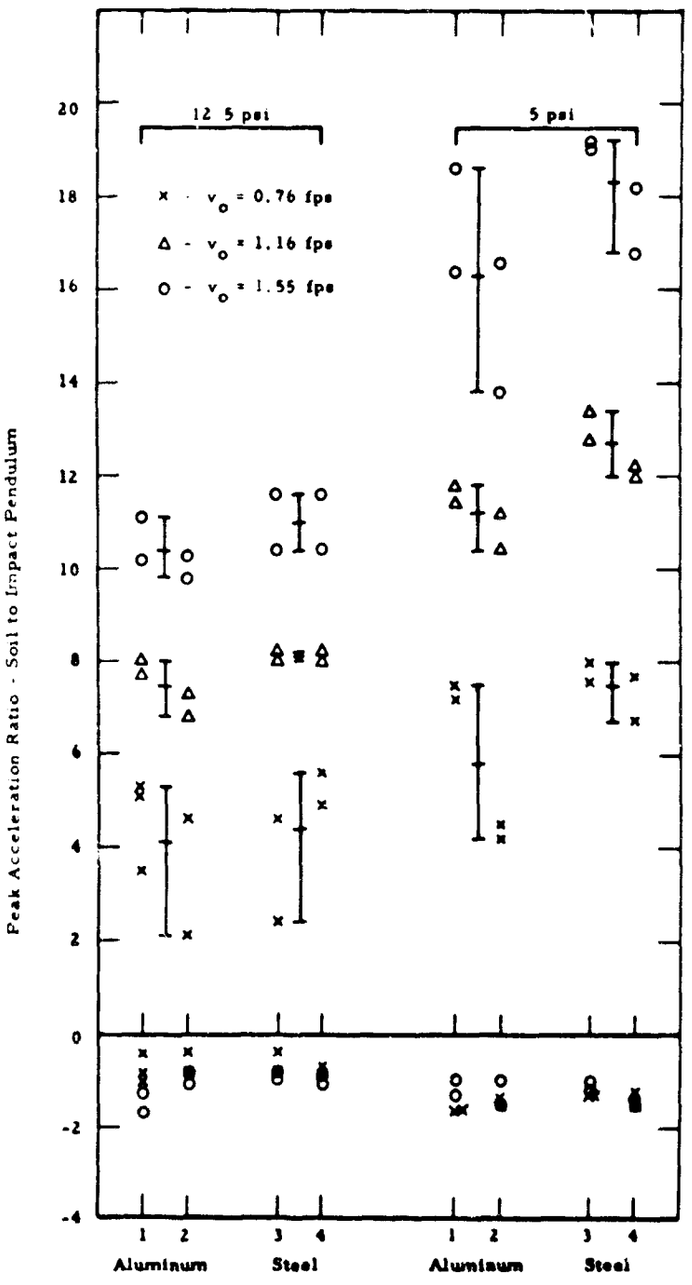


Fig. 11 Acceleration Results for Pendulum Series B

CONCLUSION

The most important factors influencing motion measurement appear to be 1) gauge density in relation to the soil, and 2) placement conditions. It is expected that acceleration measurements, expecially peak values, are much more sensitive to these factors than velocity or displacement measurements. Placement involves either grouting or soil recompaction. For many applications, for example in a deep hole, grouting may be the only suitable method. It may also permit better reproducibility, although not necessarily better accuracy. Because grouting gave apparently inconsistent results in this study, it warrants further examination.

Reproducibility of peak acceleration measurements with the pendulum apparatus (accelerometer embedded in cylindrical specimens of dry sand) was within ± 15 percent on the average. With close control on test conditions it could be kept within ± 10 percent. Reproducibility in the shock tube experiments (gauge embedded in confined specimens of compacted clay) also averaged ± 15 percent for all placement conditions.

Two accelerometer densities were used, one about 7 percent greater than that of the soil and the other about 65 percent greater. For the pendulum tests the heavier gauge recorded peak accelerations averaging 12 percent greater than those for the lighter gauge. For the shock tube tests, the increase was about 37 percent. The difference between these two sets of experiments may be due to the rate of loading. For placing the gauges in the clay two different static compaction pressures were used, 12 psi and 42 psi. The latter required in a clay density about the same as that of the rest of the specimen. The peak accelerations for the smaller effort averaged 22 percent greater than those for the higher effort.

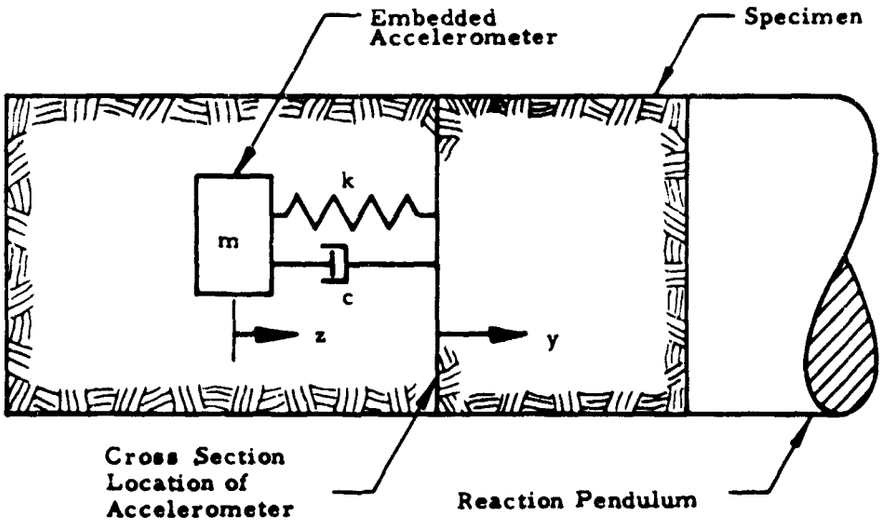
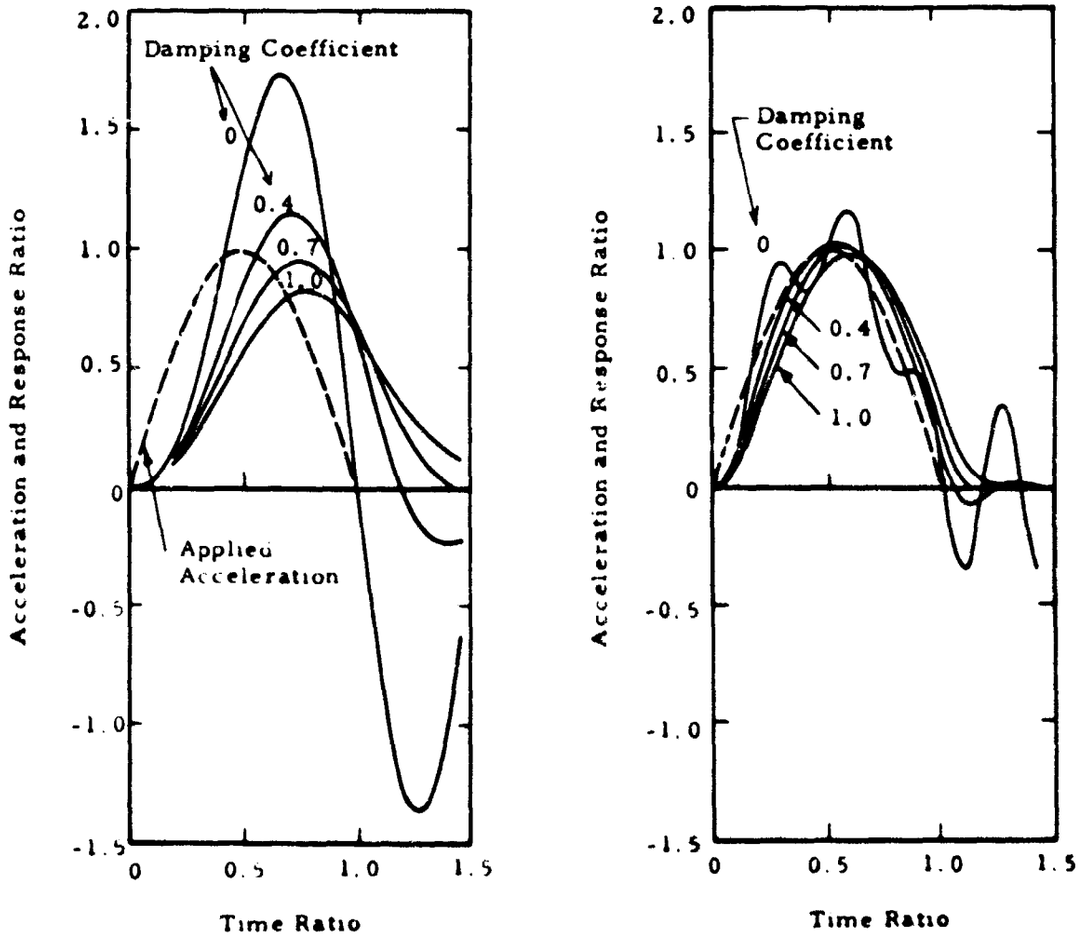


Fig. 12 Idealized Soil-Accelerometer System



(a) Accelerometer Period Equal to 1.014 times Duration of Pulse

(b) Accelerometer Period Equal to 0.338 times Duration of Pulse.

Fig. 13 Response of Accelerometer to Half-Sine-Wave Pulse

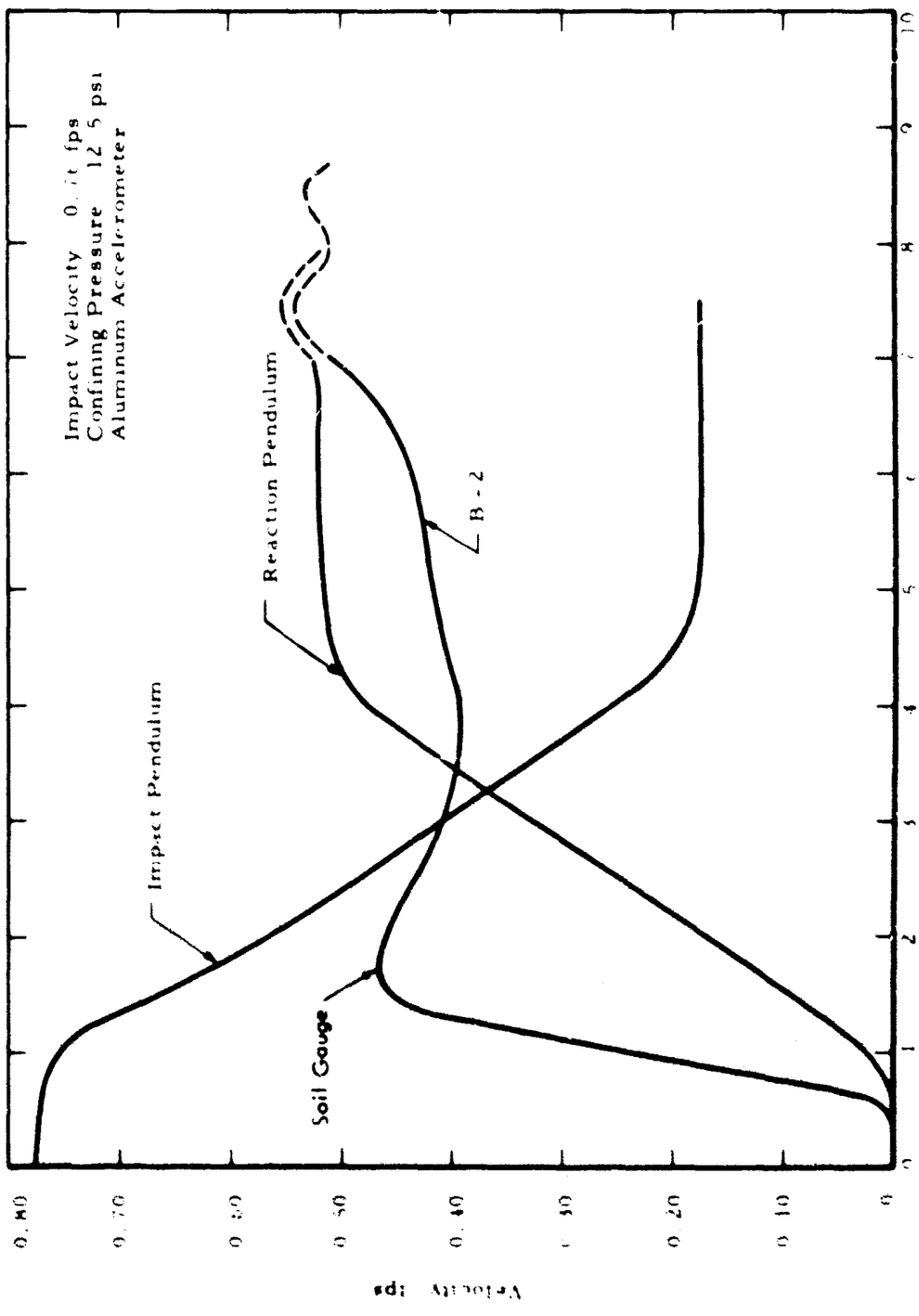
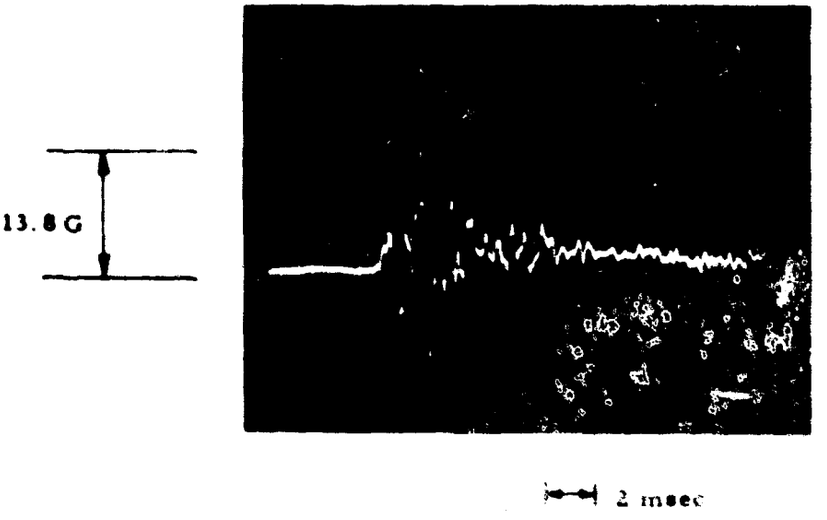
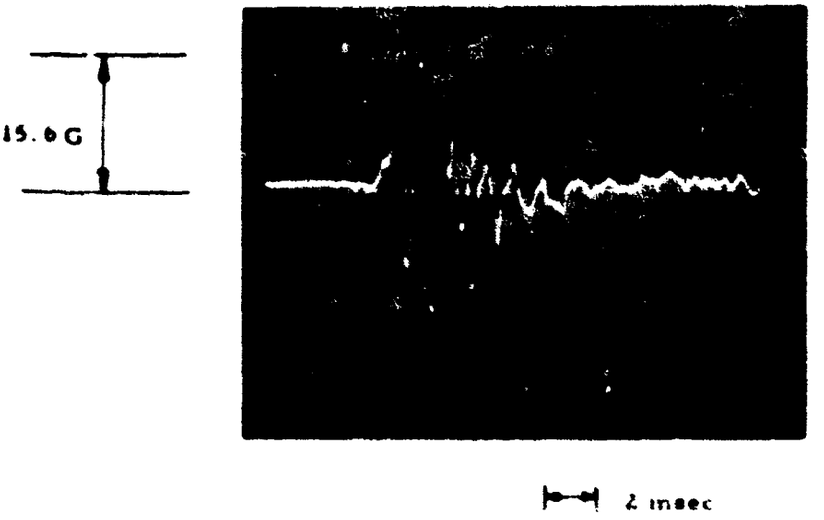


Fig. 14 Velocity Records Obtained by Integration



(a) Light Compaction



(b) Grout Placement

Fig. 15 Typical Shock Tube Accelerometer Records (Steel Accelerometer, Shock Pressure [illegible] psi)

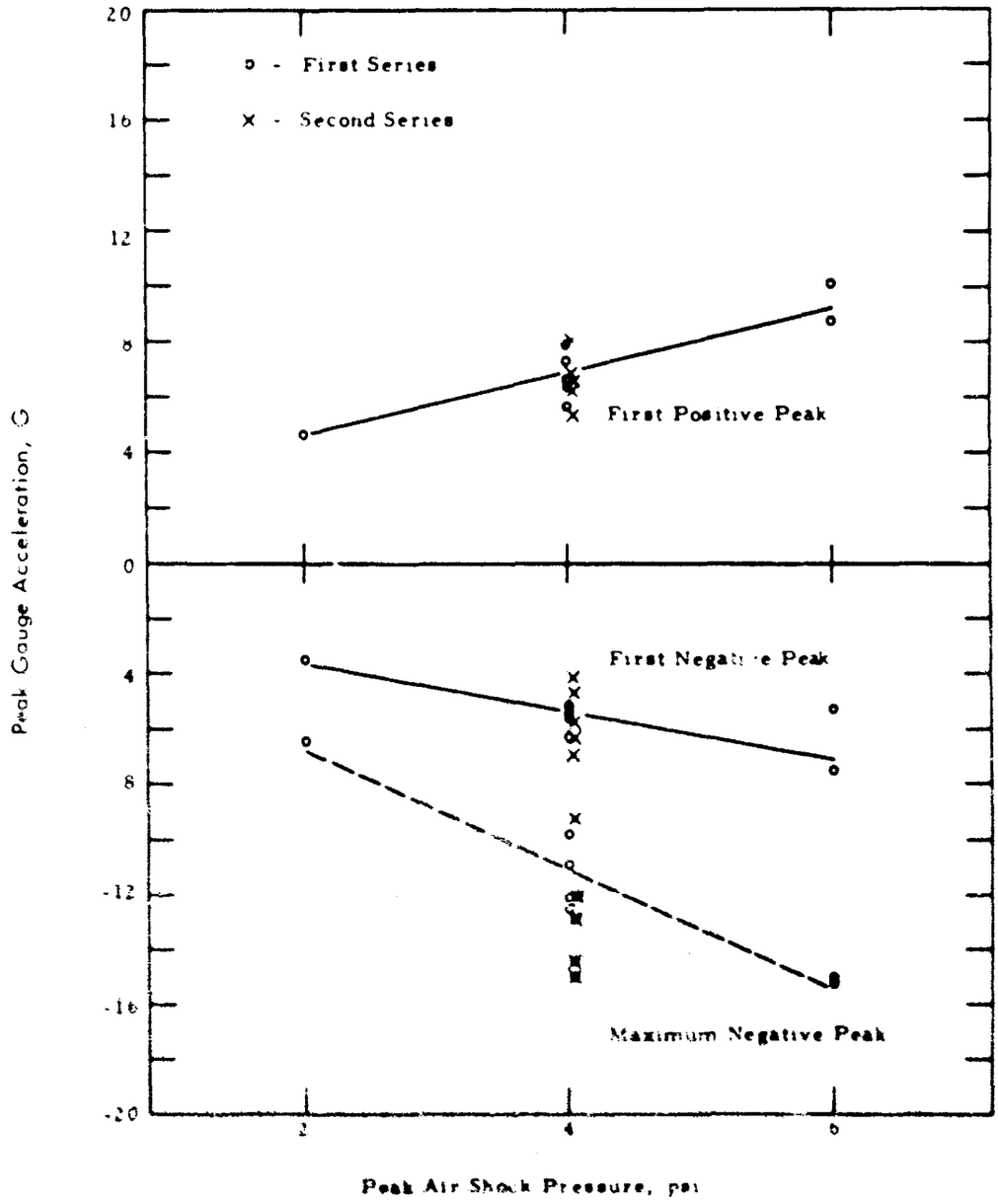


Fig. 16 Response of Aluminum Accelerometer to Shock Loading when Embedded with Heavy Soil Compaction

In general the reproducibility of gauge response for successive identical loadings was significantly improved after the first impact for all pendulum specimens. In some cases a several hundred percent increase in gauge response between the first and second impacts was observed for a relatively small change in input conditions. Because the first loading is usually of prime importance in field applications it is necessary to consider the significance of this observation. This phenomenon may likely be caused by 1) a change in specimen stiffness, which change is greatest between the first and second impacts, or 2) a change in gauge coupling as a result of placement techniques. The effect was present even with very careful control on placement procedures. If the specimen change is the cause then the first and succeeding acceleration measurements may all be correct. If the cause is placement then either the first or else the remaining measurements would be in error. The answer is not now known, but the effect appears to be significantly less with cohesive soils than with sand.

It is believed that the laboratory results are a meaningful indication of expected field performance. The relationship between pulse frequency and the accelerometer-soil system frequency lie within the spectrum existing in the field. The lateral constraints on the soil specimens are not the same, but this has basically no different affect on results than the normal variation in soil properties.

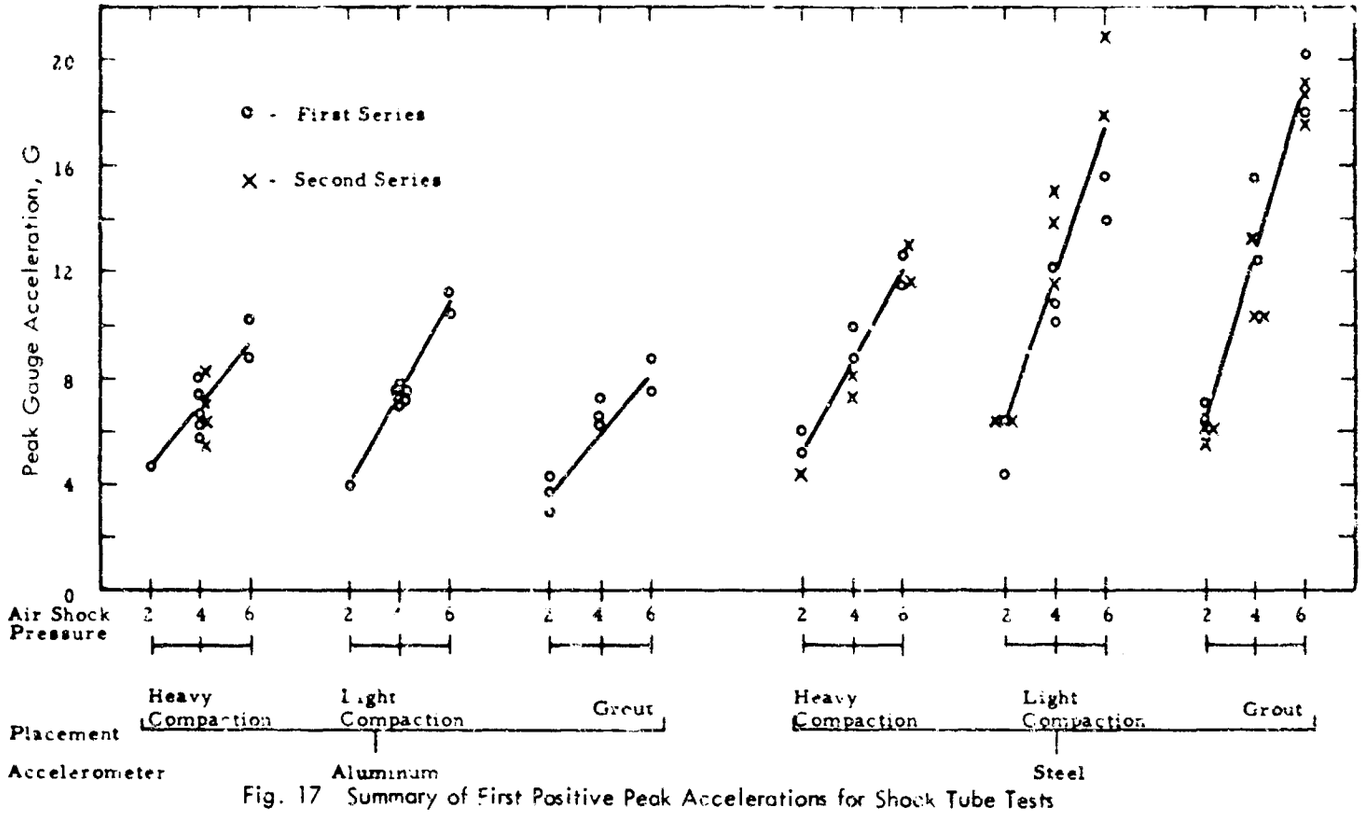


Fig. 17 Summary of First Positive Peak Accelerations for Shock Tube Tests

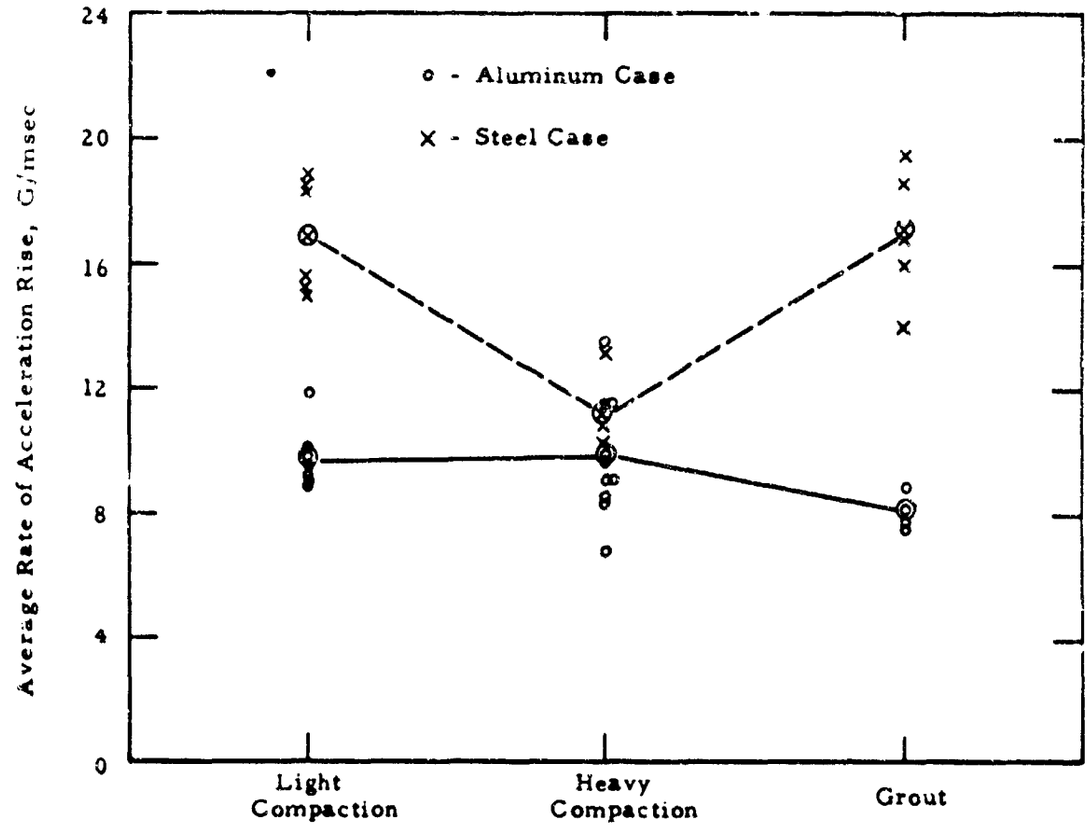


Fig. 18 Average Rate of Acceleration Rise for Shock Tube Tests

Intuition supplemented by field experience and the limited laboratory data available must still form the basis for judging the reliability of such soil-motion measurements. Unfortunately it is not generally possible to obtain suitable independent checks. On the basis of accumulated experience it is quite evident that gauge placement procedures have as great an influence on gauge response as any other factor. Therefore, further studies of this problem are desired.

ACKNOWLEDGEMENTS

The research forming the basis of this paper was sponsored by the Air Force Weapons Laboratory, Kirtland Air Force Base, New Mexico. The writers wish to express their appreciation to Lt. Bulin, the technical monitor, for his many helpful suggestions. Appreciation is also expressed to E. Stridde of IITRI for assisting with the experiments.

REFERENCES

1. "Nuclear Geoplosics, Part Three - Test Sites and Instrumentation," Prepared for the Defense Atomic Support Agency by Stanford Research Institute, February 1962.
2. Seaman, L., G.N. Boycroft and H.W. Kriebel, "Stress Propagation in Soils," Final Report, Part III for Defense Atomic Support Agency, DASA 1266-3, May 1963.
3. Levy, S. and W.D. Kroll, "Response of Accelerometers to Transient Accelerations," J. of Research of the National Bureau of Standards, Vol. 45, No. 4, October 1950.

A REVIEW OF STRESS AND STRAIN MEASUREMENT IN SOIL

by
E. T. Selig*

ABSTRACT

A review is made of the reported experience of many investigators who have been concerned with stress and strain measurement in soil. The objective has been to delineate the important factors governing gauge response and to discuss the problems involved in making the measurements. The majority of the paper is devoted to stress measurement, since this subject has received most of the attention in the past. It is concluded that accurate measurements of stress and strain in soil are difficult to make because 1) the gauge does not respond like the soil it replaces and, 2) the soil is disturbed during installation of the gauge. However, such measurements must be made if a clear understanding of many soil-structure interaction problems is to be obtained.

INTRODUCTION

In most of the experiments which have been conducted dealing with soil-structure interaction, the observed measurements have been restricted to the input loading and the structural response. The stress and strain developed in the soil have been omitted from direct consideration because of the problems involved in measuring them. However, it is the lack of knowledge of the soil behavior around the structure which is the greatest deterent to further advances in understanding the interaction phenomena. Techniques for measuring stress and strain are thus urgently needed.

The purpose of this paper is to review some of the basic types of gauges which have been used for stress and strain measurement in soil and to summarize the experiences obtained with them. It is hoped that this discussion will help to stimulate further study of the problem as well as assist experimentalists in making such measurements. For only when a much better knowledge of the soil behavior is achieved, will the many contradictory opinions of the phenomena be resolved.

There are two inherent difficulties with the use of gauges in soil: 1) the gauge does not behave like the soil it replaces, and 2) the installation of the gauge usually requires disturbance of the soil in the immediate vicinity so that this soil does not behave like the remainder of the soil mass. The first is especially true of stress gauges which to be perfect would require matching of stress-strain properties with those of the soil. The installation problem is not as severe in laboratory studies because the entire soil specimen is usually remolded. In the discussion that follows the important factors which influence gauge performance will be described. The majority of the paper is devoted to stress measurement, since this subject has received most of the attention in the past.

GENERAL CONSIDERATIONS OF STRESS MEASUREMENTS

For at least 50 years gauges have been used for measuring the stress distribution in soils and pressures produced on the surface of buried structures. The Goldbeck cell, one of the first to be widely used, was reported in the literature (1) in 1916. The cell was of the null-indicator type in which back-pressure was applied to a piston to keep it from depressing, and thereby balance soil pressure acting on it. An electrical switch was used to indicate piston movement. However, this procedure did not insure proper pressure measurement in the free field because the pressure on the gauge does not, in general, equal the correct soil stress.

The following, not necessarily arranged in order of importance, are the principal factors which must be considered in evaluating stress gauge performance:

1. application, i.e., free field or against structures,
2. overall size with respect to soil irregularities,
3. effectiveness of placement,
4. relative stiffness,
5. geometry,
6. nature of sensing element,
7. density, and
8. frequency response.

*Senior Research Engineer, IIT Research Institute, Chicago, Illinois.

GROUND MOTION AND INSTRUMENTATION

For both free field and structure applications the diameter of the sensing element must be considerably greater than the non-homogeneities of the soil locally such as discrete particles or voids. A distinction must be made between the use of the gauge for measuring stress in the free field and for measuring pressures on the surface of buried structures because the gauge requirements are different in each case. The measurement of pressures on the wall of a structure is easier than free field measurements. The primary requirement in this case is that the gauge must deflect as the structure to which it is attached. For instance if the gauge is embedded in the surface of a wall and the face of the gauge deflects either more or less than the material around it, then the pressure reading will be lower or higher respectively than the soil pressure applied to the wall. Of primary concern in this paper is the application of the gauge to free field measurements.

The stress gauge response is very sensitive to placement conditions. This is perhaps the biggest factor influencing reproducibility and consistency of measurements. If the gauge is not in proper contact with the soil or if the soil is not properly compacted around it then the readings can be significantly affected. For example a soft pocket of soil in contact with the gauge sensing element can make a rigid gauge appear to be less stiff than the soil, i.e., a gauge that would normally read too high would read too low.

Because the stress-strain characteristics of the gauge are different from those of the soil in which it is embedded, the soil immediately adjacent to the gauge will deform to a different extent than it would if the gauge were not present. Whether the soil strains would increase or decrease depends upon whether the gauge has a larger or smaller stiffness than the soil. This effect will result in a redistribution of stresses around the gauge to produce a higher pressure on the gauge if it is stiffer than the soil or a lower pressure if it is less stiff.

The magnitude of the redistribution of stress depends a great deal on the thickness-to-diameter ratio (T/D) of the gauge as well as relative stiffness--the greater this ratio, the greater the redistribution of stress. Many gauges have as their sensing element a flexible diaphragm supported at the perimeter by a rigid case. The interaction of the soil with such a gauge is often a combination of the effects of a stiff and a soft gauge. Because the gauge case is stiff the stress arches onto the gauge causing a higher than free-field value at the edge. But because the diaphragm deflection increases toward the center, the stress arches across the face of the gauge thus relieving the stress in the center, possibly even below the free-field value. These effects are illustrated in Figure 1. It is generally accepted that the T/D ratio should be as small as possible to minimize the mismatch. However, if the stress conditions are such that the soil compresses laterally and extends perpendicular to the face of the gauge, then the large dimension in the lateral direction may cause error in the gauge response.

The nature of the sensing element can influence the gauge accuracy in many ways. For example, it can determine the mode of deflection and stiffness of the gauge. It can also be sensitive to lateral and shear stresses as well as the normal stress for which it is intended. And finally, it can influence other factors such as frequency response and density.

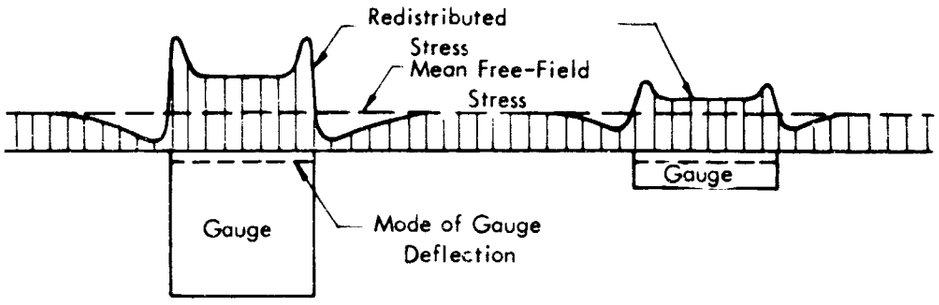
Density matching is only important for dynamic measurements. If the density of the gauge is appreciably greater than that of the soil then it will not follow the motion of the soil. The result is that the gauge inertia will produce stress on the interface which can either add to or subtract from the mean value. This effect becomes increasingly significant as the rate of loading increases and is most critical under shock loading. In addition, a shock wave will be altered in the vicinity of the gauge as it encounters the sudden density or stiffness change. For wave lengths which are long compared with the thickness of the gauge, this latter effect may not be significant. In general, density matching is not difficult to accomplish because by providing voids or ballast, or by proper selection of components, the overall weight of the gauge can be made the same as that of the soil which it displaces.

Frequency response of the gauge is another important factor in dynamic measurements. Either the transducer which converts the gauge response to an output signal or the ability of the gauge body to sense the changes in stress fast enough may be the factor limiting frequency response. These problems usually can be avoided by proper design. In contrast, piezoelectric gauges, because of the nature of the instrumentation, are usually more limited in low frequency response, i.e., the ability to sense slowly varying stresses.

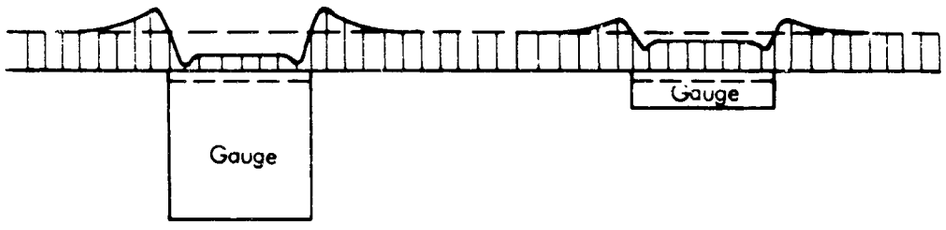
Most of these problems would not exist if the gauge behaved as the soil. It is not possible to construct such a gauge because the modulus of deformation of the soil is not a unique, constant value even for a single soil. It varies with stress level, with the relationship between the lateral and normal stress at a point in the soil, with the density and moisture content, and it is different for loading and unloading. For use under a sufficiently restricted range of conditions so that the modulus of the soil does not vary significantly, it may be possible to design a gauge to match the soil or to calibrate it for over- or under-registration. Except for this situation the only other alternative is to minimize the effects of mismatch by proper gauge design.

FIELD STRESS GAUGES

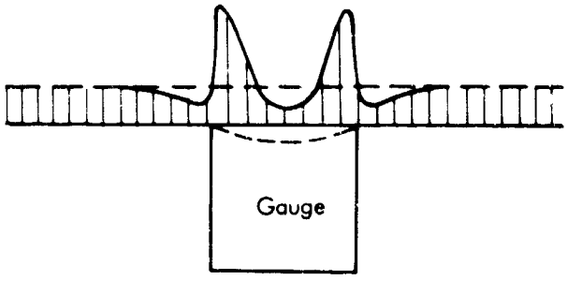
A review of some of the gauges designed to measure static earth pressures has been compiled in reference 2. The principal gauges which have been used for measuring pressure in earth masses, as distinguished from those designed for use on the face of a buried structure, include the Goldbeck cell, the Waterways Experiment Station (WES) cell, the Swedish State Power Board cell, the Road Research Lab gauge and the Plantema cell. All of these gauges are of the same general shape, a disk with a T/D ratio ranging from one for the Swedish cell to about 0.14 for the Plantema cell. For the



(a) Gauge More Stiff than Soil



(b) Gauge Less Stiff than Soil



(c) Stiff Gauge with Flexible Diaphragm

Fig. 1 Stress Distribution Around Embedded Gauges

other gauges the T/D ratio was about 0.3. No specific information is given to indicate the stiffness of the gauges, but it appears that the stiffness ratios (gauge stiffness to soil stiffness) range from less than one for the Swedish cell to values much greater than one for the WES cell.

Methods of calibration varied. For the Goldbeck cell and apparently also for the Swedish cell the pressure of fluid in the gauge was used as a measure of the soil pressure. The other gauges were calibrated under a uniform, externally applied fluid pressure; the WES and Platema cells were also calibrated in soil to obtain an indication of over-registration.

Benkelman and Lancaster (3) observed, using modified Goldbeck pneumatic cells, that there was considerable variation in the readings obtained with different types of material and different methods of embedment. It was reported that in plastic clays the physical dimensions of the cells did not produce a significant deviation in the pressure indications.

GROUND MOTION AND INSTRUMENTATION

Many of the limitations of the soil pressure gauge have been determined by studies at the Waterways Experiment Station (4). The report recommends that cells embedded in a sand mass should have a thickness-diameter ratio less than 1/5 and a diameter-deflection ratio greater than 2000.

Whiffin (5,6) reports the use of two types of gauges for measuring the stresses generated in soil by compaction equipment. Both were developed at the Road Research Laboratory in England. One gauge utilized piezoelectric quartz crystals as the sensing element. The housing was made of light alloy so that the overall density of the gauge was about the same as that of the soil. The T/D ratio was 0.17. Special precautions were taken to water-proof the gauge in order to maintain high circuit impedance. With the available instrumentation the gauges were suitable for stress of about 10 sec duration or less. The second gauge utilized an acoustic sensor consisting of a vibrating wire to measure the deflection of a steel diaphragm. The T/D ratio of this gauge was 0.27. It is suitable only for static or slowly varying stresses because of the nature of the transducer. On the basis of theoretical analysis and some field measurements, a constant over-registration of 10 per cent was reported for the piezoelectric gauge. It is unlikely, however, that this could be true for the gauge in general.

A soil pressure cell was developed by McMahon and Yoder (7) for use in the measurement of pressures in a flexible pavement subgrade. The cell is 1-1/2 in. in diameter and 3.8 in. thick, i.e., T/D ratio of 0.25. One face consists of a flexible steel diaphragm (0.015, 0.018 or 0.020 in. thick) to which SR-4 strain gauges are attached for sensing the pressure acting on the cell. Because of the difficulty of securing the diaphragm to the body of the cell, the cell and diaphragm were machined as an integral unit from round stock. The gauge was calibrated in air and embedded in clay and sand. The calibration data obtained in clay compared well with the calibration data in air. When sand was used, the data were very erratic and the correlations were very poor. The accuracy of stress measurement in clay soils was reported to be within $\pm$ 5 per cent.

The Waterways Experiment Station has reported experience gained in the measurement of stresses in soil beneath applied surface loads (8,9,10). The first series (8) were conducted in a compacted bed of clayey silt (remolded Vicksburg weathered loess with a plasticity index of 12) using 12 in. dia. WES earth pressure cells. The soil was first rolled to a depth of about 1 ft. above the level at which the gauges were to be located. A hole was then dug for each gauge and the bottom of the hole sloped to orient the gauge at the desired angle. The sensitive face of the gauge was placed in contact with the bottom of the hole and the soil replaced by hand-tamping with sufficient effort to provide a density approximately equal to that of the compacted fill. Loads were applied to the soil surface through bearing plates and stress readings taken with the embedded cells using calibrations obtained under uniform fluid pressure.

A check of the gauge performance was obtained by comparing the measured stresses with those computed from the theory of elasticity and by checking stress equilibrium within the soil. With this method of comparison as a basis, which provides only an approximate check, it was reported that the gauges read definitely within about $\pm$ 25 per cent of the expected reading and probably within $\pm$ 10 per cent, with no apparent over- or under-registration as a whole. However, the data given in the reference show scatter greater than 25 per cent in some cases. Although it is not possible to be certain how much of this effect is due to placement, on the assumption that the apparent error is randomly distributed about the expected value, the variation due to placement is probably of the same order as the total variation, i.e., $\pm$ 25 per cent.

The WES studies, were extended to compacted sand fills (9) using improved WES earth pressure cells and newly developed shear cells. Again, the soil was compacted to a height above the cell locations and then holes dug to position the gauges. The sand was carefully replaced around the gauges to match the density of the rest of the fill. Gauge response due to applied surface loads was measured and, based upon a comparison with expected stresses, information on the reproducibility and consistency of gauge performance was obtained.

Reproducibility as used in reference 9 is interpreted to mean the per cent ($\pm$) variation of the pressure readings from the average for each individual gauge upon successive identical loadings without removing and re-embedding the gauge. Reproducibility would therefore reflect the change in soil-gauge interaction upon repeated loading. The results given in Table 1 show a reproducibility of about $\pm$ 5 per cent based upon 99 per cent of the data for the pressure and shear cells.

As used in reference 9, consistency refers to the correlation of the readings between identical gauges with equivalent installations, i.e., at positions where the stress conditions should be the same. Consistency results listed in Table 2 are given in terms of the per cent ($\pm$) deviation of the gauge readings from the average values under identical conditions. The consistency of readings for the pressure cells was $\pm$ 11.9 per cent compared to a reproducibility of $\pm$ 5.6 per cent. The difference between these two values should give an indication of the minimum variation due to placement. Depending upon how the results are interpreted, on the average the variation due to placement ranged from $\pm$ 6 to $\pm$ 12 per cent.

In this case, neither consistency nor reproducibility necessarily indicates the accuracy of the stress readings. In the vicinity of the surface load the vertical stresses were higher than given by the elasticity theory and the horizontal stresses were lower; however, this may be expected because of the difference in behavior between the sand and an elastic material. If over-registration is assumed to be only a few per cent, then the accuracy of the stress readings should be about the same as the consistency, i.e., $\pm$ 12 per cent.

Table 1

REPRODUCIBILITY OF SOIL GAUGES

Type of Gauge	Reproducibility as Percent of Average Reading		Number of Readings
	50% of Data	99% of Data	
Pressure Cell	± 1.5	± 5.6	700
Shear Cell	± 1.1	± 4.2	640
Deflection Gauge	± 1.5 (high deflection)	± 5.8	500
	± 4.0 (low deflection)	± 15.2	300
Strain Gauge	± 10.9	± 41.6	290

Table 2

CONSISTENCY OF SOIL GAUGES (9)

Type of Gauge	Consistency as Percent of Average Reading		Number of Readings
	50% of Data	99% of Data	
Pressure Cell	± 3.1	± 11.9	40
Deflection Gauges	± 9.5	± 36.3	13

In the third series of WES tests (10), surface loads were produced by a moving vehicle on compacted clay. Three types of cells were used in these tests: 1) WES earth pressure cell, 2) WES fluid pressure cell, and 3) a gauge constructed from a Consolidated Electronics Corporation (CEC) pressure transducer. The geometry of these gauges is shown in Figure 2.

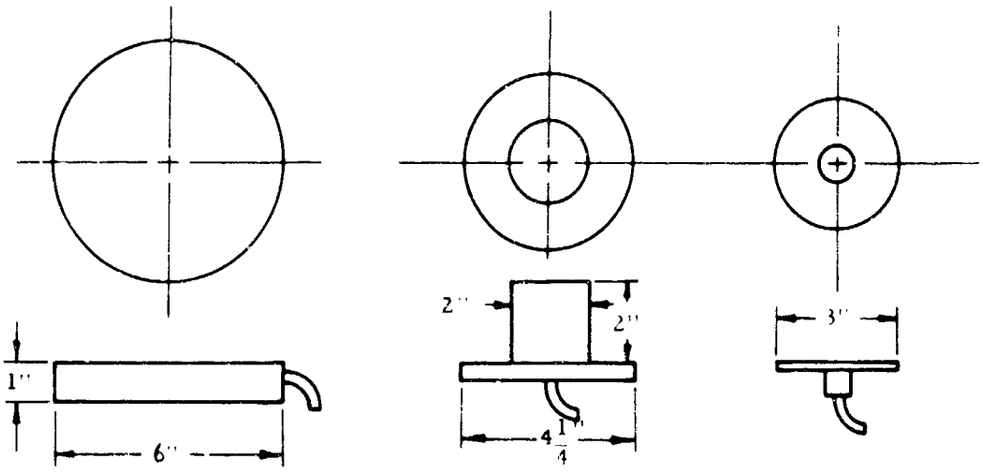
The clay fill was first compacted with rollers and then gauge holes, about 7 in. in diameter, were dug to the required depth. The soil was recompacted by hand around the gauges to the same strength as the surrounding fill. A penetrometer was used to control the compactive effort.

In the initial tests there was considerable variation in the soil strength throughout the fill. The measured stress values were very erratic, possibly for this reason, but there was also uncertainty in the applied load on successive passes because of the difficulty in controlling the alignment of the vehicle as it passed along the test strip. In the firm clay fill, several of the gauge readings were very low for the first pass or two, but increased thereafter, suggesting that the soil had not been compacted sufficiently around the gauge initially.

In the softer clay fills it appeared that placement was better since the readings were more consistent, but rutting beneath the vehicle caused considerably more movement of the gauges than in the firm clay. Some gauges showed little change in stress under successive passes while others showed an increase of as much as 100 per cent.

Another test was conducted in clay sufficiently firm that no rutting occurred. Difficulty in aligning the vehicle caused some variation in recorded pressures from pass to pass. In addition, stress recorded by similarly placed cells differed considerably for one pass. The magnitude of these inconsistencies is not indicated, but the cause is most likely associated with placement or variation in the uniformity of the fill.

The poorest results were obtained with the fluid pressure cells. Generally these cells recorded stresses too low and were difficult to place properly because of their shape. The fact that they read low values of stress suggests that they were not seated properly, because their stiffness and high effective T/D ratio would tend to cause too high readings. The experience with the CEC cell was similar. One of the shortcomings of this gauge is its very small sensitive area which makes it especially sensitive to placement and soil irregularities. In addition, however, both of these gauges had cables exiting from the back of the gauge. This is a very undesirable condition because it makes proper placement extremely difficult to accomplish.



(a) WES Earth Pressure Cell (b) WES Fluid Pressure Cell (c) CEC Cell

Fig. 2 Stress Gauges for WES Tests (10)

Studies involving the measurement of stresses in noncohesive soil masses subjected to vibratory loads have been conducted by Bernhard (11). The problem of measuring low amplitude vibratory stresses in soil appears to be less difficult than other types of soil stress measurement. This is primarily because under continued vibration the soil approaches a state of elastic equilibrium so that there is no further change in soil-gauge interaction and discontinuities and variation in placement tend to be smoothed out.

The tests were performed in noncohesive gravelly sand. The gauge was cylindrically shaped with a T/D ratio of about 1-1/2. The gauge was calibrated in terms of the deflection of a flexible diaphragm at one end of the cylinder. Both uniform pressure and concentrated load calibrations were made and the average used for obtaining the soil stress. The stress fluctuations in the soil were measured after the stable dynamic conditions were reached. In placing the gauge, as little sand as possible was removed and it was replaced to the same density using a penetrometer as a means of checking.

The accuracy of the stress measurements was determined by correlation of the experimental and theoretical results assuming that the soil behaved elastically during vibration. On the basis of this analysis it was reported that 68 per cent of the readings were within ± 5.2 per cent of theoretical and 95 per cent within ± 10.2 per cent.

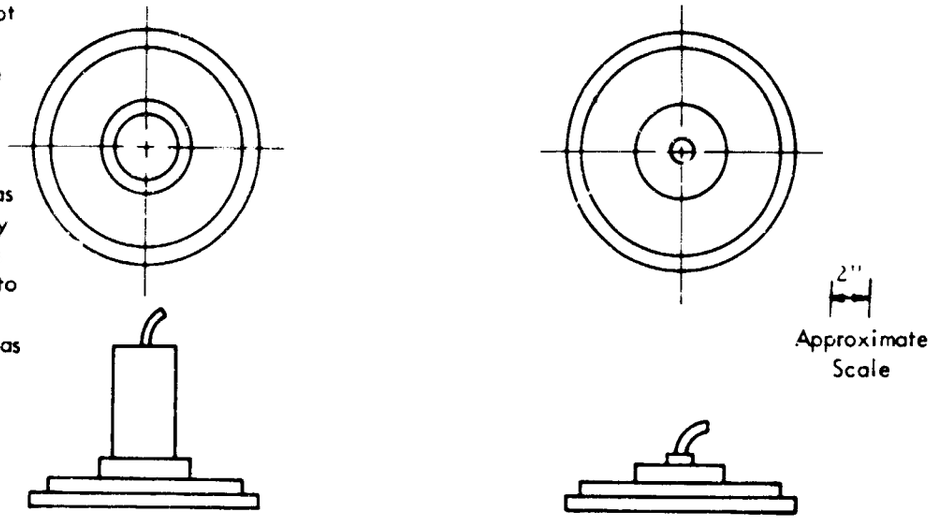
Attempts have been made to measure the stresses in soil produced by nuclear blasts in conjunction with a number of the nuclear weapons test programs. A description of the principal types of gauges used and an indication of some of the problems encountered are given in reference 12.

The Carlson-Wiancko earth pressure cell is reported to be one of the most successful used in any of the field tests. It is a diaphragm type gauge in which the deflection of the diaphragm is measured by a variable reluctance transducer and calibrated in terms of a uniformly applied pressure. The gauge is basically disk-shaped, but as originally used in the Buster-Jangle and Tumbler-Snapper field test series, there was a large protrusion on the back of the gauge to house the transducer (Figure 3). The reliability of the gauge was demonstrated in these tests, but the recorded stresses appeared higher than expected. It was thought that the transducer housing caused a stress concentration around the gauge, and so the housing was made more compact prior to further use. The modified Carlson-Wiancko cell was used in the Upshot-Knothole series and better results were reported.

For measurements in rock or hard soils the gauges were generally grouted into a prepared hole. Some attempts have been made to use grouts which match the earth as closely as possible (13). For other soil conditions the gauges were generally mounted flush with the bottom or sides of the prepared holes. Moistened and screened soil was then carefully tamped around the gauge either mechanically or by hand. Very little information indicating the effect of placement on the measured stresses is available in the test reports. However, it is generally accepted that the local variations around the gauge can significantly affect the readings, especially for stress measurement.

Another gauge concept was investigated by United Electrodynamics (14). The gauge consisted of two sections each with a disk attached to a hollow stem, one sliding within the other (Figure 4). The stem houses the transducer and the pressure sensitive element is located in the center of one of the disks. Stems are free to slide with respect to each other without resistance to prevent the stress concentration which would be caused by this housing if it were rigid. This configuration also permits measurement of strain and acceleration with the insertion of a displacement transducer in the stem to measure the relative movements of the ends and an accelerometer in the face of the disk not used for the stress sensor.

Placement of this gauge is not accomplished as easily as with other stress gauges, especially in cohesive soils, because of the difficulty in compacting the soil around the stem between the two end disks. Satisfactory performance of this gauge was reported in confined specimens of dry sand, although significant variations in results which appeared to be due to lack of adequate control of the sand density were noticed. The scatter was especially significant at high stress levels and under dynamic loading.



(a) Original (b) Modified

Fig. 3 Carlson-Wiancko Earth Pressure Cells

LABORATORY STRESS GAUGE EVALUATIONS

Taylor (15) carried out a theoretical analysis of the pressure acting on embedded gauges which relates the gauge error to its geometry and stiffness and to the soil stiffness. A more rigorous analysis was made by Monfore (16) who considered the cell to be embedded in an infinite elastic homogeneous solid. The calculated examples were extended by Peattie and Sparrow (17) to cover a wider range of parameters. From this work a number of conclusions were drawn.

1. For a given set of conditions, gauge errors are directly proportional to the T/D ratio and may be expressed approximately in the form

$$\frac{p_c - p}{p} = \frac{p_e}{p} = C_a \frac{T}{D} \tag{1}$$

where p_c = average pressure on gauge,
p = true soil stress,
p_e = gauge error,
T = gauge thickness,
D = gauge diameter,
C_c = cell action factor which depends in part on gauge-soil stiffness ratio, soil properties and T/D ratio.

2. The cell action factor, C_a, increases with increasing values of E_g/E_s, the gauge-to-soil stiffness ratio; however, as E_g/E_s increases, C_a approaches a limiting value. (For the cases studied C_a was considered approximately constant if E_g/E_s was greater than 10 providing that the ratio of gauge sensitive area to total facial area was constant.)
3. For a given value of modular ratio, C_a increases as the ratio of the gauge sensitive area, A_s, to total facial area, A_t, increases. This effect is caused by the nonuniform pressure distribution over the face of the gauge, the pressure varying from a minimum in the center to a maximum at the edge.
4. The cell action factor depends on the value of Poisson's ratio for the material in which the gauge is embedded; however, this effect is small.

A fundamental experimental study of soil stress gauges was undertaken by Peattie and Sparrow (17) in which the T/D ratio, A_s/A_t and E_g/E_s were varied independently. The gauges constructed for the test were 3 in. in diameter. The gauge stiffness was controlled by fitting composite plates of brass and rubber to the back of the standard gauge in place of the brass plates used to vary the thickness.

Effect of placement was evaluated first in the following manner. The soil container was filled to the level at which the gauges were to be located and the surface made flat. Six identical gauges were used, all stiffer than the soil. Two gauges were placed directly on this surface, two pressed into the soil an amount equal to one-half of the gauge thickness, and two pressed into the soil an amount equal to their entire thickness. The remainder of the soil was added and then the surface pressurized uniformly. The response of the gauges pressed into the soil their entire thickness was approximately 15 per cent greater than that of the other gauges. The exact condition of the soil was not indicated for these tests, but it appears that an increase in soil density across the face of the gauge increased the stress concentration in the vicinity of the gauge, thereby increasing gauge response.

The error in gauge reading was found to be a linear function of the T/D ratio and the effect of change in T/D ratio was significant. For a particular gauge of constant stiffness and diameter, an increase in T/D ratio 0.2 to 1.0 caused an increase in gauge registration ranging from 28 to 62 per cent under the same loading conditions in several soils. Over-registration as high as 180 per cent was reported in sand and 100 per cent in clay.

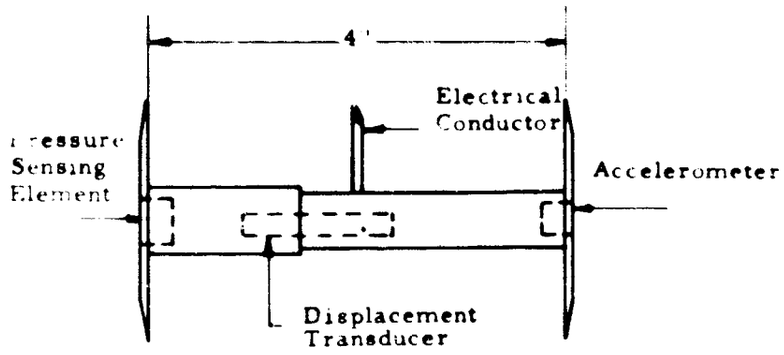


Fig. 4 UED "Soil-Filled" Stress Gauge (14)

Several factors influencing the cell action factor were investigated. For dense sand C_a varied with stress level (the direction of change was not indicated) when the sensitive area of the gauge was greater than 25 per cent of the total facial area, otherwise C_a was approximately constant for both loose and dense sand. For clay C_a decreased with stress level--more than 50 per cent in some cases. This decrease could have been caused by an increase in soil stiffness under pressure.

Since the stress was not uniformly distributed over the face of the gauge, being higher at the edge than at the center, the over-registration was found to decrease as the sensitive area was decreased in proportion to the total gauge area. For best results the report recommends that the sensitive area be less than 25 per cent of the total area for rigid diaphragm and less than 45 per cent for a deflecting diaphragm. Experiments showed a decrease in over-registration from as high a value as 48 per cent to 9 per cent due to a reduction in sensitive area from 100 per cent to 25 per cent of the total area.

The effect of a variation in the stiffness ratio, E_g/E_s, was observed by changing the gauge stiffness for a particular soil condition. It was found that when the ratio was unity the gauge indicated the true stress, but the rate of change of the over-registration with stiffness was greater, i.e., a given change in stiffness ratio produced the greatest change in over-registration for values of the ratio near unity. For one of the cohesive soils C_a was observed to decrease with time at a given stress level. This indicates a consolidation which would increase E_s thus decreasing the ratio. Since the gauge cannot be made to always match the soil stiffness the report recommends that the stiffness ratio be kept at least greater than ten to minimize the effects of changes in this ratio.

Buck (18) has investigated gauges for measuring stress in sand which were 1 in. in dia by 1/4 in. thick, with two 3/4 in. dia sensitive faces consisting of deflecting diaphragms to which were attached electrical resistance strain gauges. The embedded response of these gauges was determined by embedding them in a 9 in. dia triaxial specimen. The cell over-registration, linearity, hysteresis, and zero-set were considered and the following observations were made:

1. The more angular the sand the higher the over-registration, less hysteresis and less zero-set. However, a greater variation in reproducibility was indicated.
2. The finer the sand fraction the more linear the gauge response, the less the zero-set and the less the variation in results.
3. The wider the range of gradation of sand the less the variation and the more linear the response.
4. Variation in the naturally random packing of sand during placement of the specimen as well as gauge placement were found to be the primary cause of data scatter.
5. Less zero-set was found to result from increasing relative density. In addition the over-registration decreased and the variation in results increased.

Gauges were embedded using a fine-grained material around the gauge to give a more uniform pressure on the diaphragm. However, this technique did not give any better results.

6. It was evident from the tests that the principal stress ratio and the obliquity of strain both have a significant effect on the cell over-registration. The gauge was placed in the triaxial specimen to measure the axial stress, lateral or confining stress, and stress on the 45° plane. The gauge showed over-registration for the axial stress and under-registration for the other two stresses.

An investigation of gauges for the measurement of pressures in soils and on the face of buried structures has been reported by Trollope and Lee (19). A deflecting diaphragm-type cell was constructed for measuring pressures in soil. This type of gauge was chosen for two main reasons: ease of construction and avoidance of edge effects inherent with the piston-type cell. However, because of difficulty with strain gauge circuits and insufficient sensitivity no satisfactory results were obtained with this gauge. Some information about embedded gauge performance was obtained nevertheless.

It was concluded that to limit the effects of soil density variation on loading, unloading, and repeated loading cycles within practical requirements, the diaphragm should be designed so that the deflection to pressure ratio is less than 1×10^{-5} in./psi. If this condition is satisfied, maximum deflection-to-diameter ratio is 1:2000. It was also reported that the measurements of pressures in clay fills appear to present far less difficulty than similar measurements in sands and

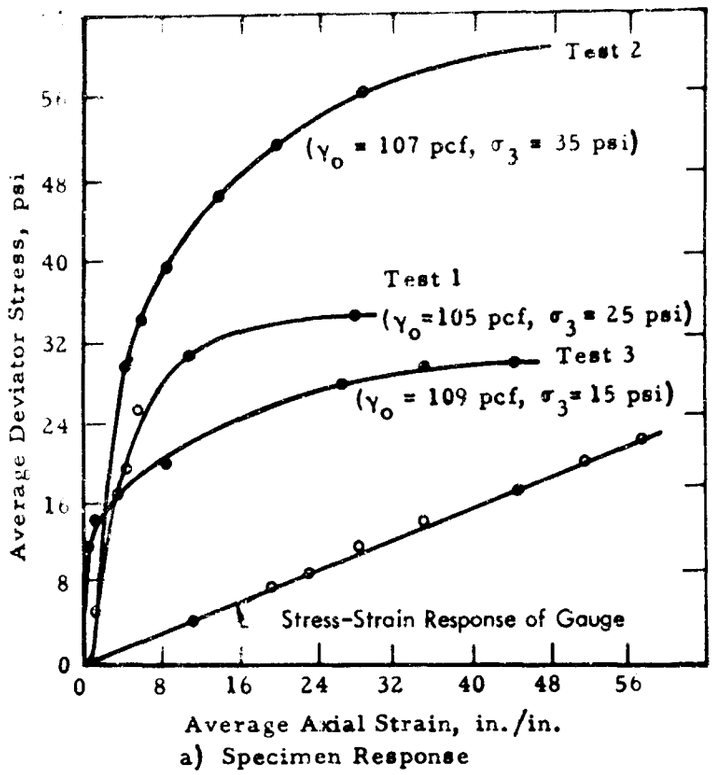
gravels.

Some tests were made by the writer (20) to determine the response of a gauge whose stiffness was much less than that of the soil. The gauge consisted of a 1 in. diameter, 1 in. long cylinder of urethane rubber molded around a small foil strain gauge, parallel to the axis of the cylinder. The gauge was evaluated using a conventional, soil triaxial chamber by embedding it in a 3 in. diameter cylinder of dry sand confined under a hydrostatic pressure. As an axial load was applied to the sand specimen the average axial stress and strain were measured together with the output of the gauge.

The average axial stress-strain curves for the sand specimen under three different conditions of density and confining pressure are shown in Figure 5a together with the stress-strain response of the soft rubber material under uniform pressure (when not embedded). The specimen response is very non-linear and the slope of the stress-strain curves is much greater than the modulus of the gauge material except near failure.

The gauge readings from these same tests are shown in Figure 5b. The output of the gauge for a given axial stress was considerably less embedded than for the same uniform stress applied directly to the gauge, i.e., there was considerable under-registration. The discrepancy decreased as the slope of the specimen stress-strain curve approached the modulus of gauge material. The point at which the two agree may be seen in Figure 5b. Beyond this point the gauge indicated a stress higher than the average specimen stress, i.e., over-registration.

A correlation of the output of the gauge with average specimen strain showed that this gauge responds roughly in proportion to specimen strain. Hence, only when the specimen stress is proportional to its strain will this gauge respond in proportion to stress. But since the under-registration is also a function of the value of the modulus and since this modulus differs for each condition of density and confining pressure, then the gauge can still not be used, in general, because a different calibration curve would be required for each situation.



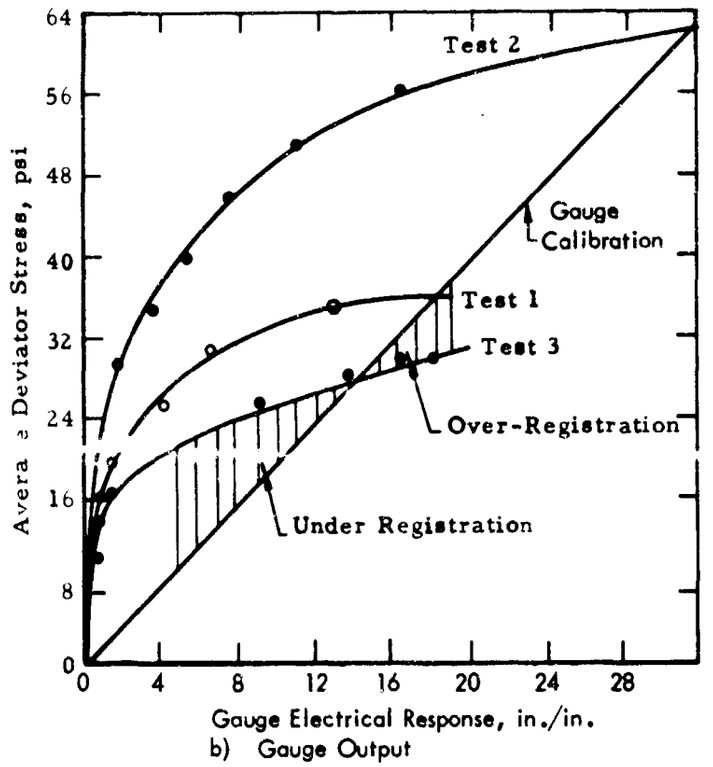
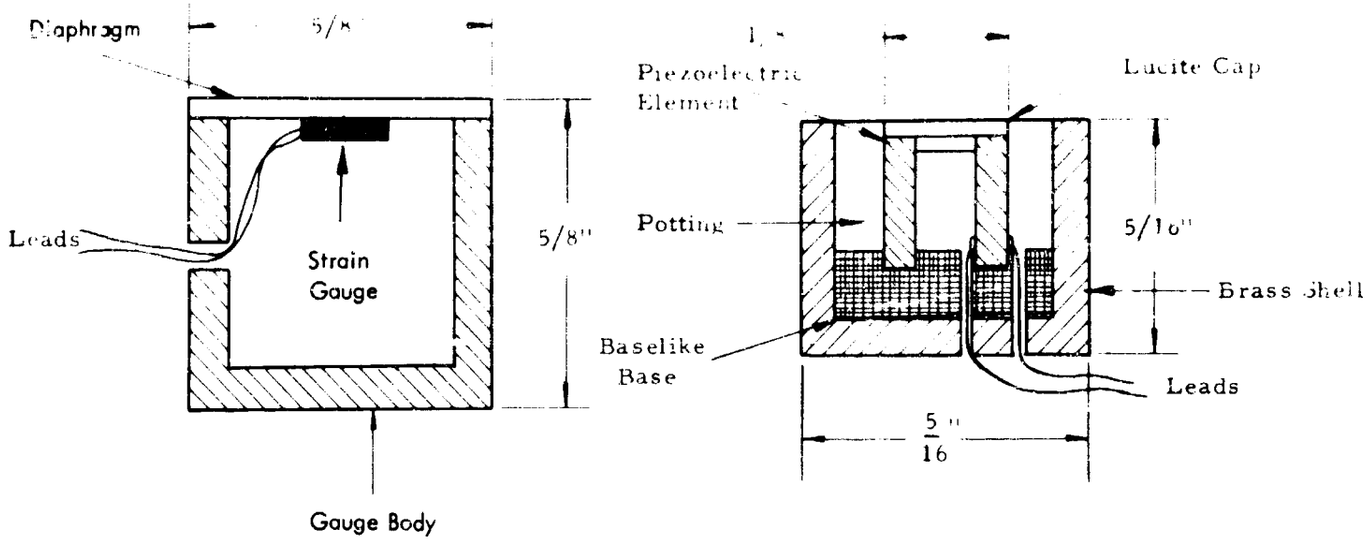


Fig. 5 Results of Tests on Soft Gauge (20)

A preliminary investigation of a small laboratory soil stress gauge was conducted (21) to determine the influence of various factors on stress measurement with embedded gauges. Two types of gauges were used, one a diaphragm type using a strain gauge transducer and the other a piezoelectric gauge (Figure 6). Both were cylindrically shaped with a T/D ratio of approximately one. The gauges were first calibrated under uniform air pressure and then embedded in soft rubber cylinders used to simulate the soil. The rubber was essentially linearly elastic in its response and it was formed around the gauge in a liquid state. Thus, both the effects of non-linear soil-gauge interaction and the placement problems were circumvented in this study.

Under static loading the diaphragm gauge showed an over-registration of about 40 per cent; under dynamic loading it was about 80 per cent. The difference between the static and dynamic results was attributed to viscoelastic behavior of the rubber. The presence of the stress concentration in the vicinity of the gauge was further illustrated by varying the



(a) Diaphragm-type

(b) Piezoelectric

Fig. 6 Preliminary ARF Stress Gauges (21)

length and diameter of the rubber specimen and the rigid loading plate. The over-registration of the gauge was found to decrease as the modulus of elasticity of the rubber was increased.

The over-registration of the piezoelectric gauge under dynamic load was about 40 per cent. No information is available on its response to static loads. The smaller over-registration for the piezoelectric gauge compared to the diaphragm gauge may be because the sensitive area of the former is restricted to the center of the gauge face, while for the diaphragm gauge the entire gauge face is sensitive to pressure.

Small disk-shaped piezoelectric stress gauges (1/2 in. dia by 1/32 in. thick) have been developed at United Research Services (22) to measure dynamic stresses in a confined column of sand. Preliminary studies of these gauges in sand indicate that the over-registration is small so that uniform pressure calibrations may be used to compute stress. The total range of data scatter including the effects of placement appears to be about $\pm$ 20 per cent. The uncertainty arises because, as a result of attenuation of stress along the length of the column, only the stress at the sand boundary is accurately known. Gauge placement was accomplished by pressing lightly on the gauges to seat them on a leveled cross section of sand at the desired depth before additional sand was added.

An extensive investigation of soil stress measurement was made at IIT in connection with a study of stress wave propagation (23). The gauges considered all utilized a piezoelectric ceramic transducer as the sensing element with a number of variations in the thickness-to-diameter ratio and methods of encasing the gauge.

The advantages of the piezoelectric transducer are 1) its short response time (microseconds) making it especially suitable for shock type loading, 2) the small size crystal possible, 3) the high electrical sensitivity and 4) high stiffness (about the same as aluminum for the gauges used in this study). But aside from the inherent difficulties of stress measurement with any type of gauge, the use of these transducers introduced other experimental problems. These were, principally, extreme sensitivity to electromagnetic radiation, temperature, and moisture. The piezoelectric ceramics are also sensitive to any impressed distortions which result from the way in which the stress from the soil is applied to the gauge. They are, therefore, sensitive to mounting and method of placement and to the manner in which the sensing element is isolated from the soil. For example, shearing stresses on the face of the transducer as well as bending moments will produce appreciable signals. The piezoelectric transducer acts as an electrical charge generating device. Because of the resistance-capacitance characteristic of the electrical circuitry, extremely high circuit resistance is required in order to measure stresses of greater than a few seconds duration and this required resistance is difficult to obtain.

The gauges studied had thickness-diameter (T/D) ratios varying from 1.0 to 0.08 with a maximum gauge diameter of 1.0 in. (23). One basic configuration of a cylinder of barium titanate mounted in a small metal cup similar to the gauge shown in Figure 6b. This gauge had been designed and constructed for use in measuring air shock pressures. The other gauges were constructed from disk-shaped piezoelectric elements (Figure 7). These gauges were constructed with and without a metal edge ring to isolate the element from the effects of lateral pressure, and with and without a teflon face covering to isolate the effects of friction on the face of the gauge. In some cases the unmounted ceramic crystals

were coated with moisture-proof materials such as epoxy.

The cylindrically-shaped N-gauge did not perform satisfactorily for measuring stress in sand. The embedded gauge sensitivity (or calibration factor) varied significantly with specimen confining pressure, sand density, stress level, and repeated loading. The gauge was also quite sensitive to placement conditions. As a result the gauge could not be calibrated so that its output could be used to reasonably predict the true stress in sand specimens.

The factors contributing to the gauge's deficiencies were that 1) the stress sensing element was not sufficiently larger than the grain size of the sand, 2) the thickness-diameter ratio was too large, and 3) the location of the electrical leads created placement difficulties. It is believed that some of these problems would be less significant in compacted clay specimens.

A disk gauge was designed to eliminate the undesirable features of the N-gauge. The sensitive area was increased, the thickness-diameter ratio was decreased and the leads were attached to the side of the gauge to simplify placement.

The sensitivity of the disk gauge was much less influenced by such factors as confining pressure, density, and placement, but these effects were still significant. The evaluation of over-registration could only be qualitative because of the large variation in values for the embedded calibration. It was observed that for stress levels well below specimen failure there was, of course, 30 per cent over-registration for the embedded gauge protected with an edge ring and a teflon covering. Without the teflon the over-registration was about 100 per cent, and without either the teflon or the edge ring the over-registration was about 200 per cent. The significant over-registration in the latter two cases was a characteristic of the gauge construction since the piezoelectric ceramic was sensitive to friction across its face and pressure on the edges. It is apparent, then, that the largest observed over-registration can be eliminated by suitable gauge design.

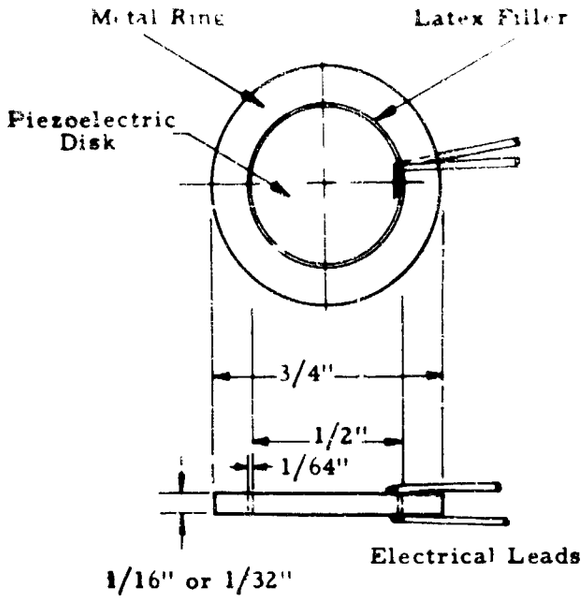


Fig. 7 Piezoelectric Disk Stress Gauge (23)

The gauge calibration curves were linear for stresses well below specimen failure, but the sensitivity increased as the failure stress was approached. The gauge response was linear, in general, only when the soil stress strain relationship was linear. Thus, a change in the soil stiffness had an appreciable effect on the gauge response whether caused by a change in confining pressure, density or by the normal stress level. This was found to be true even though the gauge stiffness itself was very high compared with that of the soil. As a consequence of this effect, the gauge calibration curves showed appreciable hysteresis for stresses near specimen failure. Also as a result the gauge performance was much better in confined specimens than in triaxial specimens. It is evident that even though the gauge stiffness was much greater than the soil stiffness (by a factor of 200 or more) a change in soil stiffness still affected the gauge response.

Gauge placement was another significant factor which affected gauge response and accounted for a significant variation in the response even though all other conditions were constant. Variations due to placement of up to ± 50 per cent were observed.

The static and dynamic sensitivities of the disk gauges were identical, but showed a ± 10 per cent variation when used in specimens having a wide range of confining pressures and densities.

It was clear from this investigation that a more elaborate piezoelectric stress gauge design is required to isolate the sensing element from the undesirable influences. The gauges used in the study were clearly affected by a complex set of circumstances as a result of their particular design features. This makes generalization of the conclusions to other gauge designs subject to some question. The study has indicated the problems involved in stress measurement with piezoelectric sensors. As a result of this information a more elaborate stress gauge has been designed which appears to give superior performance to the more simple versions. Extensive evaluation of the new gauge is currently underway.

SOIL STRAIN MEASUREMENT

Much less information is available on the performance of soil strain gauges than soil stress gauges. In the majority of studies in which strains in soil have been determined the gauge has consisted of some type of device to measure the change in spacing between two points in the soil to which it is attached. Most concepts have involved two reference points physically coupled with a displacement transducer. The physical connection required between the gauge points causes interference with movement of the soil in the region between these gauge points and complicates the placement of soil around the gauge.

It is generally considered that a suitable strain gauge should meet the following requirements (12, 20): 1) there should be a satisfactory means of attaching the gauge to the soil, and 2) the gauge should freely follow the soil movement, which means, in part, that the stiffness of the gauge should be as small as possible and the density of the gauge components should be about the same as that of the soil. Placement is one of the biggest problems with strain gauges since the gauge will only respond to the strain of the soil immediately surrounding it.

A gauge with a short base length (apparently about 6 in.) was developed by Sandia Corporation (12) for use on the Tumbler-Snapper field tests. It consisted of a telescoping tube with a disk attached to each end. A differential transformer within the tube measured the relative displacement of the disks. The principal proved satisfactory but the electromagnetic pulse from the blast caused too much interference to obtain suitable strain records. After modification the gauge was used on Upshot-Knothole and Teapot with better results.

From Plumbbob, SRI used linear differential transformers to measure relative displacements between two anchors 2 or 3 ft. apart. These were set into the side of a large hole before backfilling (25). Problems were encountered with electrical shorts in the cables thus no conclusions were reached regarding the performance of the gauge.

A tube-shaped strain gauge with no projecting end disks has been under development by SRI (26). The two end pieces are connected by sylphon bellows of the same outside diameter. The purpose of the bellows is to permit movement of the ends with little resistance while providing lateral support for the interior. Inside the bellows is a linear differential transformer for measuring the relative displacement of the ends. The entire gauge is encased in a plastic sleeve to keep the ends at the proper spacing during placement. The gauge is designed for installation in small diameter holes to measure the strain in the direction of the axis of the hole. It is suspended at the proper depth and cemented in place with a grout intended to be as stiff as, or less stiff than, the surrounding ground.

For those tests in which the strain measurements have been made in rock generally wire resistance strain gauges have been embedded in cast cement cylinders (27) or on the surface of rock cores taken from the parent material. The cores are then grouted into drilled holes in the rock.

The general procedure used for placement of short-span strain gauges in prepared holes, other than by grouting, involves recompacting the soil. Moistened and screened soil similar to that removed from the hole is carefully hand-tamped around the gauge for a depth of about one foot above the gauge (12). The remainder of the field is usually tamped mechanically.

Measurements of soil strains and displacements have been made at WES in connection with the previously described studies of stresses in soil due to applied surface loads (9). Selsyn motor-type gauges were constructed for measuring the relative movement between points on the surface and points in the soil at various depths. The core of a linear differential transformer was attached to one end of a rod and a circular disk to the other. A second disk was centered on the transformer coil. The assembled gauge had a base length of 10 in. These gauges were used only in sand; the method of placement was basically the same as used for stress gauges.

The reproducibility and consistency of the readings obtained with the strain and displacement gauges are given in Tables 1 and 2. Neither the strain nor deflection gauges performed as well as the pressure and shear cells. It was suggested in the discussion of the stress gauge results that the errors due to placement are probably on the order of the difference between consistency and reproducibility. A comparison of Tables 1 and 2 shows that, for each case represented, the consistency is about twice reproducibility, hence the errors due to placement may be about the same magnitude as the reproducibility. Thus, for the strain and displacement gauges the placement effects would be about ± 42 per cent and ± 15 per cent respectively. The considerable effect, especially pronounced for the strain gauges, may be the result of the relatively small values of strain which occur in a compacted sand fill.

Field tests in which strains were measured in the soil produced by static surface loads and by vehicles moving over the ground surface have been conducted at IITRI (28). The gauges developed for this study also used an iron-core differential transformer, but in a miniaturized version. The transformer housing was 3 in. long and 3/8 in. in diameter; the gauge length was 6 in. Differential displacements of the two ends of the gauge as small as 0.0001 in. could be detected over a range of 1/2 in. However, transverse and rotational movements of the core inside the coil could produce response corresponding to longitudinal displacements of 0.0001 in., hence the gauges could not be relied upon for such small movements.

The gauges were specially designed for embedding in natural soil deposits with as little disturbance as possible. Two different configurations were used (Figure 8), one for vertical orientation and the other for horizontal orientation, the difference being based upon the method of placement. Each end of the gauge for vertical displacements was coupled to the soil by an auger which was screwed into a pilot hole drilled into the soil. The ends of the horizontal gauge were coupled to the soil by stakes which were pressed into the bottom of a narrow vertical slot cut into the soil. In some tests, after the gauges were placed, the holes were backfilled with soil compacted to the same penetration resistance. In other tests the holes were left unfilled.

The response of two gauges as a function of static surface pressure is given in Figure 9. The horizontal gauge did not begin responding to the load immediately, indicating some small slack in the coupling. It is very difficult to place these gauges in soil, especially the horizontal ones, such that slack in the system is less than a few ten thousandths of an inch. The nonrecovery of the displacement upon loading, shown in Figure 9, is believed entirely a function of the soil

hysteresis.

A comparison of the response of sets of gauges located in identical positions with respect to the load showed an average variation of ± 23 per cent. These values primarily reflect both the effect of placement and the nonhomogeneities in the soil. However, it is expected that an appreciable part of this is due to placement. Within this data variation no differences were observed between the condition where the gauge holes were backfilled and where they were not.

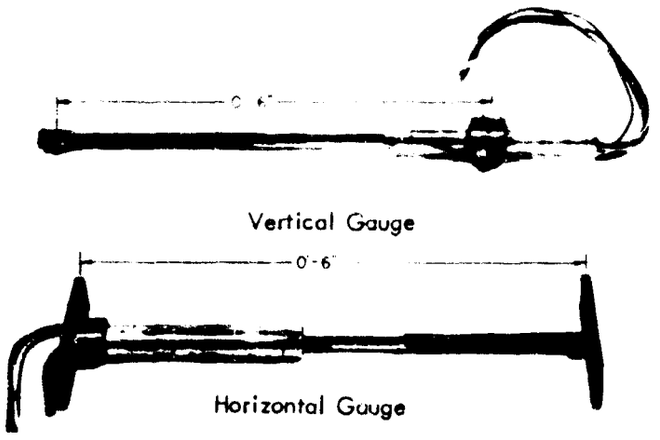


Fig. 8 IITRI Field Strain Gauges (28)

The development of an electrically coupled laboratory soil strain gauge was undertaken at IITRI (29,30) in an attempt to overcome some of the limitations of the previous gauge designs. A schematic of the gauge is shown in Figure 10. The gauge, itself, consists of four coils, two pairs in the soil and two on an adjustable micrometer mount. A detailed description of this gauge and the results of laboratory evaluation of it are contained in another paper in this symposium (31). The gauge gives promise of being a valuable tool for soil mechanics research. Further development is underway to adapt the gauge concept for field application.

SUMMARY

Previous experience with stress and strain measurements in soil has been reviewed. It is generally believed that soil stress is a very difficult measurement to make accurately, especially in the field. The most important factor effecting stress gauge response is the difference in stiffness between the gauge and the soil. The influence of this factor is significantly effected by placement conditions and gauge geometry, and is not a constant because the soil stiffness is variable.

It is evident from the past experience with stress gauges that considerable technique is involved in obtaining reliable soil stress measurements. On the basis of information available to date to appears that:

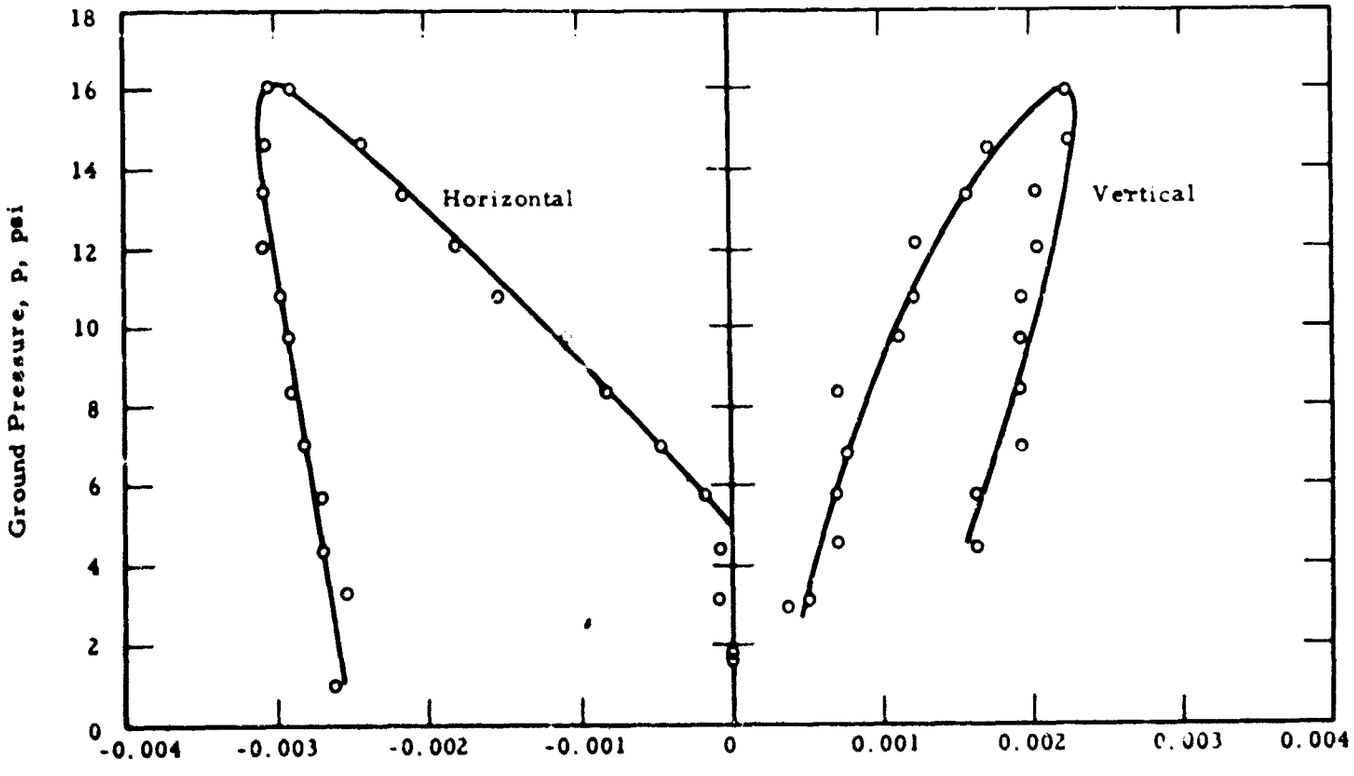


Fig. 9 Representative Strain Gauge Displacement Response in Silty Clay (28)

1. the thickness-diameter ratio of the gauge should be kept as small as possible,
2. the ratio of gauge stiffness to soil stiffness should be kept as large as possible,
3. the gauge design must take into consideration methods of placement, and
4. under ideal conditions the gauge can be expected to read the true stress within ± 10 per cent, but in the field ± 25 per cent is a more realistic estimate.

Conceptually, soil strain is easier to measure because the gauge ideally should not have any stiffness and hence should deform as the soil. However, strain gauges are generally more difficult to place because of their configuration and their presence does often constrain the soil locally. For many applications the magnitude of strains to be detected border on the precision of the gauge. For these reasons the overall accuracy of strain measurement is probably no better than stress measurement.

Although the measurements of stress and strain in soil present very difficult problems, efforts to solve these problems are to be encouraged. The attaining of such information on soil response promises to greatly assist in understanding the many complex soil-structure interaction problems.

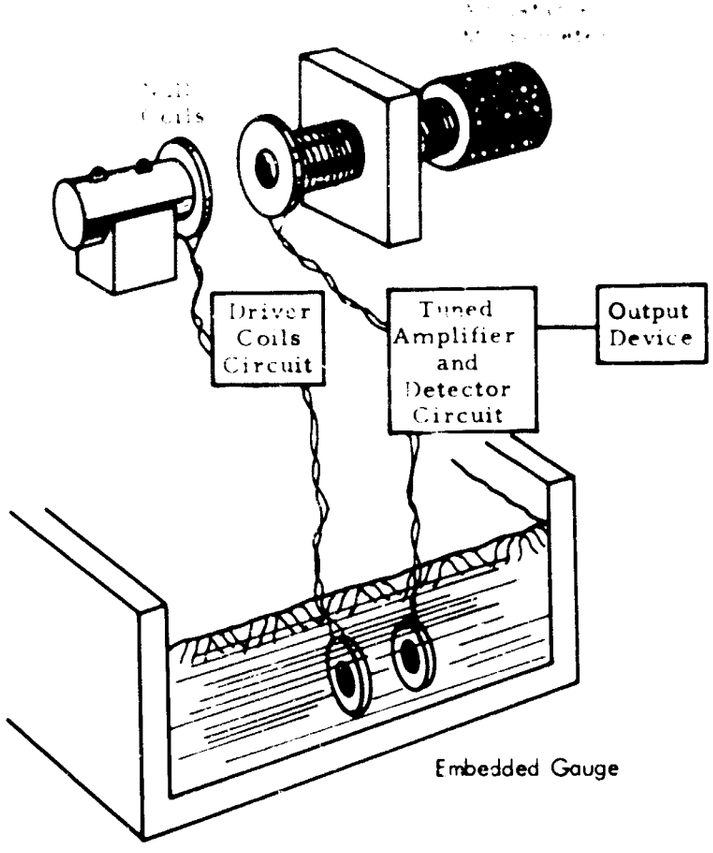


Fig. 10 IITRI Coil Strain Gauge (29)

ACKNOWLEDGEMENTS

The material for the review contained in this paper was primarily obtained in the course of research at the Illinois Institute of Technology sponsored both by the National Science Foundation and by the Air Force Weapons Laboratory, Kirtland Air Force Base, New Mexico. The support of this research by these agencies is gratefully acknowledged.

REFERENCES

1. Goldbeck, A. T. and E. B. Smith, "An Apparatus for Determining Soil Pressures," Proceedings, American Society for Testing Materials, Vol. 16, No. 2, pp. 310-319, 1916.
2. Hamilton, J. J., "Earth Pressure Cells-Design, Calibration and Performance," Tech. Paper No. 109, Division of Building Research, National Research Council, Ottawa, Canada, November 1960.
3. Benkelman, A. C. and R. J. Lancaster, "Some Important Considerations in the Design and Use of Soil Pressure Cells," Public Roads, Vol. 21, No. 12, p. 235, February 1941.
4. Corps of Engineers, U.S. Army, "Soil Pressure Cell Investigation, Interim Report," Waterways Experiment Station, Vicksburg, Mississippi, 1944.
5. Whiffin, A. C., "The Pressures Generated in Soil by Compaction Equipment," Symposium on Dynamic Testing of Soils, ASTM Special Technical Publication No. 156, pp. 186-210, 1954.
6. Whiffin, A. C. and S. A. H. Morris, "Piezoelectric Gauge for Measuring Dynamic Stresses Under Roads," The Engineer, pp. 3-7, April 1962.
7. McMahon, T. F. and E. J. Yoder, "Design of a Pressure-Sensitive Cell and Model Studies of Pressures in a Flexible Pavement Subgrade," Proceedings, Highway Research Board, Vol. 39, pp. 650-582, 1960.
8. "Stress Distribution in a Homogeneous Soil," Research Report No. 12-F, Highway Research Board, Washington, D.C., January 1951.
9. "Investigations of Pressures and Deflections for Flexible Pavements," Report No. 4, Homogeneous Sand Test Section, Waterways Experiment Station, Tech. Memo No. 3-323, December 1954.

10. "Stresses under Moving Vehicles," Waterways Experiment Station Report for [illegible], U.S. Army Engineer Waterways Experiment Station, Vicksburg, Mississippi, May 1960.
11. Bernard, R. F., Biaxial Stress Fields in Noncohesive Soils Subjected to Vibratory Loads, American Society for Testing and Materials, STP 305, Symposium on Soil Dynamics, 1961.
12. "Nuclear Geophysics, Part Three-Test Sites and Instrumentation," prepared for the Defense Atomic Support Agency by Stanford Research Institute, February 1962.
13. Goode, et al, "Soil Survey and Backfill Control in Frenchmen Flat," Waterways Experiment Station Report for Operation Plumbbob, WT-1427, November 1957.
14. Mason, H. and C. M. Wolfe, "A Soil Filled Soil Stress Gauge," Bulletin No. 28. Part III, Shock, Vibration and Associated Environments, Office of the Secretary of Defense, Research and Engineering, Washington, D.C., pp. 87-89, September 1960.
15. Taylor, D. W., "Pressure Distribution Theories, Earth Pressure Cell Investigations and Pressure Distribution Data," U.S. Army Waterways Experiment Station, Vicksburg, Mississippi, 1947.
16. Monfore, G. E., U.S. Department of Interior, Bureau of Reclamation (Res. and Geol. Div.) Research Laboratory Report No. S. P. 26, 1950.
17. Peattie, K. R. and R. W. Sparrow, "The Fundamental Action of Earth Pressure Cells," J. Mech. and Phys. of Solids, Vol. 2, pp. 141-155, 1954.
18. Buck, G. F., "An Interim Report on the Cell Action Studies Connected with Research on Pressure Measurements in Sand," Proceedings, Midland Soil Mechanics and Foundation Engineering Society, Vol. 4, pp. 95-105, 1961.
19. Trollope, D. H. and I. K. Lee, "The Measurement of Soil Pressures," Proceedings, 5th International Conference on Soil Mechanics and Foundation Engineering, Vol. II, pp. 493-499, 1961.
20. Selig, E. T., "Detection of Transient Stresses and Strains in Soil," Proceedings, Symposium on Detection of Underground Objects, Materials and Properties, Ft. Belvoir, Va., pp. 163-190, March 1962.
21. Durelli, A. J. and W. F. Riley, "Performance of Embedded Pressure Gauges under Static and Dynamic Loadings," American Society for Testing and Materials, STP 305, Symposium on Soil Dynamics, pp. 20-37, 1961.
22. Mason, H.,et al, "A Further Study of Stress Wave Transmission," United Research Services, Interim Report for DASA, URS-160-12, February 1963.
23. Selig, E. T. and E. Vey, "Piezoelectric Gauges for Dynamic Soil Stress Measurement," Proceedings, 43rd Annual Meeting, Highway Research Board, January 1964.
24. Selig, E. T., "Shock Induced Stress Wave Propagation in Sand," unpublished Ph.D. thesis, Illinois Institute of Technology, Chicago, Illinois, January 1964.
25. Swift, L. M. and D. C. Sachs, et al, "Ground Acceleration, Stress and Strain at High Incident Overpressures," SRI, Operation Plumbbob, WT-1404, May 1960.
26. Swift, L. M., "Development of Soil Displacement and Strain Gauges," Final Report prepared by SRI for DASA, 1961.
27. Anthony, M. V., "Ground Motion Measurements," ERDL, Project 26.3, Operation Hardtack-II, ITR-1704, February 1959.
28. Selig, E. T., K. E. Hofer and N. A. Weil, "Elastic Response of Soil to Tracked Vehicles," Proceedings, 1st International Conference on the Mechanics of Soil-Vehicle Systems, Turin, Italy, pp. 97-107, June 1961.
29. Truesdale, W. B., "Development of a Small Soil Strain Gauge," Final Report for Air Force Special Weapons Center, Albuquerque, N. M., AFSC-TR-63-3, December 1962.
30. Keller, R. W. and M. E. Anderson, "Development of a Soil Strain Gauge for Laboratory Dynamic Tests," TDR-64-7, Final Report for Air Force Weapons Laboratory, Kirtland Air Force Base, New Mexico, April 1964.
31. Truesdale, W. B., "A New Device for Soil Strain Measurement," Soil-Structure Interaction Symposium Session 2 (included in this volume).

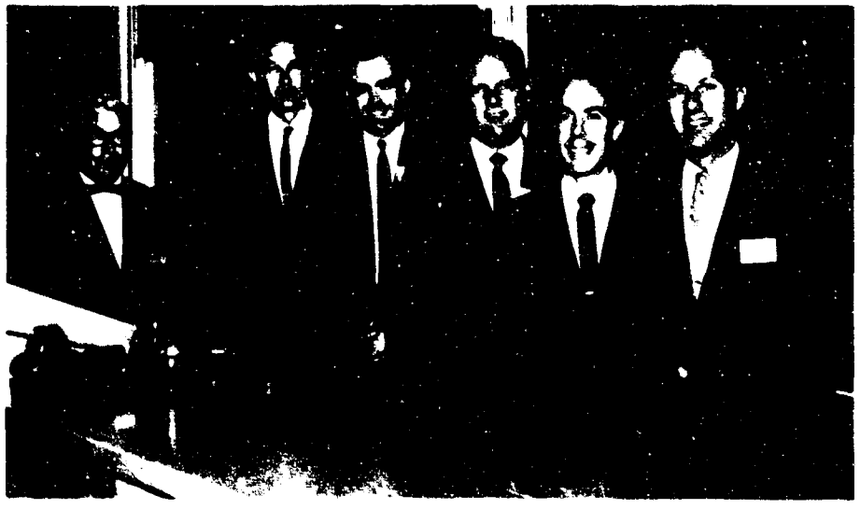
SESSION FOUR–TUESDAY PM

STATE OF THE ART

SESSION CHAIRMAN: GUY L. ARBUTHNOT

TABLE OF CONTENTS

	page
THE BEHAVIOR OF SHALLOW-BURIED CYLINDERS, Jay R. Allgood	189
BURIED TUBES UNDER SURFACE PRESSURE, P. S. Bulson	211
REVIEW OF SOIL-STRUCTURE INTERACTION, Carl K. Wiehle	239
STRUCTURAL DESIGN TRENDS IN BURIED FLEXIBLE CONDUITS, Reynold K. Watkins	246
A STUDY OF LOADS ON UNDERGROUND STRUCTURES, D. A. Van Horn	256



Participants in Session Four were, left to right, Guy L. Arbuthnot (Session Chairman); J. R. Allgood; D. A. Van Horn; P. S. Bulson; R. K. Watkins; and C. K. Wiehle.

THE BEHAVIOR OF SHALLOW-BURIED CYLINDERS

by
Jay R. Allgood*

INTRODUCTION

In designing shallow buried shelters one is usually concerned with loads in the range of 25 to 500 psi. Such loadings are, of course, much larger than those encountered in normal culvert and buried pipe design and are dynamic rather than static. These basic differences give rise to the need for an extension of the knowledge of soil-structure interaction and for development of improved methods of analysis.

To understand dynamic response it is almost axiomatic that the static behavior must first be understood. A logical route to comprehension, then, would seem to be to draw upon the accumulated knowledge of such fields as the static behavior of buried culverts and the buckling of cylinders in a hydrostatic field and to extend this information as necessary to solve the blast response problem.

This paper represents an effort to synthesize available information to gain an improved understanding of the behavior of shallow buried cylinders whose axes are parallel to the ground surface, as indicated in the sketch in Figure 1, and to define specific areas where further research is needed. The treatment is limited to thin metal cylinders in a granular non-cohesive soil field. Particular attention is given to the arching and buckling phenomena and in these areas extensions to available knowledge are offered.

In the following paragraphs, the status of culvert design and the predominant experimental work are reviewed. Then, the status of applicable buckling theory is given. Thereafter, the known aspects of static behavior are discussed to provide the basis for a limited treatment of dynamic response.

ANALYSIS OF PROBLEM

It is known from long experience that thin metal cylinders buried in earth have the capacity for resisting large surcharge and surface live loads. This is possible because of resistance provided by the confining earth media. The exact nature of the interaction has not been well understood; however, from the studies that have been performed, the dominant parameters are known to be those associated with 1) system geometry, 2) type of loading, and 3) structure and media properties. Those associated with geometry are the diameter to thickness ratio, the length to diameter ratio, the depth of cover over the crown to diameter ratio, and the depth of soil to bedrock. In addition to these parameters, it is known that the initial shape of the structure after backfill has an influence on the load capacity. As to the loading parameters, one must, of course, know whether the loading is static or dynamic. If it is a blast loading, one should know the ratio of the rise time to the natural period of the buried structure, the ratio of the positive phase duration to the natural period and the peak side-on overpressure. It also is important to know the orientation of the wave front with respect to the longitudinal axis of the structure. Likewise, one must know the velocity of the blast wave and the seismic velocity of the soil media to determine the angle of incidence of the soil stress wave to the ground surface. Structure and media physical properties of dominant concern are the structure stiffness, the moduli of vertical and horizontal soil reaction, and the soil properties affecting these moduli including the angle of friction, the density, and the cohesion. Absolute and relative densities of the bedding and backfill soil are exceedingly important--soft bedding permits developing arching, dense compaction at the sides enables the activation of large passive-sense pressures in the soil at small deflections. The influence of the cited parameters and the characteristics of failure of buried cylinders will become more apparent in subsequent discussion.

Failure of buried cylinders can occur in several possible modes including buckling, excessive deformation, joint failure, compression yielding of the tube material, and end wall collapse. What constitutes excessive deflection depends on the function of the structure. Large relative motions between a personnel shelter and the free field may result in rupture of fuel, water, and sewer lines. Control of relative deformations, obviously, is as important as assuring against buckling.

Until recently it was not acknowledged that failure could occur by buckling; yet, for the high overpressures induced by nuclear weapons, buckling is a highly probable mode of failure. The load at which buckling occurs is directly dependent on the amount of arching that occurs in the soil bridge across the structure.

Actually, little is known of buckling, arching, or other aspects of the interaction phenomenon. Part of the difficulty in comprehending the phenomenon is due to lack of knowledge of soil properties, including lack of data on the influence of surcharge pressure on the moduli of soil reaction. Without this information or knowledge of the pressure distribution around the buried cylinder it is difficult to analyze the structure.

*Structural Research Engineer, Structures Division, U. S. Naval Civil Engineering Lab, Port Hueneme, California.

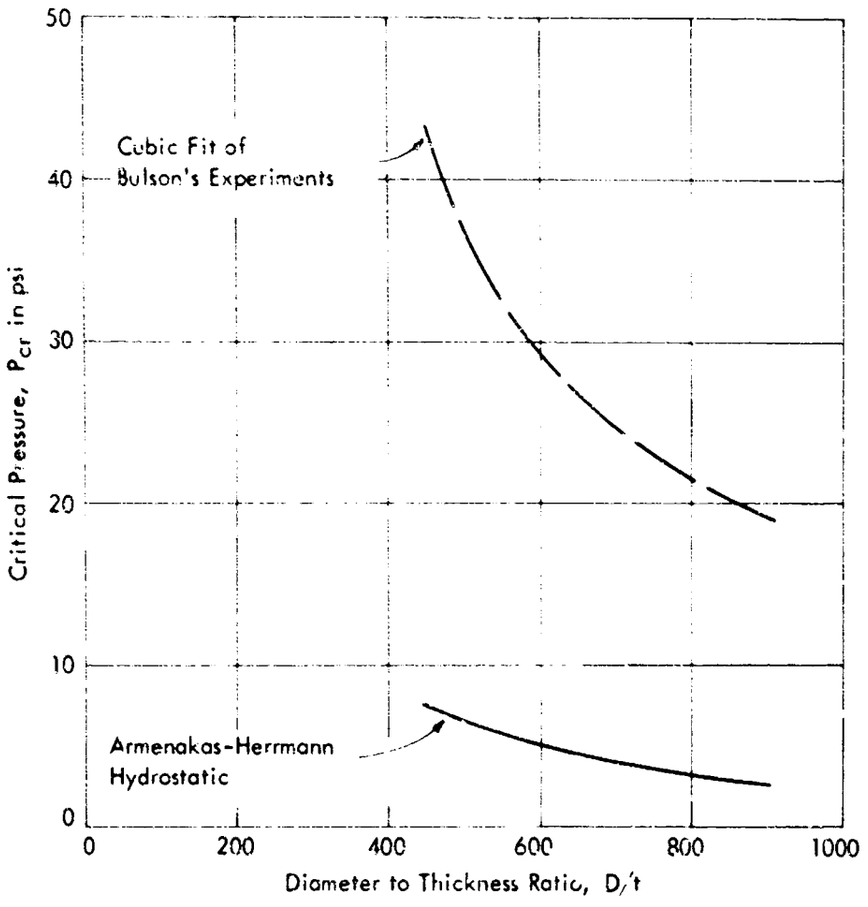


Fig. 1 Buried Cylinder Failure Load

From the preceding, one can deduce that these five items, body deflections relative to the free field, moduli of soil reaction, interface pressure distribution, buckling, and arching constitute the major unknowns and present the challenge to comprehension that is the goal of this paper. These facets of the problem will be examined following a review of previous work.

REVIEW OF PREVIOUS WORK

Status of Culvert Design

One of the more widely known methods for the design of flexible culverts is due to Spangler and his proteges and is based on limiting the horizontal deflection to an acceptable value (1). A common criteria is that the horizontal deflection shall not exceed 5 percent of the nominal diameter. This is based on the observation that the vertical crown deflection that causes collapse is about 20 percent of the nominal diameter (2). The Spangler equation, sometimes referred to as the Iowa Formula, is utilized later in this paper.

Another widely used semi-empirical method developed by Barnard attempts to define the deformation and the failure load. Barnard's development is based on the membrane method and presumes that failure occurs when the compressive stresses exceed the yield stress. The method ignores bending moments and the possibility of buckling (3).

A more elementary method, recommended by one of the largest suppliers of culverts, is the so-called ring-compression method (33). It involves treating a culvert as a pure compression ring to assure that the wall and seam strength are adequate and then making a check to determine if the stiffness is larger than a given minimum which experience has shown will insure against buckling failure.

Recently, Meyerhof and his colleagues have developed an improved design method that treats buckling in a rational way (4,32). The method is based on observations of a series of curved plates bearing against soil. Meyerhof contends that, "Experience with culverts has shown that their flexural rigidity governs mainly the installation stages and compaction of the backfill, and the compressive strength of the culvert governs its behavior under the working load." Meyerhof and Baike have proposed an equation for the stress at buckling which allows for accidental geometric irregularities (4).

Experimental Evidence

Bulson has performed static tests on small steel tubes 5 to 10 inches in diameter with diameter to thickness ratios of 454 to 909 and length to diameter ratios of 1.2 and 2.4 (5). The tubes were sheet steel 0.011 inches and 0.015 inches thick and were buried in a dry well-compacted sand. Measurements consisted entirely of applied load and radial deformation of the intrados of the tubes.

Bulson found that it was possible to express all of his results in the form of a single empirical equation. The equation, however, has several deficiencies, among which are that it contains no term to account for the soil modulus and contains the unlikely condition that the collapse pressure is inversely proportional to the cylinder length.

Less extensive experimental data but enlightening analyses have been made available by Luscher and Whitman (6,7). These investigations were on one-inch inside diameter sand cylinders, one-inch diameter thin aluminum cylinders, and a concentric aluminum sand cylinder system. A few cellulose acetate tubes also were included in the program. Measurements in these tests consisted primarily of inside and outside applied pressures and changes in volume of the inside of the cylinders. Analysis included consideration of the limiting equilibrium condition of a soil ring, buckling of a cylinderical shell, approximate interaction and arching analysis, mathematical analysis of a lined elastic ring, and buckling of an elastically supported ring. Luscher's tests showed that for relatively incompressible metal tubes very little arching was present; however, for the more compressible plastic tubes effective active arching was mobilized in the soil. In addition, it was found that the experimental data correlated reasonably well with the theory for buckling of an elastically supported ring. To achieve this the modulus of soil reaction appearing in the buckling theory was related to the geometry and material properties of the soil ring. The greatest difficulty encountered was in defining the soil moduli. It was found that the critical tube flexibilities where the failure mode changes from buckling to compressive yielding could be approximated, thus defining the boundary of the two modes of failure.

Experimental and theoretical results have been published by Watkins (8,9,10) showing, among other things, that the ring stiffness of a conduit has a minor influence on the horizontal deformations of a thin buried cylinder.

Rather extensive static (34) and traveling-blast load tests on buried tubes have been performed at the University of New Mexico, Kirtland Air Force Base Shock Tube Facility. The static experiments are described elsewhere in this publication.

More limited experiments on cylinders have been conducted at a number of other institutions and at the Nevada Test Site, including non-destructive tests at the Navy Civil Engineering Laboratory. Certain of the data from the latter tests will be included as a part of the discussion to follow.

Theoretical Contributions

To understand the behavior of confined cylinders it is helpful to utilize information from the hydrostatic theory in addition to that from the theory of cylinders in an elastic media. The hydrostatic theory will be a lower limit for buckling should the soil become saturated. Both the hydrostatic and elastic media theories are important in giving one an appreciation of the nature of the buckling problem. One of the first theoretical treatments of cylinders loaded radially was due to Southwell, (12) who showed that a tube would deform into a characteristic number of circumferential waves.

An important recent contribution to hydrostatic theory has been made by Armenakas and Herrmann who reviewed the buckling problem, cited errors in the classical solutions, and from their precise analysis developed simplified equations for the buckling load (13). They have re-emphasized that in elastic behavior a cylinder deforms into a characteristic number of circumferential waves, that the critical buckling pressure is a function of the length of a cylinder, of Poisson's ratio, of the ratio of longitudinal to circumferential shell stress, and of the thickness to diameter ratio. Their charts for determining the number of circumferential waves will be useful later in this paper and are included here as Figures A1 and A2 of Appendix A. Plots of the Armenakas-Herrmann equation for the case of zero initial uniform longitudinal shell stress are included as Figures A3 and A4. More complete plots are given elsewhere (35). As one would expect, the hydrostatic buckling equation does not agree with the experimentally determined load to produce buckling of buried cylinders as may be seen in the comparison of Figure 1. The Armenakas-Herrmann equations are for end conditions where the radial and circumferential displacements are zero and where the forces and moments normal to the original end planes are non-resistant. In practice this is achieved by using deep thin annular edge rings. Langhaar and Boresi have presented solutions, tables, and charts for the cases where the ends are simply supported, rigid, and free to warp out of their planes (28).

Hetenyi has investigated the problems of an elastically supported arch and cylinder. He gives equations for deflection, moment, shear, and thrust corresponding to various boundary conditions but not for the critical buckling load (14). A solution for the buckling load of an elastically supported cylinder subjected to hydrostatic pressure has been obtained by Czerwenka (15) and others (38). (Also see the bibliography to reference 38). A solution to the same problem has been derived by Luscher from the equations of Hetenyi (14). In addition to the solutions for the hydrostatic field and elastic media theories, other contributions containing pertinent information warrant mention.

In a particularly significant paper, Gjelsvik and Bodner showed that the energy load is a lower bound for the snap buckling of elastic systems subject to transitional buckling and containing a certain class of initial imperfections (16). In this paper a snap-buckling model was developed and the importance of two basic classes of imperfections were studied. These imperfections are 1) deviations from straightness of the member and 2) changes in basic geometry. Their studies showed that imperfections in straightness of a member reduces the upper buckling load but leaves the energy load unchanged. Gjelsvik and Bodner pointed out that there are strong indications that the energy load is a relatively insensitive function of the buckled shape.

In other studies, Anderson and Boresi, (17) have found that there is little difference in the buckling load for load distributions departing from the uniform all-around loading. This was verified by Armenakas and Herrmann who showed that the difference in the character of the applied pressure affects the buckling stress only if the shell dimensions are conducive to buckling into a small number of circumferential waves, that is, for relatively stiff- or thick-walled cylinders. Nonetheless, the effect of change during deformation of the magnitude and direction of the pressure must be considered, at least for hydrostatic conditions. Boresi and Bodner have shown that the critical values of the external constant-directional pressure acting on a ring may be one-third larger than the corresponding critical value of hydrostatic pressure where the direction and magnitude per unit of undeformed area depend on the deformation.

It remains to synthesize the reviewed information with some additional data to provide further understanding of the soil-structure interaction problem.

DISCUSSION

Static Behavior

Introduction. The discussion to follow is concerned with shallow buried cylinders in a cohesionless soil field subjected to uniform static surface load. The cylinders are considered to be thin with respect to their radius, that is, the diameter to thickness ratio in general will be presumed to be greater than 400.

There is a vast difference in the compressive strength and the moment resistance of thin walled conduits. Obviously, a conduit is an effective structure only if it behaves mainly as a compression ring. When confined in soil, experience shows that a cylinder does just that. As it attempts flexural deflection, resistance is mobilized in the soil preventing collapse. Whatever weakness the structure demonstrates, the soil tends to compensate for it. Only when excessive deflection, gross compressive yielding, joint failure, or buckling occurs does the structure finally collapse.

Deflection. Deflection of a thin-walled buried cylinder subjected to a uniformly distributed static surface load is characterized by 1) body motion of the structure with and into the soil, 2) flattening in the vertical direction, 3) reduction of the perimeter due to pure compressive strain, and 4) development of circumferential waves. These basic deformations and their superposed configurations are shown in exaggerated form in Figure 2. The body motion is the absolute vertical deflection of the undeformed cylinder and consists of the distance aa', Figure 2a, due to compaction of the soil field and y_b, the movement of the cylinder with respect to the soil. Displacement due to compaction depends on the character and depth of soil to bedrock. The relative displacement depends largely on the bedding beneath the cylinder which is exceedingly influential since it largely governs the amount of arching that may be developed.

Radial compressive deformation for metal cylinders is very small compared to deformations from other causes. For cylinders tested at NCEL, it was found that the radial compressive deformation was less than 0.01 of that from the first symmetrical mode deformation.

The first symmetrical mode deformation or flattening, indicated in Figure 2c, is due to compaction of the soil field and to difference in the compliance of the cylinder and the soil. For design purposes, flattening is usually defined by the horizontal deflection from the Iowa Formula.

$$\Delta x = D_L \left[\frac{KWr^3}{EI + 0.061E'r^3} \right] \qquad (1)$$

- r = conduit radius
- EI = pipe stiffness per inch of length
- E' = modulus of horizontal soil reaction in same units as pressure
- D_L = deflection lag factor (accounts for plastic flow in soil with time)
- K = bedding constant (accounts for differences in compaction of soil beneath a conduit)
- W = load on conduit per unit length

The correctness of the form of this equation is readily seen from the theory of curved beams and arches on elastic foundations (14) Selecting a deflection lag factor equal to 1, for dry granular backfill, a bedding constant of 0.10, and the load as the surface pressure, p, times the pipe diameter, D, times a unit length, Equation 1 may be expresses in non-dimensional form as:

$$\frac{\Delta x}{D} = \frac{0.10p}{8\frac{EI}{D^3} + 0.061_{E'}} \qquad (2)$$

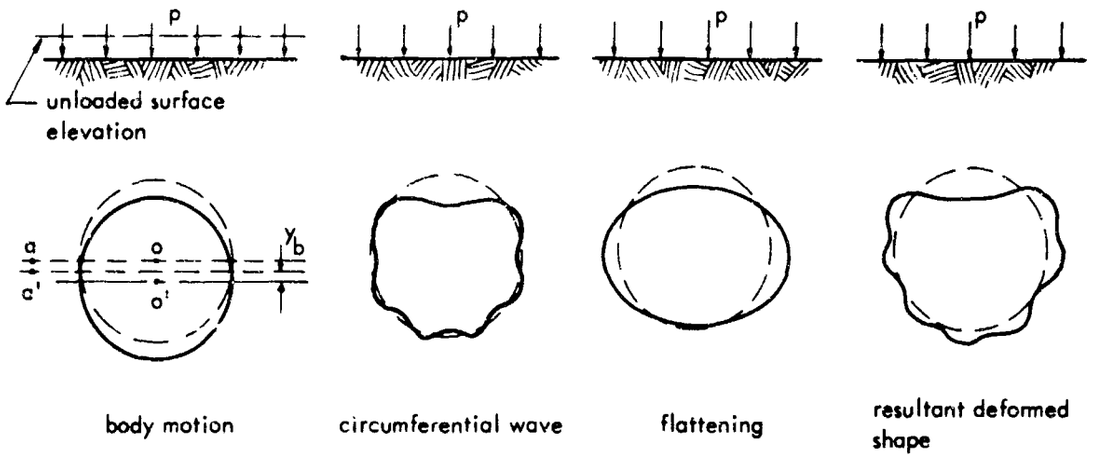


Fig. 2 Deflection of Shallow-Buried Cylinders

The bedding constant of 0.10 is the recommended value for flat bottom trenches with backfill tamped to the horizontal diameter of the culvert; the load condition assumes that the dead load is negligible compared to the live load.

It is instructive to apply the Iowa Formula to one of Bulson's test cylinders for which load-deflection curves are available. The data is as follows: D=10 in., t=0.015 in., d_o=3.75 in., and E=30 x 10^6 psi. This data is used repeatedly throughout the text to exemplify different points. Substituting in Equation 2 it is found that:

$$\frac{\Delta x}{D} = \frac{0.10p}{0.0674 + 0.061E'} \qquad (3)$$

From this equation it is evident that the first term in the denominator of the right hand side, the stiffness term, is negligible. Clearly, the cylinder stiffness has a negligible effect on the horizontal deflection for thin-walled cylinders. Equation 2, then, may be used to distinguish or define what constitutes a thin-walled cylinder; it is a cylinder whose stiffness has a negligible, say less than two percent, effect on the horizontal deflection. Applied load, diameter, and the modulus of soil reaction are the parameters which govern the deflection. Only for thick cylinders of relatively small radius of curvature would one expect shell stiffness to influence the deflection appreciably.

Equation 3 shows that the deflection varies linearly with the surface load. All available data prove this to be true, although often there is a departure from linearity for pressures less than 10 psi. Apparently this depends on the initial condition of the soil around the structure; for many tests, pressure-deflection plots as a straight line through zero.

As previously indicated, a cylinder under hydrostatic load is predisposed to buckle into a given number of circumferential waves depending on its ratio of thickness to radius and length to radius. When a cylinder is in a soil field, experiments indicate that it will tend to deform in the same number of circumferential waves as when loaded hydrostatically; however, the wave shape is modified as indicated in Figure 2b due to boundary influences. To demonstrate, consider the Bulson data previously given, $\frac{t}{r} = 30 \times 10^{-4}$, $\frac{L}{r} = 2.4$; then from Figure 2A, of Appendix A, n=7. Thus, the angle

between the circumferential wave peaks for hydrostatic loading is $\frac{360}{7} = 51.4$ degrees. The angle between circumferential deflection peaks in the Bulson experiment was about 50 degrees at the sides and 40 degrees at the bottom. An essentially identical comparison was found for the cylinders tested at NCEL. The sides buckled in the wave shape predicted by hydrostatic theory, the angle between wave peaks at the bottom was slightly less than on the sides, and the top took the shape of a pinned arch deformed in the first symmetrical non-extensional mode. With this knowledge, one may readily predict almost exactly the deformed shape including the included angle of the "arch" roof which for the above data would be $2\text{-}1/2 \times 51.4 = 128.5$ degrees. Bulson estimated the included angle at 140 degrees. The number of waves between inflection points is usually fairly obvious, particularly if one prepares a sketch of the circumferential wave deformations. Since the deflected shape can be predicted, one also knows in advance the shape of the moment diagram.

Soil Moduli. Determination of the various soil moduli presents one of the greatest uncertainties in buried cylinder analysis. This section attempts to define the moduli of direct concern; as used here they are:

1. Modulus of horizontal soil reaction, sometimes refered to simply as the modulus of soil reaction, E', in psi; as used in the Iowa Formula.
2. Coefficient of horizontal soil reaction, $k' = \frac{E'}{r}$, in, lb/in.^{2}/in.; alternately used in the Iowa Formula.
3. Modulus of vertical soil reaction, also called the modulus of foundation reaction, E_z, in psi; used in the transitional buckling equation.
4. Coefficient of vertical soil reaction, k_z, in lb/in.^{2}/in.; alternately used in the transitional buckling equation.

The different moduli in different directions, of course, are due to the anisotropic properties of soil. In addition to the above terms, it is useful to utilize constants of horizontal and vertical soil reaction as defined by Terzaghi (36). Collectively these are referred to as moduli of soil reaction.

The modulus and coefficient of horizontal soil reaction are constants unique to the buried cylinder system. They are best determined from measurements on thin-walled cylinders substituted back in Equation 3. A model conduit in any suitable soil test tank should provide good results for granular soils when the depth of burial is sufficient to avoid undue error from the surface boundary influences.

It is not advisable to try to determine the modulus of soil reaction from lateral plate bearing tests or other tests of different geometry. Gill has found in recent unpublished tests at NCEL that the modulus of horizontal soil reaction is a non-linear function of displacement width of loaded area, and surcharge pressure. As is well known, the moduli of soil reaction depend on the geometry, the physical properties of the underlying medium, the rigidity of the structure, and the position, direction, and configuration of the displacement. In view of this dependency, the odds are against correct determination of the modulus of horizontal soil reaction on any but a model of the actual system. Even the model approach may not suffice for cohesive soils where modeling is more difficult. Apparently, for the shallow buried cylinder in non-cohesive soils, the effective plate width decreases with increasing load resulting in a straight line load-deflection diagram and a constant modulus of horizontal soil reaction. The modulus, however, will vary with depth.

The modulus and coefficient of vertical soil reaction are linearly related. An equation between the two can be found by comparing the derivations for the critical elastic buckling pressure alternately employing these moduli. A derivation by Luscher (6) gives the critical pressure as:

$$p_{cr} = 2\sqrt{\frac{E_z EI}{r^3}} \tag{4}$$

where E_z = modulus of vertical soil reaction
EI = stiffness of cylinder wall
r = radius of cylinder

A derivation by Link (38) results in the expression:

$$\frac{p_1 r^3}{EI} = (4n^2-1) + \frac{1}{(4n^2-1)} \frac{k_z r^4}{EI} \tag{5}$$

where p_1 = load which produces pure compression of cylinder
$2n$ = number of circumferential waves
k_z = coefficient of vertical soil reaction

A lower bound to Equation 5 of sufficient accuracy for practical purposes for n greater than 3 is

$$p_{cr} = 2\sqrt{\frac{k_z EI}{r^2}} \tag{5a}$$

Comparing these two equations it is evident that: $k_z = \frac{E_z}{r}$ (6)

A similar relation would be expected to hold for the modulus and coefficient of horizontal soil reaction as d[illegible]y Watkins (10) in his dimensional analysis. Other than for model tests, adequate means for evaluating the modulus of horizontal soil reaction for a cylinder have not been developed although Luscher and Meyerhof have made contributions toward this end. Luscher has developed relations between the modulus of soil reaction and the modulus of elasticity* of an elastic soil of uniform thickness surrounding an elastic cylinder. He also has given a relation from the theory of elasticity between the modulus of elasticity of an idealized soil and the one-dimensional compression modulus.

Meyerhof has presented approximate relations between the modulus of horizontal soil reaction, the coefficient of soil reaction, and constants of soil reaction for clays and sands. These relations are valuable as a guide where it is economically unfeasible to perform a model test.

No sound direct method for finding the modulus of vertical soil reaction has been evolved as yet. Considering the lower one-half of a buried cylinder as a free body, one can observe that in its tendency to body motion it acts much as a hearing plate. In this case, the change in effective plate width with increase in load is small Consequently, it might be expected that the modulus of vertical soil reaction might be determined from bearing tests with surcharge pressure on a semi-cylindrical bottomed plate.

White has found in unpublished tests on 15-inch circular plates on dry NCEL sand that the static coefficient of foundation reaction is an exponential function of the surface surcharge pressure. Contrarily, buried cylinder tests at NCEL show that the absolute vertical deflection increases linearly with applied surface load which would indicate that the coefficient of vertical soil reaction is a constant. Obviously, further investigation of the modulus of vertical soil reaction is badly needed.

Thrust and Moment. Typical plots of deflection, thrust, and moment from NCEL static experiments on buried cylinders are given in Figures 3, 4, and 5. These plots are for uniform surface loading. Except near the top and bottom the distribution of thrust is nearly uniform. Significantly, the thrust is smallest and the moment is largest at the bottom of the cylinder. Magnitude of the induced moments would be expected to be very sensitive to the backfill placement. At the top, the boundary influences come into play resulting in thrust and moment distributions much the same as in the similar region of a buried arch (19).

Arching. In tests of buried arches it has been found that a large portion of the surface load is carried through arching in the soil and that the extent to which arching is developed depends on the relative motions between the structure and the adjacent free field soil (19). The relative displacement in the case of the arch depends primarily upon the footing width and it is significant that relatively small footing widths are required to permit activation of appreciable arching. The theoretical development of Luscher tends to confirm the finding: he found that in an annular soil-cylinder system, deformations of 3 to 7 percent of the inside radius are required to develop full arching (6). In concentric aluminum tube-sand systems Luscher found that there was little arching, but for plastic tube-sand systems, some active arching was experienced. In tests at NCEL, the thrust due to to ring compression, calculated on the assumption that the interface pressure was equal to the surface pressure, agreed with the measured thrust at the sides. Thus, none of the surface load was taken by the soil in arching. Indications are, then, that for shallow buried steel and aluminum tubes in a uniform soil field, the net arching will be negligible.

Arching can be achieved by controlling the compressibility of the bedding beneath the cylinder or by designing the cylinder with joints which slip under surface load. The result will be development of arching much as in the case of a buried arch (19). For stiffer structures, Mason has shown that passive arching may occur which may greatly increase the load on a buried structure (31). Obviously, the bedding stiffness should be controlled to avoid such a situation

Understanding of the arching phenomenon is greatly enhanced by studying the elementary two-dimensional trap-door system of Figure 6 and assuming that the shear stress-strain diagram is elasto-plastic as indicated in Figure 7. With this system one may obtain a first approximation for 1) the depth of cover required for all of the load to be carried by soil arching, 2) the maximum percentage of the surface load which can be carried for any lesser depth, and 3) the deformation required to develop the maximum possible arching

For this purpose arching is defined as the total shear developed on the sides of the rectangular prism, A, Figure 6; that is, the amount of the surface load on A that is transferred to the adjacent soil mass.

If the trap door in Figure 6 is displaced sufficiently, failure planes will develop in the soil mass. These may be assumed as vertical planes through the edges of the trap door. Vertical equilibrium of the prism A requires that:

$$(p - p_H) D + \gamma DH = 2\tau_f H \qquad (7)$$

* The ratio of the change in deviator stress and the corresponding change in linear strain at unaltered confining pressure in a trial shear test.

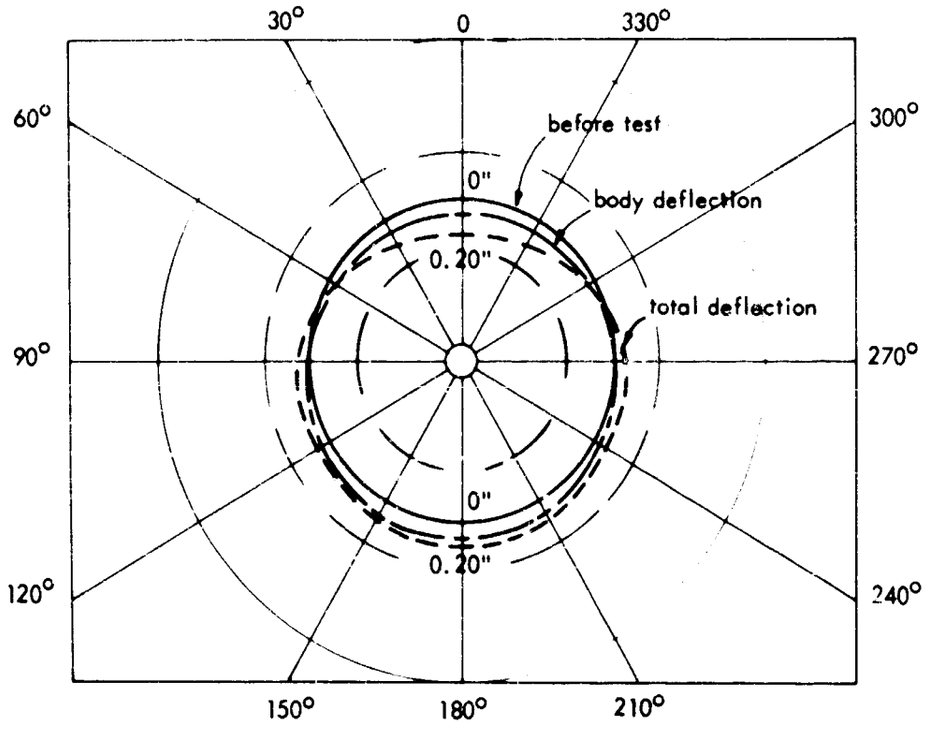


Fig. 3 Peak Cylinder Deflection at 25 psi

where p = surface pressure
p_H = average pressure on the trap door
D = width of trap door
τ_f = failure shear stress
γ = density of soil
H = depth of soil over trap door

at failure $\tau = \tau_f = c + k_o \sigma_v \tan \phi$ (8)

where c = coefficient of soil cohesion
$k_o = \frac{\sigma_h}{\sigma_v}$ = at rest coefficient of earth pressure
σ_v = vertical soil stress at a point in the soil mass
σ_h = horizontal soil stress at the same point
ϕ = angle of friction of soil

For shallow buried structures subjected to uniform surface pressures, one may take $\sigma_v = p$. This relation and Equation 8 with the condition $p = \bar{p}$, the failure load, substituted in equation 7 gives the depth for incipient shear failure as

$$\frac{H}{D} = \frac{1 - \frac{p_H}{\bar{p}}}{2k_o \tan \phi + \frac{2c - \gamma D}{\bar{p}}} \quad (9)$$

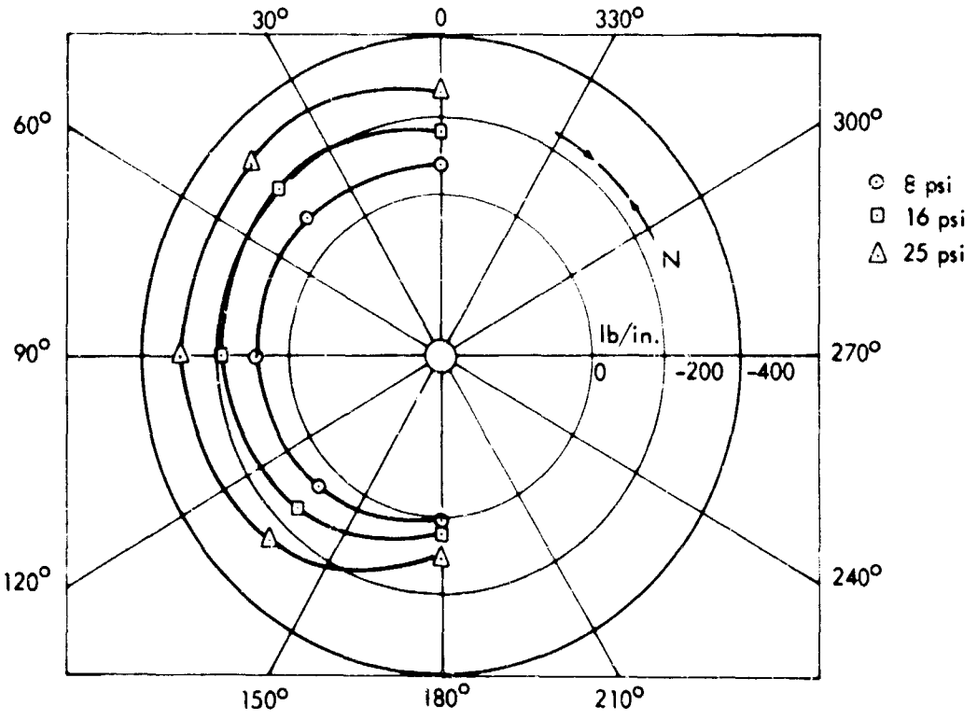


Fig. 4 Thrust Diagram

The depth of cover, $\bar{H}$, required for all of the surface load above the trap door to be carried by arching is found by setting the average pressure on the trap door, p_H, to zero. If this is done and one utilizes the knowledge that $k_o \tan \phi$ is approximately 0.3 for most all granular soils, then, for $\bar{p} >> 2c - \gamma D$,

$$\bar{H} = 1.67\ D \tag{9a}$$

Equation 9 also may be expressed in the form

$$p_a = \left[\frac{\bar{p} - p_H}{\bar{p}}\right] 100 = \left[2k_o \tan \phi + \frac{2c - \gamma D}{\bar{p}}\right] \frac{100\ H}{D} \tag{10}$$

where p_a = percent of the surface load carried by arching.

Applying the conditions and approximations imposed on Equation 9, Equation 10 reduces to

$$p_a = 60\ \frac{H}{D}\ ; \quad p_a \leq 100 \tag{11}$$

The trap-door deflection, d_f, required to develop the maximum possible arching for a given H/D is found by substituting the stress-strain condition at incipient shear failure, $\tau_f = \epsilon_f G$ in Equation 7 and noting that $d_f = \epsilon_f H$, whence,

$$d_f = \left[\bar{p} - p_H\right] \frac{D}{2G} + \frac{\gamma DH}{2G}\ , \quad H \leq \bar{H} \tag{12}$$

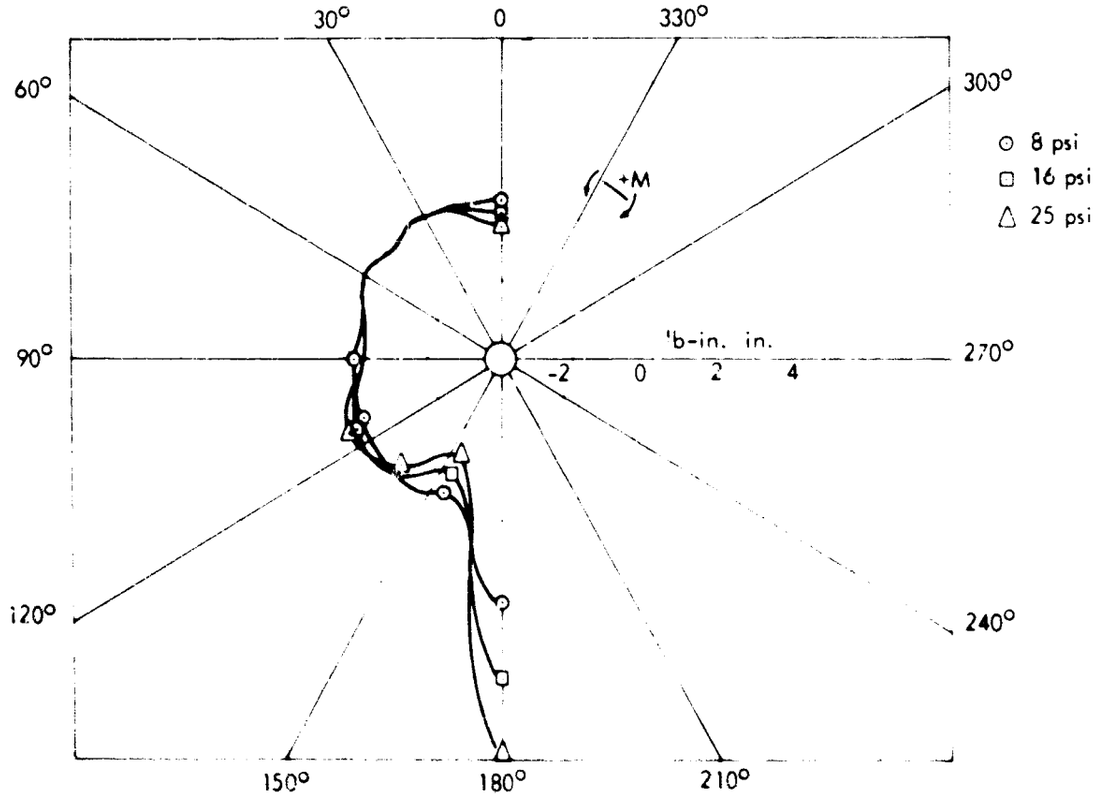


Fig. 5 Moment Diagram

but $\bar{p} - p_H$ is given by Equation 10, thus:

$$d_f = \frac{\bar{p}H}{2G}\left[2k_o \tan\phi + \frac{2c - \gamma D}{\beta}\right] + \frac{\gamma DH}{2G}, \quad H \leq \bar{H} \tag{13}$$

which for $2k_o \tan\phi = 0.6$ and $p >> 2c - \gamma D$ becomes

$$d_f = \left(0.3\beta + \frac{\gamma D}{2}\right)\frac{H}{G} = \epsilon_f H, \quad H \leq \bar{H} \tag{14}$$

It is important to observe that d_f depends on pressure and that the failure can be found only when ϵ_f is known from one-dimensional shear tests.

A more refined analytical approach to the trap-door problem than the preceeding has been developed by Finn (20), for the case of an elastic media of infinite depth. This work has been extended by Chelapati at NCEL to a finite depth of cover with a surface pressure (37).

Whether the trap door of Figure 6 is straight or curved makes little difference in the preceeding analysis providing it does not deflect as a plate. Thus, the relations hold for a buried arch or cylinder. For a cylinder: $H = r + d_o$ (15)

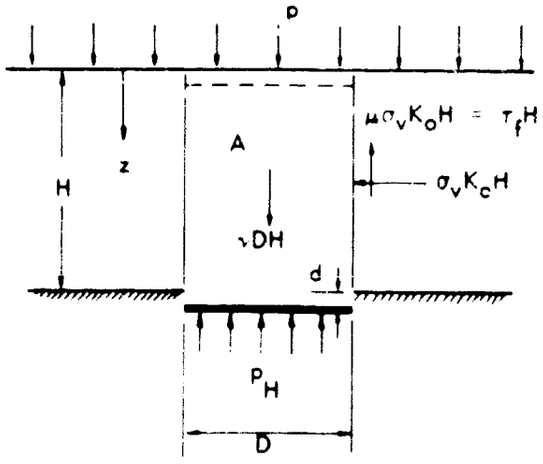


Fig. 6 Trap-Door System

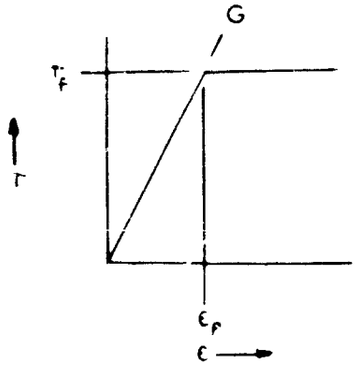


Fig. 7 Elasto-Plastic Soil

where r = radius of cylinder
d_o = depth of cover over crown

It is interesting to compare results from the preceeding equations with data from tests performed at NCEL

In the previously cited static tests on thin metal buried arches, it was found that the percent of the surface load carried by arching depended upon the footing width but for a given width was essentially constant in the pressure range of 3 psi to 25 psi (19) Geometric parameters for these arches were r = 15 in , d_o = 6 in , t = shell thickness = 0 0478 in , h = footing depth = 1.8 in , b = footing width = 1.2 inches From Equation 10:

$$p_a = 60 \left[\frac{15+6+1.8}{330}\right] = 46 \text{ percent}$$

The experimentally determined value for the 1.2 in. footing width was 60 percent and for a 2.4 in footing width was 40 percent These values are larger than those predicted by the above equation probably because the deflections of the thin metal arches permitted development of passive pressures which reduced the thrust that would otherwise have occurred at the spring line Unfortunately this is the best data that is presently available for comparison with Equation 10; it does indicate that the theory is a reasonable first approximation for shallow buried structures

Presumably the pressure, β, to develop the shear in the soil of the arch tests was 3 psi since the percent arching was constant at larger pressures Thus, the deformation required to develop the shear is from Equation 12:

$$d_f = \left[0.3 \times 3 \cdot \frac{112 \times 30}{1728 \times 2}\right] \frac{22.8}{3890} = 0.011 \text{ in}$$

where G = 3890 psi

The deformation relative to the free field required to develop the maximum possible arching at 100 psi overpressure is a sizeable 0.28 inches The deflection of the 1.2 inch footings relative to the free field for the first loading to 3 psi was 0.022 inches which was ample to develop the maximum possible arching

For a shallow buried cylinder in a uniform soil field, the maximum possible relative deflection of the horizontal center-line with respect to a point at the same original elevation in the free field will be:

$$\Delta x_c \simeq \frac{\Delta x}{2} = \frac{1.64}{2} \frac{p}{E'} \qquad (16)$$

At 3 psi load, the value of Δx_c in the 24-inch diameter cylinders tested at NCEL was 0.0005 inches for the first loading while the necessary deflection to develop full arching was 0.010 inches.

From the preceeding discussion and equation it would seem that the buried arch with strip footings is inherently superior to the buried cylinder for resisting large static loads since the arch is capable of undergoing sufficiently large deformations which increase with applied load to permit transfer of a large portion of the surface load to the soil in arching. As normally built, buried cylinders do not have this capability, however, through use of proper bedding and slip joints they can be designed to have similar capabilities to the buried arch, thus, greatly increasing their failure load. Even if this is not done and a local failure develops, arching will immediately develop in the soil.

Failure Modes. From the previous analysis of the buried cylinder problem, it is evident that there are several modes of failure including 1) joint failure, 2) compression failure of the shell wall, 3) excessive deflection of the cylinder relative to the free field, and 4) buckling. Joint failure and compression failure of the wall are relatively easy to design against. Further, excessive deflection relative to the free field is seldom a problem in buried cylinders as it is with buried arches. With buried cylinders, buckling is the least understood of the possible modes of failure, as such, it is of dominant concern. Buckling of shallow buried cylinders appears to be a phenomenon of two's: there are two basic methods of analysis, two fundamental types of buckling, and two characteristic modes of buckling failure. These are:

1. Methods of analysis
   a. Classical method
   b. Energy load
2. Types
   a. Elastic buckling
   b. Plastic buckling
3. Modes of buckling
   a. Roof caving
   b. Local snap buckling

The transitional and caving modes of buckling are illustrated in Figures 8 and 9.

Classical and Energy Buckling Loads. Fung and Kaplan have observed, "Both the classical and the energy criteria have been applied to curved beams and shells. To some cases, the classical criterion gives better results. The reason, as pointed out by Tsien, is that in some cases the energy "hump" between two equilibrium states (one buckled and one unbuckled) of the same energy level is large and in other cases it is small. If the hump is small, the ever present small disturbances will enable the structure to jump from the unbuckled state to the more stable buckled state. Otherwise this jump will not be incurred. The crucial decision of the proper criterion depends much on what one means by a "practical" experimental setup or a "practical" service condition of the structure." (21) Fung and Kaplan performed experiments and calculations for a sinusoidal arch wherein the stress at buckling was well below the yield stress of the material. The essence of their work is contained in Figure 10 where it may be noted that the experimental results agree with the classical solution for the larger

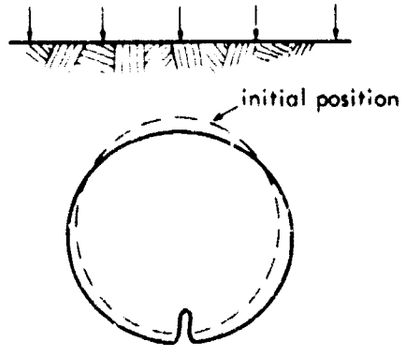


Fig. 8 Transitional Buckle

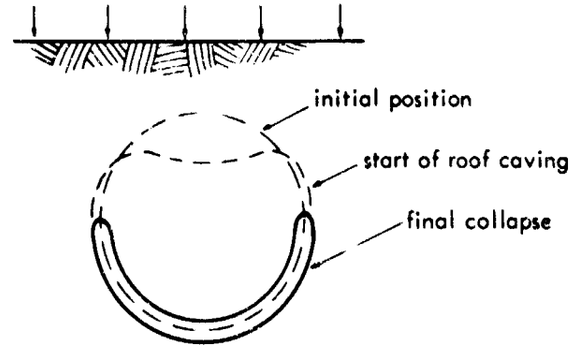


Fig. 9 Caving of Roof

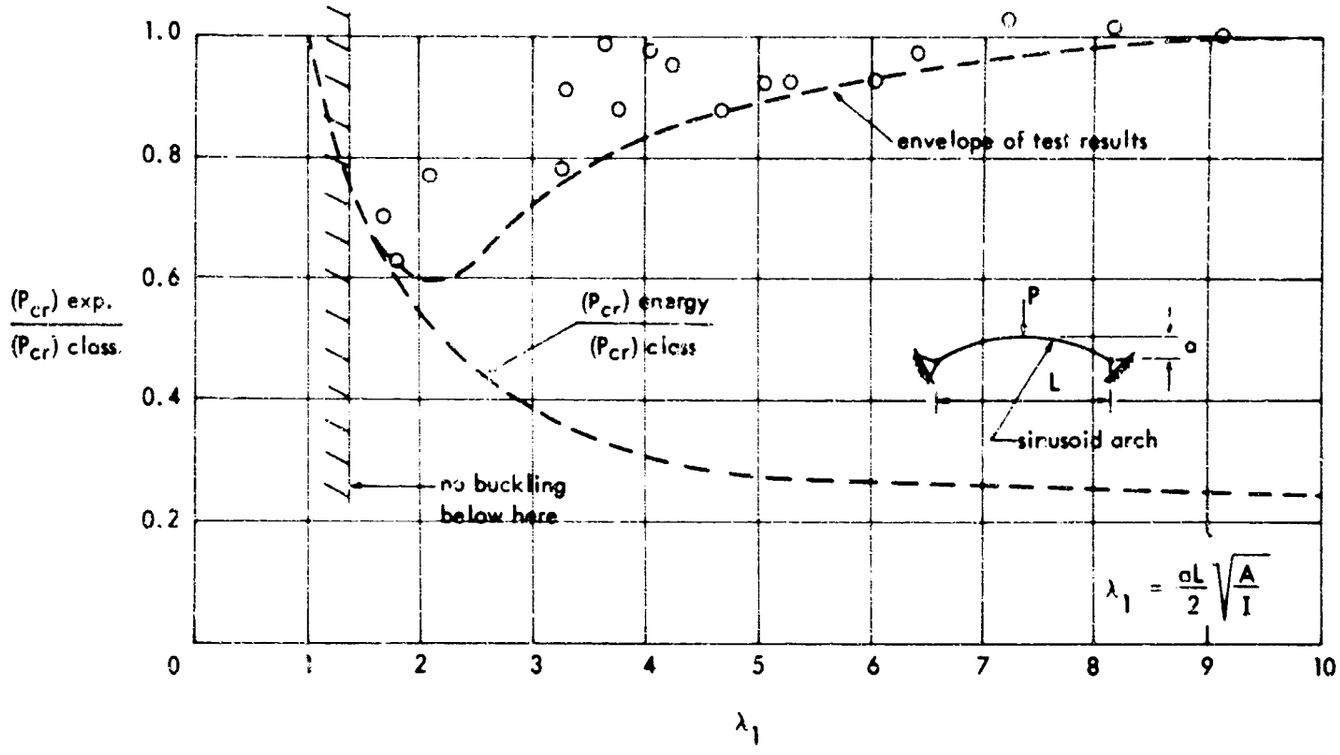


Fig. 10 Theoretical and Experimental Results for Shallow Arch. Reproduced from NACA, TN-2840.

values of λ_1 but are better defined by the energy load at smaller values of λ_1. The parameter λ_1 is defined as

$$\lambda_1 = \frac{aL}{2}\sqrt{\frac{A}{I}} \qquad (17)$$

a = rise of arch
L = span
A = area of longitudinal section per unit length
I = moment of inertia of longitudinal section per unit length

The envelope and the scatter of the experimental data of Figure 10 are of particular interest especially considering that all of the failures resulted from elastic and not plastic buckling. The data of Figure 10 illustrates that the buckling load cannot be defined with great precision, that is, there will always be considerable scatter of experimental results. It is also evident that the most suitable method of analysis of the buckling problem depends on the geometry and the range of stiffness of the structure. Fung and Kaplan have shown that very similar results to that of Figure 10 hold for the circular arch.

The preceeding information on arches is pertinent to the buried cylinder problem since the lobe consisting of one-half of a circumferential wave at the bottom may be considered as a shallow arch hinged at the inflection points. One finds difficulty in determining the snap buckling load of this small arch, however, because 1) the arch rise corresponding to a given thrust is unknown and 2) the distance between the inflection point changes with applied load.

For the Bulson cylinder the values of λ_1 may be computed based upon the measured rise of a lobe at different applied loads and for the rise of a segment of the undeformed cylinder with the same included angle. Doing this, it is found that λ_1 is in the range where the class theory gives good results. In any given case, computing λ_1 based on the undeformed geometry and the included angle corresponding to the wave shape for hydrostatic loading should provide an indication as to whether the energy load or classical method should be employed to define the buckling load.

To simplify the discussion of the buckling phenomenon, it will first be assumed that the cylinder is in a uniform soil field and that the buckling is elastic. Under these conditions, as has been shown, there will be no net arching across the structure though there will undoubtedly be local areas of active and passive pressure. For uniform soil conditions, and shallow burial, tests show that the pressure on the cylinder is essentially equal to the surface pressure. This is readily demonstrated from the thrust distribution, Figure 4, for the NCEL test cylinders. It may be observed that the thrust at the sides is very nearly equal to the pressure times the radius for any given loading. Thus, the average loading may be considered as a uniform all-around pressure equal in magnitude to the surface pressure.

Elastic Snap Buckling. Knowing the loading, one may proceed to consider the buckling load. Let us first discuss snap buckling in a lobe of one of the waves at or near the bottom of the cylinder. As previously pointed out, if one examines the deflection data from tests it is found that the period of the circumferential waves at the sides, and to a lesser accuracy near the bottom, is that predicted by the hydrostatic theory. The buckling load computed from the hydrostatic theory, however, is much less than the experimental buckling load as indicated in Figure 1.

Conversely, the buckling load from the theory for an elastically supported cylinder, Equation 4, is usually considerably larger than the actual buckling load. Such calculations must, of course, be based on appropriate values of the modulus of vertical soil reaction. Bulson's cylinder, which were relatively thin also showed this tendency; buckling was clearly inelastic. The theoretical elastic buckling load for the previously employed Bulson cylinder was about 68 psi while the experimental buckling load averaged 46 psi for a wall of 40,000 psi yield steel.

Inelastic Transitional Buckling. Most buried cylinders, particularly those with the relatively thick walls required in blast resistant design, can be expected to fail by inelastic buckling if they buckle at all. Meyerhof has given an approximate relation for the stress at incipient transitional buckling as:

$$\sigma_b = \frac{2}{A}\sqrt{\frac{k_z EI}{1-\nu^2}}\ ; \qquad \sigma_b \leq \sigma_y \tag{18}$$

where σ_b = stress at incipient buckling
σ_y = yield stress of shell material
EI = stiffness of cylinder per in. of length
ν = Poisson's ratio
A = area of unit length of cross section of wall
t = wall thickness = $A/1$ for a rectangular section
k_z = coefficient of vertical soil reaction

For a uniform soil field where the net arching is zero, the theoretical surface load to produce snap buckling for a cylinder with a rectangular section and negligible induced moments is:

$$p_{cr} = \frac{t\,\sigma_b}{r} \tag{19}$$

Meyerhof's theory is based on the classical theory of buckling of flat plates and, hence, cannot be expected to be universally applicable and accurate in predicting failure loads. Indeed, experiments have shown that considerable yielding can occur prior to buckling collapse in thicker walled cylinders (34).

Elastic Caving. In certain instances, especially if the cover is very shallow, failure in the caving mode is a distinct possibility. Tests performed at the University of New Mexico Air Force Shock Tube Facility showed consistent collapse in the caving mode under static loading for 8-inch diameter cylinders with one-inch of sand cover over the crown (34).

Prediction of the caving load is facilitated by the observation that the upper portion of the cylinder deflects in the first non-extensional symmetrical mode of a two hinged arch. Determination of the included angle of the "hinges" was previously discussed. Further, from Figure 5 it may be noted that the moments in the upper portion of the cylinder are much less than at the bottom. Because of this, buckling of the "arch" is much more likely to be elastic than for buckling of a bottom lobe.

One might question why the upper portion of a shallow buried cylinder deforms in the shape of the first non-extensional symmetrical mode of a hinged arch? The reason becomes evident if it is recognized that since the bending resistance of a thin-walled cylinder is small, it will deform as required to develop a nearly uniform radial loading on the extrados. Obviously, this can never be completely achieved because of the presence of the surface boundary and the development of circumferential waves. A detailed study of the action of successive soil elements shows that the presence of the surface boundary alters the circumferential waves near the top of the cylinder and forces deformation in three half waves as illustrated in Figures 2b and 2d (35).

The elastic caving load may be estimated from Equation 5 if the term $4n^2$ is replaced by $(2n\pi/\alpha)^2$, where α is one-half the included angle of the "arch" (38). One must, however, modify this equation to account for the presence of the surface boundary. Test results provide evidence that the failure load is very sensitive to the depth of cover up to a certain minimum value but that above this transitional value the depth of cover has little influence on the caving load. Indications are that the transition depth may be as small as one eighth of the radius depending on the wall stiffness,

although, insufficient experimental data is available to be certain. A study of Equation 5 reveals that for small EI arches with n = 3, the first term on the right is small compared with the second term, thus, the caving load is primarily dependent upon k_z, the coefficient of soil reaction. Actually, the great reduction in the modulus of soil reaction at very shallow depths of cover is not of much practical significance since depths of cover larger than the transitional depth will usually be required for radiation protection. In other words, with sufficient cover to provide radiation shielding, caving will not usually be the critical failure mode.

For the Bulson cylinder, assuming the upper portion to act as a three hinged arch, the elastic caving load is computed from Equation 5 as 93 psi. This, then, is definitely not a critical load for the cylinder considered, although, the inelastic caving load may be.

Inelastic Caving. No method is available as yet for defining the inelastic caving load. The only known criteria for this is that caving probably will not occur for practical depths of burial until the horizontal deflection reaches 15 percent of the original diameter. Such large deflections are readily avoided by proper backfill. Further, inelastic caving is not expected under blast loading.

One should be careful not to overlook the possibility of pure compression failure, especially under dynamic loading.

DYNAMIC RESPONSE

Little is known about the dynamic response of buried cylinders, however, data has been obtained in tests at NCEL and the University of New Mexico that give important clues regarding behavior. The NCEL tests show that for uniformly distributed surface loading 1) the crown and side deflection under dynamic loading is twice the value from static loading, and 2) the bottom displacement is essentially the same for the two load conditions. Another interesting observation from the static tests was that the absolute deflection of the bottom of the cylinder equalled twice the magnitude of the deflection of the crown with respect to the bottom. These values were about equal for dynamic loading. Further observations from the NCEL tests were 1) that the peak thrusts were about 0.98 pr and 1.13 pr respectively for static and blast loads of the same magnitude, and 2) the maximum moment at the crown under blast loading was 1.5 times the corresponding static moment. Strangely enough, the moment at the bottom was less for the dynamic loading than for the static loading.

The test data leads one to suspect that the soil field deforms essentially the same under static and blast loading but that the structure and its cover behave differently. This difference is primarily associated with the upper portion of the cylinder and is attributable to the presence of the surface boundary. Nearness to this boundary assures that the energy absorption and dispersion are negligible quantities, therefore, the surface pressure may be used in investigating the response of shallow-buried cylinders.

Comprehension of the nature of response is aided by recognizing that the soil mass near the crown, in effect, is resting on a spring composed of the cylinder and its supporting soil. See Figure 11. As with any spring-mass system subjected to a long-duration blast load, the maximum deflection will be twice the static value. This is true regardless of what one chooses as the effective soil mass because the mass will only affect the time to maximum displacement, not the magnitude of the maximum displacement. The analogy of Figure 11 is useful in that it permits the application of the knowledge gained about the spring-mass system to prediction and interpretation of the behavior of shallow buried cylinders (35).

The model of Figure 11b and response charts (22) developed for the single-degree-of-freedom system are valuable aids to ones judgement in predicting the influence of various parameters, including the natural period, on the motion of the crown. The natural period of an actual installation may be calculated if reasonable values for the cylinder and foundation stiffness can be found. One might also scale up the period from the known period of a model. Detonation of a small charge over the surface of the NCEL test cylinders resulted in a period of larger cylinders in field installations also is available (23).

Apart from analysis by the spring-mass analogy, more sophisticated dynamic analyses have been developed for elastic and acoustic media (24, 25, 26). No success has been achieved as yet, however, in getting such theories to predict the motion much less the failure mode and load.

Photoelastic studies have been made of plates loaded with a traveling wave on one edge which contained lined and unlined holes (27). The extent of the applicability of such tests to soil-

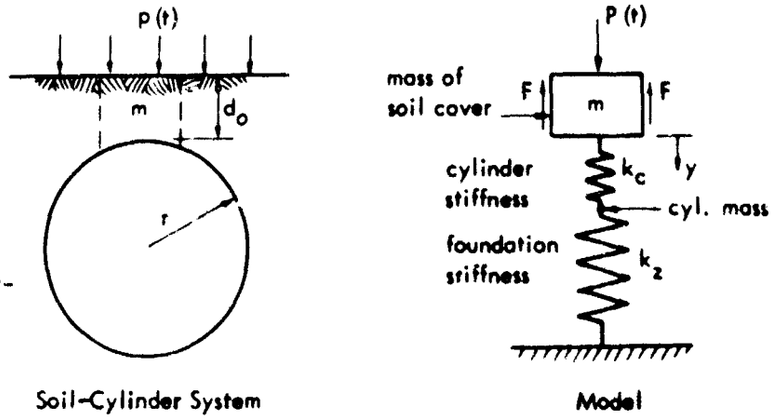


Fig. 11 Model of Soil-Cylinder System

structure system is unknown, but at the least, the resulting visual presentation of results aides ones' understanding for elastic systems. Photoelastic studies indicate that there is very little stress magnification due to dynamic loading.

From the information reviewed, it is evident that for plane wave loading:

1. Deflection of the sides and crown can be predicted from the spring-mass analogy. For long-duration loads, these deflections, and presumably the corresponding moments, will be about twice the static values.
2. The moments elsewhere will be about equal to the static values.
3. The peak thrust may be taken as 15 percent greater and, consequently, the buckling load an equal percent less than for static conditions.

It is expected that the caving load would be considerably greater under a rapidly decaying dynamic load than under static loading while the transitional buckling load would be about the same in either case. The reason is the deformation of the crown and sides requires considerable time and a short-duration load may decay to a non-critical value before the collapse deflection is reached. The thrust to produce transitional buckling, in contrast, develops very rapidly.

The influence of a traveling wave loading on response is not definitely known at the present time, although, the collapse pressure for this type of loading is not expected to be appreciably different from that for plane wave loading.

Using the preceeding guides it should be possible to achieve a reasonably good design for a blast resistant cylinderical shelter, especially if one takes care to provide an adequate factor of safety against buckling failure. Care also must be exercised to avoid "locking in" large deformations and stresses during backfilling that will be subsequently magnified by blast loading.

Other Considerations

Throughout the text, the buried cylinder problem has been treated as two dimensional when, in actuality, there will always be stresses due to a finite length and end walls. For the case of hydrostatic loading, the influence of length effects and of longitudinal compression may be seen in the charts of Appendix A. In the case of an elastically supported, or soil supported, cylinder these effects are not well defined, however, it can reasonably be surmised that length effects are less important than for hydrostatic conditions. In tests of 1.6-inch diameter soil-surrounded tubes Luscher found that changing the length from 10 inches to 6 inches produced no change in behavior. From tests of thin-wall buried arches, it is known that the end wall effects dissipate in a length approximately equal to the radius. While no such information is available for thin-wall cylinders, such information is available for thicker wall cylinders with spherical end walls (29). Unquestionably, more theoretical and experimental work is needed to define the effects of length, end walls, and longitudinal stresses.

There are, of course, numerous secondary aspects of the buried cylinder problem which eventually should be considered. Some of these are influences of a non-uniform soil field, the effect of backfill materials other than dry sand, the possible gain in resistance from the introduction of slip or yield joints, and the possibility of utilizing mechanical shielding through introduction of a liner or other material in the soil field.

It is not expected that use of other than non-cohesive granular soil will introduce any insurmountable difficulty in defining the load capacity. Indications are that the modulus of soil reaction is the dominant soil parameter, consequently, for a given modulus the load capacity should be essentially the same regardless of the character of the material comprising the soil field.

The analysis of the problem given in this paper is based upon limited theoretical and experimental information, hence, it must be expected that certain of the deductions will need alteration when more extensive data becomes available. For example, there are indications that the number of circumferential waves which develop is a function of the applied pressure and the soil modulus in addition to the length, diamter, and wall thickness. It also is possible that the influences of length are sufficiently important that they cannot be neglected in defining the action of the central transverse section. Imperfections in roundness are not expected to affect the transitional buckling load but may effect the caving load. These things can only be ultimately determined from experiments.

Factors such as rotation at the seams of bolted plates and optimum geometry for corrugated plates are not treated here despite their importance in culvert and protective construction design. These matters have been studied in some detail and information on them is available from the various manufacturers of plate.

CONCLUSIONS

This study attempts to transcend the major obstacles to comprehension of the behavior of shallow buried cylinders. The problem is dissected and analyzed to determine the dominant parameters and to define the areas in which further research is needed. The treatment and the following findings and conclusions are limited to the case of thin-metal cylinders with shallow burial in a uniform non-cohesive soil field.

STATE OF THE ART

It can be concluded that:

1. The stiffness of the wall has little influence on the cylinder deflection but does influence the buckling load.
2. The moduli of soil reaction are the dominant parameters influencing deflection and buckling.
3. The cylinder deflection is a linear function of the surface load.
4. The modulus of horizontal soil reaction, E', is a constant at a given depth of burial.
5. Circumferential waves are developed on the sides which have the same included angle as an identical cylinder loaded hydrostatically. The included angle of the waves at the bottom is slightly smaller than for side waves and the top deforms in the first symmetrical mode of a two-hinged arch due to the presence of the boundary.

A study of arching shows that:

1. For static loading a certain minimum cover is required for all of the surface load to be carried by arching.
2. For any lesser depth there is a maximum (determinable) percentage of the surface load which can be carried by arching.
3. A certain minimum relative deformation between the structure and the free field is required to develop the maximum possible arching.
4. The net arching across a thin metal cylinder is negligibly small, although, local active and passive arching exists around the perimeter.

The arching analysis and measurements show that the effective load on the structure tending to induce failure is the surface overpressure.

Buckling failure may be elastic or inelastic, in either the caving or transitional modes. The caving mode consists of a collapse of the roof while the transitional mode is characterized by a local snap buckle near the bottom of the cylinder. For thin-wall cylinders failure in the transitional mode will most likely be inelastic.

Under blast loading and for the depths of cover required to provide radiation shielding, the most probably failure mode is inelastic transitional buckling provided the structure is designed to avoid end wall, joint, or other secondary failure. Deflection of the sides and crown can be predicted from the spring-mass analogy and for long-duration loads these deflections will be twice the corresponding static values. Peak thrust and, consequently, the buckling load is expected to differ from the static values by about 15 percent--the thrust higher and the buckling load lower.

SUGGESTIONS FOR FUTURE RESEARCH

Classical and energy load solutions are needed for all of the possible modes of buckling failure. Most needed are a classical solution for the inelastic transitional buckling load and a derivation of the energy load for snap buckling. Experimental methods and data must be developed for finding the moduli of soil reaction in the buckling equations. Information is especially needed on the modulus of vertical soil reaction beneath the invert.

Eventually, experimental and theoretical work should be accomplished to define the influence of a traveling wave, behavior in non-cohesive soils, and the effect of such things as slip joints, non-uniformity of the soil field, and end walls. It also may be desireable to consider in more detail parameters such as the depth of cover, length and initial out-of-roundness.

The number of variables is so large that it would be best if most test work could be accomplished as part of a large statistically designed experiment even though different phases of the work were performed by different groups. This is probably the only way second and third order interactions can ever be defined experimentally.

ACKNOWLEDGEMENTS

Sincere appreciation is extended to those who contributed their time and talent in effecting the preparation and review of this paper. Special recognition is due to members of the Soils Division at NCEL who provided data, council, and constructive criticism regarding the soils aspects of the study. Acknowledgement is extended to Sergeant Norman Alston who typed most of the text.

REFERENCES

1. Spangler, M.G., Soil Engineering, International Textbook Company, Scranton, Pennsylvania, 1960, p. 433.
2. "Earth Loads on Steel Pipe, Chapter 8, Design and Installation of Steel Water Pipe," Journal of the American Waterworks Association, Vol. 53, No. 8, August 1961, p. 1053.
3. Barnard, R.E., "Design and Deflection Control [illegible]," Proc. ASTM, Vol. 57, 1957.
4. Meyerhof, G.G. and L.D. Baike, "Strength of Steel Culvert Sheets Bearing Against Compacted Sand Backfill," presented at the 42nd Annual Meeting of the Highway Research Board in Washington, D.C., 9 January 1963.

5. Bulson, P.S., "Deflection and Collapse of Buried Tube:," Report RES 7/1, Millitary Engineering Experimental Establishment, Christchurch, Hampshire, England, November 1962.
6. Luscher, U., "The Interaction Between a Structural Tube and a Surrounding Cylinder of Soil," Ph. D. Thesis, Massachusetts Institute of Technology, Cambridge, Massachusetts, August 1963.
7. Whitman, R.V. and U. Luscher, "Basic Experiment into Soil-Structure Interaction," Journal of Soil Mechanics and Foundations Division, Proceedings ASCE, December 1962.
8. Watkins, R.K., "Some Observations on the Ring Buckling of Buried Flexible Conduits," discussion to Reference 4, 15 January 1963.
9. Watkins, R.K., "Development and Use of the Modpares Device in Predicting the Deflection of Flexible Conduits Embedded in Soil," a report submitted to the ASCE Pipeline Division, Committee on Pipeline Crossings at Railroad and Highways, May 1962.
10. Watkins, R.K., "Failure Conditions of Flexible Culverts Embedded in Soil," Highway Research Board Proceedings, Vol. 39, 1960, pp. 361-371.
11. Defense Atomic Support Agency, Headquarters Field Command, WT-1421, Operation Plumbbob, "Evaluation of Buried Conduits as Personnel Shelters," by G.H. Albright, J.C. LeDoux, and R.A. Mitchell, NCEL, 14 July 1960.
12. Southwell, R.V., "On the Collapse of Tubes by External Pressure," Philisophical Magazine, I, May 1913, pp. 687-698; II, Sep' mber 1913, pp. 502-511; III, January 1915, pp. 67-77.
13. Armanakas, A E. and G. Herrmann, "Buckling of Thin Shells Under External Pressure," Journal of Engineering Mechanics, Proceedings of the ASCE, Paper 3552, Vol. 89, No. EM3, June 1963.
14. Hetenyi, M., "Beams on Elastic Foundation," The University of Michigan Press, Ann Arbor, Michigan, 1946, pp. 156-178.
15. Czerwenka, G., "Untersuchugen von dunnen durzen zylindern, die durch Ring-Kleinstprofile enger und mittlerer Teilung verstarkt sind und unter Manteldruck stehen," Zeifshrift fur Wissenschaft, Vol. 9, 1961, pp. 163-190.
16. Gjelsvik, A. and S.R. Bodner, "Energy Criterion and Snap Buckling of Arches," Journal of Engineering Mechanics Division, Proceedings of the ASCE, Vol. 88, No. EM5, Part 1, October 1962.
17. Anderson, R.H. and A.P. Boresi, "Equilibrium and Stability of Rings under Nonuniformly Distributed Loads," Proceedings of the Fourth U.S. National Congress of Applied Mechanics, ASME, New York, June 18-21, 1962, pp. 459-467.
18. Murphy, G., Similitude in Engineering, The Ronald Press Company, New York, 1950.
19. U.S. Naval Civil Engineering Laboratory, TR-278, "Static Loading of Small Buried Arches," by H.L. Gill and J.R. Allgood, Port Hueneme, California, 31 January 1964.
20. Finn, W.D., "Boundary Value Problems of Soil Mechanics," Journal of the Soil Mechanics and Foundations Division, Proc. ASCE, September 1963.
21. Fung, Y.C. and A. Kaplan, "Buckling of Low Arches or Curved Beams of Small Curvature," National Advisory Committee for Aeronautics, TN2840, Washington 25, D. C., November 1952.
22. "Design of Structures to Resist Nuclear Weapons Effects," Manual of Engineering Practice - No. 42, ASCE Headquarters, 33 West 39th Street, New York City, New York.
23. Sievers, R H., Jr., "Underground Structural Response Experiments," Bulletin No. 28, Shock, Vibration and Associated Environments, Part III, September 1960, p. 233.
24. Yoshihara, T., "Interection of Plane Elastic Waves with an Elastic Cylinderical Shell," Ph. D. Thesis, University of Illinois, Urbana, Illinois, 1963.
25. Forrestal, M.J., "Protection Against High Blast Overpressure and Ground Shock," MRD Division of General American Transportation Corp., OCD Contract No OCD-05-62-59, 28 February 1963.
26. Air Force Special Weapons Center, Report NT-62-30, "A Theoretical Study of Structure-Medium Interaction," by A M. Soldate and J F. Hook, NESCO, Contract AF 29(601)-2838 Kirtland Air Force Base, New Mexico, March 1962.
27. Air Force Special Weapons Center, Report TDR-62-47, "A Study of Stress Wave Interaction with Buried Structures," by W F Riley, I.M. Daniel, and J.J. Carey, ARF, Contract AF 29(601)-4312. Kirtland Air Force Base, New Mexico, May 1962.
28. Langhaar, H L., and A P Boresi, "Snap-Through and Post-Buckling Behavior of Cylindrical Shells Under the Action of External Pressure," University of Illinois Engineering Experiment Station Bulletin No. 443, 1957.
29. Air Force Weapons Laboratory, RTD TDR-63-3060, "A Study of Static and Dynamic Resistance and Behavior of Structural Elements," by R L. Marino, Jr., IIT Research Institute, Contract AF 29(601)-5372. Kirtland Air Force Base, New Mexico
30. Air Force Special Weapons Center, TDR-62-135, "Principles and Practices for Design of Hardened Structures," Air Force Design Manual by N.M. Newmark and J.D. Haltiwanger, University of Illinois. Kirtland Air Force Base, New Mexico

31. Air Force Weapons Laboratory, RTD TDR-63-3075, "A Study of the Dynamic Soil-Structure Interaction Characteristics of Real Soil Media," by H.G. Mason, O.H. Criner, R. Waissar, and N.R. Wallace, URS. Kirtland Air Force Base, New Mexico.
32. Meyerhof, G.G. and C.L. Fisher, "Composite Design of Underground Steel Structures," The Journal of the Engineering Institute of Canada, September 1963.
33. White, H.A. and J.P. Layer, "The Corrugated Metal Conduit as a Compression Ring," Highway Research Board Proceedings, Vol. 39, 1960.
34. Donnellan, B.A., "The Response of Buried Cylinders to Quasi-Static Overpressures," a paper to be presented at the Soil-Structure Interaction Symposium, Tucson, Arizona, 8-11 June 1964.
35. U.S Naval Civil Engineering Laboratory Report, "The Behavior of Shallow Buried Cylinders--A Synthesis and Extension of Contemporary Knowledge," by J.R. Allgood, Port Hueneme, California, in publication May 1964.
36. Terzaghi, K., "Evaluation of Coefficient of Subgrade Reaction," Geotechnique, Vol. 5, 1955.
37. Chelepati, C.V., "Arching in Soil due to Yielding of a Rigid Horizontal Strip," a paper to be presented at the Soil-Structure Interaction Symposium, Tucson, Arizona, 8-11 June 1964.
38. Link, H., "Beitrag zum Knickproblem des elastisch gebetteten Kreisbogenträgers," Der Stahlbau, July 1963.

LIST OF SYMBOLS

- A = area of longitudinal section per unit length
- a = rise of arch
- c = coefficient of cohesion
- D = diameter of cylinder; width of trap door; coefficient
- D_L = deflection lag factor
- d = deflection of trap door
- d_o = depth of cover over crown
- d_f = deflection required to develop the maximum possible arching
- E = modulus of elasticity of cylinder material
- E' = modulus of horizontal soil reaction
- E_z = modulus of vertical soil reaction
- F = arching shear
- G = shear modulus
- H = depth of soil over trap door
- $\bar{H}$ = minimum depth of cover for all surface load to be carried by arching
- I = moment of inertia per unit length of longitudinal section
- K = bedding constant
- K_o = $k_o = \sigma_h / \sigma_v$ = at rest coefficient of earth pressure
- k_c = cylinder stiffness
- k_z = coefficient of vertical soil reaction
- k' = coefficient of horizontal soil reaction
- L = length of cylinder; span of arch
- M = moment
- m = mass over crown acting with cylinder
- N = thrust; longitudinal stress
- n = number of circumferential waves into which a hydrostatically loaded cylinder buckles
- p = surface pressure
- p_a = percent of surface load carried by arching
- p_H = average pressure on trap door
- p_{cr} = critical buckling pressure
- p_1 = uniform radial load
- β = failure load
- P = total load
- P_{cr} = total critical buckling load
- R = r = cylinder radius
- T = initial uniform longitudinal shell stress
- t = time; wall thickness
- W = load on conduit per unit length
- y = displacement
- y_b = relative body deflection
- z = depth from the soil surface

γ = density of soil
Δ_x = horizontal deformation of a buried cylinder
ϵ = unit strain
ϵ_f = failure strain
λ_1 = parameter
μ = coefficient of friction
ν = Poisson's ratio
σ_b = stress at incipient inelastic transitional buckling
σ_n = horizontal soil stress at a point in the soil field
σ_v = vertical soil stress at a point in the soil field
σ_y = yield stress of shell material
τ = shear stress
τ_f = failure shear stress
ϕ = angle of friction of soil

APPENDIX A - DESIGN CHARTS

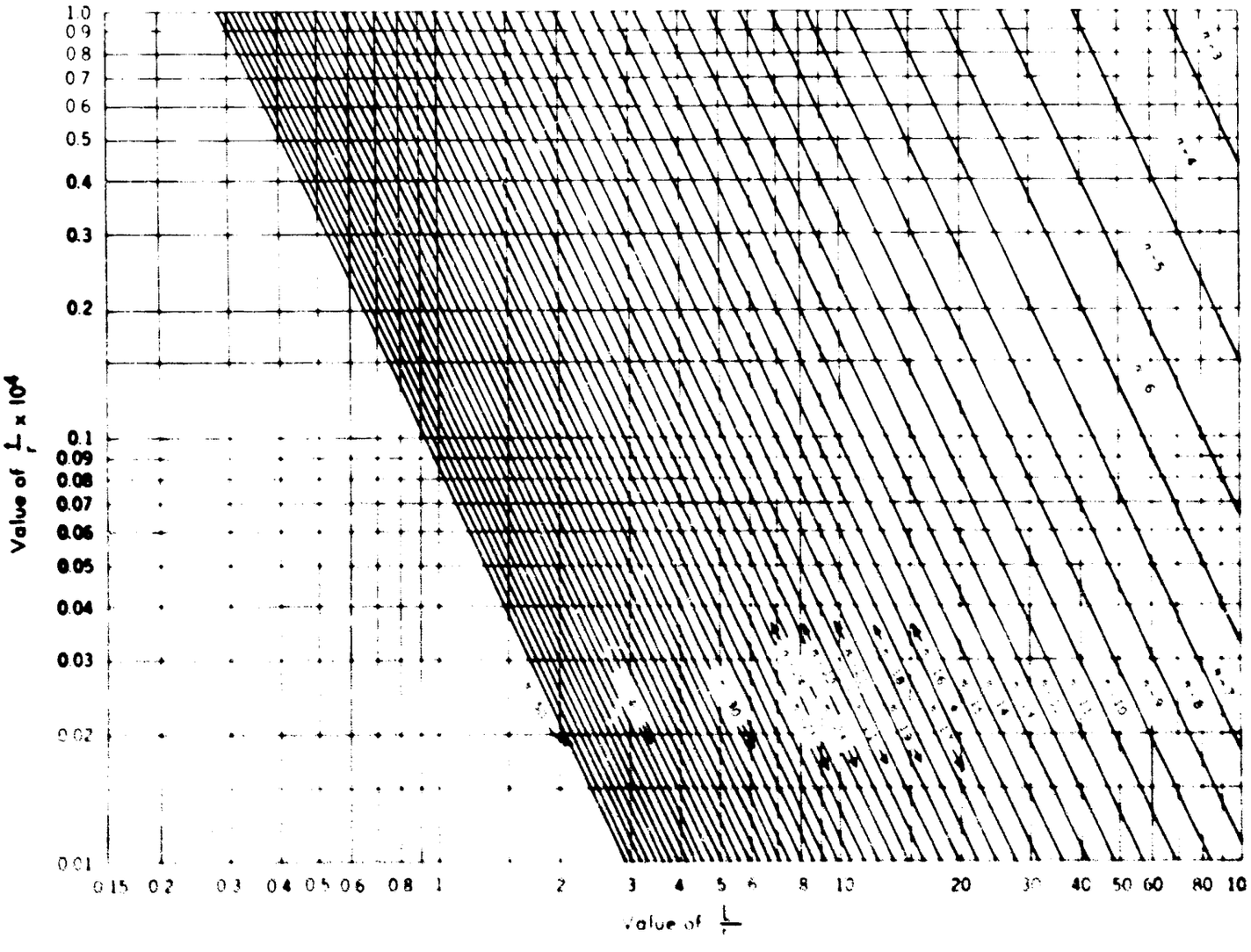


Fig. A1 Number of Circumferential Waves for All-Around or Lateral Pressure

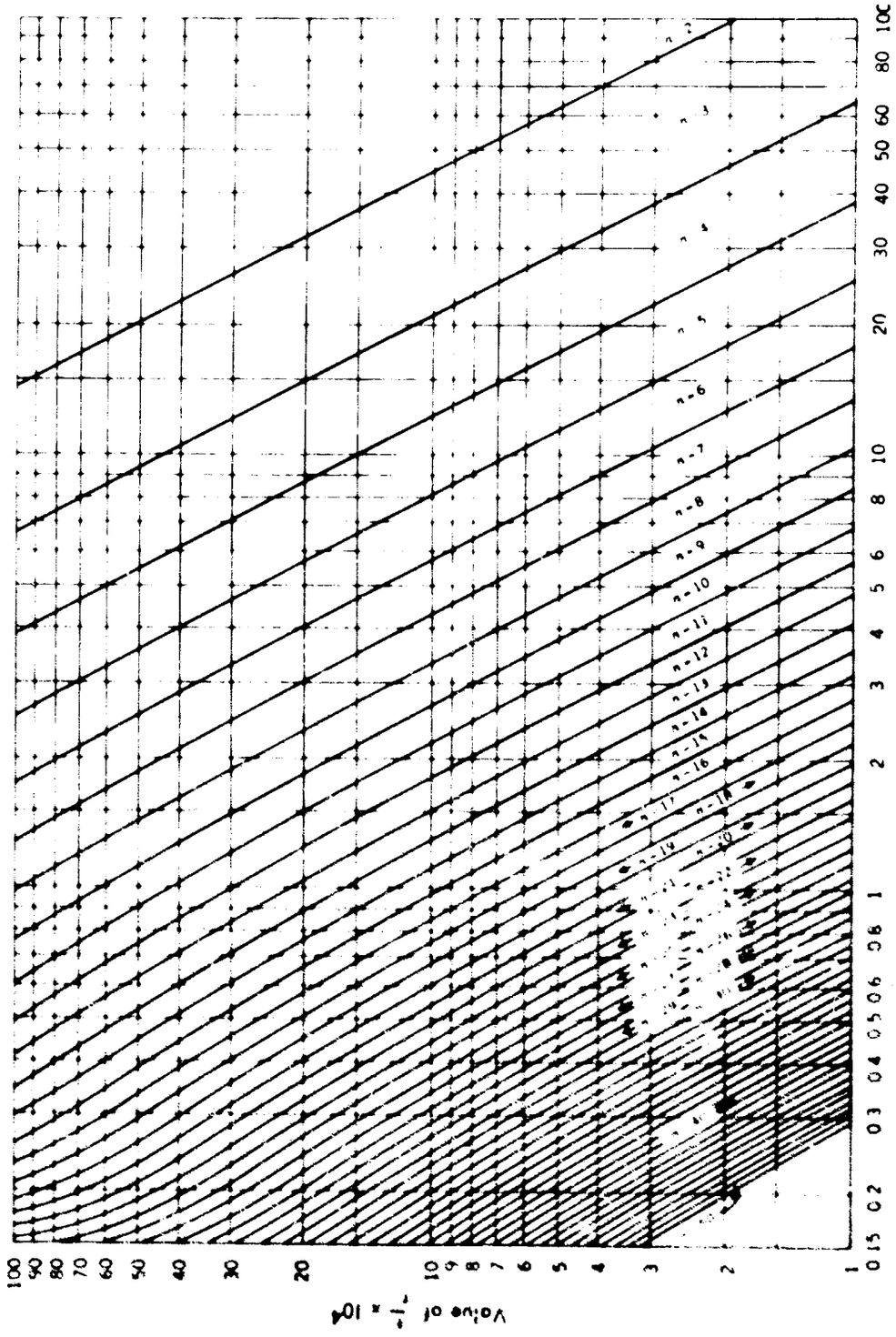
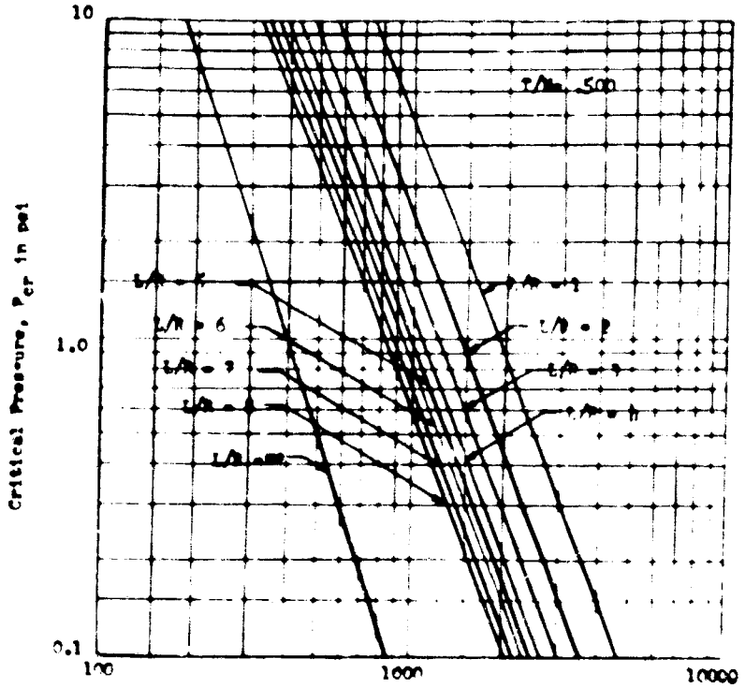


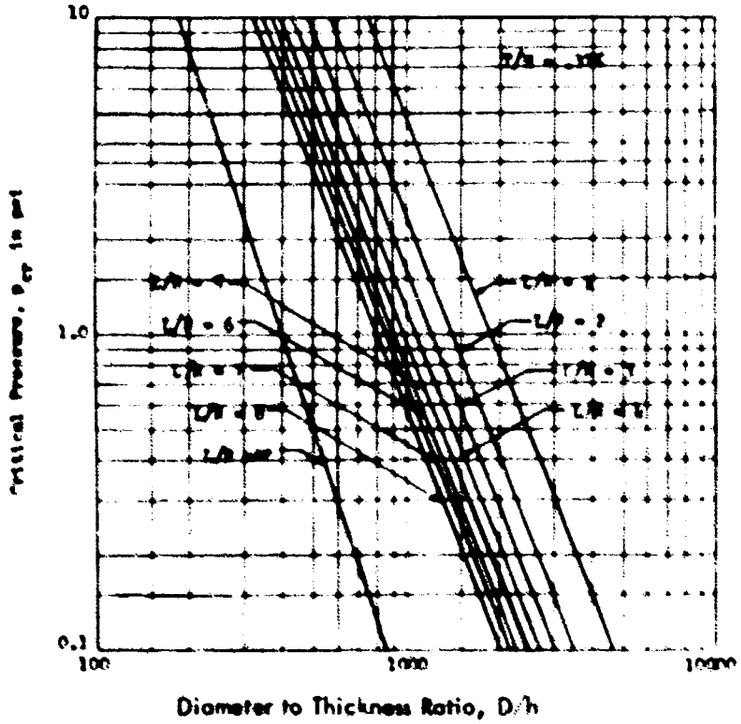
Fig. A2 Number of Circumferential Waves for Lateral Pressure



Diameter to Thickness Ratio, D/h

Poisson's Ratio = 0.330
Young's Modulus = 29 x 10^6 psi

Fig. A3 Armenakas-herrmann Formula



Diameter to Thickness Ratio, D/h

Poisson's Ratio = 0.330
Young's Modulus = 29 x 10^6 psi

Fig. A4 Armenakas-herrmann Formula

BURIED TUBES UNDER SURFACE PRESSURE

by
P. S. Bulson*

INTRODUCTION

This paper summarizes a number of recent investigations at M.E.X.E. into the deflection and collapse of thin-walled, flexible tubes buried in compacted sand, when the surface of the sand was under a static vertical overpressure. The tubes were unstiffened and open ended, and the majority were circular or square in section. Surface loading was by means of a uniform pressure applied hydrostatically.

Test specimens were made from mild steel sheet, and buried so that their longitudinal axes were horizontal. The moisture content of the sand was in the range 1% - 3.5%, and the average density after compaction was within a small percentage of 104 lbs per ft^3 for all tests.

Most of the tests have been made at a scale about 1/10th full size, so that the tubes were 8 or 10 inches diameter or side. Some tests have been made at about 1/3rd full size with tubes 30 inches diameter or side. To do this we have employed two testing rigs.

TEST EQUIPMENT

The 5 ft. rig

This is the smaller of the two, and measures 5 ft. square in plan, 4 ft. deep. It is shown diagrammatically in Figure 1. The steel container is filled with fine sand in 3 in. layers, and each layer compacted by two passes of a vibrating hammer fitted with a 6 in. square plate. This is found to give a very consistent density.

When the sand level reaches the bottom edge of two inspection ports, in opposite vertical sides of the container, the tube under test is placed on the sand so that its longitudinal axis is level, central, and in line with the ports. All tubes are 12 inches long. Inspection tunnels, made from tubes having the same section shape as the specimen are placed between the ends of the specimen and the ports, and all gaps sealed with plasticene. For very shallow depths of cover the tunnels are made with thick walls, so that they can be re-used, but at greater depth it is necessary to make the tunnels as flexible as the specimen, to eliminate earth arching across its length.

Further layers of sand are added and compacted until the desired cover is reached. In order to preserve the shape of the tube during this phase, wooden struts are placed inside (removed after compaction). A pair of soft rubber diaphragms, edged by a steel frame, is placed on the horizontal surface of the sand, and above this is a restraining structure is connected via links to the side of the container. As water is pumped into the space between the diaphragms a uniform pressure is applied over the sand surface. It is measured by a guuge included in the water supply system. The maximum working pressure of the rig is 100 psi.

Figure 2 shows the rig with the restraining structure and loading diaphragms removed, and the sand level with the base of the specimen and tunnels. Figure 3 shows a general view.

The 24 ft. rig

This is used for the one-third scale tests, and is shown diagrammatically in Figure 4. It consists of a reinforced concrete pit, 24 ft. square in plan, with vertical sides to depth of 4 ft. By building up the side walls with steel sections a total depth of 7 ft. can be obtained. Sand is layed by means of a travelling hopper, and compacted by vibrating roller. Inspection ports on opposite faces of the pit enable the behaviour of a specimen to be studied during loading. The positioning of specimens follows a similar sequence to the 5 ft. rig, and the same procedure is followed during compaction of the cover.

A similar loading system is used. In this case the diaphragms are 24 ft. square, and the restraining structure consists of large girders connected through heavy links to the side of the pit. Figure 5 shows the rig with loading diaphragm removed and a group of three girders in position. The working pressure is 50 psi.

---

* Head of Structures Group, Military Experimental Establishment, Ministry of Defence, Christchurch, Hampshire, England.

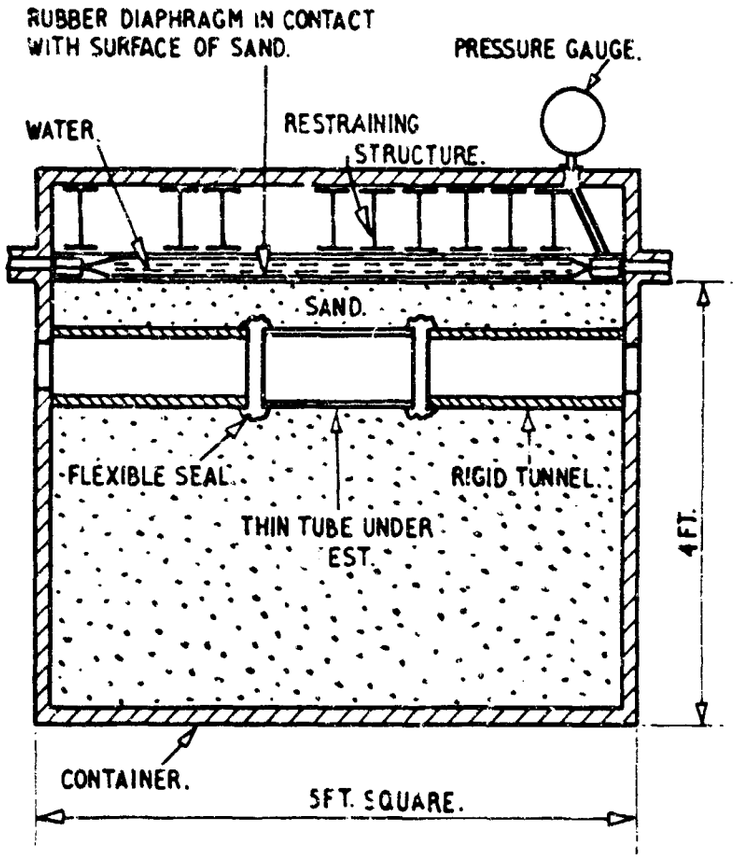


Fig. 1 Cross Section of Test Rig

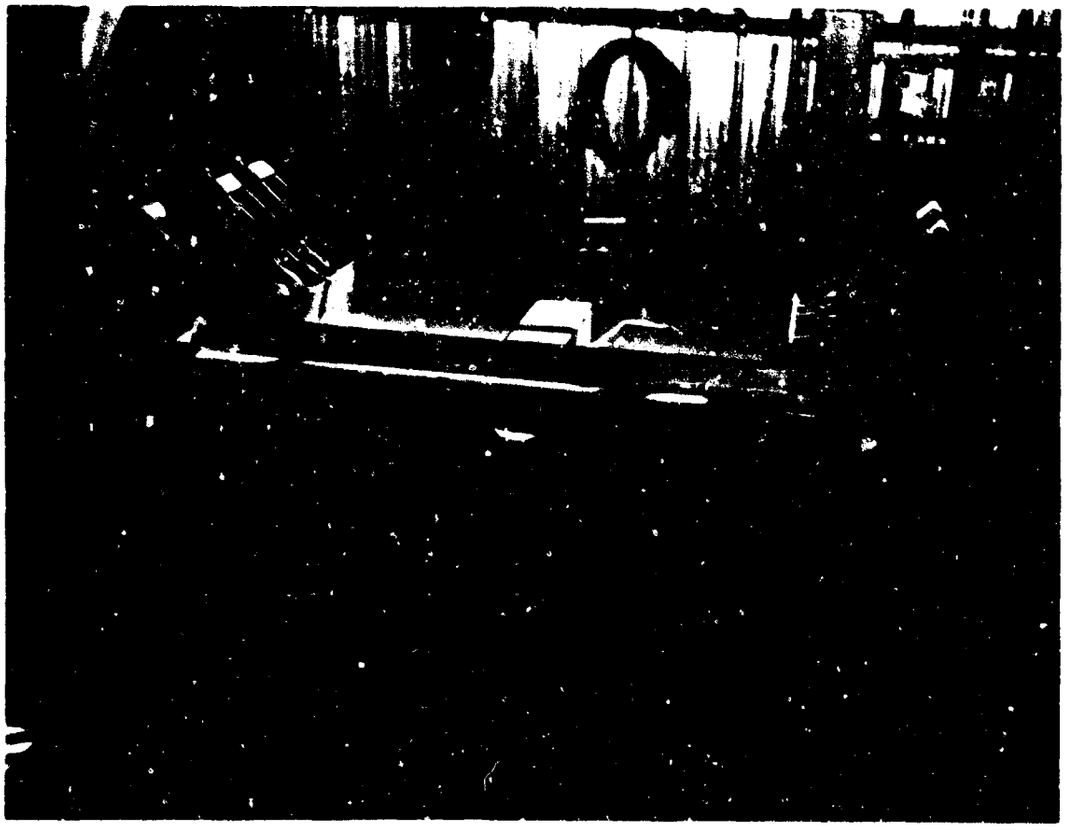


Fig. 2 Rig With Restraining Grid and Loading Diaphragms Removed, Showing Specimen and Tunnels

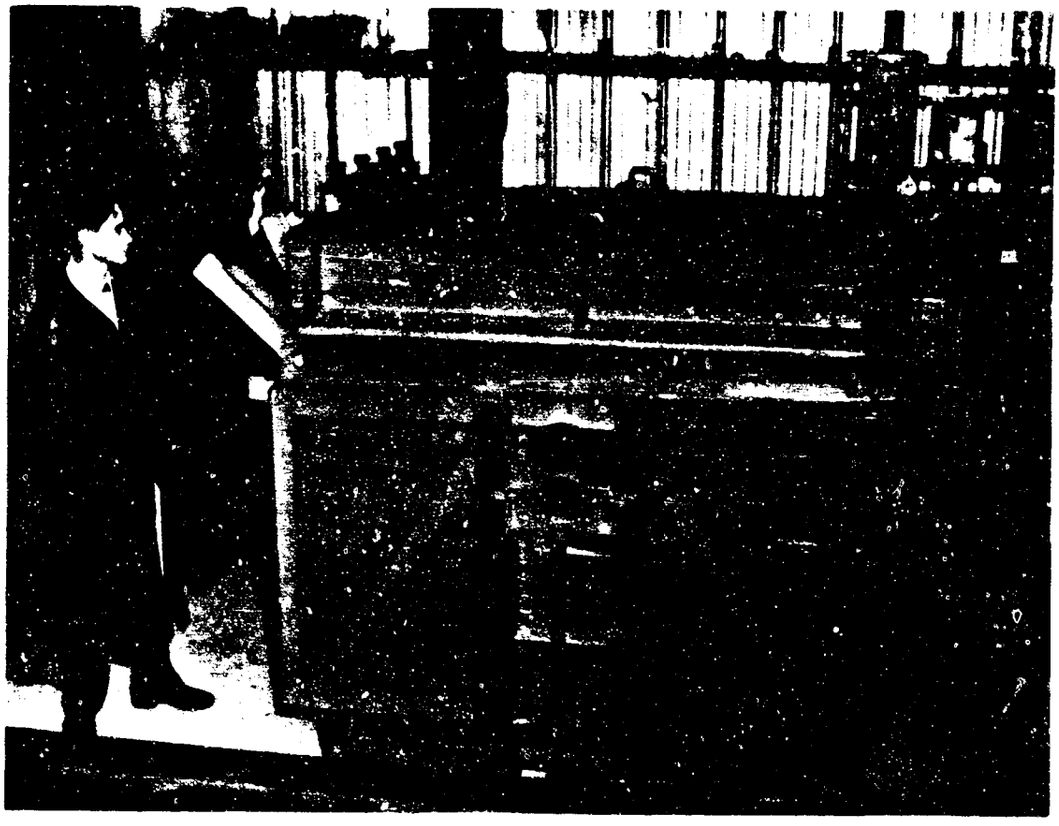


Fig. 3 General View of Test Rig

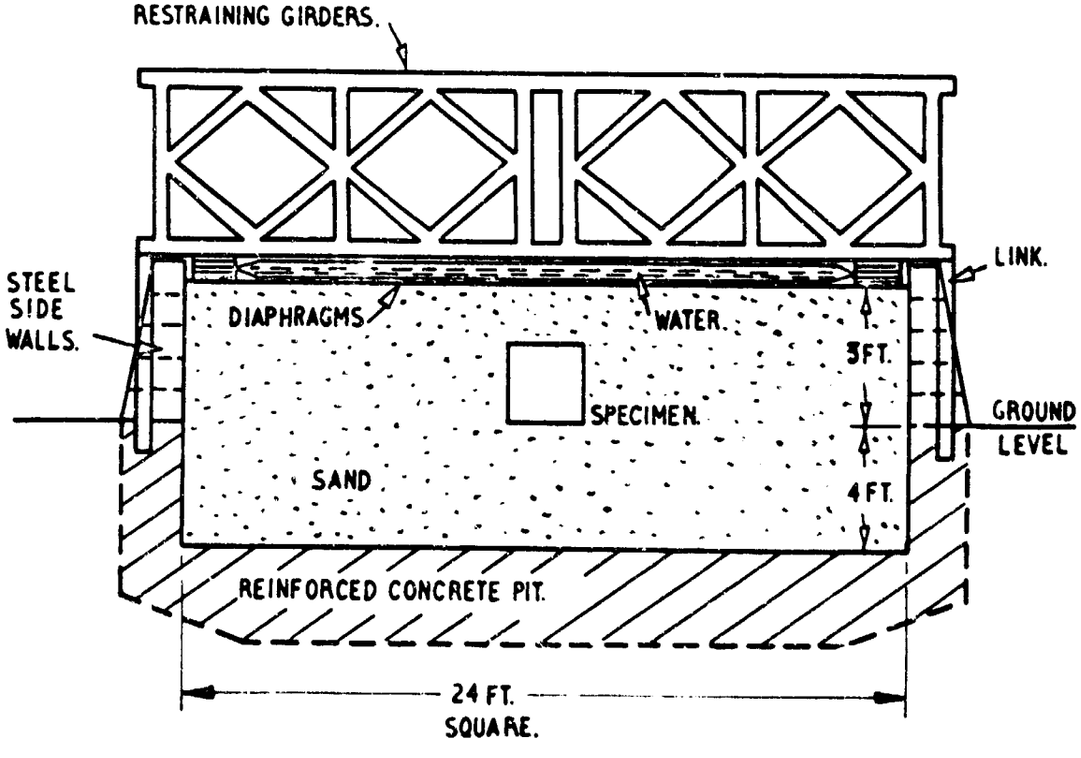


Fig. 4 Transverse Cross Section of 24 Ft. Rig

The plan area is large in relation to the size of the specimen to ensure the load on the specimen is not affected by side friction. A considerable quantity of sand is stored in large hoppers when not in use (Figure 6), and a gantry crane is used to handle the heavy apparatus. In both rigs the pit or container is completely excavated after each test, and refilled according to a strict compaction sequence. Excavation is by mechanical digger and conveyor belt. In order to keep moisture content of the sand as constant as possible, the whole installation is housed in a weathertight hangar.

Measuring apparatus

Apparatus for measuring specimen deflections in the 5 ft. rig consists of a long, heavy, stiff tube that passes through the tunnels and the specimen, and is held by bearings fixed externally to a supporting frame (Figure 7). The longitudinal centre of the tube carries a mounting for a potentiometric deflection gauge, which is placed in contact with any desired face of the specimen. As the gauge plunger moves an attached contact rides over a finely wound resistance in the body of the instrument, altering the balance of a pen-recorded bridge circuit. For circular cylinders, the gauge can

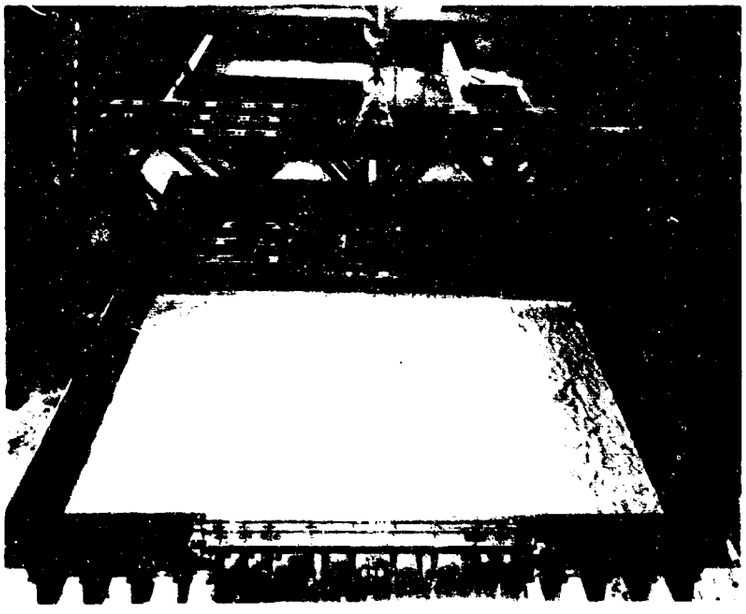


Fig. 5 24 Ft. Rig With Loading Diaphragm Removed

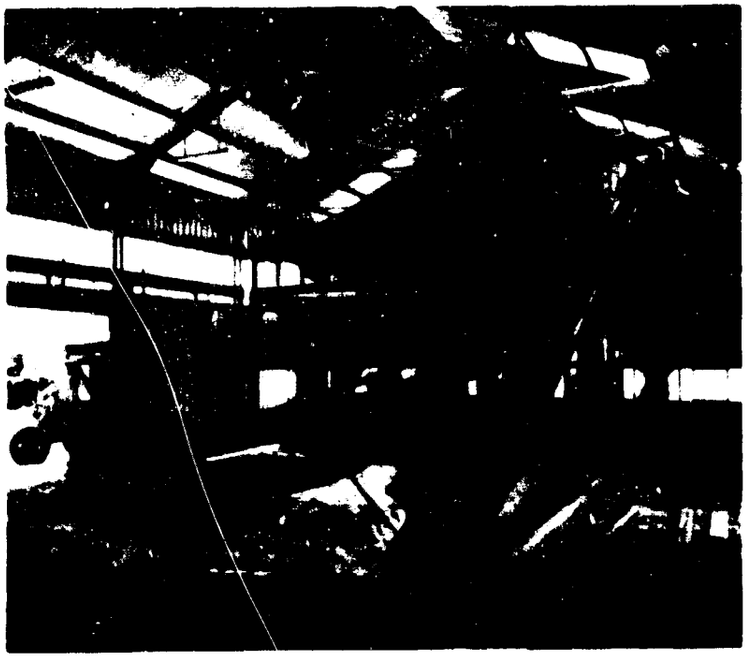


Fig. 6 Digger, Conveyors and Hoppers, 24 Ft. Rig

be rotated through 360° by rotating the main tube on its bearings, and in this way a complete record of radial deflections taken.

As deflections grow to the order of 2 inches, and collapse approaches, the apparatus is removed, and in the final stages deflections are measured by optical measuring devices (cathetometers). Sometimes the sequence is filmed using high speed cine-camera, and the film projected later in single frames. Rotations are measured by mounting graduated scales on slender rods, attached to the desired point on the specimen, and checking their movement by telescope.

All deflections so far observed in the 24 ft. rig have been by graduated scale and telescope. Facilities exist to measure strains in the walls of cylinders, using resistance strain gauges, and earth pressures, but the investigations to date have been limited to the measurement of deflections and over pressures only.

CIRCULAR TUBES

Tubes made from tin plated mild steel sheet ($E = 30 \times 10^6$ psi, $\sigma Y =$ 26,300 psi) with a thickness of 0.011 in. and diameters in the range 5 in. to 10 in. were tested in the 5 ft. rig. The depth of cover was either 3/8 or 1/4 x diameter, sand density 104 lbs per cu. ft.

As over pressure was increased each specimen buckled into a number of half waves around the circumference, and the roof simultaneously deflected inwards. Most tubes collapsed in the sequence shown in Figure 8. Large deflections of the buckles around the lower half of the circumference were followed by one half wave deflecting rapidly and failing. This was followed by collapse of the roof in a three half wave mode. In some tests roof failure occurred before the lower buckles reached ultimate capacity. Figure 9 shows a typical radial deflection plot, indicating large roof deflection and buckles around the lower rim.

Figure 10 shows the relation between over pressure at collapse (p_{max}) and the theoretical critical elastic buckling stress for the tubes under a uniform lateral pressure (q_{cr}). The experimental points are in each case the average of a number of tests, and as might be expected in tests involving instability of circular cylinders, the scatter was rather high. Bearing in mind the limited range tested, the results suggest an approximately linear relationship between p_{max} and q_{cr} for the depth of cover to tube diameter ratio (d/D) used. For d/D = 0.375,

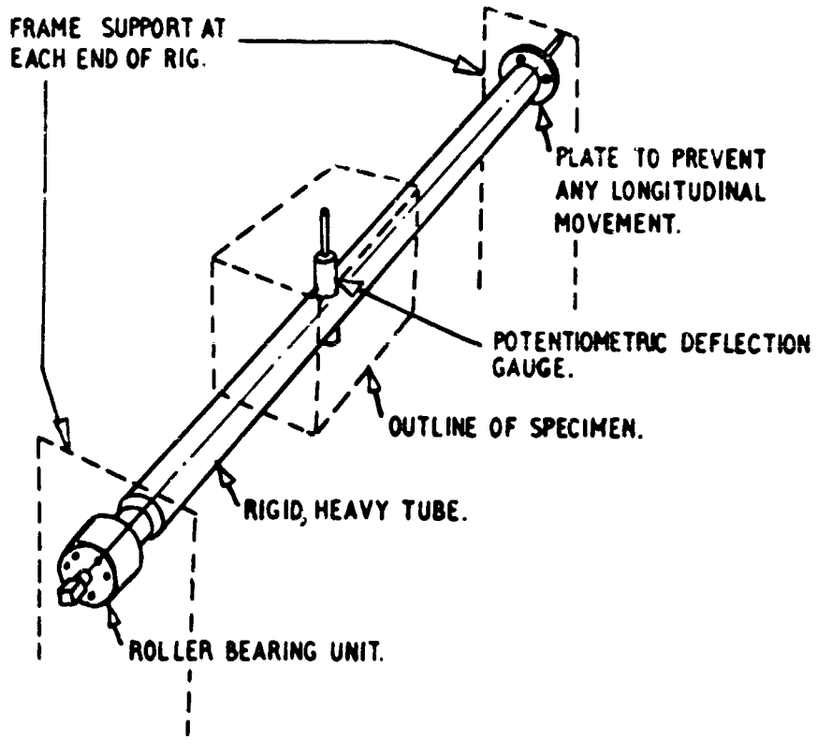


Fig. 7 Deflection Measuring Apparatus

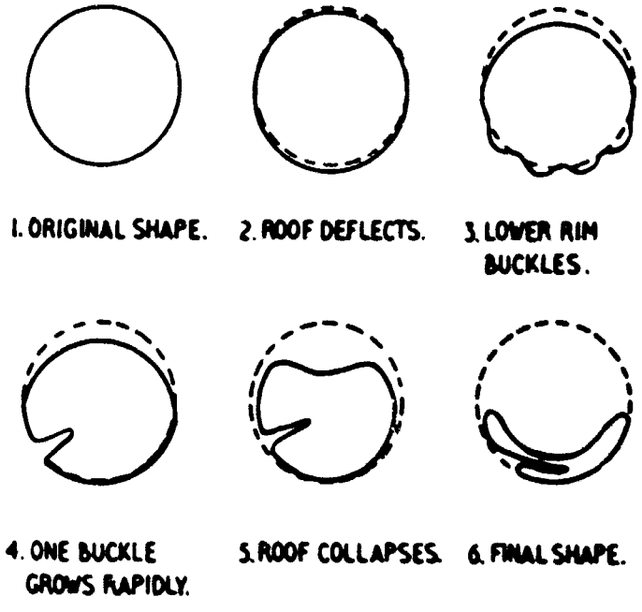


Fig. 8 Stages in Collapse of Thin Walled Tube

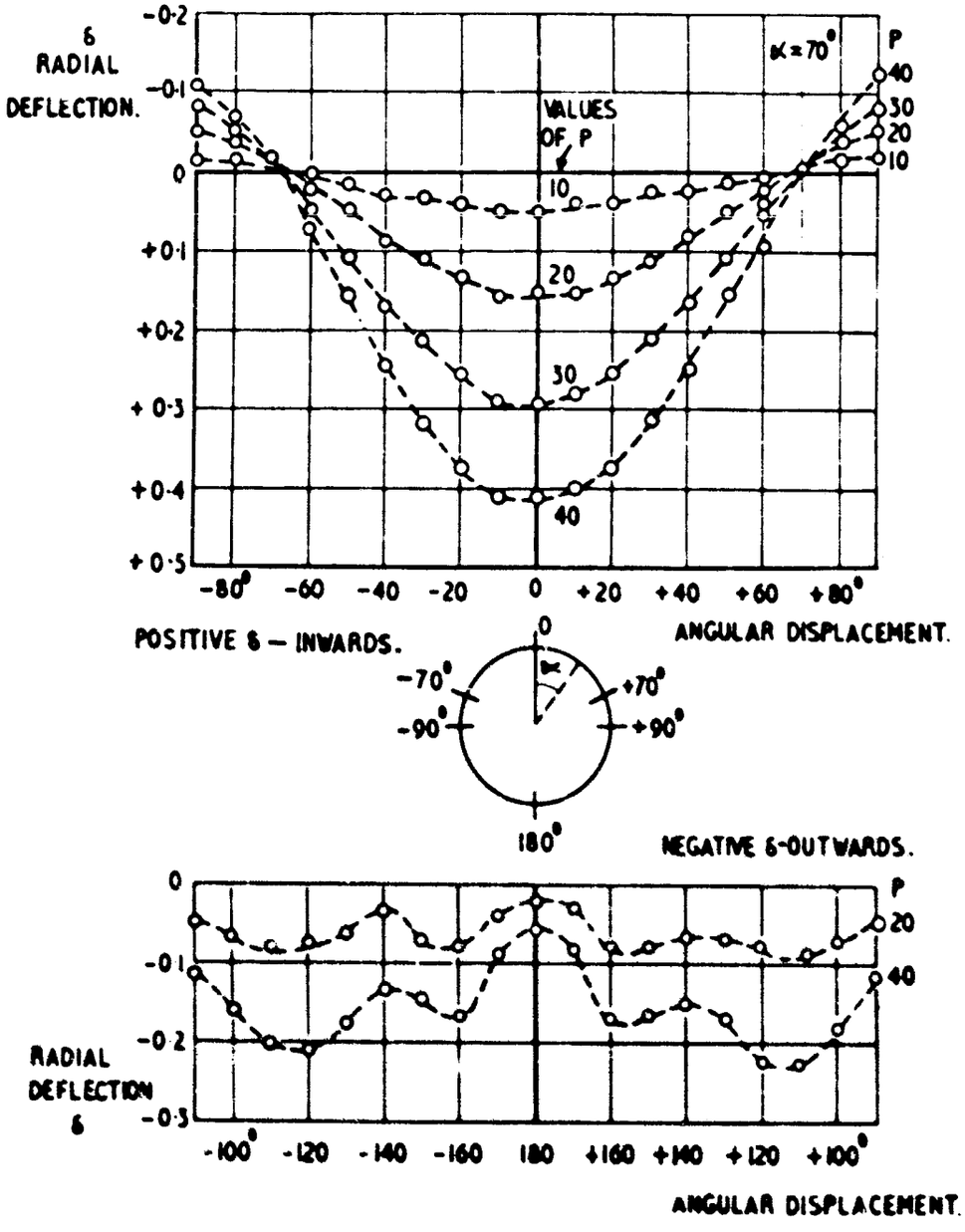


Fig. 9 Radial Deflections

P_{max}/q_{cr} = 6.2, and for d/D = 0.75, P_{max}/q_{cr} = 9.2.

Figures 11 and 12 are photographs of a specimen after formation of the local buckle (Figure 11), and after partial collapse (Figure 12). Figure 13 shows the top central vertical deflection, δ_c plotted against over pressure for three selected tubes. The relationship is linear, and the stiffnesses, P/δ_c, are: 60 psi per in. (d/D = 0.375) and 95 psi per in. (d/D = 0.75). The ratio of the stiffnesses for the two depths of cover (= 60/95), is of the same order as the ratio of P_{max}/q_{cr} (= 6.2/9.2) in Figure 10.

SQUARE TUBES 1): CONSTANT COVER, VARIABLE WALL THICKNESS

Depth of cover 3 ins.

Tubes made from mild steel sheet ($E = 30 \times 10^6$ psi, σ_Y = 30,000 psi), 8 inches square, were tested in the 5 ft. rig. In the first series, the depth of cover remained constant at 3 ins., but the gauge of the sheet varied between 0.165 in. and 0.038 in., giving side/thickness ratios in the range 210–485. Sand density was 104 lbs per cu. ft.

As the over pressure increased, the roof of each tube deflected downwards. The relation between over pressure and deflection was linear at first, then followed a large increase in deflection for a small load increment, as plastic hinges formed at the upper corners of the tube. At this time horizontal deflections of the centres of the vertical sides were negligible. Further over pressure resulted in very large roof deflections, until one vertical side collapsed under a combined end and lateral load. The collapse sequence is shown in Figure 14, and a tube after partial collapse in Figure 15.

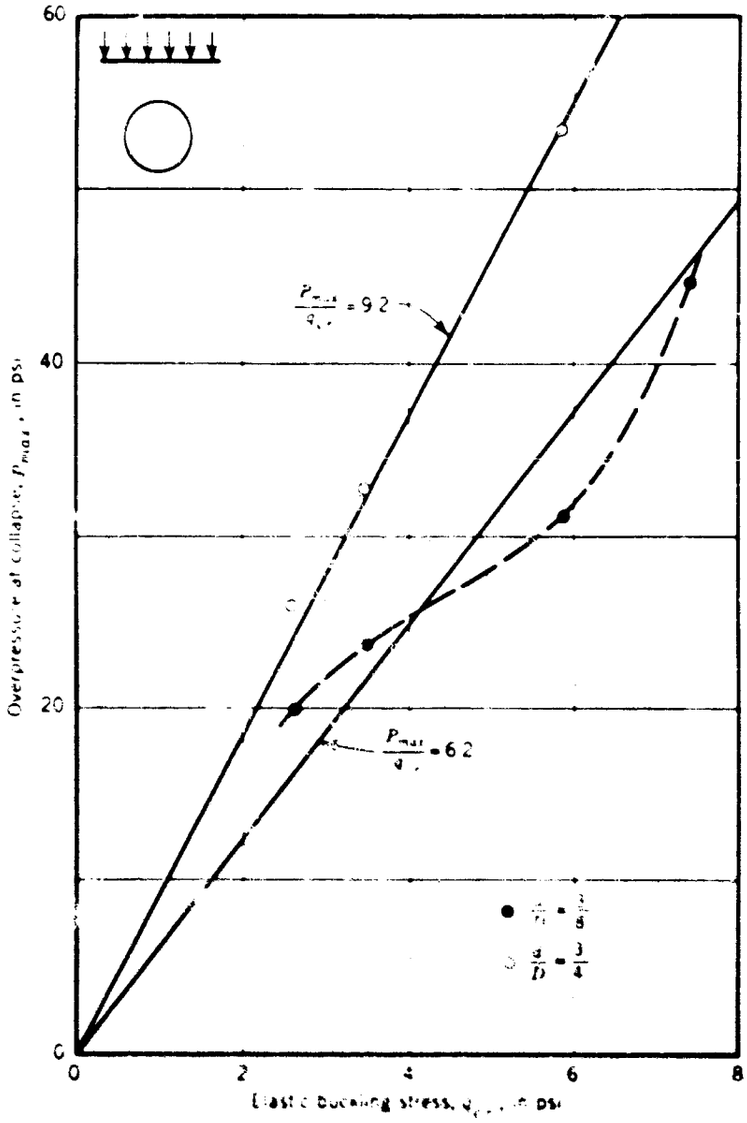


Fig. 10 Relation Between p_{max} and q_{cr} Circular Tubes

Curves of over pressure against roof deflection for a typical group of four similar specimens are brought together in Figure 16. Note that during early stages of loading the four specimens give similar readings, and that after the formation of plastic hinges the curves take the same linear form. The scatter in collapse pressures only appears at the very end of the loading sequence, suggesting variations in property of material or initial deviations from flatness rather than inconsistency in sand density. The deflection at which plastic hinges formed agrees well with the theory for a clamped roof under a uniformly distributed load.

Settlement of the whole specimen during loading was negligible. The angular rotation of the top corners of a specimen was measured optically, and the results appear in Figure 17. The sudden increase in rotation as the hinges form can be clearly seen.

As final collapse always occurred by the buckling of a vertical side, and the buckling load of a side plate under compression is a function of $(t/b)^2$, where t = wall thickness, b = wall breadth, it seems logical to compare collapse over pressure (p_{max}) with $(t/b)^2$. This has been done in Figure 18, which shows an approximately linear relation, with a proportional increase in scatter at higher values of p_{max}. The relation between roof stiffness (p/δ_c)



Fig. 11 Tube Removed From Test Rig After Formation of Local Buckle

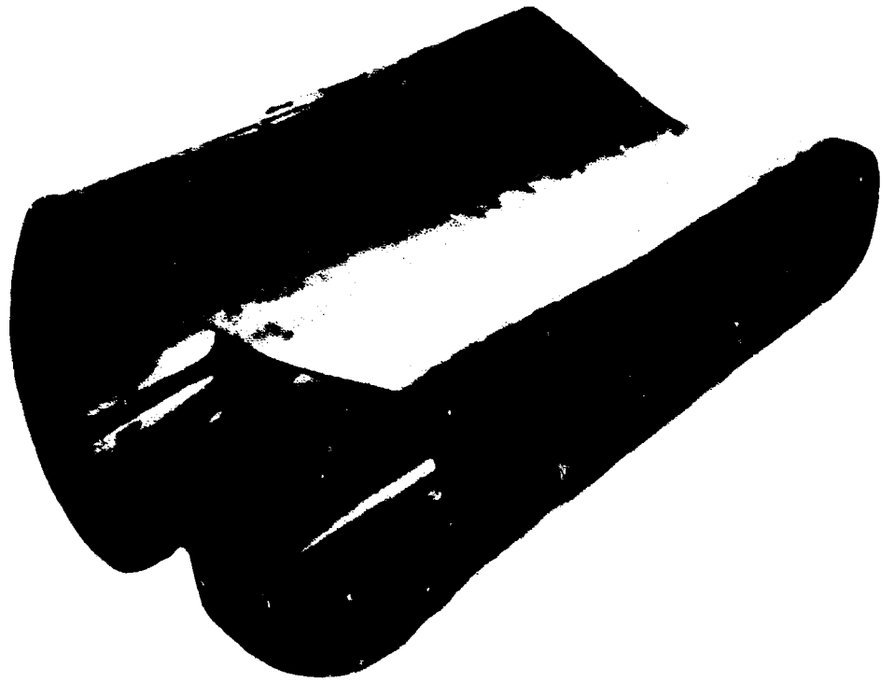


Fig. 12 Tube After Partial Collapse, Showing Local Buckle and Form of Roof Failure

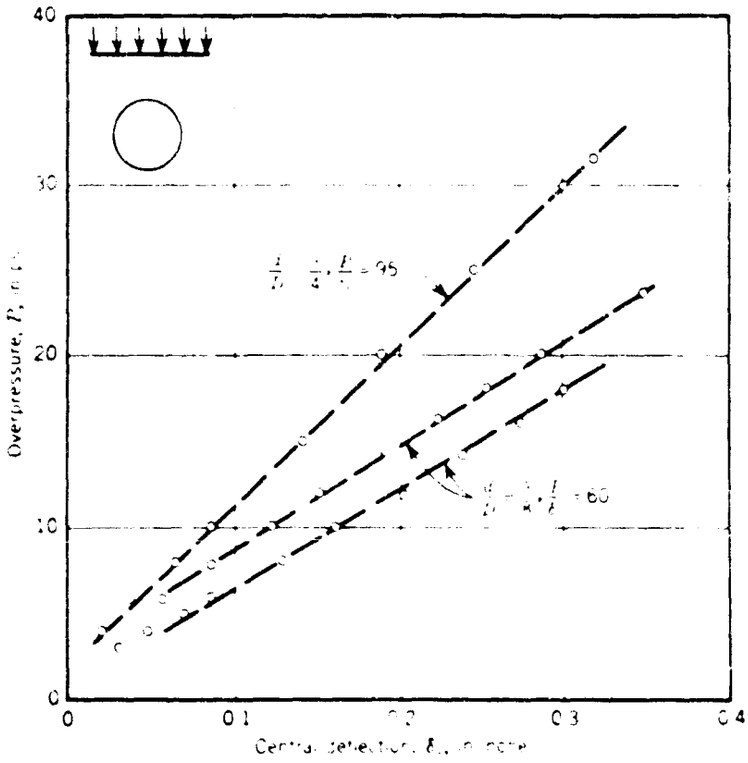


Fig. 13 Relation Between p and δ_o Circular Tubes

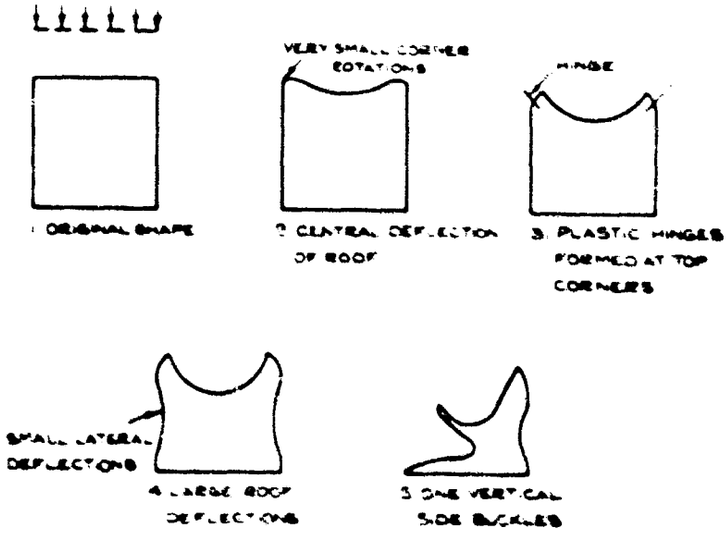


Fig 14 Stages in Collapse of 8 Inch Square Tubes Under 3 Inches Cover

and $(t/b)^2$ can also be shown to be linear.

For a second series of tests the depth of cover was increased to 6 ins., and tubes in the same range of side/thickness ratios examined. The moisture content of the sand varied between 1.3% and 2.3%, the average density being 103.2 lbs per cu. ft. As the over pressure was applied the roof of each tube deflected downwards, and the sides inwards. Roof and side deflections were in some instances of the same order, suggesting equality of vertical and horizontal pressure. This was different to behaviour at 3 ins. cover, when horizontal deflections were negligible.

As plastic hinges formed at the top corners of the tube there was a slight increase in deflection for small load increments, but much less marked. Further pressure increase resulted in large deflections of roof and sides until both vertical sides collapsed simultaneously inwards. This simultaneous collapse occurred in every test. The collapse sequence is shown in Figure 19, and a tube after partial collapse in Figure 20.

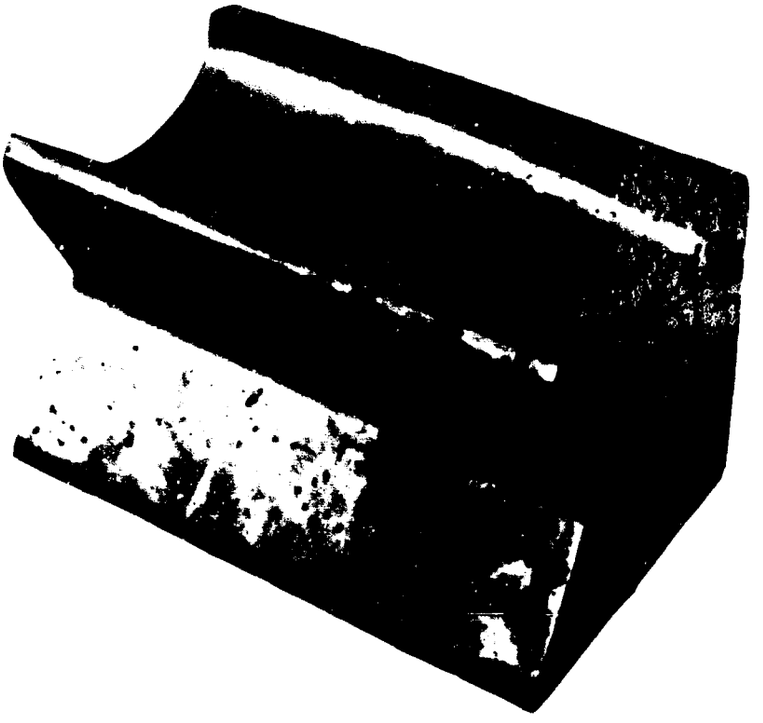


Fig. 15 Specimen After Collapse

Curves of over pressure against roof deflection for a typical group of three similar specimens are brought together in Figure 21. As in the 3 in. cover tests, the scatter in collapse pressures only appears at the very end of the loading sequence, suggesting variations in property of tube material or initial deviations from flatness. For a soil/structure experiment, the scatter of results seems quite small.

Because collapse always took place by the buckling of vertical sides, we have again compared collapse over pressure (p_{max}) with $(t/b)^2$. Figure 22 shows the linear relation that results.

Relationship between p_{max} and $(t/b)^2$

The above results suggest the relation:

$$p_{max} = k(t/b)^2 \times 10^6 \text{ psi}$$

Values of k from the tests were:

3 in. cover, k = 1.7,
6 in. cover, k = 3.0.

Before accepting these values for k an important limitation in the experimental technique should be noted. The approach tunnels at each end of all specimens were very stiff. The distance between the ends of these, across the length of the specimen, was 12 in., and this was reckoned to be large enough in comparison with the depth of cover to preclude arching across the specimen in that direction. However, as subsequent tests, described later, show, the stiffness of the tunnel does increase the collapse pressure. The measured values of k, therefore, are high.

SQUARE TUBES 2) : CONSTANT WALL THICKNESS, VARIABLE COVER

Wall Thickness .020 in; side width 8 in.

Tubes made from mild steel sheet ($E = 30 \times 10^6$ psi, $\sigma_Y = 30{,}000$ psi), with b/t ratio = 400 were tested in the 5 ft. rig. The depth of cover was increased from zero to 12 in. in increments of 3 in. Tests were first made with stiff inspection tunnels, but the collapse pressures rose so rapidly when the depth of cover exceeded 9 in. that it was clear the tunnels were offering additional support. It was decided, therefore, to make them the same thickness as the specimen - which meant new tunnels for each test. Three, and in one case four, specimens were tested at each depth. The degree of scatter was low.

In Figure 23 collapse overpressure (p_{max}) is plotted against $(d)^2$, where d is the depth of cover. The

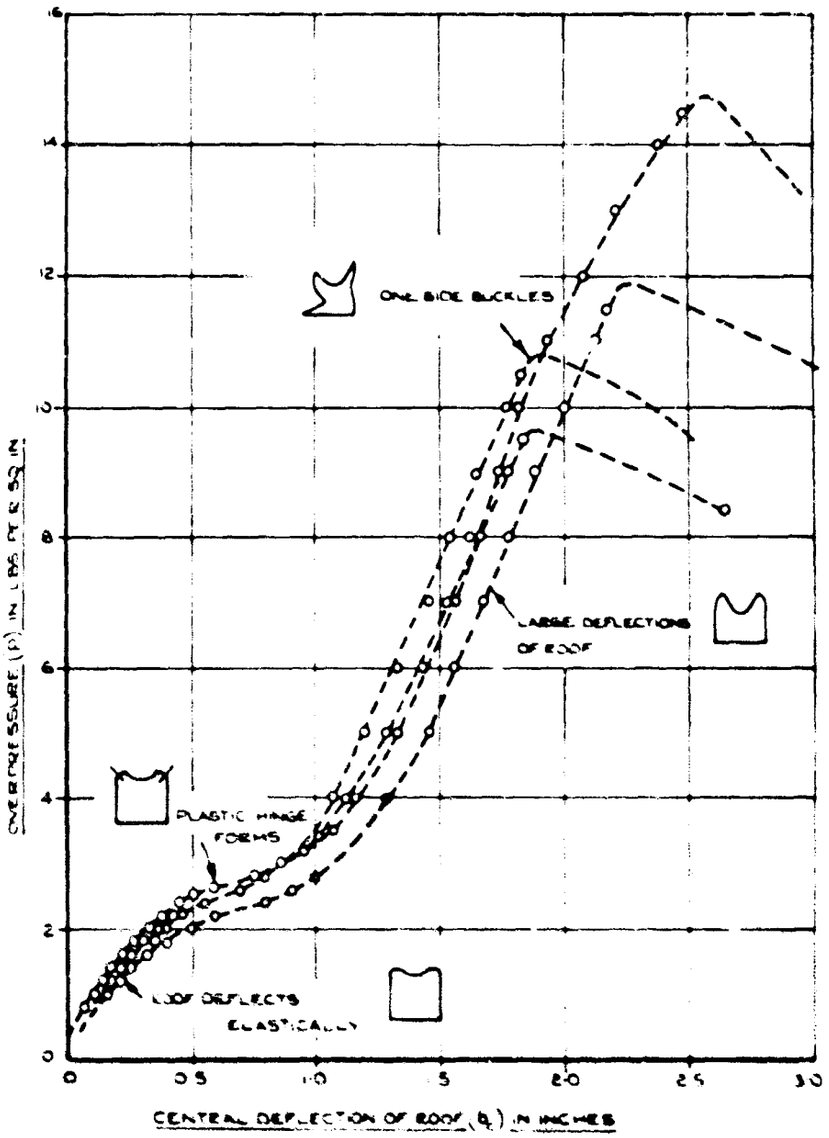


Fig. 16 Central Deflection of Roof Depth of Cover 3 Inches

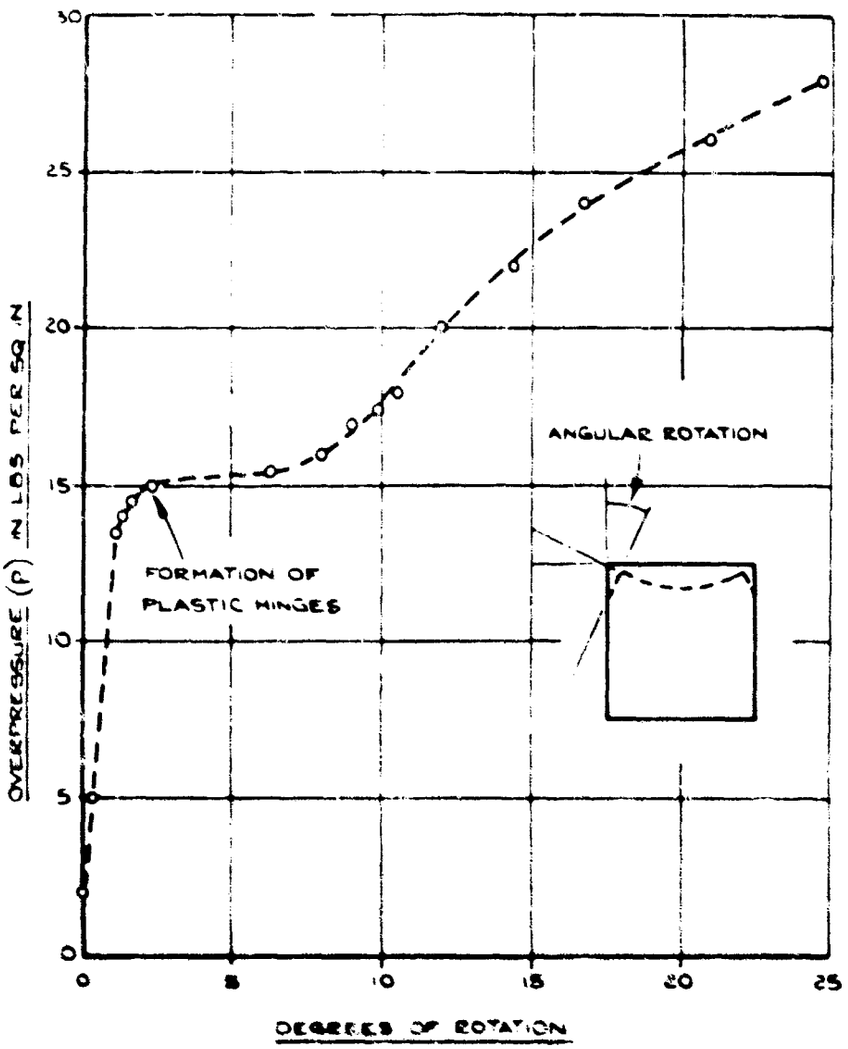


Fig 17 Angular Rotation of Top Corner. Depth of Cover 3 Inches

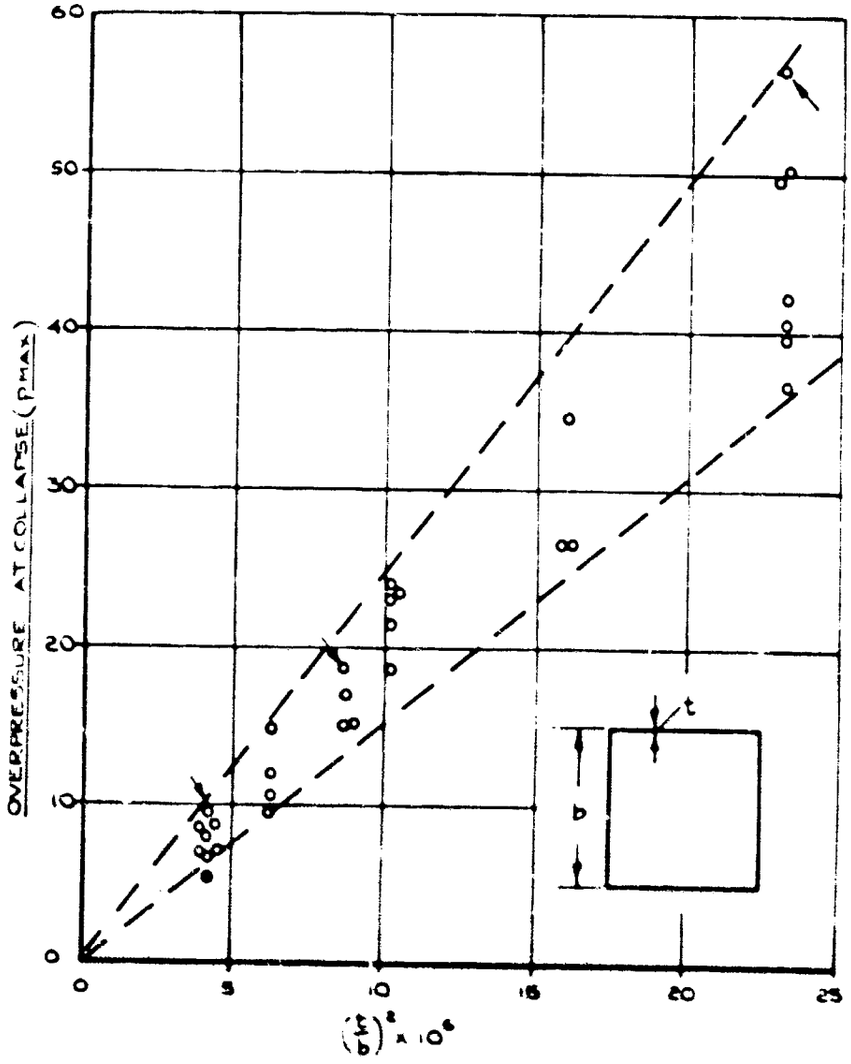


Fig. 18 Relation Between p_{max} and $(t/b)^2 \times 10^6$. (Depth of Cover 3 Inches) (Doubtful Results Arrowed)

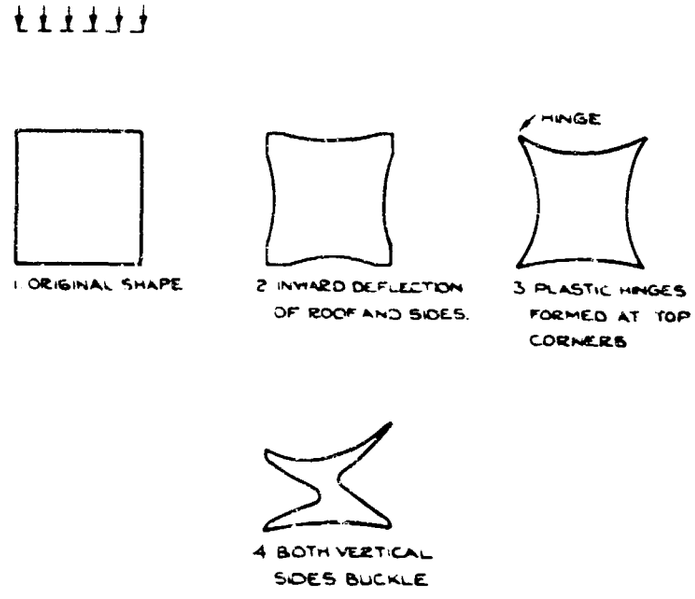


Fig. 19 Stages in Collapse of 8 Inch Square Tubes Under 6 Inches Cover

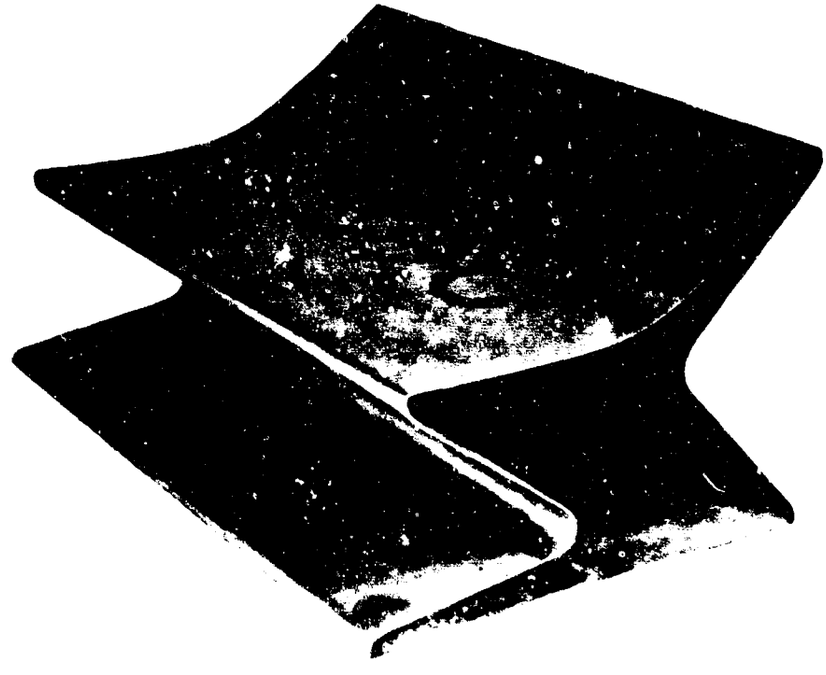


Fig. 20 Specimen After Collapse (6 Inch Cover)

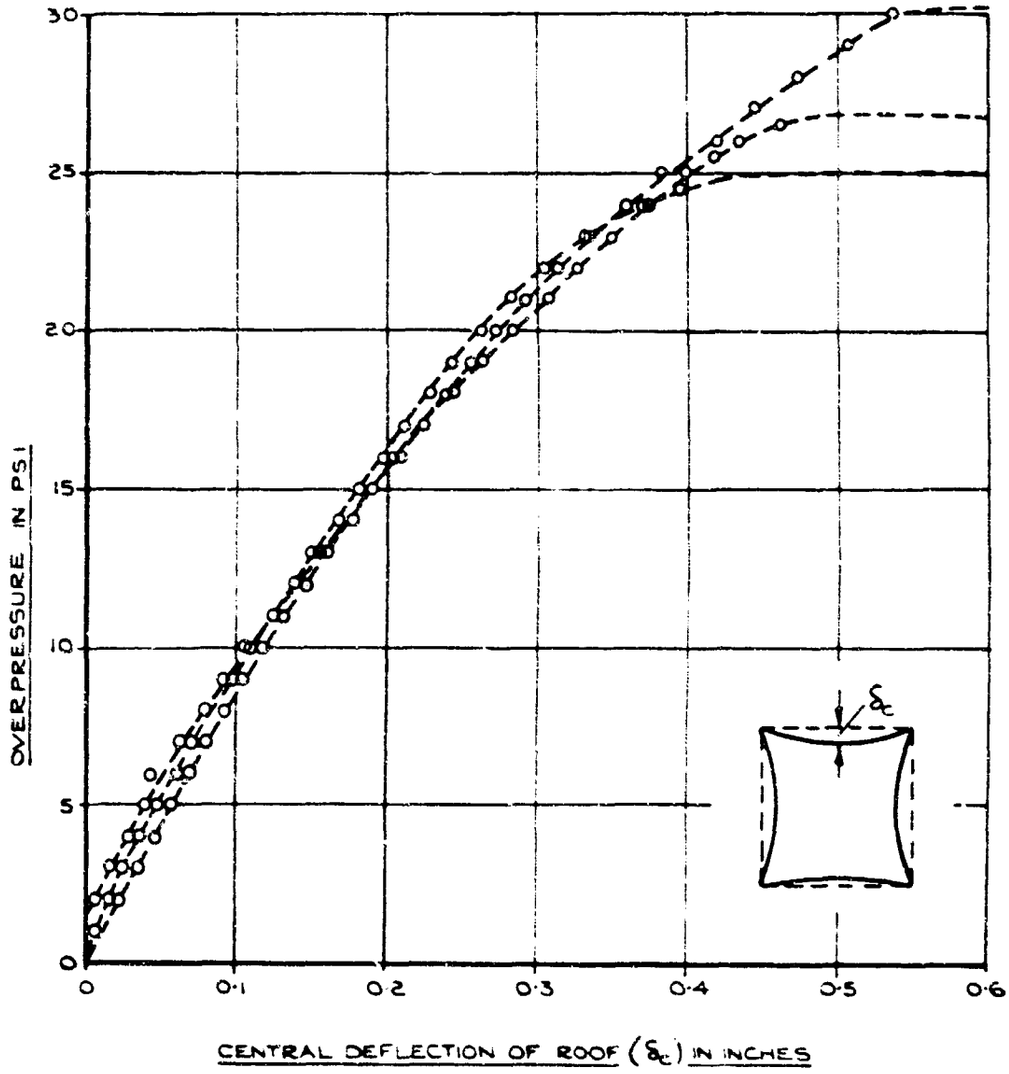


Fig. 21 Central Deflection of Roof. Depth of Cover 6 Inches.

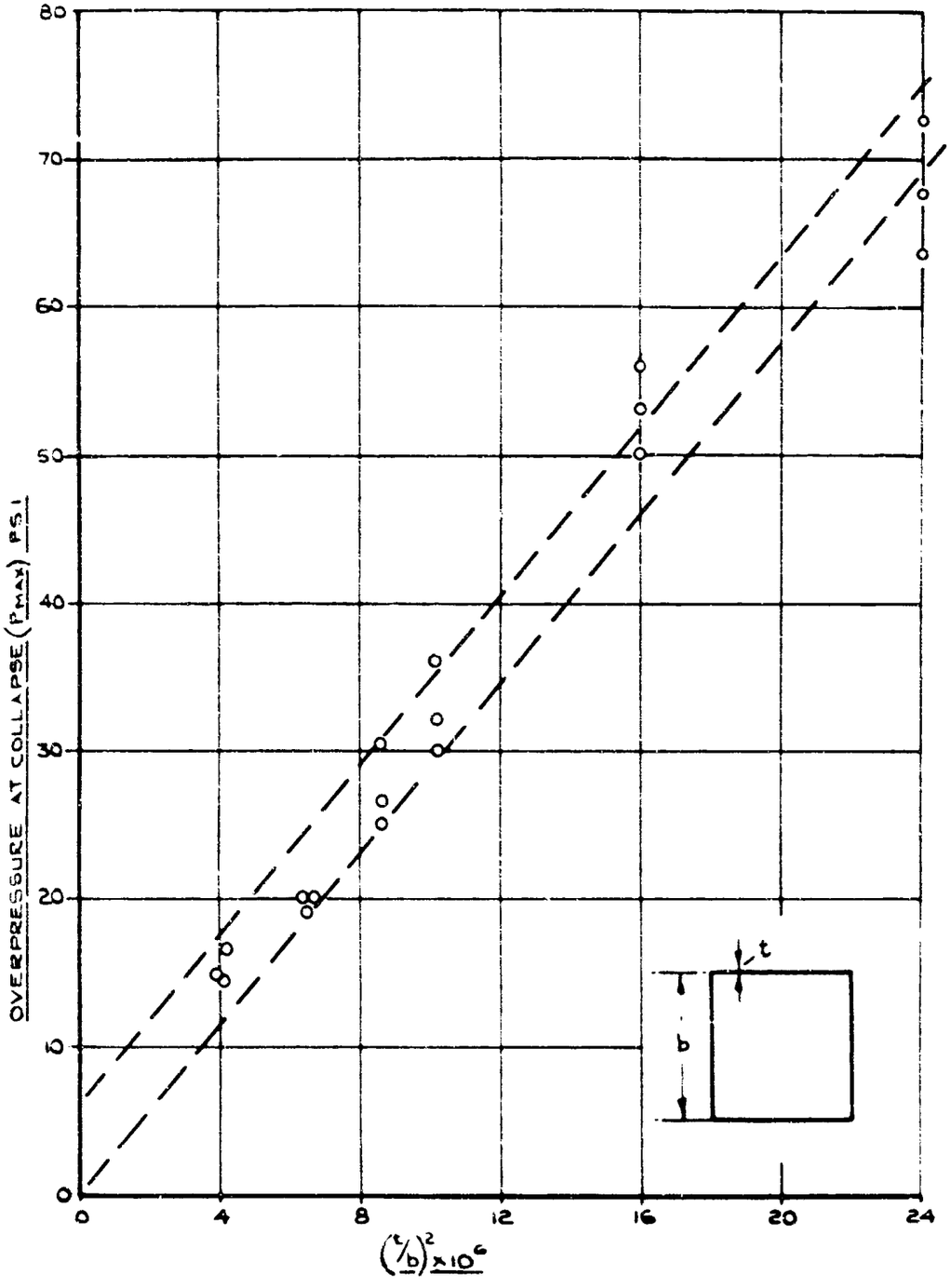


Fig. 22 Relation Between p_{max} and $(t/b)^2 \times 10^6$ (Depth of Cover 6 Inches)

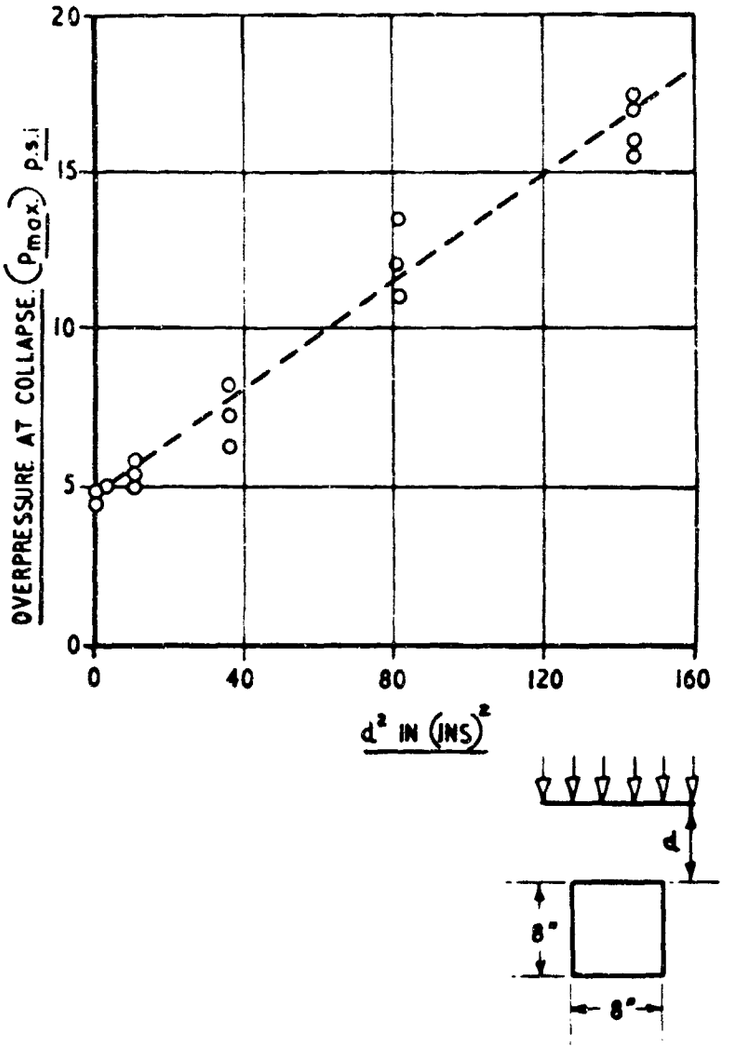


Fig. 23 Relation Between p_{max} and d^2 for Mild Steel Tube, Side 8 Inches, Thickness .020 Inch

relationship is shown to be linear over the range tested. For d = 0, 3 ins, collapse occurred by the buckling of one vertical side (as described earlier). For d = 6, 9, 12 ins. both vertical sides buckled simultaneously inwards. Figure 24 compares vertical displacement of the roof with horizontal displacement of the side for a specimen buried under 12 ins. cover.

Wall thickness .015 in.; side width 8 in.

Tests similar to those just described were also made with tubes having a wall thickness of .015 in. and a b/t ratio of 533. Figure 25 compares collapse overpressure with (d^2), and again the relationship is approximately linear.

Relationship between p_{max} and d^2

The above results suggest the form

$$p_{max} = n(d)^2 \text{ psi}$$

Values of n from the tests were

$$t = .020 \text{ ins, } b/t = 400, \; n = 0.085,$$
$$t = .015 \text{ ins, } b/t = 533, \; n = 0.10.$$

Tests are continuing to evaluate n for tubes of smaller b/t ratio, and to extend the range of depth of cover.

SQUARE TUBES 3): INCREASING CORNER RADIUS

Tests have been made in the 5 ft. rig to examine the effect on collapse pressure of increasing the corner radius of a square section thin walled tube. The depth of cover was held constant at 3 ins, and the wall thickness at 0.015 ins. All tubes were basically 8 ins. square. The corner radius was varied in the following increments: 0, 1, 2, 3, 3.5 and 4 inches. An 8 inch side tube with a 4 in corner radius is, of course, circular. The tests were planned to study the effect of tube shape on soil arching. The inspection tunnels were made the same shape as the specimen but of much thicker material, so that collapse pressures are higher than we would expect with flexible tunnels.

Figure 26 shows the basic shape of the tubes, and the mode of collapse. Note that for smaller radii, collapse is by buckling of a vertical side, but for larger radii instability first occurs in the roof. In the latter cases, it was possible to continue loading after the appearance of the roof buckle, until eventually a vertical side collapsed inwards, but we have taken roof instability as the effective limit.

Over pressures at collapse are shown in Figure 27. Pressures at 2 in. corner radius are lower than at 1 in. because of the change in failure mode. Increase in collapse pressure as the corner radius exceeds 3 in., and the tube approaches a circular form, is very steep. Conversely, the presence of a small 'flat' in a circular tube can greatly reduce collapse pressure. Judging from previous sections of this paper, when collapse occurs by instability of a vertical side, $p_{max} \propto (t/b_1)^2$, where b_1 is the flat length down the side. A curve of this form is shown to give good agreement, including the odd result at 2 in. radius where we continued loading after roof instability, until the vertical side collapsed.

Instability in the roof must be associated with a hoop stress around the curved corner. If we assume a radial pressure here, it can be shown that for the roof $p_{max} \propto (t^3/b_1^2 r)$, where r is corner radius. A curve of this form is shown to agree with test results for r = 2, 3, and 3.5. For the completely circular section the collapse mode is again different, and the maximum overpressure much higher.

The test results can be explained by considering only the structural behaviour of the tubes, without reference to soil properties. This suggests that the shape of the roof, and any effect it has on soil arching during the early stages of loading, has very little influence on collapse pressure.

SQUARE TUBES IN THE 24 FT. RIG

The first tubes tested in the 24 ft. rig were circular, but in order to examine scale effect, with special reference to the large number of square tubes tested in the 5 ft. rig, the main experiments so far have been on tubes 30 in. square. These were made from 14 or 16 gauge material (thickness .080 and .062 ins.), and buried with a cover depth of 11.25 ins. The density of the sand after compaction by roller, was 104 lbs per cu. ft., which agreed closely with sand density in the 5 ft. rig. The inspection tubes were stiff compared with specimens.

The depth of cover (d) was chosen as 11.25, to give the same (d/b) ratio already used in one of the 5 ft. rig test series (d/b = 0.375). The sheet thickness .080 ins gave a b/t ratio of 375, and the thickness .062 a ratio of 484. The latter agrees closely with one of the small scale tubes (t = .0165, b/t = 485) so the scale of the test was 30:8 in all

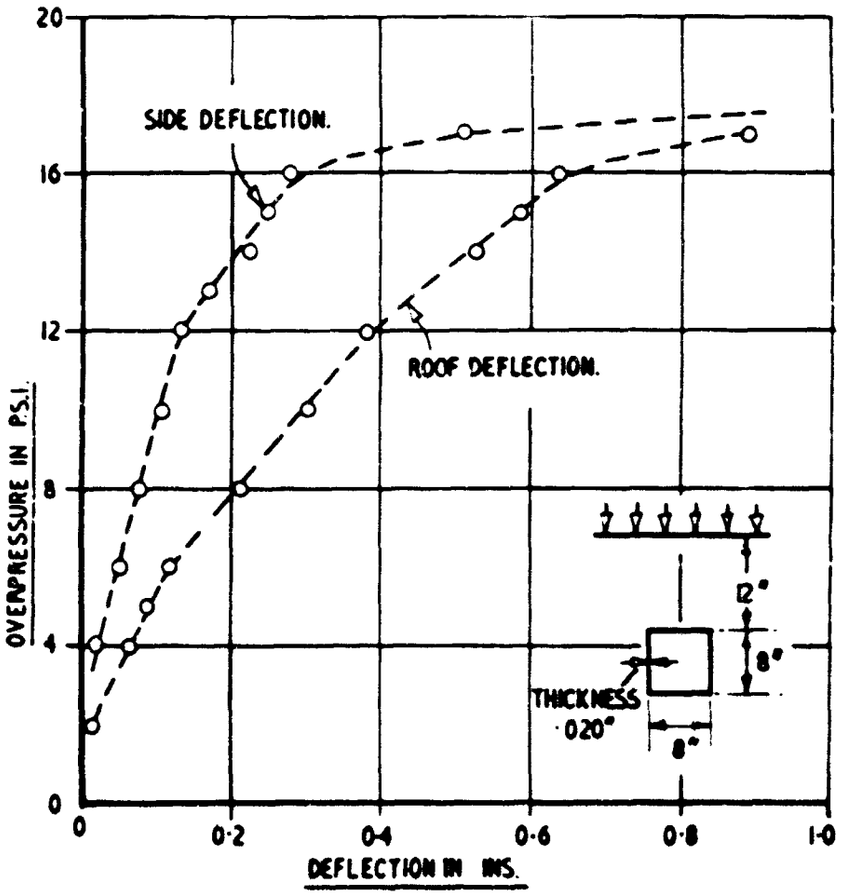


Fig. 24 Roof and Side Deflection of 8" Square Tube, 0.020" Thickness, Buried 12" Below Surface

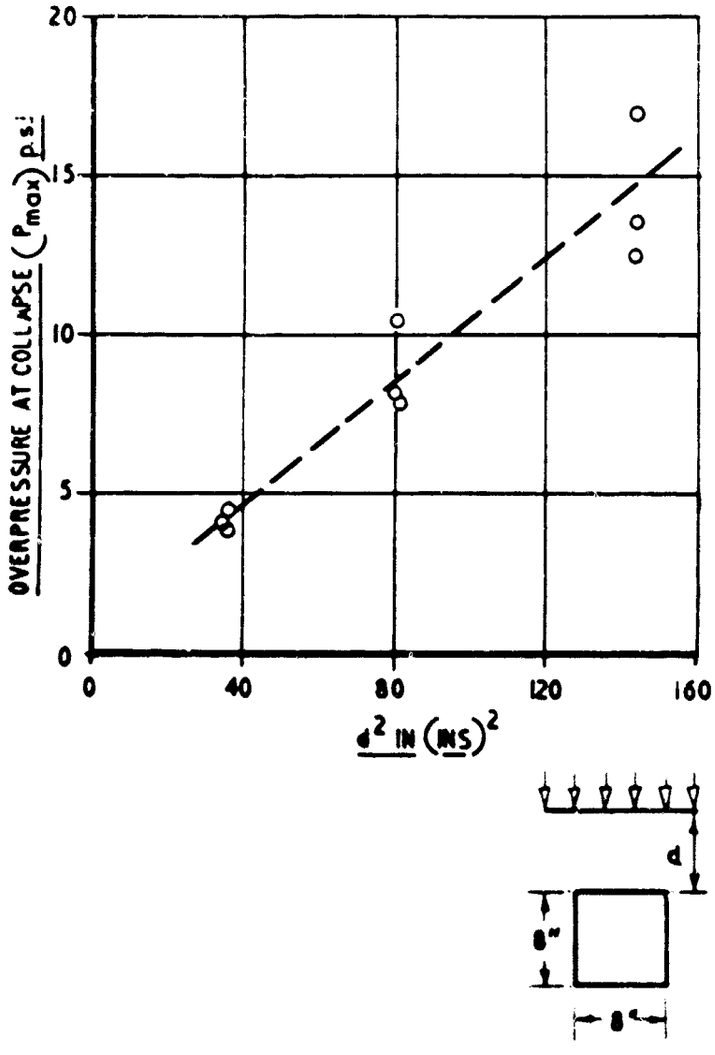


Fig. 25 Relation Between p_{max} and d^2 for Mild Steel Tube, Side 8 Inches, Thickness .015 Inch

geometrical respects.

In Figure 28, over pressure is plotted against δ/b, where δ is central deflection of the roof, for both scales. The one factor that does not scale is the dead weight of the sand, and because of this the initial deflections (before application of over pressure) are proportionately greater in the large scale test. The pressure on the shelter roof due to dead weight of sand is 0.18 psi in the 5 ft. rig, and 0.65 psi in the 24 ft. rig. The curves agree reasonably well, suggesting that roof stiffness is not affected by scale after loading begins. The collapse pressure of the large specimen is, however, considerably lower than for the specimen in the 5 ft. rig (3.5 psi as against 6.9 psi). This is thought to be again due to the dead weight of sand. When collapse finally occurs by buckling of a vertical side, the lateral pressure acting is considerably higher in the large rig, because there is a considerably heavier mass of sand moving between the slip line and the surface. Experiments are continuing to examine this explanation.

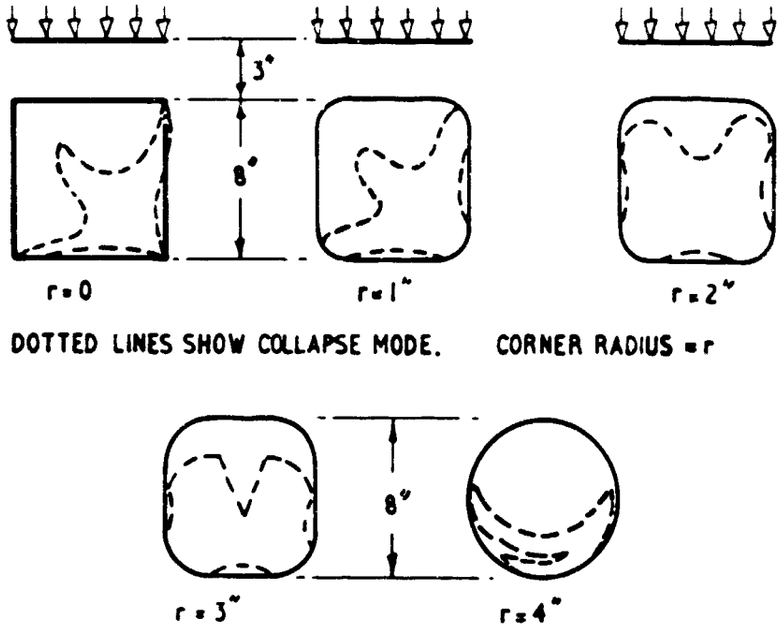


Fig. 26 Shape and Collapse Mode of Tubes With Increasing Corner Radius

TWO-DIMENSIONAL TESTS WITH GRANULAR MEDIUM

In support of the work described so far, and to investigate more fundamentally the role of a granular material surrounding a flexible structure, a third rig has been constructed. Details are shown in Figure 29. A steel frame 2 ft. 6 ins. long, 2 ft. high, 6 ins. thick, is packed with thin glass rods, about 3 mm. diameter, 5.75 ins long. The rods surround a 5.75 ins. long specimen of circular or square section thin walled tube. These specimens are shorter, but otherwise similar to those used in the 5 ft. rig. They are buried to a known depth of cover, and pneumatic loading is applied to the upper surface through a rubber air bag.

By arranging the rods in coloured layers it is possible to study their movement immediately preceding and during collapse. One face of the rig is plate glass, the other is metal. These enclose the rods but are not in contact with them. Figure 30 shows an 8 in. diameter circular specimen, buried to a depth of 3 inches, before loading. Figure 31 shows the configuration after collapse, which was sudden and catastrophic under the pneumatic load. Although the rods move with great acceleration, they remain parallel and do not break.

Figure 32 shows a square specimen after collapse of one vertical side. The slip line profile can be clearly seen. The results of a number of tests with square tubes of varying t/b ratio and depth of burial are brought together in Figure 33. The results of a large number of tests in this rig are now being analysed.

A similar rig, with higher sides, no top member, and no pneumatic loading, has been used to examine the arching of a granular material under its own weight. The results of typical experiments in this series are shown in Figure 34. In the first experiment, a thin walled square specimen (4 ins. side, .008 ins. thick) was loaded uniformly over its roof by layers of glass rods. The rods in each row were taped together with a flexible adhesive tape, to contain them as the height of the pile increased. The specimen rested on a wood base, and was held from side sway by two wood blocks that made contact with the upper corners, but allowed freedom of lateral deflection of the sides. Figure 34 shows a plot of depth of cover against roof deflection.

In the second test, wood blocks were placed to form a vertical sided trench above the specimen. Glass rods were again placed in layers so that the specimen roof was loaded, and were contained by the blocks as the height increased. Up to a depth of cover of 8 ins. there was no discernable difference in the loading curves for the two cases. In the third test, rods were placed over the whole area of specimen and side blocks. To a depth of cover of 4 ins. the cover/deflection curve remained very similar in form, but for deeper cover began to deviate. At a depth of cover of 8 inches there was only a small increase in deflection as the depth increased.

A programme of simple experiments like this has been planned to examine the behaviour of the tube under a variety of lateral supports, and with the applied load consisting of surface pressure as well as dead weight of rods. Eventually the effect of a plastic, or elastic loading media will be compared with that of the dry glass rods.

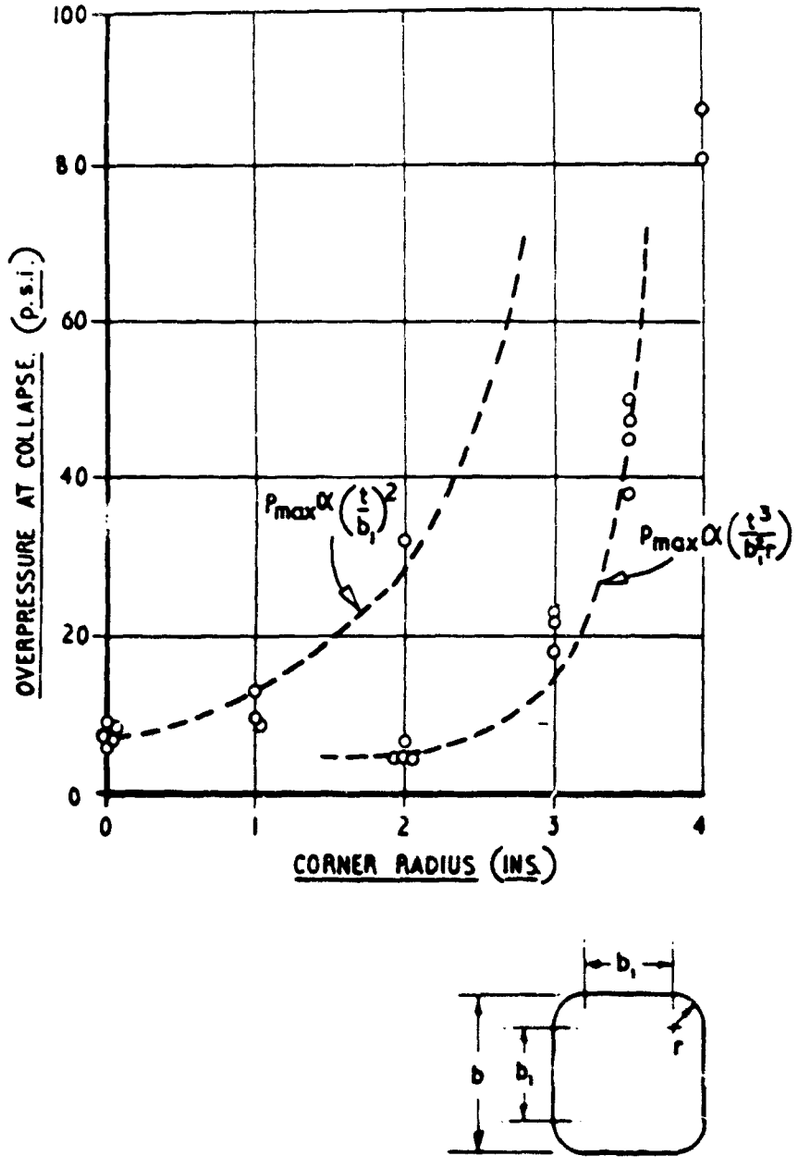


Fig. 27 Relation Between p_{max} and Corner Radius (r) for Mild Steel Tube, Side 8 Inches, Thickness .015 Inch

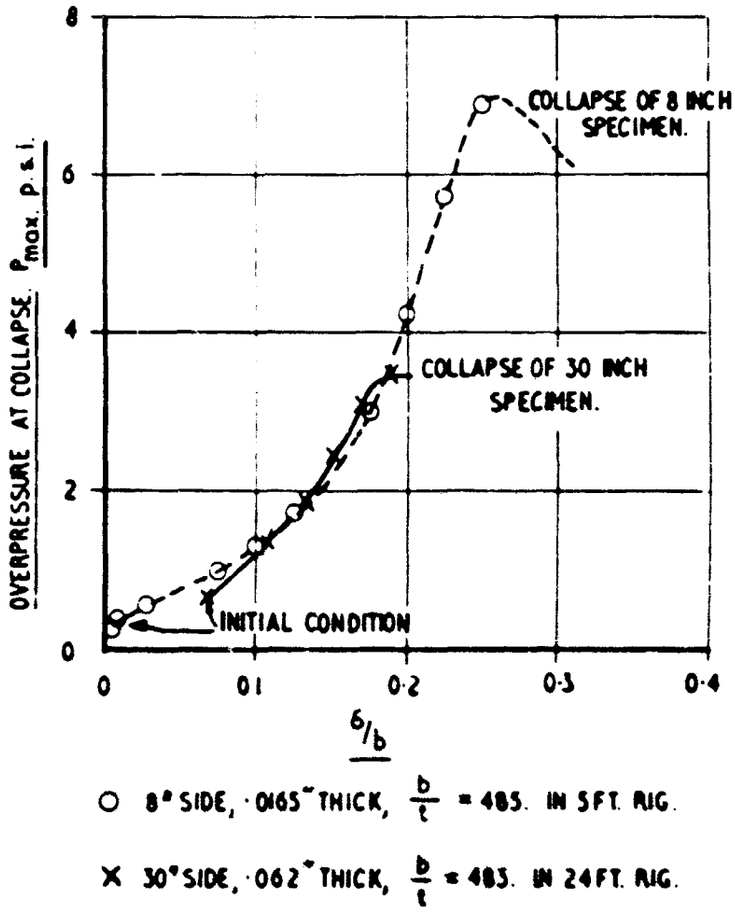


Fig. 28 Comparison of Tests at Two Scales

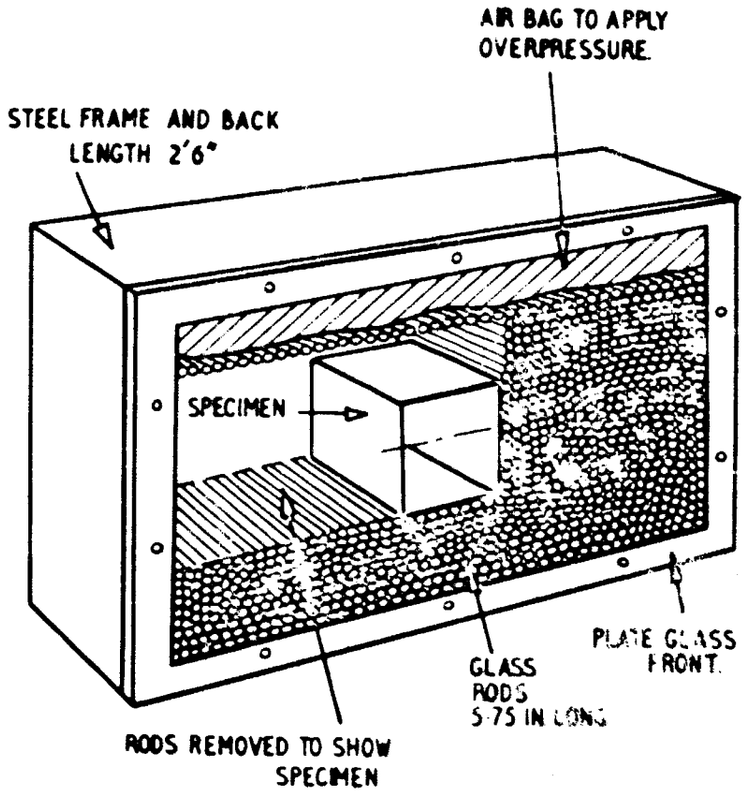


Fig. 29 Schematic View of Two Dimensional Test Rig

FUTURE PROGRAMME

The 5 ft. rig

A number of the tests so far carried out in compacted sand will be repeated with tubes of the same shapes, but made from other materials, e.g. light alloy (greater flexibility) or durestos (brittle, inflexible.

Selected tests from the whole of the above range will then be repeated in other soils, e.g. clay, loam, dry uncompacted sand. Results will be presented in a semi-empirical form, and will be useful to designers and planners who have to make a judgement between shelter material, form, and depth of cover for a specified soil.

Further experiments will investigate other shapes of tube, and the effect of stiffeners and corrugations.

The 24 ft. rig

When the scale effect due to dead-weight of soil has been satisfactorily investigated, experiments will be made with model reinforced concrete structures, and with practical forms of shelter. The scale is large enough to enable earth pressure cells to be introduced into the soil and the walls of the specimen, and it is intended to make a systematic investigation of soil pressure distribution.

Dynamic testing

All the work discussed so far has been limited to behaviour of structures under a static over pressure. How do the results compare with those from dynamic tests, and how far can they be used to predict dynamic behaviour? To answer these questions a number of courses are being followed:

1. Tubes similar to those tested in the 5 ft. rig are being tested under identical conditions of sand compaction and burial in the large field explosion of T.N.T. at Suffield, Canada, in July 1964. Instruments will give overpressure time relationships.
2. Tubes under similar conditions will be introduced in to a container in the floor of the new large shock tube facility at A.W.R.E., Foulness, England.

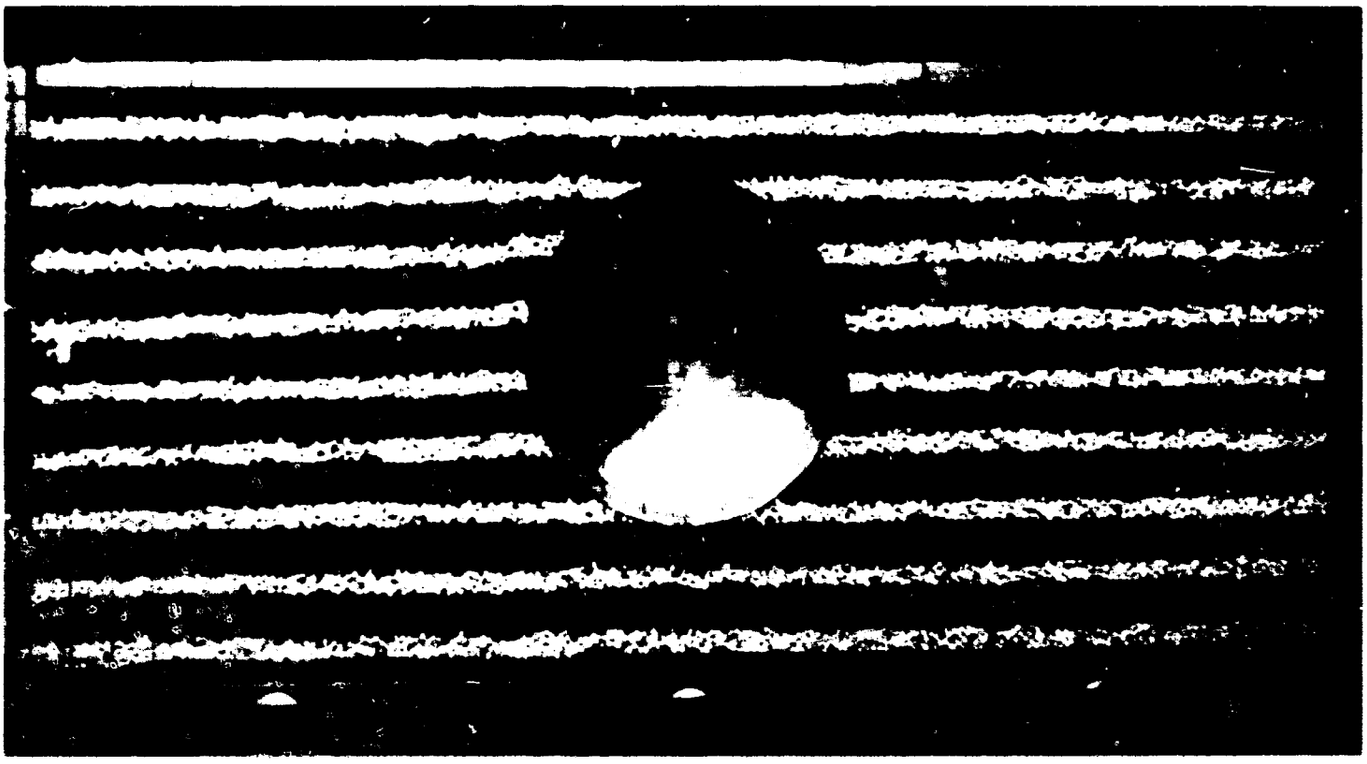


Fig. 30 Circular Specimen Before Loading

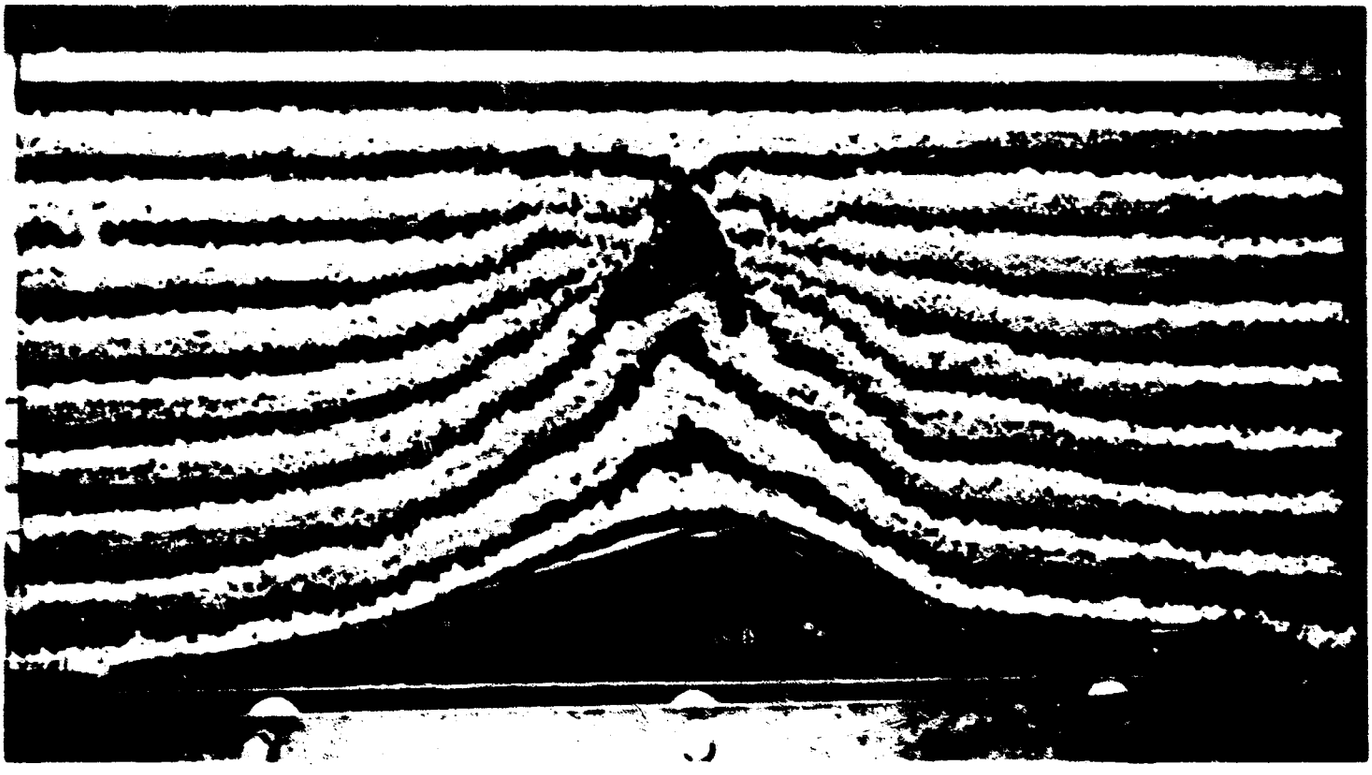


Fig. 31 Circular Specimen After Collapse

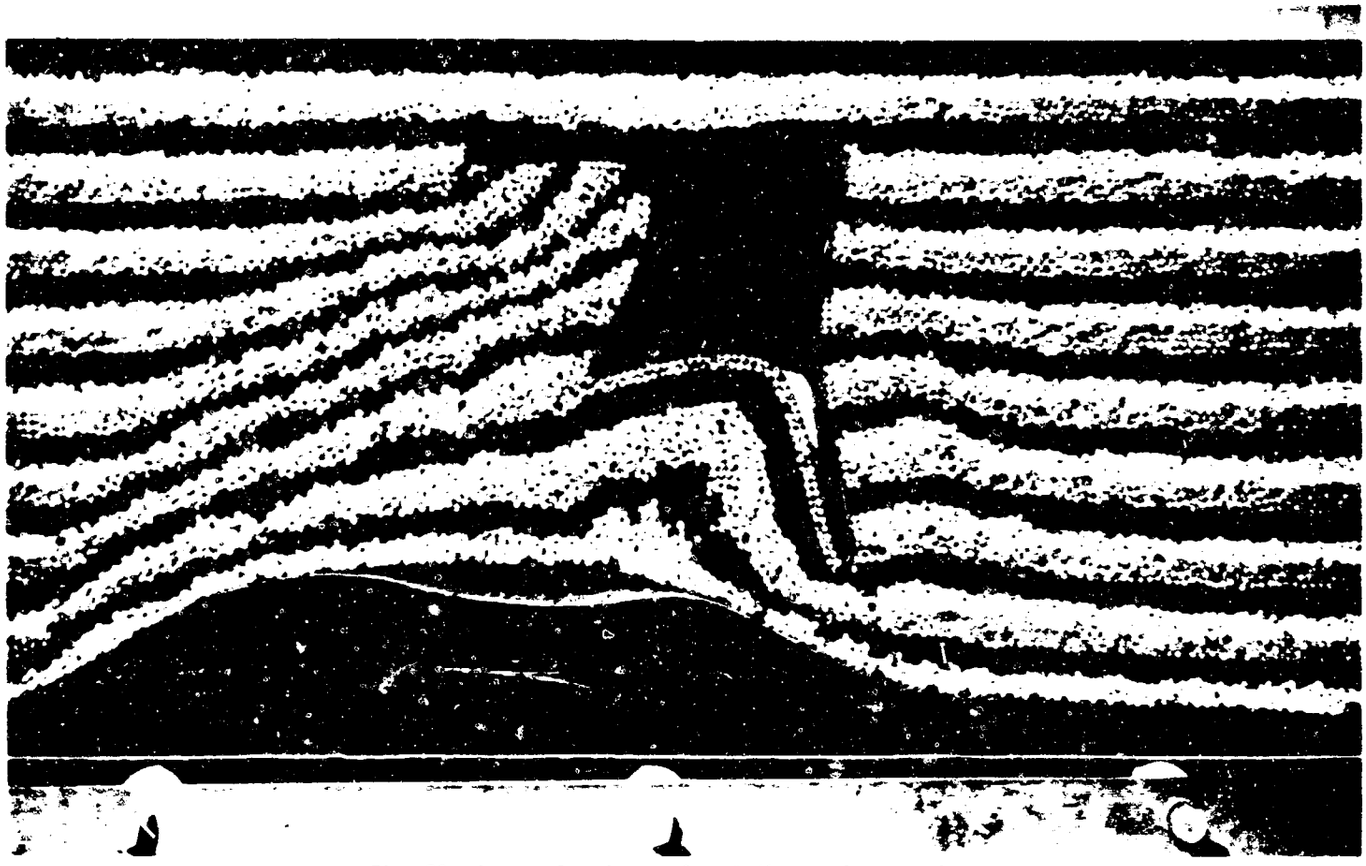


Fig. 32 Square Specimen After Collapse of Vertical Side

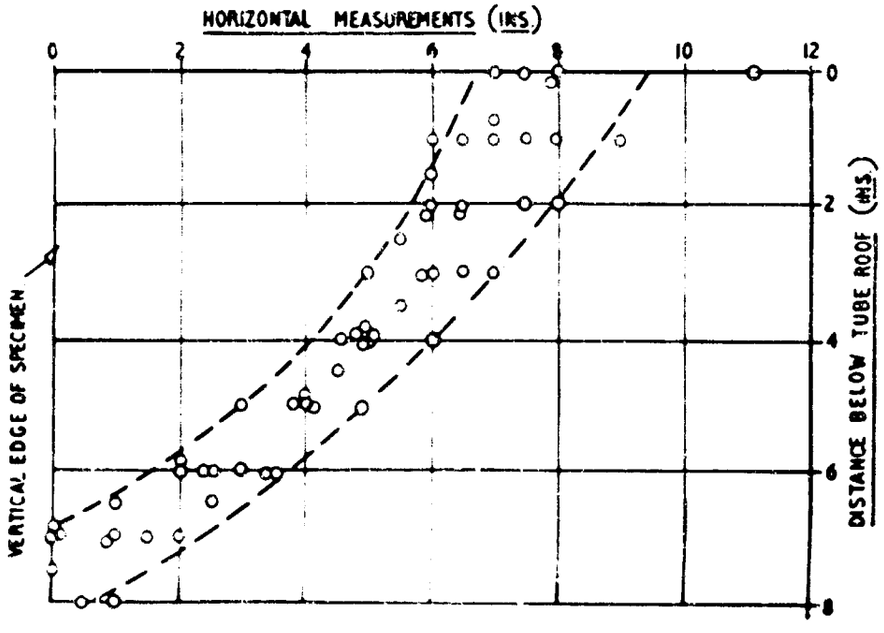


Fig. 33 Summary of Slip Line Results

3. A theoretical and experimental investigation, sponsored by M.E.X.E., is being undertaken at Southampton University, England, to study the natural frequency of vibration of structures buried in soil.

* * * * * * * * *

The work described on circular and square tubes is covered in greater detail in M.E.X.E. Reports RES 7/1, RES 48.3/2 and RES 48.3/3. Reports to be issued later will give more detail about the tests on square tubes with variable cover, with increasing corner radius, and at the larger scale.

This paper is published by permission of the British Ministry of Defence (Army Department), and the Scientific Advisors Branch of the British Home Office.

APPENDIX

The following material has been added by the editor in an attempt to present, within space limitations, additional information which was presented at this session by means of a motion picture. The motion picture illustrated the collapse and failure of numerous buried structures. Figures 35 and 36 present selected frames from two sequences which were enlarged from the 16 mm motion picture film. They have been appended to the paper in order to show the mechanism of failure from impending failure to complete collapse. It is felt that the failure sequences, as shown in the photographs, add to understanding of the soil-structure interaction. Therefore, with Dr. Bulson's permission, we have made this addition to his paper.

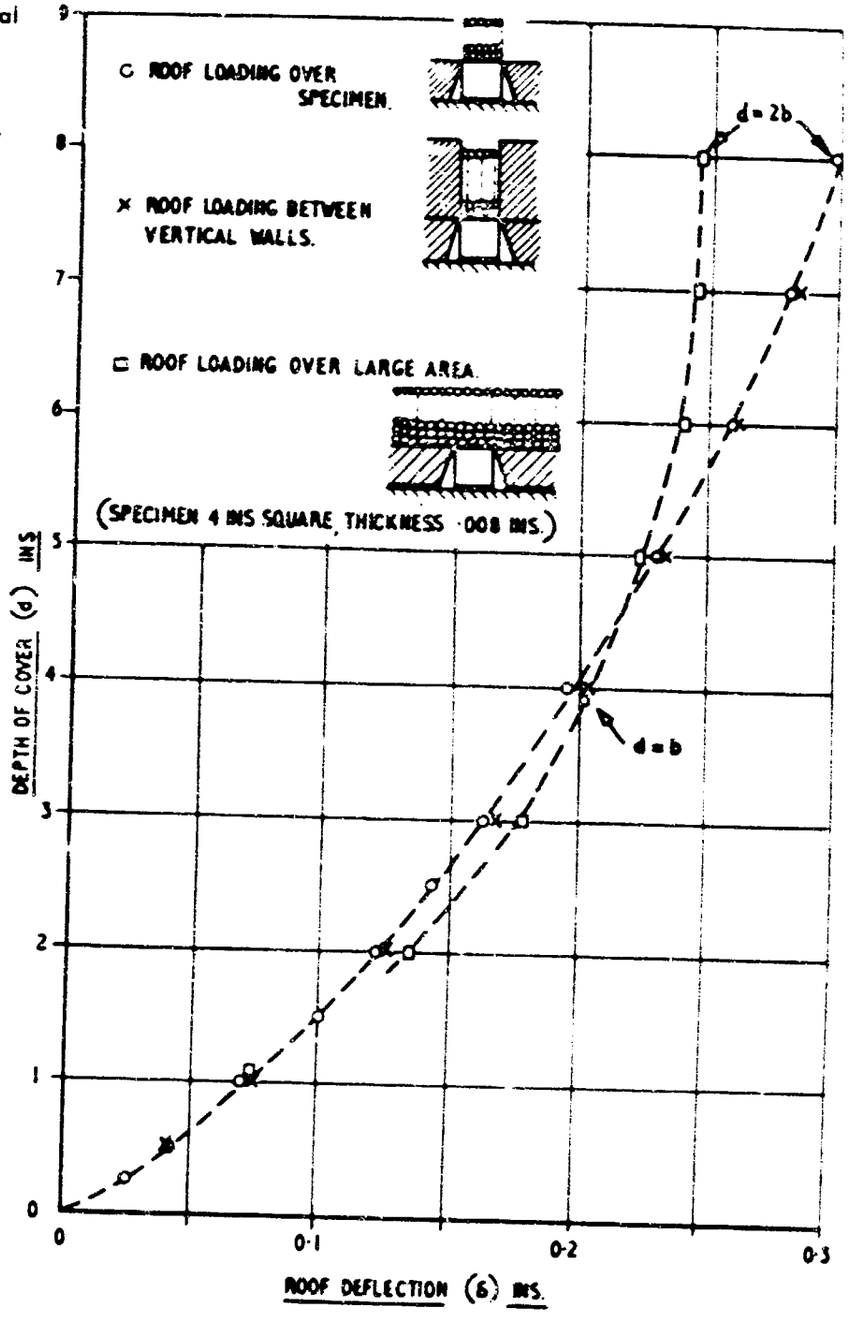


Fig. 34 Experiments With Glass Rods

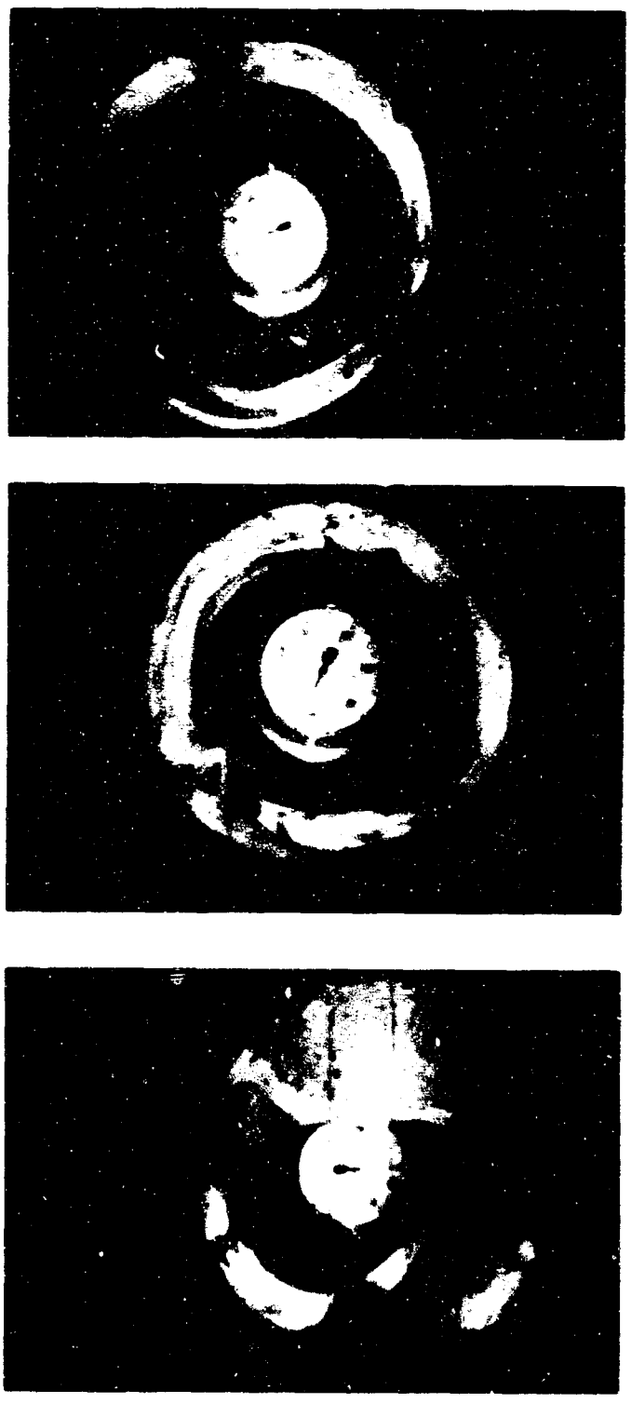


Fig. 35 Time History of the Collapse of a Circular Tube Buried in Sand, and Tested in the 24 Ft. Rig

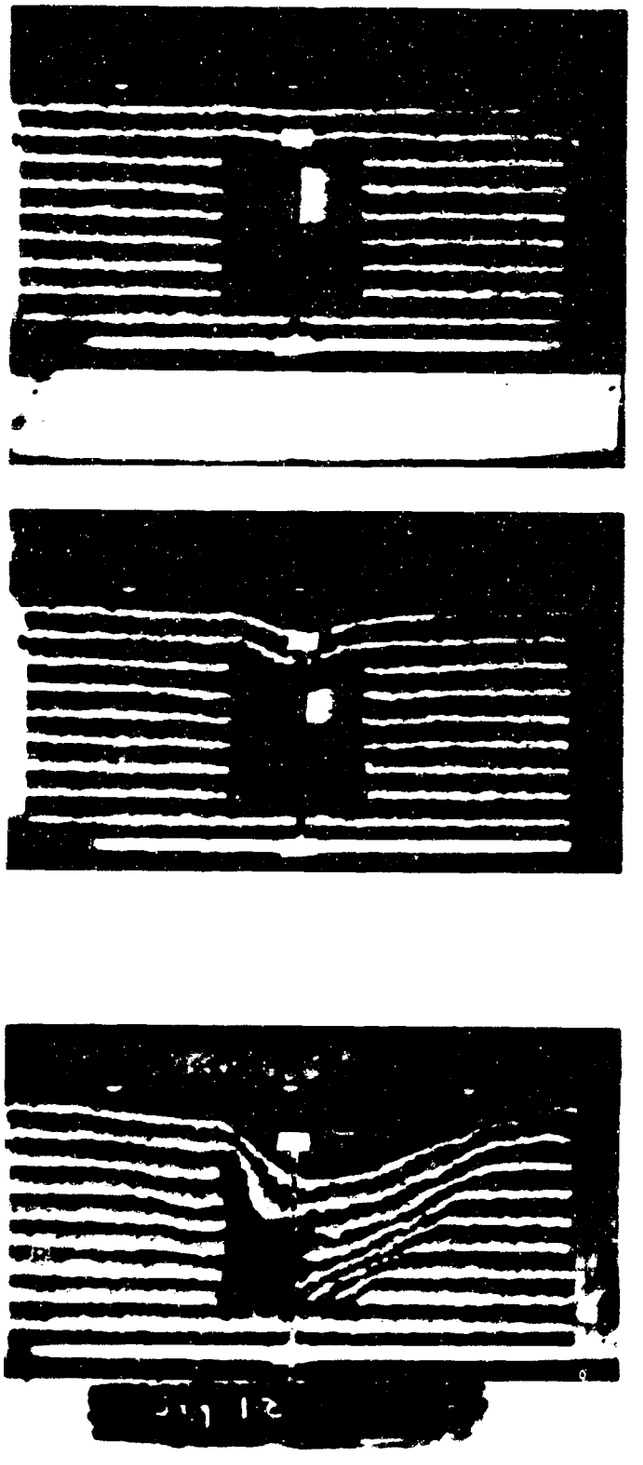


Fig. 36 Time History of the Collapse of a Square Tube in the Two Dimensional Test Rig Using Glass Rods as the Soil Medium

REVIEW OF SOIL-STRUCTURE INTERACTION

by
Carl K. Wiehle*

Interest in the problems associated with nuclear-blast loading on underground structures dates from about 1957. Prior to this, interest was concentrated on the lower air blast regions, where drag and diffraction type structures and free-field phenomena were of primary concern. Research workers were interested, insofar as structures were concerned, in such parameters as the loading and response of various basic shapes and in their effect on such air blast phenomena as reflection, diffraction, and drag. Although the term "structure-medium interaction" could have been used for these problems, there was really no need to spend extensive effort on research to describe the properties of the medium (with the exception of initial air pressure) from the standpoint of loading and response of structures; instead, in a given air shock environment it was possible to adequately describe the air blast loading on most aboveground structural shapes of interest. For analysis, the loading on the structure could be separated and investigated independently from the response of the structure; for example, for the satisfactory prediction of structural behavior, it was assumed that the compressed air in intimate contact with a responding structure had negligible effect upon the mass and effective stiffness of the structure.

In conjunction with the formulation of nuclear-blast load prediction methods for complex geometric shapes, considerable effort was also expended for determining the dynamic response of structures and structural elements (1,2,3). The result of this combined research effort was the development of design procedures for the loading and response of typical aboveground structures subjected to nuclear blast forces of 50 psi or less (4,5,6).

Although early protective structure research was primarily concerned with the aboveground situation, a number of nuclear field tests were conducted to determine the loading and response of underground structures (7-10). To design these underground test structures, the engineer utilized his knowledge of the behavior of aboveground blast-loaded structures, together with his knowledge of the behavior of ordinary underground civil engineering structures. In general, the method of design was to assume a load and then to design the structure by conventional structural design procedures. Since the assumption was usually made that the ground surface peak overpressure could be applied to the structure as a static load, these designs were seldom actual dynamic designs. Soil-structure interaction was generally not considered, although it was sometimes accounted for by modifying the load distribution applied to the structure (9).

Although many of the test structures remainder intact during a nuclear blast, it became apparent that the behavior of the structures could not be adequately predicted by the methods available. The main reason for the discrepancy between theory and experiment was due to the failure of many investigators to adequately account for the interaction of the structures with the surrounding soil media; that is, the loading and response of the underground structure could not be considered as independent phases, as was done for the aboveground structure.

Determining the dynamic loading on underground structures is exceedingly complex since it involves the physical properties of both the structure and the surrounding soil medium, as well as the characteristics of the input stress wave. The structure, by its very presence as well as by its structural response, affects the distribution of free-field stress in its vicinity. For instance, the ovalling of an underground cylindrical structure under the influence of a stress wave traveling across its diameter is dependent on the load and the properties of the structure. The load, however, is partially dependent on the deflection of the structure relative to the soil, which is itself a function of the soil properties. This interdependence of the soil response and structure response is a major difference between the aboveground and the underground nuclear blast environment.

Even though the design of underground structures subjected to nuclear blast is an extension of the design of conventional civil engineering structures such as tunnels, culverts, and retaining walls, it is somewhat surprising to examine the limitations of present knowledge regarding the response of soil-structure systems even to static loads. Although some basic concepts have been developed which have led to useful procedures for specific design problems, there are insufficient quantitative data available regarding fundamental behavior to permit development of general design procedures. Even the conventional culvert problem is difficult if the parameters are changed beyond their usual limits (11,12).

Lack of knowledge of soil-structure interaction phenomena has placed severe limitations on the ability of engineers to confidently extrapolate test information to structural and soil types that vary appreciably from the unique test conditions. It is apparent that considerable work must be done before adequate design procedures are available. In recent years, however, there has been an increased research effort to determine the basic phenomena involved. The complex problem of the interaction of stress waves with inclusions in solid media has been treated extensively both

*Senior Structural Research Engineer, URS Corporation, Burlingame, California.

theoretically and experimentally (15–25). However, because of the mathematical complexity of formulating a theory to predict the behavior of a structure in soil, it has been necessary for investigators to make a number of simplifying assumptions. These efforts have invariably resulted in solutions that are mathematically exact, but are generally restricted to a specific, highly idealized situation in elastic media. In most instances, the theories postulated do not apply directly to the design of structures in real soil. (Although the theoretical developments are very important to an understanding of soil–structure interaction, the basic approaches will not be treated in further detail in this paper.)

Even though soil–structure interaction phenomena are not completely understood, two factors are recognized as important in determining the load on the underground structure: one is the flexibility of the individual structural member and the other, the overall compressibility of the structure relative to the soil it replaces. (Of course, other factors must also be considered, such as the magnitude of the free-field stress and its attenuation with depth, reflection, refraction, virtual mass, and natural frequency of the structure.) Both involve what is commonly referred to as the arching phenomenon, i.e., the ability of the soil, probably by virtue of its shear strength, to redistribute the stress in the vicinity of an inclusion. The local arching of soil stress around a deflecting structural member and the resulting relief of a portion of the load on the member is universally accepted among investigators. (In soil mechanics, this is the arching effect, defined by Terzaghi (26) for the classical static case of the yielding platform.) What is not so universally recognized by engineers is the arching onto or away from a structure (because of its overall stiffness) and the resulting increase or decrease in the total load on the structure (24,25); that is, for a soil mass undergoing large strains, a relatively stiff structure would be subjected to a total stress greater than the free-field stress, while a relatively soft structure would be subjected to a total stress less than the free-field stress. For complex structures, it is a combination of the two types and the total stress may be either greater or less than free field. It is important that an engineer concerned with the design of blast-loaded underground structures recognizes this and, if possible, accounts for it in his design.

It should be emphasized that present knowledge does not permit a quantitative determination of numerical values for a specific soil–structure interaction problem in real soil. However, an examination of the traditional arching theory in a soil mass, together with recent investigations, can provide the engineer with a qualitative understanding of the concepts as applicable to nuclear-blast loaded underground structures.

Terzaghi (26,27) treats in considerable detail the now classical static arching effect over the yielding platform. The case considered is that of a soil mass of finite depth overlaying a rigid base. Mounted in the base is a movable strip, whose top surface is flush with the rigid base (Figure 1). An arbitrary lowering of the strip a–b results in the development of shearing resistance between the soil mass attempting to move with the strip and that which remains stationary. This is indicated in Figure 1 by the upward shear forces on the soil mass included between the assumed vertical surfaces of sliding.

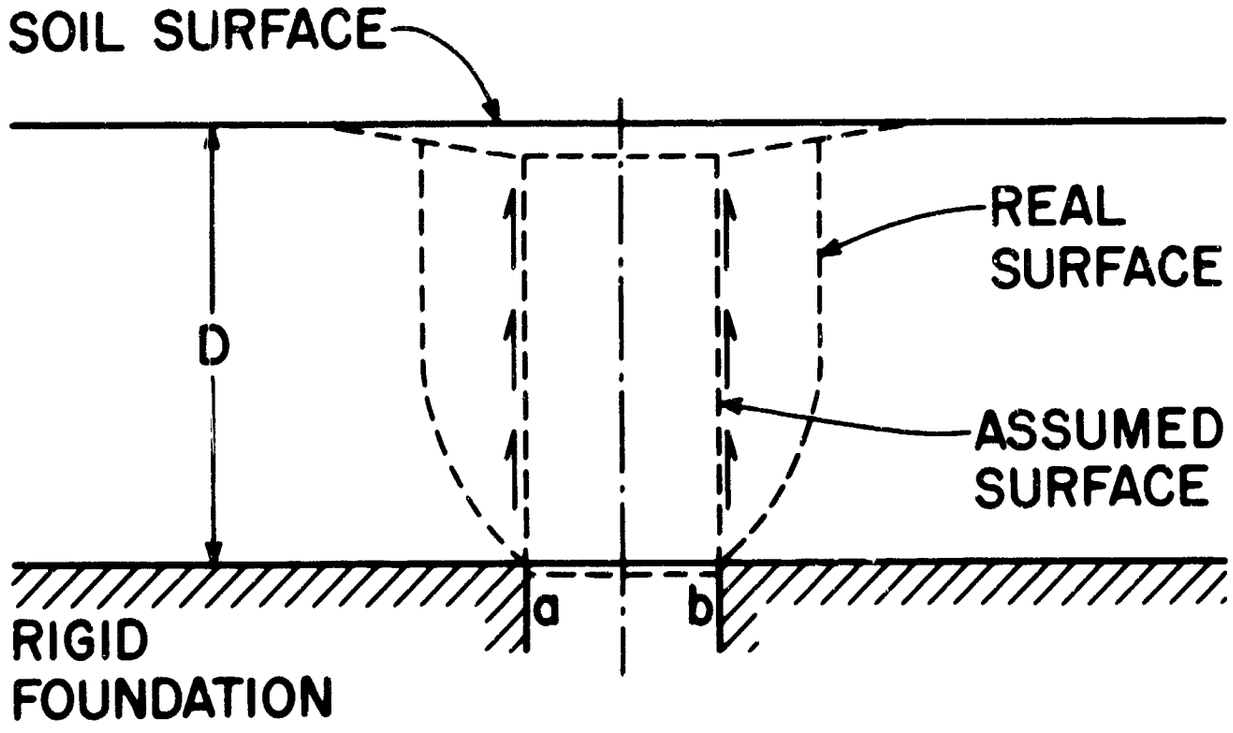


Fig. 1 Soil Failure as a Result of Downward Motion of a Movable Strip Mounted in Rigid Foundation

The net result of the lowering of the strip is a decrease in total load on the strip, and an increase of load on adjacent portions of the rigid base; the load essentially "arches" around the yielding platform. This concept of arching has been applied to nuclear blast loaded underground structures by many investigators for both static and dynamic conditions (4,21, 24,25,28); it has been defined by Mason (24,25) as the "active arching case." Terzaghi's arching effect, or active arching, would apply to an underground structure whose overall compressibility was more than the soil it replaces, as shown in Figure 2. The upper portion of the figure shows an idealized structure with uniform properties which is embedded in a soil

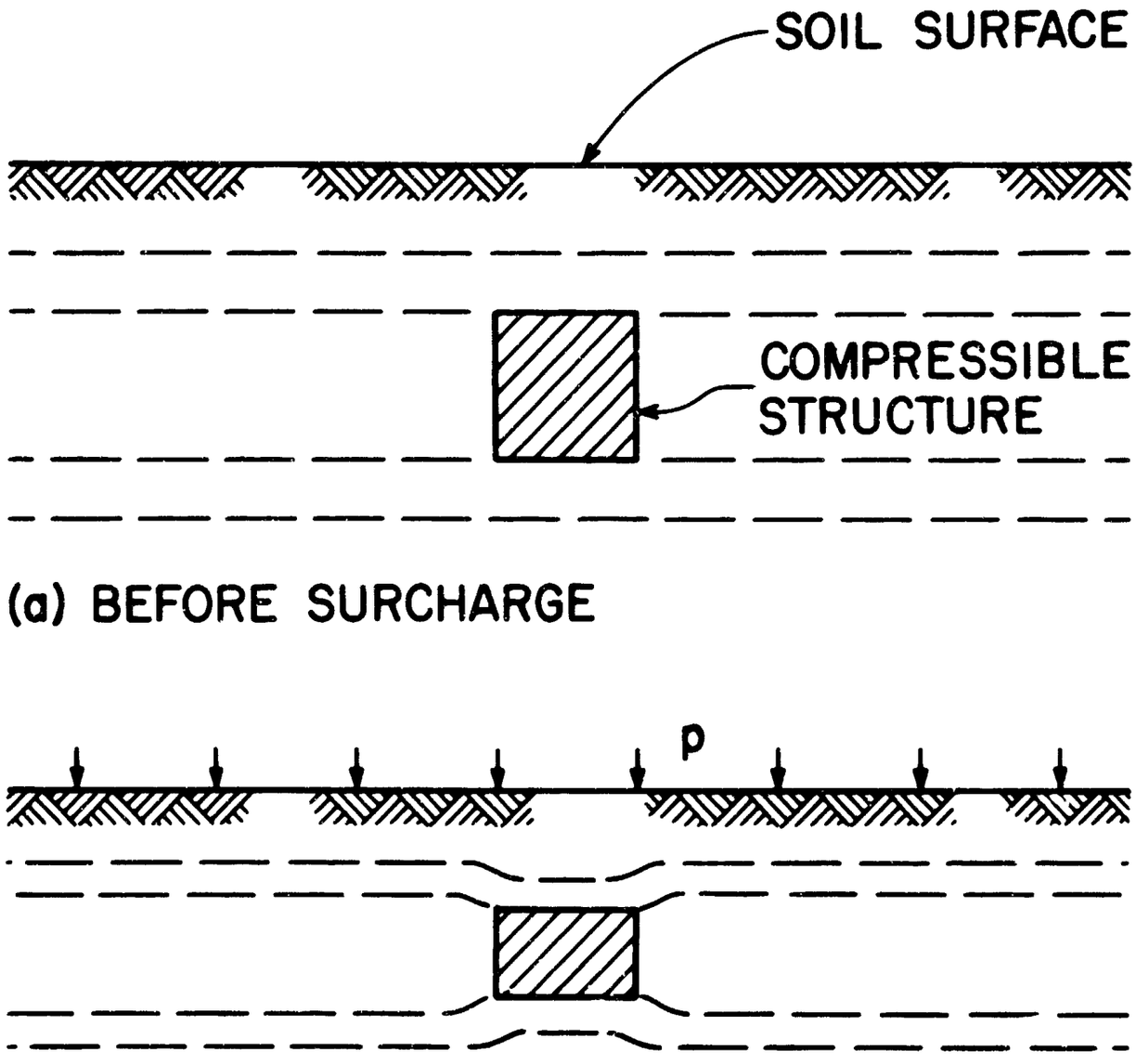


Fig. 2 Displacements Within a Soil Mass With an Inclusion More Compressible Than the Soil

mass prior to the application of a surcharge load. The horizontal dashed lines indicate typical planes of equal soil elevation. After application of the surcharge, the structure, shown in the bottom portion of the figure, has compressed vertically a greater amount than an initially equal length of soil column in the free field. The horizontal soil planes have now taken a generic shape similar to that shown, and the average stress on the structure is less than the free-field soil stress.

Active arching can also have important implications when it is necessary to determine the distribution of load on a member of an underground blast-loaded structure. For instance, consider the roof of a rectangular structure that is buried

in a soil mass undergoing an increase in stress shown schematically in Figure 3. As the roof member deflects under the loading (indicated by the dashed lines in Figure 3), it is obvious that the soil at the center of the roof tends to displace a greater relative amount than the soil over the supports. (The use of these center displacements to justify the application of the active arching case across the entire roof is disputed by some investigators, since the member has a continuously varying absolute displacement across its entire span rather than a uniform displacement as assumed in the Terzaghi arching

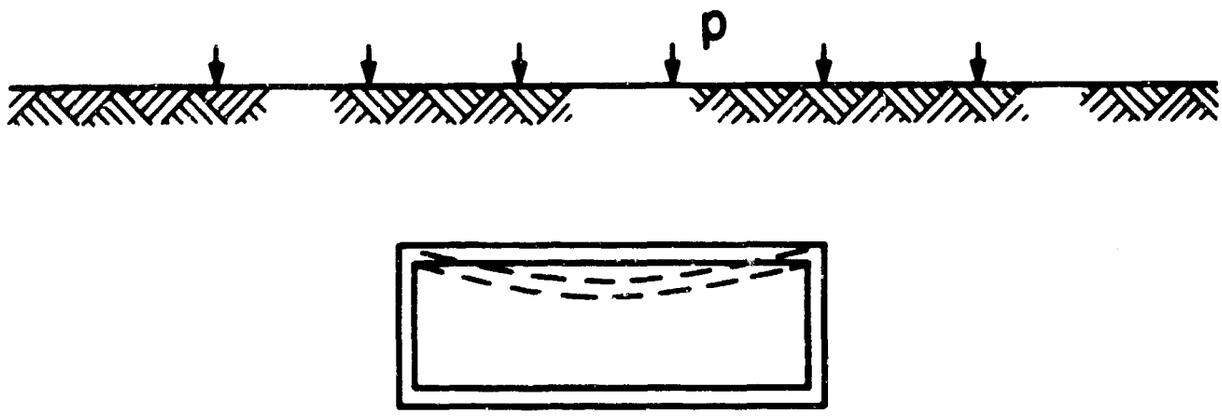


Fig. 3 Schematic of Roof Deflection of Loaded Underground Structure

theory. However, since this is somewhat analogous to the active arching case, it is quite probable that a portion of the load arches away from the center and toward the supports.) Current analytical procedures predict a decrease in the total load on such a structure. This may or may not be correct, since it should be remembered that an actual decrease in the total load for the situation described has not been corroborated by sufficient three-dimensional tests of underground structures subjected to large nuclear blast forces. In any event, a redistribution of stress on the member would occur and this in itself can be very important in the design of a specific structural member.

A problem which has been given considerable attention in civil engineering technical literature is the determination of static earth loads on underground structures such as culverts which project above the natural ground surface and are then covered with a soil fill. A review of this case is given by Van Horn (29), who shows that the pressure exerted on the top surface of a structure can be greater than the weight of soil above the structure. Mason (24,25) considered an analogous case in some detail as applicable to underground protective structures, and defined it as the "passive arching case." In this concept, if the overall compressibility of an underground structure is less than the soil it replaces, a stress wave impinging on the structure will result in an average load on the structure greater than the free-field stress; maximum load on a given structure would occur if it were rigid.

The general concept is illustrated in Figure 4, where an idealized structure with uniform properties is embedded in a soil of greater compressibility. The upper portion of Figure 4 shows a rigid structure prior to application of the surcharge load, and the horizontal dashed lines indicate typical planes of equal elevation. After application of the surcharge, the structure, shown in the bottom portion of Figure 4, has compressed vertically a less amount than an initially equal length of soil column in the free field. Again, the horizontal soil planes have some generic shape similar to that shown. Because of the differential strain between the free-field soil and the structure, there is a redistribution of stress by means of the shear strength of the soil, and a resulting increase in average stress on the structure.

To find a solution to the static passive arching case similar to that presented by Terzaghi for the static active arching case, Mason (24,25) utilized identical mathematical principles. The important difference in this concept is shown in Figure 5, where an idealized rigid structure is embedded in a soil mass subjected to a vertical load. As the loaded soil mass moves downward, a shearing resistance is developed between the adjacent soil mass attempting to move past the structure and the soil mass included between the arbitrary vertical surfaces of sliding. The net result is a decrease of the load on adjacent portions of the surrounding soil mass and an increase in the load on the structure. Although the equations developed do not include inertia effects, considerable experimental corroboration for the static case has been obtained using small structure tests (24,25). Test results indicate that the overstress for dynamic loads is even greater than for static loads.

In summary, the average load on an underground structure subjected to nuclear blast forces can be either less or greater than the free-field stress, depending on the properties of the soil and the structure. Under the concept of relative compressibility between the structure and the soil it replaces, equations have been developed that define the active and passive arching cases for static loads. In the active arching case, the overall compressibility of the structure is conceived to be greater than that of the soil, for any given stress field, and the average stress on the structure is less than

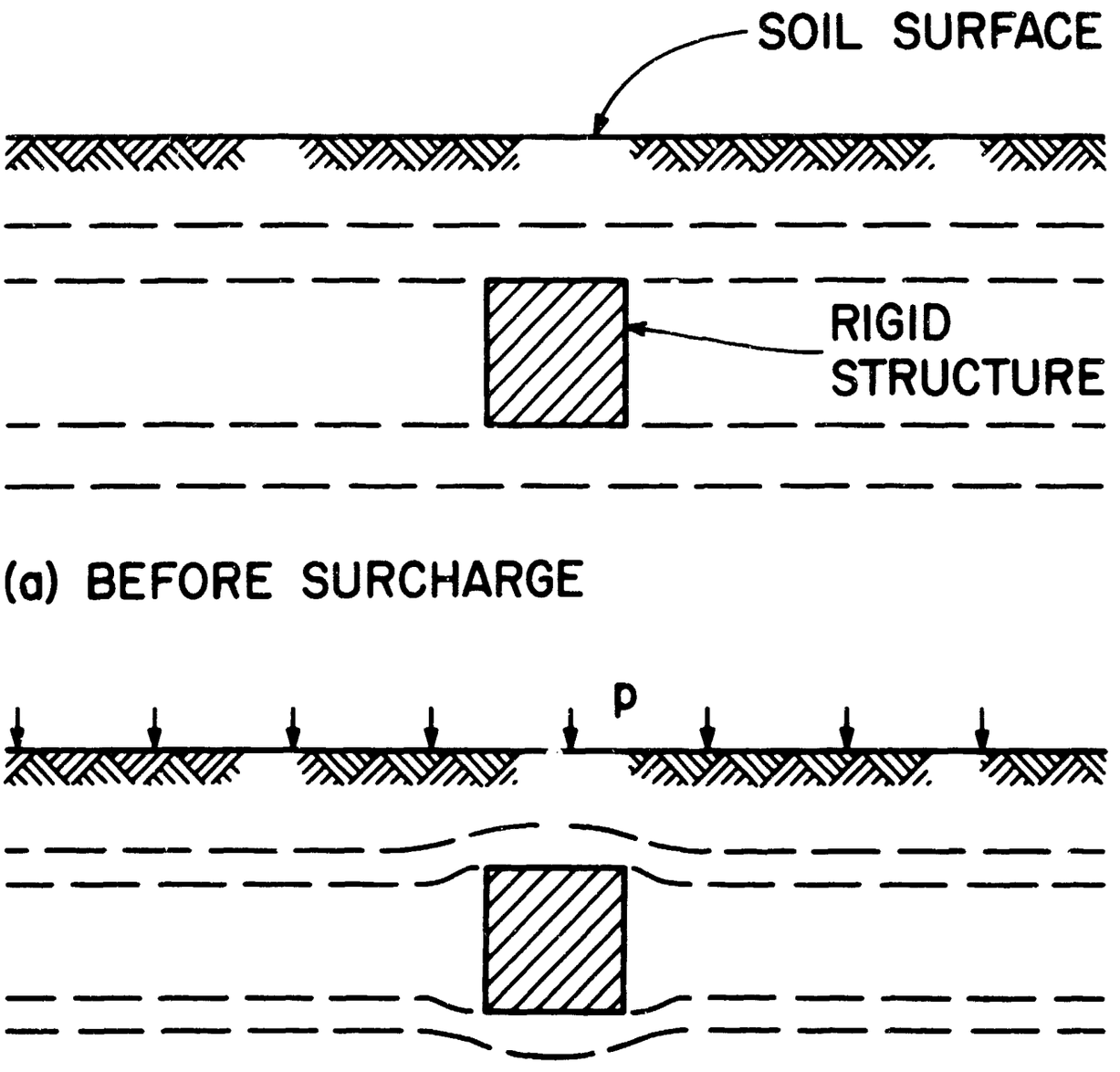


Fig. 4 Displacements Within a Soil Mass With an Inclusion Less Compressible Than the Soil

free-field stress. In the passive case, the structure is less compressible than the soil and, therefore, the average stress on the structure is greater than free field. When considering full-size underground structures, it is obvious that the load on the structure is dependent on both the structure's overall compressibility and the flexibility of individual structural members. For most protective structures, it is probable that a combination of both passive and active arching is involved; that is, the overall compressibility of the structure could be such that there would be a greater average load on the structure through passive arching, whereas, the flexibility of a structural member could result in a reduction or modification of stress distribution on the structure through active arching.

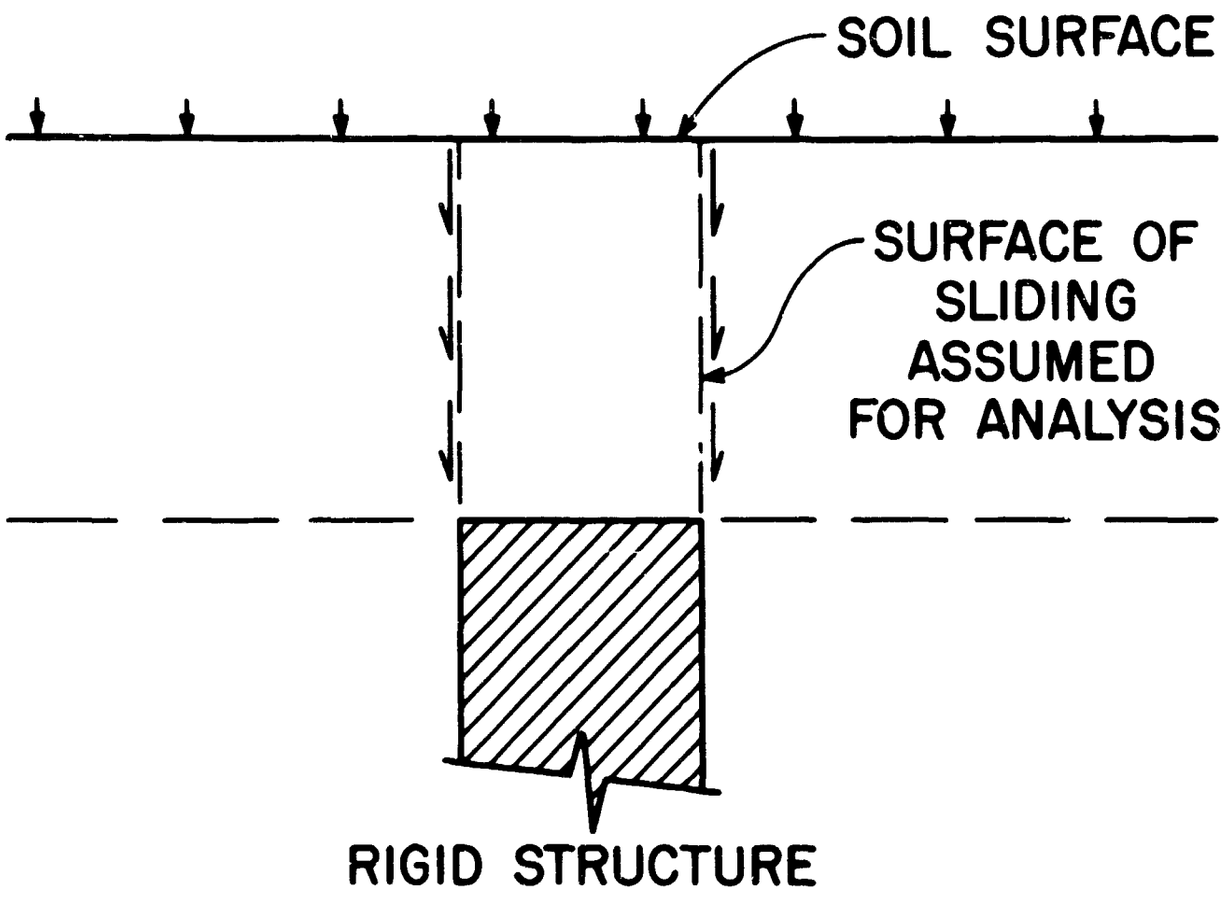


Fig. 5 Assumed Surfaces of Sliding in a Loaded Soil Mass With a Rigid Inclusion

REFERENCES

1. Wojcieszak, R. F. and J. M. Massard, "Slow and Rapid Lateral Loading Tests of Simply Supported Beams and Beam-Columns," AFSWC TR 57-21, University of Illinois for the Air Force Special Weapons Center, Kirtland Air Force Base, New Mexico, 1957.
2. Allgood, J. R. and W. A. Shaw, "Elasto-Plastic Response of Beams to Dynamic Loads," TM-130, U.S. Naval Civil Engineering Laboratory, Port Hueneme, California, 1958.
3. Duberg, J. E. et al, "Analysis and Design of Domes, Arches and Shells," two volumes, AFSWC TR 59-9, University of Illinois for the Air Force Special Weapons Center, Kirtland Air Force Base, New Mexico, 1959.
4. Newmark, N. M. and J. D. Haltiwanger, "Air Force Design Manual, AFSWC-TDR-62-138, University of Illinois for the Air Force Special Weapons Center, Kirtland Air Force Base, New Mexico, 1962.
5. "The Design of Structures to Resist the Effects of Atomic Weapons," EM 1110-345-414 to 421, Massachusetts Institute of Technology for the Office of the Chief of Engineers, U.S. Army, Washington, D.C., 1957.
6. Smith, S. B., "Design Manual-AEC Test Structures," TID-16347, Volumes I, II, and III, Holmes and Narver for the Atomic Energy Commission, Los Angeles, California, 1961.
7. Newmark, N. M. and G. K. Sinnamon, "Air Blast Effects on Underground Structures," WT-727, Operation UPSHOT-KNOTHOLE, University of Illinois for Office of the Chief of Engineers, U.S. Army, Washington, D.C., 1954.
8. Bultmann, E. H., G. F. McDonough, and G. K. Sinnamon, "Loading on Buried Structures at High Incident Overpressures," WT-1406, Operation PLUMBBOB, University of Illinois for Air Force Special Weapons Center, Kirtland Air Force Base, New Mexico, 1960.

9. Flathau, W. J., R. A. Breckenridge, and C. K. Wiehle, "Blast Loading and Response of Underground Concrete-Arch Protective Structures," WT-1420, Operation PLUMBBOB, U.S. Army Corps of Engineers Waterways Experiment Station, Vicksburg, Mississippi, and U.S. Naval Civil Engineering Laboratory, Port Hueneme, California, 1959.
10. Bultmann, E. H., G. F. McDonough, and G. K. Sinnamon, "Loading on Buried Structures in High-Overpressure Regions," WT-1614, Operation HARDTACK, University of Illinois for the Air Force Special Weapons Center, Kirtland Air Force Base, New Mexico, 1960.
11. Spangler, M. G., "Underground Conduits-An Appraisal of Modern Research," Trans. American Society of Civil Engineers, Vol. 113, 1948.
12. Spangler, M. G., "Stresses in Pressure Pipelines and Protective Casing Pipes," Proceedings of the American Society of Civil Engineers, Vol. 82, No. SM5, 1956.
13. Wiedermann, A. H., "The Interaction of Buried Structures with Ground Shock," AFSWC-TR-60-3, Appendix B, Armour Research Foundation for the Air Force Special Weapons Center, Kirtland Air Force Base, New Mexico, 1960.
14. Soldate, A. M. and J. F. Hook, "A Theoretical Study of Structure-Medium Interaction," AFSWC-TN-61-6, National Engineering Science Company for the Air Force Special Weapons Center, Kirtland Air Force Base, New Mexico, 1960.
15. Whipple, C. R., "The Dynamic Response of Shallow-Buried Arches Subjected to Blast Loading," Thesis, University of Illinois, Urbana, Illinois, 1961.
16. Riley, W. F., I. M. Daniel, and A. J. Durelli, "Stress Wave Phenomena in Semi-Solids," AFSWC-TR-61-25, Armour Research Foundation for the Air Force Special Weapons Center, Kirtland Air Force Base, New Mexico, 1961.
17. Post, D., M. Leitman, and C. C. Mow, "Photoelastic Determination of Boundary Stresses Around Tunnels of Various Cross-Sectional Shares," SR-36, The Mitre Corporation, Bedford, Massachusetts, 1961.
18. Baron, M. L. and R. Parnes, "Diffraction of a Pressure Wave by an Elastically Lined Cylindrical Cavity in an Elastic Medium," SR-44, The Mitre Corporation, Bedford, Massachusetts, 1961.
19. Robinson, R. R., "The Investigation of Silo and Tunnel Linings," AFSWC-TR-62-1, Armour Research Foundation for the Air Force Special Weapons Center, Kirtland Air Force Base, New Mexico, 1962.
20. Allgood, J. R., "Blast Loading of Small Buried Structures," TR-216, U.S. Naval Civil Engineering Laboratory, Port Hueneme, California, 1962.
21. Ang, A. and N. M. Newmark, "Computation of Underground Structural Response," Bimonthly Progress Report No. 6, University of Illinois for Defense Atomic Support Agency, Urbana, Illinois, 1962.
22. Selig, E. T., K. E. McKee, and E. Vey, "Underground Structures Subject to Air Overpressure," Journal of the Engineering Mechanics Division, American Society of Civil Engineers, New York, August 1960.
23. Whitman, R. V., Z. Getzler, and K. Hoeg, "Static Tests Upon Thin Domes Buried in Sand," R62-41, Massachusetts Institute of Technology for U.S. Army Waterways Experiment Station, Vicksburg, Mississippi, 1962.
24. Mason, H. G., O. H. Criner, R. Waissar, and N. R. Wallace, "A Study of the Dynamic Soil-Structure Interaction Characteristics of Real Soil Media," AFSWC-TDR-63-3075, United Research Services for the Air Force Weapons Laboratory, Kirtland Air Force Base, New Mexico, September 1963.
25. Mason, H. G., O. H. Criner, R. Waissar, and N. R. Wallace, "A Study of the Dynamic Soil-Structure Interaction Characteristics of Real Soil Media," presented at the American Society of Civil Engineers Annual Conference, San Francisco, California, October 1963.
26. Terzaghi, Karl, Theoretical Soil Mechanics, John Wiley and Sons, New York, 1943.
27. Terzaghi, Karl, "Stress Distribution in Dry and in Saturated Sand Above a Yielding Trap-Door," reprint from Proceedings of the International Conference on Soil Mechanics and Foundation Engineering, Volume I, No. Z-3, pp. 307-311, Harvard University, Cambridge, Massachusetts, June 1936.
28. Newmark, N. M. and J. L. Merritt, "Nuclear Geoplosics, Part Five, Effects on Underground Structures and Equipment," DASA-1285 (V), University of Illinois for Defense Atomic Support Agency, Washington, D.C., 1962.
29. Van Horn, D. A. and R. K. Tener, "A Study of Loads on Underground Structures," DASA-1406, Iowa State University for Defense Atomic Support Agency, Washington, D.C., 1963.

STRUCTURAL DESIGN TRENDS IN BURIED FLEXIBLE CONDUITS

by
Reynold K. Watkins*

The use of buried conduits will increase in the future because of the increasing use of soil as a material of construction. This is due to the obvious advantages of soil in defense installations; but it is also due to improved soil engineering and to the economy of soil structures. The cost per yard for handling soil is less than before the turn of the century. This increased use of soil will apply not only to the number of installations but the variety of installations.

Of course soil structures require buried conduits and many new shapes and unprecedented sizes of conduits will be called for in the future. Already there is an urgent demand for more accurate and more extensive design methods. Fortunately some research data is currently available. The object of this paper is to shorten the lag-time between current research and its reduction to practice.

Buried conduits are defined as structures which maintain a passageway through soil. The cross-sectional shape of the passageway may be almost anything and the passageway may be used for the transport of almost anything: electric lines, pipelines, fluid flow, traffic, etc. Buried conduits are usually classified as either rigid or flexible. In the design of rigid conduits, the conduit itself is the basic structure. In Figure 1 a free-body diagram is drawn of the rigid conduit ring which is designed to withstand soil loads. In marked contradistinction, a very flexible conduit must not be considered as the basic load supporting structure. On the contrary, it serves as a form to retain the shape of the passageway or as a reinforcement or a boundary condition for the soil, but the soil itself becomes the basic load carrying structure. Under these circumstances, a soil displacement theory of failure or a soil shear plane theory of failure is more rational than maximum stress in the conduit. It may be an enormous mathematical chore to evaluate the equations for a soil failure or a soil-conduit system failure; but as computer capability increases, solutions by numerical methods become promising. Even more important, the soil-conduit system concept emphasizes the structural importance of the soil rather than the conduit alone, and so approximate design methods will become more rational.

In the spectrum of buried conduit design, the flexible conduit will be at one end. It depends upon proper design and placement of a basic soil structure. At the other end of the spectrum will be the rigid conduit as the basic structure. It can support low grade, uncompacted soil as well as good soil. Additional studies will fill in the spectrum between. Design trends are already appearing in codes of practice and pipe manufacturers manual of design and installation.

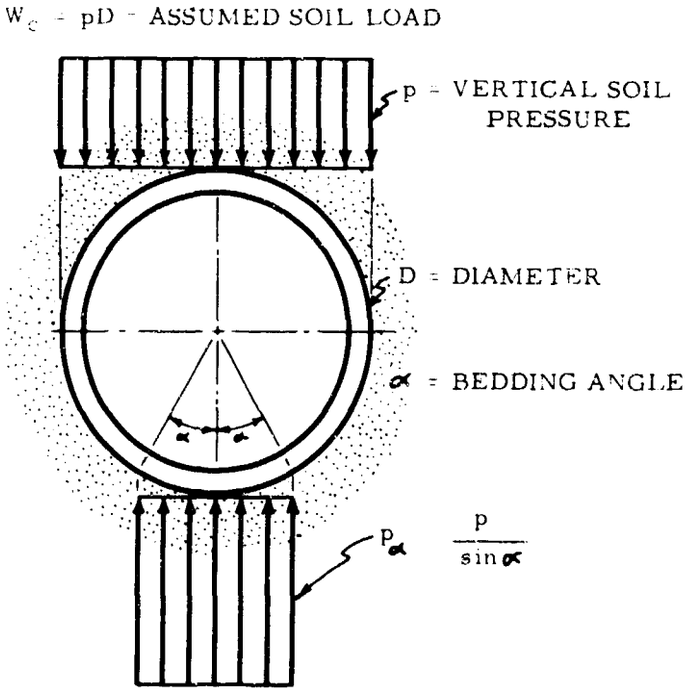


Fig. 1 Typical Soil Loading Assumptions for Buried Conduit

History of Flexible Conduit Design

Design trends spring from previous practices; so the history of buried conduit design must be reviewed. At first most flexible conduit design was based on a change in the diameter of the ring. Using the ring as a free-body diagram (Figure 2), assuming elliptical deformation, and assuming the soil load shown, M. G. Spangler (1) derived the Iowa Formula for predicting the increase in horizontal diameter ΔX of circular conduit as a function of:

*Professor and Head, Department of Mechanical Engineering, Utah State University, Logan, Utah.

p = vertical soil pressure at top of conduit,
D = conduit diameter,
EI = conduit wall stiffness, and
E' = soil modulus.

The Iowa Formula is:

$$\frac{\Delta X}{D} = 0.01 \left(\frac{pD^3}{EI}\right) \left[\frac{1}{1 + 0.008\left(\frac{E'D^3}{EI}\right)}\right]$$

A maximum deflection $\frac{\Delta X}{D}$ was specified for design. For many installations, however, it was found that $\frac{\Delta X}{D}$ was not a critical condition of failure. For example, if a very flexible ring is carefully embedded in a well-compacted granular fill, buckling of the pipe wall will occur before any significant change in diameter. The ring compression theory was recommended by Howard White (2) as an alternative design under these circumstances. The ring compression theory simply requires that the tangential compressive stress f_c in a conduit wall be less than the allowable wall strength (Figure 3); i.e., $f_c = \frac{pD}{2A} < S$

where

p = vertical soil pressure at top of conduit,
D = horizontal span of conduit,
A = cross-sectional area of the conduit wall on each side, and
S = allowable stress (strength) in the conduit wall.

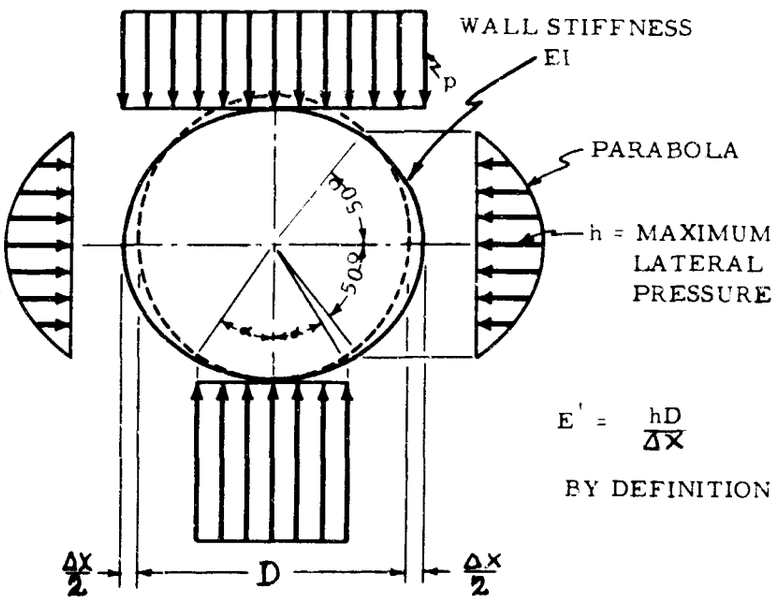


Fig. 2 Loading Assumptions for Iowa Formula

This analysis is adequate provided that the fill is so rigid that deformation of the ring is negligible. (A predictable deformation may be analyzed under special circumstances.) Such a condition is met in many compacted fill installations such as interstate highways. This condition is not met if the soil is loose, viscous or plastic. For fluid pressure, the theory of buckling by static fluid loading is best. This theory depends upon the equation

$$\frac{p'D^3}{EI} = \frac{24}{SF} \quad \text{or} \quad \frac{p'}{E}\left(\frac{D}{r}\right)^2 \frac{D}{A} = \frac{24}{SF}$$

where SF = safety factor,
p' = the radial fluid pressure, and
r = radius of gyration of cross-sectional area of conduit wall.

For the range of soil types between a very rigid fill and a fluid fill, a combination of ring compression and fluid buckling can be used (3,4). This theory is analogous to the classical theory of column design wherein the allowable stress $f_c = \frac{p}{A}$ is plotted as a function of slenderness ratio $(1/E)(L/r)^2$ as shown in Figure 4, where:

p = load on column,
A = cross-sectional area,
L = length of column,
r = least radius of gyration of cross-sectional area, and
E = modulus of elasticity.

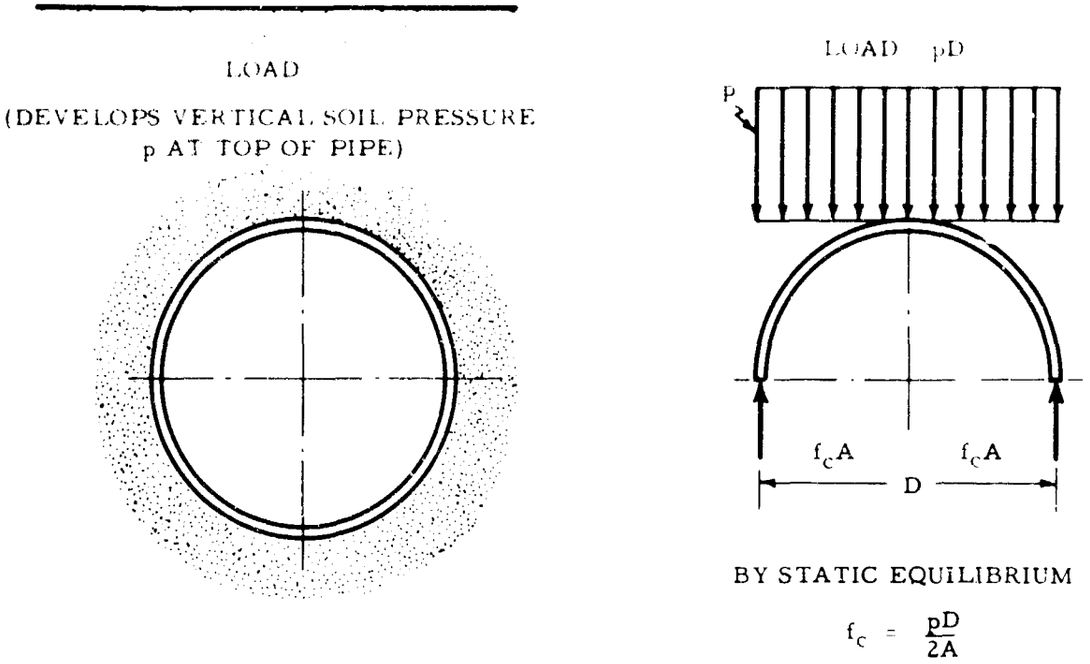


Fig. 3 Ring Compression Theory for Design of Flexible Pipe Embedded in Dense Soil

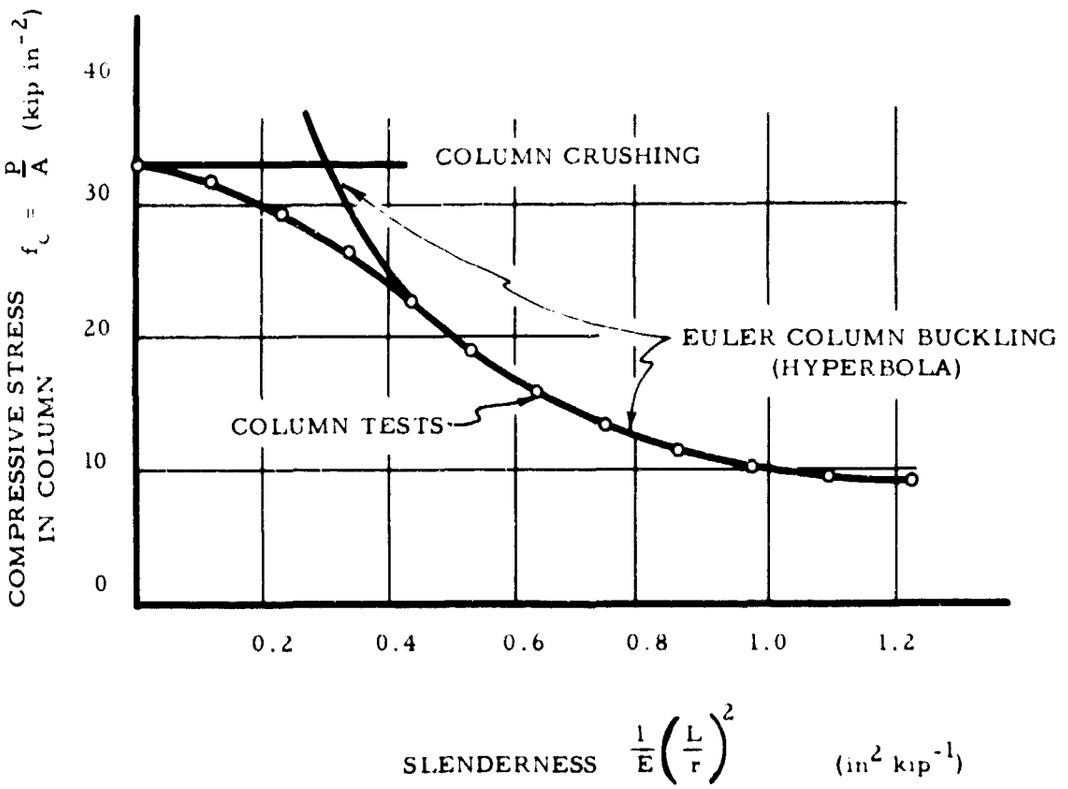


Fig. 4 Typical Column Strength Curves

In Figure 5 the allowable wall stress is plotted as a function of ring flexibility for a circular conduit configuration. Note that the ordinate $f_c = \frac{pD}{2A}$ is analogous to the column design ordinate $f_c = \frac{P}{A}$ and the abscissa $(1/E)\,(D/r)^2$ is analogous to the column design abscissa $(1/E)\,(L/r)^2$. Moreover, for a very thick-walled conduit, as for a thick column, the allowable design stress is f_c = yield strength of material; and for a very flexible conduit, as for a very slender column, the allowable stress plots as a hyperbola. This applies to static fluid fill or soil with a soil modulus of $E' = 0$. Now if the fill is soil with shearing strength, the allowable stress curve is raised above the static fluid hyperbola. For a rigid fill with a soil modulus E' approaching infinity, the allowable stress approaches the ring compression buckling. Recent tests show that the strength curves in soil approach horizontal asymptotes as conduit flexibility increases.

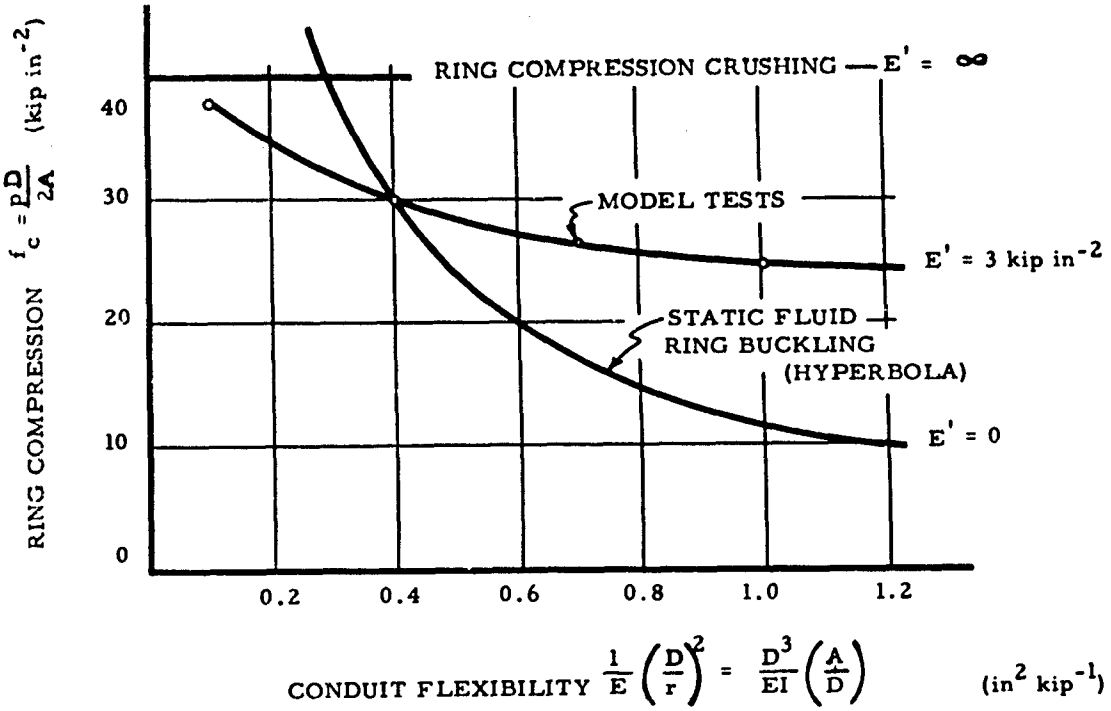


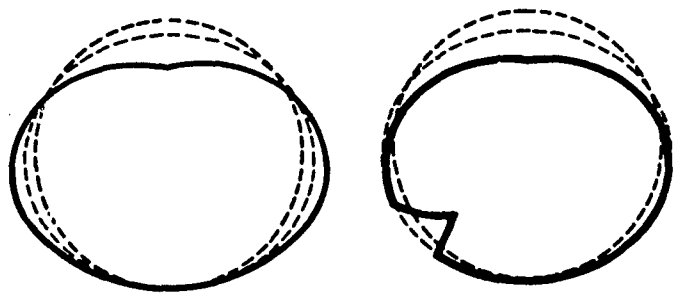
Fig. 5 Ring Buckling Curves for Buried Flexible Pipes

TRENDS IN THE STRUCTURAL DESIGN OF COMMON SOIL-CONDUIT SYSTEMS

Pipes

A pipe is a conduit with a circular cross-section. Failure occurs if the soil-pipe system does not perform as intended; for example, the system fails if the passageway is so deformed that it cannot perform its transport function. Also failure occurs if the soil surrounding the pipe is so displaced that it cannot perform its structural functions. In either event, failure may be measured by deformation of the pipe cross-section. Two basic types of deformation have been observed as shown in Figure 6: flattening of the pipe, and buckling of the pipe wall.

Of course buckling is affected by flattening. The allowable extent of deformation is left up to the design engineer with this observation: a permanent pipe deformation does not necessarily result in failure. It is true that once buckling has commenced the resistance of the pipe to soil pressure is greatly reduced; but

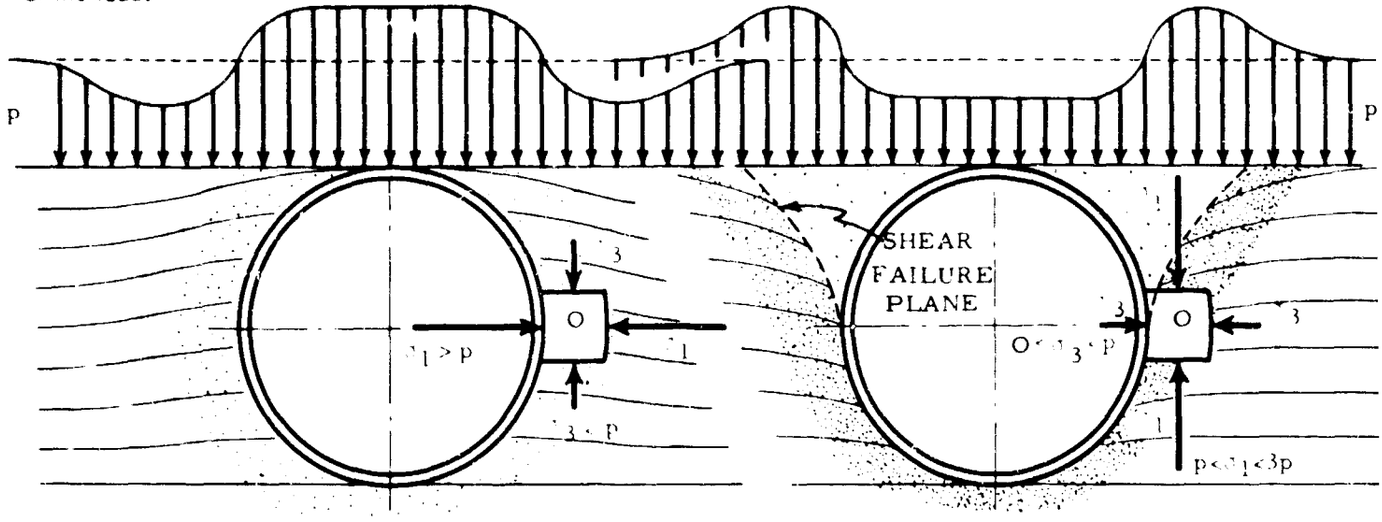


(a) RING FLATTENING (b) RING BUCKLING

Fig. 6 Two Types of Structural Ring Failure of Buried Flexible Pipes

on the other hand, buckling decreases the cross-sectional area of the conduit and so relieves soil pressure on it. The soil structure itself may be able to support the additional pressures with no distress whatsoever. In general, pipe ring buckling must be classified as failure even though the ring may not collapse by snap through. It is very probable that in the future methods will be introduced to purposely relieve soil pressures on the pipe in order to reduce chance for buckling.

If the soil cross-sectional area decreases per unit area (compressibility) more than the pipe cross-sectional area, the load on the pipe will exceed p and the tangential stress in the pipe wall will exceed pD/2A. This is shown schematically in Figure 7a. If the pipe ring is very flexible, radial soil pressure everywhere on the pipe will be constant and σ_1 on soil stress element "0" will be greater than p. σ_3 will be less than p because the conduit is carrying so much of the load.



(a) Loose Soil
Noncompressible Ring Area
Compressible Soil

(b) Dense Soil
Compressible Ring Area
Noncompressible Soil

Fig. 7 Soil Stress Element at Spring Point of Flexible Buried Conduit

If the value of $K = \sigma_1/\sigma_2$ is greater than $(1+\sin\phi)/(1-\sin\phi)$ (where ϕ = soil friction angle) then a shear failure plane will start in the soil at this point.

If on the other hand the soil is less compressible than the pipe, as shown in Figure 7b, then σ_1 may be anything between p and 3p and σ_3 may be anything between zero and p. If $K = \sigma_1/\sigma_3$ is greater than $(1+\sin\phi)/(1-\sin\phi)$ for the soil, then a shear failure plane will start at that point 0. Some simple model studies have inaicated that the shear failure plane forms as shown by dotted line in Figure 7b. This shear plane may not progress far, however, because generally the ratio $K = \sigma_1/\sigma_3$ decreases as the distance from the pipe increases. The soil below the shear plane is confined in a dense state; but as shearing action progresses, the soil above the shear plane moves down forming a zone of shear failure in which the soil is loosened. Of course a concentrated surface load over the pipe will aggravate the shear plane failure.

One way to relieve stress in the pipe ring is to reduce pipe area, i.e., slotted rivet holes in the longitudinal seam. But a more practical stress release trick may be available in the design of the soil fill. The basic concept is to construct a well compacted soil arch over the pipe as shown in Figure 8. Ideally the trench or site should be over-excavated and a solid footing for the arch should be provided. A densely compacted or stabilized structural soil arch should then be constructed up over the pipe but with a loose soil cushion immediately adjacent to the pipe to partially relieve the pipe of soil pressure. This method is promising for very large flexible conduits. Practically the cushion might be provided by specifying that hand compaction devices be kept a minimum distance away from the pipe as shown in Figure 9. Or even more ideally, in the future, machines may be devised which will: 1) compact and form the bedding; 2) place lifts of soil simultaneously on both sides of the positioned conduit while holding pipe shape; and 3) compact the soil to form a soil arch leaving a soil cushion. At present researchers are considering the design of the soil arch and in the near future may have a successful analytical method for determining the size and shape of the soil arch and the amount o compaction required for a given soil type and a given conduit.

The concept of the soil arch is important in the design of multiple parallel pipes. It is imperative that enough densely compacted soil be placed between pipes to serve as columns to support the soil arches over the pipes.

Noncircular Conduits

One additional concept is required for the design of noncircular flexible buried conduits which include arches, pipe arches, vertically elongated (VE) pipes, horizontally elongated (HE) pipes, etc. In most conduit installations, shearing stresses between the soil and conduit surface may be ignored. The coefficient of friction is generally low, and dynamic loads, especially vibrations, tend to relieve any shearing stresses that might develop. If no shearing stresses are involved, the stresses between the soil and the conduit are normal and the tangential compressive force C in the conduit wall is constant around the entire conduit (Figure 10) and is equal to: $C = p'R$ where p' = radial soil pressure at any point and R = radius of curvature at the same point.

On a noncircular cross section, if R increases, p' decreases and vice versa. As far as the conduit is concerned, design is simply $f_c = C/A <$ allowable stress.

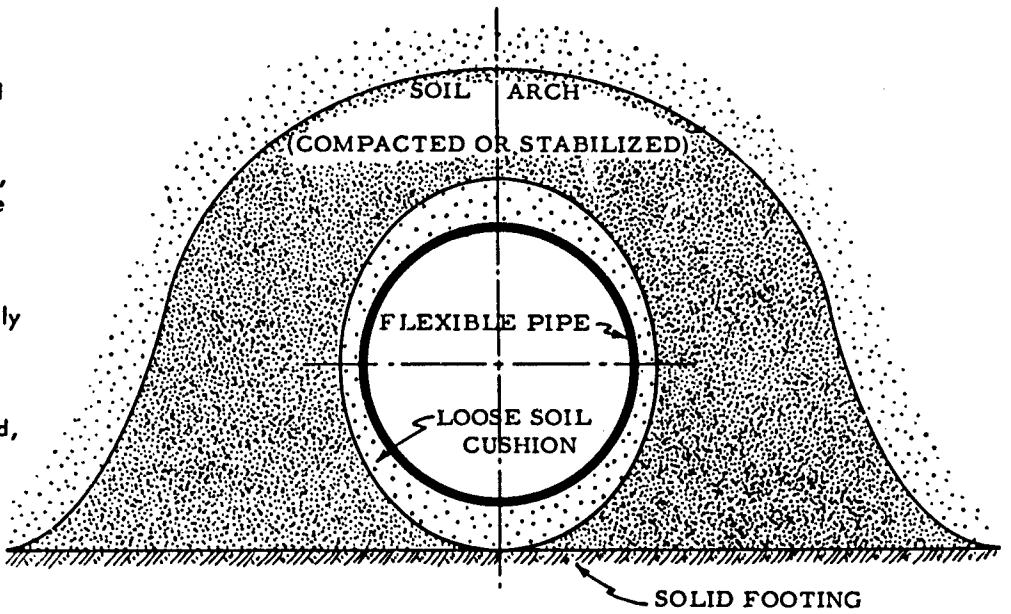


Fig. 8 Concept of Compacted Soil Arch with Cushion to Relieve Stress in Buried Flexible Pipe (Note Loose Soil Cushion)

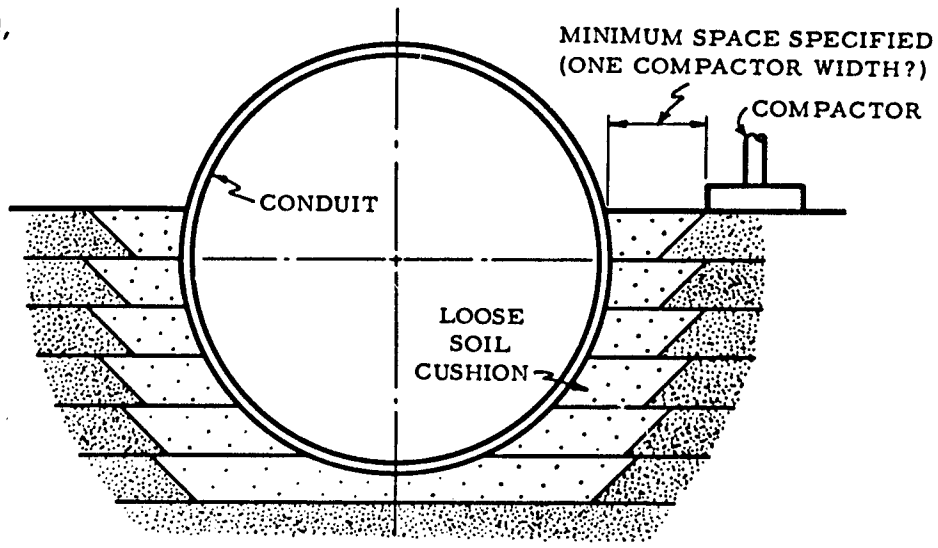


Fig. 9 Method of Compaction by Which Conduit Shape is Maintained and Ring Compression Load is Reduced by Loose Soil Cushion

TRENDS IN THE STRUCTURAL DESIGN OF SPECIAL SOIL-CONDUIT SYSTEMS

Nonsymmetrical Loads

There are many occasions where a nonsymmetrical load is applied to a soil-conduit system. One typical example is indicated in Figure 11. Tests have been conducted on nonsymmetrical loading for relatively rigid pipes; but very little work has been done on flexible conduits and non-circular conduits. An approximate solution for the special case of a uniformly distributed static load over one-half of the conduit width (Figure 11), has been used successfully. Failure is here defined as complete collapse or snap-through of the top half of the conduit. The analysis is based on a sliding wedge theory of failure with a conduit so flexible that the radial soil pressures are constant about the entire conduit ring. Shearing stresses against the conduit are ignored. The worst shear failure plane angle θ can be found by iteration. The curves shown in Figure 12 give the minimum height of soil cover mR required to resist a collapse failure due to the uniformly distributed load q acting at the soil surface over one-half the pipe diameter. This analysis is particularly important in the placement of very large, flexible pipes to ascertain the mimimum height of cover required before earth moving equipment compactors etc. can operate over the pipe. This particular loading condition is not greatly different from the worst possible loading condition.

A similar analysis has been applied to a vertically elongated (VE) pipe. The minimum computed soil cover is shown in the plot of Figure 13. Proportional values may be used for other q-loading values as determined from Figure 12.

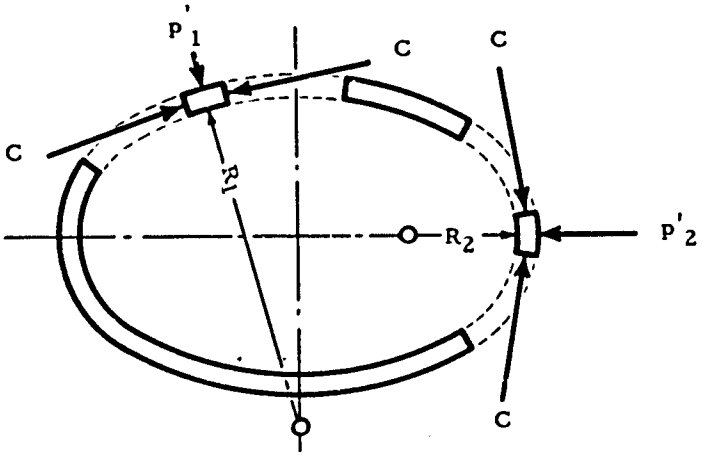


Fig. 10 Radial Pressure p' for Flexible Conduit if Shearing Pressures are Neglected (Force C is constant)

Slabs Over Buried Flexible Conduits

Oftimes it is necessary to operate equipment over the top of a buried flexible conduit with inadequate soil cover. Under such circumstances, a slab may be needed as shown in Figure 14a. In designing the slab, it should be recognized that if the soil is densely compacted, the center of the slab will have the greatest tendency to settle; and so a reasonably conservative reaction diagram for a concentrated load

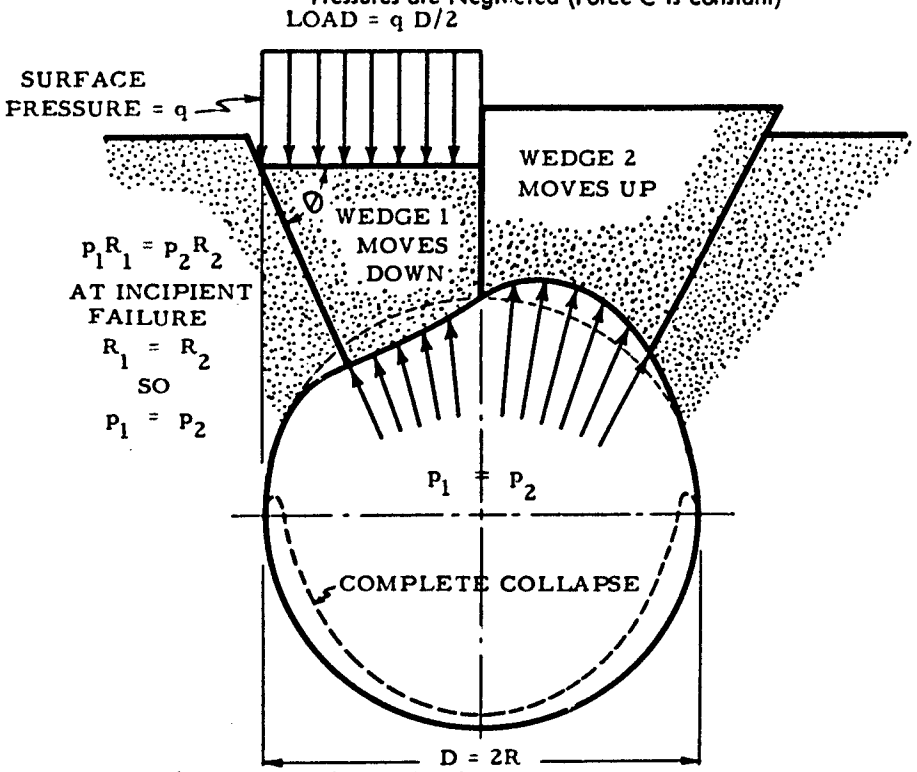
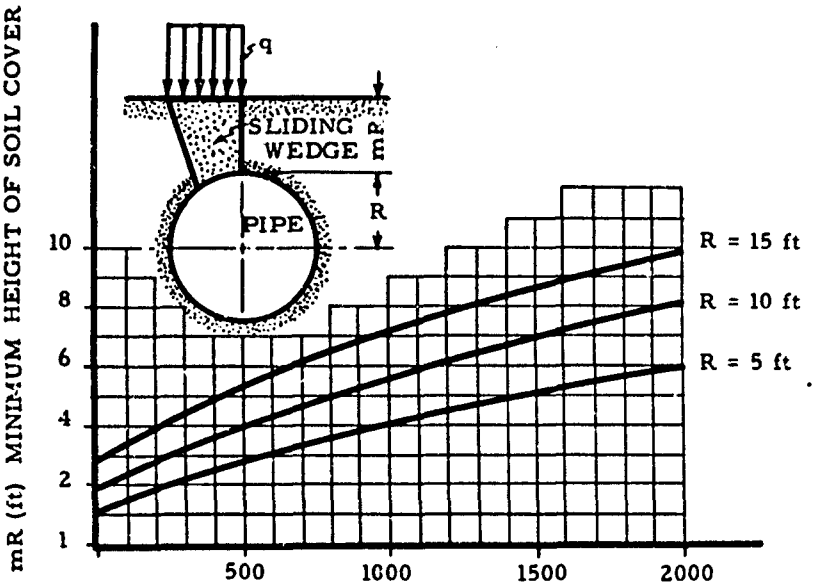


Fig. 11 Sliding Wedge Theory of Failure of Buried Flexible Conduit Due to Surface Pressure q Above Half of Pipe

in the center of the slab might be that shown in Figure 14b with a maximum moment of $M = \frac{3}{16}$ pD. This problem needs additional attention because in many installations economy justifies a stiff slab directly over the conduit rather than a higher fill or a stronger conduit. The slab should extend far enough beyond the conduit width to prevent the sliding wedge failure indicated in Figure 11. An extension of D/4 is adequate if the fill is good.

Cone-shaped Soil Pipe

For reasons of economy, more and more soil is being loaded from beneath conical stockpiles by dropping it through gates in conduits placed under the piles as shown in Figure 15a. The only new problem in this case is the determination of vertical soil pressures at the bottom of the conical pile of soil. Of course settlement of the supporting base would make some difference in the soil pressure diagram, however, the maximum pressure would occur if the base were assumed to be rigid with no differential settlement. Under this assumption, calculations show the pressure distribution diagram pressure equal to approximately two-thirds of the pressure which would be calculated using the height of the cone times the unit weight of the soil.



ASSUMPTIONS

γ = 110 P.C.F. = UNIT WEIGHT OF SOIL
ϕ = 35° = SOIL FRICTION ANGLE
C = 0 = SOIL COHESION
EI = 0 = PIPE WALL STIFFNESS
CIRCULAR PIPE CROSS SECTION

Fig. 12 Minimum Height of Soil Cover Required to Resist Failure of Buried Flexible Conduit with a Surface Pressure Over Half of the Pipe

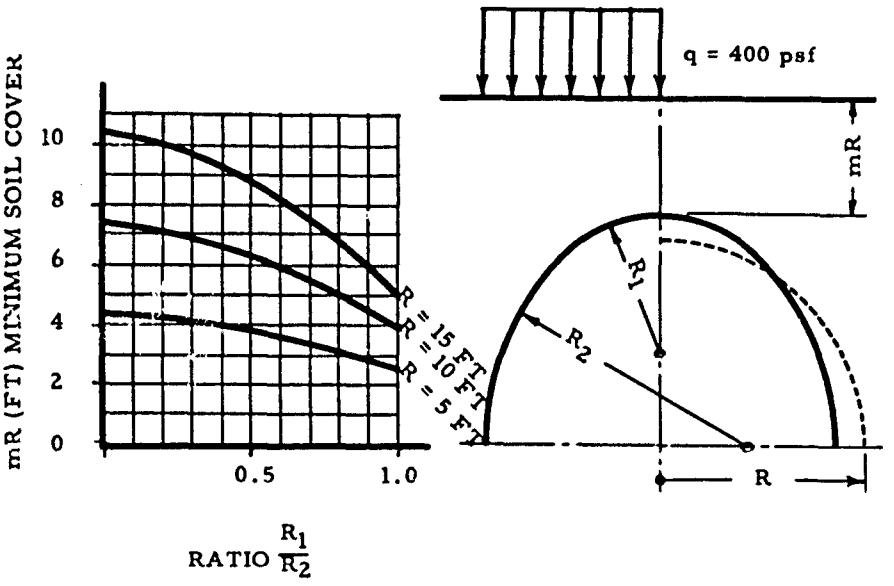
Miscellaneous Considerations

Very little has been done yet in the analysis of flexible conduits beneath the water table. There should be a distinction between drainage conduits and water tight conduits in such cases. The water not only develops hydrostatic pressure, with increased possibility of conduit buckling, but it also decreases the shearing strength of the surrounding soil by decreasing the intergranular pressure.

Analysis of cohesive soil fill is in demand. On numerous jobs the soil contains enough binder to develop cohesion which in turn may materially alter the performance of the soil-conduit system. In fact, future design might well take into account the possibility of stabilizing a soil arch over the conduit, to increase cohesion.

No theory as yet takes into account the difference in soil depth between the crown of the pipe and the spring line. Present theories are based on a soil pressure at the level of the top of the pipe. These assumptions are adequate for installations in which the height of soil cover over the pipe is large in comparison to the difference in elevation between the crown and the spring lines; but in the design of very large flexible buried conduits this assumption is not realistic.

There are but a few of the structural design trends in buried flexible conduits. Many others will be forthcoming. The need is urgent.



ASSUMPTIONS

γ = 110 P.C.F. = UNIT WEIGHT OF SOIL
ϕ = 35° = SOIL FRICTION ANGLE
C = 0 = SOIL COHESION
EI = 0 = CONDUIT WALL STIFFNESS
q = 400 P.C.F. OVER HALF CONDUIT WIDTH
m = 0.5

Fig. 13 Minimum Height of Soil Cover Required to Resist Failure of Buried Flexible Pipe with Two Different Ring Radii

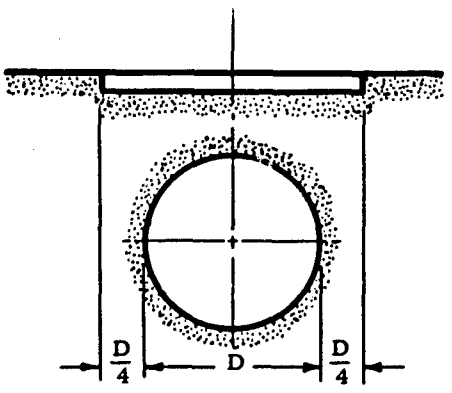
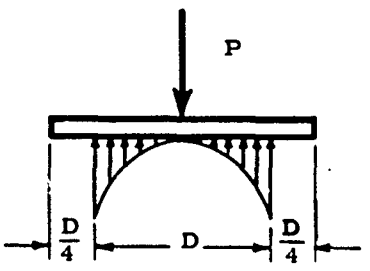


Fig. 14a Slab Over Buried Flexible Pipe



MOMENT AT CENTER

$M = \frac{3}{16} pD$

Fig. 14b Assumed Parabolic Loading on Slab

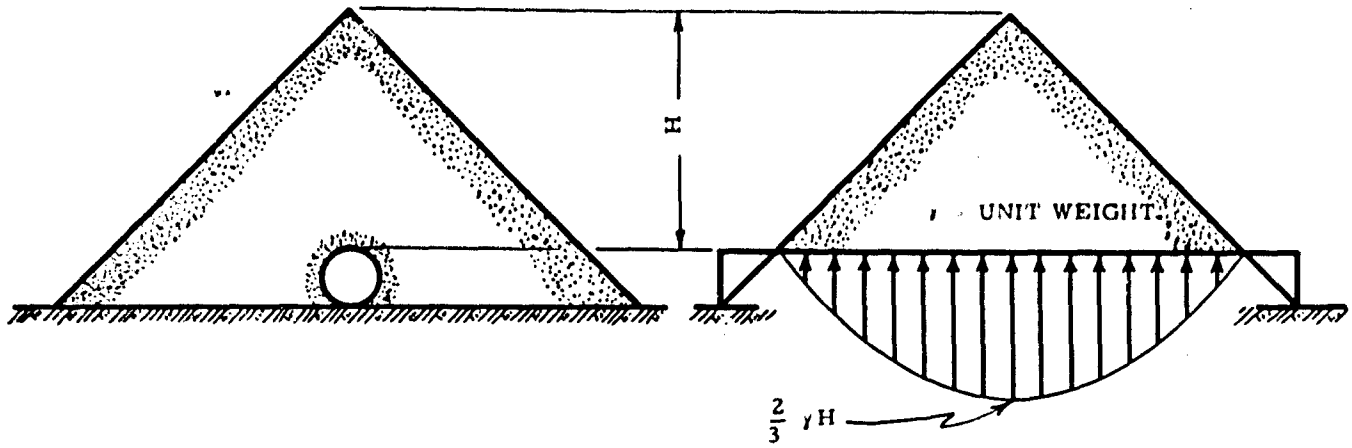


Fig. 15a Conical Pile of Soil Over Buried Flexible Conduit

Fig. 15b Soil Pressure Diagram Along Conduit Assuming No Support Settlement

REFERENCES

1. Spangler, M. G., Soil Engineering, International Textbook Company, Scranton, Pa., 1960, p. 433.
2. White, H. L., "The Corrugated Metal Conduit as Compression Ring," Armco Drainage and Metal Products, Inc., January, 1960.
3. Brockenbrough, R. L., "A Theoretical Evaluation of Two Corrugation Profiles for Corrugated Metal Pipe Culverts," ARL Project 90.12-017, Memorandum, United States Steel Corporation, Applied Research Laboratory, February 23, 1962.
4. Watkins, R. K., "Some Observations on the Ring Buckling of Buried Flexible Conduits," discussion of report "Strength of Steel Culvert Sheets Bearing Against Compacted Land Backfill," by G. G. Meyerhof and L. D. Baikie, presented 42nd Highway Research Board Meeting, January 1963.

A STUDY OF LOADS ON UNDERGROUND STRUCTURES

by
D. A. Van Horn*

ABSTRACT

In this paper an analytical method is presented for determining the loads on underground structures induced by time-dependent air overpressures of the type resulting from nuclear blasts. The first part is devoted to the development of an analytical method for evaluating the loads produced by static overpressures, and is based on principles set forth as a result of theoretical and experimental work conducted by Marston, Spangler, and associates, (1,2,4,5) at Iowa State University during the period 1908-1952. In this method, the major importance of the method of installation of the structure and the fill material is emphasized, and the effects of the various factors related to construction procedure are taken into account in the development. In the second part, the analysis is extended to include the effects of time-dependent overpressures. The method presented is based on a procedure published in 1960 (3) by engineers at the Illinois Institute of Technology Research Institute, and reflects the principles set forth in the theory of static loads.

STATIC OVERPRESSURES

Introduction

On the subject of static loads, the most extensive analytical and experimental work has been directed toward the determination of loads on underground conduits. Much of the early work can be attributed to the late Dean Anson Marston and his associates at Iowa State University. Professor M. G. Spangler, a student and long-time friend of Dean Marston, was responsible for perpetuating the work and has done much writing on the subject. The theories developed by Marston and Spangler form the core of currently accepted design practice for underground conduits. The following analysis of the effects of static loads is based on an extension of these theories to include the effect of a static uniform overpressure and the possible effect of cohesion.

In a consideration of loads on an underground structure, it would appear that the load due to the soil overburden would be equal to the weight of the soil prism directly above the structure (Figure 1). However, research and study have shown that the actual resultant load may be either greater or less than the actual weight of the soil prism. It has been found that the magnitude of the load is a function of both the weight of the prism and the shearing forces which are developed on the vertical faces of the prism. That is, for a given structure buried at a given depth, the weight of the prism depends only on the unit weight of the soil. However, the magnitude and direction of the shearing forces depend on several factors. These factors can be divided into two categories:

1. Soil Properties. Several soil properties have been found to effect the development of the shearing forces:
   a. Unit weight---directly affects the vertical pressure on any horizontal plane in the soil mass.
   b. K, the ratio of active lateral unit pressure to vertical unit pressure at a point in the soil mass---an index of the ability of a soil to develop horizontal pressure and likewise an index of the ability to develop normal forces on the vertical faces of the soil prism.
   c. Cohesion and Angle of Internal Friction---factors which reflect the magnitude of the maximum shearing forces which can be developed on failure planes in the soil mass.
   d. Stress-strain characteristics of the soil---which are important in the consideration of settlements.
2. Settlement Factors. Relative settlements of the soil prism and the soil adjacent to the prism have been found to affect not only the magnitude and direction of the shearing forces, but also the extent of the vertical surfaces of the prism over which the shearing forces act. Several factors affect the relative settlements:
   a. Settlement of the natural ground surface adjacent to the structure.
   b. Settlement of the soil directly beneath the structure.
   c. Vertical deflection of the top surface of the structure with respect to the base.
   d. Compression of the soil prism directly above the structure.
   e. Compression of the soil adjacent to the soil prism.

In the developments which follow, the relative importance of the various factors are shown.

---

*Formerly Associate Professor of Civil Engineering, Iowa State University; currently Research Associate Professor of Civil Engineering, Lehigh University, Bethlehem, Pennsylvania.

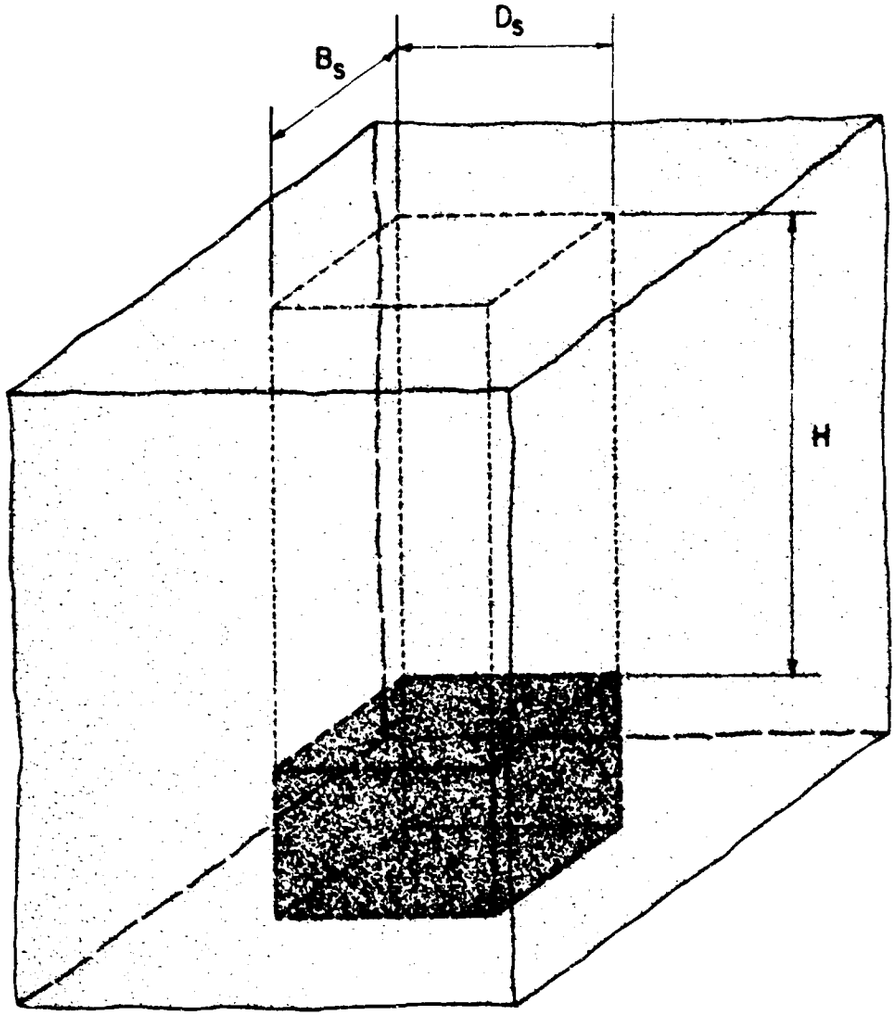


Fig. 1 Underground Structure

Classification of Underground Structures

In the development of the Marston Theory underground conduits are divided into three main classes (Figure 2) on the basis of the construction conditions of installation. The classes are:

1. Ditch Conduits---which are structures installed and completely buried in narrow ditches excavated in undisturbed or relatively passive soil,
2. Positive Projecting Conduits--which are structures installed in shallow bedding with the top projecting above the surface of the natural ground, and then covered with a soil backfill, and
3. Negative Projecting Conduits---which are structures installed in shallow ditches with the top below the adjacent natural ground surface, and then covered with a soil backfill. Expressions are developed for evaluating loads on structures in each of the three classes.

Structures in Ditch-Type Excavations

For a structure installed in a shaft-like excavation having horizontal dimensions which do not exceed two to three times the horizontal dimensions of the structure, the prism of backfill soil normally tends to settle downward. As a result of the relative movement between the soil prism and the adjacent soil, upward shearing forces on the vertical surfaces of the prism are generated (Figure 3). From a consideration of a free-body diagram of an element of the soil prism (Figure 3), the summation of vertical forces must be equal to zero.

$$P + W - (P+dP) - 2V_B - 2V_D = 0 \qquad (1)$$

where $$W = wB_dD_ddh \qquad (2)$$

If the soil is considered to exhibit the theory of failure proposed by Coulomb,

$$V_D = (c + K p \tan\phi)\, D_d\, dh \tag{3}$$

and

$$V_B = (c + K p \tan\phi)\, B_d\, dh \tag{4}$$

where

$$p = \frac{P}{B_d D_d} \tag{5}$$

Equation (1) then yields $dP = wB_dD_d\,dh - 2\left(c + K\left\{\frac{P}{B_dD_d}\right\}\tan\phi\right)(D_d + B_d)\,dh$ (6)

If $L_d = \frac{D_dB_d}{D_d+B_d}$ (7)

then Equation (6) can be reduced to $dp = dh\left(w - \frac{2c}{L_d} - \frac{2K\tan\phi}{L_d}\,p\right)$ (8)

The boundary conditions are

$$p = p_u \text{ when } h = 0 \quad \text{and} \quad p = p_H \text{ when } h = H$$

and the solution for the equation is

$$\frac{p_H}{wL_d} = \left[\left(\frac{2c}{wL_d} - 1\right)\left(\frac{e^{(-2K\tan\phi\frac{H}{L_d})} - 1}{2K\tan\phi}\right) + \left(e^{(-2K\tan\phi\frac{H}{L_d})}\right)\left(\frac{p_u}{wL_d}\right)\right] \tag{9}$$

Figures 4, 5, and 6 in a series illustrate the relationship between p_H/wL_d and H/L_d for several different values of p_u/wL_d. In Figure 4 soils having c = 0 and ϕ = 10°, 25°, and 35° respectively, are represented. In this figure $p_u = 0$ and a typical behavior is represented. That is, as the value of H/L_d is increased, each of the curves converges upon a particular value of p_H/wL_d. A comparison of the three curves shows the effect of ϕ, the angle of internal friction. As the value of ϕ is increased, the curve converges on a lower value of p_H/wL_d, and the convergence occurs more readily. The effect of cohesion can be seen in Figure 5. The three soils represented have a ϕ = 10°, and values of $2c/wL_d$ equal to 0, 0.8, and 1.2, respectively. Again, for $p_u = 0$, it is clearly illustrated that as the value of $2c/wL_d$ is increased, the curve converges on a lower value of p_H/wL_d. In fact, for $2c/wL_d$ = 1.2, the curve converges on a negative value of p_H/wL_d. The negative value illustrates the impossible occurrence of a resultant upward pressure on the top of the structure. The cohesion represented by $2c/wL_d$ = 1.2 would be 600 psi if w = 100 pcf and L_d = 10 feet. Figure 6 illustrates that for a given soil all of the curves, each representing a different value of p_u/wL_d, converge on the same value of p_H/wL_d.

On the basis of studies by Marston (2), it was suggested that cohesion be neglected because:

1. Considerable time must elapse after the backfill soil has been placed, before effective cohesion can be developed between the backfill soil and the adjacent soil, and
2. Rainfall or some other action may occur which would either eliminate or greatly reduce any cohesion that might have developed. Therefore, until it can be shown that the effect of cohesion is significant, the value of $2c/wL_d$ should probably be considered equal to zero in all calculations.

From Equation (9), or from Figures 4, 5, and 6, values of p_H can be obtained. However, p_H is the theoretical pressure on the bottom surface of the soil prism. In determining the pressure transmitted to the top surface of the structure, consideration must be given to the relative stiffnesses of the backfill soil adjacent to the sides of the structure, and of the structure itself. If the structure is very flexible, that is, sufficiently flexible that the stiffness of the structure and the adjacent soil are about the same, then p_s can be considered equal to p_H. On the other hand, if the structure is rigid, the entire load on the base of the soil prism should be considered as transmitted to the structure. Hence, the value of p_s can be determined from

$$p_s = p_H\left(\frac{D_dB_d}{D_sB_s}\right) \tag{10}$$

Even though it would probably be impractical to construct a structure at the bottom of a deep, shaft-like excavation, particularly when it is desirable to keep the horizontal dimensions of the shaft at a minimum, the development of the expression for the ditch condition forms a basis for further concepts and developments.

To illustrate the theory and use of the graphs, consider a structure having length = width = depth = 10 ft, buried in a ditch-type excavation at a depth H = 30 ft. The properties of the soil are $\phi = 25°$, K = 0.6, and w = 100 pcf. For no overpressure, $p_u = 0$.

Case I: Ditch dimensions - 20 ft x 20 ft.

$$L_d = \frac{(20)(20)}{20+20} = 10 \text{ ft} \qquad \frac{H}{L_d} = \frac{30}{10} = 3$$

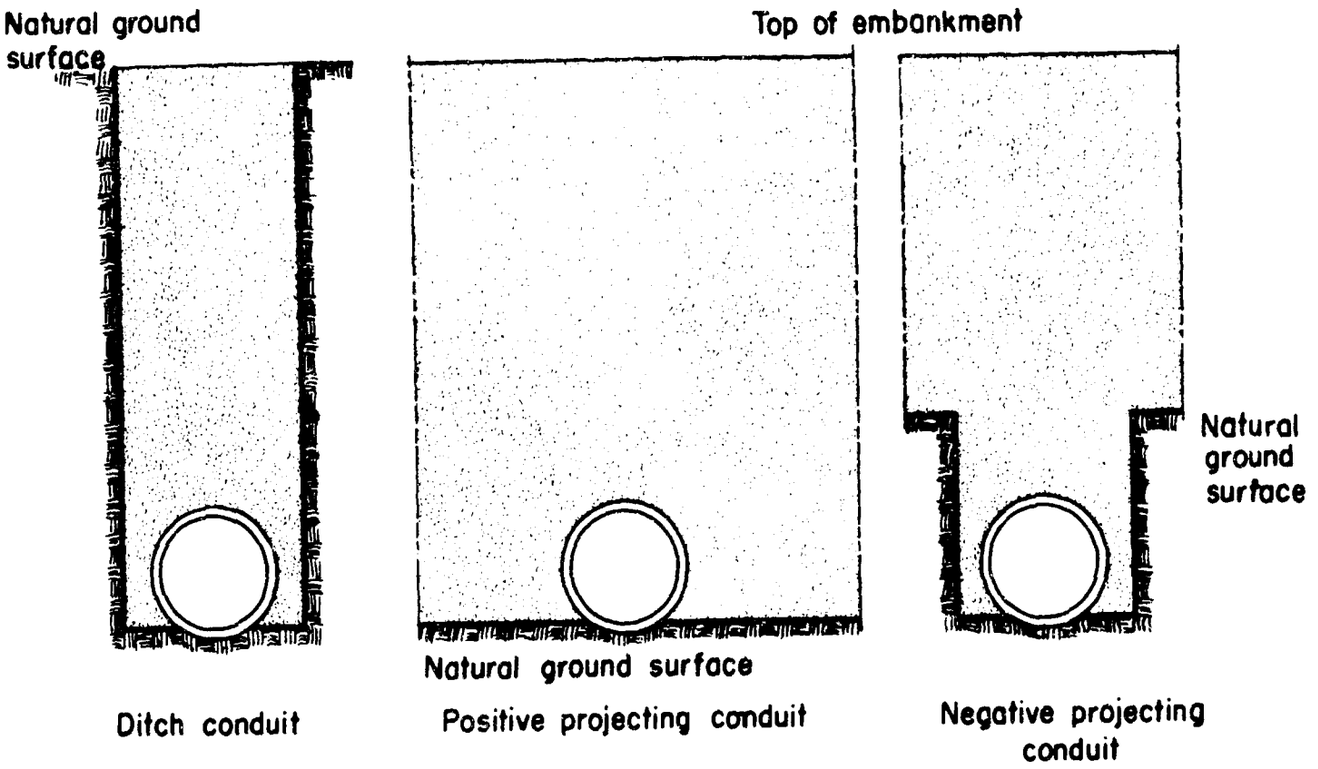


Fig. 2 Three Main Classes of Conduits

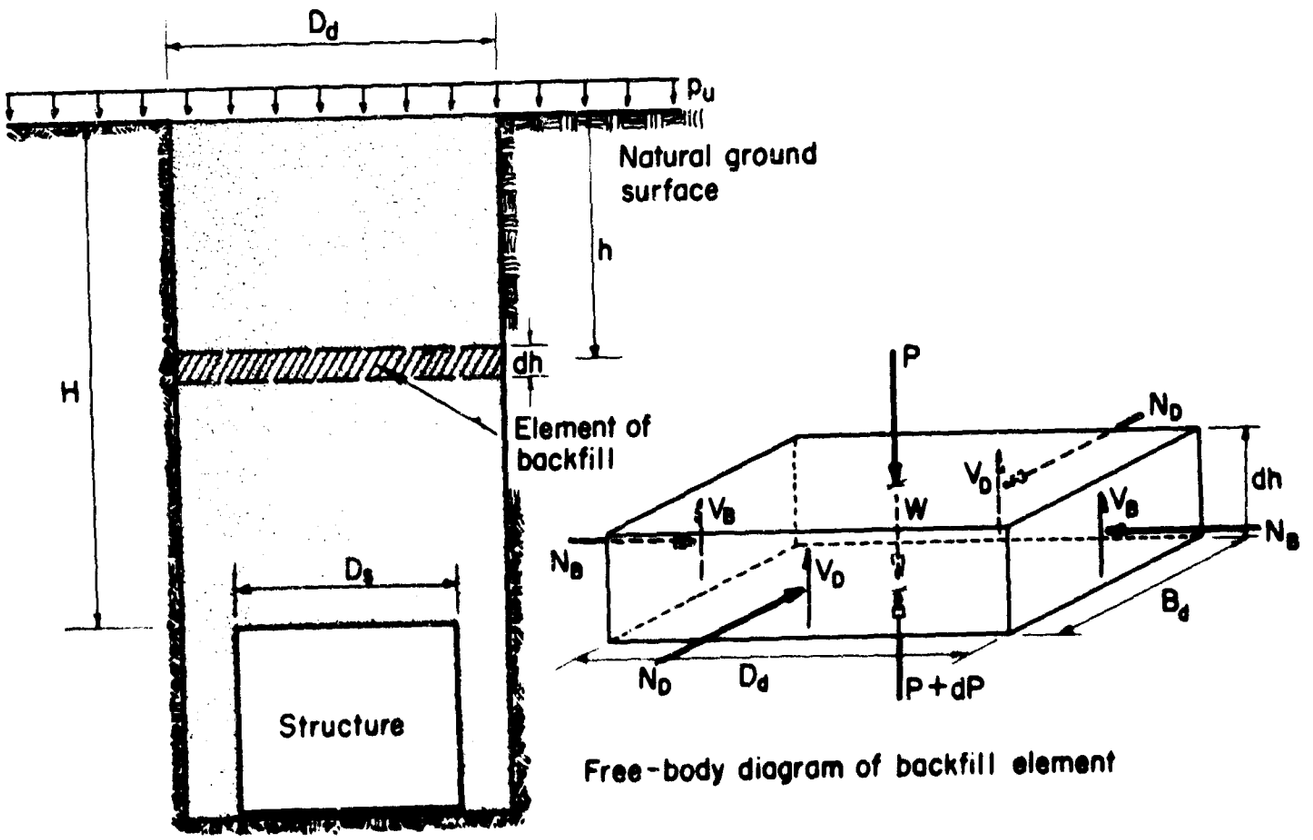


Fig. 3 Structure Buried in a Ditch-Type Excavation

From Figure 4,

$$\frac{p_H}{wL_d} = 1.44$$

Then $p_H = 1.44\ wL_d = 1440$ psf. If the stiffness of the structure and the soil adjacent to the structure are the same, then $p_s = 1440$ psf. However, if the structure is stiffer than the adjacent soil, then from Equation (10),

$$p_s = 1440 \left[\frac{(20)(20)}{(10)(10)}\right] = 5760 \text{ psf}$$

A comparison of the two values of p_s vividly illustrates the great importance of thorough compaction of the soil adjacent to the structure.

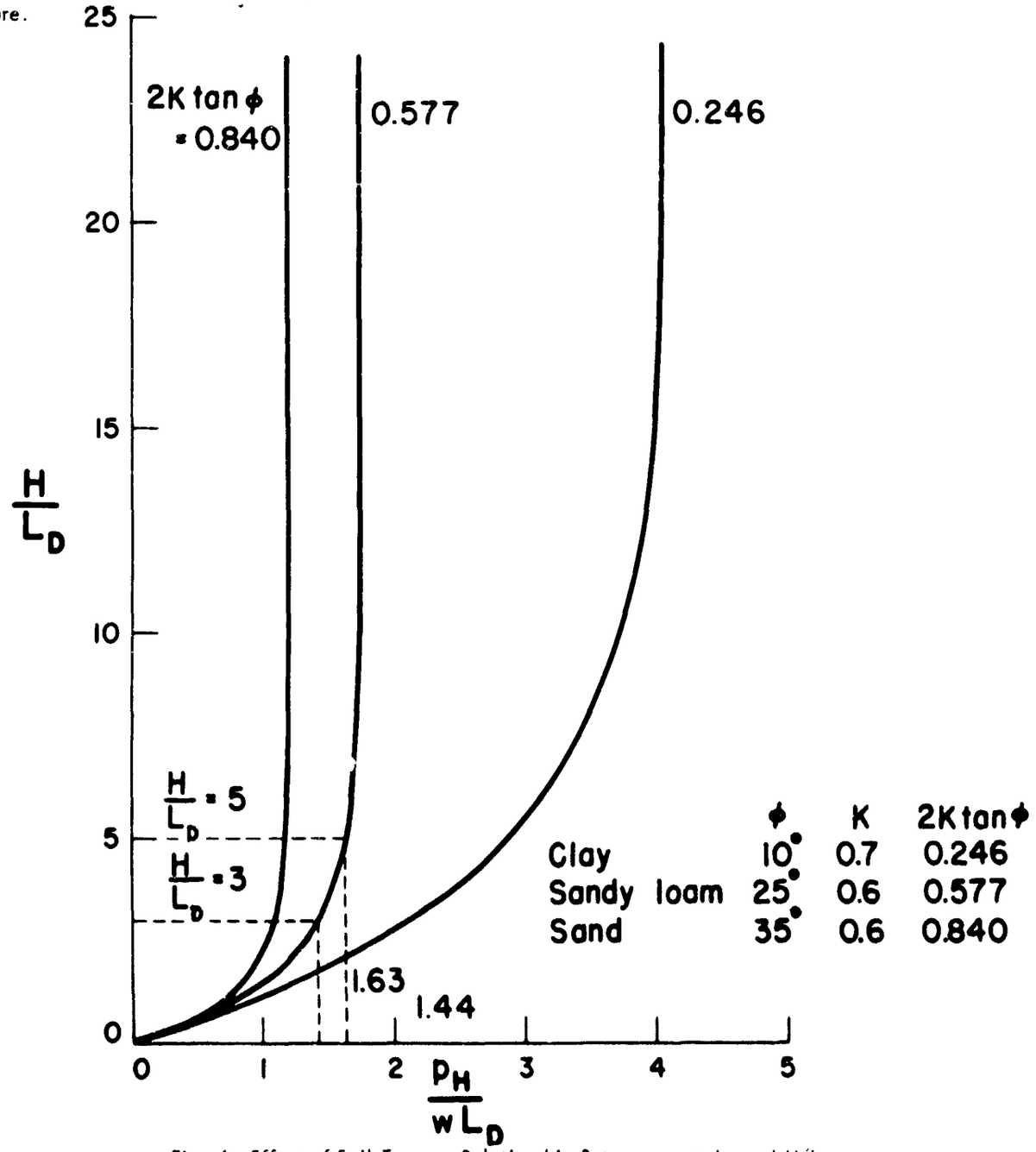


Fig. 4 Effect of Soil Type on Relationship Between p_H/wL_d and H/L_d

Case 2: To visualize the effect of the size of the excavation, suppose the dimensions of the ditch were reduced to 12 ft x 12 ft.

$$L_d = \frac{(12)(12)}{12+12} = 6 \text{ ft} \qquad \frac{H}{L_d} = \frac{30}{6} = 5$$

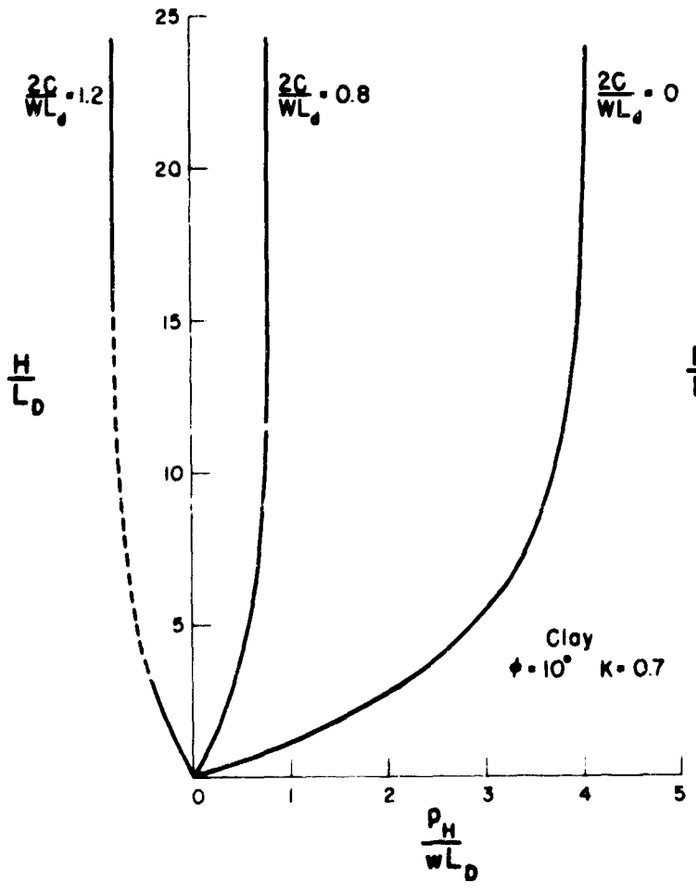


Fig. 5 Effect of Cohesion on Relationship Between p_H/wL_d and H/L

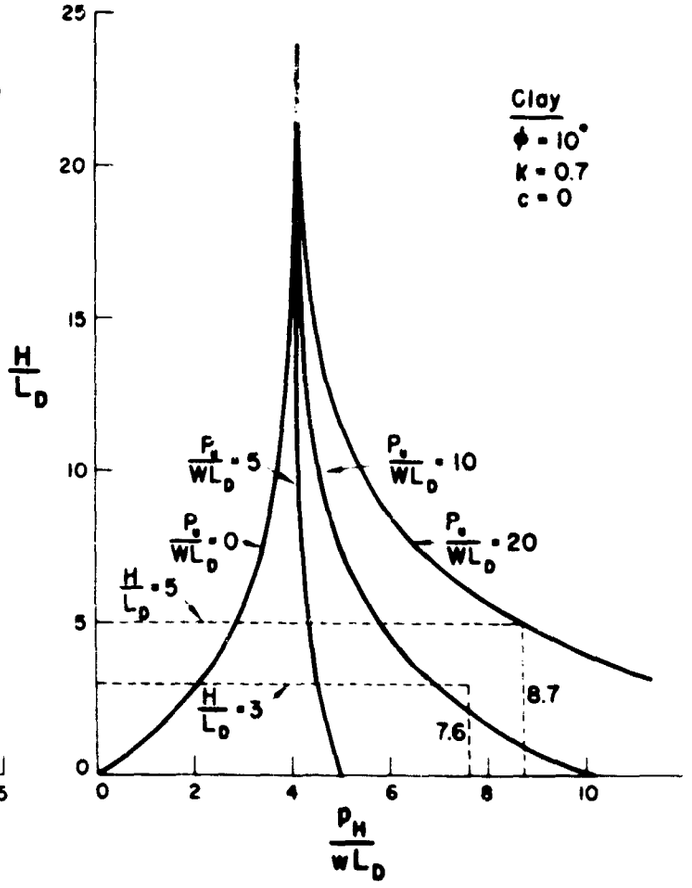


Fig. 6 Effect of Overpressure on Relationship Between p_H/wL_d and H/L_d

From Figure 4, $p_H/wL_d = 1.63$. Then $p_H = (1.63)(100)(6) = 973$ psf, which would be the value of p_s for essentially equal stiffnesses of soil and structure. If the structure is more rigid than the adjacent soil, then again from Equation (10)

$$p_s = 973 \left[\frac{(12)(12)}{(10)(10)}\right] = 1402 \text{ psf}$$

Thus, a second important feature has been demonstrated--the substantial reduction in load on the structure achieved by reducing the dimensions of the excavation.

To demonstrate the effect of a uniform overpressure, consider the same structure and burial depth as in the previous cases, but soil properties of $\phi = 10°$, $K = 0.7$, and $w = 100$ pcf. Consider an overpressure of 12,000 psf.

Case 3: $D_d = B_d = 20$ ft

$$\frac{p_u}{wL_d} = \frac{12{,}000}{(100)(10)} = 12 \frac{H}{L_d} = 3$$

From Figure 6

$$\frac{p_H}{wL_d} = 7.6 \qquad \text{Then} \quad p_H = 7600 \text{ psf}$$

Case 4: $D_d = B_d = 12$ ft

$$\frac{p_u}{wL_d} = \frac{12{,}000}{(100)(6)} = 20 \quad \frac{H}{L_d} = 5$$

Again from Figure 6

$$\frac{p_H}{wL_d} = 8.7 \qquad \text{Then} \quad p_H = 5220 \text{ psf}$$

SOIL-STRUCTURE INTERACTION

PROJECTING STRUCTURES

Positive Projecting Structures

When a structure is constructed with the top projecting above the natural ground surface and then covered with a soil fill, several new factors are introduced into the determination of loads on the structure. Most of these factors are centered around the relative settlements of the prism of soil directly above the structure and the soil adjacent to the prism. In the ditch-type excavation the soil adjacent to the prism is relatively compact compared with the backfill soil, and the development of upward shearing forces on the prism is assured. In contrast, for projecting structures the adjacent soil is also fill material, and a consideration of the relative settlements is necessary to determine the magnitude and direction of the shearing forces.

Two horizontal planes are important in further discussion. The first is the critical plane, a horizontal plane passing through the top surface of the structure when the level of the fill is at that surface. This plane changes shape during and after the placement of the remainder of the fill. The second is the plane of equal settlement, the horizontal plane above which the settlements of the soil prism and the adjacent soil are equal.

A projecting structure is in one of three classes according to the relative settlements of the soil prism and the adjacent soil (Figure 7)

1. Projection Condition---the settlement of the top of the structure is less than the settlement of the critical plane (Figure 7a), resulting in downward shearing forces on the soil prism. Therefore, the pressure on the top surface of the structure would be greater than the weight of the soil prism.
2. Transition Case---the settlements of the top of the structure and the critical plane are equal (Figure 7b). In this case, no shearing forces are developed, and the pressure on the top surface of the structure would be equal to the weight of the prism.
3. Ditch Condition---the settlement of the top of the structure is greater than the settlement of the critical plane (Figure 7c), resulting in upward shearing forces which reduce the pressure on the top surface of the structure to a value less than the weight of the prism.

The possible plane of equal settlement makes it necessary to sub-divide the projection and ditch conditions. If there is no plane of equal settlement, then the shearing forces extend to the top of the embankment and the condition is called either the Complete Projection Condition or the Complete Ditch Condition. If there definitely is a plane of equal settlement between the top of the structure and the top of the fill, the shearing forces extend only to the plane of equal settlement, and the condition is called either the Incomplete Projection Condition or the Incomplete Ditch Condition. At this point the particular factors which have an effect on the direction of the shearing forces will be related (Figure 8).

s = settlement of the natural ground surface adjacent to the structure
s_g = deformation of the fill material adjacent to the structure
s_m = settlement of the base of the structure
s_f = deflection of the top of the structure with respect to the base
d_s

The settlement ratio, r_{sd}, is defined by the relationship

$$r_{sd} = \frac{(s_m + s_g) - (s_f + d_s)}{s_m} \tag{11}$$

It can be seen (Figure 8) that for a positive value of r_{sd}, the load on the structure is greater than the weight of the soil prism. The load is less for a negative value.

For the Projection Conditions (r_{sd} positive) consider a free-body diagram of an element of the soil prism (Figure 8). The summation of vertical forces must equal zero.

$$P + W - (P + dP) + 2V_B + 2V_D = 0 \tag{12}$$

where

$$W = wB_sD_s\,dh \tag{13}$$

$$V_d = (c + K p \tan\phi)\, D_s\, dh \tag{14}$$

$$V_B = (c + K p \tan\phi)\, B_s\, dh \tag{15}$$

and

$$p = \frac{P}{D_s B_s} \tag{16}$$

Then Equation (12) yields

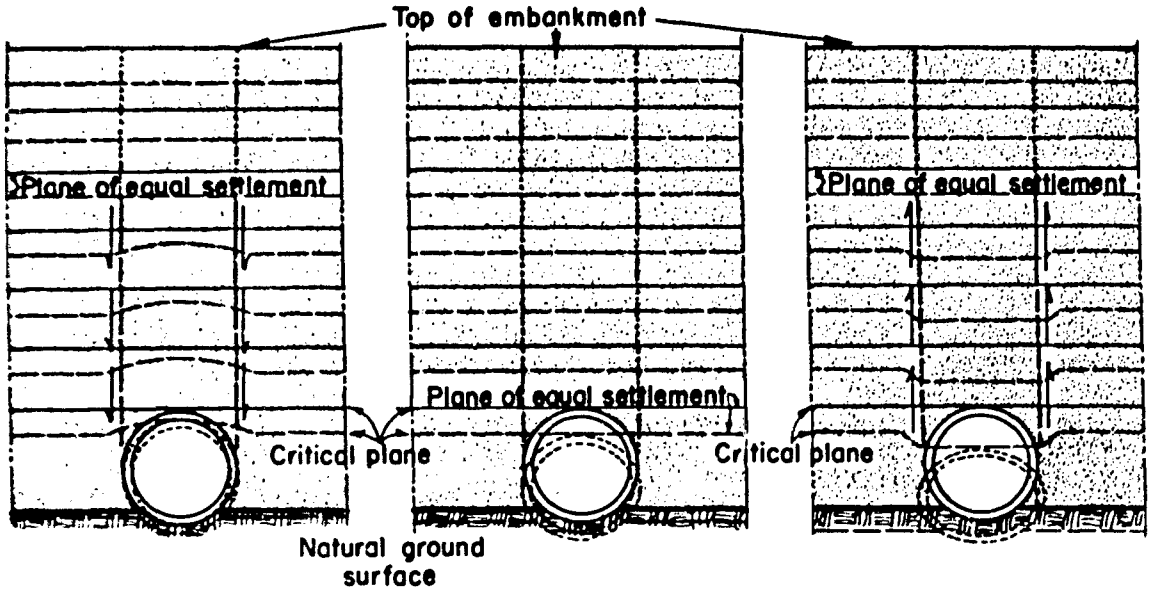
$$dP = wB_sD_s\,dh + 2\left(c + K\frac{P}{D_sB_s}\tan\phi\right)(D_s + B_s)\,dh \tag{17}$$

If

$$L_s = \frac{D_sB_s}{D_s+B_s} \tag{18}$$

then

$$dp = dh\left(w + \frac{2c}{L_s} + \frac{2K\tan\phi}{L_s}\,p\right) \tag{19}$$

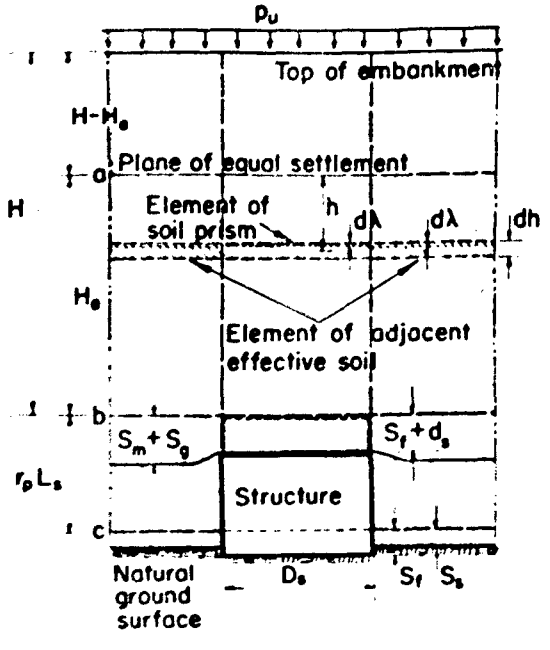


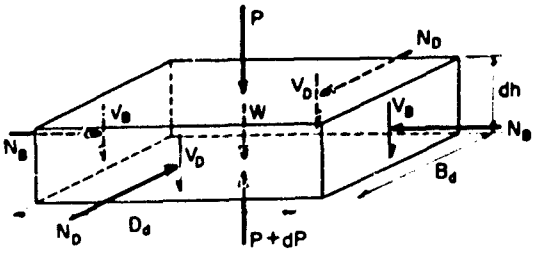
a) Incomplete projection condition — Positive settlement ratio

b) Transition case — Zero settlement ratio

c) Incomplete ditch condition — Negative settlement ratio

Fig. 7 Typical Settlement Situations Affecting Loads on Positive Projecting Structures





Free body diagram of backfill element

Fig. 8 Settlements Which Affect Loads on Positive Projecting Structures

For the Complete Projection Condition, the boundary conditions would be

$$p = p_u \text{ when } h = 0 \quad \text{and} \quad p = p_H \text{ when } h = H$$

and the solution of the equation is

$$\frac{p_H}{wL_s} = \left(\frac{2c}{wL_s} + 1\right)\frac{e^{\left(+2K\tan\phi\,\frac{H}{L_s}\right)} - 1}{2K\tan\phi} + \left\{e^{\left(+2K\tan\phi\,\frac{H}{L_s}\right)}\right\}\left(\frac{p_u}{wL_s}\right) \tag{20}$$

For the Incomplete Projection Condition, the boundary conditions would be

$$p = w(H - H_e) + p_u \text{ when } h = 0 \quad \text{and} \quad p = p_H \text{ when } h = H_e$$

and the solution is

$$\frac{p_H}{wL_s} = \left(\frac{2c}{wL_s} + 1\right)\frac{e^{\left(+2K\tan\phi\,\frac{H}{L_s}\right)} - 1}{2K\tan\phi} + \left\{e^{\left(+2K\tan\phi\,\frac{H}{L_s}\right)}\right\}\left(\frac{H}{L_s} - \frac{H_e}{L_s} + \frac{p_u}{wL_s}\right) \tag{21}$$

Now, an expression must be developed for the determination of H_e. From the definition of the plane of equal settlement, the settlement of the prism of soil extending from the top of the structure to the plane is equal to the settlement of the adjacent soil. To express this condition in equation form, two new quantities are defined:

λ = compression of the soil prism between the top of the structure and the plane of equal settlement, due to the height of fill H, and the overpressure p_u.

λ' = compression of the adjacent soil between the top of the structure and the plane of equal settlement, due to the height of fill H, and the overpressure p_u.

Then

$$\lambda' + s_m + s_g = \lambda + s_f + d_s \tag{22}$$

and since

$$r_{sd} = \frac{(s_m + s_g) - (s_f + d_s)}{s_m}$$

then

$$\lambda = \lambda' + r_{sd}\, s_m \tag{23}$$

In the derivation of an expression for λ, consider the element of the soil prism (Figure 8). $d\lambda = \frac{p}{E}\,dh$ where E = modulus of compression of the fill material, and p is given by the equation

$$\frac{p}{wL_s} = \left(\frac{2c}{wL_s} + 1\right)\frac{e^{\left(+2K\tan\phi\,\frac{h}{L_s}\right)} - 1}{2K\tan\phi} + \left\{e^{\left(+2K\tan\phi\,\frac{h}{L_s}\right)}\right\}\left(\frac{H}{L_s} - \frac{H_e}{L_s} + \frac{p_u}{wL_s}\right) \tag{24}$$

then

$$\lambda = \int_0^{H_e} d\lambda$$

$$= \frac{wL_s^2}{E}\left[\left(\frac{2c}{wL_s} + 1\right)\left(\frac{1}{2K\tan\phi}\right) + \left(\frac{H}{L_s} - \frac{H_e}{L_s} + \frac{p_u}{wL_s}\right)\right]\frac{e^{\left(+2K\tan\phi\,\frac{H_e}{L_s}\right)} - 1}{2K\tan\phi}$$

$$- \frac{wL_s^2}{E}\left(\frac{H_e}{L_s}\right)\left(\frac{2c}{wL_s} + 1\right)\left(\frac{1}{2K\tan\phi}\right) \tag{25}$$

Similarly, in the development of an expression for λ', an element of the adjacent effective soil is considered (Figure 8).

$$d\lambda' = \frac{p'}{E}\,dh$$

where p' is the average unit pressure at the level h in the adjacent effective soil (Figure 9), and is expressed as $p' = \frac{P'}{A}$

The term adjacent effective soil refers to the mass of soil which surrounds the soil prism and is considered to be affected by the behavior of the soil prism. At this point, an assumption must be made in defining a finite mass of adjacent effective soil. In the earlier work considering underground conduits, the length of the structure was large compared with that of the width, and a two-dimensional case was used in arriving at an expression for load per unit length. For the two-dimensional case, the mass of the adjacent effective soil was considered to be composed of a mass on each side of the soil prism, equal in size to the mass of the prism (Figure 10). For the three-dimensional case, the mass of adjacent effective soil is defined as the mass outlined in Figure 10. Then, in Equation (26), P' represents the total pressure on the adjacent effective soil at level h, and A the total area of the adjacent effective soil.

To evaluate λ', an expression for P' must be developed. From a free-body diagram of the adjacent soil (Figure 9), it can be seen that

$$P' = W_2 + p_u A - F \tag{27}$$

where $W_2 = wA(h+H-H_e)$ (28)

and F = summation of all vertical shearing forces acting on the soil prism. From the free-body diagram of the soil prism

$$F = P - W_1 - p_u D_s B_s \tag{29}$$

where $W_1 = wD_s B_s (h+H-H_e)$ (30)

and $P = pD_s B_s$ (31)

Then

$$p' = \frac{P'}{A} = w\left(1 + \frac{D_s B_s}{A}\right)(h+H-H_e) + p_u\left(1 + \frac{D_s B_s}{A}\right) - p\left(\frac{D_s B_s}{A}\right) \tag{32}$$

where p is given by Equation (24).

Finally,

$$\lambda' = \int_0^{H_e} d\lambda' = \frac{wL_s^2}{E}\left(1 + \frac{D_s B_s}{A}\right)\left[-\frac{1}{2}\left(\frac{H_e}{L_s}\right)^2 + \frac{H}{L_s}\left(\frac{H_e}{L_s}\right) + \frac{p_u}{wL_s}\left(\frac{H_e}{L_s}\right)\right]$$

$$- \frac{wL_s^2}{E}\left(\frac{D_s B_s}{A}\right)\left(\frac{2c}{wL_s} + 1\right)\left(\frac{1}{2K\tan\phi}\right)\left\{\frac{\left(e^{+2K\tan\phi\,\frac{H_e}{L_s}}\right) - 1}{e^{2K\tan\phi}}\right\}$$

$$+ \frac{wL_s^2}{E}\left(\frac{D_s B_s}{A}\right)\left(\frac{2c}{wL_s} + 1\right)\left(\frac{1}{2K\tan\phi}\right)\left(\frac{H_e}{L_s}\right)$$

$$- \frac{wL_s^2}{E}\left(\frac{D_s B_s}{A}\right)\left(\frac{H}{L_s} - \frac{H_e}{L_s} + \frac{p_u}{wL_s}\right)\left\{\frac{\left(e^{+2K\tan\phi\,\frac{H_e}{L_s}}\right) - 1}{e^{2K\tan\phi}}\right\} \tag{33}$$

In the derivations of expressions for λ and λ', two basic assumptions were made. The first assumption is that settlement of the soil prism, which is caused by the effects of the overpressure, by the weight of the soil, and by the shearing forces is substantially the same as would result from a uniform vertical pressure. The second is that the settlement of the adjacent soil is, likewise, substantially the same as that which would be caused by a uniform pressure.

An expression is now derived for s_m, the compression of the effective soil adjacent to the structure (Figure 8). The assumption is made that the vertical pressure is constant throughout the depth $r_p L_s$, and is equal to pH_e. Equation (32). The validity of the assumption depends mainly upon the ratio of H to $r_p L_s$---the greater the ratio, the more accurate the assumption. The expression for s_m would be

$$s_m = (r_p L_s)\left(\frac{p'}{E}\right) h \quad H_e \qquad \frac{D_s B_s}{A} \tag{34}$$

Substituting the expressions for λ, λ', and s_m into Equation (23), and letting $\beta = \frac{D_s B_s}{A}$, the following expression is obtained

$$\left[\frac{\left(\frac{2c}{wL_s} + 1\right)}{2K\tan\phi} + \frac{h}{L_s} - \frac{H_e}{L_s} - \frac{p_u}{wL_s} + r_{sd}\, r_p\left(\frac{2c}{wL_s} + 1\right)\left(\frac{\beta}{\beta+1}\right)\right]\frac{\left(e^{+2K\tan\phi\,\frac{H_e}{L_s}}\right) - 1}{e^{2K\tan\phi}}$$

$$+ r_{sd} r_p \left(\frac{\beta}{\beta+1}\right) e^{(+2K\tan\phi \frac{H_e}{L_s})} \left(\frac{H}{L_s} - \frac{H_e}{L_s} + \frac{p_u}{wL_s}\right) + \frac{1}{2}\left(\frac{H_e}{L_s}\right)^2 - \frac{H}{L_s}\left(\frac{H_e}{L_s}\right)$$

$$- \left(\frac{H_e}{L_s}\right)\left(\frac{p_u}{wL_s}\right) - \frac{\left(\frac{2c}{wL_s} + 1\right)}{2K\tan\phi}\left(\frac{H_e}{L_s}\right) - r_{sd} r_p \left(\frac{H}{L_s} + \frac{p_u}{wL_s}\right) = 0 \qquad (35)$$

For the Ditch Conditions (r_{sd} negative) the development of expressions for determining H_e/L_s and p_H/wL_s parallels the previous derivation of Equations (20), (21), and (35). The only difference between the final equations for the ditch and projection conditions would be in signs of several of the terms. Therefore, the following general expressions can be written which cover both ditch and projection conditions: For the complete conditions

$$\frac{p_H}{wL_s} = \left(\frac{2c}{wL_s}\right) \frac{e^{(\pm 2K\tan\phi \frac{H}{L_s})} - 1}{2K\tan\phi} + \left\{e^{(\pm 2K\tan\phi \frac{H}{L_s})}\right\}\left(\frac{p_u}{wL_s}\right) \qquad (36)$$

For the incomplete conditions

$$\frac{p_H}{wL_s} = \left(\frac{2c}{wL_s} \pm 1\right) \frac{e^{(\pm 2K\tan\phi \frac{H}{L_s})} - 1}{2K\tan\phi} + \left\{e^{(\pm 2K\tan\phi \frac{H_e}{L_s})}\right\}\left(\frac{H}{L_s} - \frac{H_e}{L_s} + \frac{p_u}{wL_s}\right) \qquad (37)$$

and

$$\left[\frac{\left(\frac{2c}{wL_s} \pm 1\right)}{2K\tan\phi} + \frac{H}{L_s} - \frac{H_e}{L_s} + \frac{p_u}{wL_s} \pm r_{sd} r_p \left(\frac{2c}{wL_s} \pm 1\right)\left(\frac{\beta}{\beta+1}\right)\right] \frac{e^{(\pm 2K\tan\phi \frac{H_e}{L_s})} - 1}{2K\tan\phi}$$

$$\pm r_{sd} r_p \left(\frac{\beta}{\beta+1}\right)\left\{e^{(\pm 2K\tan\phi \frac{H_e}{L_s})}\right\}\left(\frac{H}{L_s} - \frac{H_e}{L_s} + \frac{p_u}{wL_s}\right) \pm \frac{1}{2}\left(\frac{H_e}{L_s}\right)^2 \mp \left(\frac{H}{L_s}\right)\left(\frac{H_e}{L_s}\right)$$

$$\mp \left(\frac{H_e}{L_s}\right)\left(\frac{p_u}{wL_s}\right) \mp \left\{\frac{\left(\frac{2c}{wL_s} \pm 1\right)}{2K\tan\phi}\right\}\left(\frac{H_e}{L_s}\right) \mp r_{sd} r_p \left(\frac{H}{L_s} + \frac{p_u}{wL_s}\right) = 0 \qquad (38)$$

In the three equations, several of the quantities have two signs. The upper signs are valid for the projection conditions, the lower signs for the ditch conditions.

The quantity β, which is the ratio $\frac{D_s B_s}{A}$, falls within a relatively narrow range (Figure 10). It is seen that for a structure with a large B_s/D_s ratio, $\beta \approx 1/2$. At the other extreme, for a square structure $\beta \approx 1/6$. Therefore, β was taken at the intermediate value of $1/3$ for all computations.

Now let us examine a problem from the given conditions. First of all, the sign of the settlement ratio would enable classification as either the projection condition (positive) or the ditch condition (negative). The next step is to utilize Equation (38) to determine H_e. If H_e is found to be greater than H, then the complete condition exists, and Equation (36) is used to determine the pressure p_H on the structure. If H_e is less than H, then the condition is incomplete and Equation (37) is used

It is impossible to solve Equation (38) directly for H_e. Therefore, for a given case, the value of H_e/L_s would be determined by trial and error, and depending on the size of H_e as compared to H, the pressure of p_H would be determined from either Equation (36) or (37). To greatly facilitate the solution of Equations (38), and (37), graphs may be prepared which enable the direct determination of p_H/wL_s (Figures 11, 12).

Negative Projecting Structures

The next step in the development of a load theory for underground structures was a refinement of the construction procedure which combined the advantages of load reduction of the ditch-type installation with the construction ease of the positive projecting structures. In this construction procedure an area having dimensions slightly larger than the horizontal dimensions of the structure is excavated such that the top of the structure is below the natural ground surface (Figure 2). After the structure has been placed or constructed in the excavation, the fill is built up to a level somewhat above the original ground surface. The use of this method of construction normally results in a load which is less than the weight of the soil prism above the structure, plus the overpressure p_u. The major reason for the reduction in load is that the soil prism can settle more than the adjacent effective soil. Since the height of the prism is greater, the settlement will be greater, and the vertical shearing forces on the surfaces of the soil prism will be directed upward, reducing the load on the structure (Figure 13). As in the discussion of positive projecting structures, two horizontal planes need to be defined. The first is the critical plane, which, for negative projecting structures, is the horizontal plane in the embankment material which is originally level with the natural ground surface before settlements occur (Figure 14). The second is the plane of equal settlement. This is the horizontal plane above which the settlements of the soil prism and the adjacent soil are equal. For negative projecting structures, there are two cases to consider, the Complete Ditch Condition and the Incomplete Ditch Condition. If there is no plane of equal settlement, the shearing forces extend to the top of the embankment, and the condition is called the Complete Ditch Condition. If there is a plane of equal settlement, the shearing forces extend only to the plane, and the condition is called the Incomplete Ditch Condition. The factors which have an effect on the possible existence and location of a plane of equal settlement must be related (Figure 14).

s_g = settlement of the natural ground surface.

s_d = compression of the material in the soil prism between the top of the structure and the natural ground surface.

s_f = settlement of the base of the structure.

d_s = deflection of the top of the structure with respect to the base.

For negative projecting structures, the settlement ratio, r_{sd}, is defined by the relationship

$$r_{sd} = \frac{s_g - (s_d + s_f + d_s)}{s_d} \qquad (39)$$

It can be seen (Figure 14) that for a negative projecting structure, the value of r_{sd} will always be negative.

Consider a free-body diagram of an element of the soil prism in developing an expression for load on the structure. Since the shearing forces are directed upward, the free-body diagram would be the same as that for an element of the soil prism above a structure buried in a ditch-type excavation (Figure 3). The differential equation will have the same form as Equation (19).

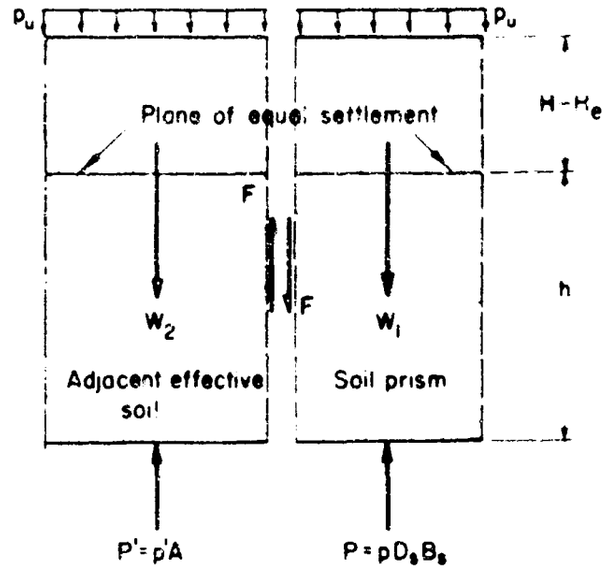
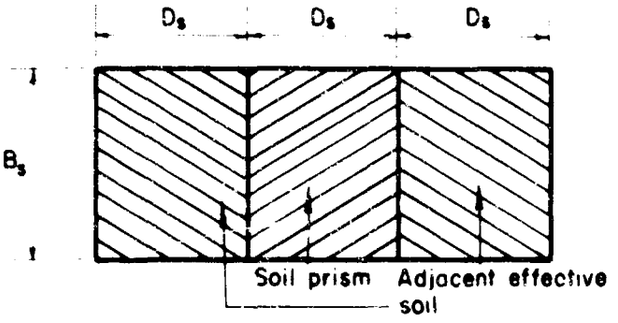


Fig. 9 Compressive Forces in the Soil Prism and in the Adjacent Effective Soil



2-Dimensional case

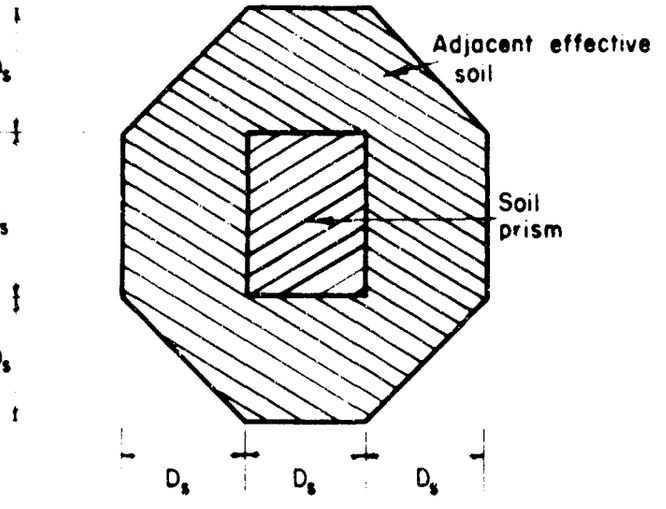


Fig. 10 Area of Adjacent Effective Soil

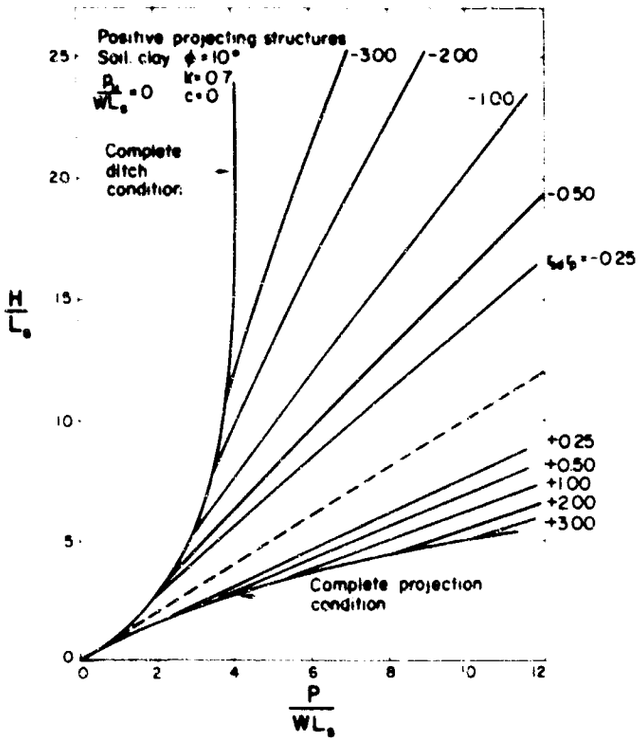


Fig. 11 Relationship Between p/wL_s and H/L_s (Eqs. 36 and 37) $p_u/wL_s = 0$

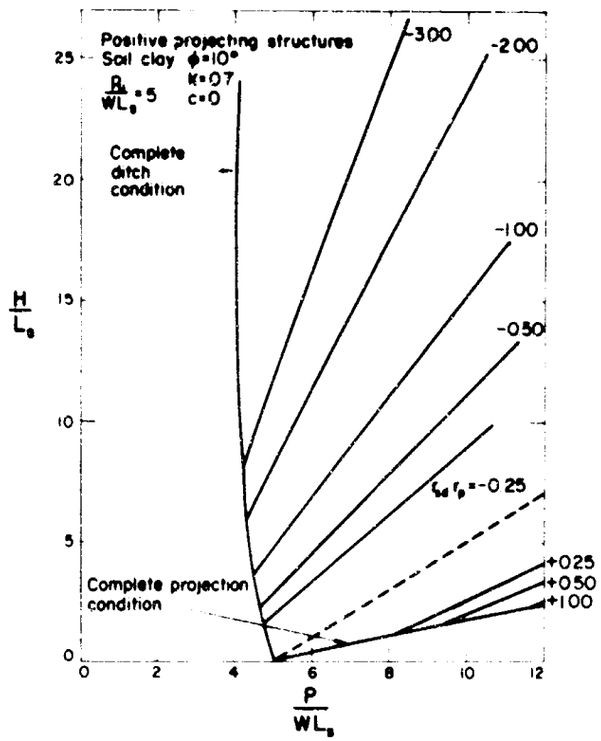


Fig. 12 Relationship Between p/wL_s and H/L_s (Eqs. 36 and 37) $p_u/wL_s = 5$

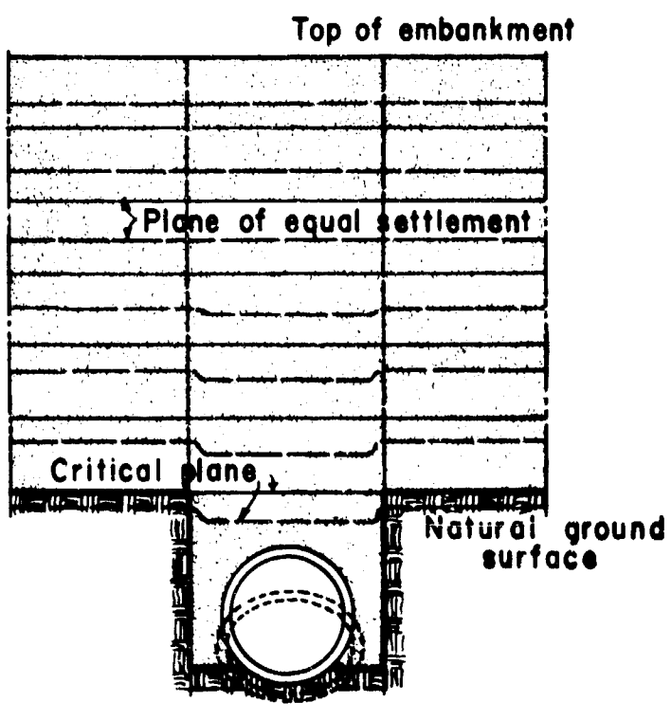


Fig. 13 Typical Settlement Situation Affecting Load on Negative Projecting Structure

$$dp = dh\left(w - \frac{2c}{wL_d} - \frac{2K\tan\phi}{L_d}\,p\right) \tag{40}$$

For the Complete Ditch Condition the boundary conditions would be

$$p = p_u \text{ when } h = 0 \quad \text{and} \quad p = p_H \text{ when } h = H$$

and the solution for the equation is

$$\frac{p_H}{wL_d} = \left(\frac{2c}{wL_d} - 1\right)\frac{e^{\left(-2K\tan\phi\,\frac{H}{L_d}\right)} - 1}{2K\tan\phi} + \left\{e^{\left(-2K\tan\phi\,\frac{H}{L_d}\right)}\right\}\left(\frac{p_u}{wL_d}\right) \tag{41}$$

For the Incomplete Ditch Condition, the boundary conditions would be

$$p = w(H-H_e) + p_u \text{ when } h = 0 \quad \text{and} \quad p = p_H \text{ when } h = H_e$$

and the solution is

$$\frac{p_H}{wL_d} = \left(\frac{2c}{wL_d} - 1\right)\frac{e^{\left(-2K\tan\phi\,\frac{H_e}{L_d}\right)} - 1}{2K\tan\phi} + \left\{e^{\left(-2K\tan\phi\,\frac{H_e}{L_d}\right)}\right\}\left(\frac{H}{L_d} - \frac{H_e}{L_d} + \frac{p_u}{wL_d}\right) \tag{42}$$

As in the previous developments, an expression must be developed for H_e. It can be seen (Figure 14) that the settlement of the prism of soil above the structure and the settlement of the adjacent soil must be equal at the plane of equal settlement. In equation form

$$\lambda + s_d + s_f + d_s = \lambda' + s_g \tag{43}$$

where: λ = compression of the soil prism between the top of the structure and the plane of equal settlement, due to the height of fill H, and the overpressure p_u.

λ' = compression of the adjacent soil between the natural ground surface and the plane of equal settlement, due to the height of fill H, and the overpressure p_u.

Since

$$r_{sd} = \frac{s_g - (s_d + s_f + d_s)}{s_d}$$

then

$$\lambda = \lambda' + r_{sd}s_d \tag{44}$$

In developing an expression for λ, consider the element of the soil prism (Figure 14) $d = \frac{p}{E}\,dh$ where E, as before, is the modulus of compression of the fill material, and p is given by the equation

$$\frac{p}{wL_d} = \left(\frac{2c}{wL_d} - 1\right)\frac{e^{\left(-2K\tan\phi\,\frac{h}{L_d}\right)} - 1}{2K\tan\phi} + \left\{e^{\left(-2K\tan\phi\,\frac{h}{L_d}\right)}\right\}\left(\frac{H}{L_d} - \frac{H_e}{L_d} + \frac{p_u}{wL_d}\right) \tag{45}$$

then

$$\lambda = \int_0^{H'_e} d\lambda$$

$$= \frac{wL_d^2}{E}\left[-\frac{\left(\frac{2c}{wL_d} - 1\right)}{2K\tan\phi} - \left(\frac{H'}{L_d} - \frac{H'_e}{L_d} + \frac{p_u}{wL_d}\right)\right]\left[\frac{e^{\left(-2K\tan\phi\,\frac{H'_e}{L_d}\right)} - 1}{2K\tan\phi}\right] - \left[\frac{wL_d^2}{E}\left(\frac{H'_e}{L_d}\right)\frac{\left(\frac{2c}{wL_d} - 1\right)}{2K\tan\phi}\right] \tag{46}$$

It should be noticed that two new terms H' and H'_e were introduced in Equation (46). From Figure 14, it can be seen that the two quantities are represented by

$$H' = H - r'_p L_d \tag{47}$$

and

$$H'_e \quad H_e - r'_p L_d \tag{48}$$

Next, an expression for λ' must be developed. Consider an element of the adjacent effective soil (Figure 14)

$$d\lambda' = \frac{p'}{E}\,dh = \frac{P'}{AE}\,dh$$

where P' is the total pressure at the level h and A is the total area of the adjacent effective soil (Figure 9). For the negative projecting structure, the direction of the shearing forces between the soil prism and the adjacent effective soil would be reversed, and the dimensions of the soil prism would be those of the excavation, B_d and D_d. From the free-body diagrams it can be seen that

$$P' = (A + D_d B_d)\left[w(h + H - H_e) + p_u\right] - P \tag{49}$$

Then

$$p' = \frac{P'}{A} = w\left(1 + \frac{D_d B_d}{A}\right)(h + H - H_e) + p_u\left(1 + \frac{D_d B_d}{A}\right) - p\left(\frac{D_d B_d}{A}\right) \tag{50}$$

where p is given by Equation (45).

Finally,

$$\lambda' = \int_0^{H_e} d\lambda'$$

$$= \frac{wL_d^2}{E}\left(1 + \frac{D_d B_d}{A}\right)\left[-\frac{1}{2}\left(\frac{H'_e}{L_d}\right)^2 + \frac{H'}{L_d}\left(\frac{H'_e}{L_d}\right) + \frac{p_u}{wL_d}\left(\frac{H'_e}{L_d}\right)\right] - \lambda\left(\frac{D_d B_d}{A}\right) \tag{51}$$

As before, in the derivations of expressions for λ and λ', the assumptions are made that the settlements of the soil prism and the adjacent effective soil are substantially the same as would result from a uniform pressure.

In deriving an expression for s_d, the assumption is made that the vertical pressure is constant throughout the depth $r'_p L_d$, and is equal to p_H, given by Equation (45). The expression for s_d would then be

$$s_d = (r'_p L_d)\left(\frac{p}{E}\right)_{h = H'} \tag{52}$$

Substitution of these expressions for λ, λ', and s_d into Equation (44), and letting $\beta = \frac{D_d B_d}{A}$, the following expression is obtained:

$$\left[-\frac{\left(\frac{2c}{wL_d} - 1\right)}{2K\tan\phi} - \frac{H'}{L_d} + \frac{H'_e}{L_d} - \frac{p_u}{wL_d} - r_{sd}r'_p\left(\frac{2c}{wL_d} - 1\right)\left(\frac{1}{\beta + 1}\right)\right]\frac{e^{\left(-2K\tan\phi\,\frac{H'_e}{L_d}\right)} - 1}{2K\tan\phi}$$

$$- r_{sd}r'_p\left(\frac{1}{\beta + 1}\right)\left\{e^{\left(-2K\tan\phi\,\frac{H'_e}{L_d}\right)}\left(\frac{H'}{L_d} - \frac{H'_e}{L_d} + \frac{p_u}{wL_d}\right) + \frac{1}{2}\left(\frac{H'_e}{L_d}\right)^2 - \frac{H'}{L_d}\left(\frac{H'_e}{L_d}\right)\right.$$

$$\left. - \left(\frac{H'_e}{L_d}\right)\left(\frac{p_u}{wL_d}\right) - \frac{\left(\frac{2c}{wL_d} - 1\right)}{2K\tan\phi}\left(\frac{H'_e}{L_d}\right)\right\} = 0 \tag{53}$$

Consideration of a particular problem parallels that of a problem involving a positive projecting structure. Equations (53), (47), and (48) are used to determine H_e. If H_e is found to be greater than H, then the complete condition exists and p_H is determined by Equation (41). If H_e is less than H, then the condition is incomplete and Equation (42) is used. As in the case of positive projecting structures, the use of graphs will greatly facilitate the solution of Equations (53), (41), and (42). Sample graphs (Figures 15, 16) enable the direct determination of p_H / wL_d.

The use of the negative projection condition in construction assures a reduction in load on the structure, but construction of the structure in the small confines of the excavation may be difficult. To permit ease of construction of the structure and, at the same time, to retain the load reduction advantage of the negative projecting condition, another method of fill construction has been suggested. It has been termed the Imperfect Ditch Method of construction. The procedure is to construct the structure at the natural ground level. The fill, built up to a level above the top of the structure, is thoroughly compacted. A part of the completed fill, equal in area and shape to the soil prism, is then excavated and replaced with loose soil or any other highly compressive material. The entire fill is then built up to a higher level, and again, a part of this layer of fill directly above the structure, is removed and replaced with loose material. The fill is built up to the desired height in several layers, and each time a part of the soil above the structure is removed and replaced with loose material (Figure 17). The settlement of the soil prism in a fill constructed in this manner will be greater than that of the adjacent soil. As a result the shearing forces on the walls of the prism will be directed upward, thereby reducing the load on the structure. The main advantage of the method is the ease of construction of the structure; but the main disadvantage would be in the additional height of fill required to provide the desired protection.

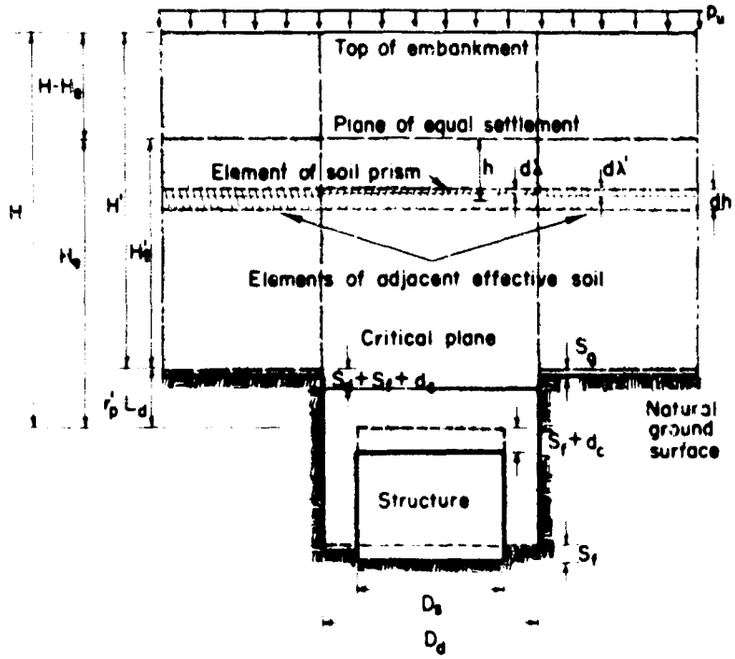


Fig. 14 Settlements which Affect Loads on Negative Projecting Structures

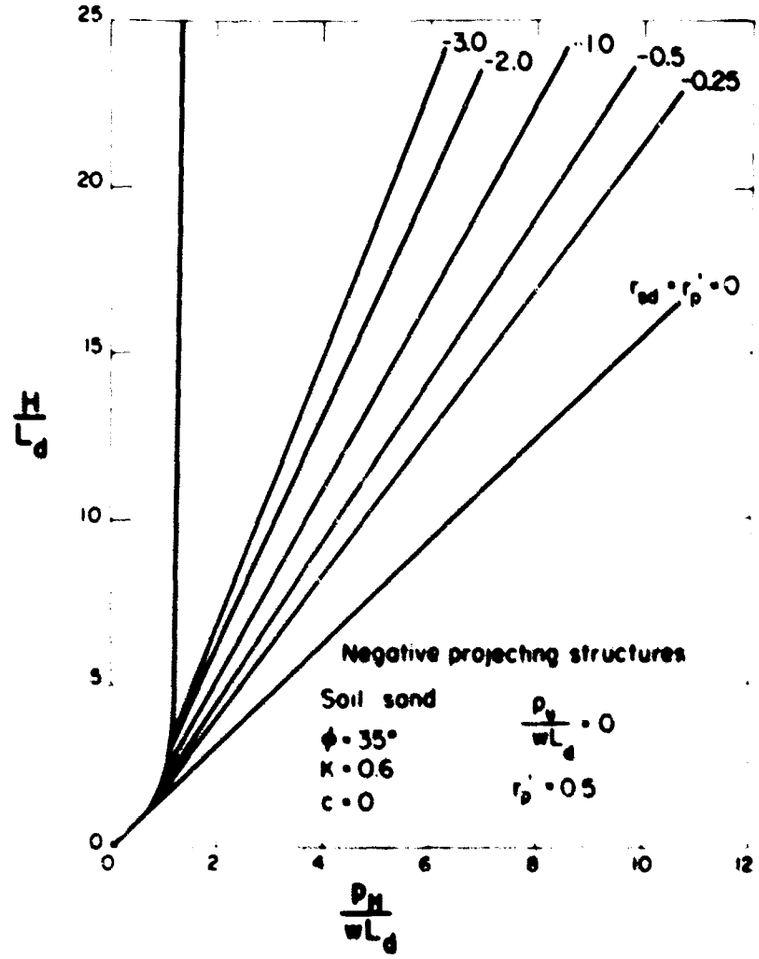


Fig. 15 Relationship between H, L_d and p_H, wL_d for Negative Projecting Structures with p_v, wL_d = 0

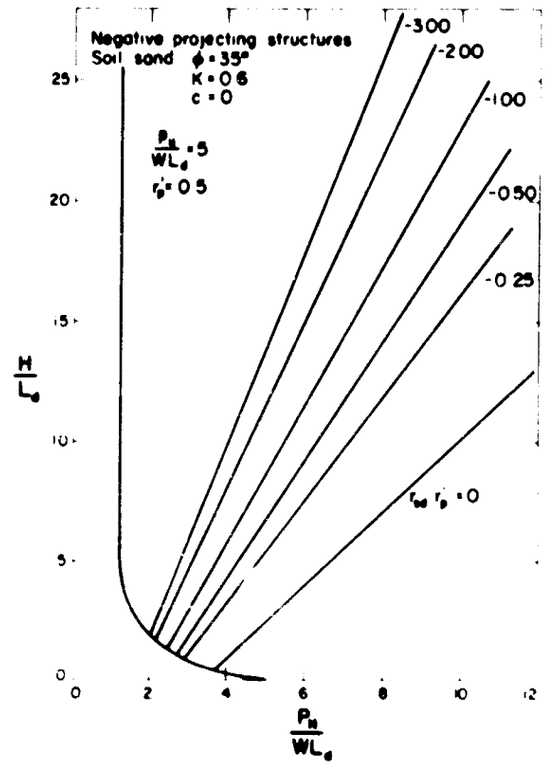


Fig. 16 Relationship between H/L_d and p_H/wL_d for Negative Projecting Structures with $p_v/wL_d = 5$

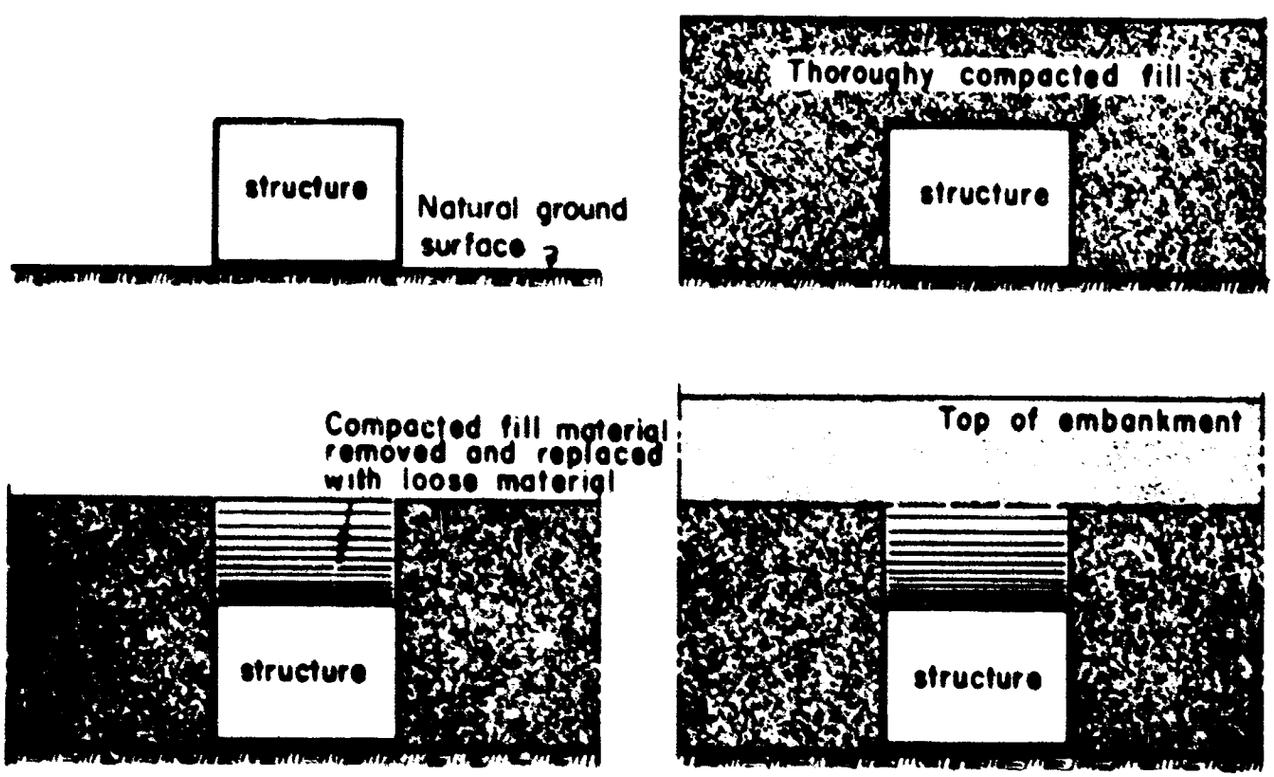


Fig. 17 Imperfect Ditch Method of Construction

STATE OF THE ART

SUMMARY

It has been shown that loads on underground structures may be materially different from the sum of the weight of the soil prism and the full effect of a uniform static overpressure. It is believed that the theories presented provide a sound approach to the determination of loads on structures installed by several different construction procedures. Of the several variables which influence the size of the loads, much information is available on the properties of the soils (w, ϕ, c, and K) and the range of values that each of the properties might have. However, the most difficult factor to evaluate is the settlement ratio. Some information has been reported (4) regarding measurements of the settlement ratios of a group of culverts, but extensive studies of the settlement characteristics of structures, either full-size structures or models, are needed to provide factual information on this important factor.

TIME-DEPENDENT OVERPRESSURES

Introduction

In 1960, an analytical method was presented for describing the behavior and possible failure modes of an underground structure subjected to a time-dependent air overpressure. This method will be referred to as the IITRI method. From the theory developed, it is possible to determine the resultant pressure on the structure produced by the time-dependent overpressure, and the weight of the soil overburden. However, the method is based on only one mode of failure, which is assumed to be independent of the method of construction. Therefore, the following development, based on the static pressure theories presented in the first part of this paper, and retaining the same basic approach and assumptions of the IITRI method, may provide a significant modification and possibly shed more light on the problem of predicting the behavior of underground structures subjected to time-dependent air overpressures.

In general, the IITRI method is based on the assumption that failure of the system takes place when the roof of the structure collapses with a downward movement of the entire mass of soil directly above the structure. The soil mass is assumed to move as a rigid body; and vertical, upward shearing forces on the soil mass are assumed to be developed throughout the entire height of the soil overburden (Figure 18). By the previously developed theory of static loads, this condition would be the complete ditch condition for a positive projecting structure, and only with the assurance of a very large settlement ratio would this type of failure be probable. In the following development, all of the methods of installation discussed in the first part of this paper will be considered.

Several assumptions related to the air overpressure-time relationship must be set forth. It has been found that the actual overpressure-time relationship resulting from nuclear explosions can be accurately represented by the equation

$$p_t = p_o e^{\frac{-t}{t_o}} \left(1 - \frac{t}{t_o}\right) \tag{54}$$

Graphical representation of this equation is given in Figure 19(a). However, it has been suggested that the relationship can reasonably be assumed to be of the simpler form

$$p_t = p_o \left(1 - \frac{t}{t_d}\right) \tag{55}$$

A plot of Equation (55) is shown in Figure 19 (b). This equivalent form is based on the same peak overpressure, p_o, and the same total impulse, which is equal to the area under the p-t curve. For the same total impulse

$$t_d = 0.736\, t_o \tag{56}$$

The assumptions related to soil behavior are precisely the same as are made in the previous development of static-load theory presented in the first part of this paper. For a more complete discussion of all of the assumptions and limitations, the reader is referred to the original paper presenting the IITRI method.

Dynamic Loads on Structures in Ditch-Type Excavations

From a consideration of the free-body diagram of the element of the soil prism (Figure 3), the summation of vertical forces must be equal to the mass of the element times the vertical acceleration.

$$P + W - (P + dp) - 2V_B - 2V_D = \frac{W}{g}\frac{d^2x}{dt^2} \tag{57}$$

where x = vertical movement of the element.

Then

$$dp = dh\left(w - \frac{2c}{L_d} - \frac{2K\tan\phi}{L_d}\,p - \frac{w}{g}\frac{d^2x}{dt^2}\right) \tag{58}$$

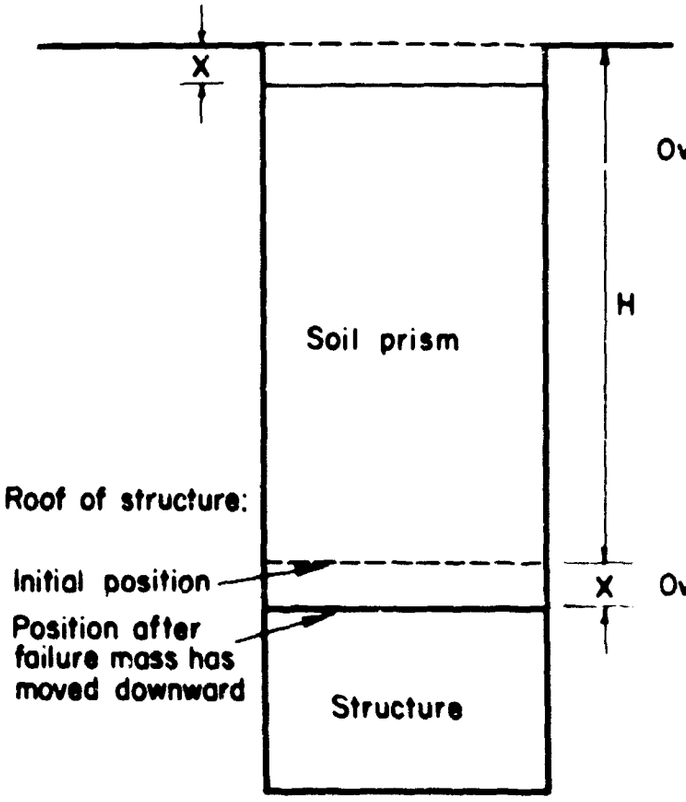


Fig. 18 Assumed Movement of Failure Mass

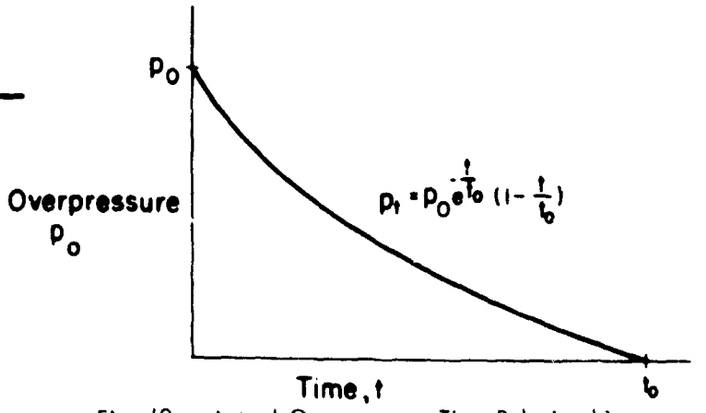


Fig. 19a Actual Overpressure-Time Relationship

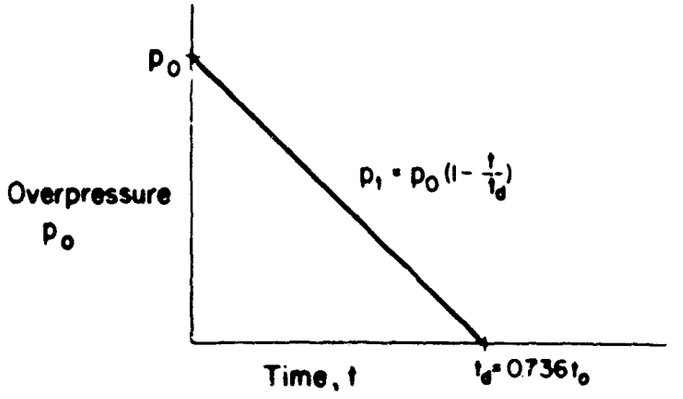


Fig. 19b Assumed Overpressure-Time Relationship

Since the entire mass is assumed to move as a rigid body, then x is independent of h, and the boundary conditions would be:

$$p = p_t \text{ when } h = 0 \quad \text{and} \quad p = p_H \text{ when } h = H$$

The solution of the equation would be

$$\frac{p_H}{wL_d} = \left(\frac{2c}{wL_d} - 1\right)\frac{e^{\left(-2K\tan\phi\,\frac{H}{L_d}\right)}-1}{2K\tan\phi} + \left\{e^{\left(-2K\tan\phi\,\frac{H}{L_d}\right)}\left(\frac{p_t}{wL_d}\right) + \frac{1}{g}\frac{d^2x}{dt^2}\right\}\left(\frac{e^{\left(-2K\tan\phi\,\frac{H}{L_d}\right)}-1}{2K\tan\phi}\right) \tag{59}$$

Solving Equation (59) for $\frac{p_t}{L_d}$:

$$\frac{p_t}{wL_d} = \frac{p_H}{wL_d}e^{\left(+2K\tan\phi\,\frac{H}{L_d}\right)} + \left(\frac{2c}{wL_d} - 1\right)\frac{e^{\left(+2K\tan\phi\,\frac{H}{L_d}\right)}-1}{2K\tan\phi} + \frac{1}{g}\frac{d^2x}{dt^2}\left(\frac{e^{\left(+2K\tan\phi\,\frac{H}{L_d}\right)}-1}{2K\tan\phi}\right) \tag{60}$$

Equation (60) may be written in simplified form

$$Q_1\frac{d^2x}{dt^2} + R_1 = S_1\left(1 - \frac{t}{t_d}\right) \tag{61}$$

where

$$S_1 = \frac{p_o}{wL_d} \tag{62}$$

$$R_I = \frac{p_H}{wL_d}\left\{e^{+2K\tan\phi\,\frac{H}{L_d}}\right\} + \left(\frac{2c}{wL_d} - 1\right)\frac{e^{+2K\tan\phi\,\frac{H}{L_d}} - 1}{2K\tan\phi} \tag{63}$$

and

$$Q = \frac{1}{g}\left\{e^{+2K\tan\phi\,\frac{H}{L_d}} - 1\right\}\frac{1}{2K\tan\phi} \tag{64}$$

It can be seen that the equation for R_I is the same as that for p_u, wL_d as given by Equation (9). It can also be shown that R_I represents the magnitude of static overpressure of infinite duration which would produce the same pressure p_H, as would the peak pressure p_o linearly diminishing in the time t_d. There are two possible solutions for Equation (59)--one for the case in which the maximum value of x is reached when $0 \le t_{max} \le t_d$, the other in which $t_{max} \ge t_d$. The solution for the first case is

$$\left(\frac{T'}{t_d}\right)^2 = \frac{4}{3}\frac{S_I}{R_I}\left(1 - \frac{R_I}{S_I}\right)^3 \qquad 1 \le \frac{S_I}{R_I} \le 2 \tag{65}$$

The solution for the second case is

$$\left(\frac{T'}{t_d}\right)^2 = \frac{1}{4}\left(\frac{S_I}{R_I}\right)^2 - \frac{1}{3}\left(\frac{S_I}{R_I}\right) \qquad 2 \le \frac{S_I}{R_I} \tag{66}$$

where:

$$T' = \sqrt{\frac{2Q_I x_{max}}{R_I}} \tag{67}$$

A plot of the relationship between $\left(\frac{T'}{t_d}\right)^2$ and $\frac{S_I}{R_I}$ is given in Figure 20.

The two basic uses of Equations (65) and (66) would be 1) in determining the peak time-dependent overpressure which would produce the same pressure on a structure as would a given static-overpressure, and 2) in designing an underground structure to withstand the effects of a given time-dependent overpressure. In the first case, the problem is very simple when it is realized that S_I/R_I is the ratio of the peak overpressure to the static pressure which would produce the same pressure on the structure. First of all, the static pressure would be computed from Equation (63), based on the given value of p_H. Then the quantity $(T'/t_d)^2$ is evaluated from Equation (67)

$$\left(\frac{T'}{t_d}\right)^2 = \frac{2Q_I x}{R_I t_d^2}$$

Next, either Equation (65) or (66), or Figure 20, can be used to determine the ratio S_I/R_I. Having this ratio, the peak pressure p_o can easily be determined.

For the design problem, the peak pressure would be known, as well as the overall dimensions. The basic problem would involve the determination of the equivalent static overpressure, p_u, and then the design of the structure. First of all, R_I could be computed, based on the assumed ratio of S_I/R_I. Then p_u could be determined from Equation (63). Based on p_u, the roof would be designed and the x corresponding to p_u could be computed. Then, from the computed R_I and x, $(T'/t_d)^2$ would be computed from Equation (67) and the theoretical value of S_I/R_I could be found from Equation (65) or (66), or from Figure 20. The sequence would be repeated until the S_I/R_I based on the initially assumed R_I is equal to the finally computed value of S_I/R_I.

For comparison, the above expressions have been used with a given structure, a 10 ft x 10 ft x 10 ft cube having different values of x. Different soils and different depths of burial were considered. For ease of computation the dimensions of the excavation were taken, ideally, the same as those of the structure. The results of the comparison are shown in Table I, and vividly illustrate the following:

1. For different soils, the difference in p_o p_u was small, no matter what the values of x and t_d.
2. The maximum and minimum values of p_o/p_u, for all cases considered, had a small range: 1.32 to 1.07. That is, for these cases the equivalent static overpressure which would be used for design would range from 76 to 93% of the peak overpressure.
3. A change in x from 1 ft to 0.1 ft resulted in a nearly constant equivalent static overpressure which was very nearly 90% of the peak value for all cases.
4. For a value of x = 0.1 ft, an increase in t_d from 1.47 sec to 2.94 sec resulted in a slight change in the nearly constant equivalent static overpressure. The percentage changed from 90 to 92% of the peak overpressure.
5. The ratio p_o/p_u changes very little with pronounced changes in H/L_d.

It appears that the major factors which influence the magnitude of the equivalent static overpressure are the vertical deflection of the structure, x, and the duration time, t_d. The equivalent static overpressure decreases as x increases and as t_d decreases.

The main point to be emphasized is that the ratio of the equivalent static-overpressure falls in the range of about 76% to 93% of the peak overpressure. Therefore, the assume-check approach should be relatively easy for a given design. Once the pressure-time relationship is established, the equivalent static pressure can be accurately estimated, the pressure on the top of the structure can be determined by the theory developed for static loads, the roof can be designed, x can be computed, and finally the ratio p_d/p_u can be checked.

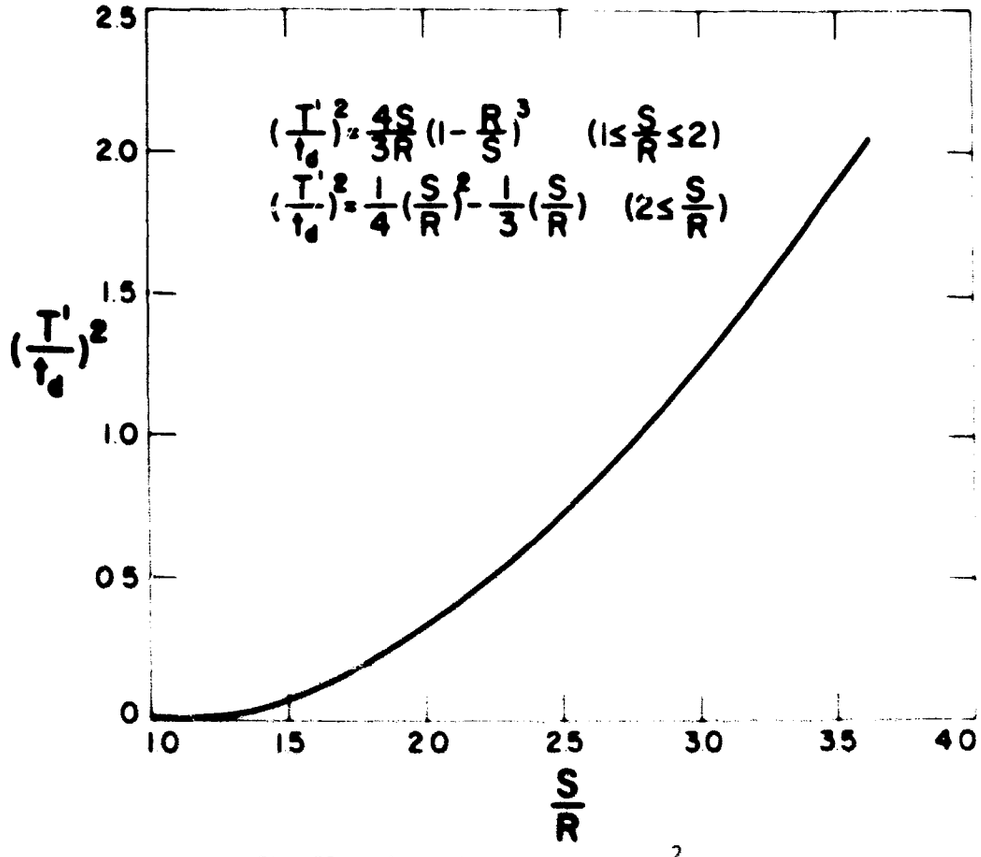
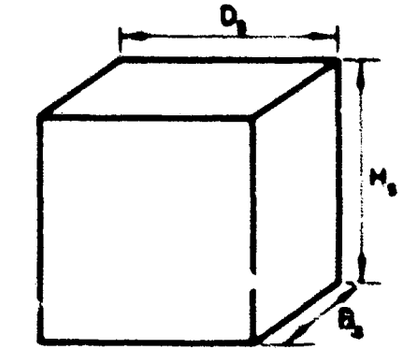


Fig. 20 Relationship between $(T' t_d)^2$ and S R

TABLE I
COMPARISON OF RESULTS



$B_s = D_s = H_s = 10$ ft
$L_s = 5$ ft

		Values of $\frac{p_d}{p_u}$						
		Clay: $\phi = 10°$ $c = 400$ psf $K = 0.7$			Sand $\phi = 35°$ $c = 0$ psf $K = 0.6$			
H	$\frac{H}{L_s}$	X = 1 t_d = 1.47	X = 0.1 t_d = 1.47	X = 0.1 t_d = 2.94	X = 1 t_d = 1.47	X = 0.1 t_d = 1.47	X = 0.1 t_d = 2.94	ft sec
15	3	1.26	1.11	1.07	1.28	1.12	1.07	
30	6	1.29	1.12	1.08	1.29	1.12	1.08	
50	10	1.31	1.13	1.08	1.30	1.13	1.08	
100	20	1.32	1.13	1.08	1.30	1.13	1.08	

It will subsequently be shown that equations of precisely the same from as Equation (61) can be developed for the projection cases. The solution and use of these equations would be exactly the same as that of Equation (61).

DYNAMIC LOADS ON PROJECTING STRUCTURES

Positive Projecting Structures

For the projection conditions (r_{sd} positive), consider the free-body diagram of Figure 9.

$$P + W - (P + dP) + 2V_B + 2V_D = \frac{W}{g}\frac{d^2x}{dt^2} \tag{68}$$

where, as before, x represents the vertical movement of the element. Then

$$dp = dh\left(w + \frac{2c}{wL_s} + \frac{2K\tan\phi}{L_s}p - \frac{w}{g}\frac{d^2x}{dt^2}\right) \tag{69}$$

For the complete projection condition, the boundary conditions would be $p = p_t$ when $h = 0$ and $p = p_H$ when $h = H$

The solution of the equation would be

$$\frac{p_H}{wL_s} = \left(\frac{2c}{wL_s} + 1\right)\frac{e^{(+2K\tan\phi\frac{H}{L_s})} - 1}{2K\tan\phi} + \left\{e^{(+2K\tan\phi\frac{H}{L_s})}\right\}\left(\frac{p_t}{wL_s}\right) - \frac{1}{g}\frac{d^2x}{dt^2}\left(\frac{e^{(+2K\tan\phi\frac{H}{L_s})} - 1}{2K\tan\phi}\right) \tag{70}$$

Solving Equation (70) for $\frac{p_t}{wL_s}$

$$\frac{p_t}{wL_s} = \frac{p_H}{wL_s}\left\{e^{(-2K\tan\phi\frac{H}{L_s})}\right\} + \left(\frac{2c}{wL_s} + 1\right)\frac{e^{(-2K\tan\phi\frac{H}{L_s})} - 1}{2K\tan\phi} - \frac{1}{g}\frac{d^2x}{dt^2}\left(\frac{e^{(-2K\tan\phi\frac{H}{L_s})} - 1}{2K\tan\phi}\right) \tag{71}$$

which can be written in the simplified form shown here

$$Q_2\frac{d^2x}{dt^2} + R_2 = S_2\left(1 - \frac{t}{t_d}\right) \tag{72}$$

where $S_2 = \frac{p_o}{wL_s}$ (73)

and

$$R_2 = \frac{p_H}{wL_s}\left\{e^{(-2K\tan\phi\frac{H}{L_s})}\right\} + \left(\frac{2c}{wL_s} + 1\right)\frac{e^{(-2K\tan\phi\frac{H}{L_s})} - 1}{2K\tan\phi} \tag{74}$$

and

$$Q_2 = -\frac{1}{g}\frac{e^{(-2K\tan\phi\frac{H}{L_s})} - 1}{2K\tan\phi} \tag{75}$$

The use of Equation (72) parallels that of Equation (61). Equation (74) is the same as Equation (36) where $R_2 = p_o/wL_s$.

For the incomplete projection condition, the boundary conditions would be

$$p = w(H - H_e) + p_t - \frac{w(H-H_e)}{g}\frac{d^2x}{dt^2} \text{ when } h = 0 \quad \text{and} \quad p = p_H \text{ when } h = H_e$$

The solution of Equation (69) would be

$$\frac{p_H}{wL_s} = \left(\frac{2c}{wL_s} + 1\right)\frac{e^{(+2K\tan\phi\frac{H_e}{L_s})} - 1}{2K\tan\phi} + \left\{e^{(+2K\tan\phi\frac{H_e}{L_s})}\right\}\left(\frac{H}{L_s} - \frac{H_e}{L_s} + \frac{p_t}{wL_s}\right)$$
$$- \frac{1}{g}\frac{d^2x}{dt^2}\left(\frac{e^{(+2K\tan\phi\frac{H_e}{L_s})} - 1}{2K\tan\phi}\right) + \left(\frac{H}{L_s} - \frac{H_e}{L_s}\right)\left\{e^{(+2K\tan\phi\frac{H_e}{L_s})}\right\} \tag{76}$$

Solving for $\frac{P_t}{wL_s}$

$$\frac{P_t}{wL_s} = \frac{P_H}{wL_s}\left(e^{(-2K\tan\phi\ \frac{H_e}{L_s})}\right) + \left(\frac{2c}{wL_s} + 1\right)\frac{e^{(-2K\tan\phi\ \frac{H_e}{L_s})} - 1}{2K\tan\phi} - \left(\frac{H}{L_s} - \frac{H_e}{L_s}\right)$$

$$-\frac{1}{g}\frac{d^2x}{dt^2}\left[\frac{e^{(-2K\tan\phi\ \frac{H_e}{L_s})} - 1}{2K\tan\phi} - \left(\frac{H}{L_s} - \frac{H_e}{L_s}\right)\right] \tag{77}$$

which can be written in the simplified form

$$Q_3\frac{d^2x}{dt^2} + R_3 = S_3\left(1 - \frac{t}{t_d}\right) \tag{78}$$

where $S_3 = \frac{P_o}{wL_s}$ (79)

$$R_3 = \frac{P_H}{wL_s}\left(e^{(-2K\tan\phi\ \frac{H_e}{L_s})}\right) + \left(\frac{2c}{wL_s} + 1\right)\frac{e^{(-2K\tan\phi\ \frac{H_e}{L_s})} - 1}{2K\tan\phi} - \left(\frac{H}{L_s} - \frac{H_e}{L_s}\right) \tag{80}$$

and

$$Q_3 = -\frac{1}{g}\left[\frac{e^{(-2K\tan\phi\ \frac{H}{L_s})} - 1}{2K\tan\phi} - \left(\frac{H}{L} - \frac{H_e}{L}\right)\right] \tag{81}$$

Equation (80) is the same as (37) where $R_3 = \frac{P_u}{wL_s}$.

For the ditch condition (r_{sd} negative), consider the free-body diagram of Figure 3.

$$P + W - (P + dP) - 2V_B - 2V_D = \frac{W}{g}\frac{d^2x}{dt^2} \tag{82}$$

Then

$$dp = dh\left(w - \frac{2c}{wL_s} - \frac{2K\tan\phi}{L_s}p - \frac{w}{g}\frac{d^2x}{dt^2}\right) \tag{83}$$

For the complete ditch condition, the boundary conditions would be $p = p_t$ when $h = 0$ and $p = p_H$ when $h = H$ and the solution of the equation would be

$$\frac{P_H}{wL_s} = \left(\frac{2c}{wL_s} - 1\right)\frac{e^{(-2K\tan\phi\ \frac{H}{L_s})} - 1}{2K\tan\phi} + \left(e^{(-2K\tan\phi\ \frac{H}{L_s})}\right)\left[\left(\frac{P_t}{wL_s}\right) + \frac{1}{g}\frac{d^2x}{dt^2}\left(\frac{e^{(-2K\tan\phi\ \frac{H_e}{L_s})} - 1}{2K\tan\phi}\right)\right] \tag{84}$$

If Equation (32) is solved for $\frac{g_t}{wL_s}$

$$\frac{P_t}{wL_s} = \frac{P_H}{wL_s}\left(e^{(+2K\tan\phi\ \frac{H}{L_s})}\right) + \left(\frac{2c}{wL_s} - 1\right)\frac{e^{(+2K\tan\phi\ \frac{H}{L_s})} - 1}{2K\tan\phi} + \frac{1}{g}\frac{d^2x}{dt^2}\left(\frac{e^{(+2K\tan\phi\ \frac{H}{L_s})} - 1}{2K\tan\phi}\right) \tag{85}$$

Equation (85) may be written in the form

$$Q_4\frac{d^2x}{dt^2} + R_4 = S_4\left(1 - \frac{t}{t_d}\right) \tag{86}$$

where $S_4 = \frac{P_o}{wL_s}$ (87)

$$R_4 = \frac{P_H}{wL_s}\left\{ e^{(+2K\tan\phi\ \frac{H}{L_s})} \right\} + \left(\frac{2c}{wL_s} - 1\right)\frac{e^{(+2K\tan\phi\ \frac{H}{L_s})} - 1}{2K\tan\phi} \tag{88}$$

and

$$Q_4 = \frac{1}{g}\left(\frac{e^{(+2K\tan\phi\ \frac{H}{L_s})} - 1}{2K\tan\phi}\right) \tag{89}$$

Equation (88) is the same as Equation (36) where $R_4 = \frac{P_u}{wL_s}$

In the case of the incomplete ditch condition, the boundary conditions would be

$$p = w(H-H_e) + p_t - \frac{w(H-H_e)}{g}\frac{d^2x}{dt^2} \text{ when } h = 0 \quad \text{and} \quad p = p_H \text{ when } h = H_e$$

and the solution of Equation (83) would be

$$\frac{P_H}{wL_s} = \left(\frac{2c}{wL_s} - 1\right)\frac{e^{(-2K\tan\phi\ \frac{H_e}{L_s})} - 1}{2K\tan\phi} + \left(e^{(-2K\tan\phi\ \frac{H_e}{L_s})}\right)\left(\frac{H}{L_s} - \frac{H_e}{L_s} + \frac{p_t}{wL_s}\right)$$
$$+ \frac{1}{g}\frac{d^2x}{dt^2}\left[\frac{e^{(-2K\tan\phi\ \frac{H_e}{L_s})} - 1}{2K\tan\phi} - \left(\frac{H}{L_s} - \frac{H_e}{L_s}\right)\left(e^{(-2K\tan\phi\ \frac{H_e}{L_s})}\right)\right] \tag{90}$$

Solving Equation (88) for $\frac{P_t}{wL_s}$

$$\frac{P_t}{wL_s} = \frac{P_H}{wL_s}\left(e^{(+2K\tan\phi\ \frac{H_e}{L_s})}\right) + \left(\frac{2c}{wL_s} - 1\right)\frac{e^{(+2K\tan\phi\ \frac{H_e}{L_s})} - 1}{2K\tan\phi} - \left(\frac{H}{L_s} - \frac{H_e}{L_s}\right)$$
$$+ \frac{1}{g}\frac{d^2x}{dt^2}\left[\frac{e^{(+2K\tan\phi\ \frac{H_e}{L_s})} - 1}{2K\tan\phi} + \left(\frac{H}{L_s} - \frac{H_e}{L_s}\right)\right] \tag{91}$$

Equation (91) is of the form

$$Q_5\frac{d^2x}{dt^2} + R_5 = S_5\left(1 - \frac{t}{t_d}\right) \tag{92}$$

where $S_5 = \frac{P_o}{wL_s}$ (93)

$$R_5 = \frac{P_H}{wL_s}\left(e^{(+2K\tan\phi\ \frac{H_e}{L_s})}\right) + \left(\frac{2c}{wL_s} - 1\right)\frac{e^{(+2K\tan\phi\ \frac{H_e}{L_s})} - 1}{2K\tan\phi} - \left(\frac{H}{L_s} - \frac{H_e}{L_s}\right) \tag{94}$$

and

$$Q_5 = \frac{1}{g}\left[\frac{e^{(+2K\tan\phi\ \frac{H_e}{L_s})} - 1}{2K\tan\phi} + \left(\frac{H}{L_s} - \frac{H_e}{L_s}\right)\right] \tag{95}$$

Equation (94) is the same as Equation (37) where $R_5 = \frac{P_u}{wL_s}$

Negative Projecting Structures

The development of similar expressions for negative projecting structures would be exactly the same as the previous developments. The resulting expressions are listed as follows

For the complete ditch condition

$$Q_6 \frac{d^2x}{dt^2} + R_6 = S_6 \left(1 - \frac{t}{t_d}\right) \tag{96}$$

where $S_6 = \frac{p_c}{wL_d}$ (97)

$$R_6 = \frac{p_H}{wL_d} \left(\frac{e^{\left(+2K\tan\phi \frac{H}{L_d}\right)} - 1}{2K\tan\phi}\right) + \left(\frac{2c}{wL_d} - 1\right) \frac{e^{\left(+2K\tan\phi \frac{H}{L_d}\right)} - 1}{2K\tan\phi} \tag{98}$$

and

$$Q_6 = \frac{1}{g} \left(\frac{e^{\left(+2K\tan\phi \frac{H}{L_d}\right)} - 1}{2K\tan\phi}\right) \tag{99}$$

Equation (98) is the same as Equation (41) where $R_6 = \frac{p_u}{wL_d}$.

For the incomplete ditch condition:

$$Q_7 \frac{d^2x}{dt^2} + R_7 = S_7 \left(1 - \frac{t}{t_d}\right) \tag{100}$$

where $S_7 = \frac{p_c}{wL_d}$ (101)

$$R_7 = \frac{p_H}{wL_d} \left(e^{\left(+2K\tan\phi \frac{H_e}{L}\right)}\right) + \left(\frac{2c}{wL_d} - 1\right) \frac{e^{\left(+2K\tan\phi \frac{H_e}{L_d}\right)} - 1}{2K\tan\phi} - \left(\frac{H}{L_d} - \frac{H_e}{L_d}\right) \tag{102}$$

and

$$Q_7 = \frac{1}{g} \left[\frac{e^{\left(+2K\tan\phi \frac{H_e}{L}\right)} - 1}{2K\tan\phi} + \left(\frac{H}{L_d} - \frac{H_e}{L_d}\right)\right] \tag{103}$$

Equation (102) is the same as Equation (42) where $R_7 = \frac{p_u}{wL_d}$.

CONCLUDING REMARKS

This paper is a part of a report prepared for the Defense Atomic Support Agency, DASA-1406. The analysis presented is based on a rational approach for predicting the behavior of underground structures subjected to time-dependent overpressures, and for determining the pressures transmitted to the structures. A close relationship is shown between the analyses of pressures produced by static overpressures and those produced by a particular type of time-dependent overpressure, thus emphasizing the importance of a thorough understanding of static load behavior. However, it must be pointed out that the procedure is based on a number of assumptions, some involving the overall behavior characteristics of the entire system and others related to the quantitative effects of factors which influence the behavior. Therefore, there is an obvious need for physical research to evaluate the method. Initial work should be directed toward determining the validity of the concept, particularly with respect to the neglecting of the stress wave effect. If the initial work serves to justify the assumed modes of behavior, the next step should be the determination of quantitative effects for simple systems. In particular, the effects of construction methods, relative settlement, structural deformation, and soil properties should be studied. After the general behavior of simple systems has been established, other variables should be introduced, variables such as the effects of ground water and the height of the water table, and the effect of layered soils. In conclusion, it is apparent that much physical research is needed to establish the behavior pattern and to form the basis for a design procedure.

ACKNOWLEDGEMENT

The author wishes to express his gratitude to several individuals whose help, suggestions, and encouragement were instrumental in making the study possible: Commander J. D. Andrews, Commander John J. Healy, and Major Merrill E. Barnes, all of the Defense Atomic Support Agency, and Dr. D. R. Boylan and Professor M. G. Spangler of the Iowa Engineering Experiment Station at Iowa State University.

REFERENCES

1. Marston, A., "The Theory of External Loads on Closed Conduits in the Light of Latest Experiments," Bulletin No. 96, Iowa Engineering Experiment Station, Ames, Iowa, 1930.
2. Marston, A., and A. O. Anderson, "The Theory of Loads on Pipes in Ditches and Tests of Cement and Clay Drain Tile and Sewer Pipe," Bulletin No. 31, Iowa Engineering Experiment Station, Ames, Iowa, 1913.
3. Selig, E. T., K. E. McKee, and E. Vey, "Underground Structures Subject to Air Overpressure," Transactions, American Society of Civil Engineers, 126: Part I: 1627-1649, 1961.
4. Spangler, M. G., "Field Measurements of the Settlement Ratios of Various Highway Culverts," Bulletin No. 170, Iowa Engineering Experiment Station, Ames, Iowa, 1950.
5. Spangler, M. G., "Underground Conduits - An Appraisal of Modern Research," Transactions, American Society of Civil Engineers, 113: 316-374, 1948.

LIST OF SYMBOLS

A = area of adjacent effective soil
B = horizontal dimension, with subscripts: d - ditch-type excavation, s - structure
c = soil cohesion
D = horizontal dimension, with subscripts: d - ditch-type excavation, s - structure
E = modulus of compressibility of soil
F = total frictional force (see Figure 9)
H = height of fill material above top of structure
H' = height of fill material above natural ground surface for negative projecting structure
H_e = height of plane of equal settlement above top of structure
H'_e = height of plane of equal settlement above natural ground surface for negative projecting structure
H_s = height of structure
h = vertical coordinate
K = lateral pressure coefficient
L = length parameter defined by $L = BD/B + D$ with subscripts: d - ditch-type excavation, s - structure
N = normal force
p = vertical pressure in soil prism at level h
p' = vertical pressure in adjacent effective soil at level h
p_H = vertical pressure in soil prism at top of structure
p_o = initial (and peak) time-dependent overpressure
p_s = vertical pressure on top of structure
p_t = time-dependent overpressure at time t
p_u = uniform static air overpressure
P = total vertical pressure in soil prism at level h
P' = total vertical pressure in adjacent effective soil at level h
Q = dimensionless ratio
r_p = ratio of height of positive projecting structure to L_s
r'_p = ratio of height of negative projecting structure to L_s
r_{sd} = settlement ratio
R = dimensionless ratio equal to p_u/wL
S = dimensionless ratio equal to p_o/wL
d_s = deflection of top of structure with respect to the base
s_d = compression of soil prism between top of structure and natural ground surface for negative projecting structure
s_f = settlement of foundation of structure
s_g = settlement of natural ground surface
s_m = deformation of fill material adjacent to positive projecting structure, between natural ground surface and top of structure

t = time

t_o = duration of actual overpressure

t_d = duration of equivalent overpressure

T' = quantity defined as $T' = \sqrt{2Qx_{max}/R}$

V = shearing force

W = weight of soil mass

w = unit weight of fill material

x = displacement of failure mass

β = ratio

λ = compression of soil prism between the top of the structure and the plane of equal settlement (positive projecting structure); and compression of soil prism between the natural ground surface and the plane of equal settlement (negative projecting structure)

λ' = compression of the adjacent effective soil between the top of the structure and the plane of equal settlement (positive projecting structure); and compression of the adjacent effective soil between the natural ground surface and the plane of equal settlement (negative projecting structure)

ϕ = angle of internal friction tor the soil

SESSION FIVE–WEDNESDAY AM

SIMILITUDE AND MODEL STUDIES

SESSION CHAIRMAN: JAY R. ALLGOOD

TABLE OF CONTENTS

page

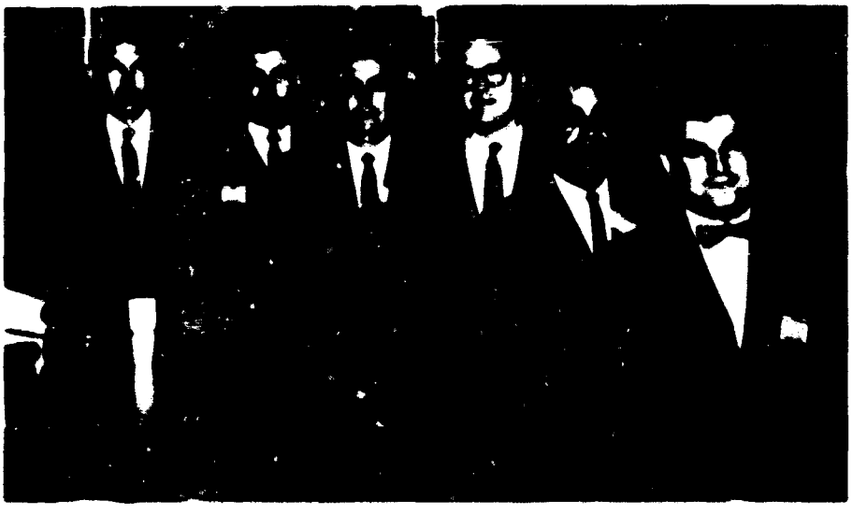
SIMILARITY REQUIREMENTS FOR UNDERGROUND STRUCTURES, Donald F. Young and Glenn Murphy 285

THE APPLICATION OF SIMILITUDE TO PROTECTIVE CONSTRUCTION RESEARCH, Robert K. Tener 296

A SIMPLIFIED SOIL STRUCTURE INTERACTION MODEL TO INVESTIGATE THE RESPONSE OF BURIED SILOS AND CYLINDERS, C. J. Costantino, R. R. Robinson, and M. A. Salmon 303

THE EFFECT OF PORE AIR PRESSURE ON SOIL-STRUCTURE INTERACTION, Delon Hampton 315

PHOTOELASTIC STUDY OF WAVE PROPAGATION AROUND EMBEDDED STRUCTURAL ELEMENTS, W. F. Riley 332



Participants in Session Five were, left to right, Jay R. Allgood (Session Chairman); R. K. Tener; D. F. Young; E. T. Selig (presented paper by C. J. Costantino, R. R. Robinson, and M. S. Salmon); D. Hampton; and R. L. Marino (presented paper by W. F. Riley).

SIMILARITY REQUIREMENTS FOR UNDERGROUND STRUCTURES

by
Donald F. Young* and Glenn Murphy**

ABSTRACT

Similarity requirements for predicting the dynamic response of underground structures are derived and checked experimentally. Dimensional analysis is used to develop the required relationships between the model and prototype systems. Tests which were performed in a two-foot diameter vertical shock tube using small hollow aluminum tubes, embedded in dry sand, as the model structures are described. The tubes were instrumented with SR-4 strain gauges, and strain-time curves were obtained for several depths of burial. Peak reflected surface pressures varied from 60 psi to 460 psi. The test results support the proposed scaling relationships.

INTRODUCTION

To establish reliable similitude requirements for a given model-prototype system, all variables that influence the phenomena must be defined. As experience is gained with a particular type of system, or general class of problems, the significant variables become well defined, and conventional model theory can be applied with confidence. Scale models are now widely used in many areas of engineering. These models find their widest application in the solution of complex problems that cannot readily be solved analytically. The use of models for the prediction of the behavior of underground structures is attractive because these problems are complex and difficult to solve. It is not feasible to test, at least extensively, the full-scale prototypes due to their large size and other factors. The use of models is desirable, therefore, since models are relatively easy to fabricate and test.

The significant soil properties that govern load transmission and soil-structure interaction are not known. Therefore, similitude requirements for predicting the response of dynamically loaded buried structures cannot be developed immediately. The purpose of the investigation reported herein was to develop similitude requirements for buried structures and to check experimentally the proposed requirements.

The experiments described in this paper were performed with a vertical shock tube having a two-foot outside diameter. This device is a cylindrical steel tube, open at both ends and mounted vertically. An explosive charge of Primacord can be suspended and exploded at the upper end creating a shock wave that propagates down the length of the tube. The lower end of the tube is located directly over a soil bin of the same diameter as the shock tube, and the resultant shock wave impinges directly on the soil surface. One of the significant characteristics of this type of loader is that the resulting variation in pressure acting on the soil surface is similar to that due to an unconfined high explosive or nuclear blast; i.e., the initial rise in pressure is practically instantaneous with a resulting exponential decay in pressure and a relatively long duration. The duration is defined as the time required for the surface pressure to decay to the ambient pressure. It is also possible with this device to obtain relatively high surface peak pressures. The highest peak pressure obtained in the series of tests to be described was 464 psi with a duration of approximately 15 milliseconds.

TEST FACILITY AND MODELS

A schematic of the basic elements of the shock tube, soil bin, and models is shown in Figure 1. The soil cover for all tests was dry Ottawa 20-30 sand. The model structures used in all tests were hollow aluminum circular cylinders of three different sizes. The average outside diameters of the test cylinders were 4.02, 2.00 and 1.00 in. with wall thicknesses of 0.253, 0.126 and 0.063 in., respectively. The cylinder length to diameter ratio was 2. The 4-in. and 1-in. cylinders were cut from 6061-T6 alloy aluminum tubing. The specific composition of the aluminum used for the 2-in. cylinder is unknown. Since the structures were not to be tested beyond the elastic range, slight differences in densities and moduli of elasticity were not considered to be significant.

The dependent variable measured in the tests was circumferential strain. Each cylinder was instrumented with two circumferential SR-4 strain gauges and one longitudinal gauge (Figure 1 c). Type A-6 gauges were used on the 4-in. cylinder, A-5 gauges on the 2-in. cylinder, and A-7 gauges on the 1-in. cylinder. The gauges were scaled in the same ratio as the cylinders. The longitudinal gauge was used to check for stresses induced due to beam action of the cylinders.

* Professor, Department of Engineering Mechanics, Iowa State University, Ames, Iowa.
** Professor and Head, Department of Nuclear Engineering, Iowa State University, Ames, Iowa

To monitor the reflected pressure acting on the soil surface, two Granath ST-2 pressure gauges were placed flush with the soil surface, 3 to 4 inches from the inside edge of the bin (Figure 1 b). Two additional pressure gauges of the same type were located in the wall of the shock tube approximately 5 inches and 25 inches above the soil surface. These gauges were used to monitor the overpressure in the tube.

The sand was loaded into the soil bin by the "raining technique" (1). With this technique, the sand is loaded into a container and allowed to "rain" or fall through a funnel and a 2-in. diameter flexible radiator hose that is capped by a No. 4 or No. 5 wire mesh. If the sand is allowed to fall freely for a distance of about 12 inches below the end of the hose, a dense and uniform state of compaction is achieved. The average specific weight of the sand was 110.5 pcf. The sand was filled to the top of the bin for each shot and covered with a thin plastic membrane. Two small holes were cut in the membrane so that the sensing surfaces of the pressure gauges were exposed to the shock wave.

The output signals from both pressure gauges and strain gauges were recorded on magnetic tape. The stored data were then played back into a sixteen-channel Miller light recording oscillograph for immediate inspection to see if all channels were operational. A final record for each gauge was obtained by playing the signal from the magnetic tape into an oscilloscope and photographing the trace with a Polaroid oscilloscope camera. The final data for the shock tube tests were obtained from these Polaroid pictures. A more detailed description of the shock tube and instrumentation can be found in a report by Holt and Crist (2).

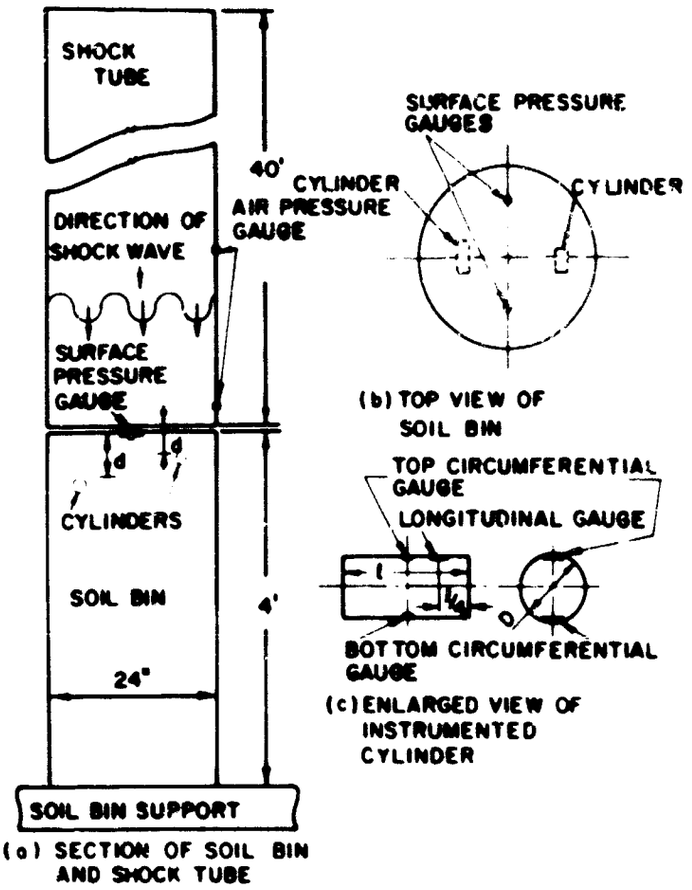


Fig. 1 Schematic of Two-Foot Shock Tube

The intensity of the shock wave was controlled by the length and the strength of the Primacord high explosive suspended from the upper end of the tube. However, it was not possible to control the duration of the pressure pulse. The minimum and maximum peak reflected surface pressures used in the tests were approximately 60 psi and 464 psi, respectively, and most of the tests were run at an average pressure of 100 psi. As noted previously, the duration time was approximately 15 milliseconds.

The 2-in. and 1-in. diameter cylinders were tested in the bin at the same time. The cylinders were placed so that their center lines were between 5-1/2, 2 and 6 in. from the edge of the soil bin (Figure 1 b). The tests with the 4-in. cylinder were run with only a single cylinder in the bin.

DIMENSIONAL ANALYSIS AND MODEL DESIGN

To establish model design conditions for this problem, the method of dimensional analysis was used. With this technique the variables that control the dependent variable, circumferential strain in this case, must be known or assumed. The chief difficulty in dealing with problems involving soils is the determination of significant soil properties. For this study it was assumed that in addition to the density of the soil all other pertinent soil parameters (η_i) have the basic dimensions of FL^{-2} (F = force; L = length) or are dimensionless. This assumption implies that a soil property related to strain rate effects need not be considered, at least not for relatively noncohesive soils. Also gravitational effects were neglected. This implies that the dead load strains (resulting from the weight of the structure and soil cover) will be small compared with the live load strains. A more detailed discussion of the soil properties and the significance of these assumptions can be found in a report by Murphy and Young (3).

The list of variables considered in the analysis of this problem is given in Table 1.

TABLE 1 - LIST OF VARIABLES

Variable	Definition	Basic Dimensions
ϵ	strain	(-)
D	outside cylinder diameter	L
b	cylinder wall thickness	L
ℓ	length of cylinder	L
d	depth of burial of structure (measured from top of cylinder to soil surface)	L
p	pressure acting on soil surface	FL^{-2}
t	time	T
ρ	initial density of soil	FT^2L^{-4}
ρ_p	density of cylinder material	FT^2L^{-4}
E	modulus of elasticity of cylinder material	FL^{-2}
G	modulus of rigidity of cylinder material	FL^{-2}
η_1	property of soil	FL^{-2}
η_i	other properties of soil	FL^{-2}

Application of the Buckingham Pi Theorem indicates that 10 dimensionless parameters (Pi terms) are required to describe the problem. One possible set is:

$$\Pi_1 = \epsilon \qquad \Pi_2 = \frac{\ell}{D} \qquad \Pi_3 = \frac{b}{d} \qquad \Pi_4 = \frac{d}{D} \qquad \Pi_5 = \frac{G}{E} \qquad \Pi_6 = \frac{\rho_p}{\rho}$$

$$\Pi_7 = \frac{\eta_1}{E} \qquad \Pi_8 = \frac{\eta_i}{E} \qquad \Pi_9 = \frac{p}{E} \qquad \Pi_{10} = \frac{\rho_p D^2}{pt^2}$$

The functional relationship between the Pi terms can be written as:

$$\Pi_1 = f(\Pi_2, \Pi_3, \ldots, \Pi_{10}) \tag{1}$$

Since the same relationship will hold for both model and prototype systems as long as the phenomena is the same in both systems it follows that:

$$\Pi_1 = \Pi_{1m} \tag{2}$$

if

$$\begin{aligned} \Pi_{2m} &= \Pi_2 \\ \Pi_{3m} &= \Pi_3 \\ &\vdots \\ \Pi_{10m} &= \Pi_{10} \end{aligned} \tag{3}$$

where the subscript m refers to the model system. Equation (2) is the prediction equation and Equations (3) represent the model design conditions.

Design conditions based on Π_2, Π_3, and Π_4 require that the models be geometrically similar to the prototype and buried at scaled depths. The geometry of the soil bin was not considered in the analysis. However, it is known that "wall effects" can cause a significant attenuation in pressure with depth and represents a potential source of distortion. If the same combination of materials is used in the model-prototype systems, design conditions based on Π_5, Π_6, Π_7 and Π_8 will be satisfied. The design condition based on Π_9 is:

$$\frac{p}{E} = \frac{p_m}{E_m} \tag{4}$$

which indicates the $p = p_m$ since $E = E_m$, i.e., the magnitude of the pressure acting on the surface of the soil must be the same in all tests. Since the surface pressure is time dependent, this condition indicates that at homologous times the pressures must correspond This means that if the time scale is other than unity then the variation in surface pressure must be of the same form for a model-prototype system but scaled in time. The design condition based on Π_{10} establishes the time scale for the problem as:

$$\frac{\rho_p D^2}{pt^2} = \frac{\rho_{pm} D_m^2}{\rho_m t_m^2}$$

$$\frac{t}{t_m} = \frac{D}{D_m} = n \qquad (5)$$

As discussed in the previous section, it was not possible to vary the duration of the pressure pulse in the shock tube, and it was apparent that the loading design condition would be distorted. However, tests performed under the specified design conditions with the recognition of the distortion in the loading term would probably give an indication of the importance of the various assumptions involved and would be of value in planning future tests.

TEST PROCEDURE

The initial step in the preparation of a given test was to remove the sand in the soil bin to a depth of 12 inches below the depth at which the bottom of the cylinder was to be placed. The sand was then allowed to "rain" into the soil bin until the proper depth was reached. The cylinder was placed on the sand surface, and the sand was allowed to "rain" around the cylinder while it was held in position. After the cylinder was covered, the raining technique was continued until the soil bin was filled to the required depth. It is estimated that the depth of burial of the cylinder was accurate to + 1/16 in. The weight of the sand added to the soil bin was recorded, and this weight combined with the volume of the soil bin provided the average sand density. As the sand was rained into the bin, some of the sand grains fell outside the bin. The sand that escaped the soil bin was collected and weighed so that a proper weight could be used. This was a source of error and could account for some of the variations in the sand density measurements. After the sand was filled to the top of the soil bin, the surface was leveled with a straight edge drawn across the top of the bin. The soil pressure gauges were then placed so that their sensing surfaces were flush with the upper surface of the sand. As much care as possible was taken in the placement of these gauges so that both gauges would be positioned in the same manner. However, some of the differences between the readings of the two surface pressure gauges were due to the inability to position each gauge in exactly the same manner. After the gauges were in position, a thin plastic membrane was stretched over the entire surface of the soil bin, and two small holes were cut in the membrane so that the sensing surfaces of the pressure gauges were exposed to the shock wave. This membrane was held tightly in position with a plastic tape. After these steps were completed, the soil bin was positioned directly under the shock tube.

The pressure gauges were calibrated by applying a static pressure at least once a day, and the strain gauges were calibrated immediately before firing. When the gauges were calibrated, the Primacord charge was loaded into the upper end of the shock tube, and the shot was fired.

In most shots, the covering membrane was torn off by the shock wave. However, little sand was thrown out of the soil bin, and the surface was only slightly disturbed. After each firing, the sand was carefully removed so that the position of the cylinder after the shot could be determined. It was noted in all cases that the cylinder moved upward and that the final depth of burial after a shot was less than the initial depth of burial. Pressure-time traces and the strain-time traces were obtained from the Polaroid pictures taken with the oscilloscope-camera system. With the test procedure described in this section, two to three shots, depending upon the depth of burial, could be completed in a given day. All tests were run and data recorded by personnel at the Air Force Shock Tube Facility.

TEST RESULTS

For the tests run in the two-foot shock tube, all design conditions assumed to be significant were satisfied with the exception of the one related to the loading. As noted previously, it was not possible to change the shape of the surface pressure-time curve. However, the peak pressures were held as nearly constant as possible for all tests in which cylinders of different sizes were to be compared. The peak strain measured on both the top and bottom gauges indicated a tensile stress. The strains indicated by the longitudinal gauge were much smaller than those measured by the circumferential gauges, and in most of the tests the peak longitudinal strains were less than 20 percent of the peak circumferential strains. The longitudinal strain traces were much more erratic or random in appearance and it appeared that the bending of cylinders, which gave rise to the longitudinal strain, was of minor importance compared with the circumferential strains. Future reference to strains will apply to circumferential strains.

SIMILITUDE AND MODEL STUDIES

An enlarged typical pressure-time trace is shown in Figure 2 and an enlarged strain-time trace in Figure 3. One of the disadvantages of recording the data on Polaroid film is that the traces are small and some accuracy is lost in reading values from the photographs. The data given in this report show the strain-time and pressure-time traces over a relatively long period of time. If a more detailed study of the response of the cylinders during the initial part of the loading is desired, the trace can be expanded by varying the sweep time on the oscilloscope, although this makes the transfer from the magnetic tape to the film more difficult. It is estimated that errors due to reading the data from the photographs used in the present study are approximately ± 3 percent for peak strains. However, rise times can be in error by approximately ± 50 percent, since they are of such short duration and are difficult to read accurately from the photographs.

An attempt was made in most of the tests to hold the peak reflected pressure at 100 psi. Variations in the recorded pressure from this value were most likely due to small differences in the explosive charges and to errors in the readings of the surface pressure gauges due to slightly different support conditions of the sand under the gauges. Figures 4 and 5 show the results of the peak strain tests for the three cylinders. For these tests, the depth to diameter ratio varied from 0.5 to 4.0. Two tests were made with a given cylinder at a specified depth of burial. The points plotted in Figures 4 and 5 represent the average value of the strain for these two runs. In addition, the average measured surface pressure, based on the average reading from the two surface gauges, fell between 79 psi and 121 psi. In most of the tests, an individual strain reading deviated from the average of a pair by less than ± 10 percent, with a maximum deviation of 32 percent from an average for one pair.

No significant difference in the peak strain predicted was noted from one cylinder to another. The variations appear to be random and fall within the range of experimental errors. There is more scatter in the data for the top gauge than for the bottom gauge, and the peak strains indicated by the bottom gauge are considerably higher than those of the top gauge. All data with the exception of the top gauge points for the 2-in. cylinder indicate a decrease in strain with depth with a possible leveling off at a depth to diameter ratio of approximately 2.

To determine the effect of peak surface pressure on peak strains, several tests were run at a depth to diameter ratio of 2.0 with the 1-in. and 2-in. cylinders. For these tests, the surface pressure was varied from approximately 50 to 500 psi (Figures 6, 7). The peak strain is plotted against peak surface pressure which is the average peak pressure measured by the two surface gauges. There appears to be a linear relationship between peak strain and pressure, and the curves that are drawn through the plotted points were obtained by at least squares fit with a zero ordinate For the bottom gauge

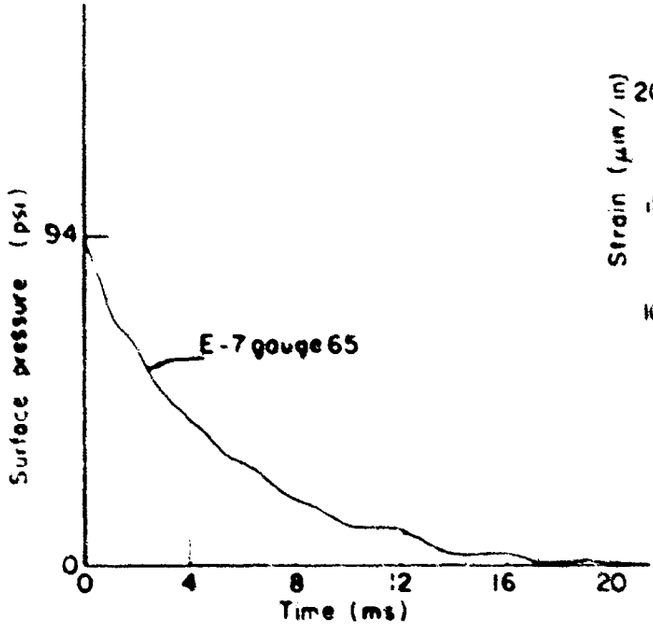


Fig. 2 Typical Surface Pressure-Time Trace

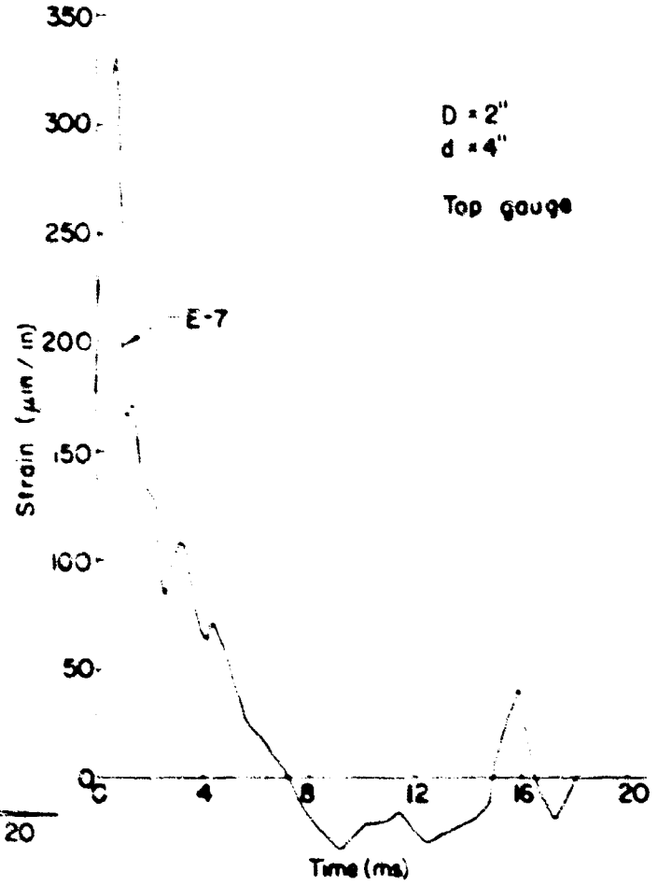


Fig. 3 Enlarged Circumferential Strain-Time Trace

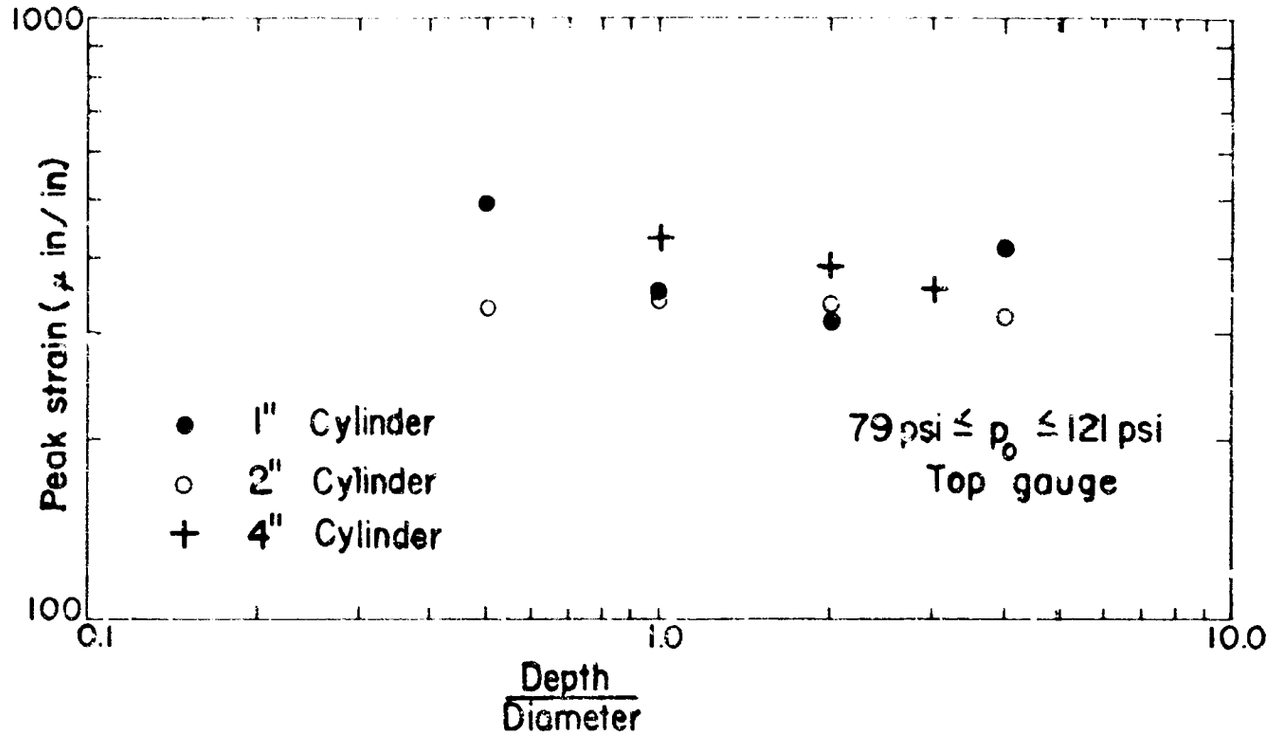


Fig. 4 Comparison of Top Gauge Peak Strain Data for Three Circular Cylinders

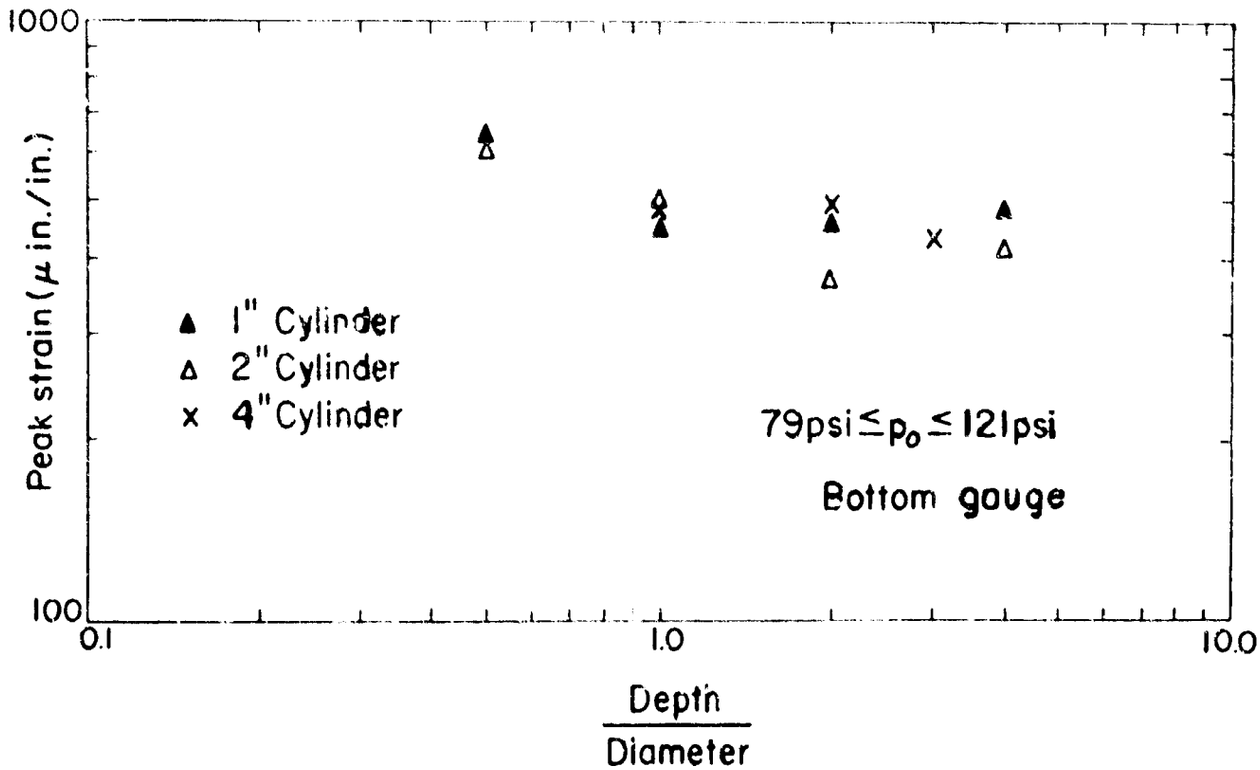


Fig. 5 Comparison of Bottom Gauge Peak Strain Data for Three Circular Cylinders

readings, there is no significant variation among the data from the three cylinders. This supports the proposed model design. The points for the 1-in. cylinder appear to be slightly higher in the top gauge data of Figure 6 than those for the 2-in. cylinder, and separate curves were drawn for these two cylinders.

If the assumption is made, which is supported by the data of Figures 6 and 7, that peak strain is directly proportional to surface pressure, then the strains which were plotted in Figures 4 and 5 can all be normalized to 100 psi. A comparison of the normalized data with the data plotted in Figure 4 and 5 shows no significant difference in results. This observation supports the conclusion that the scatter in the peak strain data of Figures 4 and 5 is due primarily to factors other than differences in surface pressures from run to run. The principal reason for this scatter is most likely the difficulty in compacting uniformly the sand in the immediate vicinity of the test cylinder.

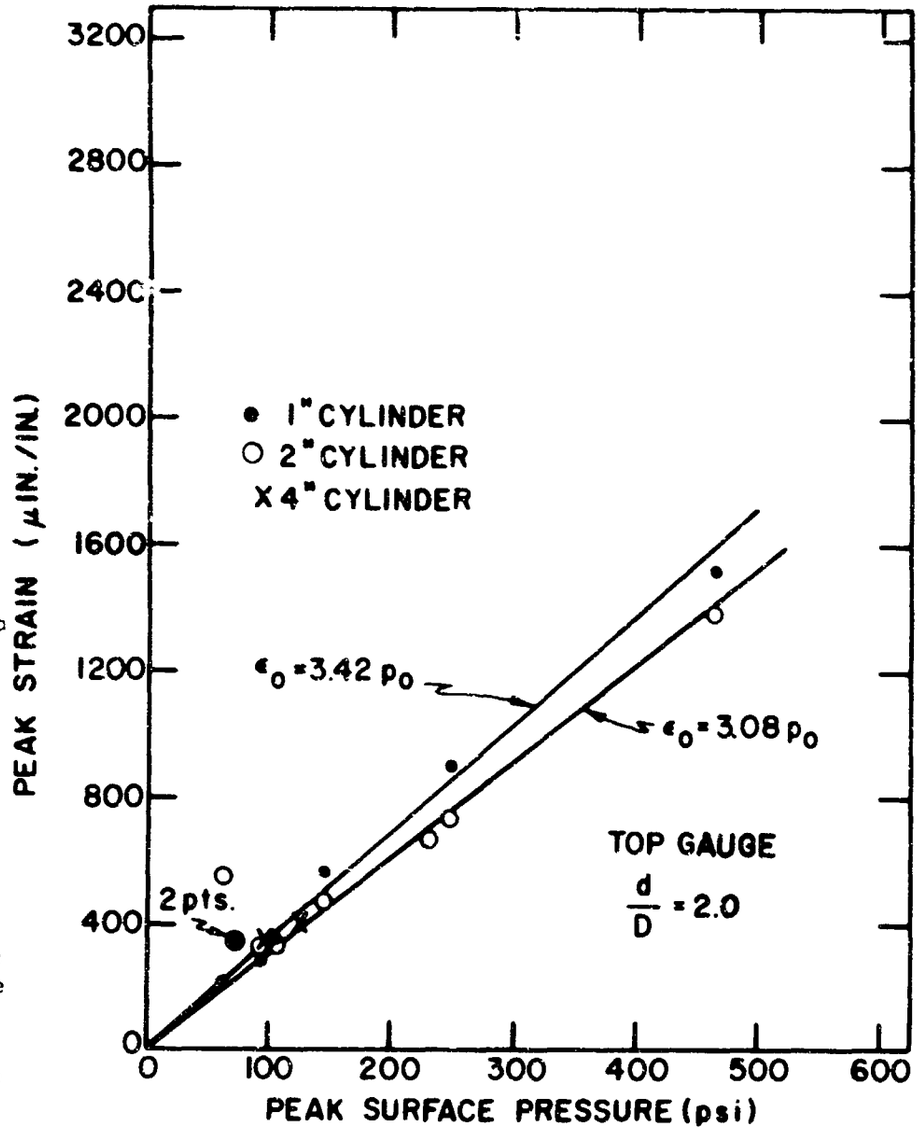


Fig. 6 Variation in Top Gauge Peak Strains with Surface Pressure

Although it is not expected that the validity of the proposed time scaling could be conclusively established, since the loading was not time scaled, it is of interest to compare the complete strain-time curves for the different sized cylinders. For this comparison, several tests in which the peak strains of the different cylinders correlated closely were considered. Figures 8 and 9 show strain-time curves for different cylinders for which all design conditions were satisfied with the exception of time scaling on loading. Although there are differences in the relative appearances of the various sets of curves shown in these two figures, for times greater than approximately the rise time (time to peak strain) the curves tend to coincide. This is especially evident in Figure 8. The rise times do not coincide but tend to deviate in a manner that could be accounted for with the proposed time scaling; i.e., the larger the model size the greater the rise time. However, as pointed out previously, the inaccuracies associated with reading the rise time from the Polaroid prints are of the same order as the value of the rise time. In most of the strain-time curves regardless of cylinder size, a pronounced hump appears in the trace at approximately 15 to 18 milliseconds after impact. The cause of this increase in strain is not known and does not appear to be directly associated with a boundary reflection, since the time interval to its occurence is too great. Another pronounced and unexplained peak occurs at 2 to 4 milliseconds after impact on most traces. In all tests, it was found that the cylinders moved upward, and the final depth of cover was less than the initial depth. The 4-in. cylinder moved up approximately 1 in., the 2-in. cylinder approximately 1.5 in., and in most of the tests with the 1-in. cylinder buried at depths of 2 in. or less the cylinder moved up to the soil surface. A complete tabulation of all data obtained in these tests can be found in a report by Murphy, Young and Martin (4).

DISCUSSION OF RESULTS

The results of the tests in the two-foot shock tube can be grouped into two categories, those which are of a more general and qualitative nature and those which apply specifically to the evaluation of the proposed similitude requirements.

The peak circumferential strain decreased with depth of burial down to a depth to diameter ratio of approximately 2 (Figures 4, 5). Beyond this depth to diameter ratio, the strains appear to approach a constant value. The reason for the near surface attenuation is not known. Near the surface of the bin it is expected that any energy dissipation caused by relative movement between sand grains, or between the sand and the boundaries, will be most pronounced. This may be the cause of the attenuation at the shallow depths of burial. The rise times did not show any significant change with depth. In most of the tests, the rise times increased with the size of the cylinder, which would be expected due to the time scale.

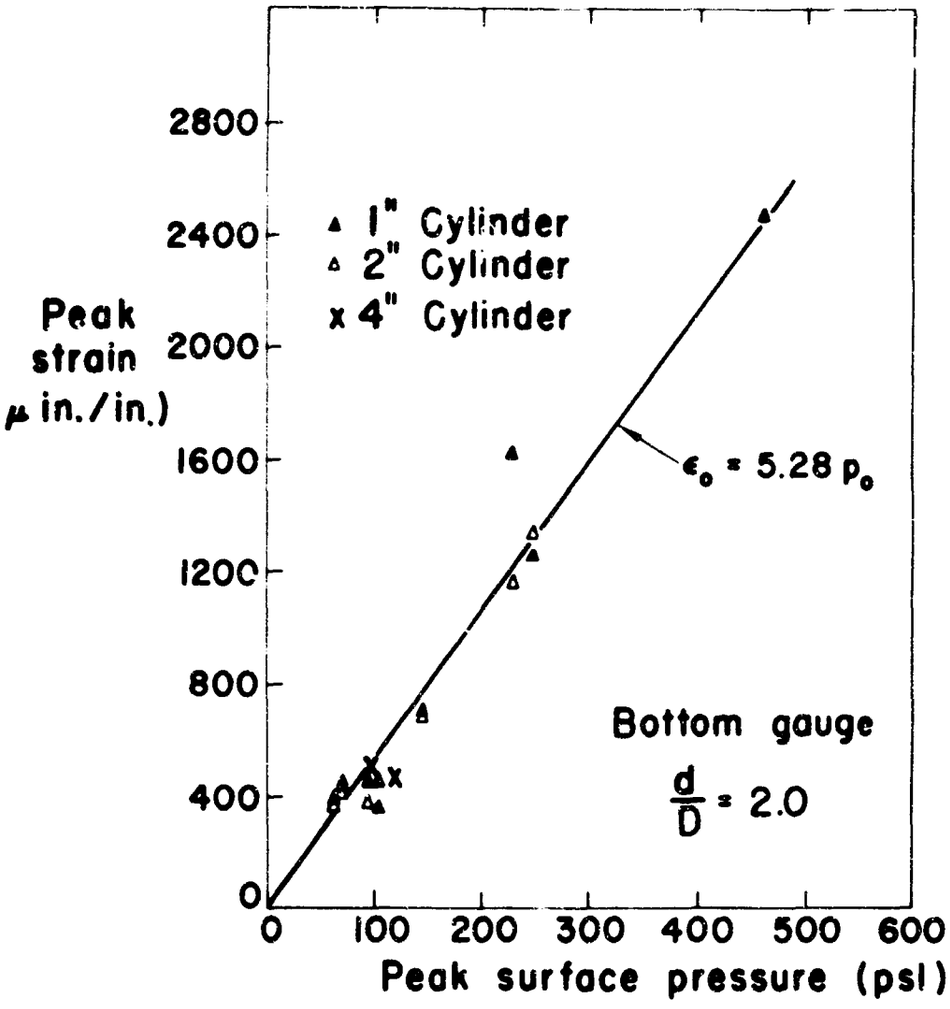


Fig. 7 Variation in Bottom Peak Strains with Surface Pressure

To evaluate the proposed similitude requirements, strains measured on three cylinders of different sizes were compared. A comparison of peak strains obtained from the three cylinders indicates that there is reasonable agreement. Tabulated values of peak strain for the tests in which all design conditions were satisfied except for time scaling the load are given in Table 2. If it is assumed that at a given depth to diameter ratio the strains from the three cylinders should be the same, then an estimate of the variation can be obtained by calculating the percentage deviation of any one strain from the average. In the strains measured by both the top and bottom gauges, the maximum deviation was less than 19.5 percent with an average deviation of 9.0 percent. Since the deviation from the average of two shots under similar conditions show approximately the same percentage variation, the differences between the peak strains can be attributed to experimental errors. More points will be required to define the peak strain curves more accurately.

Since the loading condition was distorted, the complete strain-time curves could not be expected to be compared directly. However, the results shown in Figures 8 and 9 support the proposed time scaling. During the initial impact of the pressure wave, the cylinder is expected to respond as if subjected to a step pressure pulse. The transit time, or time required for the pulse to traverse the cylinder, can be determined by dividing the diameter of the cylinder by the velocity of the wave front. For example, for the 4-in. cylinder, the transit time is approximately one-third of a millisecond based on an estimated wave speed of 1000 fps. During this short time required for the wave to pass across the cylinder, the intensity of the surface pressure pulse has decreased only slightly; therefore, the approximation of a step pressure pulse during this early period may be valid. After the cylinder is engulfed in the pressure wave, the strain will be controlled primarily by the decrease in the intensity of pressure, and during this phase the strains would be expected to follow the decaying pressure pulse. Thus, during the initial response to the approximate step pulse, the time scale must be used; since the surface load, now considered a step pulse, is properly scaled. However, as the pulse begins to decay significantly, the strain will follow this decay. If there is no time scaling of the surface pressure, there should not be time scaling on the response curve for times exceeding the rise time. Better agreement among the various curves is obtained

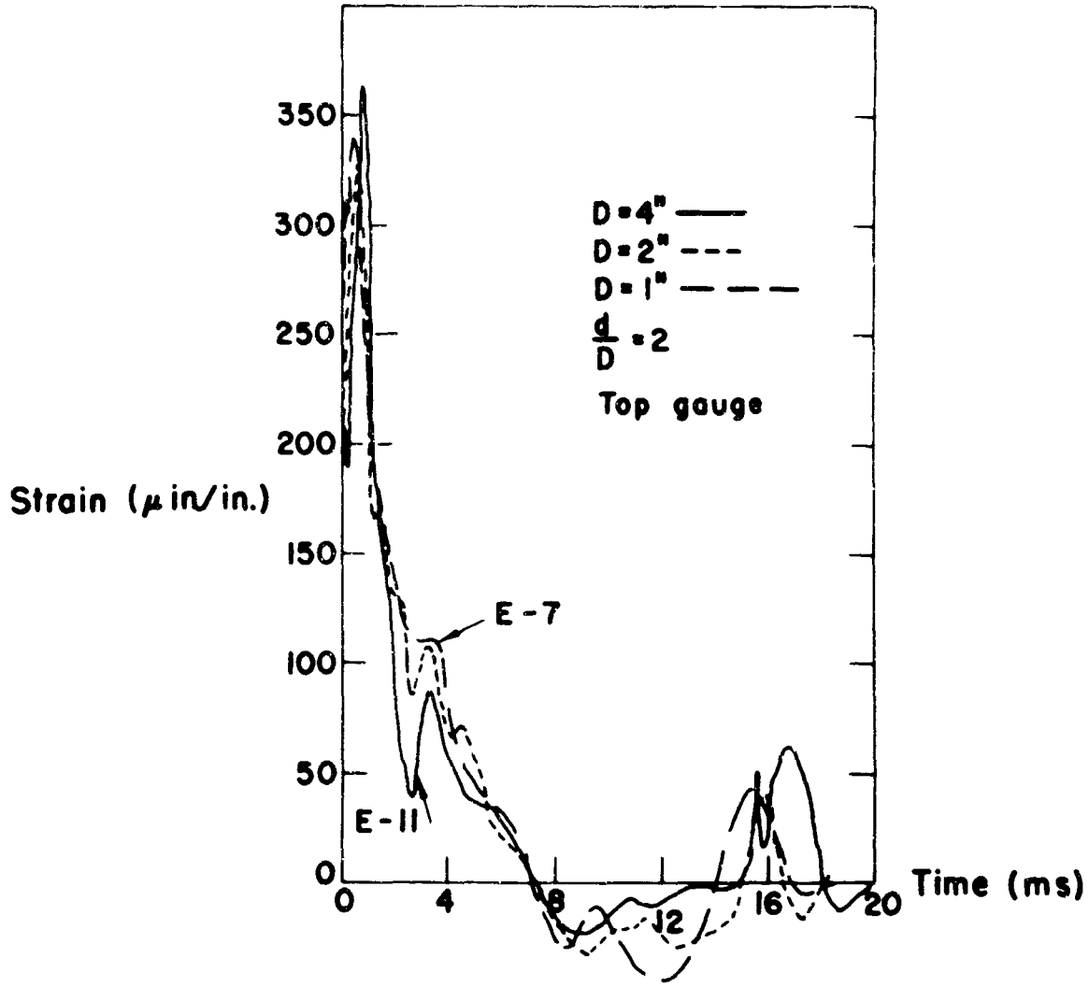


Fig. 8 Comparison of Strain-Time Curves for 1 in., 2 in., and 4 in. Diameter Cylinders

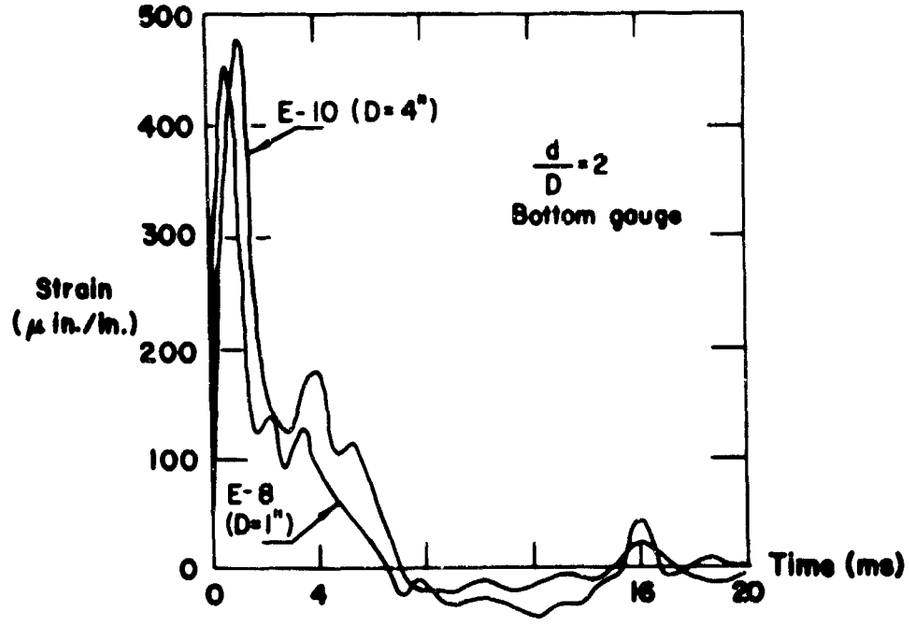


Fig. 9 Comparison of Strain-Time Curves for 1 in. and 4 in. Diameter Cylinders

after peak strain if no time scaling is used which tends to substantiate the preceding argument (Figure 8, 9). Also, it appears that for the times near to and less than the time of peak strain the use of a time scale would improve the correlation among the curves.

TABLE 2 - TABULATION OF PEAK STRAINS

Cylinder Diameter D (in.)	$\frac{d}{D}$	[a]Peak Strain ϵ_o (μin./in.)	Av. Peak Strain ϵ_a (μin./in.)	$\frac{\epsilon_o - \epsilon_a}{\epsilon_a} \times 100$ (%)
		Top Gauge		
1	0.5	485	406	+19.5
2	0.5	328		-19.5
1	1.0	347		- 6.5
2	1.0	340	371	- 8.4
4	1.0	424		+15.9
1	2.0	312		- 8.8
2	2.0	330	342	- 3.5
4	2.0	382		+11.7
1	4.0	410	363	+13.0
2	4.0	316		-13.0
		Bottom Gauge		
1	0.5	637	619	+ 2.9
2	0.5	602		- 2.9
1	1.0	445		- 6.9
2	1.0	500	478	+ 4.6
4	1.0	491		+ 2.7
1	2.0	454		+ 4.4
2	2.0	366	437	-17.3
4	2.0	490		+12.7
1	4.0	479	444	+ 7.9
2	4.0	412		- 7.2

[a]Average of two shots

SUMMARY AND CONCLUSIONS

In this paper, dimensional analysis has been used to derive a set of similarity requirements for predicting the behavior of underground structures by means of models. The analysis indicates that the behavior of a prototype structure can be predicted from measurements taken on a model structure if the following conditions are satisfied.

1. The model and prototype are geometrically similar.
2. The same combination of materials is used in both model and prototype. This condition refers to both the soil and structure.

3. The surface pressures are of the same magnitude and applied at homologous positions and times. Since the time scale is equal to the length scale the pressure variation on the model system must be time scaled.

Two major assumptions are required to arrive at these similarity requirements. These are:

1. The significant properties of the soil are adequately described by its density and one or more additional properties having the basic dimensions of FL^{-2}.

2. Gravitational effects are negligible.

Although the similarity requirements were derived from the particular system used in the test program the same general requirements as they pertain to geometry, material, and loading are applicable to other systems with different geometries and different loading environments.

Results of a series of experiments specifically designed to check the proposed similarity requirements support the analysis. Although the surface pressures used to load the structures were properly scaled with respect to magnitude, they were not scaled with respect to time. However, the peak strain data are in reasonable agreement with the predicted results. As discussed in the preceding section it is believed that the complete strain-time curves also support the proposed similarity requirements. A better understanding of the properties that govern the behavior of soils under dynamic loading conditions is necessary before models can be utilized to their fullest extent. The authors believe that the feasibility of using small scale models to predict the behavior of underground structures under intense surface loads is clearly demonstrated by the results of this study.

ACKNOWLEDGMENTS

This investigation was done under Project 432-S of the Iowa Engineering Experiment Station, Iowa State University, Model Studies of Underground Structures. The project was supported by funds from the United States Air Force through the Research and Technology Division, Air Force Weapons Laboratory.

All the shock tube tests described herein were performed by personnel at the Air Force Shock Tube Facility, Albuquerque, New Mexico, under the immediate supervision of Dr. Delon Hampton. The assistance of these personnel is gratefully acknowledged.

THE APPLICATION OF SIMILITUDE TO PROTECTIVE CONSTRUCTION RESEARCH

by
Robert K. Tener*

> I have often been impressed by the scanty attention paid even by original workers in physics to the great principle of similitude.
>
> - Lord Rayleigh, 1915

INTRODUCTION

Investigation into the design of underground protective structures has comprised a major effort in engineering research for more than ten years. During this period extensive knowledge has been gained, and the engineer is doubtless better equipped today than in 1954 to prepare with some measure of confidence a design for a practical underground structure capable of surviving the effects of a given nuclear weapon. However, it would be inaccurate to consider the state of the art of blast-resistant underground structural design to be highly refined. Rather, from the design engineer's viewpoint, two basic questions as yet require completely adequate answers: 1) for what values of input load, shock, and displacement should a specific buried structure be designed, and 2) by what means should a given design be analyzed to verify its adequacy.

The objective of protective construction research is to equip the engineer with answers to these questions. Technical requirements for investigations must be based on the goal of ultimately enabling the determination of input effects on buried structures and providing procedures for analyzing a proposed design. In order to analyze a structural design, the engineer must know how it will respond to the blast effects from a given design weapon. This means that he must be able to predict the response of the structure to the pertinent weapon effects.

The complexities of the phenomena involved in the dynamic response of an underground structure are familiar to all who have approached the problem. Research into the nature of these phenomena is being pursued by various theoretical and experimental approaches. This paper proposes that cognizance be made of a specific approach which offers rather unique advantages and potential promise in providing early answers to the problems of input effects and structural response. It is submitted that application of the theory of similitude to selected studies in protective construction research will potentially lead to information adequate to the designer's needs and at a considerable savings in research time and money.

APPLICIABILITY OF SIMILITUDE

Background

The theory of similitude encompasses those principles which govern similarity between physical systems. Similitude has its basis in dimensional analysis, and the central premise which provides for the application of dimensional analysis is the Buckingham Pi theorem (1), which may be stated as follows:

If a functional relationship exists between n variables having b basic dimensions,

$$F(x_1, x_2, x_3, \ldots x_n) = 0$$

this relationship may be expressed in terms of s independent, dimensionless products of these variables, called Pi terms:

$$F(\Pi_1, \Pi_2, \Pi_3, \ldots \Pi_s) = 0$$

where $s = n - b$.

The behavior of any physical system which is characterized completely by the variables x_i can then be represented by the function F, which may be expressed alternatively as:

*Corps of Engineers, U.S. Army Engineer Waterways Experiment Station, Vicksburg, Mississippi.

$$\Pi_1 = \phi(\Pi_2, \Pi_3, \ldots \Pi_s) \quad (1)$$

An identical relationship exists for any other system which is physically similar. One such system may be terms the model system, for which:

$$\Pi_{1m} = \phi(\Pi_{2m}, \Pi_{3m}, \ldots \Pi_{sm}) \quad (2)$$

in which the subscript m denotes the model system. If in equations 1 and 2 it is provided that $\Pi_{2m} = \Pi_2$, $\Pi_{3m} = \Pi_3, \ldots \Pi_{sm} = \Pi_s$, then, since the form of the function ϕ is identical in the two physically similar systems, it follows that $\Pi_1 = \Pi_{1m}$.

The procedure for applying the principle of similitude to the design of a model system involves four steps.

1. Determine all the variables which influence the behavior of the prototype system. This is the most important and in general the most difficult step and if of obvious necessity.
2. Form c suitable set of Pi terms involving the pertinent variables.
3. By equating the independent Pi terms $\Pi_2, \Pi_3, \ldots \Pi_s$ in the model and prototype systems, establish the conditions for the design and operation of the model.
4. Once the design conditions are satisfied, the prediction equation is established for the dependent Pi terms, $\Pi_1 = \Pi_{1m}$.

General Applications

There are two primary types of investigations in which the application of similitude principles can provide meaningful results. The first and most widely recognized usefulness is in establishing design and operating conditions for a model system of a specific prototype. Observations of the model behavior are used to predict the behavior of the prototype in the desired respect, without resorting to detailed study of the form of the functional relationships between the pertinent variables. Examples of this application are common in many fields of engineering, especially hydraulics, structures, and aerodynamics.

The second area in which similitude is of value is in basic phenomeno-logical investigations. If a selected set of variables is assumed to determine the behavior of a system, an equation such as equation 1 can be formulated. By designing and operating several experimental system of different sizes, a comparison of the behavior of the system will indicate whether or not the assumed similitude existed. In this matter the sufficiency of the assumed set of variables may be verified. These basic verification studies are generally intended to provide an understanding of the behavior of a system. Procedures are available (5) for utilizing the results of similitude studies to determine the manner in which certain of the Pi terms enter the functional relationship ϕ in equation 1. Examples of the use of similitude in basic phenomenological studies are available in the literature (21,31,32).

Two additional advantages of considering dimensional analysis in the conduct of experiments are noteworthy. In any variation of parameters study, the number of parameters which must be investigated is reduced by the number of basic dimensions involved if the pertinent variables are formed into Pi terms. Additionally, the collection of data can be systematized, the presentation of results simplified, and the usefulness of the results generalized by use of dimensionless groups of variables. Discussion of these points with reference to soil mechanics research was presented by Lundgren (29), and with reference to fluid mechanics by Van Driest (4).

The list of general references at the end of this paper constitutes a representative collection of books and papers treating similitude and dimensional analysis in their more general engineering applications.

Advantages of Similitude Approach

The objective of protective construction research is to equip the engineer with the knowledge required for the efficient design of protective structures. Research toward this objective, to a greater degree than ever before, is subjected to the constant dictates of expeditiousness and economy. The use of similitude as a research tool offers distinct advantages when considered in the light of the necessity for early usable results and an efficient research effort.

It appears that the pressing need for early reliable answers to the design engineer's questions is sometimes lost sight of in the research establishment, particularly where the time and effort required by basic research problems may lead to a lack of attention to the applied aspects. There should be an unqualified understanding that useful applied research results are in great immediate demand. If the protective structure design information presently at hand had been available ten years ago, it would not have been too soon. A valid requisite for an investigative approach then is the degree to which the approach can provide early adequate results.

In many protective construction research problems, the application of similitude offers a distinct advantage in this aspect. A properly conducted model study can usually lead to an adequate prediction of specific prototype behavior with less effort than is required to develop an adequate analytical prediction. The analytical approach requires that functional relationships based on theory and experimentation be established, which will enable calculation of the required input and response parameters. Development of these functional relationships is presently dependent upon the results of extensive

basic theoretical and experimental research yet to be conducted in many areas. These areas include static and dynamic soil mechanics, dynamic properties of structural materials, shock phenomena in real earth media, dynamic soil-structure interaction, and others. The required solutions in these areas are not being quickly reached. Thus, the value of analytical approaches to protective construction design problems may improve progressively, but at a rate dependent upon costly, time-consuming basic research.

However, if just enough is known about a particular problem to enable identification and evaluation of the specific variables which influence the phenomena, whether it be free-field effects, structural response, or otherwise, the problem can be approached by similitude. Detailed knowledge of the functional relationships involved is not essential to a model study. If a reliable model procedure can be established, as in general it can, a similitude study will provide the information needed to predict input effects for use in design and structural response for use in analysis, and in sufficient time to be of value to the designer.

Figure 1 illustrates schematically how a similitude study might be applied in the analysis of a specific proposed protective structure design. The details of the similitude study and model tests are based on the specific proposed prototype design, and the validity of the prototype design is evaluated on the basis of predictions from the model tests. This concept is analogous to applications of similitude in aircraft design, flood control studies, design of complex structures such as dams and multistory buildings, and numerous other fields.

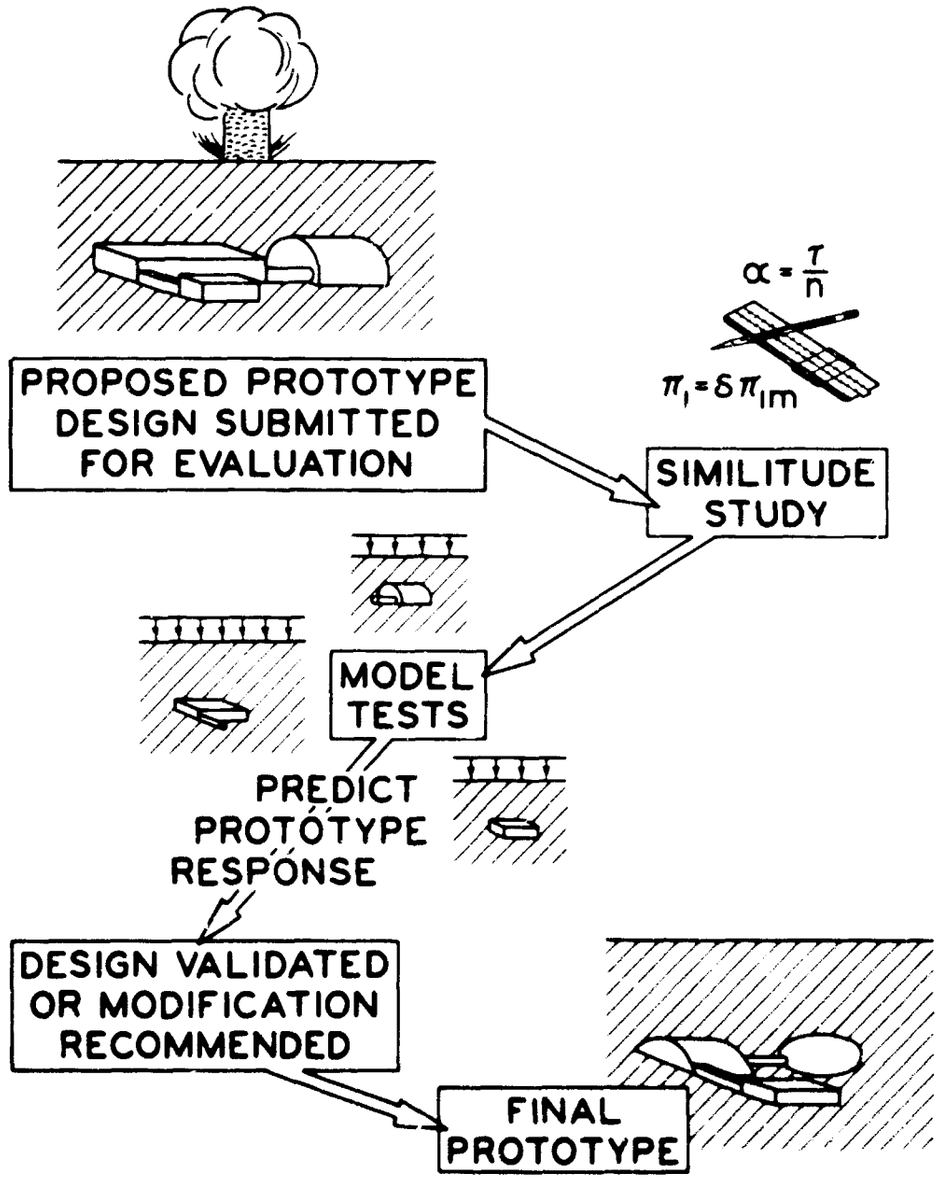


Fig. 1 Concept of Objective for Similitude Studies in Protective Construction

The advantages of the similitude approach to protective construction research may be summarized briefly. In the problems involved, which are characterized by highly complex functional relationships not yet fully understood, an urgent need exists for design information. Similitude studies are not dependent upon analytical development of these relationships, and bear promise toward providing adequate information to the designer at a savings in time and cost. Thus, potential economy of research effort is to be gained when a similitude treatment of a problem is applicable.

Additional Considerations

There must be communication and interplay among the various protective construction research efforts. Theoretical and experimental advances can and must be mutually complementary. A certain level of understanding of the nature of the phenomena involved is essential to the value and efficiency of a similitude study. Bridgeman advised, "The man applying dimensional analysis is not to ask himself 'On what quantities does the result depend?' for this question gets nowhere, and is not pertinent. Instead we are to imagine ourselves as writing out the equations of motion at least in sufficient detail to be able to enumerate the elements which enter them. It is not necessary to actually write down the equations, still less

to solve them" (3).

As more accurate knowledge of dynamic soil-structure interaction is developed, the ability to conduct more efficient and reliable model studies will improve. Likewise, similitude studies provide experimental evidence and promote theoretical understanding of the behavior of physical systems.

One point of a conservative nature should be injected. An inherent danger exists whenever predictions are made based on scale model tests. It is recognized that it is possible to operate with a model design that is quite incorrect, yet blithely predict results which are considerably in error. Thorough verification tests are important, as is correlation of observed prototype data whenever availabe.

STATE OF THE ART

Work to Date

Historically, the use of the models and scaling in protective construction dates back more than twenty years. Extensive work was done during World War II using similitude principles to study penetration and explosion of bombs and projectiles. Results of this work are reflected in an early Corps of Engineers protective design manual (11).

The argument in favor of similitude studies in nuclear weapons effects research is by no means new or profound. McCutchen before 1949 proposed such studies, and he wrote an article with the purpose "to explain enough of the basic principles of similitude between a model and an original to enable one to apply these principles to the serious problem of the effect of an atomic bomb upon an underground rock fortress" (27). This was 16 years ago, yet even today new research is being initiated applying the similitude approach to deep underground effects.

An early study of model blast effects in rock was done by Jones and McCutchen in 1948 (26). Their paper formulated a model theory based on similitude, and they investigated the use of a model medium whose strength was reduced from that of the prototype sandstone by a factor of 20, the length scale for the study. The limited results of their test demonstrated the feasibility of such investigations.

In 1946, a few months after the first atomic bomb was detonated, the Office of the Chief of Engineers initiated planning of the Underground Explosion Tests. These tests were carried out between 1948 and 1952 with the specific intent of establishing the similitude relations between TNT explosions and nuclear blast effects. Dimensional analysis was utilized to develop scaling relations for particle displacements, velocities, and accelerations and stresses in soil and rock. The effects of charge weight and depth of burial, range, and soil type were studied, and it was concluded that the test results tended to support the model law for the existing soil conditions (28).

Extensive use of similitude was made in studies of blast effects on surface structures during the earl. 1950's. The scope of current protective construction research transcends the range of weapons effects with which surface structure. are associated, so that extensive research in this area is essentially a thing of the past. An excellent treatment of the similitude considerations in modeling surface structure blast effects was presented by Jones in Canada (12).

Considerable interest in model studies of dynamically loaded buried structures within the past three years is evident. Ahlers at Armour Research Foundation (now Illinois Institute of Technology Research Institute) reported on a theoretical modeling analysis in 1961 and concluded that an exact model could not practically be built (13). An analytical similitude study on dynamically loaded buried cylinders was reported by Murphy and Young at Iowa State in 1962, and their report included a brief test program which clearly demonstrated the feasibility of such studies (14).

Another paper study on scaling relations for dynamically loaded buried structures was published in 1962 by Arentz (15). This study analyzed in some detail a number of the scaling problems inherent in the buried structure problem and discussed at length certain phenomenological relations. However, no use of similitude based on the Buckingham Pi theorem was made. The resultant approach does not readily lend itself to the practical design and performance of model tests, and is an example of the fact that overattentive consideration of basic problems can sometimes mask a practical approach to an investigation.

A model analysis of a buried arch was reported by the U. S. Naval Civil Engineering Laboratory in 1963 (19). Comparison was made between four deflections observed in a full-scale field test structure and scaled-up deflections from one laboratory test on a small arch. Although the compared values were of the same order of magnitude, a number of highly questionable assumptions were required, and no firm conclusions regarding the validity of the modeling procedure were offered.

The most significant similitude study to date on buried structure response was conducted at the Air Force Weapons Laboratory and reported by Murphy, Young and Martin (21). An extensive test program was conducted on aluminum cylinders with diameters of 1, 2, 4, and 8 inches and depths of burial in dry sand of up to ten diameters. The test results clearly demonstrated, within the range of parameters investigated, the feasibility of predicting the behavior of buried structures by the use of models. Three areas for further investigation were proposed: 1) increased length scales, on the order of 10 or greater, 2) strain-rate effects on cohesive soil behavior, and 3) a more specific means of determining pertinent soil properties. It is felt that the approach to protective construction research demonstrated in this study bears great promise.

SOIL-STRUCTURE INTERACTION

Model buried structures have been tested in full-scale field tests (20, et.al.). A recent report on a dynamic model study of one of the buildings in the NORAD underground installation is a good example of the practical usefulness of model studies (22). Valuable information and lists of references concerning general considerations of dynamic structural modeling are available (13, 16, 17, 18).

An excellent presentation of the applicability of similitude to several dynamic problems was given by Abramson and Nevill (23). Model studies are described for such problems as response of structures to vibratory and impulsive loads, cumulative penetration of foundations due to repeated dynamic loads, soil-structure interaction, and mobility of off-the-road vehicles. The special advantages and scaling considerations in similitude studies in these areas are clearly and thoroughly described in this paper. An especially good evaluation of the problems of modeling in soil dynamics is presented.

An interesting application of similitude to a problem somewhat related to soil-structure interaction was reported at Sandia Corporation in March 1964 (33). In that study dimensional analysis was applied in considering the impact and penetration of a high-speed projectile into earth media, including water and various soils.

Current Status

To date, the general goals of similitude studies in protective construction research have been to formulate and verify a model theory for structures buried in soil subjected to dynamic air-overpressure and to provide scaling relations for free-field weapons effects. The theoretical similitude relations are well established for the design of model structures and loading conditions. The primary area in which further information is needed to support structural response modeling and free-field effects scaling concerns the properties of the soil or rock medium which must be considered.

The feasibility of establishing similitude within laboratory-sized soil-structure systems for a dense dry sand soil medium has been demonstrated (21). The dynamic response of surface footings on a highly plastic compacted clay has been successfully scaled (32). Other than these studies there is no published experimental evidence of successful scaling of dynamic soil-structure interaction between similar systems of different sizes. Two of the primary recognized difficulties are first, identifying and evaluating the properties of the soil medium which influence the behavior under study, and second, providing the proper scaling of these properties between prototype and model.

The necessity for defining analytically the physical properties of the medium follows the advice attributed to Lord Kelvin (9): "When you can measure what you are speaking about, and express it in numbers, you know something about it; but when you cannot express it in numbers, your knowledge is of a meagre and unsatisfactory kind."

Progress is being made in this area. Soil mechanics research is constantly developing new means of quantitatively identifying the dynamic stress-strain relations for various soils and states of confinement. Dynamic triaxial and dynamic one-dimensional compression testing devices now being developed will provide future information which will enable a better understanding of the significance of these stress-strain curves in soil-structure interaction.

The specific properties of a medium which influence the attenuation of peak pressure as a shock wave propagates through it must be quantitatively identified. Strain-stress effects on soil strength must be thoroughly evaluated. Dynamic similitude studies may encounter less difficulty regarding this latter effect than has been anticipated, however. As long as loading times are of a magnitude considered dynamic, it is possible that little variation in soil strength with strain rate will be observed for real soils, either granular or cohesive.** This means that even if loading time is scaled between two dynamically loaded soils, strain-rate effect on soil strength may be negligible.

Similitude studies in rock and rocklike media have been conducted. This is an area where very great benefit could be derived from model studies. In these materials, too, a more thorough knowledge of medium properties is required. Martin and Murphy concluded, "Prediction of fracture caused by impacts and explosions requires more research into the strain-time conditions that cause fracture in various brittle materials" (31). Present research is taking a hard look at properties and equations of state for brittle earth materials, and results of this research are essential to knowledgeable model studies of rock phenomena.

The current status of similitude studies in dynamic soil-structure interaction includes limited theoretical consideration and a complete lack of valid experimental information regarding scaling of inelastic behavior and ultimate failure of a buried structure. Tangible results to date are limited to elastic structural behavior. Since economical protective construction will make use of plastic response and ultimate strength behavior, this is obviously an area which must receive attention.

An area of current consideration is that of time scaling. Dynamic similitude, when the model and prototype materials are the same, requires that time should scale as the length scale. At present there are no practical dynamic loading facilities available for buried structure tests in which time parameters can be widely varied and closely controlled. For the present, distortion of the design conditions on model time must be handled analytically until capabilities exist for study this effect experimentally.

To date, there has been but limited experimental correlation between the behavior of a full-scale prototype buried structure observed in a field test with the behavior predicted by a laboratory-scale model test. To successfully establish this correlation for realistic earth materials should be an early major research goal.

**A. J. Hendron, Vicksburg, Mississippi, Private Communication, 1964.

FUTURE REQUIREMENTS AND PROSPECTS

From the state of the art presentation and from a consideration of the designer's needs, a number of areas may be identified in which future similitude studies are required in order that any prototype underground installation in general might be modeled. These are presented in outline form.

1. In laboratory verification studies, establish capabilities for
   a. predicting inelastic structural response and ultimate strength.
   b. conducting studies for different prototype soils with properties varying over the range of all practical media.
   c. predicting response of various prototype structural materials and geometries.
   d. operating with length scales in excess of 10.
2. Establish correlation between laboratory and full-scale conditions by
   a. predicting behavior of prototypes already observed in field tests.
   b. conducting coordinated laboratory and field tests on practical structures.
3. In addition, for deep installations in rock
   a. formulate model theory and conduct pilot tests.
   b. develop new laboratory testing concepts.
   c. establish capability for operating with length scales on the order of 100 or greater.

As new nuclear weapons technology and capabilities are developed, the protective design concepts for defense must adapt. Protective construction research requirements should be based not upon the attack capabilities of today, but on the weapons effects against the future design will be pitted. The hardened installations to be constructed ten years hence should be based on rational, efficient design procedures already developed by then. The precept "plan ahead" could hardly be more applicable.

It must be decided in the research establishment, based upon the best available evidence, whether specific current investigations are likely to bear fruit in time to be of use. If not, an approach toward protective design problems must be found which will enable adequate solutions before the design concept being studied becomes obsolete. In view of the prospective weapon yields and attack concepts of the future, an acceptable level of hardening for prime targets will obviously necessitate very deep underground installations in rock. Design of such structures could be greatly facilitated by the results of well-founded similitude studies. It is hoped and expected that the manifold problems coupled with such investigations can be overcome, and that these studies will be successfully carried out. The future rate of progress in this field must be greatly accelerated over that of the 16 years since Colonel McCutchen proposed such research.

SUMMARY

It is not proposed that similitude studies are the panacea for every protective construction research problem. It is proposed that considerable advantage is to be gained by adopting the model approach whenever feasible, especially in view of the particular complexities inherent in the problems of behavior of protective structures.

The most reliable design is that based on credible experimental evidence. The application of similitude to protective construction research offers a potential means of providing this evidence at a considerable saving of research time and effort. This prospective saving is an essential consideration due to the particular demands for urgency and economy inherent to the field.

REFERENCES

General References

1. Buckingham, E., "On Physical Similar Systems," The Physical Review, 4, 345-376, October 1914.
2. Rayleigh, Lord, "The Principle of Similitude," Nature, 95, 66-68, March 1915.
3. Bridgeman, P. W., Dimensional Analysis, Yale University Press (rev. ed.), New Haven, 1931.
4. Van Driest, E. R., "On Dimensional Analysis and the Presentation of Data in Fluid-Flow Problems," J. Appl. Mech., 13, No. 1, A34-A40, March 1946.
5. Murphy, G., Similitude in Engineering, The Ronald Press, New York, 1950.
6. Langhaar, H. L., Dimensional Analysis and Theory of Models, John Wiley and Sons, New York, 1951.
7. Huntley, H. E., Dimensional Analysis, Rinehart and Company, New York, 1951.
8. Pankhurst, D., "Dimensional Analysis in 10 Steps," Product Engineering, 31, No. 5, 54-57, February 1960.
9. "Your Turn," Product Engineering, 33, Nos. 16-21, August-October 1962.
10. Jasiewicz, J., "Applications of Dimensional Analysis Methods to Civil Engineering Problems," Civil Engineering and Public Works Review (England), 33, Nos. 9-12, September-December 1963.

Protective Structures

11. U. S. Army, Office of the Chief of Engineers, "Fundamentals of Protective Design," EM 1110-345-405, Washington, Author, 1946.
12. Jones, G. H. S., "The Use of Models in the Study of Blast Effects of Simulated Nuclear Weapons," Suffield Experimental Station Technical Paper No. 132, Ralston, Alberta, April 1958.
13. Ahlers, E. B., "Experimental Methods of Determining the Behavior of Underground Structures Under Dynamic Loads," Armour Research Foundation, Chicago, November 1961.
14. Murphy, G. and D. F. Young, "A Study of the Use of Models to Simulate Dynamically Loaded Underground Structures," AFSWC TDR-62-2, Air Force Special Weapons Center, Kirtland Air Force Base, New Mexico, January 1962.
15. Arentz, A. A. Jr., "Study of the Use of Models to Simulate Dynamically Loaded Underground Structures," AFSWC TDR-62-3, Air Force Special Weapons Center, Kirtland Air Force Base, New Mexico, February 1962.
16. Antebi, J., H. D. Smith, S. D. Sharma and H. G. Harris, "Evaluation of Techniques for Constructing Model Structural Elements," DASA Report 1287, Massachusetts Institute of Technology, Cambridge, Mass., May 1962.
17. Harris, H. G., D. J. Pahl and S. D. Sharma, "Dynamic Studies of Structures by Means of Models," DASA Report 1320, Massachusetts Institute of Technology, Cambridge, Mass., September 1962.
18. Smith, H. D., R. W. Clark and R. P. Mayor, "Evaluation of Techniques for the Investigation of Structural Response to Blast Loads," DASA Report 1373, Massachusetts Institute of Technology, Cambridge, Mass., February, 1963.
19. Allgood, J. R., C. R. White, R. F. Swalley and H. L. Gill, "Blast Loading of Small Buried Arches," U. S. Naval Civil Engineering Laboratory Technical Report R-216, Port Hueneme, California, April 1963.
20. Swalley, R. F., "Behavior of Buried Model Arch Structures (U)," POR 2224 (CONFIDENTIAL), U. S. Naval Civil Engineering Laboratory, Port Hueneme, California, May 1963.
21. Murphy, C., D. F. Young and C. W. Martin, "Use of Models to Predict the Dynamic Response of Dynamically Loaded Underground Structures," AFWL RTD-TDR-63-3064, Air Force Weapons Laboratory, Kirtland Air Force Base, New Mexico, November 1963.
22. Johnson J. E. and R. E. Crawford, "Test of a Scaled Dynamic Model of the South Building, NORAD Combat Operations Center," Bulletin No. 32, Part III, Shock, Vibration and Associated Environments, Office of Director of Defense, Research and Engineering, Washington, D. C., pp. 88-114, December 1963.
23. Abramson, H. N. and G. E. Nevill, Jr., "Some Modern Developments in the Application of Scale-Models in Dynamic Testing," in W. E. Baker, ed., "Use of Models and Scaling in Shock and Vibration," American Society of Mechanical Engineers, New York, pp. 1-15, c. 1953.

Soils and Rock

24. Bucky, P. B., "Application of the Principles of Similitude to Design of Mine Workings," Trans. Am. Inst. Mining Met. Engrs., 109, 25-42, 1934.
25. Hubbert, M. K., "Theory of Scale Models as Applied to the Study of Geologic Structures," Bull. Geol. Soc. Am., 48, 1459-1520, October 1937.
26. Jones, B. D. and W. R. McCutchen, "Model Test of Large Scale Explosive Blast," unpublished paper, Colorado Schools of Mines, May 1948.
27. McCutchen, W. R., "Similitude in the Study of Military Geology," The Military Engineer, 41, No. 279, 7-9, January-February 1949.
28. "Underground Explosion Test," Final Report, Engineering Research Associates, Inc., St. Paul, Minnesota, Vol. I, August 1952, Vol. II, April 1953.
29. Lundgren, H., "Dimensional Analysis in Soil Mechanics," Acta Polytechnica, Civil Engineering and Building Construction Series, Vol. 4, No. 10, 1957.
30. Clark, G. B. and R. D. Claudle, "Geologic Structure Stability and Deep Protection Construction," AFSWC-TDR-61-93, Air Force Special Weapons Center, Kirtland Air Force Base, New Mexico, November 1961.
31. Martin, C. W. and G. Murphy, "Model Prediction of Fracture Due to Explosions," J. EM Division, Proceedings ASCE, 89, 133-150, April 1963.
32. Jackson, J. G., Jr. and P. F. Hadala, "An Application of Similitude to Small-Scale Footing Tests," Technical Report 3-599, Report 3 (draft), U.S. Army Waterways Experiment Station, Vicksburg, Mississippi, June 1963.
33. Thompson, L. J. and J. L. Colp, "Preliminary Evaluation of Earth Targets for Use in Impact Effects Studies," TID-4500, Sandia Corp., Albuquerque, New Mexico, DR 316-63, March 1964.

A SIMPLIFIED SOIL STRUCTURE INTERACTION MODEL TO INVESTIGATE THE RESPONSE OF BURIED SILOS AND CYLINDERS

by
C. J. Costantino*, R. R. Robinson**, M. A. Salmon***

ABSTRACT

This paper presents a summary of an approximate soil structure interaction model applicable to the problem of buried flexible circular tunnels and silos, subjected to air blast induced ground shock. Comparisons of the theory with some experimental results are presented. More complete experimental results have recently been obtained and are currently in the process of being analyzed. Application of the theory to several problems of interest is made, and particular design information evolved from the analysis is indicated.

INTRODUCTION

In the design of protective underground structures, designers are faced with an apparently overwhelming task. From a rather vague description of the threat against which they must protect, designers must evolve designs of such structures having very few tools of analysis at their disposal, the most important of these tools (and one which cannot be underestimated) being engineering judgement. The current state of affairs is similar to that which existed prior to the evolution of elementary beam theory.

The major difference between the two time periods is that in dealing with conventional structures

a. the engineer had a mass of experience to fall back on, and

b. his design, once built, could immediately be put to the test.

Clearly, both of these factors are missing from the current state of the art of protective design. Although, through both experiment and analysis, advances are slowly being made, the designer is faced with a problem which must be overcome now and which involves huge expenditures of money. Most significantly, also, a high degree of confidence must be assigned to the design to ensure that the structure will adequately perform its most important function.

In this report, we would like to describe an analysis which has been used to investigate the response of circular flexible tunnels and silos, subjected to nuclear induced ground shock waves. Although the approach is clearly approximate, it is felt that, from a design point of view, it suitably describes the phenomena involved, and can be a useful design tool to predict the gross response of such structures. Comparisons of the analysis with some experimental results are also presented.

GENERAL FORM OF DESIGN INPUTS

The inputs usually given the designer to describe the environment can be summarized as follows. A weapon size and ground range (or overpressure level) are specified against which the structure must survive. Associated with this environment is a design shock spectra which purports to describe the severity of the ground shock to which the structure will be subjected. Figure 1 is a typical example of such an input spectra. In general, depth effects are taken into account by suitably reducing the high frequency portion of the spectra with depth.

It is well known that the shock spectra formulation of the input data is incomplete and is not a unique characterization of the free-field shock displacement-time history. In addition, the variation of the spectra with depth is based upon relatively meager experimental data and includes a significant amount of engineering judgement, or "feel" for the problem.

The other conditions specified for the designer include information on site conditions (soil properties, water levels, etc) as well as thermal and nuclear radiation levels to be expected at the surface. In this paper we will neglect the radiation aspect as we are primarily concerned with the structural response problem.

From this information, the designer is expected to evolve a structural design which will, in general, satisfy two primary requirements, namely,

a. The structure will remain intact both during and after the application of the free-field ground shock;

b. the motions transmitted to sensitive equipments and personnel housed within the primary structure will remain within tolerable levels.

Satisfaction of these two criteria of design will ensure that the structure will perform its intended function before, during and after the attack. Other conditions which must be considered in the design include the number of attacks which the structure must withstand, time after the attack when the structure must be operational, etc.; and again, although

*Research Engineer, IIT Research Institute, Chicago, Illinois
**Research Engineer, IIT Research Institute, Chicago, Illinois
***Senior Scientist, IIT Research Institute, Chicago, Illinois

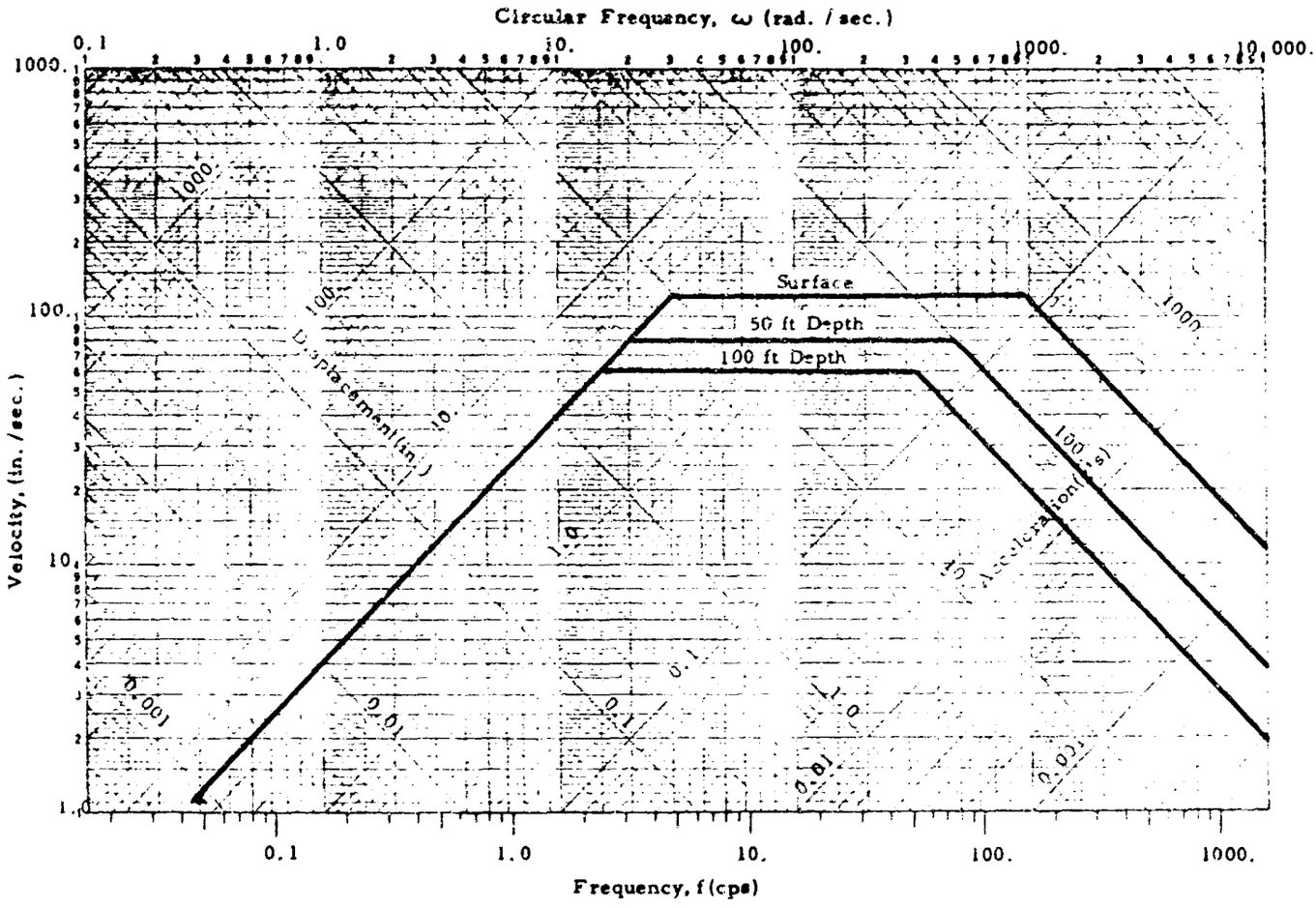


Fig. 1 Typical Free-Field Design Input Shock Spectra

important, these will not be discussed herein.

ANALYTIC INVESTIGATIGATION OF SILO AND TUNNEL LININGS

It is clear that a rigorous treatment of a cylindrical shell of finite length embedded in a semi-infinite continuous soil medium presents considerable analytic difficulties and requires a major research effort extending over a long span of time to provide the design information ultimately desired. We are currently in the early stages of such a development, what with the various elastic, (1,2) elastic-plastic (3) or finite difference (4) solutions obtained for particular aspects of the problem. Some of the prime difficulties encountered in such an analysis are the existing lack of detailed knowledge of the free-field environment, as well as the uncertainties involved in determining the response of soil to load, both static and dynamic.

Despite this shortcoming, it is possible to identify factors which principally affect silo and tunnel lining response. Consider the deformation imposed on a vertically oriented cylindrical column of soil in the free-field, sufficiently far removed from near ground zero effects. The principal deformations of the soil column (Figure 2) are:

a. shortening of the cylinder diameter in the direction of the blast-induced wave
b. horizontal displacement of the circular cross sections
c. vertical strain.

If the soil cylinder is replaced by a structural lining, the initially circular cross section is deformed (flattened), producing hoop bending and direct stresses. The variation of horizontal displacement with depth causes longitudinal bending and shear stresses in the lining, while the vertical soil strain develops longitudinal skin friction at the lining surface.

Corresponding effects are present in the case of horizontal cylinders (tunnels). That is, the displacements of the soil tend to flatten originally circular cross sections, produce longitudinal bending stress, and generate compressive axial forces in the lining. The last two effects are judged to be much less significant for tunnels than for silo linings since they can be reduced or eliminated by the use of expansion joints. The quantitative determination of the response of silo and tunnel linings to these effects has been the primary objective of past and current studies (5,6). In the following

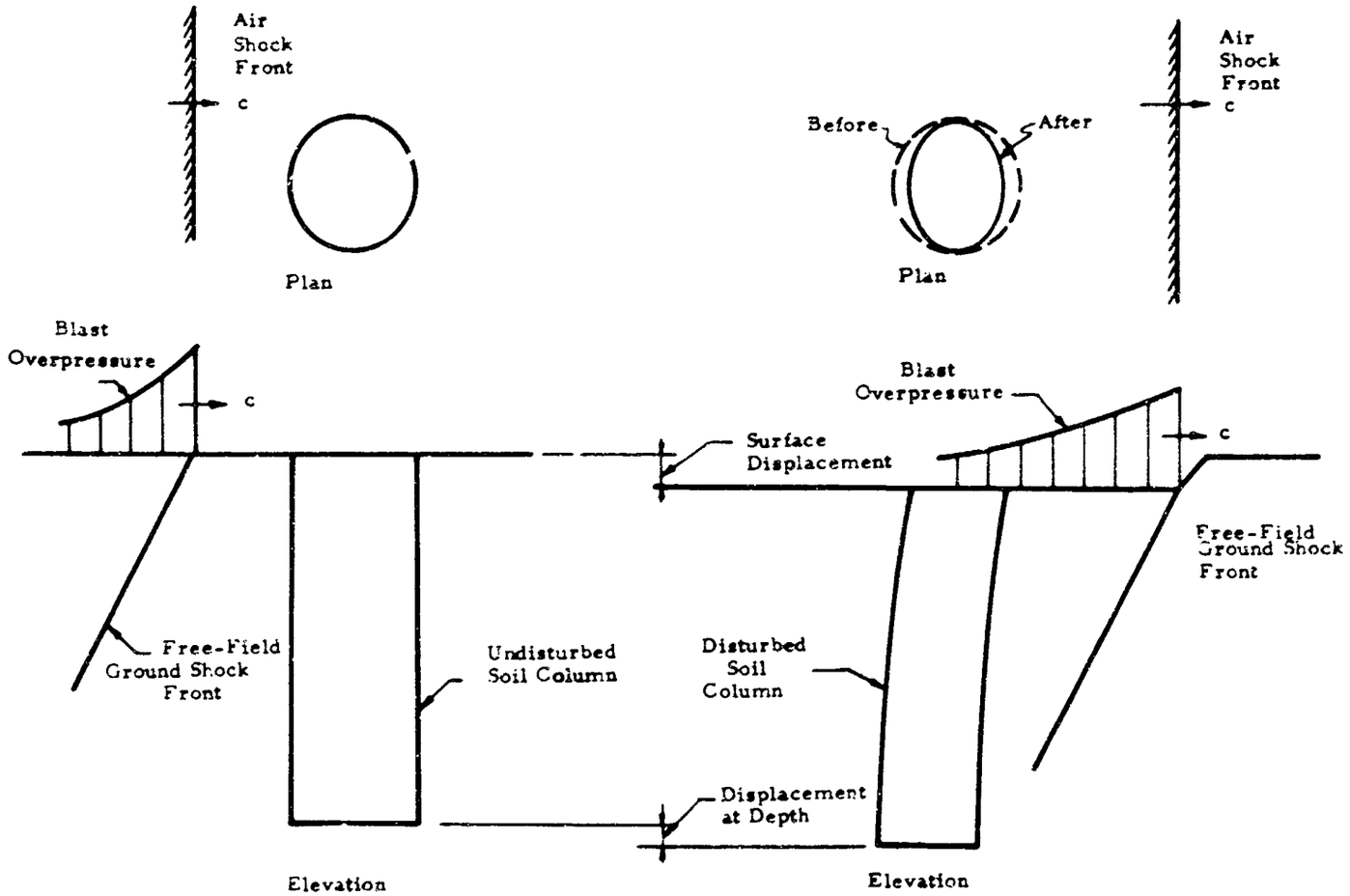


Fig. 2 Free Field Deformations Of A Vertical Soil Column

discussion, we will neglect the influence of longitudinal skin friction effects and consider only the response of the shell to radial loadings.

The loading on the structure is assumed to consist of the following radial components:

a. the free-field stress,

b. a stress dependent on the displacement of the liner relative to the free-field radial displacement,

c. a stress dependent on the velocity of the liner relative to the free-field radial velocity.

Thus the radial stress at a point on the cylindrical surface of the shell is written as (Figure 3):

$$\sigma_r = \sigma_o + k(w_o - w) + s(\dot{w}_o - \dot{w}) \tag{1}$$

where

σ_r = radial stress applied to cyljinder
σ_o = free-field radial stress
w = radial displacement of cylinder
$\dot{w}$ = radial velocity of cylinder
w_o = free-field radial displacement
$\dot{w}_o$ = free-field radial velocity

The proportionality factors k and s (foundation modulus and damping coefficient) will be discussed in a following section.

Considering the free-field stress and displacement conditions (Figure 3), the variation of the compressive stress in the x-direction, σ_x, can be written as

$$\sigma_x = \begin{cases} f_1(x-ct) & \text{for} \quad (x-ct) < 0 \\ 0 & \text{for} \quad (x-ct) > 0 \end{cases} \tag{2}$$

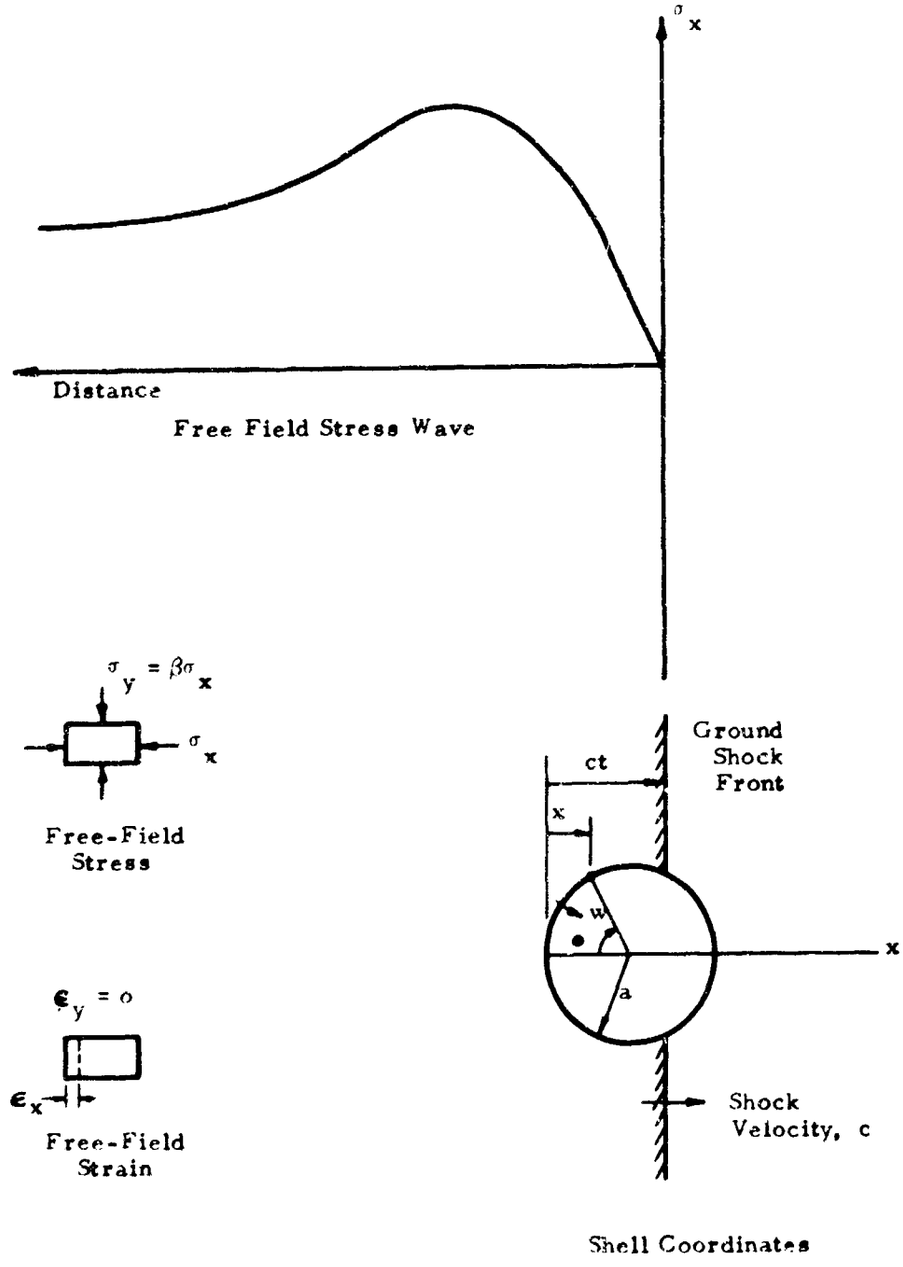


Fig. 3 Free Field Stress, Strain and Shell Coordinate System

where $f_1(x-ct)$ is a specified free-field stress function which depicts the actual passing stress wave. The compressive stress in the y direction σ_y, is assumed to be equal to $\beta\sigma_x$ for all values of x in the free-field, that is, it is assumed that

a. the "biaxiality" ratio, β, remains constant for all stress conditions, and

b. the soil is always in a state of plane strain.

The free-field strain in the x-direction, ϵ_x, is some function of the applied stress, σ_x, obtained from experiment, or

$$\epsilon_x = f_2 (\sigma_x, \sigma_{x_{max}} \ldots .) \tag{3}$$

The displacement, in the positive x-direction, of a particle originally at the point x is given by

$$u = \begin{cases} \int_x^{ct} \epsilon_x dx & \text{for} \quad (x-ct) < 0 \\ 0 & \text{for} \quad (x-ct) < 0 \end{cases} \tag{4}$$

Since $\epsilon_y = 0$, the free-field radial displacement is simply the radial component of the displacement u, or

$$w = u \cos\theta \tag{5}$$

while the free field radial velocity is

$$\dot{w}_o = \dot{u} \cos\theta \tag{6}$$

The radial stress component, σ_o, that would act on the cylinder were it to move with the free field is

$$\sigma_o = \frac{\sigma_x}{2} \left\{ (1+\beta) + (1-\beta) \cos 2\theta \right\} \tag{7}$$

EQUATIONS OF MOTION OF RING

Once the applied load on the cylinder is known, the response problem follows in a straight forward manner. We will briefly outline the procedure if we are considering plane elastic deformation in the plane of the ring. The radial and tangential shell displacements can be written in modal form as

$$w = \sum_{n=0}^{\infty} a_n \cos n\theta$$

$$v = \sum_{n=1}^{\infty} \frac{1}{n} a_n \sin n\theta \tag{8}$$

where inextensional bending behavior of the shell has been assumed. The term a_0 represents a pure radial or breathing mode, the term a_1 a rigid body displacement, while the terms a_n $(n \geq 2)$ the bending modes.

Writing the applied pressures in the form

$$\sigma_r = \sum_{n=0}^{\infty} p_n \cos n\theta \tag{9}$$

the modal equations of motion for the ring can be written as (7)

$$m_n \ddot{a}_n + b_n a_n = c_n p_n \quad (n = 0, 1, \ldots) \tag{10}$$

where $m_o = m_1 = m$, $m_n = m \left(\frac{n^2+1}{n^2} \right)$

$$b_o = \frac{\bar{E}h}{a^2} \left(1 + \frac{h^2}{12a^2} \right), \quad b_1 = 0$$

$$b_n = \frac{\bar{E}h^3}{12a^4} (n^2-1)^2$$

$c_1 = 1/2, \quad c_n = 1 \; (n \neq 1)$

m = the shell mass

h = the shell thickness

$\bar{E}$ = the shell modulus in plane strain

If it is desired to include the effect of hoop stress on the bending displacements, these coefficients may be modified to

$$b_n = \frac{\bar{E}h^3}{12a^4} (n^2-1)^2 - p_o (n^2-1) \quad (n \geq 2) \tag{11}$$

In any case, this serves to point out that the response solution can be rather easily obtained, either analytically or numerically, once the parameters k and s of Equation 1 are specified.

SELECTION OF PARAMETERS

It is shown in Reference 8, that, in the analysis of the response of a cylindrical shell submerged in an incompressible fluid, the interaction between the fluid and the shell can be completely accounted for by the addition of a virtual mass to the actual shell mass. This virtual mass is given by

$$m_{vn} = \rho a \frac{n}{n^2 + 1} \tag{12}$$

where ρ is the medium density, a the shell radius, and n the displacement mode number. It would thus seem appropriate to use some fraction of this virtual mass for an underground structure.

There is no experimental data on which to base the selection of the value of s, the parameter relating changes in load to relative velocity. The choice of s determines the magnitude of the jump in pressure at the head-on point ($\theta = 0^o$) at $t = 0$. There is, as yet, no specific evidence that such reflection effects exist in soil. However, for an elastic medium, the reflected pressure would be twice the incident pressure for the case of normal incidence of a compression wave. To obtain this result from this analysis, a value of

$$s = \rho c \tag{13}$$

would be required, where c is the velocity of the wave front.

The last parameter which must be assigned is the foundation modulus k. Static load tests on culverts ranging from 30 to 84 inches (9) in diameter indicate that the foundation modulus is a function of the cylinder radius, a. Values of the quantity ka seem to be constant for a given soil condition. Values of ka $\geq$ 200 psi are cited for various types of soil backfill. Values of the compression moduli and density of the fill material are not given so that it is difficult to relate the observed values of ka to other soil properties.

Watkins (10) obtained values of ka ranging from about 2300 to 3700 psi for various mixtures of silt and clay. These results were obtained from tests on 3-7/8 inch diameter cylinders. Increasing values of ka were observed with increasing density of the soil, so that, as would be expected, ka increases with increasing values of the soil compression modulus.

The plane strain solution for the displacements produced by the application of a radial pressure varying as cos n θ to the boundary of a hole in an infinite elastic medium (11) leads to

$$ka = \begin{cases} \left\{ \dfrac{1-2\nu}{1-\nu} \right\} E_c & \text{for } n = 0 \\ 0 & \text{for } n = 1 \\ \left\{ \dfrac{(1-2\nu)(n^2-1)}{(1-\nu)\left[(2n+1) - 2(n+1)\nu\right]} \right\} E_c & \text{for } n = 2 \end{cases} \tag{14}$$

where E_c is the elastic modulus in confined compression of the medium and ν is Poisson's Ratio. Thus, for an elastic medium the foundation modulus increases with increasing mode number (for $n \geq 2$) and is directly proportional to the modulus in confined compression. The solution for n = 1 (rigid body displacement) yields a foundation modulus equal to zero. That is, there is no resistance to the displacement of a hole as a rigid body in an infinite elastic medium. This effect can be rather easily included in the stress determination of Equation 1 by using the relation

$$\sigma_r = \sigma_o + k \left\{ w_o - w - W_1 \cos \theta \right\} + s \left\{ \dot{w}_o - \dot{w} \right\} \tag{15}$$

where W_1 is the first mode component of the relative displacement $(w_o - w)$ or

$$W_1 = \frac{2}{\pi} \int_0^{\pi} (w_o - w) \cos \theta \, d\theta \tag{16}$$

It is clear that the utility of the proposed method for the analysis of the response of silo and tunnel linings to blast-induced loadings can be best established only by demonstrating agreement between predictions of the analysis and experimental results. At this time, we are just beginning to evolve applicable experimental results, some of these being as follows.

Stress-Strain Behavior of Sands

Since the foundation modulus is dependent upon the confined modulus of the soil, some static one-dimensional consolidation tests have been performed on a Standard Ottawa sand (since this sand was used in buried cylinder tests) to determine its stress-strain behavior. The tests were performed at a high density (80 to 90 percent relative density) and a loose density (10 percent relative density) with pressures up to 300 psi. Both loading and unloading cycles were included. The test results indicated that the stress-strain behavior could be approximated by

$$\text{Loading:} \quad \sigma = A_L \epsilon^{B_L}$$

$$\text{Unloading:} \quad \frac{\sigma}{\sigma_{max}} = \left\{ \frac{\epsilon - \epsilon_{min}}{\epsilon_{max} - \epsilon_{min}} \right\}^{B_U} \tag{17}$$

$$\epsilon_{min} = C_U \epsilon_{max}$$

where σ_{max} is the maximum previous stress to which the sample was loaded, ϵ_{max} is the corresponding maximum strain, and ϵ_{min} is the residual strain remaining in the sample upon loading. The parameters found from the experiments for both the loose and dense condition are given in Table I.

TABLE I
SOIL PARAMETERS

Parameters	Loose	Dense
A_L, psi	2.08×10^5	3.18×10^5
B_L	1.751	1.704
B_U	2.038	2.694
C_U	.503	.227

Thus, as would be expected, the confined modulus (and the foundation modulus) of the soil is strongly dependent upon both the stress level to which the soil is subjected as well as its loading history. Preliminary results on similar dynamic tests (12) indicate negligible dynamic effects, at least for stress levels below 500 psi.

Static Buried Cylinder Tests

The results of a series of buried culvert tests in a variety of soils (13) has led to the Iowa formula for determining diameter changes, which is

$$\frac{\Delta}{2a} = \frac{1.5\,\sigma_o}{\left(\frac{18\,\bar{E}I}{a^3} + 1.1\,ka \right)} \tag{18}$$

where Δ is the vertical diameter change, and σ_o is the applied static overpressure. The static solution from this analysis yields the result

$$\frac{\Delta}{2a} = \frac{\sigma_o \left(1 - \beta + ka/E_c \right)}{\left(\frac{18\,\bar{E}I}{a^3} + 2\,ka \right)} \tag{19}$$

Comparison of Equation 18 and 19 indicates a significant agreement between theory and experiment, at least for the static problem. Thus, selection of the foundation modulus can be made from these experimental results (13) for the various soil types tested.

Dynamic Buried Cylinder Tests

A series of dynamic model tests of flexible buried tunnels has recently been completed (14) and comparisons between theory and experiment are currently in the process of being made. Unfortunately, no information is currently available for presentation.

APPLICATIONS OF THE THEORY TO PRACTICAL PROBLEMS

It is clear from the preceding discussion that it is not possible at the present time to assign precise values to the parameters on which the solution depends. Nevertheless, in the interim, something is to be gained by an investigation of the nature of the solutions given by the method and by the study of the effects on these solutions of variations in the parameters. We will indicate various applications to which the solution has been applied and some of the interesting results generated for these problems.

Buried Flexible Tunnels Subjected to Step Pulse Loadings

Table 2 contains the results of an analysis to determine the response of buried concrete tunnels engulfed by a step pulse pressure wave. The three parameters (virtual mass, soil damping, foundation modulus) were varied over a large range to cover the extremes of values most likely to be encountered. In addition, three values of the radius to thickness ratio were chosen to cover the range usually found in protective structures. The response value shown is the ratio of diametral shortening to cylinder diameter, a measure of the developed bending moments. It may be noted that the dynamic load factors obtained from the solution are generally less than 1.4, except for the cases where no soil damping is included (a highly unrealistic condition). Thus, these results indicate that, with the application of a low dynamic load factor, an analysis for static loading is adequate for the design of such structures of interest. Similar dynamic load factors were obtained for peak lining stress as well as applied pressures. Figure 4 contains a typical example of the pressure applied to the cylinder with time.

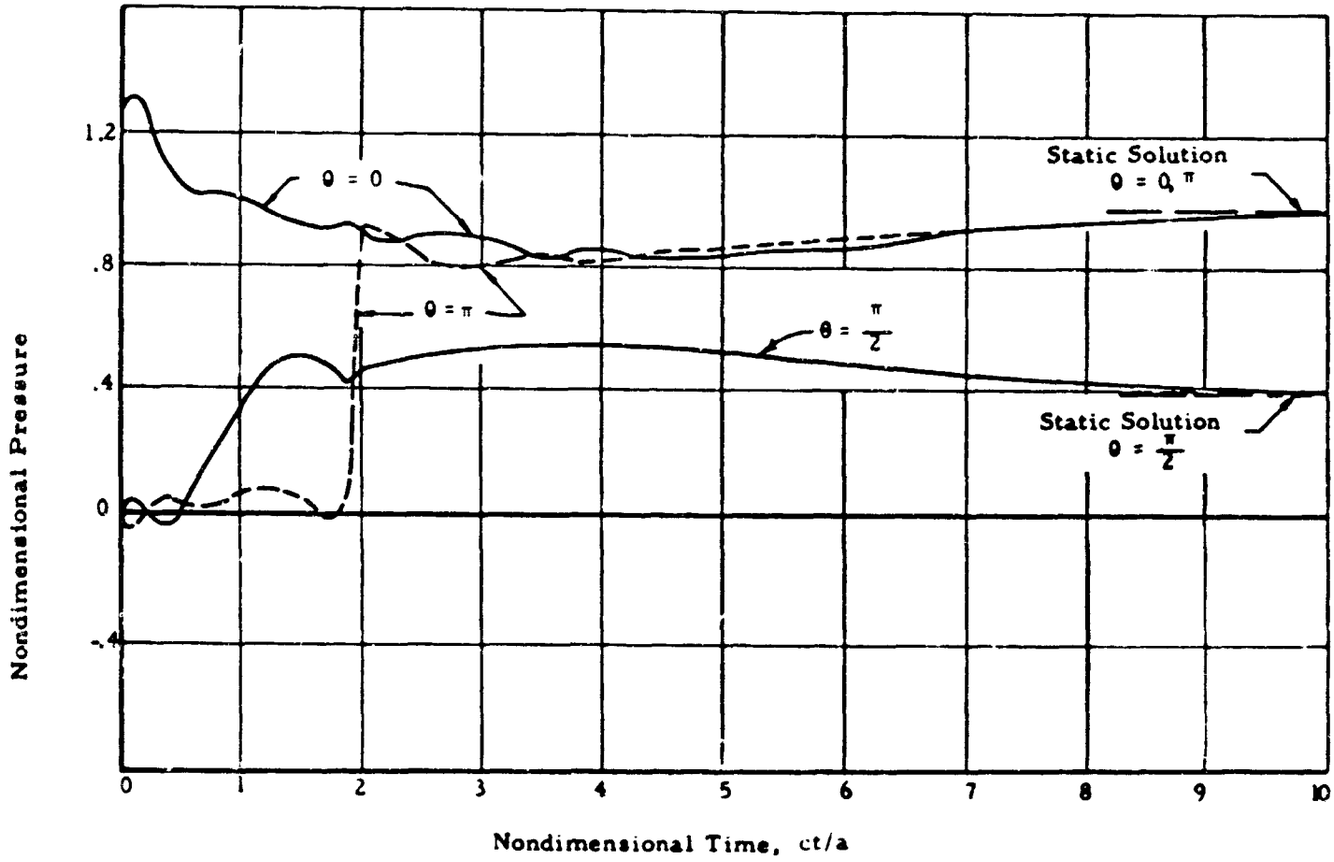


Fig. 4 Pressure-Time Variation (Case 24 of Table 2)

Static Buckling of Buried Tunnels

The analysis indicates that the pressure required to cause the cylinder to buckle in the first bending mode (n=2) is

$$\sigma_{cr} = \frac{2\left(1 + \frac{ka^2}{\bar{E}h}\right)}{\left(1 + \beta + \frac{ka}{\bar{E}_c}\right)} \left(\sigma_{cr_o} + \frac{ka}{3}\right) \tag{20}$$

where σ_{cr_o} is the ordinary buckling pressure equal to $3\bar{E}I/a^3$. From this result, it is seen that for reasonable values of ka, the buckling strength is much higher than the applied overpressures encountered in practice. In addition, it indicates that the influence of direct stress on bending can generally be neglected, simplifying the shell problem that need be investigated.

TABLE 2
MAXIMUM DIAMETRAL SHORTENING FOR STEP PULSE APPLIES TO FLEXIBLE TUNNELS (Ref. 11)

Case No.	Foundation Modulus in psi ka	Proportion of Virtual Mass used, Eq. 12 K_{mv}	Critical Damping Ratio s/ρc	Shell Radius Thickness Ratio a/h	Ratio Diametral Shortening to Diameter from Eq. 19 Static $\frac{\Delta}{2a}$	Dynamic Load Factor DLF
1	5000	0	0.5	10	.01323	.98
2			.25			1.06
3			.125			1.11
4			0.0			1.24
5		0.5	0.5			1.04
6			.25			1.21
7			.125			1.36
8			0.0			1.63
9			.125	30	.01937	1.24
10				20	.01867	1.25
11	2000	0	.25	10	.01985	1.03
12			.125			1.16
13			0.0			1.39
14		0.5	.25			1.16
15			.125			1.39
16			0.0			1.81
17			.125	30	.04563	1.21
18				20	.04084	1.21
19	500	0	0.5	10	.02943	.89
20			.25			.98
21			.125			1.14
22			0.0			1.74
23		0.5	.5			.91
24			.25			1.09
25			.125			1.32
26			0.0			1.84
27			.125	30	.3866	.411
28				20	.1836	.671

Applied Loads and Motions of Vertical Silos

This approach for taking into account the soil-structure interaction phenomena has been used to investigate the response of vertical silos (6) to engulfing ground shock waves. For this problem, the design input data was given in the form of free-field shock spectra. To convert this data to useable input for the analysis, a family of simplified ground shock wave forms were evolved which developed the given input spectra. The information required for the design of the structure was

1. loads applied to the silo structure
2. motions and accelerations transmitted to sensitive equipment housed within the silo
3. characteristics of the equipment isolation system to minimize "rattle" space requirements while maintaining peak accelerations within tolerable levels.

For this particular problem, it was found that the motions sustained by the key equipment within the silo were fairly insensitive to the particular values of the foundation parameters chosen. This was due to the fact that the silo in this case was housed in an extremely stiff medium. A typical result of this analysis (Figure 5) shows the displacement history for the silo and the free-field at the top and bottom of the silo. The silo displacements at various depths were then used to determine in-silo shock spectra at corresponding depths. Figure 6 shows the resulting in-silo and free-field shock spectra at the surface.

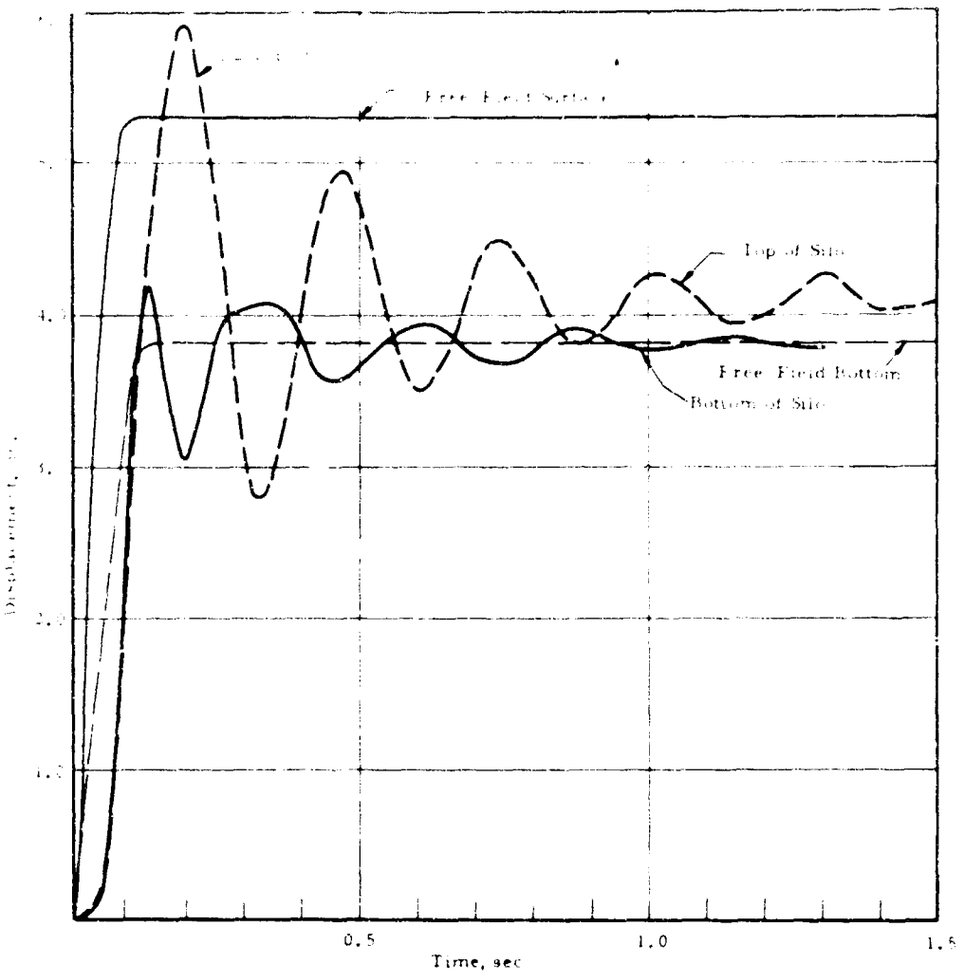


Fig. 5 Silo and Free-Field Displacement Time History

Such information is adequate for the design of simple isolation systems for equipment mounted directly to the silo wall. Previous to this approach, the only alternative open to the designer was the use of an empirical "structural attenuation factor" to decrease the high frequency end of the free-field input spectra to obtain input spectra to equipment.

Studies of Foam Encased Structures

Currently under way at IITRI is a series of dynamic experiments to determine the response of buried flexible tunnels encased in crushable foam isolation material. An analysis (and associated computer program) has been developed based upon this apprach to the soil-structure interaction problem. Preliminary comparisons of analytic and experimental results indicate a significant agreement as to applied pressure loadings, shell response and percent crushing of the isolation material. Again, these results will be reported upon when further studies are completed.

SUMMARY

We have tried to present a summary of an approximate soil-structure interaction model applicable to the problem of circular buried protective structures, as well as some of the problems to which this model has been applied. We would like to emphasize again that the primary objective of this approach has been to provide a more complete tool to designers of such structures than currently exists. Naturally, as more information, both analytic and experimental, becomes available to the designer, the model can be further improved and made more applicable to the problem at hand.

From some of the problems to which this model has been applied, it has been found that although the several open parameters involved cannot as yet be precisely specified, significant design information can be developed.

ACKNOWLEDGEMENT

The results presented in this paper have been developed as part of several different programs conducted at IIT Research Institute for the Air Force Weapons Laboratory and the Air Force Ballistic Systems Division.

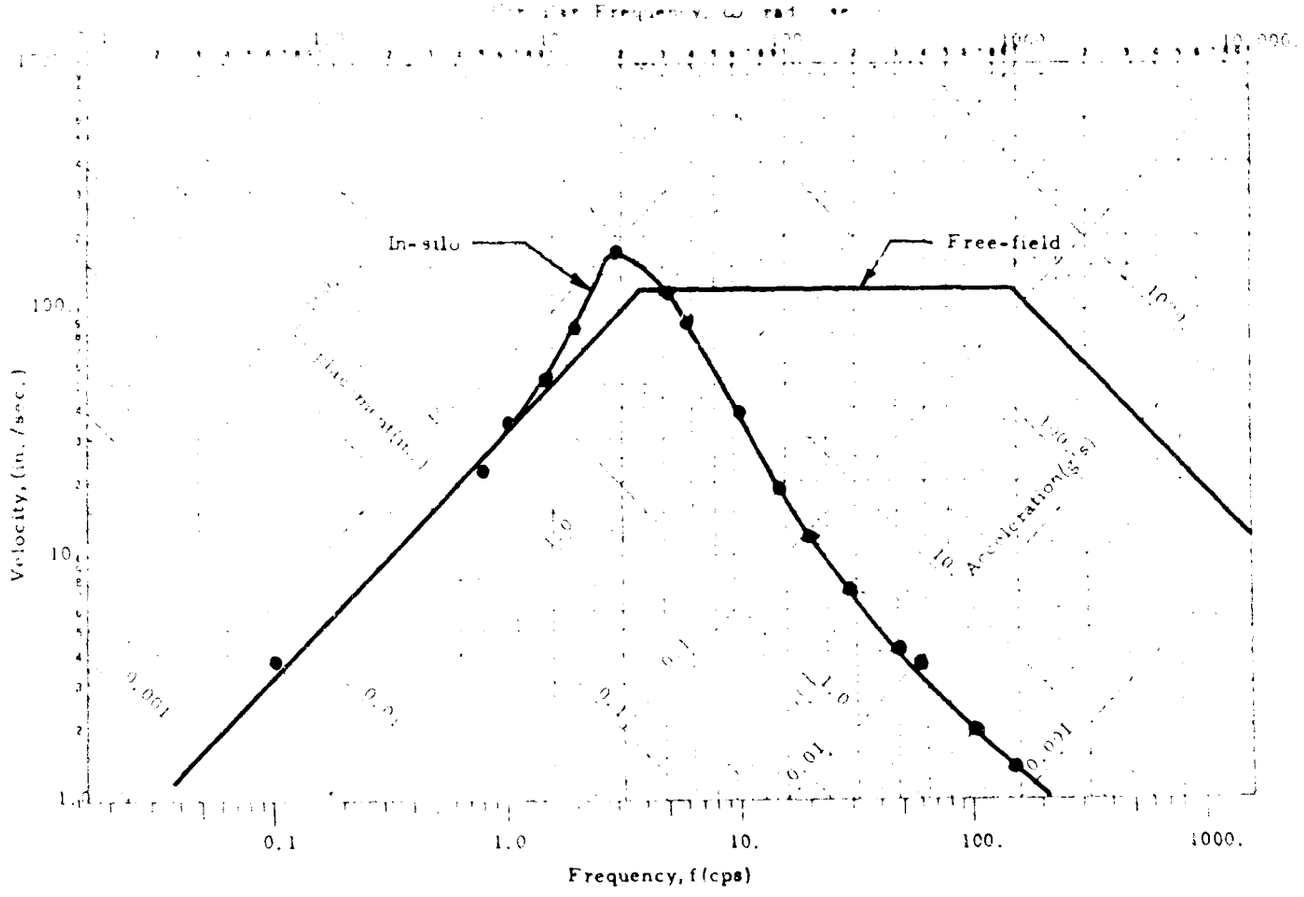


Fig. 6 Surface Shock Spectra

REFERENCES

1. Baron, M. L., H. Bleich, P. Weidlinger, "Theoretical Studies on Ground Shock Phenomena," the MITRE CORPORATION, October, 1960.
2. Soldate, A. M. and J.F. Hook, "A Theoretical Study of Structure-Medium Interaction," Report No. AFSWC-TN-61-6, for AFSWC, November 1960.
3. Soldate, A. M. and I. Miklowitz, "A Theoretical Analysis of Stress Wave Interaction in a Model Soil-Further Studies," National Engineering Science Co., for AFWL, Contract No. AF29(601)-5395, April 1964.
4. DaDeppo. D. A. and J.F. Werner, "The Influence of Mechanical Shielding on the Response of a Buried Cylinder," Dept. of Civ. Eng. Univ. of Arizona, for USNCEL Contract No. NBy-32199, February 1962.
5. Robinson, R. R., "Analytical and Experimental Investigations of Silos and Tunnel Linings," IIT Research Institute Project M270, for Air Force Weapons Laboratory, Contract No. AF29(601)-5384, Report No. RTD TDR-63-3085, February 1964.
6. Costantino, C. J., "Study of Advanced Missile Support - Isolation Systems," IIT Research Institute Project No. M6043, for AFBSD/Aerospace Corporation, Contract No. AF 04(694)-163, Final Report, August 1963, SECRET
7. Timoshenko, S. and J. Gere, Theory of Elastic Stability, 2nd Ed., McGraw-Hill Book Co., New York, N.Y. 1961.
8. Bleich, H., DiMaggio, F., "Dynamic Buckling of Submerged Plates and Shells," Columbia University Publication, Dept. of Civil Eng. Mech., ONR Contract No. NONR-266(08), Technical Report No. 12, September 1754.
9. Watkins, R. and M.G. Spangler, "Some Characteristics of the Modulus of Passive Resistance of Soil: A Study of Similitude," Highway Research Board Proc. 37, 1958.
10. Watkins, R., "Influence of Soil Characteristics on Deformation of Embedded Flexible Pipe Culverts," Highway Research Board, Bulletin No. 223, 1959.
11. Robinson, R. R., "The Investigation of Silo and Tunnel Linings," IIT Research Institute, for AFWL, Contract No. AF 29(601)-2596, Report No. AFSWC-TDR-62-1, March 1962.

12. Smith, J., Private Discussion with author, Air Force Weapons Laboratory, May, 1964
13. Spangler, M. G., "The Structural Design of Flexible Pipe Culverts," Iowa State College, Engr. Experiment Station Bull, 153, 1941.
14. Marino, R. L. and W. F. Riley, "Response of Buried Structural Models to Static and Dynamic Overpressures," IIT Research Institute, presented at Symposium on Soil-Structure Interaction, Univ. of Arizona, June 1964.

THE EFFECT OF PORE AIR PRESSURE ON SOIL-STRUCTURE INTERACTION

by
Delon Hampton*

ABSTRACT

All tests were conducted in a 4 inch diameter shock tube, and the propagation of pore air pressure in samples of soil subjected to a shock wave was studied. The soils tested were a uniformly graded pea gravel, a standard 20-30 Ottawa sand, and a well-graded silty sand. The orientation of the shock wave to the soil sample was head-on, and the maximum overpressure on the upstream end of the sample was approximately 126 psi. The effect of peak overpressure, permeability, and total impulse per unit area was ascertained. The data are reviewed in the light of their effect on laboratory experiments utilizing shock waves to load specimens of soil.

INTRODUCTION

A great amount of time, money, and effort has been and is being expended to obtain a better understanding of soil-structure interaction phenomena. Much of this research is conducted in the laboratory where soil specimens containing gauges or small buried structures are loaded by shock waves.

When a shock wave passes over the soil, air is forced into the pores of the soil and pore pressures are created. If the soil is dry, only pore air pressures result; in partially saturated soils, both pore air and pore water pressures are generated; and in fully saturated soils, pore pressures are caused by pore water only. Whatever the state of the soil, pore pressures if transmitted deep enough will alter the stress state of the soil surrounding the buried structure.

The effect of pore pressures on the effective stress at a given point in a mass of soil can be noted from an equation proposed by Bishop (1):

$$\sigma' = \sigma - u_1 + \chi (u_1 - u_2) \qquad (1)$$

where σ denotes the total normal stress;
σ' the effective normal stress;
u_1 pressure in the gas and vapor phase;
u_2 pressure in the pore water; and
χ a parameter depending principally on the degree of saturation of the soil.

the value of the parameter, χ, is unity for saturated soils and zero for dry soils. Furthermore, it should be noted that for extreme values of χ, Equation 1 reduces to the form of that originally proposed by Terzaghi (2) for a two-phase system.

It is apparent from Equation 1 that if significant pore pressures are developed by air entering or attempting to enter the pores of the soil, then the stress state of the soil will be altered. To understand soil-structure interaction phenomena, one must be able to evaluate the magnitude and nature of the stress change. To evaluate this stress change, one must also be able to evaluate the pore pressure in any given mass of soil, at any given point resulting from a shock wave with any given pressure-time history at the surface of the ground.

In addition, if one is to use data from laboratory experiments to predict phenomena which occur under full-scale conditions. And if significant pore pressures are developed in laboratory experiments, whether they are pore air pressures, pore water pressures, or a combination of pore air and pore water pressures, they have to bear the appropriate scale relationship--which is practically impossible.

Seed and Clough (3) acknowledged the difficulty of modeling pore water pressures in cohesionless soils: "The writers presented this analysis to emphasize the extreme importance of pore-pressure effects in model testing and the potential dangers of attempting to include them in a test program. It is doubtful if techniques could ever be developed for correct modeling of pore water pressures in cohesionless materials and at the present stage of knowledge the only recourse seems to be the elimination of the problem by using only dry cohesionless materials for model construction." Although this statement refers to pore water pressures in particular it is also applicable to pore pressures of all types.

From the above discussion it is apparent that the distance of propagation and the magnitude of the pore air pressures in soil specimens loaded by shock waves are of prime importance. If the penetration is deep enough to produce significant pore air pressures in the vicinity of a buried structure, the stress state of the soil surrounding the structure will

*Research Associate Engineer, Air Force Shock Tube Facility, University of New Mexico, Albuquerque, New Mexico.

...e effe... test, ... subsequently, the ... stress ... the str... re will also be effected.

PURPOSE AND SCOPE

Recognizing the importance of this problem and the lack of information about it, University of New Mexico personnel at the Air Force Shock Tube Facility, instituted a research program to explore it. The experimental program was conducted in the 4 inch diameter, compressed-air-driven shock tube which produced a shock wave that strikes the sample head-on. The maximum pressure at the upstream end of the sample was approximately 126 psi.

It should be noted that all pressures in this report are gauge pressures. In extrapolating the data to other atmospheric conditions, one must take into consideration that the average barometric pressure at the test site is 12 psia.

The soils used in this study were pea gravel, 20-30 Ottawa sand, and a well-graded silty sand; their basic properties will be given subsequently; and all were tested in an air-dry condition.

SOIL PROPERTIES

Grain-Size Distribution

Pea gravel and Ottawa sand are uniformly graded soils, and their grain-size distributions are given in Table 1.

Table 1

GRAIN-SIZE DISTRIBUTION OF PEA GRAVEL AND OTTAWA SAND

U.S. Std. sieve No.	Size of opening (inches)	Percentage passing Pea Gravel	Ottawa sand
-	0.375	99.24	
4	0.187	17.90	
10	0.0787	0.96	100.00
20	0.0331	-	99.43
30	0.0232	-	5.78
40	0.0165	0.12	0.03
100	0.0059	0.04	0.00
200	0.0029	0.00	

The grain-size distribution of the silty sand is shown in Figure 1. It can be seen that approximately 47 percent is finer than 0.074 mm (upper limit of the silt-size particles) and approximately 7 percent finer than 0.002 mm (upper limit of the clay-size particles).

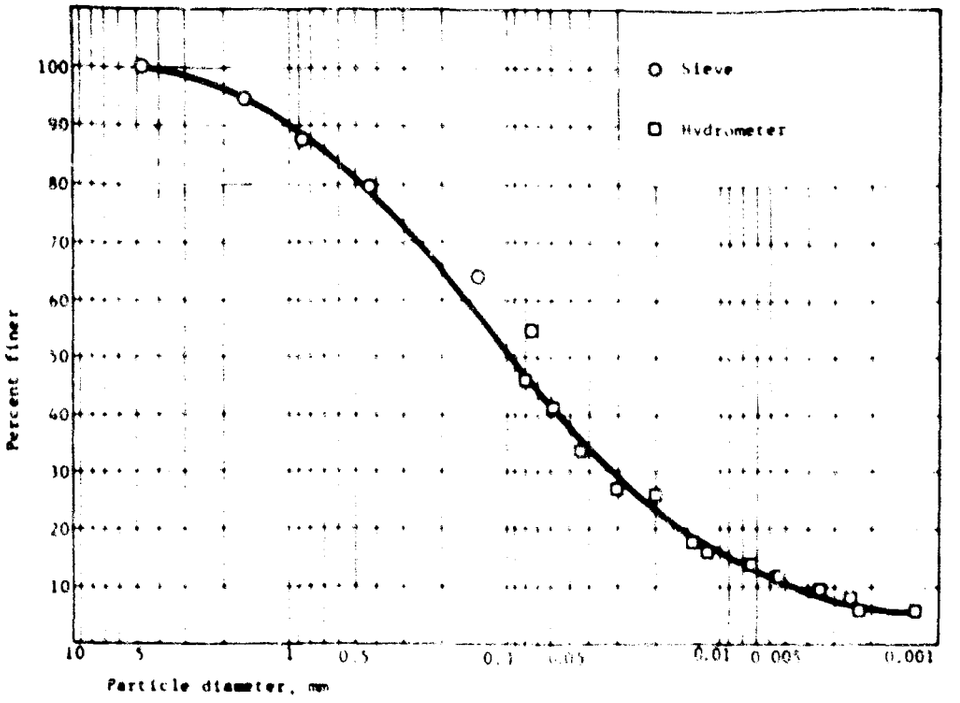


Fig. 1 Grain-Size Distribution Curve (Silty Sand,

Table 2 shows the [illegible] properties of the [illegible] tested.

Table 2

VARIATIONS IN SOIL SAMPLES TESTED

	Ottawa sand	Pea gravel
γ_{max} (lb/cu ft)	115.6	107.4
γ_{min} (lb/cu ft)	111.9	105.0
e_{min}	0.43	0.52
e_{max}	0.47	0.54

An attempt was made to determine the effect of a change in void ratio on the propagation of pore air pressure through samples of the silty sand. The extent to which the void ratio could be controlled can be seen from Table 3.

Table 3

VARIATIONS IN UNIT WEIGHT AND VOID RATIO OF SILTY SAND

Soil condition	Soil property	
	Unit weight (lb/cu ft)	Void ratio
Loose	γ_{max} = 97.6 γ_{min} = 94.8	e_{min} = 0.72 e_{max} = 0.77
Dense	γ_{max} = 105.8 γ_{min} = 101.2	e_{min} = 0.63 e_{max} = 0.66

It should be emphasized that these data indicate the extreme variation of the properties considered, and in most cases the variation was much less. It was therefore assumed that the properties of all samples tested are the same for a given soil type and relative density.

Permeability

Tests were conducted to determine the permeability of the soils to water. These were done with the constant head permeameter for the pea gravel and Ottawa sand, and with the falling head permeameter for the silty sand. The results are presented in Table 4.

Table 4

AIR-DRY UNIT WEIGHT AND PERMEABILITY OF SOIL SAMPLES

Soil	Air-dry unit weight, γ (lb/cu ft)	Permeability, k (cm/sec)	Physical permeability, K (cm^2)
Pea gravel	107.0	0.232	2.34×10^{-6}
	105.0	0.247	2.50×10^{-6}
Ottawa sand	112.0	0.060	6.06×10^{-7}
	111.0	0.061	6.16×10^{-7}
Silty sand	109.5	0.971×10^{-4}	9.81×10^{-10}

Atterberg Limits and Hydroscopic Moisture

Tests were conducted on the silty sand to determine its Atterberg limits and hygroscopic water content. The Atterberg limits were determined on the material passing the No. 40 U. S. Standard sieve. The liquid limit was found to be 21.4 percent and the plasticity index, 1.9. The hygroscopic moisture content was 3.2 percent.

Sample Preparation

The soil-test section in the 4 inch shock tube was the same diameter as the shock tube. At the start of sample preparation the soil-test section was placed in a vertical position, the end was covered with a wire mesh to retain the soil, and rested on the floor. A No. 30 sieve screen was used to hold the sample of Ottawa sand, a No. 4, for the pea gravel, and a No. 250, for the silty sand.

The Ottawa sand was poured through a funnel into a 2 inch diameter radiator hose, to the bottom of which was attached a wire mesh. The mesh distributed the falling sand and forced it to "rain down" on the soil surface, producing a high relative density. The same procedure was used for the pea gravel, except that the screen and hose were omitted.

The Ottawa-sand and pea-gravel samples produced in this manner were a minimum of 6.13 feet long for testing in the 4 inch shock tube. A screen of appropriate size was placed over the upstream end of the sample and held in place by screws. The test section was then attached to the shock tube.

In the case of the silty sand, a given amount (2 kilograms) was dropped in the test section. For the dense state, the sand was compacted by 25 blows of a 10 pound weight dropped 18 inches onto a metal plate which covered the entire surface of the soil. The process was repeated until a sample 3.13 feet long was obtained. The end of the sample was then covered with a screen and attached to the shock tube. The loose state was obtained by dropping the soil through a funnel placed at the upstream end into the soil-test section until the desired length of sample was obtained.

Test Setup

The basic test setup is shown in Figure 2. The lower portion of Figure 2 shows the gauge station numbers and the distance of the gauge stations from the upstream end of the soil-test section. The shock wave is produced by rupturing a membrane which forms one end of a compressed-air driver chamber.

For the tests on gravel, one specimen was used for a complete series of shots. This proved feasible because no disturbance of the specimen was noted. Furthermore, this approach was justified experimentally.

However, for the tests of the Ottawa sand and the silty sand, a virgin sample was used for each shot. A series of shots consisted of tests at nominal reflected pressures of 20, 40, 60, 70, 80, 105, and 120 psi on the upstream end; the

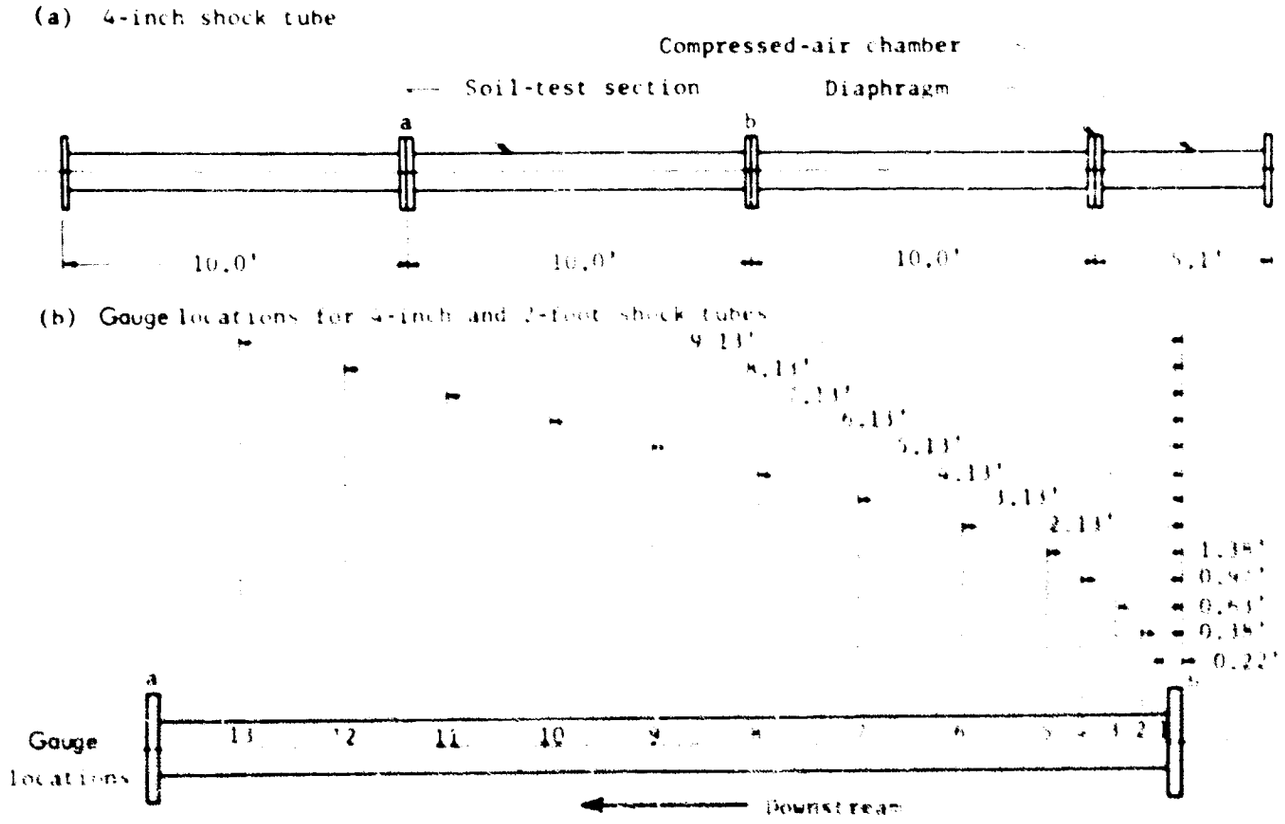
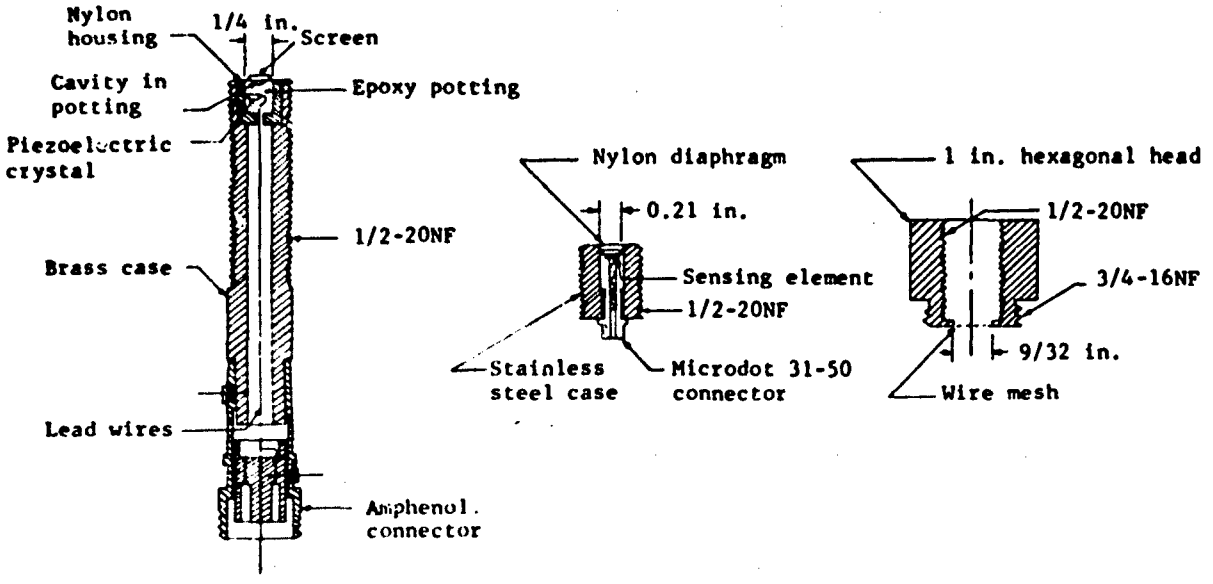


Fig. 2 Schematic Diagram of Test Setup

resulting shock waves reflecting at the sample interface were monitored by a gauge immediately preceding the sample.

Instrumentation

Initially, barium titanate gauges were used in the soil-test section to measure the pore air pressure. These gauges, assembled in the Electronics Laboratory of the Air Force Shock Tube Facility, were covered with a No. 30 sieve screen (Figure 3). There was an air gap of 0.030 inch between the screen and the sensing element.



(a) Barium titanate (b) Granath ST-2 (c) Grommet

Fig. 3 Schematic Diagram of Gauges and Grommet

Granath ST-2 gauges, manufactured by Susquehanna Instruments Company, were used in all tests to monitor the air shock pressure in the section upstream with respect to the face of the sample. The monitor gauge was 2-1/2 inches upstream of the test section in the 4 inch shock tube.

The barium titanate gauge (Figure 3a) proved satisfactory for measuring pore air pressure in testing the pea gravel. However, it proved unsatisfactory with the Ottawa sand and silty sand because the screen was forced against the sensing element, and the gauges registered a total stress instead of pore air pressure. Consequently, another method of measuring pore air pressure was required.

It was felt that the principal fault of the barium titanate gauge resulted from the method of mounting the screen over the sensing element. A more effective method of isolating the sensing element of the gauge from the soil was sought. A grommet was made to hold the gauges, over the end of which wire mesh could be cemented. The distance between the mesh and the gauge was 0.020 inch.

To increase the accuracy of the measurements, the Granath ST-2 gauge was substituted for the barium titanate gauge because the former has much less cross-axis sensitivity.

The new combination of grommet and ST-2 gauge proved satisfactory, and it was used to measure pore air pressures in all tests except those on pea gravel and Ottawa sand, a No. 30 sieve screen was used across the end of the grommets; and for tests on silty sand, a No. 250 sieve screen was used to isolate the sensing element from the soil.

For a more comprehensive description and explanation of the instrumentation, see Reference 4.

Data Recording and Processing

The data were recorded on magnetic tape with equipment whose frequency sensitivity ranges from DC to 20 kc. The data were taken from the tape by two methods. The first was to play the tape through an oscilloscope and take Polaroid pictures of the data channels. The second was to obtain a complete and simultaneous visual record of all gauges by playing the tape through a light-sensitive, multichannel recording oscillograph. The second method allowed the observer to relate the performance of the gauges in time and to see the entire history of the event.

RESULTS

General

When the shock wave strikes the soil, air is forced into the pores. In practically all cases, the rate of transmission of the air through the pores of the soil will be significantly less than the initial rate at which the air is being introduced. Consequently, near the upstream end of the specimen a buildup of quasi-static pressure will occur which may possibly increase the pore air pressure above the input pressure at the air-soil interface.

If the magnitude of this quasi-static pressure becomes appreciable, it would significantly alter the rate of attenuation, i.e., the essentially exponential decay shown in Figures 4 and 5 would not be valid.

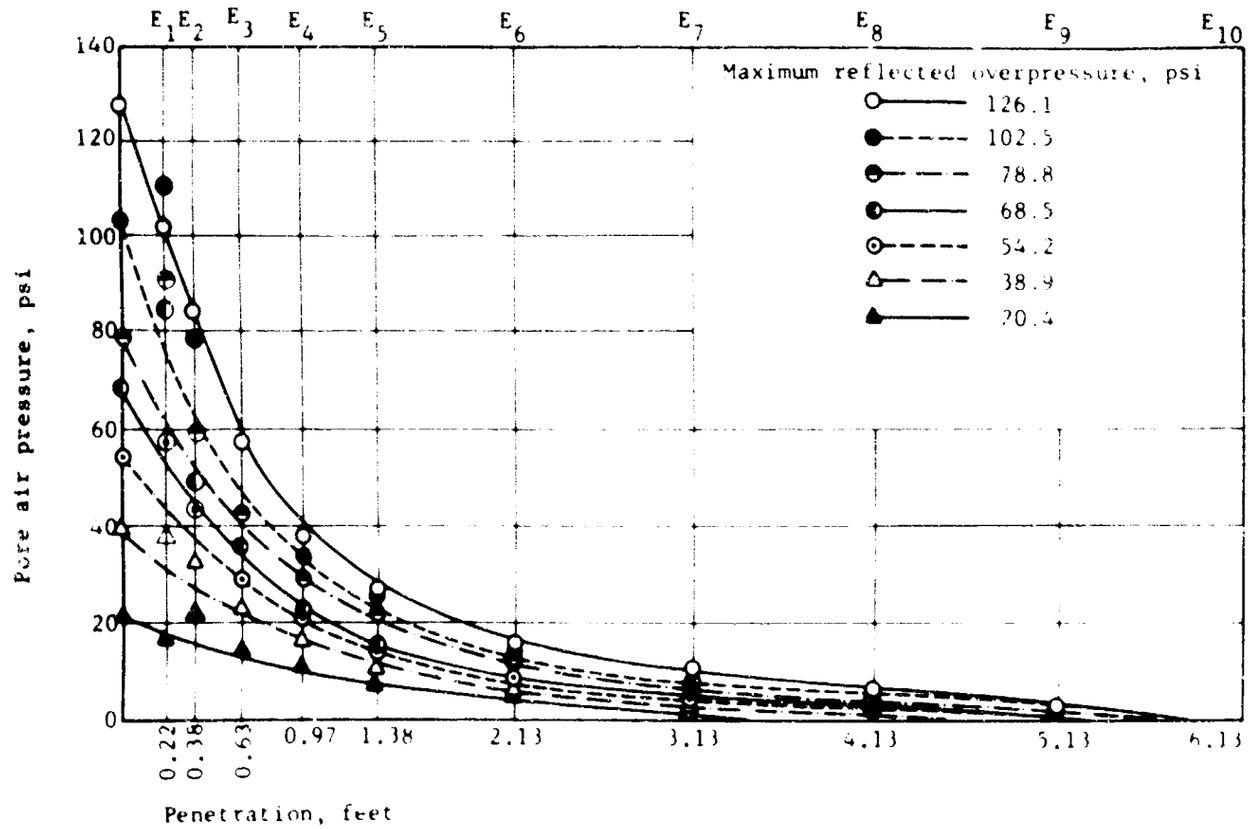


Fig. 4 Pore Air Pressure Vs. Penetration (Pea Gravel, 4-Inch Shock Tube)

The first gauge station was at a penetration of 0.22 foot. As a result the magnitude of the pore air pressure at shallower penetrations is not known. Additional research is needed to clarify the effect of quasi-static pressure on the pore air pressure at shallow penetrations. The data did not show evidence of the build-up of quasi-static pressure. In instances where the data points lie above the established curves, evidence in the following sections shows the gauge to be measuring a combination of soil and pore air pressure caused by the screen which covers the gauge having been forced back onto its sensing element.

Input Wave Shape

Figure 6 shows a typical trace from a monitor gauge in the air-test section ahead of the upstream end of the sample. Three possible input pressures could be used in analyzing the data. In order of increasing magnitude, these are 1) the incident pressure, 2) the reflected pressure, and 3) the pressure resulting from the cold gauge, represented by the peak of the curve.

The first two points need no explanation, but the third requires clarification. When the membrane breaks, two distinct fronts develop and each travels at a different velocity. The faster of these fronts, the hot-air front, results from the air originally in front of the membrane being compressed, and it travels at shock velocity. The cold-air front, resulting from the expansion of the air in the combustion chamber, travels at the particle-flow velocity.

Consequently, the monitor gauge first registers the initial passage of the hot-gas front. Before any decay can take place, the hot-gas front has reflected from the upstream end of the soil sample, and this reflected pressure is applied to the monitor gauge. Finally, before significant decay of the initial reflected pressure can occur, the gauge also feels the reflected pressure due to the cold gas. Since the cold gas has the same particle velocity but a higher density than the hot

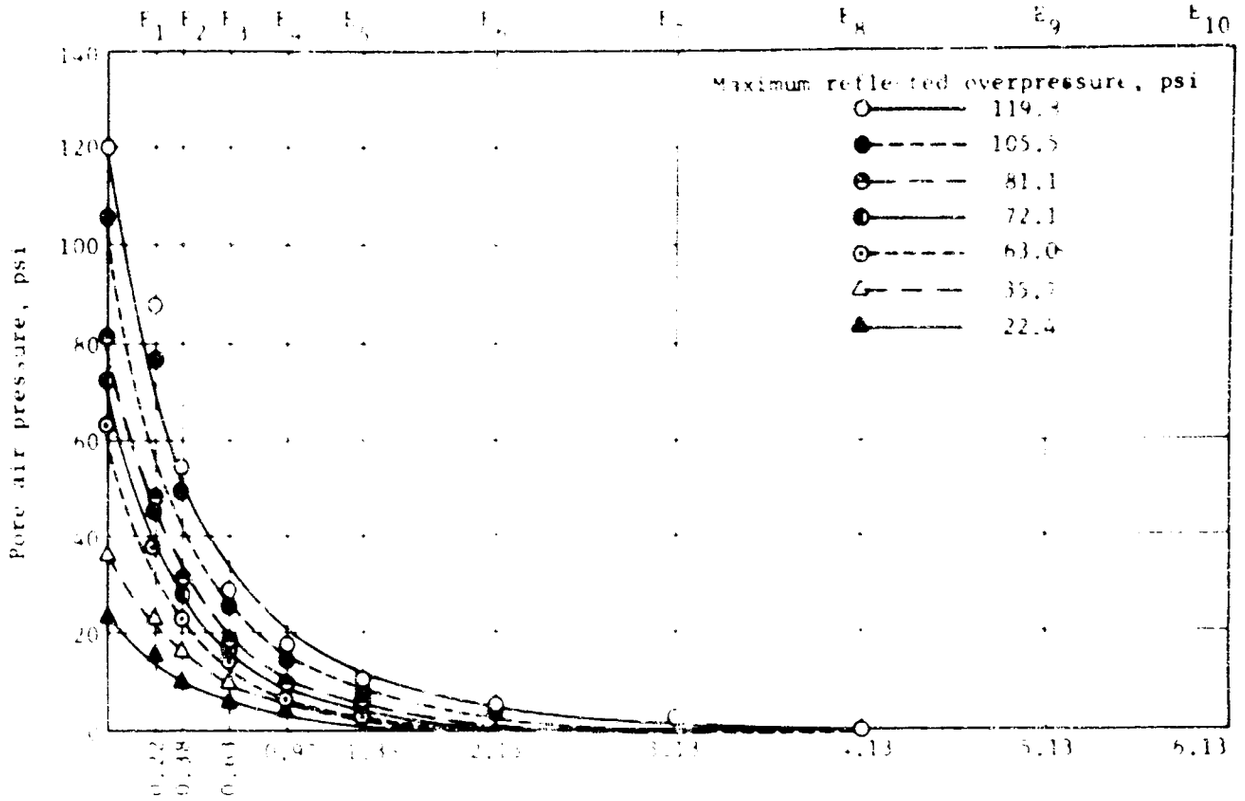
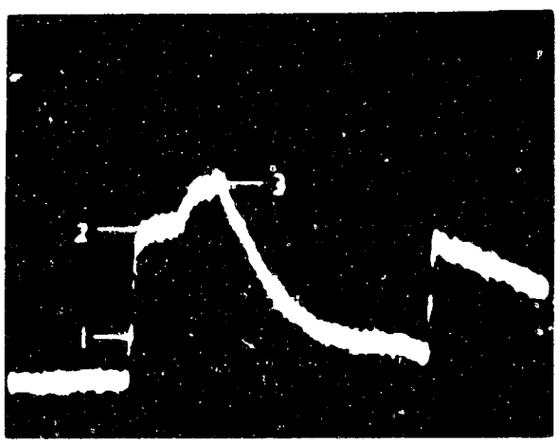


Fig. 5 Pore Air Pressure Vs. Penetration (Ottawa Sand, 4-Inch Shock Tube)

gas, it reflects to a higher pressure. The maximum pressure reflected by the monitor gauge is considered to be the input to the soil sample and will be known as the overpressure or reflected overpressure. The maximum reflected pressure was chosen as a reference because it was felt that it would relate more closely to the pore air pressure as measured at each gauge station.

The upstream section of the 4 inch shock tube represents a confined column. As a result, the shock wave reverberates in, approximately, a 30-msec cycle. Therefore, in establishing the relationship between pore air pressure and penetration, only the maximum pressure occurring in the first 30 msec after the onset of the pulse was considered.

In Figure 7, one can observe the change in shape of the pressure versus time curve of the air pressure resulting from the shock penetrates the sample. Even at a penetration of 0.22 foot the initial air shock has degenerated into a slow-rising pressure pulse (rise time of approximately 9 msec for the trace shown). For a penetration of 1.38 feet the rise time is more than twice that at a penetration of 0.22 foot, while the peak pressure has decreased, approximately, by a factor of ten. Although the data shown are for Ottawa sand, the general pattern is similar for the other soils tested.

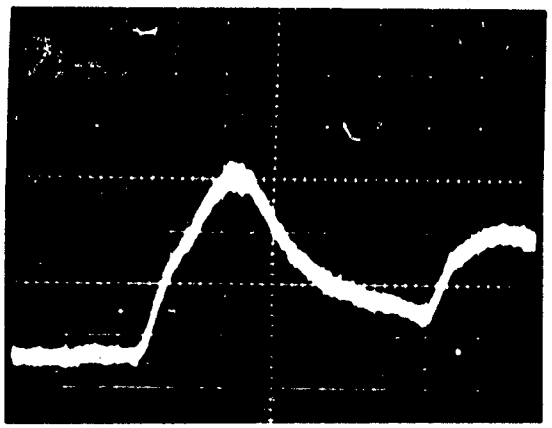


Sweep speed: 5 msec/cm
Vertical sensitivity: 100 mv/cm
Maximum pressure: 64.4 psi

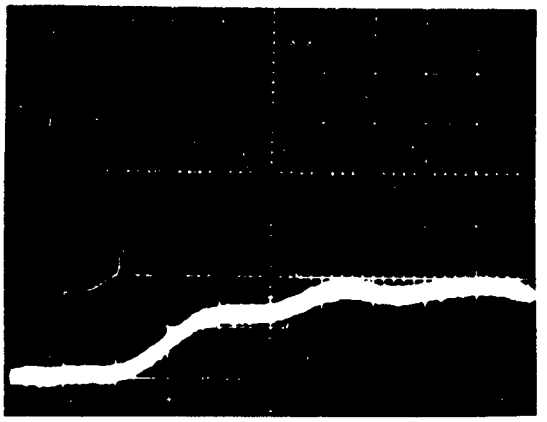
Fig. 6 Typical Air-Monitor Gauge Traces Showing Shape of Input, Pressure-Wave Form

Figures 6 and 7 also clearly show the effect of the closed, upstream end of the shock tube. One can readily see that the sample was being subjected to a reflected wave. As a result, in analyzing the data, only the first 30 msec were considered valid. This was especially important for those records on which the time of arrival of the reflections could not be discerned. This normally occurred at penetrations of 3.13 feet, but for relatively low incident pressures, it also took place at penetrations of 2.13 feet.

At least two tests were conducted at each overpressure level to check the repeatability of the data. If reasonable agreement was not obtained between the two, an additional test was conducted.



(a) Penetration, 0.22 ft.
Sweep speed: 5 msec/cm
Vertical sensitivity: 100 mv/cm
Maximum pressure: 37.9 psi



(b) Penetration, 1.38 ft.
Sweep speed: 10 msec/cm
Vertical sensitivity: 100 mv/cm
Maximum pressure: 3.2 psi

Fig. 7 Wave Shape at Penetrations of 0.22 and 1.38 Feet (Ottawa Sand, 4-Inch Shock Tube)

In all tests the maximum pressure on the upstream end of the sample (zero penetration) was assumed to be the same as that recorded by the input air-monitor gauge (2.5 inches ahead of the upstream end of the sample).

Pea Gravel

The data obtained from the testing of the pea gravel in the 4 inch shock tube are shown in a plot of measured pore air pressure versus penetration (distance from the upstream end of the sample).

As can be seen from Figure 4, most data for penetrations of 0.22 and 0.38 foot (gauge stations E-1 and E-2, respectively) appear significantly above the appropriate curve. The data show that in practically all cases with a penetration of 0.22 foot, the maximum pore air pressure exceeds the maximum overpressure.

To check the validity of these data, a series of tests were run on pea gravel and on Ottawa sand with a plastic membrane over the upstream end of the sample. In these tests the maximum possible pressure at the surface of the membrane was 125.5, 93.0, or 38.4 psi. In each case, it was found that the first three gauges (stations E-1, E-2, and E-3 which were, respectively, 0.22, 0.38, and 0.63 foot from the end of the sample) recorded a pressure.

The measured pressures could be caused by one of the following phenomena: 1) an increase in pore air pressure due to volume decrease under the applied overpressure, 2) the gauge's measuring the results of soil pressure and pore air pressure, or 3) a high-frequency shock generating on the other side of the membrane and quickly decaying. Because of the magnitude of the measured pressure at 0.22 foot penetration (approximately 12 psi for a maximum pressure at the upstream end of 126 psi) and because the membrane was in intimate contact with the sample, phenomena 1 and 3 are of no importance to this study. It can thus be concluded that the gauges were overregistering, principally because the soil pressed against the sensing element. The data discussed in this phase were obtained from barium titanate gauges without grommets.

It appears that beginning at station E-4, 0.97 foot from the upstream end of the sample, the gauges were reading only the effect of air pressure. Also, for the readings obtained at gauge station E-3 with 0.63 foot penetration, the values of measured pore air pressure were not significantly affected by the soil pressing against the sensing element. Approximately 126 psi on the surface of the sample produced a maximum pressure reading of approximately 3 psi at station E-3 when the upstream end of the sample was covered with a membrane.

As a result of the findings indicated above and in drawing the curves of Figure 4, the data collected at stations E-1 and E-2 were suspect (penetrations equal to or less than 0.38 foot). Therefore, those portions of the curves for a penetration of less than 0.38 foot were based on the shape of the curves at a greater penetration, i.e., assuming the data obtained from stations E-3 to E-9 to be valid and using the data from stations E-1 to E-2 as an upper bound.

The data for overpressures of 126.1 and 20.4 psi do not follow the aforementioned pattern. The reason in the case of the 126.1 psi shots is that they were the first two tests in which these gauges were used, and the space between the sensing element and the screen was sufficient to prevent the registration of significant soil pressure. With regard to the data from the 20.4 psi shot, the lateral effective stress in the soil was not sufficient to produce soil pressures of a detectable magnitude, due to the isolation of the gauge.

From Figure 4 it can readily be seen that the excess pore air pressure produced by the air shock striking the sample initially decays quite rapidly. For example, by the time the pore air pressure reaches station E-5, it has attenuated a minimum of 67 percent. However, the remaining 33 percent requires an additional 4.4 feet for essentially 100 percent

attenuation. The initial 67 percent attenuation is accomplished in less than 1.38 feet. The data indicate that, under the conditions of these tests, the pore air pressure in the sample will not be significantly effected by the shock wave at distances greater than 6.13 feet.

The data presented in Figure 4 have been replotted in Figure 8. The latter established the relationship between the

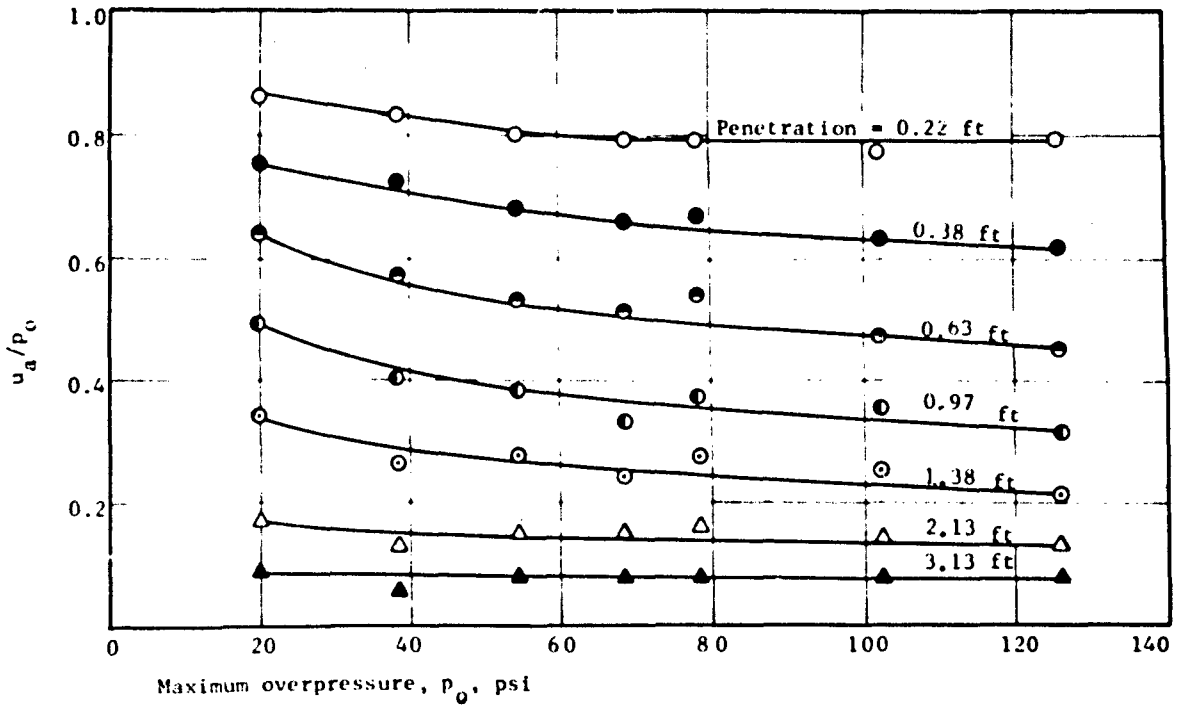


Fig. 8 u_a/p_o Vs. Maximum Overpressure, p_o (Pea Gravel, 4-Inch Shock Tube)

pore air pressure/overpressure ratio, u_a/p_o, and overpressure for a given penetration.

The shape of the curves is interesting. It implies that for large overpressures the pore air pressure/overpressure ratio reaches a constant value. In the case of the pea gravel, such a condition leads to the hypothesis that the rate of attentuation with penetration is independent of overpressure--at least at the higher overpressures of the test. The data cited above agree with data that Crist (5) obtained from tests on rock filters.

Table 5 shows the relationship between the attenuation factor and air pressure on the upstream face. The attenuation factor, F, was computed as follows:

$$F = \frac{p_m - u_a}{p_m} (100) \qquad (2)$$

where p_m is the maximum air pressure on the upstream face of the sample, as measured 2-1/2 inches from the upstream end of the sample;

u_a the gauge reading at a specific location along the length of the sample; and

F the attenuation factor (expressed as a percentage).

It should be noted that the attenuation factors shown in Table 5 are based on the curves of Figure 4. Table 5 also shows that, for the conditions of the test described, the attenuation factor is not greatly effected by overpressure and, as a first approximation, may be considered independent of overpressure. The maximum value of the standard error of the mean, as a percentage of the mean, is approximately 12 percent. Nevertheless, one should recognize that there is a tendency toward a slight increase in the attenuation factor with an increase in overpressure.

The magnitude of the increase in the attenuation factor with overpressure can be ascertained from Figure 9. In this figure two curves are shown for the pea gravel, representing overpressures of 126.1 and 20.4 psi. The vertical separation of the curves is relatively small and lends credence to the assumption that, as a first approximation, the attenuation factor can be considered independent of overpressure.

Table 5

AVERAGE ATTENUATION FACTORS (PEA GRAVEL)

Gauge location	Penetration (ft)	Maximum overpressure at upstream end (psi)							Std. error of mean (psi)	Percentage of mean
		20.4	38.9	54.2	68.5	78.8	102.5	126.1		
E-1	0.22	21.6	25.4	26.2	27.0	27.2	29.8	27.7	2.5	9.5
E-2	0.38	26.5	31.9	29.9	35.1	35.3	37.6	36.0	3.9	11.7
E-3	0.63	30.9	41.7	48.4	49.7	49.3	51.2	52.6	4.3	9.3
E-4	0.97	51.0	60.0	62.0	64.6	62.1	63.0	65.7	4.9	8.0
E-5	1.38	67.7	74.5	74.0	76.2	73.2	75.4	77.6	3.2	4.3
E-6	2.13	82.4	85.9	84.1	83.6	84.0	86.0	86.4	1.5	1.8
E-7	3.13	92.1	93.0	91.9	90.9	90.3	92.0	91.5	0.9	1.0
E-8	4.13	98.3	97.5	96.0	95.3	94.9	95.1	95.2	1.3	1.4
E-9	5.13	100.0	100.0	99.0	98.6	98.1	98.0	98.4	0.8	0.8

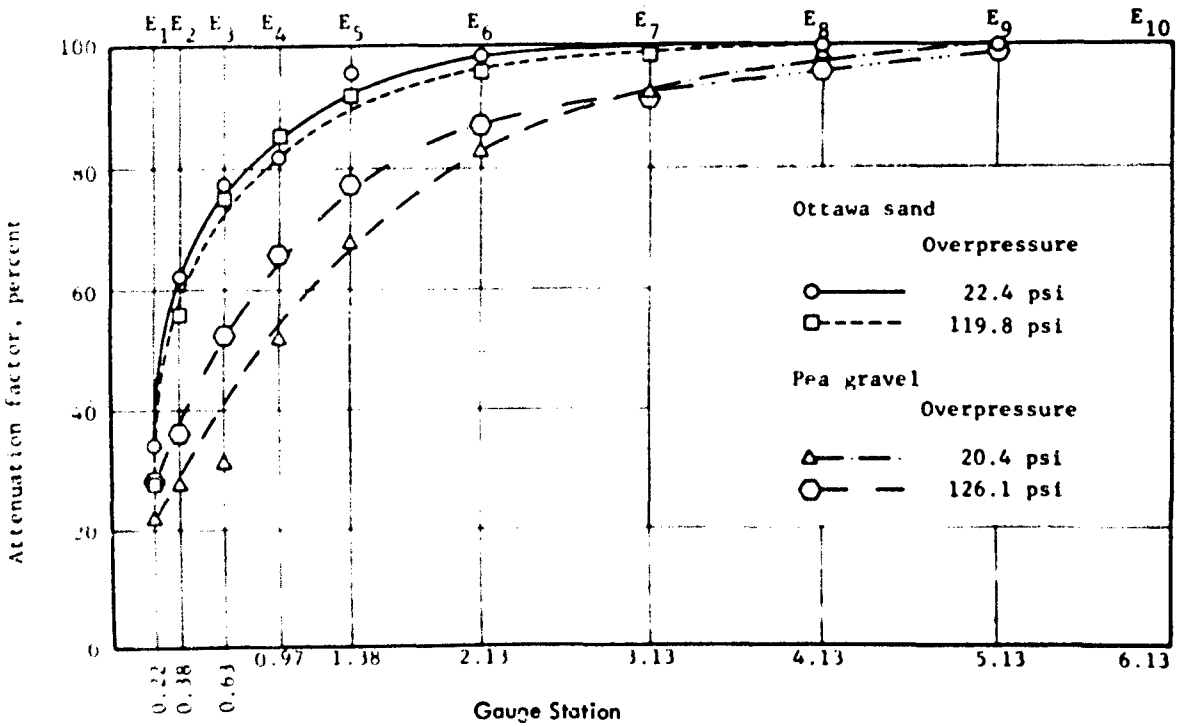


Fig. 9 Attenuation Factor Vs. Penetration (4-Inch Shock Tube)

Figure 10 is a plot of pore air pressure versus maximum reflected overpressure. For the range of overpressures tested, this relationship can be considered linear. However, the trend of the last two data points suggests that this linearity may not extend to higher overpressure levels.

The curves of Figure 10 should have a zero intercept on the Y-axis, but such is not the case. The reason for the discrepancy may be due to experimental error or the physics of the system, i.e., the linearity does not persist for low values of overpressure.

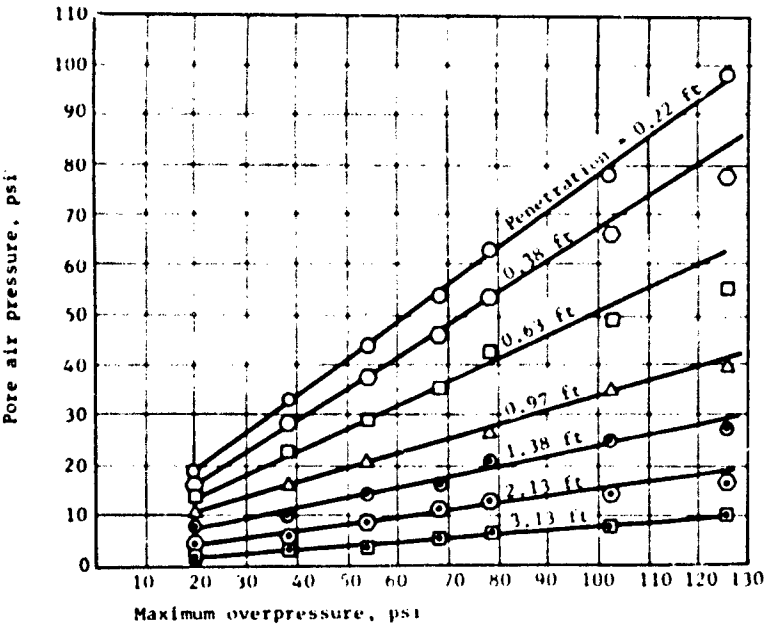


Fig. 10 Pore Air Pressure Vs. Maximum Overpressure -- Penetration Constant (Pea Gravel, 4-Inch Shock Tube)

Figure 11 is a plot of unit impulse (impulse per unit area) versus time--air-shock monitor gauge--for the pea gravel. It is apparent that as overpressure (maximum reflected pressure) increases, the unit impulse, at any given time after the onset of the shock wave, also increases. In addition, as the magnitude of the elapsed time increases, the effect of overpressure on the unit impulse also increases.

The unit impulse is a measure of the energy which is producing the flow of air through the pores of the soil. As might be expected, the higher the overpressure, the more energy. However, from Figure 4, it is evident that the effect of unit impulse dissipates rapidly with penetration; for example, the separation between the curves becomes small. It appears that unit impulse effects the magnitude of the pore air pressure to a significant degree, but only at shallow penetrations. In all probability, unit impulse would also effect the distance of penetration, but the magnitude of penetration cannot be ascertained from the data.

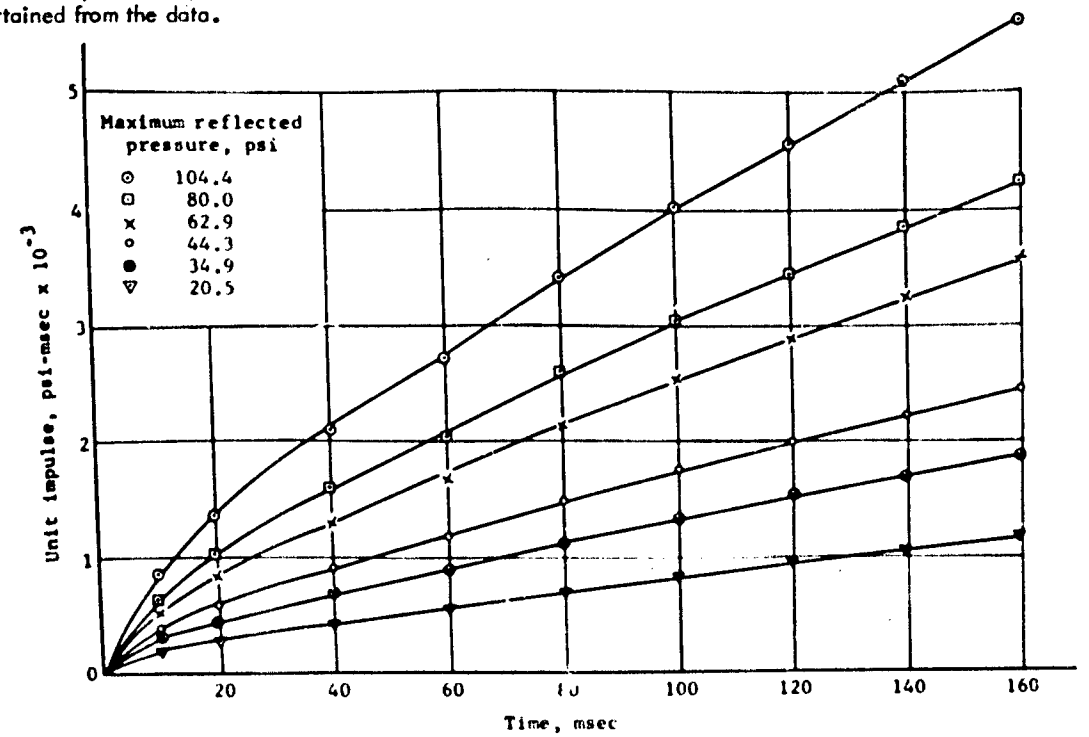


Fig. 11 Unit Impulse Vs. Time (Pea Gravel)

Figure 12 is a plot of maximum reflected pressure versus unit impulse. The relationship is linear within the limits of experimental error. It should be noted that the unit impulse under the first cycle of loading (approximately 30 msec) is much less than that at a time of 160 msec. This indicates that the reverberating shock wave maintains a large portion of its initial energy over the indicated period.

Ottawa Sand

Figure 5 is a plot of pore air pressure versus penetration for the Ottawa sand. This figure shows that the rate of attenuation of pore air pressure produced by an air shock is very high in dense Ottawa sand. Also, on the basis of the data collected and for the test conditions previously stated, a length of sample of approximately 4.13 feet would reduce the incident pore air pressure to zero.

The data in Figure 5 are plotted in a different manner in Figure 13. With the exception of the data for penetrations of 0.97 and 1.38 feet, the trend, as noted for the pea gravel, is toward a constant value of u_d/p_o for large overpressures. This implies that u_d/p_o is independent of overpressure for large values of the latter.

Table 6 presents the relationship between attenuation factor and depth of penetration. From this table one can conclude that as a first approximation the attenuation factor for a given penetration can be considered independent of overpressure. This statement is validated by the two curves for Ottawa and shown in Figure 9. They represent overpressures of 22.4 to 119.8 psi, yet their separation is a maximum of two on the attenuation-factor scale.

The values of attenuation factors shown in Table 6 for station E-1 at overpressures of 105.5 and 119.8 psi are much too low for penetrations of 0.22 and 0.38 foot. The reason is that the measured pore air pressures for these conditions were in error (too high). This error was probably caused by the screen covering the gauge being forced onto the sensing element.

As previously mentioned in the discussion of the results of tests on the pea gravel, it was thought that the possibility of the gauge measuring a combination of soil pressure and air pressure had been eliminated by the use of the screen-covered grommets. It proved to be a reasonable assumption, except for stations E-1 and E-2 at overpressures greater than 100 psi.

The validity of the previous statement is supported by Figure 14 which is a plot of maximum overpressure versus pore air pressure for a given penetration. The data points are plotted along straight lines except those for gauge stations E-1 and E-2 at pressures greater than 100 psi.

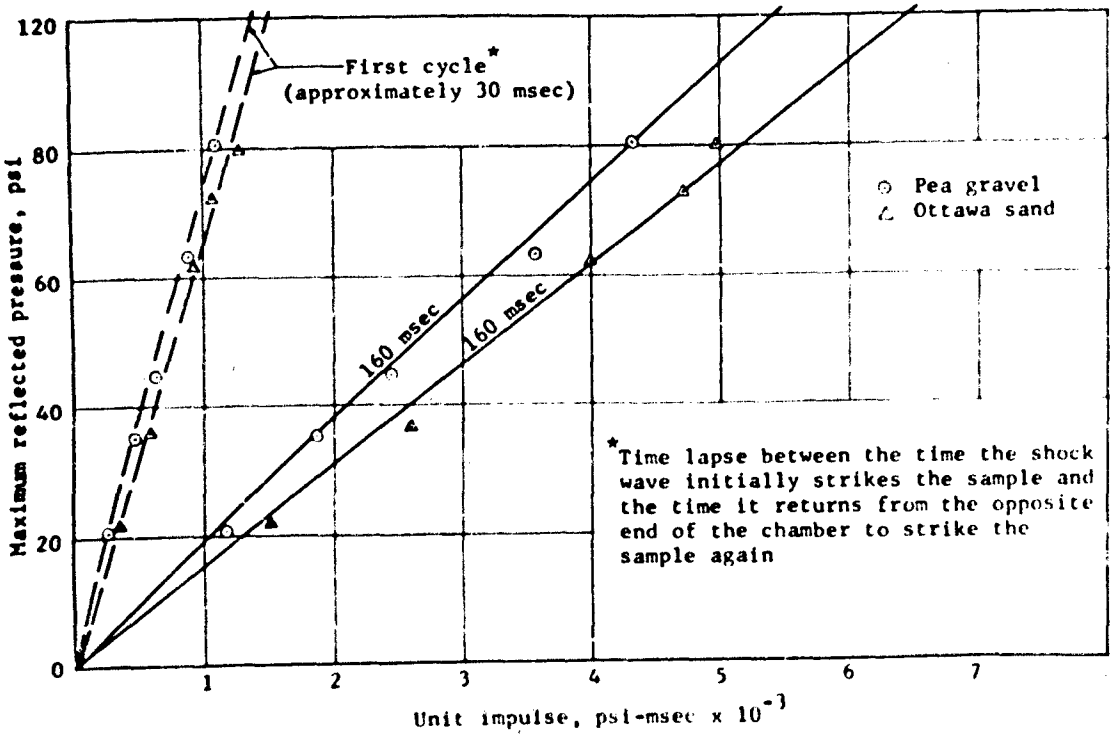


Fig. 12 Unit Impulse Vs. Maximum Reflected Pressure (Overpressure)

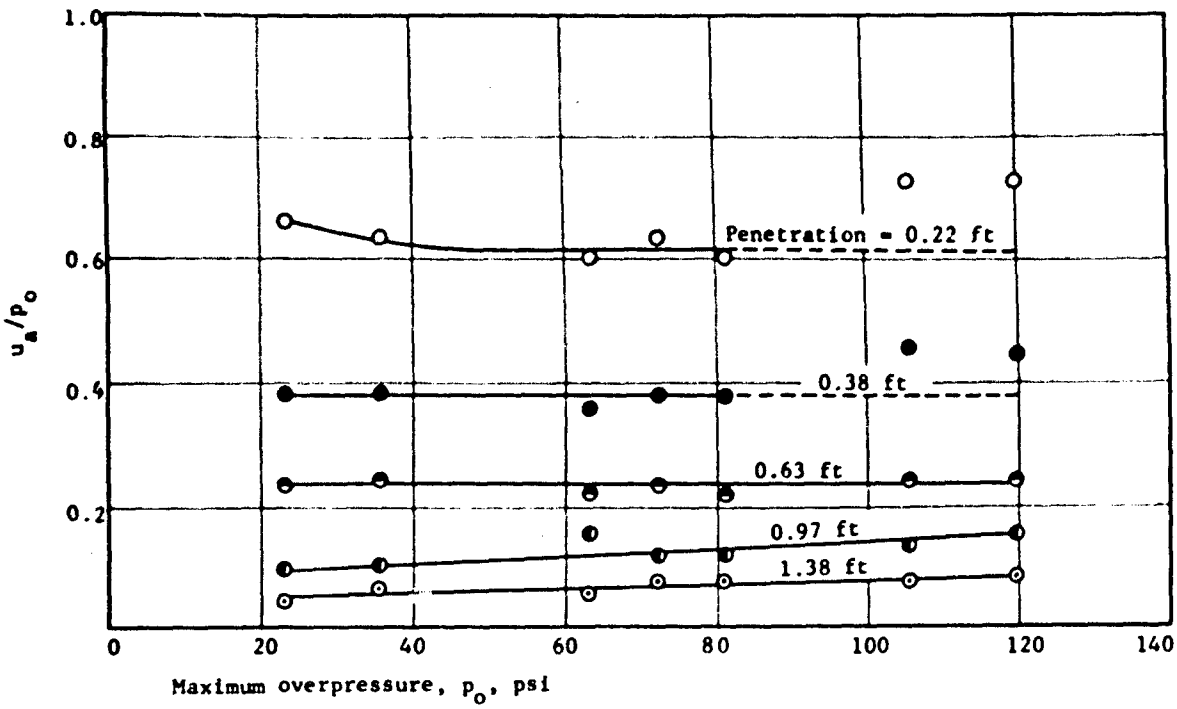


Fig. 13 u_a/p_o Vs. Maximum Overpressure, p_o (Ottawa Sand, 4-Inch Shock Tube)

Table 6

AVERAGE ATTENUATION FACTORS (OTTAWA SAND)

Gauge location	Penetration (ft)	Maximum air pressure at upstream end (psi)							Std. error of mean (psi)	Percentage of mean
		22.4	35.7	63.0	72.1	81.1	105.5	119.8		
E-1	0.22	34.0	37.2	39.8	37.0	40.2	27.2	27.0	5.4	15.6
E-2	0.38	62.0	58.7	63.7	61.9	61.9	54.2	54.9	3.8	6.4
E-3	0.63	77.2	76.2	77.6	77.2	77.7	75.6	77.0	0.8	1.0
E-4	0.97	81.7	79.9	84.5	87.6	87.9	86.8	85.5	3.1	3.7
E-5	1.38	95.5	93.8	94.9	93.0	92.6	92.9	91.6	1.3	1.4
E-6	2.13	98.2	97.1	98.1	97.2	97.0	95.6	95.6	1.1	1.1
E-7	3.13	--	--	--	99.5	99.0	98.1	98.3	--	--
E-8	4.13	100.0	100.0	100.0	100.0	100.0	100.0	100.0	--	--
E-9	5.13	100.0	100.0	100.0	100.0	100.0	100.0	100.0	--	--

Figure 15 is a plot of unit impulse versus time for tests conducted on Ottawa sand. The data were obtained by integration of the pressure-time histories of the monitor gauges. It is evident that the maximum reflected pressure (overpressure) has a pronounced effect on the unit impulse at any given period of time following the onset of the shock wave. This effect of maximum overpressure increases with time as indicated by the increased separation of the curves with time.

In comparing Figure 11 for the pea gravel and Figure 15 for the Ottawa sand, it can be seen that the curves, for a given maximum reflected pressure, for the Ottawa sand lie above those for the pea gravel. This indicates that in the Ottawa sand less air is being forced into the pores of the soil. To express this another way, the Ottawa sand provides a better reflecting surface for the shock wave.

This fact is also borne out by Figure 12 in which maximum reflected pressure is plotted against unit impulse for both the Ottawa sand the pea gravel. The Ottawa sand curves always lie to the right of those for the pea gravel. In addition, the separation of the curves increases with time, as would be expected.

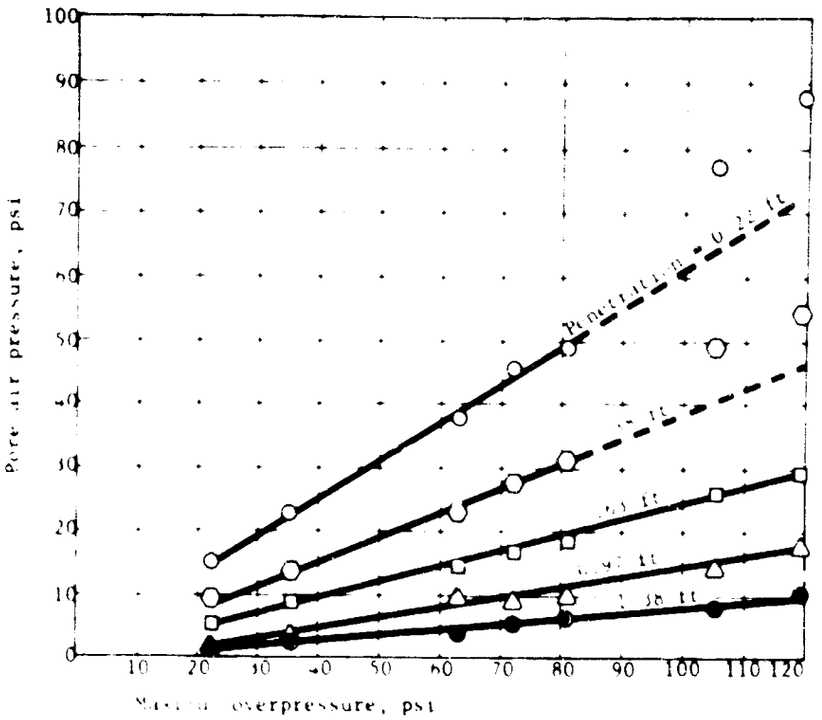


Fig. 14 Pore Air Pressure Vs. Maximum Overpressure--Penetration Constant (Ottawa Sand, 4-Inch Shock Tube)

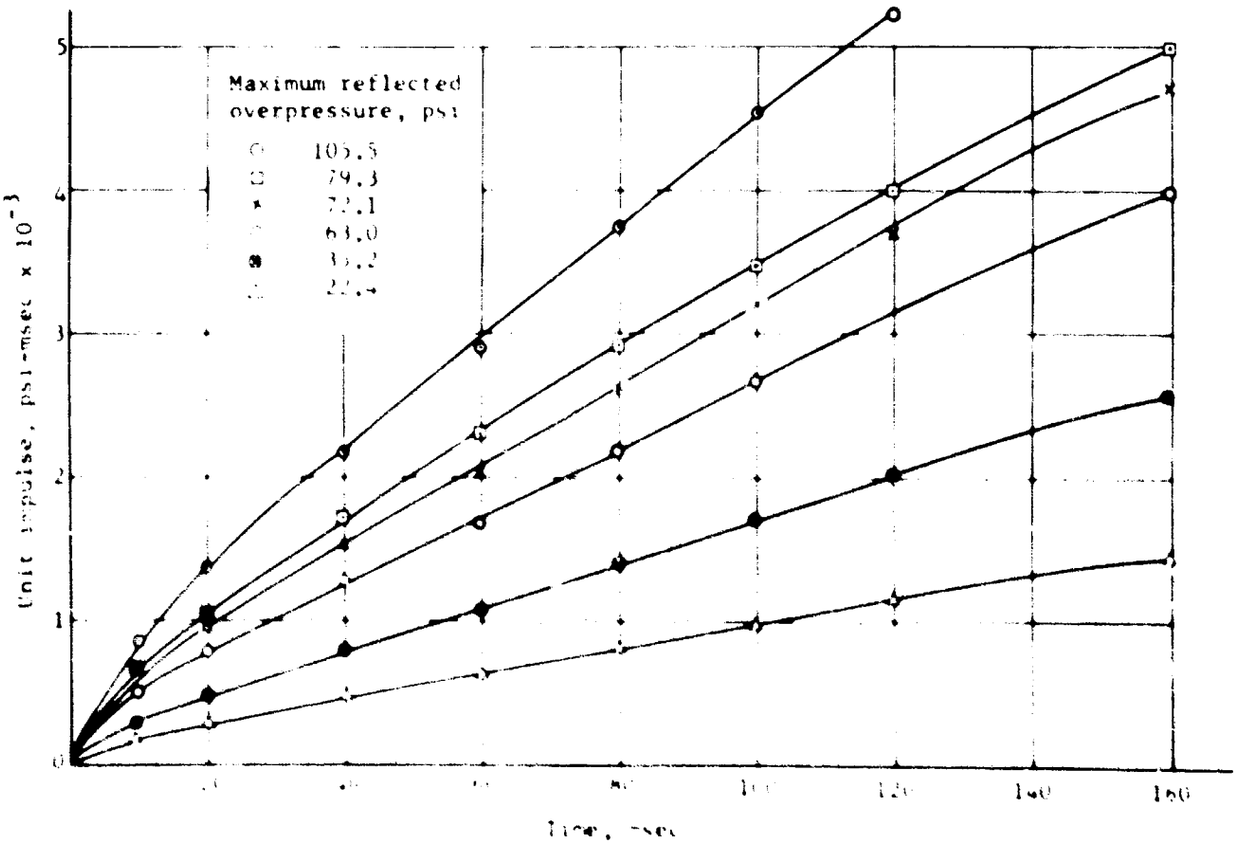


Fig. 15 Unit Impulse Vs. Time (Ottawa Sand)

Silty Sand

Tests were conducted on the silty sand, and the data are summarized in Table 7. From Table 7 it is apparent that no significant pore air pressures were generated in the samples of silty sand as a result of a maximum overpressure of approximately 122 psi.

As a result of the above it can be concluded that, for the test conditions previously stated, the magnitude of the pore air pressure generated in samples of the silty sand is negligible. In addition, the length of penetration of the pore air pressure resulting from an overpressure at the surface of the ground will also be negligible.

Table 7

SUMMARY OF PORE AIR PRESSURE ON SILTY SAND

Maximum overpressure (psi)	Void ratio	Pore air pressure (psi) Penetration (ft)		
		0.22	0.38	0.63
122.5	0.66	0.80	0.80	0.20
108.0	0.59	1.20	0.76	0.00
122.5	0.77	0.80	1.00	0.90
62.0	0.59	0.49	0.00	0.00
44.0	0.59	0.00	0.00	0.00

DISCUSSION OF RESULTS

The principal factors which could possibly effect the magnitude and attenuation of pore air pressures in soil samples are peak overpressure, wave shape, total impulse per unit area, positive-phase duration, permeability, distance of penetration, and degree of saturation. Due to the limitations of the test setup, only the effects of peak overpressure, total impulse per unit area, and permeability could be ascertained.

Based on Figures 4 and 5, it is apparent that the effect of peak overpressure (in this case, maximum reflected pressure) is very pronounced at shallow penetrations. This is evidenced by the decreasing distance of separation of the curves with penetration.

A comparison between Figures 4 and 5 gives an appreciation of the effect of void ratio and particle size. The pea gravel has a larger particle size and void ratio than the Ottawa sand. This means that its resistance to fluid flow is less, which is evident from its greater permeability ($k \approx 0.240$ cm/sec). The permeability of the Ottawa sand is approximately 0.060 cm/sec. The effect of the difference in particle size and void ratio is evidenced by the fact that it takes penetration of approximately 6 feet of pea gravel to reduce an overpressure of approximately 126.1 psi to zero, while a penetration of approximately 4 feet of Ottawa sand will accomplish the same effect.

Figures 11 and 15 show the variation of unit impulse with time and overpressure. It is apparent that large differences in unit impulse occurred with overpressure. However, due to the fact that the pore air pressure versus penetration curves converge rapidly with penetration, unit impulse must exert its maximum effect at shallow penetrations. It is also possible that unit impulse effects the distance of penetration to a significant degree for a given magnitude of overpressure. The data are not sufficient to clarify this point.

The data have proved that pore air pressures will penetrate large distances in air-dry soils with coefficients of permeability greater than or equal to 0.060 cm/sec. In addition, for soils with permeabilities equal to or less than 9.71×10^{-5}, the penetration for overpressures up to 126.1 psi will be less than 6 inches, and the magnitude of the pore air pressure will be negligible.

In fully saturated soils, the air attempting to enter the voids would create large pore water pressures; and in partially saturated soils, large pore air and pore water pressures would be produced. In either case, the stress state of the soil would be significantly altered; and, with present knowledge, it is not possible to evaluate that change.

To conduct tests from which understanding of soil-structure interaction phenomena can be obtained, it is necessary to use air-dry soil and to prevent the air in the shock wave from entering the soil. This can be accomplished by placing a membrane over the soil.

An attempt was made to determine the velocity of propagation of the shock wave and the change in velocity as the air passed through the soil sample. Unfortunately, it was not possible to do this with the desired degree of accuracy, as is evidenced by the fact that velocities as low as 250 fps were calculated for penetrations of 0.38 foot. This velocity was determined by dividing the distance between stations E-1 and E-2 (0.16 foot) by the difference in time of arrival of the wave at these two stations.

The velocity of propagation of the shock wave should at least equal the velocity of sound in air (approximately 1100 fps). Consequently, the low velocities are due either to the properties of the soil or the sensitivity of the recording system. The tortuosity of the flow path makes the distance traversed by the air much greater than the distance between adjacent gauges. In addition, the gauges may not be sensitive enough to register the first arrival of the air shock.

Regardless of the degree of accuracy of the calculated velocities, it is evident that the air forced into the soil as a result of a shock wave at the surface will travel much slower than the peak stress wave in the soil.

LIMITATIONS OF THE TEST SETUP

Boundary Effects

Since the diameter of the soil sample was small, the effect of wall friction had to be considered. Undoubtedly, sidewall friction effected the flow of air along the boundary of the soil sample. But since friction loss resulting from the roughness of the tube wall was less than that caused by the air flowing through the pores of the soil, the wall of the soil-test section did not adversely effect the flow of air at the boundary between the soil and the tube.

Another point to consider is the effect of friction between the soil and the wall of the soil-test section. This friction would reduce the magnitude of the volume decrease under a given overpressure, as a result of the arching phenomenon.

Since it has been proved (in tests conducted with a membrane over the upstream end) that the magnitude of the pore air pressure resulting from volume change is negligible, any further decrease in its magnitude is of no consequence.

Relative Density

One density state was used in the testing of the Ottawa sand and the pea gravel due to limitations of the test setup. It was impossible to make a sample of these soils in a medium-dense or loose state and still be certain at the time of testing that no significant volume change had occurred. Testing was therefore confined to soil in the dense state.

Gauge Isolation

The air gap between the sensing element and the screen which isolates the gauge from the soil had an effect on the data. Because this chamber has to fill, the rise time to maximum pressure increases while the maximum pressure decreases. But since the volume involved is small (less than 0.005 cu in.), since there is a large number of pores feeding the chamber, and since the transit time of the wave across the face of the gauge is minuscule, it was felt that the cavity did not significantly effect the data either quantitatively or qualitatively.

CONCLUSIONS

Based on the information reported on air-dry, uniformly graded, granular soils of high relative density, certain relationships became apparent. The most significant are as follows:

1. For the overpressure range tested, soil densification added little to the measured pore air pressure. Although the data are valid only for dense, granular soils over a relatively small overpressure range, it is felt that even for much higher overpressures and looser soil conditions the contribution of densification to the measured pore air pressure would still be negligible.
2. For all practical purposes, the rate of attenuation of pore air pressure may be considered, as a first approximation, to be independent of overpressure. The attenuation factor is primarily a function of the size of the pores and the depth of penetration. This conclusion is supported by the work of Crist (5) who, in studying the use of rock filters as blast attenuators, found that the rate of attenuation of air pressure with distance of penetration is independent of overpressure for a side-on orientation and a pressure range of 30 to 100 psi.
3. Initially, the rate of attenuation of pore air pressure is very high. This is caused by a large quantity of air being forced into the pores of the soil in a short period of time. The result is to increase effectively the resistance of the soil to the flow of air. However, with increased penetration, the rate of flow of air decreases as, correspondingly, the resistance to flow decreases. Therefore, the rate of attenuation decreases markedly with penetration.

This conclusion is supported by Reference 5 which discusses pressure attenuation through a rock filter as an increasing function of flow velocity.

4. The most important factors effecting the magnitude of the pore air pressure at a given point in a mass of soil are prototype peak overpressures, shock-input wave shape, permeability, and depth of penetration.
5. The effect of peak overpressure and wave shape is of prime importance at shallow depths. As penetration increases, the effect of these variables on the measured pore air pressure decreases rapidly.
6. In coarse-grained, uniformly graded soils, pore air pressures which result from an overpressure at ground surface can be of significant magnitude. Furthermore, the distance of propagation may be appreciable.
7. In well-graded soils, comparable to the silty sand tested, both the magnitude and the depth of penetration of the pore air pressure generated as a result of a shock wave at ground surface would be of no consequence.
8. As the average particle size of a soil increases, the magnitude of the pore air pressure at a given point increases, as does the depth of penetration. In other words, as the size of the pores increase, the magnitude of the pore air pressure at a given point and the distance of propagation increase.

9. Changes in unit impulse, for a given overpressure, do not significantly effect the measured pore air pressure in deep penetrations; in shallow penetrations, such changes can be significant.
10. The velocity at which the pore air penetrates the ground will be significantly less than the propagation velocity of the effective stress wave.

RECOMMENDATIONS FOR FUTURE RESEARCH

Much more work needs to be done before the phenomena involved in the propagation of pore air pressures in soils subjected to a shock wave can be fully understood. It is therefore recommended that work in the following areas be undertaken to determine:

1. The effect of long-duration shock waves on the propagation and attenuation of pore air pressures in soils.
2. The effect of high pressures on the propagation and attenuation of pore air pressures in soils.
3. The propagation and attenuation of pore air and pore water pressures in partially saturated soils.
4. The effect of wave shape on the propagation and attenuation of pore air pressures in soils.
5. Pore air pressures at depths less than 3 inches.

ACKNOWLEDGEMENTS

This paper** is based on an experimental investigation conducted at the Air Force Shock Tube Facility operated by the University of New Mexico.

The staff members of the Air Force Shock Tube Facility who contributed to this report are too numerous to mention. However, the author is especially indebted to Dr. Eugene Zwoyer, Director of the Shock Tube Facility; Mr. Robert A. Crist, Research Associate Engineer; Mr. Dwane Brewer, Research Associate Engineer; and Mr. Billy C. Brewer, Electronic Technician.

The discussion of this research with Mr. George N. Sisson, Chief of the Professional Advisory Services Branch, Office of Civil Defense, Department of Defense (formerly Technical Adviser, Protective Structures Division, Air Force Weapons Laboratory, Kirtland Air Force Base, New Mexico) and his constructive criticism are gratefully acknowledged.

REFERENCES

1. Bishop, A. W., "The Measurement of Pore Pressure in the Triaxial Test," Proceedings, Conference on Pore Pressure and Suction in Soils, Butterworth's, England, 1961 (Conference held in March 1960).
2. Terzaghi, K., Theoretical Soil Mechanics, John Wiley and Sons, New York, 1943.
3. Seed, H. B. and R. W. Clough, "Discussion of a Paper on Earthquake Resistance and Sloping Core Dams," Journal of the Soil Mechanics and Foundations Division, ASCE, Vol. 90, No. SM2, pp. 169-170, March 1964.
4. Lanza, F. J. and C. W. Hicks, "The Calibration and Interpretation of Recorded Shock-Tube Pressure Data Using Piezoelectric Sensors," Air Force Shock Tube Facility, University of New Mexico, RTD-TDR-63-3073, Albuquerque, New Mexico, November 1963.
5. Crist, R. A., "The Use of Rock Filters to Attenuate Air Shocks," Air Force Shock Tube Facility, University of New Mexico, AFSWC-TDR-63-27, March 1963.

** An abridgment of a report, WL-TDR-64-3, to be published by the Air Force Weapons Laboratory, Kirtland Air Force Base, New Mexico, 1964.

PHOTOELASTIC STUDY OF WAVE PROPAGATION AROUND EMBEDDED STRUCTURAL ELEMENTS

by
W. F. Riley*

ABSTRACT

Photoelastic methods have been used extensively in recent years to determine stress distributions associated with a propagating stress wave. In this paper a series of studies are described which have been conducted to determine stresses in the free field of a two-dimensional plane and at the boundaries of embedded structural elements in the plate during passage of a stress wave. Both explosives and traveling air shocks were used to generate the stress waves. Results for circular holes and rigid circular inclusions are presented and compared with equivalent static stresses based on the free field conditions. Important conclusions are drawn regarding dynamic stress concentration factors.

INTRODUCTION

The problem of determining the state of stress in the vicinity of tunnels or various types of buried structures has long been a subject of interest for civil and mining engineers. A considerable amount of analytical and experimental effort has been expended to develop methods and techniques suitable for making static stress determinations in elastic materials around discontinuities of any shape. Analytical studies based on the theory of elasticity and experimental studies utilizing two- and three-dimensional photoelasticity methods have yielded much useful information.

In recent years considerable effort has been directed toward the design of underground structures capable of withstanding the extremely high pressures generated by nuclear explosions. Since the loads applied to the structure in this application are transient rather than static, the problem of determining stress distributions is considerably more difficult. At the present time only a limited amount of information is available on stress wave transmission characteristics in either elastic materials or soils. Similarly, the effects of stress waves, in terms of the loads they produce on buried structures, the effects of rigidity or flexibility of the structures on the effective loads, and the overall stress wave diffraction around the boundaries of the structure are in general unknown.

In an attempt to study some of the fundamental aspects of stress wave propagation in an elastic material and to obtain some information on the interaction between a propagating stress wave and discontinuities and embedded obstructions in the wave propagating medium, Air Force Weapons Laboratory has sponsored a series of experimental laboratory type programs at IIT Research Institute. In these programs dynamic photoelasticity and moire methods were developed for making full field transient stress measurements and a number of problems were solved. In the following sections of this paper results from several of the more important studies are presented and discussed. Included are:

1. stresses generated on the boundary of a circular hole in a plate by an explosive charge which is detonated on the edge of the plate, and
2. stresses generated on the boundaries of a circular hole and a rigid circular inclusion in a plate by an air shock wave moving along an edge of the plate.

The significant features of the experimental methods employed for the study can be briefly summarized as follows.

Photoelasticity Methods

A low modulus model material was employed so that the wave propagation velocities were sufficiently low to permit photographing of the associated fringe patterns with a 16 mm Fastax camera. This type of recording gives a satisfactory picture of the overall patterns for the full duration of the loading. Microflash techniques were then used to obtain large high quality photographs of the patterns in localized regions of interest at selected times after loading. A conventional diffused light polariscope was employed for all of the measurements.

Moire Methods

The moire effect is an optical phenomenon observed when two arrays of lines are superimposed. If the arrays consist of opaque parallel lines which are not identical in spacing nor orientation then fringes will form as the lines of one array fall on or between the lines of the other array. Measurements of the spacing and direction of the fringes gives sufficient information for determining differences between the arrays. In the present study the array printed on the model

* Science Advisor, Illinois Institute of Technology Research Institute, Chicago, Illinois.

was free to deform as the model was loaded. The reference array through which the model array was viewed did not deform. Once the model deformations were determined from the moire fringe patterns, the strain field at any point of interest could easily be determined.

For a detailed presentation of results of other studies and for a complete description of dynamic photoelasticity and moire methods the reader should consult several of the previously published AFSWC reports (1,2).

EXPLOSIVE STUDY

When a time dependent load is applied at a point on one edge of a semi-infinite plate, two basic waves are produced, namely dilatational waves and distortional waves. These waves propagate radially from the point of load application with velocities C_1 and C_2 respectively.

The dilatational wave is produced by radial displacements which occur at the point of load application. The photoelastic fringes associated with this wave type tend to form circular lines with the point of load application at the center. The distortional wave is produced by transverse or circumferential displacements. The photoelastic fringes associated with this wave type form a very complex pattern. Other waves are also generated as the dilatational and distortional waves propagate along the boundary of the plate. In the model material used for the study, the distortional wave velocity is only 52 percent of the dilatational wave velocity. Thus, as a stress pulse propagates, the two waves which were simultaneously generated tend to separate. In the present work an explosive with a short detonation time was selected to effect rapid separation so that the influences of both dilatational and distortional waves could be evaluated.

The model used for this study was machined from a large sheet of low modulus urethane rubber known commercially as Hysol 4485. A 5/8 in. diameter hole was machined 4 in. from the point of load application along a radial line 30° from the centerline of the plate. A sketch of the model is shown in Figure 1. The location of the hole was chosen to give the maximum time for study before reflections return from the boundary. The 30° orientation also provided a symmetric point in the same model where free field stresses could be simultaneously determined. This symmetric point was far enough removed from the hole so that any disturbance in the stress field produced by the presence of the hole did not interfere appreciably with the free field stress distribution. The 30° orientation also placed the hole in a location where the influences of both the dilatational and distortional waves were felt. If the hole were located on the centerline of the plate, the distortional wave influence would be smaller.

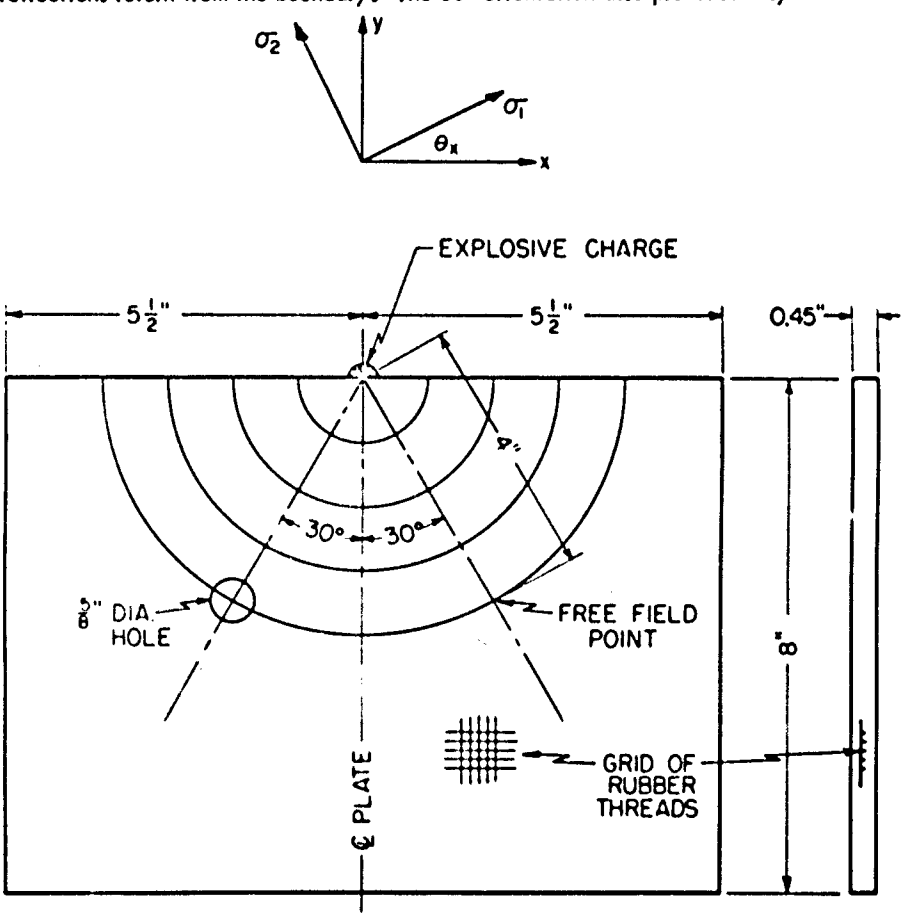


Fig. 1 Sketch of the Model Showing the Location of the Hole, and the Symmetric Free Field Point

The loading of the model was accomplished by detonating a 70 milligram charge of lead azide on the boundary. A complete photoelastic fringe pattern record was obtained using a 16 mm Fastax camera operating at 6780 frames per second. The first 20 photographs of this record are shown in Figure 2. These were the frames used in the analysis and they cover approximately 3000 microseconds. A similar series of Fastax records were obtained of the moire fringes in the region of the free field symmetric point. The printed grid used in obtaining the moire fringes in the region of the free

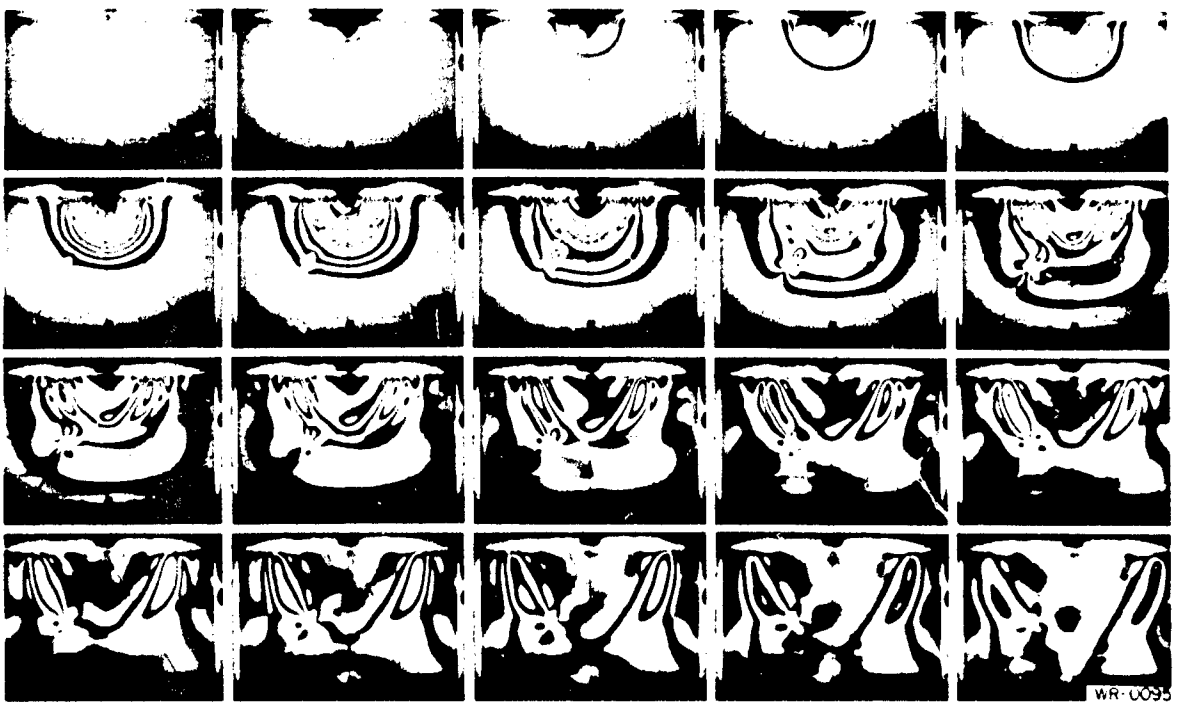


Fig. 2 Series of 20 consecutive photographs showing a compressive stress wave propagating past an open hole in a large sheet of Hysol 8705. The stress wave was generated by detonating a 70 milligram charge of lead azide on the boundary. Photographs were taken with a Fastax camera at 6780 frames per second.

field symmetric point. The printed grid used in obtaining the moire fringes had 1000 lines per inch. Typical records are shown in Figure 3. The duration of the detonation of the lead azide charge was approximately 2 microseconds. This value of the duration has been reported in the literature by Kolsky for charges of similar size.

The Fastax records were used for the free field determinations and for studying the overall wave propagation phenomena. Microflast photographs, similar to those shown in Figure 4, were used to establish the fringe order distribution on the boundary of the hole.

Ten microflash photographs were finally selected for analysis. These photographs covered the interval from 750 microseconds until

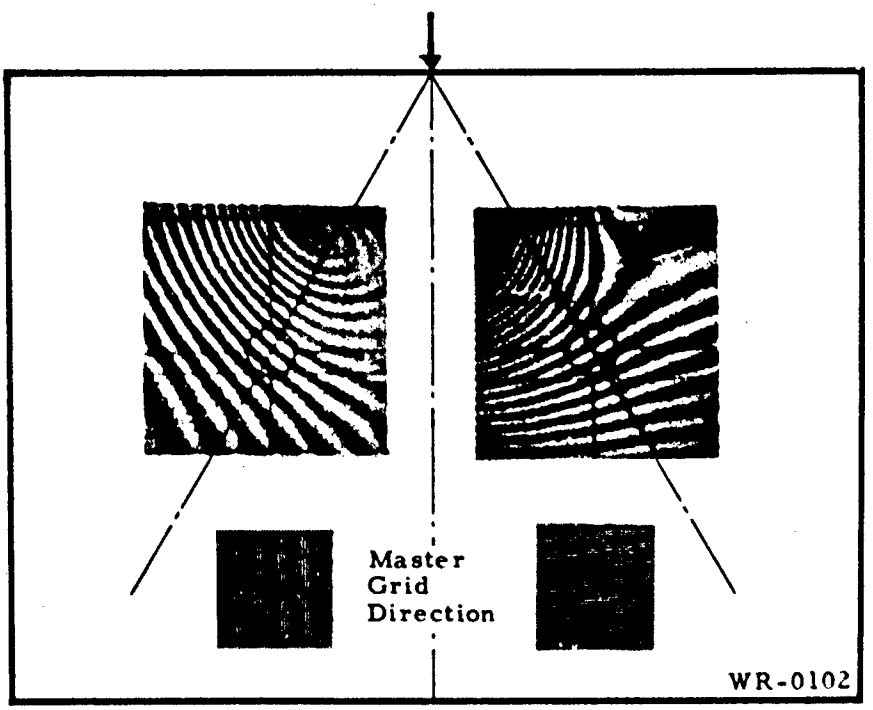


Fig. 3 Typical dynamic moire patterns obtained with the Fastax camera in the vicinity of the symmetric free field point.

2650 microseconds after the explosive charge was detonated. The beginning of the time interval was chosen when the 0.5 order fringe reached the symmetric point in the free field. This was also the time at which the response around the hole boundary was sufficiently high to allow accurate fringe order determinations. The analysis was conducted at approximately 150 microsecond intervals until the response around the hole became too low for accurate determinations.

The time duration of the pulse was sufficiently short for the major portion of the pulse to pass the hole before reflections returned from the boundary. Thus the analysis which was conducted covers about 80 percent of the pulse.

The experimentally determined values for the fringe order as a function of time at the symmetric free field point are shown in Figure 5. Similar curves for the two strains ϵ_x and ϵ_y are shown in Figure 6. These data were then used together with the material properties of the model material to obtain the two principal stresses and their directions at the free field point as shown in Figure 7. The effect of rate of loading on the modulus of elasticity of the urethane rubber material was considered in these determinations.

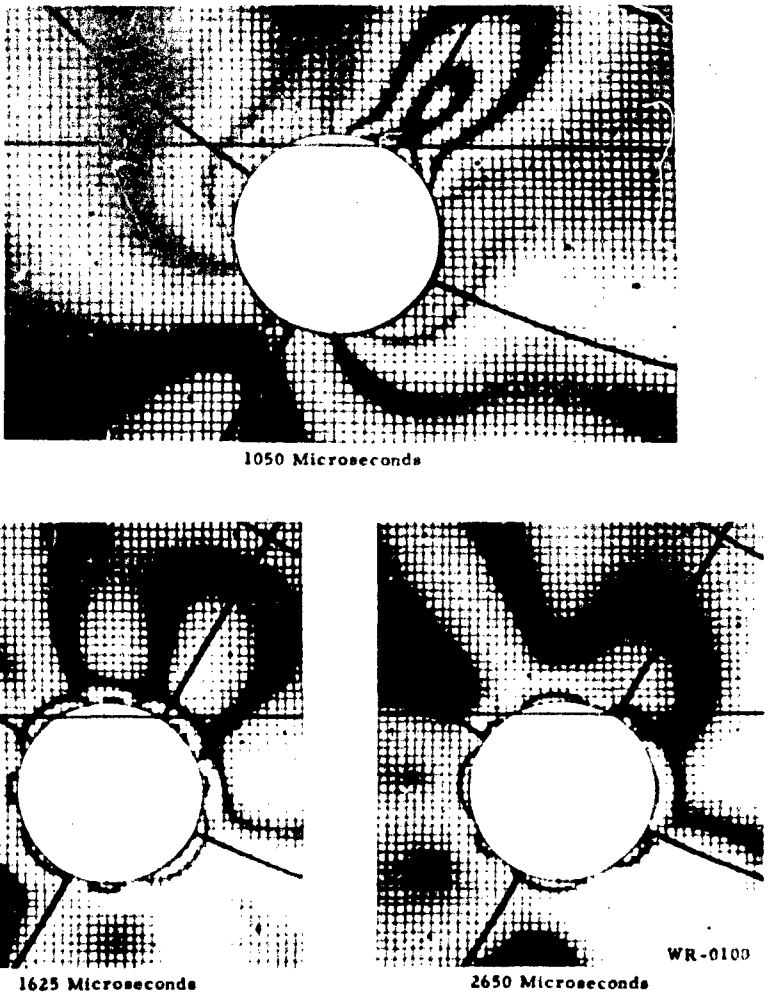


Fig. 4 Microflash photographs showing the fringe order distribution around the boundary of the hole at various times after detonation of the explosive charge.

The dynamic stresses on the hole boundary were computed directly from the isochromatic data since the radial component of the boundary stress vanishes. Typical results are shown plotted in Figures 8-10. The free field stresses at the same instant of time as shown at the center of each of these figures. The isochromatic fringe order at the symmetric free field point as a function of time was shown in Figure 5. It can be seen from this figure that the stress wave front arrived at the symmetric free field point approximately 660 microseconds after the explosive charge on the boundary was detonated. This wave front would be a dilatational type wave. Since the velocity of a distortional type wave is only 52 percent of the velocity of a dilatational wave in the urethane rubber material, the front of the distortional wave will not reach the symmetric free field point until 1250 microseconds after the charge is detonated.

The stress distributions shown in Figures 8 and 9 therefore, are produced by a compressive dilatational wave. The compressive stresses on the boundary of the hole develop and reach a maximum as the peak of the stress wave passes the hole (approximately 1100 microseconds after the charge is detonated). The tensile stresses which develop during this time interval are relatively small on the edge of the hole nearest the point where the charge is detonated. On the opposite edge of the hole the tensile stresses do not develop during this time interval. After the peak of the stress pulse passes the hole, the compressive stresses decrease and the tensile stresses increase as shown in Figure 10. After a sufficient period of time the maximum tensile and compressive stresses have equal magnitudes and their locations shift approximately 45°. This indicates the presence of a pure distortional wave.

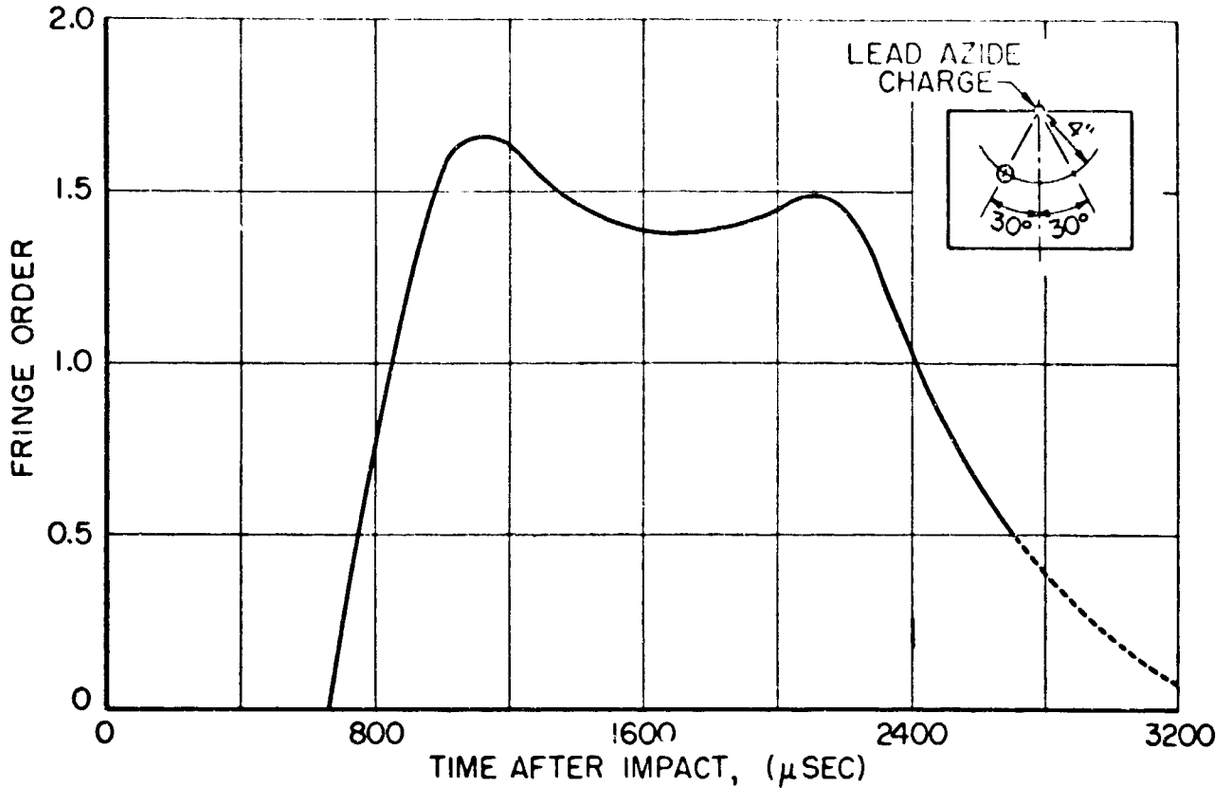


Fig. 5 Fringe order at the symmetric free field point as a function of time after detonation of the explosive charge.

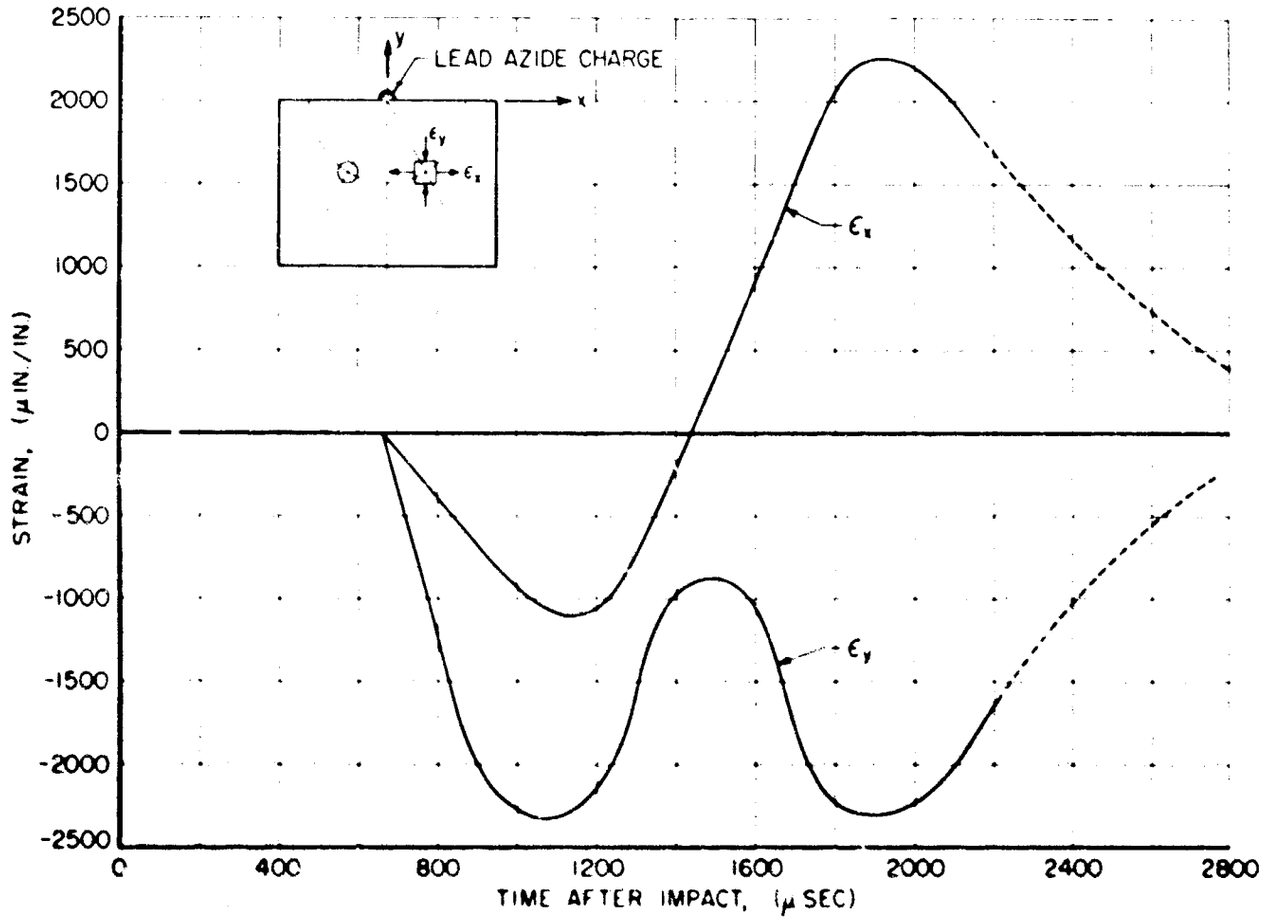


Fig. 6 Horizontal strain ϵ_x and vertical strain ϵ_y at the symmetric free field point as a function of time after detonation of the explosive charge.

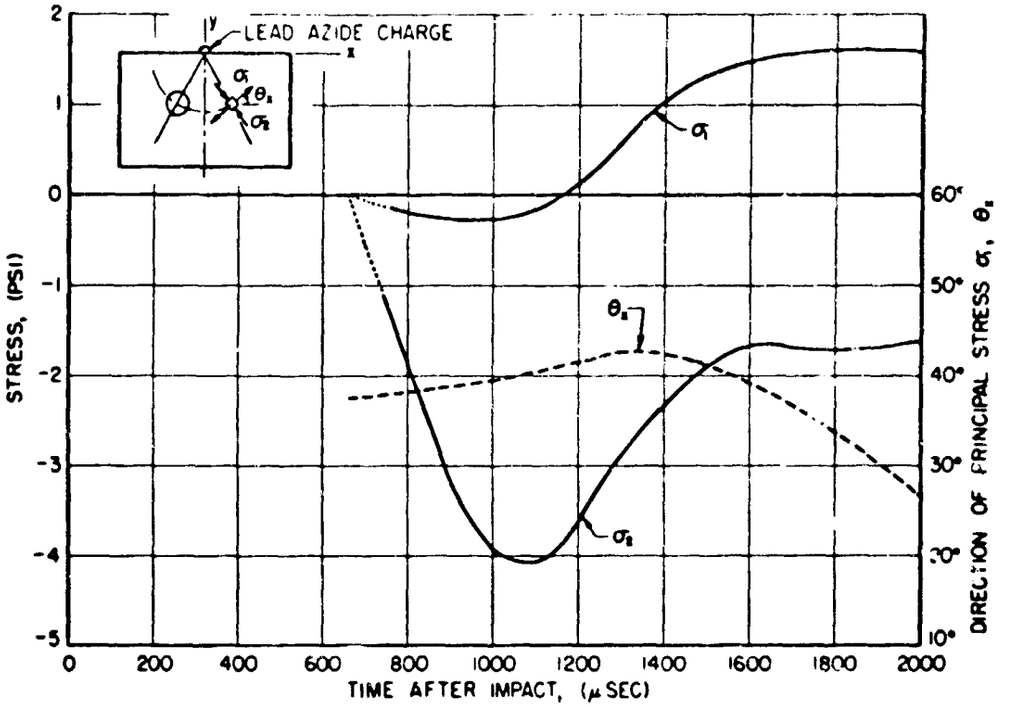


Fig. 7 The two principal stresses and their orientation at the symmetric free field point as a function of time after detonation of the explosive charge.

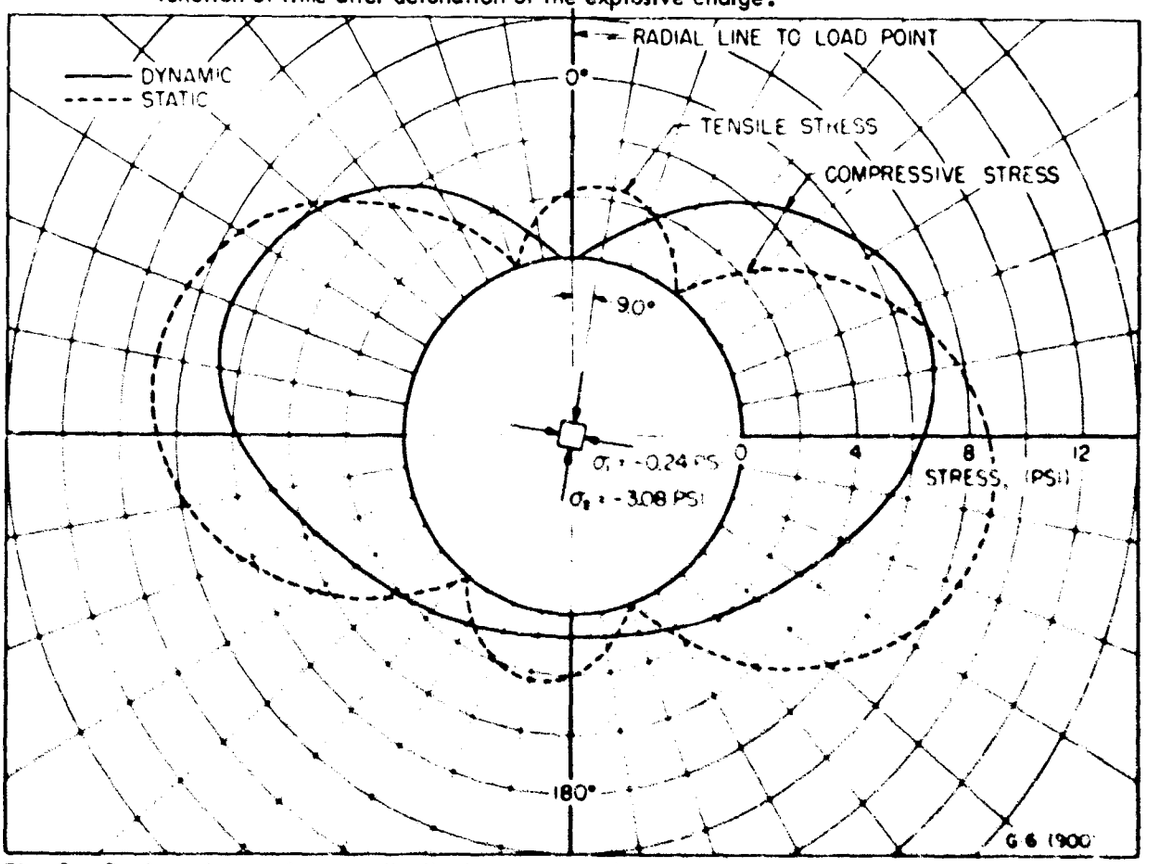


Fig. 8 Static and dynamic stress distributions on the hole boundary 900 microseconds after the explosive charge was detonated.

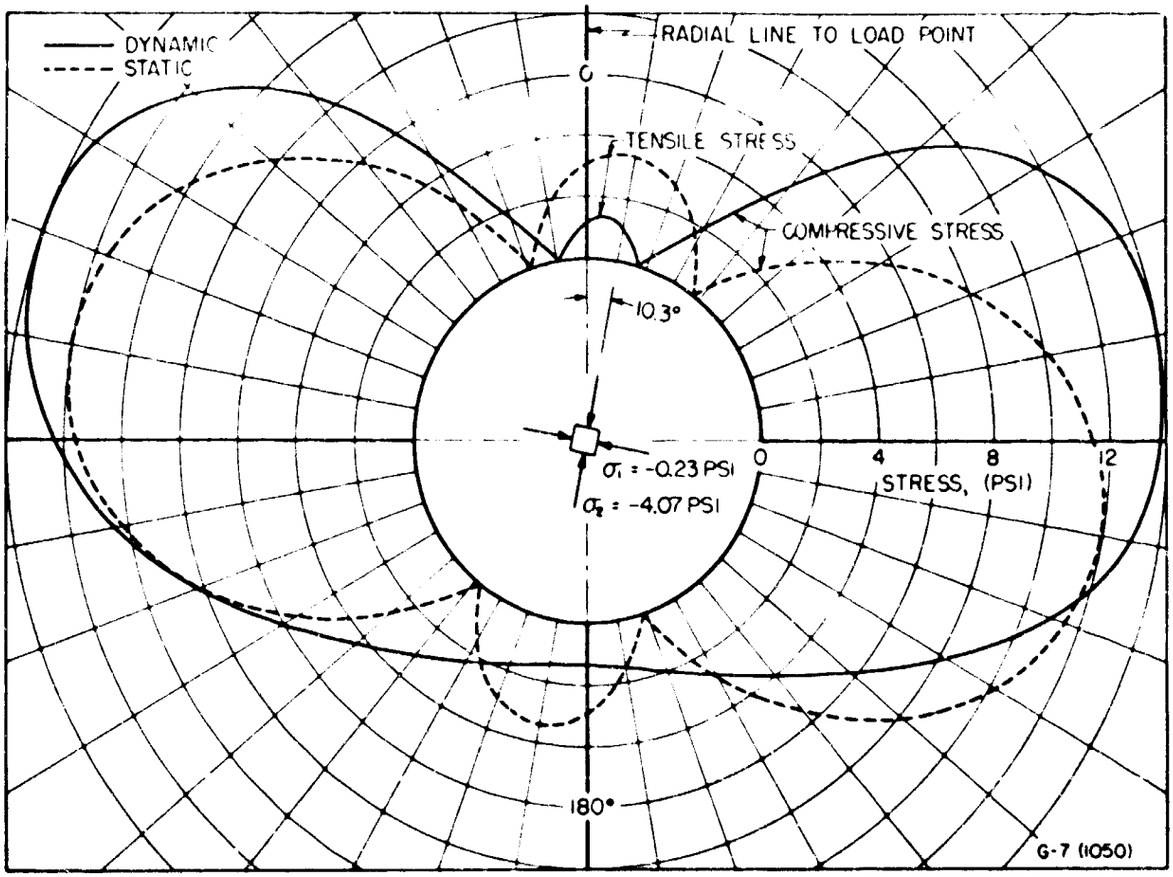


Fig. 9 Static and dynamic stress distributions on the hole boundary 1050 microseconds after the explosive charge was detonated

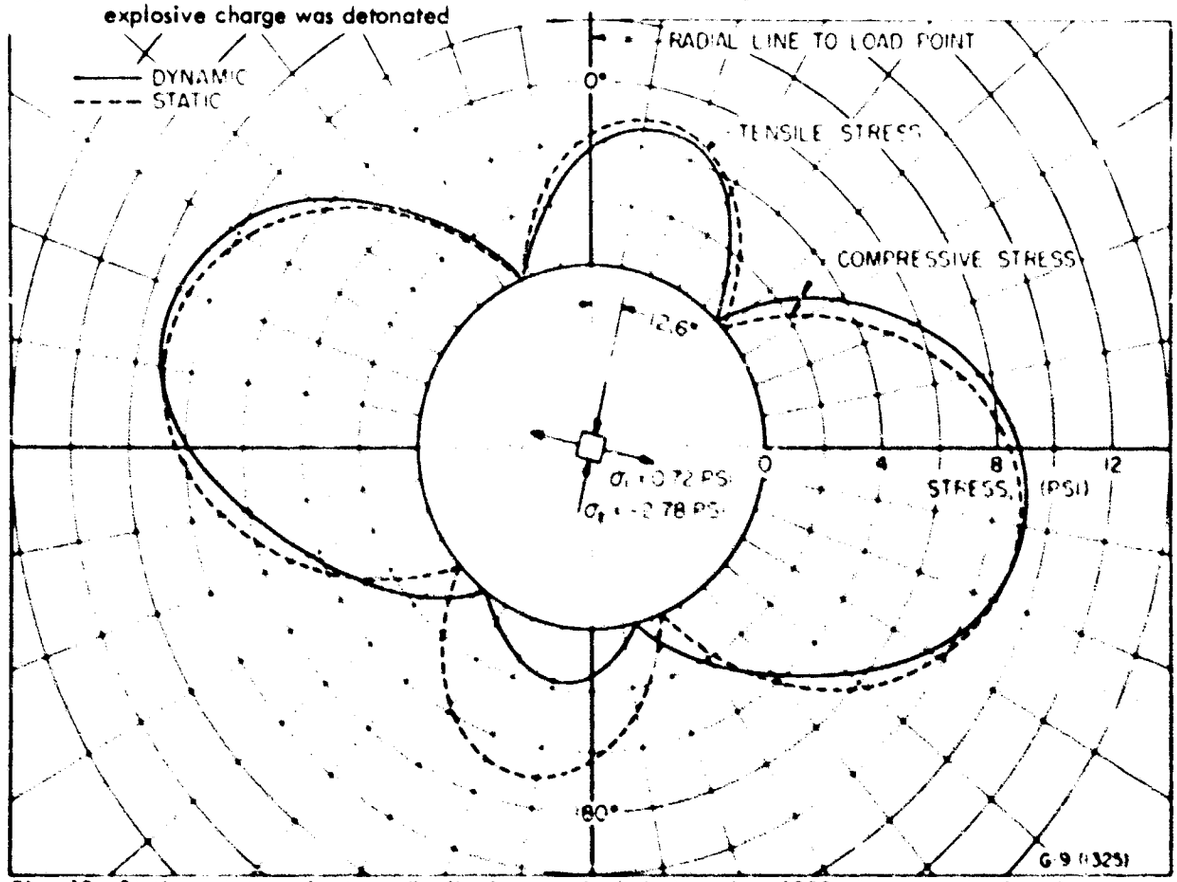


Fig. 10 Static and dynamic stress distributions on the hole boundary 1325 microseconds after the explosive charge was detonated.

SIMILITUDE AND MODEL STUDIES

Values of the boundary stress suitable for comparison with the dynamic distributions were computed at the appropriate times by using the experimentally measured dynamic free field stresses and the static Kirsch solution for a circular hole in an infinite plate. These "so-called" static distributions are also shown in Figures 8-10. In these figures it can be seen that the dynamic compressive stresses are initially smaller than the computed static values. Later as the wave front passed the hole, the dynamic compressive stress is approximately 15 percent greater than the computed static value. Much later the two values show excellent agreement. It can also be seen in these figures that the dynamic tensile stresses are always smaller than the static values.

AIR SHOCK STUDY

The model used for this study is shown in Figure 11. Both the open hole and rigid inclusion cases were studied.

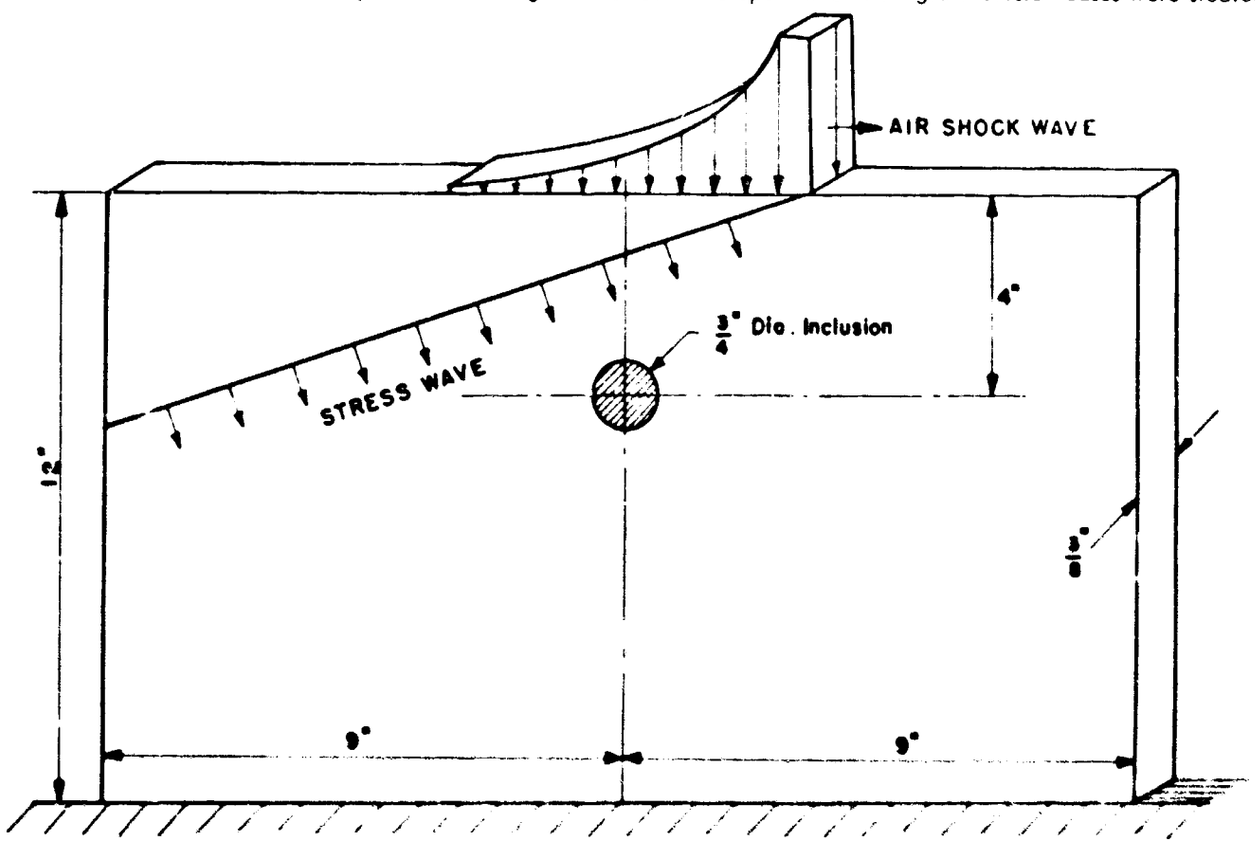


Fig. 11 Sketch of the model showing the location of the hole or inclusion with respect to the loaded edge of the plate.

The air shock loading was applied to the top edge of the model by means of a 6 in. diameter shock tube. The shock tube facility together with the model, polariscope, and assorted electronic and photographic equipment used in the study is shown in Figure 12. The model was inserted at a specially machined section which was located approximately 16 ft from the driver (pressure) section and 10 ft from the end of the tube. A section through the tube at the model location is shown in Figure 13. The thin rubber diaphragm shown in this figure was used as a seal to prevent the air in the tube from entering the spaces between the model and housing. During operation the driver section of the tube was filled with air under pressure. The air shock wave was initiated by piercing the plastic diaphragm which separated the driver section from the remaining sections of the tube.

The pressure pulse applied to the model for the study being reported was generated by a pressure of 75 psi in a 2-ft driver section. The maximum amplitude of the pulse, which was accurately measured with a Kistler type pressure gauge mounted on the wall of the tube at the model location, was 14.8 psi. The rise from zero to peak of the front of the pulse was less than 100 microseconds. The total length of the pulse was approximately 14 milliseconds. Typical oscilloscope records of the signal from the Kistler gauge are shown in Figure 14. The velocity of the shock wave was measured with a Berkeley counter which was started and stopped with signals from two pressure gauges spaced 4 ft apart. The shock wave velocity was established at 1549 ± 8 ft per second.

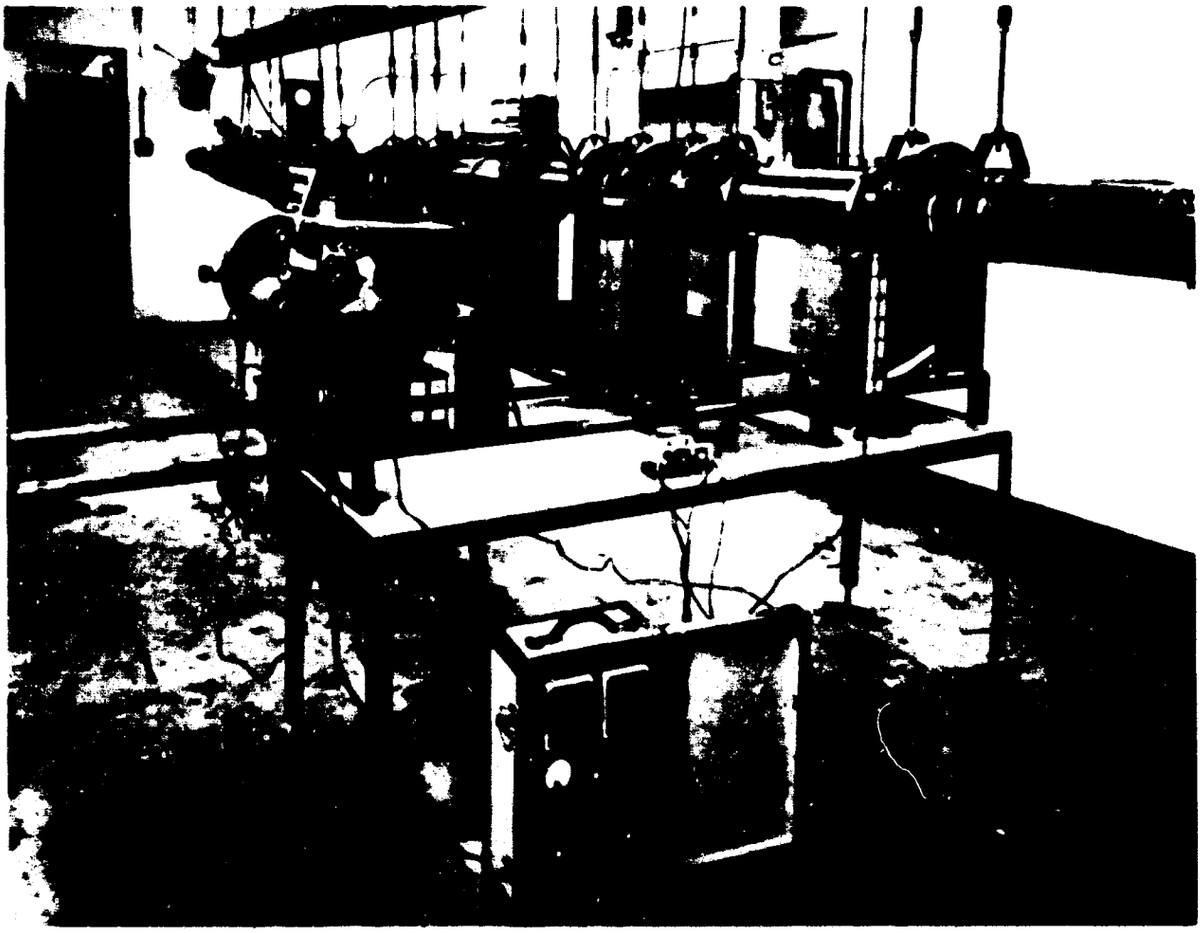


Fig. 12 Photograph showing the shock tube facility, model, polariscope, and assorted electronic and photographic equipment used in the study.

Photographic records of the photoelastic and moire fringe patterns produced as the stress wave propagated through the model were recorded with a Fastax camera operating at a speed of approximately 7500 frames per second. Twenty frames from a photoelastic fringe pattern record are shown in Figure 15. To obtain more detailed information at selected points of interest such as the inclusion boundary, a series of photographs were again taken with a microflash unit and a large studio camera.

The time when the shock wave started moving along the top edge of the plate was chosen as the origin of time. The exact time (from this origin) at which the microflash photographs were taken was accurately measured with a Berkeley counter. The counter was started with a signal from a pressure gauge in the wall of the tube opposite the edge of the model and stopped with a signal from a photocell activated by the microflash.

In this study the principal stresses and directions along the vertical centerline of the plate were determined before the hole was machined 4 in. below the loaded edge. The results are shown in Figure 16. In this figure it can be seen that both principal stresses are compressive and increase linearly with time initially for about 800 μ sec for the σ_2-stress and about 1300 μ sec for the σ_1 stress. The principal stress direction θ_o remains constant at about 10.5° from the first 800 μ sec and then decreases to 0° over the next 1000 μ sec. The attenuation of the maximum compressive stress with depth is shown in Figure 17.

Typical results for the boundary stress determinations are shown in Figure 18-21. Again the dynamic stresses are only slightly larger than the computed static stresses as the front of the stress wave passes the hole or inclusion. At later times the dynamic and static values show excellent agreement. The results for the open hole are also in agreement with the theoretical results of Baron and Matthews (3) for the stress distribution around a cylindrical cavity produced by a plane stress wave of Heaviside unit function distribution.

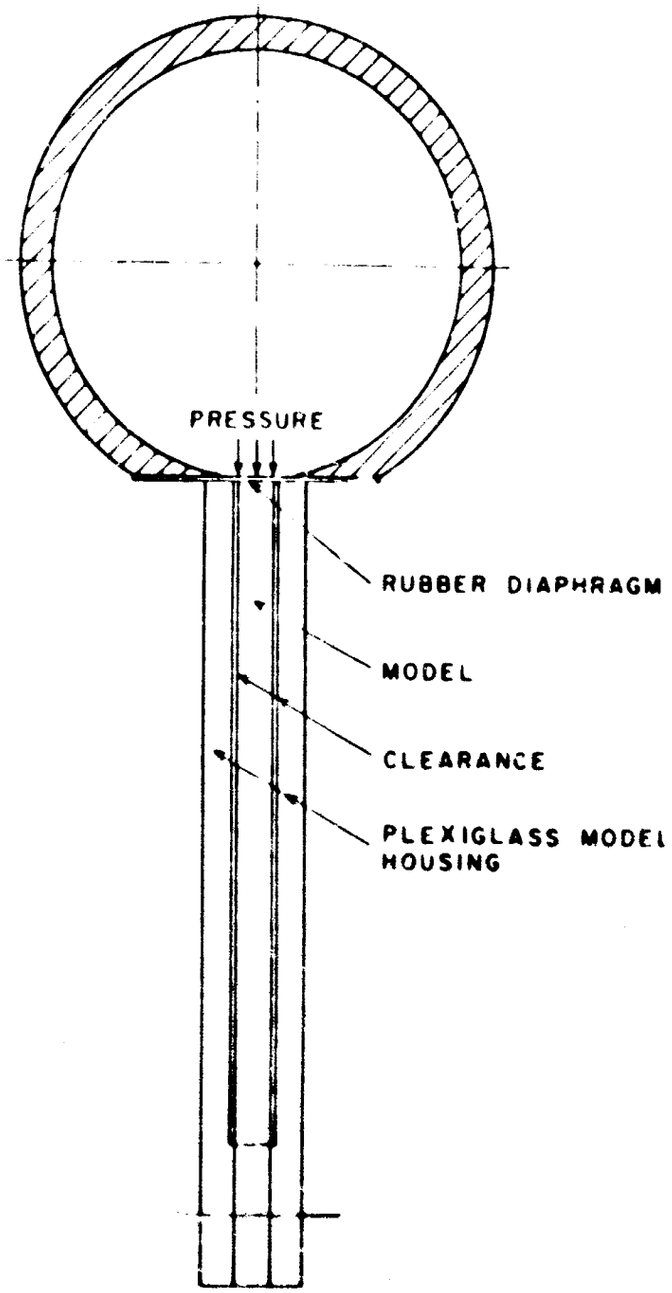


Fig. 13 Sectional view through the shock tube at the model location.

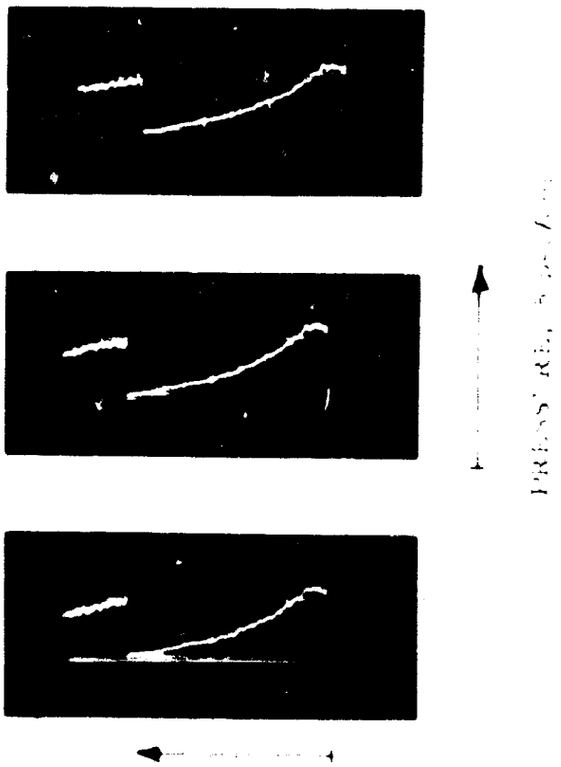


Fig. 14 Pressure-time records at the model location obtained with a Kistler type gauge.

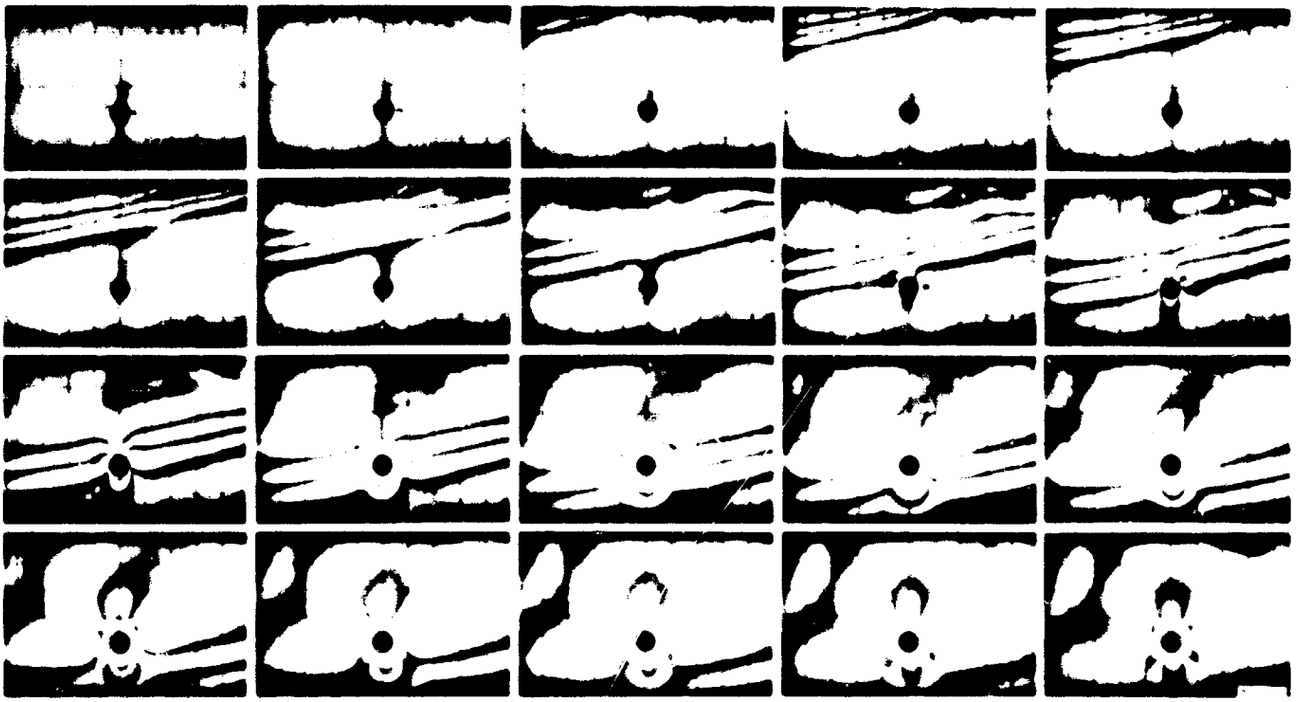


Fig. 15 Series of photographs showing the photoelastic fringe patterns produced in a plate with a circular inclusion when an air shock wave travels across the top edge of the plate.

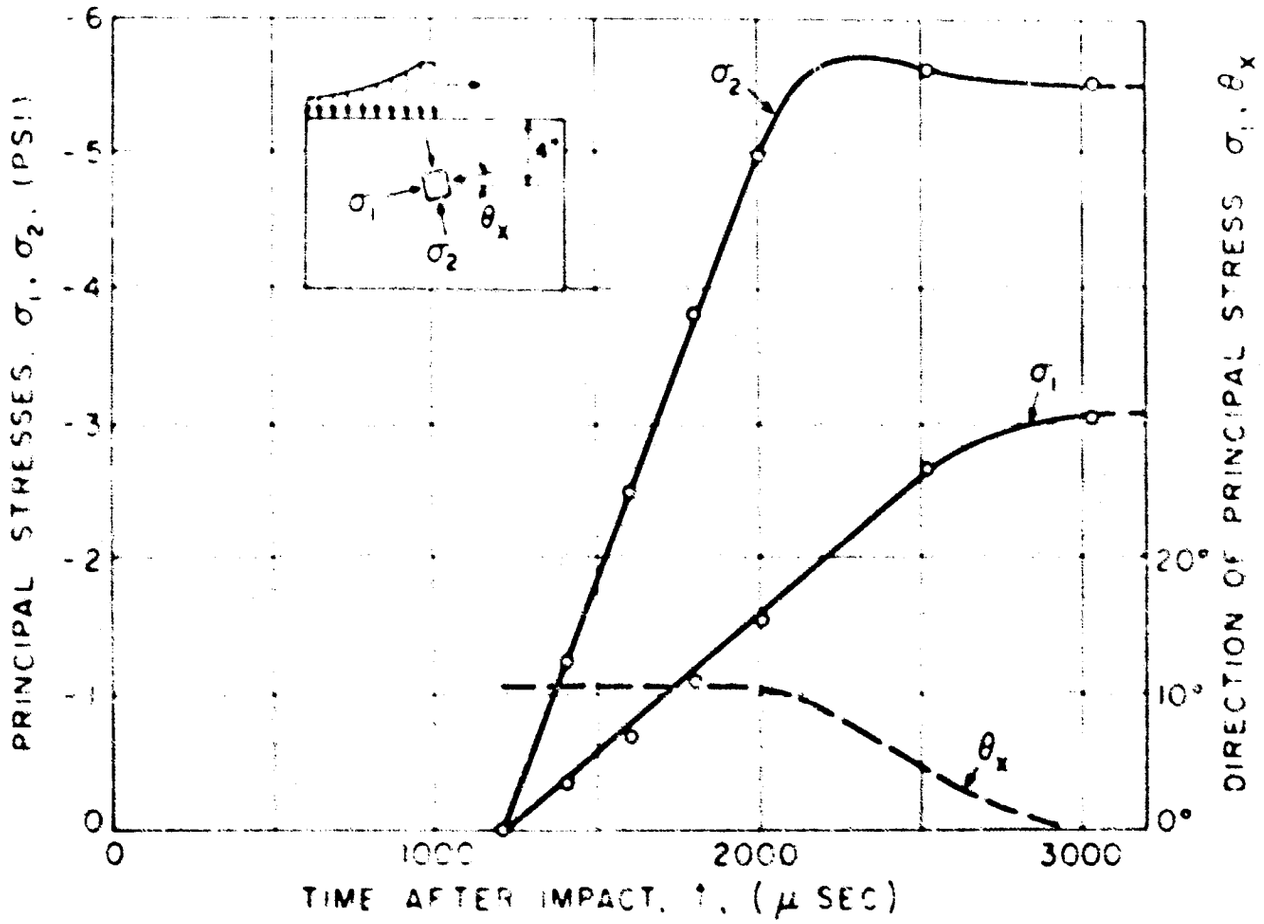


Fig. 16 The two principal stresses σ_1 and σ_2 and their orientation θ_x at a point on the centerline of the plate 4 inches below the loaded edge as a function of time after the air shock started across the top edge of the plate.

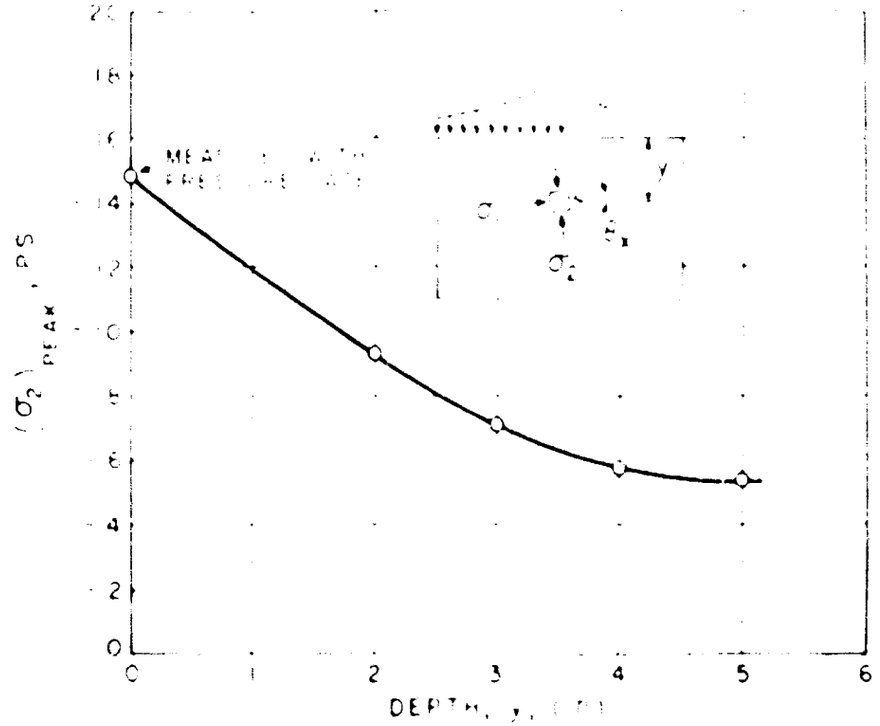


Fig. 17 Attenuation of maximum compressive stress with depth from the top edge of the plate.

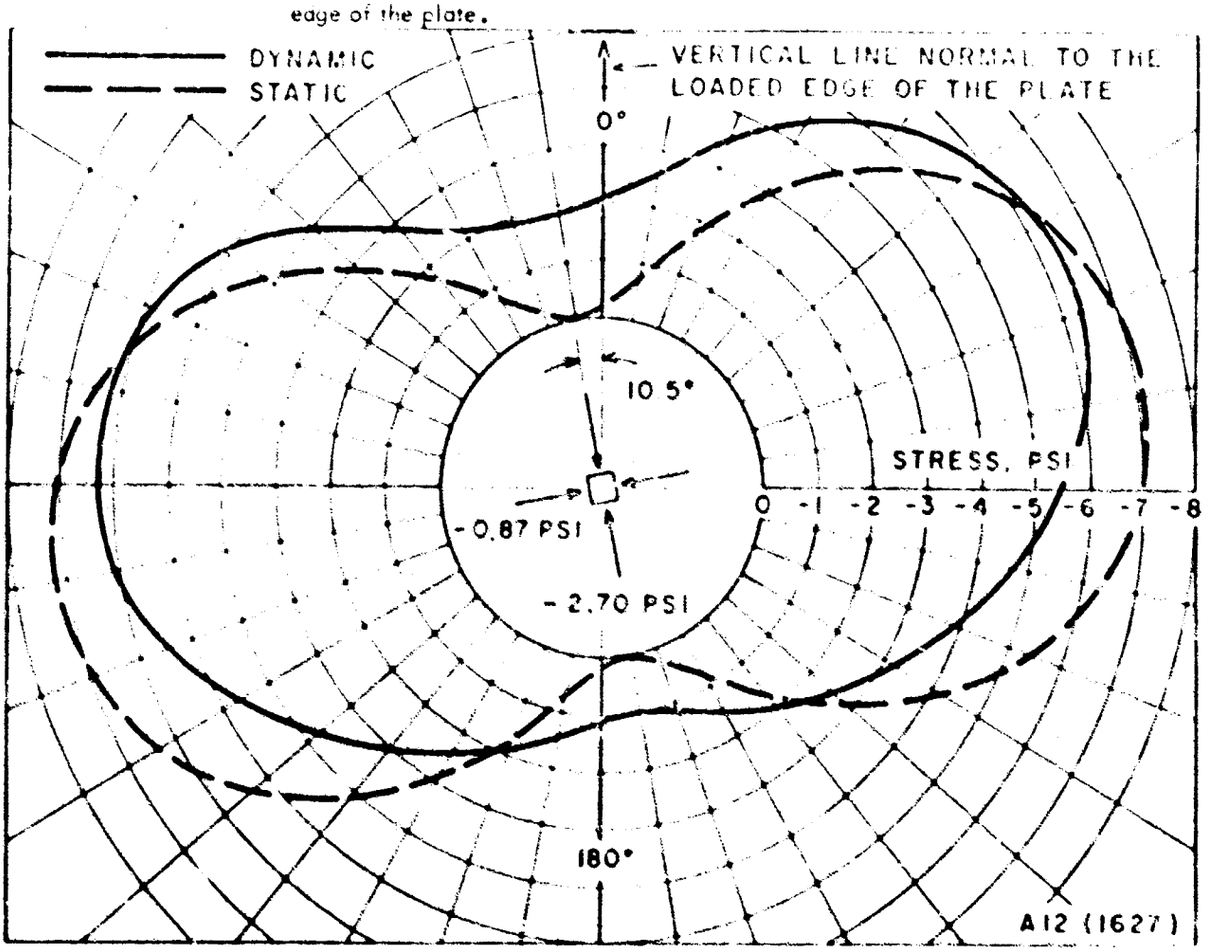


Fig. 18 Static and dynamic stress distributions on the hole boundary, 1627 microseconds after the air shock started across the top edge of the plate.

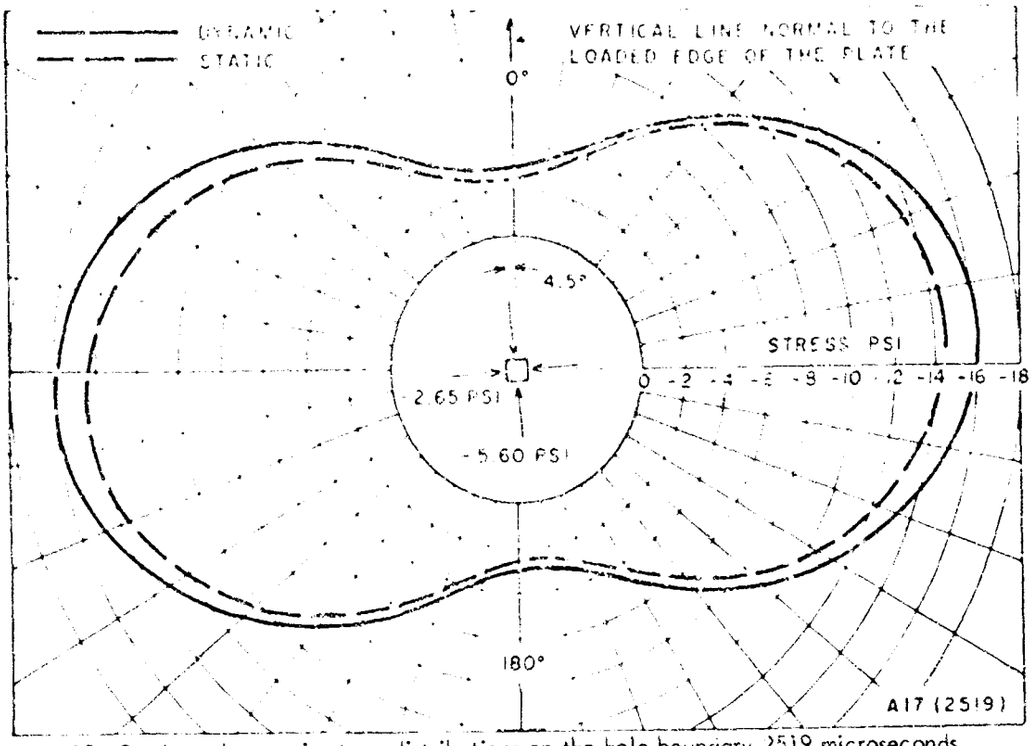


Fig. 19 Static and dynamic stress distributions on the hole boundary 2519 microseconds after the air shock started across the top edge of the plate.

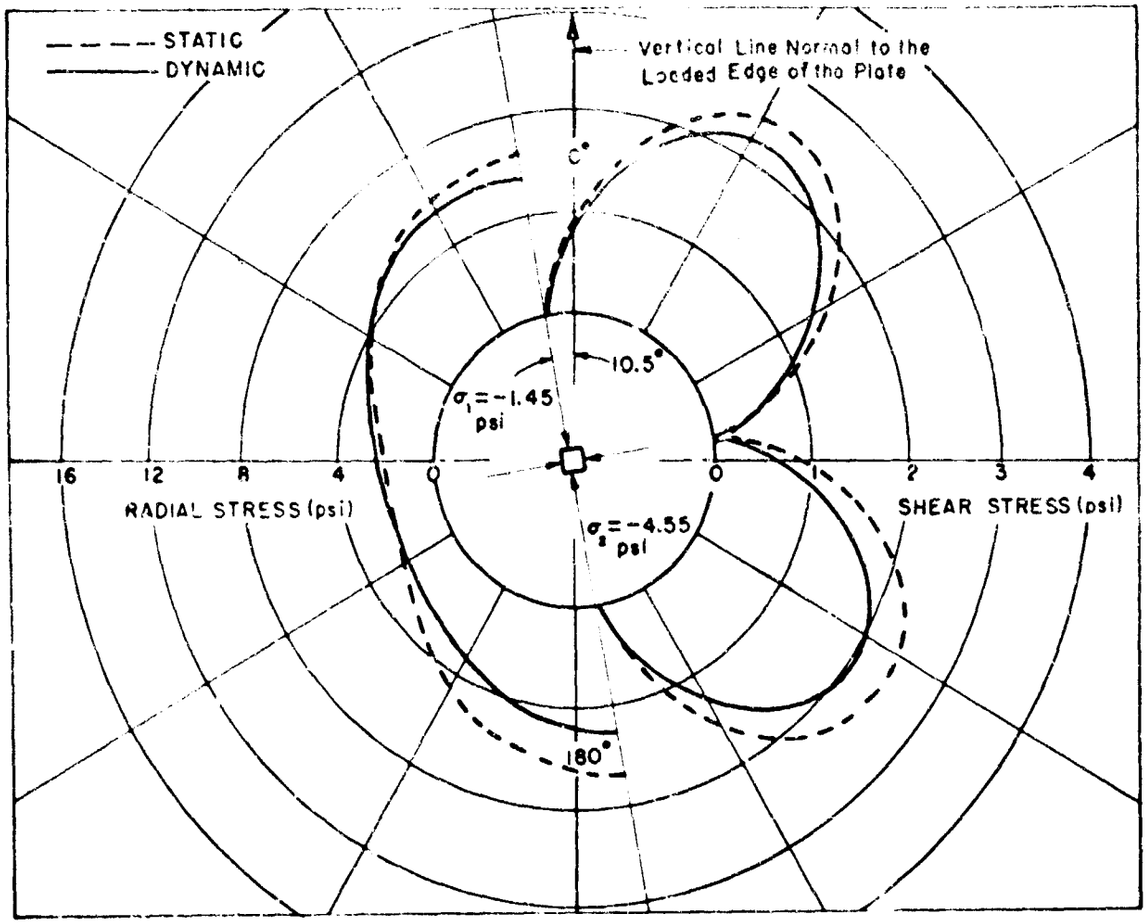


Fig. 20 Radial and shear stress distributions on the interface between the inclusion and the plate 1925 microseconds after the air shock started across the top edge of the plate.

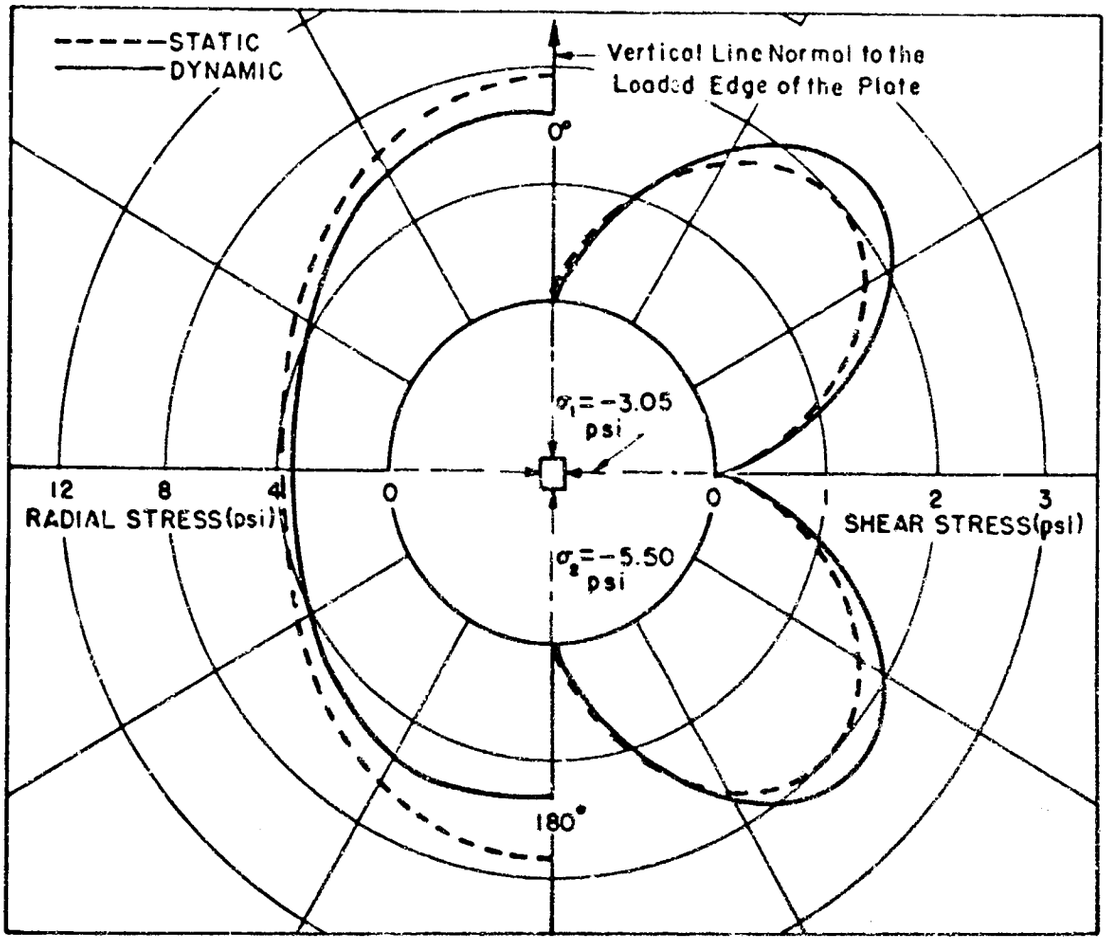


Fig. 21 Radial and shear stress distributions on the interface between the inclusion and the plate 3035 microseconds after the air shock started across the top edge of the plate.

CONCLUSIONS

The results of this experimental investigation indicate that static solutions can be used as a first approximation for computing dynamic stress distributions on the boundaries of discontinuities in elastic materials if the time-dependent free field stress distributions are known. In all of the cases studied to date the measured dynamic stress has not exceeded the computed stress based on the appropriate static solution and the measured dynamic free field stresses by more than 15 percent. Further study is needed for non-elastic materials and for pulse lengths of the order of the discontinuity diameter.

ACKNOWLEDGEMENTS

The research work described in this paper was part of a project sponsored by the Air Force Weapons Laboratory, Kirtland Air Force Base, New Mexico, and conducted at the IIT Research Institute. The author would like to express his appreciation to AFWL for their sponsorship and in particular to Lt. D. Merkle for his encouragement and cooperation.

REFERENCES

1. "Stress Wave Phenomena in Semi-Solids," AFSWC-TR-61-25, July 1961.
2. "A Study of Stress Wave Interaction with Buried Structures," AFSWC-TDR-62-47, May 1962.
3. Baron, M. L and A. T. Matthews, "Diffraction of a Pressure Wave by a Cylindrical Cavity in an Elastic Medium," Journal of Appl. Mech., Vol. 28, p. 347, 1961.

SESSION SIX–WEDNESDAY PM

ANALYTICAL AND EXPERIMENTAL STUDIES, PART I

SESSION CHAIRMAN: EUGENE ZWOYER

TABLE OF CONTENTS

page

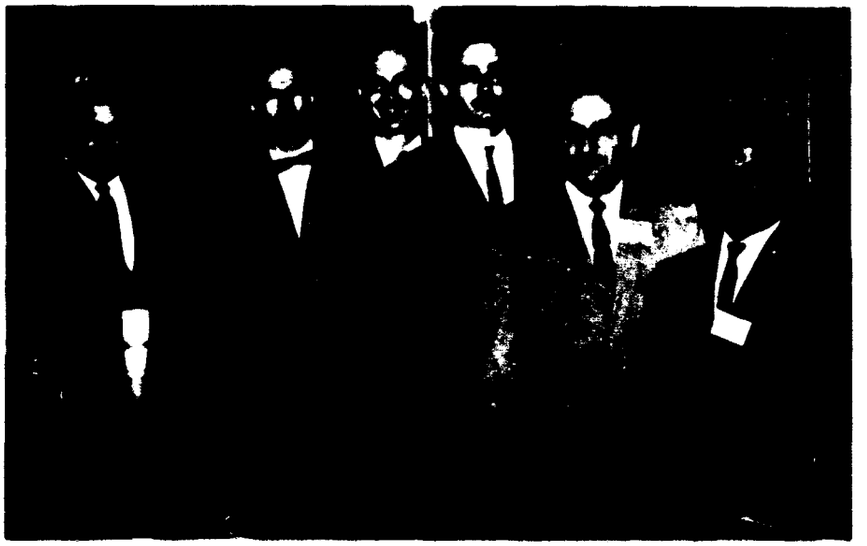
AN INVESTIGATION OF PANEL-ARCHING EFFECTS IN NONCOHESIVE SOIL, W. B. Truesdale and E. Vey 349

ARCHING IN SOIL DUE TO THE DEFLECTION OF A RIGID HORIZONTAL STRIP, Chunduri V. Chelapati 356

ATTENUATION OF STRESSES FOR BURIED CYLINDERS, Jerome Q. Burns and Ralph M. Richard 378

THE BENEFICIAL ACTION OF THE SURROUNDING SOIL ON THE LOAD-CARRYING CAPACITY OF BURIED TUBES, U. Luscher and K. Höeg 393

AN EXPERIMENTAL EVALUATION OF SOIL ARCHING, George E. Triandafilidis, Delon Hampton and Milan Spanovich 403



Participants in Session Six were, left to right, Eugene Zwoyer (Session Chairman); U. Luscher; W. B. Truesdale; J. G. Burns; G. Triandafilitis; and C. V. Chelapati.

AN INVESTIGATION OF PANEL-ARCHING EFFECTS IN NONCOHESIVE SOIL

by
W. B. Truesdale* and E. Vey**

INTRODUCTION

A buried flexible panel, for all stable loading conditions, must be in equilibrium under vertical forces. The effects of a surface applied load must be transmitted through the cover soil. Consequent deformation of the panel must if loading is to be maintained, be accompanied by deformation in the cover soil. If the effect of a surface load on a soil structure combination is such that a non-uniform distribution of shearing strains results within the soil body, a non-uniform distribution of interior stresses will also exist.

For any total shearing strain over the depth of cover soil, the stresses at localized points are related only to localized strains. In consequence, it is conceivable that the peak strengths at certain points within the soil body could be exceeded at loads much less than would be predicted by a consideration of average strains and stresses throughout the soil mass. Thus a localized failure as a result of large localized strains may limit the load-resisting capacity of the soil, rather than a general failure affecting the entire soil body.

The complexities introduced by considering stress-strain relationships within a soil body may be avoided by treating the soil as a free body subjected to specified boundary forces. The maximum load-resisting capacity can be associated with some finite total strain between the surface of the soil and its lower boundary. The internal distribution of strain, as well as the internal variation of the shearing stresses which combine to furnish total load resistance are not considered. This approach, in effect, replaces interior stress-strain considerations by a weighted averaging of the localized stresses and strains throughout the soil mass. While this is a major simplification, it involves some important assumptions as to the boundaries of the failure mass of soil. It has been assumed that the entire mass of soil between the ground surface and the buried structure, bounded by vertical planes delineating the periphery of the structure, constitutes the incipient failure mass (1,2). However, there remain the possibilities that the actual bounds may be influenced by localized stresses and strains and that failure planes other than those assumed may, in fact, prove critical.

An additional deviation is introduced when the lower boundary of the soil mass is in contact with a buried structure. When surface load is applied the soil and structure deflect as a unit as long as contact is maintained at their interface. Each material contributes some portion to total soil-structure resistance. However, in much the same way that the total shearing resistance of the soil mass is not the integrated sum of peak strengths at its interior points, the maximum load resistance of the composite soil-structure system may not necessarily be the sum of the individual peak resistances.

The solution of an exact set of analytical expressions considering all of these factors would be extremely complex. However, with the use of high-speed computers a solution can be obtained through iterative, self correcting approximations.

BASIC ASSUMPTIONS

Assumptions required to describe the soil behavior:

1. soil stress-strain relationships,
2. relation of lateral and vertical soil pressures, and
3. distribution of soil shearing strains with depth.

Coulomb's equation for ultimate shear resistance is

$$\tau_v = \sigma_n \tan \phi$$

However, the relationship of shearing resistance and shear strain up to ultimate is not known. Figure 1 shows the general stress-strain relationship assumed for this problem. The shearing resistance mobilized at any instant up to ultimate is a function of shearing strain and may be computed as shown.

Accepting that Coulomb's equation satisfactorily describes the ultimate shearing resistance of the Ottawa sand, an assumption is still required to determine the value of τ_n, the lateral stress in the soil, to be used in the equation.

*Associate Research Engineer, Soil Mechanics Section, IIT Research Institute.
**Manager, Soil Mechanics Section, IIT Research Institute.

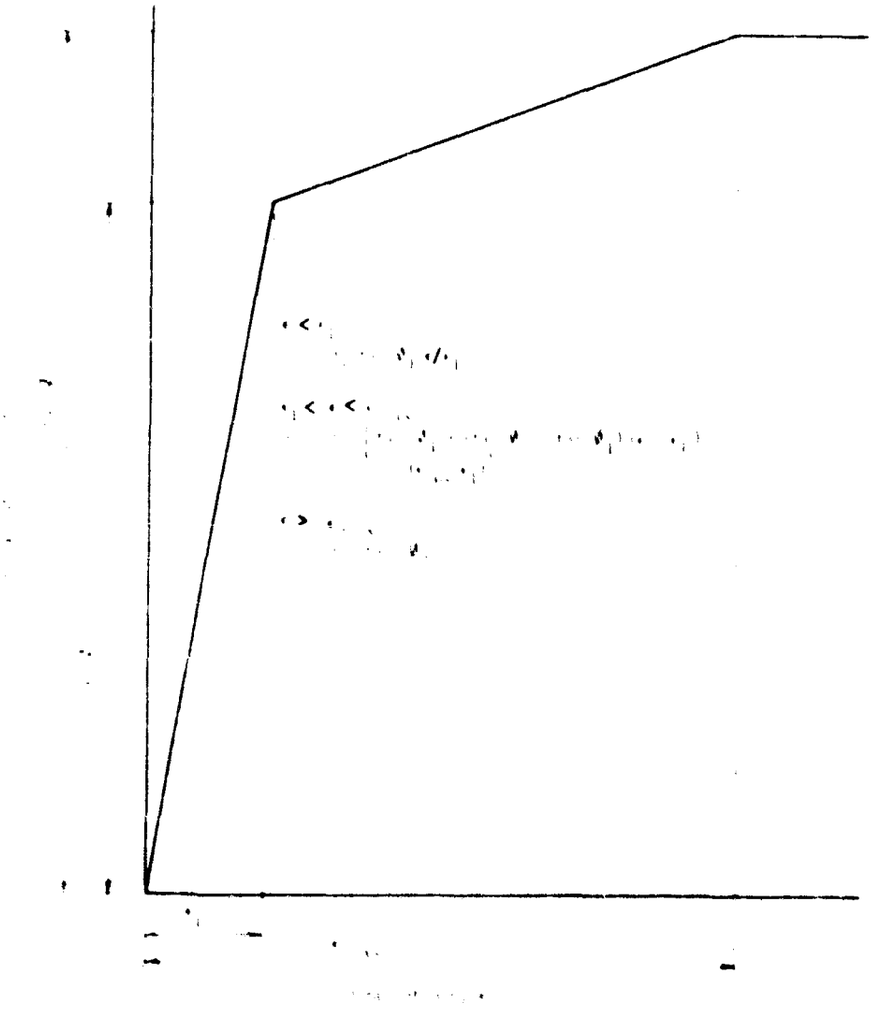


Fig. 1 Assumed Shear Stress-Strain Relationship

For specific conditions of impending failure, active and passive, Rankine's ratio relates the normal forces at a point in the soil. However, application of Rankine's ratio, either active or passive, to the buried structure problem is quite difficult. Experimental work to determine the relationship of horizontal and vertical earth pressures above a yielding structure in a cohesionless soil was conducted by Terzaghi [3]. A trap door located at the bottom of a dense sand was slowly lowered with a rigid body motion, holding it parallel to its original position, while measurements were made of lateral and vertical pressures. Figure 2 presents the ratio of lateral to vertical pressure versus burial ratio.

It is seen that a constant relationship was found between horizontal and vertical soil pressures at all depths prior to lowering the trap door, and at distances of over two panel widths above the structure when displacement occurred. Within two panel widths above the structure, although the relationship was nonlinear, the ratio of horizontal stress to vertical stress was always greater than the constant relationship above.

Because Terzaghi's study did not include any investigation of the effect of overpressure, it was decided to investigate the two following lateral and vertical soil pressure relationships:

1. $\sigma_h = 0.67\ \sigma_v$ throughout the cover soil
2. $\sigma_h = K\ \sigma_v$ where K is either 1.0 or 0.67 as shown in Figure 3.

The selection of this particular geometry was based on observations of soil deformations such as shown in Figure 4. It can be seen in the area over the panel center-line that there has been a lateral contraction and vertical extension of the grids. This would make it seem quite possible that horizontal stresses on the elements exceed the vertical. The distortion in the soil grids occur to greater heights above the structure over the panel center-line than at the edges. Based on this observation and because no experimental measurements of lateral and vertical pressures near a yielding structure's edge were available for guidance, it was decided to reduce the height above the structure for which K was greater than 1.0 near the panel edges.

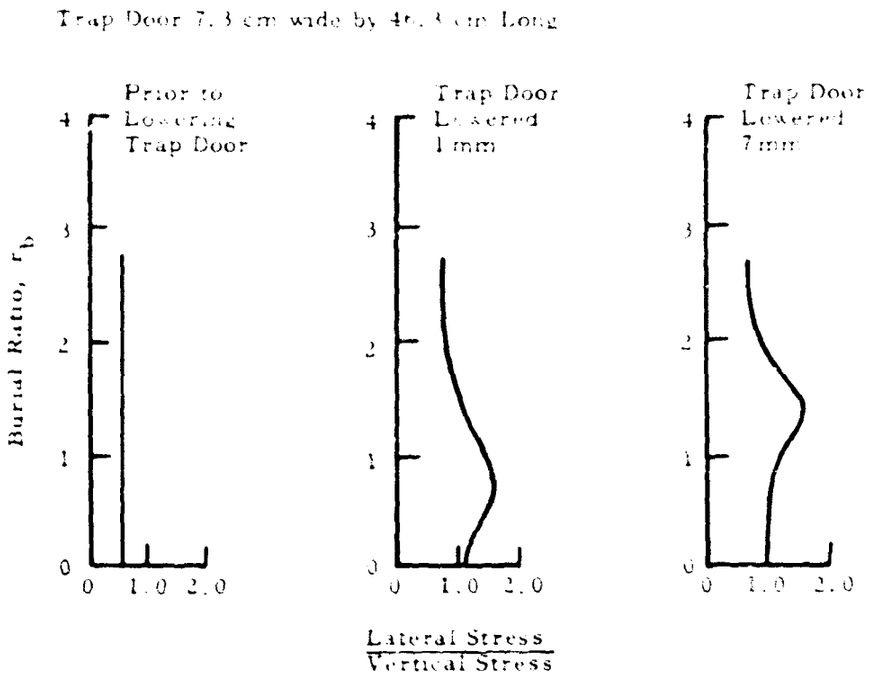


Fig. 2 Ratio of Lateral and Vertical Stress as Related to Burial Ratio (Ref. 3)

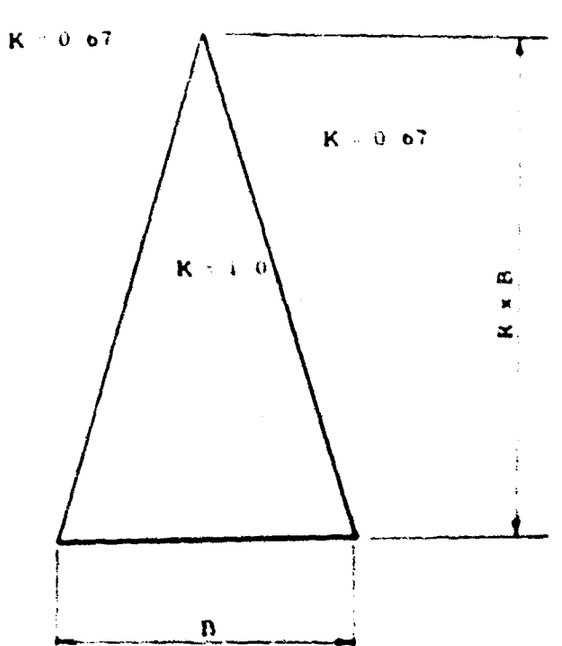


Fig. 3 Assumed K Value Distribution

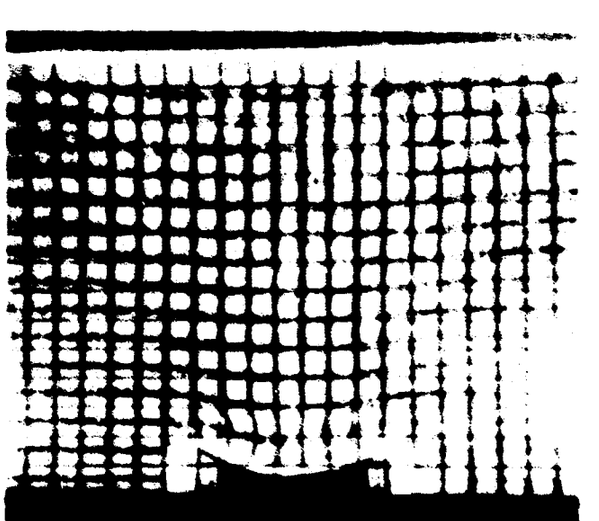


Fig. 4 Flexible Roof Panel After Pressure Yielding (ref. 5)

SOIL-STRUCTURE INTERACTION

The last required assumption to describe the soil behavior was the distribution of soil shearing strains with depth. Again in Figure 4, it can be seen that the curvature of grid lines is not constant with depth. This would indicate that straining is not uniform from the soil surface to the buried panel. It was assumed that shear strain distribution was of a form suggested by Newmark and Hall, presented in Reference 2.

$$\epsilon = \epsilon_{max} e^{-\beta (D - Z)/B}$$

where

ϵ = shear strain,
β = constant,
D = depth of burial,
Z = depth from soil surface to the element being considered,
B = width of structure

By varying β various degrees of nonuniformity of shearing strain distribution throughout the covering soil may be investigated. For any particular value of β the strains at any particular height above the structure are dependent only on the structural geometry and deformation.

COMPUTER PROGRAM

The loading is considered to be uniformly applied over a large enough area of the soil surface so that there is no dissipation of pressure with depth. The soil mass above the buried structure (of infinite length) was treated as a gridwork of individual square elements (Figure 5). This somewhat approaches a real condition in that a soil medium is composed of individual particles, however, they are not in general, either uniform in size or shape.

With a uniform loading p_o over an infinite area on the soil surface, the free-field pressure at any depth below the surface is equal to the surface overpressure plus an addition of overburden pressure of γZ. A first approximation of the loading to be carried by a structure roof panel located at a depth D below the surface might be a uniform loading of $p_o + \gamma D$. The deflected shape of the panel can be computed for this loading.

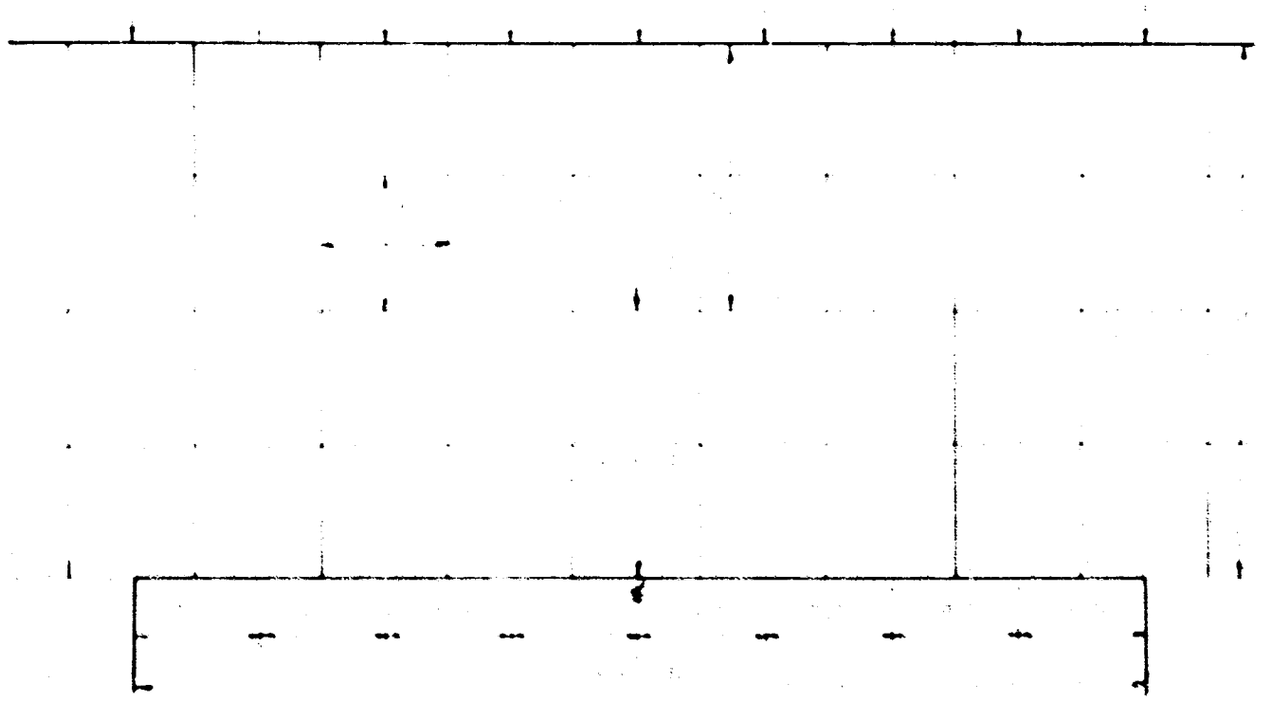


Fig. 5 Analytical Model Geometry

To maintain loading on the panel, the soil elements above must follow this deflected shape (Figure 6). In so doing, relative motion occurs between the adjacent soil elements and frictional resistance is mobilized. This results in particle to particle transfer of load around the structure, and a shift in the distribution of load transmitted to the panel towards the panel edges. Recomputing panel deflections under this new, more favorable loading system results in a decrease in the panel deformations, which results in corresponding decreases in the soil deformations. Soil shearing resistance then decreases causing an increase in panel loading. This process continues until a compatible solution is realized between the loading transmitted to the panel, panel deformations, and the deformations in the cover soil.

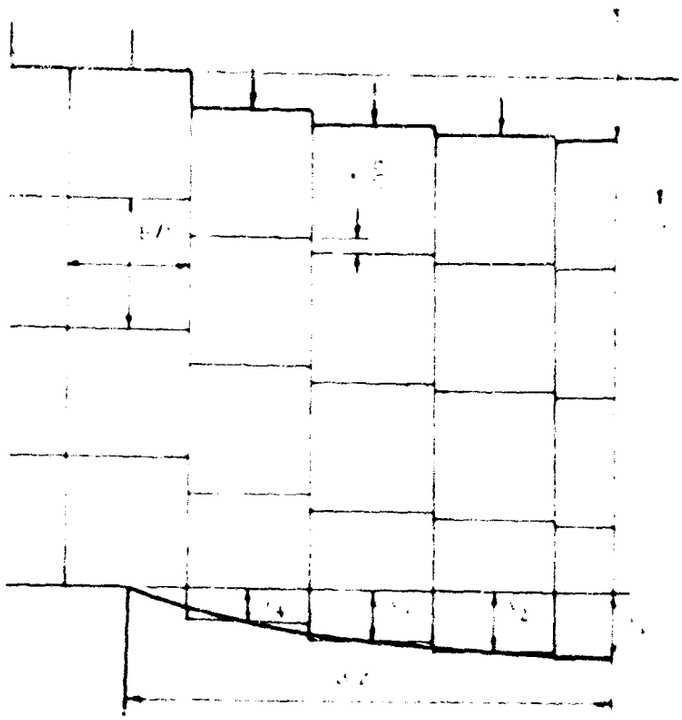


Fig. 6 Soil-Panel Deformation Relationships

The influence of the assumptions regarding soil behavior can be seen in Figures 7 and 8. These present the analytical relationships of overpressure and panel deformation for a structure located at a depth of burial of 1 panel width. The structure was selected to be of very little stiffness so that the influence of arching would be predominant.

The ratio of the panel center line deflection to panel width is computed for an idealized soil condition and for various levels of surface overpressure. The soil was assumed to be cohesionless and in accordance with the aforementioned assumptions its frictional resistance at any strain is determined by σ_{π}, $\emptyset_1$, $\emptyset_2$, ϵ_1, and ϵ_2. $\emptyset_1$, $\emptyset_2$, ϵ_1, and ϵ_2 were evaluated after study of triaxial test results so that the values selected would realistically represent a soil condition. The particular tests studied (4) were performed on a medium dense Ottawa sand. $\emptyset_2$ was determined from the slope of the failure envelope as 31°. $\emptyset_1$ was determined as 26° from the slope of the envelope of Mohr's circles plotted for the stress condition at 70 per cent ultimate load. The shear strains corresponding to the stress conditions at $\emptyset_1$ and $\emptyset_2$ were then determined, assuming that the triaxial tests were constant volume tests. On the basis of these computations ϵ_2 was evaluated as 0.10 in. in. and it was decided to examine the influence of varying ϵ_1 from 0.01 in. in. to 0.02 in. in.

Investigation was also made of the influence of various degrees of nonuniformity of shearing strain distribution in the soil mass by varying β from 0.2 to 2.0.

The panel deformation ratio under the weight of the overburden soil was almost independent of changes in either ϵ_1 or β. For a constant value of K = 0.67 (Figure 7) the curves defining the overpressure-panel deformation relationships fall within a relatively narrow band indicating that small changes in the assumptions describing the soil stress-strain relationships, or strain distribution in the soil mass do not significantly influence the results.

A change in the assumed value of K (Figure 8) does however, significantly influence the results. Also with the larger value of K changes in both the soil stress-strain relationship and strain distribution become quite important. For a given level of overpressure, the deflection ratio increases approximately proportionately with ϵ_1, and in a ratio of about 1 to 5 with β.

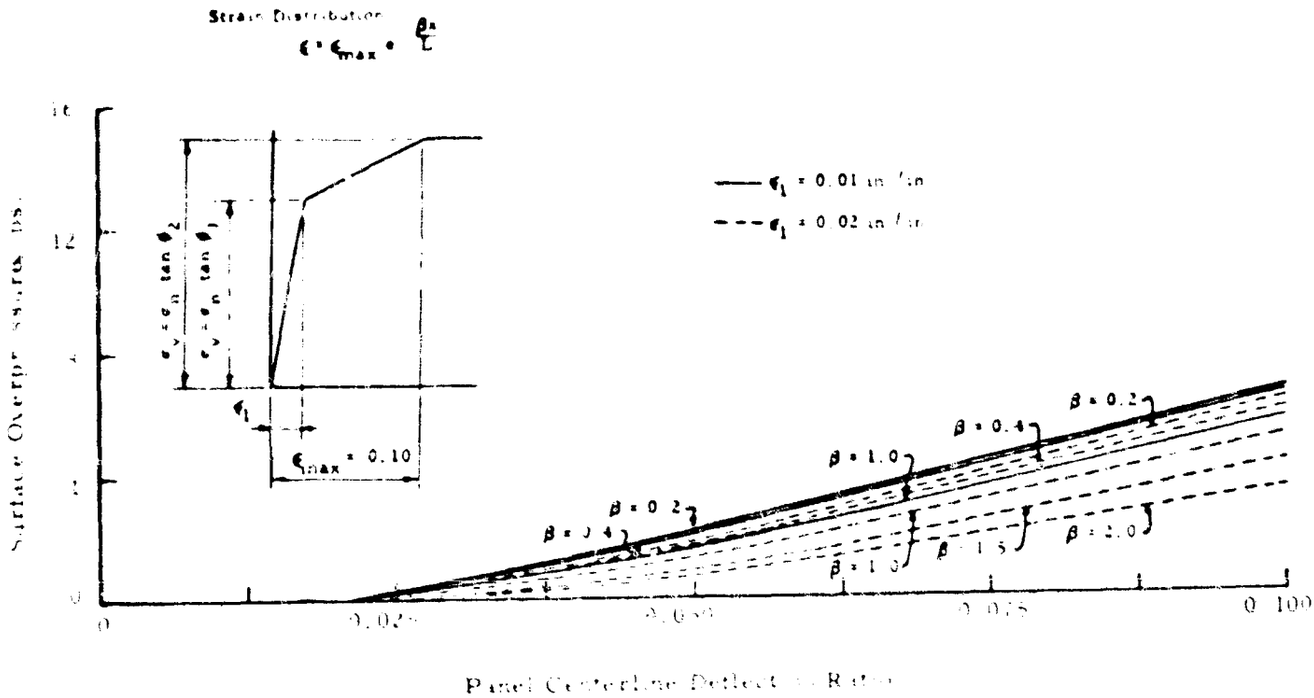


Fig. 7 Surface Overpressure as Related to Panel Centerline Deflection Ratio, $r_b = 1.0$, K = 0.67

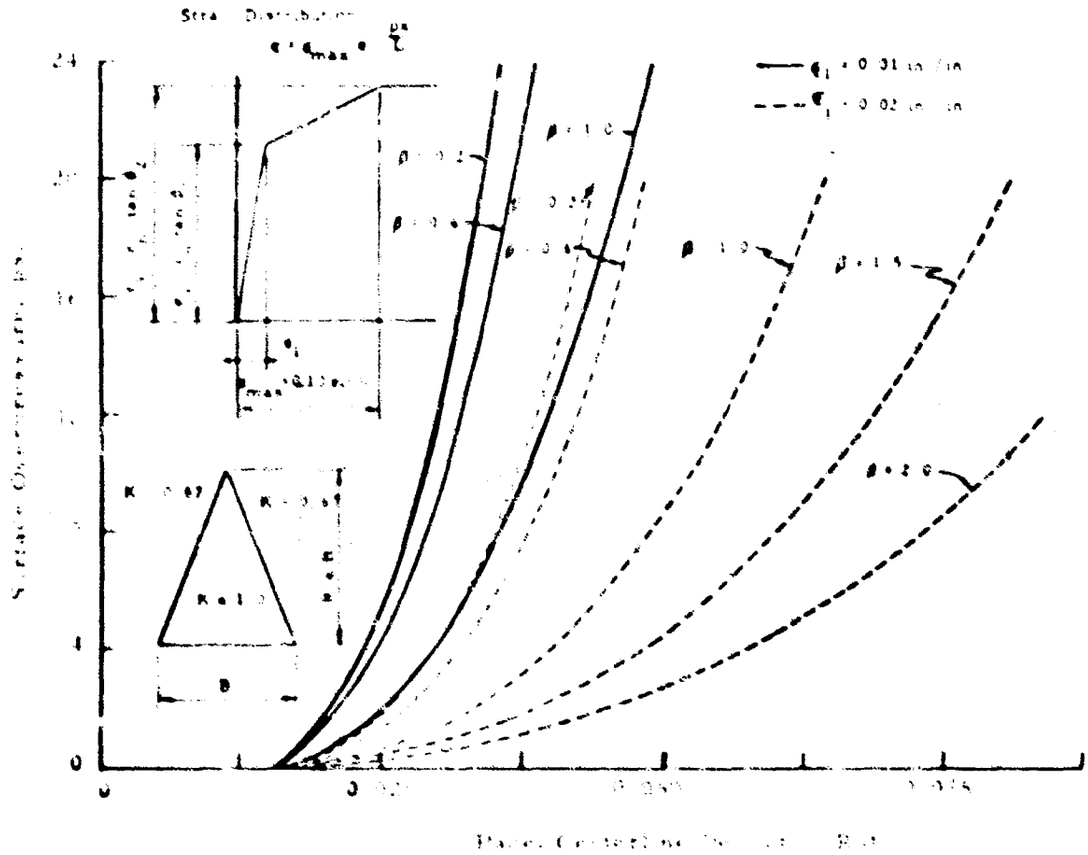


Fig. 8 Surface Overpressure as Related to Panel Centerline Deflection Ratio, r_b = 1.0, K = 0.67 1.0

CONCLUSION

Based on the Rankine Theory of earth pressures, it is postulated that the ratio of lateral to vertical stress within a soil mass may vary from

$$K = \frac{P_h}{P_v} = \tan^2 (45 - \emptyset/2), \text{ the active case, to}$$

$$K = \frac{P_h}{P_v} = \tan^2 (45 + \emptyset/2), \text{ the passive case.}$$

The development of either the full active of full passive case requires that certain conditions of deformation be realized and these cases probably represent the upper and lower bounds of the ratio of lateral to vertical stress.

For an angle $\emptyset = 30^\circ$, this means K may be between 1/3, the active case, and 3, the passive case. It was seen in Figure 4 that near the panel center-line, soil grids were shortened in the horizontal direction and elongated in the vertical direction. This pattern of deformation would indicate that K is greater than 1 and could be approaching the ratio of passive resistance. Terzaghi found experimentally that over the center-line of a yielding trap door that K was greater than 1 for a height of almost two trap door widths. However, near the panel edge (Figure 4), the deformations in the soil indicate that the vertical stresses are greater than the horizontal and hence, K is less than 1 and could approach the ratio of active resistance.

Thus, in a soil mass surrounding a deforming structure, the ratio of lateral to vertical stress changes from the coefficient of earth pressure at rest, before any deformation occurs, to a smaller or greater value between the limits of

$$\tan^2 (45 \pm \emptyset/2).$$

The results presented in this paper show that the K value selected is probably the most significant influence in the soil-structure interaction problem. Because of its affect on the problem it is not believed a constant value can be assigned, and still satisfactorily predict structural loading over any range of conditions. Also, because of the influence the K value has on the problem, one must exercise caution in accepting the validation of any theory on the basis of a limited experimental program. From Figure 8, it can be seen that reasonable assumptions, as to soil behavior and the K value, can be made which would cover a wide range of experimental results.

It is believed that for an analytical solution to successfully predict structural loading over a wide range of varying parameters, i.e., panel stiffness, burial depth, soil type, etc., it will be necessary to account for changes in K as the soil and structure interact. Terzaghi's results give some indication that these changes may be restricted to a localized area near the deforming structure. As such, it is possible that an empirical relationship could be established between structural deformation and K values at various distances from the structure.

REFERENCES

1. Selig, E. T., K. E. McKee and E. Vey, "Underground Structures Subject to Air Overpressure" Transactions ASCE, Part I, Vol. 126, 1961.
2. Newmark, N. M. and J. D. Hallinanger, "Principles and Practices for Design of Hardened Structures" AFSWC-TD2-62-138, December 1962.
3. Terzaghi, K., "A Fundamental Fallacy in Earth Pressure Computations", Journal Boston Society of Civil Engineers, April 1936.
4. Truesdale, W. B., "Strain Variations in a Triaxial Soil Test" IITRI for the AFWL, WL-TDR-64-47, February 1964.
5. Havers, J. and W. Truesdale, "Experimental Study of the Response of Buried Structural Elements to Static and Dynamic Surface Loading," Proceedings of the 32nd Symposium on Shock, Vibration and Associated Environments, Albuquerque, New Mexico, April 1963.

ARCHING IN SOIL DUE TO THE DEFLECTION OF A RIGID HORIZONTAL STRIP

by
Chunduri V. Chelapati*

SYNOPSIS

When one part of the support of the soil settles relative to the other parts of the support, the pressure on the deflecting support reduces with a corresponding increase of pressure on the neighboring parts. This transfer of pressure from the deflecting part to the neighboring soil is known as the arching effect. In the present study, the amount of arching, that is, the amount of pressure transferred to the neighboring soil when a rigid horizontal support buried under a soil cover of finite depth deflects, is investigated. The surface of the soil is subjected to high overpressure. The soil is assumed ideal characterized by modulus of elasticity E, and Poisson's ratio, μ. Solutions based on the equations of plane strain are obtained in the form of infinite series. Since soil cannot be expected to be effective in tension, a condition is imposed that the net pressure on the deflecting base cannot be tensile. It is shown that arching in this case is a function of the parameters b/h, ph/dE, and μ, where 2b is the width of this base, h is the depth of soil, p is the pressure on the base with no displacement and d is the amount of base displacement.

The first six terms of the infinite series solution are evaluated using a digital computer for a wide range of parameters. Graphs are presented showing the pressure distribution on the base, and the amount of arching over the base. An example is given to demonstrate the use of these plots.

INTRODUCTION

If the foundation of an underground structure settles, the pressure transmitted to the structure is reduced with the corresponding increase of pressure in the neighboring soil. This phenomenon is known as arching. Arching due to the displacement of a rigid horizontal strip, or yielding of a base, has been discussed by Terzhaghi (1) and formulas for the pressure transmitted to the strip or base are given based on assumed failure planes. The magnitude of the displacement to produce these failure planes is not known. If the magnitude of the displacement is below a critical value, the failure planes will not develop and the arching formulas cannot be used effectively. At zero displacement, the pressure on the strip is equal to the pressure of the soil above the strip plus any additional overpressure acting on the soil. The pressure on the strip decreases as the displacement is increased. It should be possible to displace the strip to a critical value such that all the pressure acting on the strip at no displacement is transferred to the neighboring soil. The objectives of this study are to establish the limits on the base displacement, to find the amount of arching and the pressure distribution on the base for various cases.

W. D. Finn (2) has treated various problems dealing with stresses in idealized soil media subjected to different types of boundary conditions. One such problem deals with the stresses in soils due to the displacement of a rigid horizontal strip. The depth of the soil was taken as infinite which imposes a restriction in adapting the solution to practical problems.

The present study deals with the stresses in a soil field of finite depth, h, due to the displacement of a rigid strip of width 2b. The soil mass is assumed to be a homogeneous, elastic, isotropic medium and is subjected to high overpressures. If there is no displacement of the horizontal strip, the pressure p, transmitted to the strip will be equal to the overpressure, p_o, plus the pressure due to soil above the base, γh, where γ is the density of the soil. However, if the strip is displaced by an amount d, the pressure transmitted to it will be relieved by an amount equal to the tensile forces induced on the strip due to the displacement d. Assuming that the principle of superposition is valid, the amount of arching (the amount of pressure that is transferred to the neighboring soil or the reduction of pressure on the strip) is equal to the amount of tensile forces on the base due to the displacement d. However, as the strip settles, zones of very high tensile stresses form toward the edges owing to the discontinuous displacement. Thus, when the overpressures are superimposed on the tensile forces, there will still be residual tensile stresses toward the edges of the base. Since the soil media cannot be expected to transmit tensile stresses these stresses are not considered to contribute to arching. This condition is specified when computing the amount of arching.

*Assistant Professor of Engineering, California State College at Los Angeles, Los Angeles, California.

ANALYTICAL DEVELOPMENT PROCEDURE

Figure 1 represents a section through the soil mass of depth h and infinite width subjected to an overpressure of p_o. The distance in the z direction perpendicular to the x-y plane can be considered as infinity. The width of the rigid horizontal strip is 2b, and the amount of base deflection is given by d. The total pressure on the strip with conditions given in Case (a) can be considered to be equivalent to the superposition of Case (b) and (c). Case (b) represents a uniform compression on the base exerted by the overpressure and soil above the base, ($p = p_o + \gamma h$) with no displacement of the rigid strip.

The distribution of pressure is indicated by 12. The tensile force distribution due to the displacement d alone is assumed to be 34567 as shown in Case (c). The tensile stresses at the edge are infinite due to the discontinuity of displacement. The pressure distribution for Case (a) can be assumed to be given by the superposition of Cases (b) and (c) for small displacements of the strip. It is to be noted that the tensile stresses due to the base displacement reach the value of the maximum compression p, at some critical distance $\pm x_{cr}$, from the center of the base. Beyond this region the net pressure on the base is tensile. These resultant tensile stresses in the region beyond $\pm x_{cr}$, from the center of the base are not considered effective. Thus, the net compressive force acting on the strip is given by the area 456. The objectives of this study are to find the distribution of tensile forces as shown in Case (c) by 34567, to determine the distance, $\pm x_{cr}$, at which the resultant pressures become tensile and to find the amount of arching as shown in Case (a) by 14562.

Evaluation of Stress Function

Since by assumption there are no strains in the z direction, the problem can be considered as one of plane strain, and the appropriate equations of Theory of Elasticity can be used (3). The positive directions of the stresses σ_x, σ_y, and τ_{xy} are shown in Figure 1. Since the surface is free of applied pressure, the boundary conditions for Case (c) at $y = h$ are given by:

$$\sigma_y = 0 \qquad (1)$$

$$\tau_{xy} = 0 \qquad (2)$$

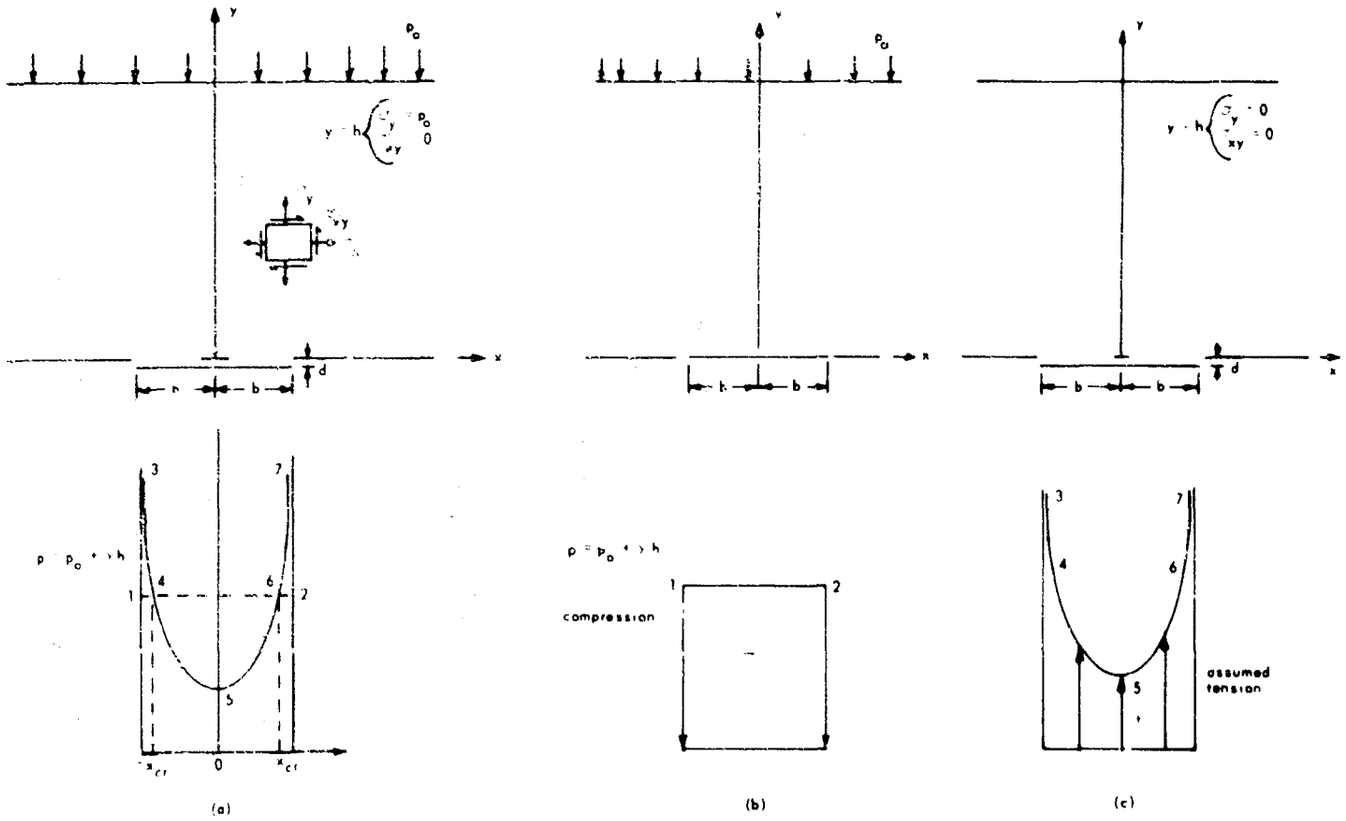


Fig. 1 Stress Distribution Across the Width of a Rigid Horizontal Strip in an Elastic Medium

The frictional resistance at the base, $y = 0$, can be assumed to prevent any elongation in the x direction at that level. Thus, the strain in the x direction at $y = 0$ is $\epsilon_{x,y=0} = \beta\sigma_x - \rho\sigma_y = 0$ (3)

where $$\beta = \frac{1-\mu^2}{E} \qquad \rho = \frac{\mu(1+\mu)}{E} \tag{4}$$

The displacement v, in the y direction at the boundary $y = 0$ is given by

$$v = -d \text{ for } -b \leq x \leq +b$$

and

$$= 0 \text{ for } x < -b \text{ and } x > +b \tag{5}$$

The displacement at the boundary can be expressed in integral form by using the Fourier cosine integral:

$$v(x) = \frac{2}{\pi}\int_0^\infty \cos\alpha x \, d\alpha \int_0^\infty v(\lambda) \cos\alpha\lambda \, d\lambda \tag{6}$$

Thus, the displacement at $y = 0$ as defined by Equation (5) can be obtained as

$$v(x) = -\frac{2d}{\pi}\int_0^\infty \frac{\sin\alpha b}{\alpha} \cos\alpha x \, d\alpha \tag{7}$$

Where α and λ are variables of integration.

The displacement, v, can be expressed in terms of strains ϵ_y in the y direction as

$$\epsilon_y = \frac{\partial v}{\partial y} = \beta\sigma_y - \rho\sigma_x \tag{8}$$

and

$$v = \int \epsilon_y dy + g(x) \tag{9}$$

To solve for the various stresses in the media, with the given boundary conditions, Airy's stress function (2) in the following form is assumed:

$$\phi = \int_0^\infty \frac{1}{\alpha^2}\left[A e^{\alpha y} + B\alpha e^{\alpha y} + C e^{-\alpha y} + D\alpha e^{-\alpha y}\right] \cos\alpha x \, dx \tag{10}$$

where A, B, C, D are constants.

It can be shown that the above stress function ϕ, satisfies the biharmonic equation

$$\nabla^4\phi = \frac{\partial^4\phi}{\partial x^4} + 2\frac{\partial^4\phi}{\partial x^2\partial y^2} + \frac{\partial^4\phi}{\partial y^4} = 0 \tag{11}$$

The stresses in the media are related to the stress function by the following relations.

$$\sigma_x = \frac{\partial^2\phi}{\partial x^2}$$

$$\sigma_y = \frac{\partial^2\phi}{\partial y^2}$$

$$\tau_{xy} = -\frac{\partial^2\phi}{\partial x\partial y} \tag{12}$$

The constants A, B, C, and D are found by using the boundary conditions (1), (2), (3), and (7) as specified above. The function g(x) in Equation 9 can be shown to be zero after appropriate substitutions and integrations using the conditions that $v = 0$ for $h \to \infty$. The relations for the constants A, B, C, and D are as follows:

$$A = \left[C(-2\alpha h - 1) + D(-2\alpha^2 h^2) \right] e^{-2\alpha h} \tag{13}$$

$$B = \left[2C + D(2\alpha h - 1) \right] e^{-2\alpha h} \tag{14}$$

$$C = D \left[\frac{e^{-2\alpha h}\left\{ (-2\alpha^2 h^2 + 4\alpha h - 2)\beta - 2\alpha^2 h^2 \rho \right\} - 2\beta}{e^{-2\alpha h}\left\{ (2\alpha h - 3)\beta + (2\alpha h + 1)\rho \right\} - \beta - \rho} \right] \tag{15}$$

$$D = -\frac{2d}{\pi} \left[\frac{\left[e^{-2\alpha h}\left\{ (2\alpha h - 3)\beta + (2\alpha h + 1)\rho \right\} - \beta - \rho \right]}{\begin{array}{l} \left[e^{-4\alpha h}\left\{ -3\beta^2 - 2\beta\rho + \rho^2 \right\} \right. \\ + e^{-2\alpha h}\left\{ (-4\alpha^2 h^2 - 10)\beta^2 + (-8\alpha^2 h^2 + 4)\rho\beta + (-4\alpha^2 h^2 - 2)\rho^2 \right\} \\ \left. -3\beta^2 - 2\beta\rho + \rho^2 \right] \end{array}} \right] \sin \alpha b \tag{16}$$

Substitution of the expressions for A, B, C, and D in Equation 10 and subsequent simplification will result in an expression for the stress function. The stresses anywhere in the medium can be found by using Equation 12. However, since the σ_y stresses over the base are of main interest, only they are evaluated in the next section.

Evaluation of Stress Due to Displacement, d

The expression for the stress σ_y is obtained by substituting stress function in Equation 12 and is given below:

$$\sigma_y = \int_0^\infty -\frac{2d}{\pi} \left[\frac{\begin{array}{l} e^{\alpha(y-4h)}\left[\alpha(\beta y + \rho y) - 2\beta \right] \\ + e^{\alpha(y-2h)}\left[\alpha^2 \left\{ 2\beta(-h^2 + hy) + 2\rho(-h^2 + hy) \right\} + \alpha\left\{ \beta(-4h + 3y) - y\rho \right\} - 2\beta \right] \\ + e^{\alpha(-y-2h)}\left[\alpha^2 \left\{ 2\beta(h^2 - hy) + 2\rho(h^2 - hy) \right\} + \alpha\left\{ \beta(-4h + 3y) - y\rho \right\} + 2\beta \right] \\ + e^{-\alpha y}\left[\alpha\left\{ \beta y + \rho y \right\} + 2\beta \right] \end{array}}{\begin{array}{l} e^{-4\alpha h}\left[-3\beta^2 - 2\rho\beta + \rho^2 \right] \\ + e^{-2\alpha h}\left[\alpha^2 \left\{ -4\beta^2 h^2 - 8\rho\beta h^2 - 4\rho^2 h^2 \right\} + \left\{ -10\beta^2 + 4\beta\rho - 2\rho^2 \right\} \right] \\ + (-3\beta^2 - 2\beta\rho + \rho^2) \end{array}} \right] \sin b\alpha \cos x\alpha \, d\alpha \tag{17}$$

This expression for σ_y can be specialized to obtain the pressure distribution across the horizontal strip by integrating and then substituting $y = 0$ in the final results. However, with some care, $y = 0$ can be substituted in some terms of the numerator of the integrand before performing the integration and the following integral is obtained for $\sigma_{y,o}$ along $y = 0$.

$$\sigma_{y,o} = -2\beta C_3 \int_0^\infty \left[\frac{e^{-4\alpha h} + 4\alpha h e^{-2\alpha h} - e^{-\alpha y}}{e^{-4\alpha h} + e^{-2\alpha h}(C_1 4\alpha^2 h^2 + C_2) + 1} \right] 2 \sin b\alpha \cos x\alpha \, d\alpha \tag{18}$$

where

$$C_1 = \left[\frac{-\beta^2 - 2\beta\rho - \rho^2}{-3\beta^2 - 2\beta\rho + \rho^2} \right]$$

$$C_2 = \left[\frac{-10\beta^2 + 4\beta\rho - 2\rho^2}{-3\beta^2 - 2\beta\rho + \rho^2} \right]$$

$$C_3 = -\frac{d}{\pi} \left[\frac{1}{-3\beta^2 - 2\beta\rho + \rho^2} \right]$$

$$C_4 dE = -2\beta C_3$$

or

$$C_4 = \frac{2\beta}{\pi E(-3\beta^2 - 2\beta\rho + \rho^2)}$$

C_1, C_2, and C_4 are dimensionless constants and C_3 has the units of pounds per inch.

The integration of the expression given by Equation 18 is achieved by expanding the denominator into series. The resulting expression is shown below.

$$\sigma_{y,o} = C_4 dE \int_o^\infty \Big\{ 1 - e^{-2\alpha h}(C_1 4\alpha^2 h^2 + C_2) + e^{-4\alpha h}\left[(C_1 4\alpha^2 h^2 + C_2)^2 - 1\right] - e^{-6\alpha h}\left[(C_1 4\alpha^2 h^2 + C_2)^3 - 2(C_1 4\alpha^2 h^2 + C_2)\right] + e^{-8\alpha h}\left[(C_1 4\alpha^2 h^2 + C_2)^4 - 3(C_1 4\alpha^2 h^2 + C_2)^2 + 1\right] - e^{-10\alpha h}\left[\ldots\right] + \ldots \Big\} \Big\{ e^{-4\alpha h} + 4\alpha h e^{-2\alpha h} - e^{-\alpha y} \Big\} \times \Big\{ 2 \sin b\alpha \cos x\alpha \Big\} d\alpha \qquad (19)$$

or

$$\sigma_{y,o} = \sum \sigma_{y,o}^{(i)} = \sigma_{y,o}^{(1)} + \sigma_{y,o}^{(2)} + \sigma_{y,o}^{(3)} + \sigma_{y,o}^{(4)} + \sigma_{y,o}^{(5)} + \sigma_{y,o}^{(6)} + \ldots \qquad (20)$$

where

$$\sigma_{y,o}^{(1)} = C_4 dE \int_o^\infty \left[1\right]\left[e^{-4\alpha h} + 4\alpha h e^{-2\alpha h} - e^{-\alpha y}\right]\left[2 \sin b\alpha \cos x\alpha\right] d\alpha$$

$$\sigma_{y,o}^{(2)} = -C_4 dE \int_o^\infty e^{-2\alpha h}\left[C_1 4\alpha^2 h^2 + C_2\right]\left[e^{-4\alpha h} + 4\alpha h e^{-2\alpha h} - e^{-\alpha y}\right]\left[2 \sin b\alpha \cos x\alpha\right] d\alpha$$

$$\sigma_{y,o}^{(3)} = C_4 dE \int_o^\infty e^{-4\alpha h}\left[(C_1 4\alpha^2 h^2 + C_2)^2 - 1\right]\left[e^{-4\alpha h} + 4\alpha h e^{-2\alpha h} - e^{-\alpha y}\right]\left[2 \sin b\alpha \cos x\alpha\right] d\alpha$$

$$\sigma_{y,o}^{(4)} = -C_4 dE \int_o^\infty e^{-6\alpha h}\left[(C_1 4\alpha^2 h^2 + C_2)^3 - 2(C_1 4\alpha^2 h^2 + C_2)\right]\left[e^{-4\alpha h} + 4\alpha h e^{-2\alpha h} - e^{-\alpha y}\right]\left[2 \sin b\alpha \cos x\alpha\right] d\alpha$$

$$\sigma_{y,o}^{(5)} = C_4 dE \int_o^\infty e^{-8\alpha h}\left[(C_1 4\alpha^2 h^2 + C_2)^4 - 3(C_1 4\alpha^2 h^2 + C_2)^2 + 1\right]\left[e^{-4\alpha h} + 4\alpha h e^{-2\alpha h} - e^{-\alpha y}\right]\left[2 \sin b\alpha \cos x\alpha\right] d\alpha$$

$$\sigma_{y,o}^{(6)} = -C_4 dE \int_o^\infty e^{-10\alpha h}\left[(C_1 4\alpha^2 h^2 + C_2)^5 - 4(C_1 4\alpha^2 h^2 + C_2)^3 + 3(C_1 4\alpha^2 h^2 + C_2)\right]\left[e^{-4\alpha h} + 4\alpha h e^{-2\alpha h} - e^{-\alpha y}\right]\left[2 \sin b\alpha \cos x\alpha\right] d\alpha \qquad (21)$$

In the present study the first six terms of the infinite series are considered adequate to represent $\sigma_{y,o}$. The expressions for $\sigma_{y,o}^{(i)}$ are evaluated individually and then y is set to zero. In the expression for $\sigma_{y,o}^{(1)}$ if the value of zero for y is substituted in the integrand, the improper integral

$$\int_o^\infty \sin b\alpha \cos x\alpha \, d\alpha$$

does not exist (4). However with the term $e^{-\alpha y}$ in the integrand, the value of the integral is given by

$$-C_4 dE \int_0^\infty e^{-\alpha y} 2 \sin b\alpha \cos x\alpha \, d\alpha = -C_4 dE \left[\frac{b+x}{y^2 + (b+x)^2} + \frac{b-x}{y^2 + (b-x)^2} \right] \tag{22a}$$

and the limiting value as $y \to 0$ is given by

$$-C_4 dE \left[\frac{1}{b+x} + \frac{1}{b-x} \right] \tag{22b}$$

The final expressions for $\sigma^{(i)}_{y,o}$ are obtained after the evaluation of the integrals in Equation 21. These expressions for $\sigma^{(i)}_{y,o}$ are non-dimensionalized by (d/h) E to give S_i's.

Thus

$$S_i = \frac{\sigma^{(i)}_{y,o}}{(d/h)\,E} \tag{23}$$

It can be noted that d/h indicates the uniform strain in the media if the base extends to infinity, and (d/h) E represents the corresponding uniform stress in the media. The following notations are used while expressing S_i's.

$$\begin{aligned}
A(i)(J) &= \left[\frac{b}{ih} \left(1 + \frac{x}{b}\right) \right]^J \\
B(i)(J) &= \left[\frac{b}{ih} \left(1 - \frac{x}{b}\right) \right]^J \\
A(i)2(J) &= \left\{ 1 + \left[\frac{b}{ih} \left(1 + \frac{x}{b}\right) \right]^2 \right\}^J \\
B(i)2(J) &= \left\{ 1 + \left[\frac{b}{ih} \left(1 - \frac{x}{b}\right) \right]^2 \right\}^J
\end{aligned} \tag{24}$$

The last two notations are used only in the denominators of the expressions for S_i's and $i \geq j - 1$. The resulting equations are:

$$S_1 = \frac{\sigma^{(1)}_{y,o}}{(d/h)\,E} = C_4 \left[0.25 \left\{ \frac{A41}{A421} + \frac{B41}{B421} \right\} + 1 \left\{ \frac{A11}{A222} + \frac{B11}{B222} \right\} - 1 \left\{ \frac{1}{A11} + \frac{1}{B11} \right\} \right] \tag{25a}$$

$$\begin{aligned}
S_2 = \frac{\sigma^{(2)}_{y,o}}{(d/h)\,E} = C_4 \Bigg[& C_1 \left\{ -\frac{1}{27} \left[\frac{3 \cdot A61 - A63}{A623} + \frac{3 \cdot B61 - B63}{B623} \right] - 1.5 \left[\frac{A41 - A43}{A424} + \frac{B41 - B43}{B424} \right] \right. \\
& \left. + 1 \left[\frac{3 \cdot A21 - A23}{A223} + \frac{3 \cdot B21 - B23}{B223} \right] \right\} \\
& + C_2 \left\{ -\frac{1}{6} \left[\frac{A61}{A621} + \frac{B61}{B621} \right] - 0.5 \left[\frac{A41}{A422} + \frac{B41}{B422} \right] + 0.5 \left[\frac{A21}{A221} + \frac{B21}{B221} \right] \right\} \Bigg]
\end{aligned} \tag{25b}$$

$$S_3 = \frac{\sigma_{y,o}^{(3)}}{(d/h)\,E} = C_4 \Bigg[C_1^2 \Big\{ 0.0117188 \left[\frac{5\cdot A81 - 10\cdot A83 + A85}{A825} + \frac{5\cdot B81 - 10\cdot B83 + B85}{B825} \right] + 0.1646091 \left[\frac{6\cdot A61 - 20\cdot A63 + 6\cdot A65}{A626} + \frac{6\cdot B61 - 20\cdot B63 + 6\cdot B65}{B626} \right] - 0.375 \left[\frac{5\cdot A41 - 10\cdot A43 + A45}{A425} + \frac{5\cdot B41 - 10\cdot B43 + B45}{B425} \right] \Big\} + C_1C_2 \Big\{ 0.03125 \left[\frac{3\cdot A81 - A83}{A823} + \frac{3\cdot B81 - B83}{B823} \right] + 0.1481481 \left[\frac{4\cdot A61 - 4\cdot A63}{A624} + \frac{4\cdot B61 - 4\cdot B63}{B624} \right] - 0.25 \left[\frac{3\cdot A41 - A43}{A423} + \frac{3\cdot B41 - B43}{B423} \right] \Big\} + (C_2^2-1) \Big\{ 0.125 \left[\frac{A81}{A821} + \frac{B81}{B821} \right] + 0.1111111 \left[\frac{2\cdot A61}{A622} + \frac{2\cdot B61}{B622} \right] - 0.25 \left[\frac{A41}{A421} + \frac{B41}{B421} \right] \Big\} \Bigg] \qquad (25c)$$

$$S_4 = \frac{\sigma_{y,o}^{(4)}}{(d/h)\,E} = C_4 \Bigg[C_1^3 \Big\{ - 0.004608 \left[\frac{7\cdot A101 - 35\cdot A103 + 21\cdot A105 - A107}{A1027} + \frac{7\cdot B101 - 35\cdot B103 + 21\cdot B105 - B107}{B1027} \right] - 0.0769043 \left[\frac{8\cdot A81 - 56\cdot A83 + 56\cdot A85 - 8\cdot A87}{A828} + \frac{8\cdot B81 - 56\cdot B83 + 56\cdot B85 - 8\cdot B87}{B828} \right] + 0.1646091 \left[\frac{7\cdot A61 - 35\cdot A63 + 21\cdot A65 - A67}{A627} + \frac{7\cdot B61 - 35\cdot B63 + 21\cdot B65 - B67}{B627} \right] \Big\} + C_1^2C_2 \Big\{ - 0.01152 \left[\frac{5\cdot A101 - 10\cdot A103 + A105}{A1025} + \frac{5\cdot B101 - 10\cdot B103 + B105}{B1025} \right] - 0.0878906 \left[\frac{6\cdot A81 - 20\cdot A83 + 6\cdot A85}{A826} + \frac{6\cdot B81 - 20\cdot B83 + 6\cdot B85}{B826} \right] + 0.1481482 \left[\frac{5\cdot A61 - 10\cdot A63 + A65}{A625} + \frac{5\cdot B61 - 10\cdot B63 + B65}{B625} \right] \Big\} + (3C_1C_2^2-2C_1) \Big\{ - 0.008 \left[\frac{3\cdot A101 - A103}{A1023} + \frac{3\cdot B101 - B103}{B1023} \right] - 0.0234375 \left[\frac{4\cdot A81 - 4\cdot A83}{A824} + \frac{4\cdot B81 - 4\cdot B83}{B824} \right] + 0.0370370 \left[\frac{3\cdot A61 - A63}{A623} + \frac{3\cdot B61 - B63}{B623} \right] \Big\} \Bigg]$$

$$+ (C_2^3 - 2C_2) \left\{ - 0.10 \left[\frac{A101}{A1021} + \frac{B101}{B1021} \right] - 0.0625 \left[\frac{2 \cdot A81}{A822} + \frac{2 \cdot B81}{B822} \right] + 0.1666667 \left[\frac{A61}{A621} + \frac{B61}{B621} \right] \right\} \Bigg] \tag{25d}$$

$$S_5 - \frac{\sigma_{\gamma_{10}}^{(5)}}{(d/h)\,E} = C_4 \Bigg[C_1^4 \left\{ 0.0020005 \left[\frac{9 \cdot A121 - 84 \cdot A123 + 126 \cdot A125 - 36 \cdot A127 + A129}{A1229} + \frac{9 \cdot B121 - 84 \cdot B123 + 126 \cdot B125 - 36 \cdot B127 + B129}{B1229} \right] + 0.0371589 \left[\frac{10 \cdot A101 - 120 \cdot A103 + 252 \cdot A105 - 120 \cdot A107 + 10 \cdot A109}{A10210} + \frac{10 \cdot B101 - 120 \cdot B103 + 252 \cdot B105 - 120 \cdot B107 + 10 \cdot B109}{B10210} \right] - 0.0769043 \left[\frac{9 \cdot A81 - 84 \cdot A83 + 126 \cdot A85 - 36 \cdot A87 + A89}{A829} + \frac{9 \cdot B81 - 84 \cdot B83 + 126 \cdot B85 - 36 \cdot B87 + B89}{B829} \right] \right\}$$

$$+ C_1^3 C_2 \left\{ 0.0051440 \left[\frac{7 \cdot A121 - 35 \cdot A123 + 21 \cdot A125 - A127}{A1227} + \frac{7 \cdot B121 - 35 \cdot B123 + 21 \cdot B125 - B127}{B1227} \right] + 0.0516096 \left[\frac{8 \cdot A101 - 56 \cdot A103 + 56 \cdot A105 - 8 \cdot A107}{A1028} + \frac{8 \cdot B101 - 56 \cdot B103 + 56 \cdot B105 - 8 \cdot B107}{B1028} \right] - 0.0878906 \left[\frac{7 \cdot A81 - 35 \cdot A83 + 21 \cdot A85 - A87}{A827} + \frac{7 \cdot B81 - 35 \cdot B83 + 21 \cdot B85 - B87}{B827} \right] \right\}$$

$$+ (2C_2^2 - 1)C_1^2 \left\{ 0.0046296 \left[\frac{5 \cdot A121 - 10 \cdot A123 + A125}{A1225} + \frac{5 \cdot B121 - 10 \cdot B123 + B125}{B1225} \right] + 0.02304 \left[\frac{6 \cdot A101 - 20 \cdot A103 + 6 \cdot A105}{A1026} + \frac{6 \cdot B101 - 20 \cdot B103 + 6 \cdot B105}{B1026} \right] - 0.0351563 \left[\frac{5 \cdot A81 - 10 \cdot A83 + A85}{A825} + \frac{5 \cdot B81 - 10 \cdot B83 + B85}{B825} \right] \right\}$$

$$+ (2C_2^2 - 3)C_1 C_2 \left\{ 0.0092593 \left[\frac{3 \cdot A121 - A123}{A1223} + \frac{3 \cdot B121 - B123}{B1223} \right] + 0.0192 \left[\frac{4 \cdot A101 - 4 \cdot A103}{A1024} + \frac{4 \cdot B101 - 4 \cdot B103}{B1024} \right] - 0.03125 \left[\frac{3 \cdot A81 - A83}{A823} + \frac{3 \cdot B81 - B83}{B823} \right] \right\}$$

$$+ (C_2^4 - 3C_2 + 1) \left\{ 0.0833333 \left[\frac{A121}{A1221} + \frac{B121}{B1221} \right] + 0.04 \left[\frac{2 \cdot A101}{A1022} + \frac{2 \cdot B101}{B1022} \right] - 0.125 \left[\frac{A81}{A821} + \frac{B81}{B821} \right] \right\} \tag{25e}$$

and,

$$S_6 = \frac{\sigma_{y,o}^{(6)}}{(d/h)\,E} = C_4 \left[C_1^5 \left\{ - 0.0009176 \left[\frac{11 \cdot A141 - 165 \cdot A143 + 462 \cdot A145 - 330 \cdot A147 + 55 \cdot A149 - A1411}{A14211} + \frac{11 \cdot B141 - 165 \cdot B143 + 462 \cdot B145 - 330 \cdot B147 + 55 \cdot B149 - B1411}{B14211} \right] \right.$$

$$- 0.0183375 \left[\frac{12 \cdot A121 - 220 \cdot A123 + 792 \cdot A125 - 792 \cdot A127 + 220 \cdot A129 - 12 \cdot A1211}{A12212} + \frac{12 \cdot B121 - 220 \cdot B123 + 792 \cdot B125 - 792 \cdot B127 + 220 \cdot B129 - 12 \cdot B1211}{B12212} \right]$$

$$\left. + 0.0371589 \left[\frac{11 \cdot A101 - 165 \cdot A103 + 462 \cdot A105 - 330 \cdot A107 + 55 \cdot A109 - A1011}{A10211} + \frac{11 \cdot B101 - 165 \cdot B103 + 462 \cdot B105 - 330 \cdot B107 + 55 \cdot B109 - B1011}{B10211} \right] \right\}$$

$$+ C_1^4 C_2 \left\{ - 0.0024979 \left[\frac{9 \cdot A141 - 84 \cdot A143 + 126 \cdot A145 - 36 \cdot A147 + A149}{A1429} + \frac{9 \cdot B141 - 84 \cdot B143 + 126 \cdot B145 - 36 \cdot B147 + B149}{B1429} \right] \right.$$

$$- 0.0300069 \left[\frac{10 \cdot A121 - 120 \cdot A123 + 252 \cdot A125 - 120 \cdot A127 + 10 \cdot A129}{A12210} + \frac{10 \cdot B121 - 120 \cdot B123 + 252 \cdot B125 - 120 \cdot B127 + 10 \cdot B129}{B12210} \right]$$

$$\left. + 0.0516096 \left[\frac{9 \cdot A101 - 84 \cdot A103 + 126 \cdot A105 - 36 \cdot A107 + A109}{A1029} + \frac{9 \cdot B101 - 84 \cdot B103 + 126 \cdot B105 - 36 \cdot B107 + B109}{B1029} \right] \right\}$$

$$+ C_1^3 (5C_2^2 - 2) \left\{ -0.0008743 \left[\frac{7 \cdot A141 - 35 \cdot A143 + 21 \cdot A145 - A147}{A1427} + \frac{7 \cdot B141 - 35 \cdot B143 + 21 \cdot B145 - B147}{B1427} \right] \right.$$

$$- 0.0060014 \left[\frac{8 \cdot A121 - 56 \cdot A123 + 56 \cdot A125 - 8 \cdot A127}{A1228} + \frac{8 \cdot B121 - 56 \cdot B123 + 56 \cdot B125 - 8 \cdot B127}{B1228} \right]$$

$$\left. + 0.009216 \left[\frac{7 \cdot A101 - 35 \cdot A103 + 21 \cdot A105 - A107}{A1027} + \frac{7 \cdot B101 - 35 \cdot B103 + 21 \cdot B105 - B107}{B1027} \right] \right\}$$

$$+ C_1^2(5C_2^3-6C_2) \left\{ - 0.001428 \left[\frac{5\cdot A141 - 10\cdot A143 + A145}{A1425} + \frac{5\cdot B141 - 10\cdot B143 + B145}{B1425} \right] \right.$$

$$- 0.005144 \left[\frac{6\cdot A121 - 20\cdot A123 + 6\cdot A125}{A1226} + \frac{6\cdot B121 - 20\cdot B123 + 6\cdot B125}{B1226} \right]$$

$$\left. + 0.00768 \left[\frac{5\cdot A101 - 10\cdot A103 + A105}{A1025} + \frac{5\cdot B101 - 10\cdot B103 + B105}{B1025} \right] \right\}$$

$$+ C_1(5C_2^4-12C_2^2+3) \left\{ - 0.0029155 \left[\frac{3\cdot A141 - A143}{A1423} + \frac{3\cdot B141 - B143}{B1423} \right] \right.$$

$$- 0.0046296 \left[\frac{4\cdot A121 - 4\cdot A123}{A1224} + \frac{4\cdot B121 - 4\cdot B123}{B1224} \right]$$

$$\left. + 0.008 \left[\frac{3\cdot A101 - A103}{A1023} + \frac{3\cdot B101 - B103}{B1023} \right] \right\}$$

$$+ (C_2^5-4C_2^3+3C_2) \left\{ - 0.0714286 \left[\frac{A141}{A1421} + \frac{B141}{B1421} \right] - 0.0277778 \left[\frac{2\cdot A121}{A1222} + \frac{2\cdot B121}{B1222} \right] \right.$$

$$\left. \left. + 0.1 \left[\frac{A101}{A1021} + \frac{B101}{B1021} \right] \right\} \right] \qquad (25f)$$

From these expressions, it can be seen that

$$S_i = S_i\,(b/h,\ x/b,\ \mu\ )$$

and

$$S = \sum_{i=1}^{6} S_i \qquad (26)$$

A digitcl computer program is written to evaluate the six terms of the series for several values of the parameters as shown below:

b/h = 0.05, 0.1, 0.2, 0.3, 0.4, 0.5, 0.6, 0.7, 0.8, 0.9, 1.0

μ = 0.1, 0.25, 0.3333, 0.5

x/b = 0 to 0.95 at intervals of 0.05

Distribution of Pressure on the Base

The results showing S versus x/b for different values of b/h and μ are given in Figures 2 through 5. In all these cases the value of S reaches infinity at x/b = 1.0 due to the discontinuity at the boundary. For smaller values of b/h, the curve in the central portion is flatter than for larger values of b/h. For the extreme case of b/h = 1.0 and μ = 0.5 the pressure at the center of the base, that is, at x/b = 0 is in compression, whereas for other portions of the strip the stresses are tensile. Comparing the plots for various values of μ, it can be seen that there is little difference in the stress distribution except for the extreme cases of b/h = 1.00.

The intensity of the resultant pressure at any point on the base when the soil of depth h is subjected to an over-pressure of p_o is given by

$$p_{resultant} = \langle\, p_o + \gamma h - \sigma_{y,o} \,\rangle = \langle\, p - \sigma_{y,o} \,\rangle \qquad (27)$$

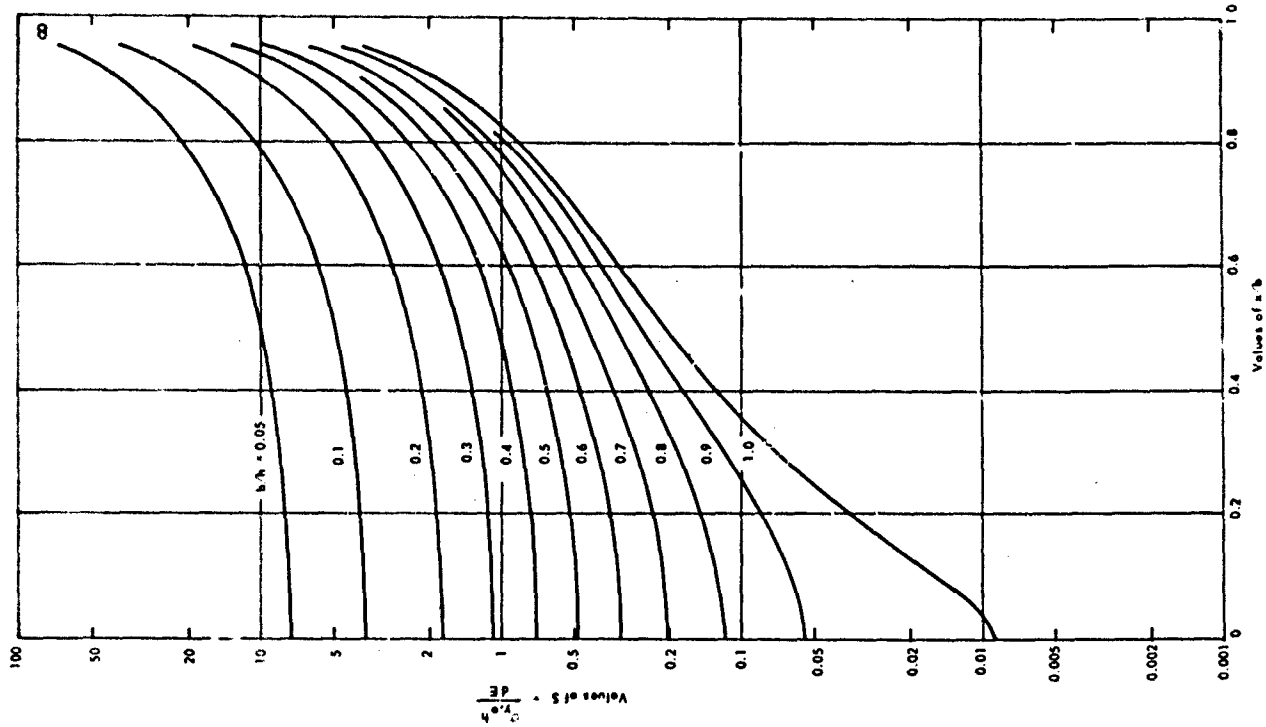


Fig. 3 Pressure Distribution on the Base for $\mu = 0.25$

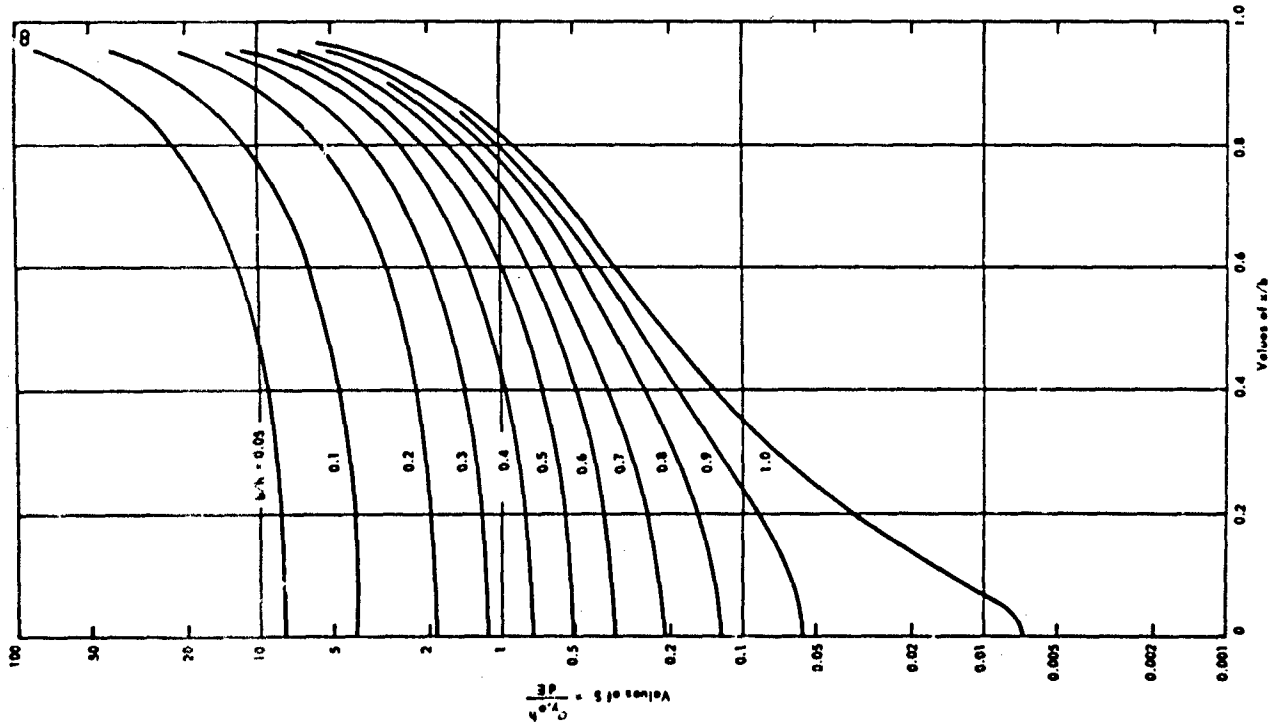


Fig. 2 Pressure Distribution on the Base for $\mu = 0.1$

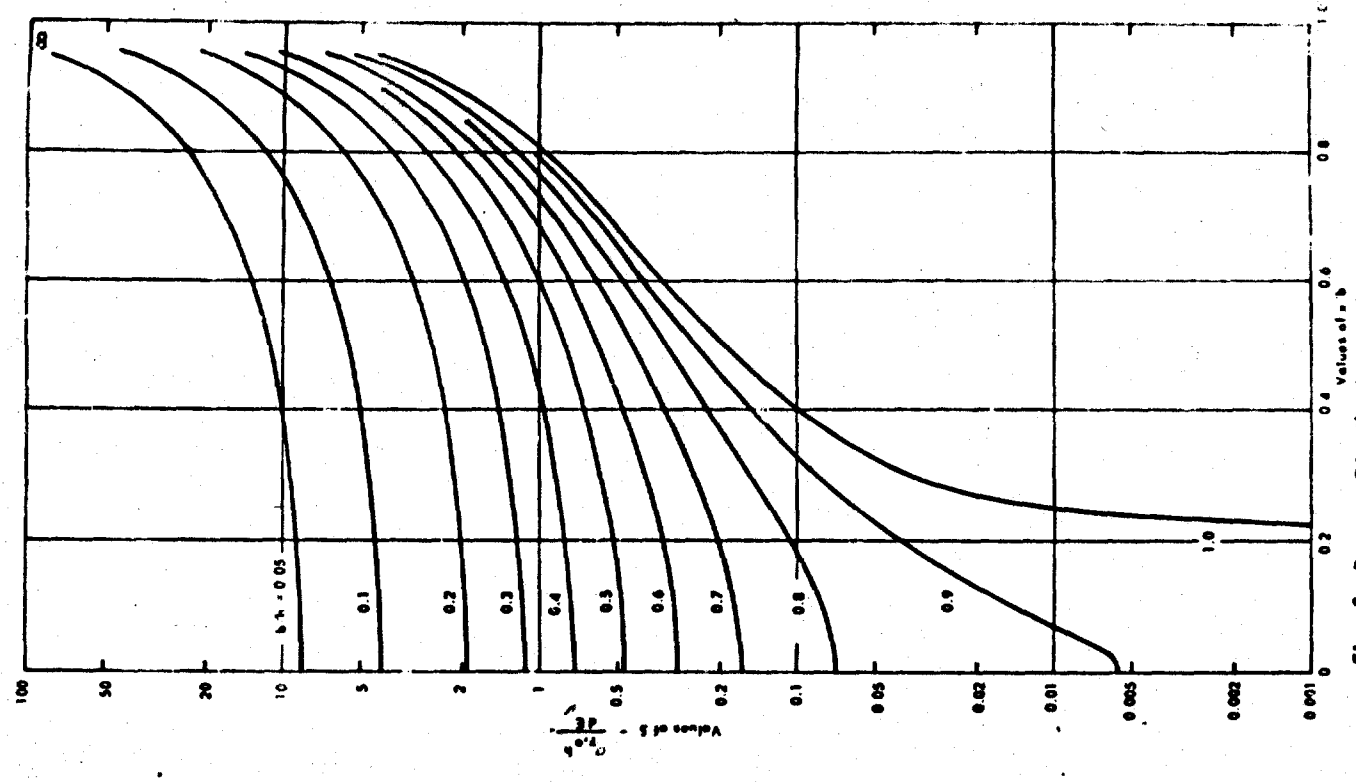


Fig. 5 Pressure Distribution on the Base for $\mu = 0.5$

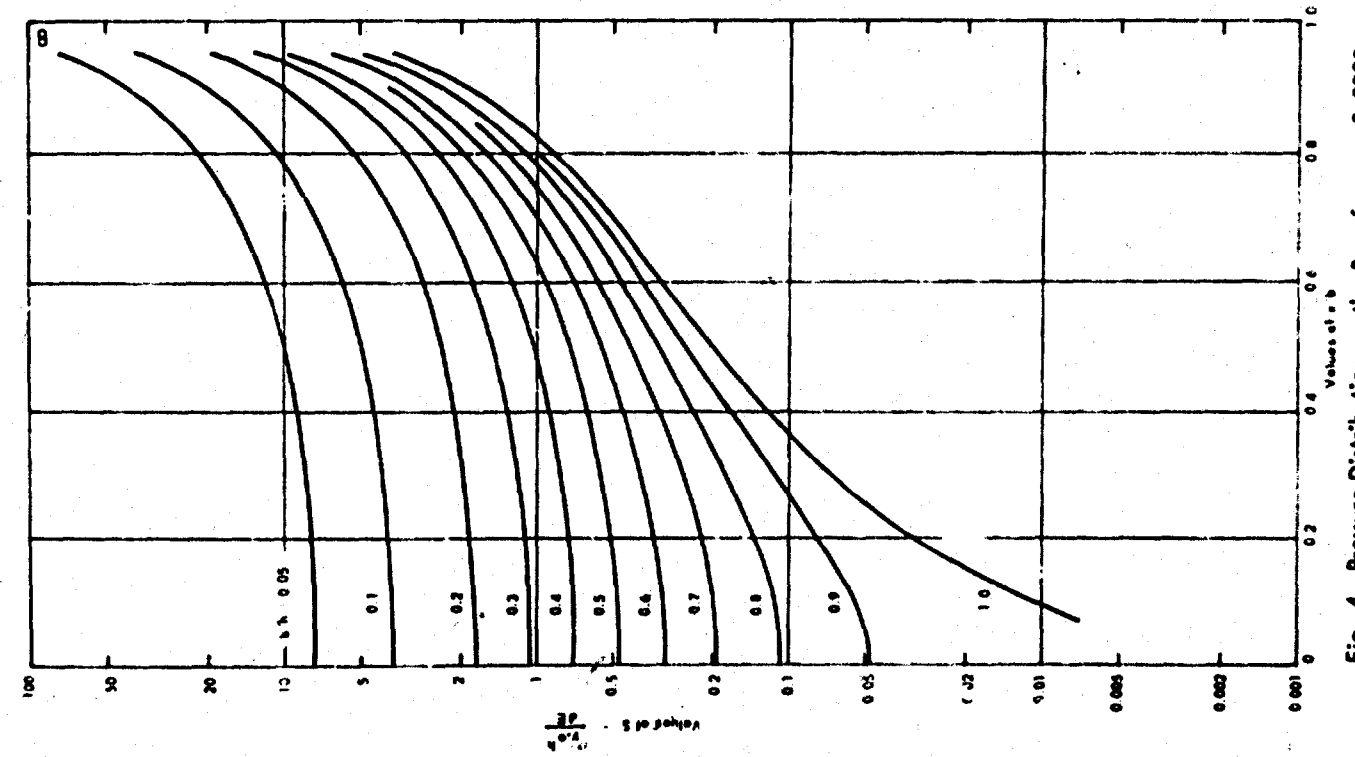


Fig. 4 Pressure Distribution on the Base for $\mu = 0.3333$

and nondimensionalizing by (d/h) $\tilde{\epsilon}$, Equation 27 can be rewritten as

$$\frac{(p_{\text{resultant}})\,h}{dE} = \left\langle \frac{ph}{dE} - S \right\rangle \tag{28}$$

The pointed brackets on the right hand side of the equation indicate that the expression is equal to zero for negative values of (ph/dE - S).

Computation of Arching

The ratio $\pm x_{cr}/b$, for which the resultant pressure becomes negative can be found for any given set of b/h, μ, and ph/dE parameters. Thus, the total tensile forces, R, over the half width of strip due to displacement d, can be obtained by integrating six stress terms as given by Equation 25, with respect to x, evaluating the definite integral from 0 to $+x_{cr}$ and adding the tensile forces from x_{cr} to b. Thus, the amount of arching, that is, the total pressure transferred to the neighboring soil, is given by

$$R = \sum P_y^{(i)} + p\,(b - x_{cr}) \tag{29}$$

where

$$P_y^{(i)} = \int_0^{x_{cr}} \sigma_{y,o}^{(i)}\, dx$$

Thus,

$$\text{percentage of arching} = \frac{R}{pb} \times 100$$

$$= \left[A + 1 - \frac{x_{cr}}{b} \right] 100 \tag{30}$$

where

$$A = \sum_{i=1}^{6} A_i = \sum_{i=1}^{6} \frac{P_y^{(i)}}{pb}$$

and

$$A_i = A_i\,(b/h, \mu, ph/dE)$$

The expressions required in Equation 29 become less involved, if the integration is first performed with respect to x and then with respect to α starting from Equation 21. The expressions for A_i's are given by Equation 32. The following notations are used in Equation 32.

$$C\,(i)\,(J) = \left[\frac{b}{ih} \left(1 + \frac{x_{cr}}{b}\right) \right]^{J}$$

$$D\,(i)\,(J) = \left[\frac{b}{ih} \left(1 - \frac{x_{cr}}{b}\right) \right]^{J}$$

$$C\,(i)\,2\,(J) = \left\{ 1 + \left[\frac{b}{ih} \left(1 + \frac{x_{cr}}{b}\right) \right]^{2} \right\}^{J}$$

$$D\,(i)\,2\,(J) \quad \left\{ 1 + \left[\frac{b}{ih} \left(1 - \frac{x_{cr}}{b}\right) \right]^{2} \right\}^{J} \tag{31}$$

Where $i \geq j$ and the last two notations are used only in the denominators except when used with logarithms.

$$A_1 = \frac{P_y^{(1)}}{pb} = \frac{C_4}{\left(\frac{b}{h}\right)\left(\frac{eh}{dE}\right)} \left[\left\{ \frac{1}{2} \log \frac{C421}{D421} + 2 \right\} - \left\{ \frac{1}{C221} + \frac{1}{D221} \right\} - \log \frac{C11}{D11} \right] \tag{32a}$$

$$A_2 = \frac{P_y^{(2)}}{pb} = \frac{C_4}{\left(\frac{b}{h}\right)\left(\frac{eh}{dE}\right)} \left[C_1 \left\{ -0.1111111 \left[\frac{-1 + C62}{C622} - \frac{-1 + D62}{D622} \right] \right.\right.$$
$$- 0.05 \left[\frac{-1 + 3\,C42}{C423} - \frac{-1 + 3\,D42}{D423} \right]$$
$$\left.\left. + 1.0 \left[\frac{-1 + C22}{C222} - \frac{-1 + D22}{D222} \right] \right\} \right.$$
$$\left. + C_2 \left\{ -0.5 \log \frac{C621}{D621} - \left[-\frac{1}{C421} + \frac{1}{D421} \right] + 0.5 \log \frac{C221}{D221} \right\} \right] \tag{32b}$$

$$A_3 = \frac{P_y^{(3)}}{pb} = \frac{C_4}{\left(\frac{b}{h}\right)\left(\frac{eh}{dE}\right)} \left[C_1^2 \left\{ 0.0234375 \left[\frac{-1 + 6\,C82 - C84}{C824} - \frac{-1 + 6\,D82 - D84}{D824} \right] \right.\right.$$
$$+ 0.1975309 \left[\frac{-1 + 10\,C62 - 5\,C64}{C625} - \frac{-1 + 10\,D62 - 5\,D64}{D625} \right]$$
$$\left. - 0.375 \left[\frac{-1 + 6\,C42 - C44}{C424} - \frac{-1 + 6\,D42 - D44}{D424} \right] \right\}$$
$$+ C_1C_2 \left\{ 0.125 \left[\frac{-1 + C82}{C822} - \frac{-1 + D82}{D822} \right] \right.$$
$$+ 0.2962963 \left[\frac{-1 + 3\,C62}{C623} - \frac{-1 + 3\,D62}{D623} \right]$$
$$\left. - 0.50 \left[\frac{-1 + C42}{C422} - \frac{-1 + D42}{D422} \right] \right\}$$
$$\left. + (C_2^2 - 1) \left\{ 0.5 \log \frac{C821}{D821} + 0.5666667 \left[-\frac{1}{C621} + \frac{1}{D621} \right] - 0.5 \log \frac{C421}{D421} \right\} \right] \tag{32c}$$

$$A_4 = \frac{P_y^{(4)}}{pb} = \frac{C_4}{\left(\frac{b}{h}\right)\left(\frac{eh}{dE}\right)} \left[C_1^3 \left\{ -0.00768 \left[\frac{-1 + 15\,C102 - 15\,C104 + C106}{C1026} - \frac{-1 + 15\,D102 - 15\,D104 + D106}{D1026} \right] \right.\right.$$
$$- 0.0878906 \left[\frac{-1 + 21\,C92 - 35\,C84 + 7\,C86}{C827} - \frac{-1 + 21\,D82 - 35\,D84 + 7\,D86}{D827} \right]$$
$$\left. + 0.1646091 \left[\frac{-1 + 15\,C62 - 15\,C64 + C66}{C626} - \frac{-1 + 15\,D62 - 15\,D64 + D66}{D626} \right] \right\}$$
$$+ C_1^2C_2 \left\{ -0.0288 \left[\frac{-1 + 6\,C102 - C104}{C1024} - \frac{-1 + 6\,D102 - D104}{D1024} \right] \right.$$
$$- 0.140625 \left[\frac{-1 + 10\,C82 - 5\,C84}{C825} - \frac{-1 + 10\,D82 - 5\,D84}{D825} \right]$$
$$\left. + 0.2222222 \left[\frac{-1 + 6\,C62 - C64}{C624} - \frac{-1 + 6\,D62 - D64}{D624} \right] \right\}$$

$$+ (3C_1C_2^2 - 2C_1) \Big\} - 0.04 \left[\frac{-1 + C102}{C1022} - \frac{-1 + D102}{D1022} \right]$$

$$- 0.0625 \left[\frac{-1 + 3\,C82}{C823} - \frac{-1 + 3\,D82}{D823} \right]$$

$$+ 0.1111111 \left[\frac{-1 + C62}{C622} - \frac{-1 + D62}{D622} \right] \Big\}$$

$$+ (C_2^3 - 2C_2) \Big\} - 0.5 \log \frac{C1021}{D1021} - 0.5 \left[-\frac{1}{C821} + \frac{1}{D821} \right] + 0.5 \log \frac{C621}{D621} \Big\} \Big] \quad (32d)$$

$$A_5 = \frac{P_y^{(5)}}{pb} = \frac{C_4}{\left(\frac{b}{h}\right)\left(\frac{ph}{dE}\right)} \Bigg[C_1^4 \Big\} 0.0030007 \left[\frac{-1 + 28\,C122 - 70\,C124 + 23\,C126 - C128}{C1228} - \frac{-1 + 28\,D122 - 70\,D124 + 28\,D126 - D128}{D1228} \right]$$

$$+ 0.0412877 \left[\frac{-1 + 36\,C102 - 126\,C104 + 84\,C106 - 9\,C108}{C1029} - \frac{-1 + 36\,D102 - 126\,D104 + 84\,D106 - 9\,D108}{D1029} \right]$$

$$- 0.0769043 \left[\frac{-1 + 28\,C82 - 70\,C84 + 28\,C86 - C88}{C828} - \frac{-1 + 28\,D82 - 70\,D84 + 28\,D86 - D88}{D828} \right] \Big\}$$

$$+ C_1^3 C_2 \Big\} 0.0102881 \left[\frac{-1 + 15\,C122 - 15\,C124 + C126}{C1226} - \frac{-1 + 15\,D122 - 15\,D124 + D126}{D1226} \right]$$

$$+ 0.0737280 \left[\frac{-1 + 21\,C102 - 35\,C104 + 7\,C106}{C1027} - \frac{-1 + 21\,D102 - 35\,D104 + 7\,D106}{D1027} \right]$$

$$- 0.1171875 \left[\frac{-1 + 15\,C82 - 15\,C84 + C86}{C826} - \frac{-1 + 15\,D82 - 15\,D84 + D86}{D826} \right] \Big\}$$

$$+ (2C_2^2 - 1)C_1^2 \Big\} 0.0138889 \left[\frac{-1 + 6\,C122 - C124}{C1224} - \frac{-1 + 6\,D122 - D124}{D1224} \right]$$

$$+ 0.04608 \left[\frac{-1 + 10\,C102 - 5\,C104}{C1025} - \frac{-1 + 10\,D102 - 5\,D104}{D1025} \right]$$

$$- 0.0703125 \left[\frac{-1 + 6\,C82 - C84}{C824} - \frac{-1 + 6\,D82 - D84}{D824} \right] \Big\}$$

$$+ (2C_2^2-3)C_1C_2 \left\{ 0.0555556 \left[\frac{-1 + C122}{C122} - \frac{-1 + D122}{D1222} \right] \right.$$

$$+ 0.064 \left[\frac{-1 + 3\ C102}{C1023} - \frac{-1 + 3\ D102}{D1023} \right]$$

$$\left. - 0.125 \left[\frac{-1 + C82}{C822} - \frac{-1 + D82}{D822} \right] \right\}$$

$$+ (C_2^4-3C_2^2+1) \left\{ 0.5 \log \frac{C1221}{D1221} + 0.4 \left[- \frac{1}{C1021} + \frac{1}{D1021} \right] - 0.5 \log \frac{C821}{D821} \right\} \Bigg] \quad (32e)$$

$$A_6 = \frac{P_y^{(6)}}{pb} = \frac{C_4}{\left(\frac{b}{h}\right)\left(\frac{ph}{dE}\right)} \Bigg[C_1^5 \left\{ - 0.0012846 \left[\frac{-1 + 45\ C142 - 210\ C144 + 210\ C146 - 45\ C148 + C1410}{C14210} \right.\right.$$

$$\left. - \frac{-1 + 45\ D142 - 210\ D144 + 210\ D146 - 45\ D148 + D1410}{D14210} \right]$$

$$- 0.0200046 \left[\frac{-1 + 55\ C122 - 330\ C124 + 462\ C126 - 165\ C128 + 11\ C1210}{C12211} \right.$$

$$\left. - \frac{-1 + 55\ D122 - 330\ D124 + 462\ D126 - 165\ D128 + 11\ D1210}{D1211} \right]$$

$$+ 0.0371589 \left[\frac{-1 + 45\ C102 - 210\ C104 + 210\ C106 - 45\ C108 + C1010}{C10210} \right.$$

$$\left. \left. - \frac{-1 + 45\ D102 - 210\ D104 + 210\ D106 - 45\ D108 + D1010}{D10210} \right] \right\}$$

$$+ C_1^4C_2 \left\{ - 0.0043714 \left[\frac{-1 + 28\ C142 - 70\ C144 + 28\ C146 - C148}{C1428} \right.\right.$$

$$\left. - \frac{-1 + 28\ D142 - 70\ D144 + 28\ D146 - D148}{D1428} \right]$$

$$- 0.0400091 \left[\frac{-1 + 36\ C122 - 126\ C124 + 84\ C126 - 9\ C128}{C1229} \right.$$

$$\left. - \frac{-1 + 36\ D122 - 126\ D124 + 84\ D126 - 9\ D128}{D1229} \right]$$

$$+ 0.064512 \left[\frac{-1 + 28\ C102 - 70\ C104 + 28\ C106 - C108}{C1028} \right.$$

$$\left. \left. - \frac{-1 + 28\ D102 - 70\ D104 + 28\ D106 - D108}{D1028} \right] \right\}$$

$$+ C_1^3(5C_2^2-2) \left\{ - 0.002040 \left[\frac{-1 + 15\ C142 - 15\ C144 + C146}{C1426} \right.\right.$$

$$\left. - \frac{-1 + 15\ D142 - 15\ D144 + D146}{D1426} \right]$$

$$- 0.0102981 \left[\frac{-1 + 21\ C122 - 35\ C124 + 7\ C126}{C1227} \right.$$

$$\left. - \frac{-1 + 21\ D122 - 35\ D124 + 7\ D126}{D1227} \right]$$

$$+ 0.015360 \left[\frac{-1 + 15\,C102 - 15\,C104 + C106}{C1026} - \frac{-1 + 15\,D102 - 15\,D104 + D106}{D1026} \right] \Big\}$$

$$+ C_1^2(5C_2^3 - 6C_2) \Big\{ - 0.0049979 \left[\frac{-1 + 6\,C142 - C144}{C1424} - \frac{-1 + 6\,D142 - D144}{D1424} \right]$$

$$- 0.0123457 \left[\frac{-1 + 10\,C122 - 5\,C124}{C1225} - \frac{-1 + 10\,D122 - 5\,D124}{D1225} \right]$$

$$+ 0.0192 \left[\frac{-1 + 6\,C102 - C104}{C1024} - \frac{-1 + 6\,D102 - D104}{D1024} \right] \Big\}$$

$$+ C_1(5C_2^4 - 12C_2^2 + 3) \Big\{ - 0.0204082 \left[\frac{-1 + C142}{C1422} - \frac{-1 + D142}{D1422} \right]$$

$$- 0.0185185 \left[\frac{-1 + 3\,C122}{C1223} - \frac{-1 + 3\,D122}{D1223} \right]$$

$$+ 0.04 \left[\frac{-1 + C102}{C1022} - \frac{-1 + D102}{D1022} \right] \Big\}$$

$$+ (C_2^5 - 4C_2^3 + 3C_2) \Big\{ - 0.5 \log \frac{C1421}{D1421} - 0.3333333 \left[- \frac{1}{C1221} + \frac{1}{D1221} \right] + 0.5 \log \frac{C1021}{D1021} \Big\} \Big] \quad (32f)$$

A digital computer program was developed to find the value of x_{cr}/b, if the parameters ph/dE, μ, and b/h are given. The program initially assumes a value of $x/b = 0$, computes the value of S and compares it with ph/dE. If the value of S is greater than ph/dE, it indicates that the net pressure on the base is tensile and an Arching of 100 percent is indicated. If the value of S at $x/b = 0$ is smaller than ph/dE, then a certain increment is given to x/b and a new value of S (x/b, b/h, μ) is computed and is compared with ph/dE. If the difference between these two is less than or equal to 10^{-5}, that value of x/b is taken as x_{cr}/b. If the difference is greater than 10^{-5}, the program assumes another value of x/b and the process is repeated until the value of x_{cr}/b is reached. For values of x/b approaching 1, the computer takes a very long time to iterate and find the value of x_{cr}/b. In cases where the number of iterations exceed more than 100, the computer prints out "number of iterations more than 100 to find x_{cr}" and proceeds with the next problem. After the value of x_{cr}/b is computed, the expression for A_i's are evaluated and the percentage of Arching is computed using Equation 30. For any problem, the value of b/h, μ, ph/dE, x_{cr}/b, A1, A2, A3, A4, A5, A6, A and Arching are printed. The following values are used for the parameter ph/dE and the range is considered adequate.

ph/dE =						
	.01	.1	1	10	100	1000
	.0125	.125	1.25	12.5	125	
	.015	.15	1.5	15	150	
	.02	.2	2	20	200	
	.03	.3	3	30	300	
	.04	.4	4	40	400	
	.05	.5	5	50	500	
	.06	.6	6	60	600	
	.07	.7	7	70	700	
	.09	.9	9	90	900	

The value of x_{cr}/b is zero when the arching is 100 percent and at zero percent arching the value of x_{cr}/b is very nearly one. Figures 6 through 9 indicate the variation of x_{cr}/b with ph/dE for Poisson's Ratio equal to 0.1, 0.25, 0.3333 and 0.5.

Figures 10 through 13 indicate the percentage of arching versus the parameter ph/dE for different values of b/h and Poisson's ratio, μ. For each value of b/h, the percentage of arching decreases with increasing values of ph/dE.

Comparing the plots of arching versus ph/dE and x_{cr}/b versus ph/dE for different values of Poisson's ratio, it can be seen that the effect of Poisson's ratio can be neglected over a wide range of ph/dE for small values of b/h.

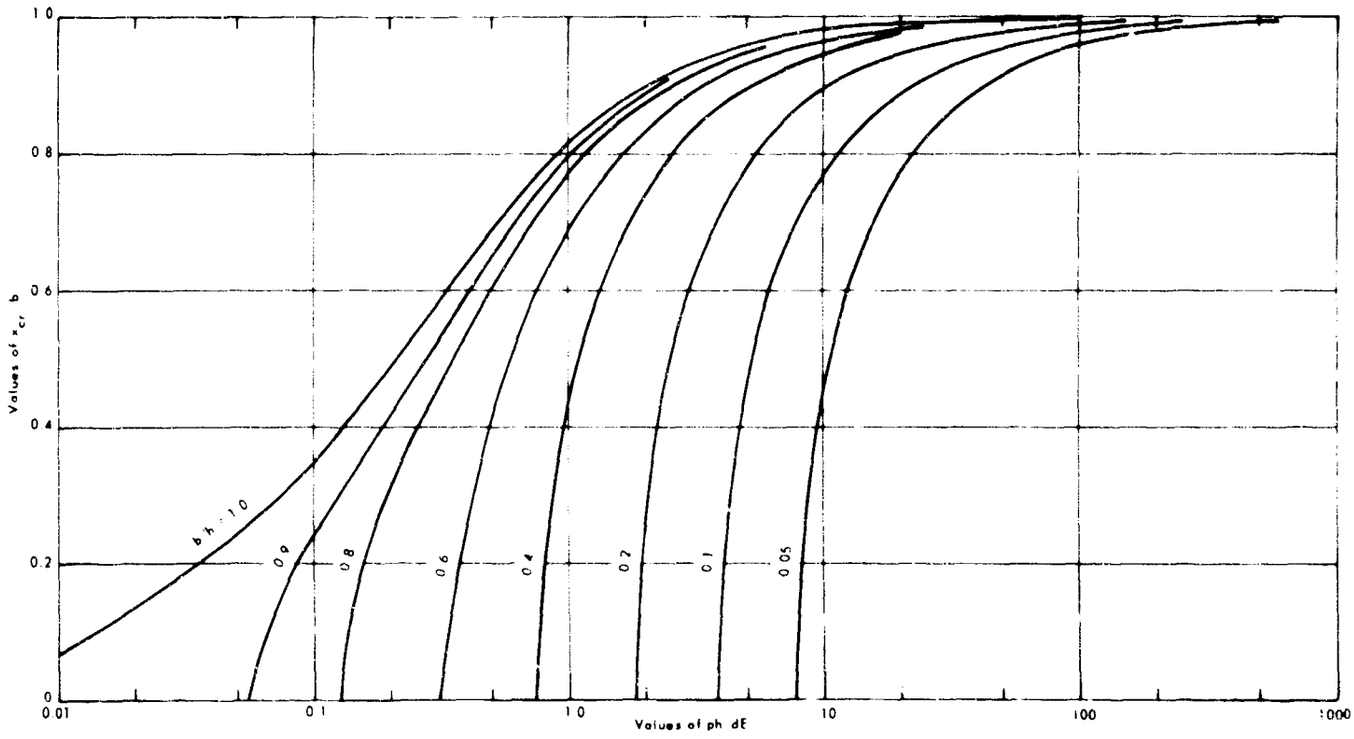


Fig. 6 Distance to Point of Zero Pressure on the Base for $\mu = 0.1$

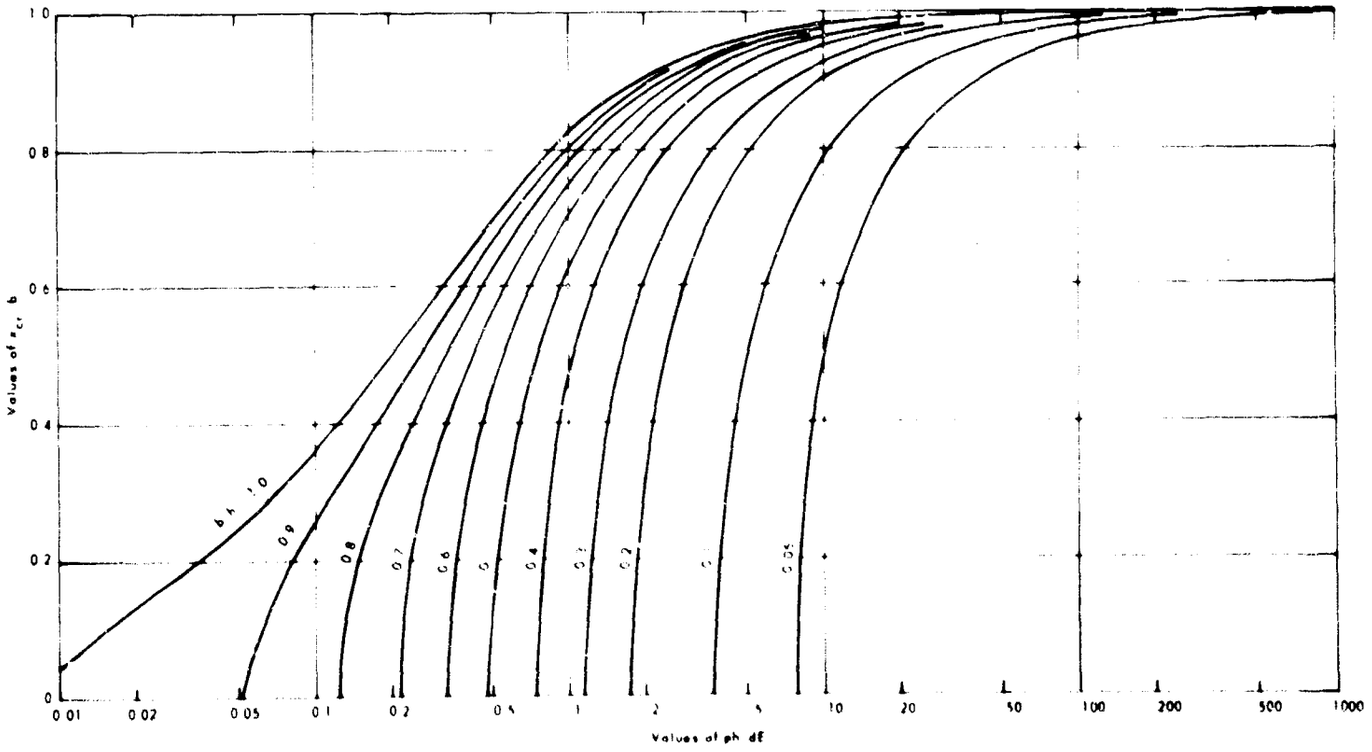


Fig. 7 Distance to Point of Zero Pressure on the Base for $\mu = 0.25$

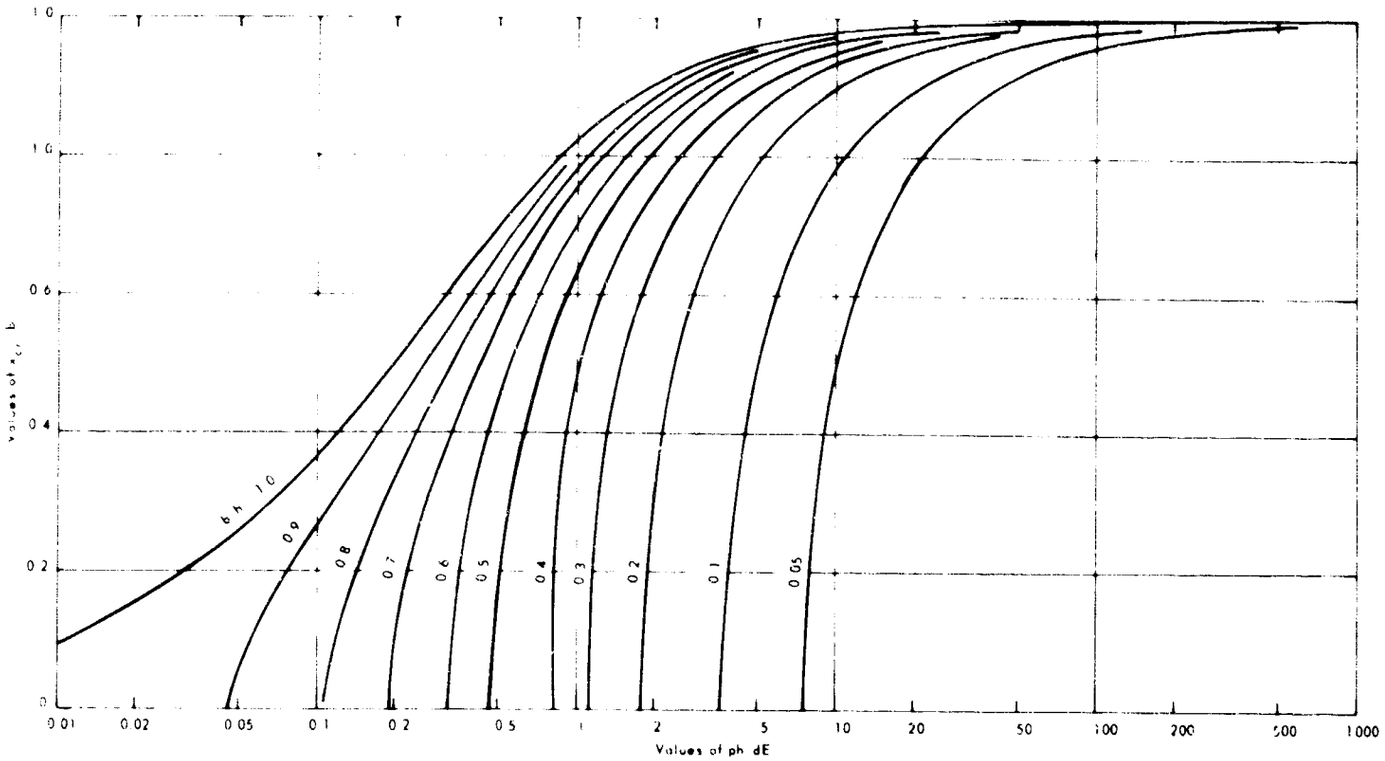


Fig. 8 Distance to Point of Zero Pressure on the Base for $\mu = 0.3333$

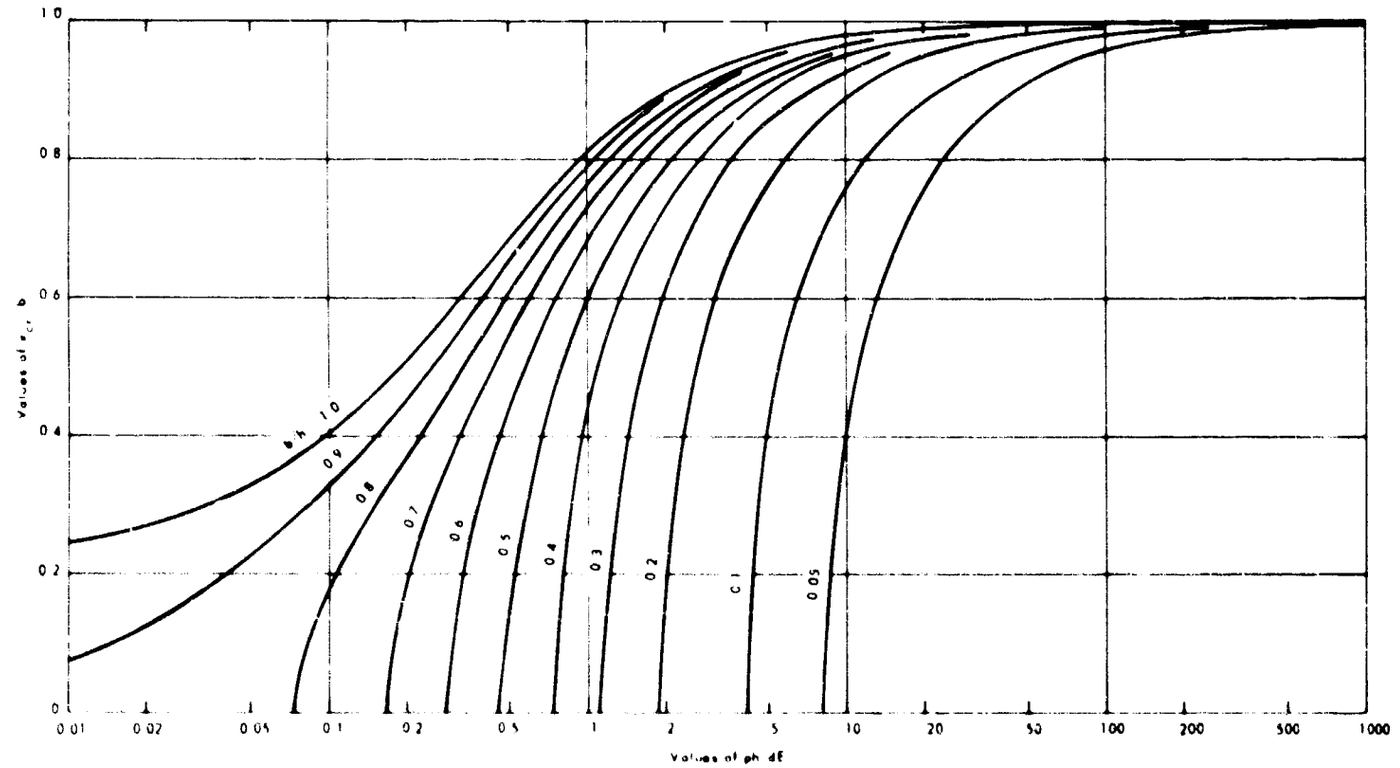


Fig. 9 Distance to Point of Zero Pressure on the Base for $\mu = 0.5$

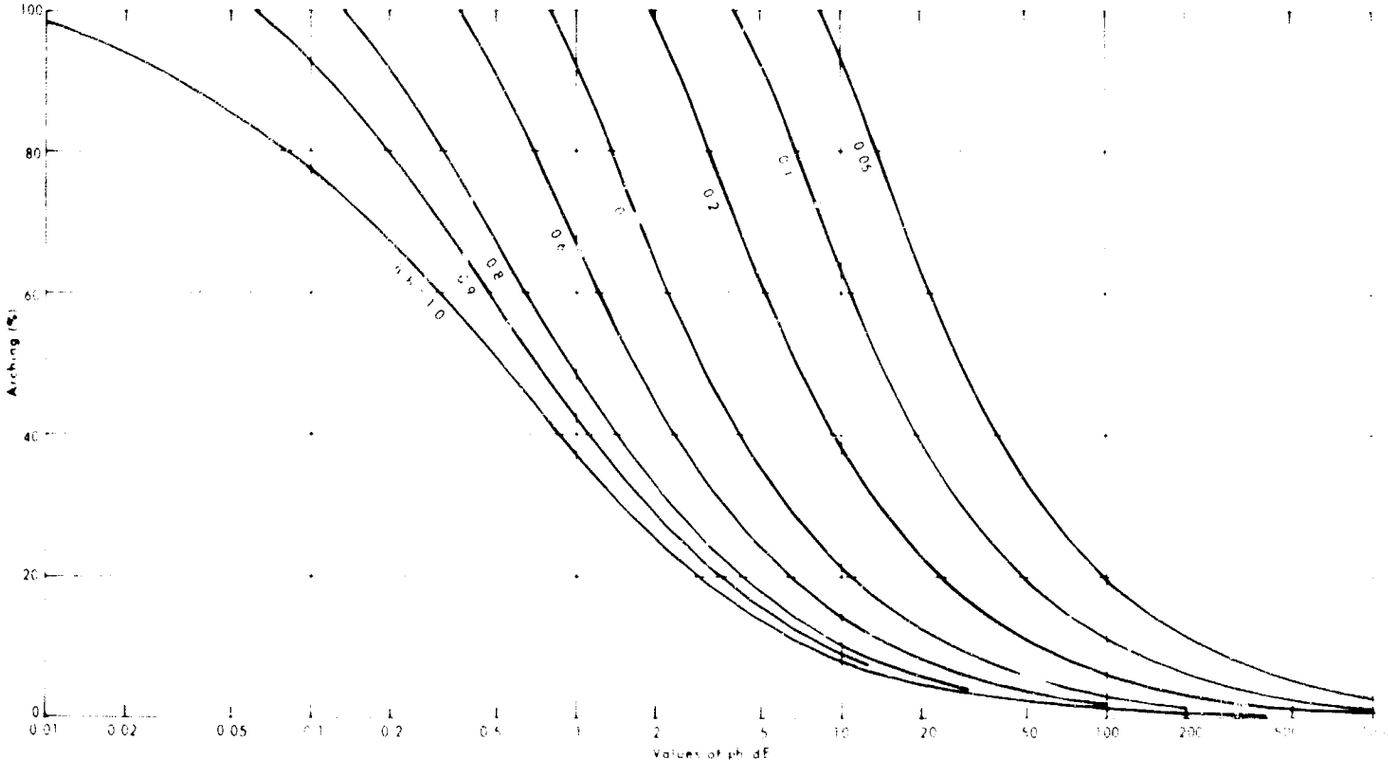


Fig. 10 Arching Due to Deflection of the Base for μ = 0.1

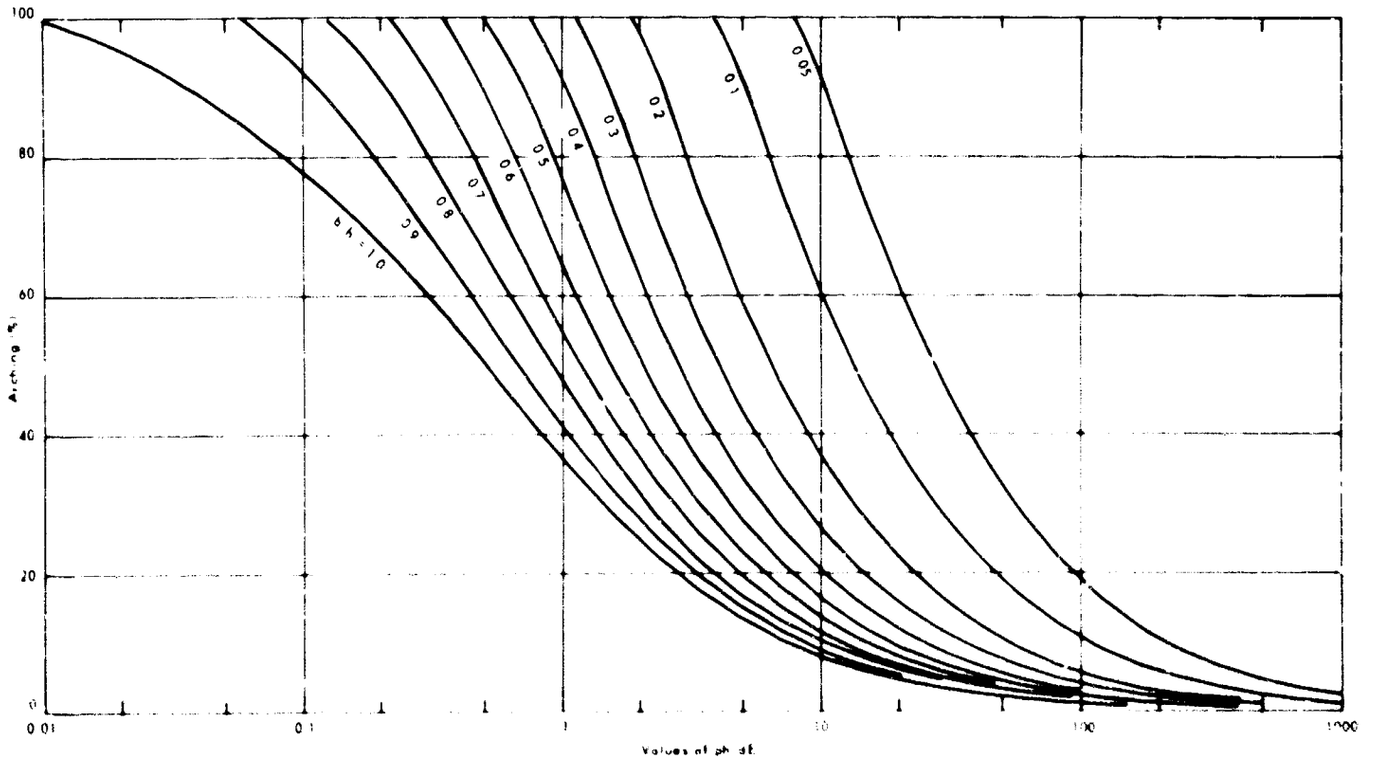


Fig. 11 Arching Due to Deflection of the Base for μ 0.25

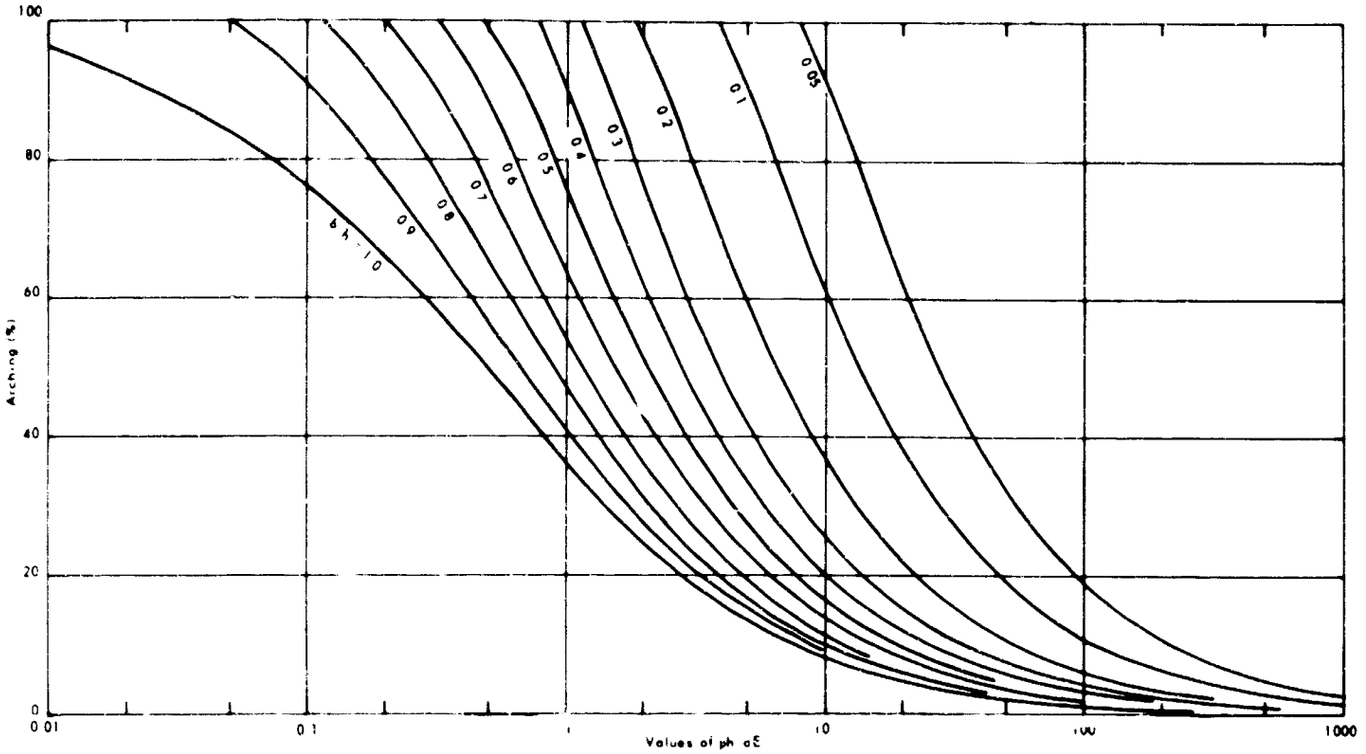


Fig. 12 Arcning Due to Deflection of the Base for $\mu = 0.3333$

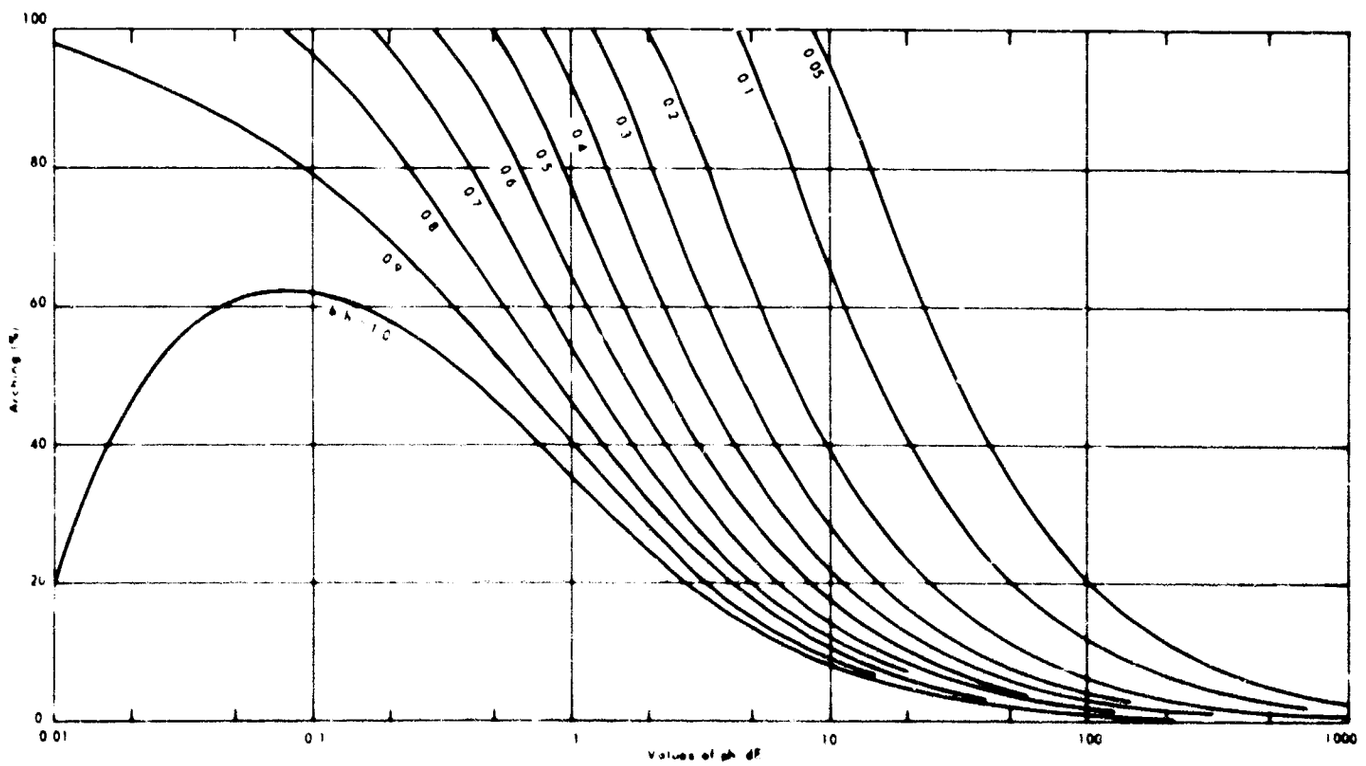


Fig. 13 Arching Due to Deflection of the Base for $\mu = 0.5$

Illustrative Example

It is desired to find the amount of arching when a horizontal rigid strip of 24 feet wide, buried under 17 feet of soil cover undergoes a yield displacement of 2 inches. The soil is subjected to an overpressure of 100 psi. The modulus of elasticity of the soil, E, is 10,000 psi, Poisson's ratio, μ is 0.25 and the density of soil, γ, is 110 pcf. Thus,

$$b = 12 \text{ feet}$$

$$h = 17 \text{ feet}$$

$$b/h = 0.706$$

$$p_o = 100 \text{ psi} \qquad \gamma = 110 \text{ pcf}$$

$$\gamma h = \frac{(110)(17)}{(144)} = 13 \text{ psi}$$

$$p = p_o + \gamma h = 113 \text{ psi}$$

$$\text{yield parameter, } \frac{ph}{dE} = \frac{(113)(17)(12)}{(2)(10000)} = 1.15$$

It can be found from the plots in Figure 7, that the value of x_{cr}/b is 0.77, and that the amount of arching is 52 percent for $b/h = 0.706$, and $ph/dE = 1.15$. The distribution of pressure on the base can be obtained from Figure 3. At $x/b = 0$, the pressure, p, at no yield displacement is reduced by $\sigma_{y,o} = 20.6$ psi where $\sigma_{y,o}$ is obtained from $S = h/dE = 0.21$. Thus the net pressure on the base at $x/b = 0$ is $113 - 20.6 = 92.4$ psi and reduces to zero at a distance $\pm 0.77 \times 12 = \pm 9.24'$ from the center of the base. Experimental data to determine the validity of the theory are not available at this time. However, these results were compared with some unpublished data obtained by U.S. Army Engineer Waterways Experiment Station for a very similar case and the trends for the amount of arching are similar to those given here.

CONCLUSIONS

The analysis indicates that arching for the case considered here varies from 100 percent to zero percent, depending upon the three parameters, b/h, ph/dE, and μ. However, for practical purposes the effect of Poisson's ratio, μ, can be neglected over a wide range of parameters. An illustrative example is given to demonstrate the use of these plots.

ACKNOWLEDGEMENTS

The author wishes to express his gratitude to Mr. Jay R. Allgood, Structural Research Engineer, U.S. Naval Civil Engineering Laboratory for suggesting the problem and for many helpful comments during the course of this investigation. The programs were checked and the results were compiled using the Honeywell 800 Data Processing System at the University of Southern California, Los Angeles. Part of the results were obtained using IBM 7090 Data Processing System at the Pacific Missile Range, Point Mugu. This paper is based on a Technical Report submitted to the U.S. Naval Civil Engineering Laboratory, Port Hueneme.

REFERENCES

1. Terzhaghi, K., Theoretical Soil Mechanics, John Wiley and Sons, New York, New York, 1943.
2. Finn, W.D., "Stresses in Soil Masses under Various Boundary Conditions," Ph.D. Thesis, University of Washington, Seattle, Washington, 1960.
3. Timoshenko, S. and J. N. Goodier, Theory of Elasticity, 2nd Edition, McGraw-Hill Book Company, Inc., New York, New York, 1951.
4. Grobner, W. and N. Hofreiter, Integraltafel, 3rd Revised Edition, 2 Volumes, Springer-Verlag, Vienna, 1961.

ATTENUATION OF STRESSES FOR BURIED CYLINDERS

by
Jerome Q. Burns* and Ralph M. Richard**

SYNOPSIS

An analysis is presented for the interaction of an elastic circular cylindrical shell embedded in an elastic medium which is loaded by a surface overpressure. Non-dimensionalized equations are presented for the interaction loads between the shell and the medium; for the thrusts, moments, and displacements in the shell; and for the stresses and displacements throughout the medium. The manner in which the circumferential extensional stiffness of the shell, the circumferential bending stiffness of the shell, and the shear load transfer between the shell and the medium influence the interaction problem is clearly indicated. The analysis is made through the use of extensional shell theory for the shell and Michell's formulation of Airy's stress function for the medium. The equations for the medium reduce to the free cavity case if the shell stiffnesses become zero, and reduce to the rigid inclusion case if the shell stiffnesses become infinite.

INTRODUCTION

It is the authors' belief that a thorough understanding of the distribution of stresses around an elastic cylinder embedded in an elastic medium will be a helpful, indeed necessary, step toward understanding the actual soil-culvert case which involves an inelastic medium. Therefore, an analysis has been made for the interaction of an elastic circular cylindrical shell in an elastic medium which is loaded by a surface overpressure as shown in Figure 1. The analysis is applicable to deeply buried conduits since the loaded surface is assumed at infinity in the derivation. The practical depth of burial for which this theory may be used is determined by noting where the resulting stress and displacement distribution in the medium becomes essentially the free-field distribution. The depth is roughly one or two diameters depending upon the properties of the shell relative to the medium. The results of this analysis are for overpressure only and are to be superimposed on those conditions existing prior to the application of the overpressure.

The overpressure effects considered in this paper are the interaction loads between the shell and the medium, the circumferential thrust and moment in the shell, the displacement of the shell relative to its axis, and the stresses and displacements throughout the medium. The analysis indicates how the following three governing parameters influence the effects listed above:

1. The circumferential extensional flexibility of the shell relative to the medium.
2. The circumferential bending flexibility of the shell relative to the medium.
3. The tangential slippage of the shell relative to the medium at the shell-medium interface; that is, the tangential shear load transfer between the shell and the medium.

The analysis is general in that it is applicable to conduits ranging from "rigid conduits" to "flexible conduits" which are embedded in any linearly elastic medium.

DEFINITIONS

The elastic medium parameters may be the elasticity constants, say, the modulus of elasticity, E^*, and Poisson's ratio, μ; or alternatively, the elastic soil constants, the constrained modulus, M^*, and the lateral stress ratio, K. These parameters are related by the following equations:

$$M^* = \frac{E^* (1 - \mu)}{(1 + \mu)(1 - 2\mu)}$$

and

$$K = \frac{\mu}{1 - \mu}$$

* Graduate Associate, Department of Civil Engineering and Engineering Mechanics, University of Arizona, Tucson, Arizona.

**Associate Professor, Department of Civil Engineering and Engineering Mechanics, University of Arizona, Tucson, Arizona.

It is convenient to define two new constants related to the lateral stress ratio; that is,

$$B = \frac{1}{2}(1 + K) = \frac{1}{2}\left(\frac{1}{1 - \mu}\right)$$

and

$$C = \frac{1}{2}(1 - K) = \frac{1}{2}\left(\frac{1 - 2\mu}{1 - \mu}\right)$$

The shell parameters are the mean radius of the conduit, R, the circumferential extensional stiffness per unit length, EA, and the circumferential bending stiffness per unit length, EI. It should be noted that these stiffnesses must be taken as plane strain stiffnesses. For example, in the case of a conduit of uniform thickness, t, the circumferential bending stiffness (D as used in shell theory) is $(E/(1 - \mu^2))\,(t^3/12)$, and, correspondingly, the circumferential extensional stiffness is $Et/(1 - \mu^2)$.

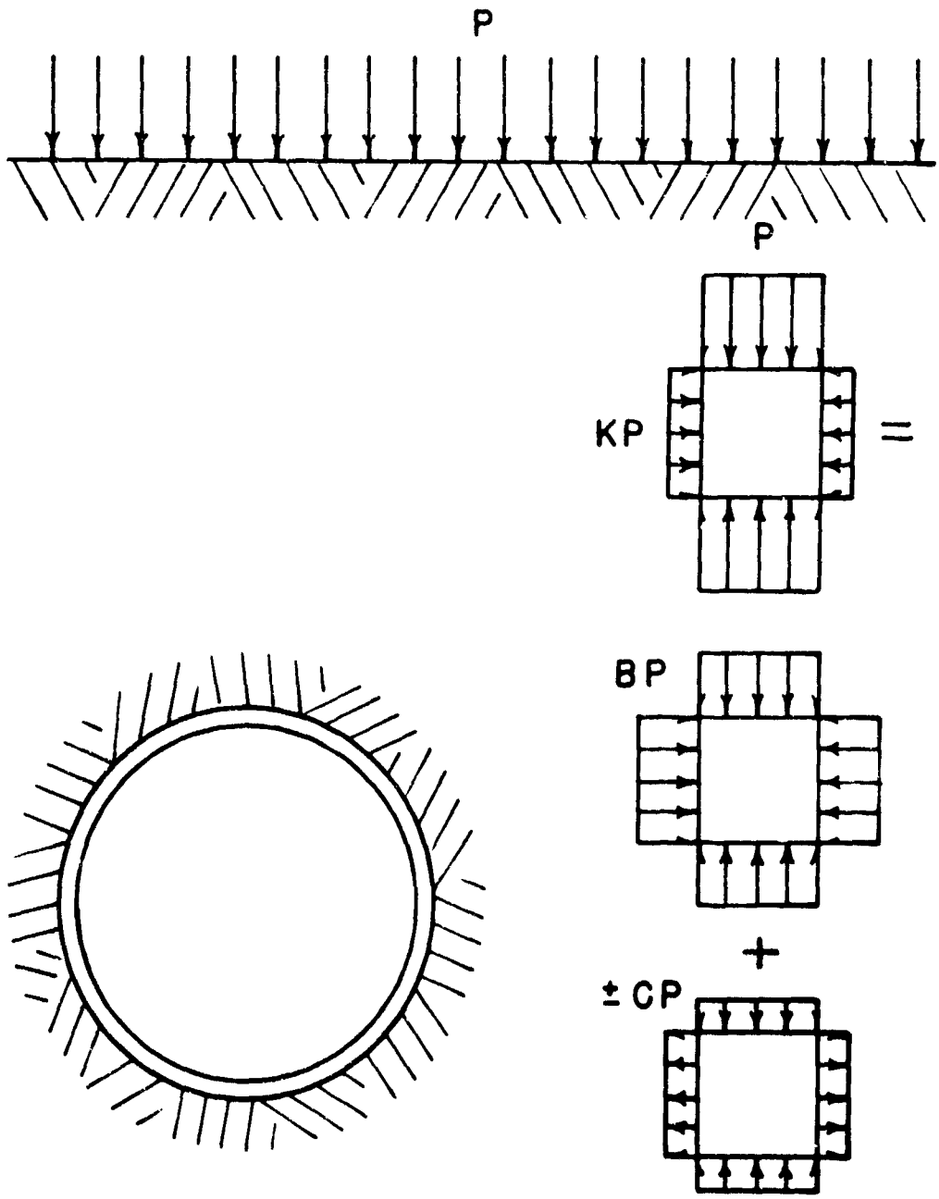


Fig. 1 Overpressure Problem and Free-Field Stress State

Convenient non-dimensional shell-medium interaction parameters are defined as the extensional flexibility ratio, UF, where:

$$UF = 2B \frac{M^*R}{EA} = (1 + K) \frac{M^*R}{EA}$$

and the bending flexibility ratio, VF, where:

$$VF = 2C \frac{M^*R^3}{6EI} = (1 - K) \frac{M^*R^3}{6EI}$$

UF is an index to the relative flexibility of the shell and the medium under uniform interaction loads. VF is an index to the relative flexibility of the shell and the medium under varying radial and tangential interaction loads.

MATHEMATICAL FORMULATION

The conduit and the medium are analyzed as a structural system. The determination of the stresses and deformations throughout this system gives the conduit thrusts, moments, and displacements, and the medium stresses and displacements; hence, the interaction loads and the arching phenomena are evaluated.

The problem is solved using Michell's stress function (1) for the medium,

$$\begin{aligned}\phi = {} & a_o \log r + b_o r^2 + c_o r^2 \log r + d_o r^2 \theta + a'_o \theta \\ & + \frac{d_1}{2} r \theta \sin \theta + (b_1 r^3 + a'_1 r^{-1} + b'_1 r \log r) \cos \theta \\ & - \frac{c_1}{2} r \theta \cos \theta + (d_1 r^3 + c'_1 r^{-1} + d'_1 r \log r) \sin \theta \\ & + \sum_{n=2}^{\infty} (a_n r^n + b_n r^{n+2} + a'_n r^{-n} + b'_n r^{-n+2}) \cos n\theta \\ & + \sum_{n=2}^{\infty} (c_n r^n + d_n r^{n+2} + c'_n r^{-n} + d'_n r^{-n+2}) \sin n\theta\end{aligned}$$

and extensional shell theory for the conduit. The notation for the shell and the medium are given in Figure 2. Note that the sign convention is completely reversed from that usually used in elasticity, so that the pressure may be considered positive in order to be consistent with the sign convention normally used in soil mechanics.

For the planar problem, the equilibrium equations for circular cylindrical shells (2) reduce to,

$$R \frac{dN}{d\theta} - \frac{dM}{d\theta} = -T_{r\theta} R^2$$

$$\frac{d^2M}{d\theta^2} + RN = P_r R^2$$

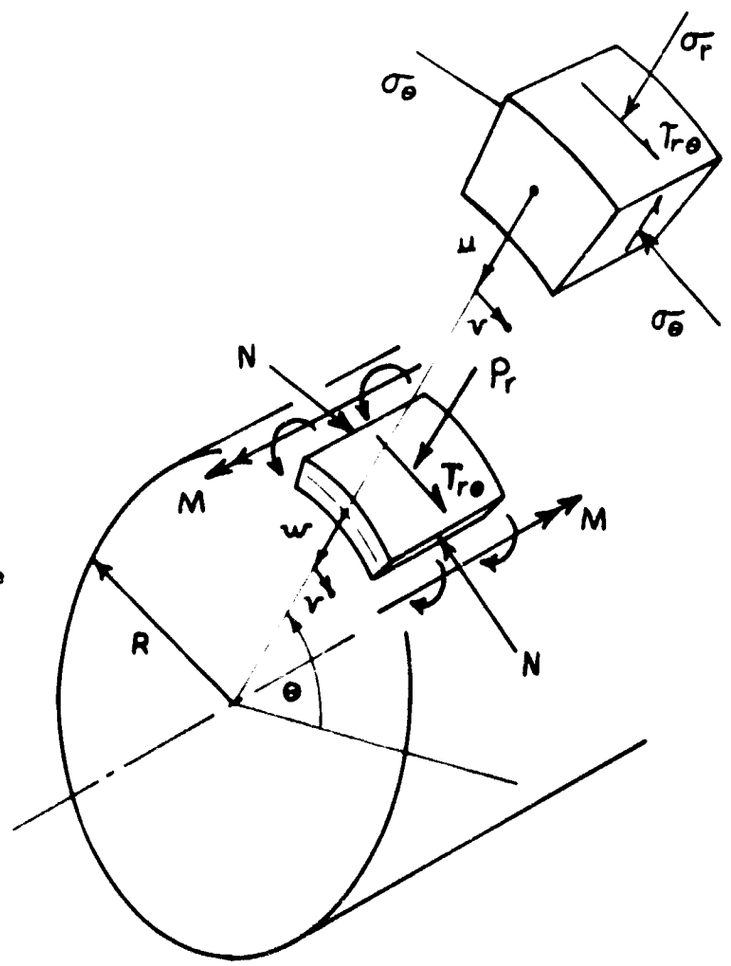


Fig. 2 Notation

from which the equations for the [illegible] may be obtained as,

$$\frac{d^2M}{d\theta^2} + M = R^2 \left[P_r + \int T_{r\theta} d\theta \right]$$

$$N = \frac{M}{R} - R \int T_{r\theta} d\theta$$

The displacement equations for circular cylindrical shells (2) reduce to,

$$\frac{d^2v}{d\theta^2} + \frac{dw}{d\theta} = -T_{r\theta} \frac{R^2}{EA}$$

$$\frac{dv}{d\theta} + w + \frac{EI}{R^2 EA} \left[\frac{d^4w}{d\theta^4} + \frac{d^2w}{d\theta^2} + w \right] = \frac{P_r R^2}{EA}$$

from which, with the addition of an additional extensionality term, the equations for radial and tangential displacement become,

$$\frac{d^4w}{d\theta^4} + 2\frac{d^2w}{d\theta^2} + w = \frac{R^4}{EI} \left[P_r + \int T_{r\theta} d\theta \right]$$

$$v = -\int w d\theta + \frac{R^2}{EA} \int P_r d\theta - \frac{1}{EA} \frac{dM}{d\theta}$$

The stresses and displacements in the medium are expressed in terms of the stress function constants by the use of the plane strain elasticity relations. That is,

$$\sigma_r = \frac{1}{r} \frac{\partial \phi}{\partial r} + \frac{1}{r^2} \frac{\partial^2 \phi}{\partial \theta^2}$$

$$\sigma_\theta = \frac{\partial^2 \phi}{\partial r^2}$$

$$T_{r\theta} = -\frac{\partial}{\partial r} \left(\frac{1}{r} \frac{\partial \phi}{\partial \theta} \right)$$

$$u = \int \epsilon_r dr = \int \frac{(1+\mu)}{E^*} \left[(1-\mu) \sigma_r - \mu \sigma_\theta \right] dr$$

$$v = \int r \epsilon_\theta d\theta - \int u d\theta = \int \frac{(1+\mu)}{E^*} \left[(1-\mu) \sigma_\theta - \mu \sigma_r \right] r d\theta - \int u d\theta$$

Certain of the unknown constants are evaluated using the free-field stress conditions at infinity:

$$\sigma_r = BP - CP \cos 2\theta$$

$$\sigma_\theta = BP + CP \cos 2\theta$$

$$T_{r\theta} = CP \sin 2\theta$$

Thus, the stress function constants b_o and a_2 are determined to be:

$$b_o = \frac{B}{2} p \quad \{1\}$$

$$a_2 = \frac{C}{2} p \quad \{1\}$$

Enforcing the conditions of symmetry and periodicity, all the rest of the constants except a_o, a_n, and b_n are found to be zero. Using the value of the medium stresses at the loci of the shell (r = R) as the loads on the shell, the deflection of the shell may be evaluated in terms of the remaining unknown stress function constants.

For the no slippage case, in which there is continuity of the radial and tangential displacements of the shell and the medium, the conditions for evaluating the remaining unknown constants are the equality of the radial and tangential displacements of the shell and the medium at the interface. Using these compatibility conditions, the stress-function constants a'_n and b'_n are found to be zero for n greater than 2. Additionally, a_o, a'_2, and b'_2 are found to be as follows:

$$a_o = -BP \left\{ \frac{UF - 1}{UF + B/C} \right\} R^2 = -BP\, a_o^* R^2$$

$$a'_2 = -\frac{CP}{2} \left\{ \frac{C(1 - UF)VF - (C/B)UF + 2B}{(1 + B)VF + C(VF + 1/B)UF + 2(1 + C)} \right\} R^4 = -\frac{CP}{2} a_2^* R^4$$

$$b'_2 = -CP \left\{ \frac{(B + CUF)VF - 2B}{(1 + B)VF + C(VF + 1/B)UF + 2(1 + C)} \right\} R^2 = -CP\, b_2^* R^2$$

For the final equations, instead of using these constants directly, it is convenient to use the bracketed factors in the above expressions. These are either unity, in the case of the first two, or the starred constants, in the case of the last three. That is:

$$a_o^* = \frac{UF - 1}{UF + B/C}$$

$$a_2^* = \frac{C(1 - UF)VF - (C/B)UF + 2B}{(1 + B)VF + C(VF + 1/B)UF + 2(1 + C)}$$

$$b_2^* = \frac{(B + CUF)VF - 2B}{(1 + B)VF + C(VF + 1/B)UF + 2(1 + C)}$$

Thus, for any shell-medium combination specified by the five parameters, M*, K, R, EA and EI, the non-dimensionalized parameters, B, C, UF and VF, may be found from which the non-dimensionalized constants, a_o^*, a_2^* and b_2^*, may be determined. The results for the no slippage case may then be expressed in terms of these constants.

The stresses in the medium are:

$$\sigma_r = P \left\{ B \left[1 - a_o^* (R/r)^2 \right] - C \left[1 - 3a_2^* (R/r)^4 - 4b_2^* (R/r)^2 \right] \cos 2\theta \right\}$$

$$\sigma_\theta = P \left\{ B \left[1 + a_o^* (R/r)^2 \right] + C \left[1 - 3a_2^* (R/r)^4 \right] \cos 2\theta \right\}$$

$$T_{r\theta} = P \left\{ C \left[1 + 3a_2^* (R/r)^4 + 2b_2^* (R/r)^2 \right] \sin 2\theta \right\}$$

The radial and tangential interaction loads are obtained by setting r = R in the above expressions for the radial and tangential medium stresses. Hence:

$$P_r = P \left\{ B \left[1 - a_o^* \right] - C \left[1 - 3a_2^* - 4b_2^* \right] \cos 2\theta \right\}$$

$$T_{r\theta} = P \left\{ C \left[1 + 3a_2^* + 2b_2^* \right] \sin 2\theta \right\}$$

The displacements in the medium are

$$u = \frac{Pr}{M}\frac{1}{2}\left\{\left[1 + (B\ C)a_o^*(R/r)^2\right] - \left[1 + a_2^*(R/r)^4 + (2\ B)b_2^*(R/r)^2\right]\cos 2\theta\right\}$$

$$v = \frac{Pr}{M}\frac{1}{2}\left\{\left[1 - a_2^*(R/r)^4 + (2\ C/B)b_2^*(R/r)^2\right]\sin 2\theta\right\}$$

The shell displacements may be obtained by setting r = R in the above expression for medium displacements. Hence:

$$w = \frac{PR}{M}\frac{1}{2}\left\{\left[1 + (B/C)a_o^*\right] - \left[1 + a_2^* + (2/B)b_2^*\right]\cos 2\theta\right\}$$

$$v = \frac{PR}{M}\frac{1}{2}\left\{\left[1 - a_2^* + (2\ C/B)b_2^*\right]\sin 2\theta\right\}$$

Through the use of identities, the important radial displacement may be written

$$w = \frac{PR}{M}\frac{1}{2}\left\{UF\left[1 - a_o^*\right] - VF\left[1 - a_2^* - 2b_2^*\right]\cos 2\theta\right\}$$

which has coefficients similar to those in the circumferential thrust and moment equations,

$$N = PR\left\{B\left[1 - a_o^*\right] + C\left[1 + a_2^*\right]\cos 2\theta\right\}$$

$$M = PR^2\left\{\frac{C}{6}\frac{UF}{VF}\left[1 - a_o^*\right] + \frac{C}{2}\left[1 - a_2^* - 2b_2^*\right]\cos 2\theta\right\}$$

The results given above for the no slippage case may be non-dimensionalized by dividing each equation through by its first term.

The full slippage case is treated similarly except that in evaluating the three constants a_o, a_2' and b_2', the stress condition of zero shear stress at the interface must be used instead of the compatibility condition of zero relative tangential displacement. For this case, the constants are:

$$a^* = \frac{(UF - 1)}{(UF + B/C)}$$

$$a_2^{**} = \frac{(2VF - 1 + 1/B)}{(2VF - 1 + 3/B)}$$

$$b_2^{**} = \frac{(2VF - 1)}{(2VF - 1 + 3/B)}$$

Thus, for any shell-medium combination specified by the five parameters, M*, K, R, EA, and EI, the non-dimensionalized parameters, B, C, UF, and VF, may be found from which the non-dimensionalized constants, a_o^*, a_2^{**}, and b_2^{**}, may be determined. The results for the full slippage case may then be expressed in terms of these constants.

The stresses in the medium are:

$$\sigma_r = P\left\{B\left[1 - a_o^*(R/r)^2\right] - C\left[1 + 3a_2^{**}(R/r)^4 - 4b_2^{**}(R/r)^2\right]\cos 2\theta\right\}$$

$$\sigma_\theta = P\left\{B\left[1 + a_o^*(R/r)^2\right] + C\left[1 + 3a_2^{**}(R/r)^4\right]\cos 2\theta\right\}$$

$$T_{r\theta} = P\left\{C\left[1 - 3a_2^{**}(R/r)^4 + 2b_2^{**}(R/r)^2\right]\sin 2\theta\right\}$$

The radial interaction load may be obtained by setting r = R in the above expression for radial stress, the tangential interaction load is, of course, zero. Hence:

$$P_r = P \left\{ B \left[1 - a_o^* \right] - C \left[1 + 3a_2^{**} - 4b_2^{**} \right] \cos 2\theta \right\}$$

The displacements in the medium are:

$$u = \frac{Pr}{M} \frac{1}{2} \left\{ \left[1 + (B/C)\, a_o^* \, (R/r)^2 \right] - \left[1 - a_2^{**} \, (R/r)^4 + (2/B) b_2^{**} \, (R/r)^2 \right] \cos 2\theta \right\}$$

$$v = \frac{Pr}{M} \frac{1}{2} \left\{ \left[1 + a_2^{**} \, (R/r)^4 + (2C/B) b_2^{**} \, (R/r)^2 \right] \sin 2\theta \right\}$$

The shell radial displacement may be obtained by setting r = R in the above expression for medium radial displacement, but the tangential displacement must be obtained directly. Thus:

$$w = \frac{PR}{M} \frac{1}{2} \left\{ \left[1 + (B/C) a_o^* \right] - \left[1 - a_2^{**} + (2/B) b_2^{**} \right] \cos 2\theta \right\}$$

$$v = \frac{PR}{M} \frac{1}{6} \left\{ \left[VF + (C/2B) UF \right] \left[1 + 3a_2^{**} - 4b_2^{**} \right] \sin 2\theta \right\}$$

Through the use of identities, the important radial displacement may be reduced to,

$$w = \frac{PR}{M} \frac{1}{2} \left\{ UF \left[1 - a_o^* \right] - \frac{2}{3} VF \left[1 + 3a_2^{**} - 4b_2^{**} \right] \cos 2\theta \right\}$$

which has coefficients similar to those in the circumferential thrust and moment equations, which are:

$$N = PR \left\{ B \left[1 - a_o^* \right] + \frac{C}{3} \left[1 + 3a_2^{**} - 4b_2^{**} \right] \cos 2\theta \right\}$$

$$M = PR^2 \left\{ \frac{C}{6} \frac{UF}{VF} \left[1 - a_o^* \right] + \frac{C}{3} \left[1 + 3a_2^{**} - 4b_2^{**} \right] \cos 2\theta \right\}$$

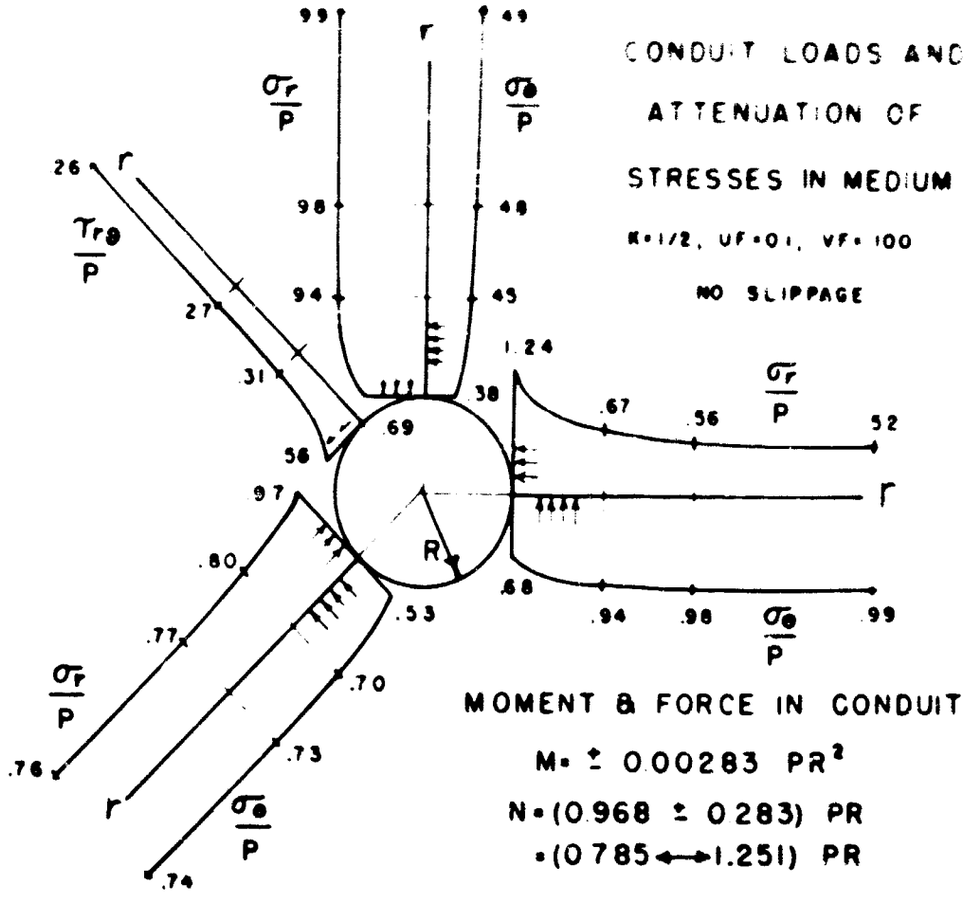
As before, the results for the full slippage case may also be non-dimensionalized by dividing each equation through by its first term.

RESULTS

The results given by these equations may perhaps be best understood graphically as shown in Figure 3 through Figure 8. These graphs are shown with radial distance as the abscissas plotted to the scale of the conduit along properly oriented radii. The stresses and displacements are plotted non-dimensionally as ordinates, thereby clearly indicating the spatial attenuation. Values are given at the interface and at distances of one-half diameter, one diameter, and two diameters from the interface.

The interaction loads are given by the values of the radial and tangential stresses at the interface. Load magnification is indicated by an increase in the stresses at the interface above the corresponding free-field stresses; conversely, load reduction is indicated by a decrease in the interface stresses below the corresponding free-field stresses. Average load magnification or reduction is indicated by the uniform radial stress values which are plotted at a 45 degree angle; it is also indicated by the first term of the circumferential thrust, N. Radial load magnification or reduction at the top and sides of the culvert is indicated, respectively, by the vertical and horizontal radial stress graphs.

Similarly, the horizontal circumferential stress graphs and the maximum value of the circumferential thrust are indicative of the arching phenomena. It is this arching which governs the load that the conduit experiences relative to the load that the medium, which the conduit is replacing, would experience in the free-field state. The arching is called positive if it transfers some of the load around the conduit, thereby resulting in a reduced load on the conduit. Conversely, the arching is called negative if it transfers additional load to the conduit, thereby resulting in an increased load on the conduit. Positive arching is indicated by an increase in the circumferential stress in the vicinity of the conduit above the free-field stress state and a corresponding decrease in the maximum thrust, N, below the value of the free-field vertical stress multiplied by the conduit radius, i.e., PR. Conversely, negative arching is indicated by a decrease in the circumferential stress in the vicinity of the conduit below the free-field stress state, and a corresponding increase in the maximum thrust, N, above the value PR.



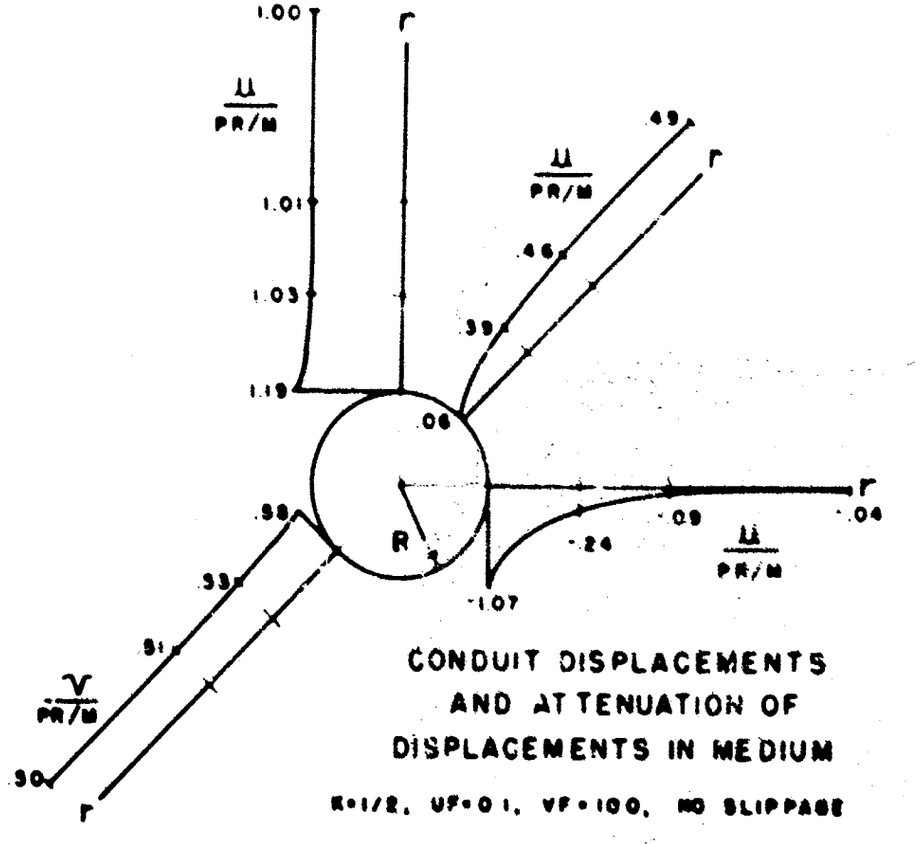
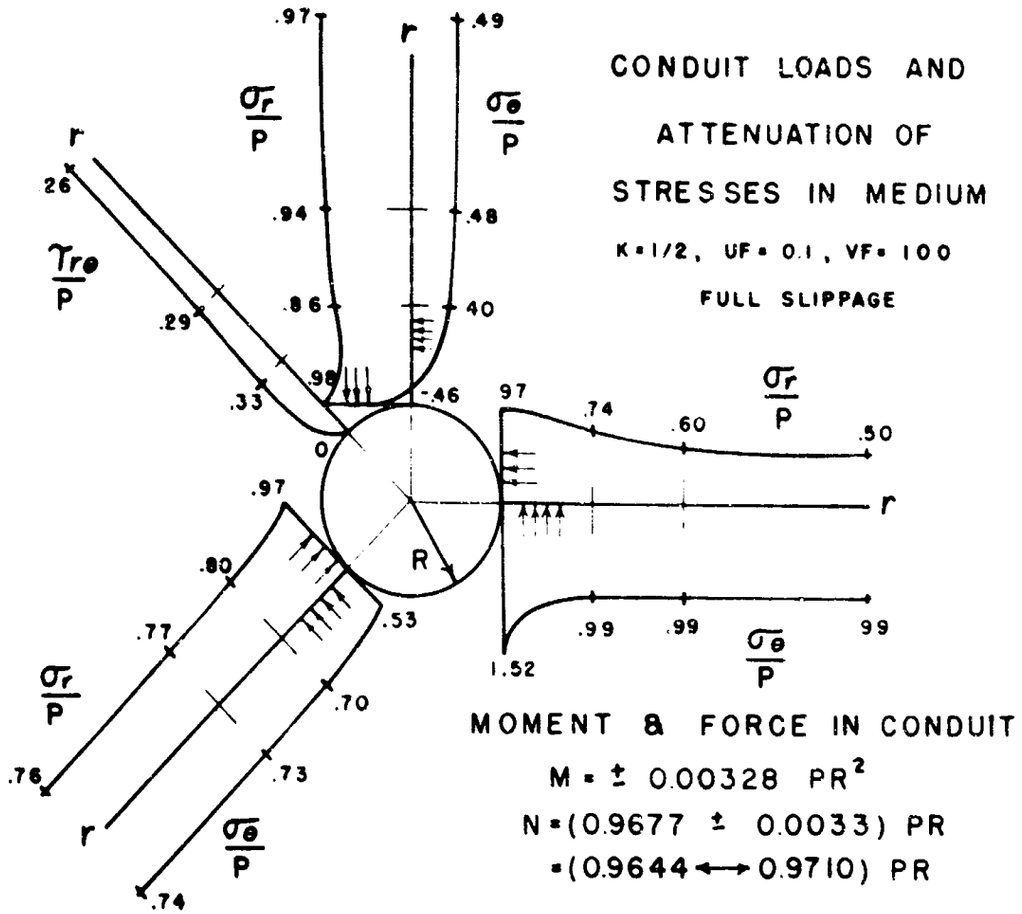


Fig. 3 Stresses and Displacements



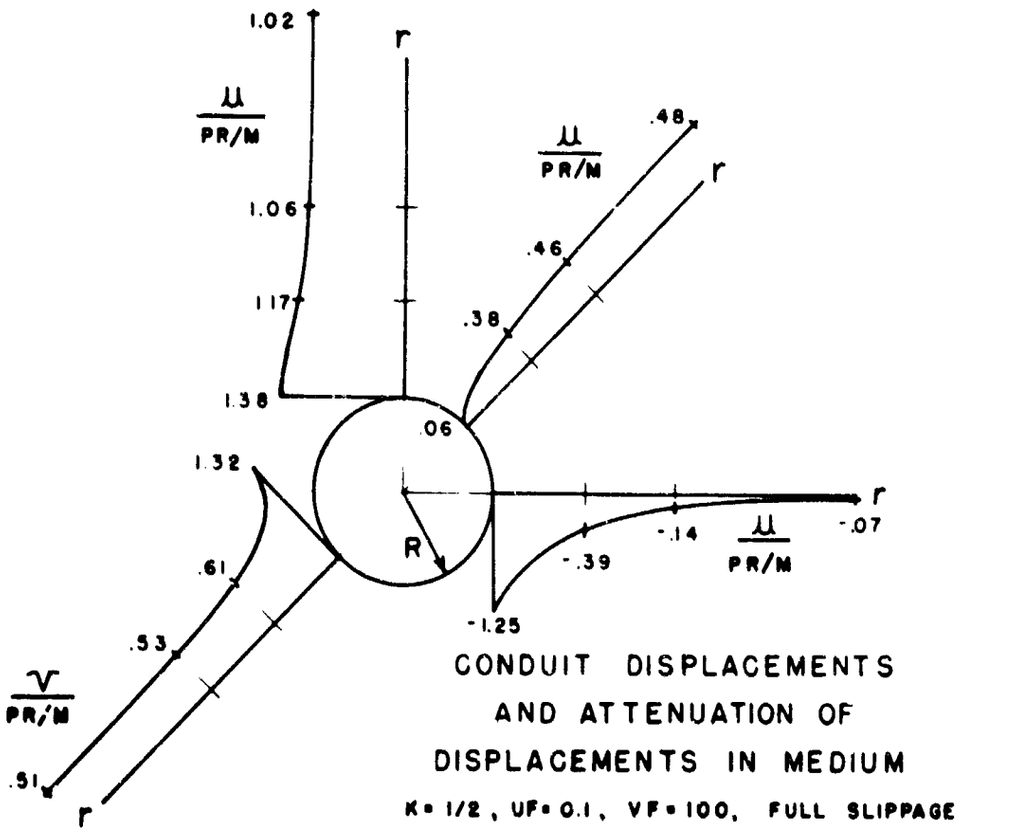


Fig. 4 Stresses and Displacements

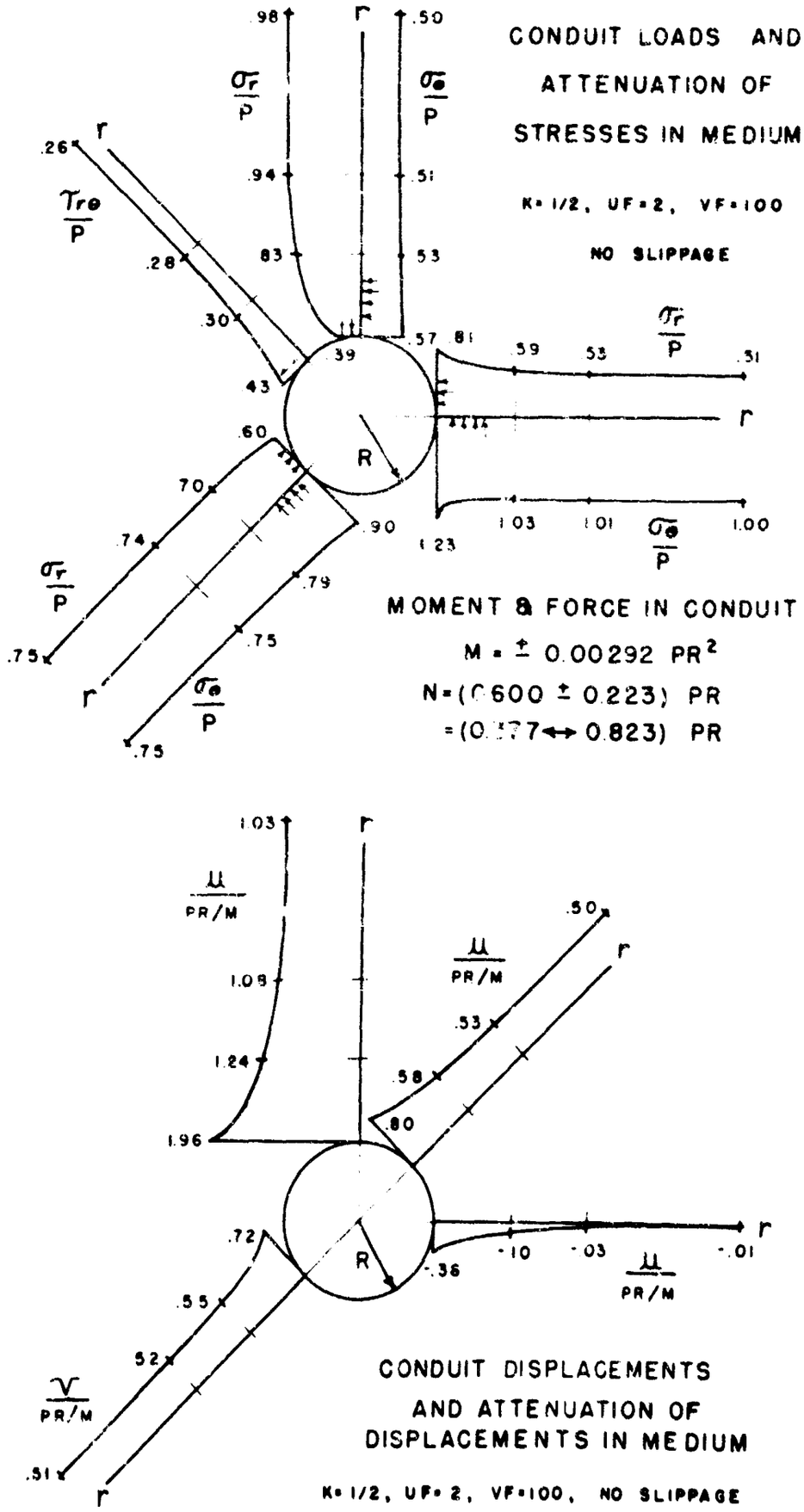


Fig. 5 Stresses and Displacements

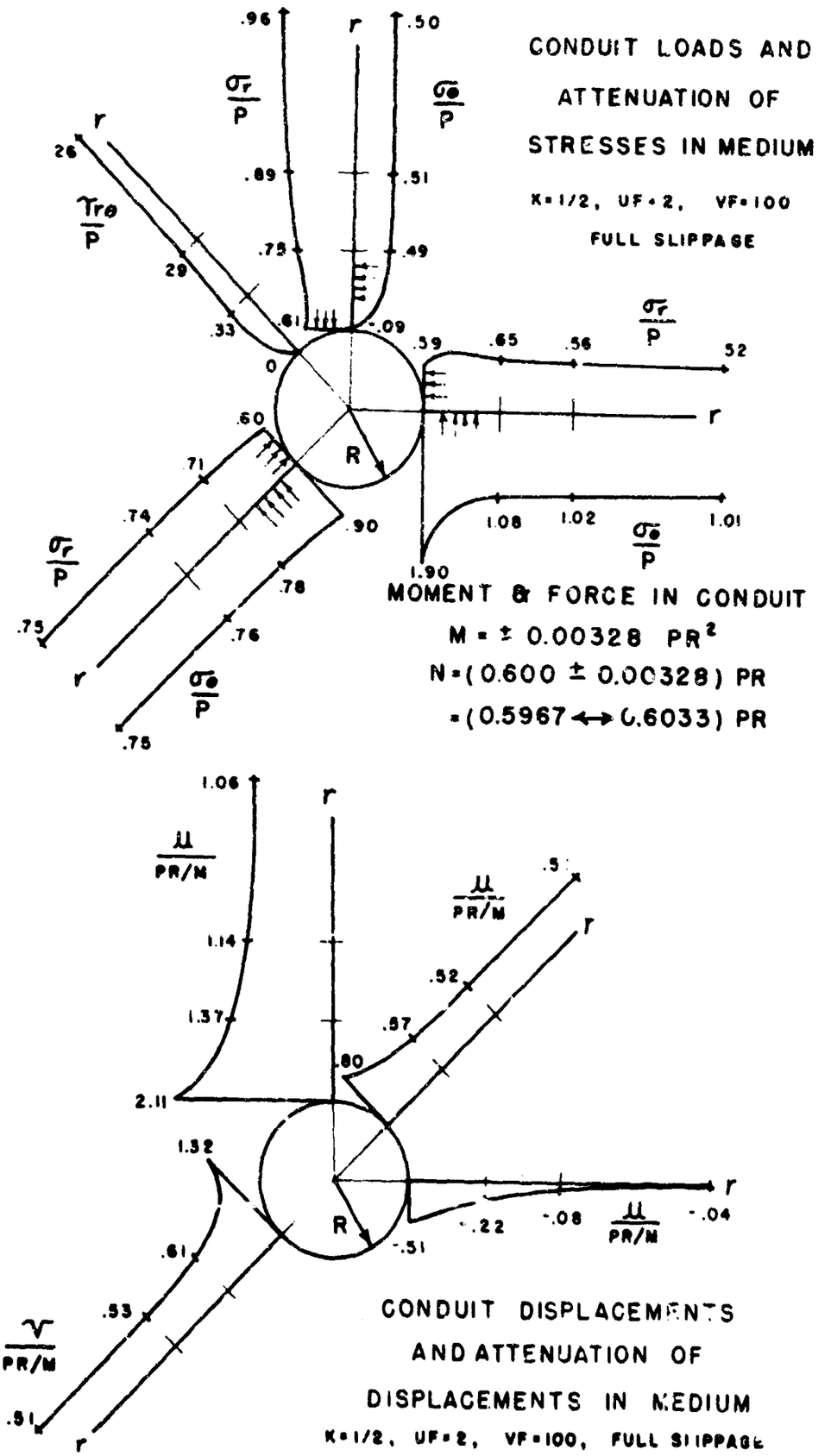
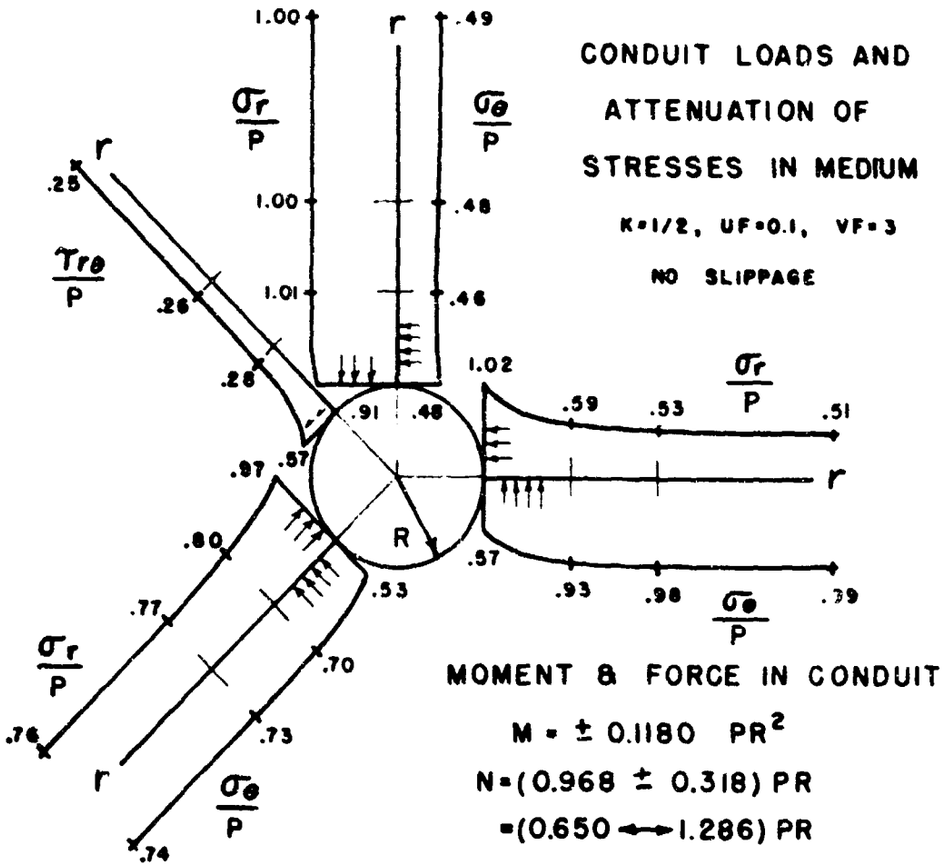


Fig. 6 Stresses and Displacements



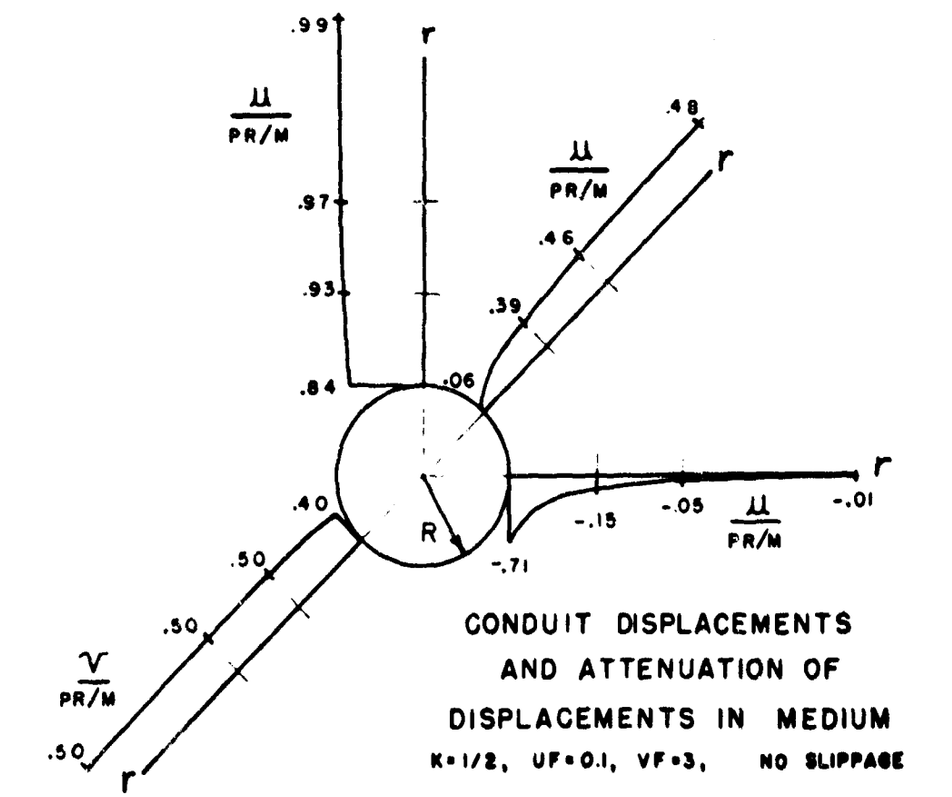
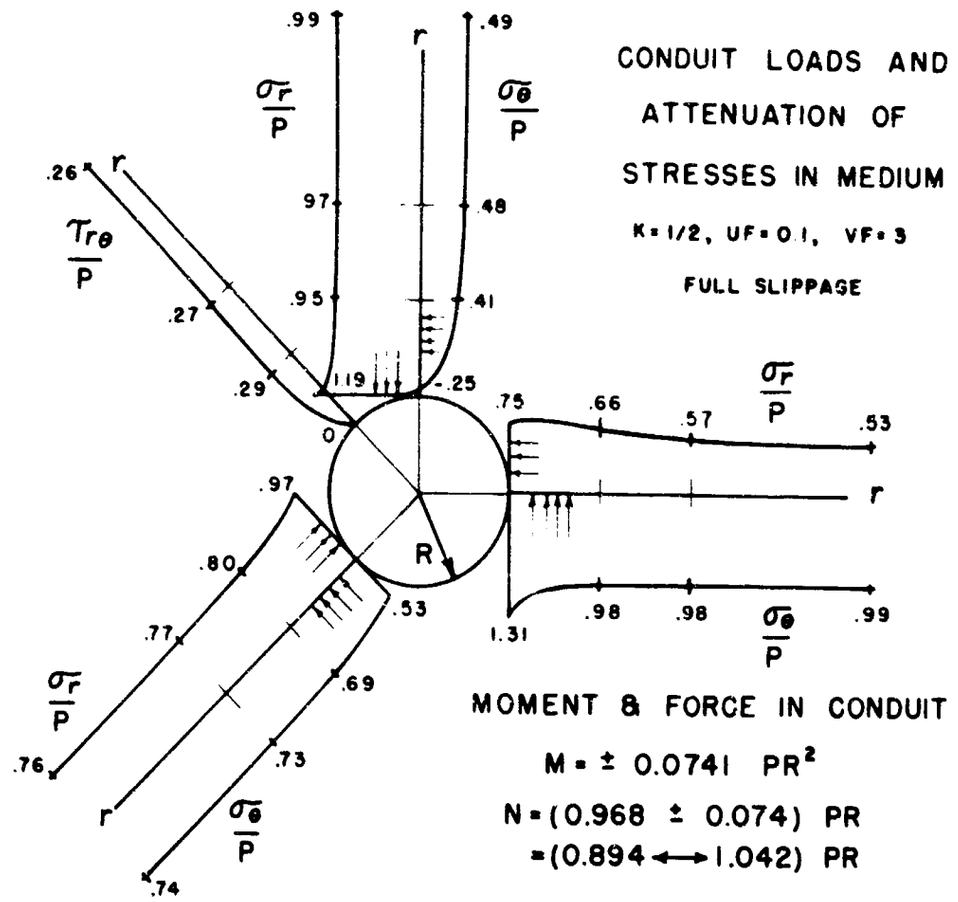


Fig. 7 Stresses and Displacements



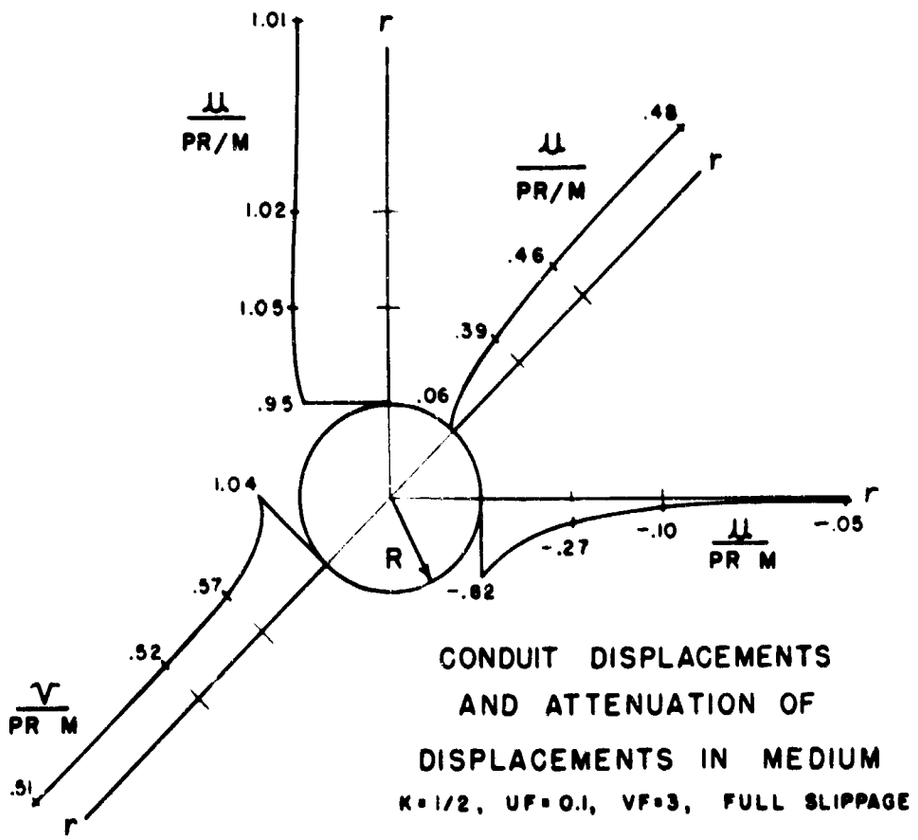


Fig. 8 Stresses and Displacements

To facilitate understanding the interaction problem, comparisons are presented wherein each of the non-dimensional flexibility parameters are varied independently. For the case UF = 0.1, VF = 100 and no slippage, it may be seen from Figure 3 that there is an average load magnification (σ_r/P = .97 at the interface compared to the free-field stress condition σ_r/P = .75) with a load reduction at the top (.69 compared to 1.00) and load magnification at the side (1.24 compared to .50). Correspondingly, negative arching is indicated by the circumferential stress distribution in the vicinity of the conduit being less than the free-field condition, and the maximum thrust occurring at the sides of the conduit being greater than PR,(N = 1.251 PR).

By varying the extensional flexibility to UF = 2 while holding VF = 100, it may be seen from Figure 5, that load reduction and positive arching is achieved. It should be noted that varying the extensional flexibility affects the interaction loads and circumferential thrust considerably, but affects the circumferential moment only slightly.

By varying the bending flexibility to VF = 3 while holding UF = 0.1, it may be seen from Figure 7 that the circumferential moment is increased substantially whereas there is only a slight increase in the circumferential thrust considering that this variation corresponds to a tremendous decrease in the bending flexibility for which the conduit has actually passed out of the "flexible conduit" range. Similarly, increasing the bending flexibility above VF = 100, while holding UF = 0.1, will decrease the moment slightly, but will cause very little decrease in thrust and load magnification. Therefore, once a fairly high bending flexibility is attained, there is a wide range of bending flexibilities for which the interaction loads and circumferential thrusts are more dependent on extensional flexibility than on bending flexibility. It should be noted, however, that reduction of the bending flexibility into the "rigid conduit" range will result in a marked increase in the importance of the bending flexibility on the interaction loads and thrusts as well as the moments.

INTERACTION CONCEPTS

It is apparent that the attenuation of the stresses and displacements is quite rapid (that is, the free-field condition is essentially reached within the depth of a diameter or two) so that this analysis may be used for conduits placed fairly close to the surface.

This analysis completely defines the stresses on orthogonal planes throughout the medium so that the principal stress trajectories and the maximum shear-stress trajectories are known. The shear-stress, and its corresponding normal stress, are known along these maximum shear-stress trajectories. Hence, if the medium is a soil with some assumed M* and K values, it may be determined whether or not slippage occurs in the soil medium. If slippage does not occur in the medium, the solution is valid and the arching follows the principal stress trajectories. If slippage does occur in the medium, insight is obtained as to where the slip zones occur, and rational assumptions can be made as to how the arches form.

An improved analysis may then be made on the basis of these assumed arches and slip zones. For instance, since slippage is a relaxation of constraints, the arches will tend to flatten thereby transferring more load to or away from the conduit--depending, respectively, on whether the continuous case caused load reduction or load magnification. Thus, even though this elastic analysis may not be the final solution, it provides a basis for more rational approaches than simply assuming vertical slip planes of uncertain height.

The effects of the relative flexibilities are clearly indicated. The advantages of a "flexible conduit" with a fairly high circumferential bending flexibility are indicated. Perhaps equally important, however, it may be seen that if the conduit is in the range of the "flexible conduit", the parameter which has the greatest influence on the load magnification or reduction, and hence the circumferential thrust, is the circumferential extensional flexibility of the conduit. For instance, if the bending flexibility is sufficient (say VF is considerably greater than 10, if K = 1/2), a further increase in bending flexibility may not be very beneficial since it will only slightly decrease the thrust in the conduit whereas it may increase the buckling hazard. However, an increase in extensional flexibility may be quite beneficial since it may decrease the conduit thrust considerably. It must be kept in mind that if buckling is not critical, increasing the bending flexibility may still be advantageous in order to decrease the bending moment even though the thrust will not be decreased appreciably.

For bolted steel culverts, which are in the "flexible conduit" range, the extensional flexibility may be increased through seam yielding. It should be noted that seam yielding obviously invalidates the continuous shell theory, and the interface tangential continuity in the limiting case of no slippage (there is no invalidity of the interface continuity in the other limiting case of full slippage). However, the effect of yielding seams may be approximated, using this analysis, by extending the definition of the extensional flexibility, UF, to include an average strain which is due to seam yielding. The justification of this approximation, as far as interface continuity is concerned, is based on the fact that the actual soil-culvert problem lies between the two limiting slippage cases; wherein, sufficient interface slippage capacity is available for the intense localized interface tangential discontinuities caused by seam yielding. The justification of this approximation, as far as the discrete degeneration of shell continuity at the yielding seams is concerned, is based on the fact that the culvert is a "flexible conduit" for which the overall decrease in circumferential length of the conduit is more important than the continuity of the extensional deformation, provided there is sufficient moment capacity to prevent buckling. This moment capacity requirement, in addition to the desirable circumferential extensionality, indicates an advantage in designing conduits with yielding longitudinal seams rather than designing circumferentially continuous

conduits, since moment capacity may be maintained in the case of yielding along overlapping seams but not in the case of uniform plastic compression. Therefore, if the thrust reaches the yield strength of the conduit, an increase in extensional flexibility through seam slippage may increase the load capacity; whereas, an increase in extensional flexibility through uniform plastic action is inviting buckling and may result in conduit failure.

Extensional flexibility becomes even more important in the actual soil-culvert problem where the passive pressure build-up at the conduit sides occurs at a higher rate than the active pressure decrease at the top; thereby resulting in smaller moments and deflections but higher circumferential thrusts in the conduit than are predicted by the linearly elastic case.

CONCLUSION

Equations are presented in non-dimensional form which completely describe the thrusts, moments, and displacements in a deeply buried conduit as well as the stresses and displacements throughout the surrounding elastic medium due to the action of an overpressure applied at the surface of the medium. The spatial attenuation of the stresses and displacements is shown to be quite rapid with the free-field condition being essentially reached within about two diameters. The separate effects of circumferential extensional flexibility and circumferential bending flexibility are clearly indicated, with the thrust being controlled principally by the extensional flexibility and the moment being controlled principally by the bending flexibility. This study of the linearly elastic soil case of the soil-culvert system is a necessary starting point and gives good insight into the actual soil problem. A brief philosophical discussion is included which mentions some of the effects of an actual soil and culvert and indicates methods for further investigation through a system of arches and slip zones. The validity of this theory and the resulting slip-zone-arch modifications which arise from it should be verified experimentally.

REFERENCES

1. Timoshenko, S. and J. N. Goodier, Theory of Elasticity, McGraw-Hill Book Company, Inc., 1951.
2. Flugge, W., Stresses in Shells, Springer-Verlag, 1960.

Author's note: A slight improvement is obtained by replacing the tangential displacement equation (p. 381) by:

$$v = -\int w\, d\theta - \frac{R^2}{EA}\iint T_{r\theta}\, d\theta d\theta$$

The only alteration will be in the two no slippage constants a_2^* and b_2^* (p. 382) which become,

$$a_2^* = \frac{C(1-UF)VF + 2B - (C/2)(C/B)UF}{(1 + B + CUF)VF + 2(1 + C) + (1 + C/2)(C/B)UF}$$

$$b_2^* = \frac{(B + CUF)VF - 2B - (C/2)UF}{(1 + B + CUF)VF + 2(1 + C) + (1 + C/2)(C/B)UF}$$

and in the full slippage tangential shell displacement equation (p. 384) in which the minor term (C/2B)UF vanishes. All other equations remain the same; the plots are only slightly affected since only the final UF term, which is the least important of the three terms in the a_2^* and b_2^* quotients, is altered by some function of (C/2) which is itself small ($C/2 \leq 1/4$).

THE BENEFICIAL ACTION OF THE SURROUNDING SOIL ON THE LOAD-CARRYING CAPACITY OF BURIED TUBES

by
U. Luscher* and K. Höeg**

ABSTRACT

This paper discusses the interaction between a buried cylindrical tube and the surrounding soil under high applied pressures. It proposes a distinction of three types of beneficial effects of soil surrounding on the strength of the buried tube, called pressure redistribution, deformation restraint, and arching. The nature of each of these three actions is examined, and suggestions are made for improvements in analysis and design of tube-soil systems.

BACKGROUND

The amazing load-carrying capacity of buried cylinders has been recognized for a long time and has been extensively used in Civil Engineering practice, predominantly for buried conduits of all kinds. Recent new applications have been primarily in protective construction, but also in the use of progressively larger conduits with shallow depth of cover for highway crossings, and of conduits under large loads from traffic or high earth embankments.

Parallel with the development of practical applications, the mechanics of buried-tube action has been extensively studied. Nevertheless, instead of a general understanding of the behavior, only practical solutions for certain classes of problems have been developed. It is thus not astonishing that extensive new research had to be initiated in support of the new applications.

At the present time, new research is being performed at many laboratories and on topics widely varying within the overall subject. Problems of communication are therefore important. This paper tries to contribute to the coherence of the many soil-structure interaction studies presently underway by presenting a general picture of the mechanics by which the surrounding soil enhances the load-carrying ability of a buried tube. It is based on an extensive review of the pertinent recent and older literature plus the authors' own research in this field.

The basic situation considered is the two-dimensional one of a long, circular cylindrical tube, buried horizontally and loaded either by the weight of a high embankment or by overpressure applied on the soil surface above it. (The two situations are equivalent if the depth of burial in the latter case is sufficient that no effect of the free surface on tube behavior is present.) Only cohesionless dry soils are specifically considered; however, the conclusions apply, in a general way, to any soil. Similarly, the concepts are developed mainly in view of static conditions, but apply also to dynamic loading conditions. However, any phenomena peculiar to the dynamic situation (e.g. inertia) have not been considered.

Any meaningful analysis of this situation must consider the interaction between the structure and the surrounding soil, and thus must investigate the load-carrying ability of the structure-soil system. This paper suggests an analysis of the soil-structure interaction in terms of three types of composite action: pressure redistribution, deformation restraint, and arching. One can think of these beneficial effects as a counteraction, by mobilization of pressures in the surrounding soil, to the tendency of the tube to deform in various modes (Figure 1): 1) The restraint against tube deformations in the second mode (i.e., counteracting the deformation from the originally circular shape into a horizontal ellipse) by mobilization of lateral passive earth pressures is called pressure redistribution. 2) The action against deformations in the third and higher modes enhances the resistance of the tube toward buckling failure, by forcing it to buckle in higher modes than in the unsupported situation; this action is called deformation restraint. 3) Finally, the reaction of the surrounding soil to tube deformations in mode one (pure compression) or zero (rigid body motion), by redistribution of pressure away from or onto the tube, is called arching. Depending on the relative compliances of tube and soil surrounding, arching is called active or passive.

The degree to which each of these three types of action is operating, and their relative importance, depends upon the characteristics of the structure-soil system. The controlling parameters are 1) the depth of soil cover over the tube, 2) the relative compressibilities of the structural tube and the soil it "replaces," 3) the general characteristics of the soil "at large" and in the immediate vicinity of the tube (i.e., bedding), and 4) the type and distribution of the load imposed on the system. Further, the relative importance of pressure redistribution, deformation restraint, and arching changes with the level of overpressure.

*Asst. Professor of Civil Engineering, Massachusetts Institute of Technology, Cambridge, Massachusetts.
**Research Assistant, Department of Civil Engineering, Massachusetts Institute of Technology, Cambridge, Massachusetts.

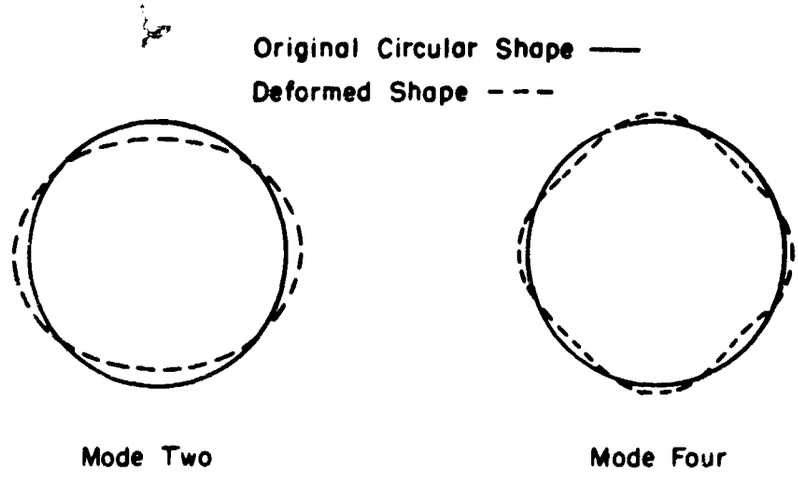


Fig. 1 Examples of Deformation of Tubes Into Modes

Before proceeding any further, it is important to identify the different ways that may lead to failure of the tube-soil system. The word failure here refers to collapse rather than merely failure to function satisfactorily under service conditions. (That is, effects such as leakage through cracks in a concrete pipe, or deformations which are excessive for an assigned purpose such as clearance, are not considered as failure.) Failure may be caused by:

1. excessive deformation leading to caving-in of the crown of the tube;
2. local instability, as for instance demonstrated by a snap-through buckling due to local decrease in curvature;
3. formation of yield hinges due to excessive bending in the tube wall, and collapse occurring when a mechanism develops;
4. over-all elastic buckling of the tube wall (under hoop stresses which are excessive for the tube rigidity and lateral support provided);
5. yielding in the wall due to excessive hoop stresses, resulting in general crushing unless such a failure is preceded by inelastic buckling due to decrease in wall rigidity.

In the following, the interaction is discussed in terms of the three interaction effects. It is realized that the distinction is somewhat artificial and arbitrary, since the effects operate simultaneously and thus undoubtedly influence each other. Nevertheless, the distinction is useful for clarifying and organizing ideas.

PRESSURE REDISTRIBUTION

Up to the present time no rigorous theoretical approach has been developed to predict the pressure distribution around a tube buried in soil. The "ring-compression theory" currently in wide use is based on intuition and extensive field experience. It postulates that the tube-soil system adjusts according to the imposed load so as to minimize bending in the tube wall.

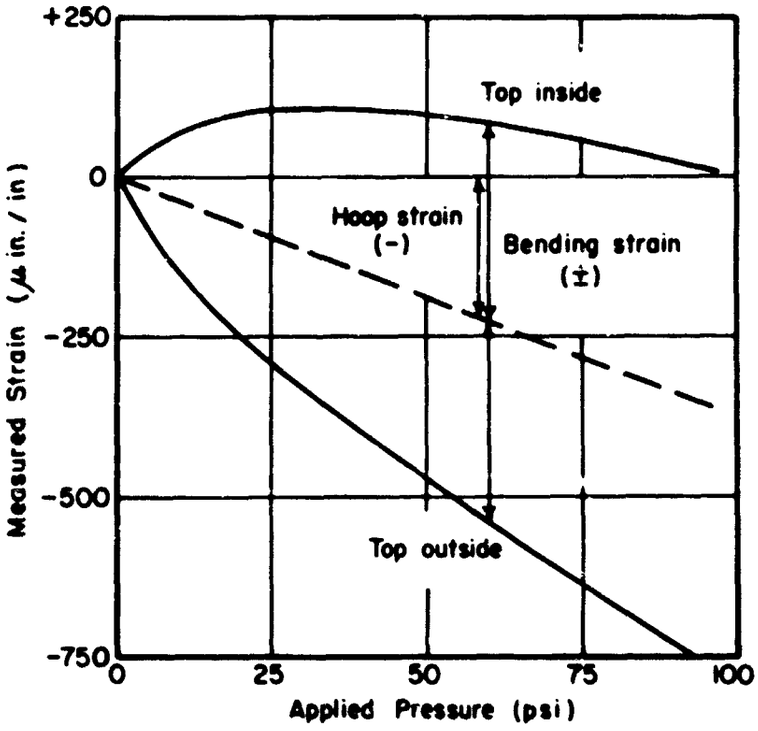
In general terms the bending moment at any point along the periphery of a circular ring can be expressed by

$$M = a\, p_{max}\, r^2$$

where $M = M(\theta)$ = bending moment
$a = a(\theta)$ = a factor dependent on the distribution of contact pressure
p_{max} = highest radial contact pressure
r = radius of ring
θ = central angle

For low loads and hence small deformations of the tube-soil system, the interface pressure between tube and soil is highly non-uniform. The factor "a" will thus be relatively high; however, since "p" is low the bending moments in the wall will not exceed the bending resistance of even fairly flexible tubes. As the applied pressure on the system is increased, the tube-soil system starts to deform and to adjust according to the imposed load; passive resistance of the soil is gradually mobilized on the sides of the tube, while simultaneously the rate of increase in contact pressure at the crown decreases. The result is that even though the average pressure "p" has increased, the bending stress in the wall may have increased very little or may conceivably have decreased because the factor "a" has been substantially reduced (see for example

Figure 2 taken from Luscher, 1964). If the tube is flexible, i.e., thin-walled or ductile, it may further deform without distress. The distribution of contact pressure will tend toward one that minimizes bending in the deformed tube section. Thus a state of pure hoop compression evolves, which is the most efficient way to carry the load.



Tube: 4-in. diameter, 0.035-in. wall thickness, aluminum

Soil: dense Ottawa sand

Cover: 1/2 in.

Fig. 2 Example of Measured Strains

There exist qualitative as well as quantitative justifications for such an interacting behavior between tube and soil, and satisfactory designs have been completed on this basis (e.g., Barnard, 1957; White, 1961). Recent small-scale experiments (Luscher and Höeg, 1963; Marino, 1963) have also confirmed the above reasoning, and of the three types of soil action discussed in this paper, pressure redistribution has been counted upon with most confidence.

However, the basic question which is of increasing importance, especially in the field of protective construction, remains to be answered: What are the criteria to ensure that a cylinder buried in a given soil is to behave predominantly in a compressive mode? Field and laboratory data (Peck, 1948; Albright, 1957; Whitman et al, 1962; Bulson, 1963; Luscher and Höeg, 1963) have shed light on the problem and design recommendations (ASCE, 1961; Newmark, 1962) have been made on the basis of data of this kind and much engineering judgement. These recommendations usually concern the depth of cover and the properties of the backfill beside the tube.

As an example of laboratory data on the effect of depth of burial, the authors (1963) observed in tests on very flexible tubes buried in sand that the applied surface pressure required to fail the tube did not vary significantly with depth of cover, provided the cover was more than approximately 1/8 D (D = diameter of tube = 1.6 inches). However, the mode of failure depended greatly on depth of burial. For a cover more than approximately 1 1/2D, the failure consisted of a narrow longitudinal buckle (a type of failure treated in the next section), and the tube could not be brought to collapse even for applied pressures three times the pressure at buckling. Under continued load only a gradual widening of the crease occurred. Tubes buried with a cover less than approximately 3/4D failed by sudden and complete collapse with caving-in of the crown. A depth of cover between 3/4D and 1 1/2D provided an intermediate condition of protection against collapse. From a structural point of view, the ductile behavior observed for the tubes buried below 1 1/2D is highly desirable.

If the conditions of burial needed to develop the capacity of a cylinder in the compression mode are not satisfied, "premature" failures may take place in the form of excessive deformations leading to caving-in, or local instabilities due to decreased curvature, or yield hinges leading to an unstable mechanism. The exact conditions, however, are not known as yet. Current research at M.I.T. aims at providing clearer understanding of the influence of conditions of burial and flexibility of the tube on the distribution and magnitude of contact pressure.

DEFORMATION RESTRAINT

Deformation restraint was defined in the introduction as the prevention of third- and higher-mode deformations of the tube. It leads to a dramatic increase of the buckling resistance in comparison to the unsupported situation. This is analogous to the increase in buckling load of a column which has lateral elastic support (Timoshenko and Gere, 1961).

Thus this effect is intuitively understandable and has been extensively relied upon in buried-tube construction practice (see "ring-compression theory"), but until recently the problem had not been accessible to analytical treatment. The important question is whether this action can always be depended upon to prevent buckling failure and thus to allow use of the yield stress of the construction material for design, or whether conceivably a high-mode buckling failure may occur. Recent experimental and theoretical research by the authors (1963) showed the following:

Buckling of an elastically supported tube is controlled by the equation

$$p^* = 2\sqrt{\frac{k_s EI}{r^3}}$$

where p^* is the uniform, radial tube buckling pressure, EI and r are the flexural rigidity and the radius of the tube, and k_s is a "modulus of soil reaction" relating the local soil pressure counteracting buckling to the strain $\Delta r/r$. Meyerhof (1963) presents an almost identical equation.

To predict p^* for a given situation, k_s has to be determined. For a circular symmetric soil surrounding (Figure 3b), chosen to eliminate the effect of pressure distribution and for simple mathematical treatment, k_s back-calculated from the experimental failure data was shown to be equivalent to the resistance of the soil ring to uniform, outward acting pressure in the cavity. Thus k_s was dependent on the ring thickness and the "elastic" soil properties; see Figure 4. Since these properties are not constants in a soil, but depend on the stress pattern, k_s is affected not only by the pressure p^* itself, but also by the arching condition in the soil ring. Only for those combinations of soil and tube for which the arching effect is negligible can the modulus k_s be expressed as a function of p^* alone, then the equation solved for p^*.

An equation of this kind was obtained for the Ottawa sand surrounding used in the study:

$$p^* = 780\left[\frac{EI\ F}{r^3}\right]^{5/6}$$

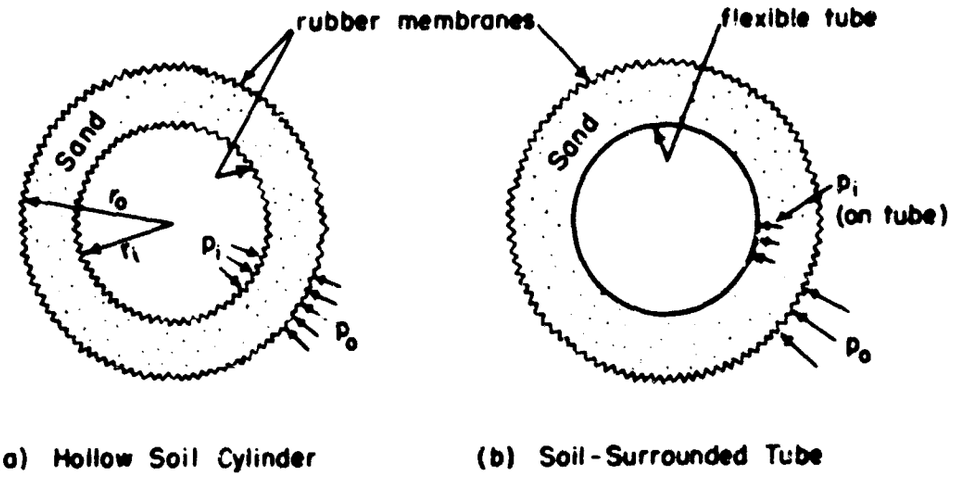
where F equals k_s/E_s as plotted in Figure 4. The application of this equation to the failure conditons of smooth-walled tubes of different materials assumed surrounded by the same soil leads to the curves of Figure 5. The figure demonstrates that the failure stress is controlled by buckling curves similar in nature to column buckling curves, also limited by the yield stress of the material. More specifically, the figure indicates, for various materials, the critical radius-to-thickness ratios at which the failure mode changes from compressive yield to buckling.

These restraining effects are more important than pressure redistribution or arching in many situations of thin-walled tubes surrounded by competent soil. Recognizing this, the authors compared directly results from buried tube tests (Luscher and Höeg, 1963 ; Bulson, 1962) with theoretical predictions based on the above theory; see Figure 6. While as expected, on account of the neglected effects, the data do not conform perfectly to the theory, the observed agreement is still encouraging. It indicates that this analysis represents a theoretical toehold on the problem, and might well lead to a rigorous solution eventually, provided it proves possible to consider in it the effects of pressure redistribution and of arching for the general case of a buried tube.

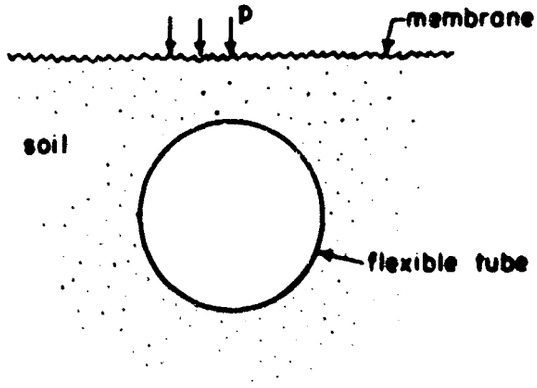
ARCHING

As an indication of the recognized significance of arching, the ratio between applied overpressure and pressure acting on the tube may, according to experimental evidence and protective design recommendation (Newmark, 1962), be as low as 0.1 under conditions favorable for active (positive) arching. Considerable experimental and theoretical effort has been expended to investigate the arching phenomena in soil, e.g. by Lane (1957), Wiedermann (1961), Whitman et al (1962), Ang and Newmark (1963), Van Horn and Tener (1963), Allgood et al (1963), and Mason (1963). However, owing to the difficulty of the problem, little basic information has been added to the state of knowledge summarized by Terzaghi (1943) some 20 years ago. The simplest of the arching theories considers the vertical equilibrium of the soil mass between assumed vertical sliding surfaces extending up from the structure (Figure 7). The magnitude of contact pressure against any buried structure is at present predicted on the basis of this same approach with some elaboration (Newmark, 1962). This section discusses and evaluates some of the assumptions involved in a vertical-sliding-surface analysis and suggests a somewhat different way of looking at the arching phenomenon.

The main uncertainty in the analysis described above is the magnitude of the lateral pressure acting normal to the sliding surfaces. In the expression for the predicted pressure at any depth (see Figure 7), the term involving the overpressure is very sensitive to the coefficient of lateral pressure K. Terzaghi states that the factor K appearing in the analysis is an empirical coefficient.



(a) Hollow Soil Cylinder (b) Soil-Surrounded Tube



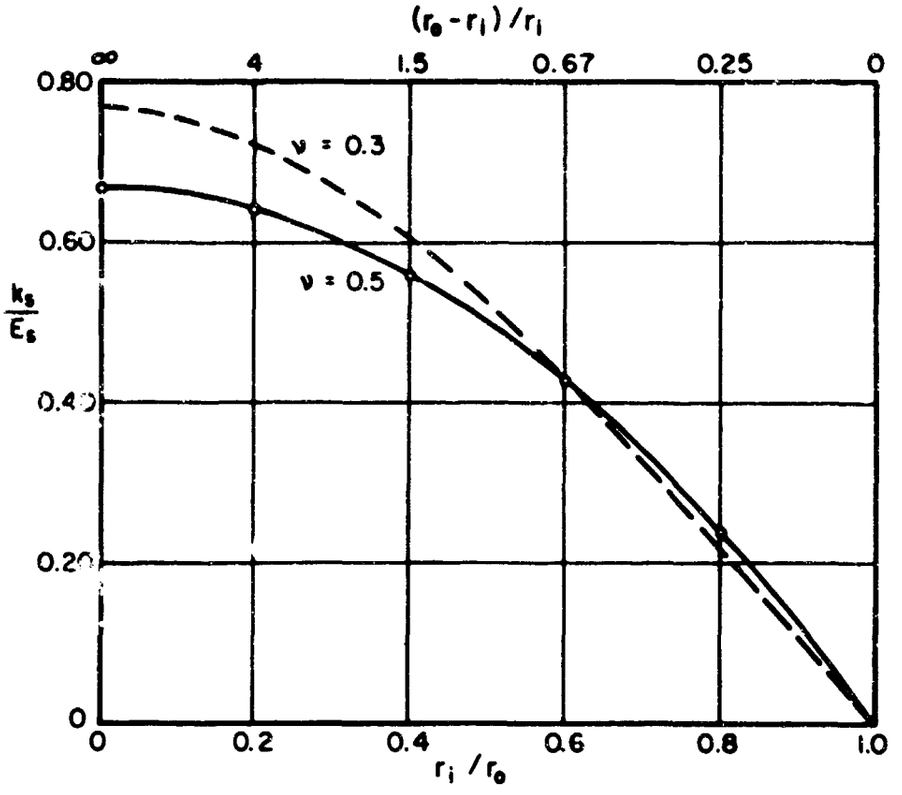
(c) Buried Tube

Fig. 3 Various Soil or Soil-Tube Configurations

However, most investigators seem to assign values of K_o (e.g. Newmark, 1962) or K_o (e.g. Spangler, 1960) where K_o is the active pressure coefficient. The reasoning behind the assumption of such values does not seem to reflect the action taking place in the structure-soil system. In Terzaghi's classical experiments (Terzaghi, 1936), the value of horizontal to vertical pressure increased with height above the trap door from 1 to 1.6 and then decreased towards K_o at a height of about 2.5 times the width of the trap door. Ang and Newmark (1963) present results from trap door tests performed with wooden toothpicks as "soil" material. By applying the sliding-surface analysis to their data, the average value of K over the depth was backfigured to be 1.5. Similarly, data from the buried dome tests by Whitman et al (1962) indicate a value of 1.2.

The vertical-sliding-surface analysis does not take into account the geometric configuration of a buried structure, although some investigators have suggested that the shape may have an influence on the magnitude of arching (Whitman et al, 1962; Newmark, 1962). In Whitman's tests a flat roof experienced approximately 50% higher total load than a hemispherical roof at the same depth of cover. In both cases the only deflection of the structure took place in the foundation, which was identical for both roofs.

The authors believe that the vertical-sliding-surface concept should be replaced by the concept of thrust-ring action, i.e., of structural arches (or domes in a three-dimensional case) forming in the soil. This concept has been stated before (Engesser, 1882; Coquot, 1934 and 1957). There exists direct evidence that soil domes may form above yielding "roofs" (Terzaghi, 1936; Jenike, 1961). Thrust-ring action in the soil around shafts and tunnels has been described and analyzed (Terzaghi, 1943), and Tschebotarioff (1951) states that "transfer of pressure by shear and arching are not synonymous."



$$\frac{k_s}{E_s} = \frac{[1 - (r_i/r_o)^2]}{(1+\nu)\,[1+(r_i/r_o)^2\,(1-2\nu)]}$$

Fig. 4 Modulus of Soil Reaction For Elastic Ring

A clear demonstration of the thrust ring that may be developed has been provided by tests on hollow sand cylinders and or mmetrically sand-surrounded tubes (Whitman and Luscher, 1962). Theoretical and experimental findings indicate that the capacity of a soil ring (Figure 3a) to carry externally applied radial pressure may be expressed as

$$p_o = p_i \left[\frac{r_o}{r_i}\right]^{\left\{\frac{2\sin\phi}{1-\sin\phi}\right\}}$$

where the notation is as shown in Figure 3a. An interior tube (Figure 3b) limits the deformation of the soil ring and thus the arching. Still, by increasing the compressibility of tubes surrounded by sand, the ratio between the pressure p_i on the tube and the applied pressure p_o could be decreased, down to a minimum of around 1/5 in those particular tests (Luscher and Höeg, 1963).

Even though the above tests investigated an idealized condition of "burial," there is no reason why the same mechanism of pressure transfer as in a soil ring or shell cannot develop in the general case of a structure surrounded by soil. The difference between the action of the soil in these laboratory experiments and in the field is one of degree, not of nature. This similarity of action has in fact been demonstrated (Luscher and Höeg, 1963) by buried tube tests in which the failure pressures were very similar to the failure pressures of identical tubes symmetrically surrounded by sand.

Returning to the vertical-sliding-surface concept, it is seen that the correct lateral force to be used is the horizontal component of the thrust in the soil arch. The ratio K between this and the vertical pressure can, of course, be quite high under favorable conditions. The exact amount of thrust mobilization depends upon the overpressure and the curvature and allowed radial deformation of the soil arch. These in turn depend directly upon the characteristics of the structure-soil system as outlined in the ... chapter.

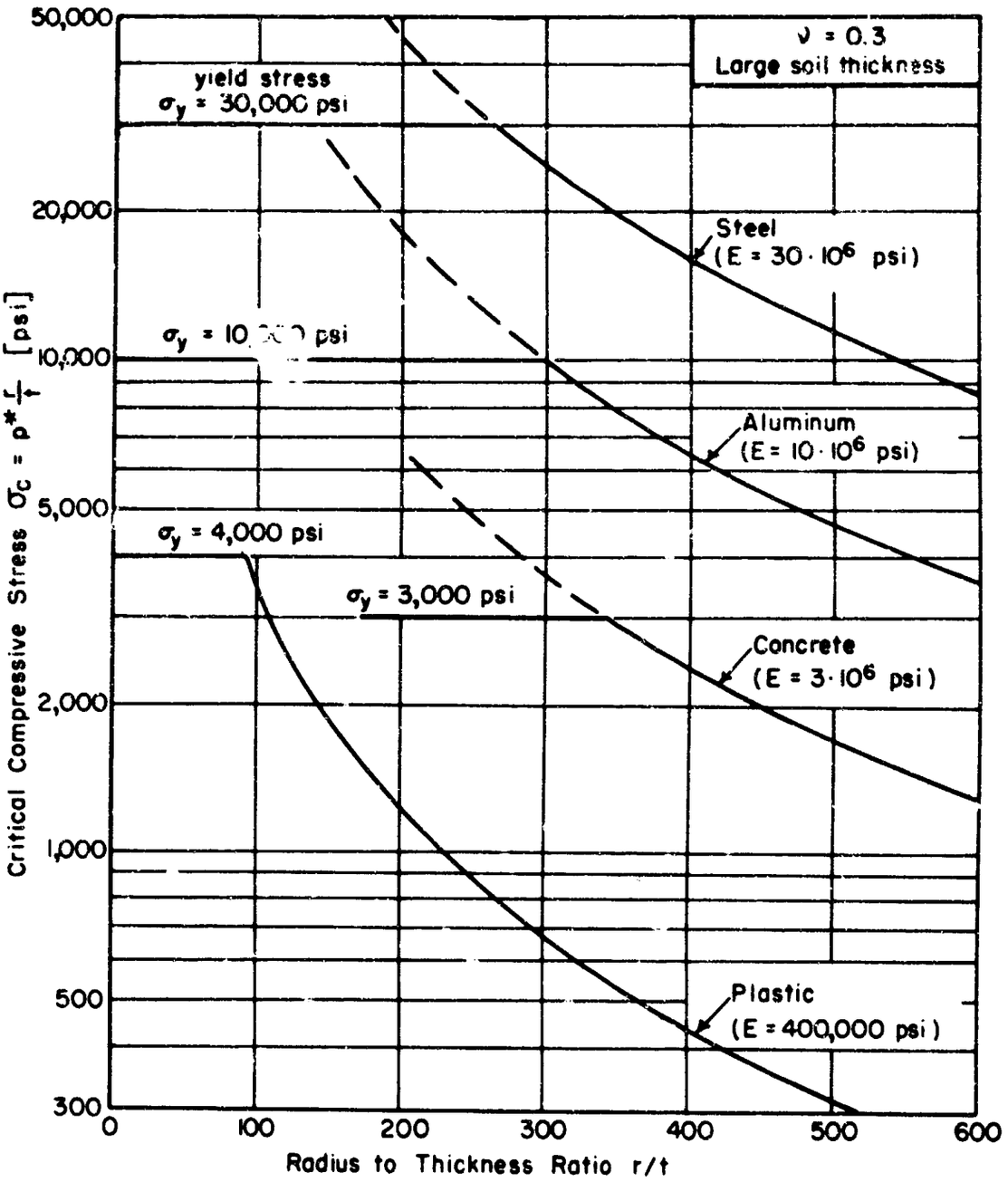


Fig. 5 Strength of Soil-Surrounded Tubes

SUMMARY AND CONCLUSIONS

This paper proposes a distinction of three beneficial effects of the surrounding soil on the load-carrying capacity of buried tubes. An analysis of the interaction between soil and tube in terms of the three effects leads to the following conclusions:

The equalization of pressures all around the tube by "pressure redistribution" can safely be depended upon if the tube-soil system is properly designed and constructed. Then failure will be initiated either by high-mode buckling or by compressive yielding of the tube. The "deformation restraint" provided by the surrounding soil is highly effective in raising the buckling resistance, but stability is still the design criterion in many cases of flexible tubes. Use of a corrugated instead of a smooth-walled tube can eliminate buckling in most of these cases. "Arching", finally, is effective in reducing the fraction of the applied load which reaches the structure. It is suggested that the soil-arch concept is more useful than the vertical-sliding-surface concept in the treatment of arching.

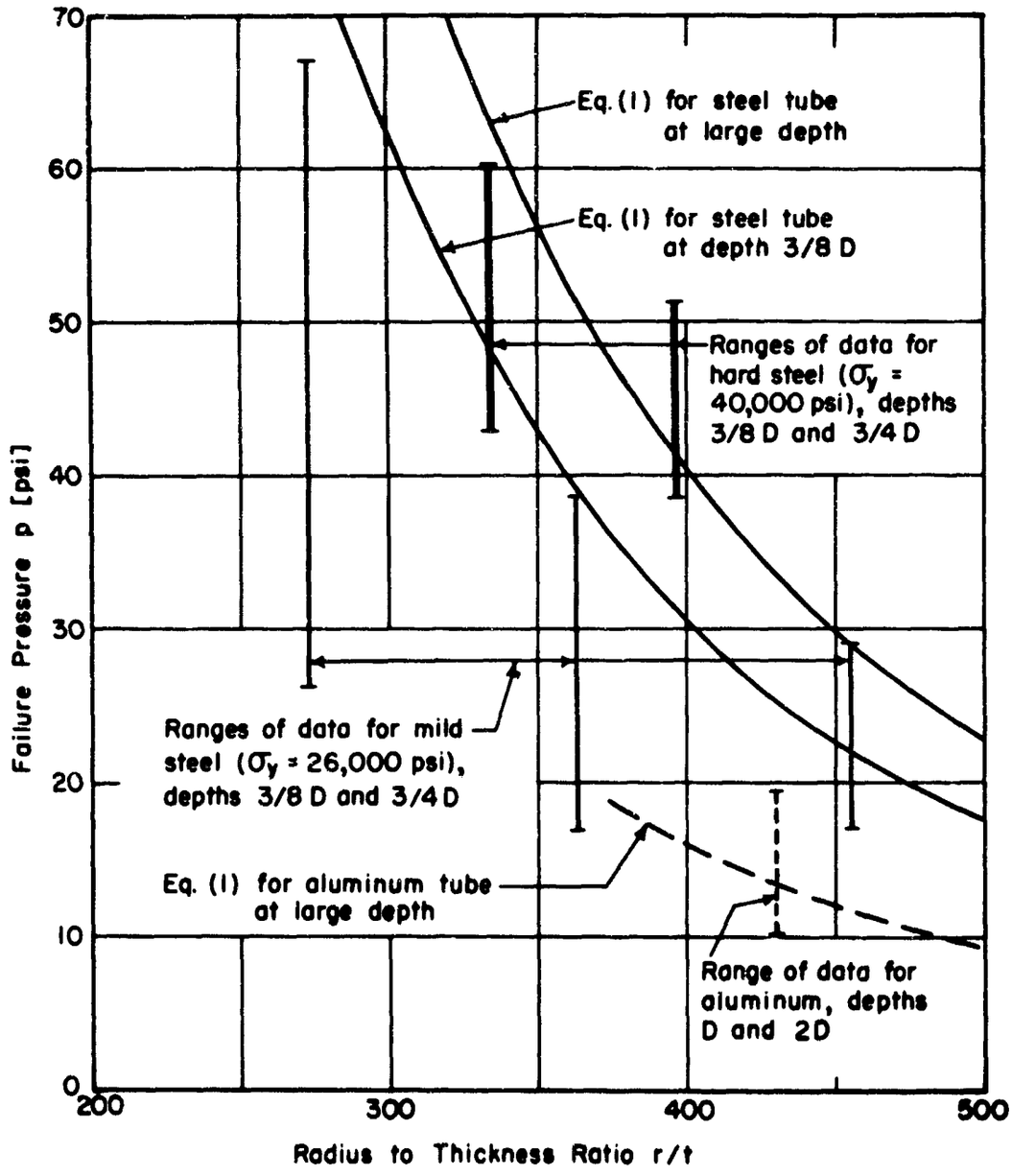
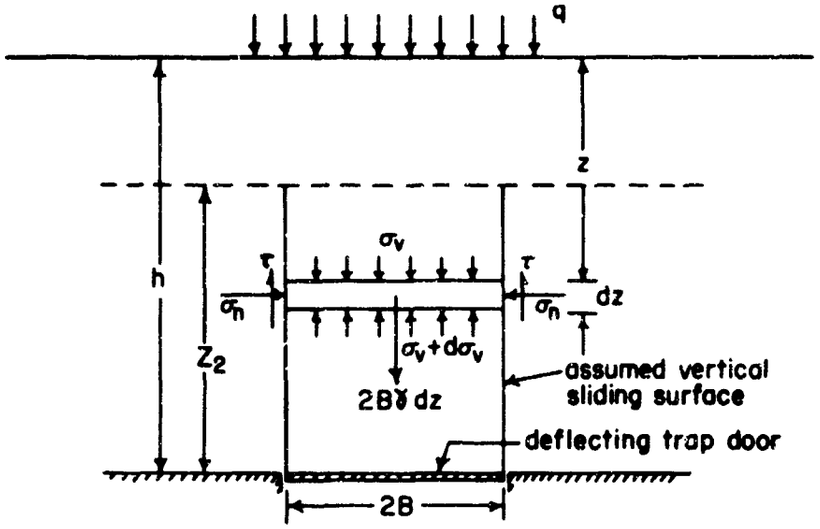


Fig. 6 Comparison of Theory with Buried Tube Data



Z_2 = assumed height of sliding surfaces

The analysis predicts pressure on trap door to be:

$$p_d = \frac{B\left(\gamma - \frac{C}{B}\right)}{k \tan\phi}\left[1 - e^{-k\tan\phi\,\frac{Z_2}{B}}\right] + \left[\gamma(h - Z_2) + q\right] e^{-k\tan\phi\,\frac{Z_2}{B}}$$

where

C, ϕ = soil strength properties

γ = unit weight of soil

Fig. 7. Vertical-Sliding-Surface Analysis

ACKNOWLEDGEMENTS

Research on soil-structure interaction has been going on for the past five years at the Department of Civil Engineering of the Massachusetts Institute of Technology, under the sponsorship of the Waterways Experiment Station of the U.S. Army Corps of Engineers and the Air Force Weapons Laboratory, U.S. Air Force Systems Command.

The authors gratefully acknowledge the guidance of Professor R. V. Whitman, who initiated and supervised much of this work.

REFERENCES

Albright, G.H., "Evaluation of Buried Conduits as Personnel Shelters," ITR 1421, 1957.

Allgood, J.R., C.R. White, R.F. Swalley, and H.L. Gill, "Blast Loading of Small Buried Arches," Technical Report R 216, U.S. Naval Civil Engineering Laboratory, 1963.

Ang. A., and N.M. Newmark, "Computation of Underground Structural Response," Report DASA 1386, Defense Atomic Support Agency, 1963.

ASCE, "Design of Structures to Resist Nuclear Weapons Effects," Manual 42 of the American Society of Civil Engineers, 1961.

Barnard, R.E., "Design and Deflection Control of Buried Steel Pipe Supporting Earth Loads and Live Loads," Proc. American Society for Testing Materials, Vol. 57, p. 1233, 1957.

Bulson, P.S., "Deflection and Collapse of Buried Tubes," Military Engineering Experimental Establishment, Hampshire, England, 1962. Summary also available in Proc. American Society of Civil Engineers, Vol. 89, No. SM5, p. 95, 1963.

Caquot, A., "Équilibre des Massifs à Frottement Interne," Gauthier-Villars, Paris, 1934.

Caquot, A., "La Pression dans les Silos," Proc. Fourth International Conference on Soil Mechanics and Foundation Engineering, Vol. 2, p. 191, 1957.

Engesser, F., "Über den Erddruck gegen innere Stützwände," Deutsche Bauzeitung, Vol. 16, p. 91, 1882.

Jenike, A.W., "Gravity Flow of Bulk Solids," Utah Engineering Experiment Station, Bulletin 108, 1961.

Lane, K.S., "Effect of Lining Stiffness on Tunnel Linings," Proc. Fourth International Conference on Soil Mechanics and Foundation Engineering, Vol. 2, p. 223, 1957.

Luscher, U., and K. Höeg, "The Interaction Between a Structural Tube and the Surrounding Soil," Report RTD TDR-63-3109, Air Force Weapons Laboratory, 1963.

Luscher, U., "Static and Dynamic Tests on 4-Inch-Diameter Cylinders," Report to Air Force Weapons Laboratory under preparation, 1964.

Marino, R.L., "A Study of Static and Dynamic Resistance and Behavior of Structural Elements," Report RTD TDR-63-3060, Air Force Weapons Laboratory, 1963.

Mason, H.G., O.H. Criner, R. Waissar, and N.R. Wallace, "A Study of the Dynamic Soil-Structure Interaction Characteristics of Real Soil Media." Paper presented at the Conference of the ASCE in San Francisco, October, 1963.

Meyerhof, G.G., and C.L. Fisher, "Composite Design of Underground Steel Structures." Reprint from the Engineering Journal, The Journal of the Engineering Institute of Canada, September 1963.

Newmark, N.M., and J.D. Haltiwanger, Air Force Design Manual, Report AFSWC-TDR-62-138, Air Force Special Weapons Center, 1962.

Peck, O.K., and R.B. Peck, "Experience with Flexible Culverts through Railroad Embankments," Proc. Second International Conference on Soil Mechanics and Foundation Engineering, Vol. 2, p. 95, 1948.

Spangler, M.G., Soil Engineering, International Textbook Company, 1960.

Terzaghi, K., "Stress Distribution in Dry and in Saturated Sand above a Yielding Trap-Door," Proc. First International Conference on Soil Mechanics and Foundation Engineering, Vol. 1, p. 307, 1936.

Terzaghi, K., Theoretical Soil Mechanics, Wiley, 1943.

Timoshenko, S., and J. Gere, Theory of Elastic Stability, McGraw-Hill, 1961.

Tschebotarioff, G.P., Soil Mechanics, Foundations and Earth Structures, McGraw-Hill, 1951.

VanHorn, D.A., and R.K. Tener, "A Study of Loads on Underground Structures," Report DASA 1406, Defense Atomic Support Agency, 1963.

White, L.W., "Largest Metal Culvert Designed by Ring Compression Theory," Civil Engineering, p. 52, January, 1961.

Whitman, R.V., and U. Luscher, "Basic Experiment into Soil-Structure Interaction," Proc. American Society of Civil Engineers, Vol. 88, No. SM6, p. 135, 1962. See also closing discussion to this paper in Proc. ASCE, Vol. 90, No. SM3, 1964.

Whitman, R.V., Z. Getzler, and K. Höeg, "Static Tests upon Thin Domes Buried in Sand," Journal of the Boston Society of Civil Engineers, Vol. 50, p. 1, 1962.

Wiedermann, A.H., "Static Experiments for the Study of the Interaction of Buried Structures with Ground Shock Waves," Report AFSWC-TR-61-32, Air Force Weapons Laboratory, 1961.

AN EXPERIMENTAL EVALUATION OF SOIL ARCHING

by
George E. Triandafilidis*, Delon Hampton**, and
Milan Spanovich***

ABSTRACT

The first phase of a sustained research effort was conducted to study the passive arching phenomenon on buried structures due to modulus mismatch**** between structure and surrounding medium. Tests were performed on buried small-scale structural models which were specially designed to measure passive arching stresses independent of side-wall friction. All tests were static, using 20-30 dry Ottawa sand at three different densities. The applied overpressure and the length of embedment of the buried structures were varied to study the influence of these parameters on soil-structure interaction.

INTRODUCTION

When the horizontal boundary of a semi-infinite soil mass is subjected to a uniform vertical pressure of infinite lateral extent, the identical applied vertical pressure is transmitted to each point of the underlying medium. However, when the continuity of the medium is interrupted by the presence of a buried structure, the stresses within the domain of the structure are no longer equal to the free-field stress since discontinuities of strain occur at the soil-structure interface whereby shear stresses are mobilized within the medium.

The principal concern of this research effort is to develop perception of the parameters that influence the arching mechanism on buried structures. When a structure is buried in the soil, there is a modulus mismatch between the structure and the surrounding soil. Consequently, when a pressure is applied to the surface of the soil, relative displacements occur between the structure and the adjacent soil. As a result, shear stresses are mobilized along the planes that experience relative displacements. The magnitude of these shearing stresses depends upon the properties of the soil, the stiffness of the structure, the magnitude of the overpressure, and the location and geometry of the buried structure.

If it is assumed that the stiffness of the buried structure is equal to that of the surrounding soil, at every overpressure level both the buried structure and the surrounding medium under the applied surface pressure should experience the same amount of deformation; and no arching stresses should develop. Thus, the buried structure will be subjected to exactly the same stress as the applied surface pressure.

If the stiffness of the buried structure is smaller than the modulus of the surrounding soil, a pressure applied at the surface will cause the buried structure to deform more than an equivalent column of soil. Thus, shear stresses will be mobilized across the planes that experience differential displacements These shear stresses will act in such a direction as to reduce the stress in the domain of the buried structure to a level below the intensity of the applied surface pressure. This phenomenon of stress transfer (reduction) will be referred to as "active arching," and the stress reduction itself will be called "active arching stress."

Finally, if the stiffness of the buried structure is greater than that of the surrounding medium, the surrounding medium will deform more than the buried structure. The mobilized shear stresses will now act in such a direction as to superimpose on the buried structure an additional stress above that of the applied surface pressure. This phenomenon of stress transfer (increase) is referred to as "passive arching," and the portion of the stress carried by the buried structure in excess of that imposed by the surface intensity will be called "passive arching stress." It should be emphasized that arching stresses can also occur due to differential displacements which do not necessarily result from superimposed surface pressure.

BACKGROUND

It appears that the significance of the arching phenomenon was first observed in connection with the bracing of open cuts. During the construction of the New York subway system at the turn of the century, field measurements of strut loads in open cuts disagreed with Coulomb's hydrostatic distribution of lateral earth pressures. Higher loads were measured in the top struts of braced, open cuts (1). Similar results were observed by Terzaghi (2) in connection with

*Assistant Professor, Rice University
**Research Associate Engineer, University of New Mexico, Air Force Shock Tube Facility
***Consulting Engineer, Pittsburgh, Pa.
****The term "modulus mismatch" in this report indicates the difference in moduli between buried structure and surrounding medium.

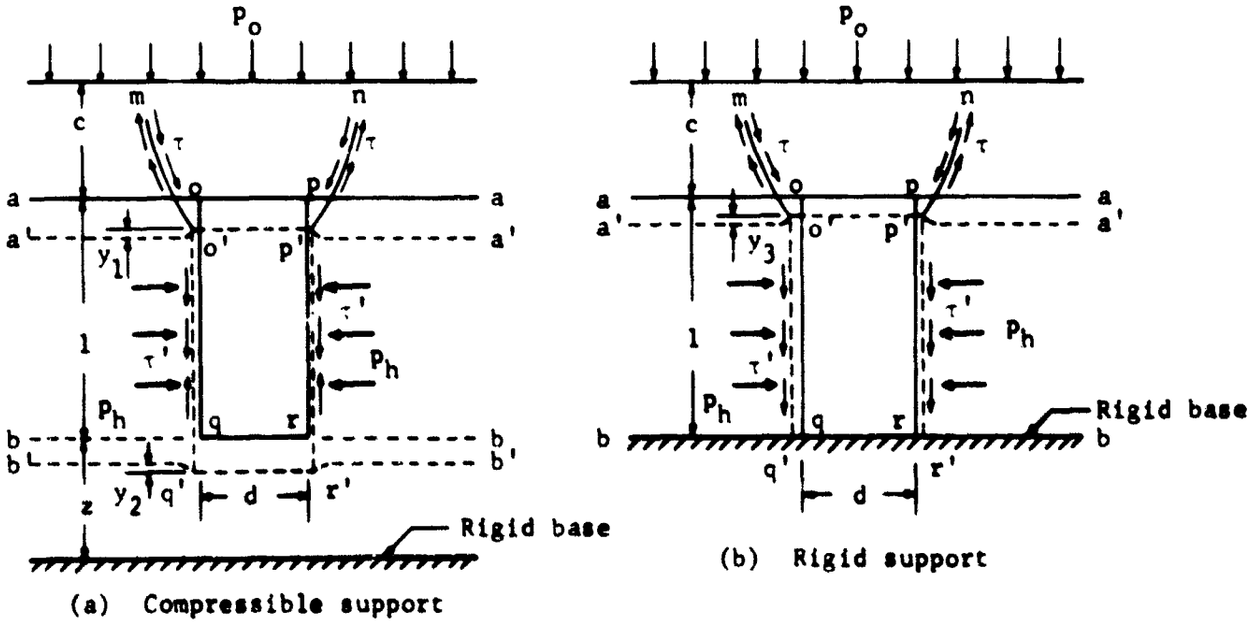
lateral earth-pressure measurements in open cuts during the construction of the Berlin subway.

The need for a more comprehensive analysis for the design of culverts and underground conduits intensified the interest in the arching mechanism of buried structures. Some of the significant work in this area has been performed by Spangler (3). More recently, the design requirements for underground protective construction have created a need for better understanding of the arching mechanism. Toward this end the Civil Engineering Branch,WLRC, has sponsored basic and applied research. Some of the results of this effort are contained in References 4 and 5. Reference 4 deals with static experiments, and Reference 5 with theoretical concepts of dynamic soil-structure interaction. Test data are presented in Reference 4 for completely buried structures and for structures pushed into 20-30 Ottawa sand. One of the more significant conclusions of these tests is that the normalized arching stress (ratio of the arching stress to the overpressure) is independent of the overpressure. Furthermore, the arching stress is expressed as a linear function of the differential displacement between the structure and the surrounding medium. No limiting value for the normalized arching stress is indicated.

Although other investigators have also made contributions toward a better understanding of the arching phenomenon, the references cited are representative and provide an overall picture of present knowledge.

SCOPE

Figure 1a shows a buried cylindrical structure of diameter, d, and embedded length, l. Before application of an overpressure, p_o, on the ground surface, the structure occupied the position, opqr, possessing a soil cover, c, and a cushion depth, z, measured from the bottom of the structure to a rigid base. The horizontal planes, a-a and b-b, are drawn so as to pass in the unloaded state through the top and bottom planes, op and qr, of the buried structure. When an overpressure is applied to the ground surface, the buried structure shown in Figure 1a is displaced to occupy a new position indicated as o'p'q'r'. If the buried structure is stiffer than the surrounding medium, plane a-a beyond the boundary of the structure will deflect more than plane op, resulting in a differential displacement, y_1, between the roof of the buried structure and the surrounding medium. As a result of this differential displacement, shear stresses, τ, will be mobilized along the planes o'm and p'n. It should be emphasized that the hypothetical rupture planes indicated in Figure 1a are diagrammatic only--and arbitrary. The actual position and shape of these planes have never been ascertained (6); furthermore, their occurrence depends on the order of magnitude of the differential displacement.



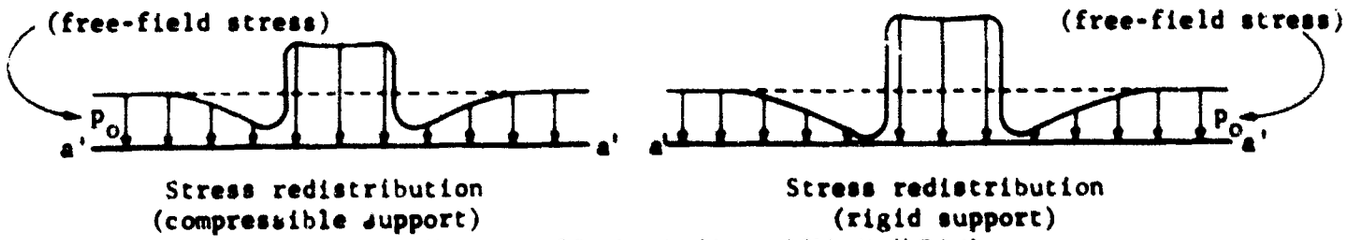


Fig. 1 Illustration of Passive Arching and Side-Wall Friction

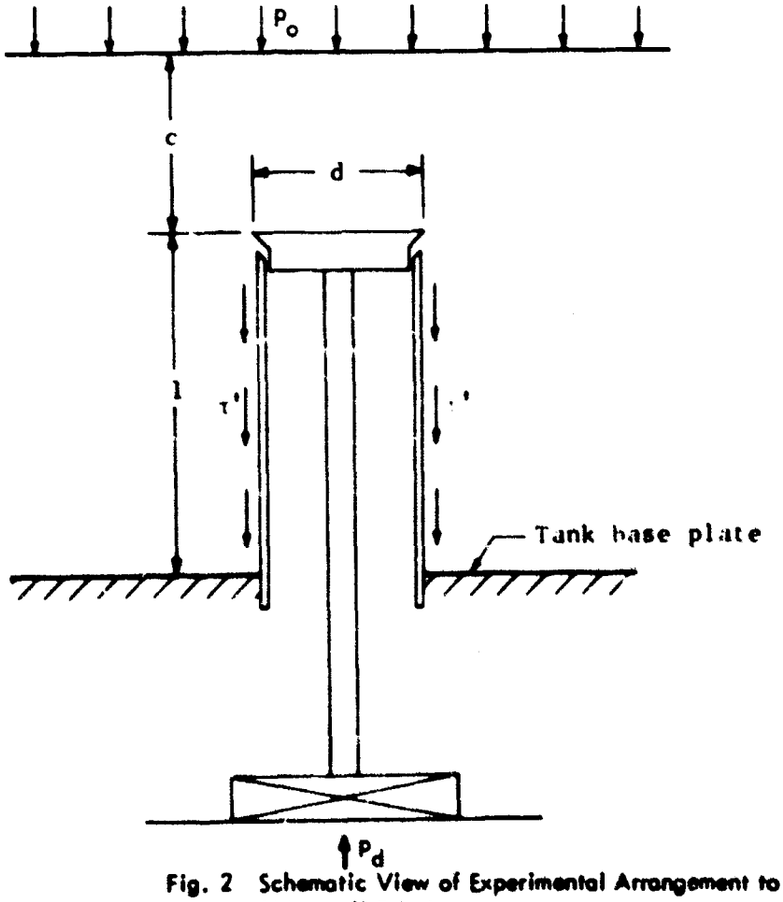
When the buried structure is stiffer than the surrounding medium, the stress on plane q-r will be larger than the free-field stress. Thus, plane b-b will be displaced to position b'-b', while plane q-r will be displaced to position q'-r', creating a differential displacement, y_2, at the bottom elevation of the structure. As a result of this differential displacement, frictional stresses, τ', will be mobilized along the vertical walls of the structure; and the direction of these frictional stresses will depend on the relative movement between the buried structure and the adjoining soil.

The total load on a buried structure consists of the separate contributions of free-field stress, arching stress, and side-wall frictional drag. Since the arching stress is caused by the mobilization of shear stresses within the soil above the buried structure, the factors that influence the arching stress for a given overpressure are the longitudinal stiffness of the structure, the modulus of the surrounding medium, and to a certain extent the rigid body motion of the structure due to the compressibility of the medium below the base level of the structure.

The total force due to side-wall friction on a buried structure is proportional to its embedded length and depends on the normal stress, p_h, exerted on the structure and the frictional properties between the structure and the surrounding medium. The normal stress depends on the radial stiffness of the buried structure as well as on the density of the surrounding medium. Furthermore, the normal stress on a buried structure depends on the overpressure and is influenced by arching in longitudinal and radial (7) directions.

During the early stages of this study, the desirability of simplifying the problem by eliminating some of the aforementioned variables became quite obvious. An experimental arrangement to simulate a conservative and relatively simpler model was designed (Fig. 1b). It consists of a buried structure whose base is supported on a stratum of infinite stiffness with respect to the surrounding medium. If it is assumed that the structure itself has an infinite stiffness in comparison to the surrounding medium, any differential displacement, y_3, between buried structure and surrounding medium will be due to the compressibility of the medium itself. The stress redistribution along plane o'p' due to arching is shown in Figure 1 for both compressible and rigid support. The pattern of stress redistribution suggested in Figure 1 is arbitrary. Its main purpose is to indicate that when a stress increase occurs on the buried structure a stress decrease must also occur immediately adjacent to the boundaries of the buried structure.

To be able to measure the influence of passive arching, a special experimental arrangement was designed which permitted the measuring of the axial load on buried structures free from any side-wall friction. For this purpose vertical cylindrical structures were used in which the roof of the structure consisted of a rigid disc supported independent of its side walls. A schematic drawing of the adapted design is shown in Figure 2. Structures of this types will be referred to as "disc structures."



The equilibrium equation for the structure in Figure 2 yields:

$$P_d = P_o + P_a$$

which can be written as:

$$\frac{P_d}{A_c} = p_d = \frac{P_o + P_a}{A_c} = p_o + p_a$$

or

$$\frac{p_d}{p_o} = 1 + \frac{p_a}{p_o}$$

where

$A_c = \pi d^2/4$

p_o = applied overpressure on surface

p_d = total pressure applied to structure

p_a = arching pressure applied to structure

Fig. 2 Schematic View of Experimental Arrangement to Separate Passive Arching from Side-Wall Friction

EXPERIMENTAL APPARATUS AND STRUCTURES

The general features of the experimental apparatus are shown in Figure 3.

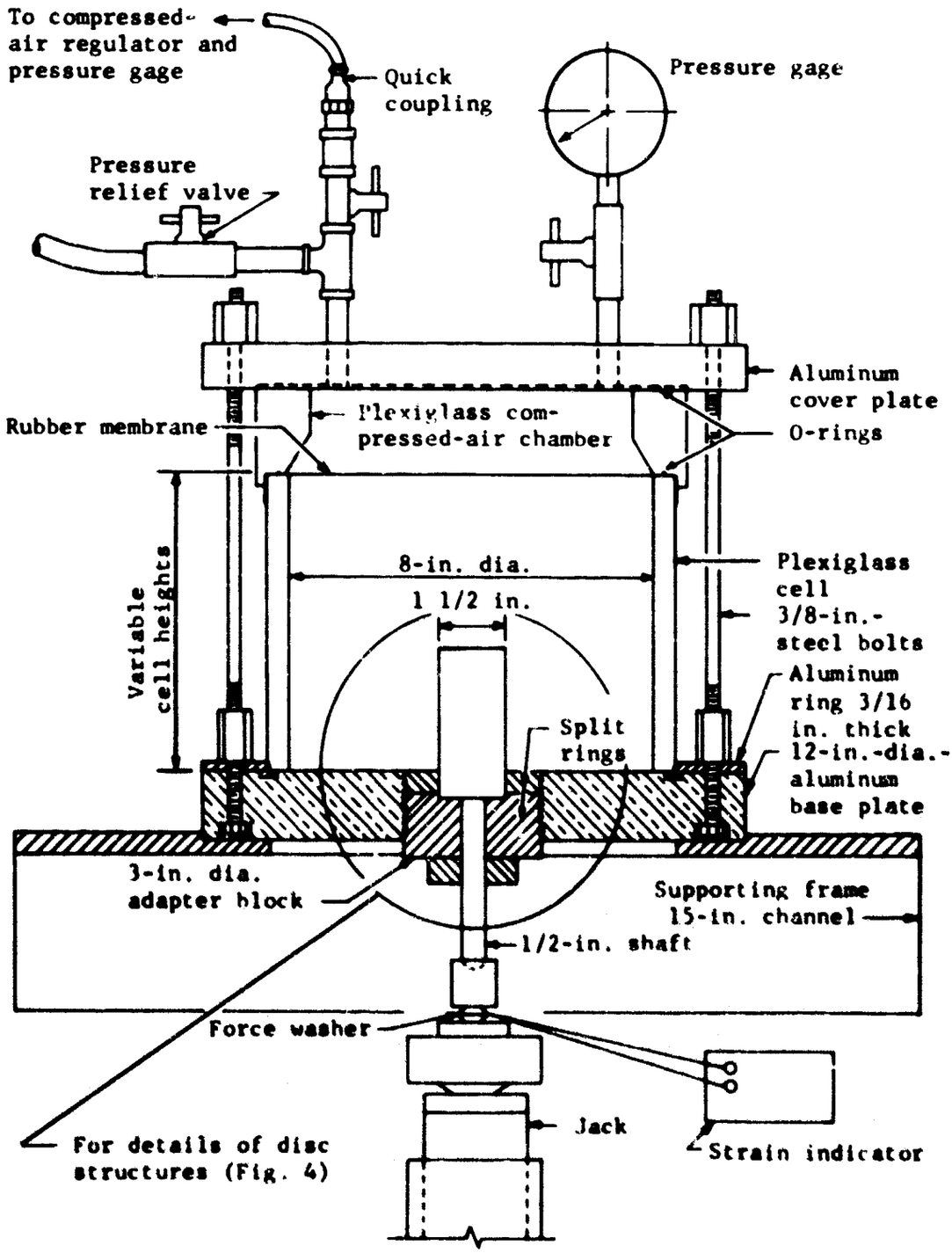


Fig. 3 General Features of Experimental Apparatus

The test tank consists of a plexiglass cylinder 8 inches I.D. and 1/2 inch in wall thickness. The lower end of the plexiglass cylinder is threaded to screw into an aluminum ring 3/16 inch thick and 12 inches O.D. The function of this ring is to connect the plexiglass cylinder to the base plate of the tank to facilitate filling the tank with sand without dislocating the plexiglass cell. This aluminum ring is attached to an aluminum base plate by means of four, 3/8-inch,

round, steel bolts, 10 inches long. The other end of these bolts is used to fasten an aluminum cover plate to the cell of the test tank. The entire assembly is connected to a base frame by four short bolts.

The supporting framework consists of a 15-inch channel with a circular hole 9 inches in diameter. The upper surface of this channel is recessed 3/16 of an inch to accommodate and center easily the 12-inch base plate of the test tank. A special ring, machined out of plate plexiglass, fits between the tank and the aluminum cover plate. This plexiglass ring provides an airtight pressure chamber, as shown in Figure 3. O-rings are provided at both rims of the plexiglass ring to seal the pressure chamber between a rubber diaphragm placed on top of the sample and the aluminum cover plate.

The aluminum base plate of the test tank has the additional function of providing independent support for the sleeves surrounding the disc structures. To obtain the required amount of structure embedment for a disc structure, sleeves of different lengths are necessary. For this purpose a series of sleeves varying between 1 and 5 inches in length was made.

Since all structures tested were 1-1/2 inches in diameter, for a given amount of embedment, the ratio of soil cover to structure diameter was varied by using different heights of test tanks. A series of plexiglass cells of different heights was made. Tests were conducted using plexiglass cells 2-1/2, 3, 4, and 5 inches high.

As shown in Figure 4, a circular hole 3 inches in diameter is provided in the aluminum base plate of the test tank. This hole is plugged with an aluminum adapter block which is split transversely into two separate rings. The upper ring has an I.D. of 1-1/2 inches and an O.D. of 3 inches. This upper ring is threaded along both the I. and O.D.'s. The threads on the O.D. are used to connect this ring to the main base plate of the test tank while the inner threads are provided to accommodate the sleeves used for the different disc structures. The lower ring of the transversely split adapter block has a 3-inch O.D. and is also threaded to screw into the base plate of the test tank. The lower portion of the adapter block houses a 1/2-inch ball bushing. The function of this ball bushing is to provide vertical alignment for the 1/2-inch shaft which supports the roof of the disc structures. It is also used to minimize friction on the shaft.

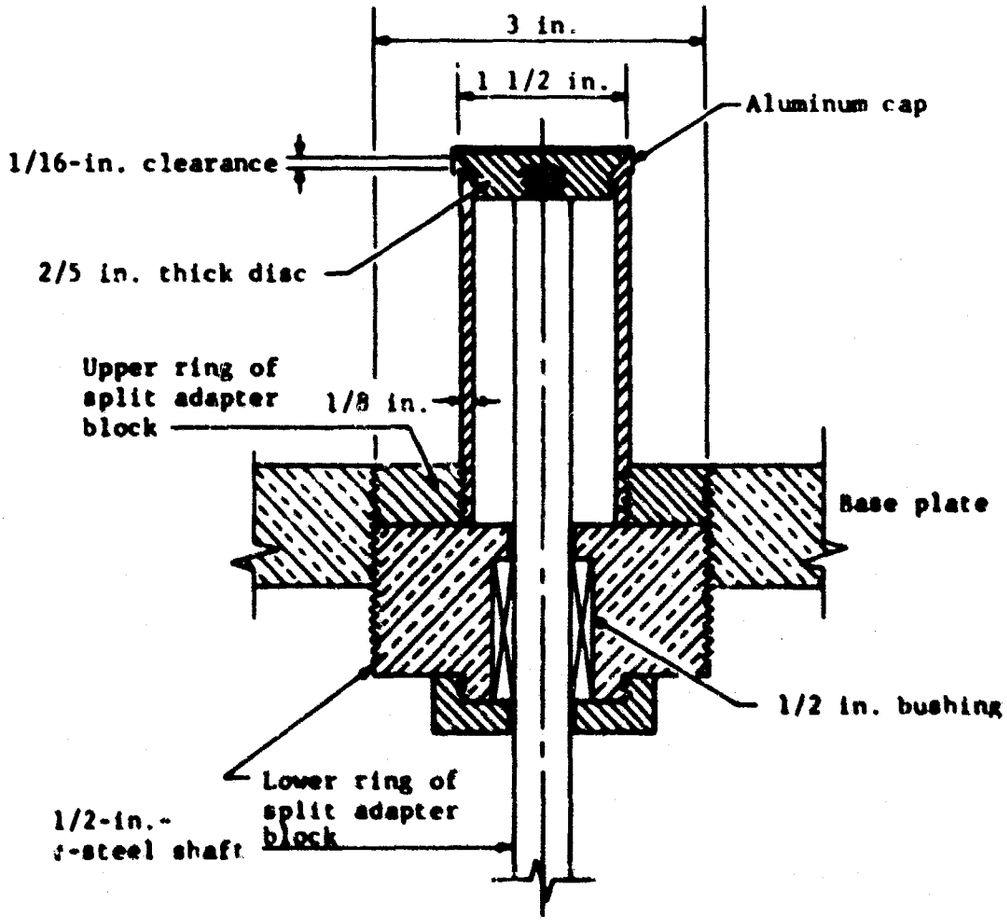


Fig. 4 Details of Test Arrangement for Buried Disc Structures

The roof of the structure consists of an aluminum disc 1-1/2 inches in diameter and 2/5-inch thick. The lower portion of the disc is tapered to contour fit inside the aluminum sleeve which is 1-1/2 inches O.D. and has a 1/8-inch wall thickness. The upper end of the sleeve is similarly tapered to accommodate the roof of the structure. The lower end of the sleeve is threaded to screw into the upper ring of the adapter block. Other details of the experimental arrangement for testing buried disc structures are shown in Figure 4.

TESTING PROCEDURE

Once the required embedment has been selected, the corresponding cell height is chosen to provide the desired cover-to-embedment, c/l, and cover-to-diameter, c/d, ratios. The appropriate cell height is then screwed onto the 3/8-inch-aluminum ring which, in turn, is connected to the base plate to form the test tank. Subsequently, the base plate of the cell is connected to the upper channel of the supporting frame. The upper ring of the transversely split adapter block is screwed to the base plate and is adjusted until it becomes flush with the upper surface of the cell base. The lower ring of the transversely split adapter block is now screwed from the underside of the base plate until it is in contact with the upper ring. The appropriate sleeve length is then screwed into the upper ring of the adapter block. The 1-1/2-inch disc which constitutes the roof of the structure is screwed into the 1/2-inch shaft, and the assembly is lowered into position from inside the tank. The disc with its supporting shaft is now adjusted to provide a clearance of about 1/16 of an inch between the tapered face of the disc and the tapered face of the sleeve. The shaft is supported on a 500-pound-capacity force washer through a cylindrical block. One end of this block is machined to accommodate the vertical shaft while the other end fits over the vertical pin of the force washer. The force washer is, in turn, supported on the platform of a mechanical jack which is raised or lowered by a variable speed motor. To provide the required length of embedment, the elevation of the upper face of the disc is adjusted by raising or lowering the jack as necessary. A metal cap made out of heavy duty aluminum foil is placed over the disc to cover the clearance between the disc and the sleeve; this cap prevents sand grains from entering the clearance.

The tank is then filled with sand until the sand surface becomes flush with the top of the cell. A rubber membrane or diaphragm is laid across the tank. The plexiglass ring, which serves as a pressure chamber, is placed on top of the rubber diaphragm. The aluminum cover plate is placed on top of the plexiglass pressure chamber, and four 1/4-inch bolts tie the assembled test tank with a quick coupling located at the cover plate of the tank. During this time the valve beneath the quick coupling should be kept closed. Before reaching the tank the compressed air passes through a control panel equipped with a pressure regulator and a pressure gauge. The pressure at the panel can be adjusted to any desired level up to 100 psi. The leads from the force washer are connected to a strain-gauge indicator, and an initial reading is taken on the indicator. The pressure at the control panel is first increased to 14.5 psi; and by opening the valve beneath the quick coupling, this pressure is transmitted from the pressure chamber onto the rubber diaphragm. The pressure is further monitored through a second pressure gauge at the top of the cell. While the pressure is maintained at this level, the strain indicator is read.

The overpressure is subsequently increased to 29.0, 43.5, 58.0, and 72.5 psi, and the corresponding strain readings are taken for each pressure level. The overpressure is then vacated by bleeding the pressure through a relief valve located on the top plate of the tank. The assembled test tank, just before a test, is shown in Figure 5.

SOIL CONDITIONS

The soil was 20-30 standard Ottawa sand used in an air-dry state. The unit weight of the soil was controlled to produce three different densities. The densities varied between 97 ± 0.4 lb/cu ft for a loose state, 106 ± 0.6 lb/cu ft for a medium-dense state, and 112.8 ± 0.4 lb/cu ft for a dense state. Assuming a specific gravity of 2.66 for the soil solids, these states correspond to void ratios of 0.71, 0.55, and 0.47 and to relative densities of 6, 66, and 96 percent, respectively. The loosest and densest states that could be obtained in the laboratory correspond to void ratios of 0.725 and 0.460, respectively.

For the medium-dense state, the sand was showered (8) through the 1/4-inch spout of a funnel maintaining a free fall of 12 inches. For the dense state, the sand was showered from the same funnel which was attached to a 2-inch-diameter, 10-inch-long radiator hose. At the free end of the hose a 1/8-inch mesh screen was provided. The free fall from the bottom of the hose was 12 inches. The sand for the loose state was placed by passing it through a funnel with a 1/4-inch spout. The tip of the funnel was kept at the center of the tank and, while the tank was being filled, it was gradually raised so as to barely touch the free sand surface at all times. Subsequently, the surface was leveled flush with the tank by carefully screening off the excess sand with a blade.

Reproducibility of soil densities was consistent. It is therefore justified to assume that the soil conditions were reasonably constant for each selected state of relative density.

ANALYSIS OF DATA

General

The approach and overall perspective of this experimental study can be best appreciated by a clear understanding of the testing arrangement and sequence. For this purpose and for a given test series, Figure 6 indicates the arrangement and sequence used to test buried disc structures. In all, four series of tests were run. In each series the soil cover is kept constant while the embedded length of the cylindrical sleeve is varied. For each cover-to-embedment ratio, the over-

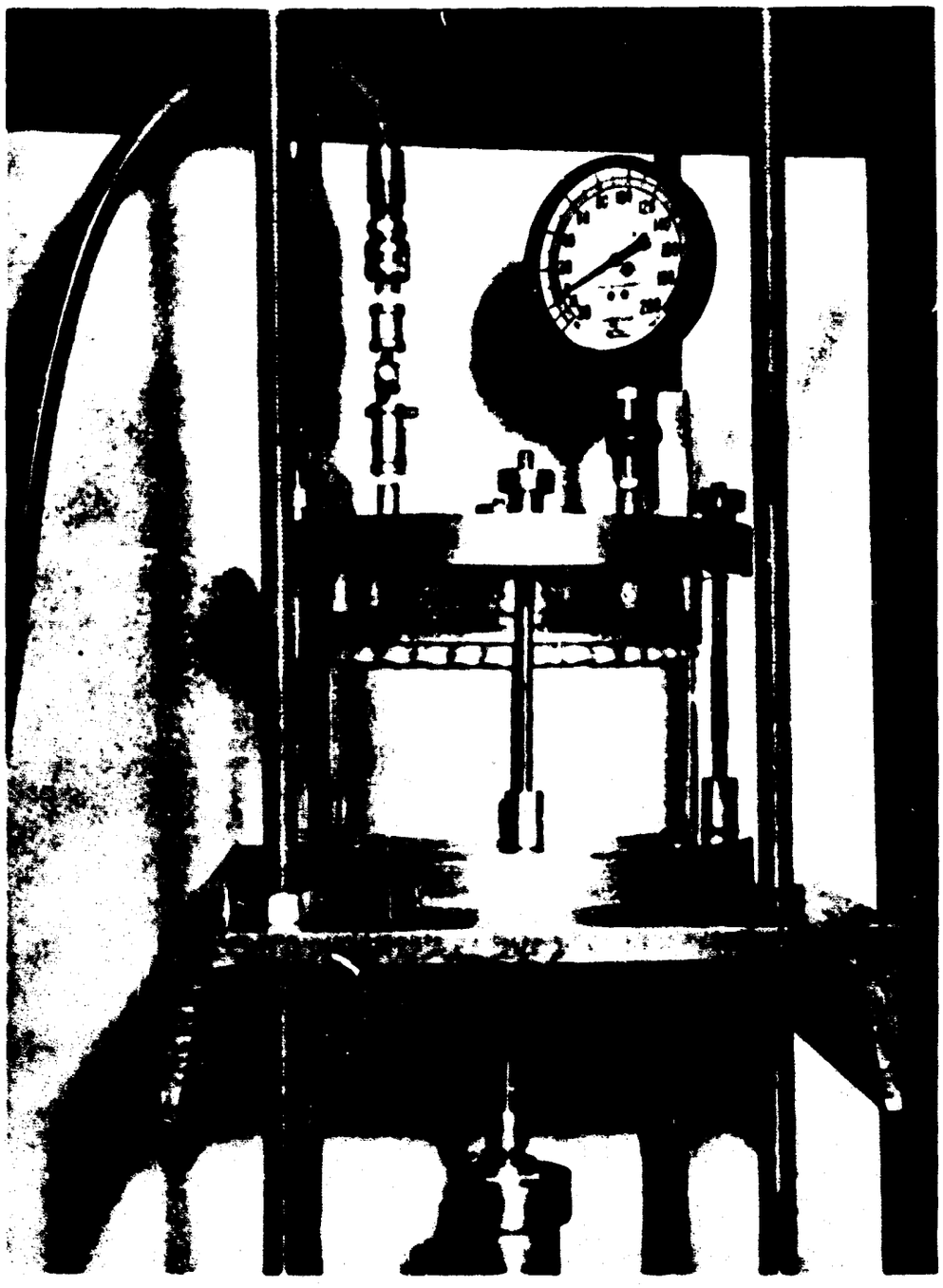


Fig. 5 View of Assembled Test Tank

pressure is raised in increments of 14.5 psi to a maximum of 72.5 psi. All tests are repeated by varying the sand density from a loose to a medium-dense and, finally, to a dense state.

Since the soil cover and structure diameter are constant in any given series, the ratio of soil cover to structure diameter is maintained constant while the ratio of soil cover to embedment is decreased by increasing the embedded length of the disc structure.

Figure 7 indicates the manner of plotting and analyzing the data obtained from testing a buried disc structure of a certain geometric configuration. In this particular example the soil cover is 15/16 of an inch; the embedment, 3-1/16 inches; and the diameter of the disc structure, 1-1/2 inches. The disc structure was tested in a tank 4 inches high, thus possessing a c/I ratio of 0.306 and a c/d ratio of 0.63. The sand was placed in a loose state at a void ratio of 0.71. The overpressure was increased using 14.5 psi increments up to 72.5 psi. The data from this test are plotted in Figure 7, using the overpressure, p_o, as abscissa versus the normalized stress carried by a disc structure, p_d/p_o, as ordinate.

Overpressure, p_o, 14.5, 29.0, 43.5, 58.0, and 72.5 psi
Cover-to-diameter ratio, c/d--constant (for a given series)
Cover-to-emedment ratio, c/l--variable
Soil density, loose, medium-dense, and dense

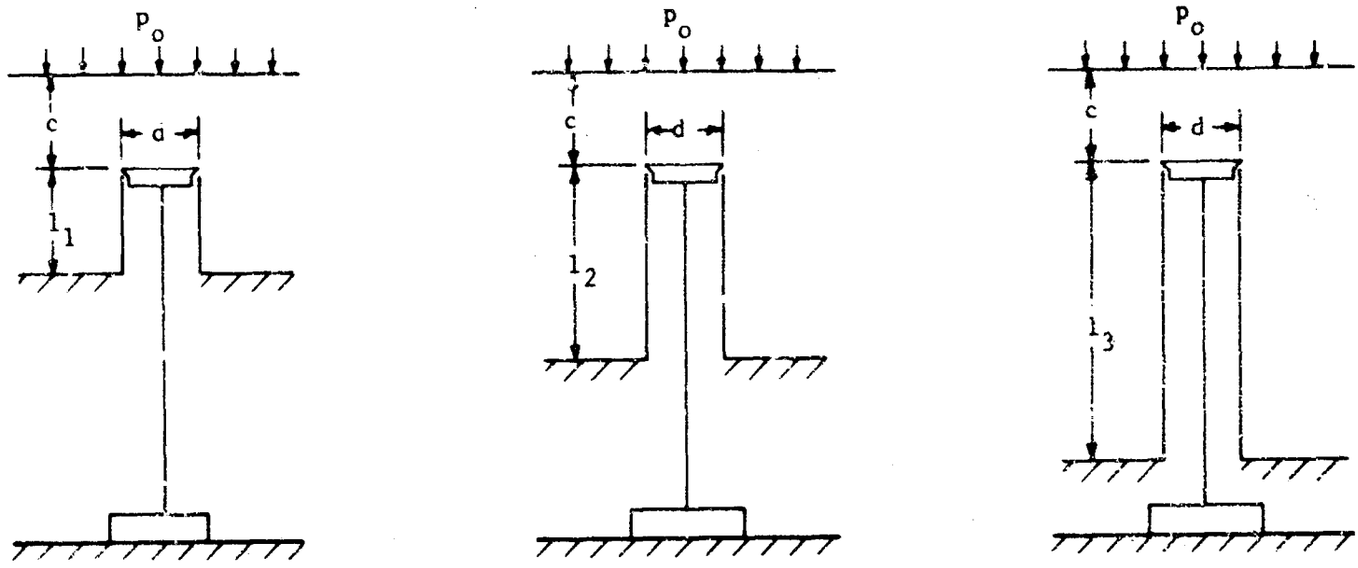


Fig. 6 Arrangement and Sequence for Testing Buried Disc Structures

The data indicate that the results can be approximated reasonably well by a straight line.

The total stress carried by the disc structure is the total force divided by the area of the disc, and it consists of the separate contributions due to arching and overpressure. Therefore, the normalized stress measured from disc structures is equal to

$$\frac{p_d}{p_o} = \frac{p_o + p_a}{p_o} = 1 + \frac{p_a}{p_o} \qquad (1)$$

in which p_o is the overpressure and p_a/p_o is the normalized arching-stress contribution. As a matter of convenience, the ratio p_d/p_o will be referred to as the "normalized arching stress." When this ratio becomes equal to unity, the buried structure is subjected to exactly the free-field stress. It is convenient to express the arching stress in this fashion since values of p_d/p_o less than unity indicate active arching, while values of p_d/p_o larger than unity indicate a passive arching case. Values of normalized arching stress were obtained for four different series of geometric arrangements and for three different densities.

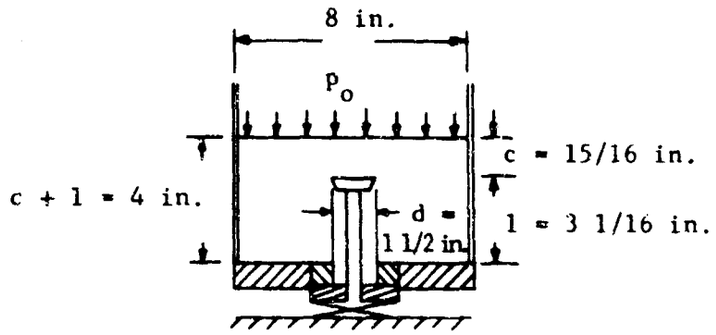
Arching Stress

Since passive arching is attributed to the mobilization of shear stresses in the soil above a buried structure and since such shear stresses can be mobilized at the expense of differential displacements due to modulus mismatch between buried structure and surrounding soil, it follows that for a given soil cover the arching stress should increase as the length of embedment increases. It should be emphasized, however, that for a given value of the c/d ratio the arching stress will reach a limiting value when the shear strength of the soil above the buried structure becomes fully mobilized.

Table I presents data for tests performed in loose sand which substantiate the above hypothesis. The same data are presented graphically in Figure 8. Examination of this figure indicates that, for a constant value of the c/d ratio, the normalized arching stress, p_d/p_o, increases at the ratio of c/l decreases (embedment increases). Furthermore, Figure 8 indicates that for any given constant value of the c/l ratio the normalized arching stress linearly decreases as the overpressure is increased. The decrease in the normalized arching stress might be attributed to the fact that the partially constrained soil modulus increases as the applied stress level is increased. However, some opposite trends were observed for similar tests performed on disc structures buried in sands of medium-dense and dense states (Figs. 9 and 10). In any event, the observed trends were neither well defined nor consistent with variations in soil density and overpressure. It appears that these deviations of the normalized arching stress are within the range of experimental error. If it is assumed that the normalized arching stress is independent of overpressure, average values of p_d/p_o could be assumed for any given constant value of the c/l and c/d ratio.

Test conditions

Loose sand, void ratio e = 0.71
c/1 = 0.306, c/d = 0.63
Overpressure, p_o, 14.5-72.5 psi



Disc structure

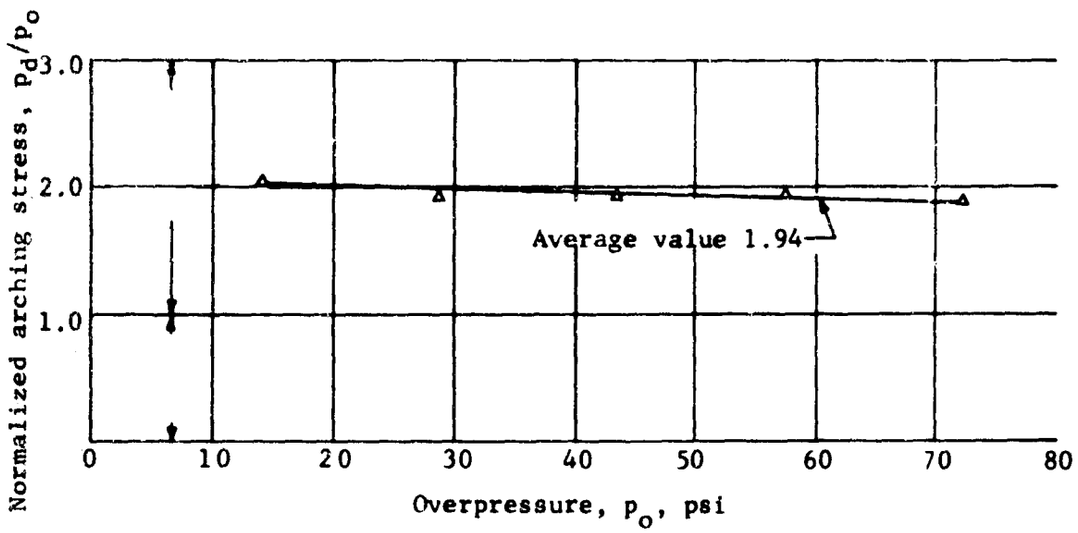


Fig. 7 Typical Data, Indicating Relationship Between Overpressure, p_o, and Normalized Arching Stress, p_d/p_o

Table I Data For Normalized Arching Stress, Loose Sand, Disc Structure

Test Series	c	c + 1	1	c/1	c/d	Overpressure, p_o					
						14.5	29.0	43.5	58.0	72.5	Ave.
						Ratio of p_d/p_o					
I	0.937	2.50	1.563	0.60	0.63	1.81	1.73	1.68	1.66	1.63	1.70
		3.00	2.063	0.453	0.63	1.92	1.81	1.85	1.79	1.79	1.83
		4.00	3.063	0.306	0.63	2.03	1.90	1.92	1.93	1.90	1.94
II	1.437	2.50	1.063	1.35	0.96	1.76	1.68	1.68	1.63	1.61	1.67
		3.00	1.563	0.92	0.96	2.24	1.98	2.01	1.99	1.96	2.04
		4.00	2.563	0.56	0.96	2.29	2.24	2.20	2.16	2.11	2.20
III	1.937	3.00	1.063	1.83	1.29	1.85	1.85	1.85	1.79	1.83	1.83
		4.00	2.063	0.94	1.29	2.34	2.29	2.28	2.22	2.19	2.27
		5.00	3.063	0.63	1.29	2.56	2.56	2.66	2.50	2.48	2.55
IV	0.0	2.50	2.500	0.0	0.0	1.06	1.06	1.06	1.06	1.06	1.06
		4.00	4.000	0.0	0.0	1.17	1.17	1.14	1.12	1.11	1.14
		5.00	5.000	0.0	0.0	1.17	1.12	1.10	1.12	1.09	1.12

To ascertain whether these deviations could be attributed to experimental errors, a series of tests was performed utilizing cell heights of 2-1/2, 4, and 5 inches. In these tests, disc structures with embedments equal to the cell height were used. The tops of the disc structures were placed flush with the sand surface bearing on the underside of the rubber diaphragm. The total load carried by the disc structures was measured while the overpressure was increased in the same manner as previously described for tests on buried disc structures. The data from these tests, which represent a case of zero soil cover, are given in Tables I, 2, and 3 for loose, medium-dense, and dense sand states, respectively. They are designated as Test Series IV. The same data are also shown graphically in Figures 8d, 9d, and 10d.

Irrespective of the longitudinal stiffness of the structure itself or of its supporting assembly, the stress measured under such circumstances should always be equal to the applied overpressure. Figure 8d indicates that for loose sand the normalized p_d/p_o ratios were always larger than unity. For the medium-dense and dense sands, Figures 9d and 10d indicate that p_d/p_o ratios larger and smaller than unity were measured. Although no specific trends are noticeable, the scatter of the data is in general somewhat less than that of the loose sand state. Stresses greater than the applied overpressure might be attributed to tensile stresses transferred by the diaphragm, but values of the normalized stress p_d/p_o smaller than unity can be attributed to experimental errors only. It should also be noted that the scatter of the data is less for tests performed with zero soil cover.

If the scatter of the data is attributed to errors inherent in the experimental technique, the normalized arching stress for the rigid structure could be assumed to be independent of the overpressure. The last column in Tables I, 2, and 3 gives the average values of the normalized arching stress for the entire range of the applied overpressures. Utilizing these average values of p_d/p_o, it is possible to present the data from Table I, loose sand state, in a more concise and comprehensive form as shown in Figure II. This figure consists of a plot of the normalized arching stress versus the c/l ratio for constant values of c/d. It confirms what one might expect: that the greater the length of embedment the more it contributes to differential displacements and, consequently, the larger the passive arching stress.

In these experiments it was not possible to increase the embedment so that, for a given soil cover, the c/l ratio would become small enough to yield a limiting value for the normalized arching stress. Under such conditions, i.e., for small c/l ratios, a substantial portion of the applied pressure would be transferred to the walls of the test tank by side-wall friction.* Although the normalized arching stress exhibits a linear variation with the range of c/l ratios attained in these tests, it is improbable that the results could be extrapolated to much larger embedments. Figure II also indicates that the normalized arching stress decreases as c/d decreases for any given value of c/l.

*This action will be referred to as "silo-type arching" in this report.

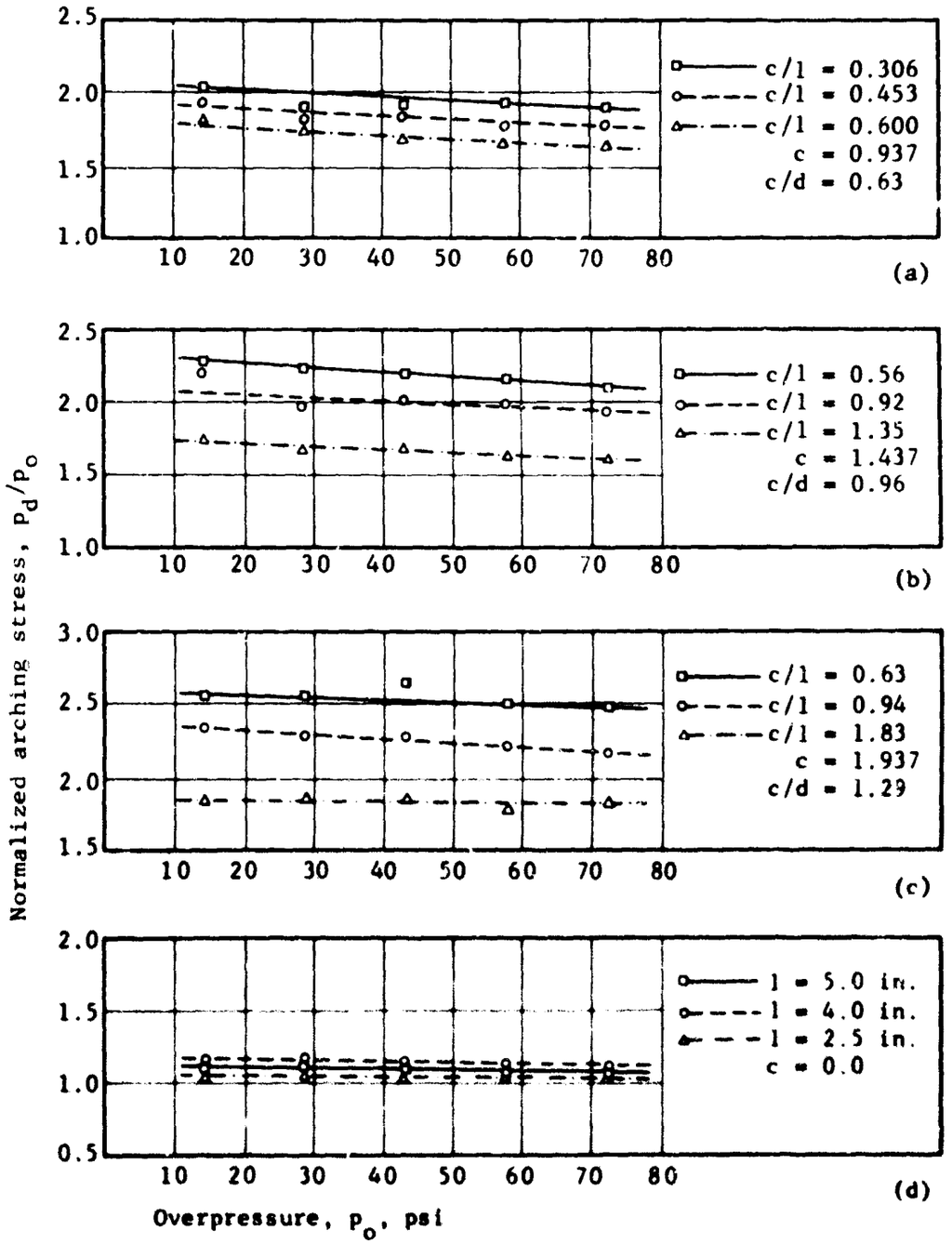


Fig. 8 Normalized Arching Stress, p_d/p_o, vs. Overpressure, p_o, For Loose Sand, Disc Structure

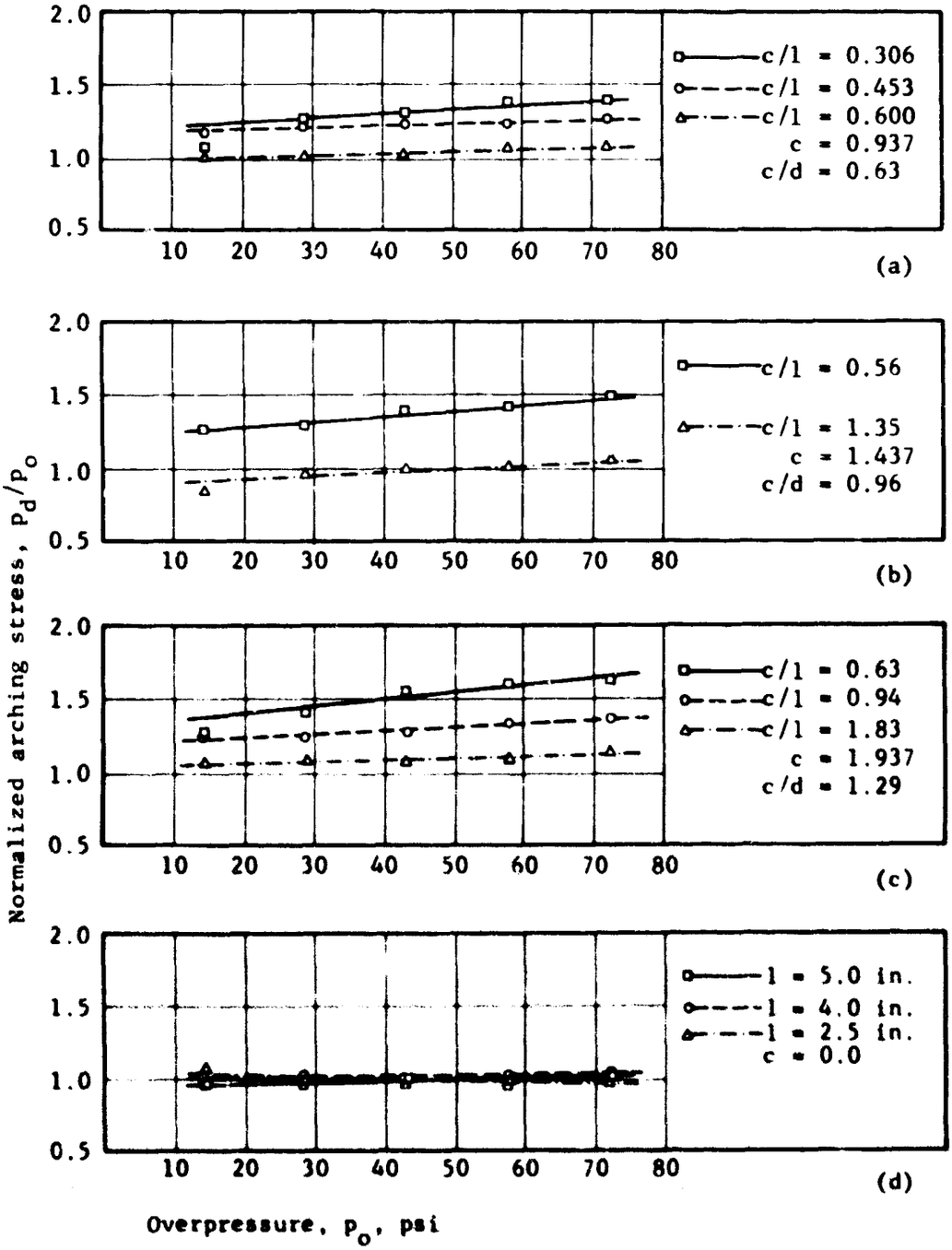


Fig. 9 Normalized Arching Stress, p_d/p_o, vs. Overpressure, p_o, For Medium-Dense Sand, Disc Structure

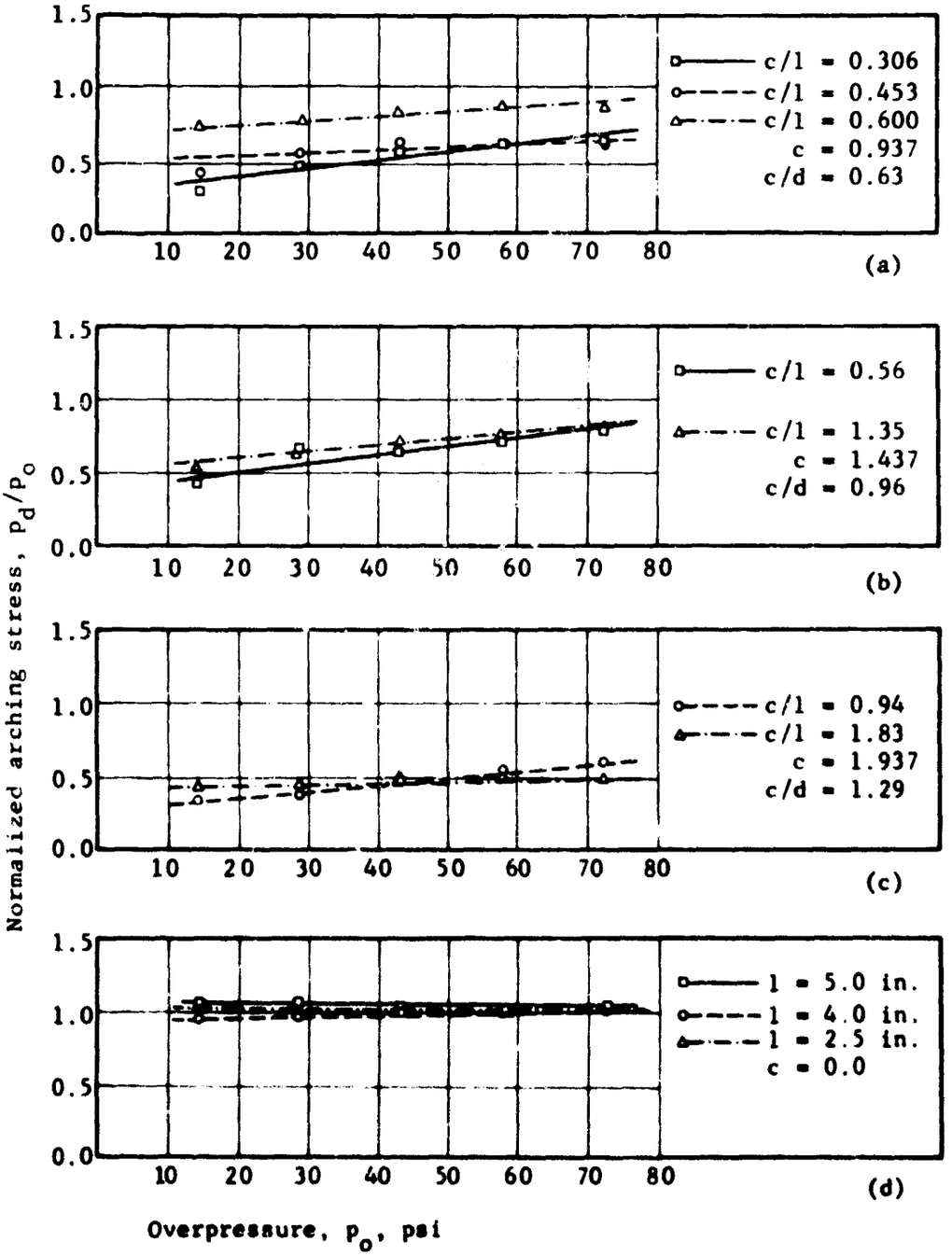


Fig. 10 Normalized Arching Stress, p_d/p_o, vs. Overpressure, p_o, For Dense Sand, Disc Structure

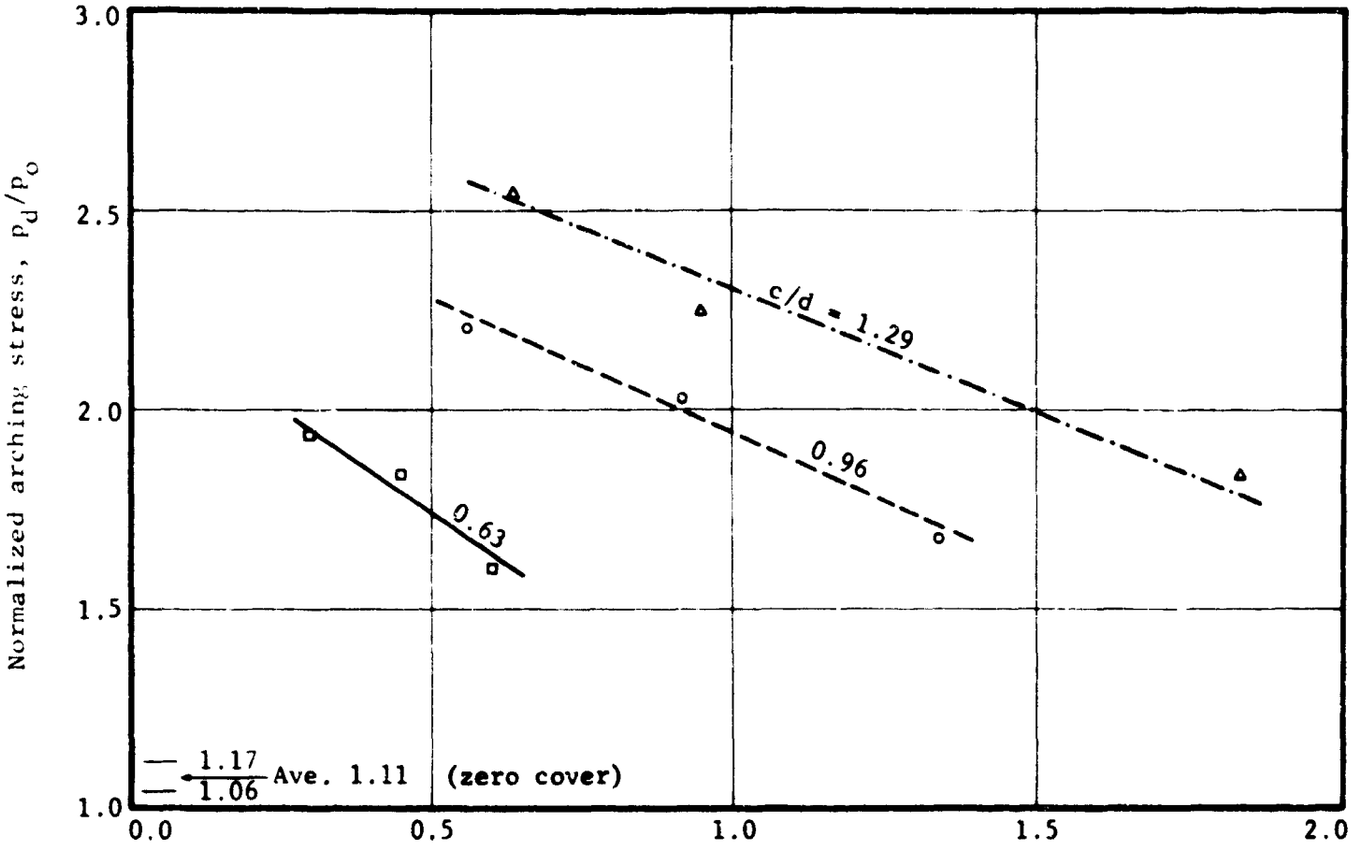


Fig. 11 Normalized Arching Stress, p_d/p_o, vs. c/l Ratio For Loose Sand

Table 2. Data For Normalized Arching Stress, Medium-Dense Sand, Disc Structure

Test Series	c	c + l	l	c/l	c/d	Overpressure, p_o					
						14.5	29.0	43.5	58.0	72.5	Ave.
						Ratio of p_d/p_o					
I	0.937	2.50	1.563	0.60	0.63	1.01	1.01	1.03	1.07	1.09	1.04
		3.00	2.063	0.453	0.63	1.17	1.23	1.24	1.24	1.27	1.22
		4.00	3.063	0.306	0.63	1.07	1.28	1.33	1.39	1.39	1.29
II	1.437	2.50	1.063	1.35	0.96	0.85	0.96	1.00	1.01	1.05	0.98
		4.00	2.563	0.56	0.96	1.28	1.28	1.39	1.41	1.48	1.37
III	1.937	3.00	1.063	1.83	1.29	1.07	1.07	1.08	1.10	1.15	1.09
		4.00	2.063	0.94	1.29	1.28	1.23	1.28	1.33	1.37	1.30
		5.00	3.063	0.63	1.29	1.28	1.41	1.55	1.60	1.64	1.49
IV	0.0	2.50	2.500	0.0	0.0	1.06	0.99	0.98	1.00	0.99	1.00
		4.00	4.000	0.0	0.0	0.96	1.01	1.00	1.01	1.04	1.00
		5.00	5.000	0.0	0.0	0.96	0.98	1.00	0.99	1.01	0.99

Table 3. Data For Normalized Arching Stress, Dense Sand, Disc Structure

Test Series	c	c + 1	1	c/1	c/d	Overpressure, p_o					
						14.5	29.0	43.5	58.0	72.5	Ave.
						Ratio of p_d/p_o					
I	0.937	2.50	1.563	0.60	0.63	0.74	0.77	0.85	0.88	0.88	0.82
		3.00	2.063	0.453	0.63	0.43	0.54	0.64	0.62	0.66	0.58
		4.00	3.063	0.306	0.63	0.32	0.48	0.57	0.62	0.66	0.53
II	1.437	2.50	1.063	1.35	0.96	0.53	0.64	0.71	0.76	0.79	0.69
		4.00	2.563	0.56	0.96	0.42	0.66	0.65	0.72	0.79	0.65
III	1.937	3.00	1.063	1.83	1.29	0.43	0.45	0.48	0.51	0.50	0.47
		4.00	2.063	0.94	1.29	0.32	0.37	0.48	0.54	0.61	0.46
IV	0.0	2.50	2.500	0.0	0.0	1.07	1.07	1.03	1.01	1.03	1.04
		4.00	4.000	0.0	0.0	0.96	0.98	1.00	1.01	1.01	0.99
		5.00	5.000	0.0	0.0	1.07	1.07	1.03	1.01	1.03	1.04

The results of tests on medium-dense and dense sands are presented in Tables 2 and 3 and in Figures 9 and 10. In contrast to the trend observed for loose sand, the data for medium-dense and dense sands indicate that the normalized arching stress increases with an increase in overpressure. It is notable that in Figure 9 the medium-dense sand exhibits the same characteristic trend of an increase in the normalized arching stress as the c/l ratio decreases. Similarly, Figure 12 shows the normalized arching stress versus the c/l ratio for medium-dense sand and for constant values of c/d. It indicates that the arching stress increases as the c/l ratio decreases. Furthermore, for constant values of c/l the passive arching stress decreases as c/d decreases. This is in accord with the result discussed previously in Figure 11 for loose sand.

Figure 10 indicates, in contrast to previously established trends, that the normalized arching stress tends to decrease as the c/l ratio decreases. This phenomenon is observed more clearly in Figure 13 where the lines for constant c/d ratios have either very flat slopes or slopes opposite to those previously discussed (Figs. 11 and 12) for loose and medium-dense sands.

It should be recognized that the plots of the normalized arching stress for dense sand fall within the zone of active arching. This indicates that the disc structures and their supporting assembly which were considered to be relatively stiff were yielding more than the surrounding dense medium. Such a supposition might seem questionable, but is probably true. Furthermore, the erratic nature of the data obtained from tests on dense sand necessitates further experimentation.

Using the data from Figures 11, 12, and 13, plots of the normalized arching stress versus void ratio are presented in Figure 14 for different values of the c/l ratio varying between 0.2 and 1.8. From the available data it is possible to draw Figure 14 for c/d ratios of 0.63, 0.96, and 1.29, respectively. The following observations can be made from the results presented in Figure 14.

(1) For a given density and c/d ratio, the passive arching stress increases as the c/l ratio decreases.

(2) For a given density and c/l ratio, the passive arching stress increases as c/d increases.

(3) For a given value of the c/l and c/d ratios, the passive arching stress decreases rather markedly as the sand density increases.

(4) When the sand density increases to a void ratio between 0.48 and 0.50, all curves indicate a transition from passive to active arching. This illustrates that although the structure itself was assumed to be more rigid than the surrounding medium, yet the framework on which the structures were supported and through which the load on the structures was monitored was presumably yielding more than the surrounding dense medium. It is also possible that in the case of dense sands, the silo-type arching was exhibiting an appreciable influence on stress transmission, thereby obliterating the occurrence of a passive arching phenomenon. No displacements were measured in this investigation; it is therefore not possible to assess the validity of either of these hypotheses. This needs further consideration with future studies. Figure 14 further indicates that within the active arching zone and for a given c/d ratio the active arching stress decreases as the c/l ratio decreases.

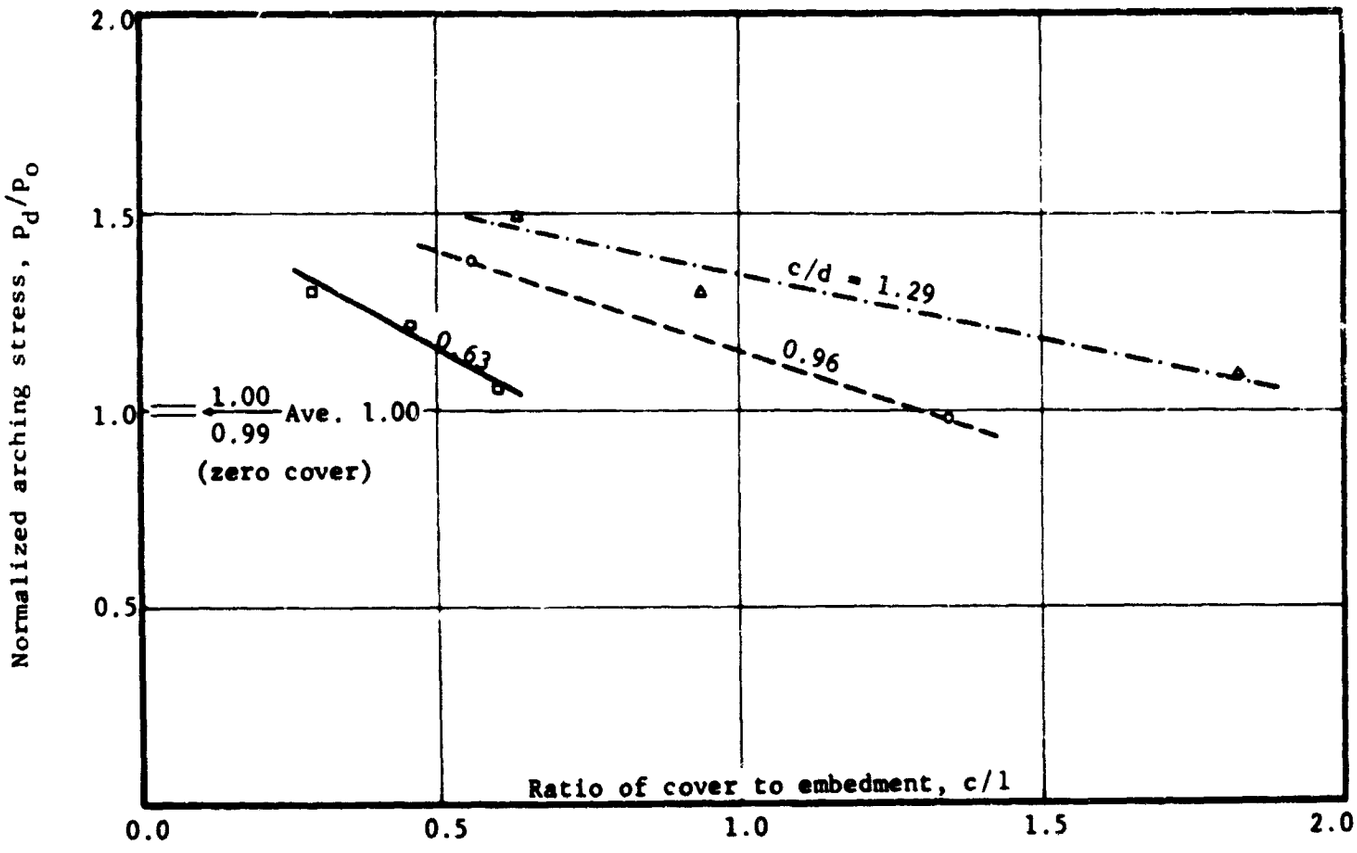


Fig. 12 Normalized Arching Stress, p_d/p_o, vs. c/l Ratio For Medium-Dense Sand

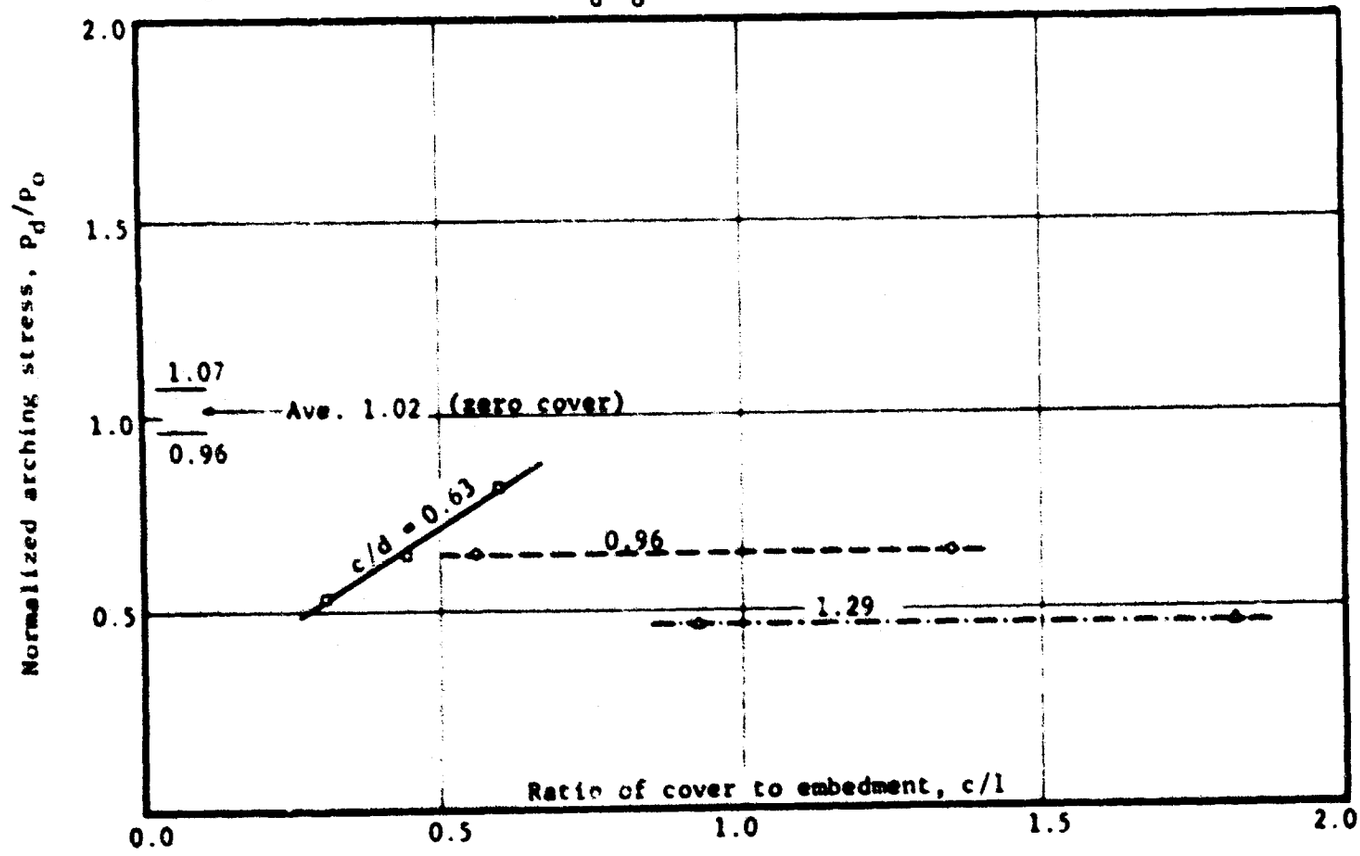


Fig. 13 Normalized Arching Stress, p_d/p_o, vs. c/l Ratio For Dense Sand

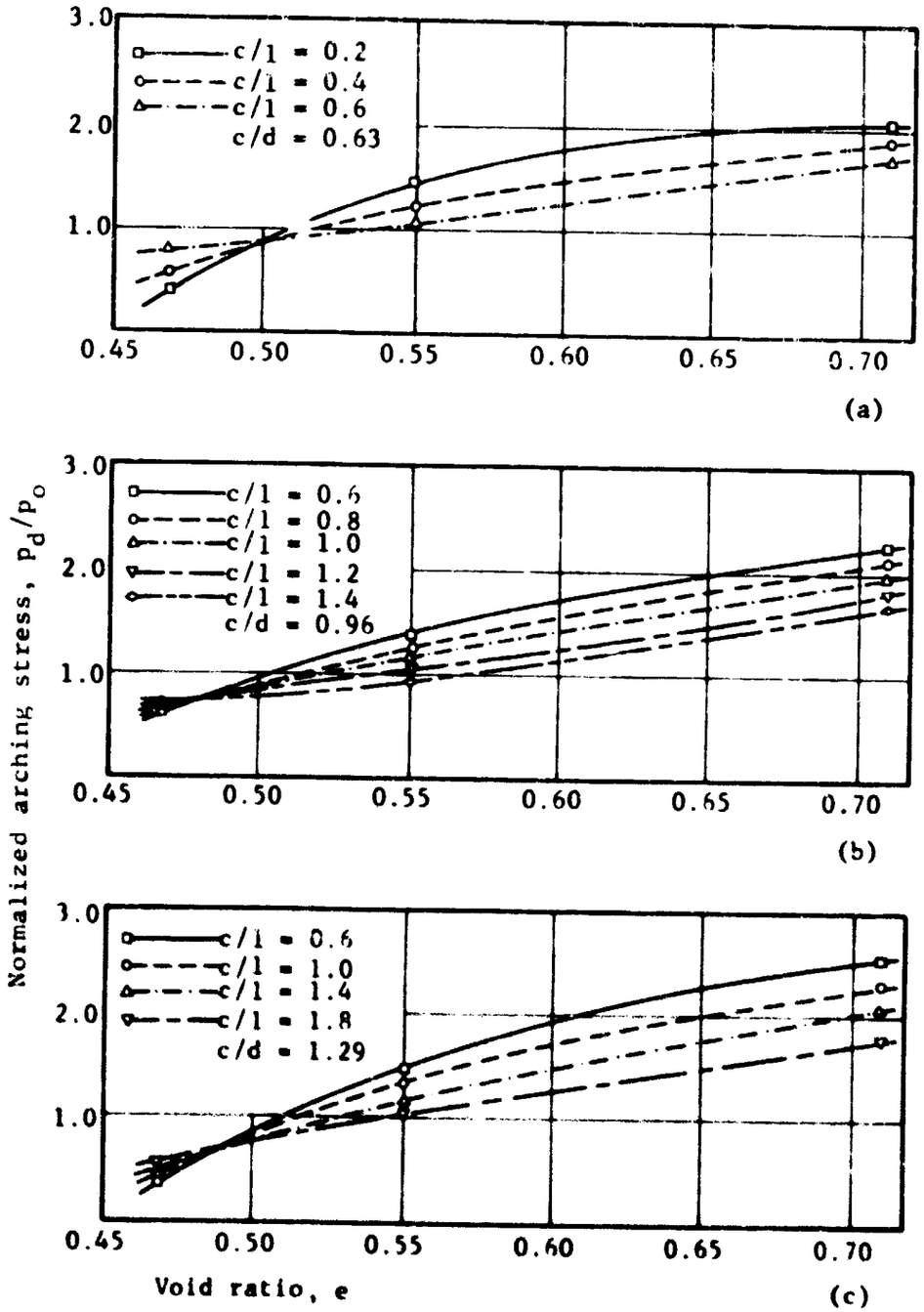


Fig. 14 Normalized Arching Stress, p_d/p_o, vs. Void Ratio, e

CONCLUSIONS

Relative density is the principal parameter affecting the passive arching stress induced on vertical cylinders buried in a granular medium. The c/l and c/d ratios are next in importance. The effect of overpressure on the normalized arching stress on rigid structures is small in comparison to the effects of any of the parameters mentioned above.

Maximum normalized arching stress ratios as large as 2.66 have been measured in this investigation. It is probable that the results represent lower bound values due to interferences with the boundaries of the tank. Although extensive input-output measurements are not as yet available to assess the performance of the test tank, some preliminary stress input-output measurements have indicated that within the aspect ratios (length-to-diameter ratio of test tank) utilized in this experimental study, which varied between a minimum of 0.12 and a maximum of 0.62, the stress transmission (output-to-input ratio) varied between 94 and 72 percent, respectively. The stress loss being mainly concentrated at the boundaries, the average loss over the structure is most likely insignificant.

For perfectly rigid structures, it is debatable that the arching stresses measured in this investigation represent absolute limiting values. It is believed that for perfectly rigid structures the absolute arching stresses could be much larger than those measured in this study.

The experimental setup and the manner of conducting the tests have fulfilled their purpose in providing an appreciation of the various parameters and their relative contribution to the passive arching phenomenon. The results of this investigation should be regarded as a guide and not as design criteria.

ACKNOWLEDGEMENTS

The experimental investigation presented in this paper was conducted at the Air Force Shock Tube Facility, operated by the University of New Mexico, and the writers wish to acknowledge their appreciation to Dr. E. M. Zwoyer, Director, for his continuous encouragement, and to Dr. B. A. Donnellan, Research Associate Engineer, for his contribution during the early stages of this study.

REFERENCES

1. Meem, J. C., "The Bracing of Trenches and Tunnels, with Practical Formulas for Earth Pressures," Transactions, ASCE, Vol. 60, 1908.
2. Terzaghi, Karl, "General Wedge Theory of Earth Pressures," Transactions, ASCE, Vol. 106, 1941
3. Spangler, M. G., "Loads on Underground Conduits," Soil Engineering, International Textbook Co., Scranton, Penna., 1960.
4. Wiedermann, A. H., "Static Experiments for the Study of the Interaction of Buried Structures with Ground Shock Waves," AFSWC-TDR-61-32, April 1961.
5. Wiedermann, A. H., "The Interaction of Buried Structures with Ground Shock of Concepts of Preliminary Design of Structure Projects for Underground Nuclear Detonations," Appendix B, AFSWC-TDR-60-3, January 1960.
6. Terzaghi, Karl, "Arching in Ideal Soils," Theoretical Soil Mechanics, John Wiley and Sons, Inc., New York, 1943.
7. Whitman, R. V. and Ulrich Luscher, "Basic Experiment into Soil-Structure Interaction," Journal of Soil Mechanics and Foundations Division, Proceedings, ASCE, Vol. 88, December 1962.
8. Kolbuszewski, J. and R. H. Jones, "The Preparation of Sand Samples for Laboratory Testing," Proceedings, Midland Soil Mechanics and Foundation Engineering Society, Vol. 4, pp. 107-124, 1961.

SESSION SEVEN–THURSDAY AM
ANALYTICAL AND EXPERIMENTAL STUDIES, PART II

SESSION CHAIRMAN: REYNOLD K. WATKINS

TABLE OF CONTENTS

page

EXPERIMENTS ON CIRCULAR CYLINDERS WITH FLEXIBLE ROOF PLATES BURIED IN SAND, C. J. Costantino and A. Longinow 423

YIELDING MEMBRANE CONCEPTS, H. P. Harrenstien and R. H. Gunderson 436

THE RESPONSE OF BURIED CYLINDERS TO QUASI-STATIC OVERPRESSURES, B A. Donnellan 449

RESPONSE OF BURIED STRUCTURAL MODELS TO STATIC AND DYNAMIC OVERPRESSURES, R. L. Marino Jr. and W. F. Riley 464

INTERACTION BETWEEN A SAND AND CYLINDRICAL SHELLS UNDER STATIC AND DYNAMIC LOADING, John Thomas Hanley 487



Participants in Session Seven were, left to right, Reynold K. Watkins (Session Chairman); R. H. Gunderson; J. T. Hanley; B. Donnellan; A. Longinow; R. L. Marino; and H. P. Harrenstien (inset).

EXPERIMENTS ON CIRCULAR CYLINDERS WITH FLEXIBLE ROOF PLATES BURIED IN SAND

by
C. J. Costantino* and A. Longinow**

ABSTRACT

A series of thirty experiments have been performed to determine the loads transmitted to vertically oriented buried circular cylinders with flexible roof plates subjected to static surface overpressures. It has been found that for depths of burial greater than one roof diameter, the load transmitted through the structure is about 1/2 of the applied surface pressure for the range of flexibilities considered. For shallow buried cylinders, sufficient flexibility must be provided in the roof plate to develop any significant load transfer. The stress distribution across the plate becomes more non-uniform with increase in deflection and depth of burial.

INTRODUCTION

In the design of buried protective structures, the designer is faced with a problem area in which the amount of available definitive information is fairly limited. In addition, present demand for superhard structures has increased the complexity of the problem. Due to the magnitudes of load which such structures are required to resist, the utilization of conventional methods of design would yield structures so greatly misproportioned as to be uneconomical or ineffective.

This study does not concern itself with methods of design as such, but rather with certain underlying aspects of soil-structure interaction on which such methods must ultimately be based. Specifically the objective of this program has been to determine in a quantitative way, the influence of structural flexibility on the loads experienced by a buried structure when the surface of the soil is subjected to static overpressures.

The structure (model) used in this study is a rigid cylinder 6-in. in diameter and 6-in. long (Fig. 1) with interchangeable flexible roof plates. The most rigid plate, 1/2-inch thick, was supported on the model in such a way that deflections were prohibited. Experiments so performed will be referred to here in as "rigid roof" experiments, to distinguish them from experiments performed with the more flexible roof panels. The soil medium was dry Ottawa sand. Experiments were performed in a 3-ft diameter by 3-ft deep pressure vessel, the walls of which were treated with bonded and loose Teflon to reduce side-wall frictional resistance. A complete discussion of the experimental set-up, and testing procedure is given in the Appendix to this paper.

Experiments were conducted considering the following variations of parameters:

1. Depth of burial
2. Flexibility of roof plates (three different flexible plates were used)
3. Surface overpressure
4. Repeated loadings
5. Soil density

The measured quantities consisted of rigid body motions of the cylinder, bending displacements of the plates, vertical displacements of the sand surface and the total load applied to the structure as a function of surface overpressure.

MODEL STIFFNESS VS. SOIL DENSITY

It is well known that the load transmitted to a buried structure is a function of the relative stiffness of the structure as compared to the soil; that is, if the structure is stiffer than the soil, load will "arch" into the structure, and if the soil is stiffer than the structure, load will "arch" around the structure. To determine which condition existed in this study, the stiffness of the model with a rigid roof plate was determined and compared to the soil stiffness obtained from confined compression tests for two density states (loose and dense). These results are shown in Figure 2.

It should be noted that for about 30 percent of the stress range shown, the model is "softer" than dense sand. Thus, in this stress range, the model, even though it has a rigid roof, would be expected to experience an under-registration of transmitted load in relation to surface overpressure. In the case of the loose density the model would be expected to experience an opposite effect. Such effects were obtained in the experimental results.

*Research Engineer, IIT Research Institute, Chicago, Illinois
**Asst. Research Engineer, IIT Research Institute, Chicago, Illinois

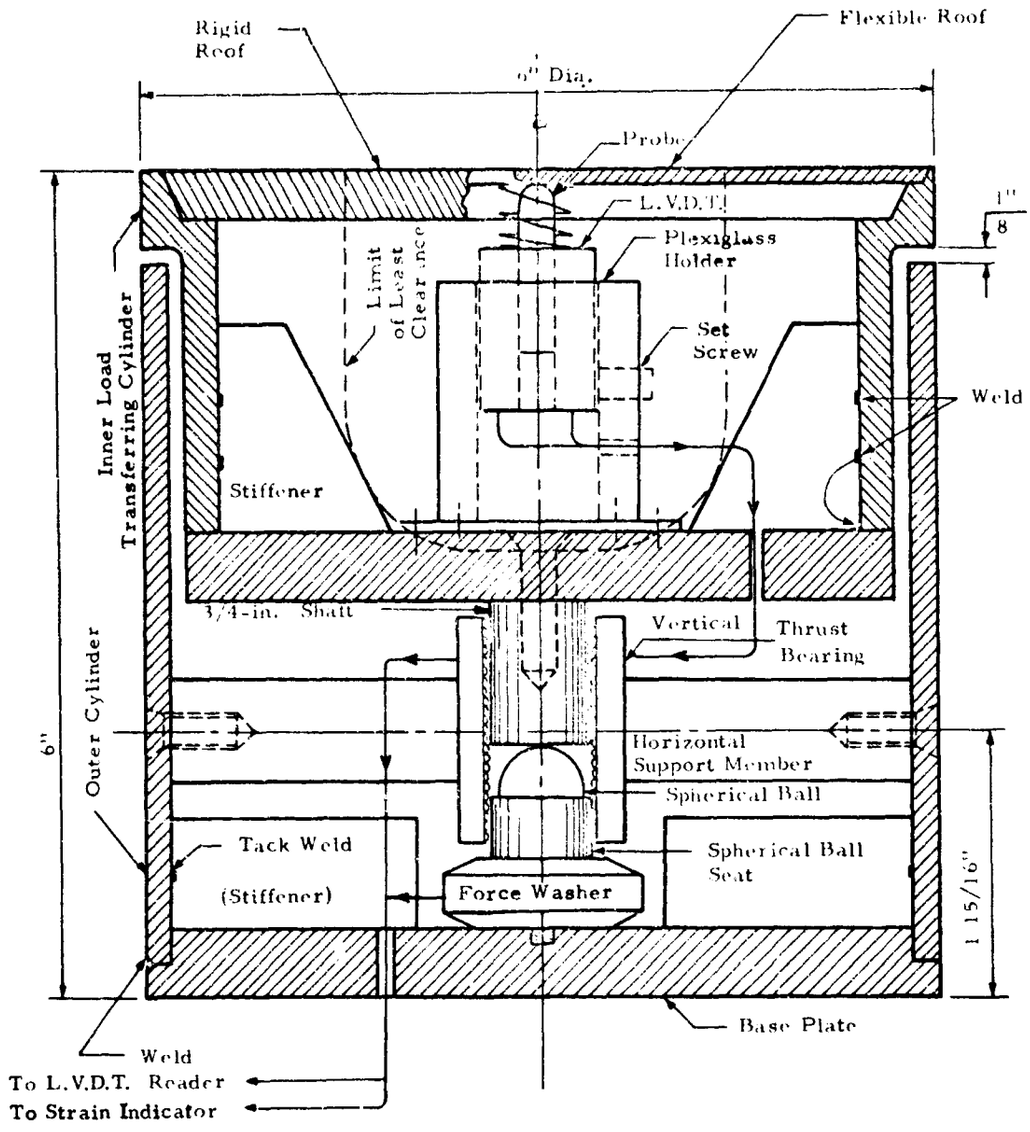


Fig. 1 Cylindrical Model

The relative densities at which the thirty experiments of this study were performed are presented in graphical form in Figure 3. With reference to density, the experiments can be divided into two categories, loose and dense. An attempt was made to keep densities constant in each of the above categories since this would facilitate a comparison of individual experiments. But as seen in Figure 3, some scatter occurred. The major cause contributing to the scatter of data was the use of a penetration type vibrator for achieving a dense sand state. The use of such a tool makes it extremely difficult to obtain a uniform density. Another contribution to this scatter is naturally error in density measurement; a 6 percent change in D_r (relative density) is equivalent to only a 1 percent change in the soil density.

RESULTS FOR RIGID ROOF PLATE SERIES

For an experiment conducted on the buried cylinder with a rigid roof plate, the total load transmitted to the plate was measured for each value of the surface overpressure. A typical result is shown in Figure 4 (for a ratio of depth of burial/roof diameter of 3). It may be noted from this curve that, upon loading the soil surface, the average pressure transmitted (total load/roof area) to the model is less than the applied surface pressure. As discussed above, this is due to the fact that this test was conducted in a dense soil (D_R = 82 percent). Upon unloading, a significant hysteresis effect develops, as is expected, with little or no residual stresses remaining.

A summary of the test series for the rigid roof is contained in Figure 5. In this figure, the ratio of the average transmitted pressure to the surface overpressure is plotted against the ratio of depth of burial to roof diameter (d/B) for surface overpressures of 60, 80, and 100 psi on the loading cycle only. It may be noted that for the higher density tests, the transmitted load is always less than the surface overpressure, while for the loose density tests, the reverse is true (as expected). In addition, as the depth of burial increases, the amount of arching (into or away from the model) appears to reach some maximum. It would be anticipated that at some critical value of d/B the "arch" would "close" and the results for deeper depths would be the same (no surface effects). Unfortunately, the scatter of these test results prevents a reasonably accurate determination of this critical depth.

To indicate this effect more graphically, two curves were sketched in Figure 5 for the loose and dense states (labeled by D_r = 40 percent and 75 percent) to represent more or less the average affect of depth of burial on transmitted pressure.

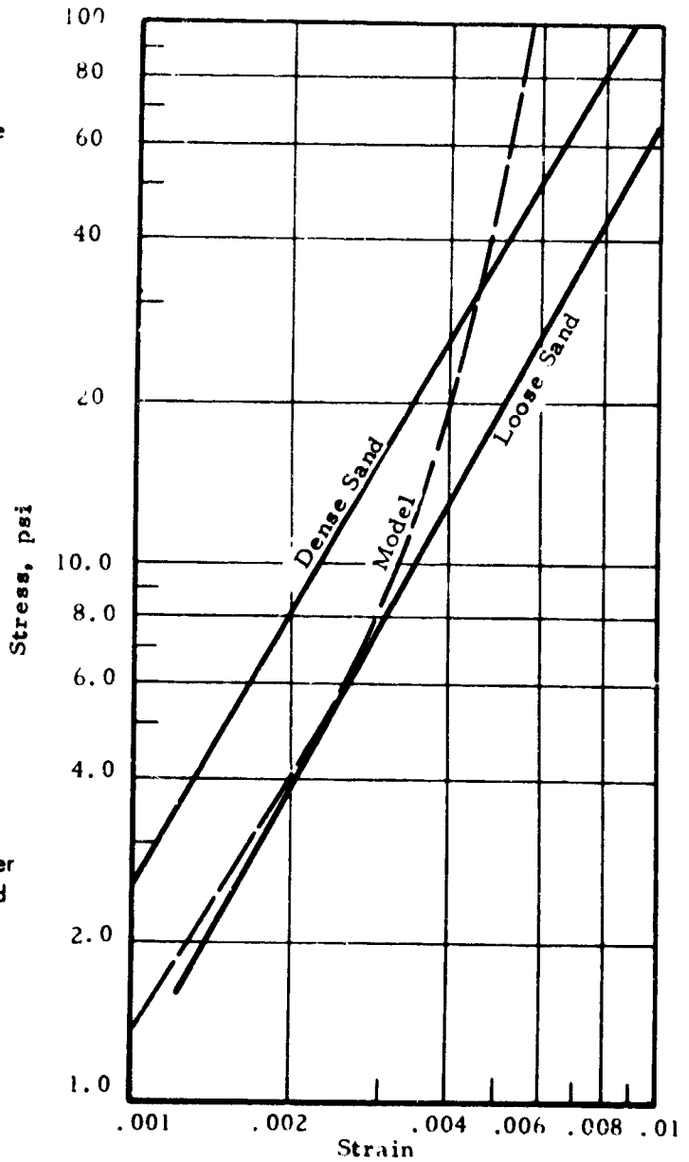


Fig. 2 Comparison of Confined Compression Tests For Sand With Model Stiffness (Rigid Roof)

RESULTS FOR FLEXIBLE ROOF PLATE SERIES

A typical set of load-deflection curves representing four cycles of loading for the model having a flexible roof disc (EI = 1054 lb-in) is shown in Figure 6. A loading cycle consisted of applying surface pressure in 20 psi increments to 100 psi and then reducing it in a set number of increments to the zero level. The cycles were conducted in succession without disturbing the experimental set-up. It may be noted especially in the loading portions of the curves that the second through the fourth cycles follow essentially the same paths, achieving greater deflection at a lesser load then in the case of the first cycle. This is as would be expected since after the first cycle both the sand and the model tend to stiffen. The magnitudes of this deviation from the first loading cycle would depend primarily on the initial sand density.

The variations of the center displacement with depth of burial for the model having the same roof disc as described is shown in Figure 7. For the case shown, displacements reach an essentially constant value for d/B > 1.0 for each level of overpressure. Manifestation of this occurrence is further illustrated in Figures 8, 9, and 10 for the roof discs considered in this study. A relatively constant center deflection for a particular load level is attained in the neighborhood of d/B approximately equal to 1.0 for all cases. This indicates the depth at which full "arching" develops which is independent of roof flexibility.

In addition, it may be noted that the pressure-center displacement curves are non-linear; this occurs from two separate effects. Firstly, the load-deflection relation for a circular plate under uniform pressure is non-linear, with the plate becoming stiffer with deflection due to the large deflection effects encountered at these displacements.* This may be noted from Figure 9 for d/B = 0. Secondly, as load is applied to the buried plate, a smaller portion of the surface pressure is transmitted to the plate due to the arching action developed by the plate displacements. Thus, for the buried plate, the effective stiffness of the system increases with surface pressure.

Furthermore, as the flexible plate is buried more deeply, it would be anticipated that the load distribution across the plate would vary. This is shown in Figure 11 in which the equivalent uniform pressure (to cause the same center displacement) is plotted against the measured total load applied to the plate (divided by the plate area). Two items may be noted from this figure. First, at any one depth of burial, the curve tends to flatten with applied overpressure indicating that the pressure distribution becomes more non-uniform (more load transferred from the center to the edges) as deflection proceeds. Secondly, as the depth of burial increased, the non-linearity again increases until the critical depth is reached (for d/B > 1.0).

*S. Timoshenko, Theory of Plates and Shells, McGraw-Hill Book Company, New York, 1940.

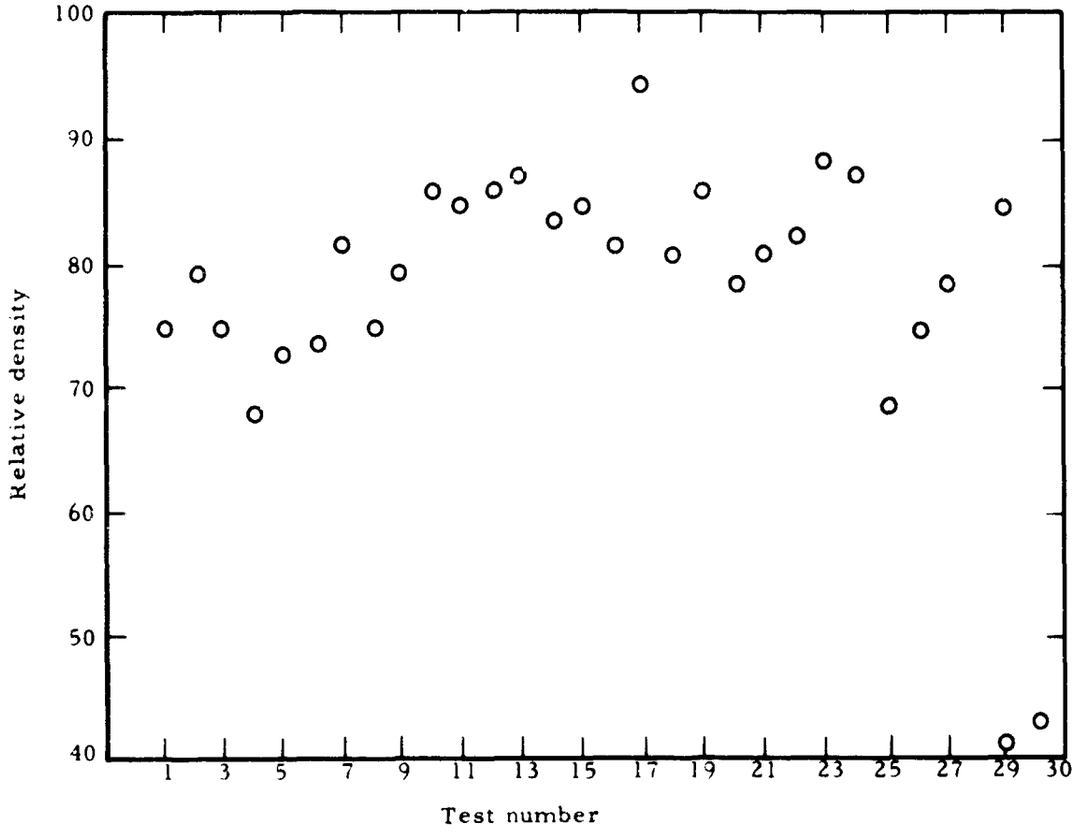


Fig. 3 Variation of Relative Density with Test

The influence of flexibility on load transfer is shown in Figure 12. From this figure it may be noted that at the shallow burial depths arching effects become significant when sufficient flexibility is included to allow for relatively large deflections. For the deeper depths of burial ($d/B > 1$), significant load transfer develops even for the stiffer roof plates. In addition, one other peculiarity may be noted in Figure 12. For the tests conducted at the various depths using the intermediate flexible plate (EI = 1054 lb-in) a characteristic hump or rise in the curves may be noted. The reason for this is not apparent and no particular significance can be attached to it at this time. Clearly, errors in measurement and nonuniformity of soil conditions could possibly produce such behavior. Further experimental work is required to investigate this problem.

CONCLUSIONS

From this limited experimental program, several conclusions may be drawn. First, and possibly most important, is the fact that experimental results obtained from small models may be misleading in that these results appear to be extremely sensitive to density variations, which are unfortunately most difficult to control. In addition, their influence on prototype structures is difficult to evaluate.

In general, however, these results indicate that for depths of burial greater than about one roof diameter the soil arch developed above the roof "closes", so that transmitted loads would be the same with deeper depths. This result appears to be independent of roof flexibility. It should be noted that in this series, pressures were not attained high enough to "collapse" the soil arch and possibly cause a reloading of the roof plates.

Further, for the range of flexibilities considered, at the deeper depths of burial ($d/B > 1$) the decrease in load transmitted to the structure is about 50 percent of the applied surface pressure. For the shallower depths of burial ($d/B < 1$), sufficient flexibility must be provided in the roof plate to allow a soil arch to form and a load transfer to occur.

The pressure distribution across the roof plate becomes more non-uniform with plate deflection and also with depth of burial.

ACKNOWLEDGEMENT

This research was performed at IIT Research Institute, Chicago, Illinois, sponsored by the Solid Mechanics Division under the direction of Dr. E. Sevin.

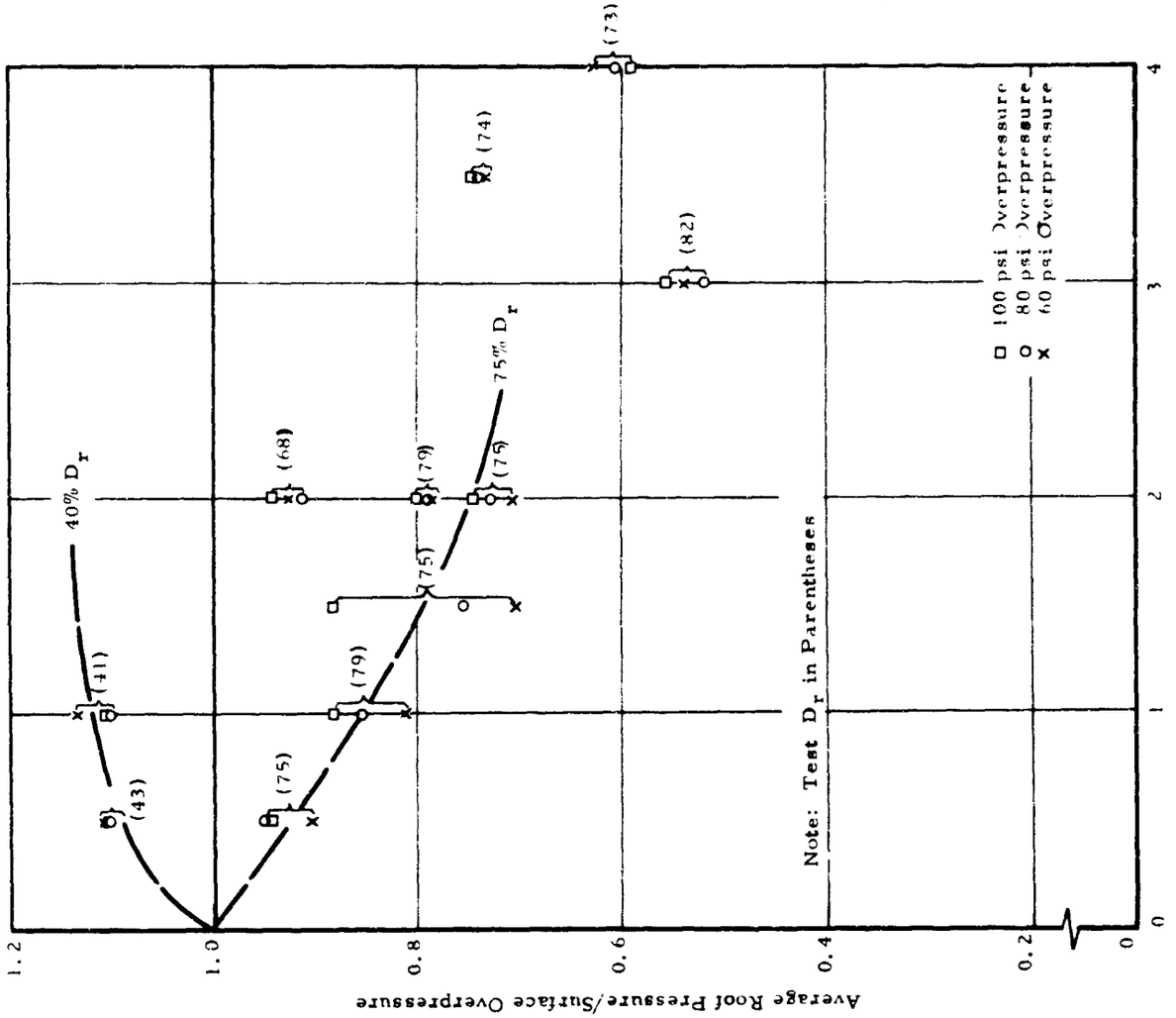


Fig. 5 Influence of Relative Density on Load Applied to Rigid Roof Plate

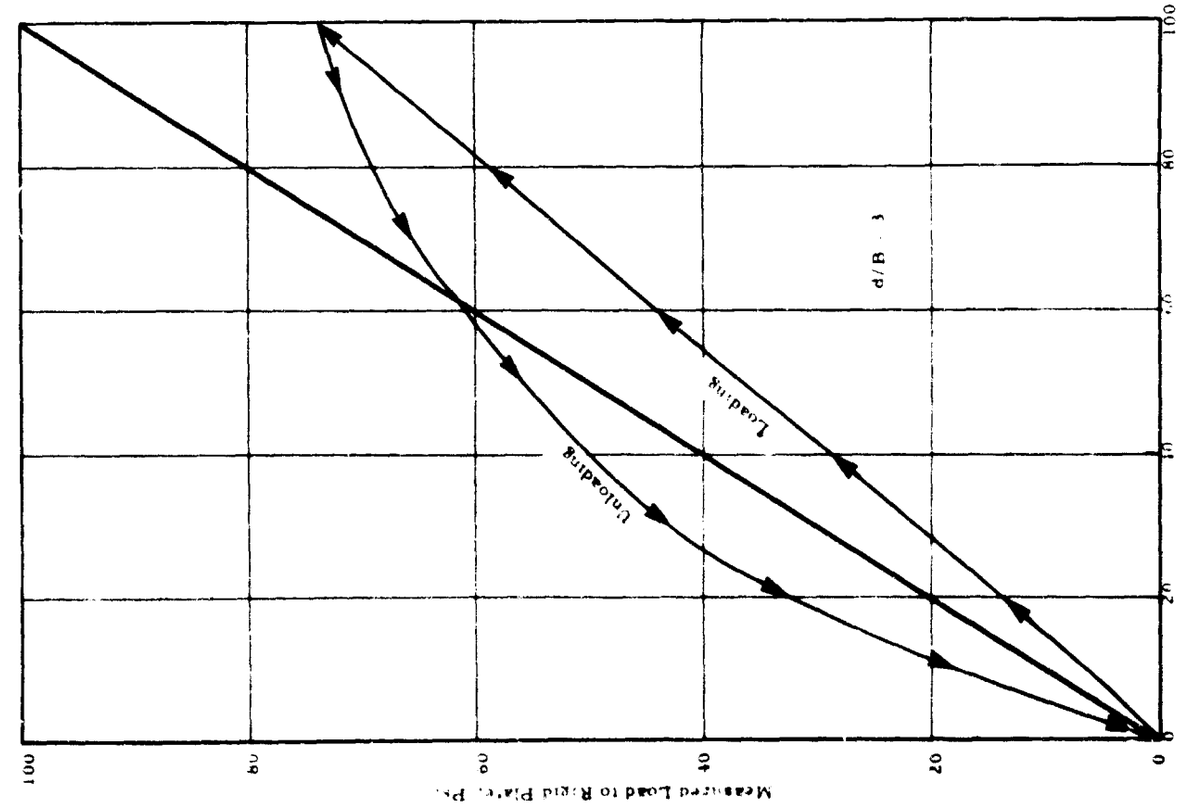


Fig. 4 Load Applied to Rigid Plate During Loading and Unloading Cycles (d/B = 3)

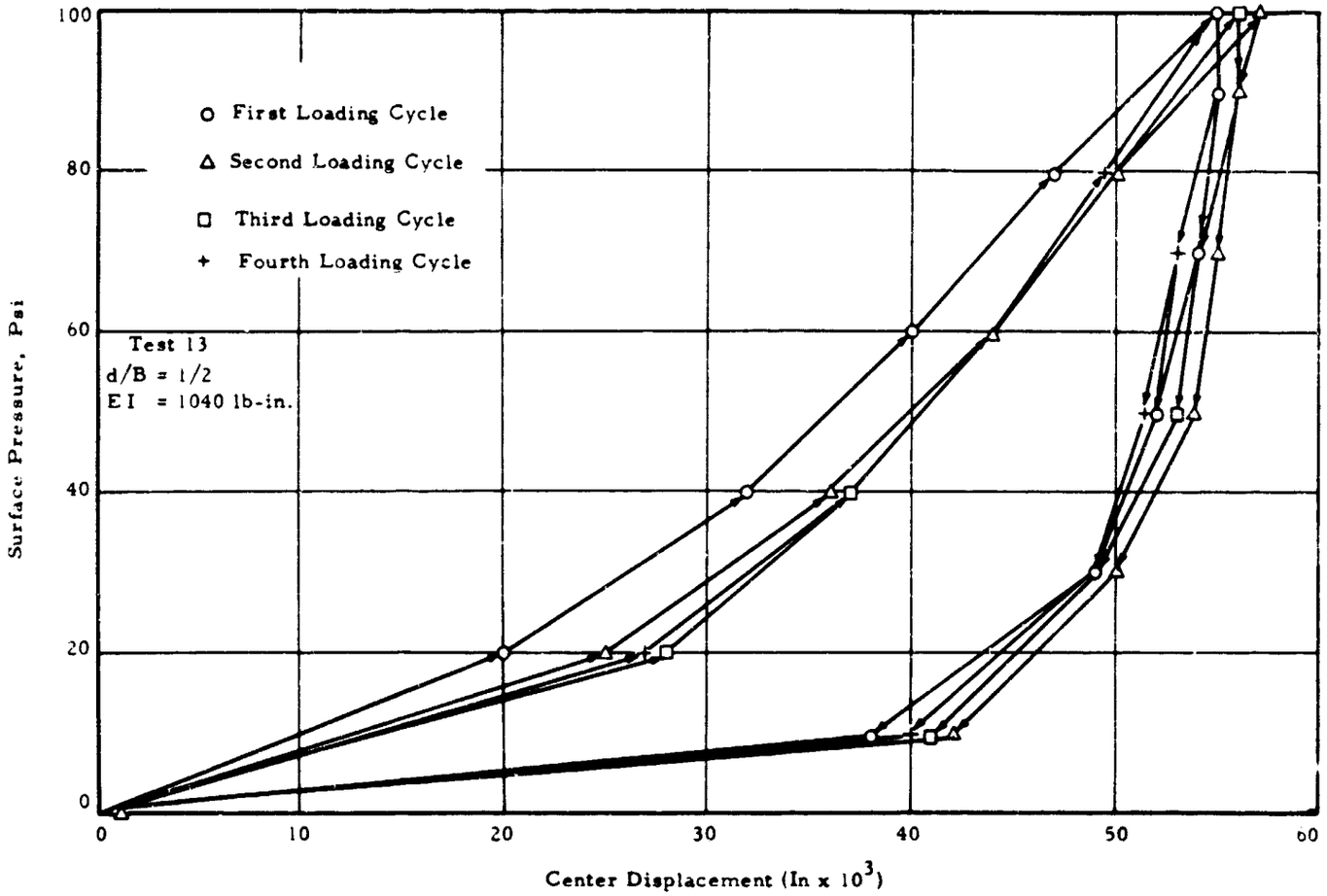


Fig. 6 Variations of Roof Displacements With Surface Pressure

APPENDIX
EXPERIMENTAL DETAILS

STRUCTURAL MODEL

The model used in the experiments is shown in Figure 1, the dimensions being 6-in. dia. and 6-in. long. The major component parts of the model were made from ordinary structural steel (type A7). The basic model consisted of an outer cylinder with a base plate welded to it, an inner load-transferring cylinder with its base plate and 3/4-in. dia. shaft, and a horizontal support member which contained a vertical thrust bearing. The inner load transferring cylinder had two support edges. The upper support edge was used in performing experiments on the model with flexible roofs, the lower support edge was used when experiments were performed on the model with a rigid roof. In order to minimize deformation of the model during experiments, four stiffeners were welded on the inside of the inner load-transferring cylinder and on the inside of the outer cylinder along four radii, 90° apart.

The shaft made contact with a spherical ball which rested in a spherical seat. The distance between the lower edge of the inner cylinder and the upper surface of the outer cylinder was 1/8-in. This space was taped during tests to prevent soil from entering the model. The only contact between the two basic parts of the model (the load transferring cylinder and the outer cylinder) was at the load cell (force washer).

The basic model was altered by changing the flexibility of the roof to obtain the following four models (Table 1). In case of the rigid roof model experiments, a 1/2-in. steel disc was placed on the lower support edge of the inner cylinder. To assure that no disc deflection would occur it was also supported at the center within the model.

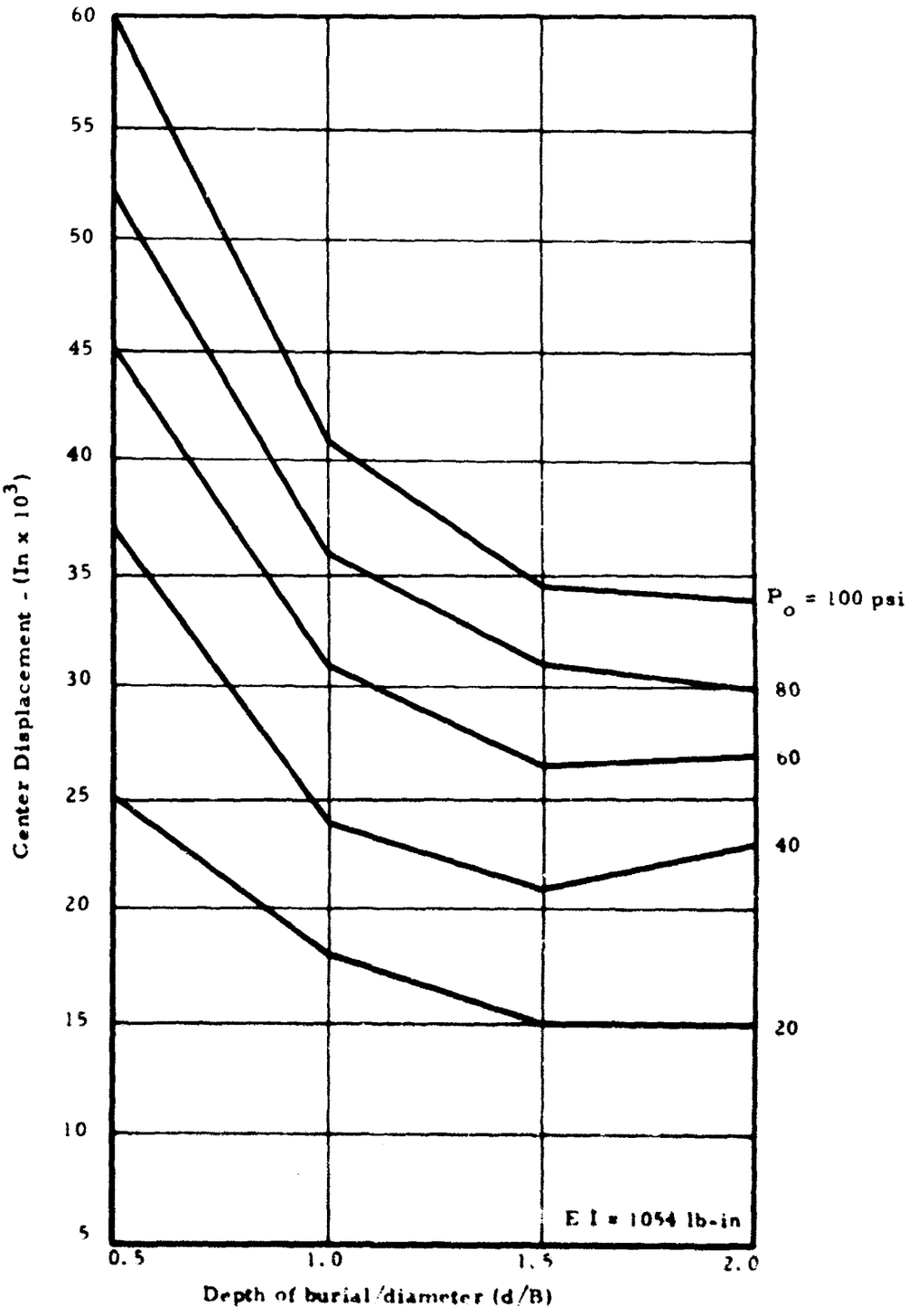


Fig. 7 Variation of Center Displacement With Depth of Burial

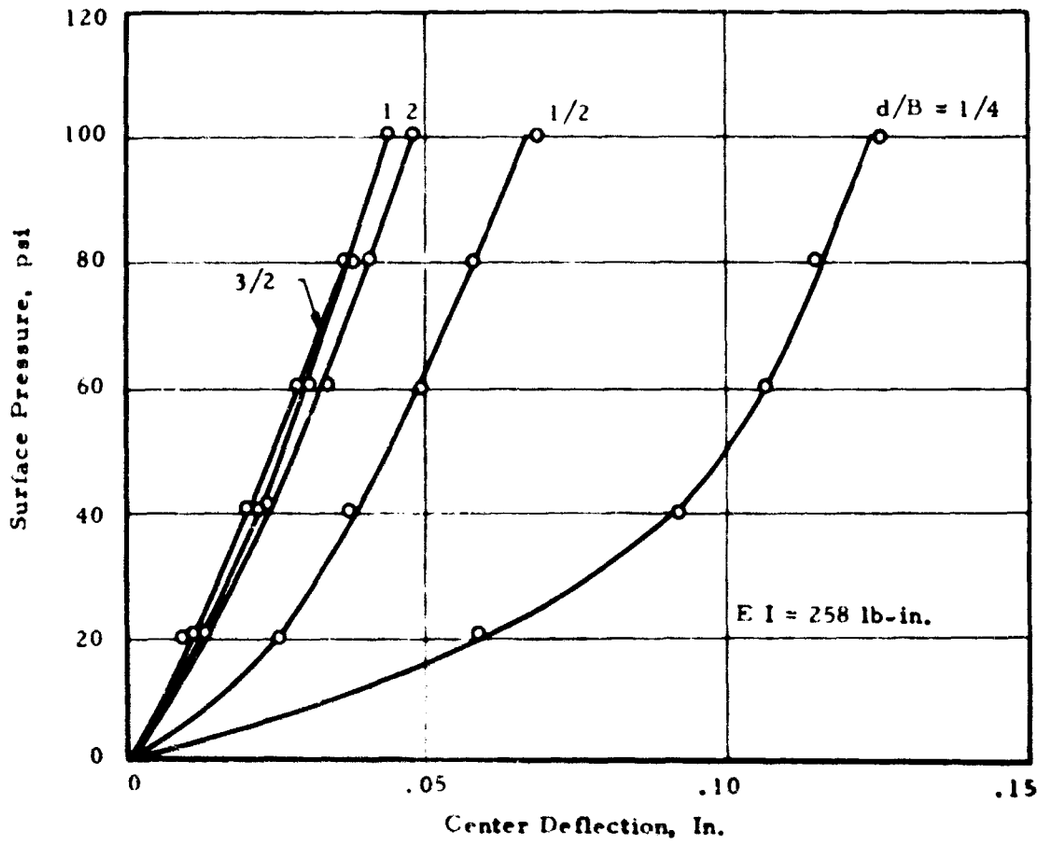


Fig. 8 Influence of Depth of Burial on Load Deflection Relations

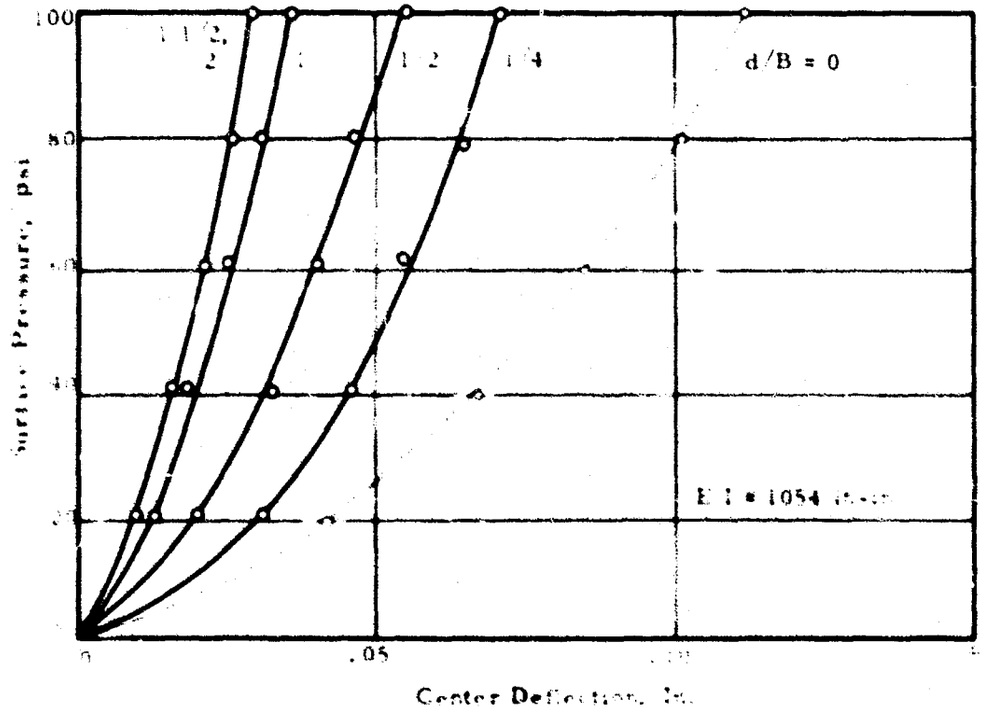


Fig 9 Influence of Depth of Burial on Load Deflection Relations

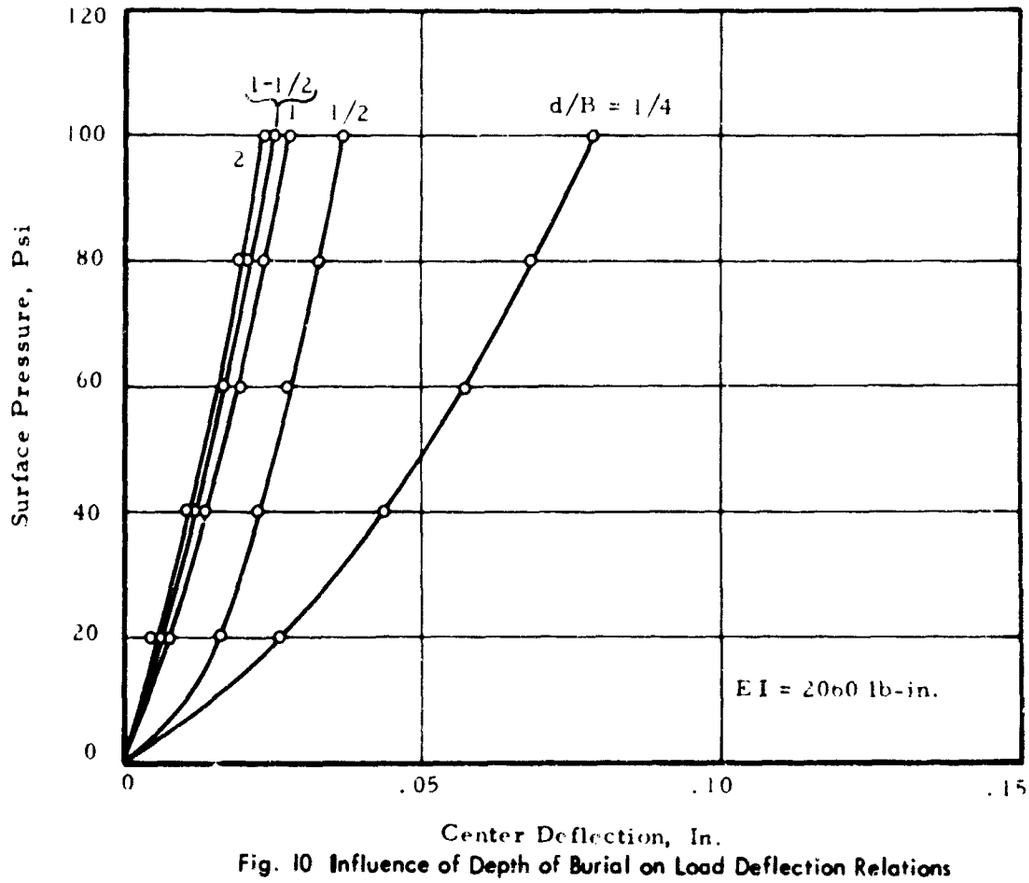


Fig. 10 Influence of Depth of Burial on Load Deflection Relations

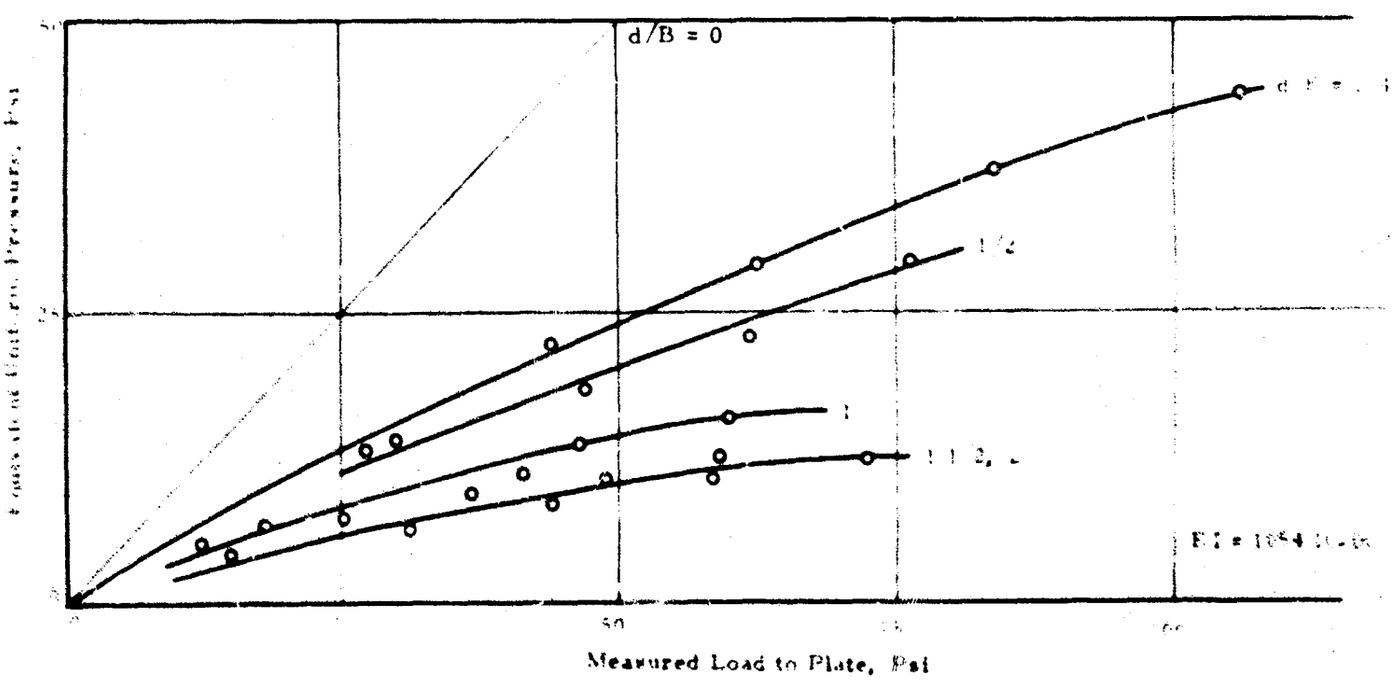


Fig. 11 Influence of Depth of Burial on Load Distribution to Flexible Plate

Table I. Roof Flexibilities

Model	Roof Thickness		Flexibility ($Eh^3/12$, lb-in)
A (Rigid)	1/2"		3.13×10^5
B	3/32"	.0938	2.06×10^3
C	3/40"	.0750	1.054×10^3
D	3/64"	.0469	0.258×10^3

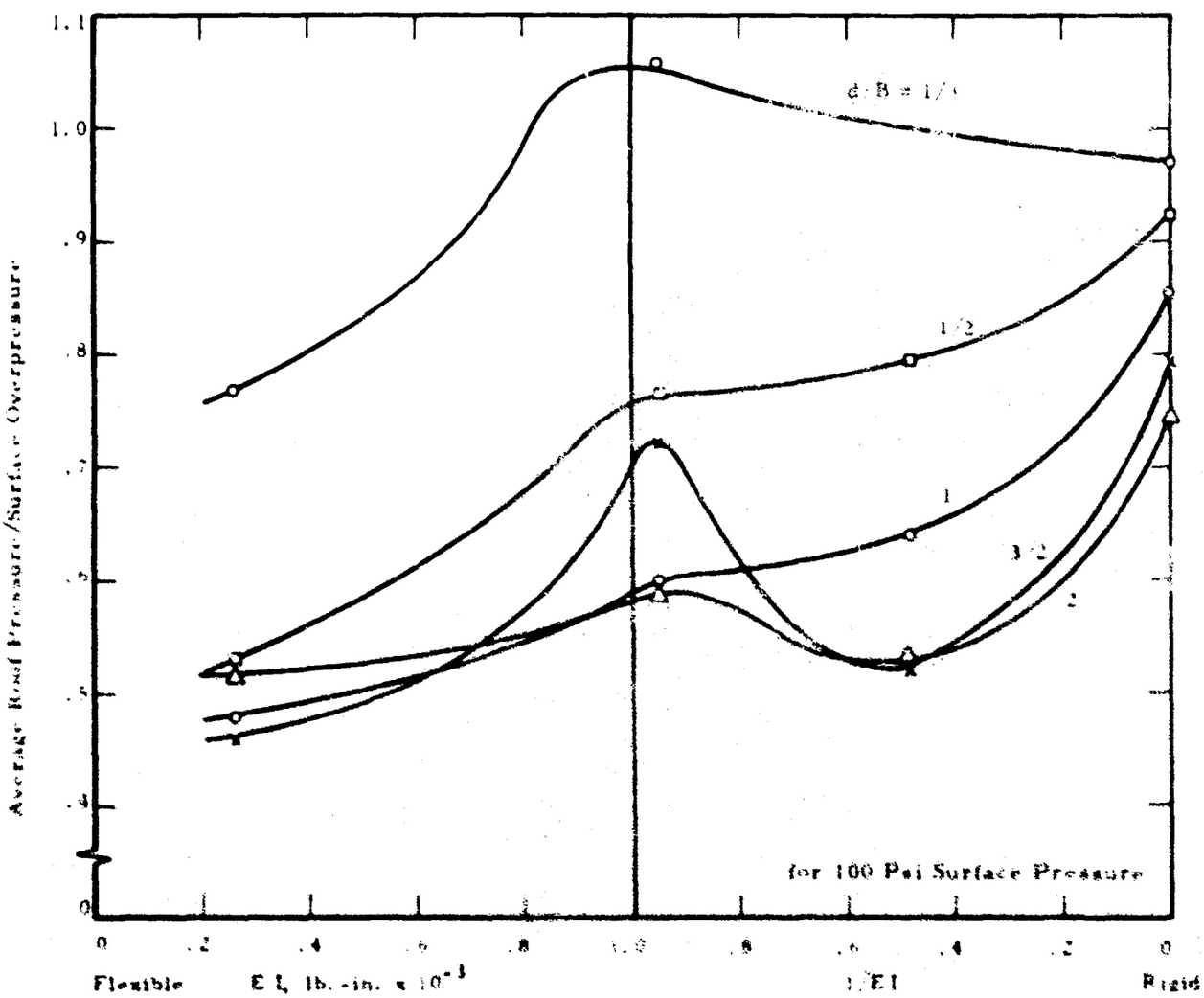


Fig 12 Influence of Flexibility on Arching Action at Various Depths

ANALYTICAL AND EXPERIMENTAL STUDIES, II

INSTRUMENTATION

In the case of the flexible roof model experiments, central deflections of the roofs at various overpressures and depths of burial were measured by means of linear variable differential transformers (L.V.D.T).

In the case of model B and C, an L.V.D.T. highly sensitive to low displacement was used. The L.V.D.T. was mounted in a Plexiglas holder, held in place with a spring and projected just far enough to make contact with the roof of the model. This assembly was then placed inside the inner cylinder and attached to its base plate with four plastic screws. A flexible roof was then placed over the model and taped at the edges with black electrical tape to prevent it from accidentally slipping off during the set-up of the experiment. The reason for using the Plexiglas holder was to prevent any metal from influencing the performance of the transformer.

In the case of model D, which had the most flexible roof disc, an L.V.D.T. with a larger range of travel was employed.

The load cell used in these experiments was a force washer, model 1636, resistance 120 ohms, gauge factor 2.0, serial no. 1683-7, manufactured by Lockheed Electronics Company, Los Angeles California.

SOIL FACILITY AND EXPERIMENT SET-UP

Experiments were performed in the IITRI Soil Facility. The pressure vessel used for the experiments has a 3-ft inside diameter with a 3-ft depth. The walls of the vessel were treated with one coat of bonded Teflon and one sheet of Teflon was placed over it. This was done to minimize frictional restraint at the vessel wall. For the performance of the experiments, the vessel was filled with soil to a desired depth. The model was then suspended into the vessel by means of two 1/4-inch rods connected to a structural angle which spanned the vessel at its top. This configuration served to locate the model and keep it in this position during the placing of the remainder of the soil. When the soil completely filled the vessel, the channel and the two 1/4-inch rods were removed without disturbing the model. A thin rubber diaphragm was then placed over the smooth sand surface and the upper projecting flange of the pressure vessel. Surface displacements were measured as follows. Four brass discs were glued to the rubber diaphragm. One disc was directly at the center, the other three were on a radial line 2, 6 and 10-inches from the center of the vessel. Wire leads were soldered to the discs and made their exit from the vessel through an airtight pipe plug in the pressure vessel cover. The vessel cover, which was bolted to the vessel by means of 36 high strength bolts, had four "through" holes drilled in it at the same locations at the brass discs. Plungers were allowed to go through these holes from the outside and contact the brass discs. Airtight "Neoprene' gaskets were placed around the plungers. A small bulb was wired to each brass disc. Thus when any plunger was moved down and touched the brass disc, the light bulb corresponding to it would light up. The source of power was a dry cell battery. A dial gauge was positioned over each plunger to measure the displacements. A schematic of the experimental set-up is shown in Figure 13.

An experiment consisted of the following: the model with a roof of a particular flexibility buried at a specified depth was subjected to a static pressure which was applied at the surface of the soil. The static air pressure was applied in increments of 20-psi up to 100-psi after which it was reduced to 90 psi and further reduced in increments of 20 psi to 10 psi, from which it was reduced to zero psi. This procedure was repeated four times in each experiment. Readings of the L.V.D.T. and the force washer were recorded at each pressure level of all four cycles.

SOIL PREPARATION

The soil used in the experiments was dry Ottawa sand whose grain size distribution is given in Figure 14. The variation of sand density with the angle of internal friction is given in Figure 15.

To obtain a dense state of Ottawa sand, the sand was first placed in one continuous layer to a height 1-ft below the depth at which the model was to be placed. It was then vibrated by means of a penetration type concrete vibrator until a desired density was reached. The sand density was determined by means of a density scoop.* After this the model was suspended into the vessel as described above and the sand was placed in 6-in. layers until the top of the vessel was reached. At each layer it was vibrated at four diametrically opposite points midway between the model and the vessel wall by the penetration type vibrator for a duration of about 3 minutes. Density scoop readings were again taken at the surface when the vessel was completely filled with sand.

The method used in obtaining a loose density for Ottawa sand was as follows. A slot 1/4-inch wide was cut in the bottom of a cylindrical metal container whose diameter and depth were 19-inches. The slot extended across the full diameter of the container. The slot was then closed from the outside and the container was filled with sand. Sand was then allowed to drop from the container through the slot into the pressure vessel while the container was moved in a circular manner within the vessel. The distance between the bottom of the container and the forming sand surface was held between 18 and 20-inches.

*Sevin, E., S. Shenkman and E. Welch, "Ground Shock Isolation of Buried Structures," Report AFSWC-TR-61-51, IIT Research Institute for Air Force Special Weapons Center, July, 1961.

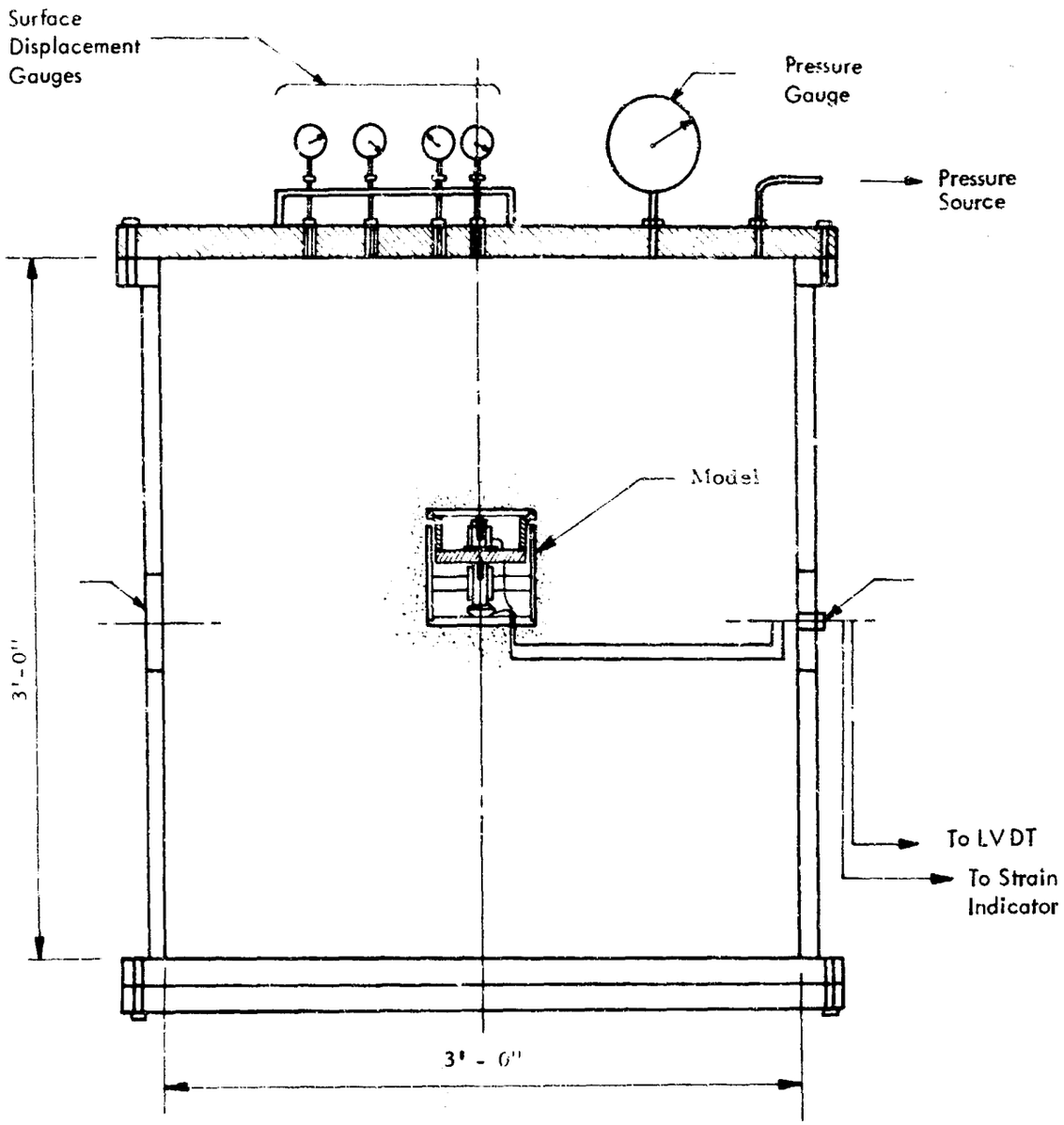


Fig. 13 Experimental Set-Up

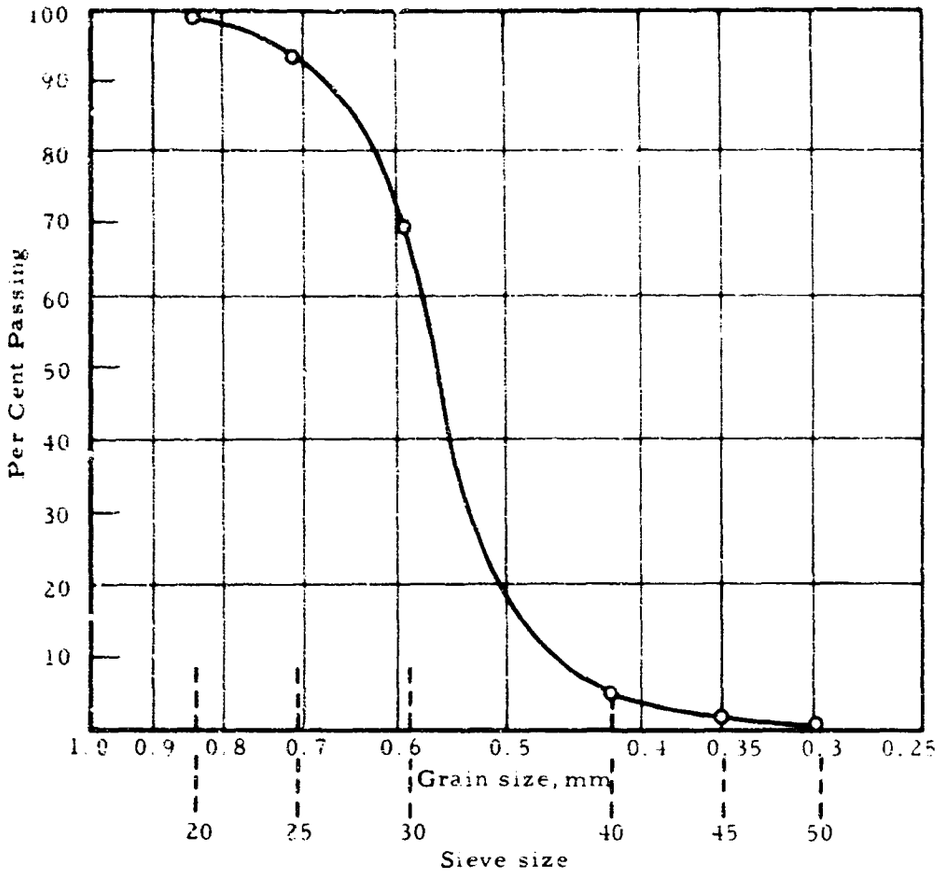


Fig. 14 Grain Size Distribution, Ottawa Sand

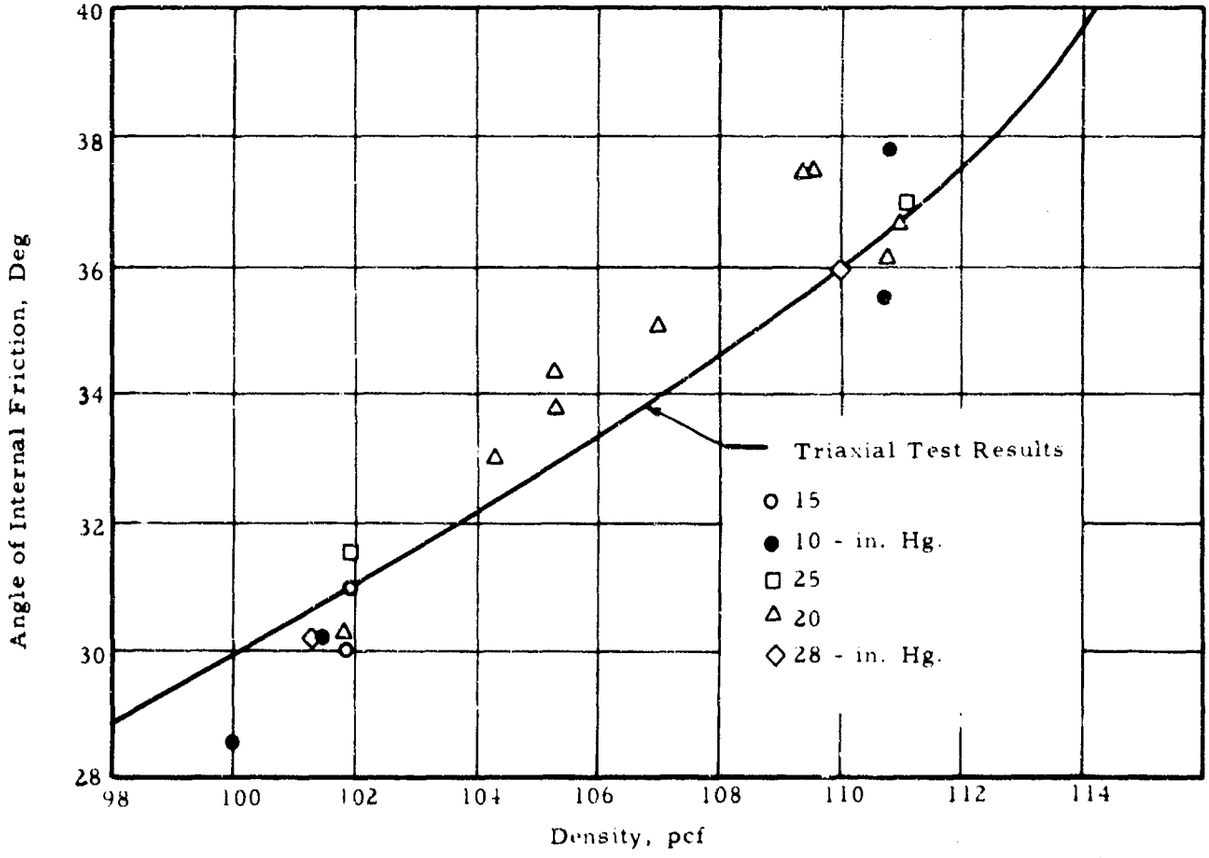


Fig. 15 Angle of Internal Friction, Density Variation (Ottawa Sand, 8 in. Specimens)

YIELDING MEMBRANE CONCEPTS

by
H. P. Harrenstien* and R. H. Gunderson**

INTRODUCTION

The presentation is concerned with the reporting of some of the ongoing research at the University of Arizona in the general area of soil-structure interaction -- specifically, the area of analysis and design of yielding steel membranes which are shallow-buried and which yield under dynamically applied overpressures. The specific contract under which the first phase of this work is being performed is Contract OCD-PS-64-187. The contracting agency is the Department of the Army, Office of Civil Defense, Washington, D. C. The contractor is the University of Arizona. The work is being performed by the Engineering Research Laboratory of the University.

A direct quote from the Contract follows:

"A. The contractor, in consultation and cooperation with the Government, shall furnish all engineering, labor, tools, equipment, materials, supplies, facilities, and services necessary for a feasibility study relating to optimizing shelter design. The work and services shall pertain to the analysis and design of flexible yielding membrane elements of a shelter to resist normal dynamic effects not unlike those which may result at the soil-structure interface as a result of a nuclear blast.

B. The general areas of investigation shall include, but not be limited to the following:

1. Investigate the theoretical prediction of the configuration of a yielding membrane and determine its application to the shelter.
2. Perform certain loading simulator studies to corroborate the intuitive fact that yielding buried structures are efficient structural systems.
3. Extend the theory of studies involving the investigations of the membrane supported on yielding boundaries.
4. Determine the feasibility for future possible exploitation in this area."

Because the contract has just started, the material presented here is more along the lines of "in-progress" reporting, as opposed to a final reporting of the results of the Contract. Such material is deemed appropriate, however, for inclusion in a symposium on the state of the art in soil-structure interaction studies.

GENERAL

When design to resist blast and other close-in nuclear weapons effects is considered, it is only logical to realize that simultaneously large amounts of initial radiation and fallout may be inevitable realities. It is this combination of effects which make buried structures most feasible. The shielding required to meet the radiation requirements and the structural strength required to meet blast requirements both point to these forms of structures as desirable and economical.

Little experience is available on this subject, but this fact is not a sufficient cause to avoid the application of judgement and engineering intuition to develop practical solutions. The economies available in such structures force engineers to develop conservative procedures for design; at the same time test data and research feed the store of knowledge necessary to refine the designs.

SOIL-STRUCTURE INTERACTION FORCES

Definition

Soil-structure interaction forces are those forces which act at the interface between a buried structure and the surrounding soil medium. These are generally considered to be normal pressures, but shearing forces also exist at this interfacial junction.

Distinction between types of forces

Normal forces are pressures which act normal to the interfacial surface and are generally in the same order of magnitude as the surface overpressures in the air medium above the ground surface. Shearing forces are those forces which are tangential to the interfacial surface and generally are in the same order of magnitude as the respective shearing forces in the soil under these conditions. In general, the normal forces produce the greater effect or response in the structure and, because of this, we will limit our discussion to the action of these structures under this interaction component only.

* Professor, Department of Civil Engineering, University of Arizona, Tucson, Arizona.
** Graduate Associate, Department of Civil Engineering, University of Arizona, Tucson, Arizona.

EFFECTIVE SOIL-STRUCTURE INTERACTION PRESSURES

Definition

The effective soil-structure interaction pressure is defined as that normal pressure distribution which at a given instant will produce a static free-field deformation in the structure equal to the deformation of the structure in the soil medium at that same instant. It follows then, if we can neglect the shearing components of interaction forces, that the moments and stresses under this effective pressure will equal those in the confined structure at the same instant.

Dependent variables

Effective soil-structure interaction pressures depend upon the characteristics and homogeneity of the soil, the nature of the loading, and the stiffness and geometry of the buried structure, in relationship to the surrounding soil.

TYPES OF BURIED STRUCTURES

Because the type of buried structure has so much to do with the nature of buildup or attenuation of the passing overpressure, it is appropriate to consider these types in some detail. The three basic types, into which categories most buried structures fall, are the rigid, rigid-flexible, and flexible types (see Figure 1). For completeness, each of these types is briefly discussed, however, the major concern of this presentation involves the flexible type structures.

Rigid buried structures

Rigid buried structures are those buried structures which by definition undergo negligible deformation upon loading. As a result of their rigidity, they have certain pecularities of interaction behavior which will be discussed in more detail later.

Rigid-flexible buried structures

A rigid-flexible structure is one which by definition exhibits rigid characteristics until some point in the rising loading cycle; at this point it yields in such a manner so as to reduce its volume or alter its shape considerably. In conjunction with this behavior are certain changes in the basic soil-structure interaction characteristics.

Flexible buried structures

Flexible buried structures are those structures which by definition exhibit yielding or other noticeable structural deformation immediately at the first sign of an overload. They continue this yielding or reduction in volume behavior throughout the rising loading cycle. As isolated structures they may be quite weak, however, in conjunction with the surrounding soil, the combined system may become very efficient at resisting dynamic overpressures.

SETTLEMENT RATIOS

To understand the nature of soil-structure interaction phenomena, it is appropriate to consider three basic types of settlement ratios. These are positive, negative, and zero ratios.

The positive settlement ratio

Definition. The positive settlement ratio by definition is associated with the change in geometry of the soil mass surrounding a buried structure such that the structure feels a vertical load in excess of the resultant of the dead and live loads immediately overhead.

Visual description. The concept of positive settlement ratio may be described visually by the idealized drawing in Figure 2. It will be observed that the soil mass surrounding the structure deflects more than the vertical column of soil in which the structure is contained. As a result of this idealized geometrical discontinuity, vertical shearing forces are produced which add to the load that is normally

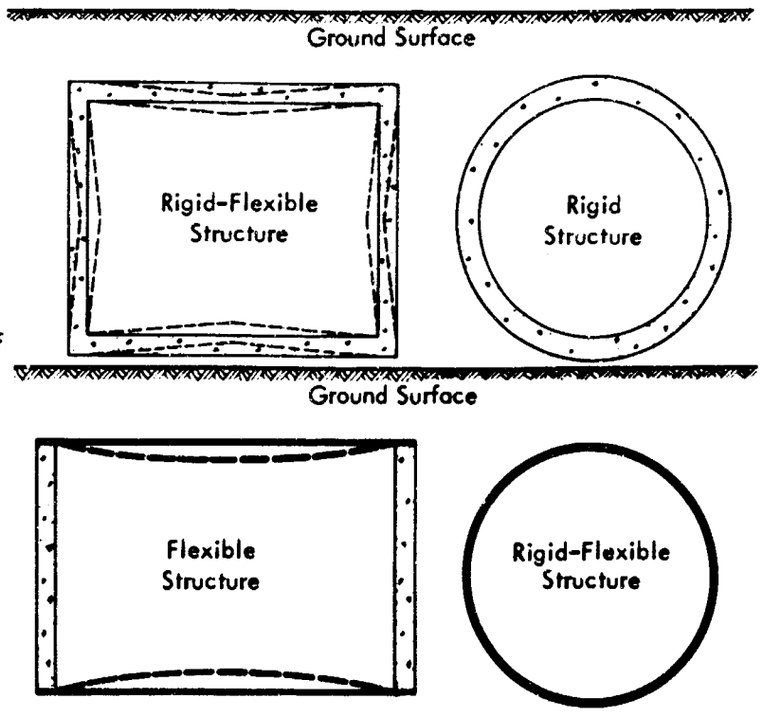


Fig. 1 Types of Buried Structures

experienced. The effective soil-structure interaction pressure for this situation is then larger than that existing in an undisturbed soil at this same depth. To be sure, this sudden discontinuity does not usually exist and more corbeling action may be observed, however the overall effect is the same.

The negative settlement ratio

Definition. The negative settlement ratio by definition is associated with the change in geometry of the soil mass surrounding a buried structure such that the structure feels a vertical load which is less than the resultant of the dead and live loads immediately overhead.

Visual description. The negative settlement ratio is shown visually in Figure 3. It will be observed that the soil mass surrounding the structure deflects less than the vertical column of soil in which the structure is contained. As a result of this idealized geometrical discontinuity, vertical shearing forces are produced which subtract from the load that is normally experienced. The effective soil-structure interaction pressure for this situation is then smaller than that existing in an undisturbed soil at the same depth. As before, the sudden discontinuity does not exist and in reality soil arching takes place but the overall effect is the same.

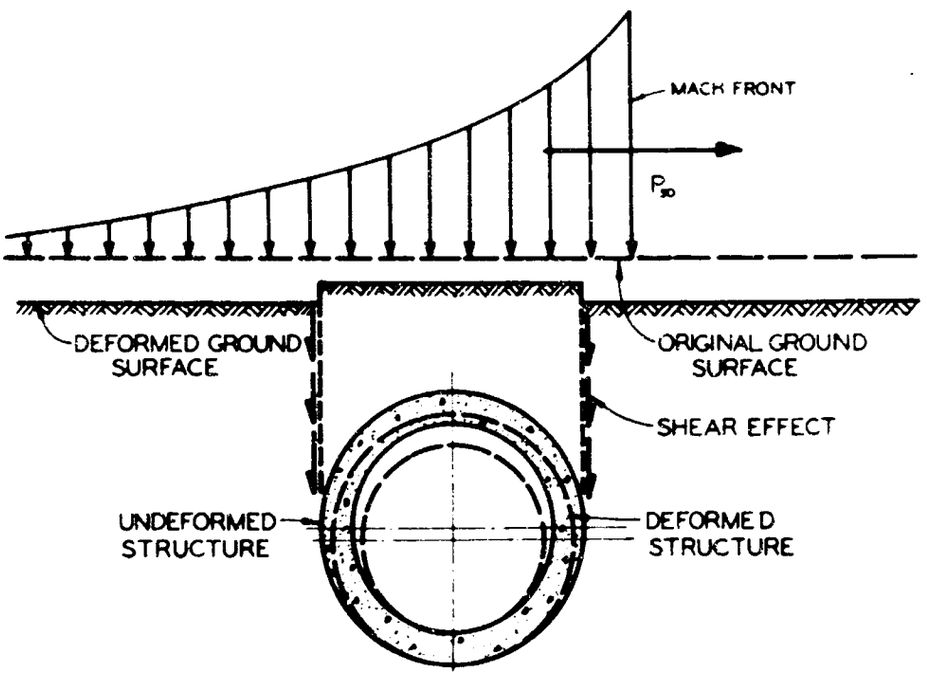


Fig. 2 Idealized Positive Settlement Ratio

Zero Settlement ratio

Definition. A zero settlement ratio is defined as being associated with that condition which exists when the surrounding soil mass and the soil column containing the structure deflect equal amounts. Under such conditions, the effective soil-structure interaction pressure is equal to that existing in an undisturbed soil medium at the same point. Figure 4 shows such a condition.

Systems conductive to zero settlement ratios. These systems are those in which the soil and structure possess equal stiffnesses. Certain types of rigid, rigid-flexible, and flexible structures may at some point in their loading cycle exhibit this behavior. In general, such situations rarely happen throughout the entire loading cycle.

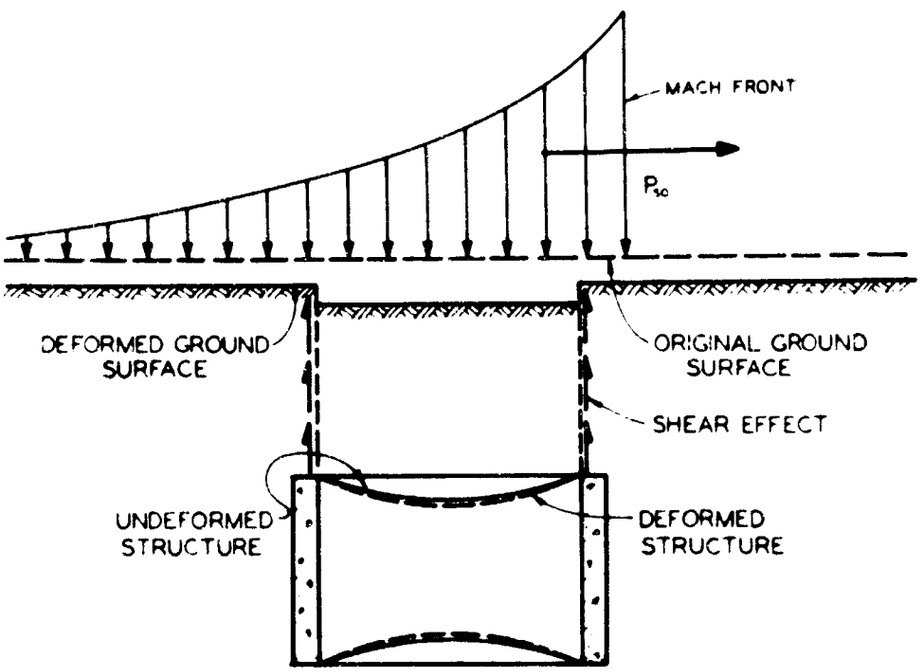


Fig. 3 Idealized Negative Settlement Ratio

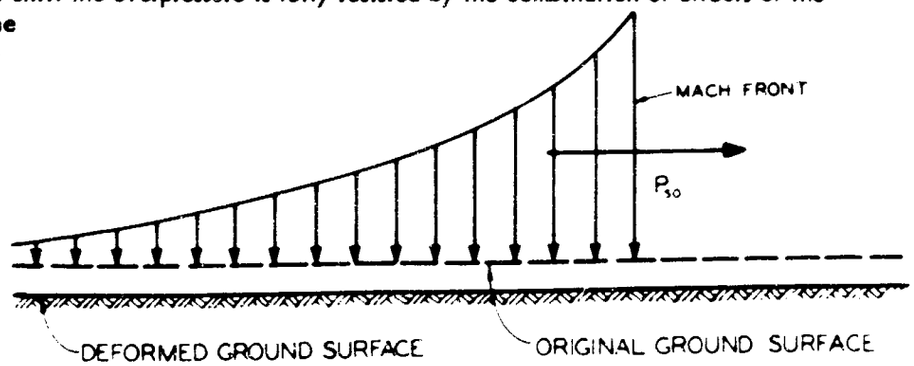
SOIL-STRUCTURE INTERACTIONS

Rigid fully-buried structures

Rigid fully-buried structures generally produce positive settlement ratio conditions and, as a result, should be designed for pressures in excess of those existing at similar points in undisturbed soils. By definition, a rigid structure is one which undergoes negligible deformation on loading. According to the AFDM definition, a fully-buried structure is one which is buried sufficiently so that transient effects of shock wave loadings may be neglected. Figure 1 shows a typical rigid buried structure. This arch, if corresponding to the fully-buried definition, can only undergo uniform compressive stress by virtue of its uniform pressure loadings. The only bending that can develop is due to the change in curvature associated with the uniform change in radius that results from this idealized loading.

Flexible buried structures

Flexible buried structures exhibit the opposite behavior to rigid structures. An example of such a structure is shown in Figure 1 as a vertically oriented circular concrete cylinder with thin steel diaphragms for the floor and roof. The diaphragms are the flexible element of the system. Yielding of these diaphragms begins almost instantly at the first sign of overpressure and such yielding continues until the overpressure is fully resisted by the combination of effects of the change in geometry of the tension membrane and the soil arching which takes place due to the development of the negative settlement ratio condition. Herein lies the real toughness of this combined soil-structure system.



Rigid-flexible buried structures

As the name implies, a rigid-flexible buried structure exhibits the qualities of each type during its loading cycle. As a result, positive settlement ratios immediately followed by negative ones may develop. Two types of rigid-flexible structures are shown in Figure 1. The first is the reinforced concrete box structure, and the second is the popular steel-culvert. The box structure gains its rigidity through the moment of inertia of the concrete mass and through beam and slab action. The flexibility is achieved through the development of yield hinges—beyond which point the resistance to overpressure is almost constant, if soil arching is neglected. The steel culvert has received much attention at this conference. It is actually ambidextrous in that it may exhibit rigid, flexible, or rigid-flexible behavior depending on the nature of loading, type of backfill, etc. Generally, however, it is relatively rigid until either large elastic deformations or buckling is experienced. Either of these latter effects simulate flexibility and thus induce negative settlement ratios.

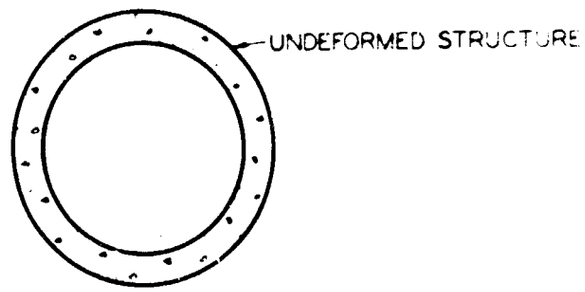


Fig. 4 Zero Settlement Ratio

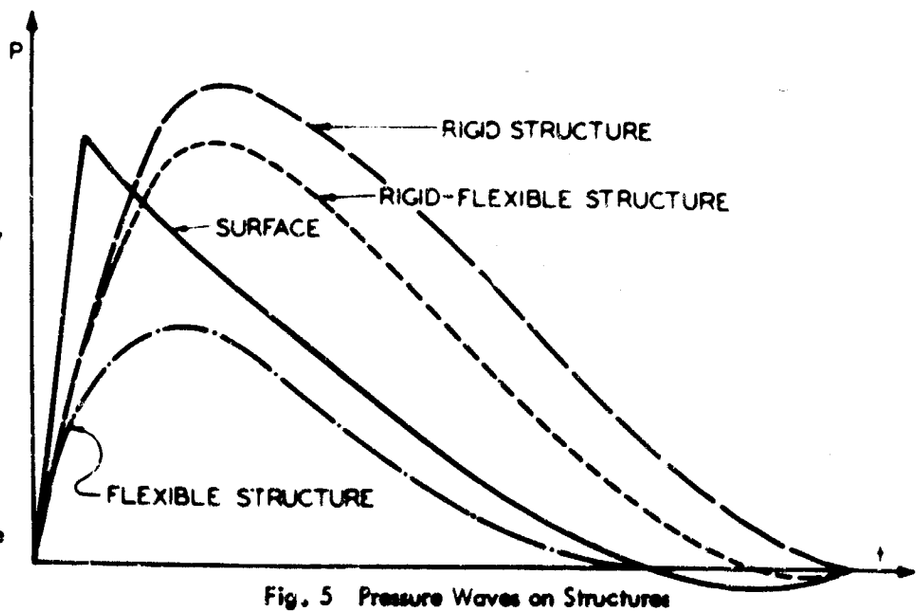


Fig. 5 Pressure Waves on Structures

Summary of effects

Figure 5 illustrates probable effective soil-structure interaction pressures which may be felt by buried structures of the three basic types. The differences in the types are due totally to soil-structure interaction

effects and relative stiffnesses of the structure and surrounding soil.

The stage has been set, by the previous discussions, for the statement that quantitative predictions of these soil-structure interaction loads are most difficult. Here we have a statically indeterminate structural problem of the worst type. Very little quantitative results of any kind are available to substantiate reliable magnitude predictions. There is a particularly intense need for more theoretical and experimental data on the soil-structure interaction phenomenon. These quantitctive predictions are necessary if hopes of meaningful analyses are real. Fortunately, however, designs may be produced from what limited knowledge we now have if we are not overly concerned about being conservative.

The ultimate in structural analysis is to find an answer, such as stress and displacement, given a structure, its supports and its loads. Obviously, for most physical systems there is generally but one answer. The analyst hopes to either find his answer exactly or else gain a close enough approximation to it that this answer is acceptable. In short, the analyst is a problem solver. In the author's opinion, the ultimate in design is to create a given structure to resist given loads over given boundaries such that an analysis is not necessary to assure that this structure will perform satisfactorily. In short, then, a designer can be a problem avoider.

A qualitative understanding of the general physical behavior of an underground structure, as we have just considered, is not sufficient for analysis. Because so little is known about the quantitative behavior of underground structures, as compared with those above-ground, we unavoidably find that our designs are conservative. This is not altogether bad, however, because the source of conservatism is generally found in the supporting strength offered by the soil. For regions in which blast overpressures are considered, close-in fallout and initial radiation will almost assuredly be such that quite a bit of mass will be required for adequate shielding. There is no more economical mass for shielding than earth and therefore, in such regions, buried structures make sense from the fallout and radiation standpoint, let alone from the blast resistance standpoint.

THE ANALYSIS AND DESIGN OF FLEXIBLE STRUCTURES

General

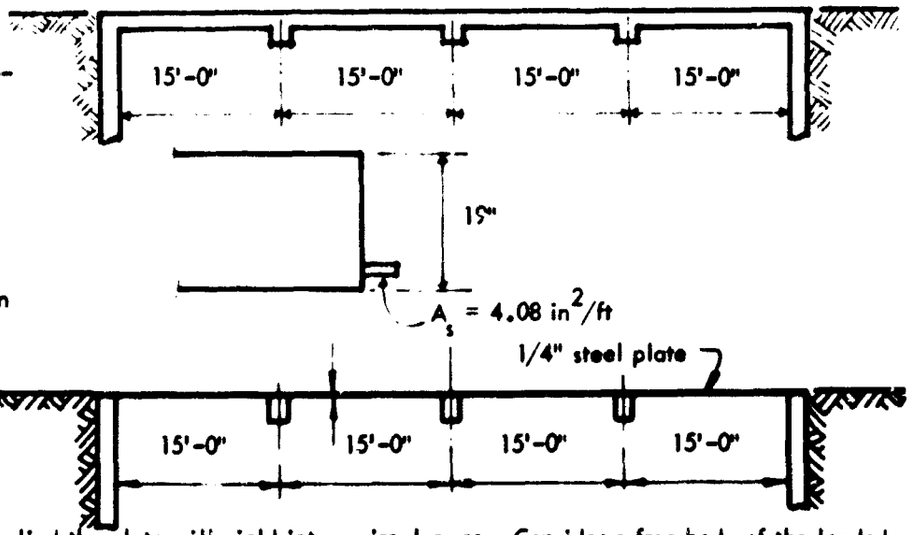
Flexible buried structures, because of yielding characteristics which produce negative settlement ratios, offer the ultimate in economy because of the way in which they force the soil to resist the overload. The most efficient flexible structure is that which simultaneously yields under constant stress at every point in its plane. The behavior of such a structure may be predicted in advance by an inverse solution of the differential equations for stress in shell structures under normal pressure loadings.

An introduction of this approach to design was made at the Sympsoium on Shell Research, Delft, The Netherlands, August 30, 1961 (1). The application at that time was directed toward the "Configuration of Shell Structures for Optimum Stress." Basically, the approach involves the initial assignment of a given final stress state, such as that of constant stress. The search is then made for the shell structure which exhibits this final state of stress under a previously assigned normal pressure loading. For the situation at hand, a uniform yield stress may be assumed under a blast pressure loading. The configuration of this yielding membrane under this blast pressure loading is then the desired result.

For an example of the structural efficiency of a system such as this, consider the following simple comparisons.

Membrane Analysis of a Thin Plate

For a comparison consider a previously designed one-way flat slab.



Where under a standard design with p_o = 50 psi the resulting section is as follows:

Now consider the same span covered with a thin steel plate.

Assume that when the load is applied the plate will yield into a circular arc. Consider a free body of the loaded section, as shown on the next page.

By static Equilibrium:

$$\sum F_v = 0$$

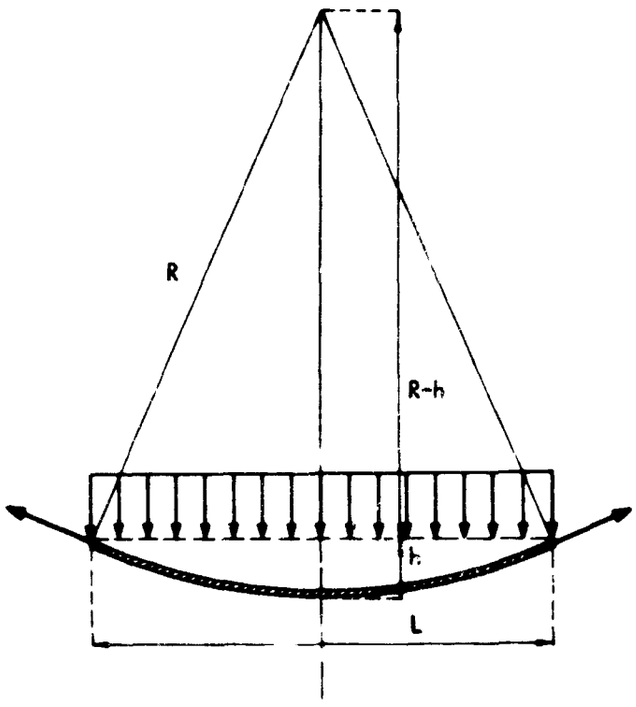
$$P_o(L) - 2(10{,}000\ \frac{L/2}{R}) = 0$$

$$P_o = \frac{10{,}000}{R} \quad \text{or} \quad R = \frac{10{,}000}{P_o}$$

For this particular case of loading:

$$P_o = 50 \text{ psi} \qquad \therefore\ R = \frac{10{,}000}{50} = 200 \text{ in.}$$

This determines the Radius as a function of the load only, independent of the length (L). This condition in itself is insufficient since no consideration is given to the percentage elongation. To determine this percentage, consider the equation of the triangle bounded by R and R-h.



$$(R-h)^2 = R^2 - (\frac{L}{2})^2$$

$$h = R - \sqrt{R^2 - (\frac{L}{2})^2}$$

At yield $T = f_s t = 40{,}000\ (1/4) = 10{,}000$ lbs./in.

h for this case is given by $h = 200 - [(200)^2 - (90)^2]^{1/2} = 200 - 178 = 22"$

Calculation of the percentage of elongation:

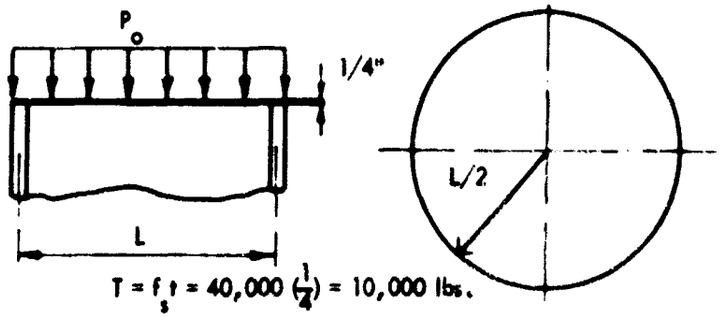
$\% e = \frac{S-L}{L}$ where S is the arc length of the membrane

$S = R\theta = (200)\ 2 \tan^{-1} \frac{90}{178} (\frac{\pi}{180}) = 187.2"$

$$\% e = \frac{187.2 - 180}{180} = \frac{7.2}{180} = 0.04 = 4\% \qquad \therefore\ \text{O.K.}$$

Thus it is seen that a 1/4" steel membrane is capable of resisting as great a load as a 19" reinforced concrete slab which is reinforced at a rate of 4.08 in^2/ft. The plate contains 3.0 in^2/ft. -- less steel than in the reinforced slab. The strain of 4% is less than the ultimate uniaxial strain capacity of most structural steel plate.

For increased efficiency of steel membrane, it may be used in a biaxial state of stress -- such as that found in a circular diaphragm, an example of which follows.



$T = f_s t = 40{,}000\ (\frac{1}{4}) = 10{,}000$ lbs.

Two-Way Circular Membrane

Consider a circular plate of diameter L subjected to a load of p_o psi and clamped around the circumference, as shown above.

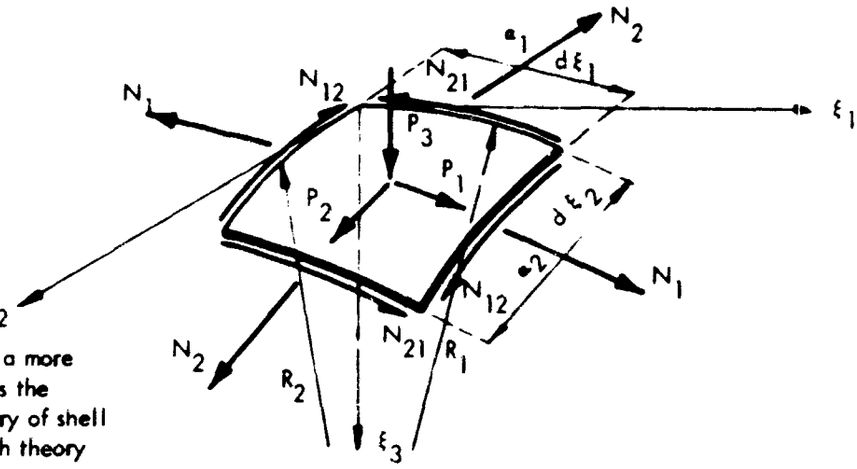
From static equilibrium:

$$\sum F_v = 0$$

$$P_o \pi \left(\frac{L}{2}\right)^2 = 10{,}000 \left(\frac{L/2}{R}\right) \pi \left(\frac{L}{2}\right)^2$$

$$\therefore \quad P_o = \frac{20{,}000}{R} \quad \text{or} \quad R = \frac{20{,}000}{P_o}$$

For $P_o = 50$ psi, $R = 400$ in.



The same examples may be solved by a more general approach. This approach involves the application of the general membrane theory of shell structures to the situation presented. Such theory may be briefly developed as follows.

Consider a free-body of an element of a shell, as shown above: From the equilibrium conditions:

$$\frac{\partial(\alpha_2 N_1)}{\partial \xi_1} + \frac{\partial(\alpha_1 N_{21})}{\partial \xi_2} + N_{12}\frac{\partial \alpha_1}{\partial \xi_2} - N_2 \frac{\partial \alpha_2}{\partial \xi_1} + \alpha_1 \alpha_2 P_1 = 0$$

$$\frac{\partial(\alpha_1 N_2)}{\partial \xi_2} + \frac{\partial(\alpha_2 N_{12})}{\partial \xi_1} + N_{21}\frac{\partial \alpha_2}{\partial \xi_1} - N_1 \frac{\partial \alpha_1}{\partial \xi_2} + \alpha_1 \alpha_2 P_2 = 0$$

$$\frac{N_1}{R_1} + \frac{N_2}{R_2} + P_3 = 0$$

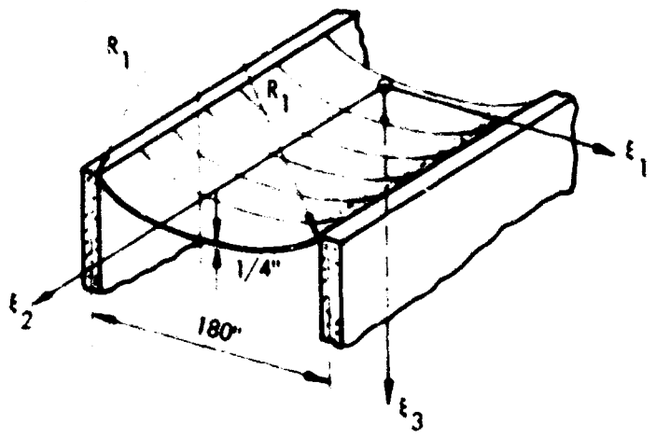
For $N_1 = N_2 = +S$ (constant), and $N_{12} = N_{21} = 0$

$$\frac{1}{R_1} + \frac{1}{R_2} = -\frac{P_3}{S}$$

Note that in this equation, R_1 and R_2 are the principal radii of curvature of the final deflected surface. P_3 is the normal pressure on the surface and S is the membrane tension in dimensions of force per unit length.

An illustration of the application of this equation is now made with reference to the previous two examples.

First example:



$R_2 = \infty$, $P_3 = P = P_o$, $S = 10{,}000$ lb/in.

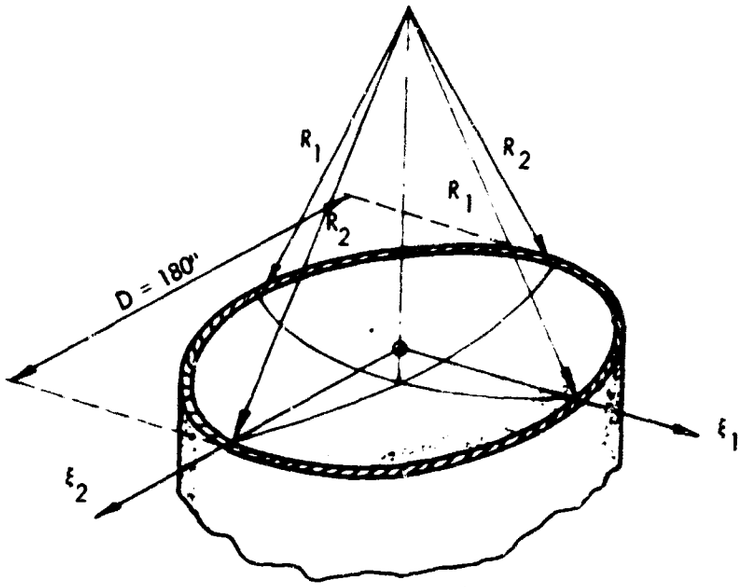
$$\therefore \quad \frac{1}{R_1} + \frac{1}{R_2} = -\frac{P_3}{S} \quad \text{becomes}$$

$$\frac{1}{R_1} + \frac{1}{\infty} = -\frac{P_o}{S}, \quad \frac{1}{R_1} = -\frac{P_o}{S}$$

$$\therefore \quad R_1 = -\frac{S}{P_o}$$

$$R_1 = -\frac{10{,}000}{50} = -200 \text{ in., as before.}$$

Second Example:



$R_1 = R,\ R_2 = R,\ P_3 = P = P_o = 50$ psi

$S = 10{,}000$ lb/in.

$\frac{1}{R_1} + \frac{1}{R_2} = \frac{P_3}{S}$ becomes

$$R = -\frac{2S}{P_o}$$

$$\therefore\ R = -\frac{2(10{,}000)}{50} = -400 \text{ in.},$$

again, as before.

Obviously, it is as simple to apply the free-body diagram approach as it is to apply the general theory, however for more complex problems, the general theory must be used in conjunction with numerical solutions on a digital computer. The following introduces this approach.

General Theory of Funicular Shells

A shell structure may be defined as a materialization of a curved surface in space. In general, the structure of structural component so formed carries its loads primarily by direct stress. By this process, such structures make maximum use of the material from which they are formed in resisting applied loads.

Among the classes of shell structures that are available for shelter application, there exist those which initially exhibit uniform direct stress characteristics under certain specified loadings. These types of shell structures possess the maximum possible structural efficiency that a two-dimensional structure is capable of providing. A structure which is of one sheet and which exhibits uniform stress characteristics under normal pressure loading is defined as a funicular shell. The particular type of such shell structures that are formed when a thin steel plate yields with "constant" stress under application of a distributed normal pressure is one such shape and is the subject at hand. The pressure need not be uniform for the funicular concept to be present.

Many authors have considered the general shape of funicular shells. As was stated, one introduction of the general theory of the configuration of such structures under load was given at the International Association for Shell Structures Sympsoium at Delft, The Netherlands in 1961 (1). The basic equation involved in this presentation was:

$$\frac{N_1}{R_1} + \frac{N_2}{R_2} + P = 0$$

Where R_1 and R_2 are the principal radii or curvature, N_1 and N_2 are the membrane forces and P is the lateral pressure load.

If it is assumed that the same stress level exists at all points in the membrane and in all directions such that $N_1 = N_2 = S$, the above equation reduces to:

$$\frac{1}{R_1} + \frac{1}{R_2} = \frac{-P}{S}$$

The exact equation of curvature derived from differential geometry for a function $z = f(x,y)$ is:

$$\frac{1}{R_1} + \frac{1}{R_2} = \frac{\left[1 + \left(\frac{\partial z}{\partial y}\right)^2\right]\frac{\partial^2 z}{\partial x^2} + \left[1 + \left(\frac{\partial z}{\partial x}\right)^2\right]\frac{\partial^2 z}{\partial y^2} - 2\frac{\partial z}{\partial x}\frac{\partial z}{\partial y}\frac{\partial^2 z}{\partial x \partial y}}{\left[1 + \left(\frac{\partial z}{\partial x}\right)^2 + \left(\frac{\partial z}{\partial y}\right)^2\right]^{3/2}} = \frac{-P}{S}$$

Solutions and Design Curves

This expression may be written in finite difference form and solved by iteration techniques on a digital computer for certain membrane shapes and specific edge conditions. The types considered in this paper are shown in Figure 6. The non-dimensionalized PD/S versus z_c/D curves, which are shown in Figure 7 are results from the computer study. Only the curves showing the center deflection are given, but these are the most important as far as design is concerned. These curves are based on the behavior of a rigid-plastic material. However, to use these curves with any other type of material the only additional information required is the appropriate stress-strain curve for the material.

The PD/S vs. z_c/D curves are based on the average stress and average strain across the center of the membrane. It is known that the strains are not uniform over a deflected membrane surface (2,3,4). However, as far as vertical deflections are concerned, the assumption of uniform stresses and strains appear justified.

The only regions where this assumption leads to appreciable errors is in the corners of rectangular membranes. If reasonable care is taken during the construction to insure proper full-strength welds and if the design strain is reasonable (less than 2.5%) the yielding membrane structural element should serve quite well.

Either the circular or rectangular problems could be programmed for the computer with a non-uniform lateral pressure. Soon, it may be possible to predict the attenuation of pressure on a yielding structural element and the resulting pressure distribution. However, in working with yielding elements, they can be built as if they were to be subjected to the full uniform lateral pressure. The yielding characteristics force the surface to take the shape it has to assume.

Although certain metals, especially mild steel have very large plastic elongation properties on uniaxial tests--sometimes greater than 30% strain--this does not mean the material will admit such large strains under biaxial conditions. In fact, most of the common yielding materials will not admit average strains greater than 9 to 10 percent even in a membrane state of stress. Since a true membrane state of stress may be difficult, if not impossible, to realize in actual construction, a maximum design strain of 2.5% is recommended. This strain corresponds to a z_c/D ratio of about 0.10.

To illustrate the use of these design curves, consider the circular membrane which was solved previously. In that example,

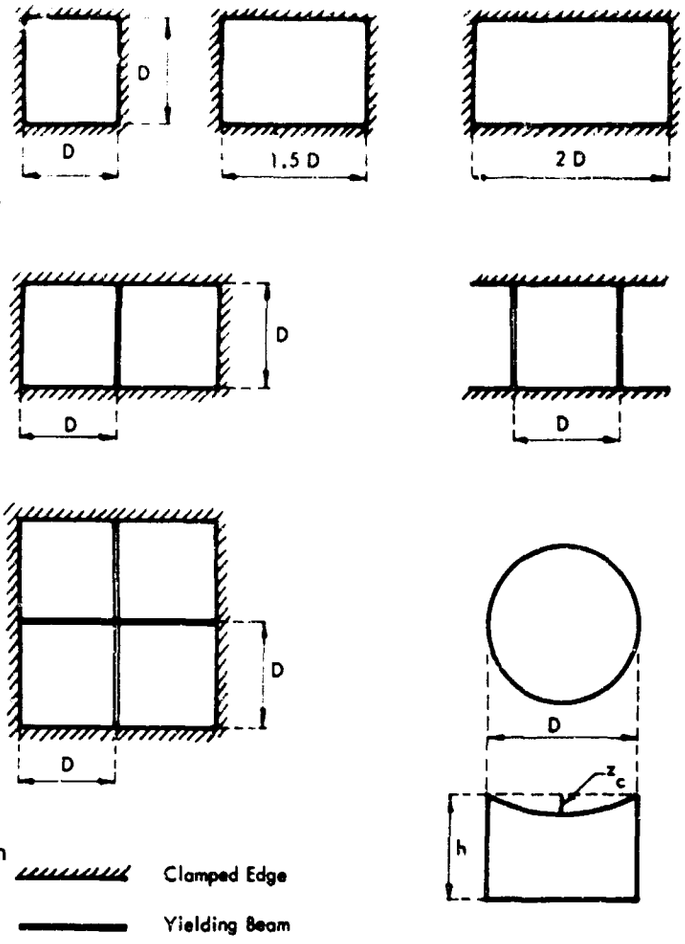


Fig. 6 Plan Views of Shapes Considered

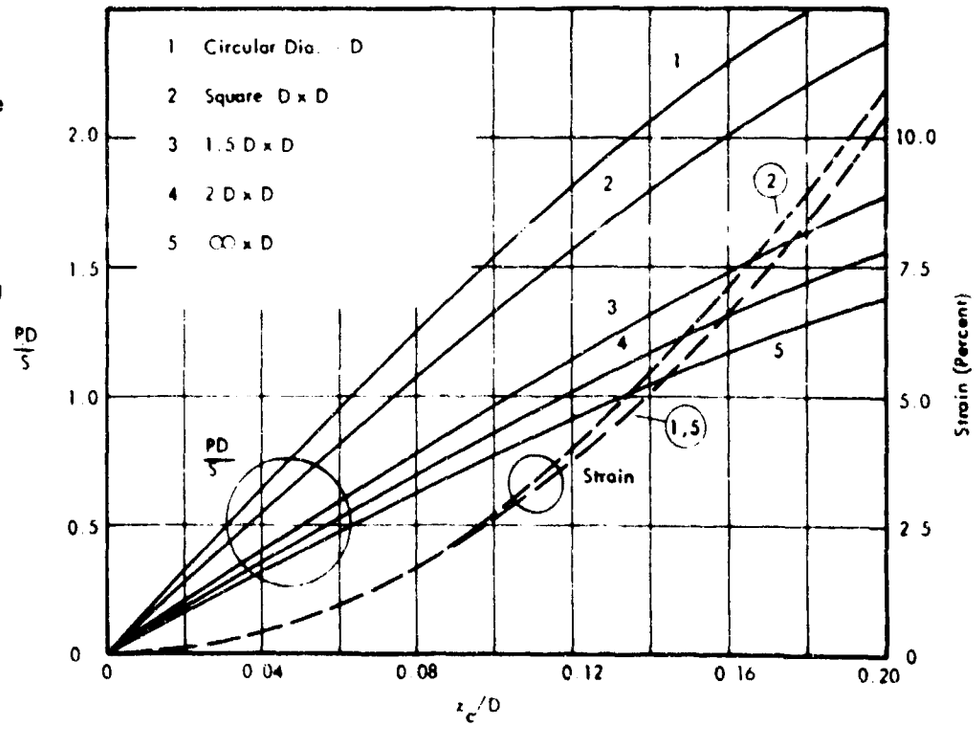


Fig. 7 PD/S versus z_c/D Curves

P_{so} = P 50 psi

D = 15 ft = 180 in.

S = 10,000 lb/in.

For this case $\frac{PD}{S} = \frac{(50)(180)}{10,000} = 0.90$

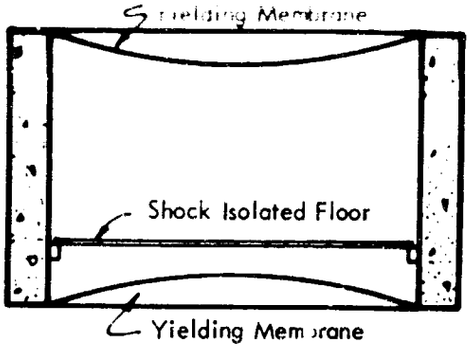


Fig. 8 Yielding Membrane Shelter

From Figure 4; $z_c/D = 0.057$, which corresponds to a strain of approximately 1%. The center deflection, z_c, is then 0.057 D, or 10.3 in.

The ultimate strength of this membrane may be easily determined by entering Figure 4 with a maximum biaxial strain requirement of 2.5%. For this strain PD/S = 1.5 and $z_c/D = 0.097$. If PD/S = 1.5, then

$$P = \frac{1.5\,S}{D} = \frac{1.5(10,000)}{180} = 83 \text{ psi}$$

The center deflection, z_c, for this condition is $z_c = 0.097\ (180) = 17.5$ in. This example demonstrates the remarkable reserve strength of these elements.

To achieve the greatest economy and overall toughness of the shelter, it is suggested that the same type of membrane be used on the floor as on the roof. Figure 8 above, illustrates this concept.

Usually the center deflection to span ratio will be the governing design factor but, also a check should be made to insure against an excessive pressure increase in the structure which may be induced by the sudden deflection on the roof.

This "back pressure" should not be greater than 4 to 5 psi. The Lovelace Foundation indicates that this is the threshold of the eardrum damage region. The back pressure curve which is shown in Figure 9 is for a circular structure but will work well for square areas. If used for other rectangular shapes, the actual pressure would be greater than the value from the graph resulting in non-conservative answers. The whole problem of back pressure can be ignored if the membrane has an initial "dish."

Membranes Supported by Yielding Beams

If yielding membranes were used in the design of blast shelters, it might be advantageous to use yielding beams across the membrane to decrease the maximum deflections. As with the yielding membrane itself, the force in the yielding beam would have to be resisted in some manner. In the following figures the behavior of such reinforced membranes is indicated.

The PD/S versus z_c/D curves (Figures 10, 11 and 12) are non-dimensionalized pressure versus deflection curves for the points of maximum deflection of the membrane and the center points on the beams for the conditions of edge constraint. The numbers inside the circles are values of the ratio F/SD where:

F = strength of beam and membrane

S = membrane strength

D = short span distance

The subscripts refer to the locations of the point. For example, $①_{9.9}$ refers to the PD/S vs. z_c/D curve for the center point of the membrane, when the ratio of beam strength to the product

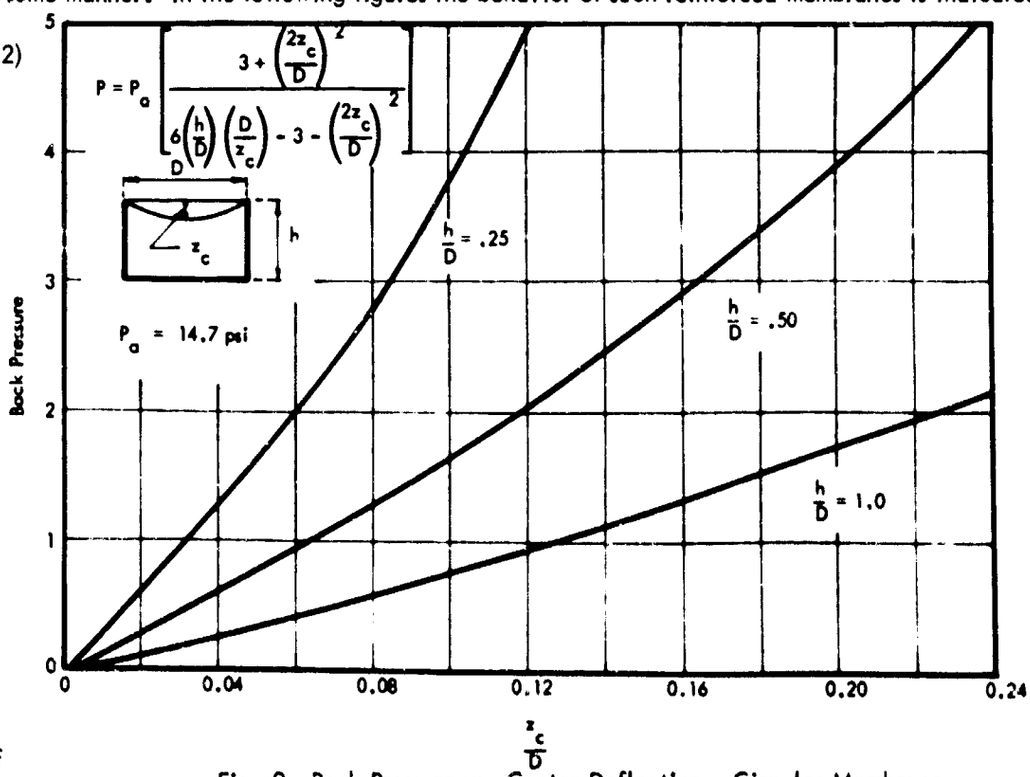


Fig. 9 Peak Pressure vs. Center Deflection - Circular Membrane

of the membrane strength and the span is one. These graphs are for symmetrical cases, i.e., it is assumed that the conditions on both sides of the supporting beams are the same (see Figures 13 and 14).

DYNAMIC TESTS

Dynamic tests were conducted in the University of Arizona blast simulator. This simulator is a plane-wave generator powered by a hydrogen-oxygen explosion. The blast chamber, shown in Figure 15, is a 300 gallon, 8 ft. by 2.5 ft. diameter tank mounted vertically on rubber bushings to a heavy concrete base. Access to the chamber is achieved by unbolting the top section of the tank and swinging the bottom section and the base around a pivot. The 2.5 ft. x 2.5 ft. soil bin is then exposed for the placement of model structures, gauges, and sand. There is also a 14 in. diameter access hole in the bottom of the soil bin and two 4 in. diameter access holes and windows in the top section.

The blast wave is caused by a hydrogen-oxygen explosion detonated by an electric spark. Predetermined quantities of hydrogen, oxygen, and air are measured in the three auxiliary tanks on the side of the chamber. The air controls the rise time of the blast wave. The gases are fed into an evacuated plastic bag at the top of the tank. The explosion is detonated by an electric spark which is triggered by the same switch that starts the recording instruments. The decay time is controlled by adjustable exhaust valves and spacing washers between the chamber sections. The decay curve is exponential. The detonating spark and the gas bag are centered in the tank to minimize dynamic imbalance during tests.

The overpressure range is from 0 to 50 psi with variable rise times from less than one millisecond to over one-tenth of a second, and decay times from one-tenth of a second and up. The blast waves could be controlled to within 10 percent from test to test. The instrumentation and recording devices included two Statham

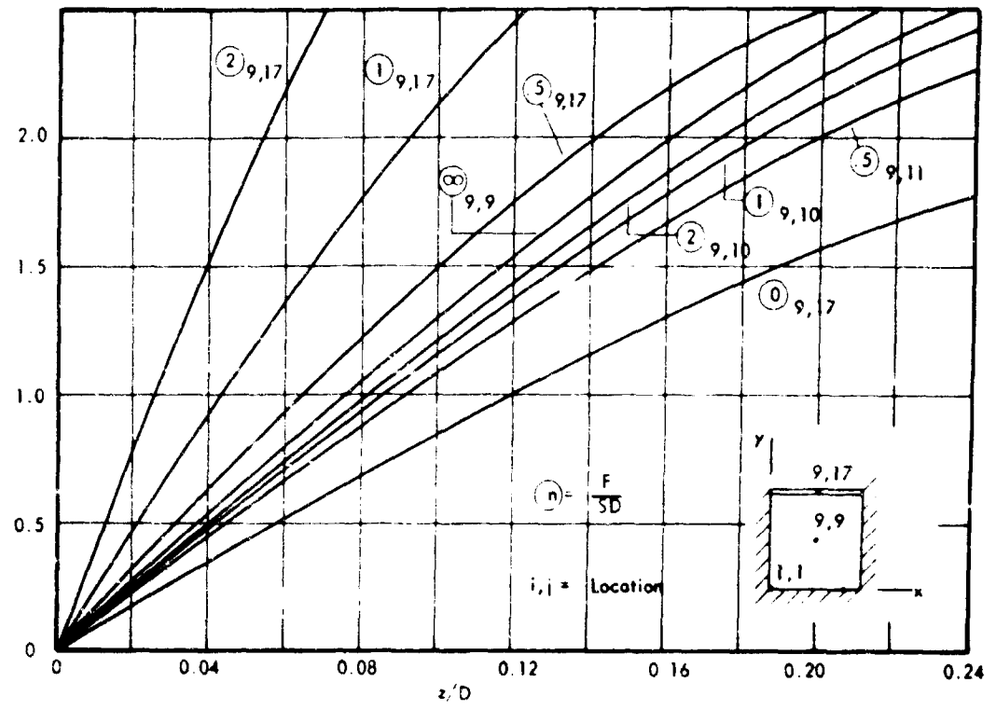


Fig. 10 $\frac{PD}{S}$ vs. $\frac{z}{D}$ Square Membrane with One Edge Beam

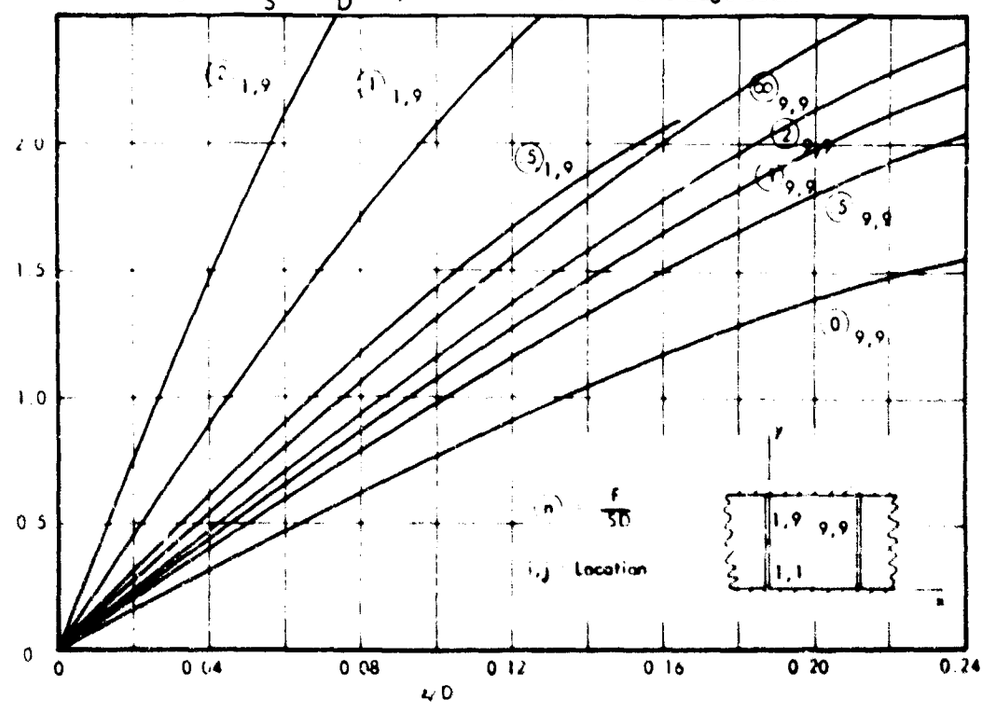


Fig. 11 $\frac{PD}{S}$ vs. $\frac{z}{D}$; Square Membrane with Beams on Two Opposite Edges

pressure transducers (0 to 50 psi), two Tectronix dual beam oscilloscopes with cameras, one six-channel Brush recorder, and one two-channel Sanborn recorder.

The blast simulator has been used to test yielding membrane models above and below ground. The test models were 3.5 to 4.0 inch cylinders which were constructed so that the edges held a membrane tightly clamped (Figure 16). The investigations were made to determine the effects of depths of burial and structural flexibility on the percentage of load carried by the yielding elements.

From the tests made in the blast chamber, some insight has been gained into the amount of attenuation of overpressure which is caused by soil cover. These tests showed that soil cover does attenuate overpressures appreciably; mainly due to an arching action in the soil as the membrane yields. Had these models been rigid they would have been subjected to pressures close to the surface overpressure. As can be seen from the test evidence, the arching action was acting well before the model was buried one-half the diameter and at one diameter only one-tenth of the overpressure is felt by the buried membrane roof (Figure 17).

These results are not useable for prototype predictions because the principles of similitude are not satisfied. They do serve to illustrate the attenuation due to soil arching. The arching, in this case, had as a point of support, the edge ring of the model structure. Had this edge ring not been present the soil would have arched from a point outside the structure,

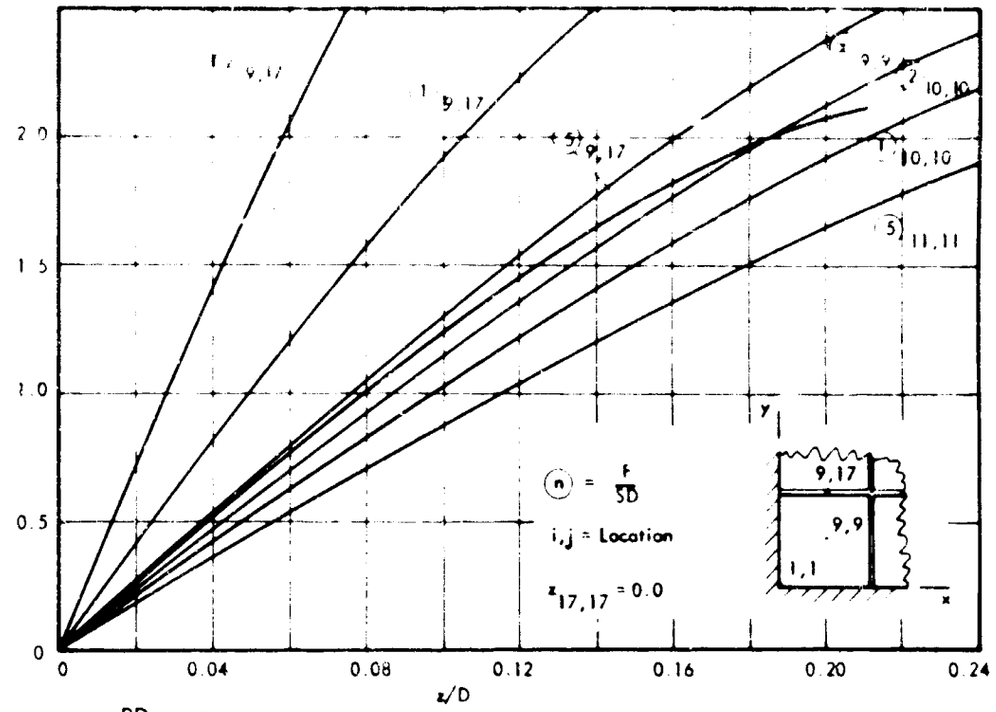


Fig. 12 $\frac{PD}{S}$ vs. $\frac{z}{D}$: Square Membrane with Beams on Two Adjacent Edges



Fig. 13 Square Membrane Test Yielding

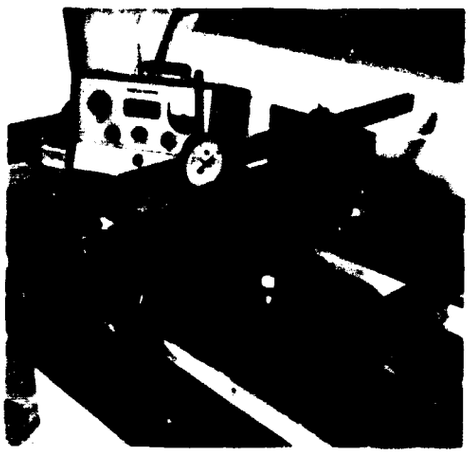


Fig. 14 Square Membrane with Two Yielding Beams

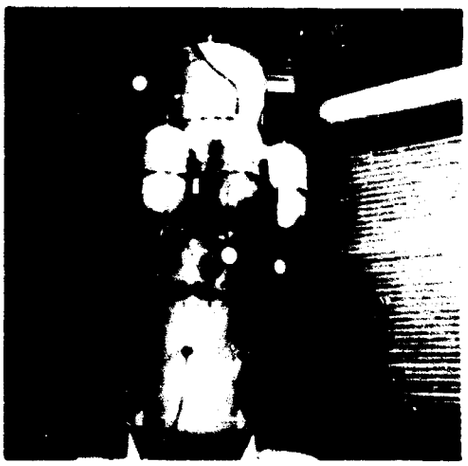


Fig. 15 Blast Simulator



Fig. 16 Model Structure and Deformed Model Shells

but the arch would have been longer and flatter and thus the attenuation of overpressure would have been less.

In tests with the circular models, it was noted that the deflected shape was nearly spherical except that near the edges where the soil arch was supported by the structure the curvature was greater. The radii of curvature along a diameter was measured and by making use of the basic formula

$$\frac{1}{R_1} + \frac{1}{R_2} = -\frac{P}{S}$$

a fairly accurate distribution of the pressure across the membrane was determined (Figure 18) Note: a thin rubber sheet was placed over the surface of the sand to prevent the blast wave from permeating the pores.

Tests have shown that yielding membranes have the ability to deform dynamic overpressure: It has been noted in the test conducted at the University of Arizona that there is 10 to 20 percent increase in deflection under a dynamic load as compared to the same magnitude of overpressure applied statically.

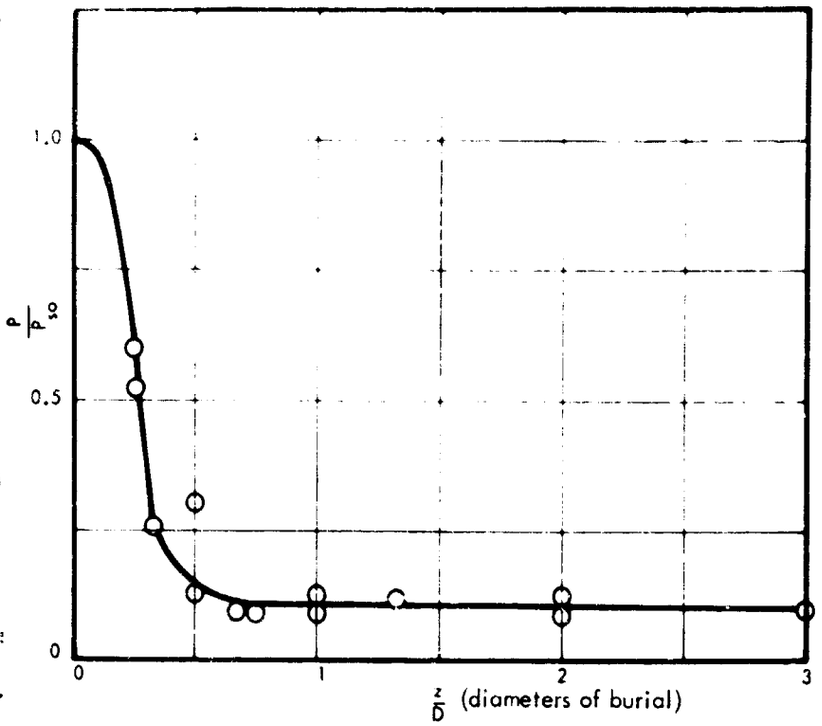


Fig. 17 Attenuation of Pressure with Depth

CONCLUSIONS

Yielding membrane structures which are supported such that they can develop maximum strength in membrane action are efficient components of a shelter structure. Preliminary studies attest to their feasibility and toughness. The true dynamic behavior of these buried components needs further study, but tests to date indicate no great differences in behavior between static and dynamic loadings. Their ability to promote favorable soil-structure interaction while remaining in stable non-buckling configurations is one of their prime assets. The probability of survival (POS) of these shapes is quite large because of their ability to stably sustain loadings in excess of design overpressures.

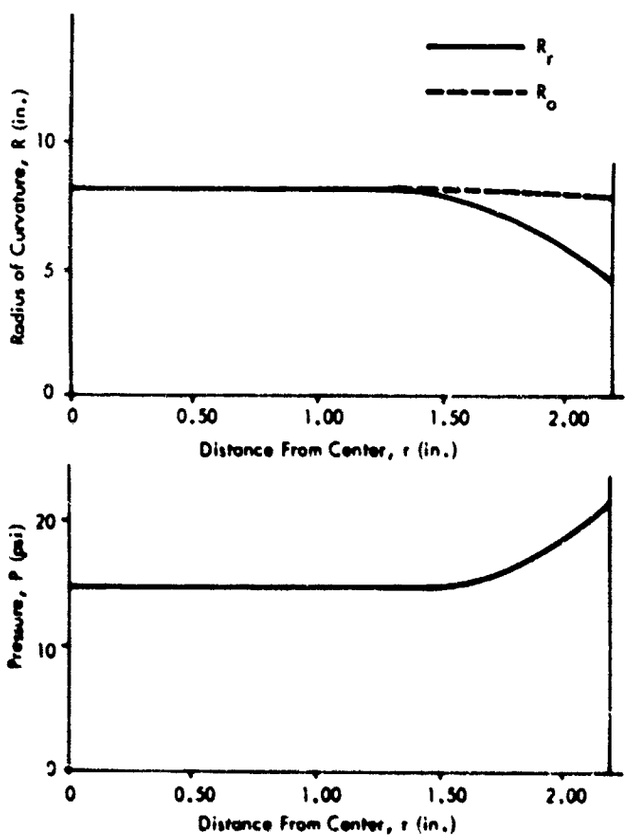


Fig. 18 Radius of Curvature and Pressure Distribution across a Circular Membrane with Soil Cover

REFERENCES

1. Harrenstien, H. P., "Configuration of Shell Structures for Optimum Stresses," Proceedings of the Symposium on Shell Research, Delft, August 30-September 2, 1961.
2. Hill, R., "A Theory of the Plastic Bulging of a Metal Diaphragm by Lateral Pressures," Philosophical Magazine, 7th series, Vol. 41, pp. 1133-42, 1950.
3. Weil, N. A. and N. M. Newmark, "Large Plastic Deformations of Circular Membranes," Journal of Applied Mathematics, Vol. 22, p. 533, 1955.
4. Gleyzal, A., "Plastic Deformation of a Circular Diaphragm Under Pressure," Journal of Applied Mechanics, Vol. 15, No. 3, pp. 288-296, September 1948.

THE RESPONSE OF BURIED CYLINDERS TO QUASI-STATIC OVERPRESSURES

by
B. A. Donnellan*

ABSTRACT

An experimental investigation was conducted into the response of small buried aluminum cylinders to quasi-static overpressures. The cylinders were 4 inches in diameter and were buried with their axes horizontal in dense, dry, 20-30 Ottawa sand.

Cylinders of two wall thicknesses (t = 0.035 inch, d/t = 114; and t = 0.016 inch, d/t = 250) were tested at depths ranging from zero to two cylinder diameters. Their behavior was evaluated quantitatively by means of radial displacement gauges and tangential strain gauges. Data corresponding to five overpressure levels up to 140 psi are presented. This maximum value exceeded the theoretical in-air primary buckling pressure of the cylinders by factors of 9.4 and 99.

Destructive tests were conducted on non-instrumented cylinders of six stiffnesses. The maximum applied overpressure was 160 psi (470 times the theoretical in-air primary buckling pressure of the most flexible cylinder). The overpressure required to cause collapse of the various cylinders was determined for as many depths of burial as the maximum overpressure would allow.

The destructive test data demonstrate the great resistance to collapse imparted to a cylinder by burial. The non-destructive test data afford a comparison between the behavior of a relatively stiff and a relatively flexible cylinder as the depth of burial and the overpressure are changed. Two zones of burial (deep and shallow), based on the behavior of the cylinders, are defined. These zones depend on the rigidity of the cylinder and the magnitude of the overpressure.

INTRODUCTION

The soil-structure interaction problem is not new. One aspect of it, that of the culvert and tunnel, has been the subject of much theoretical and experimental study. The known high load-carrying capacity of the culvert and tunnel, together with other advantages of burial, has attracted the attention of designers of protective structures.

A portion of the research effort at the Air Force Shock Tube Facility is directed toward an understanding of the parameters involved in the design of such structures. These parameters include the structure's shape and stiffness, the engineering properties of the surrounding medium, the depth of burial of the structure, and the peak magnitude and time history of the applied overpressure.

This investigation concerned the response to quasi-static overpressures of small cylindrical structures (4-inch ID) buried with their axes horizontal in dense, dry, 20-30 Ottawa sand.

The first phase of the investigation dealt with non-destructive tests on instrumented cylinders. The program allowed variations in the stiffness of the cylinders, the depth of burial, and the overpressure level.

Destructive tests on non-instrumented cylinders were conducted in the second part of the investigation. The intent was to determine the overpressure required (maximum available, 160 psi) to cause collapse of cylinders of various stiffnesses over as great a range in depth of burial as the maximum overpressure would allow.

Significant experimental investigation into the behavior of small buried cylinders has been conducted by Robinson (1), Bulson (2), and Whitman and Luscher (3).

EXPERIMENTAL PROGRAM

Scope of Investigation

The experimental program was divided into 1) non-destructive testing of instrumented cylinders, and 2) destructive testing of non-instrumented cylinders.

The test cylinders described by Robinson (1) and Bulson (2) varied from very stiff to very flexible (the equivalent aluminum d/t values ranged from 27 to 333). Testing outside of this stiffness range would have involved the problems of handling an impracticably flexible cylinder at one end of the scale and eliciting a measurable response in the range of overpressure (140-psi maximum) at the other end of the scale. For the instrumented cylinders, two d/t values (114 and 250) were chosen to fit conveniently between these two extremes.

*Research Associate Engineer, Air Force Shock Tube Facility, University of New Mexico, Albuquerque, New Mexico.

The program was designed to alleviate somewhat the paucity of information on the effects of variation in depth of burial of the test cylinders. Tests were conducted at as many as eleven different depths, ranging from zero to two cylinder diameters. The maximum overpressure in the non-destructive tests was 140 psi.

The goal of the destructive tests was to determine the collapse overpressure for cylinders of as many stiffnesses and over as great a range in depth of burial as the maximum overpressure would allow. The practical limitation on the maximum overpressure (160 psi) and the great increase in resistance to collapse imparted to a cylinder by burial combined to curtail the extent of destructive testing.

Dense Ottawa sand was used as the surrounding medium in all tests.

Description of Cylinders

All the structures tested were cylinders, 4 inches ID by 16 inches long. The ends of each cylinder were sealed by tight-fitting plates, held apart by an axial rod so that the axial forces on the plates were borne by the rod and not by the cylinder.

Instrumented cylinders of two stiffnesses were used. The stiffer cylinder was a commercially available drawn tube of 6061-T4 aluminum with 0.035-inch wall thickness. The more flexible cylinder was fabricated from 2024-0 aluminum sheet of 0.016-inch thickness, using a 1/4-inch epoxied lap joint. The d/t values of the two types of cylinders were 114 and 250, respectively. The theoretical in-air primary buckling pressure, as given by the equation $p_{cr} = [2E/(1-\nu^2)]\ (t/d)^3$, for these two cylinders is 14.9 and 1.41 psi, respectively (4). The maximum overpressure exceeded these theoretical values by factors of 9.4 and 99.

The cylinders used in the destructive tests were also manufactured from 2024-0 aluminum sheet with thicknesses of 0.010, 0.012, 0.016, 0.020, and 0.025 inches, giving d/t values of 400, 333, 250, 200, and 160, respectively.

Young's modulus for both alloys is 10×10^6 psi. The yield strength, based on 0.2 percent permanent strain, is 16,000 psi for 6061-T4 aluminum and 8,000 psi for 2024-0 aluminum (5).

Test Technique

The cylinders were tested in a horizontal orientation in a bin, 30 inches in diameter and 16 inches deep, containing dense, dry, 20-30 Ottawa sand. The sand was sieved into position by allowing it to fall free through a flexible hose, funnel, and screen (6). The height of fall from the end of the hose to the surface of the sand varied from 12 to 18 inches.

The surface of the sand was maintained as close to horizontal as possible during placement. When the sand reached a required level in the bin, the cylinder to be tested was placed on the sand surface. Care was taken to minimize the generation of failure zones in the sand. The sieving continued until the surface of the sand reached a level 1/4 inch below the top of the bin. The sand adjacent to the invert of the cylinder was deflected into place to maintain a horizontal surface and avoid local shear failures.

An air-tight rubber membrane which extended over the rim of the bin was placed on the sand surface. The top cover plate was then put in position and tightened down. The surcharge, in the form of air pressure on top of the membrane, was applied at about 5 psi per second and then released. The maximum pressure was 160 psi for destructive tests and 140 psi for non-destructive tests. Lower values were used in the testing of the more flexible, instrumented cylinder to avoid its collapse and the destruction of the displacement gauges.

The method of placing a dense sand around a flexible cylinder proved satisfactory. The average unit weight throughout the bin was 113 lb/cu ft (void ratio 0.47). In about half the tests the variation in average unit weight was less than 0.4 lb/cu ft, and in only about ten percent of the tests did it exceed 1 lb/cu ft. Figure 1 shows a plan and elevation of the test bin.

Instrumentation

The response of each instrumented cylinder throughout the loading and unloading cycles was monitored continuously by six electric strain gauges and five electric displacement gauges. Type A-14, wire-wound, paper-back strain gauges manufactured by the Baldwin-Lima-Hamilton Corporation were used. Linear potentiometers, manufactured by both Computer Instruments Corporation and Bourns, Incorporated, were used as displacement gauges. The strain gauges were mounted circumferentially at mid-length of the cylinders on both the inner and outer surfaces at the crown, springline, and invert (Figure 2a). The readings from each set of back-to-back gauges enabled the strain in the wall of the cylinder to be broken into the direct and flexural components. The displacement gauges were installed to register the relative displacement between the cylinder wall and the stiff axial rod supported by the end plates (Figure 2b). Two Dynisco Model 25-1C linear pressure transducers were installed in the cover plate to monitor the overpressure in the non-destructive tests.

The collapse overpressures of the non-instrumented cylinders in the destructive tests were read on a Bourdon gauge. The moment of collapse was marked by a sudden reduction in overpressure and a sharp report. The locations of the pressure transducers and the Bourdon gauge are shown in Figure 1.

Cautionary Remarks

In the testing of small buried structures, there are many sources of error. These include shortcomings in the test technique itself and inevitable errors in the recording and reduction of data.

There is a definite possibility that silo-type arching in the test bin itself may have influenced the behavior of the buried cylinders. In a carefully built apparatus in which total loads at both ends of a rigidly contained column of dense, 20-30 Ottawa sand were measured hydraulically, Abbott (7) reported measuring only about 85 percent of the applied load when the height/diameter value of the sand was 0.315. In the writer's investigation, the ratio between the maximum cover over the test cylinders and the diameter of the test bin was only 0.267. Hence, it is unlikely that silo effects distorted the trends in the data.

It is recognized that a cylinder length/diameter value of four would inhibit the development of the in-air primary buckling mode. However, the end restraints play a smaller and smaller role as the order of the buckling mode increases.

In addition, there are inevitable errors in the calibration of gauges and in the processing of data. Reduced data, from tests conducted under supposedly identical conditions, which differ by less than 20 percent are considered satisfactory. The reader should bear this in mind when terms like "constant" and "linear" are used in connection with the data.

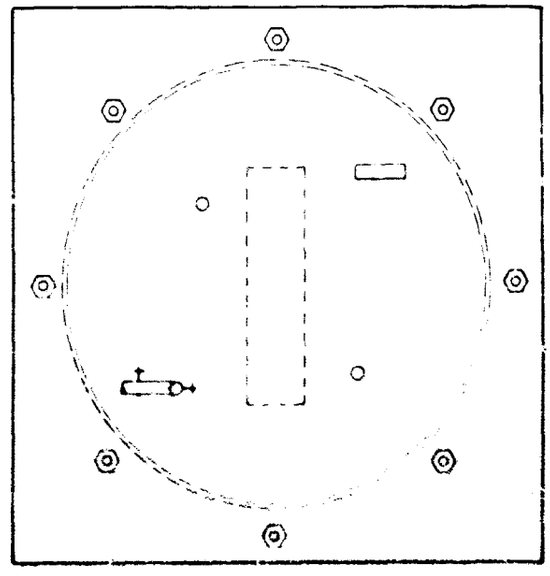
The possibility of obtaining a theoretical solution to the problem of the buried cylinder, based on realistic assumptions, is extremely remote. A theoretical analysis of the arching around a movable, rigid trapdoor has been made, assuming constant-volume plastic flow (Bedesem, et al (8)). An analysis of the arching in a dilatant sand around a flexible cylinder with an incompatibility of strain at the sand-cylinder interface would be much more complex and has not been attempted.

DATA

Data from the tests on instrumented cylinders were obtained in the form of traces of gauge output versus time on Polaroid pictures. The sweep speed was 5 sec/cm. The vertical grid lines on the pictures corresponded to the same times in any one test. No time lag between the application or release of pressure, as recorded by the pressure gauges, and the response of any displacement or strain gauge could be detected. It was thus possible to line up the pressure-time traces with the gauge output-time traces and read the output of the gauges at any desired overpressure level. Overpressure levels of 10, 30, 50, 100, and 140 psi (the maximum value) were chosen arbitrarily for the portrayal of the data. Figure 3 shows the manner in which the gauge data were correlated with the pressure-time traces.

The deflections (δ) and the depths of cover (c) were normalized by dividing by the diameter of the structure (d). The normalized deflection was then expressed as a percentage. In the majority of cases at least three tests were conducted at each depth of burial. Only the average value from each depth was plotted.

An effort was made to avoid the inclusion of many similar plots; those presented were selected to illustrate behavior of cylinders at both deep and



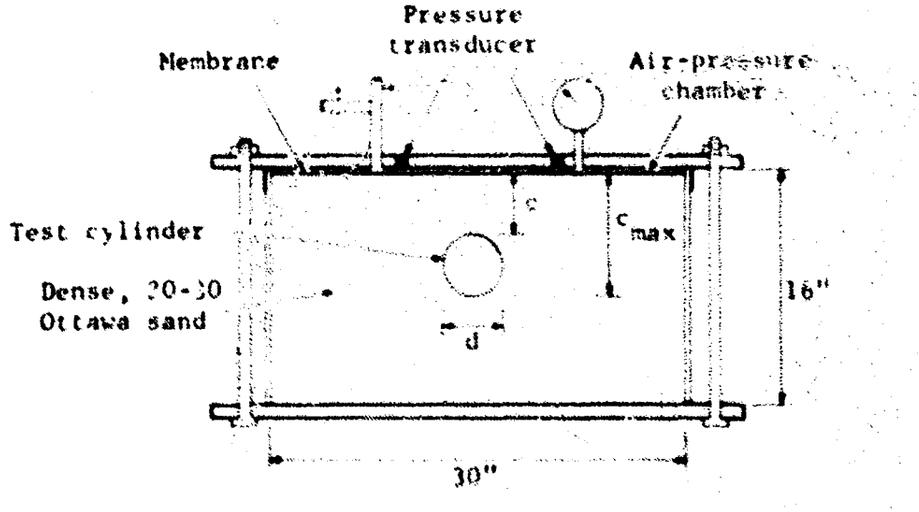


Fig. 1 Plan and Elevation of Test Bin

shallow burial. In this paper a cylinder is considered to be deeply buried when the observed phenomena are independent of or, at least, vary little with c/d in the overpressure range tested. A cylinder is considered to be buried at shallow depth when the observed phenomena vary considerably with c/d in the overpressure range tested. These definitions proved satisfactory, as the distinction was quite sharp. It was best exemplified by the displacements and strains at the crown (Figures 4a and 5).

Tests were not conducted on the more flexible, instrumented cylinder at small c/d values lest collapse of the cylinder and damage to the displacement gauges occur.

It will be observed that occasionally some data points are missing from the figures. This is due to the fact that the signals on the Polaroid pictures, for some reason, were unintelligible.

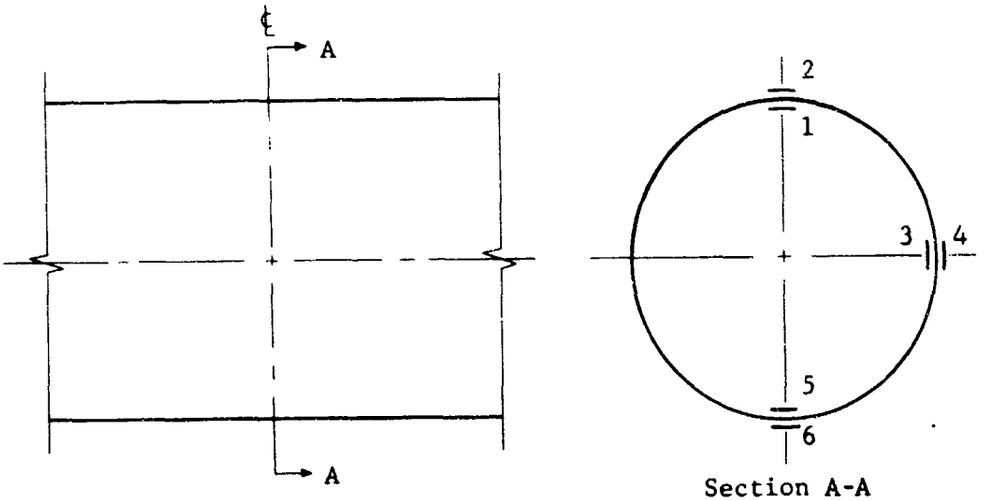
Stiff, Instrumented Cylinder (d/t = 114)

Displacements. Plots of the normalized radial displacement (δ/d) versus c/d are presented in Figure 4 for each of five overpressure levels.

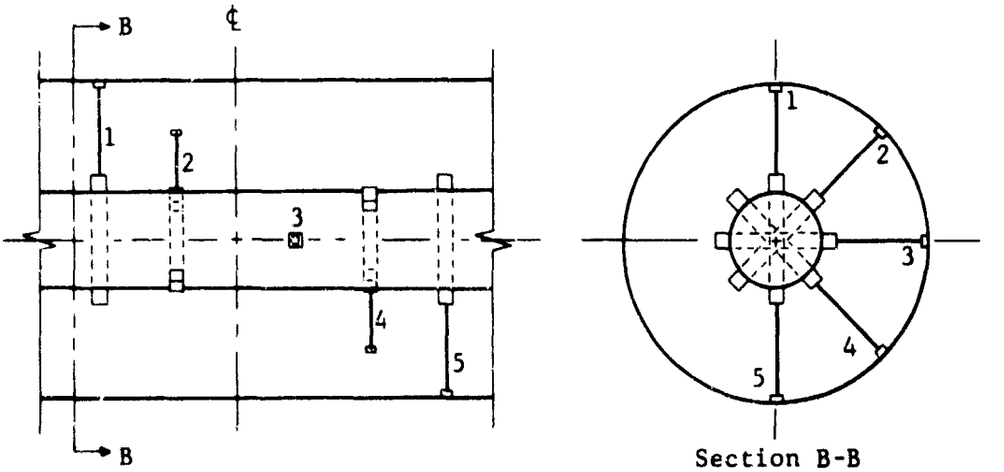
The displacements at the crown showed an essentially constant inward movement of the cylinder with depth, except for a sharp increase at small c/d values (Figure 4a). The c/d value at which this change in behavior took place increased with the overpressure. At the lowest value of 10 psi, no change in behavior with c/d is exhibited; and at the highest value of 140 psi, the change takes place at a c/d value of about 1/2.

Displacement gauge 2, inclined at 45° above the horizontal, registered an inward displacement which remained constant with depth for each overpressure level when c/d was equal to or exceeded 1/2 (Figure 4b). At smaller c/d values, the output of the gauge decreased and actually reversed sign at the higher overpressure levels. Two points are worthy of mention regarding this change in behavior. First, the c/d value at which the change took place appears to be independent of overpressure, at least in the range of overpressure considered. Second, both the inward displacement, when c/d was equal to or greater than 1/2, and the outward displacement, when c/d was less than about 5/16, increased in magnitude with overpressure.

Displacement gauge 3 monitored the movement at the springline. The response curves indicate an outward displacement at all times (Figure 4c). At the lower overpressure levels, the output of the gauge proved insensitive to c/d. However,



(a) Strain gauges



(b) Displacement gauges

Fig. 2 Arrangement of Gauges

at the maximum overpressure level of 140 psi, the o. tward movement increased significantly as c/d was reduced from 2 to 1/4. No tests were conducted at lower c/d values for this overpressure.

Figure 4d shows plots of the data from displacement gauge 4 which was inclined 45° below the horizontal. For all practical purposes it can be said that the radial displacements were outward and constant with depth for each overpressure level when c/d exceeded a certain value. This value increased with the overpressure. At low c/d values the output of the gauge decreased. At c/d equal to zero and for an overpressure of 100 psi, the displacement reversed sign. There are indications that still greater inward displacements would have occurred at higher overpressure levels.

The deflections at the invert were inward and increased in a linear manner for all overpressure levels as c/d was reduced to 1/8 (Figure 4e). At smaller c/d values, a sharp reduction in output of the gauge took place. This behavior is documented by two tests at c/d equal to 1/16 and three tests at c/d equal to zero.

Strains. Figures 5 to 7 present the strain-gauge data.

The curves in Figures 5a and 5b show the variations in strain on the interior and exterior surfaces with respect to c/d for five overpressure levels. Three facts can be noted from these plots. First, relatively large strains were recorded at low c/d values. These strains were tensile on the interior surface and compressive on the exterior surface. Second, the response of both gauges was essentially independent of the cover when c/d exceeded a value of about 1/2. In this range of c/d, the strains on the interior surface were tensile at low overpressures but compressive at the higher levels. Third, the c/d value at which the change in behavior took place increased with the overpressure and may be as large as 5/8 for the strain on the exterior surface at 140 psi overpressure.

Figures 5c and 5d show the direct and flexural components of strain at the crown plotted against c/d. The comments about the total strains can be applied equally well to the components of strain. The flexural strains increased significantly as c/d was reduced to low values.

Figure 6 shows plots of the strain-gauge data at the springline. The data are somewhat erratic, but some trends are evident. As was the case with the displacements along a horizontal radius (Figure 4c), neither the total strains nor the components of strain proved sensitive to c/d. This is significant in that the direct strain at the springline is indicative of the vertical load on the cylinder. The direct compressive strains in Figure 6c indicate that somewhat less than 50 percent of the applied overpressure was carried by the cylinder. The flexural strains are of the order of one-half the direct strains. However, Figure 6d indicates that at higher overpressures and low c/d values the flexural strain might increase significantly.

The strains at the invert were monitored by strain gauges 5 and 6, and the data were plotted in Figure 7. No significance should be attached to the fact that the curves of strain versus c/d are [illegible]s. The origin of this effect probably lies in inevitable variations in the seating of the cylinder. Little tendency toward a sudden increase in total strain or components of strain at low c/d values is exhibited by the curves. The flexural strains exceeded the direct strains by a factor of about two.

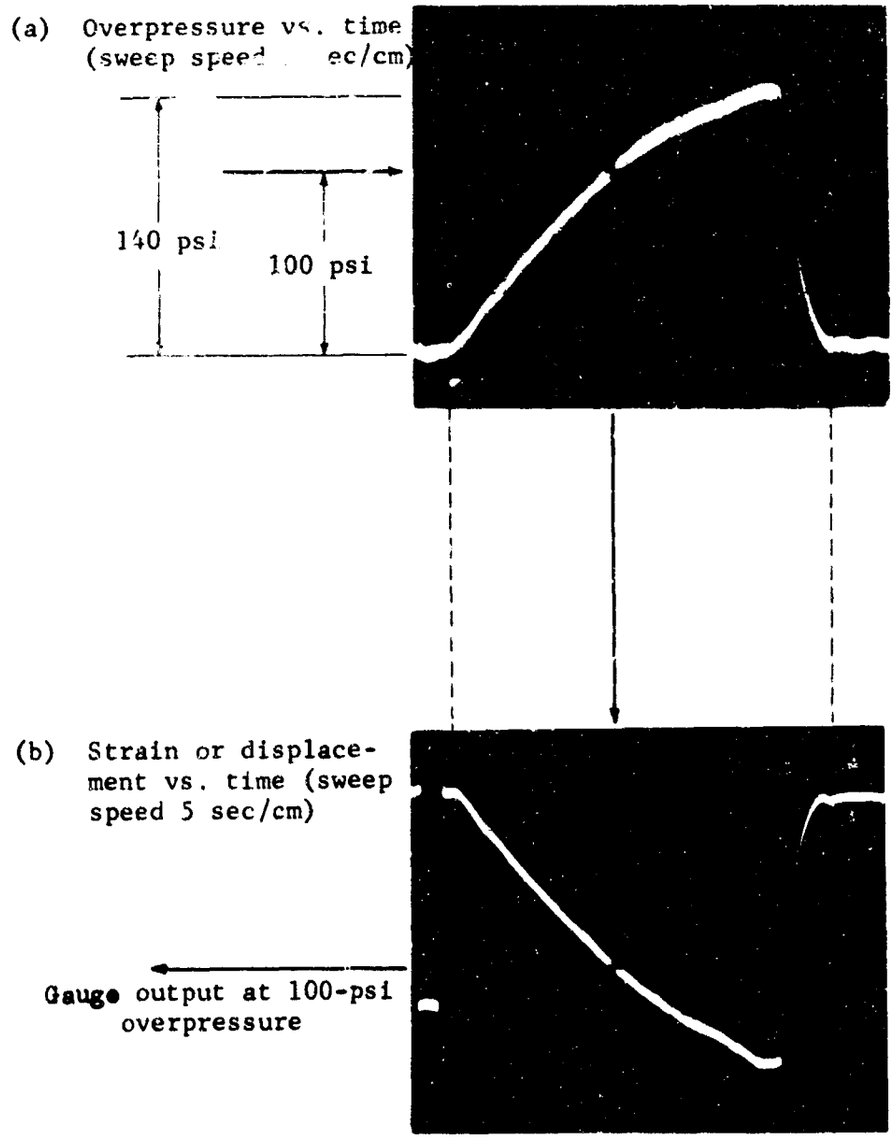


Fig. 3 Correlation of Gauge Output with Overpressure

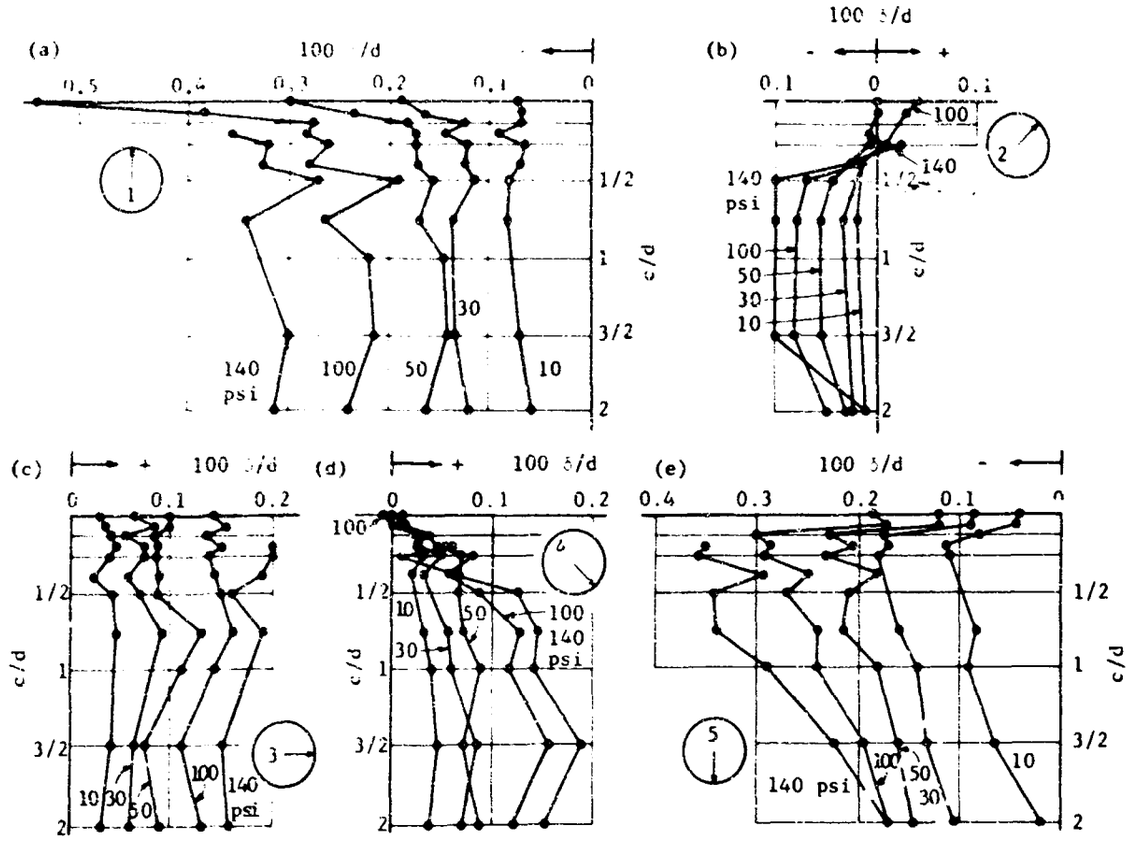


Fig. 4 Normalized Radial Displacements (d/t = 114)

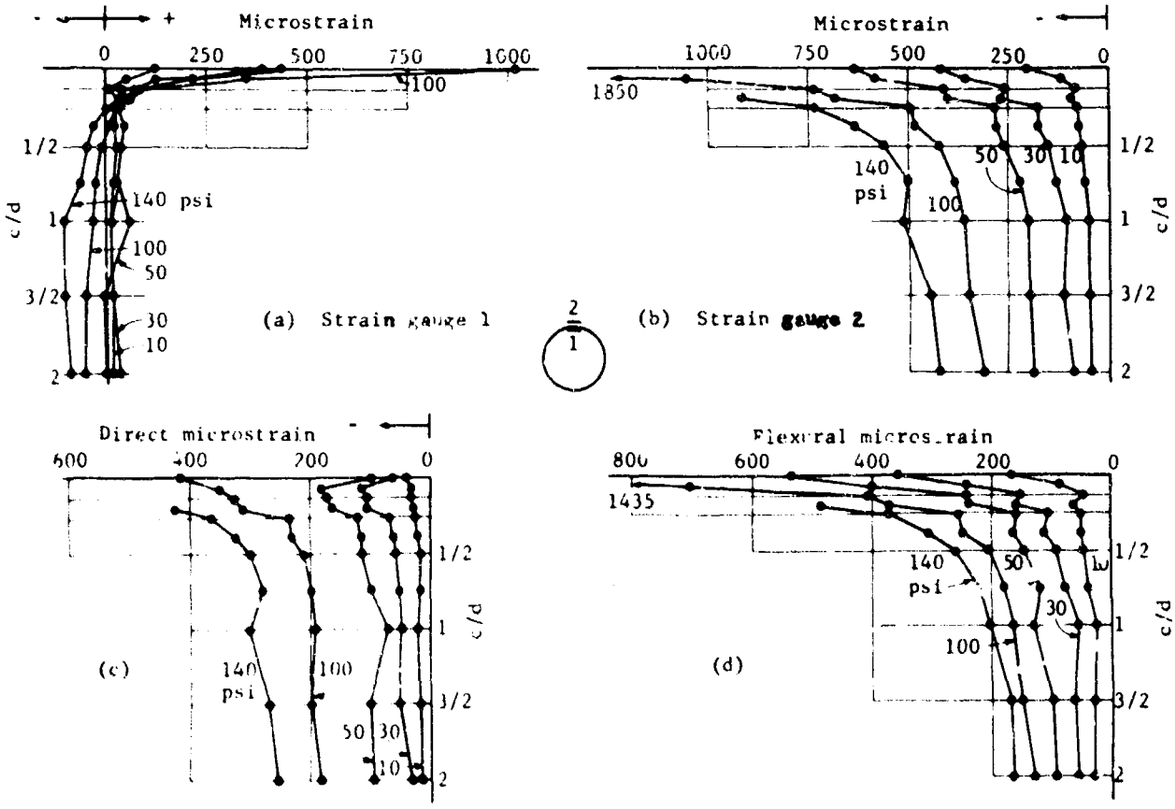


Fig. 5 Strains at Crown (d/t = 114)

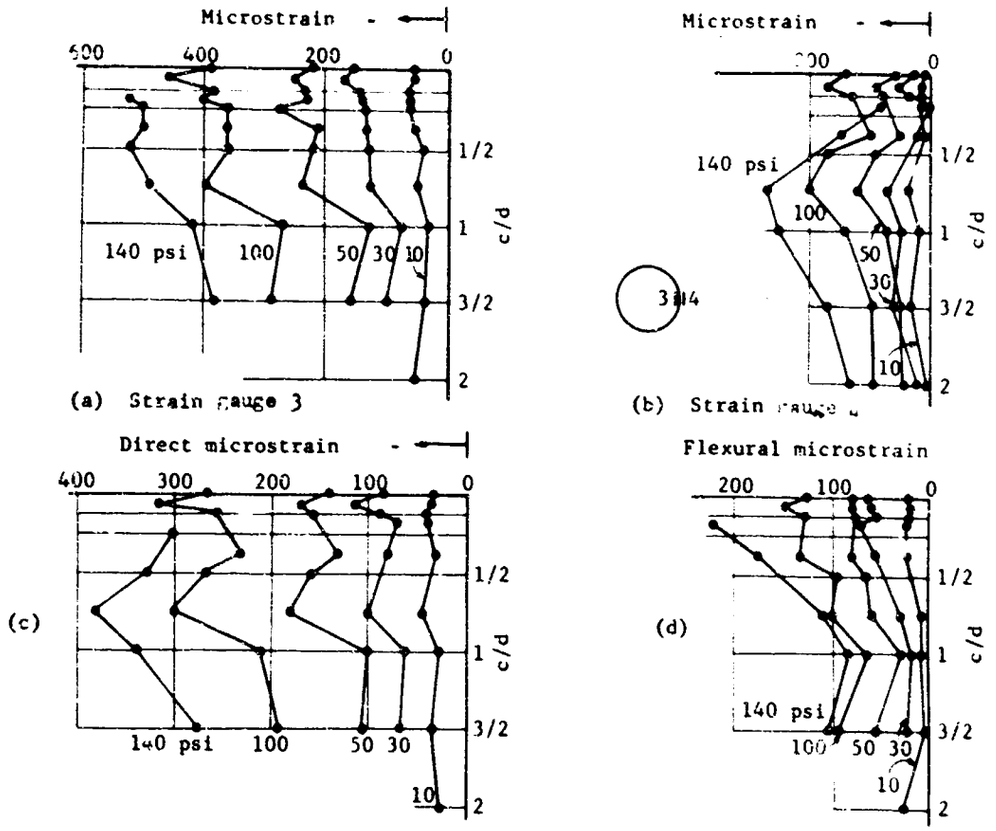


Fig. 6 Strains at Springline (d/t = 114)

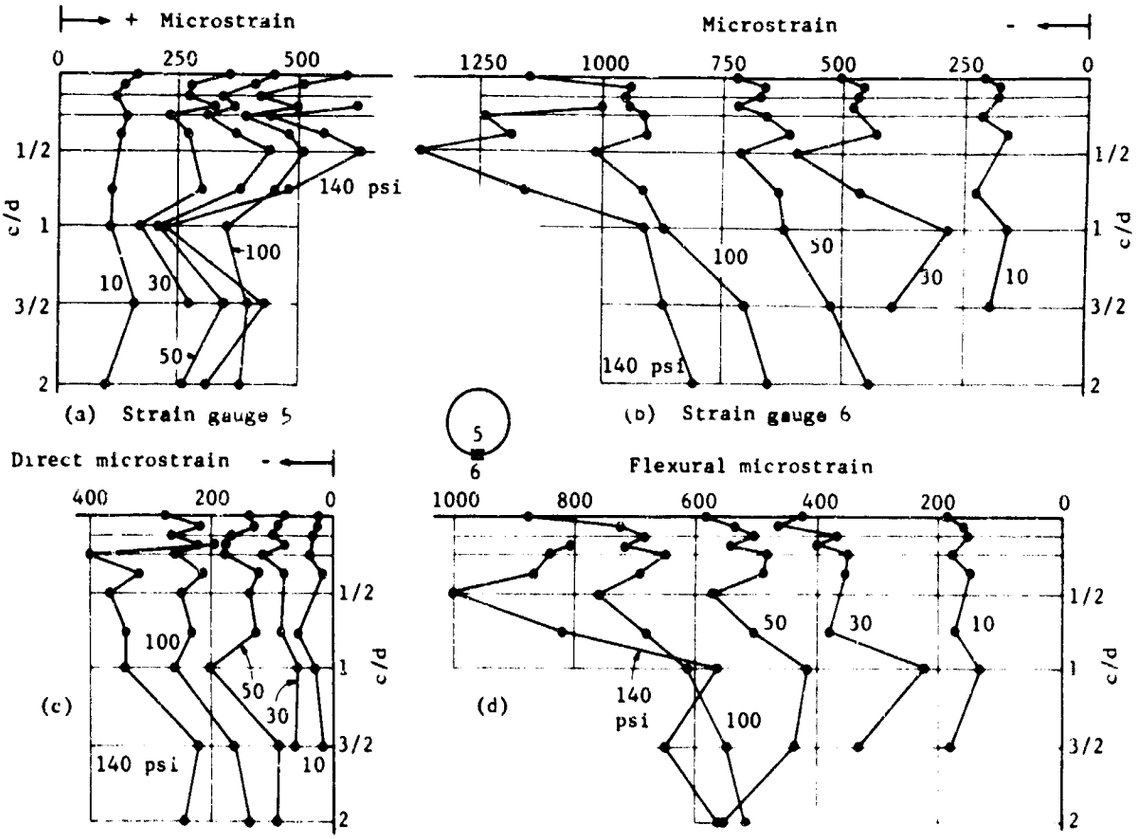


Fig. 7 Strains at Invert (d/t = 114)

General Behavior. In assessing the overall behavior of the cylinder, it was helpful to bear in mind the mode of failure in the destructive tests. Collapse in these tests was found to be initiated by snap-through at the crown. This fact is stated explicitly for two reasons. First, the very flexible cylinders tested by Bulson (2) first showed distress in the vicinity of the invert. Second, in dynamic tests at the Air Force Shock Tube Facility, in which identical buried cylinders were subjected to plane wave loading, collapse was found to take place at the invert.

There is no doubt that more information on the displacements and strains in the quasi-static test cylinders would help in establishing their overall behavior. However, some significant observations can still be made.

Figure 8 shows the normalized displacement, direct strain, and flexural strain for a deeply buried cylinder (c/d = 3/4). The displacements at the crown and invert were inward. The deflections at the springline were outward and smaller in magnitude than those at the crown. On the radii, inclined 45° above and below the horizontal, the deflections were inward and outward, respectively. The magnitude of the displacement at each of the five gauge locations increased with the overpressure.

The direct strain varied little between the three gauge locations and, bearing in mind the inherent spread in data of this type, could be considered constant. A tendency toward a somewhat greater direct strain at the springline than at either of the other two stations can be seen, especially at the higher overpressure levels.

The flexural strains were least at the springline, larger by a factor of about two at the crown, and larger still at the invert. Those at the invert exceeded those at the crown by a factor of about four. This means that the flexural strains at the invert exceeded those at the springline by a factor of seven or eight. Even though the deflections at the crown and invert were of the same order of magnitude, the curvature was greater at the invert, thus accounting for the larger flexural strains.

Similar data for a case of shallow burial (c/d = 1/16) are presented in Figure 9.

The displacements at the crown were larger than for the deeply buried cylinder (Figure 4a). The displacements at the springline remained essentially unchanged (Figure 4c). The displacements, on a radius inclined 45° above the horizontal, were zero for the lower overpressures and outward for the 100 psi overpressure level. The outward movement is indicative of the formation of a mode of relatively high order in the vicinity of the crown. Figure 4b indicates that the outward displacements would be even greater at 140 psi overpressure, provided, of course, collapse did not occur.

The deflections on an inclination 45° below the horizontal were outward but smaller in magnitude than the corresponding values for a deeply buried cylinder (Figure 8). Furthermore, as the overpressure was increased, the magnitude of the movement increased when the cylinder was deeply buried, but decreased when buried at shallow depth.

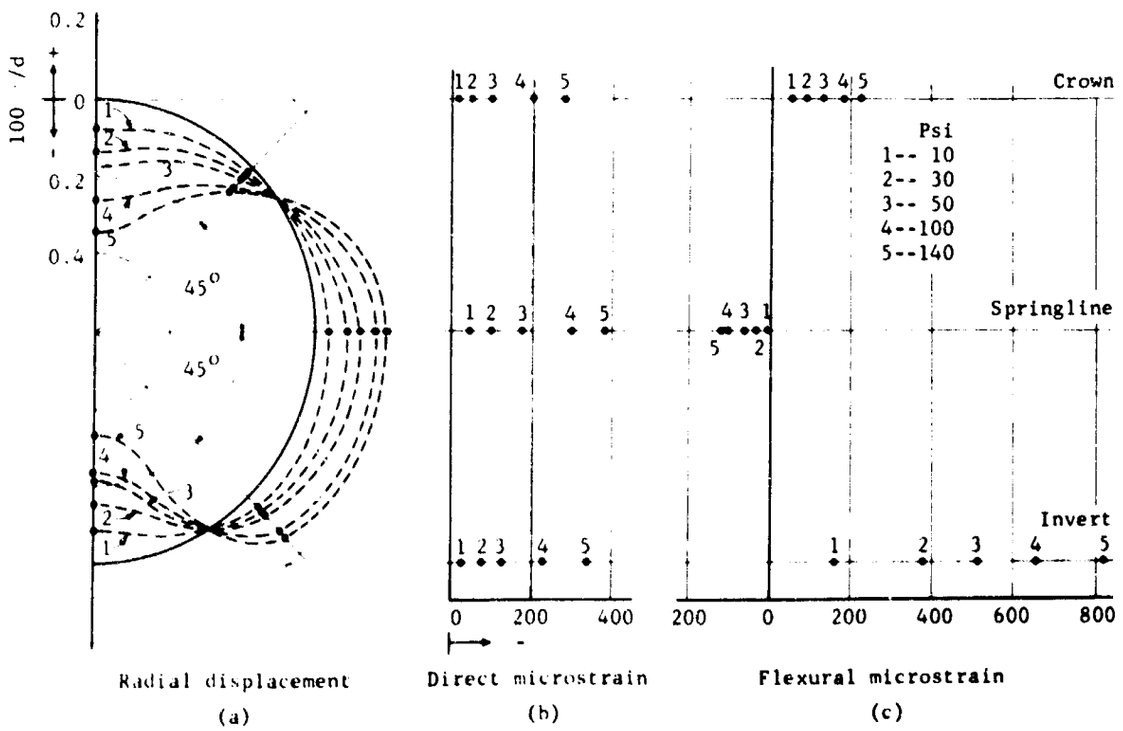


Fig. 8 Normalized Radial Displacement, Direct Strain, and Flexural Strain (d/t = 114, c/d = 3/4)

Figure 4d indicates that an inward movement would have taken place at this cover (c/d = 1/16) if higher overpressures had been used. Again, this would be dependent upon the cylinder remaining intact. At the invert the displacements were inward and also of smaller magnitude than when the cylinder was deeply buried.

Two observations are worthy of note from Figures 9b and 9c. First, the magnitudes of the direct strains and flexural strains at the springline and invert were essentially the same for shallow as for deep burial. Second, a large increase in the flexural component and a somewhat smaller though significant increase in the direct component of strain took place at the crown. The flexural strain increased by a factor of two at 10 psi overpressure and by a factor of four at 100 psi overpressure. An increase of 75 percent in the direct strain at 100 psi overpressure was recorded.

Figure 10 affords a comparison at an overpressure level of 100 psi between the displacements and components of strain in a deeply buried cylinder (c/d = 3/4) and in a cylinder at shallow depth (c/d = 1/16). The deflection diagram in Figure 10a shows the increase in the order of the deflection mode in the neighborhood of the crown, as c/d was reduced. Curiously, the reverse took place at the invert. Since collapse in this series of quasi-static tests has been found to be precipitated by snap-through at the crown, the deflections of the lower portion of the cylinder probably had little influence on the collapse overpressure.

Figure 10b indicates that the direct strain at the crown increased about 75 percent while that at the springline and invert remained unchanged when c/d was reduced from 3/4 to 1/16.

The flexural strain (Figure 10c) showed an insignificant increase at the invert, a 50 percent increase at the springline, but a four-fold increase at the crown where c/d was reduced from 3/4 to 1/16. It can be seen in Figure 5d that the flexural strain at the crown increased two-fold at 100 psi overpressure when c/d was reduced from 1/16 to zero. Thus, at this overpressure, the flexural strain at the crown varied by a factor of at least eight over the range in c/d. The indications from Figure 5d are that this factor would be even larger at greater overpressures.

Flexible, Instrumented Cylinder (d/t = 250)

Displacements. The normalized radial displacement (δ/d) was plotted versus c/d in Figure 11 for each of five overpressure levels.

In the range of c/d tested, the displacements at the crown increased linearly as the cover was reduced (Figure 11a). No tendency toward a sharp increase in deflection was detected in the range of overpressure tested.

The displacements, along a radius inclined 45° above the horizontal, were plotted in Figure 11b. All movement was inward. A reduction in the magnitude of this movement, similar to the behavior of the stiffer cylinder (Figure 4b), took place when c/d was less than one.

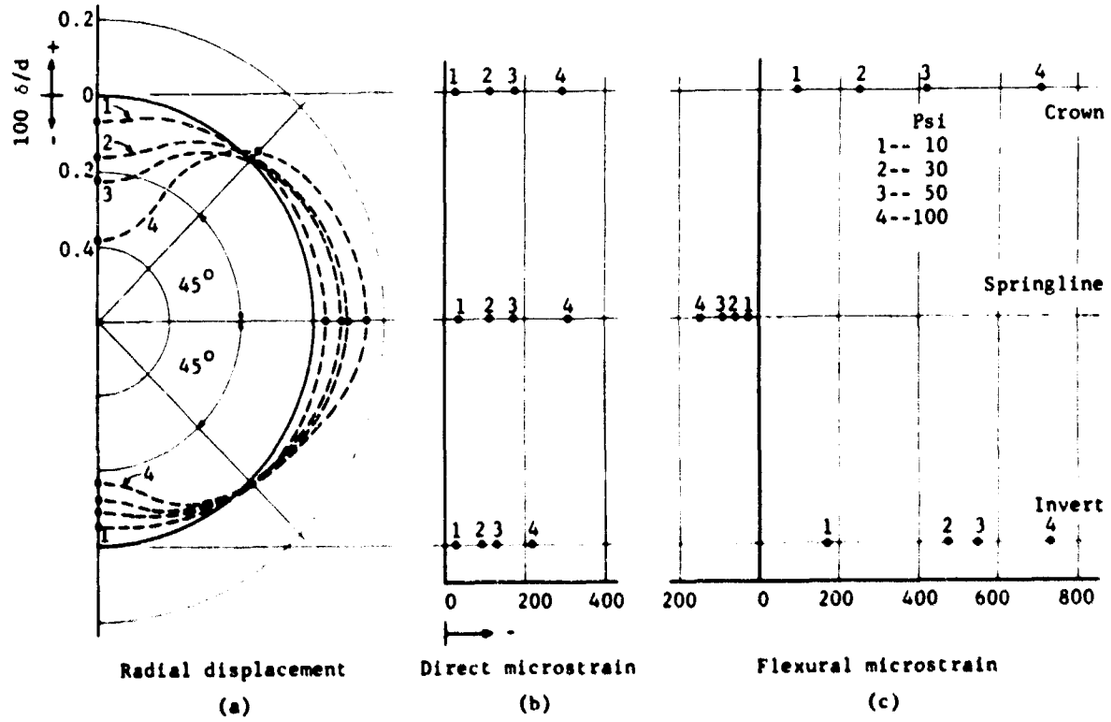


Fig. 9 Normalized Radial Displacement, Direct Strain, and Flexural Strain (d/t = 114, c/d = 1/16)

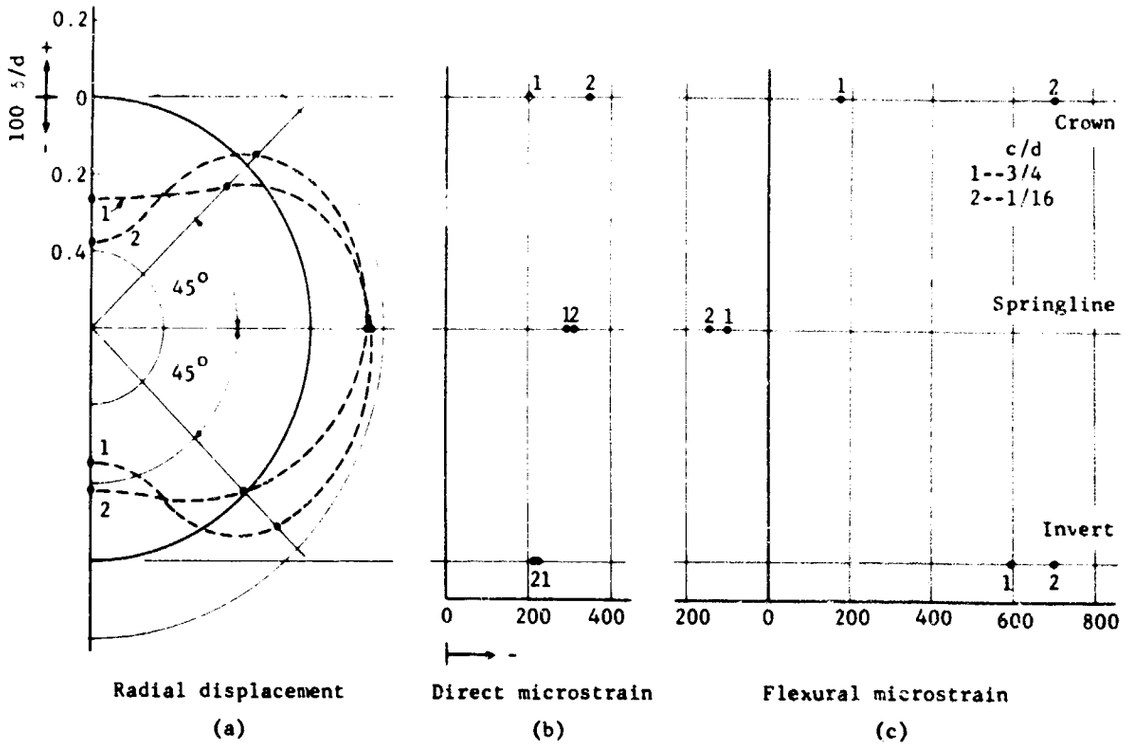


Fig. 10 Normalized Radial Displacement, Direct Strain, and Flexural Strain at 100 psi Overpressure (d/t = 114)

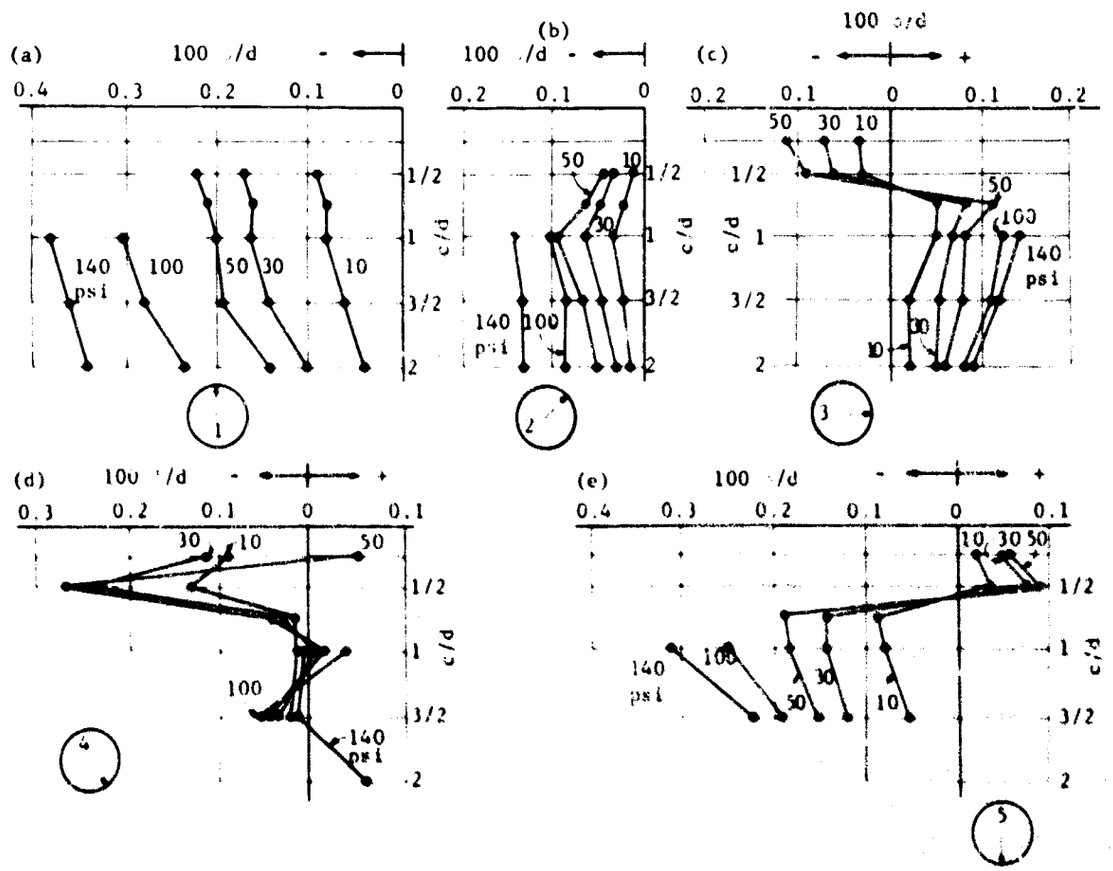


Fig. 11 Normalized Radial Displacements (d/t = 250)

In Figure 11c the displacements at the springline were plotted. The outward movement at the springline increased linearly as c/d was reduced from 2 to 3/4. At the latter value, a sudden reduction in output of the gauge took place. When c/d equaled about 5/8, zero displacement was recorded for all three overpressure levels tested. At all smaller c/d values, the gauge recorded inward movement of the cylinder. At a c/d value of 1/2, the magnitude of the inward movement was almost as great as that of the outward movement at a c/d value of 3/4. Still greater inward deflections of the cylinder were recorded when c/d equaled 1/4. No tests were conducted on cylinders of this stiffness (d/t = 250) at shallower cover. It can be seen from Figure 11c that, regardless of sign, the magnitude of the movement increased with the overpressure. These inward displacements at the springline are considered of great significance and will be discussed later.

The displacements, along a radius inclined 45° below the horizontal, were plotted in Figure 11d. The data are erratic and do not follow any pattern.

The displacement data from the invert were plotted in Figure 11e. The displacements were inward and increased for all overpressure levels when c/d was reduced from 3/2 to 3/4. At c/d values less than 3/4, a sudden reversal in sign took place; and outward movements were recorded. The significance of this behavior is not understood. It will be recalled that, for the same gauge location in the more rigid cylinder, a sudden reduction in inward displacement but no reversal in sign took place at small c/d values (Figure 4e).

Strains. The strain-gauge data are presented in Figure 12. These data are very erratic. The explanation advanced is that local buckling developed in a random manner in the very flexible cylindrical shell and resulted in spurious strains. The data are not conducive to detailed discussion, but some pertinent remarks may be made.

The interior strain gauge at the crown recorded tensile strains when c/d was less than about 1 (Figure 12a).

The output of the interior strain gauge at the springline (Figure 12c) proved very similar to that of the corresponding gauge on the stiffer cylinder (Figure 6a). The tensile strains, recorded by the exterior strain gauge at the springline when c/d was less than 3/4 (Figure 12d), are not consistent with the inward movement at the springline shown in Figure 11c. Assuming both sets of data are correct, this can be accounted for only by postulating the occurrence of local buckling.

The capricious nature of the strains at the invert is not entirely unexpected. Bulson (2) found that for very flexible cylinders it was the invert which first showed distress under load. Furthermore, irregularities in the density of the sand may have occurred near the invert.

General Behavior. To emphasize the significance of the inward movement at the springline at small c/d values (Figure 11c), two deflected shapes were drawn in Figure 13. Both correspond to an overpressure of 50 psi, but one is for deep burial (c/d = 3/4), and the other is for shallow burial (c/d = 1/2). The distinction is based on the change in behavior at the springline.

The deeply buried cylinder deflected in a low-order mode. Displacements were inward and of about equal magnitude at the crown and invert.

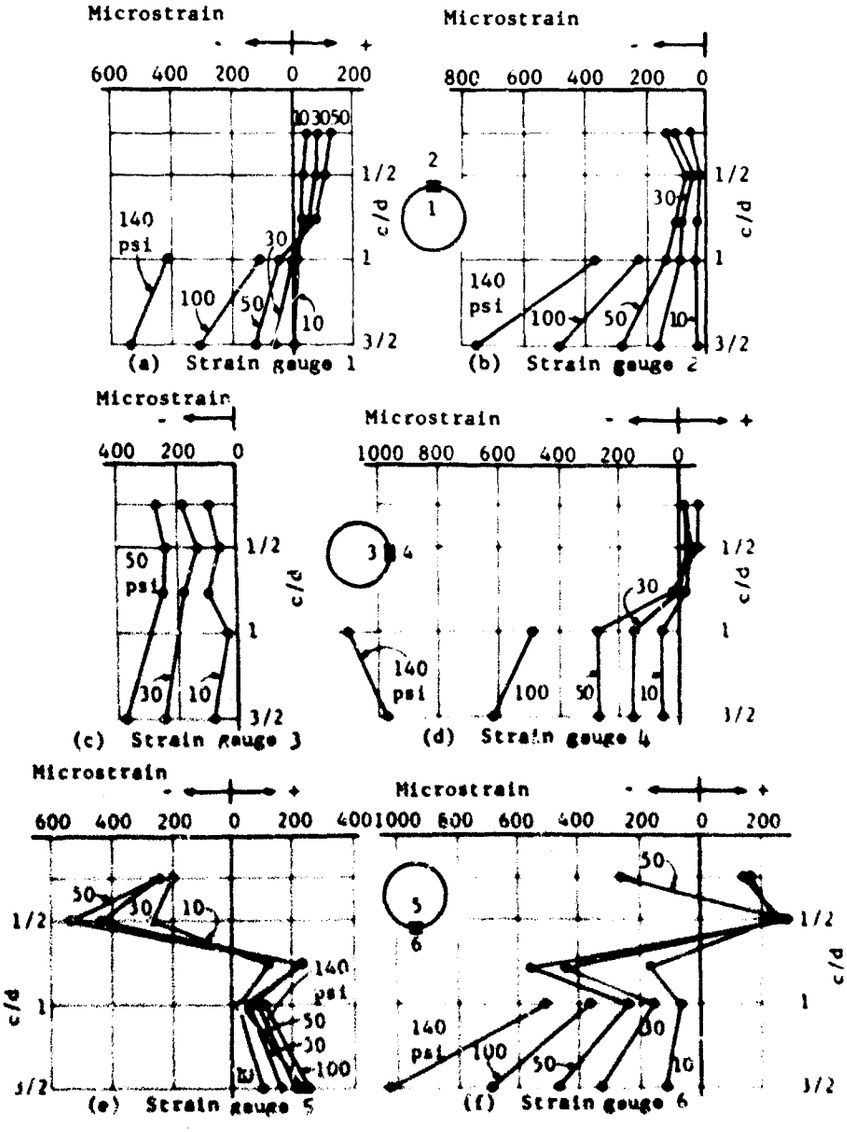


Fig. 12 Strains (d/t = 250)

At the springline, displacements were outward and equal in magnitude to about one-half of those at the crown. The movements along radii inclined 45° above and below the horizontal were both inward and equal in magnitude to about one-quarter of those at the crown.

The cylinder at the shallower cover assumed a high-order mode, at least near the crown. This is manifested by the fact that the inward movement at the crown was greater, while the inward movement along a radius inclined 45° above the horizontal was less, than the corresponding deflections in the deeply buried cylinder. At the springline, the inward displacement at shallow burial was about equal in magnitude to the outward displacement at deep burial. Furthermore, this inward displacement increased still more when c/d was reduced from 1/2 to 1/4 (Figure 11c). On a radius inclined 45° below the horizontal, the inward displacement was very large, exceeding the corresponding value at deep burial by a factor of more than six. The displacement was, curiously, outward at the invert. The reason for this is not understood. With the exception of this outward reading at the invert, all other displacement gauges recorded an inward movement of the cylinder at shallow burial.

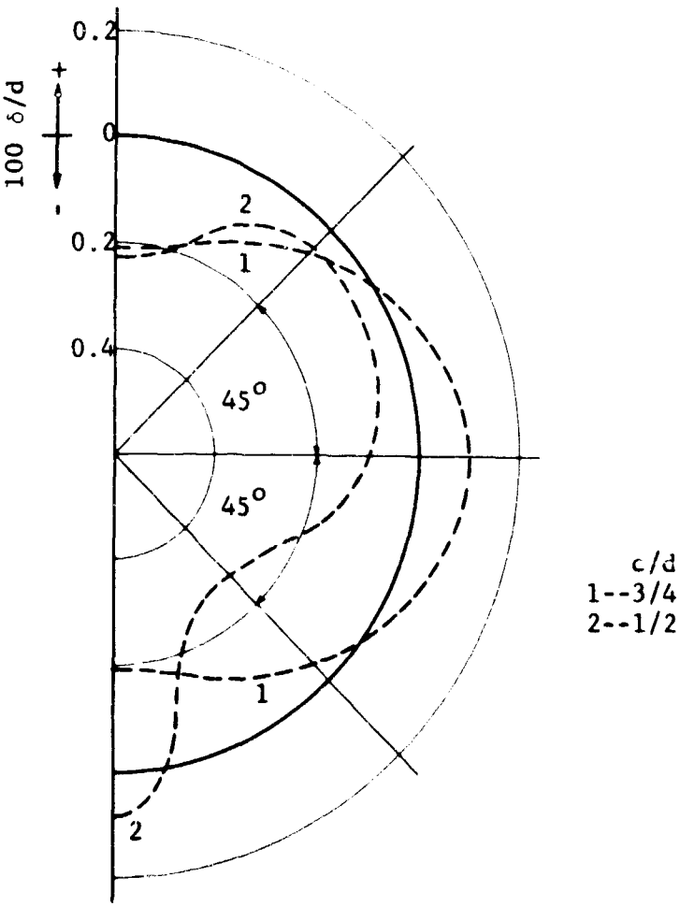


Fig. 13 Normalized Radial Displacement at 50 psi Overpressure (d/t = 250)

Comparison of Stiff and Flexible, Instrumented Cylinders

In spite of a lack of experimental data for the more flexible cylinder at small c/d values, a comparison between cylinders of both stiffnesses shows many similarities and some differences.

The deflected shapes of both cylinders for different conditions of burial are shown on the same diagrams in Figure 14. The data in both diagrams correspond to the same overpressure of 50 psi.

Figure 14a shows the displacements at a c/d value of 3/2. Both cylinders deflected outward about an equal amount at the springline. However, it is seen that the more flexible cylinder assumed a "flatter" shape, indicating a higher level of distress.

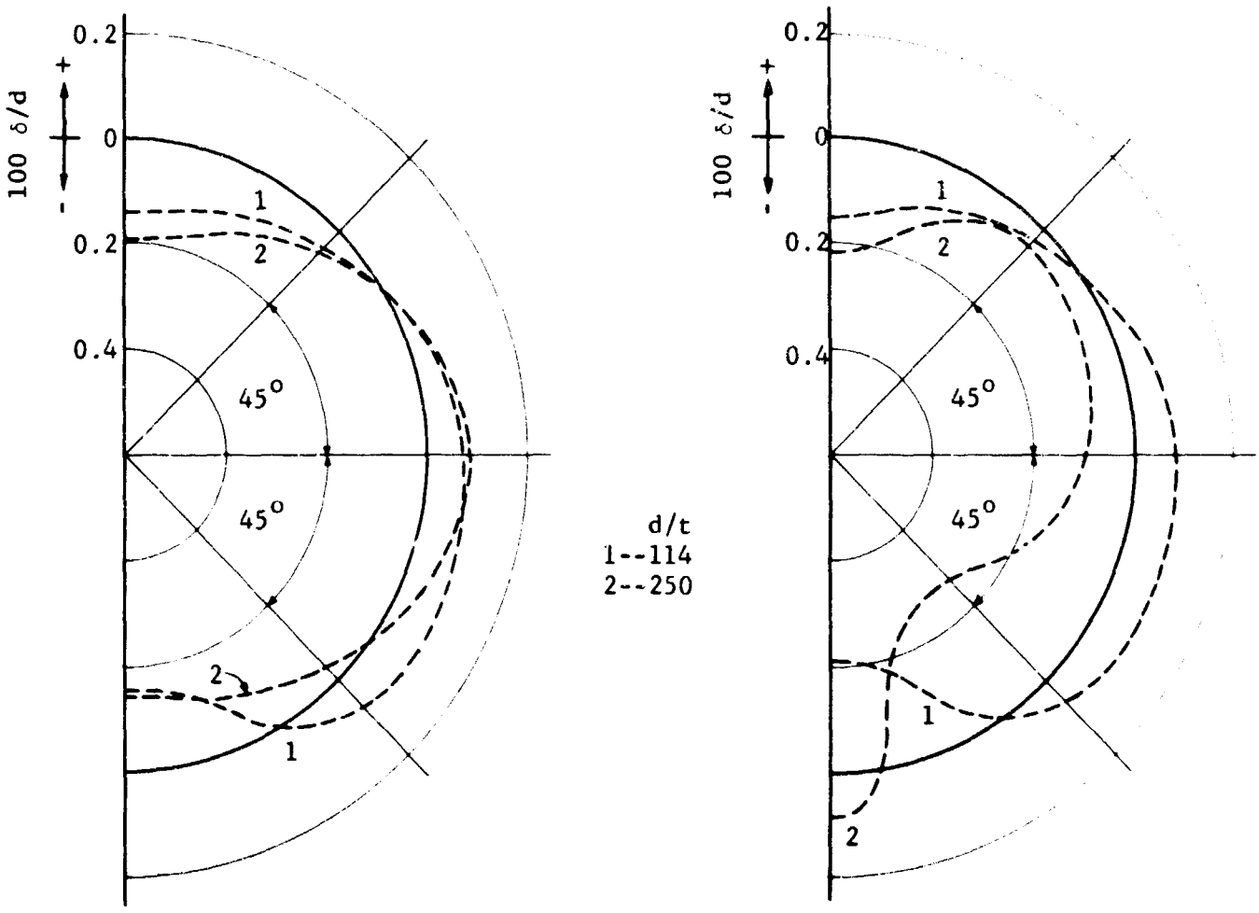
When c/d was reduced to 1/2 (Figure 14b), the stiffer cylinder showed little change. But the level of distress in the more flexible cylinder became much greater. The inward deflection at the crown increased; the outward deflection at the springline (c/d = 3/2) gave way to an inward deflection of about the same magnitude; and a very large inward deflection took place on a radius inclined 45° below the horizontal. Allusion has already been made to the outward movement of this cylinder (c/d = 1/2) at the invert. It probably would have little effect on the resistance of the upper portion of the cylinder to snap-through.

The deflected shapes in Figure 14b portray the different kinds of behavior at the springline for the two cylinders at the same overpressure and depth of burial.

A comparison between the behavior of the two cylinders at nearly the same multiple of their respective theoretical in-air primary buckling pressures can be made by comparing the response of the stiffer cylinder (d/t = 114) at 140 psi overpressure (9.4 p_{cr}) to the response of the more flexible one (d/t = 250) at 10 psi overpressure (7.1 p_{cr}). From Figures 4a and 11a it can be seen that the inward movement at the crown in the stiffer cylinder is several times greater than the corresponding movement in the more flexible one. The same is true of the inward movement on a radius inclined 45° above the horizontal (Figures 4b and 11b) and the outward movement at the springline (Figures 4c and 11c).

For the more rigid cylinder (d/t = 114), the first indication of a significant change in behavior as the cover was reduced was provided by displacement gauge 2 (Figure 4b). This gauge was inclined 45° above the horizontal. The change in behavior took place when c/d equaled 1/2 for all overpressure levels.

The displacement and strain gauges at the crown also exhibited a change in output as the cover was reduced (Figures 4 and 5). The c/d values at which these changes occurred were not always well defined; however, the greater the overpressure, the greater this c/d value. These c/d values separate zones of shallow and deep burial. The phenomenon is best illustrated by the displacements (Figure 4a), the strains on the exterior surface (Figure 5b), and the flexural component of strain (Figure 5d). A c/d value of 1/2 is again associated with the minimum value for deep burial at 140 psi



(a) c/d = 3/2 (b) c/d = 1/2

Fig. 14 Normalized Radial Displacement at 50 psi Overpressure (d/t = 114 and 250)

overpressure. Whether this value increases at higher overpressure levels is, considering the available data, subject to conjecture. No curve separating deep from shallow burial is evident from the strains on the interior surface (Figure 5a), probably because these strains represent the superposition of two components of unlike sign.

It is not possible from available data to delineate zones of deep and shallow burial for the more flexible cylinder (d/t = 250). However, this cylinder exhibited changes in behavior at depths greater than the c/d value of 1/2 associated with the more rigid cylinder. The curves of displacements at the springline and invert break sharply at a c/d value of 3/4 (Figures 11c and 11e).

Destructive Tests, Non-Instrumented Cylinders

Table 1 presents the results of the destructive tests on non-instrumented cylinders. It shows the six convenient d/t values selected for testing, the theoretical in-air primary buckling pressure (p_{cr}) of each, and the experimental collapse overpressure at three c/d values. The experimental values are also stated in multiples of p_{cr}. Within the maximum available overpressure (160 psi), only four cylinders could be collapsed even at zero cover, and not even the most flexible could be collapsed when c/d exceeded 1/8. The maximum overpressure was 470 times the theoretical in-air primary buckling pressure of the most flexible cylinder.

As expected, the overpressure required to cause collapse at a particular c/d value increased with depth of burial. However, it was the large increase in the experimental collapse overpressure for any one cylinder, when c/d was increased from zero to 1/16, that proved most interesting.

The more flexible the cylinder, the greater was the ratio between the experimental collapse overpressure and the theoretical in-air primary buckling pressure. A cylinder with a d/t value of 400 collapsed at an overpressure of 265 p_{cr} when c/d was 1/8. At the same depth of burial, a cylinder whose d/t was 250 collapsed at 97 p_{cr}.

Table 1

Results of Destructive Tests

Cylinder Stiffness (d/t)	Theoretical In-Air Primary Buckling Pressure, $p_{cr} = \left(\frac{2E}{1 - \nu^2}\right)\left(\frac{t}{d}\right)^3$ (psi)	Experimental Collapse Overpressure (psi)			
		c/d = zero	c/d = 1/16	c/d = 1/8	c/d = 1/4
400	0.34	12 (35 p_{cr})	42 (124 p_{cr})	90 (265 p_{cr})	--
333	0.59	18 (31 p_{cr})	84 (142 p_{cr})	152 (257 p_{cr})	--
250	1.41	28 (20 p_{cr})	133 (94 p_{cr})	137 (97 p_{cr})	--
200	2.75	40 (15 p_{cr})	140 (51 p_{cr})	--	--
160	5.37	--	--	--	--

It is not possible to determine from the small amount of data available if zones of shallow burial and deep burial for cylinders of various stiffnesses can be established from destructive tests.

It is worthy of note that in the stiffer instrumented cylinder (d/t = 114), very large strains were recorded at the crown at 100 psi overpressure and zero cover (Figure 5b). Yet collapse could not be induced at 160 psi overpressure and the same condition of burial.

CONCLUSIONS

The following conclusions are drawn from the results of this experimental investigation:

1. The increase in the resistance to collapse of cylinders by burial in dense sand was demonstrated. The existence of very large strains does not imply the imminence of collapse.
2. The overpressure required to cause collapse, as measured in destructive tests over a very small range in depth of burial, increased with the depth of burial. Collapse occurred by snap-through at the crown.
3. The ratio of the overpressure required to cause collapse at any depth to the theoretical in-air primary buckling pressure varied inversely with stiffness.
4. Two zones of burial were defined by the variations in the magnitudes of the displacements and strains at the crown of the stiffer, instrumented cylinder. In the first zone (shallow burial), the displacements and strains were highly sensitive to small changes in depth of burial. In the second zone (deep burial), the displacements and strains were insensitive to changes in depth of burial. The minimum depth required for deep burial increased with the overpressure.
5. The deflected shape assumed by a buried cylinder depends on its stiffness and zone of burial. Deeply buried, instrumented cylinders of both stiffnesses deformed into low-order modes. At shallow burial, the more rigid, instrumented cylinder assumed a high-order mode in the vicinity of the crown. Again at shallow burial, the more flexible, instrumented cylinder experienced inward radial displacements at the springline.
6. The direct compressive strains were uniform around the more rigid, instrumented cylinder at deep burial.
7. For the more rigid cylinder, the effect of arching, as reflected by the direct compressive strains at the springline, did not vary significantly with depth in the range of overpressure employed.
8. Local buckling of the more flexible cylinder resulted in spurious strain data.

ACKNOWLEDGEMENTS

This paper* is based on an experimental investigation conducted at the Air Force Shock Tube Facility operated by the University of New Mexico.

Special acknowledgement is made to the director of the Shock Tube Facility, Dr. Eugene Zwoyer. The writer also wishes to acknowledge the contributions of all his colleagues at the facility. He is particularly appreciative of the assistance of Mr. Dwane Brewer, Research Associate Engineer and head of the electronics department at the facility.

REFERENCES

1. Robinson, R.R., "The Investigation of Silo and Tunnel Linings," AFSWC-TDR-62-1, Research Directorate, Air Force Special Weapons Center, Kirtland Air Force Base, New Mexico, 1962.
2. Bulson, P.S., "Deflection and Collapse of Buried Tubes," Report Res. 7/1 Military Engineering Experimental Establishment, Christchurch, Hampshire, England, 1962.
3. Whitman, Robert V. and Ulrich Luscher, "Basic Experiment into Soil-Structure Interaction," Journal of the Soil Mechanics and Foundations Division, American Society of Civil Engineers, Vol. 88, No. SM6, 1962.
4. Timoshenko, S., Theory of Elastic Stability, McGraw-Hill Book Co., Inc., New York, N.Y., 1936.
5. Aluminum Company of America, Pittsburgh, Pa., Alcoa Structural Handbook, 1960.
6. Luscher, Ulrich, "Laboratory Sand-Placement Tests," Work Order 16, Air Force Shock Tube Facility, Albuquerque, New Mexico, 1962.
7. Abbott, Phillip A., Personal communication, 1963.
8. Bedesem, W.B., et al, "Studies on the Analysis and Design of Domes, Arches, and Shells," University of Illinois, Urbana, Illinois, 1963.

*An abridgment of a report, WL-TDR-64-13, to be published by the Air Force Weapons Laboratory, Kirtland Air Force Base, New Mexico, 1964.

RESPONSE OF BURIED STRUCTURAL MODELS TO STATIC AND DYNAMIC OVERPRESSURES

by
R. L. Marino, Jr.* and W. F. Riley**

ABSTRACT

This research program was conducted to determine the behavior of a number of simple structural models while buried in a soil medium which was subjected to static and dynamic overpressures. During the course of the program, studies were conducted on four cylindrical shell models. Three models had hemispherical end closures and diameter-thickness ratios (D/t) of 40, 80, and 160. The other model (D/t = 80) had an end closure system which could not transmit load to the shell. All of the work discussed was conducted using a dry cohesionless soil medium of uniformly graded silica sand (Ottawa sand). For each model a complete analysis was made of the central transverse plane of the shell. Conclusions are drawn regarding the influences of model stiffness, overpressure level, rate of loading, and end closure system on the hoop and longitudinal membrane forces and bending moments in the shells.

INTRODUCTION

The research program described in this paper was conducted to determine the behavior of a number of simple structural models while buried in a soil medium which was subjected to static and dynamic overpressures. The behavior of such a structure is greatly influenced by the pressure distribution on the interface between the structure and the soil. Part of this interfacial pressure is developed as a result of the soil overpressure plus the weight of the soil overburden which acts directly on the buried structure. This component of the interfacial pressure is commonly referred to as primary soil pressure.

Another component of the interfacial pressure is developed as a result of the deformation of the buried structure and is commonly called secondary soil pressure. If the walls of a buried structure are displaced outwardly, the surrounding soil is compressed and "soil reactions" are developed which are proportional to the amount of displacement. These "soil reactions" are particularly helpful in supporting some specific types of buried structures such as cylindrical shells. In this case, they act to keep the shell in a circular shape by resisting the outward displacement of the side walls. On the other hand, if the walls or roof of a buried structure are displaced inwardly, the primary soil pressure producing the deflection is transferred from the flexible structure to the surrounding soil. This phenomenon is commonly referred to as "arching." In this case, the secondary soil pressure can be considered to be a negative or outward "soil reaction" since it has the same effect as reducing the primary soil pressure. Since these "soil reactions" are produced by the displacement of the walls or roof of the structure, the resulting interfacial pressure distribution depends largely on the stiffness of the buried structure relative to the surrounding soil.

In an attempt to gain a clearer understanding of the interaction phenomenon on buried structures, the major efforts of this research program were directed towards determining the influence of:

1) the magnitude of the soil overpressure
2) the model stiffness
3) the end closure system, and
4) the rate of loading

on the behavior of cylindrical shell structures buried in a dry cohesionless soil medium of uniformly graded silica sand (Ottawa sand). In addition, attempts were made to evaluate the experimental procedures and techniques currently employed in the investigation of buried structures.

EXPERIMENTAL METHODS AND PROCEDURES

Models

During the course of the program four different cylindrical shell models were studied. The significant dimensions of each are listed in the following table.

The cylindrical parts of all models were manufactured from cold drawn seamless steel tubing to tolerances of ± 0.002 inch. This degree of accuracy was considered essential to eliminate any influence of nonuniformity of wall thickness or out-of-roundness of the cylinders on the overall behavior of the models under load. The end closures were

* Research Engineer, IIT Research Institute, Chicago, Illinois.
** Science Advisor, IIT Research Institute, Chicago, Illinois.

Table I. Cylindrical Shell Model Dimensions

Model No.	Overall Length in.	Diameter in.	Wall Thickness in.	D/t Ratio	Flexural Rigidity $\frac{Et^3}{12(1-\nu^2)}$	End Closure
1	15	5	0.124	40	5240	Hemispherical
2	15	5	0.062	80	655	Hemispherical
3	15	5	0.031	160	82	Hemispherical
4	18	5	0.062	80	655	Special*

*The end closure system on this model was not attached to the cylindrical shell. It was designed: a) to eliminate longitudinal membrane forces and longitudinal bending moments in the walls at the ends of the cylindrical shell, and b) to allow the end transverse cross sections of the cylindrical shell to deform freely.

machined to the same dimensional tolerances as the shells. Adhesive (Eastman 910 Cement) joints were used in assembling the models to avoid the high localized temperatures associated with welding or brazing which could damage the strain gauges and warp the thin shells. A stepped lap joint was used since it provided a positive seating arrangement.

Instrumentation

Electrical resistance foil strain gauges and linear variable differential transformers were employed to determine the response of the buried models. The foil gauges recorded the strains in the structural model while the differential transformers recorded horizontal and vertical diameter changes of the cylindrical shell.

"Two-gauge" strain rosettes (Budd Type C6-121-R2C) having a one-eighth inch gauge length were placed at a number of locations on the inside and outside surfaces of all models as shown in Figure 1. The gauges were aligned so that one recorded the strain in the hoop direction while the other recorded the strain in the longitudinal or meridional direction. On the outside surface of the model, the gauges were covered with a thin epoxy film to protect the foil grid from scratches and moisture.

Miniature displacement transducers of the differential transformer type with built-in carrier systems were employed for measuring diameter changes in the cylindrical shells under load. These transducers (Sandborn Model 7 DCDT) require 6 volts d.c. excitation and provide a d.c. output which can be read on a d.c. indicator. The output is linearly proportional to the core movement within the rated displacement range ($\pm$ 0.050 in.) of the transducers.

In the static studies the output signals from the strain gauges were recorded with a Baldwin Model 20 strain indicator and suitable switching boxes. The outputs from the differential transformers were recorded with a vacuum tube milli-voltmeter.

In the dynamic studies Consolidated Electrodynamics Corporation type 5-124 oscillographs equipped with 7-363 galvanometers and Video Instruments type 93 amplifiers were used to record the output signals from the strain gauge bridges. An Ampex Model AR-200 magnetic tape recorder was used to record the dynamic signals from a Kistler pressure gauge in the water chamber and the differential transformers in the model.

Three Tektronix type 502 dual beam oscilloscopes equipped with C-12 polaroid cameras were also used in the dynamic studies to obtain a "quick-look" at signals from selected transducers.

Soil Facility

The soil facility used for the study was built around a 48 in. diameter cylindrical tank approximately 6 ft deep. For most of the static studies a flat removable head was used as the top closure (see Figure 2). Nitrogen gas was used to apply overpressures to the soil. A rubber diaphragm placed on the top surface of the soil prevented the Nitrogen gas from entering the soil pores.

For the dynamic studies a conical water chamber and a cylindrical gas chamber were added to the soil tank as shown in Figure 3. The flexible rubber diaphragm was again used to separate the water from the soil and in addition a thin steel diaphragm was used to separate the water from the pressurized gas in the upper chamber. In order to apply a dynamic load to the surface of the soil, the gas chamber was first pressurized to the value necessary to produce the desired magnitude of soil overpressure. This chamber pressure had to be greater than the desired steady-state soil pressure because of the volume expansion of the pressurized gas which occurred as the pressurized gas filled the initial air space in the water chamber. This air space was further increased by the overall compression of the soil and water. The thickness of

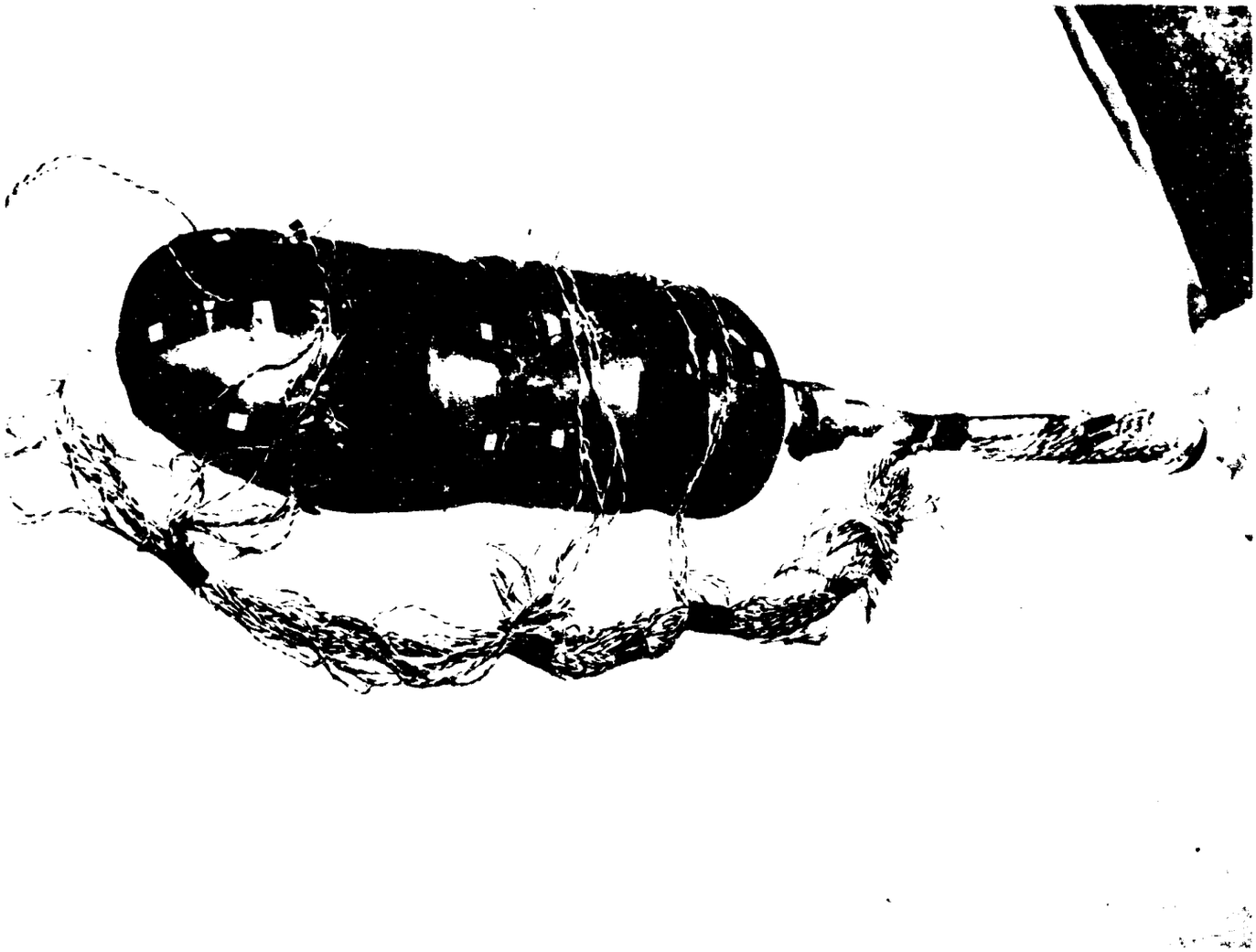


Fig. 1 One of the Cylindrical Shell Models With Hemispherical Heads

the steel diaphragm was selected to safely retain the chamber pressure. In order to release this pressure, the diaphragm was ruptured by detonating a small charge of primacord with a blasting cap. This action resulted in a rapid transfer of pressure to the water which served to transmit and distribute the dynamic pressure pulse uniformly across the soil area. The facility has the capability of generating a pulse of up to 500 psi peak pressure with a rise time of approximately 6 milliseconds.

Soil Placement

In order to obtain meaningful results from the studies of the buried structures, it was imperative that the properties of the soil be held constant for all investigations. Since most of the significant properties of a uniformly graded dry silica sand are related to its density, all of the placement efforts in this program were directed toward controlling this one parameter.

One of the commonly used methods for compacting large masses of cohesionless material utilizes vibration techniques. In all of the studies, two small protable vibrators ordinarily used in the placement of concrete were employed to compact the soil.

The sand was placed in six inch layers in the soil facility. It was poured into the vessel in a loose state and each layer in succession was compacted by inserting the vibrator probes into the sand bed at a total of approximately 6 locations. The rotating eccentric weights in the probes imposed a forced vibration on the soil and the desired degree of compaction was defined as that density which existed when resonance occurred in the soil mass. This condition was immediately evident since the forced vibrations could be felt in the walls of the soil facility. The vibrator probes were then removed and another six inch layer of loose sand was added. This procedure was continued until the vessel was completely filled.

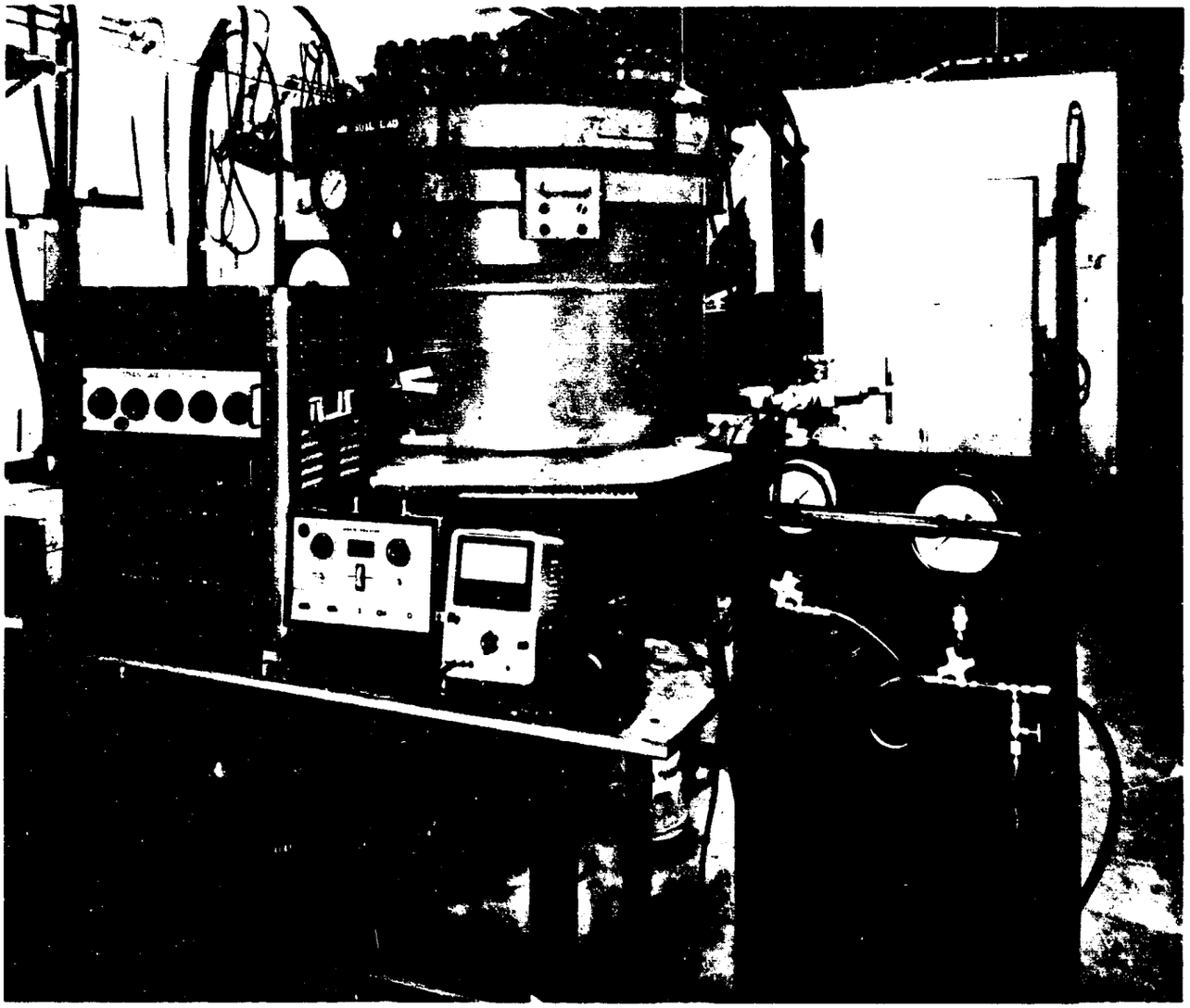


Fig. 2 Equipment Employed For Applying Pressure and For Recording the Behavior of the Buried Model

A small scoop with a known volume was used for making density measurements. These readings were taken at five positions on the top surface of the sand bed after it had been leveled following the final vibration. These density measurements gave readings in the range of 106 lbs/ft^3 to 109 lbs/ft^3 for all studies. When the head of the soil facility was removed after each model investigation, surface density measurements were again taken. It was found that the density of the soil in this final state usually increased by less than 1 lb/ft^3. These final readings were normally in the range between 107 lbs/ft^3 to 110 lbs/ft^3 for all studies.

Model Placement

Because of the importance of correctly positioning the model in the soil media, the special fixture shown in Figure 4 was designed for holding it in the proper orientation during the placement operation. This fixture consisted of a 4 in. box beam which spanned the tank and a frame having a top and bottom plate connected by three rods. A template in the form of a 90° segment of a circle and having the same radius of curvature as the cylindrical shell was attached to each end of the bottom plate. These templates held the model in the proper position while it was being buried. By correctly spacing the top and bottom plates, the depth of burial could be accurately controlled.

After the soil facility had been filled and compacted to a level slightly below the desired level of the invert of the cylindrical shell, the model placement fixture was set for the proper depth of the burial. The 4 in. square box beam was then positioned over the open end of the soil facility and the top plate of the placement fixture was attached to it by means of a standard "C" clamp. The model was held in position by hand against the templates on the bottom plate



Fig. 3 Soil Facility and Instrumentation Used For Loading and Recording The Behavior of a Buried Model in The Dynamic Studies

of the fixture and the box beam was moved so as to position the center of the model at the exact center of the soil facility. The beam was then locked to the top flange of the soil facility by means of other "C" clamps. After this positioning operation, the model was ready for burial. Loose sand was placed in the soil vessel up to the level of the mid-depth of the model and then vibrated with the model still held in place by the fixture. The next step involved adding another layer of sand so as to bring the level of the soil surface up to the crown of the cylindrical shell. This layer was also vibrated. The model was now completely buried in compacted sand and the placement fixture was removed. Exactly the same procedure as was previously described was used to place the remaining sand in the soil tank.

To insure a soil density which was uniform to the top of the soil bed, the final sand layer was piled above the rim of the soil vessel and then vibrated. A level surface, even with the rim, was struck off by using a structural angle supported on the flange of the vessel.

Exactly the same burial procedure was followed for each of the structural models. They were first placed in the soil with their LVDTs along the horizontal and vertical diameters. In this initial orientation, the strain gauges also occurred at positions on the horizontal and vertical diameters and at 45° to them

In order to determine the strains and diameter changes at locations other than the 0°, 45°, and 90° lines associated with the initial orientation, the models were also placed in the soil in a +20°, -20°, +30° and -30° orientation. These angles were measured between the initial orientation of the horizontal (vertical) LVDT and each new position of the

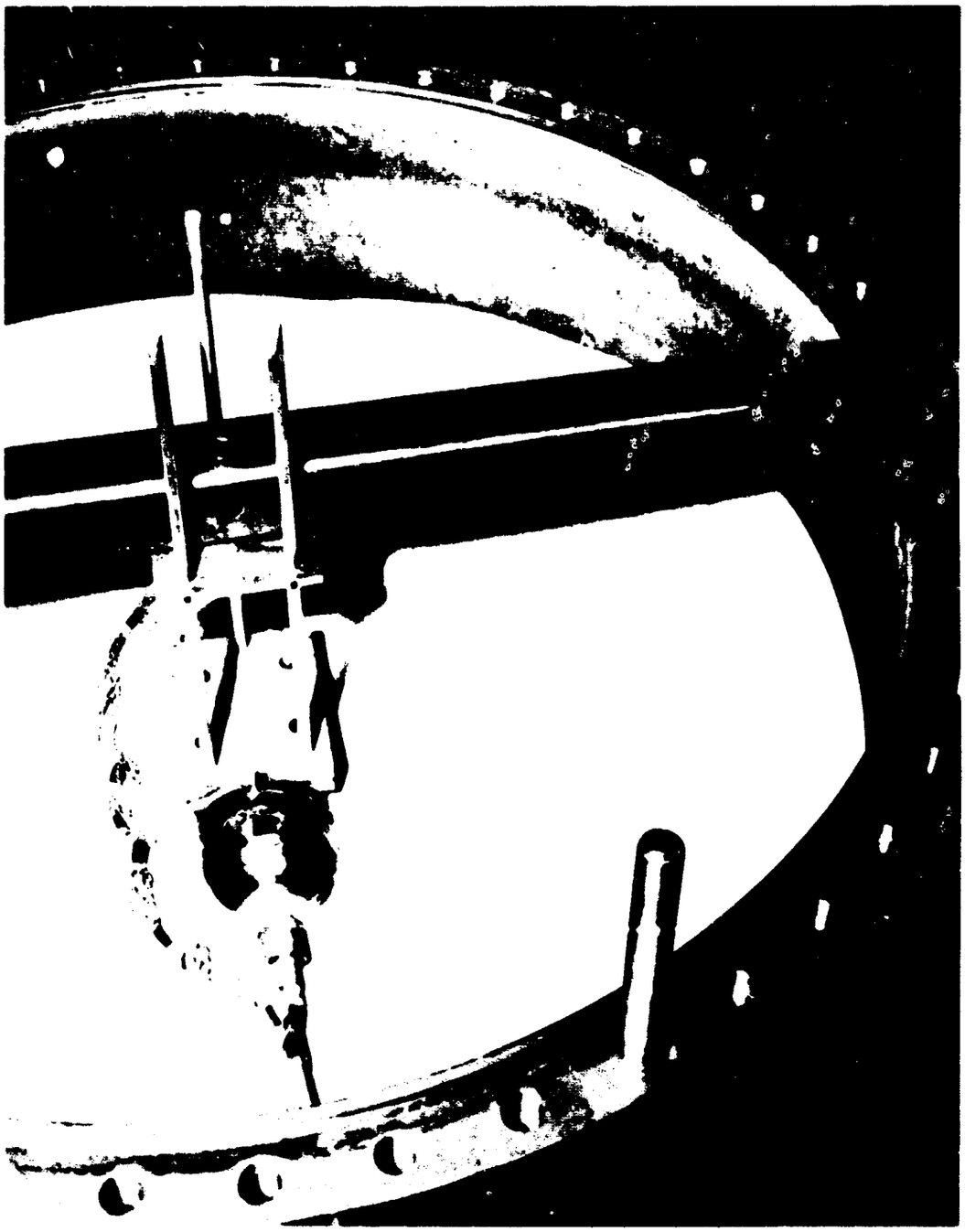


Fig. 4 The Box Beam And Fixture Used In Positioning The Model

LVDT. Positive angles represent a counterclockwise rotation of the model about its longitudinal axis and negative angles represent a clockwise rotation looking toward the end of the model which had the access hole for the lead wires. By also placing the model at a +45° and a +90 orientation, adequate checks on the reproducibility of the strains from one burial to the next were obtained.

TEST PROCEDURES

Before the structural models with hemispherical heads were buried, they were first subjected to an external hydrostatic pressure. This hydrostatic pressure was applied and released about twenty times and strain readings were taken during the cycling operation. This preliminary loading served several functions among which were:

1) to check the strain gauges to ensure that all gauges were reading correctly before the model was buried in soil,

2) to cycle the strain gauges to guarantee obtaining a reproducible signal for a given strain magnitude, and

3) to check the efficiency of the bonded closure joint.

The checks of items 1) and 3) were accomplished by comparing measured strains with theoretical strains computed for a cylindrical shell with hemispherical heads subjected to an external hydrostatic pressure. Using this procedure, several of the strain gauges were found to be improperly bonded but in no case was the bonded head joint found to be unreliable.

When the hydrostatic pressure check was completed, the first structural model was placed in the soil facility and a complete set of strain gauge and LVDT readings were taken before the model was buried. These readings corresponded to the initial or unstrained condition of the structural model. The soil facility was then filled, completely burying the model, and another set of strain gauge and LVDT readings was taken. It was found that the weight of the soil produced:

1) a change in horizontal diameter that was equal to only 1% of the corresponding change due to a 100 psi overpressure,

2) a change in vertical diameter that was equal to only 3% of the corresponding change due to a 100 psi overpressure, and

3) strains of the order of magnitude which could not be accurately resolved with the strain indicating equipment used for the study. These measured strains were of the order of magnitude of 10 μ in./in. which is equivalent to only 300 psi in steel in a uniaxial stress field. As this lower limit of strain sensing is approached, apparent strain due to thermal and electronic drift are of the same order of magnitude as the real strain and these apparent strains obscure the true behavior of the model.

The strains due to the weight of the soil were therefore neglected in the study and the readings taken on the completely buried model were assumed to be the "zero" strain readings.

Preliminary investigations conducted during the early stages of the program showed that the strain readings and the deflection readings were not reproducible for the first three or four cycles of load. This was attributed to two facts: a) the stress-strain curve for Ottawa sand is not reproducible for the initial three of four cycles of load and b) before any application of load there was probably a slight difference in density between the sand in the immediate proximity of the model and the sand in the remainder of the soil facility. As successive cycles of load were applied, however, a relatively uniform condition was finally reached after about four cycles. Figure 5 shows the vertical and horizontal diameter changes vs. the applied overpressure for one of the models for the first six load cycles. This graph gives some indication of the reproducibility of the model deformations which occurred for successive applications of load. The majority of the strain readings after four or five cycles were reproducible within $\pm$ 20 μ in./in. The maximum strains occurring in each of the models under the maximum overpressure were of the order of magnitude of 800 to 1200 μ in./in.

After the preliminary cycling operation, static pressure was applied in 100 psi increments over the range from 0 to 400 psi except for the model with a D/t of 160. The maximum pressure for this model was limited to 300 psi to keep the strains below the yield point of the model material. All of the strain gauges and the LVDTs were read at zero pressure and also at each 100 psi increment. When the readings had all been recorded at the maximum overpressure, the load was released and another set of zero load readings was taken. It was possible to take all of the measurements for one complete load cycle within a time interval of approximately 90 minutes. In most cases the amount of drift which occurred during this time interval was negligible. The data used for analysis was recorded during the fifth and sixth load cycles in all of the static studies.

For the dynamic studies, a pressure pulse was applied to the surface of the soil. The conical shaped transition section connecting the cylindrical pressure chamber to the vessel containing the soil was first filled with water to a level approximately 6 inches below the 0.030 inch thick steel diaphragm. This 6 inch air space allowed the diaphragm to deform freely without contacting the water as the gas chamber was pressurized.

In order to rapidly release the pressure in the chamber and transfer it to the surface of the soil, the diaphragm was ruptured by detonating four 6 inch lengths of 25 grain primacord. The electrical pulse used to trigger this explosive also served to trigger the oscilloscope traces employed in recording some of the signals from the model. All other instrumentation used for recording the model behavior was manually started before the explosive was triggered.

All of the pressure records indicate that a chamber pressure of 200 psi will produce a dynamic soil overpressure which reaches a peak value of about 320 psi in approximately 7 msec. A steady state value of 150 psi is maintained after 100 msec.

Both static and dynamic studies were conducted for each model burial so that a more meaningful comparison could be made between the behavior of a buried model under a dynamic soil overpressure and the behavior of the model under a static soil overpressure of the same magnitude. Four or five cycles of static overpressure was first applied to the

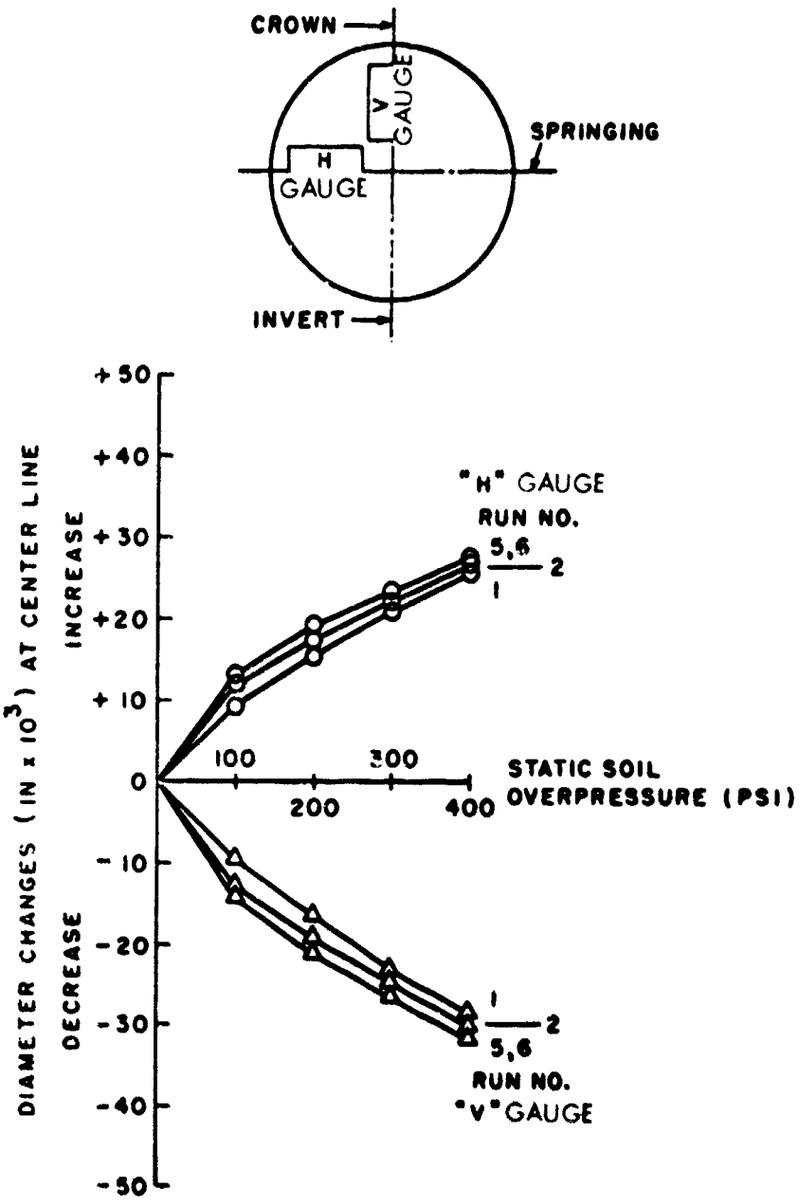


Fig. 5 Diameter Change On The Central Transverse Cross Section of The Cylindrical Shell Model With Hemispherical Heads (D/t = 40) As A Function of Soil (Ottawa Sand) Overpressure

soil and a set of model deformation readings was then obtained for a static soil overpressure of the same magnitude as the peak dynamic pressure. After these static readings had been recorded, the dynamic study was then conducted.

RESULTS

Static Studies

Since the central transverse plane of the cylindrical shell models was a plane of symmetry, the hoop and longitudinal stresses computed from the measured strains were also principal stresses. This made it possible to compute the longitudinal and hoop membrane force and the longitudinal and hoop bending moment per inch of circumference directly from the longitudinal and hoop stresses on the inside and outside surfaces of the shell. These quantities were computed for each model at each 100 psi level of static soil overpressure. Diameter changes were also measured at the central transverse plane of the cylindrical shells as a function of the angular position of the measured diameter for each 100 psi level of soil overpressure.

The cylindrical shell model with hemispherical heads having a D/t ratio of 40 had the greatest rigidity of all the models investigated. Measurements taken of the horizontal and vertical diameter changes were previously shown in Figure 5 as a function of the soil overpressure for a number of the load cycles applied to this model.

The hoop membrane force was computed for each 100 psi soil overpressure at the gauge positions for all orientations of the model having a D/t of 40. The values for the 400 psi soil overpressure are plotted in Figure 6 on only one side of the vertical axis since it is an axis of symmetry. A curve that best fitted these points was drawn and this "averaging curve" was later used on other graphs to represent the distribution of the hoop membrane force for a model with D/t of 40 buried in dense Ottawa sand and subjected to a 400 psi soil overpressure.

Exactly the same procedure was employed to obtain the distribution of the hoop membrane force at the 300 psi, 200 psi, and 100 psi values of overpressure. Similar distribution curves were drawn for the longitudinal and hoop membrane force and bending moment for each model at every 100 psi increment of soil overpressure.

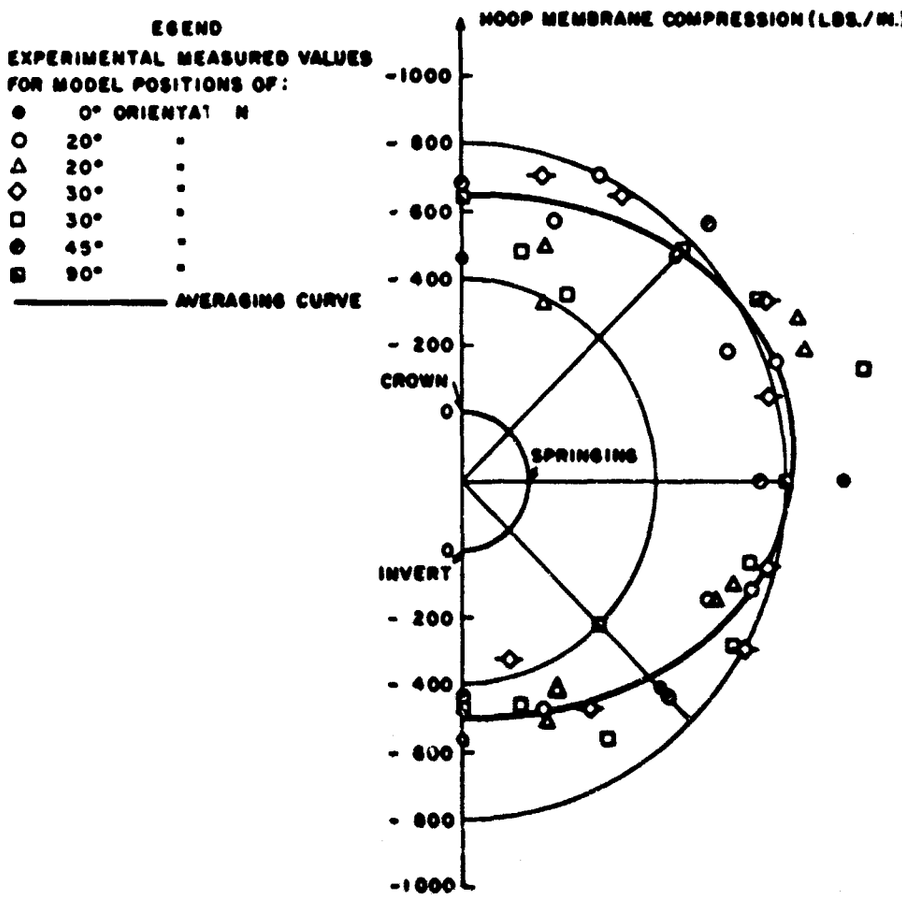


Fig. 6 Distribution Of The Hoop Membrane Force At The Central Transverse Cross Section Of The Cylindrical Shell Model With Hemispherical Heads (D/t = 40) For A Soil (Ottawa Sand) Overpressure Of 400 psi

Typical examples of the other "averaging" distribution curves for the model with a D/t ratio of 40 appear in Figures 7 to 9. These figures (6 to 9) serve to show the amount of experimental data "scatter" that occurred with the model in the various rotational orientations. Experimental points at the 0°, 45°, and 90° positions also illustrate the reproducibility that was obtained for successive burials of the model.

Typical examples of the influence of the magnitude of the soil overpressure on the behavior of a model are illustrated in Figures 10 to 14.

The diameter changes for the cylindrical shell model with hemispherical heads (D/t = 80) as a function of the angular position of the measured diameter at each 100 psi of soil overpressure are plotted in Figure 10. The "averaging" curves for the distribution of hoop membrane force for the same model (D/t = 80) at each 100 psi increment of soil overpressure are shown in Figure 11. "Averaging" curves giving the distribution of hoop bending moment, longitudinal mem-

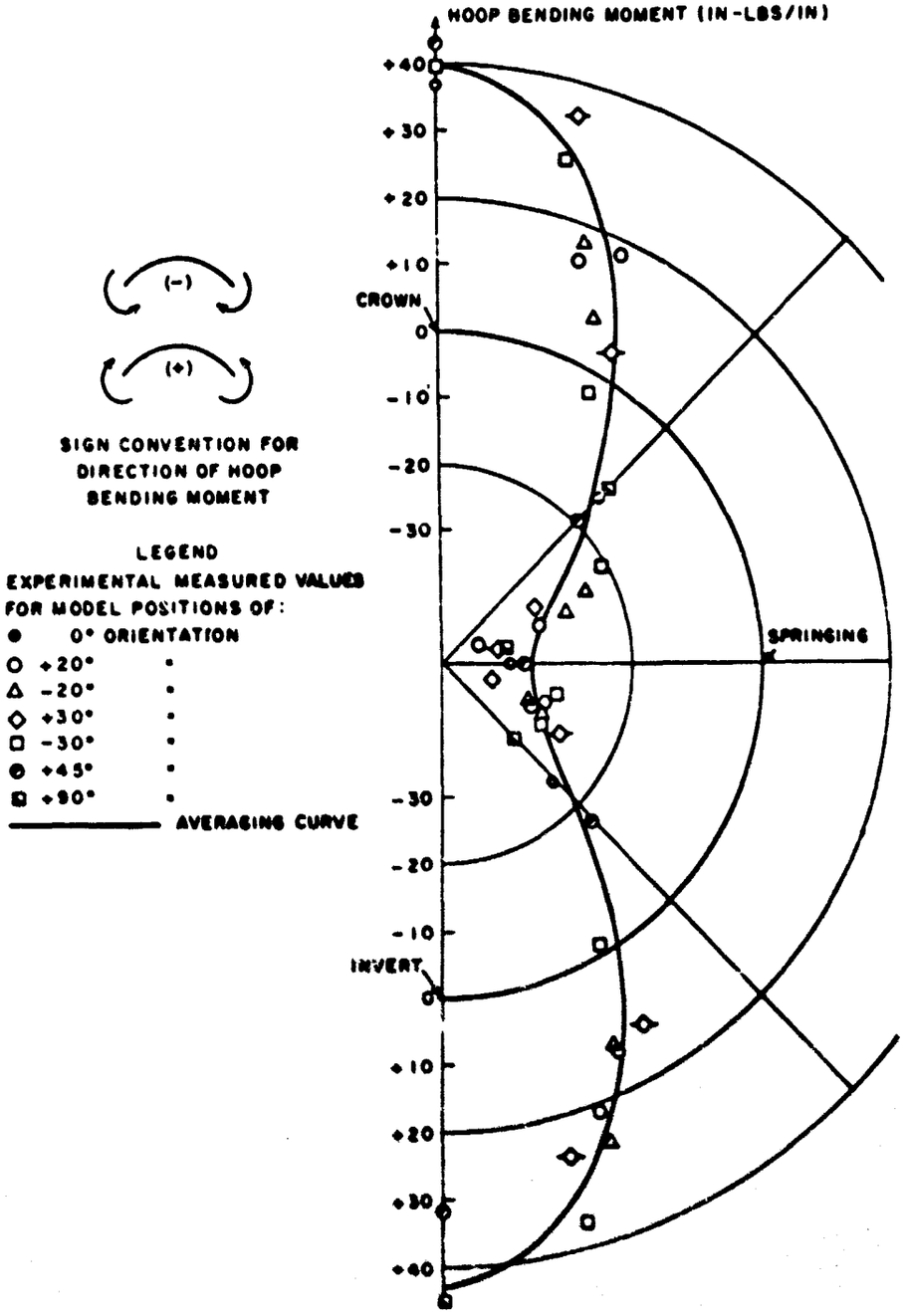


Fig. 7 Distribution Of The Hoop Bending Moment At The Central Transverse Cross Section Of The Cylindrical Shell Model With Hemispherical Heads (D. t = 40) For A Soil (Ottawa Sand) Overpressure Of 400 psi

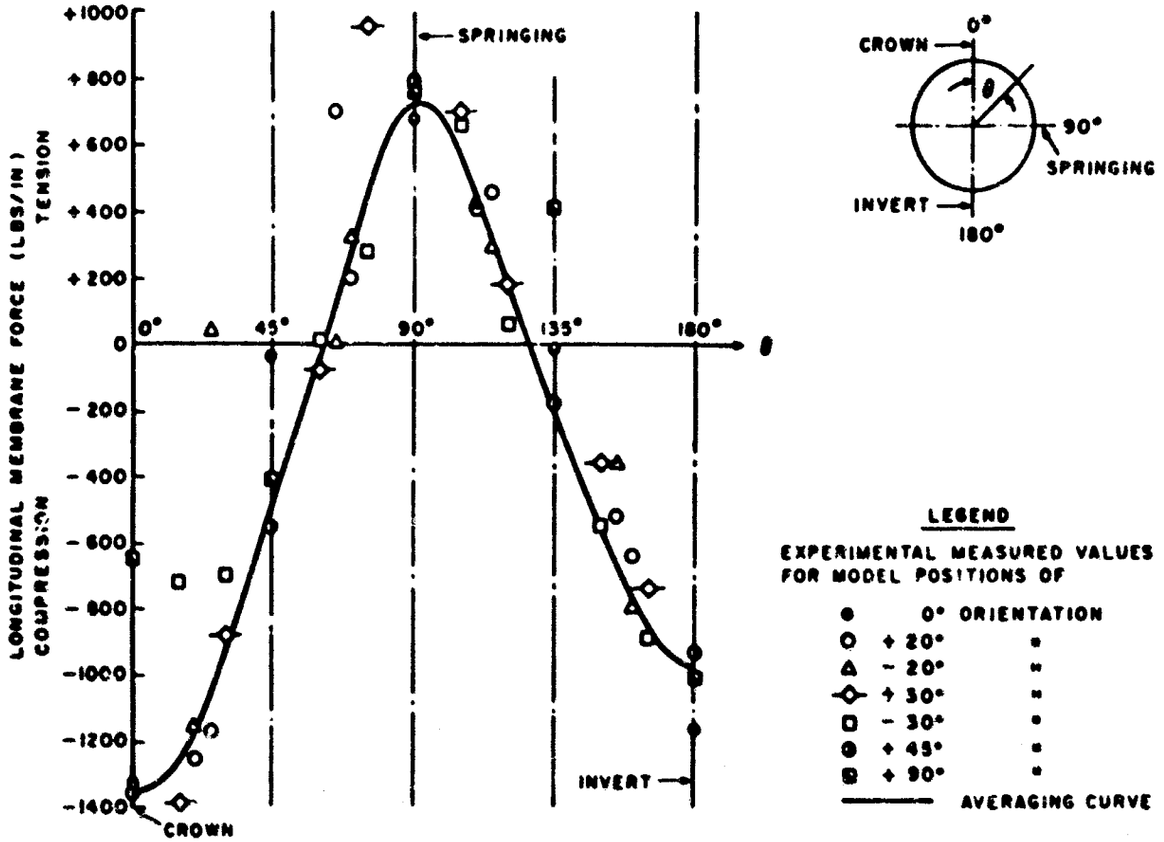


Fig. 8 Distribution Of The Longitudinal Membrane Force At The Central Transverse Cross Section Of The Cylindrical Shell Model With Hemispherical Heads (D/t = 40) For A Soil (Ottawa Sand) Overpressure Of 400 psi

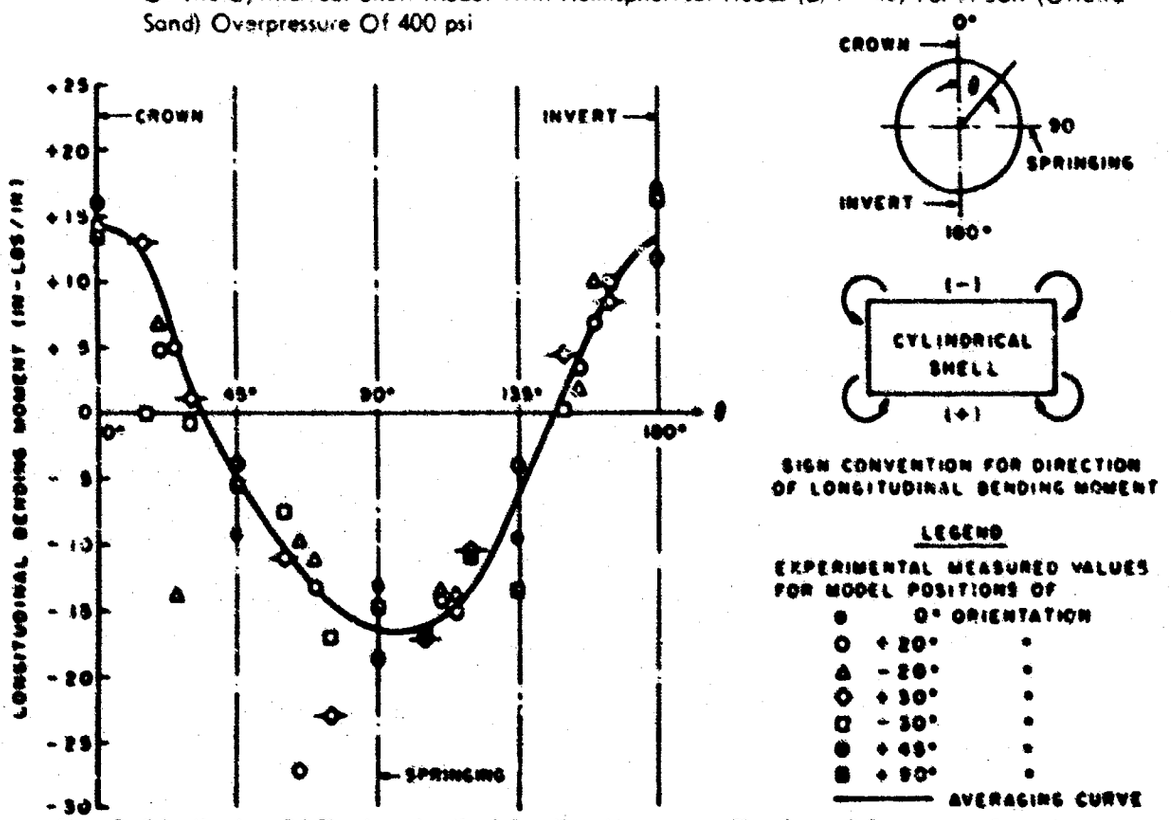


Fig. 9 Distribution Of The Longitudinal Bending Moment At The Central Transverse Cross Section Of The Cylindrical Shell Model With Hemispherical Heads (D/t = 40) For A Soil (Ottawa Sand) Overpressure Of 400 psi

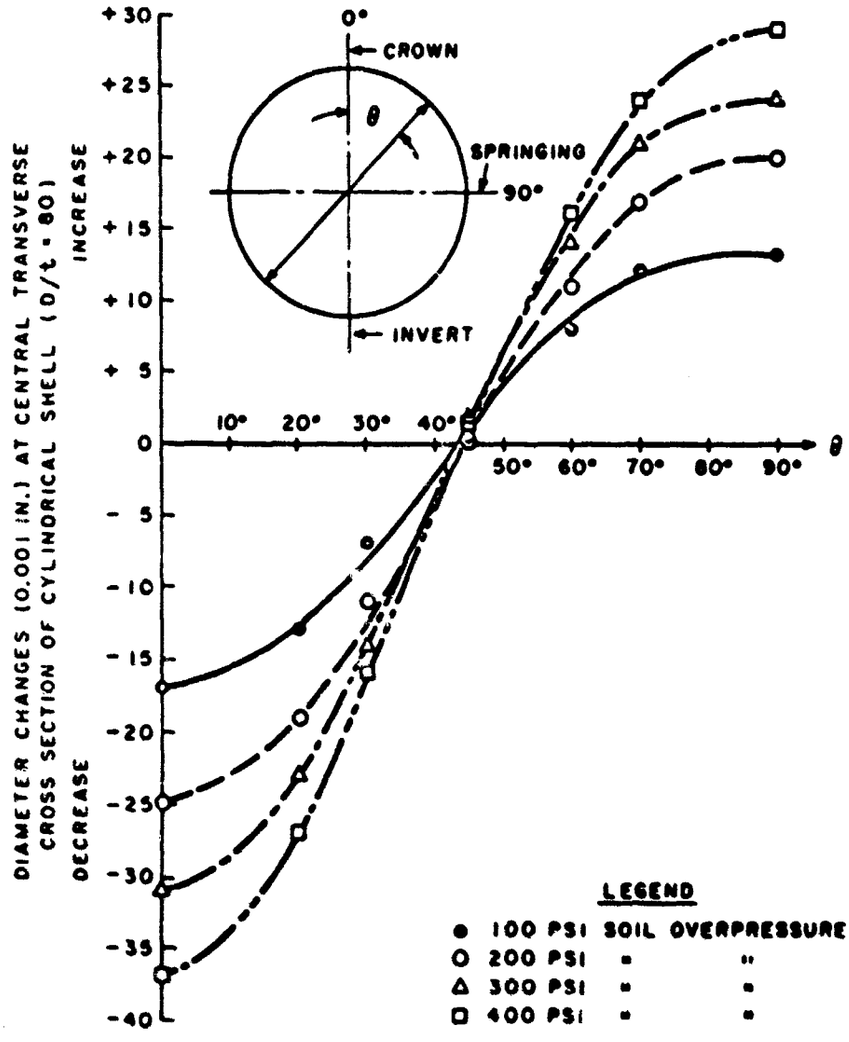


Fig. 10 Diameter Changes At The Central Transverse Cross Section Of The Cylindrical Shell Model With Hemispherical Heads (D/t = 80) For Four Different Levels Of Soil (Ottawa Sand) Overpressure

rane force and longitudinal bending moment for each 100 psi overpressure are presented in Figures 12, 13, and 14 respectively.

Figure 15 shows the hoop membrane force at the springing line of each model as a function of the static soil overpressure.

The distribution of the hoop membrane force for each of the cylindrical shell models at 300 psi soil overpressure are plotted together for comparison purposes in Figure 16. Similar comparisons of the distributions for the various models of hoop bending moment, longitudinal membrane force, and longitudinal bending moment are made in Figures 17, 18, and 19 respectively.

Dynamic Studies

The dynamic data which have been evaluated to date have been limited to the cylindrical shell model with hemispherical heads having a D/t ratio of 40. A comparison is made in Figure 20 between the distributions of hoop membrane force resulting from a static and a dynamic application of soil overpressure. In Figure 21, the hoop membrane force at the springing line is plotted as a function of the soil overpressure. The theoretical value obtained by multiplying the applied overpressure by the projected area of one-half the model is shown together with the experimental values obtained from both the static and dynamic studies. Figure 22 shows the distribution of the hoop bending moment resulting from a static and dynamic loading.

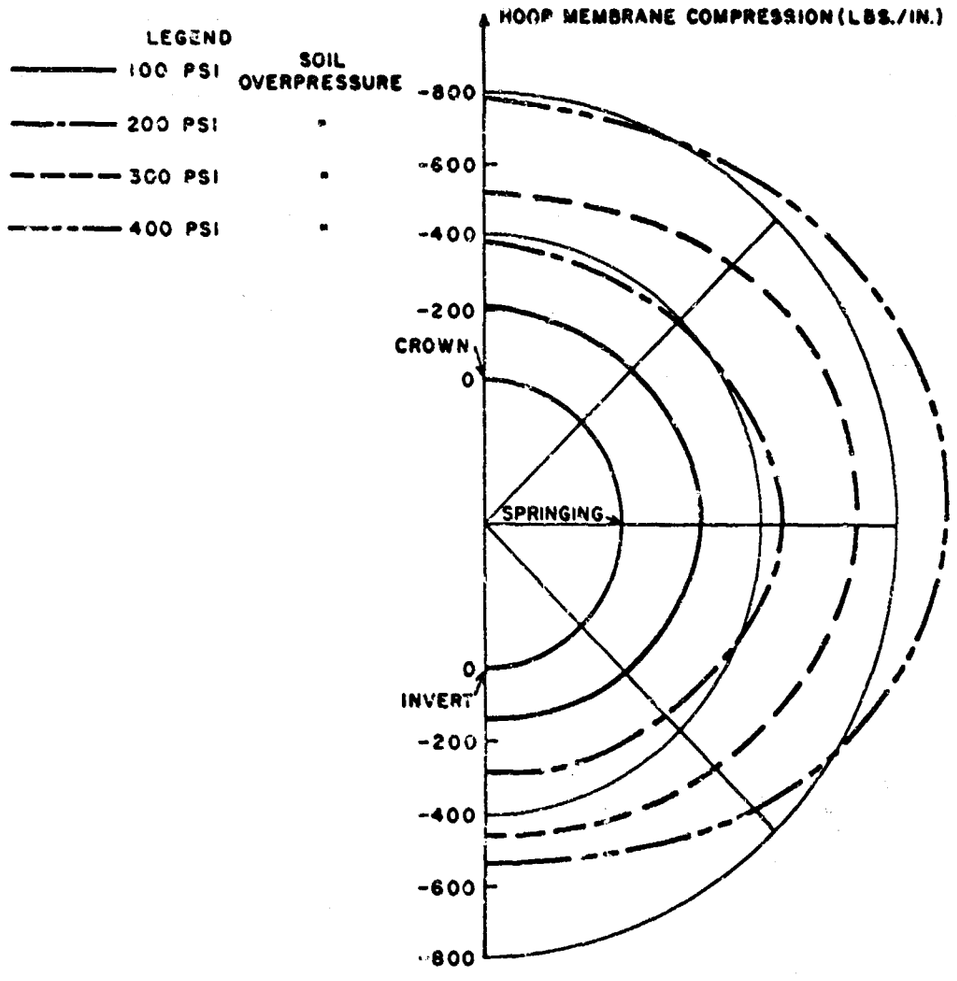


Fig 11 Distribution Of The Hoop Membrane Force At The Central Transverse Cross Section Of The Cylindrical Shell Model With Hemispherical Heads (D/t = 80) For Four Different Levels Of Soil (Ottawa Sand) Overpressure

Summary

Table II is presented in order to more clearly illustrate the influence of the magnitude of the soil overpressure on the behavior of a cylindrical shell model with no end restraints. This table gives the increase in the value of certain structural functions for each 100 psi load increment as a percentage of the value of the structural function that existed at the initial 100 psi increment.

Tables III, IV, and V are presented to show respectively, the influence of the model stiffness, the end closure system and the rate of loading.

CONCLUSIONS

The main objective of this research program were directed towards determining the influence of:

1) the magnitude of the soil overpressure,
2) the model stiffness,
3) the end closure system, and
4) the rate of loading

on the behavior of cylindrical shell structures buried in Ottawa sand. Each of these factors will be discussed in turn.

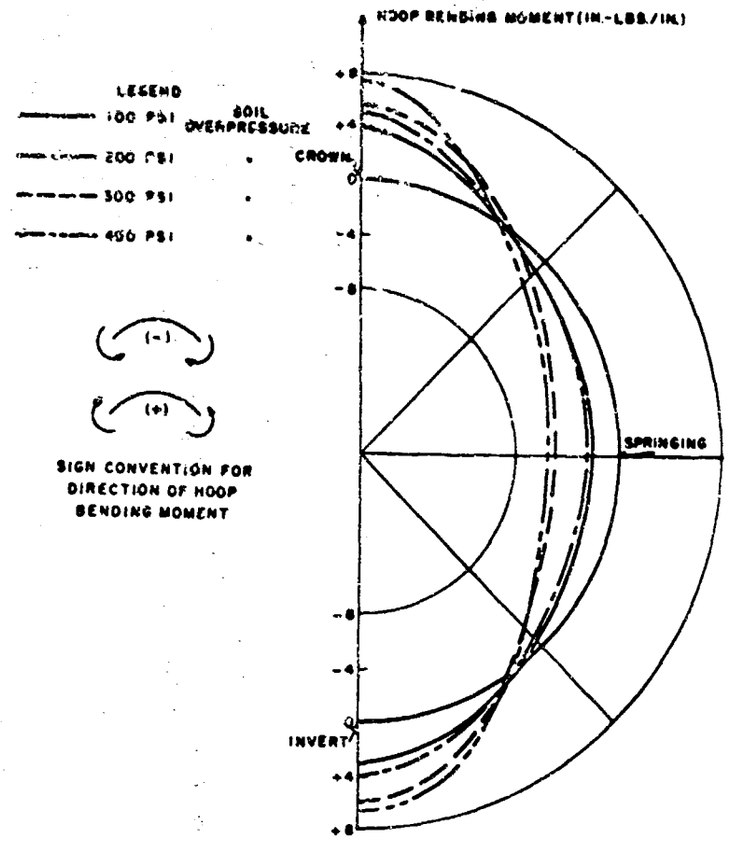


Fig. 12 Distribution of the Hoop Bending Moment at the Central Transverse Cross Section of the Cylindrical Shell Model with Hemispherical Heads (D/t = 80) for Four Different Levels of Soil (Ottawa Sand) Overpressure

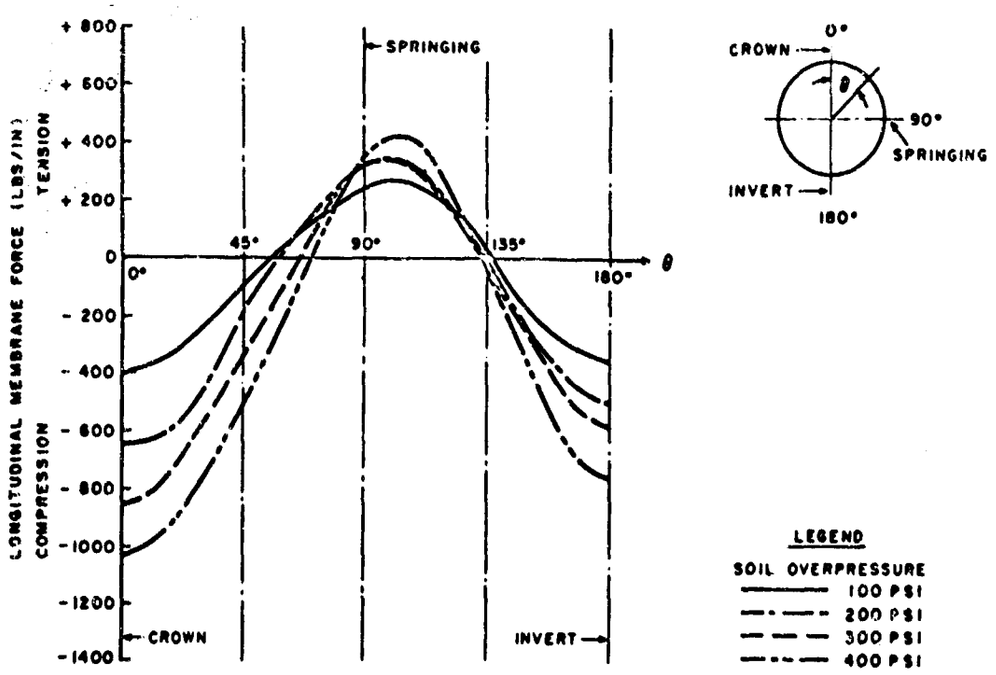


Fig. 13 Distributions of the Longitudinal Membrane Force at the Central Transverse Cross Section of the Cylindrical Shell Model with Hemispherical Heads (D/t = 80) for Four Different Levels of Soil (Ottawa Sand) Overpressure

The hoop membrane force at the springing of the cylindrical shell is a good measure of the amount of "arching" that takes place over the model since by vertical equilibrium this quantity actually shows the overpressure transmitted through the soil to the model. Figure 15 shows the hoop membrane force at the springing to be reasonably linear with increasing soil overpressure. It also shows that for all models this hoop membrane force is less than the theoretical value obtained by multiplying the applied overpressure by the projected area of one-half of the model. This indicates that part of the overpressure is borne by the surrounding soil but the percentage of the soil overpressure that the model accepts is independent of the magnitude of the overpressure. The amount of hoop bending of the cylindrical shell on the other hand is greatly influenced by increases in soil overpressure. Table II shows that the changes in diameter and the hoop bending moment are not linear functions of the soil overpressure. The initial 100 psi of load produces the greatest change and after this the change becomes less for successive 100 psi increments. This nonlinear behavior is attributed to the increased lateral (horizontal) support which occurs at the springing as the surrounding soil by virtue of its stiffness acts to oppose the increase in horizontal diameter as the cylindrical shell deforms under load. The stiffness of the soil also becomes greater with increased load and this adds further to the lateral (horizontal) soil reaction.

Figure 16 and Table III show the similarity of the hoop membrane force distributions for all of the models at 300 psi overpressure. This similarity was also observed at the 100 psi, 200 psi, and 400 psi overpressures which seems to indicate that the hoop membrane force of the cylindrical shell is essentially independent of the model stiffness.

Figure 17 shows that the hoop bending moment is not significantly influenced by the model stiffness for the models with a D/t ratio greater than 80. It can also be seen that the magnitudes of the hoop bending moments are relatively small as compared with the values which are developed in the model with a D/t ratio of 40. This phenomenon seems to indicate that all cylindrical shells up to a given value of wall rigidity will deform sufficiently under load to allow a lateral (horizontal) support to develop at the springing which acts to reduce the bending in the cylinder. This lateral force is developed as the surrounding soil acts to oppose the increase in horizontal diameter of the shell. As the flexural rigidity of the cylinder is increased, the model will deform less under load and the resistance to deformation must be taken more by the shell itself in the form of hoop bending moments.

Table IV shows a comparison between the cylindrical shell models with D/t ratios of 80 both with hemispherical end closures and with no end restraints. It can be seen that the behavior of the cylindrical shell model with hemispherical heads is very similar to the behavior of a cylindrical shell model with no end restraints with one notable exception. The distributions of the longitudinal membrane force which are further illustrated in Figure 18 are completely different for the two models. The curves of Figure 18 show:

a) there is an overall longitudinal bending of the cylindrical shell with no end restrains which tends to produce longitudinal compressive forces at the crown and tensile forces at the invert,

b) there is no tensile membrane force at the invert for the model with hemispherical heads. This can be attributed to the end thrust transferred to the cylindrical shell by the hemispherical heads,

c) the tension which occurs at the springing for the model with heads does not occur in the model without heads. The exact nature of the action producing this force can not be readily explained at this time. It is believed that these tensile forces are developed as the hemispherical heads try to maintain the shell in a circular shape and act to resist any horizontal change in diameter.

Table V shows that the greatest variation between the static and dynamic results occurs for the hoop membrane force at the springing where the dynamic value is 54% greater than the static value. It appears that the rapid (7 msec) application of overpressure does not allow the soil sufficient time to develop arching over the model. This is further illustrated in Figure 21 which shows that the load transmitted to the model, rather than being reduced as in the static case, is actually greater than the value of the overpressure multiplied by the projected area of one-half the model. This seems to indicate that load is transferred onto the model from the surrounding soil.

ACKNOWLEDGEMENT

The research program described in this paper was conducted by personnel of the soil mechanics and experimental stress analysis sections of IIT Research Institute for Air Force Weapons Laboratory under Contract AF29(601)-5372. The authors would like to express their appreciation to Mr. R.H.Atkinson of Air Force Weapons Laboratory, who monitored the work, for his numerous comments and suggestions and for his help in obtaining permission to publish the results.

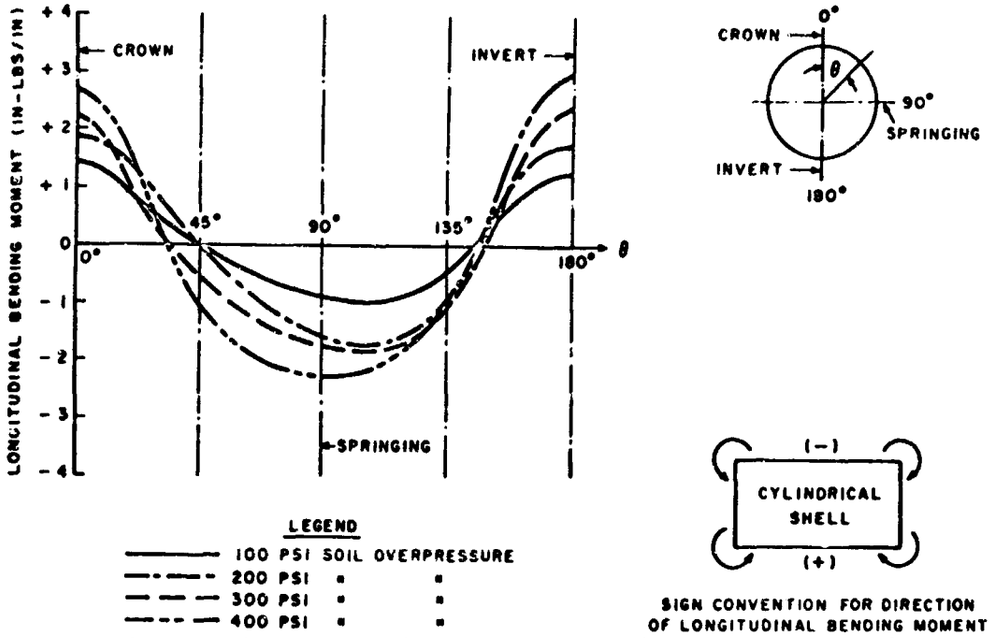


Fig. 14 Distribution of the Longitudinal Bending Moment at the Central Transverse Cross Section of the Cylindrical Shell Model with Hemispherical Heads (D/t = 80) for Four Different Levels of Soil (Ottawa Sand) Overpressure

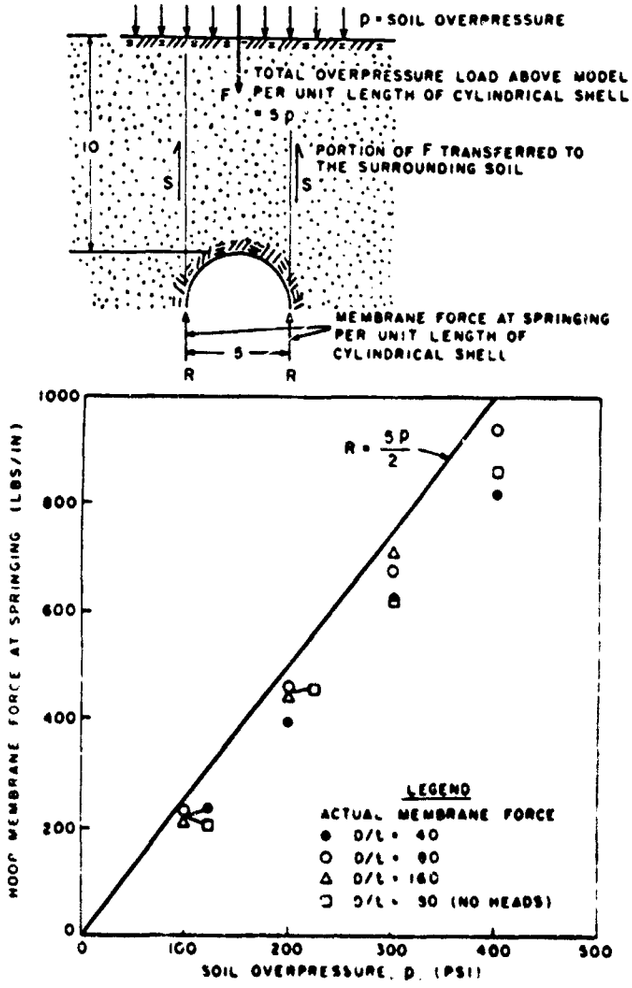


Fig. 15 Hoop Membrane Force at the Springing of the Central Transverse Cross Section of the Cylindrical Shell Vs. Soil Overpressure

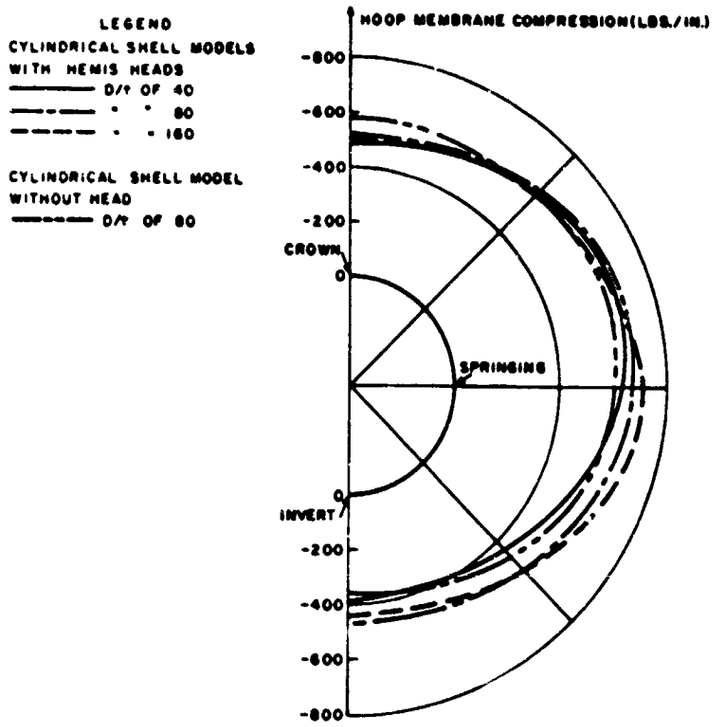


Fig. 16 Comparison of the Hoop Membrane Force Distributions at the Central Transverse Cross Sections of Four Models for a Soil (Ottawa Sand) Overpressure of 300 psi.

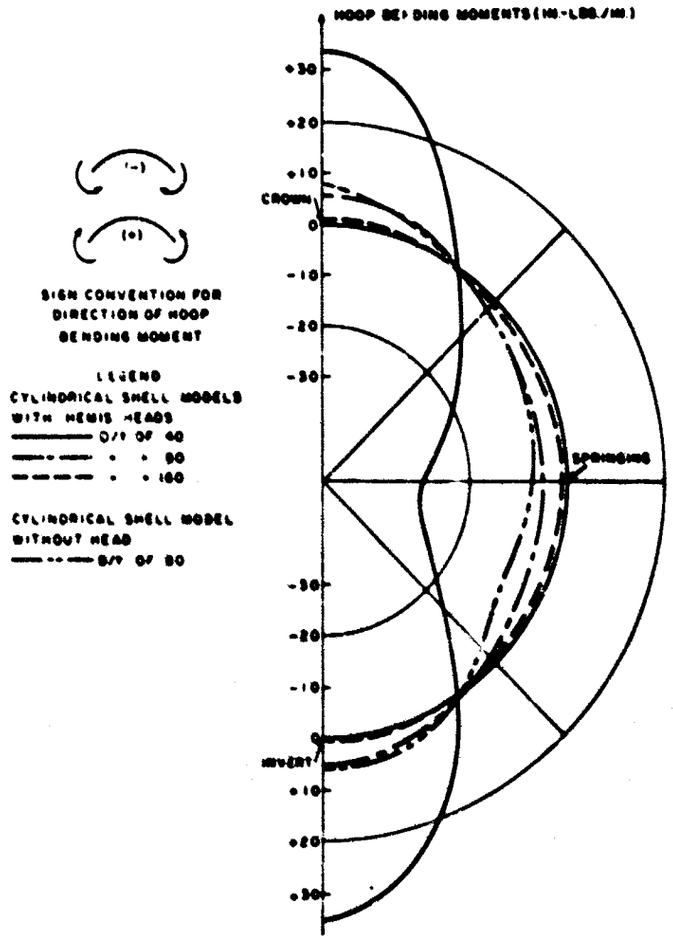


Fig. 17 Comparison of the Hoop Bending Moment Distributions at the Central Transverse Cross Sections of Four Models for a Soil (Ottawa Sand) Overpressure of 300 psi

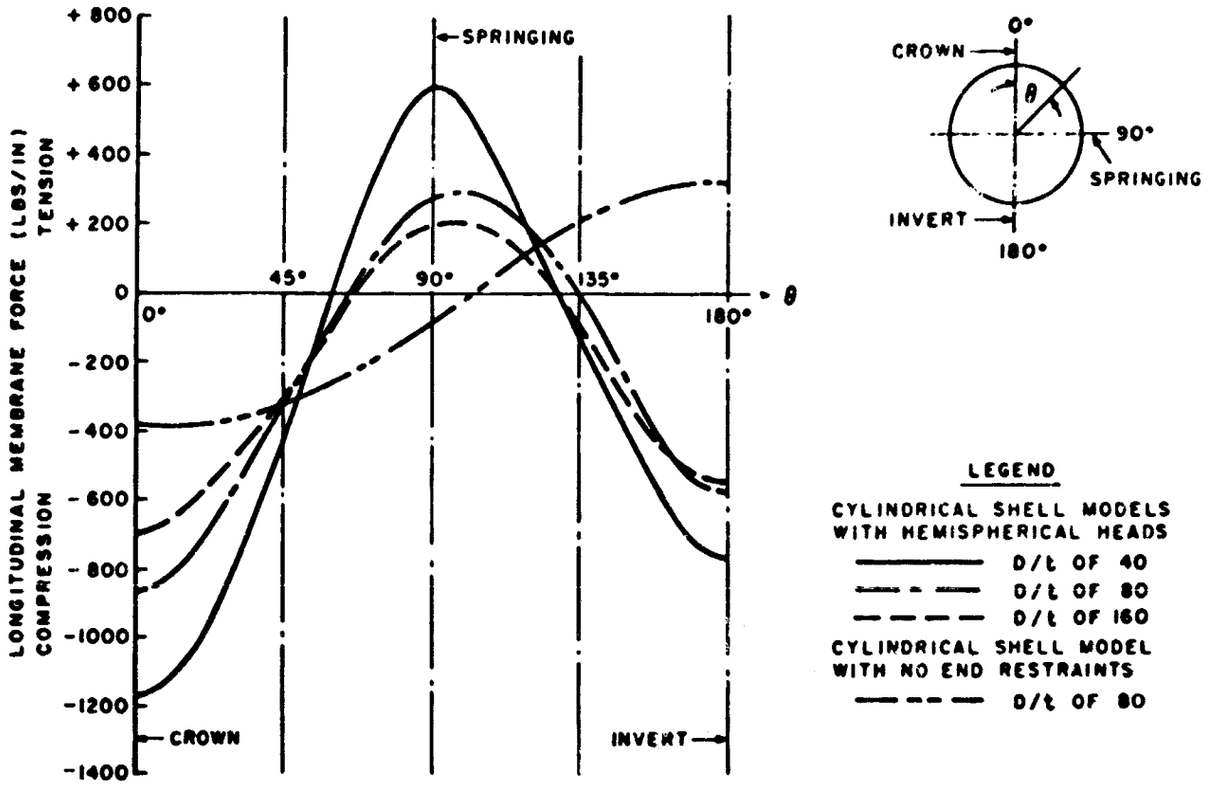


Fig. 18 Comparison of the Longitudinal Membrane Force Distributions at the Central Transverse Cross Sections of Four Models for a Soil (Ottawa Sand) Overpressure of 300 psi

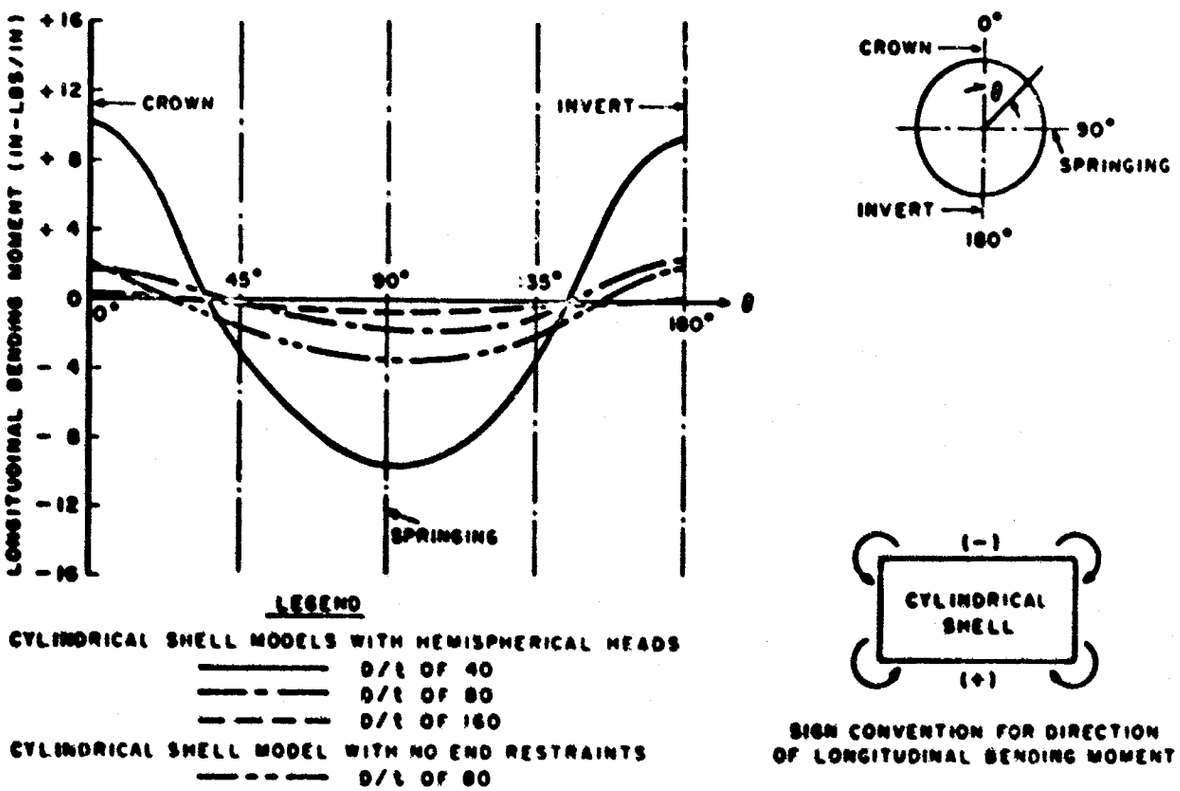


Fig. 19 Comparison of the Longitudinal Bending Moment Distributions at the Central Transverse Cross Sections of Four Models for a Soil (Ottawa Sand) Overpressure of 300 psi

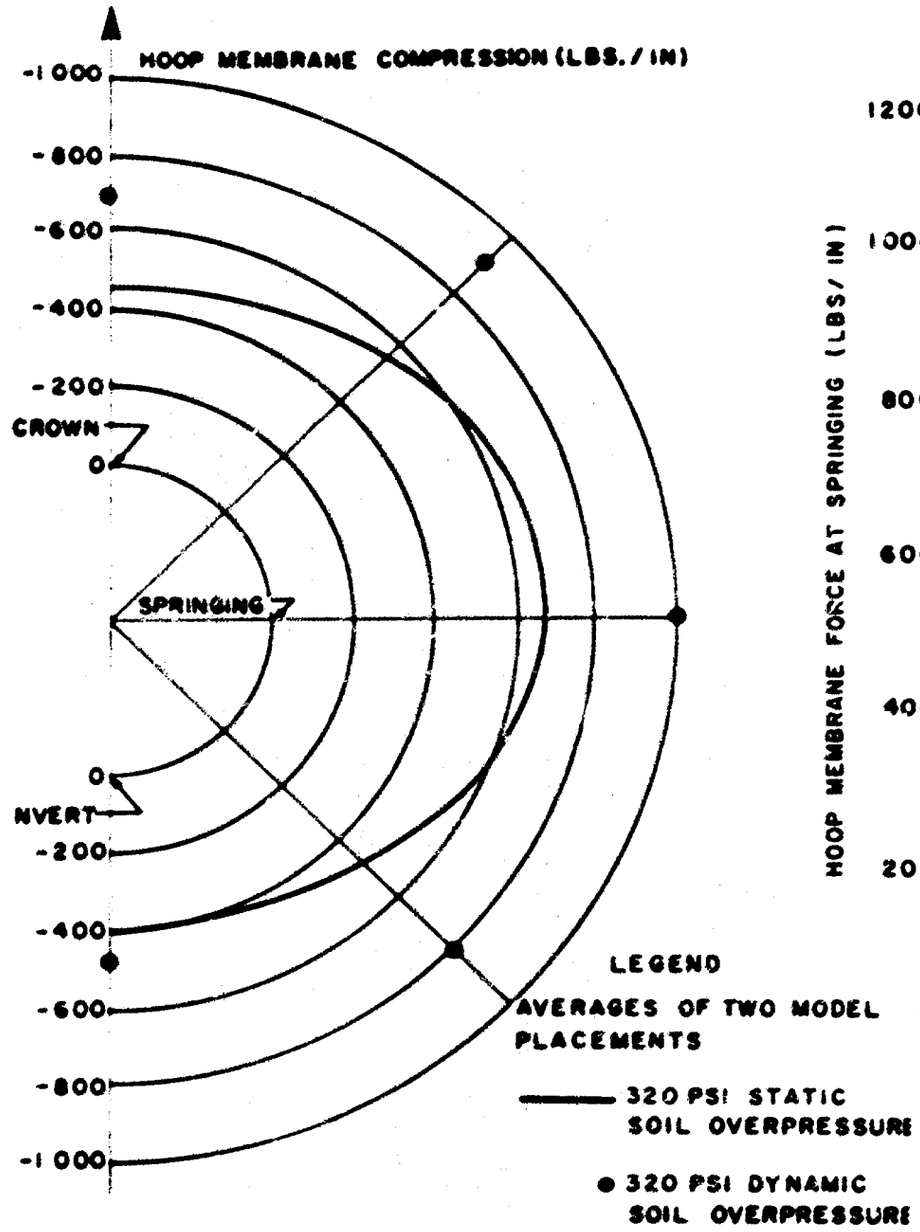


Fig. 20 Hoop Membrane Force Distribution at the Central Transverse Cross Section of the Cylindrical Shell Model with Hemispherical Heads (D/t = 40)

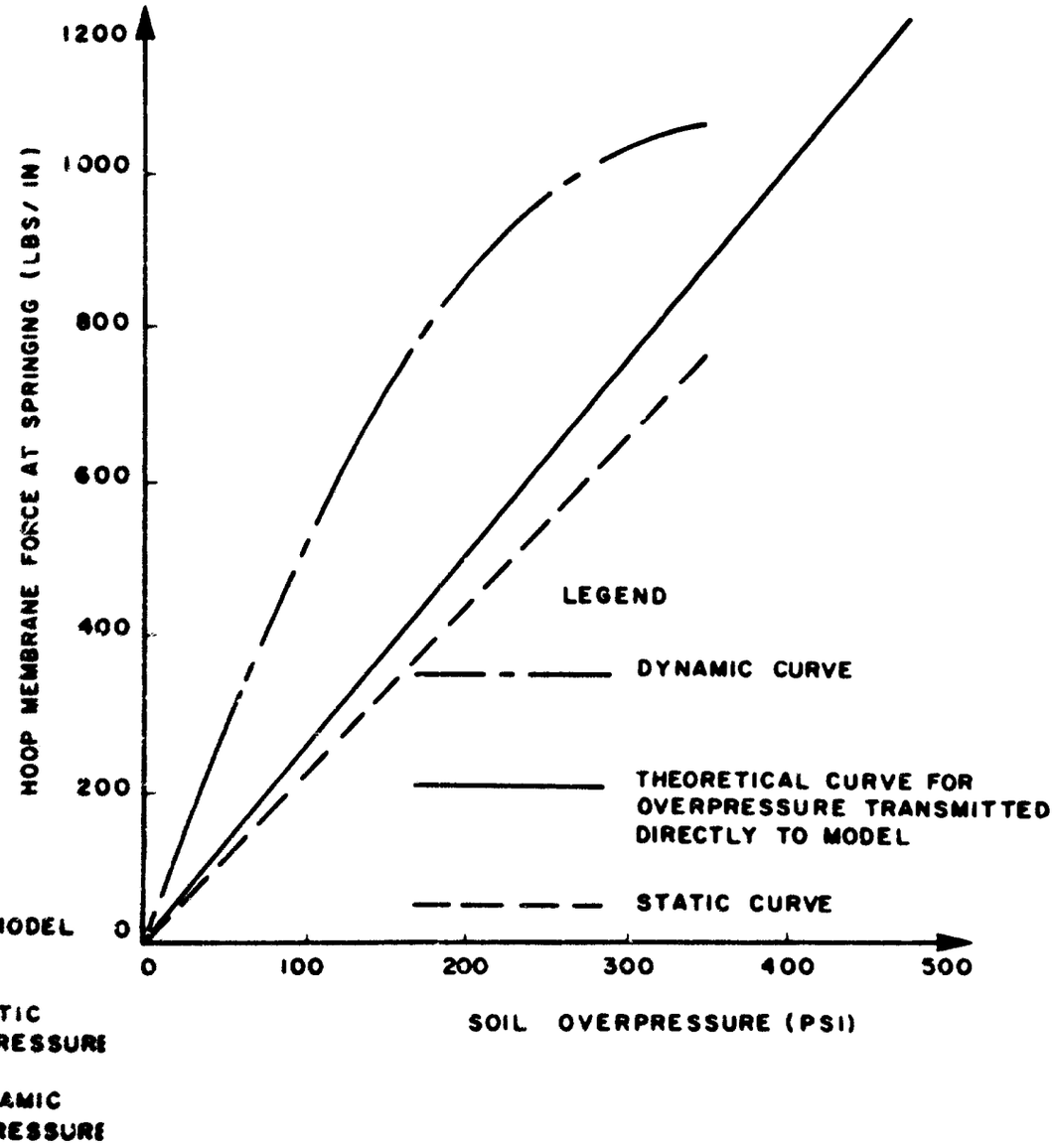


Fig. 21 Variation of Hoop Membrane Force at Springing with Soil Overpressure, Cylindrical Shell Model with D/t = 40

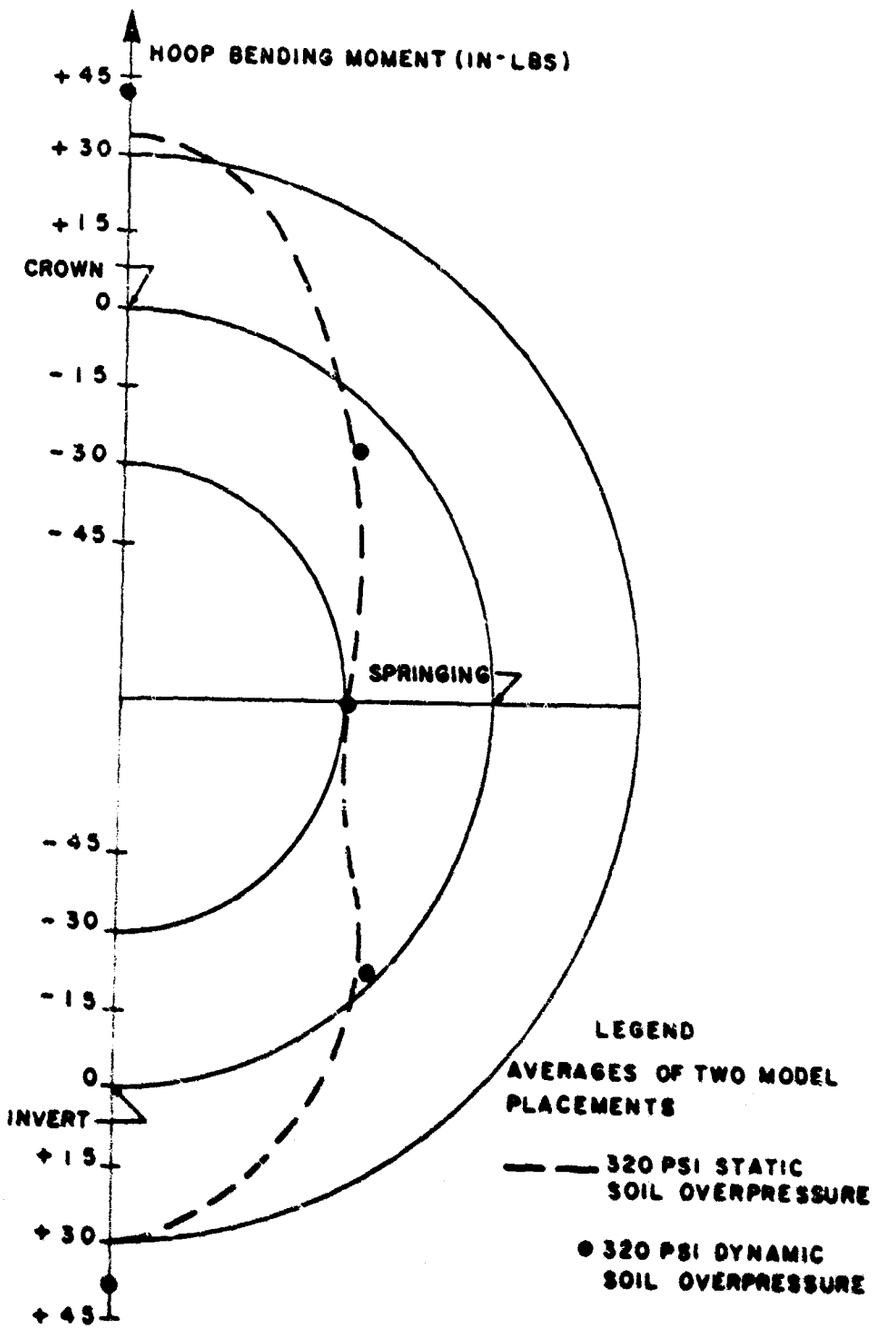


Fig. 22 Hoop Bending Moment Distribution at the Central Transverse Cross Section of the Cylindrical Shell Model with Hemispherical Heads ($D/t = 40$)

Table II

INFLUENCE OF THE MAGNITUDE OF THE STATIC SOIL OVERPRESSURE ON THE BEHAVIOR OF THE BURIED MODEL

Central Transverse Cross Section of Cylindrical Shell Model with No End Restraints

Diameter to Thickness Ratio = 80

Flexural Rigidity = $\frac{E t^3}{12 (1 - \mu^2)}$ = 655

Structural Function of Cylindrical Shell Model	Static Soil Overpressure						
	100 psi	200 psi		300 psi		400 psi	
	Value of Function	Value of Function	Increase in Value of Function as a Percentage of Value at 100 psi	Value of Function	Increase in Value of Function as a Percentage of Value at 100 psi	Value of Function	Increase in Value of Function as a Percentage of Value at 100 psi
Increase in Horizontal Diameter (inches)	0.024	0.032	33%	0.037	21%	0.041	17%
Decrease in Vertical Diameter (inches)	0.029	0.039	35%	0.045	21%	0.052	24%
Hoop Membrane Force at Springing (lbs/in.)	-220	-440	100%	-620	82%	-860	110%
Hoop Membrane Force at Crown (lbs/in.)	-190	-380	100%	-580	105%	-760	95%
Hoop Membrane Force at Invert (lbs/in.)	-120	-240	100%	-360	100%	-480	100%
Hoop Bending Moment at Springing (in-lbs/in.)	-4.0	-6.0	50%	-7.2	30%	-8.8	40%
Hoop Bending Moment at Crown (in-lbs/in.)	+5.6	+6.6	18%	+8.0	25%	+8.0	0%
Hoop Bending Moment at Invert	+4.8	+6.3	31%	+6.3	0%	+7.2	14%

Table III

INFLUENCE OF THE MODEL STIFFNESS

Central Transverse Cross Section of Cylindrical Shell Models with Hemispherical Heads

Static Soil Overpressure = 300 psi

Structural Function of Cylindrical Shell Model	Cylindrical Shell Models with Hemispherical Heads				
	D/t = 80 $\frac{E t^3}{12(1-\mu^2)} = 655$	D/t = 160 $\frac{E t^3}{12(1-\mu^2)} = 82$		D/t = 40 $\frac{E t^3}{12(1-\mu^2)} = 5240$	
	Value of Function	Value of Function	Difference as a Percentage of the Value for the Model with D/t = 80	Value of Function	Difference as a Percentage of the Value for the Model with D/t = 80
Increase in Horizontal Diameter (inches)	0.024	0.026	+ 8.5%	0.022	- 8.5%
Decrease in Vertical Diameter (inches)	0.031	0.040	+29.0%	0.026	-16.0%
Hoop Membrane Force at Springing (lbs/in.)	-680	-720	+ 6.0%	-640	- 6.0%
Hoop Membrane Force at Crown (lbs/in.)	-520	-500	- 4.0%	-480	- 8.0%
Hoop Membrane Force at Invert (lbs/in.)	-470	-440	- 6.0%	-400	-15.0%
Hoop Bending Moment at Springing (in-lbs/in.)	5	- 2	-60.0%	- 30	+500.0%
Hoop Bending Moment at Crown (in-lbs/in.)	+ 5	+ 1	-80.0%	+ 34	+580.0%
Hoop Bending Moment at Invert (in-lbs/in.)	+ 5	+ 1	-80.0%	+ 35	+600.0%

Table IV

INFLUENCE OF HEMISPHERICAL END CLOSURES

Central Transverse Cross Section of Cylindrical Shell Model

Diameter to Thickness Ratio = 90

Flexural Rigidity = $\frac{E t^3}{12(1-\mu^2)}$ = 655 lb-in^2

Static Soil Overpressure = 400 psi

Structural Function of Cylindrical Shell Model		Cylindrical Shell Model With		Difference as a Percentage of Model with No End Restraint
		No End Restraint	Hemis. End Closures	
Increase in Horizontal Diameter (inches)		0.042	0.029	-31%
Decrease in Vertical Diameter (inches)		0.052	0.037	-29%
Hoop Membrane Force (lbs/in.)	At Springing	-860	-930	+ 8%
	At Crown	-780	-780	0%
	At Invert	-480	-530	+10%
Hoop Bending Moment (in-lbs/in.)	At Springing	- 8	- 6	-25%
	At Crown	+ 8	+ 8	0%
	At Invert	+ 7	+ 7	0%
Longitudinal Membrane Force (lbs/in.)	At Springing	-200	+330	
	20° Below Springing	0	+400	
	At Crown	500	-1000	+100%
	At Invert	+400	-760	
Longitudinal Bending Moment (in-lbs/in.)	At Springing	- 4	- 2	- 50%
	At Crown	+ 3	+ 3	0%
	At Invert	+ 2	+ 3	+ 50%

Table V

COMPARISON OF STATIC AND DYNAMIC RESULTS

Central Transverse Cross Section of Cylindrical Shell Model with Hemispherical Heads

Diameter to Thickness Ratio = 40

Flexural Rigidity = $\frac{E t^3}{12(1-\mu^2)}$ = 5240 lb-in^2

Soil Overpressure = 320 psi

Structural Function of Cylindrical Shell Model	Static Value	Dynamic Value	Difference as a Percentage of Static Value
Increase in Horizontal Diameter (inches)	0.021	0.023	+ 9.5%
Decrease in Vertical Diameter (inches)	0.023	0.028	+22.0%
Hoop Membrane Force at Springing (lbs/in.)	-670	-1030	+54.0%
Hoop Membrane Force at Crown (lbs/in.)	-453	- 690	+52.0%
Hoop Membrane Force at Invert (lbs/in.)	-395	- 480	+22.0%
Hoop Bending Moment at Springing (in-lbs/in.)	- 29	- 32	+10.0%
Hoop Bending Moment at Crown (in-lbs/in.)	+ 33	+ 42	+27.0%
Hoop Bending Moment at Invert (in-lbs/in.)	+ 30	+ 39	+30.0%

INTERACTION BETWEEN A SAND AND CYLINDRICAL SHELLS UNDER STATIC AND DYNAMIC LOADING

by
John Thomas Hanley*

ABSTRACT

A series of fourteen static and twelve dynamic tests were conducted on three cylindrical shells in a fine, dry, sand. Each four-inch diameter shell (pipe) was placed in the center of a cylindrical container approximately two feet in diameter and two feet in depth; the axis of the pipe being coincident with the axis of the container. The pipe was then surrounded by the sand, which was compacted in six-inch layers up to the top of the container. A neoprene diaphragm was placed on top of the soil sample to prevent gas penetration into the soil. A uniformly distributed gas pressure was then applied to the surface of the soil sample and to the capped end of the pipe (top) both statically and dynamically to simulate loading by a plane shock wave traveling in a direction normal to the surface of the soil.

Measurements were made of the gas pressure near the surface of the soil, of the vertical pressure at various depths in the soil and of the vertical and circumferential strains in the pipes at three depths; four, ten and sixteen inches below the surface. Calculations were then made of the effective lateral pressure at the soil-structure interface at the three gauge depths and of the magnitude and direction of the shear acting between the gauge lines at that interface. Using the calculated lateral pressures and vertical soil pressures obtained from soil pressure gauge measurements, the ratios of the former to the latter (K_f) were calculated for both static and dynamic tests for two depths; four and sixteen inches below the surface.

Under static load, at four inches below the surface the value of K_f increased with applied load from about 0.5 to about 0.6. These relatively high values of K_f are believed to be caused by the depression of the surface of the soil around the top of the pipe. At a depth of sixteen inches the value of K_f increased from about 0.3 to about 0.4.

From the dynamic tests, it appeared that initially the soil was behaving much as a viscous fluid at a depth of four inches. The computed value of K_f at four inches was about 1.0 at four milliseconds. With increasing time, the value of K_f at that depth decreased to about 0.7. However, at a depth of sixteen inches, the value of K_f increased slightly with time, the average value being about 0.45.

As a consequence of the transfer of load from the soil to the structure under both static and dynamic loading, the circumferential strains in the shells were tensile rather than compressive at a depth of sixteen inches. This behavior may be predicted for large cylindrical shells in soil with similar foundation conditions and under similar loading conditions.

It was apparent from the raw data obtained, and shear calculations confirmed, that ahead of the stress wave in the soil the shells moved down with respect to the soil under dynamic load. This behavior was predicted and was caused by the high velocity of stress propagation in the shells as compared to the soil.

Additional studies are required before it will be possible to predict the dynamic interaction between a cylindrical shell, such as those tested, and soils in general. The tests conducted, however, confirmed qualitative predictions of the interaction between a fine sand and simple shell structures responding within the elastic range and furnished some data which was not previously available.

INTRODUCTION

Objectives and Scope

The interaction between a vertically oriented cylindrical shell and the soil surrounding it when subjected to a stress wave traveling in the direction of the shell's axis is a problem of practical significance. Examples of such structures are missile silos, fuel tanks, and access and ventilation shafts for underground installations (see Figure 1). Analytical considerations indicated that a cylindrical shell, properly instrumented, should permit the calculation of the lateral pressure acting at the soil-structure interface and of the load transferred to the shell by the soil, or vice versa, through shear at the interface.

Further, if the vertical pressure could be measured at various depths in the soil adjacent to the shell, it would be possible to obtain a ratio between the lateral pressure calculated from strain measurements in the pipe and the vertical pressure in the soil at the same depth. This ratio is not that denoted by K in soil mechanics literature for reasons which

*Associate Professor, Department of Civil Engineering, University of Minnesota, Minneapolis, Minnesota.

will be discussed, but it would furnish information of value.

Thus, the basic objectives of the experimental program were:

a. to obtain information regarding the ratio between the lateral pressure acting on a cylindrical shell in soil and the vertical pressure in the soil at the same depth,
b. to obtain information regarding the transfer of load between the soil and the shell through shear at the interface, and
c. to determine whether there were fundamental differences in the soil-structure interaction under static and dynamic load.

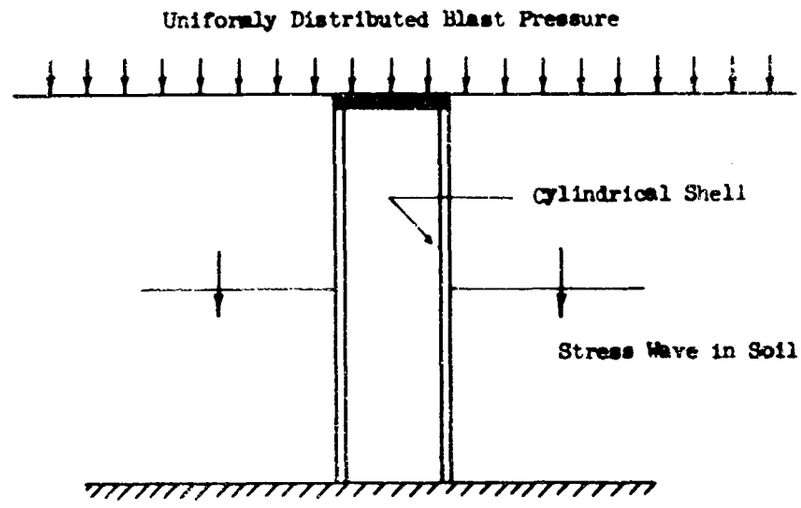


Fig. 1 Practical Problem Simulated by Experiment

Because the laboratory equipment employed has never been used for such studies an important secondary objective was to investigate the capabilities of the equipment for such studies. For this reason and because of time and cost limitations the test program was limited as follows:

a. Only a non-cohesive soil, a fine sand, was used.
b. Structural response was limited to small, elastic deflections.
c. Only one rise-time was employed for the dynamic loading.

In addition to the above it is known that gas at high pressures, such as those associated with blast loading, will penetrate a porous medium such as sand. Such penetration undoubtedly occurs in the real case. This is a problem which requires investigation. However, for these tests it was decided to prevent gas penetration primarily because the soil sample was so small that the gas penetration might be so rapid as to preclude meaningful measurements.

Finally, an inherent limitation of the laboratory equipment available is that it can not produce a shock wave at the surface of the soil sample. While this limitation is not of major significance in some respects, it is of importance in terms of structural response. It was recognized before the tests were planned in detail that the ratio of the rise-time of the pressure pulse to the fundamental natural period of vibration of the structure would be so large that there would be no dynamic amplification of structural response.

Notation

A = an area; various

$B = \dfrac{Eh^3}{12(1-\nu^2)}$, characteristic stiffness of the shell in flexure

c = velocity of stress propagation in any material

c_v = viscosity coefficient

$C, C_1, \bar{C}_1, C_2, \bar{C}_2, C_3, \bar{C}_3$ = constants of integration

$D = \dfrac{Eh}{1-\nu^2}$, characteristic stiffness of shell in compression

E = elastic modulus of shell material

f = a measure of the shear at the soil-structure interface

h = thickness of the shell in the z- (or radial) direction

k_1 = characteristic stiffness of shell in compression

k_2 = characteristic stiffness of soil column in compression

k = subgrade modulus in soil

K = ratio of lateral to vertical stress in soil under conditions of plane deformation

K_f = ratio of lateral pressure at soil-structure interface to vertical pressure in soil adjacent to shell

L = length of cylindrical shell in the x-direction

m = a constant

M = confined modulus of compression for soil

$M_x = \int_{-\frac{h}{2}}^{+\frac{h}{2}} z\,\sigma_x\,dz = -\frac{Eh^3}{12(1-\nu^2)}\,\frac{\partial^2 w}{\partial x^2}$; M_x = unit bending moment in the x-direction, $(\frac{\text{force-length}}{\text{length}})$

$N_x = \int_{-\frac{h}{2}}^{\frac{h}{2}} \sigma_x\,dz = \frac{Eh}{1-\nu^2}\left(\frac{\partial u}{\partial x} - \nu\,\frac{w}{R}\right)$; N_x = unit normal force in the x-direction, or force per unit length

$N_y = \int_{-\frac{h}{2}}^{\frac{h}{2}} \sigma_y\,dz = \frac{Eh}{1-\nu^2}\left(\frac{w}{R} - \nu\,\frac{\partial u}{\partial x}\right)$; N_y = unit normal force in the y-direction, or force per unit length

p = uniform radial pressure acting on a cylindrical shell

p_n = natural circular frequency of shell in n^{th} mode

p_o = pressure acting at the soil surface

p_v = vertical pressure in the soil

$Q_x = \int_{-\frac{h}{2}}^{\frac{h}{2}} \tau_{xz}\,dz$; Q_x = unit normal shear perpendicular to the x-axis, (force/length)

$r_k = \frac{k_1}{k_2}$, ratio of stiffnesses of shell and equivalent soil column in compression

R = radius of shell

R_t = radius of soil container

t = time

T = period of vibration

u = displacement of shell in x-direction

w = displacement of shell in radial or z-direction

x = coordinate along the axis of the shell from top

$\bar{x}$ = $L-x$, coordinate along the axis of the shell from bottom

z = radial coordinate of shell

β = damping coefficient

θ = correction factor for effect of shell thickness on radial strain

$\lambda = \sqrt[4]{12\,\frac{R^2}{h^2}}$

ν = Poisson's ratio of shell material

ρ = mass density of the shell material

σ_x = stress in shell in x-direction

σ_y = stress in shell in y-direction

ϕ = angle of internal friction of soil

ANALYTICAL CONSIDERATIONS

Before undertaking the experimental program several questions were raised, the answers to which were necessary to the design of the experiment, to the choice of structures to be tested and their instrumentation, and to the analysis of the data obtained. Among these questions were;

1. What is the variation of vertical and lateral pressure with depth in the soil sample under static load?
2. How far from the end of the shell should the first gauge line be placed to avoid flexural strains developed by the support conditions?
3. What affect would flexure induced by a variation of lateral pressure have on the strains in the shell?
4. What effect would pipe wall thickness have on the strains measured?
5. Is it possible to predict what the interaction between the soil and the structure should be under both static and dynamic load?

In addition, as the work progressed it became clear that some additional definitions were required to ensure that the data and subsequent calculations were properly interpreted and not confused with other similar expressions. In particular, the meaning of the ratio of effective lateral pressure to the vertical stress in the soil, as obtained from these experiments, required clarification. Thus a brief discussion of the meaning of the ratio defined as K_f in this document, is included.

The question of the possibility of dynamic response of the structures tested is raised and answered in Appendix A. The calculated natural frequencies of all structures tested are so high that no dynamic response of the shells could be anticipated. In one particular respect this is fortunate; the pipes used also served as soil pressure gauges and the lack of dynamic response simplified the lateral pressure calculations.

Variation of Vertical Soil Pressure with Depth-Static Case

This apparently simple problem has been given considerable attention. The simplest approach is that developed by Taylor (1). With it an expression may be developed for the variation of the "average" pressure as a function of depth under the planned test conditions. Taking the sum of the vertical forces shown in Figure 2;

$$\pi\,(R_t^2 - R^2)\,\frac{\partial P_v}{\partial x}\,dx + fKp_v\,2\pi(R_t + R)\,dx = 0$$

from which

$$\frac{d(p_v)}{dx} + \left[\frac{2fK}{R_t(1 - \frac{R}{R_t})}\right] p_v = 0$$

If it is assumed that f and K do not vary with x;

$$p_v = p_o \exp\left[-\frac{2fK}{(1 - \frac{R}{R_t})}\right]\frac{x}{R_t} \qquad (1)$$

In Equation 1, R is the radius of the shell in the tank, R_t is the radius of the tank, K is the ratio of the lateral stress to the vertical stress in the soil at the soil structure interface and f is the coefficient of friction between the sand and the wall or the tangent of the angle of internal friction in the soil whichever is smaller.

The assumption that f and K do not vary with x is a gross one and will be discussed more fully later. Even the use of the ratio K is open to discussion here. However, it will be established that if the tank wall and structure are rigid compared to the soil, the assumption that f does not vary with depth is justified. Further, defining K properly will permit its use in the expression.

Effect of End Restraint and Load Variation on Strains in the Shell

The effect of end restraint on the strains in an elastic thin shell subjected to a uniform, radially symmetric load has been investigated (2). It has been established that even assuming a "fixed" end condition the flexural strains induced are limited to a narrow zone in the vicinity of the end. To the author's knowledge the effect of an exponentially varying load on the strains in the shell has not been investigated. Since the analysis requires the assumption of boundary conditions, these two effects may be determined from an analysis of an elastic thin shell subjected to a radially symmetric load which varies exponentially with x.

The worst end condition which can be imagined for the test structure is a fixed end condition; that is, both rotation and radial displacement are prevented by the cap at the top. In fact, such restraint can not be achieved but the disturbance created by less restraint will not be felt as far from the end. Thus for the purposes of the problem at hand, the assumption of a fixed end is conservative.

Using Timoshenko's coordinate notation (3) (see Figure 3), the differential equation of static equilibrium of the shell may be written as:

$$\frac{d^4w}{dx^4} + \frac{D}{BR^2}\,w - \frac{K}{B}\,p_v(x) = 0 \qquad (2)$$

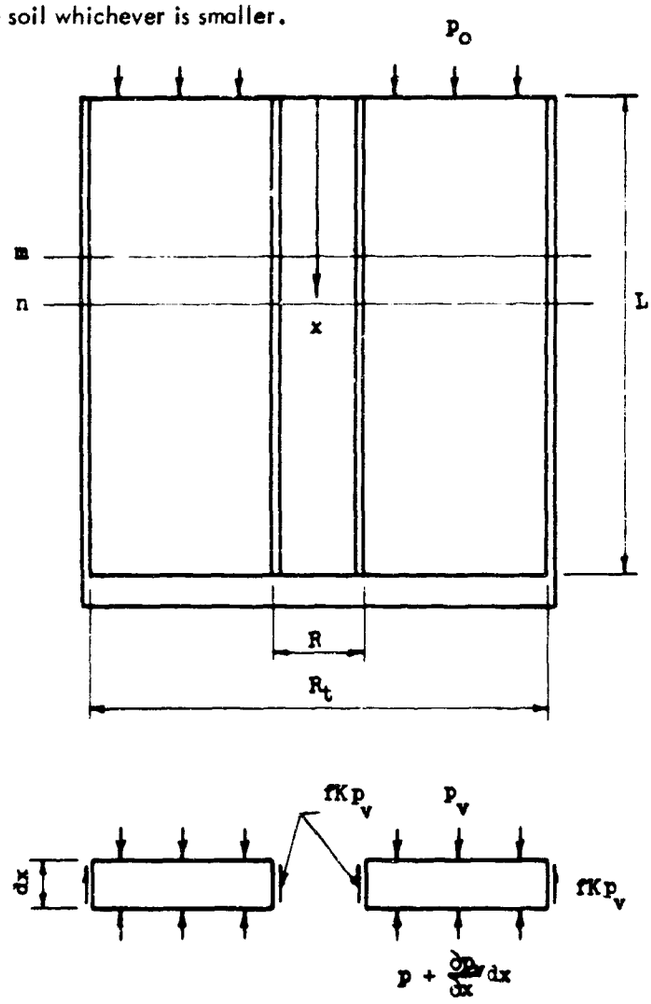
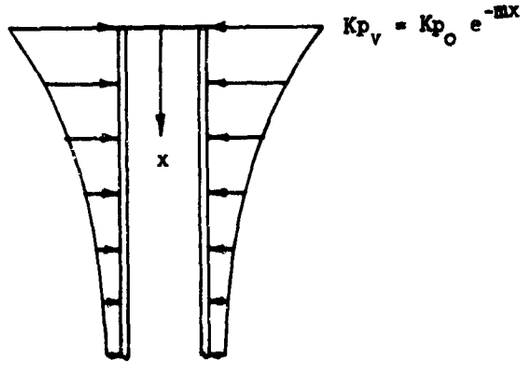


Fig. 2 Notation for Variation of Vertical Soil Pressure with Depth in Container



Equilibrium Equations:

$$\frac{\partial Q_x}{\partial x} + \frac{N_y}{R} + Kp_v = 0$$

$$\frac{\partial M_x}{\partial x} - Q_x = 0$$

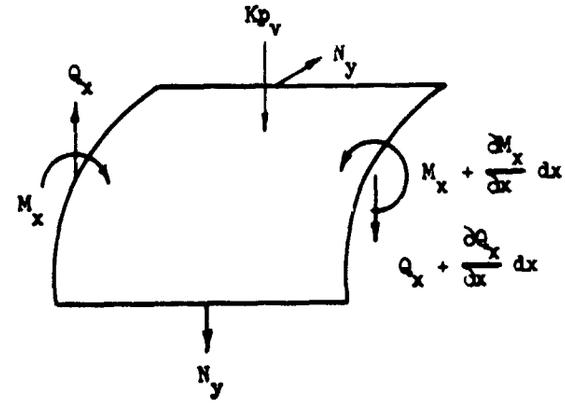


Fig. 3 Notation for Thin Cylindrical Shell Subjected to Radially Symmetric Load Which Varies Exponentially with x

The homogeneous solution of Equation 2 may be written:

$$w_h = e^{-\lambda\frac{x}{R}}\left(C_1 \cos\lambda\frac{x}{R} + C_2 \sin\lambda\frac{x}{R}\right) + e^{-\lambda\frac{\bar{x}}{R}}\left(\bar{C}_1 \cos\lambda\frac{\bar{x}}{R} + \bar{C}_2 \sin\lambda\frac{\bar{x}}{R}\right)$$

where

$$\lambda = \sqrt[4]{12\frac{R^2}{h^2}}$$

and

$$\bar{x} = L - x$$

The assumed boundary conditions are:

(a) $w\Big|_{x=0} = 0$ (b) $w\Big|_{x=L} = 0$

(c) $\left.\frac{dw}{dx}\right|_{x=0} = 0$ (d) $\left.\frac{dw}{dx}\right|_{x=L} = 0$

Assuming that the lateral pressure varies exponentially with x:

$$Kp_v = Kp_o e^{-mx},$$

a particular solution may be obtained.

Let

$$w_p = C_3 e^{-mx}$$

Substituting the assumed particular solution in the differential equation, it may be determined that:

$$C_3 = \frac{Kp_o e^{-mx}}{B\left(m^4 + \frac{\lambda^4}{R^4}\right)}$$

Now letting

$$\bar{C}_3 = \frac{Kp_o}{B\left(m^4 + \frac{\lambda^4}{R^4}\right)}$$

the complete solution may be written

$$w = e^{-\lambda\frac{x}{R}}\left(C_1 \cos\lambda\frac{x}{R} + C_2 \sin\lambda\frac{x}{R}\right) + e^{-\lambda\frac{\bar{x}}{R}}\left(\bar{C}_1 \cos\lambda\frac{\bar{x}}{R} + \bar{C}_2 \sin\lambda\frac{\bar{x}}{R}\right) + \bar{C}_3 e^{-mx}$$

where w is the radial displacement of the shell.

From boundary condition (a):

$$C_1 + e^{-\lambda\frac{L}{R}}\left(\bar{C}_1 \cos\lambda\frac{L}{R} + \bar{C}_2 \sin\lambda\frac{L}{R}\right) + \bar{C}_3 = 0$$

From (b)

$$e^{-\lambda\frac{L}{R}}\left(C_1\cos\lambda\frac{L}{R}+C_2\sin\lambda\frac{L}{R}\right)+\bar{C}_1+\bar{C}_3\,e^{-mL}=0$$

From (c)

$$-\frac{\lambda}{R}C_1+\frac{\lambda}{R}C_2+\frac{\lambda}{R}e^{-\lambda\frac{L}{R}}\left[(\bar{C}_1+\bar{C}_2)\sin\lambda\frac{L}{R}+(\bar{C}_1-\bar{C}_2)\cos\lambda\frac{L}{R}\right]-m\bar{C}_3=0$$

From (d)

$$-\frac{\lambda}{R}e^{-\lambda\frac{L}{R}}\left[(C_2-C_1)\sin\lambda\frac{L}{R}+(C_1+C_2)\cos\lambda\frac{L}{R}\right]+\frac{\lambda}{R}\bar{C}_1-\frac{\lambda}{R}\bar{C}_2-m\bar{C}_3\,e^{-mL}=0$$

Since

$$\lambda=\sqrt[4]{12\frac{R^2}{h^2}}$$

$\lambda > 2$, for any reasonable shell thickness. Further, for the shells tested

$$\frac{L}{R}\simeq 13$$

therefore $e^{-\lambda\frac{L}{R}}\simeq 0$, and an approximate solution may be obtained by ignoring those terms which contain $e^{-\lambda\frac{L}{R}}$. Thus, the equations obtained from the boundary condition reduce to;

(a) $C_1+\bar{C}_3=0$

(b) $\bar{C}_1+\bar{C}_3\,e^{-mL}=0$

(c) $-\frac{\lambda}{R}C_1+\frac{\lambda}{R}C_2-m\bar{C}_3=0$

(d) $\frac{\lambda}{R}\bar{C}_1-\frac{\lambda}{R}\bar{C}_2-m\bar{C}_3\,e^{-mL}=0$

The constants C_1, C_2, $\bar{C}_1$ and $\bar{C}_2$ may be determined from these four equations and the complete solution of Equation 2 may be written:

$$\begin{aligned}w=\;&\bar{C}_3\,e^{-\lambda\frac{x}{R}}\left[-\cos\lambda\frac{x}{R}+\left(1+\frac{mR}{\lambda}\right)\sin\lambda\frac{x}{R}\right]\\&+\bar{C}_3\,e^{-mL}\,e^{-\lambda\frac{\bar{x}}{R}}\left[-\cos\lambda\frac{\bar{x}}{R}+\left(1-\frac{mR}{\lambda}\right)\sin\lambda\frac{\bar{x}}{R}\right]\\&+\bar{C}_3\,e^{-mx}\end{aligned}\qquad(3)$$

In Equation 3, the expression containing $e^{-\lambda\frac{\bar{x}}{R}}$ is negligible near $x = 0$ (i.e., $\bar{x}\simeq L$ when $x\simeq 0$). Therefore near the surface of the soil sample the radial displacement of the shell is governed by the following expression:

$$w=\bar{C}_3\,e^{-\lambda\frac{x}{R}}\left[-\cos\lambda\frac{x}{R}+\left(1+\frac{mR}{\lambda}\right)\sin\lambda\frac{x}{R}\right]+\bar{C}_3\,e^{-mx}\qquad(4)$$

From Equation 4 it may be seen that to avoid the disturbance induced by the boundary conditions, it is necessary to locate the first line of strain gauges at a distance, x, such that the term

$$\bar{C}_3\,e^{-\lambda\frac{x}{R}}\left[-\cos\lambda\frac{x}{R}+\left(1+\frac{mR}{\lambda}\right)\sin\lambda\frac{x}{R}\right]$$

may be neglected. If this is done the radial displacement of the shell may be expressed by:

$$w = \bar{C}_3 e^{-mx}$$

or, substituting the expression obtained for $\bar{C}_3$, by

$$w = \frac{Kp_o e^{-mx}}{B(m^4 + \frac{\lambda^4}{R^4})} \tag{5a}$$

The effect of the exponential decay of lateral pressure on the radial displacement, at some distance from the end, is indicated by the term, m^4, in the denominator of Equation 5a. That equation may be rearranged as follows:

$$w = \frac{Kp_o e^{-mx}}{B\frac{\lambda^4}{R^4}(1 + \frac{m^4R^4}{\lambda^4})} \tag{5b}$$

From Equation 5b it is apparent that if $(1 + \frac{m^4R^4}{\lambda^4}) \cong 1$, the effect of the load variation on the lateral displacement is negligible.

From the preceding discussion of the variation of vertical load with depth, m may be expressed as:

$$m = \frac{2fK}{R_t(1 - \frac{R}{R_t})}$$

For static loading reasonable maximum values for f and K are 1 and 0.5 respectively. Since $R_t \cong 12$ and $R \cong 2$

$$m \cong 0.1$$

and

$$m^4 \cong 0.0001$$

Since

$$\frac{R^4}{\lambda^4} = \frac{R^2h^2}{12}, \quad R \cong 2, \text{ and } h \ll 1, \text{ then } (1 + \frac{m^4R^4}{\lambda^4}) \cong 1.$$

Therefore it is concluded that the effect of the load variation on radial displacement is negligible and that the effect of the end restraint may be avoided by placing the first line of gauges at a distance x from the end such that expression

$$\zeta_3 e^{-\lambda\frac{x}{R}} \left(-\cos\lambda\frac{x}{R} + (1 + \frac{mR}{\lambda})\sin\lambda\frac{x}{R}\right)$$

is negligible.

In a similar manner, the flexural displacement due to a constant axial load may be shown to be negligible under the assumed loading conditions.

Development of Expressions Used for Data Analysis

Having established that the structures will not respond dynamically to the applied loading and that flexural deformations induced by the end restraint and the load variation may be avoided or are negligible, the equations of equilibrium for the shell reduce to

$$D\left[\frac{\partial^2 u}{\partial x^2} - \frac{\nu}{R}\frac{\partial w}{\partial x}\right] + fKp_v = 0 \tag{6}$$

$$\frac{D}{R}\left[\frac{w}{R} - \nu\frac{\partial u}{\partial x}\right] - Kp_v = 0 \tag{7}$$

Rearranging Equation 6 and integrating with respect to x, yields

$$\frac{\partial u}{\partial x} = - \int_o^{x_1} fKp_v \, dx + \nu \frac{w}{R} + C$$

The value of the constant of integration can be obtained by evaluating $\frac{\partial u}{\partial x}$ at x = 0, noting that w = 0 at this point:

$$\left.\frac{\partial u}{\partial x}\right|_{x=0} = - \frac{p_o R}{2D}$$

Therefore

$$C = - \frac{p_o R}{2D}$$

and

$$\frac{\partial u}{\partial x} = - \frac{1}{D} \int_o^{x_1} fKp_v \, dx + \nu \frac{w}{R} - \frac{p_o R}{2D} \tag{8}$$

From (7)

$$Kp_v = \frac{D}{R} \left[\frac{w}{R} - \nu \frac{\partial u}{\partial x} \right] \tag{9}$$

The measurements which are possible on the shells are measurements of vertical strain ($\partial u/\partial x$) and circumferential strain (w/R). Thus, from Equation 9 the product Kp_v may be obtained and then, if f is assumed to be constant between two successive gauge lines the value of f may be obtained from Equation 8 as follows:

Let $\left.\frac{\partial u}{\partial x}\right|_{x_1}$ be the vertical strain at depth x_1.

$$\left.\frac{\partial u}{\partial x}\right|_{x_1} = - \frac{f}{D} \int_o^{x_1} Kp_v \, dx + \nu \left.\frac{w}{R}\right|_{x_1} - \frac{p_o R}{2D}$$

Similarly

$$\left.\frac{\partial u}{\partial x}\right|_{x_2} = - \frac{f}{D} \int_o^{x_2} Kp_v \, dx + \nu \left.\frac{w}{R}\right|_{x_2} - \frac{p_o R}{2D}$$

Then

$$\left.\frac{\partial u}{\partial x}\right|_{x_2} - \left.\frac{\partial u}{\partial x}\right|_{x_1} = - \frac{f}{D} \int_{x_1}^{x_2} Kp_v \, dx + \nu \left[\left.\frac{w}{R}\right|_{x_2} - \left.\frac{w}{R}\right|_{x_1} \right]$$

and

$$f = \frac{-D \left[\left.\frac{\partial u}{\partial x}\right|_{x_2} - \left.\frac{\partial u}{\partial x}\right|_{x_1} \right] + \nu \left[\left.\frac{w}{R}\right|_{x_2} - \left.\frac{w}{R}\right|_{x_1} \right]}{\int_{x_1}^{x_2} Kp_v \, dx} \tag{10}$$

The indicated integration was performed numerically using Newmark's (12) concentration formulas, which is equivalent to representing the variation of Kp_v with x, by a second degree polynomial of the form

$$Kp_v = ax^2 + bx + c$$

Effect of Shell Thickness on Circumferential Strain

In the foregoing analysis the shell was assumed to be a thin shell. For such shells, the circumferential strain does not vary significantly from the middle surface to the extreme fiber. However, as the thickness of the shell increases this is no longer true. Significant concentrations of strain may occur at the inner surface, particularly, where the strain gauges were placed to avoid possible damage resulting from relative displacement between the soil and the structure.

From Equation 9 it may be seen that the effect of a concentration of circumferential strain is to increase the calculated value of the effective lateral pressure. Further from the development of the basic shell equations (3) it may be seen that a resonable approximation to the correction factor required may be expressed as

$$\theta = \frac{1}{(1 + \frac{h}{2R})} \tag{11}$$

where θ is the correction factor which must be applied to the circumferential strain, h is the shell thickness and R the radius of the shell.

The preceding expression is based on an assumed linear variation of strain with distance from the middle surface. Although the actual variation is known to be not linear (4) for cases of plane strain, a more elegant approach is believed to be unwarranted in this case. There are many other variables whose effect can not be evaluated.

Definition of K and f

It is apparent from Equations 9 and 10 that it is not possible to determine the value of K from the data. What may not be so apparent is that if friction is present at the soil-structure interface, as implied, the ratio of the lateral pressure on the pipe to the vertical pressure in the soil is not the ratio, K, as defined in theoretical soil mechanics. Terzaghi (5) defines K as the ratio of the lateral pressure to the vertical pressure in soil under conditions of plane deformation; that is, under the condition that no shear exists on horizontal and vertical sections. Therefore even if the value of K could be determined from the strain data obtained from measurements on the shell, it would not be the same ratio as defined in soil mechanics literature.

To avoid confusion, then, for purposes of this investigation the ratio of the effective lateral pressure on the pipe to the vertical pressure in the soil will be designated K_f.

Vertical pressure measurements were obtained in the soil by means of a soil pressure gauge described in Appendix B.

As used in the development of the expression for the variation of vertical soil pressure with depth, it is implied that f has some constant value. This implication is obviously incorrect, because f may have any magnitude between zero and some maximum value which is either the coefficient of friction between the soil and the structure or the tangent of the angle of internal friction of the soil, whichever is smaller. If the displacement of the soil and the structure at a given depth are equal there is no transfer of load from soil to structure or vice-versa. If the displacement of the soil relative to the pipe at a given depth is sufficient to cause slipping between the soil and the structure or a shear failure in the soil adjacent to the interface, or, if either behavior is incipient, the magnitude of f will be a maximum. Further, it is obvious that f may have any absolute value between zero and this maximum.

The sign of f is arbitrary. For this analysis it was assumed that f is positive when the soil is loading the structure; that is, when the soil is moving or tending to move down with respect to the structure. Conversely the sign of f is negative when the structure is moving or tending to move down with respect to the soil.

Anticipated Soil-Structure Interaction

Even in the simplest static case, the prediction of soil-structure interaction is difficult. Consider the case depicted in Figure 1. Assume a uniformly distributed static pressure applied to the surface of a semi-infinite medium which surrounds a cylindrical shell of length, L. Both the shell and the surrounding medium are resting on a rigid foundation.

In the vertical direction, the stiffness of the shell may be characterized by

$$k_1 = \frac{AE}{L} = \frac{2\pi RhE}{L}$$

Assuming the soil to be elastic, the stiffness of a similar column of soil may be characterized by

$$k_2 = \frac{AM}{L} = \frac{\pi R^2 M}{L}$$

where M is the confined modulus of the soil in compression.

Ignoring the effect of Poisson's ratio in the two materials, the vertical deflection at all depths in the soil and the shell would be equal if $k_1 = k_2$. Under these conditions there would be no shear at the soil-structure interface (i.e., f would be zero).

The ratio of stiffnesses, then, may be used to make qualitative predictions concerning the interaction.

$$r_k = \frac{k_1}{k_2} = 2\frac{h}{R}\frac{E}{M}$$

where r_k is the ratio of stiffnesses of the shell and the soil.

When the ratio $r_k = 1$, the soil and the structure will move together. If the structure is essentially rigid compared to the soil; that is, if r_k is very large, the soil will move down with respect to the structure as load is applied. Under this condition, it may be reasonable to assume that the value of f is a maximum along the entire length of the shell and it should be possible to determine the response of the structure. However, the usual case is not so clear cut.

For reinforced concrete shafts and other similar structures, h/R ranges from about 0.1 to 0.05. Assuming $E = 4 \times 10^6$ and $M = 5 \times 10^4$, which is a reasonable value for the constrained modulus of sand (6), it may be computed that values of r_k from 8 to 16 are reasonable for reinforced concrete structures. Even lower values of r_k are not unusual, particularly for steel structures.

The vertical displacement in the soil is not dependent upon behavior of the structure at large distances from the structure so if the properties of the soil are known the vertical displacement may be computed as a function of depth at such distances. Further the vertical displacement in the shell at any depth could be determined by integrating the strains, computed by means of Equation 8, from the rigid foundation to the point of interest. However, even ignoring variations in lateral pressure resulting from radial displacements of the shell, it is simply not possible to determine the variation of f with depth in advance of the calculation. An iterative solution might be possible at some later time after more is known about soil-structure interaction.

Despite the obvious complexities of the problem and the simplicity of the approach used, such considerations do permit a qualitative prediction of the behavior of the soil-structure system under the conditions described. Assuming a structure which is only slightly stiffer than the soil it is apparent that near the surface the vertical displacement of the soil will be greater than that of the structure and that load will be transferred to the structure from the soil through shear. The increased load will produce increased strain in the structure below that depth. Such transfer should continue down to a depth such that displacement in the structure equals the displacement in the soil. Below that depth, under static load, the soil and structure displacements should remain equal. Any tendency on the part of t structure to move down relative to the soil would result in a transfer of load to the soil, thus maintaining compatible displacement.

Under dynamic loading the problem is so much more complex that no attempt will be made to discuss the general case which involves elastic vibrations of the structure as well as dynamic response of the soil. As previously stated no dynamic response of the structures was anticipated in this test program. The fundamental natural period of longitudinal vibration of a steel pipe about 2 feet long is about 0.47 milliseconds and for a steel pipe, 4 inches in diameter, the natural period in the so-called "breathing mode" is about 0.06 milliseconds. Since the planned rise-time of the pressure pulse was greater than 10 milliseconds the structural response, though rapid, would not be dynamic.

For the soil, on the other hand, the fundamental period of longitudinal vibration could not be determined prior to test. The fundamental natural period of vibration of a column of any material supported by a rigid base may be expressed as

$$T = \frac{4L}{c}$$

where T is the period in seconds, L, is the height of the column in feet and c is the velocity of stress propagation in the material in feet per second. For fine-grained sand, Barkan (7) gives a compression wave velocity of about 1000 fps. Thus for a soil sample about 2 feet long, T ≅ 8 milliseconds, and although the computed fundamental natural period of the soil sample is somewhat shorter than the rise-time of the pressure pulse, the load may be considered dynamic insofar as the soil is concerned. If the soil were elastic, some dynamic amplification of the response could be anticipated.

However, of more importance to this investigation is the fact that the stress wave traveling through the pipes will reach the base of the tank at times which are measurably earlier than the arrival of the stress wave in the soil. Thus, the pipes should tend to move down with respect to the soil prior to the arrival of the stress wave in the soil at a given depth, resulting in a transfer of load from the pipe to the soil in front of the stress wave in the soil. Then as the stress wave in the soil passes that point and the soil below becomes stressed the vertical displacement in the soil may become large enough to reverse the relative motion of soil and structure. This behavior would be reflected in a change in sign of f.

In view of the fact that very little is known about soil-structure interaction under dynamic load very little more could be said about the anticipated behavior prior to test. The test program outlined below, then, must be considered as exploratory in nature.

EXPERIMENTAL WORK

Introduction

In broad outline the experimental work consisted of a series of tests of three instrumented pipes, which were first tested in uniaxial compression to obtain information regarding the physical properties of the materials of which the pipes were made (i.e., Young's modulus and Poisson's ratio). Subsequently, the three pipes were placed in a tank, surrounded by soil (a fine, dry sand) and subjected to both static and dynamic loading. The orientation of the pipes in the tank was as shown in Figure 4.

A total of 14 static tests and 12 dynamic tests were conducted. The maximum pressure at the surface of the soil sample for each test is given in Table 1.

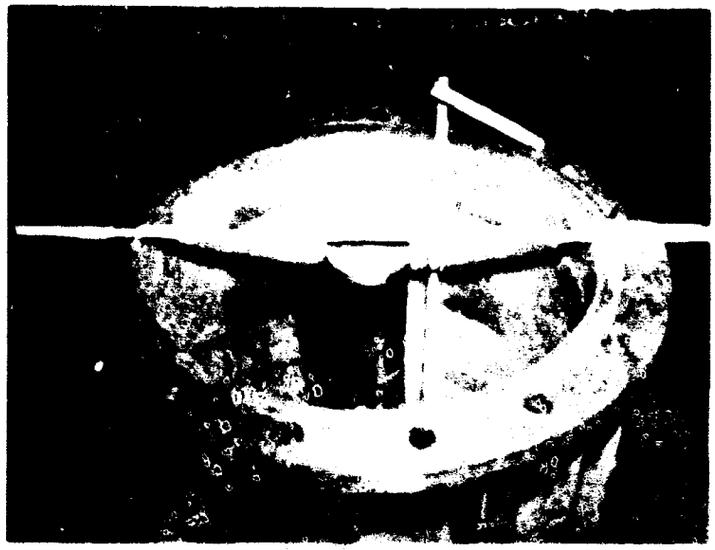


Fig. 4 View of Soil Container Showing Orinetation of Test Structure (Pipe) in Tank

Test Facilities

The facilities employed for the soil-structure interaction studies, both static and dynamic, consisted of a cylindrical steel tank (see Figure 4) mounted on a platform. For the static test the tank was fitted with a flat head, Figure 5, to conserve gas and to speed up the testing program. For dynamic tests the testing machine used in this study was a 60,000 pound capacity, gas operated, slow or rapid loading device originally designed and constructed by Egger (8). (See Figure 6 for a view of the dynamic loading machine mounted on the soil container.)

The 60 kip machine was modified to permit simulation of blast loading from a nuclear or thermonuclear weapon. Details of those modifications and the operating characteristics of the machine as mounted for these tests are contained in another document (9) and will not be repeated here. However, a brief description of the machine and its operation are in order.

The machine used for this test series consisted of one external compression or charging chamber together with its associated slide valve chamber and an octahedral transition section. The transition section, which served as the expansion chamber was connected between the 12-inch diameter slide valve chamber and the 24-inch diameter steel drum or tank mentioned above as shown in Figure 7.

A baffle and grid were placed in a transition ring as shown in Figure 8. The purpose of the baffle and grid was to achieve a uniform distribution of pressure on the surface of the soil in the tank below. This particular combination of baffle, grid and spacing between the grid and the soil surface has been investigated experimentally (9) and found to produce very good results.

Table 1

Maximum Pressure (psi) at Surface of Soil Sample For All Tests

Static Test No.	Pipe Number 1	2	3
Dynamic Test No.			

The baffle used consisted of a solid plate, 0.5 inch thick and 7 inches in diameter and was held 3.5 inches above the grid by three legs bolted to the grid. The grid used was fabricated from a 0.75 inch steel plate by drilling approximately 925 one-half inch diameter holes through it so that the area of the holes was about 40 percent of the total grid area.

A transition ring was fabricated to provide a spacing of approximately 2.0 inches from the bottom of the grid to the neoprene diaphragm separating the expansion chamber from the surface of the soil in the tank below. In addition, a hole was bored in the side of the transition ring to permit installation of a Kistler pressure transducer, Model 601, which was



Fig. 5 View of Soil Container Showing Head Used for Static Tests

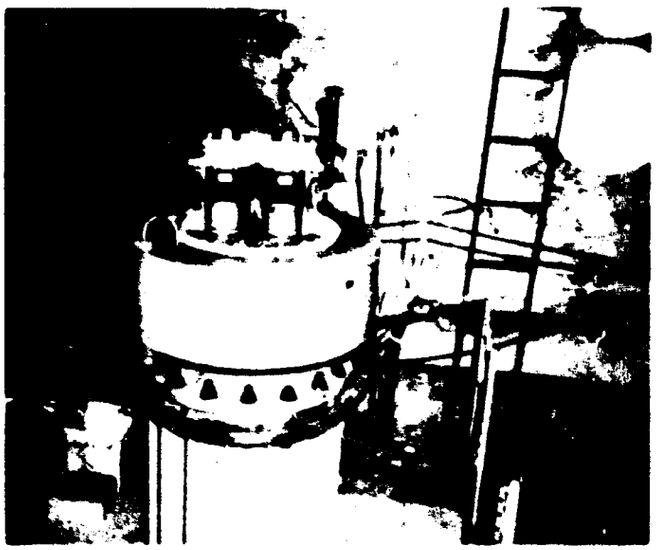


Fig. 6 View of Soil Container with 60 kip Dynamic Loading Device Used for Dynamic Tests

used to measure the gas pressure on the surface of the soil as a function of time.

To operate the dynamic loading device it was necessary to charge the external compression chamber to some predetermined pressure level, charge the auxiliary chambers which cause the piston to travel upward, and then release the piston. As the pressure in the auxiliary chamber forced the piston upward, the gas at high pressure in the compression chamber vented into the expansion chamber and, filling the chamber, loaded the surface of the soil with a relatively uniform pressure which rose very rapidly to a peak value determined by the initial pressure in the compression chamber.

Specimens

Soil As stated previously, to reduce the number of variables in this test series only one soil was employed; a fine dry sand. Using the test procedures described below, the soil was compacted to a density of about 108.5 pounds per cubic foot for each test.

The soil used, Sangamon River Sand, has recently been tested in a series of one-dimensional tests by Hendron (6). Further information regarding its properties are available in that document.

Pipes Three segments of pipe of varying stiffness were used. The dimensions and properties of each of the pipes are listed in Table 2.

Instrumentation

Soil Vertical pressure measurements were obtained in the soil at two levels in each test using the soil pressure gauges described in Appendix A. Soil pressure gauge No. 3 was placed at a depth of 1.5 inches below the surface of the sand and at the midpoint between the pipe wall and the tank wall for all tests. The location of soil pressure gauge No. 4 is listed in Table 3 for each test.

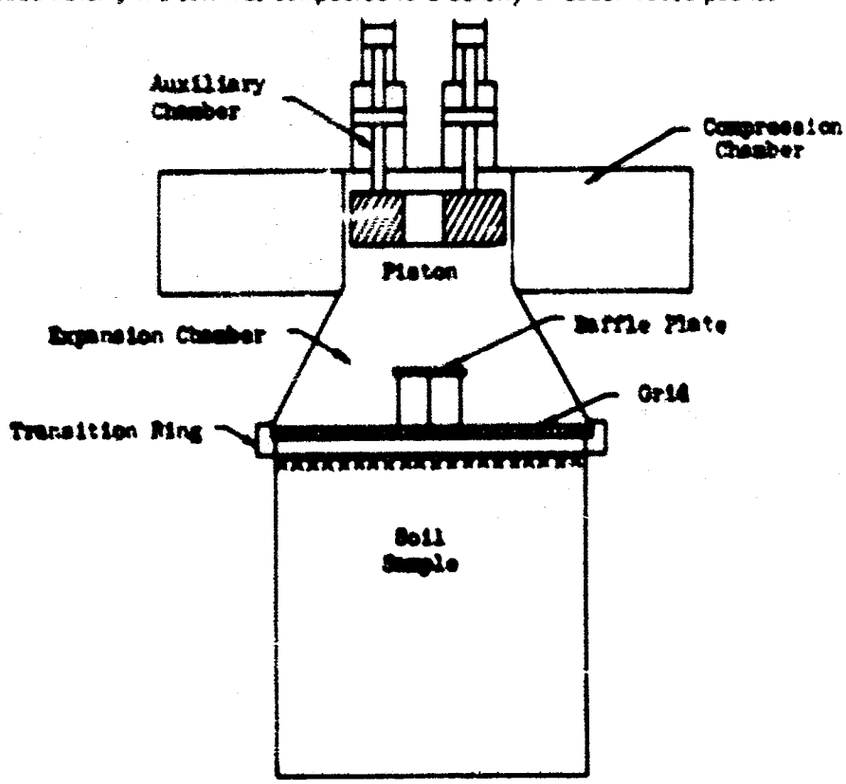


Fig. 7 Schematic of Experimental Equipment Used for Dynamic Tests

Pipes Each pipe was instrumented as shown in Figure 9. Twelve SR4 "T"-gauges, type AX-5, manufactured by the Baldwin-Lima-Hamilton Corporation, were mounted on the inside of each pipe; four at each gauge level. These gauges were used to obtain "average" circumferential and vertical strains at 4, 10 and 16 inches below the top of the pipe. That is, the four vertical and the four circumferential strain elements were connected in series and balanced by four dummy gauges outside the pipe as shown in Figure 10.

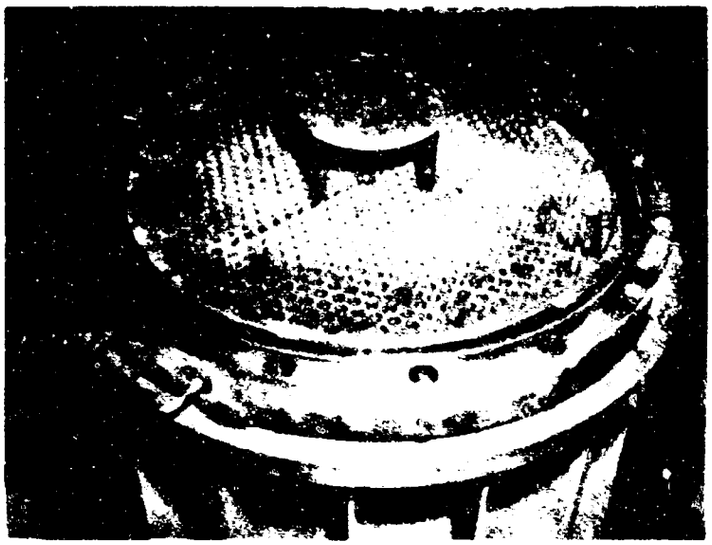


Fig. 8 View of Soil Container Showing Baffle and Grid in Transition Ring

Gas Pressure For the static tests the gas pressure on the surface of the soil was measured by mean of two gauges; a 1000 psi capacity gauge with 10 pound subdivisions and a 100 psi capacity gauge with 1 pound subdivisions. The latter, of course, was used for pressures up to 100 psi only.

For the dynamic tests the gas pressure as a function of time was measured by a Kistler pressure transducer, Model 601, which is a quartz crystal type piezo-electric sensing device, in conjunction with a Kistler preamplifier-calibrator unit. The output of the preamplifier unit was fed into the CEC (Consolidated Electrodynamics Corporation) recording oscillograph, described below.

Data Recording Data for both static and dynamic tests were recorded by means of a Type 5-124 recording oscillograph, manufactured by the Consolidated Electrodynamics Corporation, which is a multi-channel, portable, ground environment, direct-recording, photographic type instrument. It uses 7-inch wide print-out recording paper, and provides up to 18 channels of data on visible records without chemical processing. Using standard CEC Type 7-300 galvanometers, dynamic measurements up to 5000 cps are possible. Five record speeds are available; 0.25, 1, 4, 16 and 64 inches per second. The slowest speed was used for the static tests and the highest speed was used for the dynamic tests.

Uniaxial Compression Tests

A 100,000 lb capacity Baldwin-Southwark Testing Machine was employed for the uniaxial compression tests, which were conducted in a conventional manner; the load being applied in the direction of the axis of each pipe segment. Because these tests were conventional uniaxial compression tests, further discussion of the test procedure is not warranted.

Tests in Soil

The procedure employed for both static and dynamic tests in soil was as follows:

1. The pipe segment was placed in the tank as illustrated in Figure 4. The leads from the strain gauges were brought out through a hole in the bottom of the tank and connected to the remainder of the "bridge" below the platform. To avoid lateral displacement of the bottom

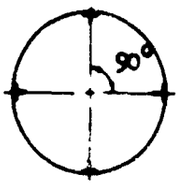
Table 2

Properties of Pipes Used

Pipe No.	1	2	3
Material	Steel	PVC*	PVC*
Nominal Size	4	4	4
OD (in.)	4.25	4.5	4.5
ID (in.)	4.010	4.026	3.826
Wall Thickness (in.)	0.12**	0.237	0.337
Approx. wgt per ft.	5.293	1.899	2.636
Length (in.)	25.75	25.75	25.75

* Ryertex Omicron PVC (Polyvinyl Chloride) Plastic Specs:
Specific Gravity, 1.35 - 1.45
Specific Volume, 20.5 - 19.1 cu.in./lb.
Tensile Strength, 5000 - 9000 psi
Elongation, 2.0 - 4.0 %
Mod. of Elast. (Tension), 3.5 - 6 x 10^5 psi
Compressive Strength, 8000 - 13,000 psi
Flexural Strength, 10,000 - 16,000 psi

** By actual measurement the pipe wall thickness for this seamless steel pipe was 0.128 in.



"T" Gauges
Type AX-5

R = 120 ± 0.5
GF = 1.99 ± 1%
AF = 1/30

Table 3

Depth (inches) of Soil Pressure Gauge No. 4 for all Tests

Static Test No.	Pipe Number		
	1	2	3
1	16	16	16
2	16	16	16
3	16	4	16
4	24	4	16
5	--	4	16
Dynamic Test No.			
1	24	16	16
2	24	16	16
3	16	4	16
4	16	4	16

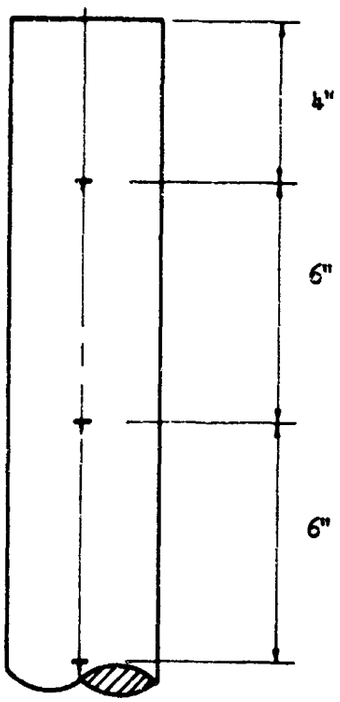


Fig. 9 Strain Gauge Locations for all Pipe Specimens

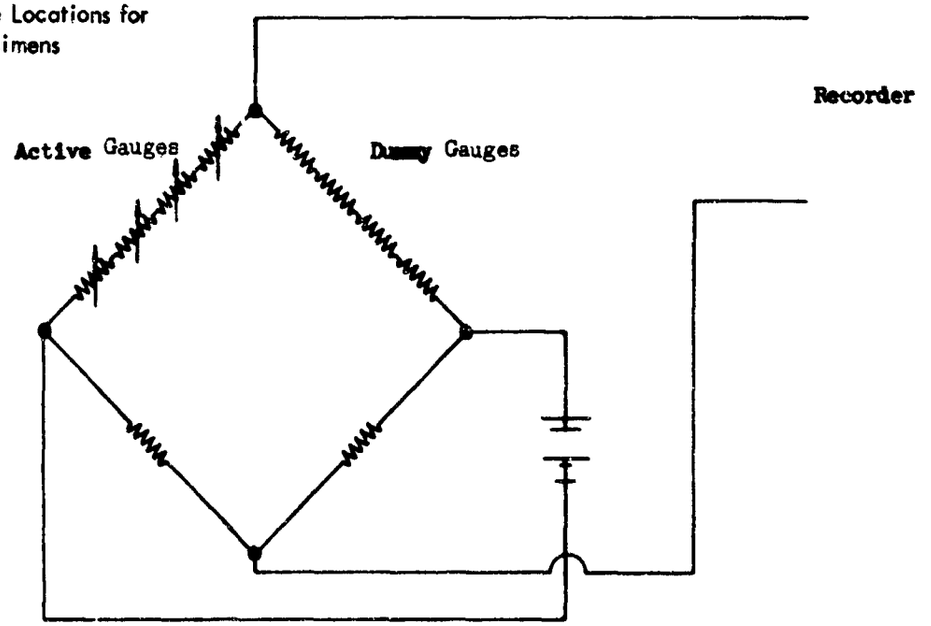


Fig. 10 Typical Circuit Diagram for Vertical and Horizontal Strain Gauges at Each Gauge Level

of the pipe a positioning disc was installed in the bottom of the tank.

2. Soil was placed around the pipe in six-inch layers and compacted by means of an electric vibrator.
3. After the tank was full the top of the sample was leveled with a steel bar (see Figure 11) and the neoprene diaphragm was placed over the surface of the soil.
4. The flat head used for the static test series was then attached to the tank and a static pressure of 100 psi was applied to the surface of the sample to compact the soil further. The purpose of this step of the procedure was to obtain as nearly uniform compaction as possible and to avoid excessive vertical deflection of the surface of the soil which could result in rupture of the neoprene diaphragm.
5. After compaction, sand was added to bring the surface of the soil flush with the top of the tank.
6. Depending on whether the test to be performed were static or dynamic, the flat head, shown in Figure 5, or the 60-kip capacity dynamic loading machine, shown in Figure 6, was attached to the tank.
7. Calibration steps were then recorded, for each test, using the recording oscillograph described above.
8. For the static tests, the pressure was increased to a maximum and then decreased in various increments depending on the pipe employed.
9. For the dynamic tests the machine was charged and fired. Records of the first 0.5 and 0.8 second of response were obtained with the recorder paper speed at 64 inches per second. The pressure was then bled from the expansion chamber and records were obtained of the strains at pressure levels employed for the static tests of the same pipe during unloading.

A sequence of two static and two dynamic tests were conducted with each pipe for the first test series. That is, static test 2 was performed without removing the pipe and soil from the container after completion of static test No. 1. After a preliminary analysis of the data obtained, three static tests of pipes 2 and 3 were conducted in sequence for the second test series. The reasons for this decision and the results obtained are discussed below.

PRESENTATION AND DISCUSSION OF TEST RESULTS

Uniaxial Compression Tests of Pipes

The uniaxial compression tests of the pipes were ordinary in every respect and no peculiarities were encountered. The load-strain relationship was linear up to the maximum strains recorded; about 0.001 inches per inch for the steel pipe and about 0.004 inches per inch for the two plastic pipes. Calculated values of Young's modulus varied within two percent of the average at the three gauge lines. This variation was probably due to variations in pipe wall thickness.

The values of Young's modulus and Poisson's ratio listed below for each pipe were obtained by averaging the vertical and circumferential strains at the three depths.

Values of ν and E for Pipes

Pipe No.	Material	E	ν
1	Steel	30.8×10^6	0.243
2	PVC	5.19×10^5	0.359
3	PVC	5.21×10^5	0.354

Static Tests of Pipes in Sand

Performance of Soil Pressure Gauges A typical, complete load-strain function for soil pressure gauge is shown in Figure 12, in which the pressure applied at the surface of the soil sample is plotted on the ordinate and the strain in the vertical element in the gauge is plotted on the abscissa. It is noteworthy that the shape of this curve is similar to stress-strain curve for a confined sand. The curve shown was prepared from data obtained from static test No. 3 of Pipe No. 3, during which the gauge was located 16 inches below the surface of the sand. In subsequent figures the unloading cycle will be omitted only to avoid confusion.

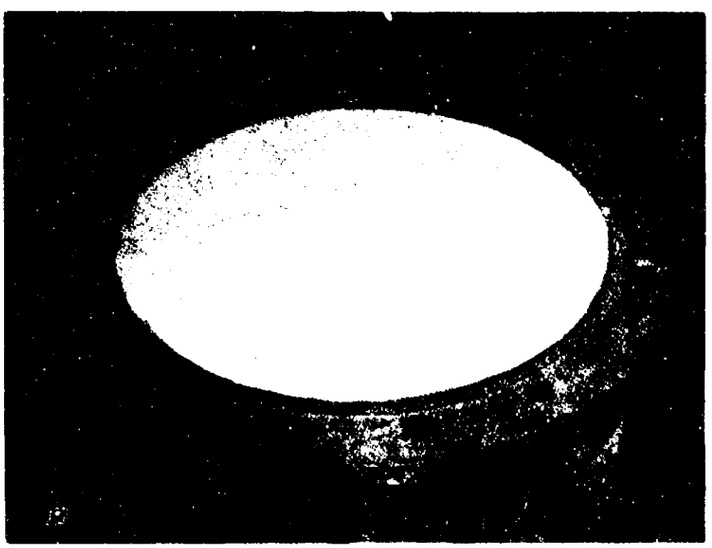


Fig. 11 View of Soil Container Showing Soil Surface Before Test

In Figure 13, the strains recorded in Gauge No. 4 are plotted as a function of applied surface pressure, during loading only, for three depths; 4, 16 and 24 inches below the surface. Only one static test was conducted with soil pressure gauge No. 4 at 24 inches below the surface. However, three static tests were conducted with that gauge at 4 inches below the surface and 9 were conducted with the gauge at a depth of 16 inches. There was less scatter in the data obtained at these depths than at the 1.5 inch depth (see Appendix B). These data were subsequently used with the

gauge calibration curve in Appendix B to obtain the vertical soil pressure existing at the depths noted as a function of the applied surface pressure. Then they were used with corresponding lateral pressure calculations to obtain values for the ratio K_f.

The scatter in the data obtained with soil pressure gauge No. 3, which was placed at a depth of 1.5 inches for all tests, was much the same as that obtained during the calibration tests. Since these data were not used in subsequent calculations they will not be discussed further.

Strain Data from Pipes Figure 14 shows the vertical and circumferential strains recorded at the three gauge lines as a function of applied pressure at the surface for a typical test of the steel pipe. Compressive strains are plotted as positive and tensile strains are plotted negative. Only strains recorded while the load was increasing are shown to avoid confusion. A complete load-strain function (for the 16-inch gauge line Pipe No. 2, Test No. 5) is shown in Figure 15. All strains recorded exhibited the same general shape but the area within the loop was much larger for the plastic pipes than for the steel pipes.

The recorded vertical strains in the pipes increased with depth at all pressure levels indicating that load was being transferred to the pipes from the soil through shear at the interface as anticipated. The total load transferred was less for the second of the two tests in the sequence. This difference is believed to be caused primarily by the fact that the soil density was greater for the second test of the sequence.

It is noted that the decrease in vertical strain in the case of the steep pipe (Pipe No. 1) was very small but that the decrease was significant for both plastic pipes. The steel pipe was essentially rigid compared to the soil so that, for the second of the two tests, the relative displacement between the soil and the pipe was virtually the same despite the increased soil stiffness resulting from the additional compaction afforded by the first test. This hypothesis was confirmed by the shear calculations which are discussed later.

At the 4-inch gauge depth the circumferential strains were compressive for all tests. At the 10-inch depth the circumferential strains were small and both tensile and compressive, varying from one test sequence to another. However, at the 16-inch depth (4 pipe diameters) the circumferential strains were tensile for all tests. At this depth the load transferred to the pipes was so large that:

$$\nu \frac{u}{x} > \frac{R}{D} K_f p_v$$

Variation of Vertical Soil Pressure with Applied Load and Depth Figure 16 shows the vertical soil pressure plotted as a function of the applied load (load increasing only). The dashed line represents the average of all test data obtained at the depth indicated. Despite the large scatter in the data at low pressure levels particularly, the relationship appears to be linear. The data for the 24-inch depth is not shown because only one test was conducted with soil pressure Gauge No. 4 at that depth.

The average value of p_v/p_o for each test depth is shown in Figure 17 as a function of depth in the tank. The solid line represents exponential decay of pressure with depth:

$$\frac{p_v}{p_o} = e^{-mx}$$

where

$$m = \frac{2.3\, fK}{R_t}$$

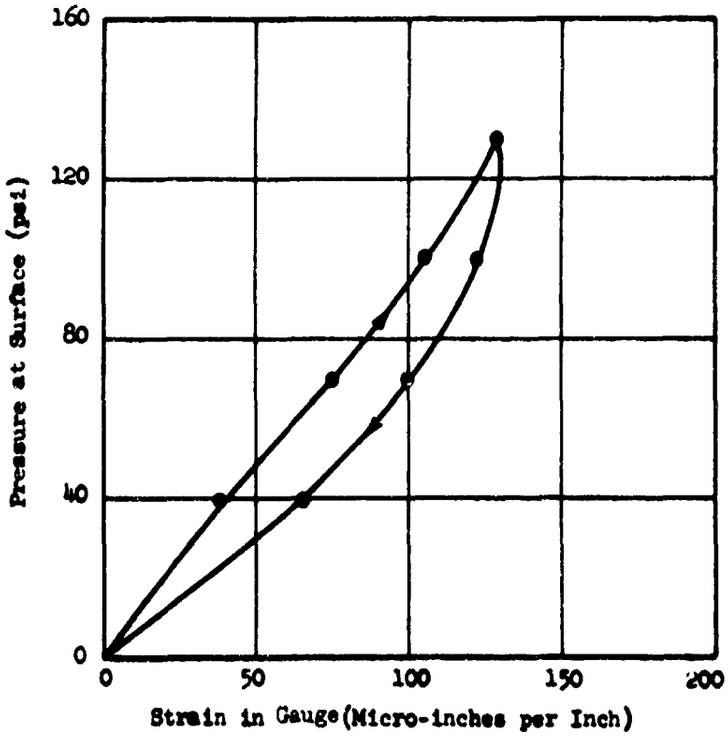


Fig. 12 Typical Complete Load-Strain Function for Soil Pressure Gauge No. 4 - Static Tests

For this calculation, values of 0.93 and 0.4 were assumed for f and K, respectively; which are reasonable as will be demonstrated later.

Although the average of all data obtained at a depth of 4 inches does not fall on this line the averages of data obtained at the 16- and 24-inch depths do so.

Variation of Lateral Pressure on Pipes with Applied Load and Depth Calculations of the effective lateral pressure on the pipes at the three gauge depths (4, 10 and 16 inches) were made using Equation 9 after correcting for the concentration of circumferential strain by means of Equation 11. Values of Young's modulus, E, and Poisson's ratio, ν, obtained from the uniaxial compression tests of the pipes were used.

There is good correlation between the calculated lateral pressures on the two plastic pipes at the same applied surface pressures and depths. However, the calculated lateral pressures on the steel pipe was considerably less than the values obtained from the plastic pipes at the same depths and applied surface pressures. This was not anticipated and the cause has not been determined. Assuming that the difference is real and not an odd statistical variation, an explanation may be found in the difference in the boundary conditions at the soil-structure interface. The value of the shear at that interface was much higher for the tests of the steel pipe than for the tests of the plastic pipes, as will be demonstrated.

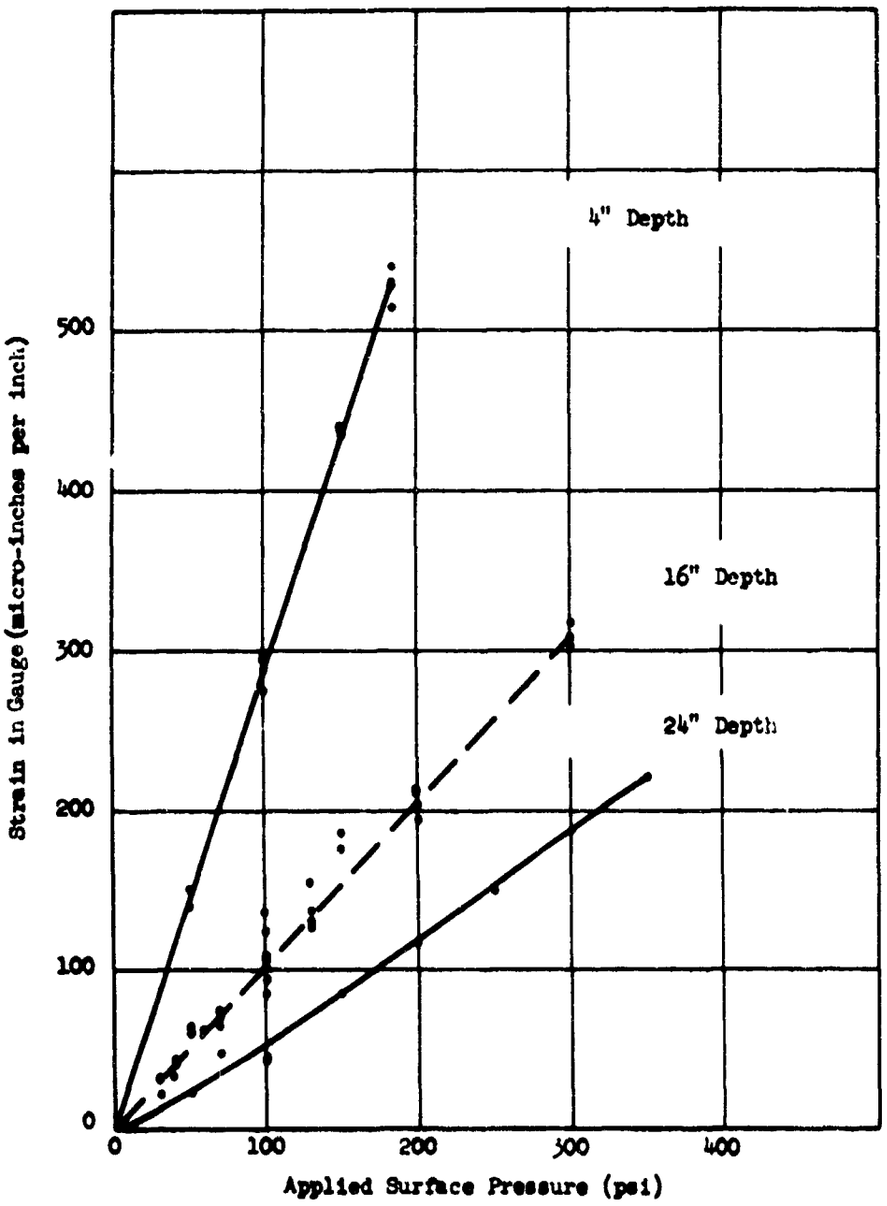


Fig. 13 Strain in Soil Pressure Gauge No. 4 as Function of Applied Load for Three Depths - Static Tests

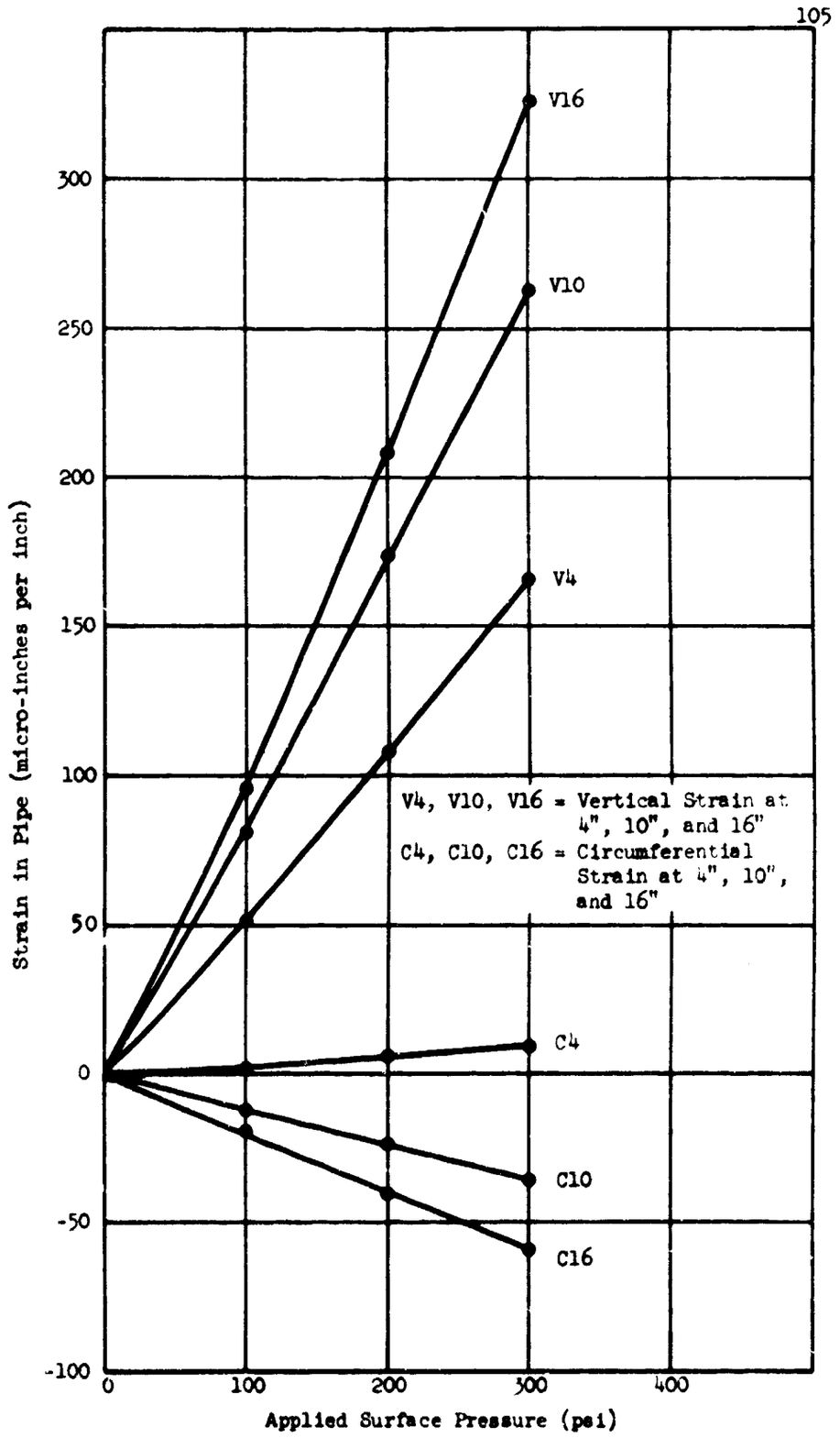


Fig. 14 Vertical and Circumferential Strains as a Function of Applied Pressure, Pipe No. 1, Static Test No. 1

Figure 18 shows the variation of lateral pressure on the plastic pipes as a function of depth for various surface pressures. The average values of the effective lateral pressure on the steel pipe at the three gauge depths are plotted as a function of applied surface pressure in Figure 19 and the same data are plotted for both plastic pipes in Figure 20. Note that the effective lateral pressure on the pipes does not appear to be a linear function of the applied surface pressure. From this, and the fact that the vertical soil pressure at the depths of 4 and 16 inches appeared to be linear functions of the applied surface pressure, it may be expected that the ratio "K_f" will vary with the applied surface pressure.

Variation of K_f with Applied Load and Depth Defining K_f to be the ratio of the calculated, effective lateral pressure on the pipe to the vertical pressure in the soil at the same depth (obtained by means of the soil pressure gauge) it is possible to obtain values for that ratio for two gauge depths; the 4-inch and 16-inch depths. The value of K_f increases during unloading. A similar increase in the value of K has been noted by others including, most recently, Hendron (6).

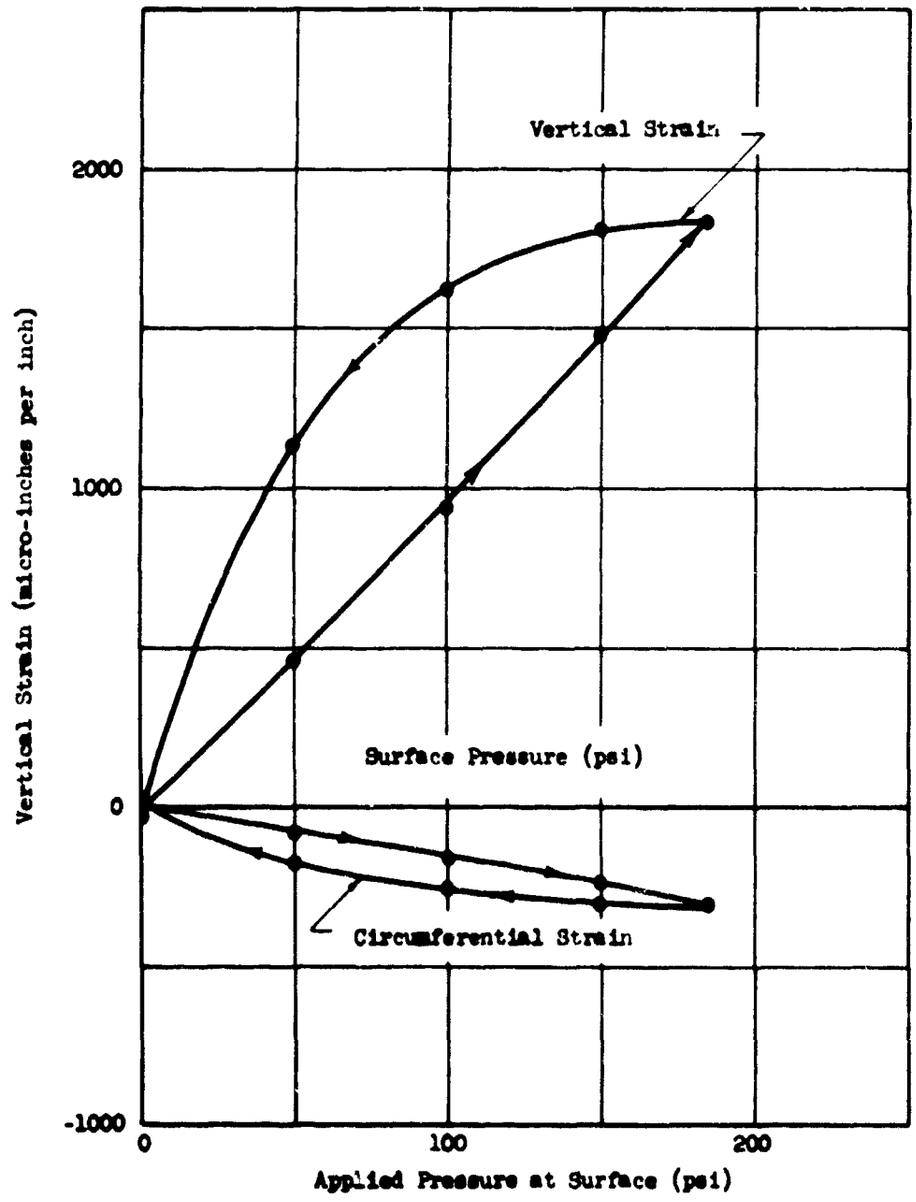


Fig. 15 Typical Complete Load-Strain Function for Pipes in Soil, 16-inch Gauge Depth - Static Tests

Average values of K_f (for increasing pressure) obtained from each test series are plotted as a function of applied surface pressure in Figure 21. Despite the variation in test data there is a clear indication that the value of K_f increases with increasing pressure. Further, there is some indication, though the data is more limited, that the value of K_f decreases with depth. The fact that the computed value of K_f must be higher than 0.5 at a depth of 4 inches may be confirmed by analytical considerations.

It is believed that the lateral pressures acting on the pipes were proportionately higher at the 4-inch gauge line than at the 16-inch gauge line because the surface of the soil sample was displaced vertically downward with respect to the pipe during test. From the dish-shaped appearance of the surface of the soil after test, Figure 22, it is concluded that there must have been a lateral component of the applied surface pressure near the top of the pipe.

Variation of f with Applied Load and Depth As explained, the coefficient f is a measure of the magnitude and the direction of the shear force acting against the side wall of the cylindrical shell (pipe) between any two gauge lines. Values of f were calculated from Equation 10 for each pressure level of each test. A summary of these calculations for the plastic pipes is included in Table 4.

Before discussing this test data, it is appropriate to point out that the relative stiffnesses of the selected pipes to the soil can not be established with accuracy because the modulus of the soil has not been established under these particular conditions of confinement. Based on data obtained by Hendron (6) in one-dimensional compression tests, a modulus of 50,000 psi is not unreasonable. Using this value the relative stiffness ratios were computed:

Pipe No.	r_k
1	76.8
2	3.5
3	2.5

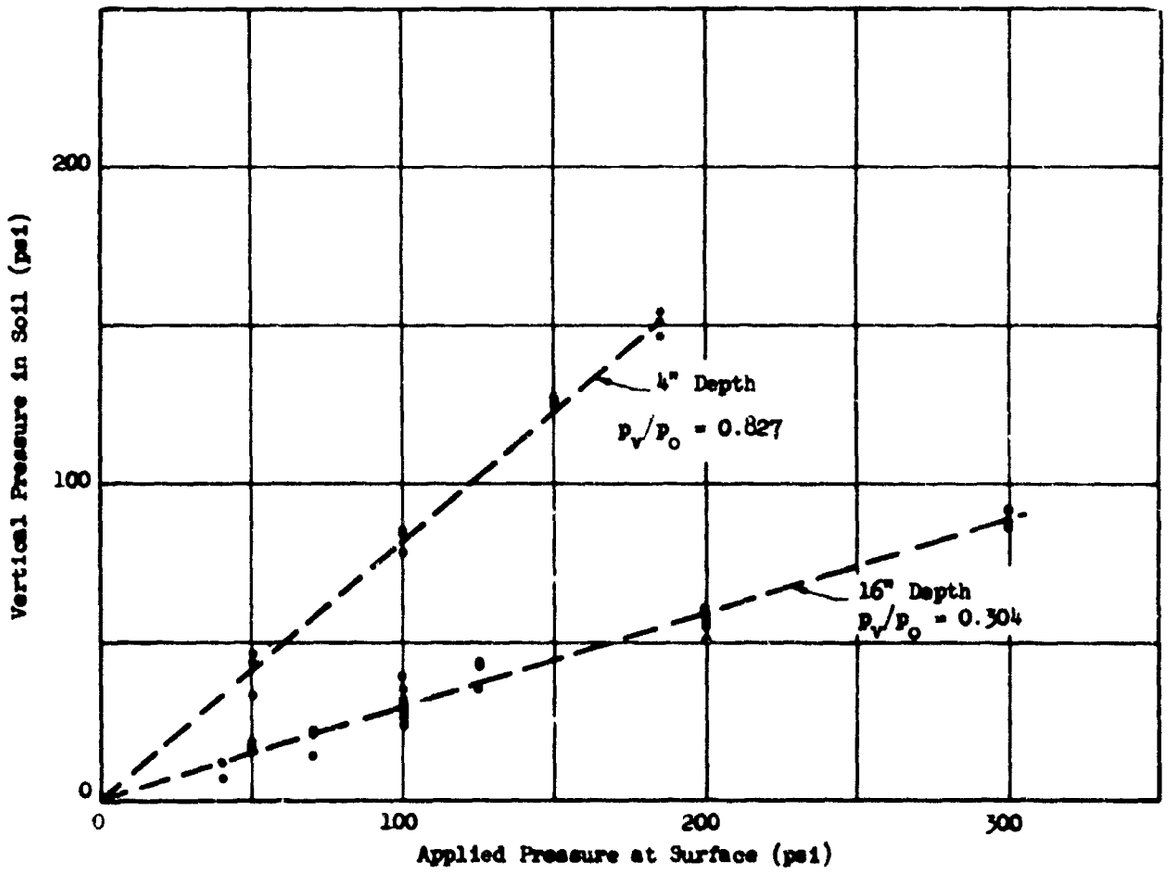


Fig. 16 Vertical Pressure in Soil as a Function of Surface Pressure for Two Depths - Static Tests

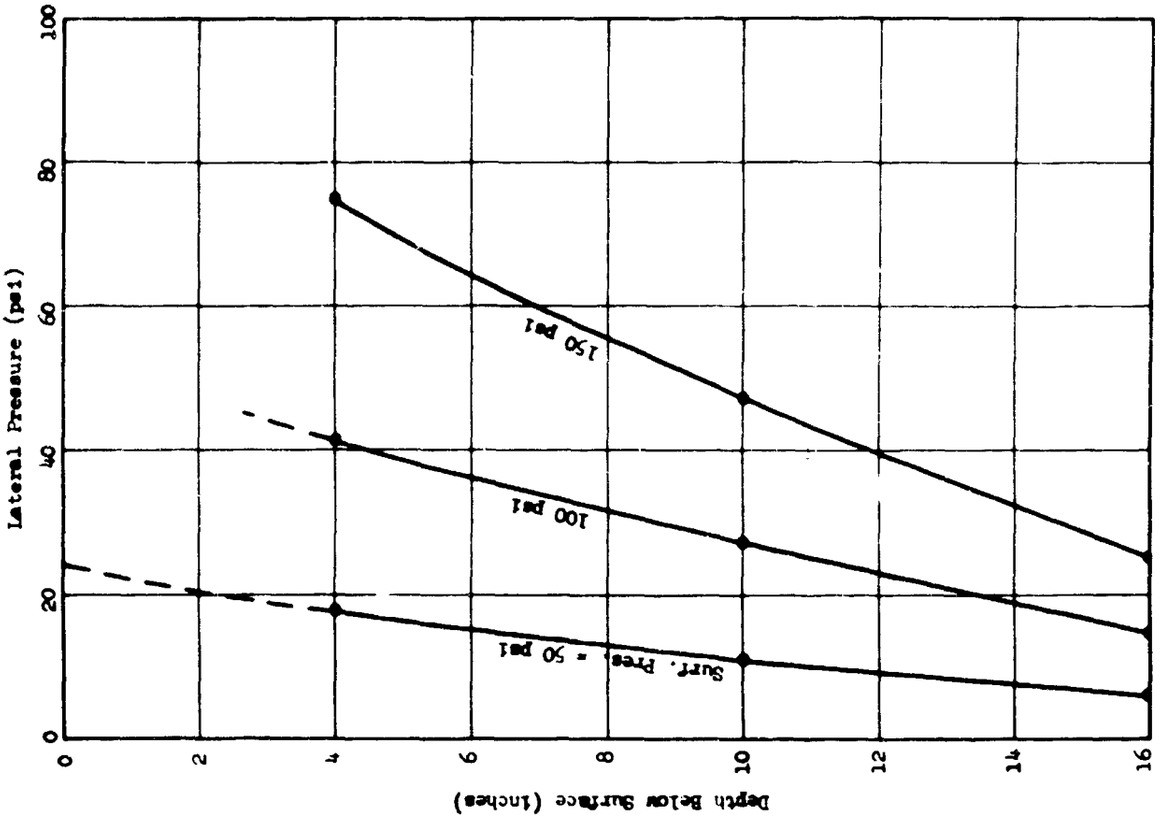


Fig. 18 Lateral Pressure on Plastic Pipes as a Function of Depth for Various Applied Pressures – Static Tests, Load Increasing

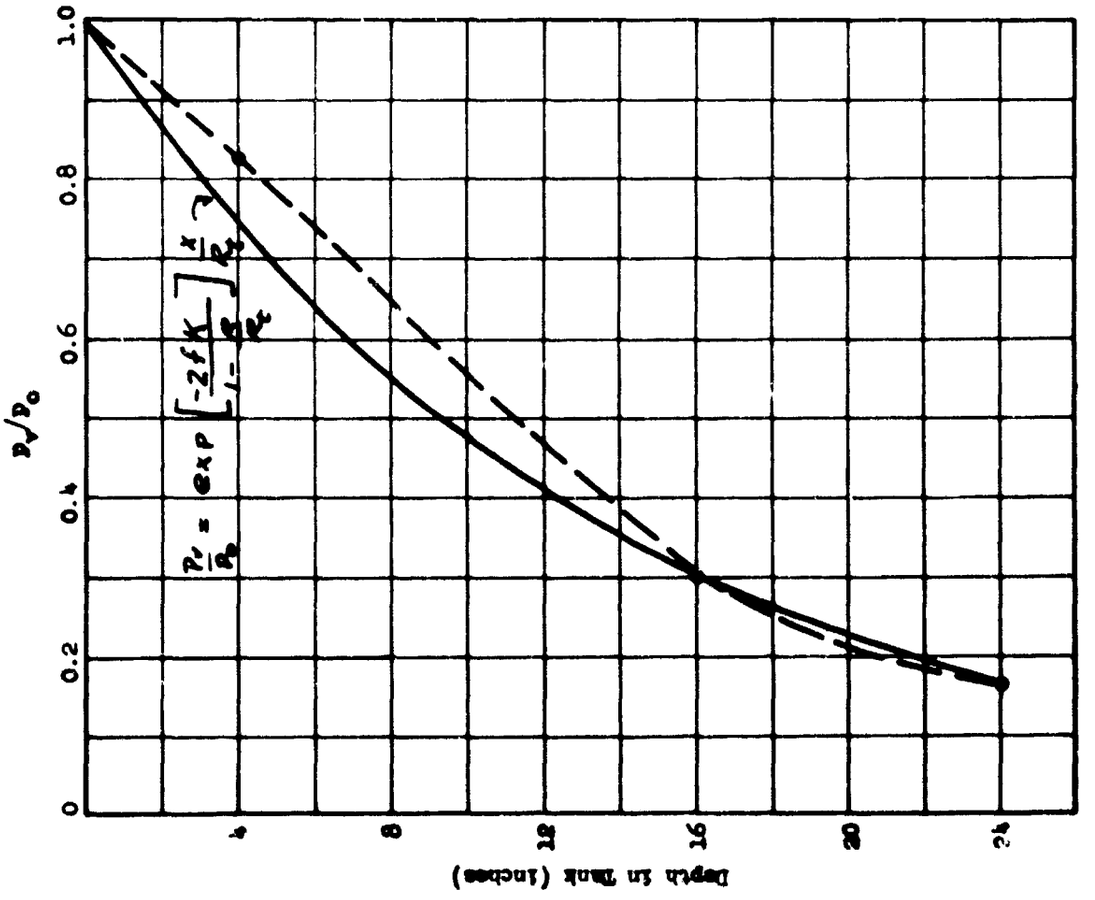


Fig. 17 Variation of Vertical Soil Pressure with Depth in Tank – Static Tests, Loading Increasing

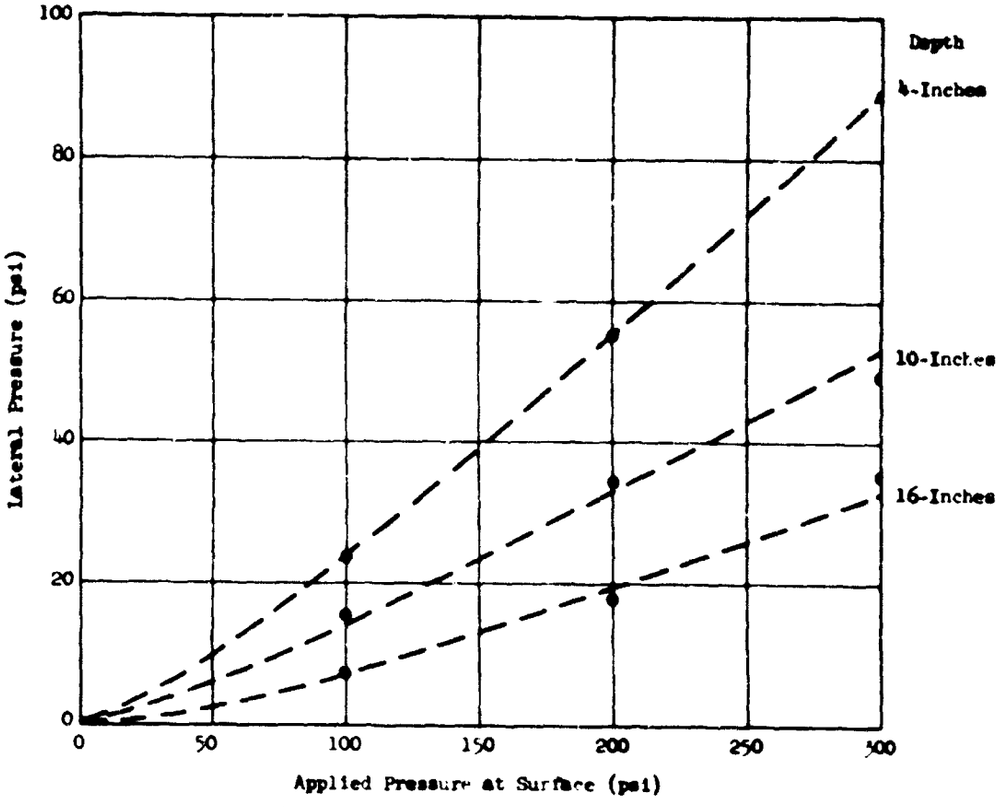


Fig. 19 Lateral Pressure on Steel Pipe as a Function of Applied Surface Pressure - Static Tests, Load Increasing

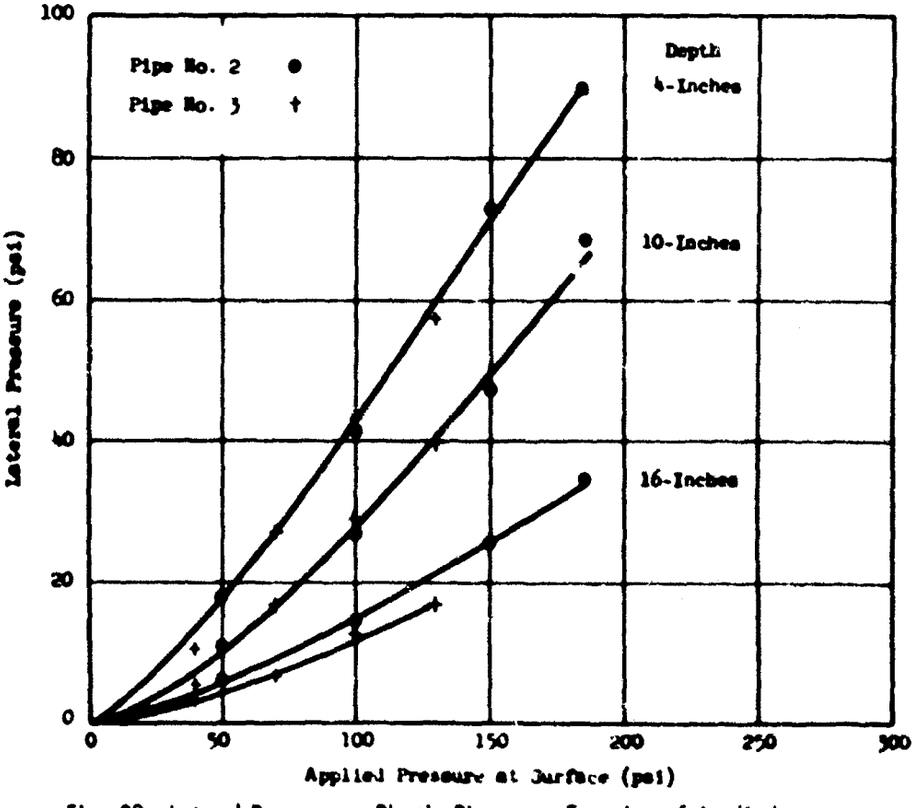


Fig. 20 Lateral Pressure on Plastic Pipes as a Function of Applied Surface Pressure - Static Tests, Load Increasing

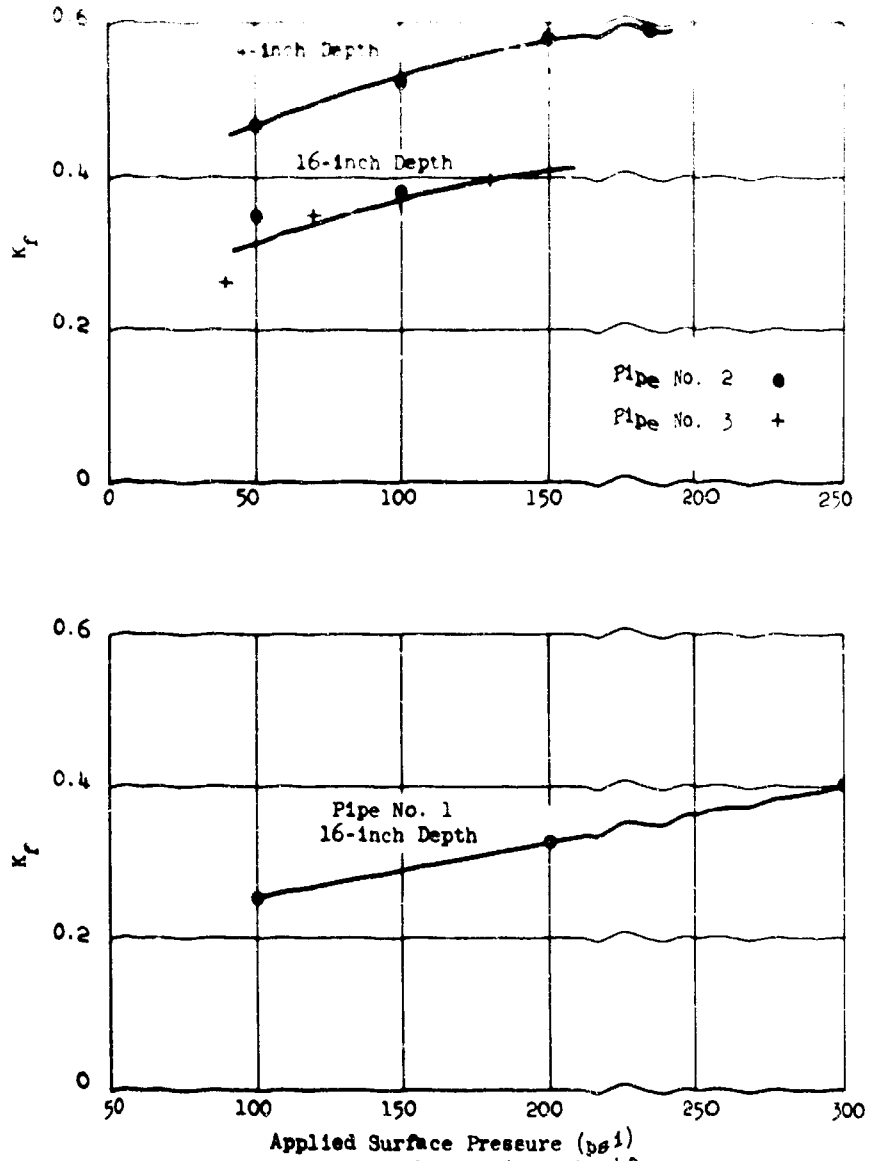


Fig. 21 Variation of K_f with Applied Surface Pressure - Static Tests, Load Increasing

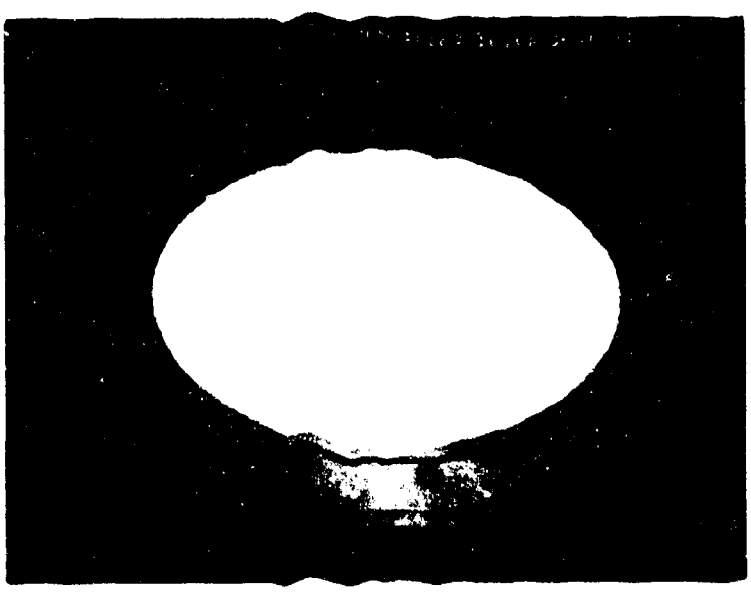


Fig. 22 View of Surface of Soil After Test

From these values it may be concluded that the steel pipe (Pipe No. 1) was essentially rigid with respect to the soil, whereas pipes No. 2 and No. 3 were only a little stiffer than the soil. The specific values listed are not to be interpreted as known facts but the relative values are important to an understanding of the discussion which follows.

The date for Pipe No. 1 (the steel pipe) indicate that the shear force on the pipe is a constant regardless of the pressure level. There was a slight difference in the average value of f with depth. The average value of f between the 4-inch and 10-inch gauge lines was 0.959, and that between the 10-inch and 16-inch gauge lines was 0.905. This difference is not satistically significant, but is probably real since the soil was undoubtedly better compacted between the 4- and 10-inch gauge lines than between the 10- and 16-gauge lines.

From the appearance of the surface of the soil sample after test it may be concluded that during tests of the steel pipe the sand did not slip along the pipe wall and that the transfer of load to the pipe was limited by the shear strength of the soil. Assuming that for the tests of the steel pipe f = tan ϕ and using the average of all data:

$$\tan \phi = 0.934$$

or

$$\phi \simeq 43^\circ$$

Table 4

Summary of Shear Calculations (f) - Static Tests

Test No.	Applied Pressure						
	50	100	150	185	150	100	50
			Pipe No. 2; 4 inches to 10 inches				
1	0.629	0.426	0.336	---	---	0.537	0.468
2	0.656	0.245	0.204	---	---	0.551	0.711
3	0.380	0.280	0.297	0.325	0.418	0.394	0.494
4	0.428	0.234	0.153	0.167	0.232	0.422	0.580
5	0.546	0.248	0.138	0.138	0.187	0.371	0.680
Avg.	0.528	0.287	0.226	0.210	0.279	0.455	0.587
			Pipe No. 2; 10 inches to 16 inches				
1	0.517	0.149	0.275	---	---	0.488	1.110
2	0.480	0.088	0.239	---	---	0.418	0.804
3	0.095	0.035	0.232	0.275	0.394	0.404	0.447
4	0.278	0.043	-0.013	0.075	0.104	0.227	0.541
5	0.230	-0.088	-0.051	-0.030	0.009	0.112	0.750
Avg.	0.320	0.045	0.136	0.107	0.169	0.330	0.730
	40	70	100	130	100	70	40
			Pipe No. 3; 4 inches to 10 inches				
1	0.824	0.313	0.341	0.339	0.485	0.505	0.400
2	0.799	0.233	0.198	0.210	0.286	0.450	0.496
3	0.989	0.285	0.228	0.238	0.374	1.024	0.915
4	0.704	0.307	0.181	0.154	0.270	0.402	0.741
5	0.766	0.339	0.209	0.152	0.239	0.392	0.747
Avg.	0.816	0.295	0.231	0.259	0.331	0.555	0.660
			Pipe No. 3; 10 inches to 16 inches				
1	0.065	-0.083	0.088	0.268	0.442	0.374	0.366
2	0.898	-0.035	-0.060	0.050	0.178	0.243	0.418
3	-0.062	-0.051	0.123	0.185	0.185	0.317	0.936
4	0.309	-0.031	-0.072	-0.016	0.075	0.172	0.581
5	0.224	-0.009	-0.065	-0.042	0.022	0.113	0.462
Avg.	0.287	-0.042	0.003	0.089	0.180	0.244	0.552

Although an angle of internal friction of 43° is large, it is not unreasonable for the sand employed, at a density of about 110 lbs per cubic foot (6).

Because the plastic pipes were more flexible, the calculated values of f were less than those calculated for the steep pipe. In fact, the values of f varied not only with depth as expected but also with pressure, as is readily apparent in Table 4.

Note that as the load was increased the calculated values of f between the 10-inch and 16-inch gauge lines approached zero for both plastic pipes indicating that there was little relative displacement between the pipes and the soil between these gauge lines during loading. Then, as the load on the surface of the sample was decreased the values of f increased indicating that the pipe was moving upward with respect to the soil during unloading. This behavior is consistent with the anticipated response of both the structure and the soil. That is, strains in the structure (pipe) were kept within the elastic range whereas the soil suffered some permanent plastic displacement. Thus, as the load was reduced it is reasonable to expect that the pipe would tend to move upward with respect to the soil producing a shearing force acting downward on the pipe.

Dynamic Tests of Pipes in Soil

Performance of Soil Pressure Gauges The performance of the two gauges under dynamic loading conditions was especially gratifying. Gauge No. 3 was used primarily to determine whether this type of gauge placed just below the surface (1.5 inches below) would record accurately the pressure at the surface. If so, some faith could be placed in data obtained at other depths.

Comparing the records obtained by means of the Kistler gauge with those obtained with soil pressure gauge No. 3 in Figure 23, it is clear that the soil pressure gauge recorded essentially the same pressure as a function time as did the Kistler gauge. The fact that the corresponding records for each test are not exactly the same is not disturbing because the two gauges were not at the same point and it is highly unlikely that the variation in pressure with time was identical at all points on the surface of the soil sample.

The ten curves in Figure 23 were obtained from records of the four dynamic tests of the thin plastic pipe (Pipe No. 3) and are typical. Note that the Kistler gauge records are plotted as pressure, in pounds per square inch, as a function of time, whereas the records from the soil pressure gauges are plotted as vertical strain (in the gauge) as a function of time so that the differences in amplitude are not important. The important factors are: (a) the shapes of the curves obtained with soil pressure gauge No. 3 and the Kistler gauge are essentially the same, and (b) the scatter in the data obtained with the soil pressure gauges is small.

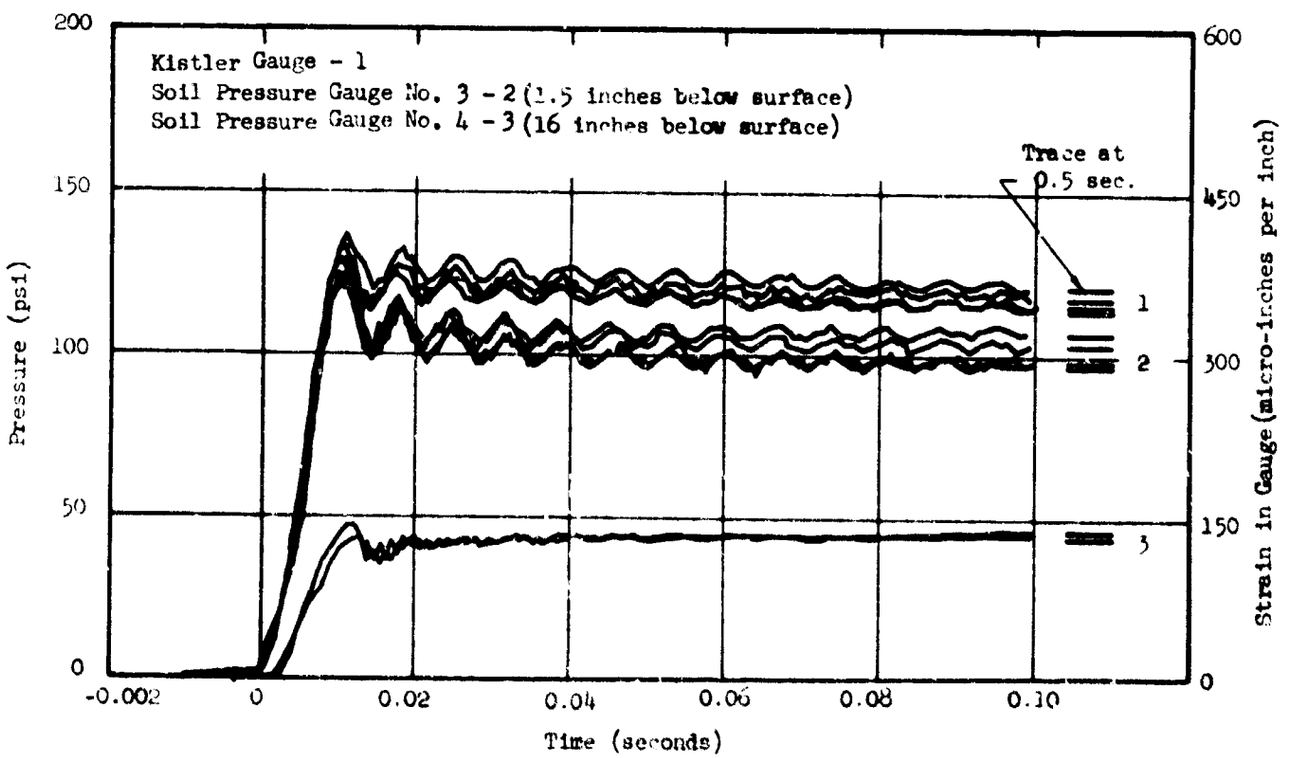


Fig. 23 Kistler Gauge and Soil Pressure Gauge Records From Four Dynamic Tests, Pipe No. 3

Soil pressure gauge No. 4 - 4 located at a depth of 4 inches below the surface for all four tests of pipe No. 3. It appears that the high frequency gas pressure fluctuations have almost damped out at this depth. (No records were obtained with soil pressure gauge No. 4 for dynamic tests No. 3 and No. 4 of Pipe No. 3.)

This apparent damping of the high frequency gas pressure fluctuations was confirmed by the test series with Pipe No. 2. Figure 24 shows the four records obtained with the Kistler gauge and soil pressure gauge No. 4 (at the 16-inch depth) during dynamic tests No. 1 and No. 2. Unfortunately, no readable record was obtained with soil pressure gauge No. 3 during these two tests. The corresponding records obtained during dynamic tests No. 3 and No. 4 of Pipe No. 2 are shown in Figure 25. The top two records are gas pressure measurements at the surface obtained by means of the Kistler gauge, and the two lower records are soil pressure measurements obtained with soil pressure gauge No. 4 at 4 inches below the surface.

Comparing these last two figures it may be seen that the gas pressure fluctuations at the surface were transmitted with relatively little diminution to a depth of 4 inches but that at a depth of 16 inches the pressure fluctuations are barely discernible. Another point of interest, which will be discussed later in connection with the transfer of load to the pipes, is that the strain in the soil pressure gauge at the 4-inch and 16-inch depths increased with time as indicated by the record trace at 0.5 seconds.

Strain Data from Pipes The vertical and circumferential strains recorded as a function of time at the three gauge lines for three tests are shown in Figures 26 through 28. Here, again, compressive strains are plotted as positive and tensile strains, negative. These records were traced from the original test records using a Moseley Autograf Model No. 3, and plotted to the more convenient scales shown.

Preliminary study of these figures reveals that in some respects the interaction between the soil and the pipes was similar to that observed in the static tests. The circumferential strains were compressive at the four-inch gauge depth, nearly zero at the 10-inch gauge depth and tensile at the 16-inch gauge depth. Further, the vertical strains at the 10-inch depth were greater than those at the 4-inch depth, and, for the steel pipe, the vertical strains at the 16-inch gauge depth were greater than those at the 10-inch depth, except at very early times. However, for the plastic pipes the strains recorded for the 16-inch depth were less than those recorded for the 10-inch depth for tests 2 and 4 of Pipe No. 2 and for tests 2 and 4 of Pipe No. 3. For tests 1 and 3 of Pipe No. 3 the vertical strain at the 16-inch gauge depth was less than that at the 10-inch gauge depth up to the peak (at about 12 milliseconds).

As noted previously, the steel pipe was essentially rigid with respect to the soil whereas the plastic pipes were not. Thus except at very early times the vertical displacement of the steel pipe at any given depth should not be as large as the displacement in the soil at the same depth once the stress wave has passed that depth in the soil. However, the plastic pipes were much more flexible in vertical compression as demonstrated by the static tests. The observed

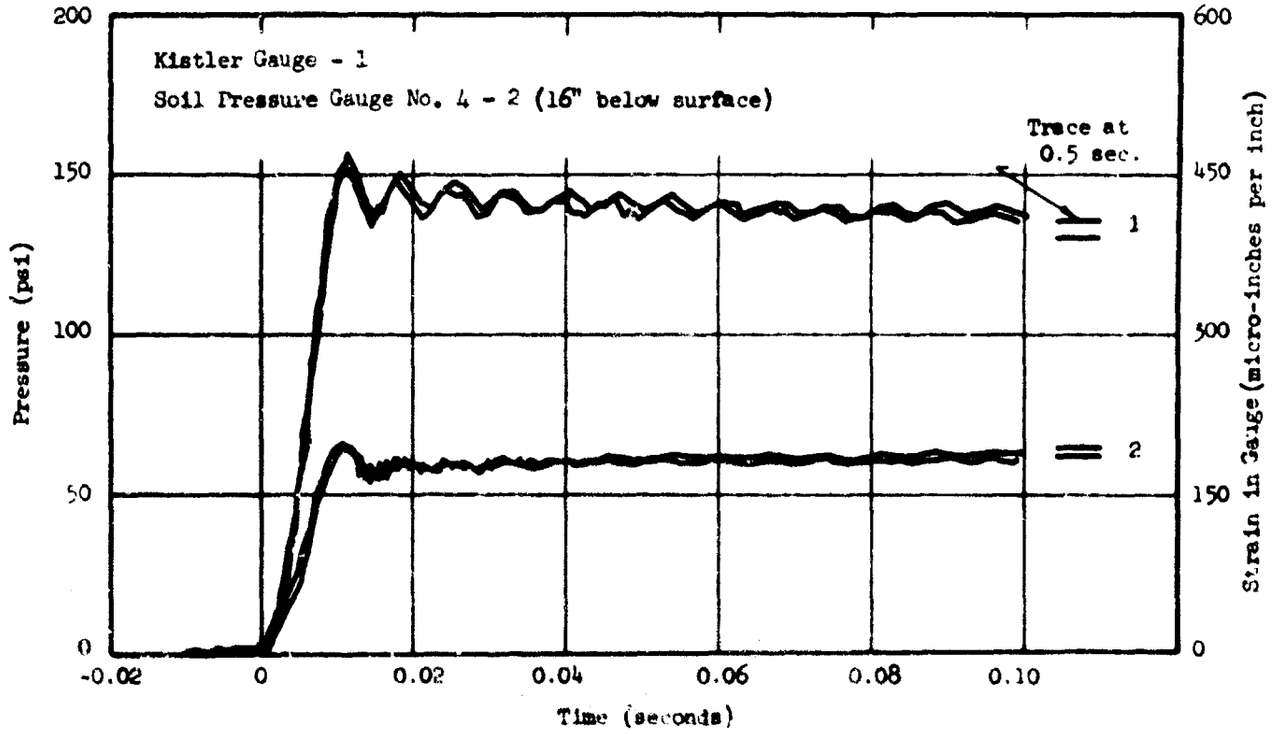


Fig. 24 Kistler Gauge and Soil Pressure Gauge Records From Dynamic Tests No. 1 and No. 2, Pipe No. 2

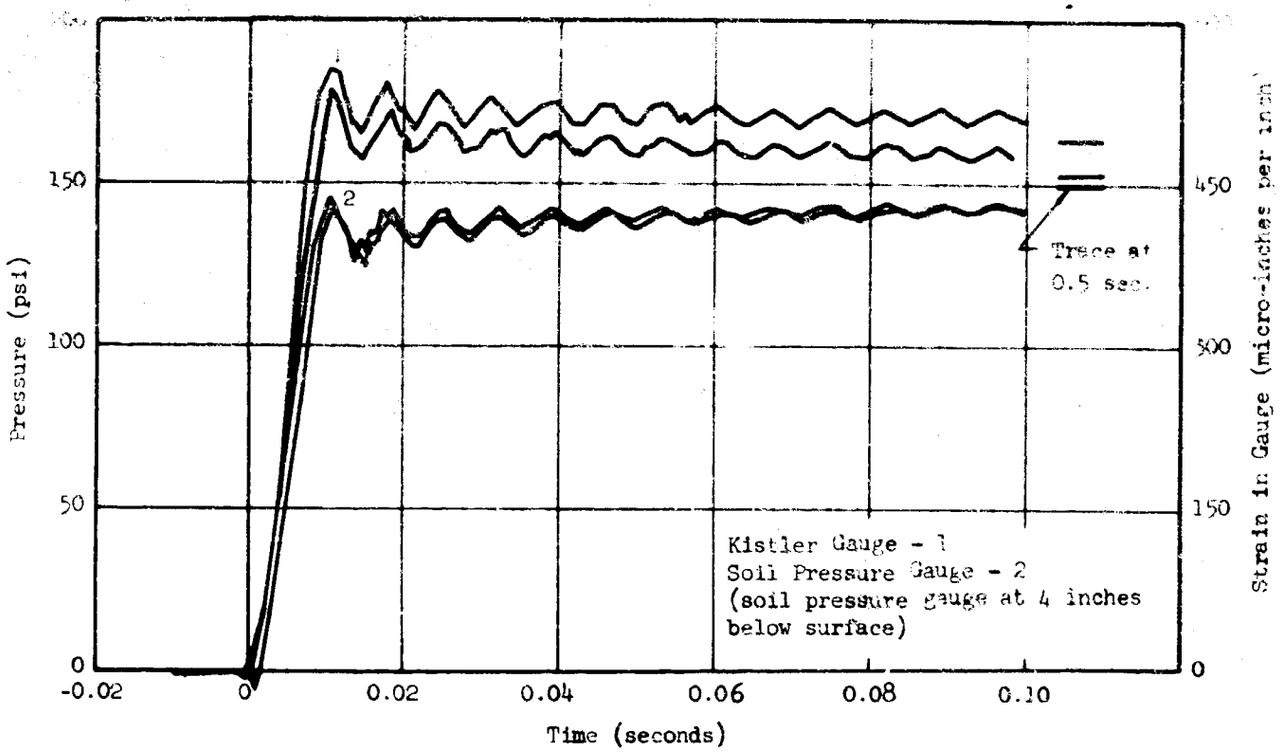


Fig. 25 Kistler Gauge and Soil Pressure Gauge Records From Dynamic Tests No. 3 and No. 4, Pipe No. 2

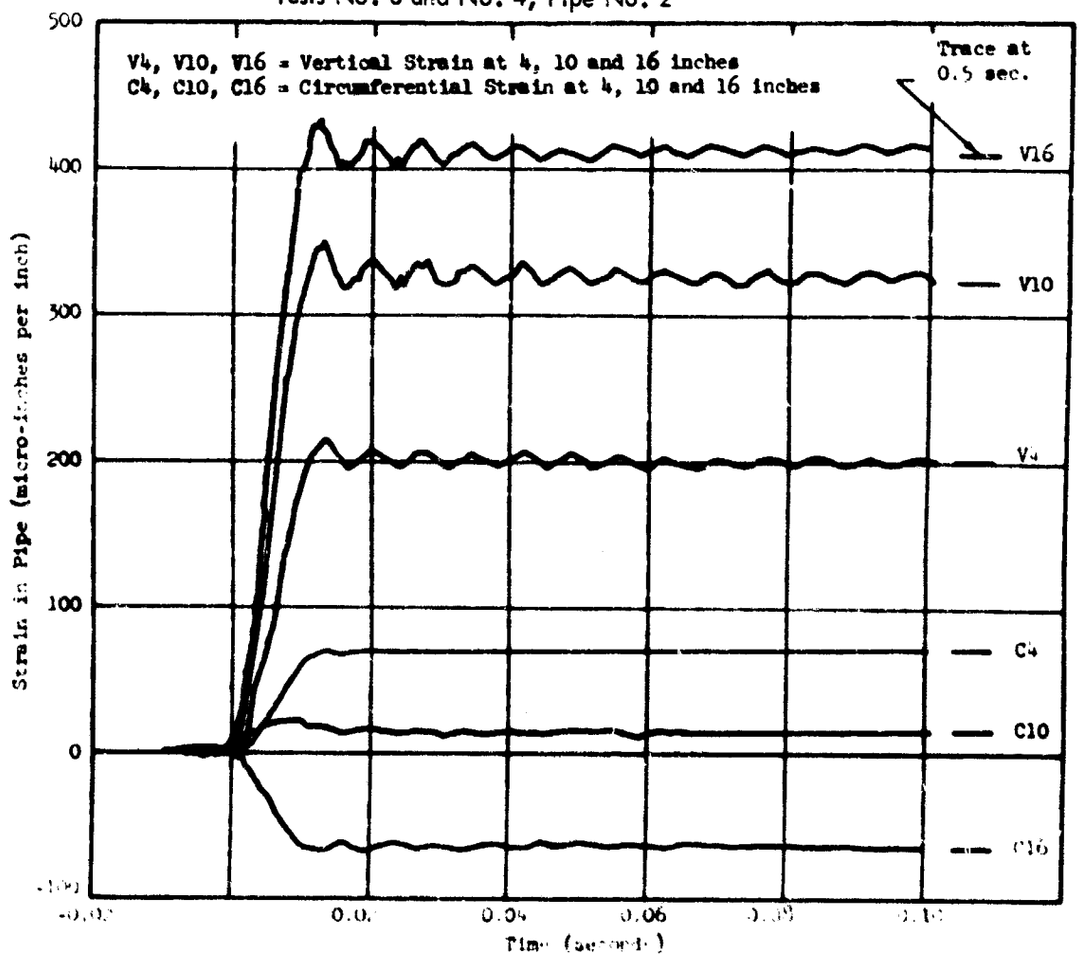


Fig. 26 Vertical and Circumferential Strain Records, Pipe No. 1, Dynamic Test No. 2

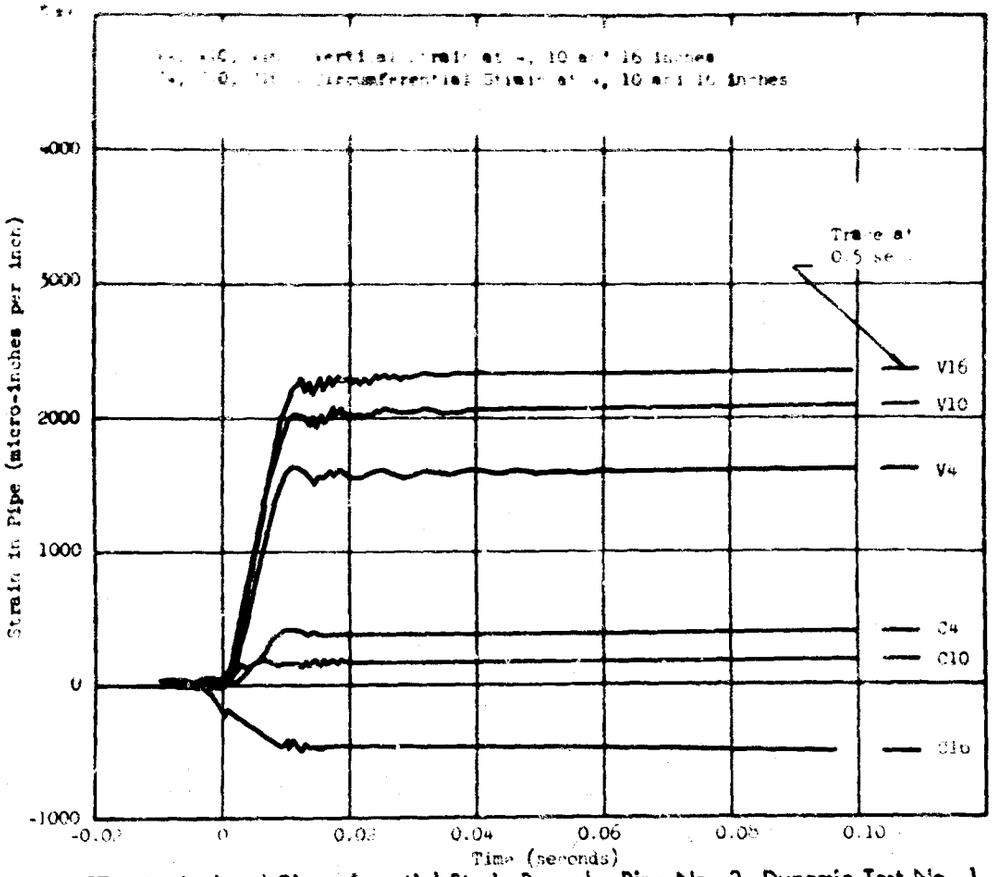


Fig. 27 Vertical and Circumferential Strain Records, Pipe No. 2, Dynamic Test No. 1

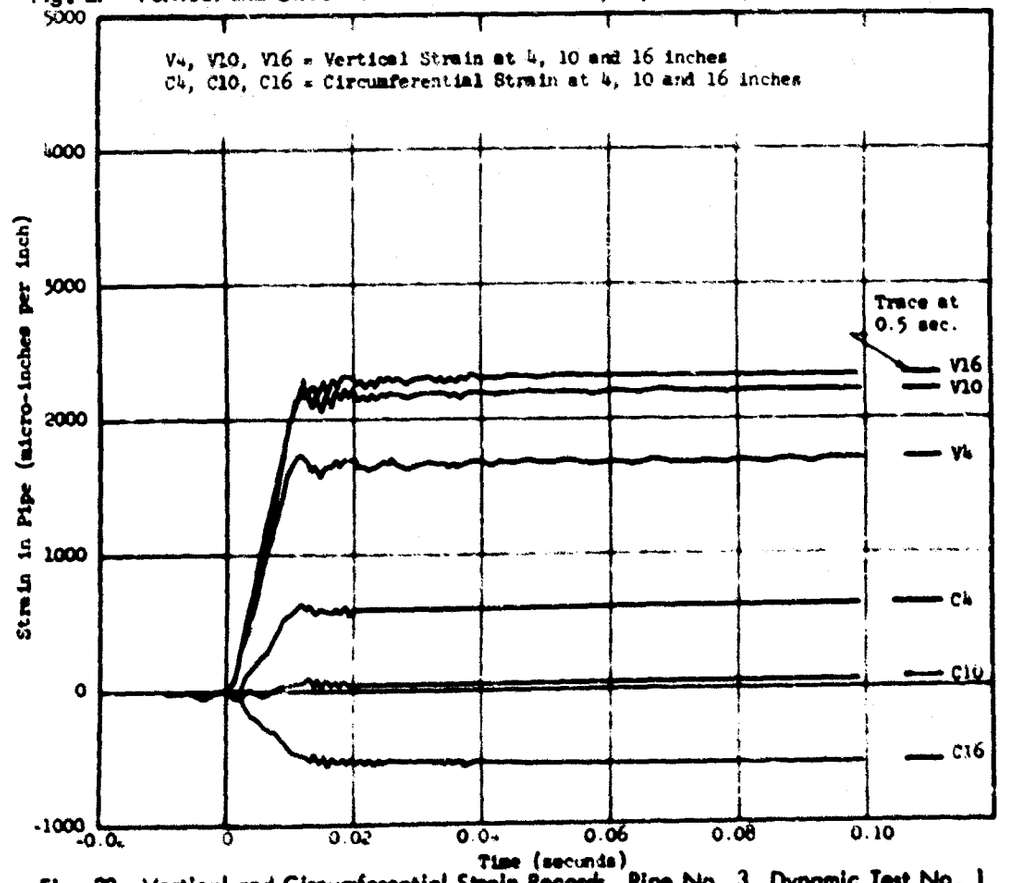


Fig. 28 Vertical and Circumferential Strain Records, Pipe No. 3, Dynamic Test No. 1

difference in behavior is clearly related to this difference in stiffness. This matter will be discussed more fully in the section dealing with the results of the shear calculations.

During the preliminary planning of this test program it was realized that owing to the design of the dynamic loading device and the method of connecting it to the tank, or soil container, a stress wave would be transmitted through the walls of the tank prior to the arrival of the gas pressure pulse at the surface of the soil sample. Further, there was some concern as to the magnitude of the stress wave which would be transmitted to the soil or the structure in the tank, either through shear at the tank walls, or, as a consequence of motion of the platform on which the equipment was mounted. Referring to Figures 26 through 28, it may be seen that a small signal was received just prior to the arrival of the gas pressure pulse ($t = 0$ sec.). This small disturbance is most noticeable in the vertical strain records for the 10- and 16-inch gauge lines. If this disturbance were due to noise in the recording circuits it would be apparent, and of approximately the same magnitude, in all circuits, including the circuits used for the Kistler gauge and the two soil pressure gauges. Since it was not, it is assumed that signal is, in fact, the anticipated disturbance. In any event, it is small and did not materially affect the records obtained. One further point should be mentioned. Just after the peak, a very high frequency oscillation appears in all of the vertical and some of the circumferential strain measurements on the pipes. This oscillation also appears in some of the records obtained with the soil pressure gauges. The computed natural frequencies of the pipes and pipe caps are much higher than the observed frequency. Further, the rate of load application is such that the natural frequencies of the pipes should not be excited. Therefore it is not logical to assume that it is a transient natural vibration excited by dynamic loading.

Although the source of this apparent vibration can not be established with certainty, it is possible that it is due to the oscillation of gas between the baffle plate and the surface of the soil sample immediately over the pipe cap. This explanation would account for the fact that the frequency of the oscillation is constant for all tests and for the fact that the oscillation is barely discernable in most of the Kistler gauge records. That gauge was located in the side wall of the expansion chamber about one inch above the surface of the soil sample, and at a considerable distance from the edge of the baffle plate.

Variation of Vertical Soil Pressure with Time and Depth The time of arrival of the stress wave in the soil at the various gauge depths can not be established with great accuracy from the records obtained. However, measurements indicate that the pressure pulse traveled from from the surface to a depth of 16 inches in about 2 milliseconds which corresponds to a stress propagation velocity of about 670 feet per second in the sand. Thus, assuming the soil to be elastic, the pressure at any time at a depth of 16 inches would correspond to the pressure at the surface two milliseconds earlier.

The ratio p_v/p_o is the ratio of the vertical pressure in the soil obtained by means of the soil pressure gauge to the pressure at the surface two milliseconds earlier obtained from the Kistler gauge records. No data was obtained for Tests No. 3 and No. 4 of Pipe No. 3 because soil pressure gauge No. 4 has become defective and no valid soil pressure data was obtained. Initially this ratio is larger than that obtained from the static tests at the 16-inch depth. However, it decreases with time approaching the value of approximately 0.3 obtained from the static tests at the same depth. The average of all data is plotted as a function of time in Figure 29.

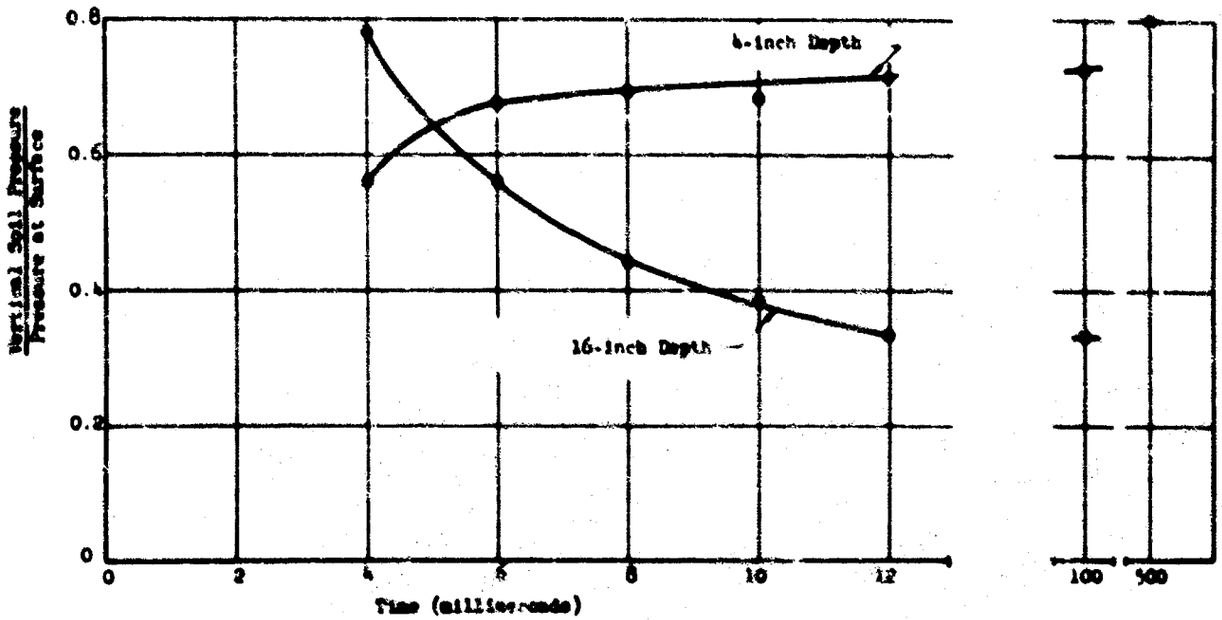


Fig. 29 Normalized Ratios of Vertical Pressure in Soil to Gas Pressure at Surface as a Function of Time for Two Depths - Dynamic Tests

Table ...

Summary of Lateral Pressure Calculations - Dynamic Tests

Test No.	Time (milliseconds)								Surf. Pres. (psi)	
	2	4	6	8	10	Peak	100	500	200	100
Pipe No. 1; 4-inch Depth: Peak Pressure at Surface ≈ 275 psi										
3	5.1	22.6	44.2	64.2	82.5	93.0	82.5	82.5	61.6	26.2
4	5.2	12.8	31.1	52.2	76.2	96.2	86.4	87.2	54.3	27.2
Pipe No. 1; 10-inch Depth										
3	4.2	--	14.6	32.1	46.4	52.9	52.9	49.6	39.4	21.2
4	4.1	9.1	17.0	32.8	45.6	55.3	47.5	48.5	41.6	22.8
Pipe No. 1; 16-inch Depth										
3	4.8	9.3	13.8	19.9	28.7	35.2	33.4	31.2	24.8	19.4
4	-0.4	5.0	18.4	22.3	30.0	37.3	35.7	32.6	28.8	23.9
Pipe No. 2; 4-inch Depth: Peak Pressure at Surface ≈ 155 psi									100	50
1	4.8	15.3	40.1	60.1	74.5	82.1	77.8	76.9	63.1	36.7
2	4.9	15.0	35.1	52.3	69.0	75.6	72.7	73.7	60.6	24.3
Pipe No. 2; 10-inch Depth										
1	1.2	12.2	23.1	35.6	46.8	49.0	49.4	50.4	57.6	43.0
2	4.1	12.1	21.2	31.0	43.7	49.0	47.6	47.2	42.0	31.5
Pipe No. 2; 16-inch Depth										
1	0.2	2.9	13.2	20.0	27.9	30.4	31.0	31.1	26.0	19.4
2	0.7	1.5	11.6	17.2	24.4	28.5	27.1	28.1	25.6	19.2
Pipe No. 2; 4-inch Depth: Peak Pressure at Surface ≈ 180 psi										
3	8.2	31.4	48.8	75.2	91.1	96.3	93.0	94.0	73.2	46.1
4	8.5	22.2	43.8	66.2	84.6	91.9	90.4	93.3	69.0	41.3
Pipe No. 2; 10-inch Depth										
3	4.9	21.1	32.9	53.0	65.3	70.6	67.7	68.7	61.3	40.7
4	5.6	18.5	32.8	46.1	59.9	63.9	64.3	63.9	56.6	39.2
Pipe No. 2; 16-inch Depth										
3	4.3	10.6	14.2	23.9	31.9	31.2	32.7	32.4	29.3	22.2
4	0.9	6.6	12.5	18.4	24.8	27.6	28.3	28.3	25.1	19.4
Pipe No. 3; 4-inch Depth; Peak Pressure at Surface ≈ 130 psi									70	40
1	4.5	21.6	36.9	54.3	71.0	78.7	73.7	73.4	55.7	39.2
2	5.2	17.7	34.4	51.3	65.5	72.4	68.6	69.3	52.3	36.2
3	4.3	17.1	30.4	46.2	57.9	62.8	59.7	60.4	44.3	29.2
4	5.1	16.7	31.5	46.6	57.0	61.3	58.5	58.8	44.4	28.9
Avg.	4.8	18.3	30.8	49.6	62.9	68.7	65.1	65.5	49.1	33.4
Pipe No. 3; 10-inch Depth										
1	3.6	15.8	23.2	34.5	45.9	52.2	49.8	51.6	43.6	33.2
2	4.1	12.6	20.5	31.5	42.9	49.2	45.4	45.1	39.6	32.5
3	2.9	11.7	18.9	28.8	36.5	42.0	38.7	38.3	30.6	24.8
4	5.1	12.8	19.9	29.3	37.0	42.2	38.9	38.1	33.0	26.7
Avg.	3.9	13.2	20.4	31.0	40.6	46.4	43.2	43.3	36.7	29.3
Pipe No. 3; 16-inch Depth										
1	0.8	4.9	7.2	11.6	18.2	20.1	19.4	19.4	17.7	14.3
2	0.8	5.4	6.9	11.0	15.0	16.9	17.6	18.0	15.9	12.4
3	0.4	5.2	7.3	12.3	16.8	17.9	16.8	16.5	15.3	13.1
4	0.5	3.9	7.8	10.9	16.4	16.7	16.1	17.2	14.1	11.6
Avg.	0.6	4.4	7.1	11.5	16.6	17.4	17.5	17.9	15.7	12.9

Using the approach on data obtained at the 4-inch depth, that is, dividing the vertical pressure in the soil at 4 inches by the pressure existing at the surface 0.5 milliseconds earlier, a different picture is obtained. For this depth, the ratio is initially lower than obtained in the static tests and increases with time to the value of about 0.8 obtained from the static tests.

This behavior was not anticipated and an obvious explanation of it cannot be offered. The fact that the initial value of p_v/p_o at the 16-inch depth is greater under dynamic load than under static load cannot be explained by a reflection of the stress wave from the bottom of the tank. If the soil were elastic, the stress wave (at a velocity of 670 fps) would have returned to the gauge depth at 4 milliseconds. It is possible that the reflected stress wave would travel faster than the incident because it is traveling in a compressed medium which exhibits a locking stress-strain relationship when confined. However, this would not explain the initially low value of the ratio p_v/p_o at a depth of 4 inches.

It is also possible that the initially high value of p_v/p_o at the 16-inch depth and the initially low value at the 4-inch depth are related to the soil-structure interaction.

Variation of Lateral Pressure on Pipes with Time and Depth The results of dynamic lateral pressure calculations are shown in Table 5. Only the tests which were conducted at the same nominal peak pressure are included for purposes of comparison. Again, the fact that there appears to be less scatter in the dynamic test data than in the static test data, is noted. The lateral pressure was calculated every two milliseconds for t = 0 sec. to the time at which the peak pressure was reached (11 or 12 milliseconds) and at t = 0.1 sec. and at t = 0.5 sec.

In Figure 30, the average lateral pressures calculated at 2, 4, 6, 8 and 10 milliseconds for the four tests in Pipe No. 3 are plotted as a function of depth. The propagation of the stress wave in the soil is evident. For example, at 2 milliseconds, the approximate time of arrival of the stress wave at a depth of 16 inches, the average lateral pressure at that depth was about 0.6 psi. However, there is no evidence of a significant reflection at the stress wave from the bottom of the soil container, here.

Variation of K_f with Time and Depth A summary of the calculations of the value of the ratio of the effective lateral pressure to the vertical pressure in the soil at the same time and depth are included in Figure 31. Of particular importance is the fact that the average value of K_f at the 4-inch depth was approximately 1 at t = 0.004 sec. and that, initially at least, the soil appeared to behave as a viscous fluid. Note that the value of K_f at this depth decreased with time.

At the 16-inch depth the value of K_f appeared to increase slightly with time,

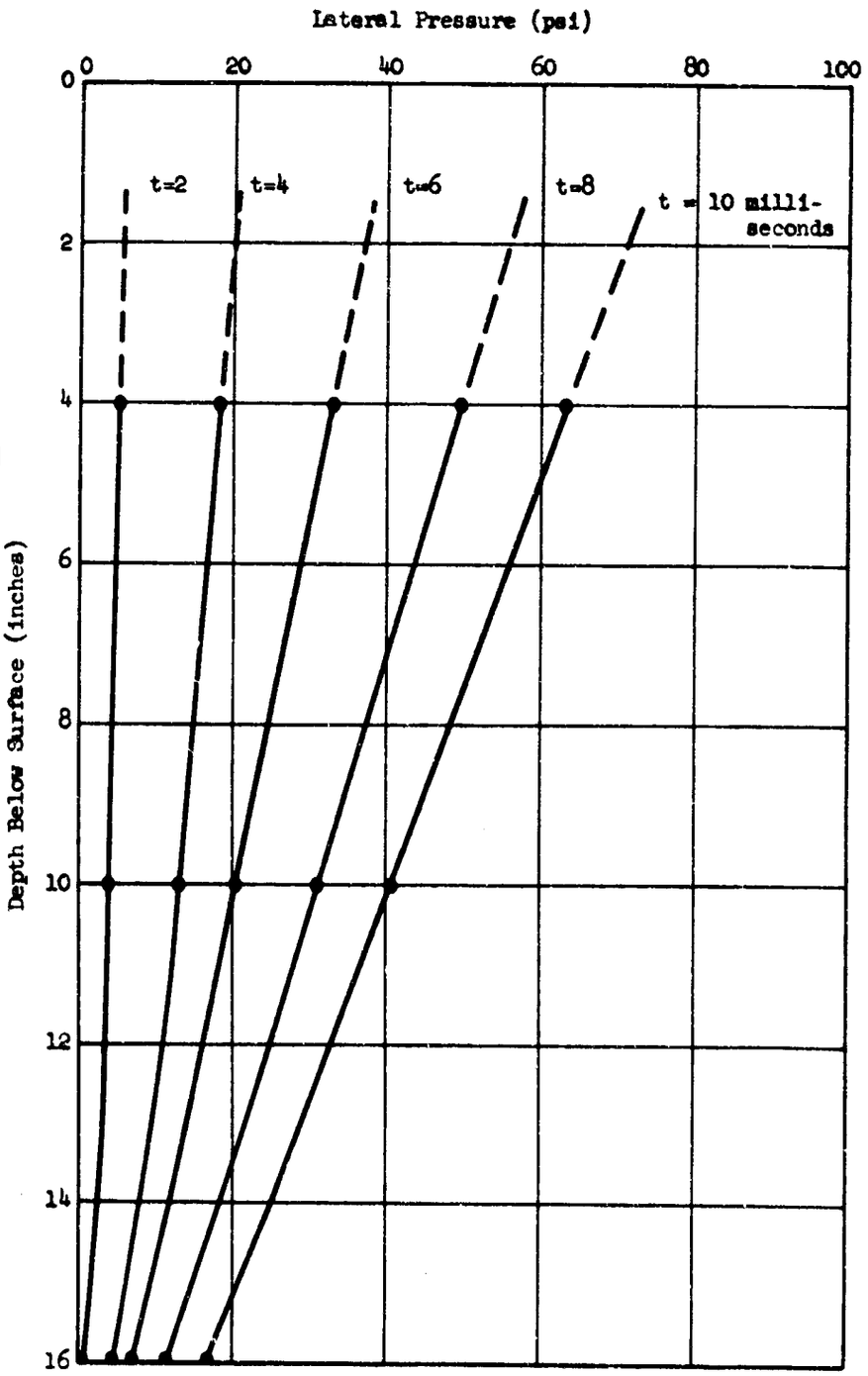


Fig. 30 Lateral Pressure as a Function of Depth at Various Times, From Dynamic Tests of Pipe No. 3

the average value for all times being about 0.45 which is about 10 to 15 percent higher than the value obtained from the static tests.

Variation of f with Time and Depth A complete summary of the shear calculations for the dynamic test series is contained in Table 6. Although there is considerable scatter in the computed value of f at 2 milliseconds, the results are notably consistent after that time. Again it is noted that the value of f is obviously dependent upon the state of compaction of the soil sample; the first and third and the second and fourth tests of Pipe No. 3 produced very similar results. The same pattern is evident in the tests of Pipe No. 2 even though the peak pressure was different for the two sequences. In each case the soil was better compacted for the second test of the sequence than for the first as explained previously.

The average values were computed to show the trend of the data and to assist in the interpretation of the test results. Because of the change in density from one test to another these data are obviously not from the same population.

Referring first to the tests of Pipe No. 1; between the 4-inch and 10-inch gauge lines the computed values of f are initially very nearly the same as those obtained from the static tests. After that, the value of f decreased with time until the time at which the peak pressure was reached. After the peak, the computed values of f increased as anticipated.

Table 6

Summary of Shear Calculations (f) - Dynamic Tests

Test No.	Time (milliseconds)								Surf. Pres. (psi)	
	2	4	6	8	10	Peak	100	500	200	100
Pipe No. 1; 4-inch to 10-inch Gauge Line										
1	0.95	1.00	0.81	0.79	0.76	0.76	0.80	0.80	0.84	0.62
2	0.85	1.11	0.85	0.80	0.77	0.78	0.80	0.80	0.99	0.73
3	0.95	0.73	0.68	0.65	0.66	0.64	0.62	--	0.69	0.74
4	0.92	1.53	0.98	0.80	0.75	0.70	0.73	--	0.84	0.88
Avg.	0.92	1.09	0.83	0.76	0.74	0.72	0.79	0.80	0.84	0.74
Pipe No. 1; 10-inch to 16-inch Gauge Line										
1	-1.10	0.52	0.69	0.76	0.74	0.78	0.78	0.81	1.01	1.34
2	-0.58	0.22	1.48	0.77	0.85	0.88	0.83	0.91	1.08	1.40
3	0.14	0.41	0.37	0.39	0.43	0.39	0.46	--	0.57	0.77
4	-0.25	-0.07	0.39	0.36	0.53	0.53	0.51	--	0.69	0.89
Avg.	-0.45	0.22	0.74	0.57	0.64	0.65	0.65	0.86	0.84	1.08
Pipe No. 2; 4-inch to 10-inch Gauge Line									100	50
1	-0.52	0.72	0.13	0.08	0.10	0.10	0.15	0.16	0.26	0.41
2	0.40	0.25	0.08	0.02	0.03	0.05	0.08	0.07	0.20	0.93
3	0.53	0.20	0.14	0.08	0.08	0.09	0.12	0.12	0.25	0.36
4	0.13	0.27	0.12	0.04	0.04	0.04	0.07	0.06	0.20	0.41
Avg.	0.14	0.36	0.12	0.06	0.06	0.07	0.11	0.10	0.23	0.53
Pipe No. 2; 10-inch to 16-inch Gauge Line										
1	0.96	0.42	-0.17	-0.10	0.01	0.12	0.16	0.16	0.24	0.34
2	-1.50	-1.25	-0.42	-0.31	-0.20	-0.10	-0.07	-0.06	0.08	0.25
3	0.30	0.03	-0.12	-0.08	-0.06	-0.04	0.01	0.00	0.07	0.36
4	-0.94	-0.48	-0.35	-0.34	-0.26	-0.22	-0.19	-0.21	-0.12	0.12
Avg.	-0.39	-0.32	-0.25	-0.21	-0.13	-0.06	-0.02	-0.03	0.07	0.27
Pipe No. 3; 4-inch to 10-inch Gauge Line										
1	0.23	0.24	0.12	0.09	0.09	0.11	0.14	0.14	0.31	0.43
2	0.34	0.27	0.12	0.07	0.05	0.08	0.09	0.09	0.24	0.39
3	0.43	0.22	0.09	0.05	0.05	0.07	0.10	0.10	0.25	0.50
4	0.39	0.20	-0.01	0.01	0.01	0.02	0.04	0.04	0.18	0.38
Avg	0.35	0.23	0.08	0.06	0.05	0.07	0.09	0.09	0.25	0.43
Pipe No. 3; 10-inch to 16-inch Gauge Line										
1	-0.01	-0.08	-0.28	-0.26	-0.13	-0.06	-0.03	-0.03	0.10	0.32
2	-0.98	-0.61	-0.65	-0.44	-0.37	-0.23	-0.21	-0.22	0.10	0.38
3	-1.15	-0.29	-0.38	-0.27	-0.19	-0.09	-0.09	-0.09	0.10	0.22
4	-1.04	-0.70	-0.43	-0.48	-0.34	-0.29	-0.27	-0.25	--	--
Avg.	-0.79	-0.42	-0.43	-0.36	-0.26	-0.17	-0.15	-0.15	0.10	0.31

Between the 10- and 16-inch gauge lines, the computed value of f was negative at t = 0.002 indicating that at this time the pipe was moving downward relative to the soil. This behavior is not unreasonable since the time of arrival of the pressure pulse in the soil at a depth of 16 inches was 2 milliseconds. Subsequently the value of f increased and at 4 milliseconds was positive indicating a reversal of relative motion between the soil and the pipe.

Turning to the results obtained from tests of Pipe No. 2, between the 4- and 10-inch gauge lines the soil was apparently moving down relative to the pipe initially. With increasing time the computed values of f decreased approaching zero for the period between 6 milliseconds and 12 milliseconds, indicating that the soil and the pipe were moving together for all practical purposes. Between the 10- and 16-inch gauge lines, the pipe was moving down relative to the soil during the entire period of loading. The fact that the computed values of f increased to about zero by the time the peak was reached indicates that the pipe and soil were moving together by that time.

The results of the tests of Pipe No. 3 were essentially the same as those obtained from the tests of Pipe No. 2. The differences noted can all be explained by the fact that Pipe No. 2 was stiffer. In fact, the relative behavior of all of the pipes was the same under dynamic loading as under static loading when due consideration is given to the differences in the velocities of stress propagation in the soil and the pipes.

Values of f computed for the period of unloading after the dynamic tests were somewhat less than those obtained from the static tests but, in general, followed the same trend; that is, the computed values increased during unloading.

SUMMARY AND CONCLUSIONS

Summary

Though there was some scatter in the data obtained (see Figure 13), it is considered that the soil pressure gauges performed satisfactorily under static load and their performance under dynamic load was even more consistent (see Figures 23 through 25). Gauge No. 3, placed 1.5 inches below the surface for all tests, recorded essentially the same pressure-time function as the Kistler gauge which was placed 1 inch above the surface of the soil in the side wall of the transition ring. Gauge No. 4, which was variously located at depths of 4 inches, 16 inches and 24 inches below the surface gave markedly consistent results.

The vertical load transfer at the soil-structure interface was strongly affected by the compaction of the soil for the tests of the plastic pipes. Although the soil was compacted by vibration during placement and by static application of a gas pressure equal to about 100 psi prior to test, the vertical strain in both plastic pipes was much less in the second of the two tests conducted in each sequence. This behavior was not marked in the tests of the steel pipe, primarily because the steel pipe was essentially rigid compared to the soil.

The fact that the circumferential strains were tensile rather than compressive at a depth of 16 inches below the surface is considered important. This behavior was observed in both static and dynamic tests of all pipes, and, it can be predicted for full scale structures so long as the structural response is within the elastic range.

To extrapolate the results of these tests into the range of plastic behavior of full scale structures could lead to erroneous conclusions. However, it does appear that at depths below one diameter, for cylindrical shells surrounded by soil and resting on a "rigid" foundation (such as bedrock) the longitudinal strain in the shell must reach the proportional limit before compressive circumferential strains can be developed. Whether the development of plastic response in longitudinal strain would constitute failure of the structure would depend on its function and the material of which it is made, among other factors.

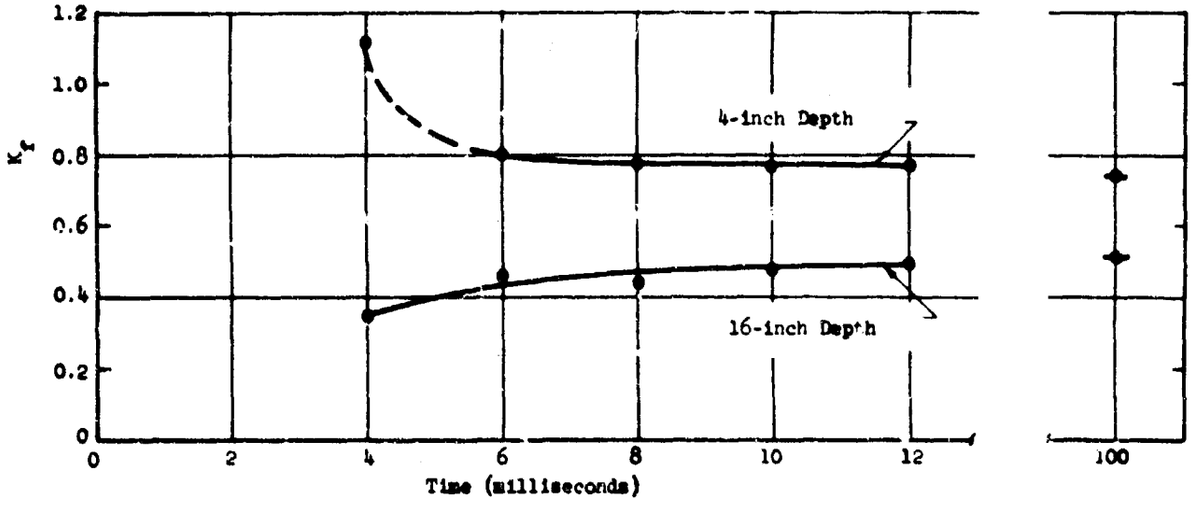


Fig. 31 Variation of K_f with Time for Two Depths, Dynamic Tests

The variation of vertical pressure in the soil in the container can be predicted with reasonable accuracy, under static load, using a simple exponential expression (Figure 17). However, under dynamic load the normalized vertical stress in the soil was initially higher at a depth of 16 inches than at a depth of 4 inches (see Figure 29). With time, both approached the values obtained during static load. This peculiar behavior may be related to the soil-structure interaction under dynamic load and it affected significantly the values of K_f at a depth of 4 inches.

Lateral pressure calculations for the static tests are summarized in Figures 18 through 20, and those for the dynamic tests in Table 5. Figure 30 shows the variation of the average lateral pressure with depth for various times during the four dynamic tests of Pipe No. 3. The propagation of the stress wave in the soil is clearly reflected in those curves but there is no indication of a significant increase in lateral pressure which would result from the reflection of the stress wave from the bottom of the tank.

As explained under Analytical Considerations, the ratio designated K_f herein is not the same as K as defined in theoretical soil mechanics because of the anticipated shear at the soil-structure interface. Calculated values of K_f obtained from the static tests are summarized in Figure 21. Those obtained from the dynamic tests are summarized in Figure 31. The values of K_f obtained from the static tests appear to vary with pressure and depth. It is interesting that when the shear calculations indicate that the value of the shear at the interface is very small, the average value obtained from the five tests of Pipe No. 3 at a depth of 16 inches approach the value (K = 0.41) obtained by Hendron (6) in one-dimensional compression tests of the same sand.

Under dynamic loading, the average value of K_f at the 4-inch depth was about 1 at t = 0.004 sec. then decreased to a value of approximately 0.7 at t = 0.5 sec. At the 16-inch gauge line, the average value of K_f increased from about 0.35 at t = 0.004 sec. to a value of about 0.5 at t = 0.5 sec. (see Figure 30). These data are perplexing. If the initially high value of K_f at the 4-inch depth were the result of a difference in the interaction between the soil pressure gauge and the soil under dynamic as compared to static loading, the same trend should be apparent in the results obtained with the same gauge at a depth of 16 inches. However, exactly the opposite behavior is indicated at the latter depth. Comparing the lateral pressures calculated at the four-inch depth under static and dynamic load for the same applied surface pressure, it may be seen that the lateral pressures are approximately equal. This is confirmed by the circumferential strain data. Therefore it is tentatively concluded that, at the 4-inch depth, the vertical pressure in the soil is lower initially under dynamic load than under static load; then approaches the static value with time as indicated in Figure 29. This behavior may or may not be important, depending on whether it is a function of the dimensions of the structure or confined to a shallow layer of soil near the surface. However, it is believed to be worth further investigation.

As used in this document, f is a measure of the magnitude and direction of the shear at the soil-structure interface. Its absolute value should be limited by the coefficient of friction between the soil and the structure or the tangent of the angle of internal friction in the soil, which is smaller. For the static tests the shear calculations are summarized in Table 4 and for the dynamic tests in Table 6.

From the static tests of the steel pipe it may be concluded that the angle of internal friction of the soil was about 43° which is high but not unreasonable for the sand employed in its highly compacted state. The average value of f obtained from these tests was 0.934. During the dynamic tests of the steel pipe, the values of f computed at 2 milliseconds between the 4- and 10-inch gauge lines were approximately equal to the values obtained from the static tests. However, after 4 milliseconds the computed values of f at the same depth decreased to about 0.75. This difference may be due to the fact that the soil is in motion.

Between the 10- and 16-inch gauge lines on the steel pipe the initial value of f was negative indicating that between these gauge lines the pipe was moving down relative to the soil at two milliseconds. This behavior is different from that observed during the static tests but is consistent with the fact that the pressure pulse took approximately 2 milliseconds to reach a depth of 16 inches in the soil, whereas the time required for the stress wave to reach the bottom of the pipe was on the order of 0.1 milliseconds. At 4 milliseconds the computed values of f were positive and then continued to rise to a value of about 0.65 by 12 milliseconds, and, subsequently to a value of about 0.86 by 0.5 sec.

In a similar fashion, values of f obtained from both static and dynamic tests of the plastic pipes may be used to explain, and can be explained by, the interaction between the soil and those structures. However, the specific values obtained have no general application and will not be repeated here.

A significant difference in behavior was observed between the static and dynamic tests of the plastic pipes in the soil. Under static test load the pipes tended to move with the soil between the 10- and 16-inch gauge lines. Further, the vertical strain at the 16-inch gauge line was greater than that at the 10-inch gauge line for all tests indicating that load was being transferred from the soil to the pipe as the soil-structure system sought equilibrium at each pressure level.

Under dynamic loading, however, the vertical strain at the 16-inch gauge line was initially less than that at the 10-inch gauge line and the shear calculations confirmed that the pipes moved down with respect to the soil between these gauge lines. This behavior was anticipated and can be explained by the fact that the velocity of stress propagation in the pipe was very much higher than in the soil. As a consequence of the difference in arrival times, the pipe underwent vertical displacement prior to the arrival of the stress wave in the soil.

Conclusions

Despite the limited number of tests performed several conclusions may be drawn. However, before presenting them, it should be stated that one of the most significant facts demonstrated by this investigation is that the equipment employed may be used effectively to study soil-structure interaction under static and dynamic loading. Although a pressure rise-time of 11 to 12 milliseconds was employed for this test series, the dynamic loading device is capable of producing equal pressures with a rise-time of only 3 to 4 milliseconds. The shorter rise-time is still not sufficient to excite dynamic response in the structures employed but is short enough to produce greater dynamic response in the soil sample.

It is concluded that:

1. The performance of the soil pressure gauges justifies further development effort. It is believed that improved performance can be obtained by reducing the length of the gauge to about 0.25 inches.
2. In addition to performing their primary function as test structures, the pipes were very effective gauges.
3. Under static load, the value of K_f at 4 inches below the surface was higher ($K_f \cong 0.5$ to 0.6) than at a depth of 16 inches. This relatively high value of K_f is believed to result from the depression of the surface of the soil around the top of the pipe. At a depth of 16 inches below the surface the value of K_f increased from a value of about 0.3 at low pressures to about 0.4 at higher surface loads.
4. Despite the limited number of tests conducted with a soil pressure gauge at a depth of 4 inches, there is reason to conclude that initially the soil behaved much as a viscous fluid down to a depth of at least 4 inches, under dynamic load. At a depth of 16 inches the computed values of K_f were only slightly higher than those obtained during the static tests ($K_f \cong 0.45$).
5. Under both static and dynamic loading, as a consequence of the transfer of load from the soil to the structure, circumferential strains at a depth of 16 inches were tensile rather than compressive. This behavior can be predicted for large cylindrical shells in soil, with similar foundation conditions and under similar loading conditions. Further, at all depths the vertical strains recorded were much larger than the circumferential strains. Additional research is required to determine the significance of these facts to the design of such structures.
6. Additional studies are required before it will be possible to predict the dynamic interaction between a cylindrical shell, such as those tested, and soils in general. The tests conducted, however, confirmed qualitative predictions of the interaction between a fine sand and simple shell structures responding within the elastic range, and furnished some data which was not previously available.

ACKNOWLEDGEMENT

The author is indebted to his advisor, Professor N. M. Newmark, Head of the Department of Civil Engineering, and to Professor G. K. Sinnamon, who developed the laboratory equipment used for these studies. In addition, the guidance and assistance of Associate Professor V. J. MacDonald, in matters pertaining to instrumentation, is gratefully acknowledged.

REFERENCES

1. Taylor, D. W., "Research on Consolidation of Clays," Publication No. 82, Publications of the Department of Civil and Sanitary Engineering, Massachusetts Institute of Technology, Cambridge, Massachusetts, 1942.
2. Timoshenko, S., Theory of Plates and Shells, McGraw-Hill, 1959.
3. Timoshenko, S., Theory of Elastic Stability, McGraw-Hill, 1956.
4. Timoshenko, S. and J. N. Goodier, Theory of Elasticity, McGraw-Hill, 1951.
5. Terzaghi, K., Theoretical Soil Mechanics, John Wiley and Sons, 1943.
6. Hendron, A. J., Jr., "The Behavior of Sand in One-Dimensional Compression," Ph.D. Thesis, University of Illinois, Urbana, Illinois, 1963.
7. Barkan, D. D., Dynamics of Bases and Foundations, McGraw-Hill, 1962.
8. Egger, W., "60 Kip Capacity, Slow or Rapid Loading Apparatus," Tech. Report to Research Directorate, Air Force Special Weapons Center, Contract No. AF33(616)-170; Structural Research Series No. 158, June, 1957, University of Illinois, Urbana, Illinois.
9. Sinnamon, G. K., J. T. Schamaun, and J. T. Hanley, "Feasibility Study of a Facility for Laboratory Investigations of Effects of Dynamic Loads on Soils and Buried Structures," Final Report to Defense Atomic Support Agency, Contract DA-49-146-x2-023, Department of Civil Engineering, University of Illinois, Urbana, Illinois, May 1961.
10. Leonards, G. A. (ed.), Foundation Engineering, McGraw-Hill, 1962.
11. Timoshenko, S., Vibration Problems in Engineering, McGraw-Hill, 1953.
12. Newmark, N. M., "Numerical Procedure for Computing Deflections, Moments, and Buckling Loads," Transactions of the American Society of Civil Engineers, Vol. 108, Paper No. 2202, 1943.

APPENDIX A

LATERAL VIBRATION OF A CYLINDRICAL SHELL SURROUNDED BY SOIL

Effect of Soil on Natural Frequencies

The vibration of cylindrical shell subjected to a dynamic, radially symmetric pressure is governed by the following equations of equilibrium:

$$\frac{\partial N_x}{\partial x} = \rho h \frac{\partial^2 u}{\partial t^2} \tag{A-1}$$

$$\frac{\partial Q_x}{\partial x} + \frac{N_y}{R} + N_x \frac{\partial^2 w}{\partial x^2} + P = \rho h \frac{\partial^2 w}{\partial t^2} \tag{A-2}$$

From Equation A-3:

$$\frac{\partial M_x}{\partial x} - Q_x = 0 \tag{A-3}$$

Therefore Equation A-2 may be written:

$$\frac{\partial^2 M_x}{\partial x^2} + \frac{N_y}{R} + N_x \frac{\partial^2 w}{\partial x^2} + P = \rho h \frac{\partial^2 w}{\partial t^2} \tag{A-4}$$

Now, for the case of a cylindrical shell in soil, any motion in the radial of z-direction will change the value of the lateral pressure at the soil-structure interface with which the structure is in equilibrium. If the shell moves inward (i.e., w is positive according to the notation established) the value of p would decrease; if it moves outward the value of p would increase. Assuming the soil to be a visco-elastic medium this variation might be expressed as:

$$p = K_o p_v - kw - c_v \frac{\partial w}{\partial t} \tag{A-5}$$

where, according to standard terminology in soil mechanics, $K_o p_v$ is the lateral earth pressure at rest and k is the subgrade modulus. The term $c_v(\partial w/\partial t)$ accounts for the viscous properties of the medium and serves as a mechanism by which energy may be dissipated into the soil from the structure.

Substituting Equation A-5 into A-4 the following equation is obtained

$$\frac{\partial^2 M_x}{\partial x^2} + \frac{N_y}{R} + N_x \frac{\partial^2 w}{\partial x^2} + K_o p_v - kw - c_v \frac{\partial w}{\partial t} = \rho h \frac{\partial^2 w}{\partial t^2} \tag{A-6}$$

M_x, N_y and N_x may be expressed as:

$$M_x = -\frac{Eh^3}{12(1-\nu^2)} \frac{\partial^2 w}{\partial x^2}$$

$$N_x = \frac{Eh}{1-\nu^2} \left(\frac{\partial u}{\partial x} - \nu \frac{w}{R} \right)$$

$$N_y = -\frac{Eh}{1-\nu^2} \left(\frac{w}{R} - \nu \frac{\partial u}{\partial x} \right)$$

Letting $B = \frac{Eh^3}{12(1-\nu^2)}$ and $D = \frac{Eh}{1-\nu^2}$ and substituting as appropriate in Equation A-6 yields:

$$-B\frac{\partial^4 w}{\partial x^4} - \frac{D}{R}\left(\frac{w}{R} - \nu\frac{\partial u}{\partial x}\right) + N_x\frac{\partial^2 w}{\partial x^2} + K_o p_v - kw - c_v\frac{\partial w}{\partial t} = \rho h\frac{\partial^2 w}{\partial t^2}$$

Assuming that only lateral vibrations are involved and that $N_x = \nu\frac{\partial u}{\partial x} = 0$, the preceding equation may be written as:

$$\frac{\partial^4 w}{\partial x^4} + \left(\frac{D}{BR^2} + \frac{k}{B}\right)w - \frac{K_o p_v}{B} + \frac{c_v}{B}\frac{\partial w}{\partial t} = -\frac{\rho h}{B}\frac{\partial^2 w}{\partial t^2} \qquad \text{(A-7)}$$

Equation A-7 is recognized to be the equation of damped vibration of a beam on an elastic foundation which may be solved by separation of the variables. For hinged ends the solution is:

$$w = \sum_{n=1}^{\infty} e^{-\beta p_n t}\left[C_1 \sin\sqrt{1-\beta^2}\, p_n t + C_2 \cos\sqrt{1-\beta^2}\, p_n t\right]\sin\frac{n x\pi}{L}$$

where

$$p_n = \frac{n^2\pi^2}{L^2}\sqrt{\frac{B}{\rho h}}\left\{\left[1 + \frac{DL^4}{n^4\pi^4 BR^2} + \frac{kL^4}{n^4\pi^4 B}\right]^{1/2}\right\}$$

Note that the natural circular frequencies of vibration of a beam are

$$p_n = \frac{n^2\pi^2}{L^2}\sqrt{\frac{B}{\rho h}}$$

so that the entire expression within the brackets amounts to a correction factor which must be applied to the beam frequencies to obtain the shell frequencies.

Since p_n is the natural circular frequency of vibration of the shell in the n^{th} mode, the effect of the subgrade modulus on the frequencies of vibration may be obtained by examining the terms within the brackets. The term $DL^4/n^4\pi^4 BR^2$ accounts for the stiffening effect of the curvature of the shell on the "beam" and the term $kL^4/n^4\pi^4 B$ accounts for the stiffening effect of the soil. Dividing the latter term by the former yields a ratio, kR^2/D, by which the relative importance of the subgrade modulus can be evaluated for a given case. Values of k, obtained by others (10) for well-compacted cohesionless soils are on the order of 200 psi per inch of deflection. For the shells employed in this test program $R^2 \cong 4$ and D varies from about 125,000 to about 3.6×10^6. Thus, for these shells, the effect of the soil on their natural frequencies in lateral vibration is negligible. Therefore, the equation for the undamped natural frequencies of lateral vibration may be expressed as:

$$p_n = \frac{n^2\pi^2}{L^2}\sqrt{\frac{Eh^2}{12(1-\nu^2)\rho}}\left\{\left[1 + \frac{12L^4}{n^4\pi^4 h^2 R^2}\right]^{1/2}\right\} \qquad \text{(A-8)}$$

The fundamental natural period of lateral vibration, then is:

$$T = \frac{2\pi}{p_1} \qquad \text{(A-9)}$$

Using Equation A-9 the fundamental natural periods of lateral vibration of the pipes used for these experiments were calculated. The fundamental natural period for the steel pipe is about 0.06 milliseconds whereas the same period for the two plastic pipes is about 0.2 milliseconds. Since the rise time of the applied dynamic pressure pulse would be on the order of 10 milliseconds it was apparent that no dynamic response of the shells could be anticipated unless the fact that the pulse would be traveling along the shell excited some resonant frequency.

Effect of a Travelling Load

The problem of the response of a simply supported beam to a moving constant force has been solved (11). If the damping effect of the soil is ignored, that solution is valid for the response of a cylindrical shell to a radially symmetric force moving in the direction of the axis of the cylinder when Equation A-8 is substituted for the beam frequencies. Performing the substitution it may be seen that the deflections will go to infinity (i.e., a resonant condition exists) when:

$$n^4 = \frac{DL^4}{B\pi^4 R^2} = \frac{n^2 c^2 \rho h L^2}{B\pi^2}$$

where c is the velocity of the stress propagation in the soil.

Solving for c:

$$c = \frac{n\pi}{L}\sqrt{\frac{B}{\rho h}}\sqrt{1 + \frac{DL^4}{n^4\pi^4 BR^2}}$$

and since $B = Eh^3/12(1-\nu^2)$, and $D = Eh/(1-\nu^2)$ the critical velocities are a function of the shell properties and dimensions. Specifically, the critical values of c are defined by

$$c = \frac{n\pi}{2\sqrt{3}}\sqrt{\frac{E}{\rho(1-\nu^2)}}\sqrt{\frac{h^2}{L^2} + \frac{12L^2}{n^4\pi^4 R^2}}$$

Note that h^2/L^2 is very small for the pipes tested and that $\sqrt{E/\rho}$ is the velocity of stress propagation in the shell so that for the lowest modes the critical velocities may be expressed as follows:

$$c \simeq \frac{1}{n\pi} \cdot \frac{L}{R}\sqrt{\frac{E}{\rho}}$$

The approximate critical velocities for the first five modes of the steel pipe and the two plastic pipes are listed below on the right.

The anticipated velocity of stress propagation in the soil was about 1000 fps, which would excite only very high frequency response. The response contributed from the very high frequencies which might be excited is not only small but would undoubtedly be heavily damped.

Mode Number	Pipe	
	Steel	PVC
1	70,350	21,330
2	35,175	10,66[illegible]
3	23,450	7,11[illegible]
4	17,590	5,33[illegible]
5	14,070	4,27[illegible]

APPENDIX B

A GAUGE FOR MEASURING VERTICAL PRESSURE IN SOIL

Introduction

The problem of the measurement of stress or strain within a soil mass has plagued soils research from its beginnings and has not been solved satisfactorily as yet. The ideal instrument for making such measurements would have properties that match perfectly those of the soil surrounding it, would respond perfectly to static and dynamic loads and be inexpensive and small. No single gauge now available embodies these features although a great amount of research effort has been expended on the development of such a pressure gauge.

When the experimental program described in the body of this report was conceived there was no small, reliable, inexpensive, soil pressure gauge available. Recognizing the many problems involved, an attempt was made to develop such a gauge.

Description of Gauge

In its final form the soil pressure gauge consisted of a solid cylinder of epoxy resin, about 1 inch in diameter and 1 inch in height, in which two Tatnall Metalfilm Epoxy-Back, C6-121, strain gauges were imbedded. One of the strain gauges was oriented to measure strain along the vertical axis and the other, at right angles to the first, was oriented to measure radial strain in the cylinder. A photograph of one such gauge is shown in Figure 32.

The gauge was made by pouring a disk of epoxy resin about 0.25 inches thick in a 1-inch diameter mold. After it has set for at least 24 hours the disk was taken from the mold and cut into two pieces exposing the centerline of the cylinder. The surfaces of the disk to which the gauges were to be attached were then polished and cleaned. The strain gauges were then glued to the half-disk of epoxy resin using Eastman 910 adhesive. Leads were soldered to the gauges after the glue had set.

The above with leads attached was then placed in the mold and 1.5-inch extensions were cast, one at a time to each end so that the over-all length of the gauge was about 3 inches. This length was chosen to avoid the effect of end restraint during the uniaxial compression tests to be described. At this stage the gauge was baked at 250°F for 24 hours to relieve shrinkage stresses. The baking was found to be necessary to raise the proportional limit of the gauge to 500 psi.

After obtaining the characteristic properties of the gauge under uniaxial compression, approximately one inch was cut off each end producing the gauge shown in Figure 32.

Uniaxial Compression Tests

Uniaxial compression tests of each gauge were conducted by means of a modified platform scale. The total load on the gauge was raised in 40 pound increments from 0 to 360 pounds and the vertical and horizontal strains were measured on SR-4 strain indicators at each load increment. From these tests the value of the modulus of elasticity (E) and Poisson's ratio (ν) were obtained for the gauges subsequently used in the experimental work discussed in the body of this thesis.

Four such tests were conducted on each gauge. The results obtained were within two percent of the average value of strain at each load level.

Calibration Tests in the Soil Environment

For these tests the gauges were placed at various depths in the same sand and in the same tank subsequently used for the soil-structure interaction studies. The objective of the tests was to establish a calibration curve which could be used to determine the pressure as a function of depth in the soil.

It was recognized that because the plastic cylinders were stiffer than the soil they would "attract" load so that the vertical strain in the gauge corresponding to a given pressure in the "free-field" would be higher than that obtained for the same pressure under uniaxial load. That is, the existence of the gauge in the soil would disturb the "free-field" stress distribution and the total load on the plastic cylinder would be greater than the load on an equivalent area in the "free-field" at the same depth.

Further, as a consequence of this "negative arching" action, the lateral pressure on the sides of the plastic cylinder would be less than might be predicted in the free-field. However, the laterally oriented strain gauge was not used to determine the ratio of lateral to vertical stress in the soil. This measurement was used only to determine whether the arching around the gauge was constant as a function of depth in the soil.

It was reasoned that so long as the soil pressure gauge were at a sufficient distance from any boundary, arching should not vary as a function of depth but only as a function of pressure. If this were true the gauge could be calibrated to measure the pressure in the soil. However, it was also clear that it would have to be calibrated for the soil in which it was to be used.

A total of 25 tests were conducted with soil pressure gauge 4 at various depths; 4 at the surface, 6 at 1 inch, 4 at 2 inches, 4 at 4 inches, and 7 at 16 inches below the surface. The results of these tests are plotted in Figure 33 where each data point represents the average of data obtained at the depth indicated.

The vertical strain recorded as a function of surface pressure showed considerable scatter particularly at a depth of 1 inch (see Figure 34). As a consequence of this scatter and the limited number of tests it was not possible to establish by statistical analysis that the data obtained at the one-inch and two-inch depths are not part of the same population.

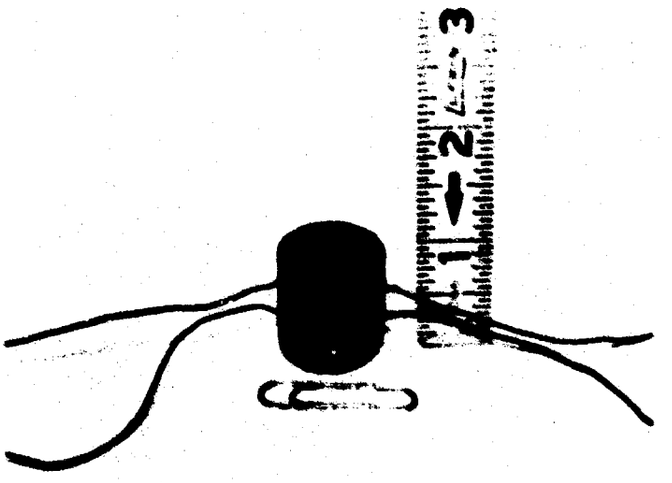


Fig. 32 Soil Pressure Gauge Developed for Experimental Program

The ratio of lateral strain to vertical strain in the gauge was calculated at three depths (see Table 7). A significant and interesting point is that at depths below the surface the lateral strain in the soil pressure gauges was tensile at all pressure levels. The arching of the soil around the gauge was such that the effective lateral pressure on the gauge was very nearly zero.

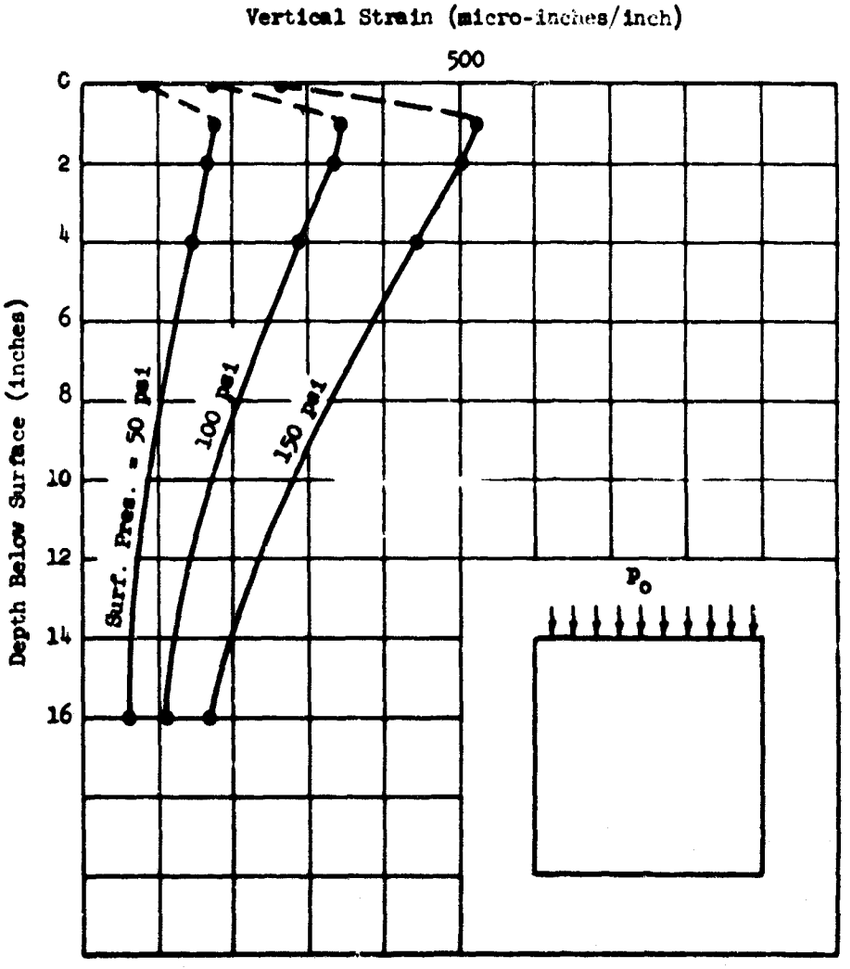


Fig. 33 Variation of Vertical Strain in Soil Pressure Gauge No. 4 with Depth

Table 7

Comparison of Ratio of Lateral to Vertical Strain in Gauge No. 4 at Three Depths

Surface Pressure (psi)	Gauge Depth = 0"			Gauge Depth = 1"			Gauge Depth = 2"		
	Lateral Strain	Vertical Strain	Lateral / Vertical	Lateral Strain	Vertical Strain	Lateral / Vertical	Lateral Strain	Vertical Strain	Lateral / Vertical
50	-35	-85	0.41	25	-174	-0.14	17	-149	-0.11
100	-5	-175	0.03	63	-546	-0.12	90	-521	-0.16
150	-15	-265	0.06	77	-525	-0.15	84	-490	-0.17
200	10	-350	-0.03	110	-686	-0.16	116	-654	-0.18
250	25	-440	-0.06	146	-859	-0.17	147	-820	-0.18
300	60	-545	-0.11	175	-1009	-0.17	177	-1005	-0.18
350	80	-630	-0.13	206	-1180	-0.18			
400	105	-735	-0.14	250	-1357	-0.17			

Notes: (1) All strains given in micro-inches per inch.
(2) Data given are averages of all tests at each depth.

However, when the top of the gauge was flush with the surface the lateral strain in the gauge was compressive at lower levels of pressure and tensile at higher levels of pressure. It is not clear why this reversal occurred, but the fact that it did occur indicates that the interaction between the soil and the gauge is significantly different from that at depths such that arching can occur.

Based on the results obtained from these limited tests, additional tests were conducted with pressure gauges No. 3 and No. 4 at a depth of approximately 1.5 inches. Calibration curves for these two gauges were prepared assuming that the vertical strain obtained at this depth corresponded to a free-field pressure equal to that applied to the surface of the soil. That is, it was assumed that the load transferred to the walls of the tank (approximately 24 inches in diameter) would have a negligible effect on the vertical pressure in the soil at a depth of 1.5 inches near the center of the soil sample. The calibration curve for gauge No. 4 is shown in Figure 35.

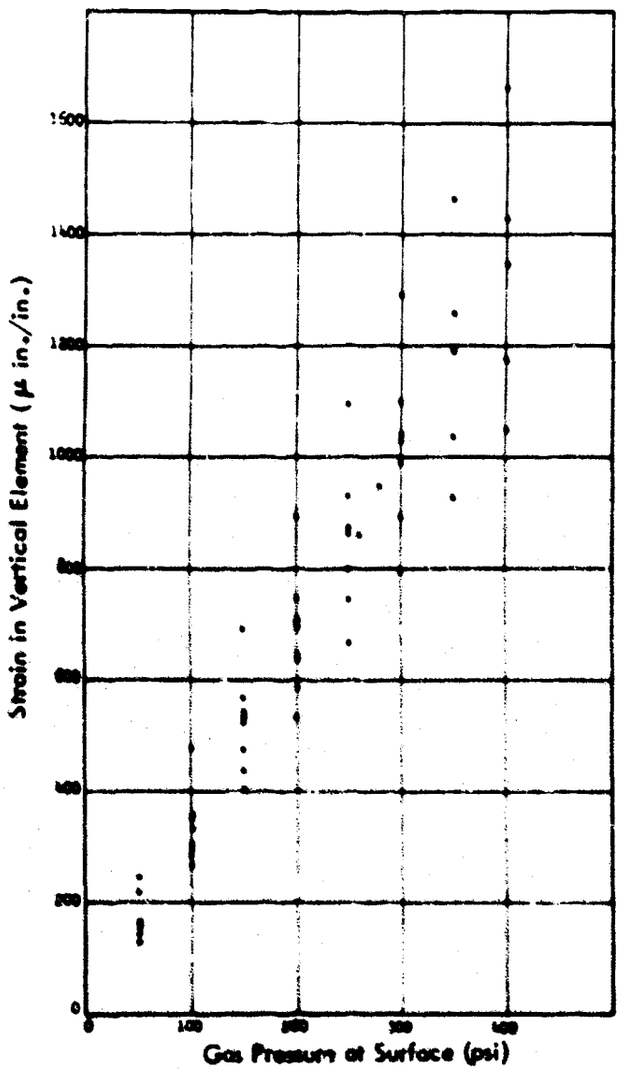


Fig. 34 Vertical Strain in Soil Pressure Gauge No. 4 as a Function of Surface Pressure - 1-inch Depth

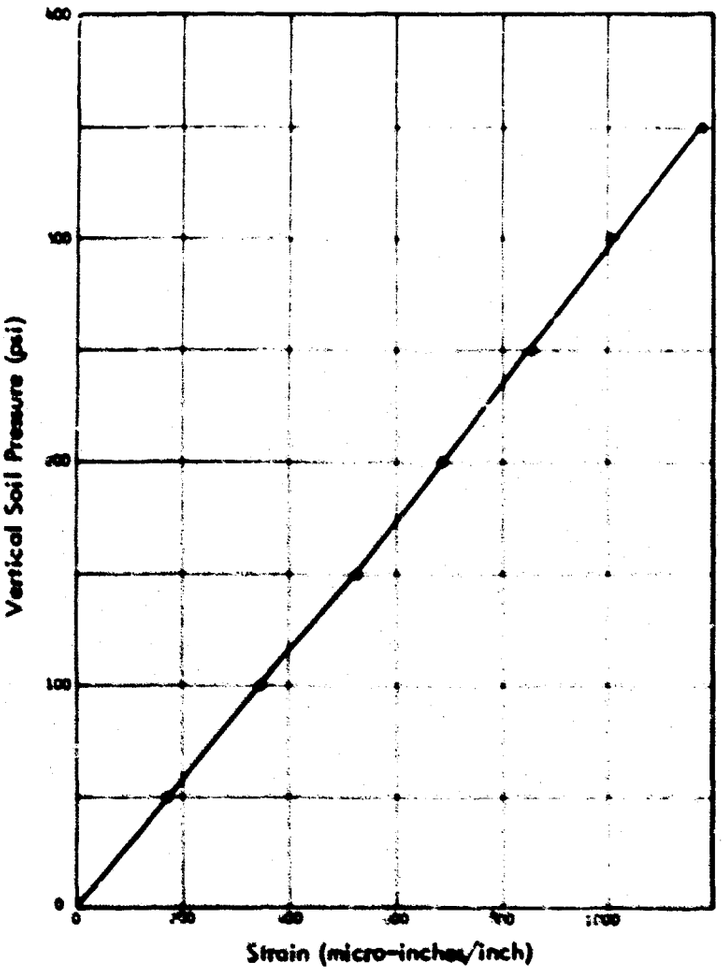


Fig. 35 Calibration Curve for Soil Pressure Gauge No. 4

SESSION EIGHT–THURSDAY PM
DESIGN AND PROTOTYPE STUDIES

SESSION CHAIRMAN: DON A. LINGER

TABLE OF CONTENTS

	page
PROTECTION OF UNDERGROUND STRUCTURES BY ARCH ACTION ASSOCIATED WITH THE IMPERFECT DITCH METHOD OF CONSTRUCTION, Merlin G. Spangler	531
MEASUREMENTS OF SOIL-STRUCTURE INTERACTION ON PROTOTYPE PROTECTIVE STRUCTURES, Ralph H. Sievers, Jr.	547
THE DESIGN OF BURIED ARCHES TO RESIST BLAST LOADS, William J. Flathau and Richard A. Sager	554
FORCE TRANSMISSION DUE TO COHESIVE SOIL-FOUNDATION INTERACTION UNDER VIBRATORY LOADING, Robert L. Kondner	574
THE THEORY OF LIMITING EQUILIBRIUM FOR AXISYMMETRIC PROBLEMS: A COMPARISON WITH EXPERIMENT ON SILO SKIN FRICTION, C. J. Costantino and A. Longinow	583



Participants in Session Eight were, left to right, Don A. Linger (Session Chairman); C. E. Eckberg (presented paper by M. G. Spangler); R. H. Sievers; R. L. Konder; A. Longinow; and W. J. Flathau.

PROTECTION OF UNDERGROUND STRUCTURES BY ARCH ACTION ASSOCIATED WITH THE IMPERFECT DITCH METHOD OF CONSTRUCTION

by
Merlin G. Spangler*

Marston's Theory of Loads on Underground Conduits is a classical procedure for the evaluation of arching phenomena in the soil overburden above an underground structure. It has a history of more than fifty years of theoretical and experimental research, and of successful application and experience in the sewerage and allied fields of engineering practice.

Arch action and the equal and opposite arch support play a tremendously important role in the development of earth load on a structure. Under some circumstances, such as the case of a pipe in a trench, its effect is favorable; that is, it reduces the load as compared to the dead weight of the prism of soil lying above the structure. In other cases, such as some installations of culverts under embankments, arch action may be inverted and the load on the structure may be considerably greater than the weight of the overlying prism of soil. The purpose of this paper is to review the various aspects of the Marston Theory, giving special attention to the Imperfect Ditch Method of Construction, by which the principles of arch action and arch support are employed to minimize the load on a buried structure. This method of construction has been rather widely used to reduce the static earth load on highway culverts, and its use is growing as heights of embankments increase due to upgrading of standards for sight distance and curvature to accommodate faster and greater volumes of highway traffic. To the best of the author's knowledge, the method has not been employed in connection with structures subjected to shock or dynamic loads. However, it is his opinion that the basic principles of the method may be effective in minimizing loads of this character, as well as static earth loads.

For purposes of load calculation, underground conduits are conveniently classified on the basis of their construction environment which influences differential settlements of the structure and its overlying prism of soil, in relation to settlements of the adjacent masses of soil. This classification is given in Table 1 and illustrated in Figure 1.

TABLE 1
CLASSIFICATION OF UNDERGROUND CONDUITS

I. Ditch Conduits

II. Projecting Conduits

  A. Positive
    1. Complete Projection Condition
    2. Incomplete Projection Condition
    3. Complete Ditch Condition
    4. Incomplete Ditch Condition

  B. Negative
    1. Complete Ditch Condition
    2. Incomplete Ditch Condition

III. Special Cases

  A. Imperfect Ditch Conduits
    1. Complete Ditch Condition
    2. Incomplete Ditch Condition

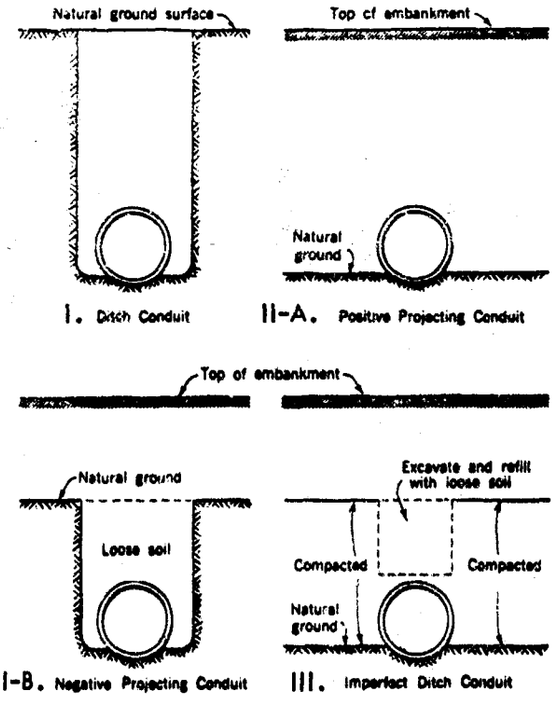


Fig. 1 Classification of Underground Conduits

*Research Professor of Civil Engineering, Iowa State University, Ames, Iowa.

A Ditch Conduit is defined as a structure which is placed at the bottom of a ditch and then covered with backfill up to the natural ground surface. Sewers and drains are typical examples of this type of installation. Projecting Conduits are structures installed with their tops at an elevation near the natural ground surface and then covered with an embankment. If the top of the structure projects above the ground surface it is a Positive Projecting Conduit. If it is placed in a shallow trench and the top lies below the ground surface, it is a Negative Projecting Conduit. A transition case which is sometimes recognized is the Zero Projecting Conduit, wherein the top of the structure is level with the natural ground surface. Highway and railway culverts are typical examples of these classes of structures. Imperfect Ditch Conduits are first installed as positive projecting conduits. Then the soil at the sides and for some distance above the top is thoroughly compacted, after which a trench is excavated directly above the structure. This trench is refilled with highly compressible material and the embankment is completed to grade in a normal manner. The deeper the imperfect ditch and the more compressible the backfill soil, the greater will be the reduction in load on the structure. Or, saying it another way, the greater will be the arch support action by which a portion of the weight of the prism of soil above the structure is transmitted to and carried by the adjacent columns of soil.

In connection with the development of load on an underground structure, arch action is considered to be the resultant of lateral thrust and vertical shearing forces which are mobilized on certain vertically oriented planes in the soil overburden. In the case of ditch conduits and negative projecting conduits, the vertical planes are coincident with or rise above the sides of the trench. In the case of positive projecting conduits and imperfect ditch conduits, the planes in question rise vertically above the sides of the structure.

The magnitude of arch support can be evaluated by means of the Marston Theory. It represents the algebraic difference between the dead weight of the overburden soil and the earth load to which the structure is subjected, as indicated by the load formula. For ditch conduits, this load formula is derived by considering the forces acting on a thin horizontal slice of backfill material, as shown in Figure 2. The summation of vertical forces on the slide equal zero. Therefore

$$V + dV + 2Ku'\frac{V}{B_d}dh = V + wB_d dh \tag{1}$$

This is a linear differential equation, the solution for which is

$$V = wB_d^2 \frac{1-e^{-2Ku'(h/B_d)}}{2Ku'} \tag{2}$$

At the elevation of the top of the conduit, h = H; and by substituting this value in Equation 2, we obtain an expression for the total vertical pressure on the horizontal plane through the conduit top. Thus Equation 2 may be written,

$$W_c = C_d w B_d^2 \tag{3}$$

in which

W_c = load on conduit, plf
w = unit weight of backfill, pcf
B_d = width of ditch at top of conduit, ft.

$$C_d = \text{a calculation coefficient} = \frac{1-e^{-2Ku'(h/B_d)}}{2Ku'} \tag{4}$$

e = base of natural logarithms
K = ratio of lateral pressure to vertical pressure
u' = coefficient of friction between backfill and sides of ditch
u = tan ϕ, the coefficient of internal friction of the backfill soil

Values of C_d can be taken from the curves in Figure 3.

As stated above, the magnitude of arch support is the algebraic difference between the weight of backfill and the load on the structure. For the case of ditch conduits, this difference is

$$A_s = wB_d(H - C_d B_d) \tag{5}$$

in which

A_s = arch support, plf (support derived from both sides of the ditch).

The lateral and vertical forces which constitute the arch action and arch support at any point below the ground surface are shown in Figure 4. The force B is the lateral pressure of the backfill against the side of the ditch and B' is its equal and opposite reaction. The force A is the shear force at the point and is equal to B times the coefficient of friction between the backfill and the ditch side, while A' is its equal and opposite reaction. The force C and its reaction C' are the resultants of A and B and of A' and B' respectively.

The maximum value of the vertical shearing force and resistance (forces A and A' in Figure 4) is the shear strength between the backfill and the ditch sides. This maximum value defines the limiting amount of arch support which is available to help carry the weight of the backfill. All of the backfill weight in excess of the arch support is transmitted to the pipe at the bottom of the ditch. The shearing strength of the soil is fully mobilized by downward movement of the backfill, due to settlement of the structure into its bedding plus compression strain or consolidation of the backfill. The magnitude of this downward movement will normally be sufficient to fully mobilize the shear strength of the soil; and having been mobilized, it continues to be effective because of the tendency for downward movement, even though actual finite movements have ceased. The permanent character and effectiveness of shear strength and accompanying arch action in the overburden soil has been demonstrated by experiments at Iowa State University, wherein the measured loads on three underground conduits remained nearly constant over a period of 21 years.

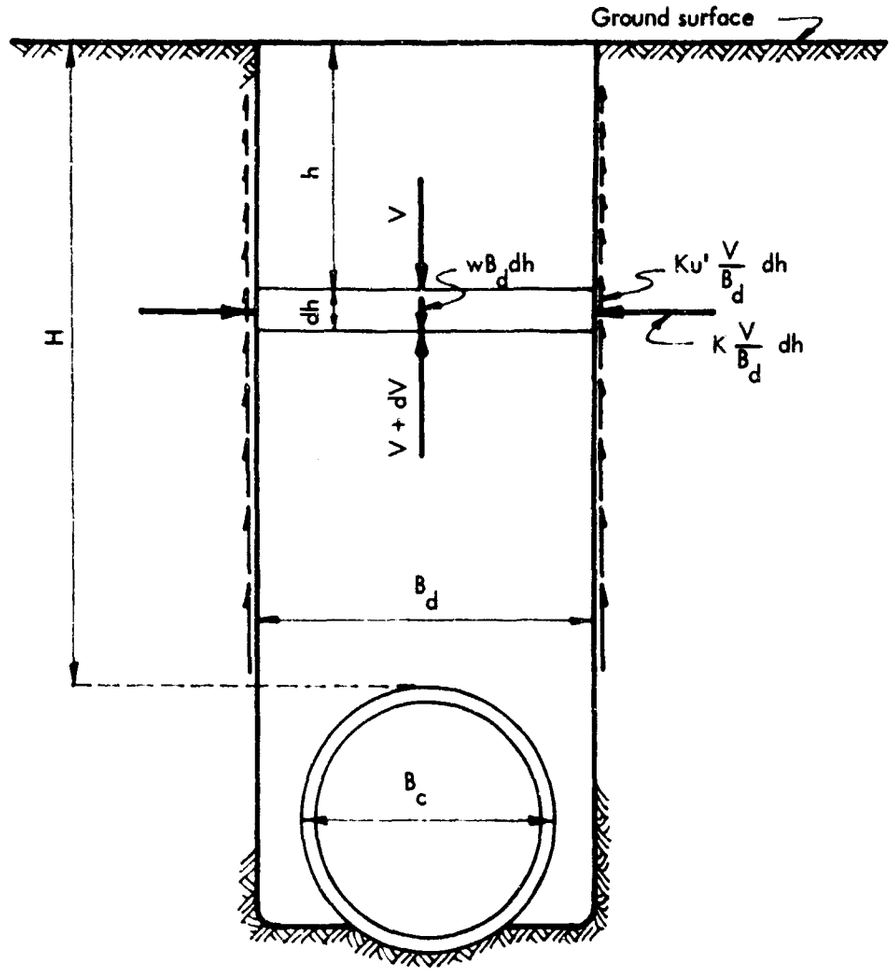


Fig. 2 Free Body Diagram Ditch Conduit

If the conduit is installed in a tunnel in such a manner that the overburden soil is undisturbed, it may be appropriate to consider that cohesion is an effective contributor to arch support of the overlying soil. The load formula, taking cohesion into account and derived in a manner similar to that indicated above is

$$W_t = C_t B_t (wB_t - 2c) \tag{6}$$

in which

W_t = load on conduit, plf
w = unit weight of overburden soil, pcf
B_t = width of tunnel, ft.
$C_t = C_d$ = a calculation coefficient
c = cohesion of overburden soil, psf

Note that C_t equals C_d, and values can be taken from the curves in Figure 3. Suggested values of cohesion for some typical soils are shown in Table 2. Again, the magnitude of arch support can be evaluated by subtracting Equation 6 from the weight of the prism of soil above the tunnel. This gives

$$A_s = B_t \left[wH - C_t (wB_t - 2c) \right] \tag{7}$$

TABLE 2
RECOMMENDED VALUES OF COHESION

Soil Material	c, psf
Clay, very soft	40
Clay, medium	250
Clay, hard	1,000
Sand, loose, dry	0
Sand, silty	100
Sand, dense	300
Topsoil, saturated	100

When a conduit is installed as a positive projecting conduit, shearing forces also play an important role in the development of arch action and the resultant load on the structure. In this case the planes along which relative movements are assumed to occur and on which shearing forces are generated, are the imaginary vertical planes extending upward from the sides of the conduit, as indicated in Figures 5 and 6. The width factor in the development of the load formula is the outside breadth of the structure, designated as B_c. The vertical distance from the natural ground surface to the top of the conduit is expressed as pB_c in which p is the Projection Ratio.

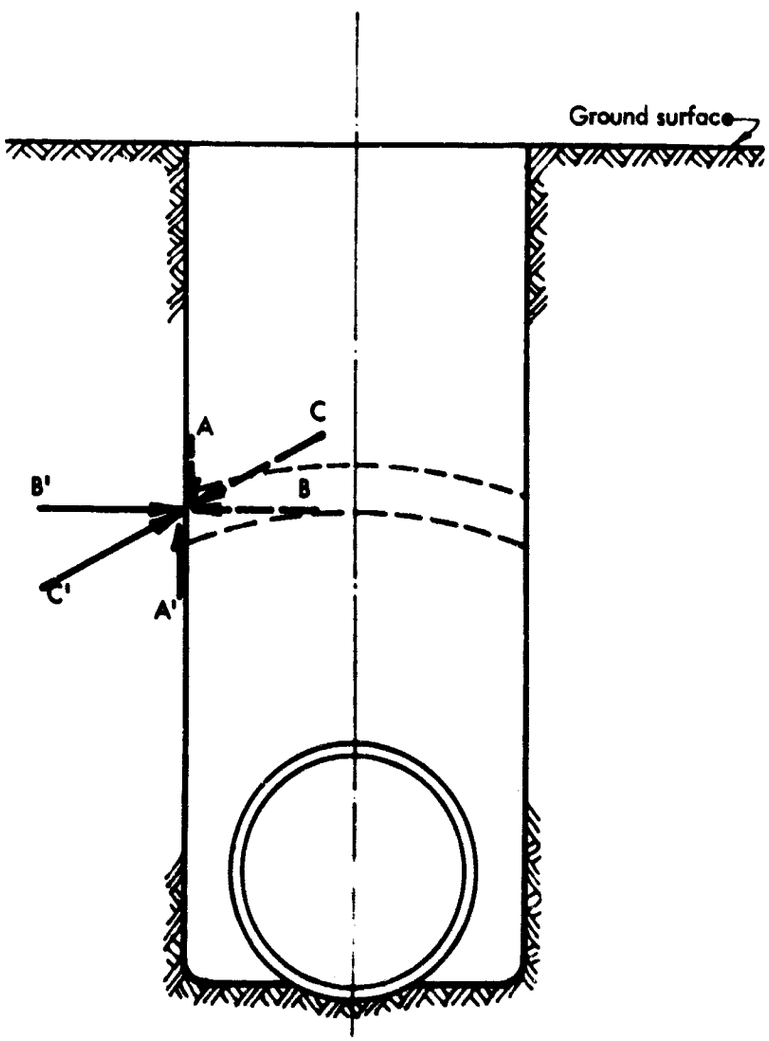


Fig. 4 Arch Action in Backfill Over a Ditch Conduit

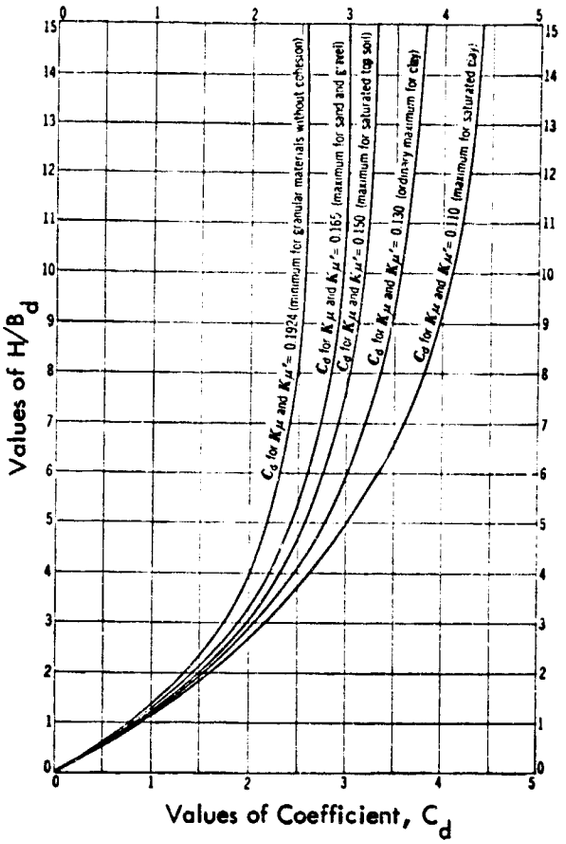


Fig. 3 Diagram for Coefficient C_d for Ditch Conduits

The magnitude and direction of relative movements between the interior prism ABCD, Figures 5 and 6, and the adjacent exterior prisms are influenced by the settlement of certain elements of the conduit and the adjacent soil. These settlements are combined into an abstract quantity, called the Settlement Ratio, according to the formula

$$r_{sd} = \frac{(s_m + s_g) - (s_f + d_c)}{s_m} \qquad (8)$$

in which (see Figures 5 and 6)

r_{sd} = settlement ratio
s_m = compression strain of the side columns of soil of height pB_c
s_g = settlement of the natural ground surface adjacent to the conduit
s_f = settlement of the conduit into its foundation
d_c = shortening of the vertical height of the conduit

In connection with the influential settlements, it is convenient to define a critical plane, which is the horizontal plane through the top of the conduit when the fill is level with its top, that is, when H = 0. During and after construction of the embankment, this plane settles downward. If it settles more than the top of the pipe, as illustrated in Figure 5, the settlement ratio is positive;

the exterior prisms move downward with respect to the interior prism; the shearing forces on the interior prism are directed downward; the arch action in the overfill is inverted and the resultant load on the structure is greater than the weight of the prism of soil directly above it. This is known as the Projection Condition.

If the critical plane settles less than the top of the Conduit, as in Figure 6, the settlement ratio is negative; the interior prism moves downward with respect to the exterior prisms; the shearing forces on the interior prism are directed upward; arch action is similar to that in the case of a ditch conduit and the resultant load is less than the weight of the soil above the structure. This is called the Ditch Condition.

In the case of a ditch conduit the shearing forces extend all the way from the top of the pipe to the ground surface, as shown in Figure 2. In a projecting-conduit installation, however, if the embankment is sufficiently high, the shearing forces may terminate at some horizontal plane in the embankment which is called the Plane of Equal Settlement. A plane of equal settlement develops because a part of the vertical pressure in the exterior prisms is transferred by shear to the interior prism, or vice versa. This transfer of pressure causes different unit strains in the interior and exterior prisms, and at some height above the conduit the accumulated strain in the exterior prism plus the settlement of the critical plane will just equal the accumulated strain in the interior prism plus the settlement of the top of the structure. Above the plane of equal settlement the interior and exterior prisms settle equally, and since there are no relative movements between the adjacent prisms, no shearing forces are generated in this zone.

When the height of the plane of equal settlement above the top of the conduit, designated as H_e, is less than the height H of the embankment, the plane of equal settlement is real. This is called either the Incomplete Ditch Condition or the Incomplete Projection Condition, because the shearing forces do not extend completely throughout the total height of embankment. If H_e is greater than H, the plane of equal settlement is imaginary. This is referred to as either the Complete Ditch Condition or the Complete Projection Condition, because the shearing forces do extend completely to the top of the embankment. (See Table 1 and Figure 7).

By a process similar to that employed in the case of ditch conduits, Marston derived a formula for the vertical load on a positive projecting conduit. For the complete ditch or projection condition, the formula is

$$W_c = C_c w B_c^2 \qquad (9)$$

in which

$$C_c = \frac{e^{\pm 2Ku(H/B_c)} - 1}{\pm 2Ku} \qquad (10)$$

the plus signs are used for the complete projection condition, and minus signs are used for the complete ditch condition.

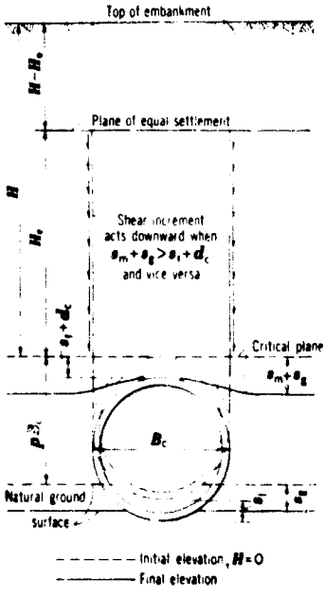


Fig. 5 Settlements which Influence Loads on Positive Projecting Conduits (Incomplete Projection Condition)

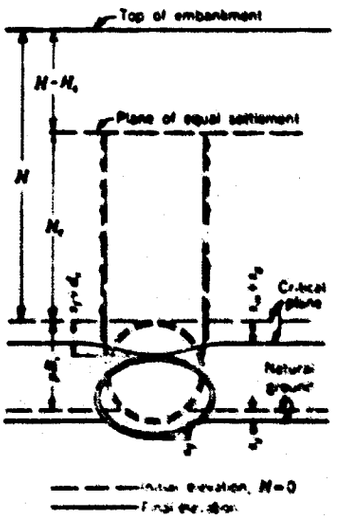


Fig. 6 Settlements which Influence Loads on Positive Projecting Conduits (Incomplete Ditch Condition)

Also, for the incomplete ditch or projection condition,

$$C_c = \frac{e^{\pm 2Ku(H_e/B_c)} - 1}{\pm 2Ku} + (H/B_c - H_e/B_c)\, e^{\pm 2Ku(H_e/B_c)} \qquad (11)$$

The plus signs are used for the incomplete projection condition, and the minus signs are used for the incomplete ditch condition.

In Equations 9, 10 and 11,

W_c = load on conduit, plf
w = unit weight of embankment soil, pcf
B_c = outside width of conduit, ft.
H = height of fill above conduit, ft.
H_e = height of plane of equal settlement, ft.
K = lateral pressure ratio
u = tan ϕ = coefficient of friction of fill material
e = base of natural logarithms

A formula for evaluating H_e is derived by equating an expression for the sum of the total strain in the interior prism and the settlement of the top of the conduit to a similar expression for the sum of the total strain in an exterior prism and the settlement of the critical plane. This formula is

$$\left[1/2Ku \pm (H/B_c - H_e/B_c) \pm \frac{r_{sd}p}{3}\right] \frac{e^{\pm 2Ku(H_e/B_c)} - 1}{\pm 2Ku}$$
$$\pm 1/2(H_e/B_c)^2 \pm \frac{r_{sd}p}{3}(H/B_c - H_e/B_c)\, e^{\pm 2Ku(H_e/B_c)}$$
$$- 1/2Ku \cdot H_e/B_c \pm H/B_c \cdot H_e/B_c = r_{sd}p\, H_e/B_c \qquad (12)$$

Use the upper signs for the incomplete projection condition, for which the settlement ratio is positive, and use the lower signs for the incomplete ditch condition, for which the settlement ratio is negative.

It is difficult and time-consuming to solve Equations 11 and 12. Fortunately the results can be given in a relatively simple diagram from which values of the load coefficient C_c can be obtained for substitution in Equation 9. Such a diagram is shown in Figure 7. It will be noted that C_c is a function of the ratio of the height of fill to the width of the conduit, H/B_c, and of the product of the settlement ratio and the projection ratio, $r_{sd}p$, as well as of the friction characteristics of the soil. However, Marston pointed out that the influence of the coefficient of internal friction, u, is relatively minor in this case, and it is not considered necessary to differentiate between various soils as for ditch conduits. Therefore, in constructing Figure 7, it was assumed that Ku = 0.19 for the projection condition, in which the shearing forces are directed downward, and Ku = 0.13 for the ditch condition, in which the shearing forces are directed upward. This diagram gives reasonable maximum loads, the accuracy of which is within the degree of precision of the assumptions upon which the analysis is based.

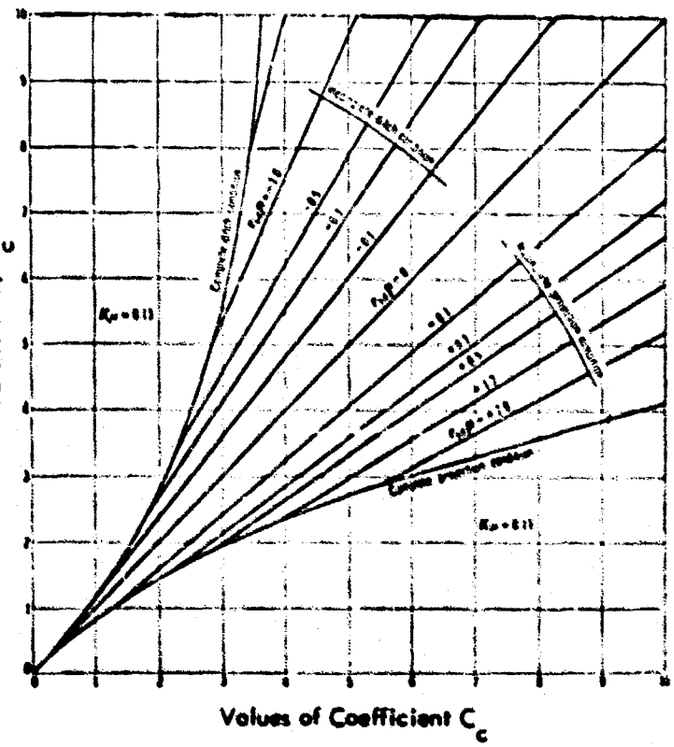


Fig. 7 Diagram for Coefficient C_c, for Positive Projecting Conduits

The ray lines in Figure 7 represent values of C_c versus H/B_c according to Equation 11, whereas the envelope curves correspond to Equation 10. The ray lines intersect the envelope curves at points where $H_e = H$. Therefore, this diagram can be used to estimate the height of the plane of equal settlement in a particular case, as well as to estimate the load on the conduit.

Although the settlement ratio, r_{sd}, is a rational quantity in the development of the load formula, it is difficult, and impractical to predetermine the actual value which will be developed in a specific case. Therefore, this ratio is considered to be an empirical quantity and working values for design purposes are determined from observations of the performance of actual culverts under embankments. Such observations have been made, and the values recommended in Table 3 are based on them.

TABLE 3
DESIGN VALUES OF SETTLEMENT RATIO

Conditions	Settlement Ratio
Rigid culvert on foundation of rock or unyielding soil	+1.0
Rigid culvert on foundation of ordinary soil	+0.5 to +0.8
Rigid culvert on foundation of material that yields with respect to adjacent natural ground	0 to +0.5
Flexible culvert with poorly compacted side fills	-0.4 to 0
Flexible culvert with well-compacted side fills*	-0.2 to +0.8

*Not well established

Examination of the load coefficient diagram in Figure 7 indicates that when the product of the settlement ratio r_{sd} and the projection ratio p equals zero, then $C_c = H/B_c$. When this value of C_c is substituted in Equation 9, the load formula reduces to $W_c = HwB_c$; that is to say, the load is equal to the weight of the prism of soil directly above the conduit and there is no arch action and no arch support. The settlement ratio is equal to zero when the critical plane settles the same amount as the top of the conduit, that is, when $s_m + s_g = s_f + d_c$. The projection ratio is equal to zero when the structure is installed in a narrow and shallow trench so that its top is approximately level with the adjacent natural ground. This is the transition case between positive and negative conduits, as previously discussed on Page 532.

Attention is directed to the fact that in the incomplete projection condition, that is when the settlement ratio is positive, the shearing forces mobilized along the vertical planes in the embankment are directed downward, the arch action is inverted and the load on the structure is greater than the weight of the overlying prism of soil. In the incomplete ditch condition the arch action is normal. The magnitude of arch action, either normal or inverted, is indicated in Figure 7 by the deviation of the various ray lines from the diagonal line for $r_{sd}p = 0$, which represents the weight of the overlying prism of soil.

Analysis of loads on imperfect ditch conduits was first published by the author in 1950. It follows the same general philosophy and approach as that previously employed by Marston for other classes of conduits. The elements of an imperfect ditch conduit are shown in Figure 8. There are two cases to be considered; the complete ditch condition in which the shearing forces and arch action are effective all the way to the top of the embankment, and the incomplete ditch condition, wherein they terminate at a plane of equal settlement.

A free body diagram for the first case is shown in Figure 9. Setting the summation of vertical forces equal to zero,

$$V + dV = V + wB_c\,dh - 2Ku(V/B_c)dh \tag{13}$$

The boundary conditions are when $h = 0$, $V = 0$, and the solution is

$$V = wB_c^2\,\frac{e^{-2Ku(h/B_c)} - 1}{-2Ku} \tag{14}$$

At the top of the conduit, $V = W_c$ and $h = H$, whence

$$W_c = C_n wB_c^2 \tag{15}$$

in which

$$C_n = \frac{e^{-2Ku(H/B_c)} - 1}{-2Ku} \tag{16}$$

Next, consider the incomplete ditch condition in which $H = H_e$ as illustrated in Figure 10. Equate the vertical forces on a thin horizontal element at distance h below the plane of equal settlement.

$$V + dV = V + wB_c dh - 2Ku(V/B_c)dh \tag{17}$$

when $h = 0$, $V = (H-H_e)wB_c$ and the solution of Equation 17 is

$$V = wB_c^2 \left[\frac{e^{-2Ku(h/B_c)} - 1}{-2Ku} + (H/B_c - H_e/B_c)\, e^{-2Ku(h/B_c)} \right] \tag{18}$$

At the top of the conduit, $V = W_c$ and $h = H_e$, whence

$$W_c = C_n w B_c^2 \tag{19}$$

in which

$$C_n = \frac{e^{-2Ku(H_e/B_c)} - 1}{-2Ku} + (H/B_c - H_e/B_c)\, e^{-2Ku(H_e/B_c)} \tag{20}$$

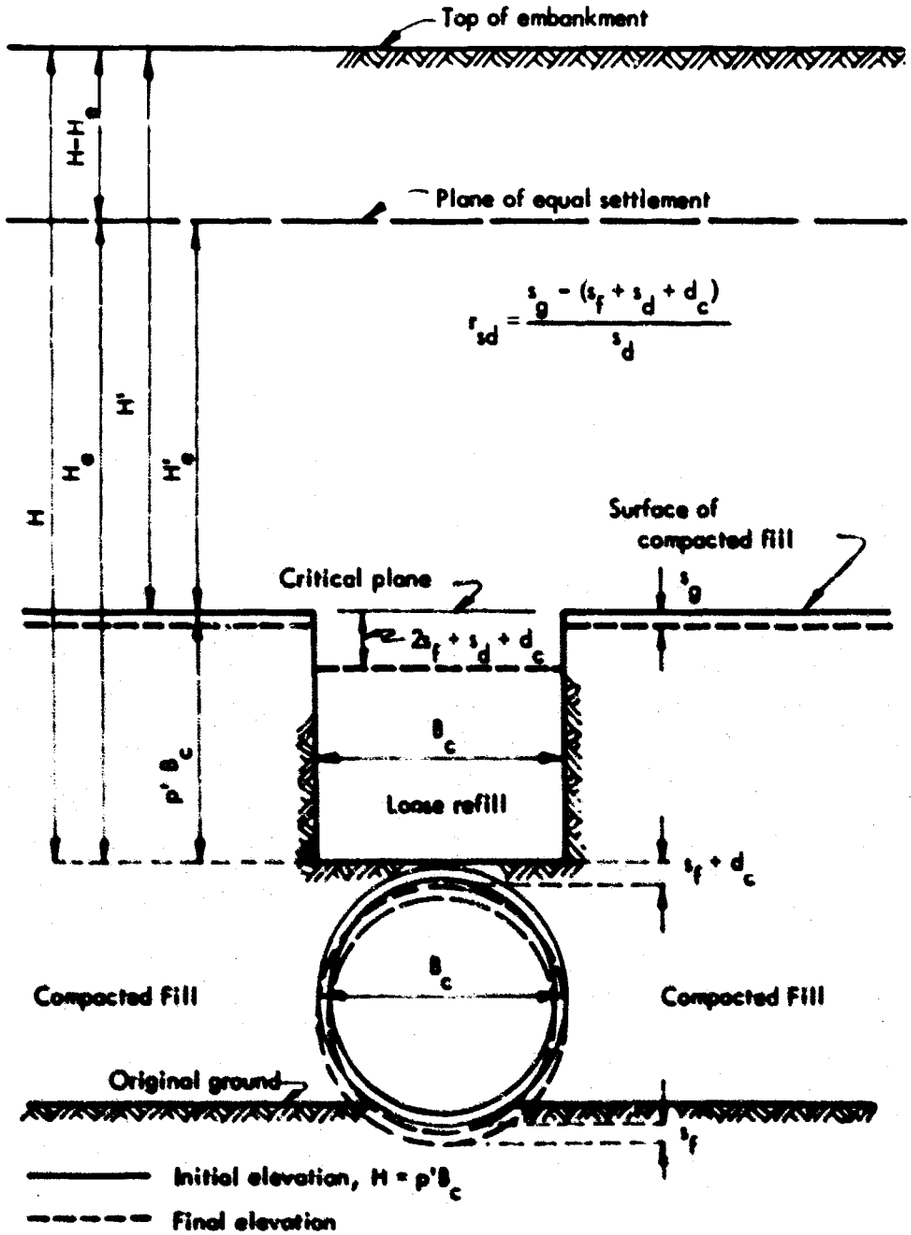


Fig. 8 Elements of an Imperfect Ditch Conduit

In order to solve Equation 20, it is necessary to know the value of H_e. An expression for determining H_e may be derived by equating the total settlement of the interior prism ABCD at the plane of equal settlement to the total settlement of the exterior prisms at this plane. The settlement ratio in this case is defined as

$$r_{sd} = \frac{s_g - (s_d + s_f + d_c)}{s_d} \tag{21}$$

in which (see Figure 8)

r_{sd} = settlement ratio
s_g = settlement of surface of compacted fill
s_d = compression strain of the ditch backfill of height $p'B_c$
s_f = settlement of the conduit into its foundation
d_c = shortening of the vertical height of conduit

Note that the settlement ratio is always a negative quantity in a properly constructed imperfect ditch conduit, because of the relatively compressible trench backfill.

The equality referred to above is

$$\lambda + s_d + s_f + d_c = \lambda' + s_g \tag{22}$$

In this expression, λ and λ' are the total compression strains in the interior and exterior prisms respectively, within the vertical height H'_e. Substituting Equation 21

$$\lambda = \lambda' + r_{sd} \cdot s_d \tag{23}$$

To derive expressions for λ and λ' the following assumptions are employed:

1. That the internal friction in the fill materials distributes the infinitely small decrements of pressure from shear into the interior prism below the plane of equal settlement in such a manner that the effect on settlement is substantially the same as for uniform vertical pressure.
2. That the internal friction in the fill materials distributes the infinitely small increments of pressure from shear into each of the exterior prisms below the plane of equal settlement in such a manner that the effect on settlement is substantially the same as though the pressure were distributed uniformly over a width of prism equal to the width of the conduit, B_c.

Referring to Figure 10, the expression for λ, the compression of the prism ABCD is derived as follows:

$$d\lambda = \frac{V}{B_c E} dh \tag{24}$$

in which

E = modulus of compression of soil material substituting Equation 18 in Equation 24,

$$d\lambda = \frac{wB_c}{E}\left[\frac{e^{-2Ku(h/B_c)}-1}{-2Ku} + (H'/B_c - H'_e/B_c)\, e^{-2Ku(h/B_c)}\right] dh \tag{25}$$

Integrating between the limits $h = 0$ and $h = H'_e$,

$$\lambda = \frac{wB_c^2}{E}\left(\frac{H'-H'_e}{B_c} - \frac{1}{2Ku}\right)\frac{e^{-2Ku(H'_e/B_c)}-1}{-2Ku} + \frac{wB_c^2}{E}\left(\frac{1}{2Ku} \cdot \frac{H'_e}{B_c}\right) \tag{26}$$

In a similar manner

$$\lambda' = \frac{3wB_c^2}{2E} \cdot \frac{H'_e}{B_c}\left(\frac{H'-H'_e}{B_c} + \frac{1}{2}\frac{H'_e}{B_c}\right) - \frac{wB_c^2}{2E} \cdot \frac{1}{2Ku} \cdot \frac{H'_e}{B_c}$$

$$- \frac{wB_c^2}{2E}\left(\frac{H'-H'_e}{B_c} - \frac{1}{2Ku}\right)\frac{e^{-2Ku(H'_e/B_c)}-1}{-2Ku} \tag{27}$$

The expression for s_d is

$$s_d = \frac{p'wB_c^2}{E}\left(\frac{e^{-2Ku(H'_e/B_c)}-1}{-2Ku}\right) + \frac{H'-H'_e}{B_c}e^{-2Ku(H'_e/B_c)} \qquad (28)$$

Substituting Equations 26, 27 and 28 in Equation 23 gives

$$\left[(H'/B_c - H'_e/B_c) - \frac{1}{2Ku}\right]\frac{e^{-2Ku(H'_e/B_c)}-1}{-2Ku} - \frac{H'_e}{B_c}\left[(H'/B_c - H'_e/B_c) + \frac{H'_e}{2B_c} - \frac{1}{2Ku}\right] = \frac{2}{3}r_{sd}p'\left[\frac{e^{-2Ku(H'_e/B_c)}-1}{-2Ku} + (H'/B_c - H'_e/B_c)e^{-2Ku(H'_e/B_c)}\right] \qquad (29)$$

Values of H'_e/B_c corresponding to H'/B_c for various values of $r_{sd}p'$ may be obtained from Equation 29. Then since $H = H' + p'B_c$ and $H_e = H'_e + p'B_c$ (see Figure 8), it is possible to determine values of C_n from Equation 20. Substituting C_n in the load formula, Equation 15, loads on imperfect ditch conduits may be obtained. Diagrams showing values of C_n versus H/B_c for various values of r_{sd} have been drawn for values of $p' = 0.5$, 1.0, 1.5 and 2.0 and are shown in Figures 11, 12, 13 and 14. C_n for intermediate values of p' may be obtained by interpolation with sufficient accuracy for design purposes. Empirical measurements of values or r_{sd} for this type of conduit installation are very meager at the present time. The few measurements which have been made indicate that values in the range of -0.3 to -0.5 are appropriate.

When Marston first invented the imperfect ditch method of construction, approximately 45 years ago, he suggested that straw, hay or cornstalks might be incorporated in the ditch backfill to increase its compressibility. If such materials are used, the settlement ratio will be decreased, the load on the structure will be decreased and the magnitude of arch support will be increased.

As in previous cases, the developed arch support is equal to the algebraic difference between the weight of the central prism of soil and the load on the structure. Thus

$$A_s = wB_c(H - C_nB_c) \qquad (30)$$

Assume a numerical example in which an 84 in. O.D. pipe is installed as an imperfect ditch conduit under 80 ft. of fill. Also $r_{sd} = -0.4$, $w = 120$ pcf. Then $H/B_c = 80/7 = 11.4$. From Figure 14 $C_n = 5.2$.

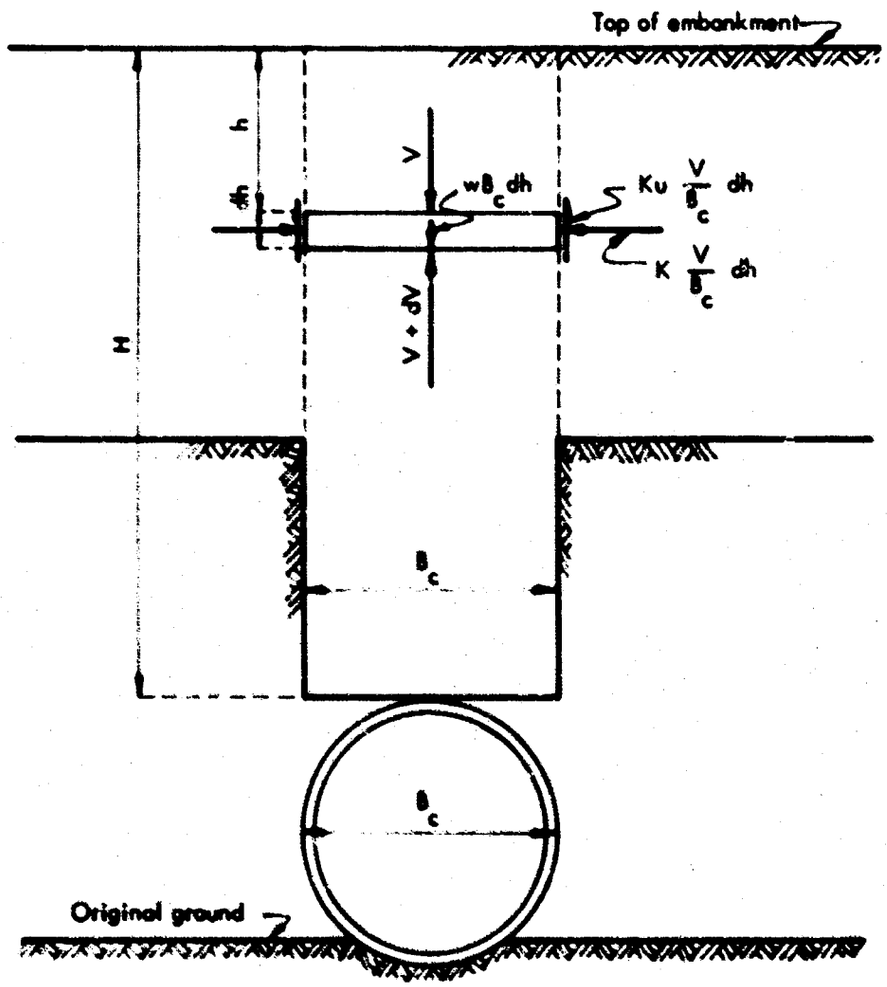


Fig. 9 Free Body Diagram Imperfect Ditch Conduit (Complete Ditch Condition)

The load on the structure is, by Equation 15

$$W_c = 5.2 \times 120 \times 7^2 = 30,600 \text{ plf}$$

Also, by Equation 30, the arch support is

$$A_s = 120 \times 7(80 - 5.2 \times 7) = 36,600 \text{ plf}$$

The weight of the central prism of soil is

$$W_s = 80 \times 120 \times 7 = 67,200 \text{ plf}$$

It is indicated that under conditions assumed in this example, arch action and arch support account for 54 percent of the weight of overburden soil, while the remaining 46 percent is carried by the structure.

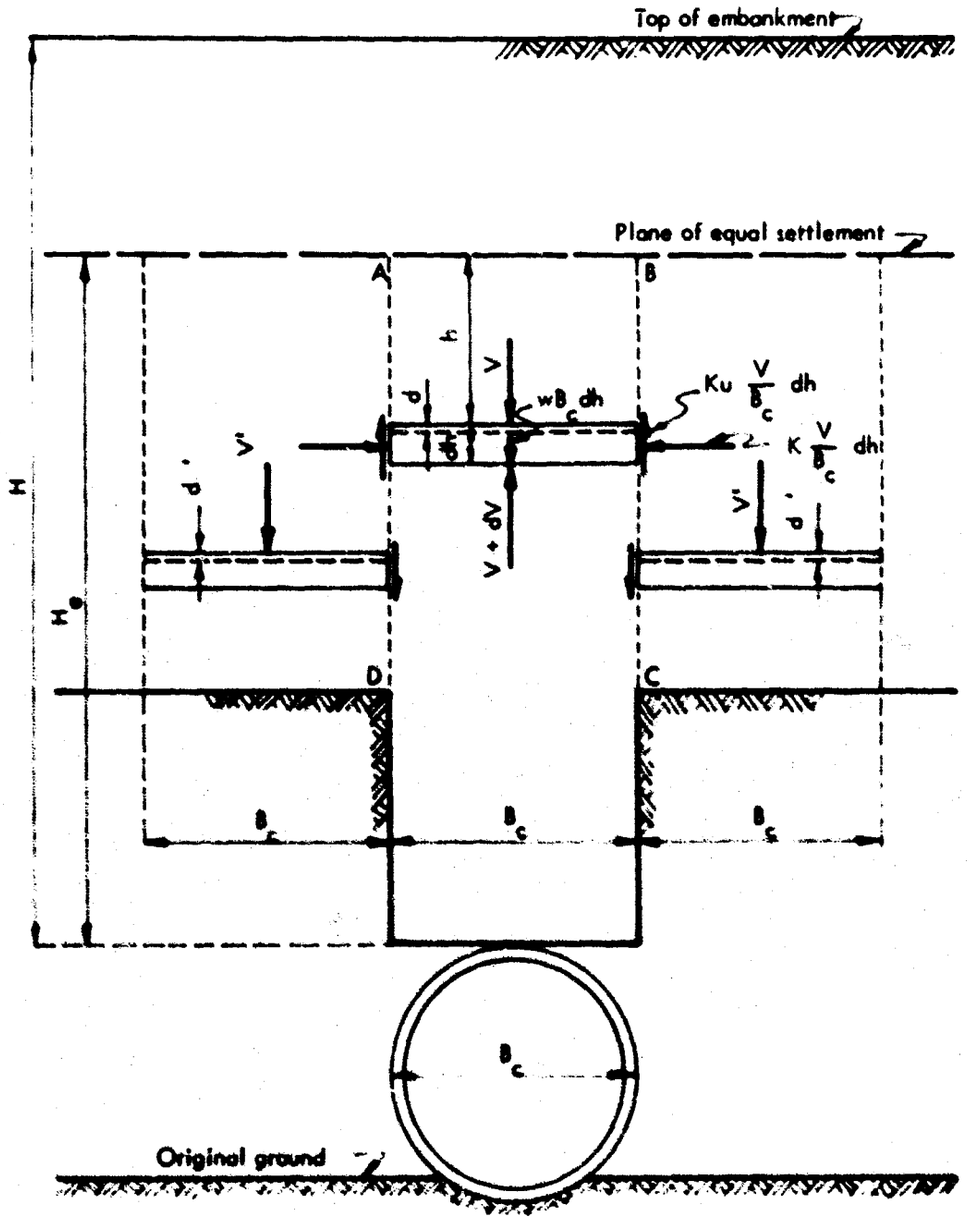


Fig. 10 Free Body Diagrams Imperfect Ditch Conduit (Incomplete Ditch Condition)

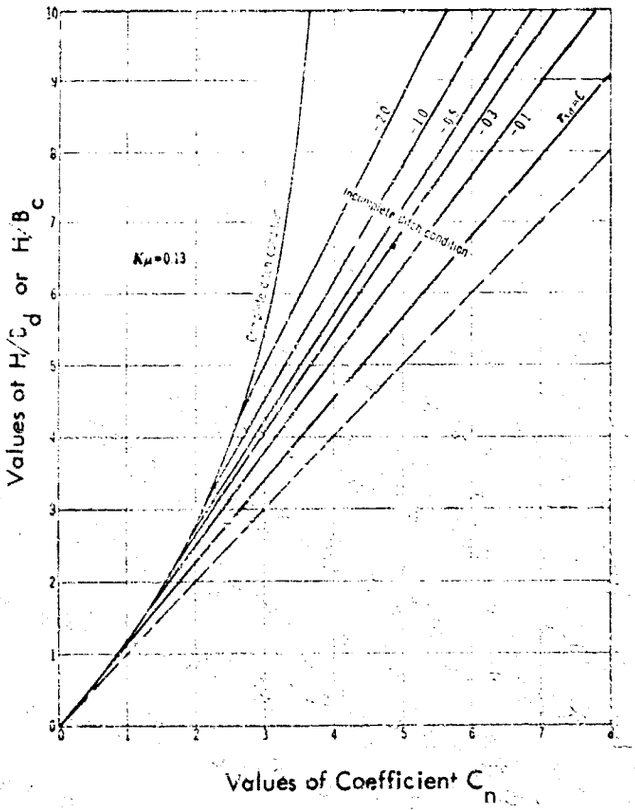


Fig. 11 Diagram for Coefficient C_n for Imperfect Ditch Conduits and Negative Projecting Conduits, $p' = 0.5$

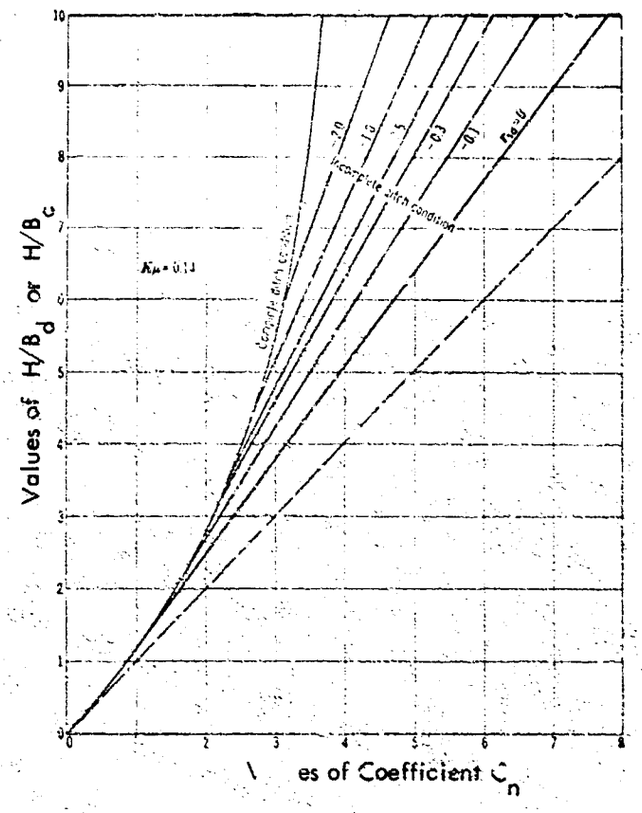


Fig. 12 Diagram for Coefficient C_n for Imperfect Ditch Conduits and Negative Projecting Conduits, $p' = 1.0$

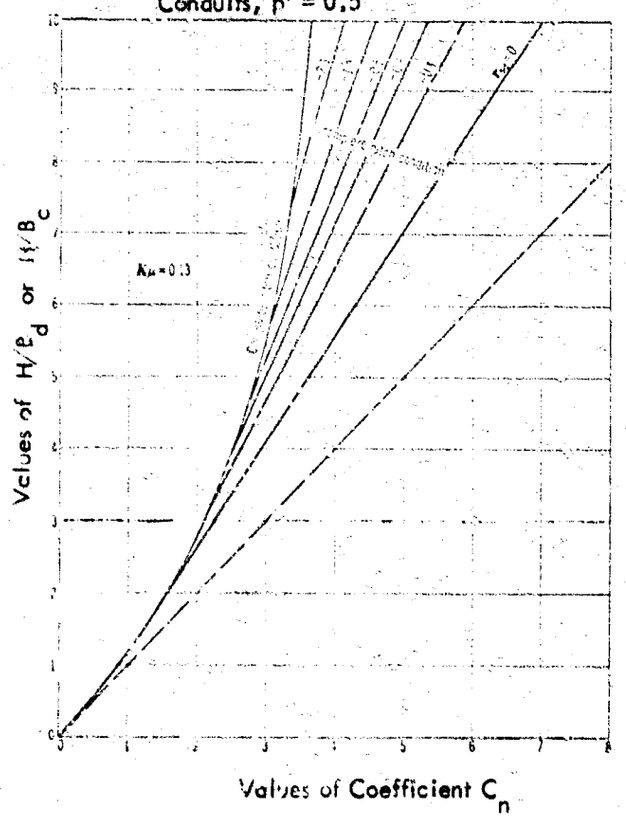


Fig. 13 Diagram for Coefficient C_n for Imperfect Ditch Conduits and Negative Projecting Conduits, $p' = 1.5$

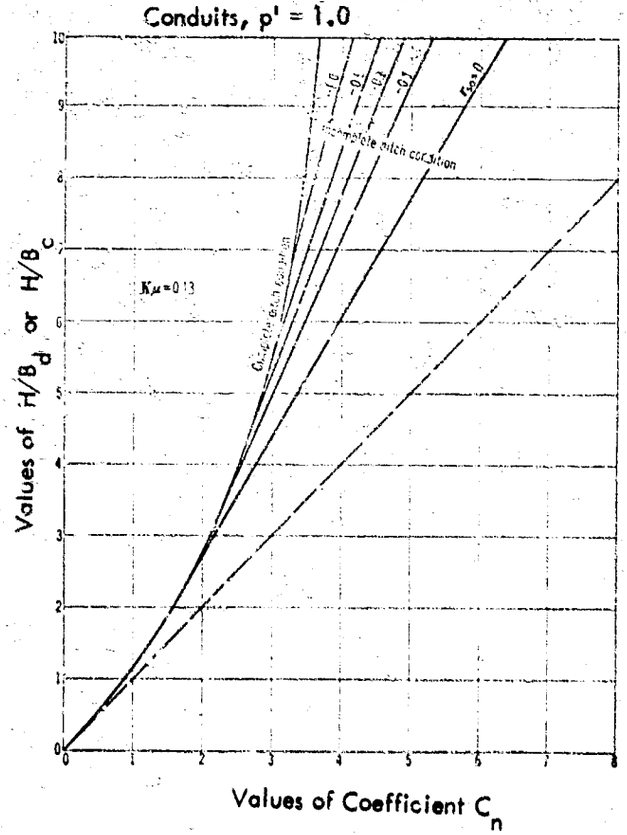


Fig. 14 Diagram for Coefficient C_n for Imperfect Ditch Conduits and Negative Projecting Conduits, $p' = 2.0$

The load formula, Equation 15, can also be used in the case of negative projecting conduits, by substituting B_d, the width of ditch in which the conduit is laid, for B_c. The values of C_n can be obtained from Figures 11, 12, 13 and 14 by using the ratio H/B_d instead of H/B_c.

Quantitative experimental evidence of loads on imperfect ditch conduits is very meager. Marston first demonstrated the effectiveness of the procedure in experiments conducted in 1919, 1920 and 1921, in which loads on a culvert consisting of ten 2 ft. long sections, 3-1/3 ft. in diameter were weighed. The embankments over the culvert were 20 ft. high and the fill material weighed 96 lb. per cu. ft. The projection ratio in these experiments was 0.9. The influence of the settlement ratio had not been discovered at that time, and it was not measured. It has since been estimated to have been in the neighborhood of +0.9 to +1.0. The following is quoted from his "First Progress Report," presented on November 28, 1921, to a meeting of the Joint Concrete Culvert Pipe Committee consisting of two representatives of each of the following organizations.

American Concrete Institute
American Association of State Highway Officials
American Railway Engineering Association
American Society for Testing and Materials
American Society of Civil Engineers
American Concrete Pipe Association
Bureau of Public Roads

"The outstanding result of the work of 1919-1920 was the very heavy weights per lineal foot of culvert imposed upon the culvert by the weight of the embankment material, amount, as already stated, approximately to 1-3/4 times the total weight of the embankment material immediately over the culvert.

"Hence, it was decided to attempt to find a special method of construction of the embankment which would reduce the load transmitted to culvert.

"Accordingly, beginning the latter part of July 1920, an embankment was built of sandy loam top soil, over the culvert and to a level 4 feet above its top, taking special care to consolidate this embankment over the culvert, and on each side, using a road roller for that purpose and depositing the material in layers.

"On completion of this embankment to a height of 4 feet above the top of the culvert, as above described, a vertical trench 4-1/2 feet wide was dug immediately over the top of the culvert itself, which was entirely cleared of material. This trench should have been 3-1/3 feet wide to secure the best results, but it was found necessary to make it 4-1/2 feet wide to permit readjusting the 2 feet sections of the culvert which had become disarranged by the road roller in making the fill.

"On completion of this trench it was refilled with material deposited in the loosest possible condition.

"Immediately after refilling this trench with loose material, the construction of the embankment was resumed and carried on until the embankment reached a total height of 20 feet on September 29, 1921 . . . . .

"During this process it was found that the weights imposed upon the culvert by the embankment at different heights were much less than those in the work of the preceding year. In other words, constructing the trench over the culvert (loose filled, and with consolidated sides) as above described materially lightened the pressure imposed upon the culvert by the embankment material."

The weight of the prism of soil over the culvert was 5400 plf. In the first experiment, the average measured load was 11,500 plf. Inverted arch action increased the load on the structure in this experiment by about 80 percent. When the special method of construction, (later called the imperfect ditch method) was employed, the measured load was reduced to 7200 plf indicating that the inverted arch action had been practically eliminated. It is probable that the load would have been further reduced, if the imperfect trench could have been held to the same width as that of the culvert.

Later, in 1951, Schlick published the results of load experiments on three rigid pipe culverts (2 concrete and 1 cast iron) in which the imperfect ditch method of construction was employed, with values of the projection ratio, p', equal to 0.25, 0.5 and 0.75. These pipes were 3.5 and 3.67 ft. in outside diameter, and the height of fill, a sandy loam top soil, weighing 116 pcf, was 15 feet above the top of the structure. Settlements of the various elements which constitute the settlement ratio were measured in these experiments.

Several years earlier the author had developed the theory of loads on negative projecting and imperfect ditch conduits as given above on Pages 537 to 540. Schlick compared his measured loads with loads calculated by this theory, as indicated in Table 4.

TABLE 4
COMPARISON OF MEASURED AND CALCULATED LOADS
IMPERFECT DITCH CONDUITS

	Culvert A (Concrete) $p' = 0.25$	Culvert B (Cast Iron) $p' = 0.5$	Culvert C (Concrete) $p' = 0.75$
Measured	4610 plf	3200 plf	2660 plf
Calculated	5290 plf	4550 plf	3900 plf

The comparison indicates that the measured loads were less than the calculated loads, although they were of the same order of magnitude. In other words the arch support developed by this method of construction was somewhat greater than that indicated by the theory; as much as 50 percent greater in the case where $p' = 0.75$.

As stated on Page 504, Marston suggested that straw, hay or cornstalks might be incorporated in the imperfect ditch backfill to augment the compressibility of this material. This idea was accepted very slowly at first by the engineering profession, but has gained in popularity in recent years. The first use of such material of which the author has knowledge, was in connection with a project in Atlanta, Georgia.

The City of Atlanta had constructed the Proctor Creek Sewer, a 48 inch reinforced concrete interceptor, in 1937. The depth of cover ranged from 17 to 35 feet. Later, in 1955, it was proposed to fill the area to an elevation which would increase the cover to a maximum of 95.5 feet above the top of the pipe. Rather than re-construct the sewer with stronger pipe to carry the additional load, the City elected to employ the principles of the imperfect ditch method to protect the existing sewer.

The general plan was to excavate a ditch directly above the pipeline, to a depth of 15 feet and to a width of 4.75 feet, which is the outside diameter of the pipe. This ditch was refilled with alternate layers of soil and tree leaves or pine straw up to the ground surface. Then as the fill above was placed and compacted, additional trenches were excavated in 10 to 15 ft. lifts of the soil. These trenches were about 5 ft. deep and 4.75 ft. wide and were also centered over the pipeline. After excavation, the trenches were refilled with loose soil before the next lift of the embankment was constructed. The diagram in Figure 15 illustrates the plan, and the photograph in Figure 16 was taken during construction.

The pipeline was inspected a number of times during and after construction of the added height of fill and was found to be in good condition. There was no evidence of increased load on the pipe and it is still functioning satisfactorily. Apparently sufficient arch action and arch support were mobilized to protect the sewer from the greatly increased weight of soil added above the line (approximately 17 tons per lineal foot of pipe).

The California Division of Highways has developed a method of protecting highway culverts under high earth fills by using baled straw to obtain a modified form of imperfect ditch construction. After a pipeline is installed, backfilling is completed adjacent and up to the top of the pipe. Then bales of straw are placed over the line to form a layer whose width is equal to the outside diameter of the pipe. Soil is placed and compacted up to the top of the bales, after which the wires are cut and another layer of bales installed. Again the soil is compacted up to the top and the wires cut. This process is repeated until the desired depth of "imperfect ditch" is obtained. The the embankment is completed in the normal manner. A photograph of this procedure is shown in Figure 17.

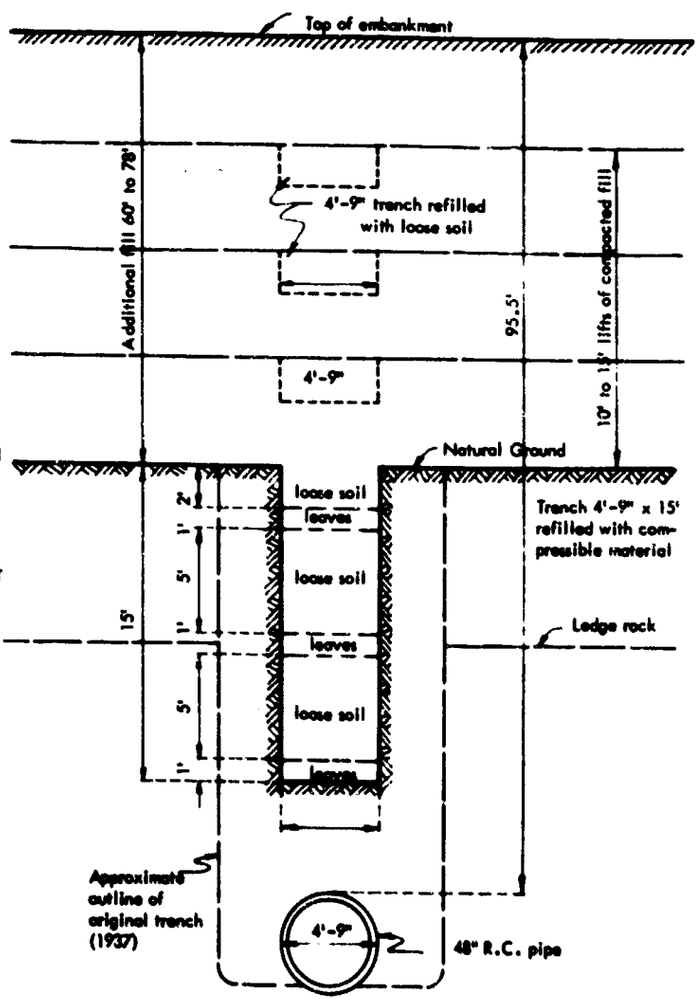


Fig. 15 Imperfect Ditch Method of Constructing Additional Fill over Proctor Creek Sewer, Atlanta, Georgia

Comparisons between distortion of the pipes in three culverts installed with baled straw as described above, and three culverts in the same county without straw are shown in Figure 18. These measurements indicate a substantial development of arch support and protection against embankment load by the baled straw treatment.

A number of additional imperfect ditch installations could be cited, some in which nothing but loose soil was used as trench backfill and others in which organic material was added to enhance the compressibility of the trench backfill. In all cases the procedure has successfully protected the pipes against excessive loads due to high fills. Figure 19 shows an imperfect ditch over a culvert being partially filled with sawdust on a highway project in Texas. In Figure 20, baled straw is placed at the bottom of an imperfect ditch in Michigan.

It is the author's conclusion that theory, experimental evidence and successful practical experience, all indicate that the imperfect ditch method of construction is effective in substantially reducing static earth loads on underground structures by inducing the development of arch action and arch support in the overlying soil. It is his belief that this method, or modifications thereof, will prove effective in reducing the load transmitted to such structures from dynamic or shock loads applied at the ground surface. Also, modifications of the method probably can be devised to protect structures from lateral shock loads. A great deal of experimental work will be required to demonstrate or prove the validity of this hypothesis.



Fig. 16 Placing Loose Soil over a Layer of Leaves, Atlanta, Georgia



Fig. 17 Soil Compacted Against Baled Straw to Create an Imperfect Ditch - California

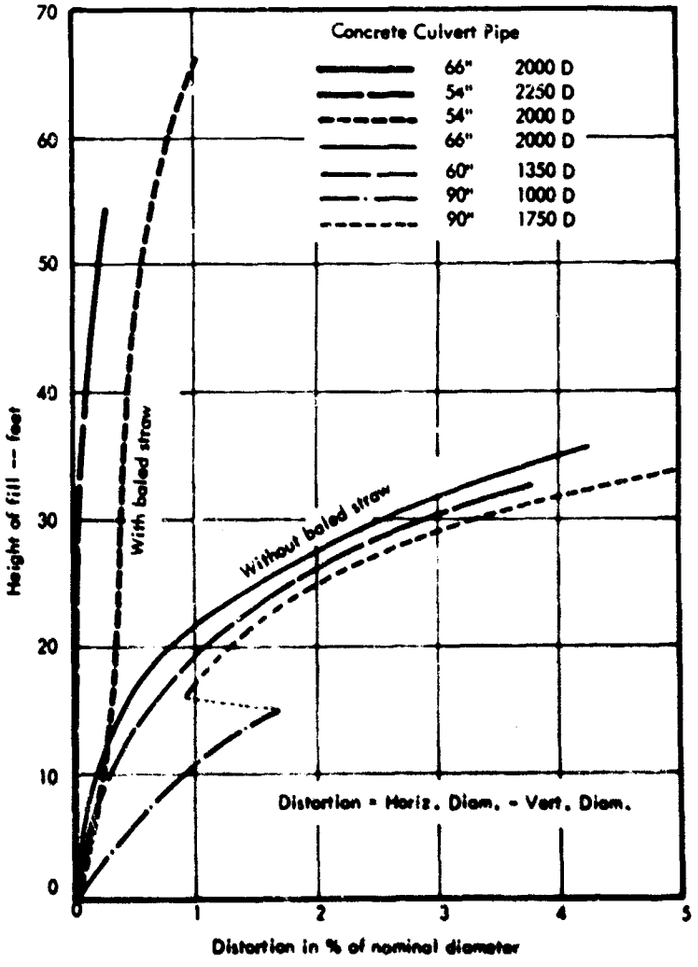


Fig. 18 Distortion of Humboldt County, California, Pipe Culverts



Fig. 19 Sawdust in Imperfect Ditch Construction, Texas



Fig. 20 Baled Straw in Imperfect Ditch Construction, Michigan

REFFRENCES

1. American Concrete Pipe Association, Concrete Pipe News, Vol. 16, No. 3, March 1964.
2. Larsen, Norman G., "A Practical Method for Constructing Rigid Conduits Under Hill Fills," Proc. Highway Research Board, Vol. 41, 1962.
3. Marston, Anson and A. O. Anderson, "The Theory of Loads on Pipes in Ditches and Tests of Cement and Clay Drain Tile and Sewer Pipe," Bulletin 31, Iowa Engineering Experiment Station, Ames, Iowa, 1913.
4. Marston, Anson, First Progress Report to Joint Concrete Culvert Pipe Committee, Mimeo, November 28, 1921.
5. Marston, Anson, "The Theory of External Loads on Closed Conduits in the Light of the Latest Experiments," Bulletin 96, Iowa Engineering Experiment Station, Ames, Iowa, 1930.
6. Schlick, W. J., "Loads on Negative Projecting Conduits," Proc. Highway Research Board, Vol. 31, 1952.
7. Spangler, M. G., "A Theory of Loads on Negative Projecting Conduits," Proc. Highway Research Board, Vol. 30, 1950.
8. Spangler, M. G., "A Practical Application of the Imperfect Ditch Method of Construction," Proc. Highway Research Board, Vol. 37, 1958.

MEASUREMENTS OF SOIL-STRUCTURE INTERACTION ON PROTOTYPE PROTECTIVE STRUCTURES

by
Ralph H. Sievers, Jr.*

INTRODUCTION

Prediction of soil-structure interaction is essential to efficient and adequate design of nuclear warfare protective construction. Test structures have been exposed to the immense loads of nuclear blasts and theories exist to explain the actions which caused or prevented failure of these structures. Laboratory tests with static and dynamic loadings provide some experimental verification of these theories; however critical assumptions which are used to predict sidewall loadings, mass of earth responding with the structure, and "arching" of earth over the structure have inadequate experimental verification. This paper presents procedures used to obtain soil-structure response characteristics of actual buried protective structures by non-destructive testing. These procedures could be employed to test full-size structures to verify or disprove theories required for effective shelter design.

This project (1) was an extension of nuclear weapons effects studies conducted through 1958 by exposure of prototype protective structures to actual nuclear detonations. These structures were not always adequately located or successfully instrumented to provide time-histories of dynamic response, nor were measurements made to specifically prove or disprove response theories which were simultaneously being developed. The conclusion of aboveground testing has left many undamaged prototype protective structures at the Nevada Test Site, available for non-destructive dynamic testing. The Defense Atomic Support Agency (DASA) sponsored a project at the US Army Engineer Research and Development Laboratories (ERDL), Ft. Belvoir, Virginia, to study the mode and period of dynamic response of certain of these structures. Principal object of the study was to investigate the relative significance of flexural and compressive modes of underground arch type structures.

Theoretical bases of the study were that

1. The response of a structure to dynamic blast-induced loadings is largely dependent upon the stiffness of the structure and the mass of the responding structural elements and earth acting with them.

2. The fundamental mode of vibration of a buried structure is apt to be the mode in which principal response and failure to nuclear shock loadings takes place.

3. Determination of the fundamental mode and period of response, in that the period of this vibration is determined by stiffness and mass, would be of vital importance in predicting the response of the structure to dynamic loadings and would thereby permit more efficient structural design.

4. Natural modes of vibration of a structure or structural element are independent of the means of excitation, or amplitude of vibration, insofar as the responding mass remains unchanged and the structural elements remain elastic. Therefore, if measurements are made with adequate sensitivity, very small amplitudes of vibration may be used and exciting forces need only be a small fraction of the safe working load of the structure.

PROCEDURE

Procedures had to be developed and tested prior to conducting tests on the extremely stiff buried structures to be studied at the Nevada Test Site. These procedures were developed through trial and error by non-destructive testing of structures and structural elements at and near Fort Belvoir. Appropriate sensors, recording equipment, and means of exciting the structure had to be selected, tested, and proved feasible.

The initial non-destructive vibration test was conducted on a beam forming part of the roof support system of a warehouse type building (Figure 1). Fifteen hundred pounds of lead bricks on a pallet were suspended to provide two point loading and a resultant initial deflection of the beam. The weight was applied by raising the pallet with turn-buckles and was instantaneously released by use of a bomb release. Dynamic measurements of resulting vibrations were made by strain gauges and by an accelerometer. Good results were obtained in that the periods of vibration of the fundamental and first three harmonics were identified, were duplicated on repeated tests, and approximated the computed periods. Use of lead weights proved to be impractical however and subsequent tests were conducted to develop light equipment which could impose an initial deflection which could then be instantaneously released.

Concrete and steel structures of varying sizes, stiffness and shapes were tested in the feasibility study. One excitation scheme developed employed wire ropes tightened by turnbuckles, and held by a quick release (Figure 2). This permitted two, three, and four point loading of circular steel structures and loading of arch structures as permitted by

*Major, USA, Office of Chief of Research and Development, McLean, Virginia.

anchoring capabilities. A load column was fabricated with a screw jack to apply the load and thereby the required deflection, and a quick release to provide a means of vibrating concrete structures. The load column permitted two point loading of circular structures and one point loading of rectangular, arch or dome roof systems.

Sensor and recording equipment was selected on a basis of that available at ERDL or obtainable at low cost. Patch type strain gauges proved to be impractical due to the extremely low strains created. Variable inductance and piezoelectric accelerometers were tried, however variable resistance accelerometers of ± 1g range were selected and purchased for the field test program. Recording equipment with three kilocycle carrier, galvanometer mirrored light traces and film speeds of up to fifty inches per second was available and fully suitable for the test program. All testing could be and was accomplished by three project personnel. Procedures were proof tested by exciting measurable vibrations of a seven-foot thick, nine-foot span reinforced concrete slab roof of a gun emplacement magazine. A load of less than two tons imposed by the load column provided measurable vibrations when the load was released. As the stiffness of this structure far exceeded that of any of the Nevada structures, the procedures which had been developed were considered to be adequate for the field test program.



Fig. 1 Initial Non-Destructive Vibration Test

TESTS ON THE NEVADA PROTECTIVE STRUCTURES

During a two-week program eleven structures were tested under thirty-one different mechanical excitation schemes or variations in structural conditons and by fourteen explosive detonations. One hundred eleven runs with three accelerometers employed on each were put on record. Structures chosen and tested were an aboveground 6" thick 36' radius reinforced concrete 45° dome; an underground reinforced concrete flat slab prototype dual-purpose garage (Figure 3); two semi-buried, 180° arch, 25' span corrugated steel Navy ammunition magazines, one having steel arch ribs providing additional support, each with 5' of earth cover over the crown of the arch; two 8' diameter, circular corrugated steel and two 8' diameter circular 8" thick reinforced concrete shelters with 7-1/2' of earth cover; and three corrugated steel "cattlepass" structures with 5, 7-1/2, and 10' of earth cover respectively.

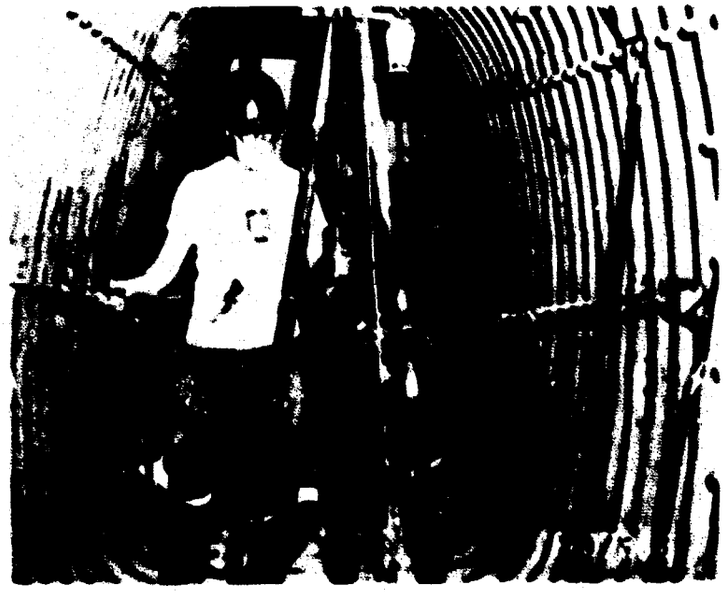


Fig. 2 Four Point Loading of Cattlepass Structure Accelerometer shown mounted at right

Mechanical testing schemes were employed in an effort to cause measurable response in the fundamental and principal harmonic flexural modes of vibration. Explosives were used to provide correlation or verification of the mechanically-induced results by providing a form of loading similar to that caused by the nuclear blast. The explosive charges were 2-1/2 to 5 pounds of 40% dynamite suspended from 5 to 8 feet above the ground surface (Figure 4). The explosive was generally centered over the test structure; however tests with the concrete dome and one test with three different culverts instrumented were run with

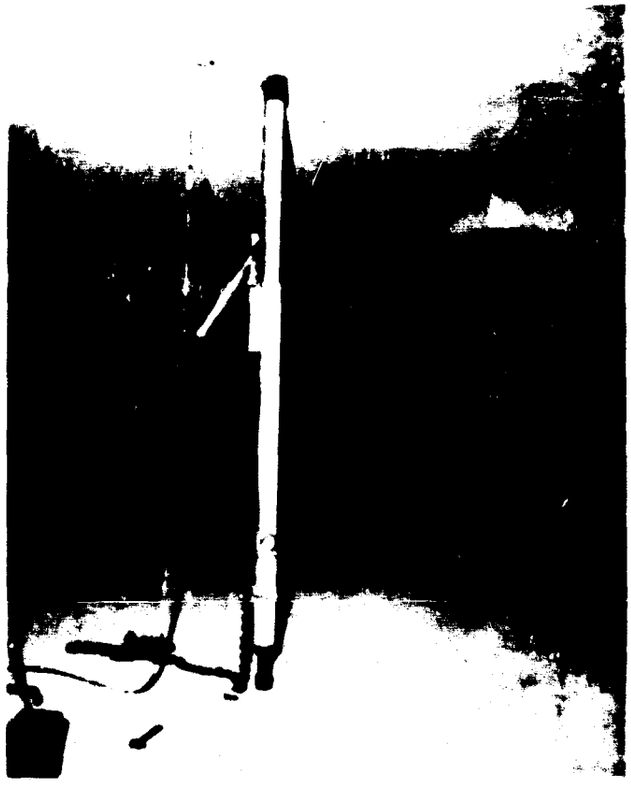


Fig. 3 Test in Dual-Purpose Garage Load Column and One Accelerometer Shown



Fig. 4 Five Pounds of Dynamite Over a Corrugated Steel Arch Structure

the explosive displaced 100 feet from the structure. The explosive tests provided a low level air-induced ground shock creating measurable vibrations in the structures. The remote character of the test site would have permitted all runs to have beem made with high explosives, however it was desirable to field test the mechanical excitation procedure and it was important to determine the relative significance of the flexural and compressive modes of vibration. Mechanically deforming the structure into its fundamental flexural mode prior to instantaneous release of this deformation should have provided the greatest opportunity for identifying and measuring the characteristics of this mode.

NEVADA TEST RESULTS

The most significant results were obtained in the tests of the 180° corrugated steel arch structures. Periods measured from the test records are given in Table I. Part of the record for one test run is shown in Figure 5. The tests showed the dominance of the compressive mode of vibration, even when the structure was deflected into its fundamental flexural mode (Figure 6). The explosive tests gave close correlation of these results. The arch rib reinforced structure had an average period of 62 ms (milliseconds) obtained from mechanical excitation and 66 ms obtained from the explosive run. The unreinforced structure had an average period of 69 ms obtained separately from the mechanical and explosive runs.

The period of vibration in the compressive mode of an exposed arch structure may be taken as the circumference divided by the velocity of sound in the material. On this basis each of the arch structures would have had approximately the same period in the compressive mode, neglecting any effect of the earth backfill. In the flexural mode the 16 to 1 ratio of stiffness between the rib reinforced and unreinforced structures would have caused an approximately 1 to 4 ratio in the respective periods of the exposed structures. Burial of the structures should cause the period to vary from the exposed value as the square root of the ratio of the mass of structure and earth responding with it to the mass of the vibrating structure itself. By these considerations the period of the unreinforced structure should have been almost five times larger than that of the ribbed structure in the flexural modes, while only 20% greater in the respective compressive modes. This calculation, the closeness of the measured periods of the two types of structures and comparison of computed periods with those measured indicated that the periods measured were those of the compressive mode. The mass of earth vibrating with the structure could also be calculated, by comparing measured periods with those computed for the case in which only the mass of earth vertically along the structure responded with it. For the reinforced structure, a mass of soil approximately 2.7 times the mass of that immediately over the structure apparently vibrated with the structure. For the ribbed structure this ratio was 3.3.

Table 1

ANGLE OF TEST RESULTS OBTAINED
Record of Measured Periods for the Corrugated Steel Arch Structures

Structure	Excitation	Run No.	Measured Periods (milliseconds)		
			Accel. No. 102	Accel. No. 103	Accel. No. 104
14' Corrugated Steel Arch reinforced with steel ribs 1' earth cover	Wire rope, 2 point loading [illegible] and [illegible] from horizontal	5	4.7	61, 8.3	NR*
	Load column, 60° from horiz.	7	NR	6[illegible], 6.6	[illegible].6
	Explosive, 5 lb., 5' above-ground	116	64, 67, 13.6, 13.7	66	66, 5.5, 5.7
14'[illegible] Corrugated Steel Arch 5' earth cover	Load column, vertical	88	68	NR	67
		89	67	68, 6	68
		90	67	NR	69.4
	Load column, 60° from horiz.	91	NR	NR	69
		95	70, 3.5	NR	NR
		96	70 (Approx)	70	NR
		97	69, 6.4	71, 6.5	71, 7.4
	Explosive, 5 lb., 5' above-ground	99	70	69	68

*Negligible response or not measurable.

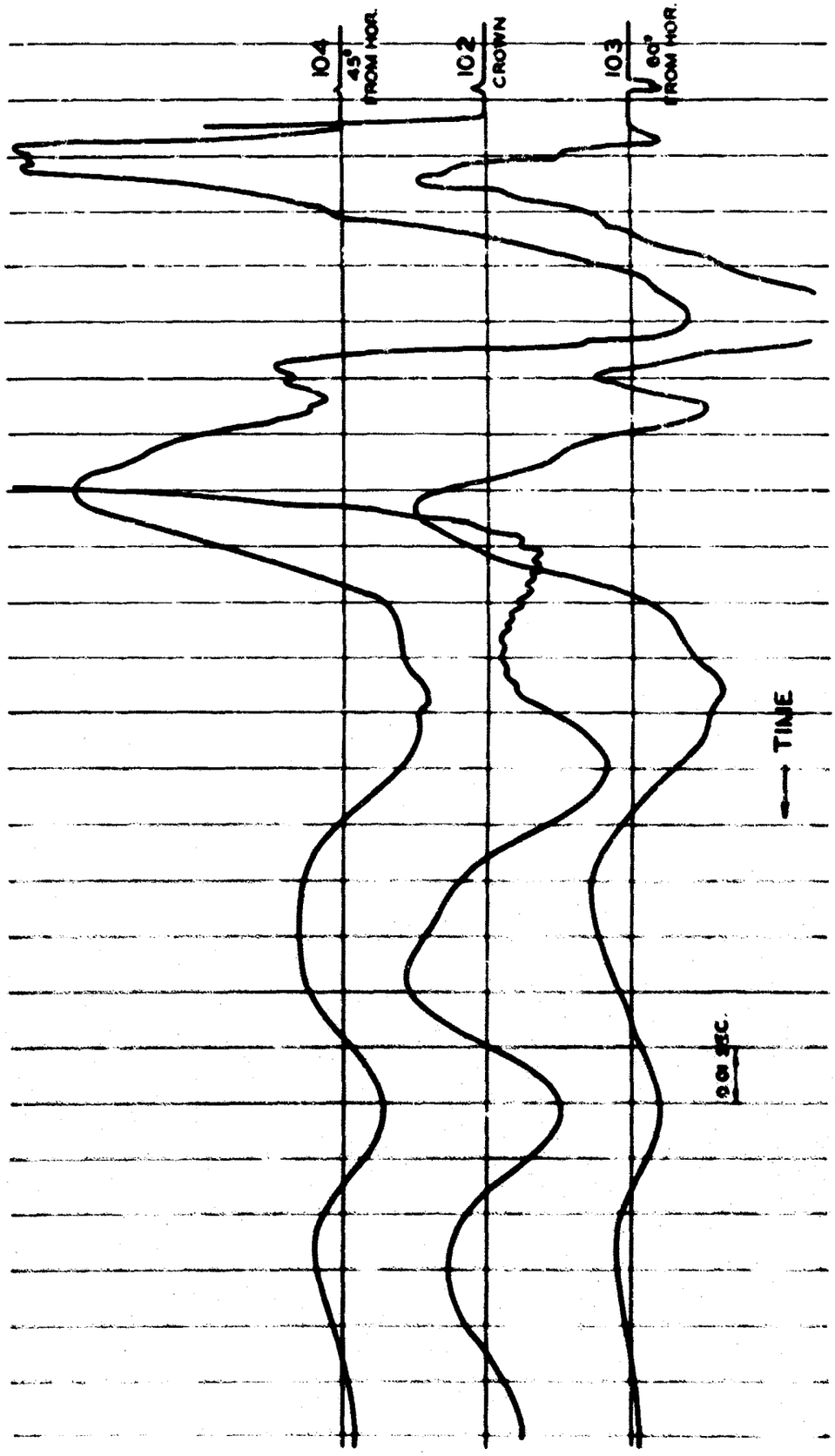


Fig. 5 Recorded Accelerometer Traces for Explosive Run 99 on Unreinforced Steel Arch

Results with the smaller steel and concrete structures did not provide as close correlation as did those for the arch structures. Damping was measured for both mechanically and explosively induced vibrations in the steel culvert sections. An average logarithmic decrement of damping for the mechanical runs was Ln 1.25, i.e., the amplitude of each cycle was 1.25 times that of the following cycle. Greater damping was evident in the explosive runs. The tests indicated that for the 8' diameter circular corrugated steel sections with 7-1/2' earth cover over the crown, a mass of earth approximately equal to that vertically above the structure responded with it in the compressive mode.

Test procedures proved adequate in that measurable vibrations were induced by mechanical means in all the underground structures studied. The recording procedure gave traces on high-speed film which could be analyzed by direct measurement. This film was developed during the test program to insure adequacy of collected data. The results obtained, principally those from the tests of the arch structures, were employed to assist development of a system of field productive construction (2).

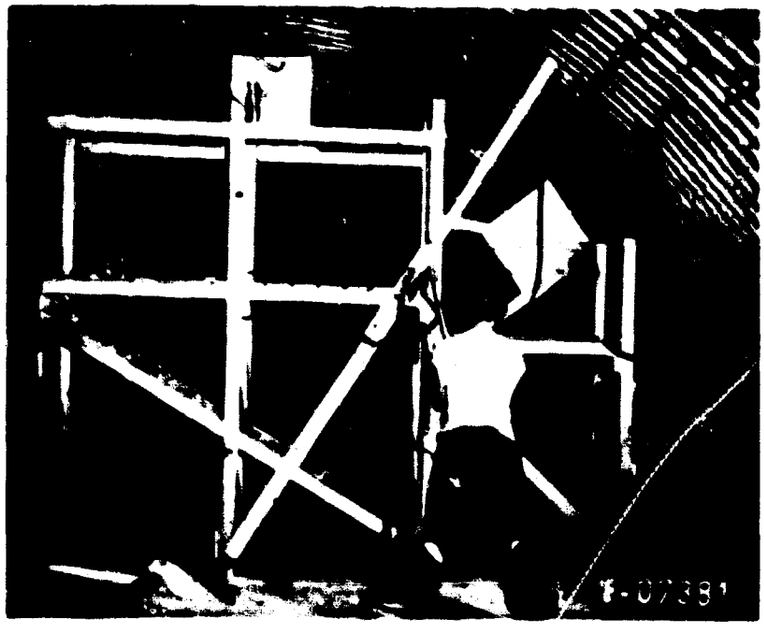


Fig. 6 Load Column in Corrugated Steel Arch Structures

APPLICATION OF PROCEDURES

The procedures and equipment employed met the requirements for the specific tests conducted. No significant errors are thought to have been introduced by the measurement and recording equipment itself. This was determined by separate tests of the significance of the natural frequency of the accelerometer itself; damping of accelerometer; the natural frequency of the accelerometer mount in the various configurations employed; linearity and hysteresis of response; variation in the time standard superimposed on the recording film; and accelerometer calibration. The mechanical equipment used to induce vibration should have had no significant effect on the subsequent vibrations, however the weight of the man operating the equipment and standing in the structure may have influenced some of the results of the small corrugated steel structures.

Test equipment for future work may employ similar means of exciting the structure, however some changes could be made in the instrumentation and recording equipment. If excitation is to be solely by mechanical means, more sensitive accelerometers would be desirable. Those used were ± 1g range and less than 10% of this range was normally used on the mechanical runs. A recording oscillograph with film speed of 5 to 10 inches per second should be adequate for most underground structures. When feasible, explosive excitation should be used. Minimum charge size was not studied in the Nevada tests but results indicated that charges of one pound or less detonated in the air above the structure could have provided fully measurable response. The equipment for any test program must be tailored to the objectives and measurements sought to meet those objectives.

CONCLUSIONS

For various reasons the results obtained in the test program described do not answer basic questions of soil-structure interaction. Some of these are due to limitations of measurement made and limited size of sample and variety of structures studied. These deficiencies could be addressed by future similar non-destructive testing. Another restriction to validity is that the nature of the soil surrounding the structure may, and probably does, have its properties changed under the nuclear shock loading. The non-destructive tests discussed here do not simulate conditions where the foundations of the structure are being permanently displaced or the shear capacity of the soil is being temporarily increased due to increase in confining pressures. However the principal modes of response may be identified by such tests, the relative significance of different modes can be examined, and indications of soil response in conjunction with the structure can be studied.

DESIGN AND PROTOTYPE STUDIES

The procedures illustrated here can be employed to assist in the verification of theories of reaction to dynamic loads of underground, and aboveground, structures. Structures such as shelters, subways, bridges and multistoried buildings, excited by simple mechanical means, traffic, or wind can be examined without nuclear testing. Such studies can greatly increase our present capabilities for effective structural design for the dynamic loadings of nuclear detonations and natural forces of wind, wave and earthquake.

REFERENCES

1. R. H. Sievers, Jr., A. R. Stacy, WT-1708, Structural Response and Permanent Displacement Measurements, Operation HARDTACK II.
2. R. H. Sievers, Jr., ERDL 1689-TR, Protective Construction by Proved Components.
3. ERDL, Research Film, RF-1907.

THE DESIGN OF BURIED ARCHES TO RESIST BLAST LOADS

by

William J. Flathau* and Richard A. Sager**

SYNOPSIS

It has long been known that certain types of buried structures interacting with the surrounding soil medium are very efficient in resisting loads. During full scale weapons tests, it has been shown that buried arches are very efficient structural types to resist moderate and high overpressures. For such structures it is first necessary to design the structure to resist dead loads using current allowable design stresses. The structure is then designed to resist the dynamic blast loads.

Equations were developed for determining the reactions resulting from dead loads, i.e., earth cover, concrete, and temperature changes, at any section for a two-hinged buried, semicircular arch of uniform cross section. These equations were plotted and presented as figures.

The equivalent surcharge loading method for designing against blast loads is presented. Two general solutions, i.e., the threshold method and upper bound method, are presented for the case where a structure is located above and below the ground water table respectively. Example calculations are included.

Calculations to determine the overpressures that should cause failure to various sizes of arch structures were made and summarized in the form of convenient graphs. One graph relates arch thickness with span to overpressure for structures located above and the other pertains to structures located below the ground water table.

INTRODUCTION

With the advent of nuclear weapons, underground structures became a necessity in the field of protective construction. Full-scale tests have shown that for underground protective construction the arch-type structures is one of the most efficient and economical in the moderate and high overpressure regions.

Since data presently available do not reveal exactly how air-induced ground shock is transmitted through soil or what effect various soils have in attenuating such shock, the actual loading of buried structures is not known with certainty. Therefore, for design purposes, it is necessary to assume certain loading conditons. Once the shape and magnitude of this load are assumed, the actual structural design is relatively straightforward. However, shock is only one important nuclear effect to consider in the design of protective installations; the other is nuclear radiation. Provision for sufficient shielding against nuclear radiation must be considered as a part of the design. However, the design of structures to resist nuclear radiation is not included in this paper.

Before designing any structure against dynamic loads, it is first important to design the structure to resist dead loads using current allowable design stresses. The structure is then designed or evaluated to determine its resistance to dynamic loads (blast loads) using the dynamic strength properties of the construction materials. Therefore, procedures for both dead and dynamic loads are presented for the design of buried, reinforced-concrete two-hinged barrel arches. The design of the associated footings, end-walls, and entraceways have not been included in this paper.

DEAD LOAD DESIGN METHODS

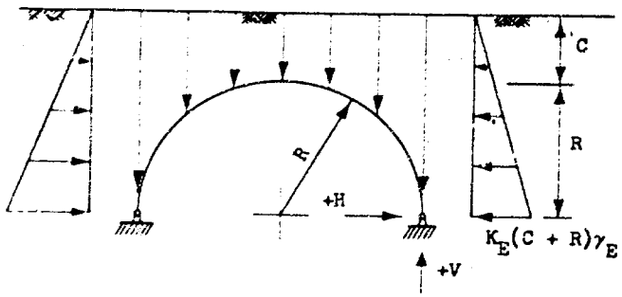
Equations were derived using the principal of virtual work for determining the reactions resulting from dead loads, i.e., earth-cover, concrete, and temperature changes, at any section for a two-hinged buried, semicircular arch of uniform cross section. The derived equations for reactions at the springing line and at any location on the arch are summarized, respectively, in Tables 1 and 2 for a two-hinged arch. In addition, a program for the various equations was written and processed in an IBM 650 computer to derive the design charts shown in Figures 1 through 9. These charts make it possible to compute rapidly the reactions caused by dead loads at any section around a two-hinged arch.

*Chief, Structural Dynamics Section, Corps of Engineers, U.S. Army Engineer Waterways Experiment Station, Vicksburg, Mississippi.

**Project Engineer, Structural Dynamics Section, Corps of Engineers, U.S. Army Engineer Waterways Experiment Station, Vicksburg, Mississippi.

Table 1

Springing Line Reactions From Dead Loads for a Two-Hinged Arch



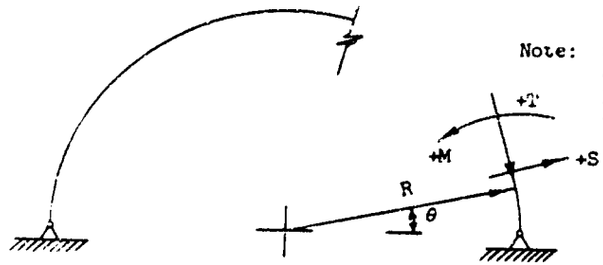
Note: Positive (+) moment causes tension on outer face.

b = unit width of section, ft
C = depth of earth cover over arch crown, ft
E_c = modulus of elasticity of concrete, lb/ft^2
I = moment of inertia, ft^4
K_E = horizontal load factor for earth load
R = radius to center line of arch, ft
t = thickness of arch, ft
γ_c = unit weight of concrete, lb/ft^3
γ_E = unit weight of soil, lb/ft^3
ΔF^o = change in temperature, ^oF
η = temperature coefficient of linear expansion for concrete, $ft/ft/^oF$

Springing Line Reactions	
Earth Load	$V_E = \gamma_E \cdot b \cdot R\,(0.21460R + C)$
	$H_E = \gamma_E \cdot b \cdot R\,[0.29941R \cdot K_E - 0.049413R + 0.42441C\,(K_E - 1)]$
Temperature Load	$V_T = 0$
	$H_T = \dfrac{-1.27324 \cdot \eta \cdot \Delta F^o \cdot E_c \cdot I}{R^2}$
Concrete Load	$V_c = 0.5\pi \cdot \gamma_c \cdot b \cdot R \cdot t$
	$H_c = -0.5 \cdot \gamma_c \cdot b \cdot R \cdot t$

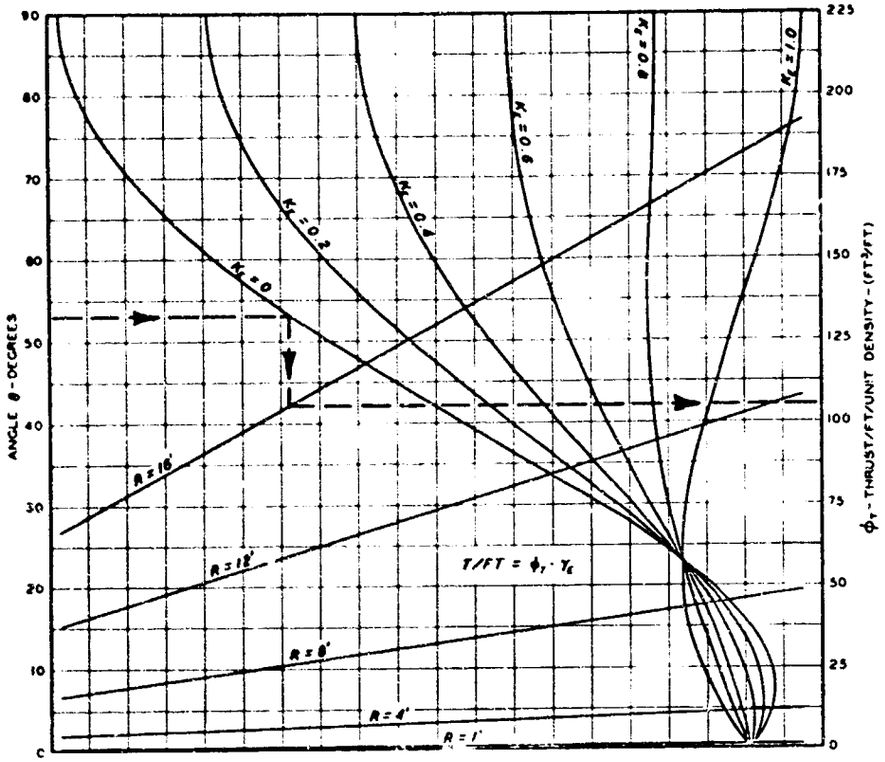
Table 2

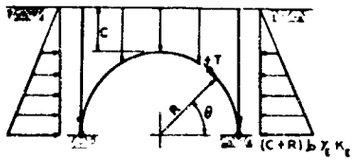
General Equations for Reactions at Any Angle θ for a Two-Hinged Arch



Note: See table 1 for explanation of terms.
Positive (+) moment causes tension on outer face.

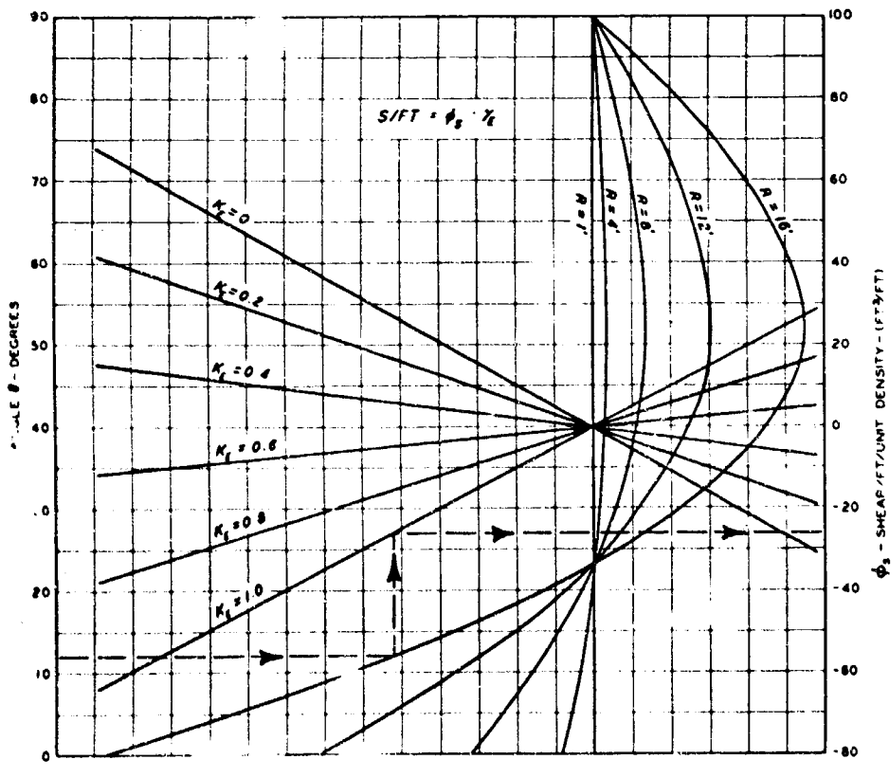
Reactions at θ	
Earth Load	$T_E = \gamma_E \cdot b \cdot R\{[K_E(-0.5R \sin^2\theta + (C + R)\sin\theta - 0.42441C - 0.29941R) + 0.049413R + 0.42441C]\sin\theta - [R(0.25\pi - 0.5\theta - \cos\theta + 0.25\sin 2\theta) - C\cos\theta]\cos\theta\}$
	$S_E = \gamma_E \cdot b \cdot R\{[K_E(-0.5R \sin^2\theta + (C + R)\sin\theta - 0.42441C - 0.29941R) + 0.049413R + 0.42441C]\cos\theta + [R(0.25\pi - 0.5\theta - \cos\theta + 0.25\sin 2\theta) - C\cos\theta]\sin\theta\}$
	$M_E = \gamma_E \cdot b \cdot R^2\{(K_E - 1)[-0.16667R \sin^3\theta + 0.5(C + R)\sin^2\theta - 0.29941R\sin\theta - 0.42441C\sin\theta] - 0.75R\sin\theta + (0.5\theta - 0.25\pi)R\cos\theta + 0.78540R\}$
Temperature Load	$T_T = \dfrac{1.27324 \cdot \eta \cdot \Delta F^o \cdot E_c \cdot I \cdot \sin\theta}{R^2}$
	$S_T = \dfrac{1.27324 \cdot \eta \cdot \Delta F^o \cdot E_c \cdot I \cdot \cos\theta}{R^2}$
	$M_T = \dfrac{1.27324 \cdot \eta \cdot \Delta F^o \cdot E_c \cdot I \cdot \sin\theta}{R}$
Concrete Load	$T_c = \gamma_c \cdot b \cdot R \cdot t\,[0.5\sin\theta - (\theta - 0.5\pi)\cos\theta]$
	$S_c = \gamma_c \cdot b \cdot R \cdot t\,[0.5\cos\theta + (\theta - 0.5\pi)\sin\theta]$
	$M_c = \gamma_c \cdot b \cdot R^2 \cdot t\,[1.5\sin\theta - (\theta - 0.5\pi)\cos\theta - 0.5\pi]$

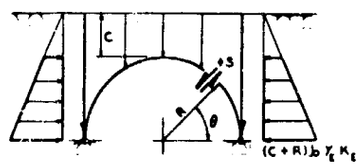




NOTE:
C - R/2 DEPTH OF COVER
R - ARCH RADIUS, FT
b - UNIT WIDTH, FT
γ_t - SOIL DENSITY, LB/FT³
K_t - HORIZONTAL LOAD FACTOR

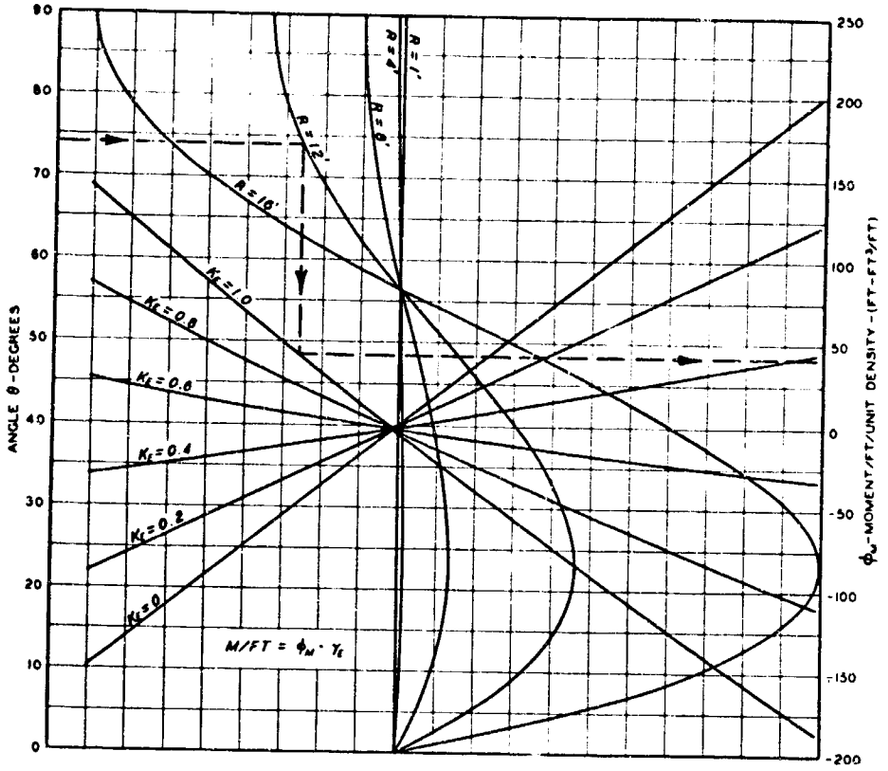
Fig. 1 Thrust (T) Due To Earth Loads For A Hinged Arch

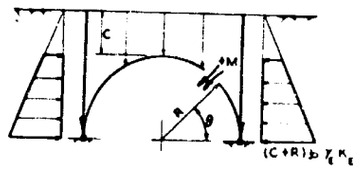




NOTE
See Figure 1 for list of terms

Fig. 2 Shear (S) Due To Earth Loads For A Hinged Arch

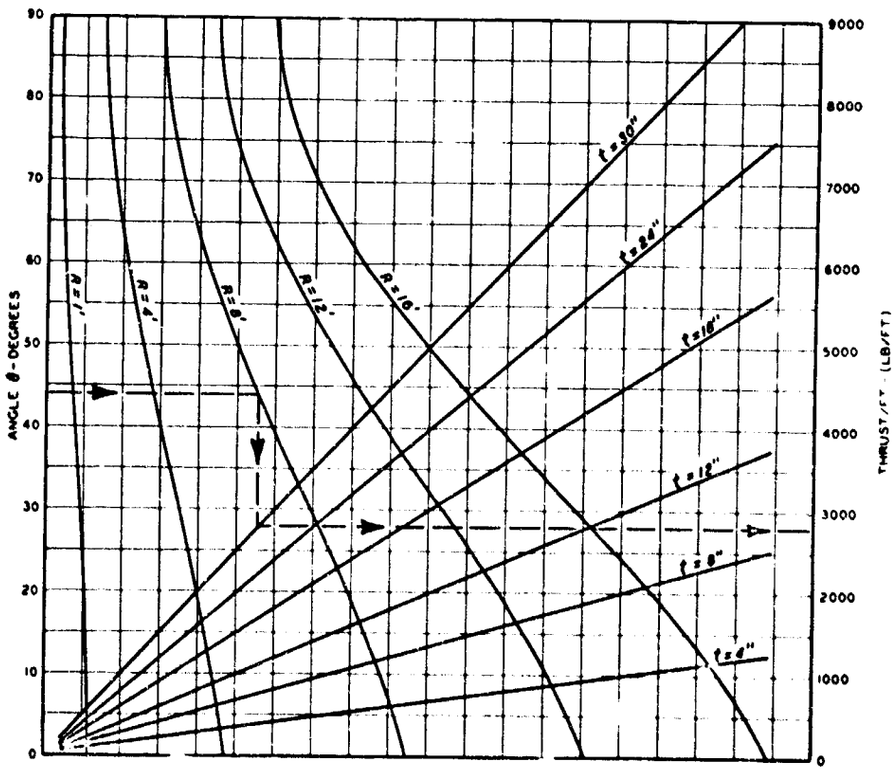


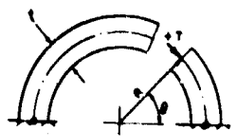


NOTE See Figure 1 for list of terms

POSITIVE (+) MOMENT CAUSES TENSION IN THE OUTER FIBER

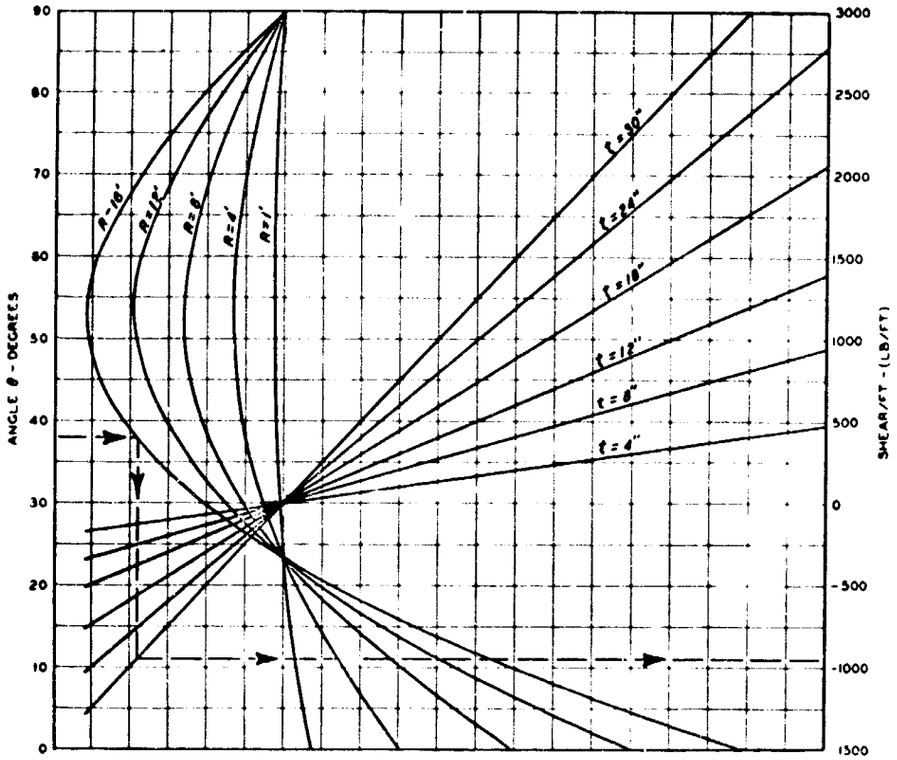
Fig. 3 Moment (M) Due To Earth Loads For A Hinged Arch

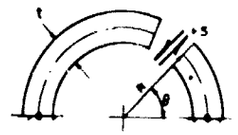




NOTE
UNIT WEIGHT OF CONCRETE (γ_t) = 150 LB/FT³

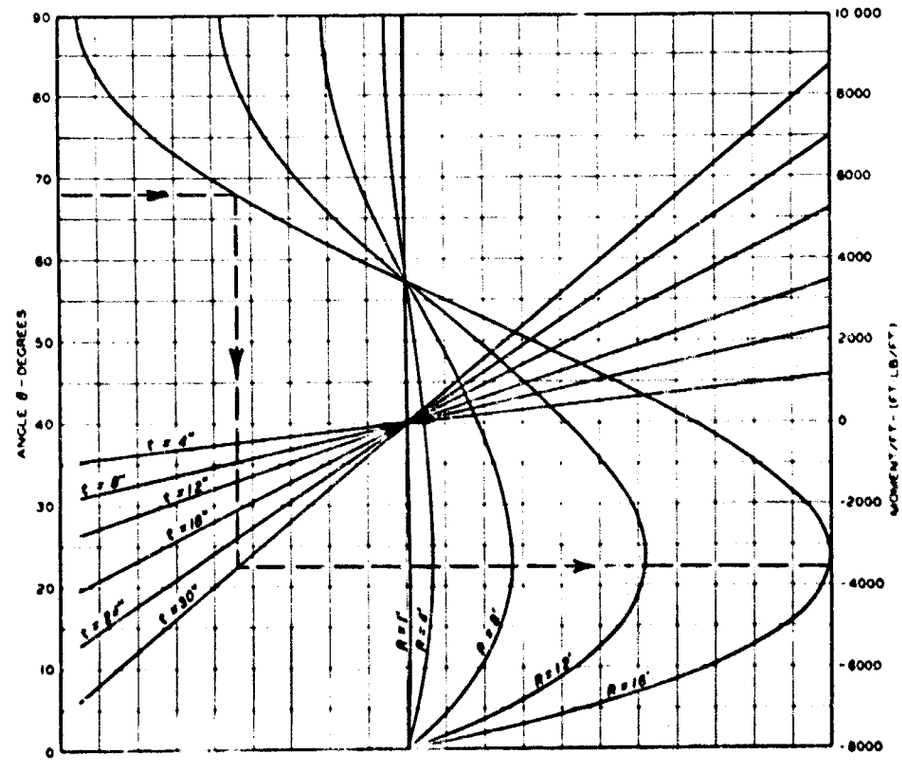
Fig. 4 Thrust (T) Due To Dead Load Of Concrete For A Hinged Arch

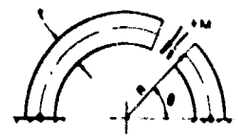




NOTE See Figure 4 for list of terms

Fig. 5 Shear (S) Due To Dead Load Of Concrete For A Hinged Arch

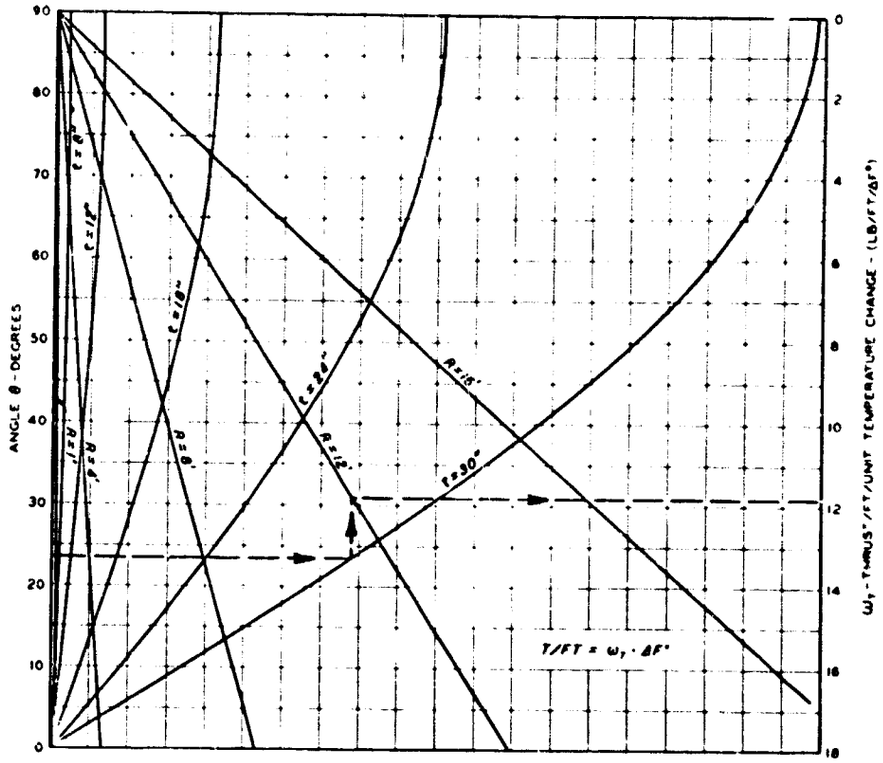


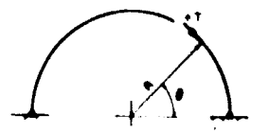


NOTE See Figure 4 for list of terms

POSITIVE (+) MOMENT CAUSES TENSION IN THE OUTER FIBER

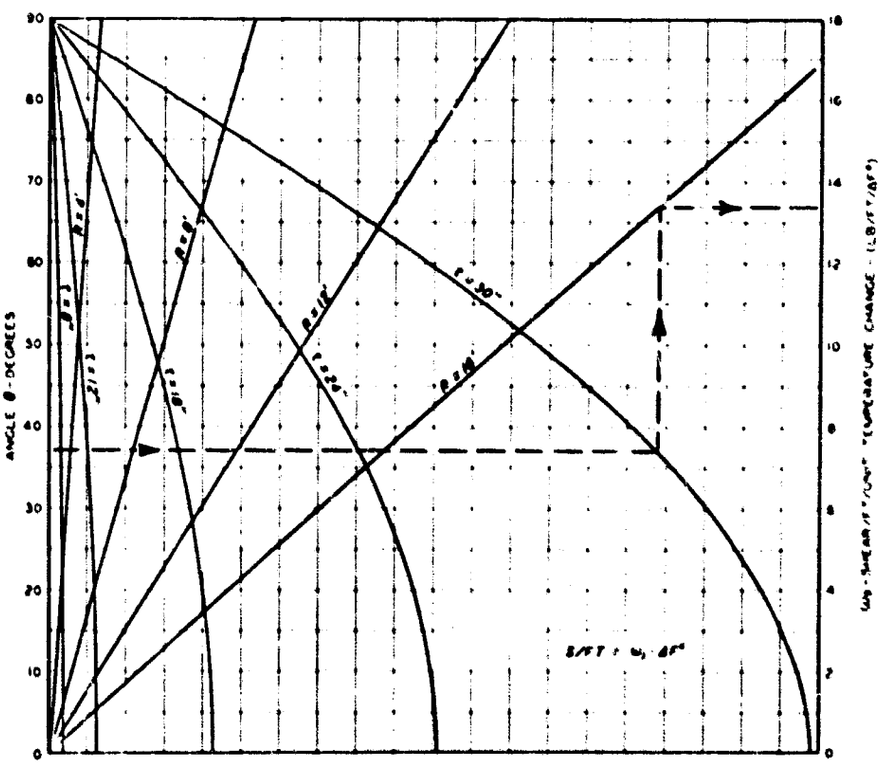
Fig. 6 Moment (M) Due To Dead Load Of Concrete For A Hinged Arch





NOTE
R - RADIUS TO C L OF SECTION
t - THICKNESS OF ARCH
ΔF° - CHANGE IN TEMPERATURE - DEGREES FAHRENHEIT

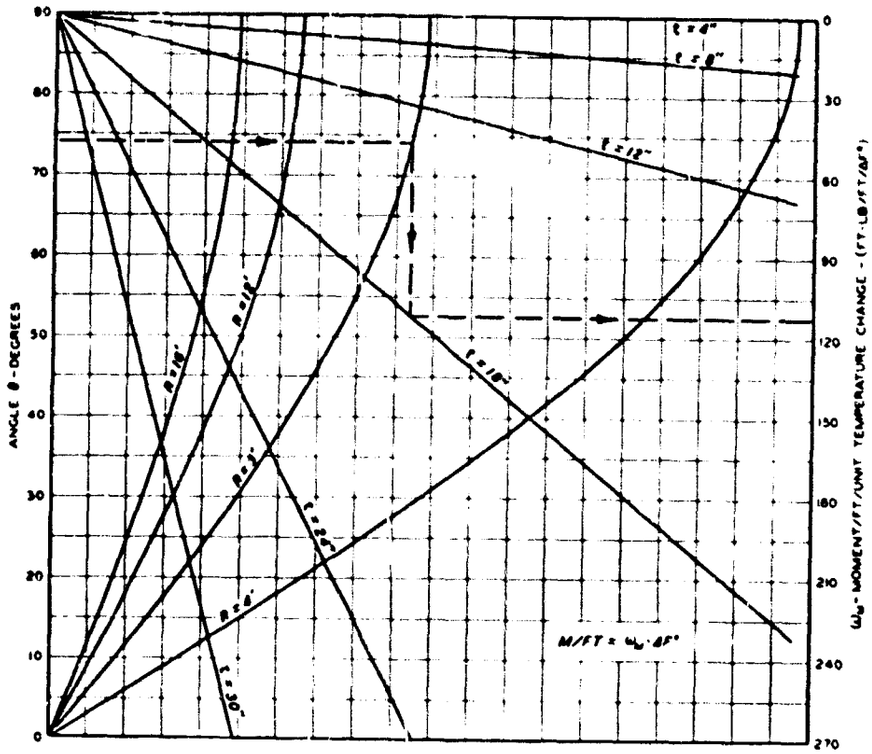
Fig. 7 Thrust (T) Due To Temperature Change (ΔF°) For A Hinged Arch

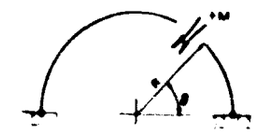




NOTE
See Figure 7 for list of terms

Fig. 8 Shear (S) Due To Temperature Change (ΔF°) For A Hinged Arch





See Figure 7 for list of terms

NOTE

POSITIVE (+) MOMENT CAUSES TENSION IN OUTER FIBER

Fig. 9 Moment (M) Due To Temperature Change (ΔF°) For A Hinged Arch

Earth Loads

In the derivation of the various reactions resulting from earth loads, it was assumed that the total vertical earth load was equal to the weight of soil directly above the arch. It was assumed also that the lateral soil pressure was same function of the vertical pressure (see Table 1). Figures 1 through 3 describe thrust, shear, and moment, respectively, for earth loads. The plots were developed for an arch having a depth of cover over the crown equal to one-half the radius of the arch, by using the appropriate equations shown in Table 2.

Concrete Load

The reactions at any section for various combinations of arch thickness, arch radius, and unit weight of concrete are shown in Figures 4 through 6 for thrust, shear, and moment, respectively. These plots were developed by using the appropriate equations shown in Table 2.

Temperature Changes

A uniform change in temperature was assumed to exist across a section through the arch ring to determine the reactions caused by temperature changes. Figures 7 through 9 describing thrust, shear, and moment, respectively, were prepared by using the appropriate equations shown in Table 2.

DYNAMIC LOAD CONSIDERATIONS

Assumptions

In general, there are two main assumptions regarding transient load distribution on a buried arch. The first is that the load over the arch surface is uniform and acts radially inward, resulting in compression of the arch ring. The other assumption, which has several variations, is that the load is not uniform over the surface of the arch, resulting in a combination of bending and compression of the arch ring. It is generally assumed also that an arch will fail either in a compressive or flexural mode depending upon the direction of the airblast wave with respect to the long axis of the structure. For underground arches, it is believed that the buttressing action of the adjacent soil limits flexural failure; therefore, the direction of travel of the blast wave is not as important for underground as for aboveground structures. This phenomenon was observed for arches tested in Project 3.1 of Operation PLUMBBOB.

Soil Conditions

It is believed that the restraining action of the soil is some function of the soil type as well as the moisture content of the soil. Also, it is reasonable to assume that the response of a buried structure located beneath the ground-water table will be different than if it were above the water table.

Structural Properties

In dealing with the response of structures to dynamic loads, there are more parameters requiring consideration than for ordinary static loads. For instance, under transient-blast loads it is possible to allow a structure to yield into the plastic range of response thus permitting a great deal of energy to be absorbed. Also under rapidly applied dynamic loads the yield strengths of concrete and steel tend to increase and can be appreciably greater than the static yield strengths. Under combined stress conditions caused by moment and axial thrust, the combination of moment and thrust caused by static loads that will produce yield stresses for a particular input-loading geometry must be determined.

In addition, a dynamic load factor (DLF) and a ductility factor (μ) must be determined for transient response. The DLF relates a static load to an equivalent dynamic load that will cause the same response to the structural system as the static load. The ductility factor relates the deflection of the structure at yield to the deflection at failure.

Blast Loads

The peak ground surface air overpressure (P_{so}) resulting from the detonation of a nuclear weapon is some function of the weapon size and the distance from ground zero (3). The duration time (t_d) is some function of pressure and weapon size. The variation in ground surface air overpressures with horizontal distance for two weapon sizes is shown in Figure 12. Also shown in the figure is a typical sketch of an air blast wave. The pressure decay is exponential with the positive phase duration of the blast wave ending at time "t_d." Since a peak triangular input force is used in the dynamic analysis (see Figure 11), an effective duration (t_e) is sued to equate the actual force pulse to an equivalent triangular force pulse. An expression (5) was developed relating the variation of effective duration time with pressure and is shown in Figure 13 for two weapon sizes.

Interaction Diagram

A dimensionless interaction diagram relating internal moment and thrust for compression members subjected to both bending and direct stress was developed and is shown in Figure 10. The diagram was constructed for the geometry shown in the typical section and was selected for several reasons: (a) the value of "G" of 0.7 results in practical dimensions providing sufficient concrete cover over the steel for most cases and (b) the percentage of steel of 1 percent provides a sufficient section for bending action.

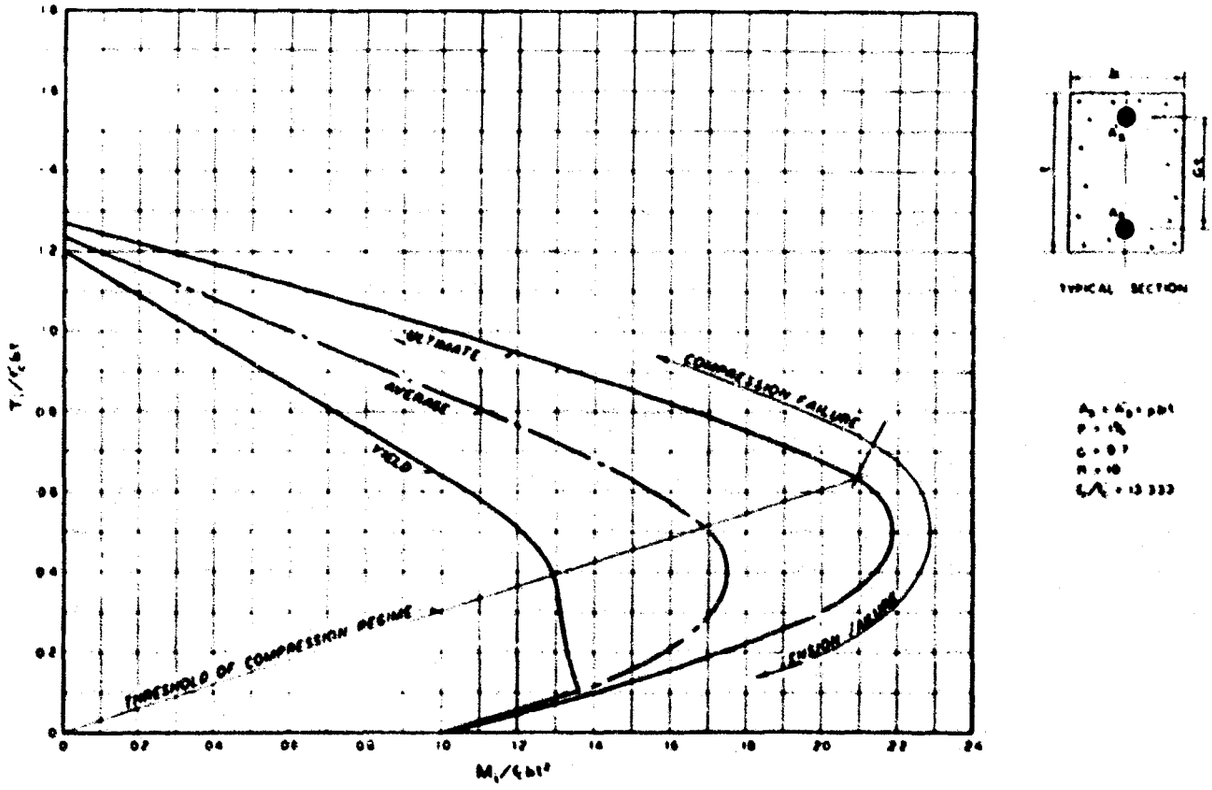
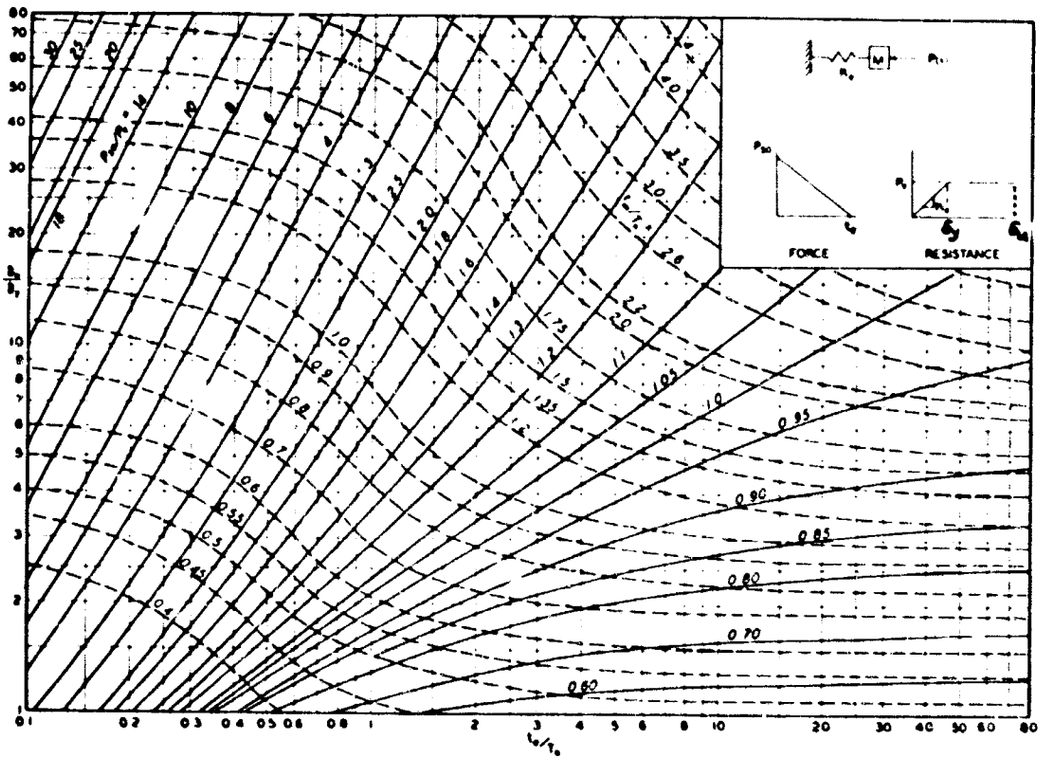


Fig. 10 Dimensionless Interaction Diagram For Moment and Axial Thrust



NOTE RESPONSE CHART BY DR. N. M. NEWMARK, SEE REF. 3

Fig. 11 Maximum Response Of Simple Spring-Mass System To Initially Peaked Triangular Force Pulse

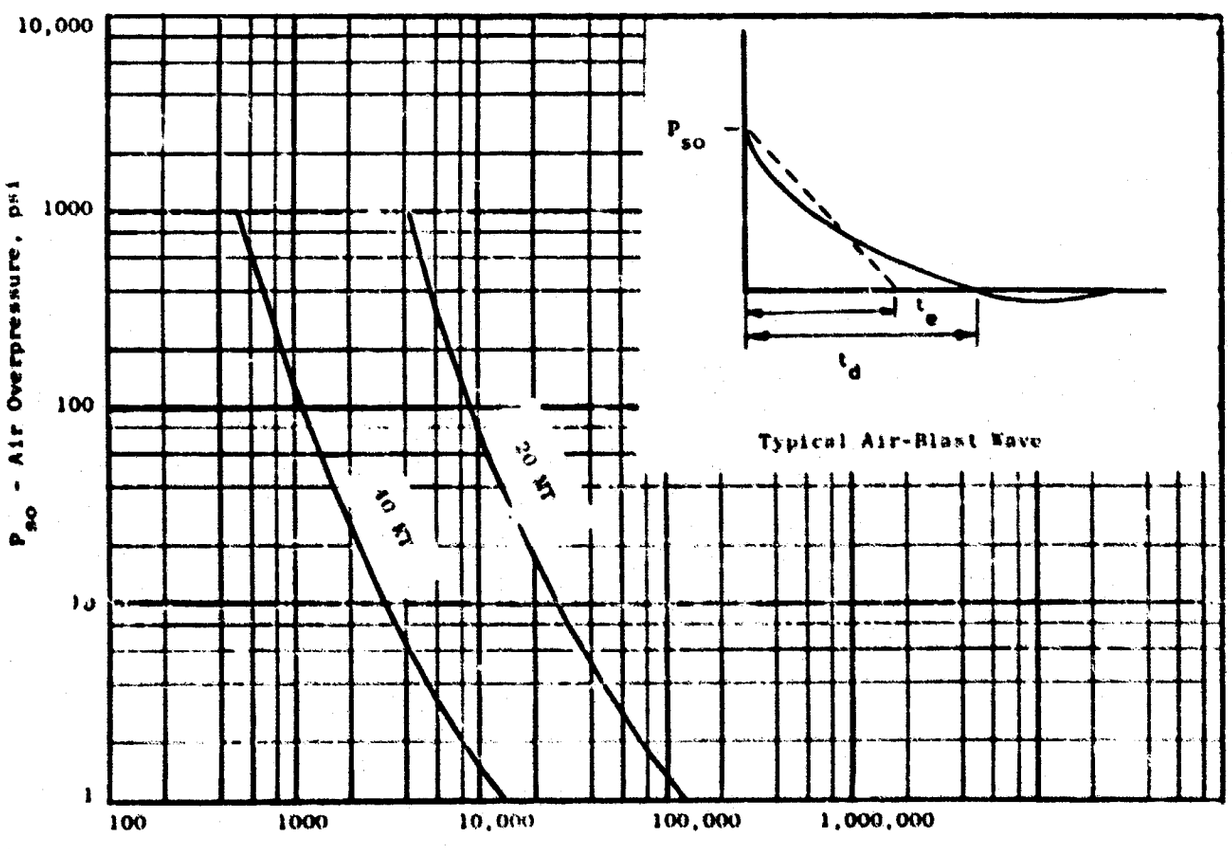


Fig. 12 Ground-Surface Air-Overpressure Vs. Horizontal Distance for A 20 MT and 40 MT Weapon

It should be noted that in making the calculations to construct the interaction diagram, the concrete area displaced by the presence of reinforcing steel was neglected for the purpose of simplifying the calculations. This omission results in an error less than 2 percent and is considered negligible.

The yield curve was prepared for various combinations of moment and thrust that caused yield stresses to occur. The ultimate curve was determined for combinations of moment and thrust that caused ultimate stresses to occur. A third curve was drawn which is the average of the other two. It is useful when an elasto-plastic response is assumed for structural analysis purposes. The portion of the curve where tensile and compressive failure occur are marked on the figure.

Dynamic Response

In determining the dynamic response of a structure it is often conveneient to substitute an equivalent spring-mass system for the structure in question. Dr. N.M. Newmark has developed a response chart (4) for a single-degree of freedom, spring-mass system, having an elasto-plastic resistance function and a peak triangular force pulse. This chart is shown in Figure 11. This chart makes it possible to determine rapidly the ovepressure load (P_{so}) that will cause the same response as the static or resistance load (P_q). It is therefore apparent that once the ratio of ^{so} the duration time (t_e) to the natural period of the system (T_n) is $_q$ determined, the ratio of some ultimate deflection (δ_u)to the yield deflection (δ_y), and the static resistance (P_q) are determined, the value of the overpressure load (P_{so}) can be calculated readily.

DYNAMIC LOAD DESIGN METHOD

Equivalent Surcharge Loading

In this method, the transient overpressure load is considered as an equivalent surcharge of soil. It is assumed that a buried concrete arch will fail in a compression regime as indicated by limited field tests (1, 2). As bending occurs and the arch ring deflects outward, a passive soil resistance develops that drives the arch into a compression regime of response. Equations essentially the same as those shown in Table 2 for earth loads were developed for predicting reactions at any point on a two-hinged buried arch subjected to overpressure loads. These equations relate pressure, arch radius, and the horizontal load factor (K). The load factor, K, relates horizontal as a function of vertical pressure. The equations were used to develop the curves shown in Figures 14 through 16 for a two-hinged arch for thrust, shear, and moment, respectively. In general, the combination of moment and thrust developed at a critical arch section (section at which the combination of the values of moment and thrust develop the maximum stress condition for a given loading) will depend upon the value of K. Since it is assumed that a buried arch subjected to overpressure loads will fail in compression, two limiting cases for the Equivalent Surcharge Loading Method were selected for design purposes. The minimum case hereafter called the threshold method was selected as one that would result in combination of moment thrust that would drive the arch to failure at the threshold of the compression regime of failure, see Figure 10. The maximum case hereafter called the upper bound mehtod is selected as one that will drive the arch to failure in pure thrust.

Threshold Method. The threshold condition represents a special combination of moment and thrust such that the concrete reaches ultimate stress when the tensile steel reaches yield stress and is shown in Figure 10 at the point where the straight line intersects the ultimate interaction diagram. Since an equivalent spring mass system having an elasto-plastic response as shown in Figure 11 is assumed, it is convenient to use the average interaction diagram of Figure 10 for computations. The general equations for internal moment and thrust at the threshold of the compression regime are determined from the average interaction diagram shown in Figure 10 are as follows:

$$M_i = 0.168 f'_c\, bt^2 \tag{1}$$

$$T_i = 0.515 f'_c\, bt \tag{2}$$

From Figures 14 and 16 for the two-hinged arch, it is evident that the critical section for producing the maximum fiber stress in the arch resulting from a combination of thrust and moment occurs where θ is 25°. At this critical section ($\theta = 25°$), thrust is independent of K; therefore, a general equation for external thrust at this section can be written:

$$T = 144R\, P_q \tag{3}$$

The total static resistance, P_q, for the two-hinged arch is then determined by equating equations 2 and 3, adding the dead load thrust (T_{dl}), and solving ^{q} for P_q:

$$P_q = \frac{0.515 f'_{dc}\, bt - T_{dl}}{144R} \tag{4}$$

The natural period of vibration of the arch for the equivalent surcharge loading is assumed to be some function of K and to be some value between that computed for an arch in the compression mode (T_c) and that for the flexural mode (T_f) of an equivalent beam.

$$T_n = T_f - (T_f - T_C)\ K \tag{5}$$

where (from Reference 4):

$$T_f = \frac{1}{42{,}500\ \frac{in}{sec}\sqrt{\rho}}\ \frac{\pi^2 R^2}{9d} \tag{6}$$

$$T_c = \frac{R}{1800\ ft/sec} \tag{7}$$

T_c is computed according to methods described in Reference 4 for an above-ground arch. In determining T_f for a two-hinged arch, the effective length of an equivalent beam equal to 1/3 the developed length of the arch is assumed. This length has been selected since the inflection point for moment occurs where θ is approximately equal to 60° (see Figure 16). The value "K" is determined by solving β_m shown in Figure 16.

$$\beta_m = \frac{M_i - M_{dl}}{P_q}$$

M_i and P_q are determined from Equations 1 and 4 respectively. The dead load moment (M_{dl}) is determined by using Figures 3, 6, and 9 where θ is 25°. After β_m is determined, enter Figure 16 and find K at the critical section, i.e., where θ equals 25°. Since the arch is buried, the period determined by Equation 5 must be modified to include the effect of earth cover according to the following expression:

$$T'_n = T_n \sqrt{\frac{m'}{m}} \tag{8}$$

In Equation 8, T_n is determined from Equation 5, whereas m is the mass of concrete per unit length, and m' the mass of concrete plus the mass of earth cover per unit length.

A ductility factor (μ), i.e., ratio of ultimate deflection (δ_u) to yield deflection (δ_y), of 5 was determined for use with the threshold method. For a detailed explanation see Appendix C of reference 7.

Upper Bound Method. The Upper Bound Method represents the upper limit for the equivalent surcharge loading. In this method "K" is numerically equal to unity resulting in a uniform inward radial loading around the arch surface. This results in the same loading condition as described in References 4 and 6, as the uniform compression mode loading. Because of the brittle type failure associated with this type of loading the internal thrust (T_i) for this case was determined by using the yield interaction diagram shown in Figure 10 and is as follows:

$$T_i = 1.20 f'_{dc}\ bt \tag{9}$$

The total external thrust (T) caused by the applied loading and the dead load thrust (T_{dl}) can be written as follows:

$$T = 144RP_q + T_{dl} \tag{10}$$

The total dead load thrust (T_{dl}) is determined by using Figures 1, 4, and 7. The total static resistance (P_q) can be solved by equating Equations 9 and 10 as the internal (T_i) and external thrust (T) must be equal. Therefore:

$$P_q = \frac{1.20 f'_{dc}\ bt - T_{dl}}{144R} \tag{11}$$

The natural period of vibration (T_c) for an arch in the compression regime is calculated by using Equation 7. The value for the period is then modified to include the effect of soil cover according to the following equation:

$$T'_c = T_c \sqrt{\frac{m'}{m}} \tag{12}$$

The values for m and m' are the same as those described in Equation 8. Since this is a brittle type of failure a ductility factor (μ) no greater than 2 is used for this method.

Example Problem

For example purposes an arch having a radius of 8 ft and a thickness of 4 in. is selected. The structure is then analyzed to determine the values of ground-surface, air-overpressure resulting from both a 40 KT and a 20 MT weapon

that would cause failure (collapse). Both methods, i.e., threshold and upper bound, for the equivalent surcharge type loading are presented. The geometry for the arch including values for various design parameters are shown in Figure 17.

Threshold Method

In this method for the equivalent surcharge loading (see Figures 14 through 16), it is assumed that when the arch is loaded a horizontal load factor (K) is developed that will cause the arch to reach ultimate stress at the threshold of the compression regime of failure, see Figure 10. The thrust and moment due to dead loads are determined first.

Dead load thrust and moment

Determine thrust and moment due to dead loads at the arch section where $\theta = 25^{\circ}$ (critical section for overpressure loads). By using the appropriate equations shown in Table 2 or the convenient curves shown in Figures 1 through 9, the following values were determined:

$$M_{dl} = 10.3 \frac{\text{in-kips}}{\text{ft}}; \quad T_{dl} = 4.72 \frac{\text{kips}}{\text{ft}} \qquad (13)$$

Static Overpressure (P_q)

An expression for static overpressure is presented in Equation 4 and rewritten:

$$P_q = \frac{0.515 f'_{dc} bt - T_{dl}}{144R} = 66.9 \text{ psi/ft} \qquad (14)$$

Determine horizontal load factor (K)

The total moment (M_t) is comprised of the dead load moment (M_{dl}, Equation 13) and the moment due to the overpressure load (M).

$$M_t = M + M_{dl} \qquad (15)$$

Substitute Equation 1 into Equation 15 then

$$M = 0.168 f'_{dc} bt^2 - M_{dl}$$

$$= \frac{6700 t^2 - M_{dl} \times 1000}{12} \text{ (ft - lbs/ft)} \qquad (16)$$

However, from Figure 16,

$$M = \beta_m \times P_q \qquad (17)$$

Substitute Equation 16 into 17 and solve for β_m

$$\beta_m = \frac{(6.7 t^2 - M_{dl})(1000)}{12 P_q} \qquad (18)$$

$$= 120.7 \frac{\text{ft - in.}^2}{\text{ft}}$$

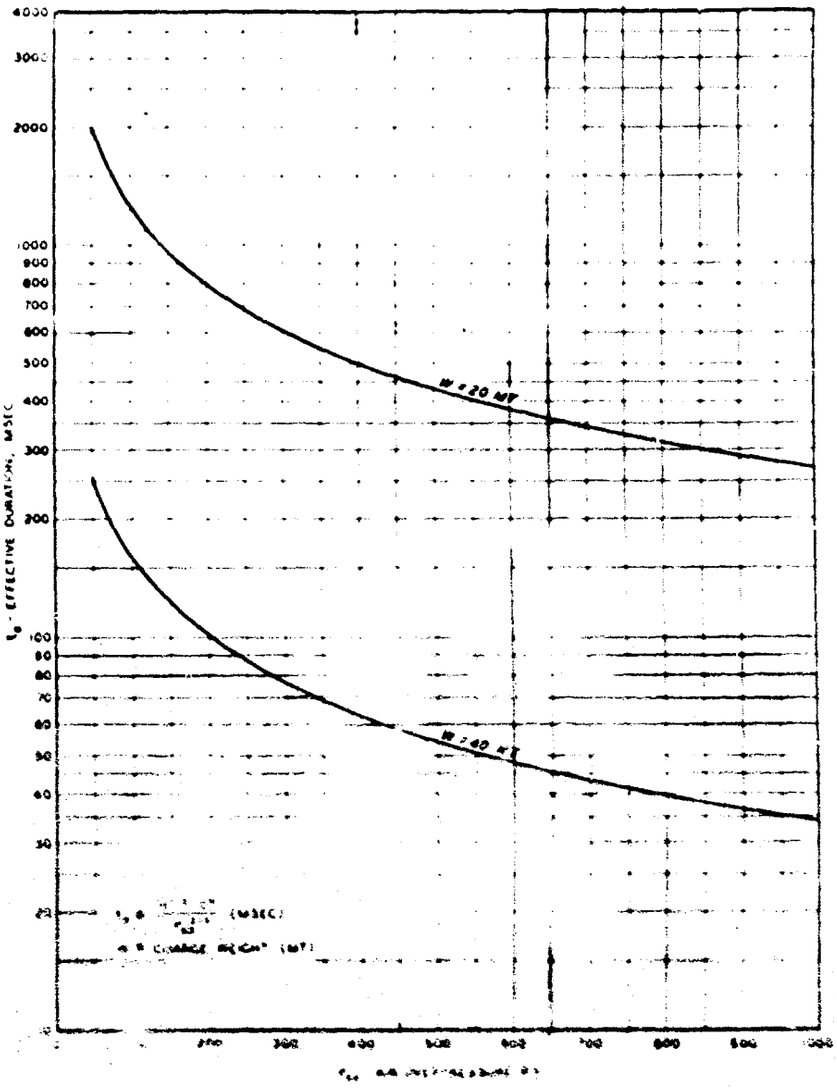


Fig. 13 Effective Durations vs Various Air-Overpressures For A 20 MT And 40 KT Weapon

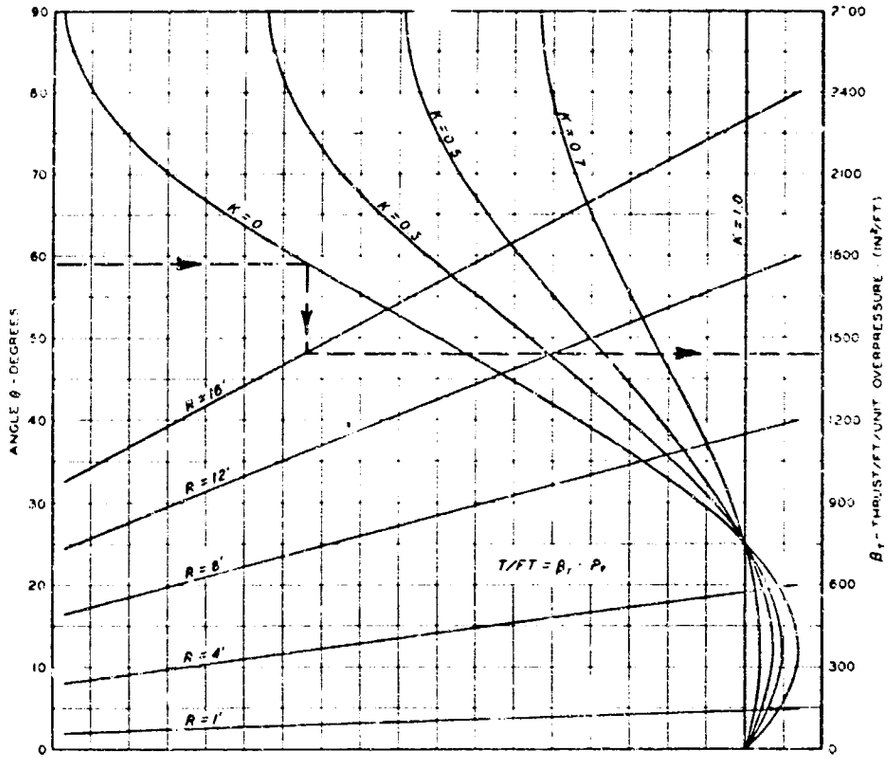


Fig. 14 Thrust (T) Due To Ground-Surface-Air Overpressure (P_q) For A Hinged Arch

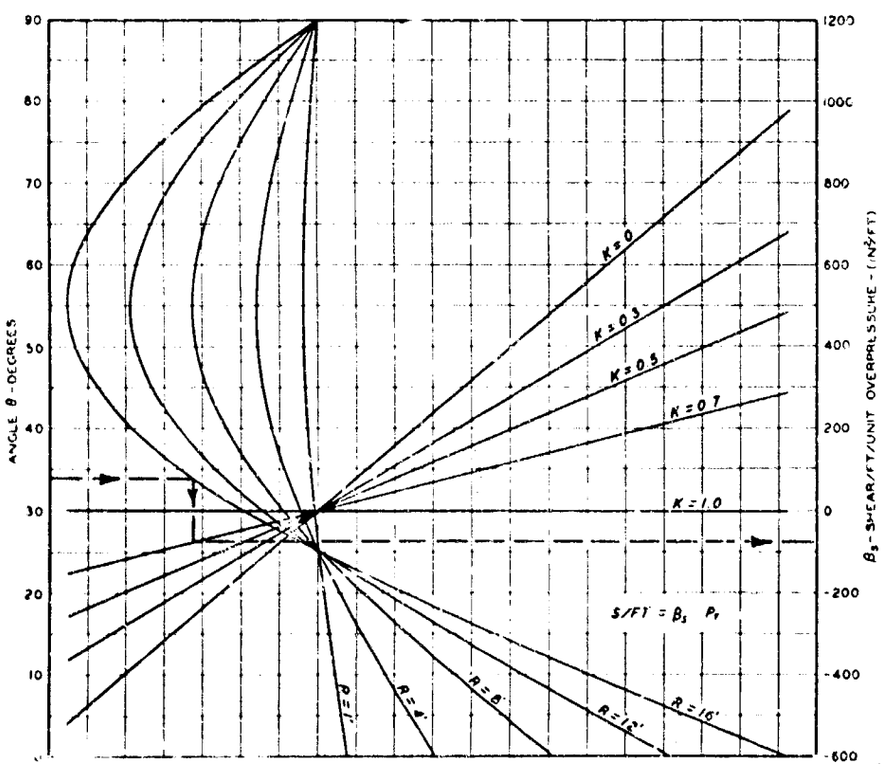
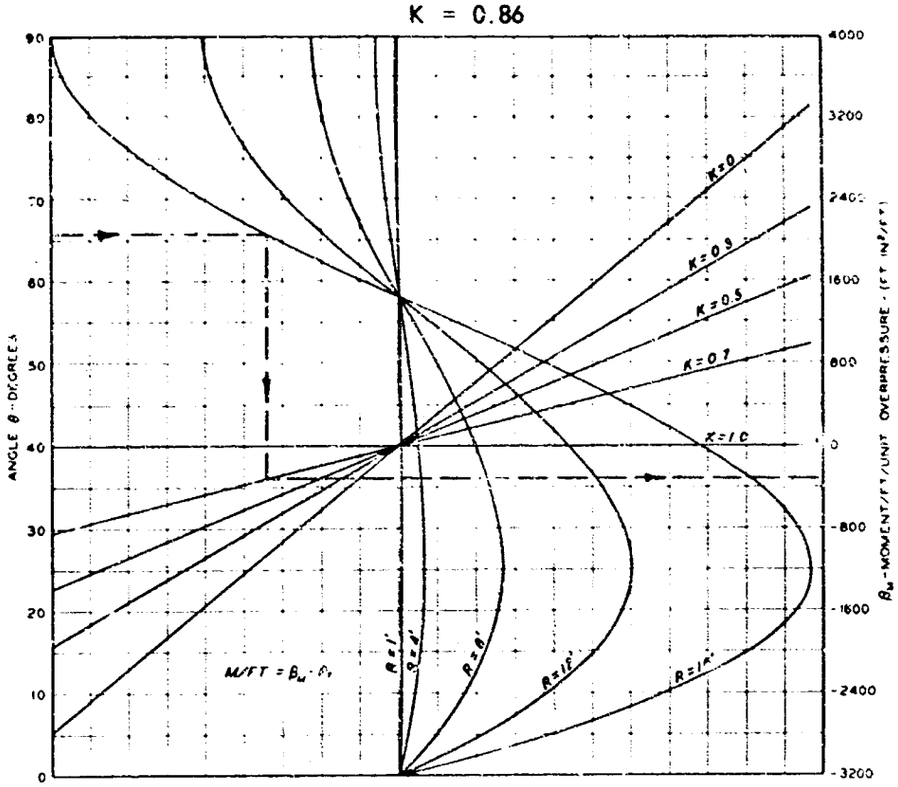
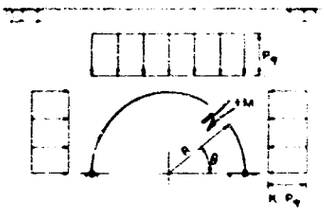


Fig. 15 Shear (S) Due To Ground-Surface-Air Overpressure (P_q) For A Hinged Arch

Determine K from Figure 16:

$$K = 0.86 \tag{19}$$





NOTE: See Figure 14 for list of terms

POSITIVE (+) MOMENT CAUSES TENSION IN OUTER FIBER

Fig. 16 Moment (M) Due To Ground-Surface-Air Overpressure (P_q) For A Hinged Arch

Natural period of vibration (T'_n)

Determine the natural period of vibration by using Equation 5 repeated as follows:

$$T_n = T_f - (T_f - T_c)\,K \tag{20}$$

From Equation 6:

$$T_f = \frac{1}{42{,}500 \frac{\text{in}}{\text{sec}}\sqrt{P}} \frac{\pi^2 R^2}{9d} \tag{21}$$

$$= 70 \text{ msec}$$

From Equation 7:

$$T_c = \frac{R}{1800 \text{ ft/sec}} \tag{22}$$

$$= 4.45 \text{ msec}$$

Substitute 19, 21, and 22 into 20 and solve T_n.

$$T_n = 70 - (70 - 4.45)\,(0.86) \tag{23}$$

$$= 13.6 \text{ msec}$$

Correct the value of T_n to include the effect of earth cover (see Equation 8).

$$T'_n = T_n \frac{m'}{m} \tag{24}$$

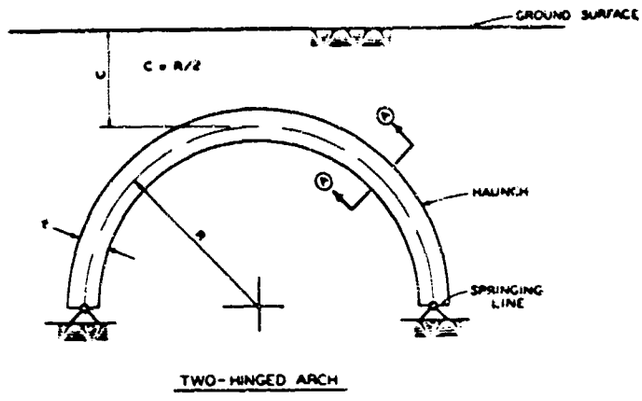
where: $m = tb\,\gamma_c/g$

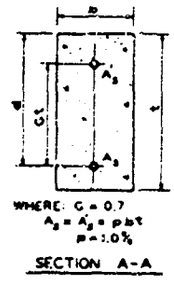
$= 50/g \text{ lbs-sec}^2/\text{ft}^2$

$$m' = \frac{(0.7R - 0.4t)\,(R + t/2)\,(b)\,(\gamma_E)}{g\,\pi\,R/2} + m$$

$= 356/g \text{ lbs-sec}^2/\text{ft}^2 + 50/g \text{ lbs-sec}^2/\text{ft}^2 = 406/g \text{ lbs-sec}^2/\text{ft}^2$

$$\sqrt{\frac{m'}{m}} = 2.87 \tag{25}$$





ASSUMED DESIGN PARAMETERS

DESIGN STRENGTHS:	STATIC	DYNAMIC
	f_c = 1350 PSI	f_{dc} = 3315 PSI
	f'_c = 3000 PSI	f_{dy} = 44,300 PSI
	f_s = 20,000 PSI	
	f_y = 40,000 PSI	
	E_c = 3.0 x 10^6 PSI	
	n = 10	
UNIT WEIGHTS:		
	γ_c = 150 LB/FT^3	
	γ_s = 100 LB/FT^3	
OTHER VALUES:	μ_c = 0.40	
	ΔF = ± 25°F	
	α = 6.0 x 10^{-6} IN/IN/F°	

Dimensions: R = 8 ft
t = 4 in.
b = 12 in.

Fig. 17 Geometry and Design Parameters For Example Problem

Therefore,

$$T'_n = 13.6 \times 2.87 = 39.0 \text{ msec} \tag{26}$$

Failure Overpressure (P_{so})

The ground surface air-overpressure (P_{so}) that would cause structural collapse was determined for two weapon sizes, i.e., 40 KT and 20 MT.

40 KT Weapon

Assume P_{so} = 67 psi
From Figure 13, t_e = 210 msec
Therefore: $t_e/T'_n = \frac{210}{39} = 5.4$
from Figure 11, at $\delta_u/\delta_y = 5$, $P_{so}/P_q = 1.0$
using P_q from Equation 14 solve P_{so}

P_{so} = 66.9 x 1.0 = say 67 psi which is equal to the assumed value and is therefore the required pressure resulting from a 40 KT weapon to cause failure.

20 MT Weapon

Assume P_{so} = 59 psi

from Figure 13, t_e = 1800 msec

Therefore: $t_e/T'_n = \frac{1800}{39} = 460$

from Figure 11 (extrapolation necessary) at $\delta_u/\delta_y = 5$,
$P_{so}/P_q = 0.88$
using P_q from Equation 14 solve P_{so}

$P_{so} = 66.9 \times 0.88 = 58.8$ psi which is close enough to the assumed value of 59 psi and is therefore the pressure required to cause failure for a 20 MT weapon.

Upper Bound Method

In this method for the equivalent surcharge loading, it is assumed that when the arch is loaded a horizontal load factor (K) of unity is developed causing the load to be applied uniformly and radially around the arch. This results in a pure compression in the arch.

Dead load thrust and moment

The critical section for dead loads, i.e., earth, concrete, and temperature changes, was found at $\theta = 23^\circ$ by using the equations shown in Table 2 or could have been found more conveniently by Figures 1 through 9. The total dead load moment and thrust were then computed for the critical section and are as follows:

$$M_{dl} = 10.56 \frac{\text{in.-kips}}{\text{ft}}; \quad T_{dl} = 4.79 \text{ kips/ft} \tag{27}$$

Static overpressure (P_q)

The static overpressure is determined by using Equation 11.

$$P_q = \frac{1.20 f'_{dc} bt - T_{dl}}{144R} = 162 \text{ psi} \tag{28}$$

Natural Period of Vibration (T'_c)

The natural period of vibration is the same as that computed in Equation 22.

Therefore: T_c = 4.45 msec
Correct the value of T_c to include the effect of earth cover according to Equation 12.

$$T'_c = T_c \sqrt{\frac{m'}{m}} \tag{29}$$

where the value under the radical is the same as shown in Equation 25, therefore:

$$T'_c = 4.45 \times 2.87 = 12.8 \text{ msec} \tag{30}$$

Failure Overpressure (P_{so})

The ground surface air-overpressure that would cause structural collapse was determined for two weapon sizes, i.e., 40 KT and 20 MT.

40 KT Weapon

Assume P_{so} = 125 psi

from Figure 13, t_e = 140 msec

Therefore $t_e/T'_c = \frac{140}{12.8} = 11.0$

from Figure 11, at $\delta_u/\delta_y = 2$, $P_{so}/P_q = 0.77$

Using p_q from Equation 28, solve P_{so}

Therefore $F_{so} = 162 \times 0.77 = 125$ psi which is equal to the assumed value and is therefore the pressure required to cause failure for a 40 KT weapon.

20 MT Weapon

Assume P_{so} = 121 psi

from Figure 13, t_e = 1100 msec

Therefore: $t_e/T'_c = \frac{1100}{12.8} = 92$

from Figure 11, at $\delta_u/\delta_y = 2$, $P_{so}/P_q = 0.75$

Using P_q from Equation 28, solve P_{so}

Therefore: P_{so} = 162 x 0.75 = 121 psi which is equal to the assumed value and is therefore the pressure required to cause failure for a 20 MT weapon.

Design Graphs

Graphs for use in the design of buried arches having a depth of soil over the crown of the arch equal to one-half the arch radius are presented in Figures 18 and 19 for the threshold and upper bound methods respectively. These graphs are reliable for arches having radii up to twenty feet and can be used regardless of the orientation of the blast wave. If a structure is located above the ground water table, use the threshold method, Figure 18. If it is known that a structure will always be located below the water table, use the upper bound method, Figure 19. Since the overpressure values in the graphs represent pressures that should cause structural collapse, for simplicity it is recommended that any factor of safety if used, be included in the overpressure value (P_{so}).

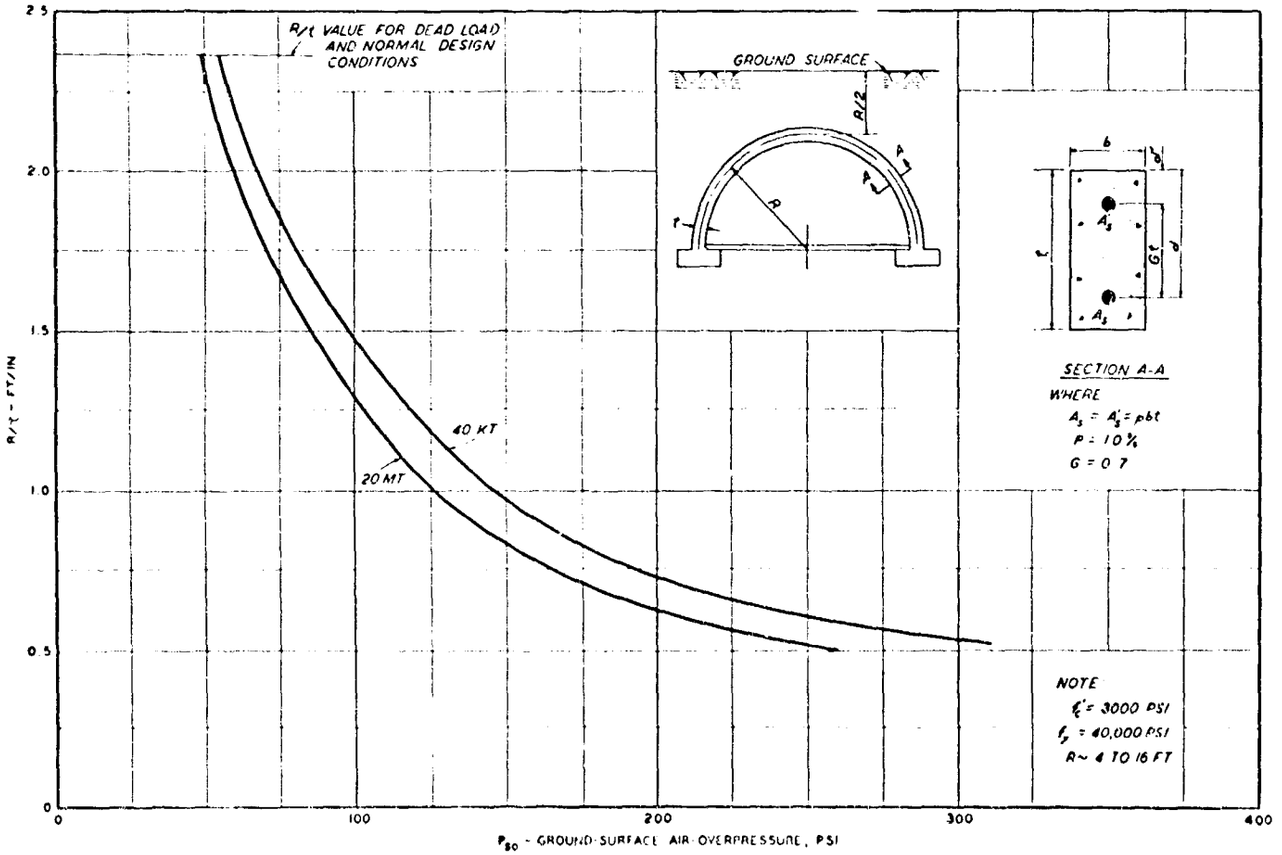


Fig. 18 Failure Overpressures Predicted by the Threshold Method

DISCUSSION AND CONCLUSIONS

Discussion

A study of detailed calculations for various arch geometries revealed that the inclusion of stresses due to dead loads had little influence in determining the failure overpressures shown in Figures 18 and 19. It is believed that the plots shown in Figures 18 and 19 offer an expedient approach to the design of buried arches that is rational and in keeping with field data presently available for such structures.

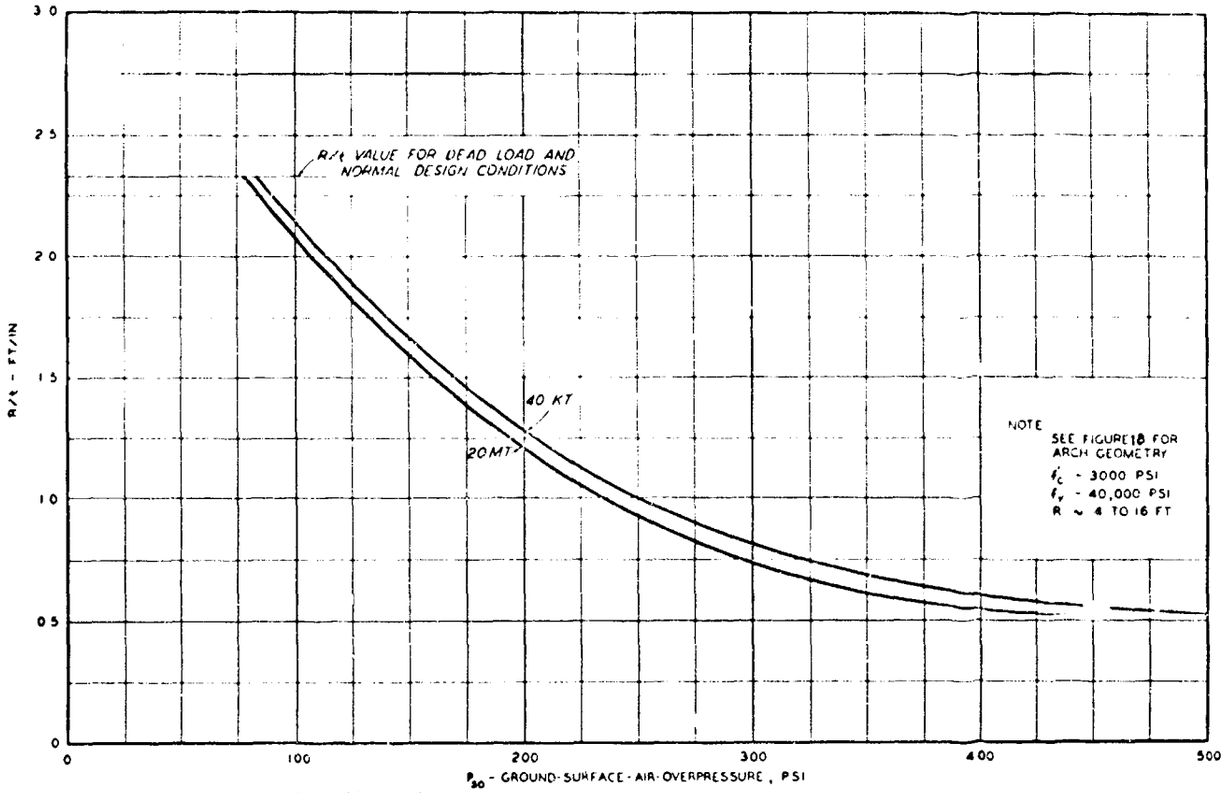


Fig. 19 Failure Overpressure Predicted By The Upper Bound Method

A study was conducted to determine the difference in the response of a fixed end arch having the same general geometry and strength characteristics to that of the two-hinged arch discussed in this paper. It was found that the overpressure to cause failure was about the same (10 percent difference approximately) regardless of the end condition, i.e., fixed or hinged.

Conclusion

Buried arches of the geometry discussed herein are able to withstand overpressures of at least 50 psi when designed to withstand dead loads alone, i.e., earth, concrete, and temperature changes, using standard design strengths for steel and concrete.

The predicted overpressure (P_{so}) necessary to cause failure of buried structures is not changed appreciably if the dead load stresses are omitted in the response calculations.

The overpressure necessary to cause failure is approximately the same geometry and strength characteristics. Therefore, the graphs shown in Figures 18 and 19 can be used for either fixed or two-hinged arches.

ACKNOWLEDGEMENT

This paper is based on a report prepared by the authors entitled "Design and Analysis of Underground Reinforced-Concrete Arches" (7), under the authority of an overall research project dealing with the effects of nuclear weapons on engineering structures, terrain, and waterways. Appreciation is expressed to all personnel of the U.S. Army Engineer Waterways Experiment Station who assisted in preparing the report. Colonel Alex G. Sutton, Jr., Corps of Engineers, was director and Mr. J. B. Tiffany the Technical Director of the Waterways Experiment Station during the preparation of this paper.

APPENDIX I: NOTATIONS

A_s	Area of tension steel in reinforced-concrete member, in.^{2}
A'_s	Area of compression steel in reinforced-concrete member, in.^{2}
b	Width of section, in. or ft.
C	Depth of earth cover for arch crown, ft
d	Depth from extreme compressive fiber to tensile steel, in.
d'	Depth from extreme compressive fiber to compressive steel, in.
DLF	Dynamic load factor
E_c	Modulus of elasticity of concrete, psi or lb/ft^2

f_c Allowable static compressive strength of concrete, psi

f'_c Static ultimate compressive strength of concrete, psi

f'_{dc} Dynamic ultimate compressive strength of concrete, psi

f^{dy} Dynamic yield strength of steel, psi

f^{s}_{y} Allowable static tensile stress of steel, psi

g Static yield point stress of steel, psi

G Acceleration due to gravity, ft/sec^2

H Ratio of distance between compressive and tensile steel to thickness of arch section

I Horizontal reaction at arch springing line, lb/ft

k_e Moment of inertia, $in.^4$ or ft^4

K^e Equivalent spring constant, lb/in.

K_E Horizontal load factor for overpressure load

KT Horizontal load factor for earth load

m Kiloton, 1000 tons

m' Mass of concrete per unit length, $lb\text{-}sec^2/ft^2$

M Mass of concrete plus mass of earth cover per unit length, $lb\text{-}sec^2/ft^2$

M_{dl} External moment, ft-lb/ft or equivalent mass in a simple spring mass system, $lb\text{-}sec^2/ft^2$

M_i^{dl} Dead-load moment, in.-kips/ft or ft-lb/ft

MT Resisting or internal moment section can develop at idealized yield for an elastoplastic response, in.-kips/ft

n Megaton, 10^6 tons

p Ratio of modulus of elasticity of steel (E_s) to the modulus of elasticity of concrete (E_c)

P Ratio of tensile reinforcement in reinforced-concrete member to concrete area

P^q Static resistance or static overpressure, psi

P^{so} Ground-surface air-overpressure, psi

$R^{(t)}$ Load applied to a structural element as a function of time

S Radius to center line of arch, ft

t External shear, lb/ft

t_d Thickness ofarch, in.

t^e Positive phase duration of blast wave, msec

t^m Effective duration of the dynamic load, msec

T Time to maximum response, msec

T_C External thrust, lb/ft

T'_C Natural period of vibration of an arch for a compression mode of loading, msec

T_{dl} Natural period of vibration of an arch for a compression mode of loading corrected for earth cover, msec

T_f Dead-load thrust, kips/ft

T_i Natural period of vibration for a flexural model of loading, msec

T_n Resisting or internal thrust section can develop at idealized yield for an elastoplastic response, kips/ft

T' Natural period of vibration, msec

V^n Natural period of vibration corrected for earth cover, msec

W Vertical reaction at arch springing line, lb/ft

β_M Charge Weight, MT

β_S Coefficient for hinged arch, M/P $(ft \times in.^2/ft)$

β_T Coefficient for hinged arch, S/P^q $(in.^2/ft)$

γ_c Coefficient for hinged arch, T/P^q $(in.^2/ft)$

γ_E Unit weight of concrete, lb/cu ft

δ_u Unit weight of soil, lb/cu ft

δ_y Ultimate arch crown deflection, in.

ΔF^o Yield arch-crown deflection, in.

η Change in temperature, ^oF

θ Temperature coefficient of linear expansion for concrete, $in./in./^oF$

μ Central angle of arch, degrees

ϕ_M Ductility factor

ϕ_S Coefficient for hinged arch, M/γ_E (ft^4/ft) $(ft\text{-}ft^3/ft)$

ϕ_T Coefficient for hinged arch, S/γ_E (ft^2)

Coefficient for hinged arch, T/γ_E (ft^2)

ω_M	Coefficient for hinged arch, $M/\Delta F^\circ$	$(\frac{ft-lb}{ft \times \Delta F^\circ})$
ω_S	Coefficient for hinged arch, $S/\Delta F^\circ$	$(\frac{lb}{ft \times \Delta F^\circ})$
ω_T	Coefficient for hinged arch, $T/\Delta F^\circ$	$(\frac{lb}{ft \times \Delta F^\circ})$

APPENDIX II: BIBLIOGRAPHY

1. Albright, G.H., "Evaluation of Earth-Covered Prefabricated Ammunition Storage Magazines as Personnel Shelters." WT-1422, Project 3.3, Operation PLUMBBOB, 1957, Dept. of the Navy, Washington 25, D.C. CONFIDENTIAL
2. Flathau, W.J., Breckenridge, R.A , and Wiehle, C.K., "Blast Loading and Response of Underground Concrete-Arch Protective Structures (U)." WT-1420, Project 3.1, Operation PLUMBBOB, U.S.Army Engineer Waterways Experiment Station, CE, Vicksburg, Miss., and U.S.Naval Civil Engineering Laboratory, Port Hueneme, Calif., June 1959. CONFIDENTIAL
3. Glasstone, S., "The Effects of Nuclear Weapons." United States Department of Defense. Published by the United States Atomic Energy Commission, June 1957.
4. Merritt, J.L., and Newmark, N.M., "Design of Underground Structures to Resist Nuclear Blast." Vol. II of final report, University of Illinois, for Office of the Chief of Engineers, Urbana, Ill., April 1958.
5. Newmark, N.M., Briscoe, J.W., and Merritt, J.L., "Analysis and Design of Flexible Protective Structures." Vol. I of Interim Report, Newmark and Associates, for the U.S.Army Engineer Waterways Experiment Station, CE, Vicksburg, Miss., May 1960.
6. Office of the Chief of Engineers, U.S.Army, "The Design of Structures to Resist the Effects of Atomic Weapons," EM 1110-345-414- to -421, Washington, D.C.
7. U.S.Army Engineer Waterways Experiment Station, CE, "Design and Analysis of Underground Reinforced-Concrete Arches," January 1962, Technical Report No. 2-590, Vicksburg, Mississippi.

FORCE TRANSMISSION DUE TO COHESIVE SOIL-FOUNDATION INTERACTION UNDER VIBRATORY LOADING

by
Robert L. Kondner*

SYNOPSIS

The influence of footing size and mass on the dynamic forces or stress transmission due to cohesive soil-foundation interaction is presented for the particular situation of vibratory loading. The methods of dimensional analysis in conjunction with kinematic and force parameters in phase diagram form are shown to be useful in analyzing and formulating dynamic stress transmission-deflection response. The results of prototype tests were analyzed for reinforced concrete, circular footings with diameters ranging from 5 ft-2 in to 10 ft-4 in, total weights of the foundation system ranging from 6.41 tons to 25.64 tons, and applied dynamic force amplitudes varying from approximately 0.26 tons to 26 tons. The static stress level about which the dynamic stress perturbations were applied was maintained constant at 4.25 psi. Although the response is nonlinear, the dynamic stress amplitude transmitted to the supporting cohesive soil is related to the displacement, x, by a power relation. This is expressed in terms of a non-dimensional displacement amplitude parameter, x/d, which conveniently accounts for the effects of footing diameter, d, as well as the transmission factor, (T.F.), of the soil-foundation system. The dynamic stress transmission is given in both graphic and analytic form. The analysis and results contained herein may provide insight on the dynamic force or stress transmission to supporting cohesive soils as well as the associated displacement consequence of such transmission due to soil-structure interaction under dynamic loading.

INTRODUCTION

The effects of foundation size and mass, properties of the soil supporting the foundation, magnitude and nature of the excitation function and static stress level are important considerations in studying the response of a system due to cohesive soil-structure interaction under dynamic loading. These factors are important aspects of both surface and buried soil-structure systems. It is generally recognized that the response of a soil-foundation system is a nonlinear problem of a highly indeterminate nature. The interrelated effects of the above factors on the dynamic response of such systems have not yet been determined clearly in broad terms, either theoretically or experimentally. In addition, most experimental studies are on models or relatively small scale foundations with prototype investigations quite limited in scope. It is highly desirable to be able to estimate the displacements of the foundation system in order to compare them with acceptable displacement tolerances of the foundation. The magnitude of the dynamic stresses transmitted to a cohesive soil by the foundation system may have a very important effect on the total displacements of the foundation.

The present paper deals with the effects of cohesive soil-structure interaction on the dynamic force or stress transmission to the supporting soil. These interaction effects are expressed in terms of the size and mass of the foundation, excitation level, and damping of the system for the particular case of sinusoidal loading of reinforced concrete, circular, prototype footings with diameters ranging from 5 ft-2 in to 10 ft-4 in. Total weights of the foundation systems range from 6.41 tons to 25.64 tons and applied dynamic force amplitudes vary from approximately 0.26 ton to 26 tons.

Although soil-foundation-loading interrelationships may be of a highly indeterminate nonlinear nature, it may be possible to express the response of output directly in terms of the input or physical variables of the system without knowing the mechanistic interaction between input and output. This is analogous to the "black box" approach in which input information is fed into the box and output is obtained without knowing how the box actually functions. Although such an approach may leave something to be desired academically, knowing the response for a set of physical variables may be quite satisfactory from the practical viewpoint. In addition, the relations between input and output response may be helpful in determining the mechanistic interaction among soil, footing system and loading.

A practical example where such an approach might be applied is the problem of determining the vertical displacement response of a footing supported on the surface of a cohesive soil and subjected to vertical sinusoidal loading. Classical approaches to this problem frequently consider an equivalent mass of soil as participating in the vibration and, hence, the inertial forces of such a mass must be included in the analysis. Such a soil mass is obviously a function of the footing size and mass, excitation function, and properties of the supporting soil. To date, the author knows of no reliable relations giving the magnitude of the vibrating soil mass as a function of the above variables. However, the effects of such a

*Associate Professor of Civil Engineering, Technological Institute, Northwestern University, Evanston, Illinois.

vibrating equivalent mass might possibly be limped into the effects of the other physical variables. Such an approach is used herein.

In general, when a cohesive soil is deformed by means of external forces, part of the work is stored elastically and part is dissipated. For simplicity, consider such combined elastic and flow response as viscoelastic behavior and a material exhibiting such behavior as a viscoelastic material. It is recognized that the response of a viscoelastic material subject to oscillating stresses or deformations may be markedly influenced by the magnitude of the static stress level about which the stress or deformation perturbations are taking place. Since a cohesive soil may be considered viscoelastic, it is important to recognize the possible influence of static stress level on the transmitted dynamic stress response of cohesive soil-foundation systems subjected to a pulse type of loading as well as an oscillating excitation of a nature prevalent in the present investigation. However, the effects of static stress level on the displacement response of the cohesive soil-foundation system considered are complex and beyond the scope of the present paper.

THEORETICAL ANALYSIS

Consider the case of a rigid circular footing supported on the surface of a cohesive soil and subjected to a harmonic forcing function, F_d, of the form

$$F_d = F_D \sin(\omega t + \delta) \qquad (1)$$

where F_D is the dynamic force amplitude, ω is the frequency, t is the time of loading, and δ is the phase angle between the displacement and F_D. The dynamic response of the soil-footing system is generally recognized as a nonlinear phenomenon. However, the assumption of a harmonic wave form for the steady state displacement-time response inherently leads to the concept of linearity, since the motion in nonlinear vibration may be periodic but not harmonic. Nevertheless, depending upon the degree of nonlinearity, it is possible to use a harmonic approximation for the response, particularly when only amplitude data are being considered on an individual point by point basis.

It is often advantageous to represent a simple harmonic function in terms of a rotating vector. Figure 1 is a vector diagram of the displacement, velocity, and acceleration with force leading the displacement by the angle δ. Since the displacement is assumed to be a sine function, the velocity is a cosine function and the acceleration is a negative sine function; the velocity and acceleration are 90° and 180°, respectively, out of phase with the displacement. The angles between the vectors are called phase angles and the diagram itself is called a phase diagram. Since all of the vectors in Figure 1 are rotating at the same frequency, they may be considered as turning like the spokes of a wheel, preserving their relative positions in the wheel.

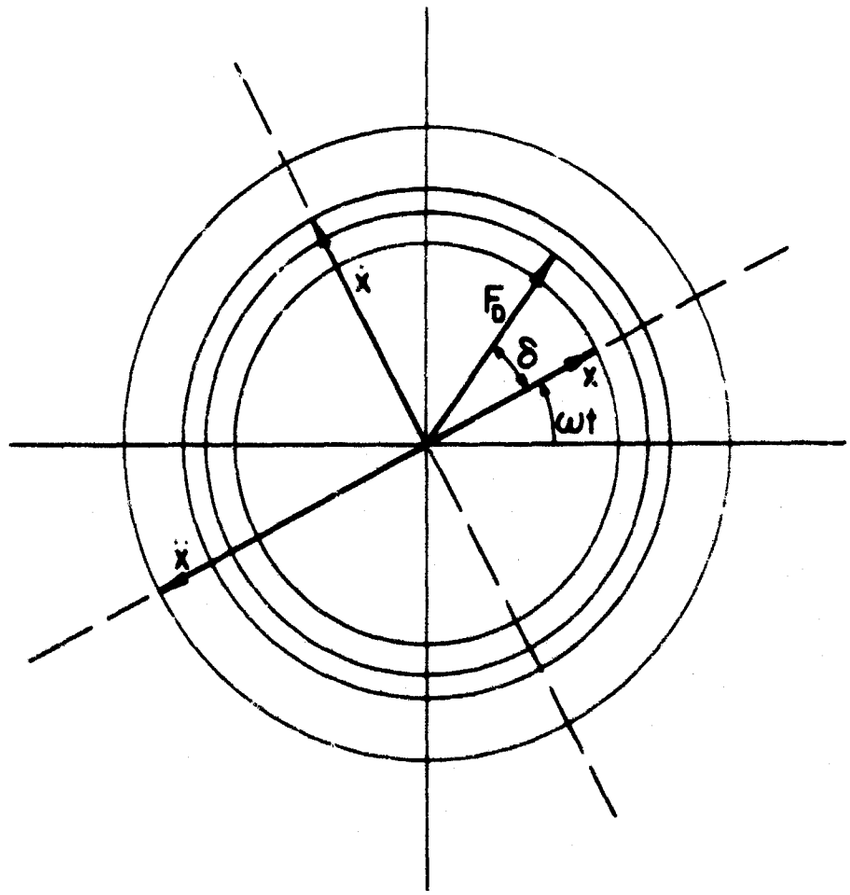


Fig. 1 Phase Diagram: Kinematic Parameters and Force

For a foundation system of mass, m, the inertial term $m\ddot{x}$ is a force whose direction is opposite to that of the acceleration vector. Consideration of the soil as a viscoelastic material allows the soil resisting force to be divided into two component forces--a dissipation or damping force of amplitude R_1 and a restoring force of amplitude R_2. The restoring force vector R_2 is opposite to that of the displacement and the dissipation force vector R_1 is in the opposite direction to the velocity. Since the response is considered to be harmonic, the force system can be represented in phase diagram form as given in Figure 2 for the situation in which the forcing function F_d leads the displacement function by the phase angle δ. By resolving the forcing function into two components perpendicular and parallel to the

displacement vector and then applying the equilibrium conditions at an instant of time, one obtains the following relations for the dissipation and restoring force amplitudes, respectively;

$$R_1 = F_D \sin \delta \tag{2}$$

$$R_2 = m\ddot{x} + F_D \cos \delta \tag{3}$$

The same relations can be obtained directly from the equation of motion for $\omega t = 0$ and $\omega t = \pi/2$.

By analogy with conventional static loading, one may consider the amount of displacement of the footing to be a function of the amount of force transmitted to the cohesive soil supporting the footing. This transmitted force, F_T, is made up of the two components R_1 and R_2, as indicated in Figure 2; that is, the transmitted force is the vector sum of the force transmitted through the dissipation mechanism or damper and the force transmitted through the restoring mechanism. The amplitude or modulus of the transmitted force vector is denoted as F_T. Figure 3 is a vector force polygon for the response given in Figure 2. All force vectors are shown in Figure 3. However, F_T is equivalent to the vector sum of R_1 and R_2 and can be combined with the applied force amplitude, F_D, and the inertial force amplitude to form a force triangle. From Newton's second law, the resultant of all the external forces acting on the footing system must be exactly equal to the product of the mass and acceleration with the direction of the acceleration. Thus, the external resultant force vector cannot have a component normal to the acceleration vector. This leads to the relation

$$F_T \sin \alpha = F_D \sin \delta \tag{4}$$

and the transmitted force amplitude is

$$F_T = F_D \frac{\sin \delta}{\sin \alpha} \tag{5}$$

As indicated in Figure 3,

$$\alpha = \tan^{-1} \left[\frac{R_1}{R_2} \right] \tag{6}$$

Substitution of Equations 2 and 3 into Equation 6 gives

$$\alpha = \tan^{-1} \left[\frac{F_D \sin \delta}{m\ddot{x} + F_D \cos \delta} \right] \tag{7}$$

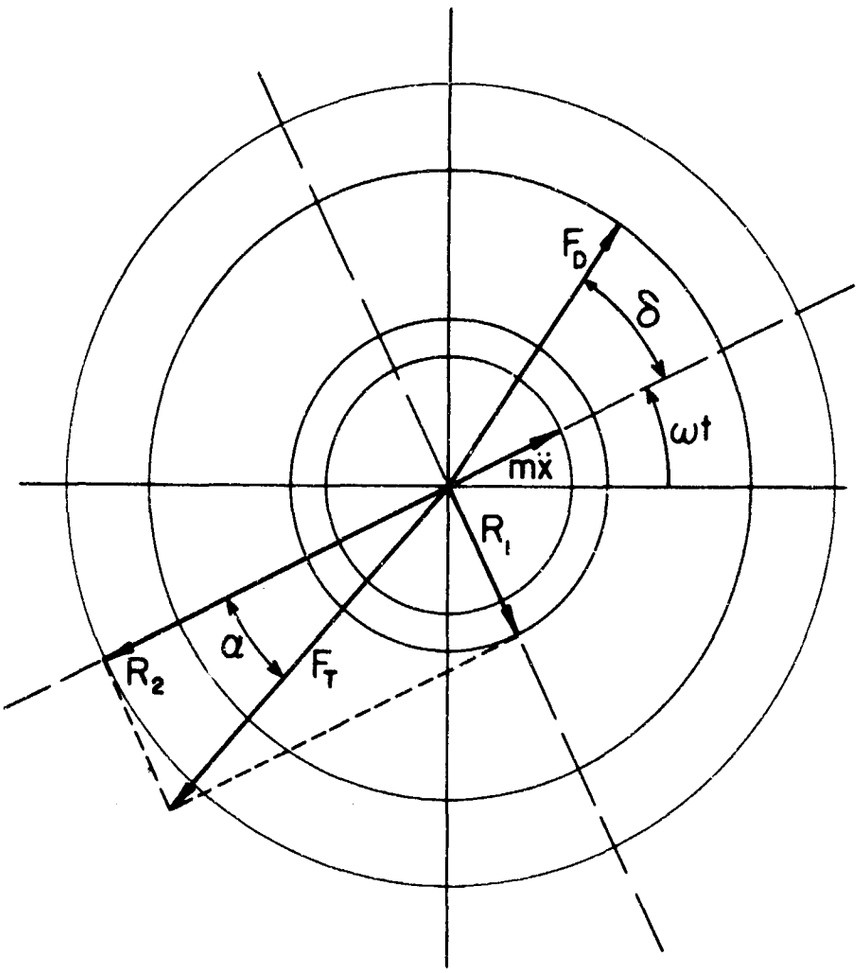


Fig. 2 Phase Diagram: Force Parameters

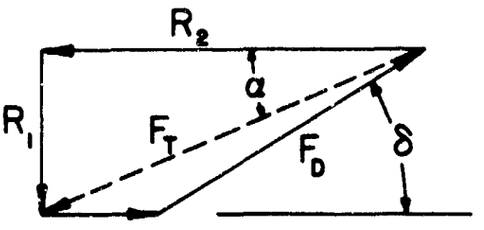


Fig. 3 Force Vector Polygon

The value of $\sin \alpha$ can be conveniently obtained from a table of the values of the trigonometric functions.

The transmission factor, (T.F.), is the ratio of the transmitted force to applied force and can be written as

$$(T.F.) = \frac{F_T}{F_D} = \frac{\sin \delta}{\sin \alpha} \tag{8}$$

and the transmitted force amplitude can be written

$$F_T = F_D\ (T.F.) \tag{9}$$

Dividing the transmitted force amplitude by the cross-sectional area of the footing gives the dynamic stress amplitude transmitted to the supporting soil as

$$\sigma_{DT} = \frac{F_D\ (T.F.)}{A} \tag{10}$$

It is interesting to note that the transmission factor is both non-dimensional and a measure of the energy dissipation parameter of the system.

A convenient form of expressing the physical phenomena in terms of a finite number of physical quantities can be obtained using dimensional analysis. The functional relationship obtained can be written

$$\frac{x}{d} = \psi\left[\frac{\sigma_{DT}}{q}, \frac{\sigma_s}{q}, (T.F.), \frac{\omega}{p}\right] \tag{11}$$

where d is the footing diameter, σ_s is the static stress, p is the natural frequency of the system, and q is a restoration parameter of the soil system. The explicit form of the functional relation may be investigated experimentally.

ANALYSIS OF EXPERIMENTAL RESULTS

The author has been involved in the analysis of the results of a number of prototype footing tests conducted using vertical sinusoidal forces generated by the centrifugal force due to a rotating eccentrically mounted mass. The test results analyzed in this paper were obtained from reinforced concrete circular footings with diameters of 5 ft–2 in, 7 ft–4 in, 9 ft–0 in, and 10 ft–4 in supported on the surface of a relatively uniform silty clay. Unfortunately, extensive soil test data were not available from the test area. Available information indicates the following typical soil characteristics; average weight density of 120 lbs per cu ft, compression modulus varying with depth from approximately 10,500 psi near the surface to 22,000 psi at 29 ft, and a shear modulus ranging from approximately 4,000 psi to 8,500 psi over the same depth. Moduli were determined using seismic methods. Each footing was loaded to a static pressure of 4.25 psi with ballast symmetrically placed and secured to the footing. The static pressure included the weight of the footing, weight of the vibrator, and ballast load. The areas included were 20.97, 41.94, 62.92, and 83.89 sq ft, while the static weights included 12,820, 25,640, 38,460, and 51,280 lbs, respectively. The dynamic force amplitude applied to the footing can be written

$$F_D = M_o r \omega^2 \tag{12}$$

where M_o is the eccentrically mounted rotating mass and r is the eccentricity. For a footing test, a particular eccentricity was selected for a constant magnitude of eccentric mass and steady state conditions were obtained for various values of frequency. Four values of eccentricity or excitation level were used for each footing. Sinusoidal forces were applied for frequencies ranging from approximately 6 cps to 30 cps, subject to the limitations of the vibrator. This corresponds to force amplitude, F_D, ranging from approximately 525 lbs to 52,000 lbs, depending upon the magnitude of the eccentric mass, the eccentricity, and frequency of oscillation. All footings were carefully instrumented with various configurations of transducers and pick-ups for both test control and displacement measurement. Special instrumentation was used to measure the phase angle, δ, between the applied force and the footing displacement. Thus, for each frequency of oscillation, the force amplitude, vertical displacement amplitude, and phase angle between force and displacement were obtained.

Dividing Equation 12 by the cross-sectional area of the footing gives the applied dynamic stress σ_D. Figure 4 is a typical plot of applied dynamic stress as a function of frequency. A typical displacement amplitude–frequency response with four levels of excitation is given in Figure 5 for a footing diameter of 9 ft–0 in. The total weight of the footing system is 19.23 tons and corresponds to a static stress of 4.25 psi.

The dissipation and restoration force amplitudes corresponding to the response of Figure 5 can be calculated with Equations 2 and 3 using the measured phase angles associated with particular values of frequency. The corresponding values of the angle α and transmission factor (T.F.) can be determined using Equations 6 and 8, respectively. Dynamic stress amplitudes transmitted to the supporting soil were determined using Equation 10 and are presented in Figure 6 as a function of frequency. Comparison of Figures 4 and 6 indicate that although the applied dynamic stress continually increases as the square of the frequency, the energy dissipation of the cohesive soil-foundation system causes the transmitted dynamic stress to tend to level off at increased values of frequency. It is interesting to note that the values of σ_{DT} were determined using phase angles and not displacement amplitudes. Thus, comparison of Figures 5 and 6 indicate that one may consider that the values of the displacement amplitudes are primarily functions of the dynamic stresses σ_{DT} felt by the cohesive soil.

Since all of the footings were supported on the same cohesive soil, the restoration parameter of the soil may be considered a constant. Thus, the non-dimensional parameter $\sigma_{DT/q}$ is proportional to σ_{DT}, the dynamic stress amplitude transmitted, while $\sigma_{s/q}$ is proportional to the static stress level (4.25 psi) about which the dynamic load perturbations take place. Lumping the transmission factor and x/d together simplifies Equation II. Figure 7 is a plot of σ_{DT} versus x/d (T.F.) for footing diameters of 7 ft-4 in, 9 ft-0 in, and 10 ft-4 in, constant excitation of $M_o r$ equal 0.368 lbs per sq sec and a constant static stress of 4.25 psi. This corresponds to total weights of 12.82 tons, 19.21 tons and 25.64 tons. Normalizing the displacement amplitudes by the footing diameter apparently accounts for the effect of the size of footing on the dynamic response. Figure 7 also tends to indicate that the inertial forces of the system take into account variations in total weight for a constant level of static stress. The correlations are good for displacements at frequencies less than resonance while the maximum deviations occur at high frequencies where the phase angle measurements are less reliable with variations in ω. Figure 8 gives the variation of σ_{DT} as a function of x/d (T.F.) for footing diameters ranging from 5 ft-2 in to 10 ft-4 in, total weights from 6.41 tons to 25.64 tons, and excitation levels ranging from 0.368 to 1.470 lbs per sq sec. No phenomenological pattern of size, total mass, or excitation level is apparent.

Since the resonant amplitudes are the critical displacement values, it is interesting to examine the resonant response of the systems tested. Figure 9 is analogous to a conventional static type of stress-deflection plot for the footings tested. In this case, the stress considered is the resonant dynamic stress amplitude transmitted to the supporting cohesive soil and the deflection used is the resonant amplitude of footing displacement, Δ. The response given in Figure 9 is similar to that obtained from conventional static loadings; namely, for a constant value of transmitted dynamic stress amplitude the deflection amplitude is larger for the larger size footing. The results of the single test for the 5 ft-2 in diameter footing do not fit in with the trends of the other 12 tests. However, the reliability of the test on the small footing is highly questionable because of improper functioning of the phase angle instrumentation, leading to doubtful values of the phase angles for this particular test. Thus, one must question the reliability of that particular point on Figure 9.

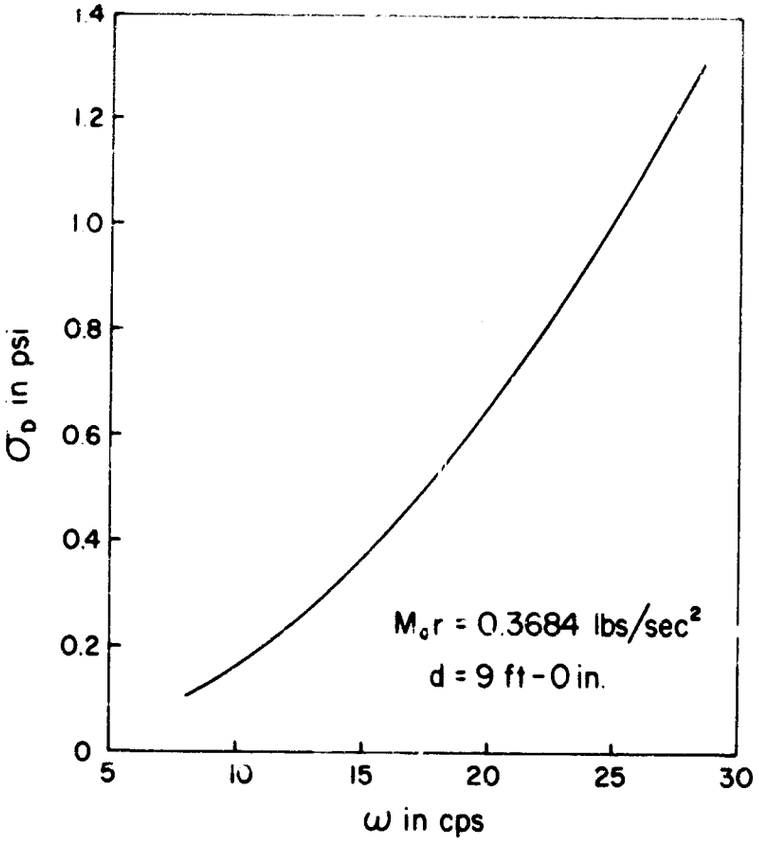


Fig. 4 Applied Dynamic Stress Amplitude vs Frequency

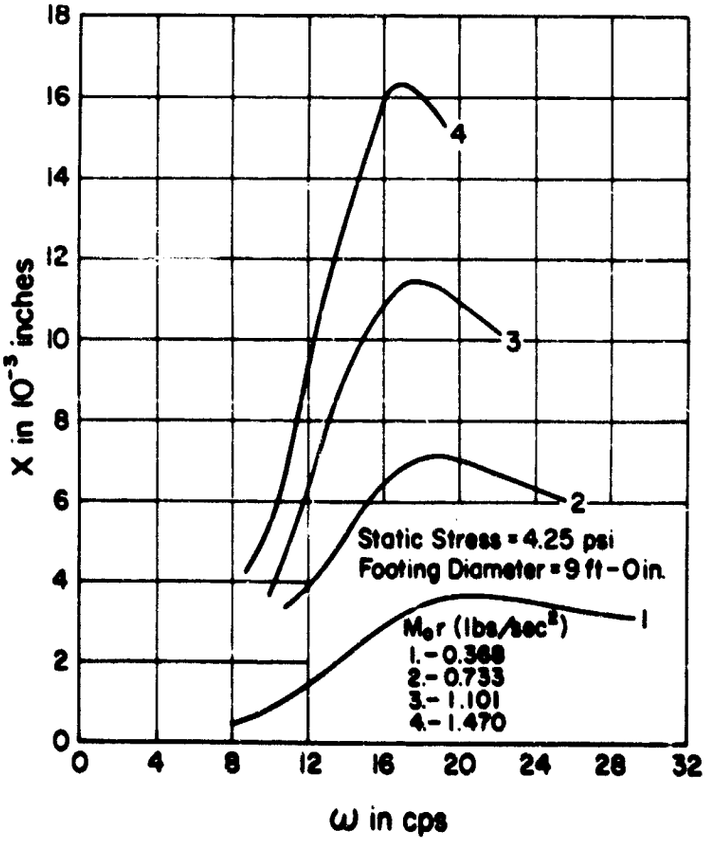


Fig. 5 Displacement Amplitude vs Frequency: Different Excitation Levels

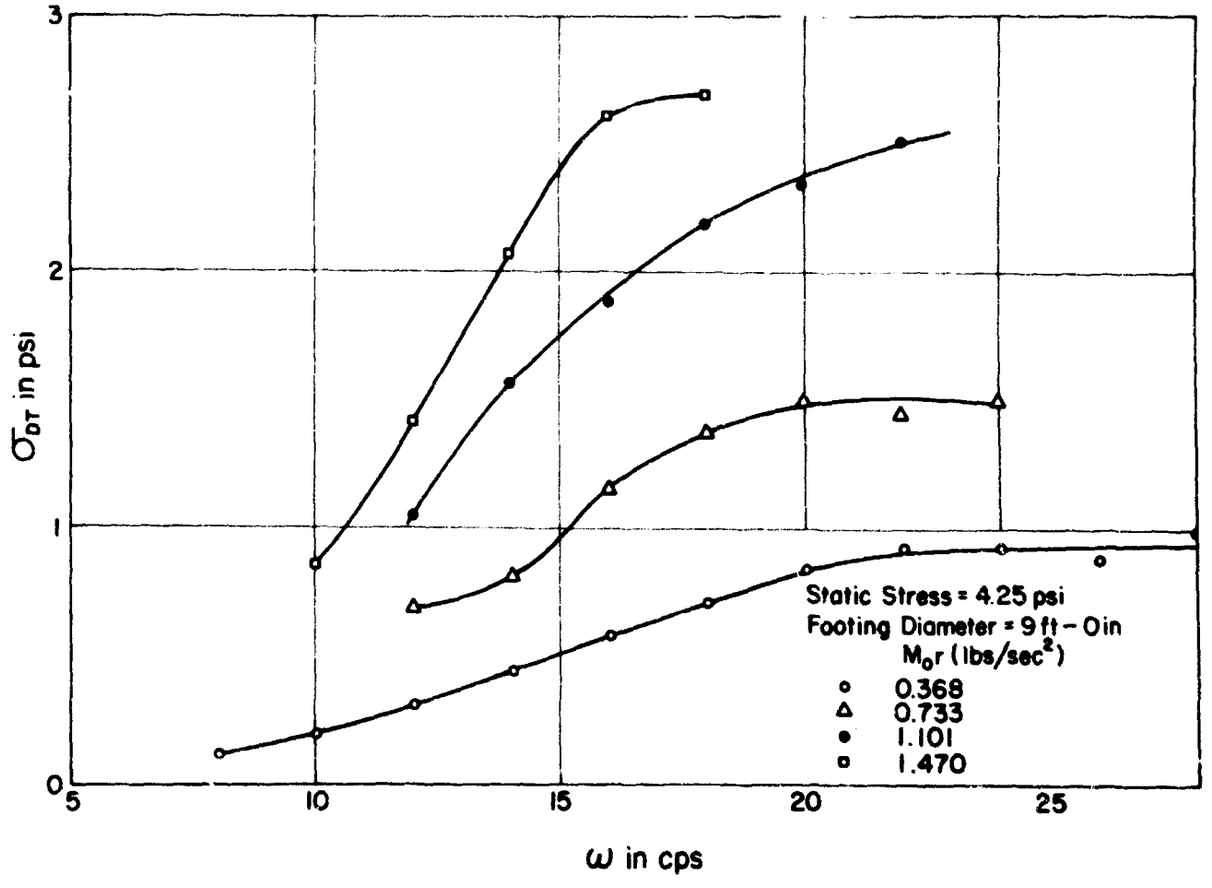


Fig. 6 Transmitted Dynamic Stress Amplitude versus Frequency

Figure 10 is a plot of the non-dimensional resonant amplitude parameter, $\Delta/d\,(T.F.)$, as a function of σ_{DT}. The response of the three large footings given in Figure 9 seem to collapse in a single band or curve in Figure 10 with no apparent phenomenological order. The advantage of the non-dimensional formulation is quite apparent. Since σ_{DT} is proportional to $\sigma_{DT/q}$, Figure 10 is essentially a plot of $\sigma_{DT/q}$ versus $\Delta/d\,(T.F.)$ for a normalized value of σ_s. The value of the resonant transmission factor, $(T.F.)_r$, varies from 1.03 to 1.40.

Consideration of the resonant response ($\omega/p = 1$) for σ_s = 4.25 psi leads to a simplification of Equation 11 to the form

$$\frac{\Delta}{d\,(T.F.)} = \Psi\left[\frac{\sigma_{DT}}{q}\right] \tag{13}$$

Equation 13 also can be rearranged so that $\sigma_{DT/q}$ is the dependent variable. Assuming a normalized value of q = 1, one can express the resonant response graphically by plotting log (σ_{DT}) versus log $\left[\Delta/d\,(T.F.)\right]$ as given in Figure 11. Approximation of the response in Figure 11 with a straight line leads to an expression of the form

$$\sigma_{DT} = B\left[\frac{\Delta}{d\,(T.F.)}\right]^C \tag{14}$$

where B is the intercept and C is the slope of the straight line. The particular values of B and C would seem to be functions of the particular cohesive soil-mass system. Thus, σ_{DT} can be expressed in terms of the resonant displacement amplitude as given by Equation 14 or in terms of the size and mass of the footing as well as the dissipation of the system, as obtained from Equations 7, 8, and 10.

In order to use the results given in Figures 10 and 11 or Equation 14 for a particular vibratory loading on a footing with the static stress level considered and supported on the cohesive soil tested, it is necessary to know the value of the resonant transmission factor in order to calculate the values of σ_{DT} as well as the deflection parameter. However, the resonant transmission factor is a function of the soil-foundation system and the manner of loading.

From the conventional analysis of the forced vibration of a linear damped spring-mass system, it can be shown that the resonant value of the transmission factor can be written

$$\left[T.F.\right]_{-1} = \sqrt{1 + \left[\frac{\Delta}{\epsilon}\right]^2} \qquad (15)$$

where ϵ is the eccentricity factor defined as

$$\epsilon = \frac{M_o r}{M} \qquad (16)$$

with M_o the eccentric mass, r the eccentricity, and M the total mass of the footing-structure system. Since Δ is an expression of the influence of the soil-foundation system and ϵ relates to the footing-loading system, Equation 15 may be related to the actual resonant transmission factor associated with the prototype dynamic soil-foundation system. Comparison of the resonant transmission factors determined by Equations 8 and 15 indicate that those determined by Equation 15 are approximately 89 percent higher than those given by Equation 8. The values determined with Equation 15 range from 1.28 to 1.74 while those determined by Equation 8 range from 1.03 to 1.40. If the resonant transmission factors calculated with Equation 15 are used in Equation 10 to determine the transmitted dynamic stress amplitudes, σ_{DT}, the results given in Figure 12 are obtained. Approximation of the results of Figure 12 with a straight line representation leads to an equation of the form of Equation 14 with different values of the coefficients B and C. In Figure 12, the response of the 5 ft-2 in diameter footing is more compatible with the results of the other footing tests. This would seem to indicate the phase angle measurements for the small footing were indeed in error.

For the prototype study conducted, the response can be represented by Figure 12 and Equation 15. It can also be represented by Figures 10 and 11 or Equation 14 along with the values of (T.F.) determined from the phase angle response of the soil-foundation system.

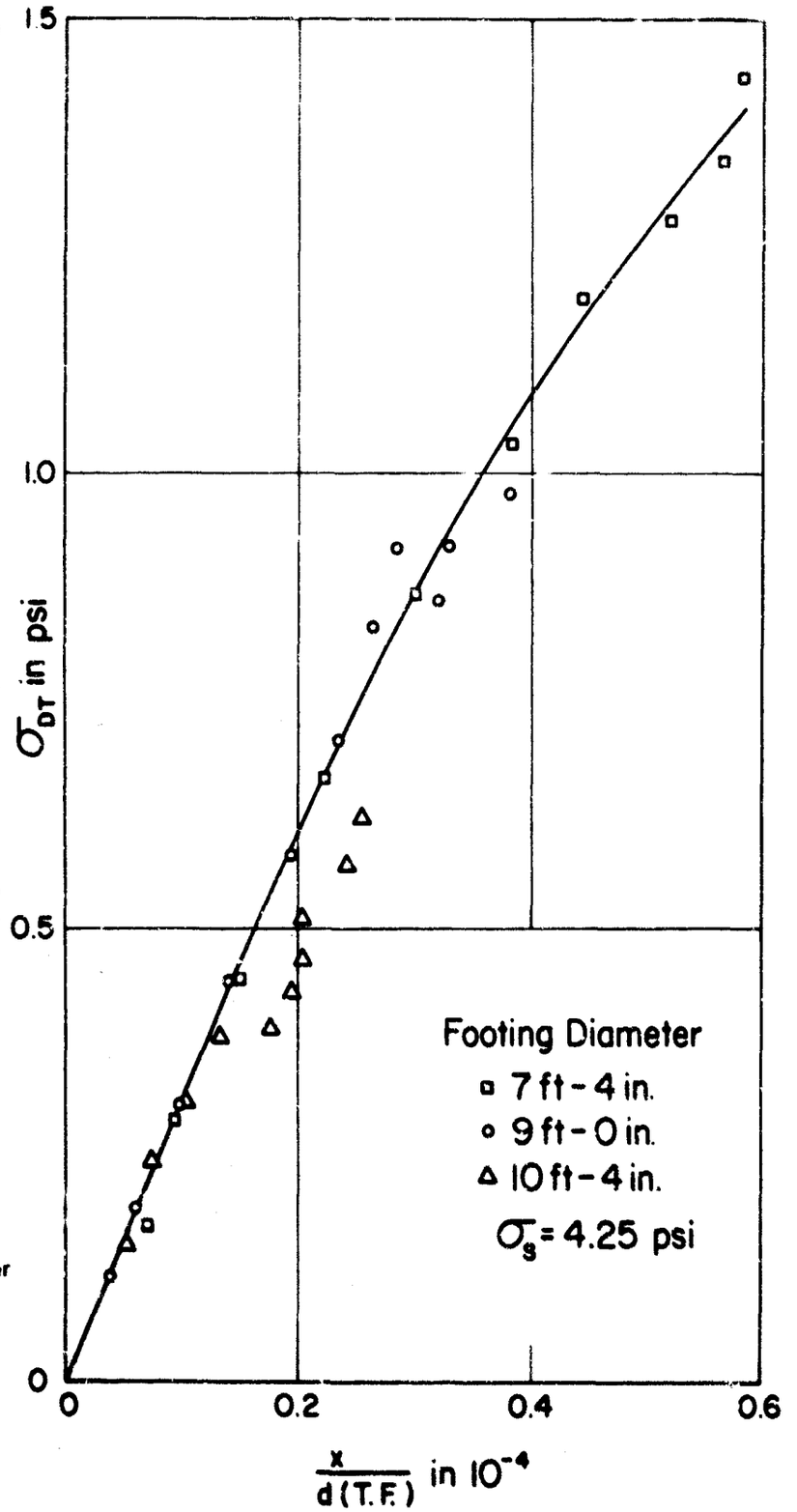


Fig. 7 Transmitted Dynamic Stress vs Dimensionless Displacement Parameter: Constant Excitation Level

It is felt that these analyses and representations shed insight on the estimation of dynamic force or stress transmission to the supporting cohesive soil as well as the displacement response associated with transmitted stresses due to cohesive soil-foundation interaction under dynamic loading. The effects of footing size and total mass are included; however, the possible effects of the static stress level are not necessarily included as the static stress was maintained constant for the present study. Additional aspects such as the effects of resonant frequency, static stress level, and response at frequencies other than resonance remain to be investigated.

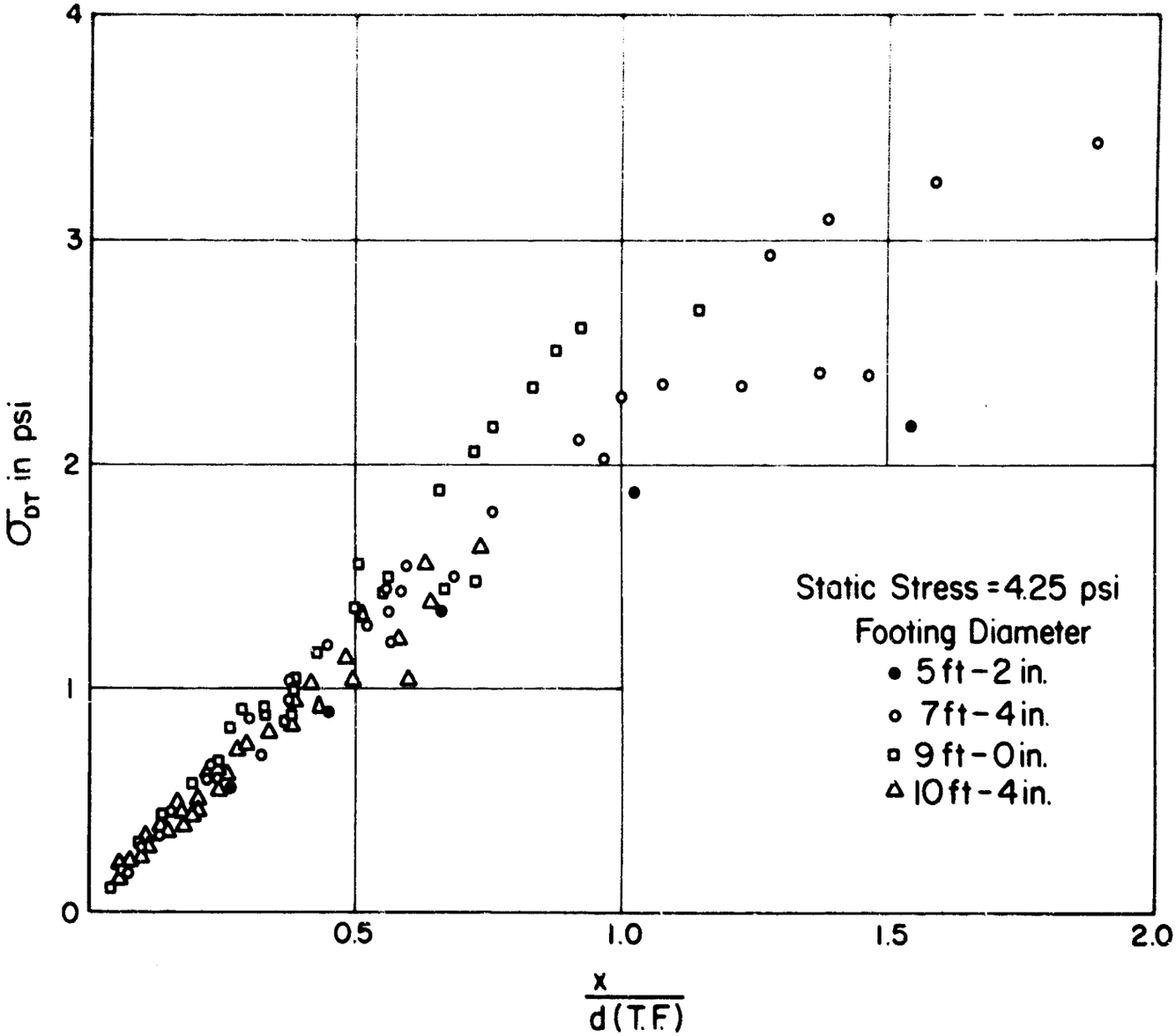


Fig. 8 Transmitted Dynamic Stress vs Dimensionless Displacement Parameter: Different Diameters and Excitation Levels

Work is currently being conducted to develop laboratory test techniques to determine the energy storage and energy dissipation properties of cohesive soil specimens, with the hope that these properties can be used in theoretical solutions to estimate transmission factors and, hence, dynamic stress transmission due to soil-structure interaction.

CONCLUSIONS

The influence of footing size and mass on the dynamic force or stress transmission due to cohesive soil-foundation interaction is presented for the particular situation of bibratory loading. The methods of dimensional analysis in conjunction with kinematic and force parameters in phase diagram form are shown to be useful in analyzing and formulating dynamic stress transmission-deflection response. The results of prototype tests were analyzed for reinforced concrete, circular footings with diameters ranging from 5 ft-2 in to 10 ft-4 in, total weights of the foundation system ranging from 6.41 tons to 25.64 tons, and applied dynamic force amplitudes varying from approximately 0.26 ons to 26 tons. The static stress level about which the dynamic stress perturbations were applied was maintained constant at 4.25 psi. Although the response is nonlinear, the dynamic stress amplitude transmitted to the supporting cohesive soil is related to the displacement, x, by a power relation. This is expressed in terms of a non-dimensional displacement amplitude parameter, x/d, which conveniently accounts for the effects of footing diameter, d, as well as the transmission factor, (T.F.), of the soil-foundation system. The dynamic stress transmission is given in both graphic and analytic forms. The analysis and results contained herein may provide insight on the dynamic force or stress transmission to supporting cohesive soils as well as the associated displacement consequences of such transmission due to soil-structure interaction under dynamic loading.

ACKNOWLEDGEMENT

The author is indebted to the U. S. Army Engineers, Waterways Experiment Station, Vicksburg, Mississippi, for their support of the analysis presented in this paper. However, the results of the analysis do not necessarily represent the views of the sponsoring agency.

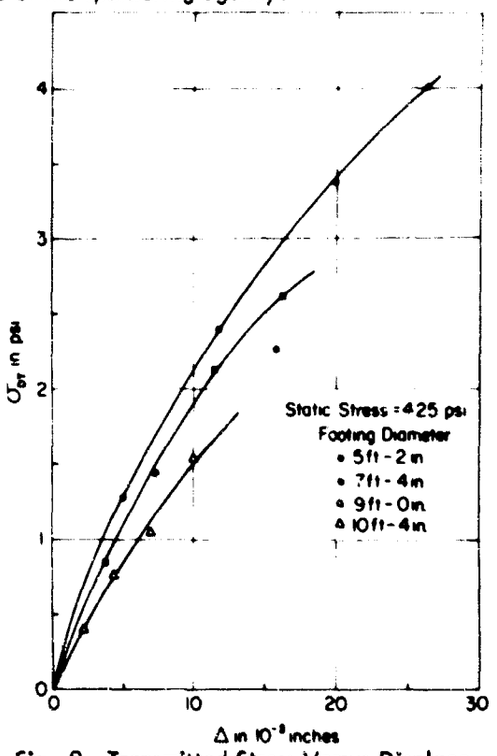


Fig. 9 Transmitted Stress Versus Displacement: Resonant Amplitude Response

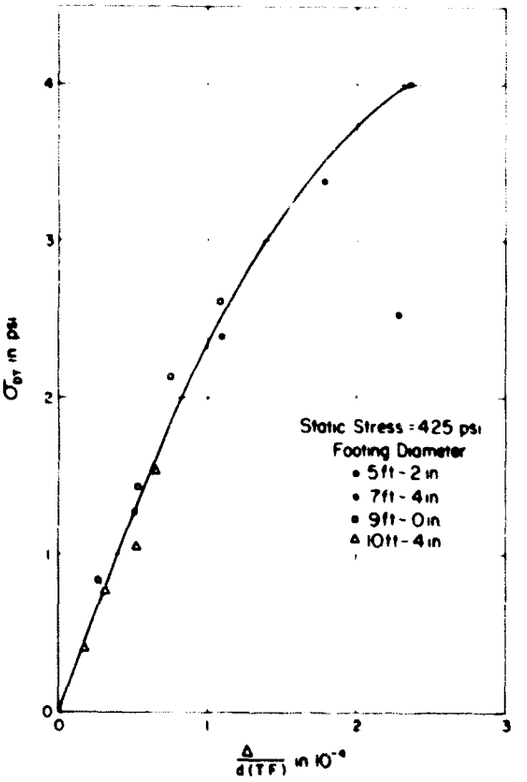


Fig. 10 Transmitted Stress Versus Dimenionless Displacement Parameter: Resonant Amplitude Response

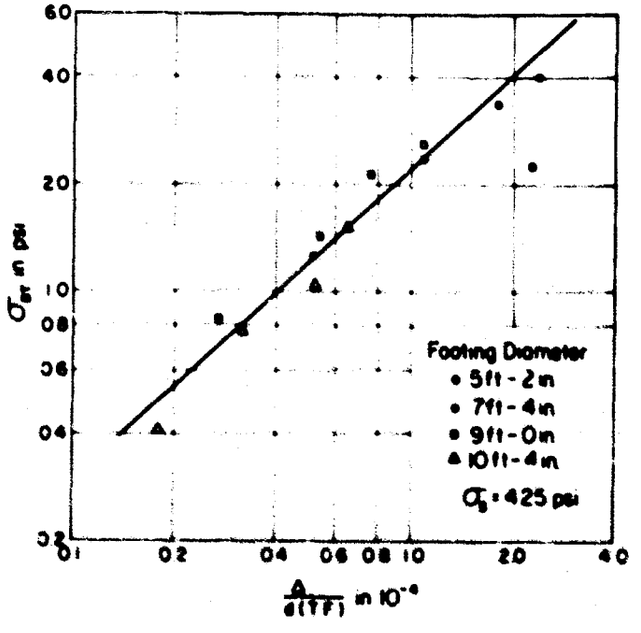


Fig. 11 Resonant Amplitude Response: Measured Phase Angles

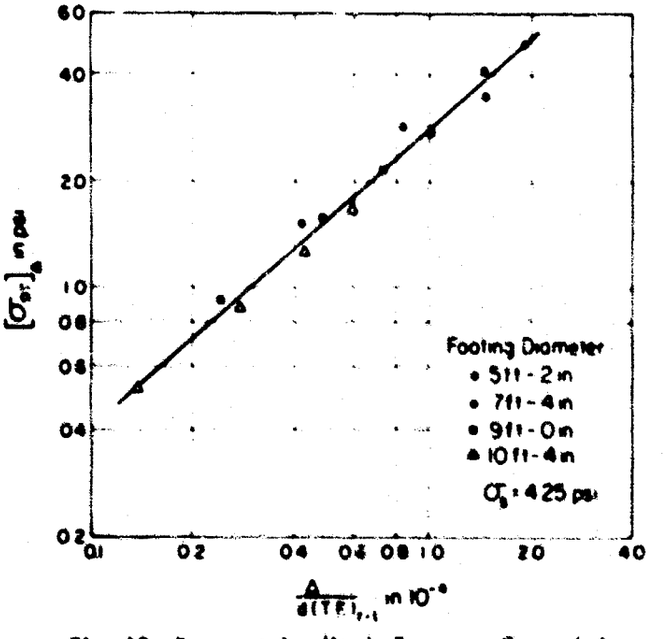


Fig. 12 Resonant Amplitude Response: Transmission Factor from Amplitude and Excitation

THE THEORY OF LIMITING EQUILIBRIUM FOR AXISYMMETRIC PROBLEMS: A COMPARISON WITH EXPERIMENT ON SILO SKIN FRICTION

by
C. J. Costantino* and A. Longinow**

ABSTRACT

The theory of limiting equilibrium is used to obtain theoretical predictions of skin friction developed along vertical cylindrical silos embedded in soil which is subjected to a uniform static surface overpressure. Comparison of the results is made with experiments conducted in an Ottawa sand subjected to surface overpressures up to 100 psi. It is found that reasonable agreement between theory and experiment is obtained for tests conducted in dense sands where passive type shear failures are obtained. The results of the tests in loose sands do not corroborate the theory, as would be anticipated based upon volume change effects accompanying shearing action. Both the analytic and experimental results indicate that the developed skin friction forces are significantly higher than those usually taken into account by current design methods.

INTRODUCTION

A major problem encountered in the design of underground structures, both conventional and protective, has been the determination of the loads transmitted by or through the soil. The uncertainties involved in this area have developed due to the incomplete understanding of the response of soil to load, both static and dynamic, as well as the influence of structural flexibility on load distribution (arching effects).

Various theories have been evolved in an attempt to approximate soil behavior, it being possible to categorize these into two separate groups. The first group is concerned with stress states wherein a small change in magnitude of the applied forces does not violate equilibrium of the system. Into this category fall the various consolidation theories for cohesive soils, as well as the solutions based upon the theories of elasticity and viscoelasticity.

The second category of analysis is concerned with stress states wherein a small change in the applied loads will cause a loss of equilibrium (stability type problems). This group includes the studies of earth pressures on retaining walls, ultimate resistance of foundations, the various methods of trial failure (or slip) surfaces, and, an approach becoming widely known of late, the theory of limiting equilibrium.

This latter theory attempts to develop a more rigorous approach to the problem of critical equilibrium than has heretofore been used in the field of soil mechanics. An extensive exposition of the theory can be found in the text by Sokolovski (1), in which he deals exclusively with the plane-strain problem, although many other studies have appeared in the open literature (2,3,4,5,6) concerning this problem. Very few solutions, however, may be found concerning the axisymmetric problem, the principal contribution in this area being made by Berezantsev (7).

The application of this theory of limiting equilibrium to practical problems eventually depends upon the success with which experimental results check the theoretical conclusions and determine the limits of its applicability. The purpose of this study, therefore, has been to compare experimental results for a particular problem with the theoretical predictions obtained by the theory of limiting equilibrium.

VERTICAL SILO SKIN FRICTION STUDIES

One problem encountered in the design of hardened silos is the determination of the axial load transmitted to the silo through skin friction developed between the soil and the structure. This loading is caused by differential vertical displacements (Figure 1) of the structure and the soil due to a passing surface air shock wave.

To investigate this problem, a series of static tests were performed on small scale silo models. These cylindrical models were embedded in the soil (Figure 2) and relative motion between the soil and model was induced by pushing the models upward through the soil until failure occurred. For these tests (termed push-out tests), a range of static surface overpressures up to 100 psi was applied to the soil prior to application of the push-out thrust.

Four models made of steel tubing were used with length-diameter ratios of 1.0, 3.58, 7.16, and 16.6. The lateral surface of each silo model was roughened by cutting 20 V-grooves per inch (1/32 in. deep) to assure that failure

* Research Engineer, IIT Research Institute, Chicago, Illinois.
** Assistant Engineer, IIT Research Institute, Chicago, Illinois.

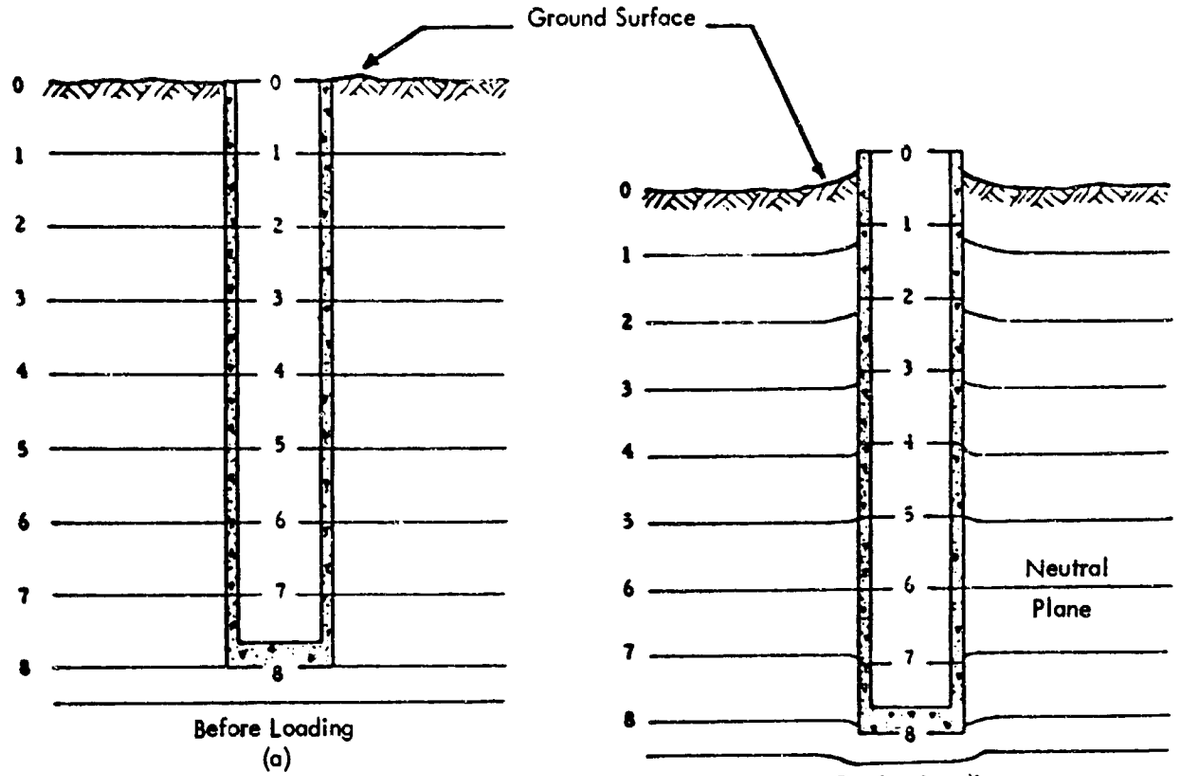


Fig. 1 Silo-Skin Friction Development

would occur within the soil. In all tests, a granular soil (Standard Ottawa sand) was used, with tests being conducted at both a low (9 percent) relative density and a high (100 percent) relative density.

A grain size curve for the sand is shown in Figure 3. Details of the test procedure and fixtures are contained in the Appendix to this report.

ANALYTICAL STUDY

To further investigate this problem an analytic solution for the push-out test was obtained using the theory of limiting equilibrium. The aim of this approach is naturally to determine, by comparison with experimental results, the regions of its applicability, if any, so as to allow its use for more general skin friction problems of interest. We describe in the following poragraphs this analytic solution.

EQUATIONS OF AXISYMMETRIC EQUILIBIRUM

The positive stress state is defined in Figure 4 for the axisymmetric case. The two equations of equilibrium become (7)

$$\frac{\partial \sigma_r}{\partial r} + \frac{\partial \tau_{rz}}{\partial z} + \frac{\sigma_r - \sigma_\theta}{r} = 0$$

$$\frac{\partial \sigma_z}{\partial z} + \frac{\partial \tau_{rz}}{\partial r} + \frac{\tau_{rz}}{r} = \gamma \qquad (1)$$

From the conditions of the problem, it follows that σ_θ is a principal stress.

CONDITIONS OF LIMITING EQUILIBRIUM

From the Mohr failure theory (8), the maximum shear stress that a soil can sustain a given plane is given by

$$|\tau_n| = c + \sigma_n \tan \phi \qquad (2)$$

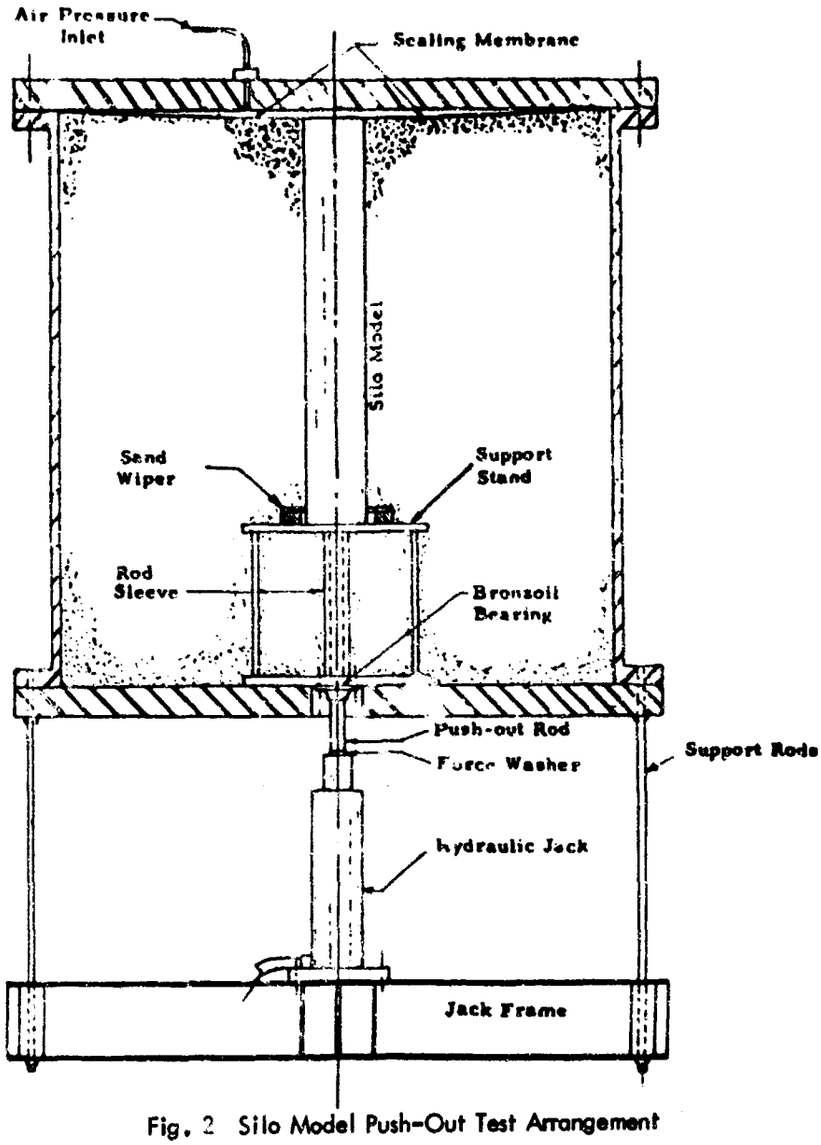


Fig. 2 Silo Model Push-Out Test Arrangement

where τ_n is the shear strength of the soil along the plane with normal n, c is the cohesion, ϕ, is the angle of internal friction, and σ_n is the normal stress on the plane. Written in terms of the principal stresses, Equation 2 becomes

$$c = \frac{\sigma_1 - \sigma_3}{2\cos\phi} - \frac{\sigma_1 + \sigma_3}{2}\tan\phi \qquad (3)$$

where σ_1 and σ_3 are the maximum and minimum principal stresses, respectively. In addition it is assumed that either

$$\sigma_\theta = \sigma_2 = \sigma_3 \qquad \text{or} \qquad \sigma_\theta = \sigma_2 = \sigma_1 \qquad (4)$$

Equations 3 and 4, therefore, make up the two equations of limiting equilibrium. It is assumed by these equations that in the "critical" zone failure is impending and that the maximum shear strength of the soil is being developed throughout the zone. In this zone, it is possible to construct surfaces whose tangent planes at every point coincide with the corresponding slip planes. Such surfaces form a system of two curvilinear families and are called "slip surfaces."

The assumptions of limiting equilibrium (Equations 3 and 4) make the problem statically determinate in that the stress distribution within the critical zone can be determined from the given stress boundary conditions. Using the substitutions

$$\sigma = \frac{1}{2}\,\frac{\sigma_1 - \sigma_3}{\sin\phi} \qquad (5)$$

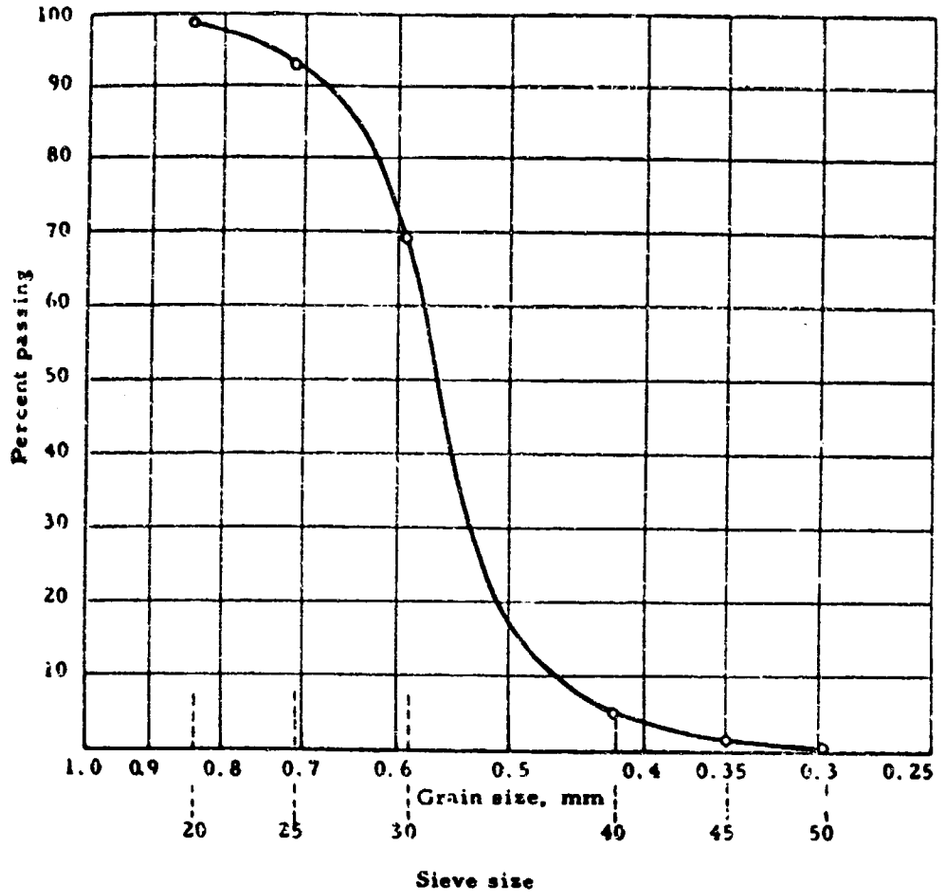


Fig. 3 Grain Size Distribution, Ottawa Sand

$$\zeta = \frac{\cot \phi}{2} \log \sigma/\bar{\sigma} + \alpha \tag{6}$$

$$\eta = \frac{\cot \phi}{2} \log \sigma/\bar{\sigma} - \alpha \tag{7}$$

$$\mu = \frac{\pi}{4} - \frac{\phi}{2} \tag{8}$$

α = inclination of σ_1 with respect to the OR axis

$\bar{\sigma}$ = any convenient measure of stress

the equilibrium equations become

$$\frac{d\zeta}{d\beta_1} = f_1 \frac{dr}{d\beta_1} \quad (a) \qquad \frac{d\eta}{d\beta_2} = f_2 \frac{dr}{d\beta_2} \quad (b) \tag{9}$$

where

$$f_1 = \frac{\gamma}{2\sigma} \frac{\cos(\alpha - \mu)}{\cos(\alpha + \mu)\sin\phi} - \frac{1}{2r} \frac{\sin(\alpha + \mu) \mp \sin(\alpha - \mu)}{\cos(\alpha + \mu)}$$

$$f_2 = -\frac{\gamma}{2\sigma} \frac{\cos(\alpha + \mu)}{\cos(\alpha - \mu)\sin\phi} + \frac{1}{2r} \frac{\sin(\alpha - \mu) \mp \sin(\alpha + \mu)}{\cos(\alpha - \mu)} \tag{10}$$

The upper sign in Equation 10 refer to the "passive" case or movement away from the OZ axis, while the lower sign refers to the "active" case or movement toward the OZ axis. β_1 and β_2 are coordinates measured along the "slip" or characteristic lines of the critical zone which are related to the (r,z) coordinate directions through

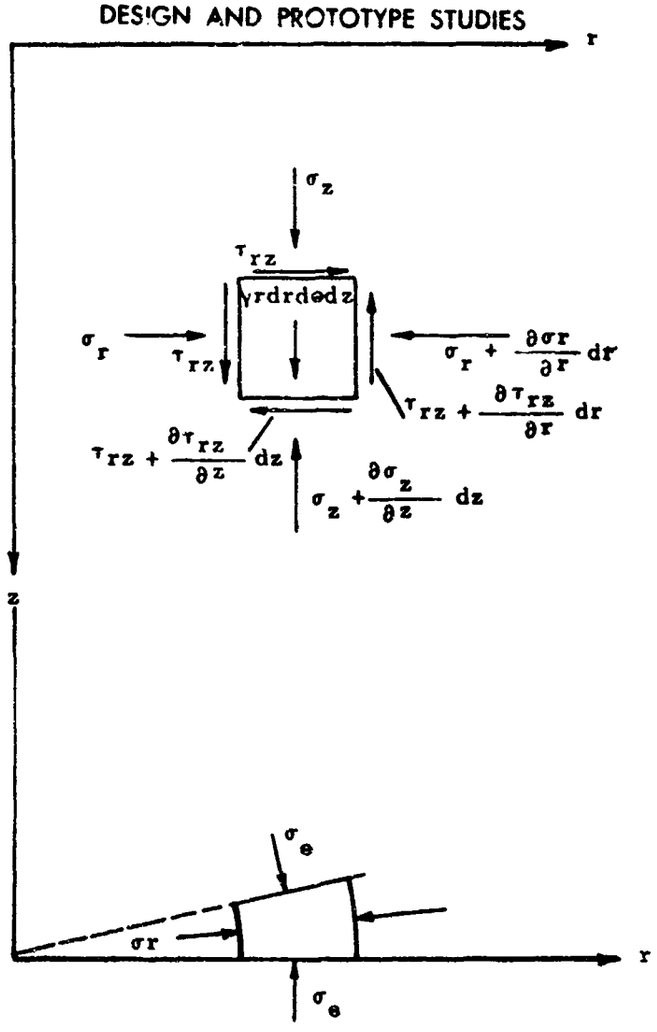


Fig. 4 Definition of Positive Stress Directions

$$\frac{dz}{d\beta_1} = \tan(\alpha + \mu)\frac{dr}{d\beta_1} \quad (a)$$

$$\frac{dz}{d\beta_2} = \tan(\alpha - \mu)\frac{dr}{d\beta_2} \quad (b) \qquad (11)$$

Equations 9, 10 and 11 allow for solution for a particular problem together with the required stress boundary conditions.

For the push-out test (see Figure 5), the cylindrical surface AC becomes a slide surface when the force F becomes large enough to overcome the developed shear stresses between the cylinder and the soil. In addition, if the angle of wall friction is equal to the angle of internal friction of the soil, the cylindrical surface becomes a characteristic surface.

The boundary conditions for this problem are: along AB: $\alpha = 0^\circ$; $\sigma_3 = p$ (12)

along AC: $\alpha = -(45^\circ + \phi/2)$

The governing equation along AC is (Equations 9b and 11b)

$$\frac{d\eta}{dz} = \frac{f_2}{\tan(\alpha - \mu)} \qquad (13)$$

which upon substitution of the boundary condition becomes

$$\frac{d\eta_1}{dz} = \frac{\gamma \cot\phi}{2\sigma} + \frac{1 - \sin\phi}{2r_o} \qquad (14)$$

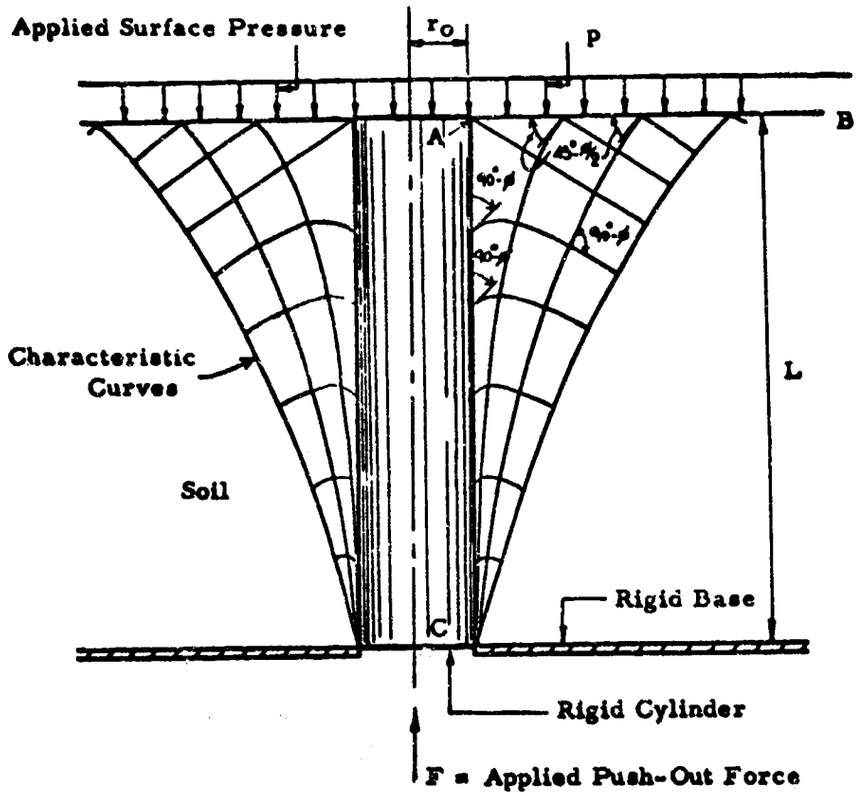


Fig. 5 Schematic Diagram Of Push-Out Test

Eliminating η from this equation by Equation 7, the equation for stress along AC becomes

$$\frac{d\sigma}{dz} = \gamma + \frac{\sigma}{r_o}\left(\frac{1-\sin\phi}{\cot\phi}\right) \tag{15}$$

The solution to this equation is

$$\sigma = \left(\sigma_o + \gamma\frac{r_o}{A}\right) e^{A\,z/r_o} - \gamma\frac{r_o}{A} \tag{16}$$

where $A = \dfrac{1-\sin\phi}{\cot\phi}$

and σ_o is the initial mean stress at point A on surface AC.

To determine σ_o, we use the boundary condition that $\eta_{AC} = \eta_{AB}$ at point A (17)

From the given conditons of the problem, a singularity exists at point A, since the stress conditions assumed along AC are not compatible with those assumed along AB.

From Equation 17 the initial condition is found to be

$$\sigma_o = p\,\frac{e^{-(\pi/2+\phi)\tan\phi}}{1-\sin\phi} \tag{18}$$

The shear stress along the wall is

$$\tau = \sigma_r \tan\phi = \sigma \sin\phi\cos\phi \tag{19}$$

and integrating along the area of the cylinder we find

$$\frac{F}{p} = 2\pi\, r_o \sin\phi\cos\phi \left\{\left(\frac{r_o}{A}\right)\left(\frac{\sigma_o}{p}+\frac{\gamma r}{pA}\right)\left(e^{A\,L/r_o}-1\right) - \frac{\gamma r_o L}{pA}\right\} \tag{20}$$

Defining the average shear stress as $\tau_{av} = \dfrac{F}{2\pi r_o L}$

we arrive at

$$\frac{\tau_{av}}{p} = \sin\phi\cos\phi\ \left(\frac{r_o}{AL}\right)\left\{\left(\frac{\sigma_o}{p} + \frac{\gamma L}{p}\left(\frac{r_o}{AL}\right)\right)\left(e^{\left(\frac{AL}{r_o}\right)} - 1\right) - \frac{\gamma L}{p}\right\} \qquad (21)$$

NUMERICAL RESULTS

Figure 6 contains a plot of the average failure skin friction as a function of length-radius ratio of the cylinder for various values of the parameters ϕ and $\gamma L/p$. From these curves, the following items may be noted:

(a) the average shear stress developed along the sides of the cylinder increases rapidly with the length-radius ratio of the cylinder;

(b) as the angle of internal friction of the soil increases, the developed skin friction increases, reaches a maximum and then decreases. The angle of friction at which this peaking occurs increases with an increase in L/r_o

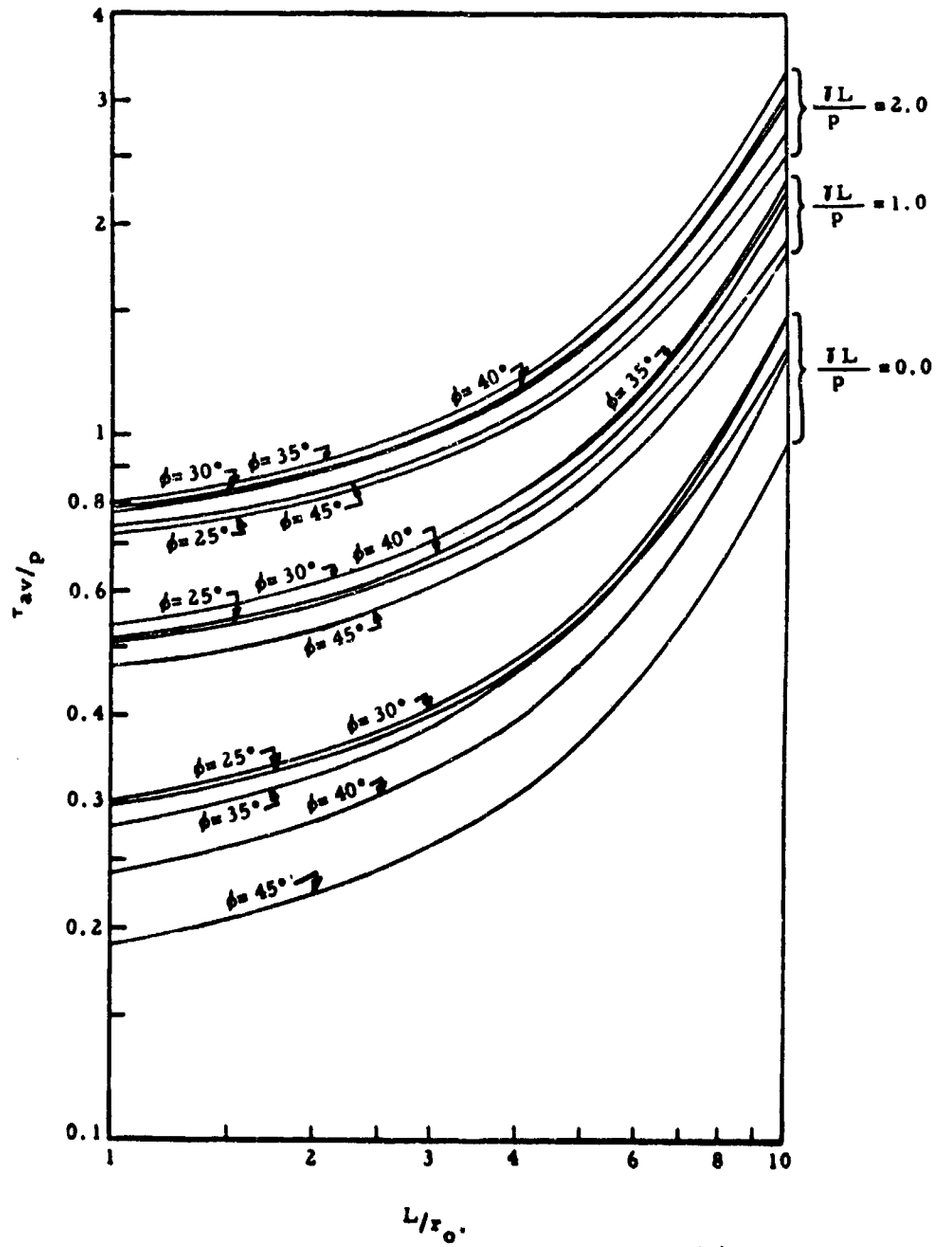


Fig. 6 Average Shear As A Function Of Length/Radius Ratio

Figure 7 contains a plot of the radial stress along the cylinder wall as a function of depth, for various values of the angle of internal friction. From these results, it may be noted that the stress increases rapidly with depth. In addition, as the soil friction angle increases, the applied radial stress decreases, at least for the depth ranges shown. At much larger depths, this is no longer true.

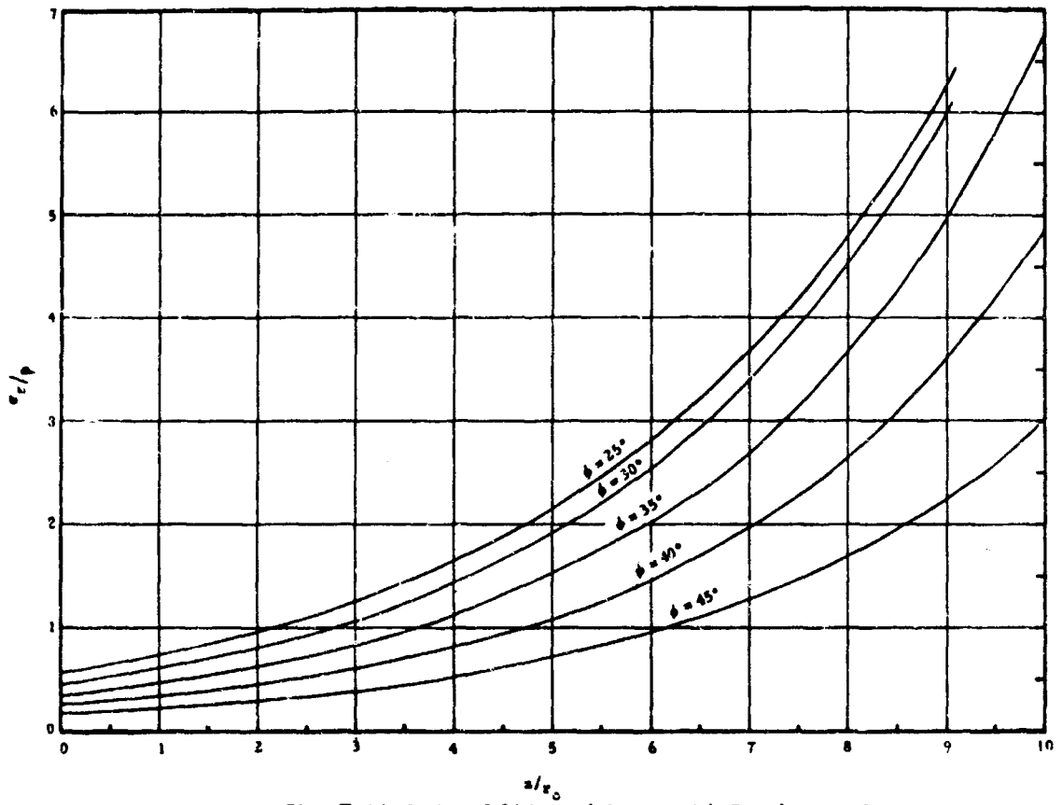


Fig. 7 Variation Of Normal Stress With Depth, $\gamma = 0$

Of more direct interest, however, is the comparison of the theoretical and experimental results, which are shown in Figure 8. The results of two series of tests are presented, one conducted in dense sand and the other in loose sand. It may be noted that for high values of L/r_o (>10) the theoretical predictions of developed shear are much higher than those found experimentally. In the lower range of L/r_o (<10), the experimental and theoretical predictions are of the same order of magnitude, at least for those tests conducted in dense sands.

The experimental results obtained from the tests conducted in loose sands are lower than the corresponding results for dense sands and are in further disagreement with the theory. An explanation of this result may be given as follows. For the soil in the dense state, a volume expansion accompanies the shearing action. This in turn induces a passive resistance of the soil to motion, corresponding to the theoretical development. In the loose state, however, this is no longer true, since a volume decrease accompanies shearing action of the soil. Further experimental work is required with low friction angle soils exhibiting dilatency during shearing to justify this statement.

CONCLUSIONS

It is felt that a powerful tool is available to investigate many foundation problems of interest to the designer. However, its application to practical problems, as with all theories, must be made judiciously, so as to ensure that the phenomena assumed in the theory at least in a gross sense approximates the behavior under actual conditions.

From the preceding results, it is felt that the following conclusions may be drawn:

(a) the radial stress along the cylinder wall is predicted by the analysis to increase exponentially with depth (Figure 7). Clearly, this result cannot be valid for the deeper depths of interest. This is also indicated by comparison with the experimental results (Figure 8). Thus, it would appear that the assumption of passive behavior of the soil is not valid over the entire length of the cylinder, at least for values of $L/r_o > 10$.

(b) It may be noted that the solution depends upon the surface overpressure applied at the edge of the cylinder only, and is independent of the surface pressure applied at other locations. This is due to the fact that the cylinder surface is taken to be a slide or characteristic surface. This would indicate that some soil moves with the cylinder and failure actually takes place at some distance away from the cylinder. This is similar to the results obtained from pile pull-out tests.

(c) In the range of interest of currently designed silos ($L/r_o < 10$), the analytic and experimental results are comparable. Current design methods use the following procedure for estimating skin friction effects. The radial stress is taken to be equal to a fraction (about 1/3) of the applied surface overpressure, and the developed shear stress to be equal to tan β times the radial stress. This leads to the design relation

$$\frac{\tau_{av}}{p} = \frac{1}{3} \tan \phi \qquad (22)$$

which by comparison with Figure 8 may significantly underestimate the skin friction forces in th[illegible]alls.

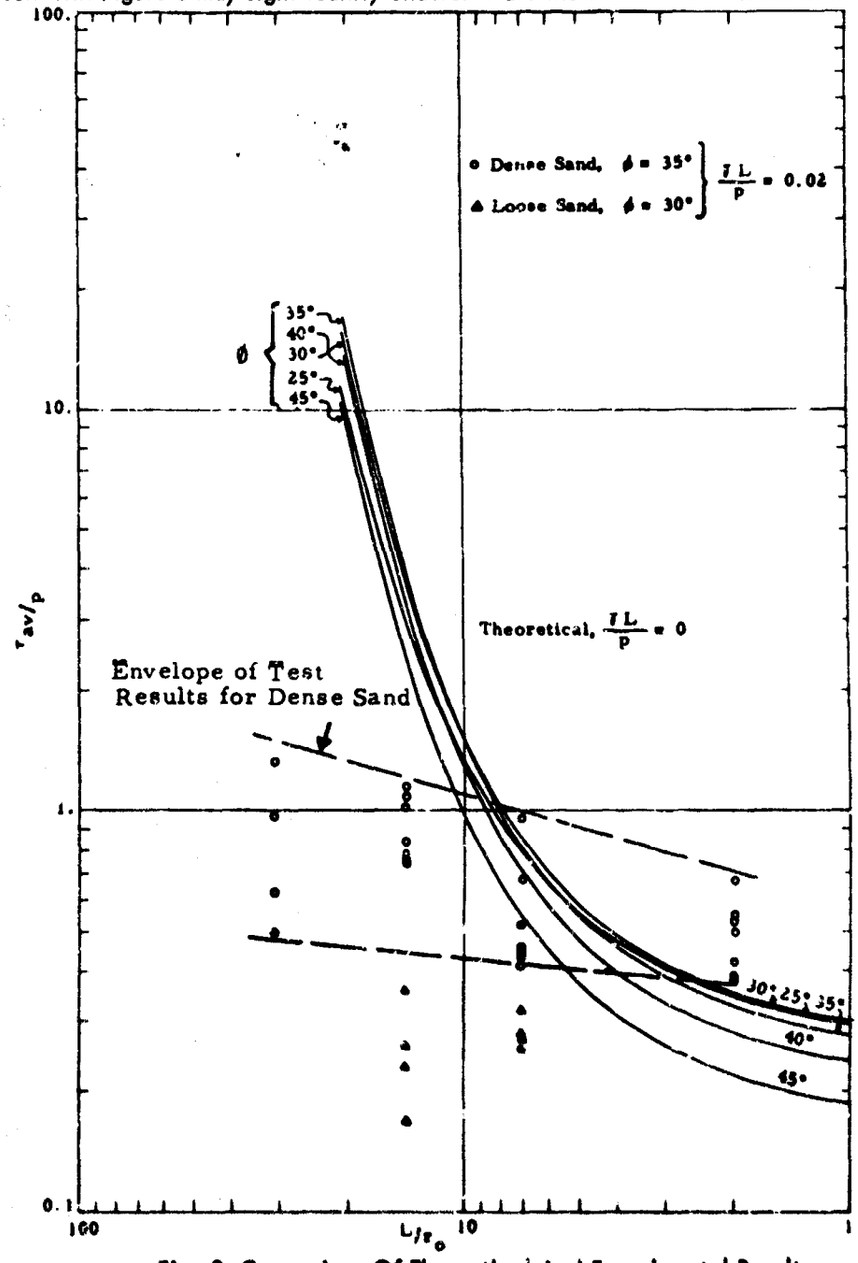


Fig. 8 Comparison Of Theoretical And Experimental Results

ACKNOWLEDGMENT

This research was conducted at IIT Research Institute for the Air Force Weapons Laboratory as part of a much more comprehensive program conducted under Contract Number AF29(601)-2596.

APPENDIX

Tests were performed in a 3 ft diameter by 3 ft deep pressure vessel. The walls of the vessel were coated with 3/2 mil thick coatings of bonded Teflon and a single sheet of Teflon 0.005 in. thick was loosely attached over the surface. This arrangement is the result of a series of tests performed on various types of surface coatings to determine the surface treatment that reduces frictional restraint at the walls of the pressure vessel to a reasonable minimum.

The general test set-up is illustrated in Figure 2. The silo model was placed on a supporting stand and the 3/4 in. push-out rod passed through a pipe sleeve to prevent frictional contact with the soil. At the lower cover of the pressure vessel, the rod passed through a "Bronzoil" bearing and the lower end of the rod made contact with a force washer which rested on a hydraulic jack head. A sand wiper assembly served to prevent sand from flowing under the model when it was lifted off the base during a test. The "Bronzoil" bearing provided lateral support to prevent possible buckling of the push-out rod.

The load measuring assembly consisted of a spherical ball, ball seat, force washer and a nipple type force washer seat. Two Lockheed Electronics Company force washers with capacities of 40,000 lb (Type SK-TR-47) and 10,000 lb were used interchangeably, depending on the magnitude of load anticipated. The force washer was securely placed on a nipple which was screwed into the head of a Lyner hydraulic jack which provided the push-out thrust. A spherical ball, which made contact with the push-out rod, rested on the spherical seat of the force washer insert. The hydraulic jack was supported on an X-frame fabricated from 12 in. WF structural members. The jack frame was supported by eight high strength rods which screwed into the bottom flange of the pressure vessel. The soil used for these tests was Ottawa sand. Two soil states were used, dense and loose. To obtain the dense state, the sand was placed in the pressure vessel, in 12 in. layers. Each lift was vibrated with a penetration type concrete vibrator for twelve minutes in four symmetrical places along the periphery of the vessel. The depth of penetration of the vibrator probe was a maximum of 18 in. Two density measurements were taken with a Density Scoop for each lift after vibration. To obtain the loose sand state, the sand was placed in the pressure vessel with a hand scoop, which was held at a height of approximately 12 in. while being moved in a symmetrical manner around the silo model. Two scoop density readings were also taken for each 12 in. increment of height as was done in the case of the dense state.

The upper surface of the sand was made concave to allow approximately 1 in. between the silo cover and the pressure vessel cover. A rubber sealing membrane was placed over the surface to prevent leakage of air pressure through the sand. Surface overpressures of 0, 20, 50, 75, and 100 psi were employed in the tests. The pressure vessel cover was secured in place by 30 high-strength bolts torqued to 130 ft-lb.

The procedure used in performing the tests is as follows: The base of the silo model was lifted off the stand by the use of the hydraulic jack a distance of about 0.2 in. during the placement of the soil. After the containment vessel was filled with soil and the diaphragm and pressure vessel cover were securely in place, the jack head was lowered and surface overpressure was applied. This procedure was followed to reduce the initial skin-friction generated by compression of the soil prior to application of the monitored hydraulic jack force. That is, if the silo model were allowed to rest on the stand during application of surface pressure, large relative displacement between the soil and the model would occur at the top of the model. This relative displacement could conceivably be great enough to create shear failure at the interface prior to application of the push-out thrust.

To obtain the load at which the skin friction on the model is a maximum, the model was pushed through the sand by the use of the hydraulic jack at an average rate of 0.1 in. per minute. Deflection readings of the jack head were taken by the use of a dial gauge attached to the bottom of the vessel. Deflection readings were taken at 0.005 in. increments. Force washer load readings, taken simultaneously with the deflection readings, were obtained from a Hathaway (Type RS-20) Strain Gauge indicator.

REFERENCES

1. Sokolovski, V.V., Statics of Soil Media, Butterworths Scientific Publications, London, England, 1960.
2. Ivlev, D.D., "On the General Equations of the Theory of Ideal Plasticity and of the Statics of Granular (Pulverulent) Media", PMM, Vol. 22, No. 1, 1958, pg 97.
3. Filonenko-Borodich, M.M., "On the Plane Problem for a Wedge", PMM, Vol. 26, No. 3, 1962, pg 874.
4. Stroganov, A.S., "Plane Plastic Deformation of Soil", Conference on Earth Pressure Problems, Proc., Brussells, 1958.
5. Pechere, M., "Equilibre Limite dans les Sols," Annales Ponts et Chaussees, 131(6), 1961, pg 771.
6. Perlin, P.I., "On the Equations of Plasticity for a Certain Limiting Condition," PMM, Vol. 26, No. 3, 1962, pg 580.
7. Berezantsev, W.G., "The Limiting Equilibrium of a Medium Possessing Internal Friction and Cohesion in a State of Stress Symmetrical with Respect to the Axis," PMM, Vol. 12, 1948, pg 95.
8. Terzaghi, K., Theoretical Soil Mechanics, John Wiley and Sons, New York, 1943.

DISCUSSION

INTRODUCTION

The following material was recorded on tape during the formal sessions of the Symposium. In most instances, the speaker has had an opportunity to verify the validity of the transcription as it appears.

Temporal significance of questions, answers, and other remarks has been preserved for the reader by using the same headings as those in the earlier divisions of this Proceedings. For example, the discussion which occurred after presentation on "State of the Art," Tuesday PM, appears after the heading, "Session Four - Tuesday PM." All material within these divisions is presented in order as it actually occurred. In some sessions, questions followed the individual presentation; in other sessions the questions were saved until after the formal presentations were completed. Wherever possible, slides or other illustrations which were used in the discussion are reproduced with this material. No attempt has been made at this point to duplicate illustrations which appear in the formal papers.

TABLE OF CONTENTS

	Page
SESSION TWO - MONDAY PM	
Wave Propagation in Soil Media	594
SESSION THREE - TUESDAY AM	
Ground Motion and Instrumentation	600
SESSION FOUR - TUESDAY PM	
State of the Art	605
SESSION FIVE - WEDNESDAY AM	
Similitude and Model Studies	609
SESSION SIX - WEDNESDAY PM	
Analytical and Experimental Studies, Part I	614
SESSION SEVEN - THURSDAY AM	
Analytical and Experimental Studies, Part II	618
SESSION EIGHT - THURSDAY PM	
Design and Prototype Studies	621
Raymond J. Krizek, Formal Paper	625
Index to Authors and Discussion Participants	634
Symposium Register	635
Memorabilia	640

SESSION TWO – MONDAY PM*

WAVE PROPAGATION IN SOIL MEDIA

SESSION CHAIRMAN: Robert V. Whitman

The Chairman of this session on "Wave Propagation in Soil Media," Dr. R. V. Whitman, is Professor of Civil Engineering at the Massachusetts Institute of Technology. This year he has been on sabbatical leave from MIT while continuing his research activities at the Stanford Research Institute. Dr. Whitman has done considerable research and written many publications in the field of soil dynamics.

ROBERT V. WHITMAN: This afternoon's session is concerned with wave propagation in soil media. Dr. Newmark in this talk this morning set the stage for this session. He first pointed out to you the complexity of the problem of predicting free field motions and stresses. He then indicated some of the steps one must go through in simplifying this problem to make it a tractable engineering problem. Dr. Newmark first demonstrated to us that at the overpressure levels with which we are interested in with this session, the direct induced ground shock effects are of minor importance and that we can concentrate upon the free field motions and stresses induced by the passage of the air blast wave over the surface of the ground. He discussed some of the implications of thinking of the soil as an elastic material and pointed out that because of the two or three dimensional aspect of the problem, there can be an attenuation of peak stress with depth. He further drew upon concepts from theory of elasticity to formulate equations for peak displacement, peak particle velocity, peak particle acceleration in a way that would properly take into account such variables as the size of the explosion, the overpressure level, and the properties of the material and, finally, by calling upon the results of the rather limited field test data that are available to us, came up with empirical factors to stick into these equations to make them work. Dr. Newmark observed, for example, in regard to the peak particle velocity, that these procedures ought to be good enough to get us within a factor of three or four of the proper answer. We are faced with the problem, for example, that the empirical factors that we draw upon are based mainly upon tests in a very limited set of soil or earth materials and we are, hence, drawing heavily upon our intuition when we try to use these for other earth materials. I think most of us will agree that we need to do somewhat better than the facter of three or four. Being limited as we are today in the ability to conduct field tests in a variety of earth materials, I think we must, then logically turn to the laboratory as a means for firming up our ideas about stress wave propagation through soil. We would, for example, like to be able to answer questions such as: How important are time-dependent effects upon the wave propagation patterns through soil? How important are non-linear aspects of the stress-strain properties of soil upon wave propagation patterns through soil? These are the kinds of questions that can be answered by laboratory experiments. This afternoon we are going to have four papers all of which are aimed at the general question: what are the aspects of the stress-strain behavior of soil that bear most heavily upon the pattern or nature of wave propagation through soil?

The first speaker this afternoon is Dr. E. T. Selig who is a senior research engineer with the Illinois Institute of Technology Research Institute, better known as IITRI. Dr. Selig has been involved in weapon's affects research now for seven years. He is a graduate of Cornell University and has pursued graduate work at the Illinois Institute of Technology. The title of his paper is "Characteristics of Stress Wave Propagation in Soil."

E. T. SELIG: Presentation of formal paper, see pages 27-61.

ROBERT V. WHITMAN: Our next speaker this afternoon is Mr. J. V. Zaccor, senior research engineer with the URS Corporation of Burlingame, California. Mr. Zaccor is a graduate of the University of California and has been at URS Corporation for approximately eight years and has there been engaged in research on soil behavior under dynamic loading conditions and into the potential explosive hazards of missile propellents. Prior to joining URS, he had spent seven years studying the nature of fallout material processes in connection with a nuclear weapon test program. Mr. Zaccor will speak to us this afternoon on the subject "Laboratory Stress Wave Propagation Studies in Granular Materials."

J. V. ZACCOR: Presentation of formal paper, see pages 62-72.

ROBERT V. WHITMAN: Our third paper this afternoon has been written by A. J. Hendron, Jr. and M. T. Davisson. Dr. Davisson is Associate Professor of Civil Engineering at the University of Illinois. He is a graduate from the University of Akron and has performed graduate studies at the University of Illinois. In addition to his contributions in the area of nuclear weapons effects, he has a wide experience in general soil engineering problems. The paper will be presented by Lt. A. J. Hendron, Jr. of the United States Army. Lt. Hendron is a graduate of the University of Illinois both at the undergraduate and at the graduate level. He holds the rank of Assistant Professor of Civil Engineering at that university while he is on military leave of absence. He is currently stationed at the U. S. Army Engineer Waterways Experiment Station. The title of their paper is "Static and Dynamic Strain Moduli of Frenchman Flat Soils."

A. J. HENDRON, JR.: Presentation of formal paper, see pages 73-97.

ROBERT V. WHITMAN: Our final speaker for the organized portion of this afternoon's session is Dr. Lynn Seaman, civil engineer from the Stanford Research Institute in Menlo Park, California. Dr. Seaman is a graduate of the University of California and performed graduate work at the Massachusetts Institute of Technology. For the past three years, he has been engaged in both military and commerical research. The title of his paper is "Propagation of Dynamic Stresses in Soils."

LYNN SEAMAN: Presentation of formal paper, see pages 98-106.

ROBERT V. WHITMAN: I would like to thank all of the speakers this afternoon, not only for their excellent papers but for their cooperation in meeting the challenge that I set to them on the time limit. I would like to make one comment about these papers. You may have noticed that these four speakers said relatively little about their experimental apparatus and the difficulties they had in making these experimental apparatus work. I can assure you that the problems in making them work were far from trivial, but, I think it is perhaps of some significance that if this meeting had been held two years ago we would have heard a lot about apparatus, and the difficulty in

* Additional material, pertaining to this session, appears on pages 625-633.

making them work, and very little about results. Today we have been able to hear a good deal about meaningful results and I think this by itself is a real indication of the progress that has gone on in this particular area within the last two years.

I would now like to invite questions from the audience.

ERIK SOLLID: I would like to have an explanation of the results with reference to depth of burial. The confinement of the various samples as shown necessarily represents only one stratum level in the ground. In other words, when operating on these cylinders, what effort was made to simulate the variableness of confinement from depth to depth?

E. T. SELIG: In my experiments, of course, there was no effect of depth. I had a constant confining pressure. The boundary condition will be different than that for what you are asking and it would have to be taken into account by possibly an increase in lateral pressure with depth. This is more like the condition that Lynn Seaman simulated with his vertical column in which he prevented lateral deformation. He had the overburden pressure and zero lateral deformation giving a one-dimensional effect so, in a sense, he would be incorporating the field conditions into his experiment as it was set up.

LYNN SEAMAN: In my tests, I had a certain amount of geostatic stress down to 15 feet though the static compression test data indicate that the alpha value, the attenuation factor, is not dependent on the stress level. So you may interpret this to say also that alpha would not depend on precompression which occurred and, therefore, would be independent of the geostatic stress. The results for the wave propagation tests indicate that you can predict the stress attenuation on the basis of an alpha value, which doesn't take into account the geostatic stress. It is assumed that the material properties are the same at all depths. The stress attenuation apparently is predictable on that basis.

J. V. ZACCOR: I believe that I covered a part of this question in the talk that I presented in which I suggested that by shifting the origin of the curve that I presented, one could get a feeling of how the stress-strain characteristics with that level of overburden might go. I don't know how you get at the potential affects of cementation that may occur with long periods of heavy overburdens. There is nothing in the present system that we use that would allow us to look at this sort of thing.

ROBERT V. WHITMAN: Perhaps as Chairman I'll just make a comment. Life is clearly not one dimensional, and even if it were, it would be neither simply constrained as in Dr. Seaman's tests or free to expand against constant pressure as in Dr. Selig's tests. Mr. Zaccor's tests are essentially the same as Dr. Seaman's tests. These men are, if you will, starting with the simpliest tests to see what can be learned about wave propagation. We have to go on to the effects of more than one dimension but we are really in our infancy in learning how to handle wave propagation, non-elastic, in anything more than one dimension.

ERIK SOLLID: I was merely curious about the effect of the increase in the velocity of pressure propagation as it travels down through denser and denser material.

ROBERT V. WHITMAN: Unfortunately, at the laboratory scale, it is difficult to get sufficient depth to really make that effect show up, although it begins to. As Dr. Seaman pointed out in his comment, the effect of the 15 feet of geostatic stress in his tests can be seen in his results.

R. H. SIEVERS: This morning it seemed that Dr. Newmark in referring to the component of the pressure upon the structure stated that the reflection of this pressure was of little significance; however, this afternoon the magnitude of the reflected pressure was shown to be quite significant in some of these one dimensional tests. Dr. Selig and Mr. Zaccor both showed these. I would like to know how this reflection shows up as a change of the impulse that would likely be felt by a concrete roof of an underground structure. Doesn't this reflection provide a very significant increase in the impulse or the pressure experienced by the structure?

J. V. ZACCOR: I think it is going to be significant and that is why I presented the information; however, there is a lot more that goes with the question which has to do with whether or not you can have a rigid receiver as a structure and what the effective modulus of the structure actually is. In addition, the structure is going to be finite and the wave is going to pass around it; and, eventually, the whole structure will be accelerated to a free-field particle velocity. It is only when there is a change in the particle velocity that you have this momentum transfer, so that as the structure starts to move with the free-field particle velocity the "reflection factor" will go back down again; and all that I say applies to shock loadings. Does that help?

R. H. SIEVERS: Well, I still have a question. It seemed that in the essentially rigid box concrete structure you have to at least accelerate the entire roof portion of the structure up to this velocity before you have the reduction in the reflection factor; and, by the time this is accelerated and you reach such a velocity, hasn't the pressure wave gone past and the time of such a reflection gone past as well? In other words, wouldn't this reflection occur much more rapidly than the structural slab would accelerate to a velocity which reduces reflection rate?

E. T. SELIG: I think Mr. Zaccor answered the question fairly well, but you are certainly right. Basically, the effect would be to add a little bit of impulse, maybe a lot of impulse, when this wave first hits because the effect will drop off as soon as you get motion of the panel. It will depend a great deal upon the stiffness of the panel and the duration of the pulse as to how significant it is in terms of the overall effect. I would like to add just one other comment, that with these analytical techniques, such as the one I used in predicting my results, I can equally well predict what these reflection factors are. Mr. Zaccor can as well, by taking into account not simply a fixed or free end, but intermediate boundary conditions. Therefore, it is possible to make some estimates of these effects by such analytical techniques.

HAROLD G. MASON: There is one other factor that hasn't been mentioned. It is the fact that these are one-dimensional tests. In the real structure, you also have a rarefaction or unloading wave which starts at the edge, propagating across the structure as the soil moves

past it as a result of the difference in compressibility between the soil and the structure. This will help to relieve any reflections which do occur, which is another reason that you may have not seen it in the field. As Mr. Zaccor said, the reflection factors apply only to shock loadings. If you don't have a shock loading, you simply get an increase in the slope of the stress-time pulse (rise time) rather than a large over-registration, such as those occurring under shock loadings in the one-dimensional case.

BILL PERRET: There are two things that I think might make a difference here. One of them is the fact that the kind of shock wave, or better yet the pressure wave, going by a structure will have a wave length very much greater than the dimensions of the structure so that reflections will not be particularly so serious. In other words, the structure will be enveloped by the wave and only portions of the wave will actually affect the structure. The other thing is that the bulk density of the structure is probably much less than that of the material it displaces so it acts as a light point rather than a mass of the same density, consequently, it will not move as a hard higher density structure would.

ROBERT V. WHITMAN: If Dr. Newmark were still here, I would call upon him to comment on this situation. Let me, in his absence, paraphrase what I understood him to say this morning. He started out by observing that if you have rigid boundary, as was true with all these laboratory experiments, you must get reflections and this is what the laboratory experiments have shown. Now, if you have something that is not rigid and any structure that you have in the ground almost invariably is not rigid either because of its own properties or because of what lies underneath it and supports it, you will have something less than complete reflections. I believe he said that he had studied a variety of typical conditions and, because of the factors that Mr. Perret has just enumerated, for the majority of those typical conditions no reflected wave of measurable duration should be expected. I believe that he also said that in a few of the structures field tests that have been carried out it appeared that something which had the nature of the influence of this reflection did appear, but in the majority of cases that have been encountered, it would, for these reasons, not be of consequence. We know it is always there and we always have to be on the lookout for it. Most of the time, if we forget about it, we are all right, but we always have to worry about those few times when we can't forget them.

MERIT WHITE: I have a question of Dr. Selig and that is whether or not the lateral inertia may have had some effect on the results he attained in his tests?

E. T. SELIG: Lateral inertia certainly may have influenced the results, and I tried to evaluate the significance of it essentially by comparison of the stress-strain response and the wave propagation behavior with the use of the analysis. All I could determine was that the effect did not appear to be significant. For example, I could not sustain a stress exceeding the static strength for any observable distance into the specimen, hence, there was no dynamic effect, be it lateral inertia, or anything else acting there, that was significant. I did, however, find in order to justify the difference between the virgin static triaxial stress-strain curve and the propagation velocity of the wave, that some dynamic effect had to be present--at least to make my data consistent. This was because on the first loading, the initial tangent modulus was too low to predict the right velocity but, on subsequent loadings, they came into agreement and it appeared that there were time-dependent effects. There are many explanations for this and one of these is lateral inertia. I also made some calculations using the theory of determine what the magnitude of lateral inertia might be and it also indicated that probably the effect would not be significant beyond two diameters from the end of the specimen. There undoubtedly was some effect, but it appeared minor. This is not too surprising especially because the soil was a dry sand.

F. J. TAMANINI: My question is concerned with the interesting correlation of Dr. Seaman's reported data. Some of his points coincide with alpha equal to .15 I believe; however, that he was hoping for a better fit with alpha equal to .2. I note that in his pressure-time curve, where he established T to be arbitrarily .368 of the maximum value, the correlation is very sensitive to the T/T_0. I wonder about the establishment of the .368 value. Could there not have been a better figure than .368? I was wondering if there is a firm basis for selecting .368 which just seemed to be out in orbit by itself. If a larger value had been established perhaps the alpha 0.2 curve could have been a better fit.

LYNN SEAMAN: I don't think so. The value of .368 is certainly an arbitrary number just to give an idea of the lengthing of the stress-strain curve. This same number was used both in treating the analytical results and the experimental results. If there were 1 to 1 correlation, the analytical curve and the experimental points would have lined up on the graph that was referred to. I think that there was a number of effects which can explain this discrepancy and one which I mentioned is the non-linearity of the stress-strain curve. This explains the bulk of the difference. I don't think I want to go into detail on a vast number of effects which may tend to bring the data into closer correlation with analysis.

HEINZ LEISTNER: I hesitate to bring this up since Dr. Newmark isn't here, and the papers that we heard this afternoon were on one-dimensional wave propagation; but, I believe that Dr. Newmark said this morning in discussing the wave setup by moving the air (pressure wave) made a certain angle with surface, which he said was a factor of the velocity of the air wave and the seismic velocity. However, then he said that this was not an indication of the directional components of the stress moving through the soil, he referred to it as simply a vertical pressure. A while later, he brought out a chart in which he gave horizontal component of the vertical pressure as a factor of seismic velocity. Wouldn't the horizontal component be a result of the slope of the stress wave moving into the soil? Or have I mised something?

A. J. HENDRON, JR.: I think there are two sources of the lateral pressure. One of them is indeed what you mentioned but there is also another one. We have the front inclined at an angle which Dr. Newmark called alpha. You do, I think, have the lateral pressure caused by this front being slanted the way it is; however, if this front were horizontal and moving down, you would also have a horizontal component of pressure which is the same as what I indicated on those curves of those confined specimens of Playa Silt. As the axial stresses increase, you have approximately a coefficient of lateral earth pressure from .47 to .56. Even if the front were plane and moving down, you would get a certain percentage of the vertical pressure as a horizontal pressure. For the particular soil I reported on today it should be somewhere around .5. Does that answer your question?

DISCUSSION

HEINZ LEISTNER: Are you saying that the slope of the wave moving down through the soil has nothing to do with the magnitude of the horizontal component?

A. J. HENDRON, JR.: I'm saying there are two components. It is partly due to the slope of the front and also, even if the front was moving vertically you would have a horizontal pressure because it is completely restrained.

HEINZ LEISTNER: Yes, I realize that.

A. J. HENDRON, JR.: I think it is due to two things. Partly what you say, and even if it were moving down vertically, there would be component of horizontal pressure.

ROBERT V. WHITMAN: I can't answer this question but maybe we have somebody in the audience that is familiar with this particular theory for wave sweeping over the surface in an elastic half space. The answer for your question comes from what this theory says. I refer to Dr. Newmark's comments that despite the inclination of the wave, the principal stresses are still more or less horizontal and vertical at least during the early passage of the wave, but if we have somebody who knows the theory, we've got the answer.

J. HANLEY: It is a question of interpretation of what he said. He said specifically that if we start the shock in the air at this point and then the wave moves to this point (see Figure 3, Opening Address), and we were attempting to locate the front of the stress wave in the soil, the time it take for the stress wave which is acting in a vertical direction at this point to reach this depth is equal to the time it takes the shock wave in the air to reach this point. He further said that the stress wave in the soil was not normal at this front. The basis for the specific calculation is solely the question of the time required for the stress wave to move through the soil from the surface to this point; and the shock wave in the air to move from this point to this point.

BILL PERRET: I think there is another point here and that is for the wave front which makes the angle alpha to the horizontal, and here Hal Mason and I agree, there is a stress gradient along the line representing the ray path because the pressure represented by the first arrow is greater than the pressure represented by the arrow at the convergence of the two lines.

J. HANLEY: That's right, the air pressure is being degraded as it moves along. The statistical interpretation of Dr. Newmark's remark is that the stress wave is not necessarily normal to that front. There is a horizontal component to the stress wave at all points.

MICHAEL ANTHONY: I think that what he has done here is that he has computed vertical stresses at a given depth due to a point source loading the surface, but he has fancied it up by adding the extra components of the stress wave sweeping out. He has just computed the vertical pressure at its given distance below the surface by the old soil mechanics method of an influence chart; but he has added a few other things. He was not talking about horizontal components but vertical components.

ROBERT V. WHITMAN: This is another point at which we regret that Dr. Newmark was unable to remain for the balance of the program. However, if I may just comment once more, I think that there are at least three separate things going on here that we perhaps tend to get confused.

The first is this concept of superseismic versus subseismic waves. Pictures like this are very useful for getting across this concept, that is to say, explaining whether or not you expect the soil to start moving before the air blast wave passes over the soil. It was my understanding that in drawing that particular picture that concept was the main thing that Dr. Newmark wished to get across.

There are theories that have been worked out for a wave sweeping over the surface. The earliest theories assumed a wave with constant velocity and constant amplitude. Since then, various attempts have been made to make that condition more realistic; to have both the shock wave velocity and the amplitude changing with distance. Those theories are available in the literature. And, while I haven't looked at them, I suspect that they predict an increasingly complicated kind of stress field depending upon how many of these kinds of refinements you get into. The third point is the computations that Dr. Newmark and his colleagues made some years ago to get some idea of the nature of attenuation of peak stress with depth. These are, as he explained, essentially a static kind of calculation. I suppose superimposed on that would be, having made this kinds of crude but useful estimate of what the peak vertical stress it might be that one would then introduce essentially coefficients of lateral earth pressure at rest a la Dr. Newmark's chart, to get some feel of the magnitude of the horizontal stress.

R. H. SIEVERS: Referring to the figure on the board (see Figure 3, Opening Address), this is for the superseismic case, apparently, but for all of the structures which are, I think, assembled here to consider, are not the ones which are superseismic but the subseismic case, which going back to Dr. Newmark again, he showed that the air blast might follow the pressure wave in the ground. How else can the soil pressure be developed in advance of the air shock other than by the soil stress primarily being in the horizontal direction? If we have a structure in advance of such a shock wave, is not this a much larger horizontal and lateral load against the structure than in comparison with that it receives on the roof? Isn't it much larger with the subseismic case than it is with the superseismic condition you saw earlier?

GLEN BERG: Mr. Chairman, would you please define for me what you mean by the subseismic, seismic and superseismic case? I seem to be confused.

ROBERT V. WHITMAN: That I can do! The superseismic case is the case in which the velocity with which the shock wave in the air is moving over the ground is greater than the seismic wave velocity in the soil; hence, superseismic. Subseismic is the reverse in which the air shock is moving less rapidly than the dilatational seismic wave velocity in the ground. On top of this, we have transeismic which has to do with shear wave velocities and dilatational wave velocities. Now, who is going to answer Major Sievers' question for us? I suppose we should really ask Earl Sibley's permission to do this. This is getting off into his area.

MICHAEL ANTHONY. The main point is that this is not a case of interest at the overpressures we are talking about. Direct induced ground shock is important. This would be an extremely hard structure.

ROBERT V. WHITMAN: If once again I can just paraphrase my understanding of what Dr. Newmark said this morning. It's nice to have someone like that to blame all your opinions on, you know. The fact that the first energy arrives in this way does not necessarily mean that the stresses associated with that first arrival will be the largest stresses associated with the structure. It still may well be; and, in fact, will be in a large number of cases, true that the stresses induced once the air blast finally arrives are the larger ones. The problem is with regard to the phasing of some of the motions and the implications that this may have with regard to the design of shock isolation equipment or the analysis, shall we say, of the dynamic response of the equipment or the people housed within that structure. Whereas in the superseismic case, one can usually presume that the first thing that will happen to the structure is that it will move downward. In the subseismic case, one cannot safely make the presumption, if the phasing of the horizontal-vertical motions is important from the standpoint of the shock isolation effects.

R. H. SIEVERS: I believe I am correct though in stating that in the lower overpressure regions the subseismic case is the one in which we would be principally concerned, say if we are dealing with structures designed for 50 psi, or less than 100 psi, in relationship to some of the charts we saw this morning as to the sound velocities in the various materials. Apparently, the effects you are seeing would be to provide a precursory or a more gradual loading of the structure in this subseismic case.

D. A. LINGER: Did all this come about from your question concerning lateral pressure? Dr. Newmark mentioned Mu over one minus Mu in which case that is the lateral pressure in a three dimensional triaxial condition when it is fully constrained. The figure which he had on the board which indicated K, the lateral pressure coefficients are obtained from this type of analysis which, of course, leads one from this three dimensionally constrained, loading it in one dimension, the other two dimensions are constrained. The pressure from which the other two dimensions feel is the factor K which he has in that tabular form. It all came around from that and that's where those came from.

HEINZ LEISTNER: What I really wanted to ask was whether we have, since Dr. Newmark developed this theory, been able to improve on it?

D. A. LINGER: Most of the discussion was the difference of opinion on this.

E. T. SELIG: If I can interject a comment on this point. Getting back to the original question, I think it might help to point out that discussion of seismic, superseismic and subseismic is generally thought of in terms of the conventional elastic half-space solution. This is very convenient because the wave propagation of the dilatational wave is a constant and a function only of the material properties; hence, the wave front will travel out in all directions at a constant velocity. Then we can tabulate values for a half-space, assuming equivalent elastic performance. But they only approximate the real situation. If I can infer some comments here from our one dimensional studies, in the real soil condition the propagation velocity, in the direction of the front, will be very much a function of the stress conditions existing there and these vary because the stress-strain curve is a non-linear thing; hence, your velocity is continually changing as it propagates from any point. The front will, in effect, really deform and it will deform downward as well as outward as the peak stress changes. For example, if you have an upward curving stress-strain relationship, as the peak stress comes down the velocity slows down. Going laterally, the same thing really applies; as the stress-strain condition in this direction changes, the velocity changes as well. We think we can say more about this problem, at least infer more on the basis of our one dimensional tests, but the three dimensional or even two dimensional analysis is extremely complex when you get away from the elastic solution.

ANDREW THOMPSON: These empirical relations are based on the Nevada Test Site data for the air induced ground shock. I am thinking about materials other than those of the Nevada Test Site. I was wondering how low an HE change we might go to in evaluating some of these relations for predicting air induced ground shocks. Can we go as low as 50 tons, 20 tons? The relations, I believe, are originally based on some of the fairly larger yields and I noticed, of course obviously, megatons, that is one thing I would like to hear about. Another thing, when he talked about attenuation with depth, he said that they were also based upon empirical attenuation of stress data with depth. That was also based upon empirical data to some extent and I was wondering what stress data this was based upon and if this stress data wasn't good, how would that affect the attenuation of depth relations? I might quote Fred Sauer of SRI in this regard. He says when you look at the test data in Frenchman's Flat, the data from the 256 pound charges were quite different from the data from all the larger charges, so he is sure than 256 pounds is too small. He's also convinced that 20 tons is big enough but he doesn't know just where the boundary might be between these two. These are explosion sizes that could be used to answer meaningful questions, not necessarily to provide data to be directly extrapolated without interpretation.

A. J. HENDRON, JR.: I have two slides that show data accumulated at the Waterways Experimentation Station and it confirms some of the things that Lynn Seaman and Mr. Zaccor have observed in their experiments on sands. I have two little slides up if you are ready to project them. These are some records that were obtained at various depths in our blast load generator at the Waterways Experimentation Station which is essentially a sand column restrained so that it is a one-dimensional test. There is an explosion set off at the surface, and at the top, there is a finite rise time which is about one millisecond. The wave is shocked up at a depth of one foot, it appears to be shocked up at depths of three and four feet but the shock does break at 8-1/2 feet when the stress level is somewhere between 20 and 40 psi. The next graph is a picture of the static stress-strain curve in one-dimensional compression which was measured on this sand. The upper graph is the dynamic stress-strain curve which we have determined from these experimental results. You can calculate by impulse-momentum relationships and so forth that if you have a shock, it should propagate as the secant modulus. If the pressure, shock propagation velocity, and density are known we can roughly locate one point on the dynamic stress-strain curve. We also know from the pressure measurement, which you can believe within plus or minus 10 psi, that the shock broke somewhere between 20 and 40 psi so that we know that there is an inflection point somewhere between those two stress levels. When the shock breaks, it propagates at the tangent modulus rather than the secant modulus when stress level is below the inflection point. This is a limited amount of data and the curve shown is the

dynamic stress-strain curve we interpreted from the data. Since these plots were made, Capt. Tener has made some shots in the large blast load generator. One shot, in particular, was 30 psi at the surface. This is the first shot out of about some 40 shots in the generator that did not show shocking up. These data substantiate that the inflection point for this particular sand is probably between 20 and 40 psi.

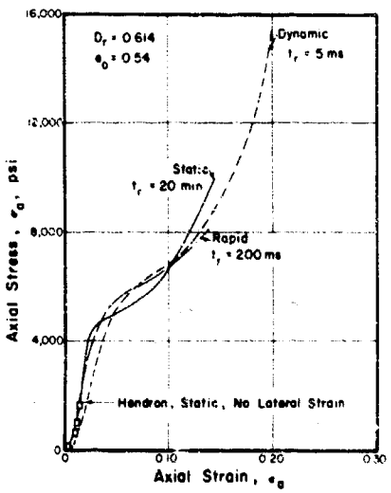
ROBERT V. WHITMAN: I would like to comment on this question of shock wave formation and degeneration as it has been observed in tests at the Stanford Research Institute where I have been cooperating with Dr. Seaman and his work. The records that he saw were very similar to those that were on the previous slide showing a tendency for the wave front to steepen in the upper part of the column and then to degenerate from that shock wave condition into a plastic wave in the lower part of the column. In the tests at the Waterways Experiment Station, which you just saw, there was a decrease in the peak stress with depth, an attenuation owing to the side friction effects between the sand and the container. The same pattern was observed in tests at SRI in which there was essentially no decrease of the peak stress with depth. The same phenomena of shock wave formation followed by shock wave degeneration can occur independently of the attenuation of peak stress with depth. I think there are two factors that come in here. One of them is the existence of this initial bump, this yielding portion of the stress-strain curve, and the second one is the effect of the increasing geostatic stress with depth. Because of the work we've done back at MIT, we've shown that the stress level at the inflection point is related to the initial stress. If you are at the surface where the initial stress is almost zero, the height of that bump is almost zero. If you are down 10 or 15 feet in the sand, then the height of that bump increases. As you go deeper and deeper, that initially yielding bump gets more and more important and eventually a wave which started out at the surface seeing the material like a locking material at some depth ends up seeing it like a yielding material.

M. T. DAVISSON: In view of the preceding discussion, I would like to illustrate some additional facets of the behavior of sand in one-dimensional compression, particularly at high stress levels. The one-dimensional stress-strain curves on the slide are for a Minnesota sand with an initial relative density of 61.4 percent and an initial void ratio of 0.54. Ninety-five percent of the rounded silica sand passes the No. 10 sieve and is retained on the No. 20 sieve.

Four tests are shown on the slide: A static test was performed by Hendron in the device, described here today by Lt. Hendron, wherein the lateral strains are eliminated. A series of three tests were performed on specimens confined in thick rings, also as described here today by Lt. Hendron. The three tests are labeled Static, Rapid and Dynamic and required 20 minutes, 200 milliseconds, and 5 milliseconds to reach the peak stress, respectively.

The static test performed by Hendron did not exceed 3,300 psi; however, up to this stress level there is essentially no difference between the stress-strain curve for Hendron's test and that obtained by using a thick ring to confine the specimen. Up to a stress level of approximately 3,000 psi the sand behaves as a locking medium, but beyond 3,000 psi and in particular at 5,000 psi, the curvature of the stress-strain is reversed. This occurs because the sand grains are crushed to powder. At a stress level of approximately 6,000 psi to 7,000 psi the curvature reverses again, and the powder behaves as a locking medium, at least up to a stress of 16,000 psi which is the maximum observed. Thus, we have two "bumps" in the stress-strain curves for granular soils, one corresponding to slipping of the grains at relatively low stress levels and one corresponding to crushing of the grains at much higher stress levels.

Whether or not a strain-rate effect is evident depends on one's point of view. As an engineer, it may be concluded that no strain-rate effect exists. As a scientist, the difference between the stress-strain curves, especially in the zones where crushing occurs, would be of interest.



Axial Stress-Strain Curve for Minnesota Sand in One-Dimensional Compression

The stress-strain curves presented for the rounded Minnesota sand are more likely to be quantitatively representative of a mass of marbles or ball bearings than they are to be representative of a normal sand. Qualitatively, however, the behavior is representative of all granular media. For normal sands crushing would occur at lower stress levels, namely, 2,000 psi to 4,000 psi. As the grain size increases into the gravel range, the stress level at which crushing begins should decrease progressively. Furthermore, angular grains will crush at lower stress levels than rounded grains.

ROBERT V. WHITMAN: We have now looked at bumpy curves twice. Lt. Hendron showed you a bumpy curve but his bump was down at very low stress levels. We are seeing here another bumpy curve but the bump is up at very high stress levels. I think these are two different phenomena, at least in a sand, which have to be distinguished. The one, as Professor Davisson has pointed out, is due to the crushing of the material, whereas the other bump which occurs at very low stress levels is the result of the particles simply starting to slide past one another overcoming some initial friction between the particles. I am sure that as we go to more real materials these two effects start to merge and perhaps begin to become indistinguishable. Now I must attempt to summarize the results of this session.

From these and other results that have become available within the last several years, I think several significant conclusions can be drawn. The first of these is that it increasingly appears possible to describe wave propagation patterns through dry granular materials by models which do not involve time dependent effects. This is not to say that everything can be explained simply by rate independent non-linear hysteretic models, but so many of the significant features such as attenuation of peak stress can be so explained. I point out to you now that there are at least three carefully conducted sets of tests--those which Dr. Selig and Dr. Seaman have described today plus the ones that were reported by Dr. Heierli of Switzerland, in the literature several years ago--all of which have come to the same conclusion. From the standpoint of wave propagation behavior in dry granular materials, the significant thing that can be said today is that you need to take into account hysteretic effects and non-linear effects, however, you don't need to take into account any time dependent effects to explain the significant features of the patterns.

The second conclusion is that, if we accept this first conclusion and the model it implies, we then have a model that allows us to estimate how important attenuation of peak stress might be in one-dimensional wave propagation due to hysteretic type of energy losses. Any attenuation of peak stress from this source would presumably be superimposed on top of any attenuation that came about as a result of two or three dimensional effects. The conclusion that is reached here is that if you look at the results of the kiloton-size explosions which are used in field tests, you should expect such attenuation of peak stress effects to be of considerable consequence.

If you go to megaton and multimegaton size weapons, they are still there; but the magnitude of the attenuation of peak stress because of such a source of energy loss begins to become insignificant, compared to the other things that you do not know about the order of magnitude of the stress that might be applied.

The third conclusion I would draw has to do with the relationship between the seismic dilatational-wave velocity through a soil and what has been referred to here today as the "effective wave velocity," i.e., the velocity at which some stress level like a couple of hundred psi might propagate. There have now been several sets of experiments ranging from those on sand, such as Dr. Seaman described, to the results for the Playa Silt that Lt. Hendron and Professor Davisson described here today. These tests show that, for those two soils, the "effective wave velocity" is a number considerably less than the seismic level wave velocity.

Finally, as a fourth conclusion, I would say that in a number of tests in clean, dry sands, we have observed the formation of shock waves. We have also seen that those shock waves at nominal stress levels of a couple hundred psi, and less, only persist to rather shallow depths before they decay into non-shock waves, waves with a plastic type of front, a finite rise time, perhaps a rise time increasing with depth. The point I want to make is that you can get shock waves, they've been seen, but when you start thinking of them in terms of practical application to real structure and real soil, everything combines to make them disappear, at these nominal pressure levels anyway. Despite the fact that within the last couple of years we, for the first time, have seen shock waves in soil, I still think that the evidence all indicates that shocking up effect, at the very high accelerations that would be associated with shock up, are not factors of great consequence in practical applications.

While there are many areas in which we need to have progress go forth, there are a few areas that clearly stick out in my mind. We first of all need to do for cohesive type soils something comparable to what has now been done for dry granular soils. When we move into cohesive soils, there is every reason to suspect, as Mr. Anthony has today, that time dependent effects which may introduce dispersive types of phenomena may be of some importance. I think we need fundamental studies aimed at finding out just how important they are in propagation over distances of 10 or 15 feet that we can accomplish in laboratory tests. A second need is for further comparison of seismic velocity and "effective wave velocity" in soils other than the Playa Silt in Frenchman's Flat, and other soils that can be tested in that similar location. This must be done in situ, because we've got to be sure that it isn't the soil disturbance effects that are giving rise to this difference and there is a great need for imaginative ways of making this comparison between wave propagation velocity for seismic level stress and wave propagation velocity for high level stress in other natural materials.

Finally, the discussion today has been restricted almost entirely to one-dimensional wave propagation phenomena. We know that two important questions creep in as soon as we try to go into two- or three-dimensional affects and get away from elasticity, and a start has to be made over the years on this question although clearly it is going to be slow going.

SESSION THREE — TUESDAY AM
GROUND MOTION AND INSTRUMENTATION

SESSION CHAIRMAN: E. A. Sibley

D. A. LINGER: I would like to introduce the Session Chairman for this morning, Earl A. Sibley. He is a vice president of the firm of Shannon and Wilson. He was a co-author of the paper by Wilson and Sibley on free field ground motion and, of course, has been working in this field for quite some time. With no further ado, let me introduce Earl Sibley.

E. A. SIBLEY: Good morning gentleman. We're going to run this session a little differently than yesterday. We don't have a discussion and summary session; therefore, we will pick up the questions at the end of each paper. As the individual speaker is through speaking and while the material is still fresh in his mind and his slides are still available, you may ask questions at that time. Perhaps if we have a little time at the end, we may have a few questions of a general nature to ask the various groups who are presenting papers this morning. I wonder if many of you who are attending this Symposium know the definition of, or have looked up the word "symposium"? I happened to just the other day. Trying to get some idea as to what I was going to get involved in, I read to you from Webster's New World Dictionary of the American Language, College Edition, 1960: "Symposium, an entertainment characterized by drinking, music and intellectual discussion." I think we've had all three so far. It does us well to look at some of these words that we so commonly accept. We were given sufficient information yesterday in the session on wave propagation to actually make a ground motion prediction. When we consider soil structure interaction, this is one of the inputs we have to consider; i.e., to predict what the ground is going to do. We have to know something about the stress-time-depth relationships and yesterday this was the prime concern. We also considered the constrained modulus of deformation. It occurs to me that if anyone were to make a prediction of the ground motion based only on what was discussed yesterday, his method would raise a number of serious questions because there is another phase we have to look at. That is, how does the ground actually react to a dynamic load? What are the field observations? What are the field measurements of ground motion? What instruments are available for measuring ground motion both in the laboratory and in the field? This is what we will be looking at today. This approach of trying to back up our answers and approaches with field observations is not new. It has been done and is continuing to be done in the field of soil mechanics today. As a result, most of our design in soil mechanics today is based on field observation, experience, and judgement. However, it seems that in the emerging field of soil dynamics, we haven't had sufficient field observation or data from which to gain experience so that we can use this wonderful talent of judgement that we have. I think it was mentioned yesterday that with what we know about soil dynamics today, we're perhaps fortunate if we can arrive at an answer within a factor of 3 or 4 of reality. Of course, I think we all want to improve, but we shouldn't be too discouraged with that because in the field of soil mechanics there are many areas where we perhaps can do no better. This is also true in the field of rock mechanics. We have been tinkering in these fields for a long time. Our first talk will be on "Observed Free Field Ground Motion from Large Explosions," given by Bill Perret. I like to think of Bill as the grandfather of free field ground motion, because when we first started in this field it was his literature that we scanned, analyzed, and waded through. He has been in this field for a good number of years. Bill is a graduate of MIT, with an M.S. and a B.S.; he also has done graduate study in physics at the Universities of Berlin and Munich. He has done soil pressure instrumentation and geophysical exploration at the Waterways Experiment Station for about 12 years, and most recently he has been studying for 13 years the underground effects of nuclear and large chemical explosions with the Sandia Corporation.

DISCUSSION

BILL PERRET: Presentation of formal paper, see pages 107-117.

E. A. SIBLEY: The next paper, "Inertial Effects and Soil Strength Criteria" will be given by Bruce Schimming, Assistant Professor at the University of Notre Dame, Civil Engineering Department. This paper was also prepared by Mr. Saxe, the Head of the Civil Engineering Department at Notre Dame. Bruce has a Ph.D. in soil mechanics from Northwestern and has been at Notre Dame since 1962.

BRUCE SCHIMMING: Presentation of formal paper, see pages 118-126.

E. A. SIBLEY: We have time for a few questions directed to both Bruce and Bill.

ARTHUR FELDMAN: This is not a question but a comment. The inertia effect you have been discussing has been observed, the same type of peak, in the dynamic tensile tests of steel reinforcing bars for concrete, the flexural dynamic testing of reinforced concrete beams of normal proportions and of what we call deep beams. I don't want to challenge your interpretation of why this phenomenon happens, but I would like to say, if you can eventually explain why it happens, it will give us some insight into why it occurs in these other materials.

R. H. SIEVERS: This refers to Mr. Perret and his last slide. It appears from that slide that there was an initial or measurable drop-off in overpressure--the overpressure dropped off considerably within the first few feet of the surface which apparently is contrary to what Dr. Newmark said in his Opening Address. He stated that there was no significant drop-off in this overpressure as you came down from the surface. It appeared from your observations of the Priscilla Shot that there was a significant drop-off in the first 3 or 4 feet of the ground surface of this overpressure, maybe even up to 30% of the overpressure as felt above the surface.

BILL PERRET: This probably occurs within a distance of considerably more than that 3 or 4 feet, but, in general, it probably is a result of the restrictions inherent to the size of source we are able to work with in the field. I suspect that the same sort of thing might occur for megatons in several 100 feet and for Priscilla it was within about 30 or 40 feet. For smaller shots, it might be observed within a shorter distance. It probably is more serious for the smaller shots because of the higher proportion of energy that is within the higher frequency region of the shock spectrum. If a megaton burst with a positive phase duration of the order of a couple of seconds, this pressure loss would probably be a minor sort of a thing. For a kiloton or a fractional kiloton where the positive phase duration may be at most a hundred or two hundred milliseconds, the portion of the energy in the high frequency end of the spectrum is relatively much greater and consequently it would cause a more serious pressure loss effect. This is one of the two things we're faced with in large explosion tests. One of them is that we aren't allowed to use big enough sources (megatons) and the other one is that we can never fire any tests in an area where soils are of the type in which we're interested in building. People are just too damn stuffy--they wouldn't let us shoot big shots in their backyards.

DALIM MAJUMDAR: The hydrodynamic domain -- what percent of the total domain do you consider this?

BILL PERRET: It is really defined by how fast the pressure will fall off in there. Usually it is not very large. For a TNT shot in soil or rock for instance, it probably extends only a few feet beyond the boundary of the charge. For a nuclear shot, it would extend out to a distance at which the pressure would fall to a certain value. For instance in Frenchman's Flat or Yucca Flats soils, it would probably extend out to a point where the stress would fall below about 5 to 10 kilobars. This might be 30-40-50 feet from a confined shot. It isn't very far and certainly it's not of any concern to structures because the stresses are all so high that you couldn't design a structure, at least with present materials, that would withstand such loading.

STAN BEMBEN: I should like to ask Bruce a question. Did you make any pore-pressure measurements in your shear box?

BRUCE SCHIMMING: No.

STAN BEMBEN: Do you think then, perhaps, that the behavior which you interpreted to be an increase in shear strength is not merely a shifting of the shear envelope to the left due to the origination of negative pore-pressures? This would tend to indicate then that the shear strength has not really changed but that your measurement of the stresses was incomplete. This might be kind of important because in application it would mean that the shear strength would be the same and that we would have to be concerned also with the rates of loading, and not only with that, but also with the drainage characteristics of the materials.

BRUCE SCHIMMING: Which set of slides are you referring to?

STAN BEMBEN: To both. For instance, when you started with sand, you showed that the curves were going higher and then when you showed the composite slide in which the shear strength of the one clay varied with water contents, the wetter material appeared to have a higher shear strength. I was wondering if perhaps this was just a larger negative pore-pressure. It appears that there is a consistency between both materials and it appears that you really didn't have any differences in shear strength if you consider the effective stress concept.

BRUCE SCHIMMING: Unless we are able to measure a pore-pressure under appropriate drainage conditions and examine this effect, I suspect that for that material and for those rates of loading, there should not be that kind of variation in pore-pressure.

DWAYNE NIELSON: Referring again to this pore-pressure, the Ottawa sand apparently has a much larger permeability or air permeability than the clays. In the Ottawa sand with the higher permeability, the effect between the two was comparatively small; whereas for the clays which you showed on the slides (especially the wet ones, which would tend to prevent the air from getting into the sample as the sample expanded) would tend to build up this large negative pore-pressure (tension) which has been mentioned. Does this sound reasonable, and if so, would it tend to bring these two curves closer together?

E. A. SIBLEY: Our next paper was prepared by Mr. W. B. Truesdale and Mr. Anderson entitled "A New Device for Soil Strain Measurement" and will be presented by Mr. Truesdale. Mr. Truesdale is an associate research engineer at IITRI and also has his B.S. and M.S. in Civil Engineering from IIT. Mr. Anderson, who is not present, is manager of the instrumentation and recording section at IITRI.

W. B. TRUESDALE: Presentation of formal paper, see pages 127-137.

E. A. SIBLEY: We are open for questions.

P. L. HUMMEL: What is the size of these coils?

W. B. TRUESDALE: The coil wire windings are encapsulated in epoxy to give them strength and to insulate them from moisture effects in the soil. The thickness of the encapsulated coils is a 1/16 inch, the outside diameter is 3/4 inch.

P. L. HUMMEL: Have you utilized this device in measuring these strains in various field applications?

W. B. TRUESDALE: The gauge, as is, is strictly a laboratory device. We are currently modifying it to come up with a field gauge based on the same principle.

ALBERT KNOTT: I would like to know what kind of problems you are experiencing in trying to place these in the field when you have compaction problems and trying to recreate in your disturbed hole?

W. B. TRUESDALE: Again, it is strictly a laboratory device this far. In the laboratory, the only uses in cohesive soil which require compaction have been in triaxial specimens, and specimens to be tested in unconfined compression. As a check on how well we place the coils, we cut the specimens apart after testing and measure mechanically the coil separation and compare this with the spacing as determined by the electronic outfit. The recorded spacing was consistently within 2% of the measured spacing indicating that we could consistently place the coils within the limits of alignment necessary to obtain accurate measurements.

As to the problem of duplicating the soil conditions, the gauge has been used in remolded specimens and the coils were placed as the specimen was built up. We would first lay one coil on the soil surface and compact soil above it and then place the second coil and compact additional soil. We had to maintain a rod through the center of the coils while applying the compactive effort, otherwise the coils would move freely since they are uncoupled. You must also exercise care in applying compactive effort in the vicinity of the gauge. In triaxial specimens, we found that we could place the gauge well with a single rod through the center of the coils to hold orientation using a Harvard miniature compaction device with a 20 lb. spring. You certainly couldn't use a Proctor Hammer or any heavy type of compaction device and hope to place the gauge within the necessary requirements on alignment because the coils are uncoupled and they will move as the soil moves. To use the gauge in the field, the problem of duplicating soil conditions is a less critical one than with a stress gauge where one has to rely on the pressure of the replaced soil on the gauge. In this case, the soil must be replaced in exactly the same condition as you removed it to obtain an accurate in situ measurement. The strain gauge can be coupled to the natural soil surrounding the excavation made for the gauge. With the field gauge, coil separation of 6 or 8 inches will be used. Perhaps, we could take a core out, which we could replace. Again, over the area of the core, certainly we would have changed the stress condition, which would be a free sort of condition on the area of the core. However, compressively it would replace the cored sample. The field problems we haven't started to get into yet since we just started to revise the gauge for use in the field.

MARC CASPE: What are the upper and lower limits of the dimension L between the coil disks? Is this instrument amenable to strain rosette arrangement? Can you align these things to get your three dimensional effects?

W. B. TRUESDALE: The upper limit of L is, with the current gauge, about one inch. In our work toward developing a field gauge, we have been modifying the black box and it may be that spacing can be increased about two diameters of the coil--whatever the coil diameter that we selected. We are working right now with a 6 inch coil; however, I don't think we will go that large with the field gauge. But with 6 inch diameter coils reasonable sensitivity is obtained at about a 12 inch spacing. There is no limit electrically on the minimum spacing which can be used. You couldn't get spacing smaller than the soil particle size. This is certainly a lower limit, but because requirements on placement become extremely crucial as the coils come very close together, around 0.3 inch is a reasonable lower limit. I would say roughly you can combine things like 5 or 6 degrees rotation and lateral displacement of 10 percent of the axial spacing and not introduce much error. Ten percent at 1/2 inch is only 0.05 inch, less than 1/16 of an inch. When compacting soil around the coil disks, this can be a pretty difficult tolerance to hold. At an inch, spacing lateral misalignments of about .15 inch have essentially no effect on the ability to accurately measure differential changes. Thus, 0.15 inch gives us in excess 1/8 of an inch at a 1 inch spacing.

As for trying to measure strain in more than one direction at one point, this is not currently possible. The reason for this is that the coils interfere with one another when they are placed in close proximity to one another. One gauge cannot be placed within 2 or 3 inches of another without interference between the magnetic fields. By the same token, they cannot be placed extremely close to materials which have magnetic properties. The distance within which they can be placed near materials with magnetic properties varies, depending on the type of material and the relative position. Directly behind a coil is much worse than to the side because the magnetic field extends to greater distances to the rear than to the side. Steel is directly behind the gauge. A clear spacing of 3 or 4 inches is required in proximity to steel--one of the worst materials; to the side, 1 to 1-1/2 inches is necessary.

MARC CASPE: This then would have no use as far as the experiment Mr. Schimming just presented?

W. B. TRUESDALE: Do you mean to measure shear strain--to measure the lateral movement of the coils, one in relationship to the other? The sensitivity of the coils to closing is so much greater than to lateral movement that I think that dilatational effects in the soil as it is sheared would introduce large errors in the lateral motions measured.

DISCUSSION

HAROLD G. MASON: I have three questions--first, what is the diameter of the rod used to space the plates?

W. B. TRUESDALE: It is of stepped diameter. The larger diameter is 0.10 inch and the smaller is 0.04 inch.

HAROLD G. MASON: The one between the two end plates of the gauges is the larger diameter one?

W. B. TRUESDALE: Yes. The one between the 2 gauges is the larger diameter. We've made much thinner ones, but in compacting in clay specimens we would break the tip off. I've also placed the coils by running a vertical string down through a test chamber and just sliding the coils down the string to rest on the soil surface. I did not remove the string, but on the compressive measurements made, I don't think that the string hurt.

HAROLD G. MASON: I'm worried though about the cases where you did use the drill as a centering rod. On pulling the rod out after placing the soil, it would seem to me that this would create a rather large distrubance of the soil and thus negate all the care given to placing it between the end plates, and not make it very representative of true free-field strain. The second question--what about disturbance of the end effects of the plates themselves? In triaxial samples for instance, we try and maintain a length-to-diameter of greater than 2 to minimize the end effects. Since the end plates of the gauge are much closer together, only one diameter apart, I should think this would be rather critical and have a large effect on the ability of the gauges to read true free field.

W. B. TRUESDALE: In the triaxial specimen there is definitely quite a bit of end effects on specimen strain in spite of the fact that we use a two or one length to diameter ratio. This ratio was selected on the basis of consideration of the stress conditions in the failure zone in accordance with St. Venant's Principle.

HAROLD G. MASON: No. I'm worried about the gauges themselves. They don't have that aspect either.

W. B. TRUESDALE: Right. Essentially what we have is a maximum of 1.33 to 1. We're attempting to study the influence of the gauge presence on the strain occurring in the soil. It appears to vary with the soil stiffness. In sand, there appears to be more effect in dense sand than in the loose sand. In clay, the opposite appears true but it is difficult to study because it is hard to generate a uniform strain field to investigate what effect the gauge has on it. The triaxial specimen definitely does not have a uniform strain field. The most suitable test we have been able to devise has been by placement of the gauges at the edge of a triaxial specimen. The check on influence gauge presence was accomplished as follows: A number of points were marked along the surface of the specimen. The original position of each point along the specimen was plotted as the abscissa, as shown in Figure 1 (see page 127), versus the corresponding measured absolute displacement of each point, at a common time. The curve obtained permits graphical determination of the strain at any point along the specimen. Strain at a point being the slope of the curve, x/x, at the point. The curve obtained for the length of the specimen could be examined for distortions consistently appearing in the vicinity where gauges were located. Figure 1 presents typical test results. In this test, three gauges were installed in the specimen; near the top, midheight, and bottom. The gauge output is represented on the figure by the slope of the straight lines superimposed on the curve of absolute point displacements. The curves do not show obvious distractions in the vicinity where gauges were located and, in general, the slope of the gauge output is a satisfactory tangent to the curve. This technique is suitable only for small strains, however, because of the formation of shear lines on the specimen surface which distort the curve of point displacement.

HAROLD G. MASON: The third question--what was the size of the triaxial specimen?

W. B. TRUESDALE: It was a 2.8 inch diameter specimen.

HEINZ LEISTNER: I believe you said you were planning to use this for dynamic tests. Have you?

W. B. TRUESDALE: Yes. The greatest use has been in a study of strain variation in the triaxial test, we ran some rapid triaxial tests (Truesdale, W. B., "Strain Variation in a Triaxial Soil Test," IITRI for the AFWL, WLTDR 64-47, March 1964). However, whether or not you would call them dynamic is questionable. They were of the same sort of loading rates Schimming was talking about with the direct shear tests. The gauges also have been used in some pressure vessel tests at IITRI on buried tunnels, but this work has not yet been reported. It is going on right now.

HEINZ LEISTNER: No wave propagation of any sort through the tunnel?

W. B. TRUESDALE: No. We are hoping to use the gauge in this type of study. As yet, we have no information on this.

E. A. SIBLEY: Thank you Mr. Truesdale. George Hoff, Civil Engineer at the Waterways Experiment Station, and a graduate of the University of Illinois will review the "Shock Isolation Materials--State of the Art." Note that the title reads isolation materials--we are still outside the structure.

G. C. HOFF: Presentation of formal paper, see pages 138-154.

E. A. SIBLEY: The next paper will be by Dr. E. T. Selig, who was introduced to you during yesterdays session. The paper is entitled "Stress, Strain, and Motion Measurements in Soil."

E. T. SELIG: Presentation of formal paper, see pages 155-171.

E. T. SELIG: Presentation of formal paper, see pages 172-188.

E. A. SIBLEY: Before we take any questions, we have one other item. It is a repeat performance for 30 seconds on negative pore-pressures in sand by Bruce Schimming.

BRUCE SCHIMMING: I think there was a slight misunderstanding. For the dense sand which expands upon shearing you stated that possibly therefore you could develop a negative pore-air-pressure; however, due to the permeability of the sand this would not occur so therefore the strength was not affected in contrast to cohesive soil where its permeability would be such that you could develop this negative pore-pressure. However, with all the cohesive soils tested, we did not notice any expansion of this type. If anything, it was constant volume and if you look at 40 seconds or 4 milliseconds this is basically a constant volume test. It seems to me that it would be conceivable that you might get a lag in the development of positive pore-pressures in the dynamic case which could explain some of that variation.

E. A. SIBLEY: Now, we'll take questions on the last two papers.

HAROLD G. MASON: In Mr. Truesdale's evaluation of the soil strain gauge, he compared the measurement taken by means of the gauge with a physical measurement between end plates of the gauge when he took the sample apart. Did he made any measurements to compare these readings with a sample undisturbed by the presence of the gauge? In other words, was another sample prepared and a comparison made? Because otherwise his evaluation to determine the influence of the presence of the gauge means only that the gauge sees what happened in its presence, but it doesn't mean that it has any relation to the free-field strain.

E. T. SELIG: Mr. Truesdale may want to comment on this too. Actually, all we gained when we cut it apart was to see if the gauge was where it says it was—which, as it turns out, it is in fact. The problem is to have an independent check of what the uniform strain field should be without the gauge there and I don't know that we found any procedure which was satisfactory for doing this. We tried everything—average strains, and measuring the variations on the surface. All we could probably assure ourselves was that the strain we were comparing it to was probably no better than what the gauge was telling us.

W. B. TRUESDALE: There is no way of measuring the final displacement and saying what effect this had on the strains. The only check that I could think of was measuring surface point displacements and seeing what effect the presence of the gauge had on the otherwise free movement of these points. I did run tests with and without gauges along the surface of the specimen. In the clay specimens on some tests, I would get a nice uniform curve along the length of the specimen for maybe 1% or 1-1/2% strain. At larger strains, however, shear lines start showing up on the surface of the specimen and cause little jags and jumps in the plot of these surface point displacements; therefore, it is very difficult for much more than very small strains to try and look at any type of known strain field to determine whether or not the gauge is restricting the free movement of the soil.

HAROLD G. MASON: But what I'm worried about is that if you take these out in the field or build a field version and you apply this information without knowing how you have distorted the field, you could be orders of magnitude off. Right now, I can't suggest any way of evaluating it against free-field conditions, but I think you must before you suggest that it is free-field.

W. B. TRUESDALE: Orders of magnitude—no I don't think so. Let's suppose that there is a restriction on the compressive movement of the soil. The soil around the gauge is going to create arching of load onto the gauge. Granted, there certainly is the possibility that there can be some effect. But, I don't think it can be orders of magnitude and it may in fact be negligible. It is not, in my opinion, comparable to stress gauge over-registration in soil. The soil pressures do not influence gauge output and the arching phenomena will tend to move the coil disks with the soil.

HAROLD G. MASON: All this is a distortion so that you are not reading free field stress.

W. B. TRUESDALE: There is undoubtedly some distortion. We don't know whether or not it is significant. We haven't been able to generate a test where we can tell for more than strain. The point you are making is a good one. I'm not trying to brush it aside, but I do not have sufficient information to make a comprehensive statement on gauge-presence effects. Over the range we have been able to investigate detrimental effects do not appear to be critical.

HAROLD G. MASON: My other question, Ernie, is did you ever change the diameter-to-thickness ratio on the accelerometers? Most types derive their sensitivity from forces applied to them; therefore, at least during rise time, they should have an acceleration that is proportional to the total force, which includes an arching force. With a diameter-to-thickness ratio of say 1, this could be a very large over-registration during the early times, which would have an effect on the accelerations read during the rise time.

E. T. SELIG: It could be. We didn't change this as one of our variables, partly because of the work that Dr. Seaman was doing with this variable. Again I think it depends largely on the wave length of the pulse with respect to the wave transit times. Also looking at theories of inclusions in solids, it appears that even with over-registration you will follow the motion although a stress concentration can be developed. If the time for the first passage of the wave is of any significance, I expect the accelerometer could be very sensitive to it.

HAROLD G. MASON: As long as there is a differential force between the two surfaces there is an error.

E. T. SELIG: Yes. But, of course, you have this on both sides once the wave engulfs the gauge, and prior to this the arching has not yet developed.

HAROLD G. MASON: Once you get the equilibrium. But I'm saying during the rise time you always have a differential.

E. T. SELIG: That is true.

DISCUSSION

HAROLD G. MASON: I would like your opinion. Basically, I found that the biggest problem in developing a gauge has been inadequate capabilities to evaluate it's ability to read the true free-field conditions, in other words, to devise a test in which you know the conditions well enough to evaluate the gauge.

E. T. SELIG: Your comment I think is very significant, especially since we had that problem with strain gauges, having spent many hours trying to assure ourselves that we had a test that was sufficient to evaluate the gauge. It is probably not as much a problem in stress measurement--you can visualize, for example, a large chamber and the walls a long way off. But I think in looking back at much of the work that has been done, one can find a lot of questions about the way the gauges have been evaluated, and this raises a great deal of question as to the validity of the conclusions--how well the gauges were really working.

E. A. SIBLEY: As Chairman, perhaps I should summarize this session. However, since time is running out and we are all anxious to get to lunch, perhaps the shortest conclusion is the best; therefore, we must conclude that nothing can be concluded.

SESSION FOUR -- TUESDAY PM
STATE OF THE ART
SESSION CHAIRMAN: G. L. Arbuthnot

D. A. LINGER: The next session is on the state of the art of soil-structure interaction. The Chairman of this session is Mr. Guy L. Arbuthnot. He is the Chief of the Engineering Research Branch of the Nuclear Weapons Effects Division of the U. S. Army Waterways Experiment Station, Vicksburg, Mississippi. Mr. Arbuthnot has had long and varied experience in the fields of weapons effects and underground structures, and is exceptionally qualified to chair this session.

G. L. ARBUTHNOT: Up until now our sessions have dealt mostly with free field phenomena. We've had sessions on wave propagation, stresses, strains, ground motions and instrumentation connected therewith, with the exception of the paper presented by George Hoff. This afternoon the emphasis is going to shift a bit to get a little closer to the problem of soil-structure interaction; we're going to take up a series of papers dealing with research efforts referred to by Dr. Newmark yesterday morning as being fashionable at the moment. This research involves tests of buried tubes, buried cylinders, buried conduits and so forth. Professor Linger, with the possible exception of the Chairman, has done a very fine job in selecting the speakers for this afternoon's session. I think it would be extremely difficult to select a better qualified group of people to bring us up to date on this currently fashionable research field. We hope to have a little time at the end of each paper for discussion and questions. I hesitate to introduce our first speaker as the grandfather of this business, because first of all he isn't as old as Bill Perret. Our first speaker is Jay Allgood and most of you know Jay. He is a structural research engineer in the Structures Division at the Naval Civil Engineering Laboratory at Port Hueneme, and he is going to speak on "The Behavior of Shallow-Buried Cylinders--A Synthesis and Extension of Contemporary Knowledge."

J. R. ALLGOOD: Presentation of formal paper, see pages 189-210.

G. L. ARBUTHNOT: Thank you Jay. We have a couple of minutes here for questions.

PETE WESTINE: To obtain these results you have done dynamic modeling. I would like to know if this represents Reynolds-Froude, or geometric scaling? I assume a similitude analysis was made.

J. R. ALLGOOD: To avoid intruding on the session of tomorrow morning, I think I will just say that we may consider these as small structures rather than models. I think this point will be well clarified by Dr. Young's paper and others. I'm sorry to hedge on you but I think it will be best not to be more direct at this time.

MERIT WHITE: In comparing the hydrostatic buckling with the observed buckling load, would it be reasonable to consider that when a structure such as a curved cylinder buckles certain parts, of course, must move in under the loading that's applied? Other parts must move out against the soil and when they move out against the soil they are pushing and it's harder for them to move out because they must overcome a passive soil resistance so to speak. So that in effect your active, working, causal load is the load you apply to the surface, whereas the resistance that is built up causing the buckling is six, eight, ten times as much.

J. R. ALLGOOD: I think you're certainly correct. And this is undoubtedly the reason that, although the period of these circumferential waves is the same as in hydrostatic loading, buckling does not occur until much higher loads. In other words, buckling does not occur until loads corresponding to a much larger value of n, the number of circumferential waves. Unfortunately we don't have good solutions to tell us just what this load is at the present time, although we certainly can make better approximations than we could have a year ago. Because of Bulson's and other experiments that will be presented at this Symposium, we have a much better idea of what these buckling loads are for these cylinders and we know where they lie with respect to the critical buckling load as calculated from the equations of Gjelsvik and Luscher I showed you, and where it lies between the hydrostatic case and this elastic support case.

ALBERT KNOTT: First of all, would you define what the end condition of these shelters were and what effect you felt it had on the structural action of the models or small structures? Secondly, would you comment on the concept that if a structure deflects an appreciable distance, the soil will then arch over it, thus relieving the loads on the structure and eliminating buckling or complete collapse of the structure? This would correspond to Dr. Newmark's comments about the fact that he felt the buckling was not too great a problem in buried semicircular arches.

J. R. ALLGOOD: Perhaps Dr. Newmark was speaking in a different context. Buckling is a real possibility. This was first shown, as far as I know, by Reynold Watkins, and it has been shown subsequently by several others, some of whom are in this room. At present we don't

know how to accurately determine buckling, so one usually uses a large corrugated plate with ample stiffness to help prevent such failure.

In response to your second question, if you study this problem you find that it's impossible to get sufficiently large deflections of a metal cylinder to develop arching. Consequently even at failure you're going to have the surface load acting on the structure, unless you resort to some method such as allowing slip in the bolt holes if you have a bolted section, or unless you put a soft bedding material at the invert. This is almost another lecture. You find that when you do this there are several deleterious effects which occur. One of which is, if you have a soft bedding and you allow the cylinder to move downward, then the soil over the top develops a momentum. When it tries to stop, its inertia loads the structure and so you may not have improved things one iota. As far as your first question is concerned about the number of circumferential waves and what their consequence is, I'm not sure I can give you any answer beyond telling you that they did appear to be exactly the same on the side as the hydrostatic case. I think n was 7 or 8 for these particular cylinders. For every bit of data that I've checked against, including Bulson's, we do get this agreement and I think that a cylindrical shell has a stiffness such that this is the way that it wants to behave.

G. L. ARBUTHNOT: In the interest of time I think we had better get on to the next paper. Any discussion on the results of tests on buried cylinders would not be complete unless we heard from our next speaker. Again, Professor Linger has even arranged for that. Dr. Bulson is head of the structures group at the Military Engineering Experimental Establishment at Christchurch, in South England. It's a part of the Army Department of the United Kingdom, Ministry of Defense. He will speak to us on "Buried Tubes Under Surface Pressure."

P. S. BULSON: Presentation of formal paper, see pages 211-238.

G. L. ARBUTHNOT: Thank you Dr. Bulson. Let's move on to the next paper, and then perhaps we can come back and ask questions to both of the last two speakers. Our next speaker is Mr. Carl Wiehle, who is a senior structural research engineer at the United Research Services Corp., and he has had a long record of work in protective research in general. Mr. Wiehle will speak to us on "A Review of Soil-Structure Interaction."

C. K. WIEHLE: Presentation of formal paper, see pages 239-245.

G. L. ARBUTHNOT: Before we go on to the next speaker, I wonder if there are any questions or discussion concerning the papers by Dr. Bulson and Mr. Wiehle?

PETE WESTINE: I would like to ask Dr. Bulson what influence he felt the membrane had on the pressures measured as opposed to the pressures transmitted to the soil? It seems to me that the deflection and curvature of the membrane were significant, and thus an important portion of the load was carried by the membrane. Are the pressures that you are measuring the pressures applied to the soil?

P. S. BULSON: Yes, we did look into this before we had started and made some calculations on this and we're pretty confident that the pressures we showed are pressures applied to the surface of the soil.

PETE WESTINE: This was then a very weak plastic membrane?

P. S. BULSON: It had a lot of extension.

ULRICH LUSCHER: I found in my work that it was always one of the greatest difficulties to develop tubes which could be used in the test. For instance, difficulties of getting them round and making the joints. I wanted to ask you, how you rolled your square tubes with the rounded corners, and how the joint was manufactured.

P. S. BULSON: The joint was a welded joint in the steel tubes and we always had it in the center of the lower face of the tube. The rolling was done pretty accurately in our work shops, but I don't know the exact details of the procedure. We measured tubes after rolling and they were very accurate. They were formed on very small rolls by hand. There was no mass production.

KAARE HOEG: As I understand it, your approach tunnels were rigid, while your test sections underwent large deflections. As you are actually attempting to simulate a two-dimensional condition with a non-varying pressure along the axis of the cylinder, what effect do you think the mismatch in the stiffnesses had on your results?

P. S. BULSON: I didn't really have a chance to make this clear in the paper but it will be clear in the report. This is very important, but for the depths of cover shown in the film, they were rigid and there was very little difference between rigid and flexible tunnels; however, when we started using deep depths of cover we had to make the tunnels the same flexibility as the specimen, otherwise there was arching along the longitudinal lengths. We did some tests, which will appear in a later report showing the effect of non-flexible and flexible tunnels. This was done mainly, I might say, as the result of your comments when you visited us.

ERIK SOLLID: It seems to me that Dr. Bulson's experiments indicate that there couldn't be any arching as evidenced by the cave-in nature of the roof collapse. Could there possibly be a time factor which would indicate where you could consider arching or where you could not? It seems to be a subject for argument whether or not arching is reliable under long time load applications.

P. S. BULSON: I prefer not to answer that, but certainly there must be an effect with square sections because of an increase in collapse pressure with depth of cover. We used a small specimen loaded over a very large area, and one assumes that the free field pressure with no specimen must be uniform all the way through. If there is any discrepancy with depth, it must be due to some effect which you could put under the general heading of arching. I don't know how else you would explain this.

ERIK SOLLID: It seems to me that with time the soil grains would realign themselves and ruin the arching effect.

DISCUSSION

P. S. BULSON: I think you're asking a question that no one can answer. The whole fundamental theory of arching is not very clear.

MERIT WHITE: This refers to the same question. I think the fact that the square tubes began to buckle on the top and then finally collapsed on the sides, is proof that there was arching.

G. L. ARBUTHNOT: Let's go on to the next paper. It will be presented by Reynold K. Watkins, Professor and Head of the Department of Mechanical Engineering at Utah State University. The title of his paper is "Design Trends in Buried Flexible Conduit."

R. K. WATKINS: Presentation of formal paper, see pages 246-255.

G. L. ARBUTHNOT: Thank you, Dr. Watkins. I think we have time for questions if we have some.

G. F. WEISSMANN: Did you consider the price in comparing installed flexible conduits with rigid conduits? I am pretty sure that installed flexible conduits become more expensive than the rigid one if special trench preparations have to be made or selected backfill has to be used.

R. K. WATKINS: I have not been concerned with prices personally, but those for whom we should reduce this to practice are connected with prices. And I'm sure the great demand for more information on flexible culverts as well as rigid culverts would confirm the fact that there are areas in which flexible culverts can compare very favorably. Others of you have much more experience in this than I, and I would welcome some help.

H. P. HARRENSTIEN: I'm your help. We've considered cost effectiveness of applying this type of structure to actual survival shelters and I think when you consider the extra toughness that the flexible material has over and above the rigid conduit, the cost effectiveness of this system is much better because a flexible culvert can resist much higher loads, particularly in blast, than it is designed for by these procedures, and the rigid tend to have their problems with this active settlement ratio.

MARC CASPE: Do you feel there is any application of this soils arch concept in areas of high seismisity?

R. K. WATKINS: I'm sure there is. I hesitate because I don't know the degree to which it would be applicable. I like to think in terms of a masonary arch design, in the design of our soil. Masonary arches seem to work fairly well in areas of seismic activity. So long as we have something to reinforce the hole, or to reinforce the soil, then I believe we can get by, although I don't know the degree to which we can get by.

R. H. SIEVERS: It appears there is a direct conflict between the manner in which you recommend that the earth be compacted over this flexible arch structure, to that which has appeared in recent design manuals for protective construction of such structures. These manuals say that the soil should be very highly compacted adjacent to the structure, I think up to the 2/3 point, and loose above it, over the structure and to the sides. Perhaps Professor Haltiwanger would be more capable than I at resolving this. Is it true that your structures are primarily for highway and not blast design, whereas these are more in the protective structures line?

R. K. WATKINS: This is true. I'm interested more in the standpoint of highway, airport, earth-fill design. I wonder if the concept of loose soil above the pipe follows somewhat the "imperfect ditch method of placement" so that we can reduce the load on the top of the pipe. If this is true, then I would add that the way to reduce this load is to somehow support the soil above the pipe by a method other than the pipe itself. It seems to me that somehow we've got to come to the soil arch, one way or the other.

L. H. GABRIEL: The terms "flexible" and "rigid" conduit are somewhat illusive. If you'll permit me a definition, then I may have a comment to make. If we consider a flexible conduit as a structure less still than the surrounding soil, and a rigid conduit a structure more still than the surrounding soil, then I'll proceed.

R. K. WATKINS: I would like to extend to you the privilege of proceeding. I think you have to define what you mean by still. If you mean this reduction in area concept, the compressibility, this would be different from talking about the flexibility stiffness.

L. H. GABRIEL: I'm thinking of flexibility stiffness.

R. K. WATKINS: All right.

L. H. GABRIEL: I would like to report very briefly on some work that has been going on at Sacramento State College. It was here that we ran into a phenomenon that at first we thought was the impingement of a buckling phenomenon but we're coming to the conclusion that it can probably be more aptly described as a wedging type action taking place. With a circular conduit, flexible in handling stiffness, as compared to the surrounding soil, first with low loads (these are static highway loads) we found a shortening of the vertical diameter and a lengthing of the horizontal diameter, as one would expect. We tried very hard to arrive at compatibility between what we found in some assumed parameters for an elasticity solution on this pipe, which was made out of concrete, but having found no compatibility, we looked for areas where we might rectify our assumptions. We found that if we were to increase the passive pressure of the very stiff walls of the side by increasing the load, the pipe would settle into a narrower area, narrower cross-section. What we did find eventually was a complete reversal. We found that the horizontal diameters started going in the other direction with heavier loads now being imposed upon the pipe, and that the vertical diameters lengthened, which of course completely reverses the stress field and the strain field, as one might expect. We're continuing with these things and we hope that this in itself may lead to some idea of why these pipes carry so much more load than they're expected to, if one just wanted to superimpose the elasticity solution on them.

J. D. HALTIWANGER: Perhaps I should comment, or more appropriately, perhaps I should go back and read the Air Force Design Manual, with which I have had some contact. I don't remember seeing in that manual the reference that you made. I think it rather unlikely. If my memory serves me correctly, I think we suggested, that in back-filling around culverts or cylindrical structures of this sort, the back-fill be made uniformly dense in order to avoid soft spots, and thereby reduce the possibility of failure by buckling. I don't know what other manual you may have been referring to.

R. H. SIEVERS: Here you have a circular structure or an arch structure. You could compact very highly up to this 2/3 ds. point, although it's very hard to compact above this point in any case, but the compaction above this point was not really so essential. What you're trying to do is provide the resistance for this structure, to build up a resistance to pressure at the sides. The compaction at the top was less significant and it may not be as critical as that achieved at the sides. That is not taking into consideration the possibility or desire to achieve any soil arching over the structure.

HOWARD WHITE: In your own state here, across the northwest corner, there is a 15 foot diameter pipe under 80 feet of fill, which might be of interest to you. I would like to suggest that I believe there is a good deal of information, not perhaps directly for blast shelters but certainly in the design of these conduits, that probably could be gained by installations already in the field. When you're talking about the deliberate building-in at the sides of the structure of a soft or yielding situation, this is good for extreme cases of high fills in which it might be more economical to do than it would be to put it in the metal. But you must look at that in view of the use of this structure. If the cover is reasonably shallow on top of the structure, it may be more desirable to put more metal in the structure and compact very hardly all around the structure in order to save the roadway, which after all is the reason for holding the fill up there.

G. L. ARBUTHNOT: Now we should go on to the last presentation of this session. Our last speaker is Dr. Van Horn. He is currently a Research Associate Professor of Civil Engineering in the Concrete Division of the Fritz Laboratory at Lehigh University. Dr. Van Horn will speak on "Analysis of Time Dependent Loads on Underground Structures."

D. A. VAN HORN: Presentation of formal paper, see pages 256-282.

G. L. ARBUTHNOT: Are there any questions or comments for Dr. Van Horn?

PETE WESTINE: On the previous paper, we have a question concerning whether or not one could depend upon arching under seismic loadings. In his book, Dynamics of Bases and Foundations (translated from Russian into English by Dr. Tschebotarioff), Barkan reports that under vibrations of certain frequencies, granular soils lose all shearing strength and become essentially a fluid. In such a media, I hardly believe one could depend on arching to occur. I do not know what frequencies are involved; however, earthquakes with their spectra of frequencies could initiate such a phenomena.

R. K. WATKINS: Do the Russians say anything about a critical density of material? I can see if the material is of sub-critical density, that is, if on vibration it will reduce its volume that this would easily be the case. However, if the soil is compacted sufficiently so that any vibration would cause it to increase in volume a different situation would exist.

WALTER LUM: We have all quoted Terzaghi today but we never followed him up; what he says in his book, Theoretical Soil Mechanics, and what he does in the field is something different. One paper that I've found on the static loads on tunnels and on the design of underground structures that has gone unnoticed today is a paper that Terzaghi had written on the Chicago subways in 1943 in the ASCE Transactions. In this paper, he tells you all the parameters that affect the loads on an underground structure: the soil above, the soil on the sides, the soil below, and the manner in which the work is done. Arching is a temporary effect and in plastic soils because of creep, the full overburden load can be expected. The main thing that Terzaghi brings out in the importance of how the work is done and its effect on arching. Depending upon the workmanship in the field, arching above an underground structure can have a wide range of values.

MARC CASPE: As far as Barkan's reference is concerned this is quite correct and this has been substantiated by the Japanese in "shaking table" analyses. The comment as far as density is concerned, this is basically true that there is no increase in lateral pressure on a dense soil as you would get in a loose, unconsolidated soil. But the arching action, the actual $\emptyset$, you have to consider this as completely destroyed. I think this applies also to the paper that Dr. Van Horn has presented. He mentioned that the c would be destroyed, and I'm afraid the $\emptyset$ would also be destroyed. In passing, as far as open cut design, which we are doing right now on the San Francisco rapid transit district, using soldier beams and lagging, this is a typical case in point where you consider the arching from soldier pile to soldier pile. In this case we feel we have to take into account for the lagging design such an occurrence since it might be a year or so before the actual support might be in position. The lagging must be designed for some degree of lateral pressure, which is not usually the case.

DWAYNE NIELSON: I might shed some light on this seismic loading. Here at the University of Arizona we have a small blast simulator that we have been testing in the labs. In this simulator, we have a small cell about 4 to 6 inches in diameter. The cell has three rigid posts on which strain gauges have been placed to measure the loads transmitted to the structure. Static and dynamic tests were made and it was found that a larger static pressure was transmitted to the buried structure than dynamic pressure. Our dynamic pressures were usually about 75% of the magnitude of the static pressures transmitted to that structure at any given depth. The rise time of these dynamic tests was of the order of 1 millisecond. The duration of the impulse was about 1 second duration. In each case the material used was a clean concrete sand.

D. A. VAN HORN: Was the peak pressure the same in both cases, that is to say, was the peak pressure in the dynamic tests equal to the maximum pressure in the static test?

DWAYNE NIELSON: That's right. In the static test the pressure was held constant or raised up over a relatively long period of time, say 5 to 10 minutes, and in the dynamic tests it was set off with the hydrogen-oxygen mixture and allowed to decay in the matter of

approximately a second. The rise time was about one millisecond.

D. A. VAN HORN: With what kind of an h/ℓ , or a depth-dimension ratio?

DWAYNE NIELSON: It didn't seem to make too much difference about what depth the structure was buried.

D. A. VAN HORN: This is exactly what this analysis will show. I'm certainly not saying that this is a last word; I'm just saying that for a few different cases that I computed by this method, which I did not show, I found that the percentage gain, that is, going the other way, taking a peak overpressure which would produce the same effect, is roughly 25% greater for sand, which would be the same thing. If you pulled the peak overpressure time-dependent down, you would produce only about 80% of the effect. So this is definitely in line with this analysis. I'd like to see your data.

DWAYNE NIELSON: There is one other consideration I would like to point out. Although the structure was rigid, it did have a flexible or membrane type roof over the surface, so the surface would dish down in a membrane configuration.

G. L. ARBUTHNOT: The five papers presented in this session indicate that there is indeed appreciable attention being directed toward tests of buried cylinders. Also indicated are some encouraging research results for small cylinders buried in dry sand. Whether or not these efforts are currently fashionable, they stem from a real and urgent need for design procedures applicable to economical protective underground structures. Buried cylinder studies are an initial approach to a solution of the problem of designing real structures to be located at various depths in both soil and rock. The discussions that followed the presentations of the five papers pointed out many of the real problems with which we are faced.

In order to advance significantly the state of the art, it is necessary that we move from the dry sand case to other types of soil as well as other types of structures. In addition, it is necessary that the results obtained from these small structures, or model tests, be scaled to the real situation, thus other needs are indicated. There is an urgent need for the development of procedures for modeling structures buried in soil or rock, from which test results can be obtained and analyzed with a fair degree of confidence. Currently there are several simulation devices suitable for tests of small buried structures or small models; however, sizes of the structures are extremely limited. Therefore, we need blast simulation devices in which high overpressures of long duration over a large surface area can be produced in order that larger model structures can be tested.

The cost of full scale tests are such that we can never hope to solve all of our problems at the Nevada Test Site, even if the current test ban is lifted and we are able to go back to above ground and surface bursts of full scale weapons.

SESSION FIVE — WEDNESDAY AM
SIMILITUDE AND MODEL STUDIES

SESSION CHAIRMAN: J. R. Allgood

D. A. LINGER: The Session Chairman for this session on model studies is Mr. Jay Allgood, who is quite well known to all of us for his extensive and outstanding contributions in testing underground structures. He is presently a Research Engineer with the Naval Civil Engineering Laboratory at Port Hueneme. With no further ado, let me introduce Jay Allgood.

J. R. ALLGOOD: Thank you Don. Gentlemen, the session this morning treats the modeling problem. Our first speaker is eminently qualified in this area of knowledge; he is an associate of Glenn Murphy, who is co-author of the paper, who has as you know, authored a book on this subject, and has long experience in modeling work. Dr. Young, who will present the paper, has his Master's degree and his Ph.D. degree from Iowa State University. We are very pleased to have Don with us to present his paper, "Similarity Requirements for Underground Structures."

D. F. YOUNG: Presentation of formal paper, see pages 285-295.

J. R. ALLGOOD: We have time for a few questions here.

HAROLD G. MASON: This is not a question, bur rather a comment. I think the bump furthest out of the traces may be a reflection from the bottom of your tank. It works out to be about the right time based on velocities that we have for this sand. The first bump, the one closest to the peak, I think, may be the effect of rarefaction due to side-wall friction. You get a rarefaction wave traveling in toward the center when the container has side-wall friction. At shallow depths, the loss due to side-wall friction is small so the rarefaction or unloading from the incident stress is small. At greater depths, the effect of side-wall friction becomes greater, and therefore the unloading wave is greater, the effect appearing on the stress-time trace as a larger bump. Your one-inch structure having, I gather, two-inch burial is pretty shallow so the rarefaction coming from the side wall has very little or no effect. The deeper you go for the larger structures, the larger the effect.

D. F. YOUNG: May I ask you a question? How did you calculate the time to the second bump?

HAROLD G. MASON: Using 650 feet per second for the velocity down to the bottom and back, you've lost some of the stress magnitude due to side-wall friction. My guess is you've lost something around 70% of the peak stress down and probably something coming back.

D. F. YOUNG: We tried to check this. It's an obvious thing to check. I don't remember what numbers we were using, but it didn't look like it was a bottom reflection. This is the thing I first suspected. Maybe we didn't use the right number for the seismic velocity.

HAROLD G. MASON: I don't know what sand you were using. I just took the numbers that we'd gotten for this stress level.

J. R. ALLGOOD: Are there other questions?

R. H. SIEVERS: It would seem that the period of vibration in the fundamental mode of these very small structures would be very critical in determining whether or not you do have an instantaneous rise time. I wondered if these had been computed and compared to the measured rise time of this shock wave?

D. F. YOUNG: We do know approximately what the periods are, but these are for cylinders in air. I'm not sure what the period is when they are buried and I think this is an important unknown. Maybe some of the people here have information on that, but we don't know what the natural period is for the buried structures. We do know what they are in air, but they could be quite different, and in my opinion may be quite different.

J. R. ALLGOOD: We have set off small charges of high explosives over cylinders in our test pit and while we were able to determine the buried frequency of similar sized arches, we were not successful in determining the frequency of the cylinders. Oscillations damp out rather rapidly, thus, I would suspect frequency determination would be doubly difficult for the relatively thick-walled cylinders that you are working with.

J. I. BUSTAMANTE: I think you mentioned that the time variable was very important; however, it seems that you didn't take it into proper consideration. If your geometric ratios are from 1 to 4, the time should be included in the same ratio. The fact that you found very good agreement, at least statistically, seems to indicate then that you should take this agreement into consideration and not say from it that the time is not an important variable. Time is usually very important and would seem to be very important in this case. However, when you had differences in geometry which is another one of four important variables, and you didn't take time into consideration, and the agreement was so good, wouldn't that seem to indicate that the time is not important. My question is essentially, did you take into consideration the time units?

D. F. YOUNG: The shape of the loading pulse is important and this is, of course, time dependent. I think the reason that we ended up with good agreement here, even though the duration of the pulse was not scaled, is the fact that as far as the cylinder is concerned, the pulse looks like a step pulse, so we were scaling it. Other tests we have run where we did not have an instantaneous rise but a rise time of a fraction of a millisecond, indicate that you do have to scale the loading pulse in order to get good results. So the time is important. We neglected it here because we had to, but I think because of the shape of the loading pulse it took care of itself, but it is an important parameter.

J. R. ALLGOOD: I think that about takes care of our time. As Don pointed out, I'm sure the important parameter is the ratio of natural period to the duration of the load, and if one has an effective step load, as far as the cylinder is concerned, that is the important thing. Our next speaker, to add further enlightenment to the comprehension of the modeling problem, is a gentleman who is currently completing the requirements for his Ph.D. degree at Iowa State University. He is Captain Robert Tener, currently at the Waterways Experimental Station. He is presenting a paper entitled, "The Application of Similitude to Protective Construction Research."

R. K. TENER: Presentation of formal paper, see pages 296–302.

J. R. ALLGOOD: Are there questions for Captain Tener?

E. T. SELIG: This question probably could be answered by either of the first two speakers. I think Ottawa sand or, in fact, any sand, has a particular property with respect to scaling, if it's parameter of strength, which is taken as ϕ, is dimensionless in itself. Have you noticed or do you anticipate problems of scaling with cohesive soils where the scale factors, the dimensionless groups, will be such that some scaling of cohesion will be required in the test?

R. K. TENER: That is a very pertinent question. I think not for this reason. The dimensional analysis which leads you to scale material properties having the dimensions of a stress as 1 indicates that if cohesion is a significant variable in the analysis then cohesion can scale as 1. Then the proper provision for modeling the strength properties of the cohesive material will enable you to use the same material in model and prototype. There is a draft of a report presently at the Waterway Experiment Station to be published soon which regards the scaling of the material properties of buckshot clay, a highly plastic clay, and which has some very fine considerations regarding the scaling of these materials. Since you've opened the subject, I would like to point out one other thing. We are fortunate as long as we test in dry granular material regarding time scaling. As Dr. Young pointed out, his cylinders, likewise our arches, are hit by a virtual step pulse because of "shocking up" in sand. Thus the ratio of the rise time to the natural period of the structure is virtually zero except for very very small structures. When we get into cohesive materials, this will not be the case. The rise time will be finite and may well be of the order of magnitude of the natural period of the structure. Here is where time scaling is going to become much more significant than we have seen in any of our studies yet.

PETE WESTINE: When investigating the strain rate effects of clays, were any of your soils partially or completely saturated?

R. K. TENER: Yes, the work reported by Carroll for the University of Illinois and done at WES involved partially saturated plastic clay. These were dynamic triaxial compression tests.

PETE WESTINE: In dynamic problems under high rates of loading, negative pore pressures may develop. Once negative pore pressures develop, cavitation may occur. Do you feel pore pressure and cavitation effects can be modeled?

DISCUSSION

R. K. TENER: It is only necessary to model if it is important to the response which you are trying to predict. Present tests, in general and almost without exception, are run in loading devices which involve membranes above the test specimen to prevent dynamic pore pressures from being a large factor; that is, most of the stress is transmitted by effective or intergranular stress. Effectively then, in our test media, I think pore pressures have not yet been overly significant. As far as the need for scaling their effect goes, I think this is a matter for conjecture. In my opinion, it's not going to be too important.

PETE WESTINE: How can you say that pore pressures are unimportant when we are unable to measure them dynamically? You have no idea what pore pressures you had.

R. K. TENER: I agree but the proof is in the pudding. If you don't worry about it and you can successfully predict by means of a scale model, then I hold that you do not need to consider it.

ABNER SACHS: In the last two days, people have been using the word "steel" without giving us any indication of the physical properties of the types. Now you've shifted to "aluminum" and you've changed the physical properties of your arch considerably. Are you going to be able to correlate your answers or are you going to give us another set of variables that can't be used?

R. K. TENER: The first point I would like to make is that the work which we are doing at WES, and I think I speak for Dr. Young's study also, is not intended to be specifically related to any field prototype situation. These are basic scaling studies to verify the similitude relationships. With particular caution and exceptions, what holds for aluminum elastically should hold for steel elastically as long as we do not exceed the yield point. Now when we get into inelastic behavior, there are going to be additional considerations, and presently I am not qualified to extend my observations into this area.

DWAYNE NIELSON: I think Dr. Watkins pointed out yesterday that the effects of the pipe wall were negligible in predicting the deflections of these pipes.

R. K. TENER: I believe he was restricting himself to flexible pipe structures. I'm considering more the intermediate range of flexibility. A D/t ratio of 80 in aluminum might be flexible or rigid depending on who the speaker is. So I think his observation must be limited to flexible, or very flexible, structures.

J. R. ALLGOOD: Our next speaker is a gentleman of renown, who hands down takes the prize for having appeared before this group the largest number of times. Dr. Selig will present the paper, written by C. J. Costantino, R. R. Robinson, and M. S. Salmon, at the Illinois Institute of Technology Research Institute. The title of the paper is "A Simplified Soil Structure Interaction Model to Investigate the Response of Buried Silos and Cylinders."

E. T. SELIG: Presentation of formal paper, see pages 303-314.

J. R. ALLGOOD: Thank you Dr. Selig. That was most interesting indeed. We have checked our experimental data against one elastic theory of a wave engulfing a cylinder and find very poor agreement. The thrusts agree well enough, but the action of the shell isn't taken into account properly, apparently because the moments are in vast disagreement. It appears that this solution offers a good possibility of overcoming this difficulty.

N. J. EVERARD: I think what you just said is a very pertinent point, viz. that we have been looking at these structures as arches; whereas in fact, they are not arches. Most of these structures are shells. The problem that Captain Tener discussed is actually a barrel shell with ten diaphragms and I believe the structural action had better take into account a three dimensional stress distribution representing the arch action.

E. T. SELIG: I think this pretty much agrees with our view in trying to carry out such an approach. The simplest thing one can do is to take the free field condition and try to indicate how they are modified by the presence of the structure in a general way, and it seems to be reasonably successful. This solution, of course, is two dimensional and it assumes an infinite cylinder, but we have adapted it, I believe, to both tunnels and silos subjected to ground shock.

J. R. ALLGOOD: Well gentlemen, I hope you realize that the speakers have been very considerate of your time. Realizing they are using 3 man hours a minute, they have kept exactly on schedule. Now we will proceed to the next paper to be delivered by Delon Hampton. Dr. Hampton has his Ph.D. from Purdue University, and is a Professor at Kansas State University. He is currently working at the Air Force Shock Tube Facility, University of New Mexico, in Albuquerque. He will depart slightly from the modeling theme and present a paper entitled, "Effect of Shock Wave Induced Pore-Air Pressure on Small Buried Structures."

DELON HAMPTON: Presentation of formal paper, see pages 315-331.

J. R. ALLGOOD: Are there questions for Dr. Hampton?

P. L. HUMMEL: You mentioned earlier something about the relative velocities of the wave through the air versus that through the pore water and through the solids. Could you comment further on that?

DELON HAMPTON: The attempt was made to ascertain the magnitude of the rate of propagation of the pore-air pressures in the soil samples. The maximum velocity of propagation was determined to be approximately 250 fps. Actually, the velocity of propagation should be equal to or greater than the velocity of sound through air (approximately 1100 fps). The low value of the computed velocity is due either to the inability of the instrumentation to pick up the initial arrival of the shock wave or to the nature of the passage of a shock wave through small pores.

Regardless of the reason, it is safe to say that the propagation of pore air pressure through the pores of the soil will occur at a slower rate than the propagation of the effective stress wave. The difference between the two propagation velocities will increase with time, and the peak pore pressure at any given point will manifest itself at a later time than the peak effective stress. Exactly how much later will depend principally upon the properties of the soil and the characteristics of the shock wave.

MERIT WHITE: I'm glad you made your last remark about the importance of the shape of the wave. I have been thinking all the time that this is extremely important. The duration of the pulse is just as important as the peak pressure. This is one case where you can't talk about scaling the test unless you scale the time factor at the same time. For an infinitely long pulse, that is a step pulse, there would be no attenuation at all within any pore; even the tiniest hole in the soil would let this pressure in.

R. K. TENER: Dr. Hampton, would you suggest that the use of a membrane over the test medium in laboratory loading devices is a realistic procedure in view of the possible extent to which pore-air pressure in field test prototypes extends to depth and the possible effects of these pore-air pressures on prototype structures?

DELON HAMPTON: A membrane over the soil effectively prevents air from entering the pores of the soil. This simulates the case when the structure is buried so deep that pore air pressures resulting from air entering the pores of the soil would not be present. However, if it happens that in the field one is dealing with a relatively shallow structure, then pore air pressures will impinge on the structure.

In uniformly graded granular soils, the distance of propagation can be large. Therefore, for shallow buried structures pore air pressures may impinge on the structure, but what is more important is its effect on the stress state of the soil surrounding the structure.

L. H. GABRIEL: Are you sure that you're picking up pressure waves and not shear waves?

DELON HAMPTON: Yes, I am sure.

L. H. GABRIEL: How do you make the geometry of these long narrow columns of soil compatible with the occurrence of these pressure waves hitting the boundary, stress free or not, and breaking up by reflection into shear and pressure waves both? You say that the arrival times of your waves were slower than the waves you expected. Shear waves travel at a slower velocity and only one singular wave goes straight through without hitting the boundary. If the column is considered infinitely long, which it isn't of course, but suppose we consider it to be, the others would have to hit the boundary and then we would get reflections of shear and pressure waves both and just going tortuously through this, breaking up as they go every time, they hit the boundary into some more shear and pressure waves.

DELON HAMPTON: During the initial phase of this research it was found at penetrations of 0.22 foot and 0.38 foot, the measured pore air pressure was much larger than was to be expected based on the general trend of the data. It was felt that this was due to inadequate isolation of the soil from the sensing element of the gauge.

To check this theory, an impermeable membrane was placed over the upstream end of the samples which effectively isolated the air in the shock wave from the soil. In doing this, any pressure measured by gauges placed along the length of the soil specimen would have to be the result of the lateral pressure exerted by the soil; i.e., the soil must be acting on the sensing element of the gauge.

In these membrane tests, it was found that the first two gauges did register a pressure. Therefore, due to the nature of the test conditions, those gauges must have been showing the effect of the soil pressing against the sensing element.

The realization that the gauges were showing the effect of the effective stress in the soil prompted the change from the barium titanate gauge where the isolation of the soil from the gauge was not effective to the Granath ST-2 gauge with grommet which was found to be satisfactory. The adequacy of the new gauge system was confirmed by the membrane experiment; therefore, effective stress-wave propagation through the soil column would have no effect on the gauge readings.

L. H. GABRIEL: I didn't quite follow all of that. I will just ask this one question. I just don't have a clear picture of what the instrumentation was. This is probably beside the point, but I will ask this question anyway. Would you agree that there were shear waves within the soil mass? And could it not be the case that the sensing elements were also picking up the components of the shear waves?

DELON HAMPTON: Whether or not shear waves were present in the soil is of no importance. If the soil is isolated from the sensing element of the gauges, it is impossible for the gauge to register any component of the shear wave.

L. H. GABRIEL: I accept your word certainly, but perhaps I could just conclude with a claim. I would claim that whenever a pressure wave hit any boundary it would break up into a shear and pressure wave.

DELON HAMPTON: If the sensing element of the gauge is effectively isolated from the soil, the fact that a shear wave may exist in the soil is of no consequence to this study.

L. H. GABRIEL: I can understand that. OK.

R. H. SIEVERS: You say that in the shock tube work we ought to have a membrane over the beginning of the sample to avoid a secondary effect perhaps of this air pulse going through the cavities. Do you know if you experience a reduction in pressure felt by a pressure gauge which would be subject to both the intergranular pressure and the pore pressure within the soil when you do not have a membrane over it as opposed to the time when you do have a membrane over it? In other words, without the membrane are you just receiving the intergranular pressure and a later arrival of pore pressure?

DELON HAMPTON: The critical factor is not so much the magnitude of the pressure that is on the structure since this can be measured. The most important effect of the pore pressure is its effect on the stress state of the soil surrounding the structure which, in turn, will effect the soil-structure interaction.

DISCUSSION

R. H. SIEVERS: It would seem though that the pore pressure would be arriving at such a later time after the significant effects have taken place that maybe the significance of it's arrival at all has been lost or is much reduced.

DELON HAMPTON: This will depend on the length of response time of interest and the depth of burial of the structure. The change in the stress state of the soil surrounding the structure will not be important if it occurs a sufficient time after the phenomena of concern.

R. H. SIEVERS: Let's say we have a shallow-buried, flat-roofed structure. If we reduce the peak pressure which was experienced by the roof of that structure by adding a highly porous granular material over it with no membrane surface across the top of the ground, is this a way of reducing the pressure on the structure?

DELON HAMPTON: The answer to this question depends upon circumstances. It depends upon the properties of the soils, e.g., whether active or passive arching will occur and on the depth of cover; therefore, a yes or no answer is not possible.

J. R. ALLGOOD: I think we're about out of time so we'll thank you again and proceed to our next paper. Our next speaker is Mr. R. L. Marino, who will be presenting Mr. Riley's paper. Mr. Marino has his B.S. and M.S. degrees from IIT and, of course, is presently with the Illinois Institute of Technology Research Institute. The paper he will present is entitled "Photoelastic Study of Wave Propagation Around Embedded Structural Elements."

R. L. MARINO: Presentation of formal paper, see pages 332-346.

J. R. ALLGOOD: Are there questions for Mr. Marino?

ALBERT KNOTT: Could you give us an estimation of what you think the effect would be if you extrapolate this information, which I realize is a narrowly defined study, into a soils material that has different elastic and plastic properties?

R. L. MARINO: I would say that this particular study would probably apply more to tunnels buried in rock. At the present time, we're extending our studies into actual viscoelastic materials and I don't really have anything to report on this as yet. I think I pointed out that this elastic analysis could be used as a first approximation depending on the nature and condition of the soil. I don't know if I can answer your question.

N. J. EVERARD: Do you think it would be possible to simulate soil conditions and, using powered acrylic isolated between two plates, use this method?

R. L. MARINO: I have never tried this particular approach. There is a possibility that acrylic chips or acrylic powder could be used to simulate real granular soil. In attempting to use plastic chips or powder, however, you might be creating more problems than you would be solving. Using the Photoelastic Method, it would be more difficult to determine the stress distribution in a plastic chip medium than it would be in a solid plastic plate because of the photoelastic principles involved. It might also be difficult to determine the properties of granular plastic which would certainly have to be done before any problems could be solved. A more reasonable approach might be to bury a two-dimensional photoelastic model of a tunnel cross section in a glass box with a real soil medium such as Ottawa sand. In this case, it would be possible to determine the stress distribution in the plastic model.

J. R. ALLGOOD: Perhaps it would be appropriate to summarize what has been said in brief form. We're fairly confident that modeling can be accomplished in dry granular material but such modeling requires the following: a similarity of geometry, use of the same material, pressures in the model equal to the pressures in the prototype, and care with time scaling particularly where we have very short time pulses.

The needs for future work were pointed out quite ably and quite thoroughly and those areas of major importance were cited for us. It was brought out particularly that we need more information on modeling of cohesive material. Indications are that modeling can be successful with such materials. We saw a new, and I think an excellent, theoretical approach to the treatment of these buried structures which holds new hope for our successful analysis. We have been cautioned that the elastic wave propagation solutions probably are not correct, and that photoelastic analyses and theoretical analyses for purely elastic materials are not strictly correct. Certainly the described photoelastic studies are an important first step in developing techniques and they do give an interesting visual interpretation of what is happening. We've learned something of the effects of pore pressure and have been cautioned that in prototype structures where the relatively fine grained soils are used, the pore pressure probably will not act on the structure. The dynamic response of the structure will usually be completed before the pore pressure becomes significant, but we must be cautious in our models because the models are much closer to the surface and if we do not isolate pore pressures by using a plastic sheet on the surface, we may get erroneous results. These are a few of the things that have been presented to us. I certainly hope they have contributed to your understanding as they have to mine. I would like to thank our speakers for their excellent presentations and for keeping within the time limit. Dr. Hampton would like to make one last statement.

DELON HAMPTON: I forgot to mention in my presentation the propagation of pore-air pressures in silty sand samples. The reason that I did this was principally because the propagation was practically nil. In the silty sand samples, the maximum pore pressure that I could measure was 1/2 psi and this was really taxing my instrumentation. At a distance of approximately 6 inches it was zero; this 1/2 psi was down to zero; therefore, for all practical purposes then, we forgot all about the silty sand and concentrated our efforts on the Ottawa sand and the pea gravel.

J. R. ALLGOOD: I thank you for the addition Delon. Thank you all.

SESSION SIX – WEDNESDAY PM
ANALYTICAL AND EXPERIMENTAL STUDIES, PART I
SESSION CHAIRMAN: Eugene Zwoyer

D. A. LINGER: The session for this afternoon is titled "Soil Structure Interaction: Analytical and Experimental Studies, Part I." The Session Chairman is Dr. Eugene Zwoyer, who is presently Director of the Air Force Shock Tube Facility, which is a nuclear effects laboratory. Dr. Zwoyer received his doctorate from the University of Illinois in 1953. He is presently Professor of Civil Engineering at the University of New Mexico, in addition to his duties as Director of the Shock Tube Facility. He is the principal in the consulting firm of Zwoyer and Associates, and his widely diversified background and present research responsibilities make him well qualified as this afternoon's Session Chairman.

EUGENE ZWOYER: As Dr. Linger mentioned, the session this afternoon is the first of two sessions devoted to papers on analytical and experimental studies related to soil structure interaction. This afternoon we have five papers. The first paper has been written by Mr. W. B. Truesdale and Dr. E. Vey. Dr. Vey is a Professor of Civil Engineering at IIT and the Manager of the Soil Mechanics Division of IITRI. You met Mr. Truesdale yesterday when he discussed soil strain gauges. Mr. Truesdale has completed his undergraduate and graduate work at IIT. He is an Associate Research Engineer in Soil Mechanics at IITRI and for the past three years has been working on problems related to soil structure interaction. This afternoon he will present the paper entitled, "An Investigation of Panel-Arching Effects in Non-Cohesive Soi."

W. B. TRUESDALE: Presentation of formal paper, see pages 349-355.

EUGENE ZWOYER: Do we have any questions for Mr. Truesdale?

R. L. MARINO: What sort of pressure gauges did Terzaghi use thirty years ago?

W. B. TRUESDALE: The way he made the measurement was by pulling steel tapes at various levels above the structure and then measuring the force required to overcome the friction at resistance. I can't detail the exact procedure because I've never seen the paper in which Terzaghi described the techniques employed (speaker's note added: "A Fundamental Fallacy in Earth Pressure Computations," Journal of the Boston Society of Civil Engineers, April, 1936).

EUGENE ZWOYER: Are there any other questions?

MARC CASPE: Dr. Newmark has mentioned that distortions are of prime consideration here, yet all the laboratory research that has been presented so far has dealt with the measurement of stress, rebounds, attenuation, etc. Would strain be a proper criterion? Since we are speaking of distortion, could we, from a laboratory test, extrapolate to the site conditions in terms of strain?

W. B. TRUESDALE: Well, I don't know how to answer your question but I think that deformation is important and can't be left out of consideration in any design problem. For example, if one designs a retaining wall for active earth pressures, he must make allowances for sufficient movement of the wall to develop the active case.

MARC CASPE: It is not so much a matter of how, but whether it would be a valid approach. The answers aren't here at this meeting. There is no question that there is work to be done. The question is whether the approach from the strain viewpoint is valid as opposed to stress. Things like pore water pressures, etc., cannot be measured, but strains can.

W. B. TRUESDALE: Personally, I feel it is essential that consideration be given to the deformations required to develop soil shear resistance.

STAN BEMBEN: As long as someone else has brought up the topic of strain, I would like to mention one more complication. In your comparison with your stress-strain curve, the triaxial tests that you used had strain in three directions and the test program had strain in two directions.

W. B. TRUESDALE: Obviously, it is a different case. We know that soil stress-strain properties vary with degree of confinement, whether it is two dimensional or three dimensional. What I was trying to do was to select some values that would realistically represent a granular soil. I also looked at some results from direct shear tests to see if at some stress level below the maximum the envelope of Mohr's circle for a series of tests was linear. You do get a fairly linear type of relationship. It is not as good at values below maximum load as it is at maximum, but it was not too bad. You obtain a different value of ϕ, at least I did, between the triaxial and direct shear test. They are two different types of test. The direct shear is two dimensional while the triaxial is three dimensional. However, I only wanted to select values representative of real soil and to establish that the stress-strain relationship established was reasonable.

STAN BEMBEN: I'm also doing work in this area of plain stress and the ϕ results are significantly different for the plain strain. Some of the results will be published in next years International Conference on the papers from Cornell. I think that the results do indicate that we really shouldn't be using the triaxial tests, the setup that you are using here. For instance, I am talking of changes in ϕ of maybe 5 degrees and when you apply a 5 degree change this makes a difference in the answers for stress.

DISCUSSION

W. B. TRUESDALE: I agree, but I did not get that big a difference between the two tests. There was only a couple of degree difference in ϕ between the triaxial and direct shear results. Because of the limitations which exist in the direct shear test, it is difficult to determine if this difference is due to the difference in the two and three dimensional condition or is simply due to techniques of the test.

STAN BEMBEN: It depends mostly on the relative density and it is only at higher relative density that the 5 degrees occur.

G. E. TRIANDAFILIDIS: I would like to make a comment about this k_o coefficient and how it was determined. I think that Tschebotarioff in his book gives a detailed account of Terzaghi's test arrangement. Actually, what Terzaghi did was to pull out of a consolidometer a thin metal strip which in one test was oriented horizontally. He measured the total force required to pull out the thin metal strip. He subsequently rotated the strip 90° and again measured the force necessary to pull the strip out from the ratio of the two forces. This allowed him to determine the order of magnitude of the k_o coefficient.

P. S. BULSON: I have a question for Mr. Truesdale. Did you measure deflections against overpressure for the sand model you demonstrated, and also how do they compare with the theoretical curves and the given linear relationship?

W. B. TRUESDALE: The tests we performed were in the glass box type apparatus and we didn't discuss qualitative results because of the fact that there are definitely side wall friction effects in the narrow glass box apparatus. We were primarily observing deformation patterns in the soil, but the results, as one might expect, fit in the general second type of curve. Tomorrow Mr. Longinow from IITRI will present some results he obtained in pressure vessel tests on circular panels and, although it is a different case, the same general trends are observed. The results you showed yesterday also were generally of this. Continual increase in surface overpressure can be obtained if you can keep allowing the panel to deform. However, as the results show, a sudden collapse occurs if the ultimate structural resistance is overcome. Arching requires some support from the structure.

EUGENE ZWOYER: Our next paper this afternoon will be presented by Dr. C. V. Chelapati, Assistant Professor of Engineering at California State College. Dr. Chelapati completed his undergraduate work at Andhra University in India and started his graduate work at the Indian Institute of Science. He completed it at the University of Illinois where he worked on an elasto-plastic response of structures to earthquakes and other simple pulses. This afternoon he will present a paper entitled "Arching in Soil Due to Yielding of a Horizontal Support." Last summer and again this summer he has been working with the Naval Civil Engineering Laboratory in soil structure interaction.

C. V. CHELAPATI: Presentation of formal paper, see pages 356-377.

BRUCE SCHIMMING: I have just one question about the assumption of small strains consistent with the type of boundary condition you impose there on a 17 foot layer with a 2 inch displacement where there is a sudden discontinuity at the edges of the door. Do you think that it may have a serious effect on your assumption of small strains?

C. V. CHELAPATI: I don't think so. Further, we are not integrating to the end of the strip; the stresses at the end are infinite. We are integrating only from zero to x_{cr}.

EUGENE ZWOYER: Our next speaker this afternoon is the first to be presented by our hosts from the University of Arizona. Dr. Ralph Richard is an Associate Professor of Civil Engineering here and has been directing the work that will be reported by Jerry Burns. Jerry Burns is a Research Assistant in Civil Engineering and has been the principle who is responsible for the construction of the plain wave blast generator here at the University. This afternoon, he will present a paper entitled "Attenuation of Soil Stresses for Buried Cylinders."

J. Q. BURNS: Presentation of formal paper, see pages 378-392.

N. J. EVERARD: I think this is a very good approach and I think actually we need to take an approach similar to this with respect to structures that are rectangular in shape and structures of that type because in our civilian construction program, we are building structures in which the basements are going to be our survival shelters. If this approach were taken with the rectangular structures, it would be very helpful.

E. T. SELIG: By slippage or no slippage you are talking about action around the wall of the cylinder when the soil compresses?

J. Q. BURNS: By slippage I mean any arbitrary relative tangential displacement between the soil and the conduit shell wall. For full slippage there would be no tangential load transfer between the soil medium and the shell wall.

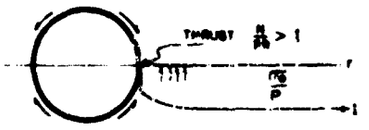
E. T. SELIG: In the examples of the no slipppage case, the stress distributions indicated, if I read the diagrams right, a reduction of vertical stress at the crown and at the springing or the horizontal diameter in the vertical direction. This means there is load transfer out of the region, but none picked up elsewhere to compensate. Have I misinterpretated the diagram?

J. Q. BURNS: The vertical component of load carried in the vertical shell wall will be greater in the no slippage case than in the full slippage case. For in the no slippage case, a load component is transferred into the shell directly by shear; whereas, in the full slippage case, the only load is the radial load. Does this answer your question?

E. T. SELIG: Perhaps, but I would like to think about this a bit more. I am just summing up forces over a horizontal plane and, of course, we don't have the complete distribution, but the vertical stresses have to sum up to the pressure on the surface. If it is relieved from the region of the hole, its got to show up somewhere else.

J. Q. BURNS: Right. They will recall the cases where this occurred. Notice that the circumferential stresses along a horizontal plane in the vicinity of the shell when they are reduced. If we integrated over the horizontal plane, we would find that we have less than the total vertical load. What else did we notice? At the sides of the shell, we noticed that the circumferential thrust in the shell was greater than unity. In other words, the shell was carrying more than just the load over its radius. Thus, the shell wall was carrying the stress which was not being carried by the soil. That is, what I call negative arching. That is, the shell was taking more load than the free field loading. Conversely, if this circumferential stress was greater than unity there was a reduced thrust in the shell wall.

R. M. RICHARD: The analysis of the stresses and displacements in a soil conduit structural system is a complex problem. A solution to this problem wherein the soil is treated as a linearly elastic medium necessarily has its limitations, however, such a solution provides insight as to which parameters or variables are of primary importance. In nonlinear systems, the mathematical expressions are far more complex than those for linear systems and advantage must be taken of certain idealizations and simplifications in order to solve nonlinear systems. Appropriate equations or functions, either algebraic or differential, must be found to relate all the variables of the system. Plotted empirical relations derived from experimental measurements (such as stress-strain curves) must be represented in the form of mathematical equations. Approximations having sufficient accuracy should be made in order to keep these expressions as simple as possible.



As a result, if a reduced simplified mathematical model of the soil-conduit system is to be derived in order that certain nonlinear effects may be determined, this model should exemplify the response of the linear system with a reasonable degree of accuracy so that confidence may be placed in the results obtained when the model is extended into the nonlinear range.

EUGENE ZWOYER: This next paper has two authors, Dr. Ulrich Luscher and Kaare Höeg. Mr. Höeg is a native of Norway and began his undergraduate training there and completed it at the Massachusetts Institute of Technology. Since that time, he has been engaged in graduate study and research work at MIT. Senior author, Dr. Luscher, is a native of Switzerland where he received his undergraduate education in Civil Engineering at the Swiss Federal Institute of Technology in Zurich. Since then, he has come to the Massachusetts Institute of Technology where he completed his graduate work, and for the past five years he has been working in soil structure interaction as well as teaching. He will present the paper this afternoon entitled "The Beneficial Action of the Surrounding Soil on the Load-Carrying Capacity of Buried Tubes."

ULRICH LUSCHER: Presentation of formal paper, see pages 393-402.

J. D. HALTIWANGER: I want first to observe that I found your paper very interesting. Now I would like to comment not only on your paper but also on an earlier statement that was made. I strongly suspect that buried structures, properly constructed as you noted, are designed to resist normal dead load pressures at ordinary allowable stresses or factors of safety, and designed also to resist blast-imposed pressures in ring compression at yield level, will produce a tube wall sufficiently thick as to be on the left-hand side of your Figure 5. This would mean in effect that buckling would not occur except at yield stress level. In this case as far as a design criterion is concerned, I don't see that the buckling mode itself becomes particularly critical. It does mean, of course, that one dare not presume large inelastic deformations in ring compression for fear that it will buckle unelastically. Consequently, as a design criterion, it would mean that we would have to curtail the permitted ductility factor.

ULRICH LUSCHER: I would agree with Dr. Haltiwanger that probably in most current design practices for protective construction his comments are applicable; however, we might think of a new material, for instance plastic, which is much more susceptible to buckling than metals. Also I did not restrict my comments to the protective construction industry; I have other conventional applications in mind too. I think that these types of effects do come in other types of applications. I am sure that we agree on that point.

R. L. BROCKENBROUGH: I would like to comment on the derivation of the equation that you gave for buckling pressure. Looking at the equation, as I understand it, you have given an equation which gives the buckling pressure for a tube that is surrounded by a two way elastic foundation; in other words, the soil behind the tube is able to take compressive forces as well we tensile forces that might develop as a tube tends to go into a buckling mode. It would seem to me that this is one of the refinements that would be quite significant in refining this theory as you mentioned needs to be done.

ULRICH LUSCHER: I think that any tensile stress is really superimposed over the compressive stress which is there anyway, and while I have not established magnitudes because buckling is an instability problem and the magnitude of stresses does not come in, I feel confident that we don't develop any tensile stress but rather just reduce the compressive radial stress which is applied to the tube.

J. Q. BURNS: I would like to make a comment on the previous question of extensional flexibility in which it was stated that inelastic extensional flexibility probably should not be relied on because it will cause buckling. I would agree with that as far as inelastic extensional flexibility due to uniform plastic yielding is concerned, since this would result in no moment capacity to resist buckling. If however, yielding occurs at certain specific points due to seam yielding at riveted or bolted connections, such that if sliding of overlapping plates occurs rather than uniform plastic yielding throughout the shell wall; then moment capacity is preserved. Thus some inelastic extensionality due to uniform plastic compression may not be.

ULRICH LUSCHER: I just want to make a brief comment in connection with the raining technique which is presently so universally used for placing sand in laboratory tests. I would like to give credit to Professor Z. Getzler who actually developed the technique in connection with tests on buried domes at MIT. The research project was supervised by Professor R. V. Whitman and is described in the report, "Static Tests Upon Thin Domes Buried in Sand," by R. V. Whitman, Z. Getzler and K. Höeg, Report No. R 62-41 of the Department of Civil Engineering, MIT, December 1962.

DISCUSSION

EUGENE ZWOYER: The final paper this afternoon is based on the work conducted by the University of New Mexico at the Air Force Shock Tube facility. There are three authors. The second author, Dr. Hampton, you met this morning when he presented his paper on pore-air pressure. The third author Milan Spanovich was a Research Assistant Engineer at the University of New Mexico when the work was conducted in the laboratory and is presently a consulting engineer in Pittsburgh, Pennsylvania. The senior author, Dr. George Triandafilidis, will present the paper. He received his undergraduate degree at Robert College in Istanbul, Turkey. He did his graduate work at the University of Illinois. He has been on the faculty at the University of Illinois and for the last three years on the faculty of Rice University and has spent the last four summers working at the Shock Tube Facility. Dr. Triandafilidis will present the paper entitled "An Experimental Evaluation of Soil Arching."

G. E. TRIANDAFILIDIS: Presentation of formal paper, see pages 403-420.

PETE WESTINE: I would like to know at what degree of saturation these tests were run?

G. E. TRIANDAFILIDIS: Perfectly dry.

PETE WESTINE: Absolutely dry? Were these dynamically or statically loaded?

G. E. TRIANDAFILIDIS: These are all static tests.

PETE WESTINE: I think we should add that the degree of saturation, water content, and even pore air pressure play a major role in arching. How can static tests which permit pore pressure alleviation answer dynamic arching problems? In the similar dynamic area of "off-the-road mobility of vehicles," water content has proven to be a very important, if not the most important, variable.

G. E. TRIANDAFILIDIS: I agree absolutely with what you have to say and I think I have mentioned that this study consists of the first phase of a sustained research effort. We are looking into this problem more extensively now.

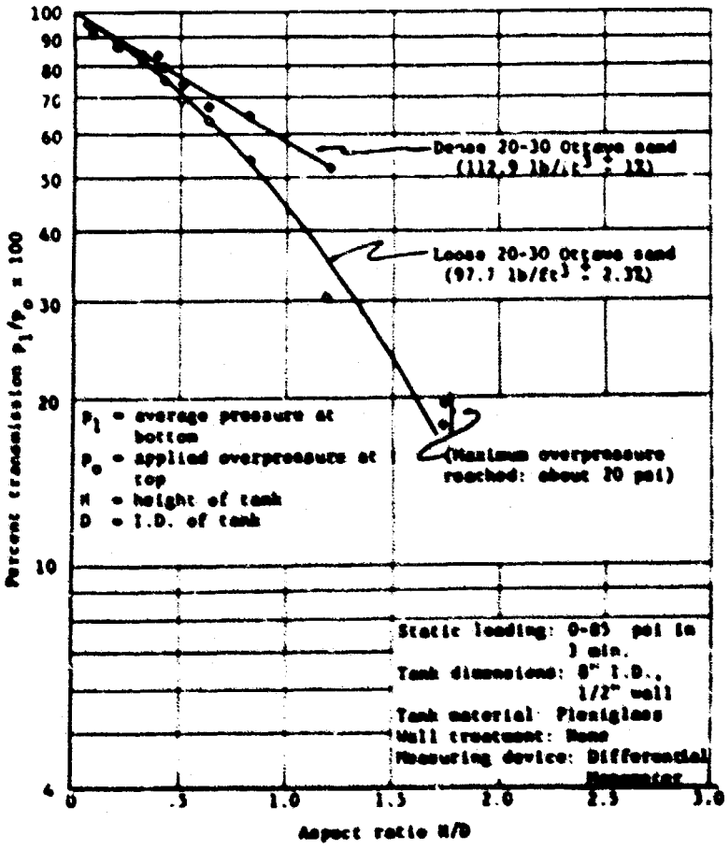
J. I. BUSTAMANTE: You have mentioned that you were planning to go ahead with more tests of this type. I was wondering if you planned on doing some experimental design of the things you are testing to have some knowledge of statistical results? When you mix all these variables, it is very difficult to say that there is not some interaction between one variable and the other. Taking, for instance, sand and saying that this is constant for the different variables. Are you planning on doing some experimental design to get a statistical statement of the conclusions?

G. E. TRIANDAFILIDIS: I think Dr. Hampton can answer this question better.

DELON HAMPTON: The data presented in this paper were independently analyzed by two different methods. The first was as presented to you by Dr. Triandafilidis, and the second was by the use of statistical methods. The statistical approach supports the assumptions and conclusions contained in our paper and presented orally by Dr. Triandafilidis to this Symposium.

D. F. YOUNG: Maybe I missed this in your talk, but it would seem that an important parameter here might be the diameter of the container that you used or the ratio of the diameter of the inner cylinder to the container so that all of your study would be restricted to this one value. Would you care to comment?

G. E. TRIANDAFILIDIS: I would like to mention that in these tests we used these tanks all of which were 8 inches in diameter but of various heights. The height was varying somewhere from about 2-1/2 inches to as much as 4-1/2 to 5 inches. We have made an independent study in which we tried to evaluate the influence of the aspect ratio on the stress transmissibility in such test containers. I don't have a slide for this but I can show this plot. For instance, for an aspect ratio of about .2 without any friction reduction walls, the transmission ratio is about 90 per cent. If we use an aspect ratio of about .5 which represents the case for the majority of the tests performed, the transmission ratio is of the order of about 78 per cent. I would suspect that most of the stress loss occurs adjacent to the wall of the test tank and chances are that the input stress is probably not greatly influenced close to the center of the tank. If you want more detailed information, Mr. Phillip Abbott has made a more detailed study of this matter.



Effect of tank aspect ratio on static transmission

(AFSTP, P. A. Abbott 7-15-64)

HAROLD G. MASON: We have run some tests on losses due to side-wall friction in steel containers with and without teflon liners. Our numbers fall in the same range as yours, for instance, at one-half diameter depth we get a loss of about 30 percent. We have done some work with structures that were of the rigid type, but placed in the free field rather than against a base, and found some similar results. However, don't you feel that for a given length you will reach maximum over-registration due to passive arching?

G. E. TRIANDAFILIDIS: I feel that I should, but ...

HAROLD G. MASON: We did with our rigid structures placed in the free field. That is why I was wondering if you had. The increase of load on the structure seems to follow an exponential passive arching form similar to Terzaghi's active arching case except opposite in sign increasing with depth to some maximum depth below which it remains constant. We have also conducted tests on the same shaped structure having greater compressibility. We found that the load on the structure decayed with depth following the form of Terzaghi's active arching case. We have shown the two extremes of load on the structure for the rigid structure (maximum passive arching) and for the soft structure, maximum active arching. We are now investigating the relations between these two arching extremes. We have recently found a theoretical relationship for predicting the amount of overstress one might expect based on the geometry of the structure.

G. E. TRIANDAFILIDIS: I would like to point out that Mr. Abbott from the Shock Tube Facility at the University of New Mexico has done an extensive study. Since I wasn't around for the last nine months, I think that he would like to comment.

P. A. ABBOTT: Dr. Triandafilidis mentioned that this was a continuing research project and it certainly has been. I have been working on it for a year. With respect to Mr. Mason's comment, is there some depth of variable at which passive arching reaches a maximum? Yes, about 3-3/4 inches for these tests. Now these tests aren't identical to the ones that he is talking about. I am not working on exactly what he worked on. I am changing the variables. I am introducing a stiffness variable into the structure and eliminating the side wall friction variable. In other words, by putting a greased membrane around the housing of the disc structure that Dr. Triandifilidis was talking about, I can reach a point at about 3-3/4 inches depth of burial at which passive arching reaches a maximum.

HAROLD G. MASON: Is that for a given size structure or is that for any size structure?

P. A. ABBOTT: No, for that particular 1-1/2 diameter structure. This is a very important variable, but neither one of us has looked at it yet.

HAROLD G. MASON: For one of the structures that we had, it had a larger diameter but a fairly close correspondence to your length. It had a diameter of about 6 inches and we found the maximum someplace in the same order of numbers; therefore, it is affected not only by diameter but probably more realistically by length, which you would expect because it has to do with the amount of compressibility.

P. A. ABBOTT: I failed to mention one thing — Mr. Robert E. Lynch at the Shock Tube Facility has tested a stress gauge which really is exactly what we are talking about. It is a right circular cylinder buried in dense Ottawa sand. Full depth of burial is about 1.2 inches in diameter and 1-1/2 inches in length, if I'm not mistaken was about 1 inch. So it is definitely affected by the dimensions of the structure.

EUGENE ZWOYER: Again, I would like to thank the authors and co-authors who presented the very excellent papers this afternoon on soil structure interaction. This session will now stand in adjournment.

SESSION SEVEN — THURSDAY AM
ANALYTICAL AND EXPERIMENTAL STUDIES, PART II
SESSION CHAIRMAN: R. K. Watkins

D. A. LINGER: This session is a continuation of our Wednesday afternoon session on analytical and experimental studies. The Session Chairman is Dr. Raynold K. Watkins, Head of the Department of Mechanical Engineering at Utah State University. He is the chairman of the Highway Research Board Committee on underground structures. He has done a considerable amount of work on underground structures, research and design, and consulting. He did his doctoral work under Prof. Spangler at Iowa State University.

R. K. WATKINS: Thank you Dr. Linger. We must proceed immediately for I know we have a heavy schedule for this morning. The first paper is entitled, "Experiments on Circular Cylinders with Flexible Roof Plates Buried in Sand," by C. J. Costantino and Andrew Longinow. Mr. Costantino is unable to be with us. The paper will be presented by Mr. Longinow, who is an assistant research engineer at IITRI. He graduated from Valparaiso University and is currently doing graduate work at IIT. He is working in the area of structural mechanics.

ANDREW LONGINOW: Presentation of formal paper, see pages 423-435.

HEINZ LEISTNER: I was interested in the hysteresis that appeared on several of your curves. Could you elaborate on the loading rates you used?

ANDREW LONGINOW: We did not measure the rate at which it was loaded. Pressure was brought up to a particular level, held for five minutes after which readings were taken. The pressure was then slowly brought up to another level.

E. T. SELIG: Let me comment on this point. This test was run very slowly and was conducted in dry sand. I think most of this hysteresis is just a characteristic of the stress-strain relationship of the sand because it looks, as you'll note, almost the same as the one-dimensional

compression stress-strain curve for sand. The test was slow enough so I don't think time effects had a great deal of influence on the results.

HAROLD G. MASON: We've observed the same thing in unloading of one-dimensional tests. We get a reversal of ratio of lateral confining pressures to axial stress. It appears that you get a sort of locking when you unload the axial stress and you actually get a reversal of the principle stresses.

KAARE HOEG: Just to elaborate a little more on the same point, I believe Dr. Hendron has already given the best explanation for such an unloading curve and is exactly the line with Dr. Selig's comment. Let me add that MIT some time ago, under Dr. Whitman's supervision, performed tests on domes buried in sand. We observed this same phenomenon as mentioned above independent of the rate of loading and unloading (static loading).

ROY BUTTERFIELD: The four loading cycles -- were these the first four or were they four after you have loaded it previously?

ANDREW LONGINOW: They were the first four.

ROY BUTTERFIELD: One would feel that you wouldn't get the first loading repetitive hysteresis, for the first loading would be different, I would have thought.

ANDREW LONGINOW: The first was a bit different.

ROY BUTTERFIELD: Were not these the first four you chose? Were there just four after it had already been loaded once?

ANDREW LONGINOW: Each experiment had four loading cycles and there was no preloading.

R. K. WATKINS: The second paper, "Yielding Membrane Concepts," by H. P. Harrenstien and R. H. Gunderson, will be presented by by Dr. Harrenstien. The co-author, Mr. Gunderson, is here also. Dr. Harrenstien is Professor of Civil Engineering and Engineering Mechanics at the University of Arizona. He was the engineer on the team which won the grand prize in 1962 for the fallout school design competition. He is presently chairman of the architectural engineering division of ASEE, and a member of the ASEE advisory committee to civil defense. I might also add that he is the man who wrote the proposal which resulted in this Symposium.

H. P. HARRENSTIEN: Presentation of formal paper. see pages 436-448.

ALBERT KNOTT: I noticed on the slides of the shells that were loaded by sand that the center deflection was not as great as it was on the shells that did not have this material over them. Yet it appeared that the edge of both sets of shells had a similar slope. It appears that a shearing action has occurred at the edges of these shells. Do you find that the strength of these is similar?

H. P. HARRENSTIEN: You are correct in your observation. This is discussed in the written text. The strength of the shells is similar which indicates more soil arching and less direct shear at the edges.

ALBERT KNOTT: Did you get some arching action being supported by these sharply-curved edge areas?

H. P. HARRENSTIEN: We can take this membrane now, measure its curvatures and predict the overpressure at each point which formed that curvature. We had to create a place for the arching to start. I think this goes back to some of Reynold's work where he was creating these arches and separating the tubes so they would have this arching. We have the same problem here. We need this support.

R. R. FOX: The paper by Harrenstien and Gunderson presents interesting possibilities in the use of yielding membranes in protective structures. Several questions come to mind which may be answered by the authors to complete the effectiveness of their presentation.

Since membranes of various metallic materials are suitable in conjunction with a variety of support conditions and materials, it would be helpful if some discussion of the membrane support could be included in these proceedings.

The need for an advantage of pre-forming or "dishing" the membrane is not clear since this operation normally removes some of the energy-absorption capacity of the membrane. Additional comments by the authors would be helpful.

Data on comparative costs of this mode of shelter construction versus more standard construction of above- or below-ground shelters would be of significant worth if such data is available.

H. P. HARRENSTIEN: Some answers to these questions are given in the written presentation. More complete answers must wait until the final report to the contract (OCD-PS-64-187) which will be published May 1, 1965.

ALBERT KNOTT: The other question I have is when you have a rectangular structure and a membrane force applied at the edge it will be necessary to have an appreciably large edge member. Do you find that the required size of this edge member is large enough to offset the savings in cost which you obtained from the use of the membrane?

H. P. HARRENSTIEN: It needn't if the outer bays contain reinforced concrete as the floor and ceiling. It is possible to arrange the interior walls in a grid pattern and pull the membrane everywhere. The rigid concrete around creates essentially beam action which carries the thrust over to the walls which take it on through. The end panel has to be of something rigid like concrete. There is no saving at all in this if you only have two bays each way and hence no membrane. If you have 50 bays by 150 bays you have quite a bit of membrane which is only supported around the outer boundaries.

MERIT WHITE: In the curves that you showed relating pressure to deflection, I assume that these were statically obtained curves?

H. P. HARRENSTIEN: Yes.

MERIT WHITE: Of course, there is a multiplication factor for a sudden applied load, so if your membranes are exposed to blast and the load is applied suddenly, there is a factor which I believe is 2.

H. P. HARRENSTIEN: Yes, this is for elastic systems. Right?

MERIT WHITE: For a linear elastic system, yes. For a membrane deflecting elastically but by a large amount, the factor is about 4. For a plastic membrane the factor, I think, is again 2 so that your 50 psi is equivalent to 25 psi suddenly applied.

H. P. HARRENSTIEN: We haven't observed that in our tests, but very possibly the error is in our gauging devices which are depended upon to yield correct effective pressure readings.

MERIT WHITE: Yes, it's a matter of duration, of course, too. If you have a mass there such as sand, then the thing reacts slowly and the factor is less than 2, but if it's a long duration pulse, suddenly applied, and a thin membrane which reacts almost instantaneously, then I think the factor becomes, theoretically at least, 2.

R. H. SIEVERS: Do you feel that materials can presently be fabricated in such thicknesses in such spans that you will be able to achieve in steel or aluminum these true membrane actions?

H. P. HARRENSTIEN: This needs research, but what we are suggesting now is that they be fabricated and dished before hand, as you see on the model back there, so that you put a static forming pressure on them which is equivalent to that pressure that you expect in the application later due to blast. If there is this factor of 2, it has to be taken into account.

R. H. SIEVERS: I don't think anything presently could be rolled in the widths you're referring to.

H. P. HARRENSTIEN: No, we have to go to welding. But you see, if we weld these plates together and take two plates and drive them apart with fluid pressure, we form two shells that we know are capable of resisting the pressure that formed them. Then if this pressure is sufficient to be applied in design we can rest assured that it will take it again. Now as far as fatigue goes, we plead with the Russians not to multiple burst us to the point of fatiguing these things. It would have to be actually tested full size by forming until we get more data on how the welds correspond or go through this rapid yielding.

DWAYNE NIELSON: I would like to make one comment. In the load cell which Dr. Harrenstien discussed as the basis for the experimental results, the dynamic loads which were transmitted through the rigid posts (as measured by the strain gauges) were roughly only 75% of the load transmitted from the static load due to the same peak pressure. The rise time of the pressure in the dynamic test was in the order of one millisecond and the duration of the impulse was approximately one second.

HEINZ LEISTNER: Have you given any thought to the action of the floor slabs under these conditions?

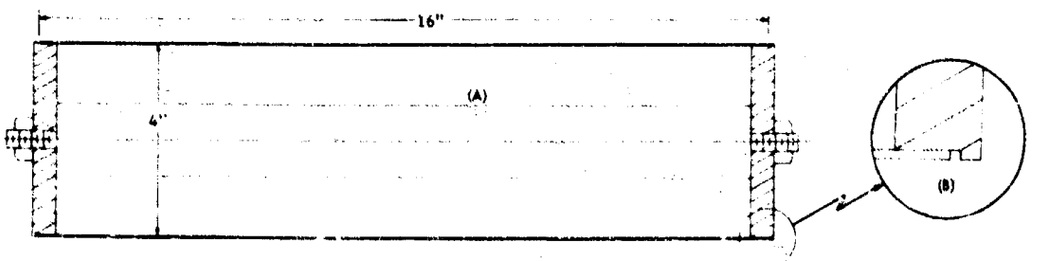
H. P. HARRENSTIEN: Yes, just in design. We thought that possibly the floor slab could be of the same sort of system; however, then we would have to allow for vertical downward motion of the walls and anything that was attached to the walls in developing the full yield of the floor. We have underdesigned the foundation of this model and let it punch and then put a floor slab on grade and let it crack. It will crack under the regular settlement of the overburden, but by not having any strength, we feel that the punching would add to the soil structure interaction. I would suggest membranes on both faces, but here, of course, we have water problems.

R. K. WATKINS: The third paper, "The Response of Buried Cylinders to Quasi-Static Overpressures," will be presented by Dr. Barry Donnellan. Dr. Donnellan is a research associate engineer at the University of New Mexico Air Force Shock Tube Facility. He just completed the requirements for a Ph.D. in soil and foundation engineering at the University of Illinois.

BARRY DONNELLAN: Presentation of formal paper, see pages 449-463.

ALBERT KNOTT: Would you take time to indicate how the end panels of these cylinders are actually built?

BARRY DONNELLAN: I can briefly indicate the details of the end panels with the appended figure. This figure (shown below) shows a longitudinal section of an aluminum cylinder with end plates. The stiff axial rod (A) rigidly holds the end plates in position and carries the axial forces. The clearance shown in the inset (B) insures this. Very close tolerances were used in fitting the cylinder over the portion of the end plate which slips into the cylinder.



Longitudinal section of 4-inch-ID aluminum cylinder

DISCUSSION

ALBERT K NOTT: In the location of your gauges that measured the deflections, did you feel that the gauges that were nearer these end supports had free motion?

BARRY DONNELLAN: Yes I do. The displacement gauges were spaced over a 4-1/2 inch length at the mid-length of the cylinder and the reason I say I feel they have free motion is because of the collapsed shape of the cylinders. I am cognizant of the fact that the collapsed shape and the shape prior to the collapse are two different things. One of the improvements that we will make in future testing is that we will deal with much longer cylinders; however, I feel that the end displacement gauges were not materially effected by the restraint of the ends of the cylinders. Bear in mind that we are talking about very small deflections. The deflections are in the order of 1/200 of an inch.

ALBERT KNOTT: Were these other gauges approximately at the quarter points? I can't recall your original sketch.

BARRY DONNELLAN: This figure is Figure 2 in my text (page 452). Here is mid-length and they were over a 4-1/2 inch length at the mid-lengths. There were two on one side of the mid-length and three on the other as shown in Figure 2. The dimensions are 3/4, 1-3/4, 2-3/4, so that there was 2-3/4 inches here and 8 inches here.

P. S. BULSON: I am interested in the radial inward displacement of the springing which you got on your flexible cylinder. In how many tests did you get this?

BARRY DONNELLAN: We conducted a minimum of three tests at each depth of burial. The data points I showed here were the average of at least three tests at each depth, and in many cases the average of more than three tests. We observed this phenomenon in all tests when depth of burial was less than 1/2 the diameter of the cylinder. We observed it at two different depths of burial, you will recall, 1/2 and 1/4 of the cylinder diameter so that it has been substantiated by quite a few tests.

P. L. HUMMEL: You indicate that the sand was placed initially in a very loose condition, and I was wondering if it was compacted prior to the test?

BARRY DONNELLAN: No sir. The sand was placed initially in a dense condition. The sand was allowed to fall through the flexible hose equipped with an inverted funnel and a screen. This gives the most dense condition that one can obtain. The void ratio was approximately 0.47 which for a uniform sand is quite dense. I don't think you can obtain a denser sand by vibration. It also has the advantage that you can obtain a dense sand around a flexible structure without any material damage to the structure.

R. K. WATKINS: The next paper is entitled, "Response of Buried Structural Models to Static and Dynamic Overpressures." The co-author, Mr. W. F. Riley, is unable to attend and the paper will be presented by Mr. R. L. Marino who has been introduced to you previously. He has had two to three years experience with the IITRI. He is associated with the experimental stress analysis sectio there.

R. L. MARINO: Presentation of formal paper, see pages 464-486.

R. K. WATKINS: The concluding paper is "Interaction Between a Sand and Cylindrical Shells Under Static and Dynamic Loading." This is to be presented by Dr. J. T. Hanley, now of the University of Minnesota. He has spent 14 years with the Navy Civil Engineering Corp including a tour of duty in AFSWP, the headquarters which later became DASA. He has spent five years at the University of Illinois before going up to Minnesota.

J. T. HANLEY: Presentation of formal paper, see pages 487-528.

NOTE: See the Thursday Afternoon Session for the discussion of the last two papers.

SESSION EIGHT — THURSDAY PM
DESIGN AND PROTOTYPE STUDIES
SESSION CHAIRMAN: D. A. Linger

D. A. LINGER: Since the shortage of time limited the discussion of this morning's papers, please feel free to ask questions about them during this session. The first paper this afternoon was written by Prof. M. G. Spangler who is a research professor of Civil Engineering at Iowa State University and has been working in this field a number of years. He did his original work with Marston, and I don't know how many of you go back far enough to know the Marston-Spangler theory of underground conduits. Professor Spangler is the author of many papers and a textbook on soil mechanics. He was the recipient of the Highway Research Board research medal. His paper will be presented by Dr. Carl Ekberg who is Head of the Department of Civil Engineering at Iowa State University.

CARL EKBERG: Presentation of formal paper, see pages 531-546.

D. A. LINGER: Are there any questions?

PETE WESTINE: Do you feel that creep endangers such a design procedure which makes use of a layer of straw as a backfill material above the buried structure?

CARL EKBERG: In Prof. Spangler's paper, he mentions this point and he cites a case where this condition was maintained for 21 years or so. I don't know anything about the tests. I would gather than there was a sustained load for that long a period, whether it was just the dead weight of soil or whether it was surcharge plus weight of soil I can't say. I would be glad to relay this question to Prof. Spangler.

D. A. LINGER: I think it is a little unfair to ask Dr. Ekberg to back up Prof. Spangler's theory, but I think the decomposition of the straw is in his favor in that condition.

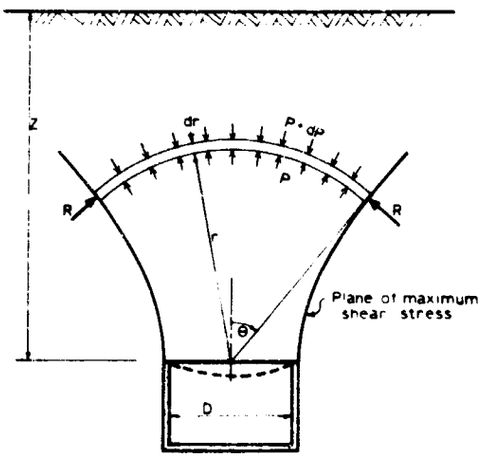
DWAYNE NIELSON: I have a question concerning the validity of the assumption in the derivation of the equation for loads on underground structures. If one assumes that soil can't take tension, is this horizontal differential element a valid assumption?

CARL EKBERG: I think you have a point there. Certainly, the shear forces are mobilized and are similar. Wouldn't you agree to that?

DWAYNE NIELSON: Yes. They are mobilized along the edge.

CARL EKBERG: They are mobilized along the edge. Just how this inverted arch action can occur is something else again. I am afraid I couldn't explain that arching within the prism itself. That is what you're referring to.

DWAYNE NIELSON: The horizontal element is the differential element used in the derivation of the equation. It is generally assumed that soil can't take tension and the differential element, as assumed in the original derivation, will have tension in the lower part. Maybe this has been discussed someplace else; if it has, I am not aware of it. I would like to suggest the following as a modification to the original derivation. If it is assumed that soil cannot take tension then some other type of differential element with only compressive stresses and shear stresses must be used. The compressive arch is one type structure that has only compressive stresses and shear strosses. It is possible to assume that a compressive arch forms over the buried conduit. The shape of the differential arch depends on the loading distribution. The top of the differential arch is free to change it's location through the soil mass as the stress level changes. The assumption that the arch acts only through a prism of soil directly above the pipe is not justifiable unless the pipe is in the ditch conduit type of installation. The maximum shear stresses do not occur along these prism planes. If one makes use of the theory of elasticity, the region of maximum shear stress can be shown to be at an angle of approximately 45° from the vertical. The arch should possibly be extended to this region of maximum shearing stress because this is the region where the friction forces of the soil are first mobilized. The proposed system could then be integrated to determine the load on the underground structure. From data on model studies, the support or stress at the support is not either the active or passive soil stress but is someplace in between the exact value, being closer to the active soil stress (see figure at right).



I have one more question for Prof. Spangler. How is the compatibility between the soil and the buried conduit taken into account? Is this done with the settlement ratio? I am currently working on this problem.

CARL EKBERG: I'll have to relay that one to Prof. Spangler also.

MARC CASPE: Have there been any considerations in the use of the imperfect ditch in open cut construction? That is, where you are not back-filling but you are actually trenching with side supports not just an open trench. Is there any possibility of developing this shear reliability?

CARL EKBERG: In answer to your first question, I am not personally aware that there has been any applications of this type of construction. I don't know of any applications along that line that would help in answering the second question either.

D. A. LINGER: Our next author is Major Ralph H. Sievers who is currently assigned to OCRD. OCRD is the Office of Chief, Research and Development, United States Army. Major Sievers received his bachelor's degree at MIT. His master's degree work was done at the University of Illinois. He has done a great deal of work on this subject. This particular work was done, I believe, at the Nevada Test Site on prototype structures as full-scale structures. The title of his paper is "Measurements of Soil-Structure Interaction on Prototype Protective Structures."

R. H. SIEVERS: Presentation of formal paper, see pages 547-553.

STAN BEMBEN: For the figures that you quoted for the equivalent mass, are they identical for both techniques for the 3,4 point loading compared to the blast loading?

R. H. SIEVERS: Yes. I got a very good correlation, particularly with the 180° arch between the mechanical loads, the mechanical means of excitation, and the blast loadings. As you can see from the sketches, I tried to get these things to vibrate in the flexural mode. The initial deflection where I apply a load and deflect the structure should be a fundamental mode of flexural vibration. The measured period was this compressive mode. I wouldn't go into the reasons why I'm sure it is a compressive mode but they were compatible both in comparison with computed, and also in comparison between the rib and the unreinforced steel arched structure. In the latter, you would expect a great difference between the fundamentals for flexural mode where the steel ribs would provide a tremendous amount of more flexural resistance; whereas, they provide an almost negligible amount of change in the compressive mode. I got 69 milliseconds for the unreinforced and 64 milliseconds for the ribbed structure.

D. A. LINGER: The next paper is on the design of reinforced concrete buried arches and is entitled "Buried, Reinforced-Concrete Arches Equivalent Surcharge Loading Device Procedure." The paper was written by W. J. Flathau and R. A. Sager and Bill Flathau will present the paper. Bill is from the Waterways Experiment Station. He is a graduate of the University of Illinois and has been with the

Waterways Experiment Station for 10 years. He is currently Chief of the Structural Dynamics section of the Nuclear Weapons Effects Branch.

W. J. FLATHAU: Presentation of formal paper, see pages 554-573.

H. A. MIKLOFSKY: Were secondary stresses such as rib shortening of the arch taken into account in developing the interaction diagrams?

W. J. FLATHAU: No.

D. A. LINGER: Any other questions? Our next paper is "Force Transmission Due to Cohesive Soil-Foundation Interaction Under Vibratory Loading." It will be presented by an author who has done a great deal of work in this area. He has all his degrees from Johns Hopkins University and is currently at Northwestern University. I would like to present Dr. Robert L. Kondner.

R. L. KONDNER: Presentation of formal paper, see pages 574-582.

D. A. LINGER: Are there any questions?

R. H. SIEVERS: Did you make any calculations as to the amount of soil which apparently was vibrating in conjunction with the footing?

R. L. KONDNER: No, I did not, but it is my understanding that the U. S. Army Engineers Waterways Experiment Station made such calculations and for some cases obtained negative values.

D. A. LINGER: Our next speaker this afternoon is from IITRI. The title is "On the Theory of Limiting Equilibrium for Axially Symmetric Soils Problems." The authors are C. J. Costantino and Andrew Longinow. Mr. Longinow will present the paper.

ANDREW LONGINOW: Presentation of formal paper, see pages 583-592.

ALBERT KNOTT: Could either you or Mr. Hanley give me some indication of the effect that you think the shock wave that is transmitted down through the cylinder from the top surface would have on the shear stresses at the structure soil interface?

ANDREW LONGINOW: I would like to point out that the tests performed here are static; I cannot answer your question.

D. A. LINGER: Is there any discussion on the paper presented by Mr. Marino?

P. S. BULSON: You showed some tests on cylinders where you measured the change in vertical diameter of the cylinder. When you plotted these, you plotted them symmetrically about the horizontal center line. Is there any justification for this?

R. L. MARINO: When I talk about change in diameter along the zero degree position, I am talking about vertical diameter. When I talk of change in diameter of the 90 degree position, I am talking about the horizontal diameter. I obtained these various diameter changes in the static tests by placing the model in the sand with the LVDTs oriented along the vertical and horizontal diameter and then obtaining a set of readings. For the next test, the model was rotated in the 20 degree position; therefore, I was measuring the change of diameter across at 20 degrees from the horizontal and vertical and it gave the displacements to me in these two positions. For each test I obtained two sets of points.

P. S. BULSON: You mentioned the diameter change, but how do you know it didn't all occur at the top of the cylinder?

R. L. MARINO: I don't. In one of the other tests, for model d/t of 160, which is the thinnest model, I had a different system. In this system I constructed a shaft that went through the end of the cylindrical shell. The shaft had sulphur lining ball bearings and was connected to a flexible shaft which went out through the soil and through the pressure vessel itself. On the outside it was connected to a protractor device and a pointer. As I applied each increment of load I could then sweep the LVDTs and measure the changes in the radius with respect to the longitudinal axis of the shell. Now this is a different set-up than the one I am reporting here. In this case one side of the LVDT presses against one wall and a probe against the other wall. The probe has a ball pressed into a little plastic fitting so it wouldn't hang up but which was spring loaded so it would follow the contours of the wall. Even though I could sweep it the whole 360 degrees in the present device I only put it in four positions and took averages to find out what the actual wall deflection was. In the other device, I measured the actual wall deflection and found that a typical oblong or elliptical shape resulted.

P. S. BULSON: Did you measure the total settlement of the whole specimen?

R. L. MARINO: The model in the soil? No, I did not.

D. A. LINGER: There is a chap here, Roy Butterfield, who would like to tell us what he is doing at Southhampton University in England.

ROY BUTTERFIELD: There are two points I would like to mention. First, we are trying to evolve a method of relating static test results and dynamic tests on buried cylinders in sand. Someone did mention this morning this business of dynamic load factor and I think it is worth a bit more emphasis. If you know the fundamental resonant frequencies of a structural system, you can calculate the response of the system to any loading function you care to apply, providing you make the usual assumptions of elastic behavior. Major Sievers has shown that you can vibrate even large structures relatively easily and it ought to be possible to calculate the response, or an approximation of it, of these structures to any blast wave pulse loading that you would like to impose. We are trying to do this on a model scale. We've

run an extensive series of tests on the lines of Prof. Kondner's with base plates on the sand and our results agree closely with what he put up this afternoon. We then intend burying some of Dr. Bulson's cylinders in this sand and finding the response of this soil–sand structural system to the same dynamic surface loading. We hope to be able to predict from this data the response of some of Dr. Bulson's structures when he tests them in a shock tube assembly. We buried the first cylindrical tube last week, and the preliminary results suggested that the system behaved approximately as if it had two degrees of freedom. (This behavior has not been observed in any subsequent tests during June and July 1964 and must be attributed to faulty instrumentation in the initial test. In fact, for 16 tubes tested to date under harmonic dynamic loading, two salient features are demonstrated in all tests: i) a decrease in the resonant frequency of the system is caused by burying the tube, ii) the tubes all fail by excessive crown deflection at a combined static and dynamic overpressure less than 5 lb/in^2.) The tubes were all similar to those tested statically by Dr. Bulson.

The second point is related to arching which may be of some interest to Mr. Truesdale who is studying this problem. We also looked around for results which had been published on trapdoor experiments and we couldn't find any either. We therefore turned our attention to grain and cement silos, the behavior of which are very much a related phenomenon. We have been considering an idealized model of uniform discs in a regular packing (see Figure 1 below). From a study of the limiting solutions of interparticle forces and friction at the silo wall, you can develop graphs of pressure on the wall against depth of filling. The lower limit solution agrees with Jansen and with Prof. Spangler's exponential pressure distributions; it is a geometric series but plots as essentially the same curve (see Figure 2 below). Considering the upper limit solution, you obtain the other curve shown in Figure 2. All the published results that we have found on silos fall in the area between the maximum and minimum curves. The point I really want to make about this is that you can get from maximum to minimum wall pressures in this idealized model with a very small amount of relative particle movement. If there is a trend for the particles to move as in Figure 3a (below), you tend to get the minimum wall pressure and maximum base pressure case, and if the trend is for the particles to move as in Figure 3b relative to each other, you can get ideally maximum wall pressures and minimum base pressures. (This is what happens with diaphragm type stress gauges and accounts for the under-registration.) It also arises in silos because if you start emptying a silo from the bottom, you are essentially encouraging relative movement of Figure 3b type. Silo results do show these trends of stress level when filling and when emptying the silo as shown in Figure 2. The minimum wall pressures correspond to a K value of 1/3 and the initial envelop of maximum pressures gives a K of the order of about 2. Current silo design tends to work with a K of about 2. I make this point because it means that K can fall anywhere between these limits, and in the idealized model it is purely a matter of relative movement between the discs. If you have a silo half full, if it is standing having been filled for some time, the wall pressure could be given by point A (Figure 2). If the silo is being emptied, then the wall pressure could be given by point B (Figure 2). The two apparently identical situations can have highly different stress patterns. Point B, of course, is unstable and if the material were disturbed it would tend to revert to point A. This is what I consider to be meant by arching. Arching, as I understand it, has some degree of impermanence. It can readily be upset from the arched to the "non-arched" state. I would suggest that this arching is a phenomenon related solely to granular materials where interparticle "cohesive" forces are negligible. Up to now a number of papers have discussed idealized elastic media and stress concentrations around lined holes, and described this as arching action. I would suggest that this is not arching. It is either stress concentration or stress relief and I feel we will mislead ourselves if we confuse these terms. The case of an elastic plate with a hole produces stress concentration or stress relief. It is permanent, and it is not affected by vibration, whereas arching is purely a granular material phenomenon. It is impermanent and the two are not in any way related. I think that using the term "arching" as a word to cover all these phenomena is confusing and incorrect.

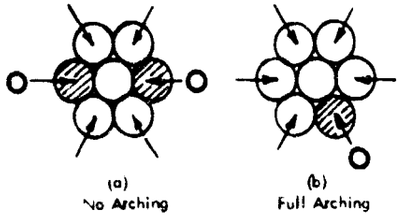


Figure 1

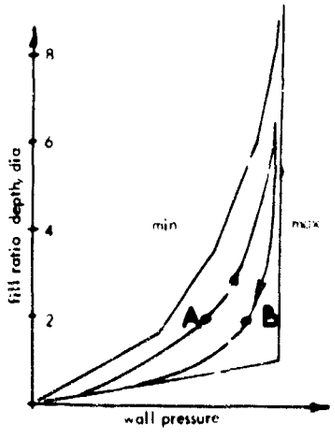


Figure 2

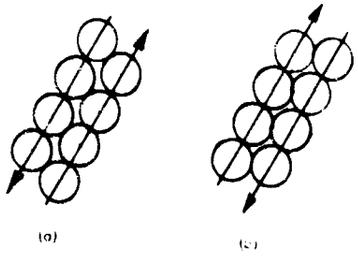


Figure 3

D. A. LINGER: This afternoon's session, on Design and Prototype Studies, has rather thoroughly considered design aspects of much of the research presented in earlier sessions. In addition, some prototype testing results have been presented which are directly involved with underground shelter design procedures. Some of the material presented this afternoon deals with theory and procedure presented in the late 1920s and early 1930s. It is indicated that very little has been done in the interim toward improving the understanding of the design of underground structures until the quite recent general realization of extreme loading criteria resulting from the threat of the nuclear weapons effects.

For some time we have designed underground structures with little knowledge of the distribution or redistribution of pressures resulting from soil or structure characteristics, or the beneficiation effects of the soil on the structure itself. Many aspects of questions relating to basic soil–structure interaction phenomena, often somewhat in conflict, have been discussed here. It is hoped that the primary objective of this Symposium (to provide a forum wherein researchers, engineering educators, and practicing professionals may meet to review the current state of the art and to present their contribution to advancement of the subject of soil–structure interaction as applied to protective construction) has been fulfilled. The published Proceedings should be of great interest to persons engaged in research and design involved with underground structures.

Editor's note: An abbreviated version of the following presentation was given during the Monday Afternoon Session on "Wave Propagation in Soil Media." It is presented here as a formal paper with pertinent discussion appended.

APPLICATION OF THE ONE-SIDED FOURIER TRANSFORM TO DETERMINE SOIL STORAGE AND DISSIPATION CHARACTERISTICS

by

Raymond J. Krizek*

INTRODUCTION

Theoretical developments in soil dynamics are very restricted in their ability to represent actual field conditions due to the complexity of soil as a structural material and the complicated interaction of the soil and the structure being supported. One aspect of considerable interest to the engineer concerned with earthquake or blast-resistant design is the determination of the frequency-dependent energy storage and dissipation characteristics of the soil. Among other things, these properties influence the propagation velocity and attenuation of generated waves and play a major role in the problem of soil-structure interaction. It is the object of this study to present a method by which experimental results from a conventional creep test may be utilized in conjunction with the one-sided Fourier transform to yield information regarding dynamic soil properties required in the solution of any boundary value problem in soil-structure interaction.

THEORETICAL CONSIDERATIONS

Complex Viscoelastic Parameters

If a linear viscoelastic material is subjected to a sinusoidally varying stress of amplitude σ_D at a given frequency of oscillation, ω, its steady state response will be a sinusoidally varying strain of amplitude ϵ_D at the same frequency but lagging the stress by a phase angle δ. The existence of a phase angle leads to the consideration of the strain components in phase and out of phase with the applied stress. The component of strain in phase with the stress divided by the stress is called the storage compliance J' and can be written

$$J' = \frac{\epsilon_D \cos \delta}{\sigma_D} \tag{1}$$

The storage compliance is related to the energy stored and completely recovered for a single cycle of deformation. The component of strain in quadrature with the stress divided by the stress is called the loss compliance J" and can be expressed

$$J'' = \frac{\epsilon_D \sin \delta}{\sigma_D} \tag{2}$$

The loss modulus is associated with the energy dissipated for a single cycle of deformation. The storage and loss compliances can be combined vectorially in the complex plane to give a complex compliance J* written as

$$J^* = J' - i\,J'' \tag{3}$$

The absolute value of the complex compliance $|J^*|$ is expressed as

$$|J^*| = |J' - i\,J''| = \sqrt{(J')^2 + (J'')^2} \tag{4}$$

Substitution of Equations 1 and 2 into Equation 4 gives

$$|J^*| = \frac{\epsilon_D}{\sigma_D} \tag{5}$$

In terms of the components of the complex compliance, the loss tangent (or tan δ) can be written

$$\tan \delta = \frac{J''}{J'} \tag{6}$$

In a similar manner, material response may be expressed alternatively in terms of storage, loss and complex moduli, given as

$$E' = \frac{\sigma_D \cos \delta}{\epsilon_D} \tag{7}$$

$$E'' = \frac{\sigma_D \sin \delta}{\epsilon_D} \tag{8}$$

and

$$E^* = E' + i\,E'' \tag{9}$$

* Assistant Professor of Civil Engineering, The Technological Institute, Northwestern University, Evanston, Illinois.

respectively. The magnitude of the complex modulus $|E^*|$ may be written

$$|E^*| = |E' + i\,E''| = \sqrt{(E')^2 + (E'')^2} = \frac{1}{|J^*|} = \frac{\sigma_D}{\epsilon_D} \tag{10}$$

while the loss tangent is given as

$$\tan \delta = \frac{E''}{E'} \tag{11}$$

Although $E^* = 1/J^*$, their individual components are not reciprocally related, but are connected by the equations

$$E' = \frac{J'}{\left[(J')^2 + (J'')^2 \right]} \tag{12}$$

and

$$E'' = \frac{J''}{\left[(J')^2 + (J'')^2 \right]} \tag{13}$$

or

$$J' = \frac{E'}{\left[(E')^2 + (E'')^2 \right]} \tag{14}$$

and

$$J'' = \frac{E''}{\left[(E')^2 + (E'')^2 \right]} \tag{15}$$

Transformations

There are two distinct methods of obtaining the complex compliance of a material. The first is based on a series of dynamic tests to investigate the steady-state response under sinusoidal stresses of various frequencies. In this case, discrete pairs of values for $|J^*|$ and δ are obtained. These may then be approximated by representative expression for J^*. The second method is based on applying a known stress $\sigma(t)$ to a material and measuring the resulting strain $\epsilon(t)$ which consists of both transient and steady-state components. The applied stress $\sigma(t)$ and resulting strain $\epsilon(t)$ may then be approximated by appropriate equations and transformed into the frequency domain by means of one-sided Fourier transforms. The ratio of the transformed strain to the transformed stress yields directly the complex compliance J^* in analytical form. Hence, a single transient test can produce all the information contained in an extensive series of variable frequency tests.

The one-sided Fourier transform expressions for stress and strain may be given as

$$\sigma^*(\omega) = \int_0^\infty \sigma(t)\, e^{-i\omega t}\, dt \tag{16}$$

and

$$\epsilon^*(\omega) = \int_0^\infty \epsilon(t)\, e^{-i\omega t}\, dt \tag{17}$$

where ω is expressed in radian frequency. The theoretical development of Fourier transforms and the conditions under which they exist may be found in texts by Titchmarsh (1937) and Sneddon (1951). Although the functions $\sigma(t)$ and $\epsilon(t)$ in Equations 16 and 17 may not meet the existence requirements and thereby not possess rigorously defined transforms, as long as they are sufficiently well-behaved (as in a great number of viscoelastic problems) the transforms of closely related expressions can be obtained. For example, the Fourier transform of a step function is not rigorously defined, but multiplication of a step function by the "convergence factor" e^{-kt} (where k is positive), as explained by Wylie(1951), may be used as an artifice to handle such cases wherein the process of letting k go to zero is postponed until after the transform has been safely taken. Another technique of considering a slightly different problem has been employed by Lockett (1961) to circumvent this same difficulty. Such manipulations allow formal integration and do not seriously affect results in the region of the time spectrum considered. Thus, Equations 16 and 17 may be formally integrated by parts to give

$$\sigma^*(\omega) = \frac{\sigma(0)}{\omega} + \frac{1}{i\omega} \int_0^\infty \dot{\sigma}(t)\, e^{-i\omega t}\, dt \tag{18}$$

or

$$\epsilon^*(\omega) = \frac{\epsilon(0)}{\omega} + \frac{1}{i\omega} \int_0^\infty \dot{\epsilon}(t)\, e^{-i\omega t}\, dt \tag{19}$$

where $\sigma(0)$ and $\epsilon(0)$ are the "instantaneous" values for stress and strain, and $\dot{\sigma}(t)$ and $\dot{\epsilon}(t)$ are the time derivatives of stress and strain, respectively. The complex compliance J^* assumes a form given by Equation 3 and may be expressed

$$J^*(\omega) = \frac{\epsilon^*(\omega)}{\sigma^*(\omega)} \tag{20}$$

DISCUSSION

A more rigorous mathematical treatment of the preceding theory has been given by Gross (1953), and applications of Fourier transforms to viscoelastic analyses have been reported by Read (1950), Bland (1957) and Lockett (1961).

EXPERIMENTAL PROCEDURE

Soil Tested

The soil investigated is a remolded plastic clay whose characteristics have been previously reported by Krizek and Kondner (1964) as liquid limit 46%, plastic limit 30%, shrinkage limit 20%, plasticity index 16% and specific gravity 2.74.

Description of Test

The experiment used in this investigation is the uniaxial compression creep test. To study the creep response of a material a stress is instantaneously applied to the specimen and maintained constant while strain is measured as a function of time.

The test reported herein is actually a constant load test and not a constant stress test. This procedure is commonly used by many investigators due to complications involved in the determination of the magnitude and distribution of area variations along the length of the specimen and the difficulty of automatic load variation to compensate for such changes. For small strains, the use of a constant load test seems quite reasonable. The constant stress is taken as the constant load divided by the initial area of the specimen, and the strain is taken as the time-dependent deformation divided by the initial length.

Conduct of Test

The particular test reported herein was conducted in a direct load apparatus where the load was applied through a hanger system by use of weights and transferred to the specimen by a vertical shaft passing through a ball bushing. The deformation was measured with an indicator dial placed at the top of the apparatus. In order to reduce moisture losses throughout the test, the specimen was protected by a thin rubber membrane and enclosed in a standard triaxial cell without lateral pressure. Due to the short duration of the test (ten minutes), it was deemed unnecessary to take further precautions, such as multiple membranes or various coatings. After the creep test was completed, a conventional constant strain rate unconfined compression test was conducted on the specimen.

In order to obtain a record of deformation response during the short time portion of the test, the indicator dial was photographed with a Wollensak Sixteen Model 93 movie camera. The camera was started several seconds before the load was applied and continued to operate for approximately ten seconds after load application. Beyond this time, dial readings were recorded manually at designated intervals throughout the ten minute duration of the test.

Specific values for the parameters of the reported test are: specimen length 8.20 cm, specimen diameter 3.60 cm, moisture content 30.5%, unconfined compressive strength 2.12 kg per sq cm, and applied load 12.5 kg.

ANALYSIS OF EXPERIMENTAL DATA

General Approach

A major problem of analysis lies in obtaining suitable analytic expressions which describe sufficiently well the experimental results and are amenable to mathematical manipulation; that is, the transforms can be obtained. While it is true that for a creep test, as was conducted, the stress varies slightly with time due to changes in cross-sectional area, these changes are small and not uniformly distributed o over the specimen length. Therefore, the approximation of $\sigma(t)$ by a constant stress, $\sigma(0)$, applied "instantaneously" at zero time lies well within the limitations of experimental work. Utilizing the fact that $\sigma(t)$ can be considered a constant, $\dot{\sigma}(t)$ vanishes and the transformed stress may then be written from Equation 18 as

$$\sigma^*(\omega) = \frac{\sigma(0)}{i\omega} \tag{21}$$

The strain response, $\epsilon(t)$, may be approximated by a series written as follows:

$$\epsilon(t) = [a + bt] - \sum_{n=1}^{N} c_n e^{-d_n t} \tag{22}$$

where $[a + bt]$ is the steady-state response and the last term represents a series of N exponential terms required to adjust the steady-state response for small times. Data reported by Kondner and Krizek (1962) for creep tests conducted for times in excess of 20,000 minutes indicate that such a steady-state response is never attained, but rather the strain rate is constantly decreasing throughout the duration of the test. With regard to the curve-fitting procedure to be utilized, $[a + bt]$ represents a "datum" which is adjusted by means of the exponential terms to yield the experimental strain response. Hence, it could be represented equally well by a constant which may be taken as the "ultimate" strain at very large time or some other suitable value as deemed applicable by the individual investigator for the particular analysis. As may be expected, the effect of this term is manifested primarily in the region of large time or low frequency. In Equation 22 c_n and d_n are constants to be determined by curve-fitting techniques and N is the number of terms required to produce the desired accuracy. The advantage of such a form is that it permits the experimental data to be fit to any desired accuracy and yet lends itself to simple transformation techniques. Such an approach has been employed by Papazian (1962) in an investigation of the constitutive behavior of asphaltic concrete.

Upon differentiation with respect to time, Equation 22 becomes

$$\dot{\epsilon}(t) = b + \sum_{n=1}^{N} c_n d_n e^{-d_n t} \tag{23}$$

Substitution of Equation 23 into Equation 19 yields the transformed strain as

$$\epsilon^*(\omega) = \frac{\epsilon(0)}{i\omega} + \frac{1}{i\omega} \int_0^\infty \left[b + \sum_{n=1}^{N} c_n d_n e^{-d_n t} \right] e^{-i\omega t} \, dt \tag{24}$$

Formal integration of Equation 24 and substitution of limits gives

$$\epsilon^*(\omega) = \frac{1}{i\omega} \left[\epsilon(0) + \frac{b}{i\omega} + \sum_{n=1}^{N} \frac{c_n d_n}{d_n + i\omega} \right] \tag{25}$$

Substitution of Equations 21 and 25 into Equation 20 gives the complex compliance as

$$J^*(\omega) = J'(\omega) - i\,J''(\omega) = \left[\frac{\epsilon(0)}{\sigma(0)} + \frac{1}{\sigma(0)} \sum_{n=1}^{N} \frac{c_n d_n^2}{d_n^2 + \omega^2} \right] - i \left[\frac{b}{\omega \sigma(0)} + \frac{1}{\sigma(0)} \sum_{n=1}^{N} \frac{c_n d_n \omega}{d_n^2 + \omega^2} \right] \tag{26}$$

Equating real and imaginary parts, the storage and loss compliances may be written as

$$J'(\omega) = \frac{\epsilon(0)}{\sigma(0)} + \frac{1}{\sigma(0)} \sum_{n=1}^{N} \frac{c_n d_n^2}{d_n^2 + \omega^2} \tag{27}$$

and

$$J''(\omega) = \frac{b}{\omega \sigma(0)} + \frac{1}{\sigma(0)} \sum_{n=1}^{N} \frac{c_n d_n \omega}{d_n^2 + \omega^2} \tag{28}$$

Specific Application

Figure 1 gives the results of a typical test during the first second after load application. As can be observed, the actual load application was not "instantaneous" but required somewhat less than one-fifth of a second. Utilizing the extrapolated dashed curve, the time interval for all subsequent calculations is taken as 0.18 seconds less than the actual elapsed time. This is significant only in the region of short time.

The creep strain versus time response for the entire ten minute duration of the test is shown in Figure 2. If the constants a and b in Equation 22 are taken as 0.0225 and zero, respectively, the strain difference between the "datum level" and the actual experimental value [that is, $0.0225 - \epsilon(t)$] may be plotted as shown in Figure 3. The data beyond 150 seconds may be approximated by the equation

$$\epsilon_1 = 0.0046\ e^{-0.00345t} \tag{29}$$

Figure 4a shows the next successive strain difference (that is, $0.0225 - \epsilon(t) - \epsilon_1$) plotted versus time, and the equation approximating the data beyond 25 seconds may be written

$$\epsilon_2 = 0.0027\ e^{-0.0226t} \tag{30}$$

In similar manner, three more such approximations are shown in Figures 4b, 4c and 4d; these yield the equations

$$\epsilon_3 = 0.0058\ e^{-0.234t} \tag{31}$$

$$\epsilon_4 = 0.0028\ e^{-2.62t} \tag{32}$$

and

$$\epsilon_5 = 0.0056\ e^{-9.60t} \tag{33}$$

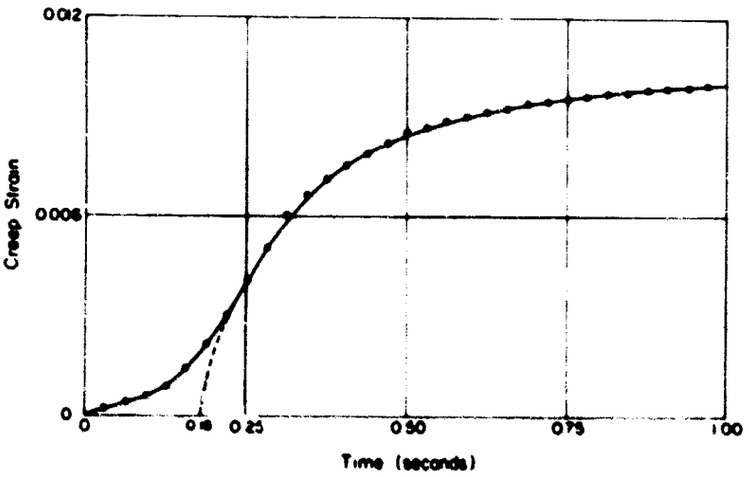


Fig. 1 Creep Strain versus Time: Short Time Region

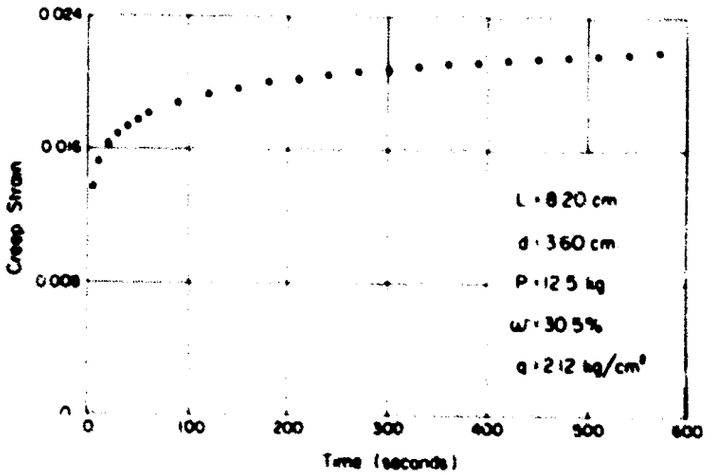


Fig. 2 Typical Creep Strain Response

Hence, the particular form of Equation 22 applicable to this test is

$$\epsilon(t) = 0.0225 - 0.0046\, e^{-0.00345t} - 0.0027\, e^{-0.0226t} - 0.0058\, e^{-0.234t} - 0.0028\, e^{-2.62t} - 0.0056\, e^{-9.60t} \quad (34)$$

By letting time vanish in Equation 34, the "instantaneous" strain is found to be

$$\epsilon(0) = 0.0010 \quad (35$$

Dividing the constant load of 12.5 kg by the initial specimen area of 10.18 sq cm, the "instantaneous" stress (which is assumed constant throughout the test) may be expressed in kg per sq cm as

$$\sigma(0) = 1.23 \quad (36)$$

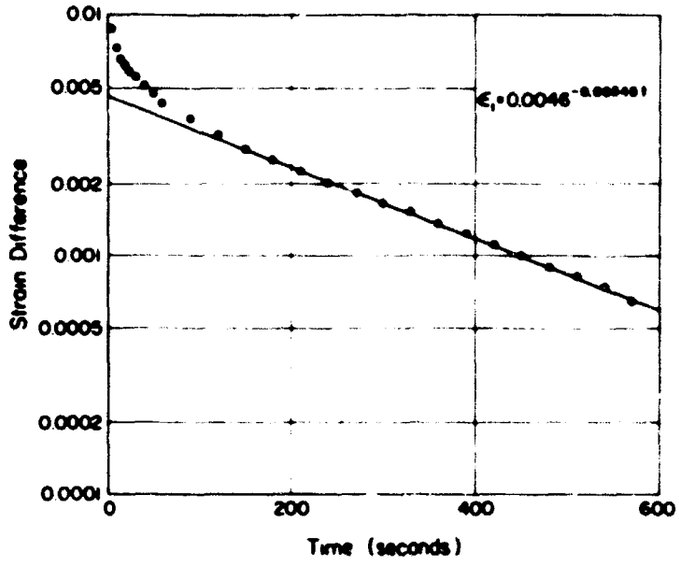


Fig. 3 Strain Difference versus Time: First Approximation

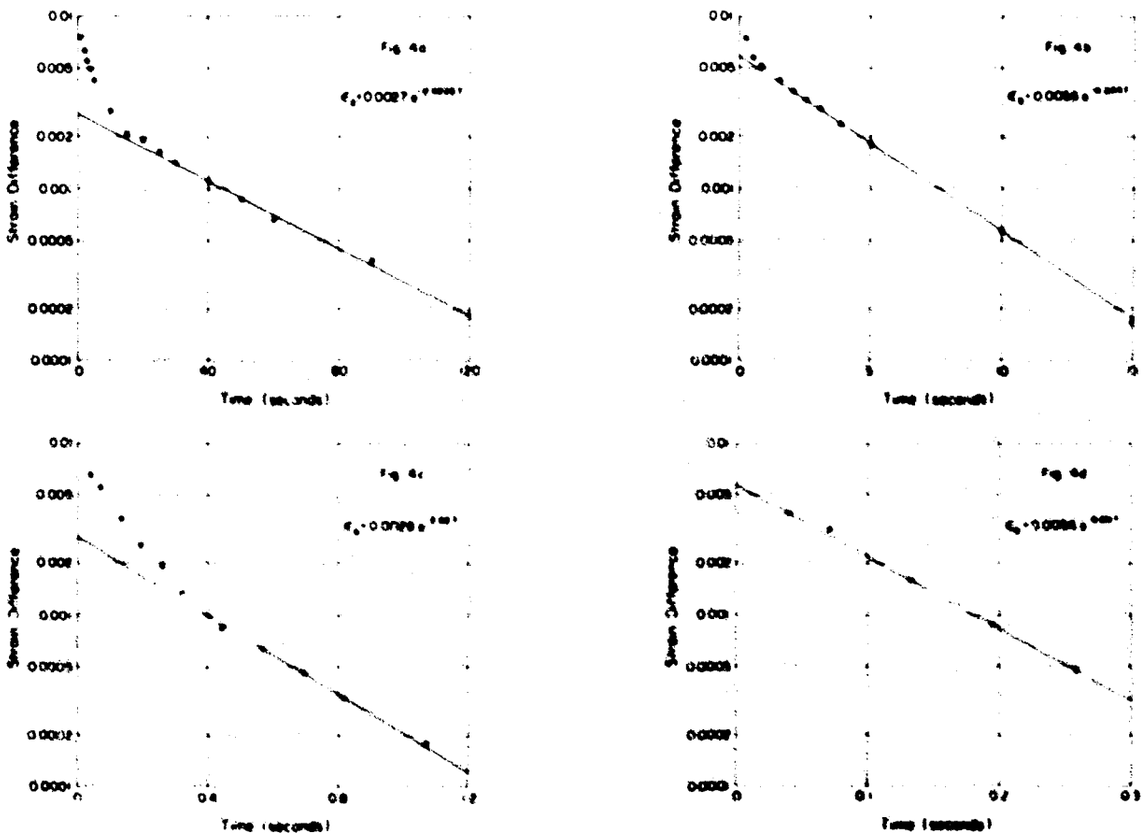


Fig. 4 Strain Difference versus Time: Successive Approximations

Compliance Function Representation

Utilizing the quantitative values given in Equations 34, 35 and 36, specific forms of Equations 27 and 28 (the storage compliance and loss compliance) may be written as

$$J'(\omega) = \left[813 + \frac{0.0445}{0.0000119 + \omega^2} + \frac{1.1212}{0.000511 + \omega^2} + \frac{258.2}{0.05476 + \omega^2} + \frac{15626}{6.8644 + \omega^2} + \frac{419590}{92.16 + \omega^2}\right] 10^{-6} \quad (37)$$

and

$$J''(\omega) = \left[\frac{12.90}{0.0000119 + \omega^2} + \frac{49.61}{0.000511 + \omega^2} + \frac{1103}{0.05476 + \omega^2} + \frac{5964}{6.8644 + \omega^2} + \frac{43707}{92.16 + \omega^2}\right] \omega \quad 10^{-6} \quad (38)$$

These parameters are associated with the energy storage and dissipation characteristics of the material. The forms of Equations 37 and 38 are quite sensitive to the accuracy of the analytic approximation to the experimental data, and this in turn is governed primarily by the number of terms utilized in Equation 22.

Since the particular test data analyzed extends over a time range from a fraction of a second to six hundred seconds, extrapolation beyond this range must necessarily be approached with caution until such time as a comprehensive experimental and analytical study provides confirmation one way or the other. The integrals given in Equations 16 and 17 (or equations derived therefrom) depend on all values of stress or strain in the entire interval from zero to infinity and cannot, in general, be expressed in terms of a portion of the time spectrum. A rigorous transformation can be determined if, and only if, the measured response is known over the entire time scale and can be formulated in an analytical expression amenable to subsequent mathematical treatment. The artifice employed herein to allow formal integration implies that the material response for long times contributes relatively little to the response spectrum. In any experiment covering a limited range of the time scale, the observable time-dependent effects are controlled primarily by those processes whose relaxation or retardation times are of the same order of magnitude as the time scale of the experiment. Hence, the subjective significance of any functional relationships derived from limited experimental data must take recognition of this fact. As one example, Treloar (1958) reports that an overwhelming contribution to the relaxation spectrum for butyl rubber arises from very short relaxation times. These mechanisms with relaxation times between 10^{-8} and 10^{-7} seconds contribute about 10,000 times as much as those with relaxation times between 0.1 and 100 seconds. The preceding comments are not intended to suppress the use of such techniques to investigate soil response characteristics, but rather to establish a thorough appreciation of the restrictions associated with this approach. This general procedure of analysis has been utilized with much apparent success by workers in the field of polymers despite the presence of some of the same problems. Not enough is really known about the constitutive response of soils to be overly optimistic or pessimistic concerning the feasibility of such an approach, but it does appear to offer a very rational starting point for obtaining a phenomenological description of soil behavior.

Assuming that data is available over a sufficiently large time scale to eliminate any adverse effects due to erroneous extrapolation, a single transient test on a linear viscoelastic material in the time domain is sufficient to obtain the corresponding stress-strain relationship (as expressed herein by the complex compliance) in the frequency domain. In general, soil will exhibit a nonlinear constitutive response, and a single test will not suffice to determine uniquely the components of the complex compliance function. A series of tests will have to be conducted at a variety of stress levels, and each test, when analyzed in the manner presented, will yield relationships qualitatively similar to those given in Equations 37 and 38. Thus, for a nonlinear material, the storage and loss compliance functions will be both frequency and stress dependent, and a family of curves will be obtained.

The time range selected for the test analyzed herein is not to be construed as a limitation of the technique presented. The range was chosen primarily for convenience since the only intent of the test was to provide typical data for illustrating a technique of analysis. Using the qualitative equivalence of $\omega \approx 1/t$ (ω in radian frequency) as explained by Ferry (1961), the time range from a fraction of a second to six hundred seconds corresponds approximately to a frequency range of 2 to 0.0002 cycles per second. Longer times in a creep test are easily obtained; shorter times are limited to some extent by the ingenuity of the investigator. While the creep test technique does not lend itself to direct determination of high frequency response, it is possible that data may be obtained over a sufficiently wide region of the time spectrum to justify its application to many dynamic soil problems of interest.

WAVE PROPAGATION

Field Equation

The field equation for one dimensional dilatation wave propagation through a material may be written

$$\frac{\partial \sigma}{\partial x} = \rho \frac{\partial^2 u}{\partial t^2} \quad (39)$$

where σ is the stress, u is the longitudinal displacement, and ρ is the mass density. Differentiation of Equation 39 with respect to x and substitution of the standard Cauchy expression for strain allows the field equation to be written as

$$\frac{\partial^2 \sigma}{\partial x^2} = \rho \frac{\partial^2 \epsilon}{\partial t^2} \quad (40)$$

In addition to suitable boundary and initial conditions, the solution of Equation 40 requires the use of some form of constitutive relation for the material. In general, there is no simple equation expressing stress in terms of strain for a real "viscoelastic" soil, and consequently no tractable expressions for the propagation of an arbitrary disturbance in such a material can be given.

DISCUSSION

Sinusoidal Waves

Considering the propagation of a train of sinusoidal waves, stress can be related to strain by means of a complex modulus, as given by Equation 9. Thus, for a sinusoidal disturbance in a linear viscoelastic material, Equation 40 assumes the form

$$E^* \frac{\partial^2 \epsilon}{\partial x^2} = \rho \frac{\partial^2 \epsilon}{\partial t^2} \tag{41}$$

According to Kolsky (1960), the solution of Equation 41 for a progressive sinusoidal wave of radian frequency ω whose displacement at the origin is $\epsilon_0 \cos \omega t$ is given by

$$\epsilon = \epsilon_0 e^{-\alpha x} \cos \left[\omega \left(t - \frac{x}{c} \right) \right] \tag{42}$$

where c is the wave propagation velocity given by

$$C = \left[\frac{|E^*|}{\rho} \right]^{1/2} \sec \frac{\delta}{2} \tag{43}$$

and α is the attenuation written as

$$\alpha = \frac{\omega}{c} \tan \frac{\delta}{2} \tag{44}$$

Propagation of Pulses

If the propagation constants c and α are known functions of frequency over a sufficiently wide frequency range, Kolsky (1960) has inferred the propagation of an arbitrary disturbance in linear materials by means of Fourier synthesis. If $f(\omega)$ is a complex function of ω which defines the shape of the disturbance, the displacement produced by the disturbance at the origin is expressed by the Fourier integral

$$u(0) = \int_0^\infty f(\omega) e^{i\omega t} \, d\omega \tag{45}$$

Then at a distance x along the filament, the displacement is given by

$$u(x) = \int_0^\infty f(\omega) e^{-\alpha x + i\omega (t - x/c)} \, d\omega \tag{46}$$

If the values of $|E^*|$ and δ are known from experiment over the relevant frequency range, the shape of the pulse can be calculated numerically by use of Equations 43, 44 and 46 since, in general, the substitution of theoretical expressions into Equation 46 does not lead to tractable integrals.

The preceding approach is concerned with the propagation of plane waves and is applicable for a longitudinal disturbance along a filament where the relevant Fourier spectrum of the disturbance contains only components whose wavelength is large compared with the diameter of the filament. A plane wave propagated through an unbounded viscoelastic medium can be treated similarly in terms of a complex modulus involving the bulk modulus. While little theoretical work on general three-dimensional wave propagation in viscoelastic materials has been done, a detailed discussion of the problems involved has been given by Hunter (1960).

There are few accounts in the literature of experimental work on the problem of pulse propagation in viscoelastic materials. Kolsky (1954, 1956) has reported some measurements on the change in shape of longitudinal stress pulses as they travel along rods of polymethyl methacrylate and polyethylene. These results have been analyzed numerically using the Fourier synthesis technique and replacing the Fourier integral by a Fourier series.

Experimental Results

Substitution of the quantitative analytical results given by Equations 37 and 38 into Equations 6 and 10 allows the magnitude of the complex modulus $|E^*|$ and the phase angle δ to be expressed as functions of frequency for a given stress level. These relationships are shown in Figures 5 and 6. It is felt that the "irregularities" in the phase angle plot of Figure 6 are manifestations of the limited number

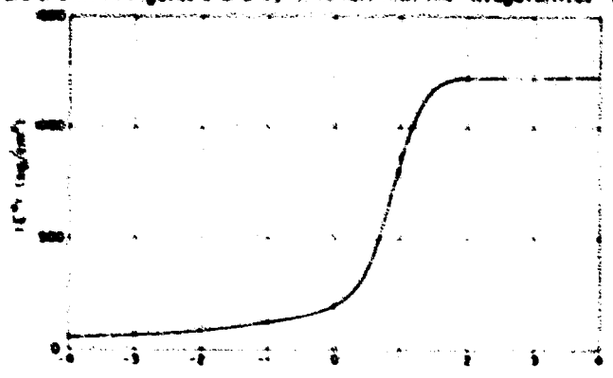


Fig. 5 Complex Modulus versus Frequency

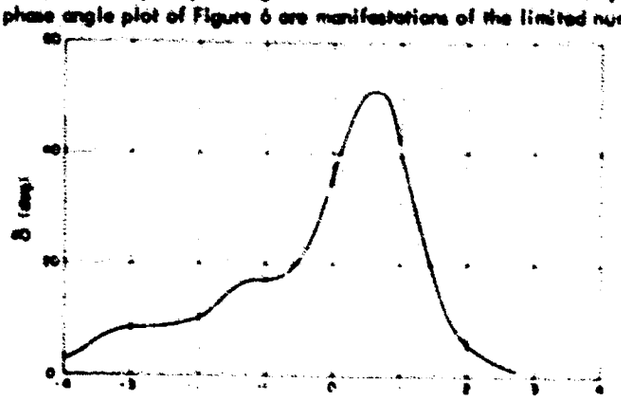


Fig. 6 Phase Angle versus Frequency

of terms in the curve fit rather than the fundamental behavior of the soil. Assuming that the soil response can be approximated by linear viscoelastic theory, the curves given in Figures 5 and 6 will be unique; that is, independent of stress. Use of Equations 43 and 44 in conjunction with previous results for $|E^*|$ and δ allows the wave propagation velocity c and attenuation α to be expressed as shown in Figures 7 and 8.

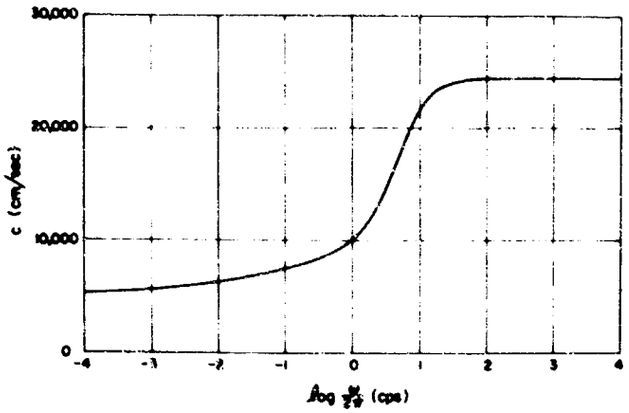


Fig. 7 Wave Propagation Velocity Versus Frequency

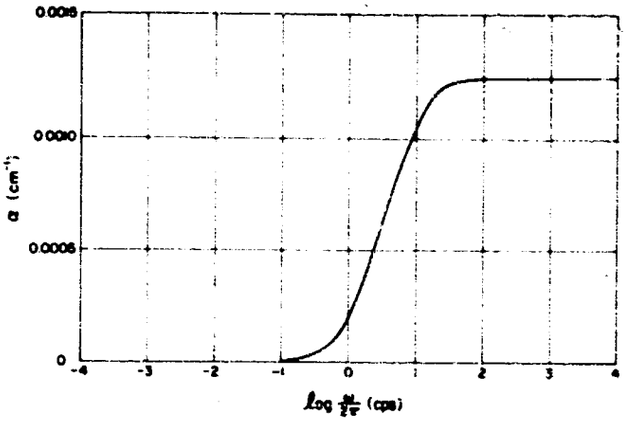


Fig. 8 Wave Attenuation Versus Frequency

Similar information on $|E^*|$, δ, c, and α has been obtained by Kondner (1962) over a more restricted range by use of steady-state vibratory techniques.

Utilizing the concept of logarithmic decrement, a study of the propagation and dissipation of elastic wave energy in granular soils has been made by Richart, Hall and Lysmer (1962) and Hall and Richart (1963). Heierli (1962) reported a similar study taking into account the complex nonlinear and inelastic stress-strain relationship for soils.

Nonlinear Approach

To date, the theory of nonlinear viscoelastic wave propagation has received little attention. One study by Malvern (1951) concerns the problem of plastic wave propagation in a metal which exhibits a strain rate effect. Hillier and Kolsky (1949) carried out some experimental work on the propagation of longitudinal sinusoidal waves of small amplitude in filaments of polyethylene, nylon and various rubbers which had been statically drained out of the region of linear viscoelasticity. By measuring the "tangent" dynamic modulus at large strains, it was found that the velocity of propagation increased considerably in some cases. For one synthetic rubber (Neoprene), $|E^*|$ increased more than one hundredfold as the specimen was stretched to six times its original length. Consequently, the propagation velocity increased more than ten times.

As previously mentioned, the constitutive response for many soils is often sufficiently nonlinear to preclude the direct application of theories of linear viscoelasticity. However, when utilized with a proper realization and respect for its limitations, linear theory can provide valuable insight to general modes of approach to nonlinear soil problems.

For a nonlinear material, the relations for $|E^*|$ and δ shown in Figures 5 and 6, as well as the expressions for J' and J" given by Equations 37 and 38, would be stress dependent and a family of curves would result — each corresponding to a particular stress level. Once obtained for a given material, these storage and dissipative functions would have to be utilized in conjunction with the field equation given by Equation 40 to determine a solution. Although quite complex and analytically unfeasible, the problem may lend itself to a numerical approach similar in nature to that utilized by Petrof and Gratch (1964) and Wolosewick (1962). However, their approaches would have to be modified by an iterative procedure to account for the additional feature of stress dependence.

SUMMARY

The work reported herein has illustrated the use of one-sided Fourier transform techniques to transform the results of constant stress experimental test data for a remolded plastic clay into the frequency domain and thereby obtain approximate expressions for the storage and loss compliance functions. These parameters are associated with the energy storage and dissipation properties of the soil, and they may be utilized as the constitutive relations in the solution of the one-dimensional field equation for dilatation wave propagation and attenuation.

The use of such techniques on a linear viscoelastic material requires only a single transient test in the time domain to obtain the corresponding stress-strain relationship in the entire frequency domain. Although most soils are not "linear viscoelastic," results obtained by means of this assumption may provide valuable insight into the analysis of available data and the development of new test procedures. Consideration of the actual nonlinear constitutive response will produce a family of curves or equations for the frequency-dependent complex compliance — each corresponding to a particular stress level. The use of discrete points for this compliance function in conjunction with the field equation may lend itself to a "marching" type iterative numerical solution to one-dimensional wave propagation problems.

ACKNOWLEDGEMENTS

Grateful appreciation is extended to Mr. John Schmidt for his capable assistance in the conduct of the test.

Acknowledgement is given to the Northwestern University Computing Center and the National Science Foundation whose funds helped in the establishment of the Center.

The method of analysis presented is the result of research activities directed by Professor Robert L. Kondner for the U. S. Army, Corps of Engineers, Waterways Experiment Station, Vicksburg, Mississippi, and pursued by Mr. Michael M. K. Ho.

DISCUSSION

BIBLIOGRAPHY

Bland, D. R., "Application of the One-Sided Fourier Transform to the Stress Analysis of Linear Viscoelastic Materials," Proceedings of the Conference on the Properties of Materials at High Rates of Strain, Institution of Mechanical Engineers, London, pp. 156–163, 1957.

Ferry, J. D., Viscoelastic Properties of Polymers, John Wiley and Sons, Inc., New York, pp. 54–56, 1961.

Gross, B., Mathematical Structure of the Theories of Viscoelasticity, Hermann, Paris, 1953.

Hall, J. R. and F. E. Richart, Jr., "Dissipation of Elastic Wave Energy in Granular Soils," Proceedings of the American Society of Civil Engineers, Journal of the Soil Mechanics and Foundations Division, Volume 89, Number SM6, pp. 27–56, 1963.

Heierli, W., "Inelastic Wave Propagation in Soil Columns," Proceedings of the American Society of Civil Engineers, Journal of the Soil Mechanics and Foundations Division, Volume 88, Number SM6, pp. 33–64, 1962.

Hillier, K. W. and H. Kolsky, "An Investigation of the Dynamic Elastic Properties of Some High Polymers," Proceedings of the Physical Society of London, Volume 62, Section B, pp. 111–121, 1949.

Hunter, S. C., "Viscoelastic Waves," Progress in Solid Mechanics (edited by I. N. Sneddon and R. Hill), North-Holland Publishing Company, Amsterdam, pp. 1–57, 1960.

Kolsky, H., "Attenuation of Short Mechanical Pulses by High Polymers," Proceedings of the Second International Congress on Rheology (edited by V. G. W. Harrison), Academic Press, Inc., New York, pp. 79–84, 1954.

Kolsky, H., "The Propagation of Stress Pulses in Viscoelastic Solids," Philosophical Magazine, Volume 1, Series 8, pp. 693–710, 1956.

Kolsky, H., "Viscoelastic Waves," International Symposium on Stress Wave Propagation in Materials (edited by Norman Davids), Interscience Publishers, Inc., New York, pp. 59–60, 1960.

Kondner, R. L., "Vibratory Response of a Cohesive Soil in Uniaxial Compression," Proceedings of the Second Symposium on Earthquake Engineering, University of Roorkee, Roorkee, India, pp. 109–129, 1962.

Kondner, R. L. and R. J. Krizek, A Rheologic Investigation of the Dynamic Response Spectra of Soils, Report 1: Basic Concepts, Equipment Development and Soil Testing Procedures, by Northwestern University to the U. S. Army, Corps of Engineers, Waterways Experiment Station, Vicksburg, Mississippi, 1962.

Krizek, R. J. and R. L. Kondner, "Strength-Consistency Indices for a Cohesive Soil," Presented at the 43rd Annual Meeting of the Highway Research Board, Washington, D. C., 1964.

Lockett, F. J., "Interpretation of Mathematical Solutions in Viscoelasticity Theory Illustrated by a Dynamical Spherical Cavity Problem," Journal of the Mechanics and Physics of Solids, Volume 9, pp. 215–229, 1961.

Malvern, L. E., "Plastic Wave Propagation in a Bar of Material Exhibiting a Strain Rate Effect," Quarterly of Applied Mathematics, Volume 8, Number 4, pp. 405–411, 1951.

Papazian, H. S., Response of Linear Viscoelastic Materials in the Frequency Domain, Engineering Experiment Station Bulletin Number 192, Ohio State University, Columbus, Ohio, 1962.

Petrof, R. C. and S. Gratch, "Wave Propagation in a Viscoelastic Material with Temperature-Dependent Properties and Thermomechanical Coupling," Transactions of the American Society of Mechanical Engineers, Journal of Applied Mechanics, Paper Number 64-APM-8, 1964.

Read, W. T., "Stress Analysis for Compressible Viscoelastic Materials," Journal of Applied Physics, Volume 21, pp. 671–674, 1950.

Richart, F. E., J. R. Hall and J. Lysmer, Study of the Propagation and Dissipation of "Elastic" Wave Energy in Granular Soils, Report by the University of Florida to the U. S. Army, Corps of Engineers, Waterways Experiment Station, Vicksburg, Mississippi, 1962.

Sneddon, I. N., Fourier Transforms, McGraw-Hill Book Company, Inc., New York, 1951.

Titchmarsh, E. C., Introduction to the Theory of Fourier Integrals, Clarendon Press, Oxford, 1937.

Treloar, L. R. G., The Physics of Rubber Elasticity, Clarendon Press, Oxford, 1958.

Wolosewick, R. M., Transient Wave Propagation in a Thermoviscoelastic Material, Master of Science Thesis, Department of Mechanical Engineering, Northwestern University, Evanston, Illinois, 1962.

Wylie, C. R. Jr., Advanced Engineering Mathematics, McGraw-Hill Book Company, Inc., New York, pp. 145–149, 1951.

* *

MICHAEL ANTHONY: I wonder if Dr. Krizek could tell us what kind of materials he used and whether he thinks there is any dispersion.

R. J. KRIZEK: The answer to your first question is easy. It was a very fine grained, remodeled plastic clay. Would you state the second part of the question again?

MICHAEL ANTHONY: What I was trying to say is that it seems we have neglected dispersion effects due to different frequency components in the major part of our analysis and I was wondering if anyone would like to present some comments on this.

R. J. KRIZEK: I think it is a generally accepted fact that all of these moduli, if you will, or compliance functions, are frequency or time dependent, and any modulus which neglects this necessarily introduces an error. How to remedy this is, of course, another question. Even a bigger question is the fact that in what I presented, I only got as far as talking about linear theory (that was another one of your questions, I believe). The presentation is restricted to one stress level, the particular stress level indicated in Figure 2. In order to test a non-linear material, it is my opinion that you have to run similar tests at other stress levels and thereby get families of such curves, each one corresponding to a particular stress level.

INDEX TO AUTHORS AND DISCUSSION PARTICIPANTS

	Page
ABBOTT, P. A.	618
ALLGOOD, J. R.	189, 605, 609–613
ANDERSON, M.	127
ANTHONY, M.	597, 598, 633
ARBUTHNOT, G. L.	605–609
BEMBEN, S.	601, 614, 615, 622
BERG, G.	597
BROCKENBROUGH, R. L.	616
BULSON, P. A.	211, 606, 607, 615, 621, 623
BURNS, J. Q.	378, 615, 616
BUSTAMANTE, J. I.	610, 617
BUTTERFIELD, R.	619, 623
CASPE, M.	602, 607, 608, 614, 622
CHELAPATI, C. V.	356, 615
CONSTANTINO, C. J.	303, 423, 583
DAVISSON, M. T.	73, 599
DONNELLAN, B.	449, 620, 621
EKBERG, C.	621, 622
EVERARD, N. J.	611, 613, 615
FELDMAN, A.	601
FLATHAU, W. J.	623
FOX, R. R.	619
GABRIEL, L. H.	607, 612
GUNDERSON, R. H.	436
HALTIWANGER, J. D.	608, 616
HAMPTON, J. D.	315, 403, 611–613, 617
HANLEY, J.	487, 597
HARRENSTIEN, H. P.	436, 607, 619, 620
HENDRON, A. J., JR.	73, 596–598
HOEG, K.	393, 606, 619
HOFF, G. C.	138
HUMMEL, P. L.	602, 611, 621
KNOTT, A.	602, 605, 613, 619, 620, 621, 623
KONDNER, R. L.	574, 623
KRIZEK, R. J.	625, 633
LEISTNER, H.	596–598, 603, 618, 620
LINGER, D. A.	598, 600, 605, 609, 614, 618, 621–624
LONGINOW, A.	423, 583, 618, 619, 623
LUM, W.	608
LUSCHER, U.	393, 606, 616
MAJUMDAR, D.	601
MARINO, R. L.	464, 613, 614, 621, 623
MASON, H.	595, 603–605, 609, 610, 618, 619
MIKLOFSKY, G.	623
MURPHY, G.	285
NIELSON, D.	601, 608, 609, 611, 620, 622
NEWMARK, N. M.	1
PERRET, BILL	107, 596, 597, 601
RICHARD, R. M.	378, 616
RILEY, R. M.	332, 464
ROBINSON, R. R.	303
RUSIN, R.	172
SACHS, A.	611
SAGER, R. A.	554
SALMON, M. S.	303
SAXE, H. C.	118
SCHIMMING, B.	118, 601, 604, 615
SEAMAN, L.	98, 595, 596
SELIG, E. T.	27, 155, 172, 303, 595–598, 604, 605, 610, 611, 615, 618
SIBLEY, E. A.	600–605
SIEVERS, R. H.	547, 595, 598, 601, 607–610, 612, 613, 620–623
SOLLID, E.	595, 606
SPANGLER, M. G.	531
SPANOVICH, M.	403
TAMANINI, F. J.	596
TENER, R. K.	296, 610–612
THOMPSON, A.	598
TRIANDAFILIDIS, G. E.	403, 615, 617, 618
TRUESDALE, W. B.	127, 349, 602–604, 614, 615
VAN HORN, D. A.	256, 608, 609
VEY, E.	349
WATKINS, R. K.	246, 607, 608, 618–621
WEISSMANN, G. F.	607
WESTINE, P.	605, 606, 608, 610, 611, 617, 621
WHITE, H.	608
WHITE, M.	596, 605, 607, 612, 619, 620
WHITMAN, R. V.	594–600
WIEHLE, C. K.	239
YOUNG, D. F.	285, 609, 610, 617
ZACCOR, J. V.	62, 595
ZWOYER, E.	614–618

SYMPOSIUM REGISTER

PHILIP A. ABBOTT
A. F. SHOCK TUBE FACILITY
BOX 188, UNIVERSITY STATION
ALBUQUERQUE, NEW MEXICO

JOSEPH T. ADAMS
CITY, COUNTY OF SAN FRANCISCO
2683 46th AVE.
SAN FRANCISCO

EDWARD J. ALBREN
DEPARTMENT OF THE NAVY
BUREAU OF YARDS AND DOCKS
CODE 50.710
WASHINGTON, D. C.

JAY R. ALLGOOD
STRUCTURAL RES. ENGINEER
U.S. NAVAL CIVIL ENG. LAB.
PORT HUENEME, CALIF.

PROF. LOREN B. ALMY
DEPT. OF CIVIL ENGINEERING
WASHINGTON STATE UNIV.
PULLMAN, WASHINGTON

MICHAEL ANTHONY
BOEING COMPANY
505 1/2 W. MERCER PLACE
SEATTLE, WASHINGTON

GUY L. ARBUTHNOT, CHIEF
ENGINEERING RESEARCH
U.S. ARMY WES
VICKSBURG, MISSISSIPPI

DONALD B. BALDWIN
PROT. STRUCT. DEV. CENT.
BLDG. 2591
FORT BELVOIR, VIRGINIA

RUSSELL E. BARNARD
ADVISORY ENGINEER
ARMCO STEEL CORP.
6401 SHEPHERD HILLS
TUCSON, ARIZONA

MAJOR M. E. BARNES
HQ DASA
IB693 PENTAGON
WASHINGTON, D. C.

PROF. STANLEY M. BEMBEN
DEPT. OF CIVIL ENGINEERING
UNIVERSITY OF MASSACHUSETTS
AMHERST, MASS.

PROF. LEON L. BERATAN
DEPT. OF CIVIL ENGINEERING
DREXEL INST. OF TECHNOLOGY
32nd AND CHESTNUT STREETS
PHILADELPHIA, PA.

DR. GLEN V. BERG
DEPT. OF CIVIL ENGINEERING
UNIVERSITY OF MICHIGAN
ANN ARBOR, MICHIGAN

DR. WILLIAM B. BICKFORD
DEPT. OF CIVIL ENGINEERING
UNIVERSITY OF ARIZONA
TUCSON, ARIZONA

DARRELL N. BLAKE
SALES MANAGER, CULVERT DIV.
EATON METAL PROD. CORP.
13th AND WILLIS
OMAHA, NEBRASKA

PROF. ALBERT J. BONAR
DEPT. OF CIVIL ENGINEERING
UNIVERSITY OF HOUSTON
3801 CULLEN
HOUSTON, TEXAS

CHARLES M. BONNEAU
RICKETT, REAVES AND WARD
2901 "H" STREET
BAKERSFIELD, CALIF.

R. L. BROCKENBROUGH
ENG. APPLIED RES. LAB.
U.S. STEEL CORPORATION
MONROEVILLE, PA.

GORDON V. BROWN
ARTHUR T. BROWN, ARCHITECT
726 N. COUNTRY CLUB ROAD
TUCSON, ARIZONA

DR. PHILIP S. BULSON
MIL. ENG. EXPER. ESTAB.
CHRISTCHURCH, HAMPSHIRE
ENGLAND

J. Q. BURNS
DEPT. OF CIVIL ENGINEERING
UNIVERSITY OF ARIZONA
TUCSON, ARIZONA

PROF. JORGE I. BUSTAMANTE
INSTITUTO DE INGENIERIA
CIUDAD UNIVERSITARIA
MEXICO 20 D. F.

ROY BUTTERFIELD
DEPT. OF CIVIL ENGINEERING
THE UNIVERSITY
SOUTHAMPTON, ENGLAND

DEL CALHOUN
RESEARCH ASSOC. ENGINEER
A. F. SHOCK TUBE FACILITY
UNIVERSITY OF NEW MEXICO
ALBUQUERQUE, NEW MEXICO

T. F. deCAPITEAU
DRAINAGE PROD. ENGINEER
REPUBLIC STEEL CORP.
1315 ALBERT STREET
YOUNGSTOWN, OHIO

DR. T. A. CARLTON, JR.
DEPT. OF CIVIL ENGINEERING
UNIVERSITY OF ALABAMA
P. O. BOX 6204
UNIVERSITY, ALABAMA

MARC S. CASPE
PARSONS, BRICKERHOFF,
QUADE & DOUGLAS
25 KEARNY STREET
SAN FRANCISCO, CALIF.

DR. C. V. CHELAPATI
CALIFORNIA STATE COLLEGE AT L.A.
LOS ANGELES, CALIF.

GEORGE G. CHORMANN, JR.
4717 PERSHING
FORT WORTH, TEXAS

PROF. GEORGE M. CLARK
OHIO STATE UNIVERSITY
COLUMBUS, OHIO

C. R. CLAUER
CHIEF PRODUCT ENGINEER
REPUBLIC STEEL CORP.
1315 ALBERT STREET
YOUNGSTOWN, OHIO

E. L. CORP
MINING METHODS RES. ENGR.
BUREAU OF MINES
SPOKANE MINING RES. LAB.
N. 1430 WASHINGTON STREET
SPOKANE, WASHINGTON

DR. D. A. DADEPPO
DEPT. OF CIVIL ENGINEERING
UNIVERSITY OF DETROIT
DETROIT, MICHIGAN

PROF. STUART R. DANIELS
DEPT. OF CIVIL ENGINEERING
UNIVERSITY OF TENNESSEE
213 PERKINS HALL
KNOXVILLE, TENNESSEE

DR. M. T. DAVISSON
DEPT. OF CIVIL ENGINEERING
UNIVERSITY OF ILLINOIS
206 TALBOT LABORATORY
URBANA, ILLINOIS

WALTER J. DOHANEY
DEPT. OF CIVIL ENGINEERING
UNIVERSITY OF NEW BRUNSWICK
FREDERICKTON, NEW BRUNSWICK

DR. B. A. DONNELLAN
UNIVERSITY OF NEW MEXICO
BOX 188, UNIVERSITY STATION
ALBUQUERQUE, NEW MEXICO

CAPTAIN ALBERT F. DORRIS
U.S. ARMY CORPS OF ENGINEERS
WATERWAYS EXPERIMENT STATION
VICKSBURG, MISSISSIPPI

JOHN DOTIS
4909 E. TOWER
TUCSON, ARIZONA

RONALD DRAWSKY
KAISER A & C SALES, INC.
300 LAKESIDE DRIVE
OAKLAND, CALIF.

DR. CARL E. EKBERG, JR.
PROFESSOR AND HEAD
DEPT. OF CIVIL ENGINEERING
IOWA STATE UNIVERSITY
AMES, IOWA

DR. NOEL J. EVERARD
ARLINGTON STATE COLLEGE
ARLINGTON, TEXAS

TERRILL C. EWBANK
DEPARTMENT OF ENGINEERING
UNIVERSITY OF ARIZONA
TUCSON, ARIZONA

ARTHUR FELDMAN
MARTIN COMPANY
2045 S. FILLMORE
DENVER, COLORADO

PEDRO FERNANDEZ
APDO 51
NAVOJOA
SONORA, MEXICO

NEAL FITZSIMONS
DIRECTOR, ENG. DEV. DIV
OFFICE OF CIVIL DEFENSE
ROOM 3A334 PENTAGON
WASHINGTON, D. C.

WILLIAM J. FLATHAU
U. S. WES
P. O. BOX 631
VICKSBURG, MISSISSIPPI

JOHN W. FOSS
SUPERVISOR
BELL TELEPHONE LABS
WHIPPANY, NEW JERSEY

RICHARD L. FOSS
CONSOER, TOWNSEND & ASSOC.
360 E. GRAND AVENUE
CHICAGO, ILLINOIS

RAYMOND R. FOX
DEPT. OF CIVIL ENGINEERING
GEORGE WASHINGTON UNIVERSITY
WASHINGTON, D. C.

LEWIS A. FRANK
INSTITUTE FOR DEFENSE ANALYSES
400 ARMY-NAVY DRIVE
ARLINGTON, VIRGINIA

H. A. FUTTRUP
CHIEF STRUCTURAL ENGINEER
R. M. PARSONS COMPANY
617 W. 7th STREET
LOS ANGELES, CALIF.

PROF. LESTER H. GABRIEL
DEPT. OF CIVIL ENGINEERING
SACRAMENTO STATE COLLEGE
SACRAMENTO, CALIF.

MAJOR JOHN T. GAFFEY, II
MISSILE BR., CONST. DIV.
HQ USAF, PENTAGON
WASHINGTON, D. C.

PROF. CHARLES N. GAYLORD
DEPT OF CIVIL ENGINEERING
UNIVERSITY OF VIRGINIA
1531 WESTWOOD ROAD
CHARLOTTESVILLE, VIRGINIA

H. A. GILLESPIE
DEPARTMENT OF ENGINEERING
UNIVERSITY OF ARIZONA
TUCSON, ARIZONA

STANLEY F. GIZIENSKI
VICE PRESIDENT – WOODWARD,
CLYDE, SHERARD & ASSOCIATES
3467 KURTZ STREET
SAN DIEGO, CALIF.

LT. JAMES G. GOVAIA
U. S. ARMY
U. S. ARMY EXPER. STATION
FORT BELVOIR, VIRGINIA

GEORGE E. GRAY
GENERAL ENGINEER
O. C. D. REGION 7
SANTA ROSA, CALIF.

JOHN F. GUARINO
PROJECT MANAGER
ATOMIC WARFARE DEFENSE
BUREAU OF YARDS AND DOCKS
CODE 42.332
WASHINGTON, D. C.

DEAN GUENTHER
DEPT. OF CIVIL ENGINEERING
UNIVERSITY OF ARIZONA
TUCSON, ARIZONA

DR. RICHARD H. GUNDERSON
DEPT. OF CIVIL ENGINEERING
UNIVERSITY OF HOUSTON
HOUSTON, TEXAS

PAUL F. HADALA
U. S. WES
VICKSBURG, MISSISSIPPI

DR. J. R. HALL, JR.
DEPT. OF CIVIL ENGINEERING
UNIVERSITY OF MICHIGAN
ANN ARBOR, MICHIGAN

DR. J. D. HALTIWANGER
DEPT. OF CIVIL ENGINEERING
UNIVERSITY OF ILLINOIS
213 CIVIL ENGINEERING HALL
URBANA, ILLINOIS

DR. DELON HAMPTON
IIT RESEARCH INSTITUTE
10 W. 35th STREET
CHICAGO, ILLINOIS

DR. JOHN T. HANLEY
DEPT. OF CIVIL ENGINEERING
UNIVERSITY OF MINNESOTA
MINNEAPOLIS, MINNESOTA

STANLEY HANSEN
DEPT. OF CIVIL ENGINEERING
UNIVERSITY OF ARIZONA
TUCSON, ARIZONA

DR. BOBBY OTT HARDIN
DEPT. OF CIVIL ENGINEERING
UNIVERSITY OF KENTUCKY
LEXINGTON, KENTUCKY

DR. H. P. HARRENSTIEN
DEPT. OF CIVIL ENGINEERING
UNIVERSITY OF ARIZONA
TUCSON, ARIZONA

DR. JOHN A. HAVERS
IIT RESEARCH INSTITUTE
10 W. 35th STREET
CHICAGO, ILLINOIS

LT. ALFRED J. HENDRON, JR.
U. S. ARMY WES
VICKSBURG, MISSISSIPPI

WALFRED E. HENSALA
SENIOR ENGINEER
EL PASO NATURAL GAS CO.
P. O. BOX 1526
SALT LAKE CITY, UTAH

GEORGE J. HERMAN
ASST. DEAN OF ENGINEERING
MONTANA STATE COLLEGE
BOZEMAN, MONTANA

KAARE HÖEG
RESEARCH ASSOCIATE
MASSACHUSETTS INST. OF TECH.
CAMBRIDGE, MASSACHUSETTS

GEORGE C. HOFF
U. S. ARMY WES
P. O. DRAWER 2131
JACKSON, MISSISSIPPI

RANDON E. HOLBEN
STRUCTURAL ENGINEER
BLANTON AND COLE
P. O. BOX 1711
TUCSON, ARIZONA

PAUL L. HUMMEL
DEPT. OF CIVIL ENGINEERING
UNIVERSITY OF HAWAII
HONOLULU, HAWAII

PROF. JOHN H. HUNTER
VIRGINIA POLYTECHNIC INST.
BLACKSBURG, VIRGINIA

F. M. ISENBERG
RALPH M. PARSONS CO.
617 W. 7th STREET
LOS ANGELES, CALIF.

LOWELL B. JACKSON
DEPT. OF ENGINEERING
PURDUE UNIVERSITY
525 DEXTER LANE
WEST LAFAYETTE, INDIANA

JAMES A. KANEMOTO
CORPS OF ENG. BALLISTIC-
MISSILE CONST. OFFICE
P. O. BOX 4187
NORTON A. F. B., CALIF.

RONALD E. KELLEY
E. D'APPOLONIA ASSOC.
710 SWISSVALE AVENUE
PITTSBURGH, PA.

GEORGE KIZNER
TECHNICAL STAFF
BELL TELEPHONE LABS
WHIPPANY, NEW JERSEY

ALBERT KNOTT, DIRECTOR
SHELTER RES. & STUDY PROG.
PENN STATE UNIVERSITY
101 ENGINEERING A
UNIVERSITY PARK, PA.

DR. R. L. KONDNER
DEPT. OF CIVIL ENGINEERING
NORTHWESTERN UNIVERSITY
EVANSTON, ILLINOIS

PROF. RAYMOND J. KRIZEK
DEPT. OF CIVIL ENGINEERING
TECH-NORTHWESTERN UNIVERSITY
EVANSTON, ILLINOIS

DR. E. M. LAURSEN, HEAD
DEPT. OF CIVIL ENGINEERING
UNIVERSITY OF ARIZONA
TUCSON, ARIZONA

L. R. LAWRENCE
REYNOLDS METALS CO.
6601 W. BROAD STREET
RICHMOND, VIRGINIA

HEINZ G. LEISTNER
THE BOEING COMPANY
P. O. BOX 3707
SEATTLE, WASHINGTON

DR. DON A. LINGER
DEPT. OF CIVIL ENGINEERING
UNIVERSITY OF ARIZONA
TUCSON, ARIZONA

DR. FRANK A. LINVILLE
CHIEF RESEARCH ENGINEER
HOLMES & NARVER, INC.
3030 S. HIGHLAND
LAS VEGAS, NEVADA

A. LONGINOW
ITT RESEARCH INSTITUTE
10 W. 35th STREET
CHICAGO, ILLINOIS

WALTER LUM
WALTER LUM ASSOCIATES
1019-A UNIVERSITY AVENUE
HONOLULU, HAWAII

DR. ULRICH LUSCHER
DEPT. OF CIVIL ENGINEERING
MASSACHUSETTS INST. OF TECH.
CAMBRIDGE, MASSACHUSETTS

MILTON LUTCHANSKY
TECHNICAL STAFF
BELL TELEPHONE LABS
WHIPPANY, NEW JERSEY

ROBERT E. LYNCH
A. F. SHOCK TUBE FACILITY
UNIVERSITY OF NEW MEXICO
1712 TOMASITA, N. E.
ALBUQUERQUE, NEW MEXICO

JOHN N. MACADAM
RESEARCH ENGINEER
ARMCO STEEL CORP.
RESEARCH CENTER
MIDDLETOWN, OHIO

PROF. DALIM K. MAJUMDAR
DEPT. OF CIVIL ENGINEERING
NORTH DAKOTA STATE UNIVERSITY
FARGO, NORTH DAKOTA

R. L. MARINO
IIT RESEARCH INSTITUTE
10 W. 35th STREET
CHICAGO, ILLINOIS

CHARLES E. MARTIN
WHEELER, PETTERSON & COFFEEN
7505 E. 22nd STREET
TUCSON, ARIZONA

HAROLD G MASON
DIV. MANAGER
URS CORPORATION
1811 TROUSDALE DRIVE
BURLINGAME, CALIF.

COL. J. A. MCDONOUGH
DEPT. OF CIVIL ENGINEERING
VIRGINIA MILITARY INST.
LEXINGTON, VIRGINIA

JOE B. MCKEE
6605 FOXHALL LANE
HUNTSVILLE, ALABAMA

PROF. HAAREN A. MIKLOFSKY
DEPT. OF CIVIL ENGINEERING
UNIVERSITY OF SOUTH CAROLINA
COLUMBIA, SOUTH CAROLINA

PROF. WILLIAM M. MILLER
DEPT. OF CIVIL ENGINEERING
UNIVERSITY OF WASHINGTON
SEATTLE, WASHINGTON

J. ALAN MYERS, MANAGER
HIGHWAY CONST. MKTG.
U.S. STEEL CORP.
5 GATEWAY CENTER
PITTSBURGH, PA.

PROF. CHARLES NEWLIN
ARIZONA STATE UNIVERSITY
TEMPE, ARIZONA

DR. N. M. NEWMARK, HEAD
DEPT. OF CIVIL ENGINEERING
UNIVERSITY OF ILLINOIS
205 CIVIL ENGINEERING HALL
URBANA, ILLINOIS

E. F. NIELSEN
KAISER ENGINEERS
300 LAKESIDE DRIVE
OAKLAND, CALIFORNIA

DWAYNE NIELSON
DEPT. OF CIVIL ENGINEERING
UNIVERSITY OF ARIZONA
TUCSON, ARIZONA

EDWARD A. NOWATZKI
DEPT. OF CIVIL ENGINEERING
UNIVERSITY OF ARIZONA
TUCSON, ARIZONA

PROF. BERTEL O. OLSON
DEPT. OF CIVIL ENGINEERING
WASHINGTON STATE UNIVERSITY
PULLMAN, WASHINGTON

WILLIAM R. PERRET
SANDIA CORP.
DIV. 5412
ALBUQUERQUE, NEW MEXICO

JAMES H. POELLOT
DEPT. OF CIVIL ENGINEERING
CARNEGIE INSTITUTE OF TECH.
PITTSBURGH, PA.

WILLIAM F. QUINN
ENGINEER
EL PASO NATURAL GAS CO.
P. O. BOX 1492
EL PASO, TEXAS

DR. R. M. RICHARD
DEPT. OF CIVIL ENGINEERING
UNIVERSITY OF ARIZONA
TUCSON, ARIZONA

PROF. JAMES E. ROBERTS
DEPT. OF CIVIL ENGINEERING
SAN JOSE STATE COLLEGE
SAN JOSE, CALIF.

DR. ABNER SACHS
ENGINEERING ECONOMIC ANALYST
INSTITUTE FOR DEFENSE ANALYSES
400 ARMY-NAVY DRIVE
ARLINGTON, VIRGINIA

JOHN R. SALMONS
DEPT. OF CIVIL ENGINEERING
UNIVERSITY OF ARIZONA
TUCSON, ARIZONA

DR. BRUCE SCHIMMING
UNIVERSITY OF NOTRE DAME
NOTRE DAME, INDIANA

CAPT. S. E. SCHULTZ
DEPT. OF MECHANICS
U. S. AIR FORCE ACADEMY
COLORADO

STUART A. SCHWAM
UNIVERSITY OF PENNSYLVANIA
TOWNE SCHOOL OF CIVIL
AND MECHANICAL ENGR.
PHILADELPHIA, PA.

DR. LYNN SEAMAN
STANFORD RESEARCH INSTITUTE
MENLO PARK, CALIF.

DR. E. T. SELIG
IIT RESEARCH INSTITUTE
10 W. 35th STREET
CHICAGO, ILLINOIS

GEORGE M. SHEETS, LLB.
EDITOR/WRITER
ENGINEERING RESEARCH LAB.
UNIVERSITY OF ARIZONA
TUCSON, ARIZONA

EARL SIBLEY
SHANNON & WILSON, INC.
105 N. 38th STREET
SEATTLE, WASHINGTON

MAJOR R. H. SIEVERS, JR.
USAR&DORAG-OCRD
C/O RES. ANALYSIS CORP.
MCLEAN, VIRGINIA

ROGER E. SKJEI
JOHN A. BLUME & ASSOCIATES
612 HOWARD STREET
SAN FRANCISCO, CALIF.

PROF. R. L. SLOANE
DEPT. OF CIVIL ENGINEERING
UNIVERSITY OF ARIZONA
TUCSON, ARIZONA

AL SMOOTS
PARTNER
DAMES & MOORE
2333 W. 3rd STREET
LOS ANGELES, CALIF.

PROF. ELMIRA S. SMYRL
SCHOOL OF ARCHITECTURE
MONTANA STATE COLLEGE
BOOZEMAN, MONTANA

LOUIS L. SNEDDEN
PRESIDENT MANAGER - R. P. E.
MASON & HANGER
SILAS MASON CO., INC.
33 S. HOGAN STREET
JACKSONVILLE, FLORIDA

ERIK J. SOLLID
1600 S. JOYCE STREET
A605
ARLINGTON, VIRGINIA

ALBERT E. STOLTZ
DEPUTY DIRECTOR
CIVIL DEFENSE AGENCY
112 W. PENNINGTON
TUCSON, ARIZONA

F. J. TAMANINI, JR.
CHIEF STRUCTURAL ENGINEER
ARCHITECTURAL AND DEV. DIV.
DEPARTMENT OF DEFENSE
OFFICE OF CIVIL DEFENSE
WASHINGTON, D. C.

PROF. THEODORE K. TANG
COLLEGE OF ARCHITECTURE
UNIVERSITY OF WASHINGTON
SEATTLE, WASHINGTON

CAPTAIN ROBERT K. TENER
CORPS OF ENGINEERS
WATERWAYS EXPERIMENT STATION
VICKSBURG, MISSISSIPPI

CAPTAIN JOHN P. THOMAS
CIVIL ENGINEERING BRANCH
AF WEAPONS LAB.
KIRTLAND AFB, NEW MEXICO

ANDREW A. THOMPSON
GEOPHYSICIST
BALLISTIC RESEARCH LABS
ABERDEEN PROVING GROUND
ABERDEEN, MARYLAND

PROF. J. NEILS THOMPSON
DIRECTOR - BALCONES RES. CENTER
UNIVERSITY OF TEXAS
173 TAYLOR HALL
AUSTIN, TEXAS

WILLIAM H. TOWNSEND
BALLISTIC RESEARCH LABS.
ABERDEEN PROVING GROUND
ABERDEEN, MARYLAND

DR. GEORGE TRIANDAFILIDIS
DEPT. OF CIVIL ENGINEERING
UNIVERSITY OF NEW MEXICO
ALBUQUERQUE, NEW MEXICO

WILLIAM B. TRUESDALE
IIT RESEARCH INSTITUTE
10 W. 35th STREET
CHICAGO, ILLINOIS

A. R. TURK
DEPARTMENT OF CIVIL ENGINEERING
UNIVERSITY OF ARIZONA
TUCSON, ARIZONA

DR. D. A. VAN HORN
DEPT. OF CIVIL ENGINEERING
LEHIGH UNIVERSITY
BETHLEHEM, PA.

RICHARD G. VAUGHAN
UNIVERSITY OF NEW MEXICO
AF SHOCK TUBE FACILITY
ALBUQUERQUE, NEW MEXICO

PROF. HARVEY E. WAHLS
DEPT. OF CIVIL ENGINEERING
NORTH CAROLINA STATE
RALEIGH, NORTH CAROLINA

DR. REYNOLD K. WATKINS, HEAD
MECHANICAL ENGINEERING DEPT.
UTAH STATE UNIVERSITY
LOGAN, UTAH

W. R. WAYMENT
MINING METHODS RES. ENG.
BUREAU OF MINES
SPOKANE MINING RESEARCH LAB.
N. 1430 WASHINGTON STREET
SPOKANE, WASHINGTON

OLIVER WEBER
6010 LEWIS STREET
ARVADA, COLORADO

G. F. WEISSMANN
TECHNICAL STAFF
BELL TELEPHONE LABS.
MURRAY HILL, NEW JERSEY

PETER S. WESTINE
SOUTHWEST RESEARCH INST.
CULEBRA ROAD
SAN ANTONIO, TEXAS

H. L. WHITE
CHIEF ENGINEER
ARMCO METAL PRODUCTS DIV.
ARMCO STEEL CORP.
4112 FISCHER AVENUE

DR. MERIT P. WHITE, HEAD
DEPT. OF CIVIL ENGINEERING
UNIVERSITY OF MASSACHUSETTS
AMHERST, MASSACHUSETTS

DR. ROBERT V. WHITMAN
MASSACHUSETTS INSTITUTE OF TECH.
CAMBRIDGE, MASSACHUSETTS

C. K. WIEHLE
UNITED RESEARCH SERVICES
1811 TROUSDALE DRIVE
BURLINGAME, CALIF.

RONALD D. WILLIAMS
THE MARTIN COMPANY
2909 FLOWER TREE
ORLANDO, FLORIDA

GILBERT R. WILLIAMSON
OHIO RIVER DIV. LABS.
CORPS OF ENGINEERS
5851 MARIEMONT AVENUE
CINCINNATI, OHIO

PROF. T. H. WU
DEPT. OF CIVIL ENGINEERING
MICHIGAN STATE UNIVERSITY
EAST LANSING, MICHIGAN

DR. DONALD P. YOUNG
DEPT. OF THEORETICAL AND
APPLIED MECHANICS
IOWA STATE UNIVERSITY
AMES, IOWA

J. V. ZACCOR
UNITED RESEARCH SERVICES
1811 TROUSDALE DRIVE
BURLINGAME, CALIF.

DR. EUGENE ZWOYER
DIRECTOR, AF SHOCK TUBE FACILITY
UNIVERSITY OF NEW MEXICO
ALBUQUERQUE, NEW MEXICO



